NAC-V

DAE-BRNS Fifth Symposium on

Nuclear Analytical Chemistry

January 20-24, 2014

Bhabha Atomic Research Centre
Mumbai, INDIA

Editors

R. Acharya
A.V.R. Reddy
A. Goswami
A. Chatt
K.L. Ramakumar

Sponsored by
Board of Research in Nuclear Sciences (BRNS), DAE

Organised in cooperation with
International Atomic Energy Agency (IAEA)

Co-organised by
Indian Association of Nuclear Chemists and Allied Scientists (IANCAS)

For further details contact:

R. Acharya
Secretary, NAC-V
Radiohemistry Division
Bhabha Atomic Research Centre
Trombay, Mumbai 400 085, INDIA
E-mail: racharya@barc.gov.in

Printed by Mr. Vilas Sangurdekar

at

Perfect Prints
22/23, Jyoti Industrial Estate
Nooribaba Darga Road
Thane 400 601, INDIA
Tel.: 022-2534 1291
E-mail: perfectprints@vsnl.net

Published by

Bhabha Atomic Research Centre
Department of Atomic Energy
Trombay, Mumbai 400 085, INDIA

Please Note:

The authors of the papers are alone responsible for
technical content of the papers and references therein.

रतन कुमार सिन्हा
Ratan Kumar Sinha

भारत सरकार
Government of India

अध्यक्ष, परमाणु ऊर्जा आयोग
व
सचिव, परमाणु ऊर्जा विभाग
Chairman, Atomic Energy Commission
&
Secretary, Department of Atomic Energy



Message for NAC-V

I am glad to learn that the Fifth Symposium on Nuclear Analytical Chemistry (NAC-V), sponsored by the Board of Research in Nuclear Sciences (BRNS), Department of Atomic Energy (DAE), is being organised at Bhabha Atomic Research Centre (BARC), Mumbai, during January 20-24, 2014. I am also happy to know that the Symposium is being held in cooperation with the International Atomic Energy Agency (IAEA), and that the Indian Association of Nuclear Chemists and Allied Scientists (IANCAS) is a co-organiser of the event. The application of Nuclear Analytical Chemistry principles and techniques has an important role in both the front and the back end of nuclear fuel cycle. The theme of NAC-V aptly chosen as '**Analytical Chemistry in Nuclear Science and Technology**' will help project the status and advances in the field as well as future prospects. It is learnt that the scope of coverage is wide and includes topics like conventional and prompt gamma-ray activation analysis, alpha, X-ray and gamma-ray spectrometry, ion beam analysis, solid state nuclear track techniques, actinide and trace element speciation studies, environmental radioactivity, nuclear forensics and safety, and QA/QC and uncertainty in measurements.

I am pleased to know that 240 contributed papers will be presented in various technical sessions and as Posters, apart from invited talks to be delivered by experts from India and abroad and that NAC-V will also facilitate close interaction among R & D specialists, academia and industry.

I hope that the Symposium will help in evolving fruitful deliberations and charting out future directions for applications of nuclear analytical chemistry in R&D work in different fields and also provide guidelines for adopting the best practices and QA/QC to support the Indian atomic energy programme.

It gives me great pleasure to know that K.C. College, Mumbai, is hosting a one day technical programme during NAC-V Symposium, as a part of its Diamond Jubilee Celebrations, and I convey my compliments and best wishes to K.C. College.

I wish all the delegates of NAC-V a scientifically stimulating experience during NAC-V and wish the Symposium all success.

(R.K. Sinha)

अणुशक्तिभवन, छत्रपति शिवाजी महाराज मार्ग, मुंबई - 400 001, भारत
दूरभाष : +(91) (22) 2202 2543 • फैक्स : +(91) (22) 2204 8476 / 2284 3888 • तार: एटमर्ग
Anushakti Bhavan, Chhatrapati Shivaji Maharaj Marg, Mumbai - 400 001, India
Phone: +(91) (22) 2202 2543 • Fax: +(91) (22) 2204 8476 / 2284 3888 • Grams: ATOMERG
E-mail: chmn@dae.gov.in

शेखर बसु
Sekhar Basu

सत्यमेव जयते
भारत सरकार
Government of India

निदेशक, भाभा परमाणु अनुसंधान केंद्र
Director, Bhabha Atomic Research Centre
सदस्य, परमाणु ऊर्जा आयोग
Member, Atomic Energy Commission



MESSAGE

I am glad to learn that Fifth symposium on Nuclear Analytical Chemistry (NAC-V)sponsored by Board of Research in Nuclear Sciences (BRNS), DAE, is being organised at Bhabha Atomic Research Centre (BARC), Mumbai during January 20-24, 2014 with the theme as **Analytical Chemistry in Nuclear Science and Technology**. I am also happy to know that NAC-V is organised in cooperation with International Atomic Energy Agency (IAEA) and co-organised by Indian Association of Nuclear Chemists and Allied Scientists (IANCAS). It gives me a great pleasure to know that K.C. College, Mumbai is hosting a one day special technical session during this symposium as part of its Diamond Jubilee Celebrations.

DAE has been in the forefront in standardising and applying nuclear analytical techniques (NATs) like conventional and k_0-based neutron activation analysis, prompt gamma-ray neutron activation analysis, charge particle activation analysis, energy dispersive and total reflection X-ray fluorescence, particle induced X-ray emission, particle induced gamma ray emission, nuclear reaction analysis and α and γ-ray spectroscopy for characterisation of materials that are important to nuclear technology. Neutron and proton based techniques in conjunction with high resolution gamma ray spectrometry methods are used to determine almost all the elements of the periodic table in various samples for R & D work as well as quality control of finished reactor materials. NATs can also be effectively employed to non-destructively determine trans-uranium elements. Speciation of actinides as well as trace elements, which are important for environmental studies, can be carried out by nuclear analytical methods. I am happy to know that BARC and other DAE units have got state of the art facilities for Nuclear Analytical Techniques. The techniques are also part of our departmental programme of effective utilisation of research reactors and accelerators.

I am happy to know that technical program consists of two plenary talks and 35 invited talks by eminent scientists from India and abroad and 240 contributed papers covering all the aspects of nuclear analytical chemistry.

It is heartening that more than 300 delegates will participate in NAC-V. I hope that young researchers from DAE and academic institutes will immensely benefit from the deliberations and take up new challenges which have direct applications towards societal benefits. I hope that delegates will have fruitful discussions during the deliberations.

I wish this Symposium a grand success.

Sekhar Basu
(Sekhar Basu)

15.1.2014

राष्ट्र की सेवा में परमाणु
BARC
ATOMS IN THE SERVICE OF THE NATION

भाभा परमाणु अनुसंधान केंद्र, ट्रॉम्बे, मुंबई - 400 085, भारत • Bhabha Atomic Research Centre, Trombay, Mumbai 400 085, India
दूरभाष / Phone: +(91) (22) 2550 5300, 2551 1910 • तार: बार्क - मुंबई - 400 085 • Gram: BARC-MUMBAI - 400 085
फैक्स / Fax: +(91) (22) 2559 2107, 2550 5151
ई-मेल / E-mail: basus@barc.gov.in / director@barc.gov.in

Dr. P. RAMA RAO
FASc, FNA, FREng.
Formerly Secretary to Govt. of India, DST

INTERNATIONAL ADVANCED RESEARCH CENTRE FOR POWDER METALLURGY AND NEW MATERIALS (ARCI)

(An autonomous R&D Centre of Dept. of Science & Technology, Govt. of India)

Balapur PO, Hyderabad-500 005, India

January 15, 2014



MESSAGE

I am glad that Fifth Nuclear Analytical Chemistry Symposium (NAC-V) is being organized at Bhabha Atomic Research Centre (BARC), Mumbai during January 20-24, 2014 which is cosponsored by Board of Research in Nuclear Sciences (BRNS). The theme of NAC-V is '**Analytical Chemistry in Nuclear Science and Technology'** and I am happy that this theme based symposium is supported by BRNS. Nuclear Analytical Chemistry is of multidisciplinary nature that finds applications in several areas of science and technology. The Nuclear Analytical Techniques (NATs) can be deployed in various fields like agriculture, nuclear medicine, forensics and material science which can immensely benefit our society. I hope that DAE and BARC will work towards popularization of these techniques by initiating collaborative research programs with Universities and improving the accessibility of these techniques.

I sincerely hope that NAC-V will act as a catalyst in promoting the growth of Nuclear Analytical Chemistry and NATs in the country. The one day special technical session at K.C. College will provide the college students an overview of these techniques, and their possible applications. Activities involving Colleges and educational institutions would generate interest among young academics and scientists and provide impetus to take up research in this field.

I am happy that IANCAS is associated with this important theme based symposium. It is heartening to note that more than 300 delegates are participating in NAC-V. I am sure that this symposium will give them a good platform for interaction and future collaborations among different academic institutes and Universities in India and abroad. I wish NAC-V all success.

P. Rama Rao.

(P. Rama Rao)
Chairman, BRNS

Phone : (O) 24443572/24443167, (R) 66614475, (M) 98497-65123
Fax : 0091-40-24441468, 24443168, E-Mail : pallerama_rao@yahoo.co.in

एस.जी. मार्कंडेय,
नियंत्रक
S.G. Markandeya,
Controller

सत्यमेव जयते

सेंट्रल कॉम्प्लेक्स,
ट्रॉम्बे, मुंबई - 400 085
Central Complex,
Trombay
Mumbai - 400 085

भारत सरकार
GOVERNMENT OF INDIA
भाभा परमाणु अनुसंधान केंद्र
BHABHA ATOMIC RESEARCH CENTRE



No. BARC/CONT/PERS/2013/ **January 15, 2014**

MESSAGE

I am extremely happy to know that the 5th Symposium on "Nuclear Analytical Chemistry - (NAC-V)" is being organized at Bhabha Atomic Research Centre (BARC), Mumbai, during January 20-24, 2014 in cooperation with the International Atomic Energy Agency (IAEA) and the Indian Association of Nuclear Chemists and Allied Scientists (IANCAS). It also gives me great pleasure to know that the K.C. College, Mumbai is hosting a one day special technical programme of NAC-V as a part of their Diamond Jubilee Celebrations this year.

Under the mandate of DAE's programme to exploit the nuclear energy at its full potential for the country's progress and prosperity, Nuclear Analytical Chemistry undoubtedly plays a very important role due to its wide applications in both the front and the back end of nuclear fuel cycle. In my view, some of the important analytical techniques such as; conventional and prompt gamma-ray activation analysis, Alpha, X-ray and gamma-ray spectrometry, Ion beam analysis, Solid state nuclear track techniques, Radioisotope production and applications, Actinide and trace element speciation studies, Environmental radioactivity, Nuclear forensics and safety, QA/QC and uncertainty in measurements, etc. need constant update considering the latest in the their state-of-the-art world over. I am sure that this will be best accomplished during the deliberations of the symposium with the strong participation of experts from abroad and also from within the country. I have observed that as in the past, the technical contents of the symposium are of very high quality and I wish that the interactions among the experts for the five days during the symposium will result into future directions of research in this very important field.

The association of BRNS in supporting such an important national event always brings great pride to DAE and to me personally. I consider it as my privilege and pleasure to be associated with NAC-V and wish all the delegates a scientifically stimulating experience during this symposium. I thank the organizers for giving me such an opportunity of association with NAC-V.

I wish the symposium a grand success.

(S. G. Markandeya)

दूरभाष / Telephone : +(91) (022) 2550 5354 • फैक्स / Fax : +(91) (022) 2550 5354, 2550 5151
ई-मेल / E-mail : sgmarkan@barc.gov.in

Preface

Analytical Chemistry is a branch of science that finds applications in almost all fields of science and technology. The demand for accurate and precise data are ever increasing, particularly in the areas like material sciences, life sciences, environmental studies and industry. Rapid developments in electronics, computers and instrumentation provided the required impetus to meet the demand to decrease the detection limits and resulted in the evolution of software that could decipher and extract reliably the signal from noise.

Most of the analytical techniques are wet chemical based and therefore not free from reagent blank. Chemical dissolution is often difficult for the samples like alloys and ceramics. Besides for the compositional analysis of finished products, a non destructive analytical method is preferred. Nuclear Analytical Techniques (NATs) meet this requirement as NATs are often non-destructive techniques.

George de Hevesy was the first to use radioisotopes as tracers and also discovered neutron activation analysis and applied it for trace element determination in a variety of samples. Horizons of nuclear analytical techniques (NATs) expanded by leaps and bounds with the availability of nuclear reactors and particle accelerators. Today Nuclear Analytical Techniques find applications in all the branches of science and technology due to their properties like inherent accuracy, precision and selectivity. Most of the techniques are non-destructive and capable of simultaneous multielement determination. Neutron and proton based techniques in conjunction with high resolution gamma ray spectrometry methods can be used to determine elements from H to U. NATs can also be effectively employed to non-destructively determine trans-uranium elements. Techniques like activation analysis using neutrons (NAA and PGNAA) and protons (CPAA), ion beam analysis (PIXE, PIGE and NRA), X-ray Fluorescence (XRF) analysis are extensively used in various R&D programs as well as for material characterization in nuclear technology. DAE is one of the leaders in developing and deploying nuclear analytical methods like Activation analysis methods using n, p and photon. IBA methods like PIXE, PIGE, RBS and NRA, EDXRF, TXRF, and and -ray spectrometry are in continuous use for characterization of materials that are important to nuclear technology. Developments in NATs and their applications are expanding at a study pace in DAE, India and various institutes abroad. It is appropriate to pause, review the progress made and evolve strategies to identify areas that find unique applications of radiotracers, radiations and Nuclear Analytical Techniques (NATs). This prompted the organisation of Symposia series of Nuclear Analytical Chemistry (NAC). NAC-I to NAC-III were held in Canada. NAC-IV was organized at BARC during November 15-19, 2010 and the current symposium, NAC-V is organized at BARC during January 20-24, 2014.

NAC-V is aimed at reviewing the current status of NATs as well as other related Nuclear Analytical Techniques used for nuclear material analysis. Thus the theme of NAC-V is Analytical Chemistry in Nuclear Science and Technology. Both fundamental and applied aspects of the subject area will be covered in various technical sessions. Topics like utilization of research reactors and accelerators, and applications of NAC to geological, biological, environmental, archaeological, pharmaceutical, industrial, nutritional and nuclear materials, speciation studies, nuclear forensics and safety aspects will be covered in this symposium.

Success of any symposium depends on the technical content. It is satisfying that a large number of contributions have been received from abroad, Indian academic Institutes and DAE Units. Technical Contents comprise of two plenary talks, 25 invited talks and 10 invited orals (short talk) by experts in the field. Contributed papers (240) will be oral and poster presentated in 15 technical sessions. Organisers will present IANCAS awards for the best poster and oral paper presentations to young academics, scientists and research students.

We received continuous support and guidance from authorities which enabled us to organize NAC-V. We profusely thank Dr. R. K. Sinha, Chairman, Atomic Energy Commission and Secretary,

Department of Atomic Energy, Government of India for providing guidance and encouragement for organizing this symposium as Chairman of the Advisory Committee and giving a message. He has kindly agreed to inaugurate special one day technical programme of NAC-V at K C College, Mumbai on 22nd January, 2014. We are grateful to Shri Sekhar Basu, Director, BARC for his support and consenting to Inaugurate NAC-V. We thank Prof. P. Rama Rao, Chairman, Board of Research in Nuclear Sciences (BRNS) for his encouragement.

NAC-V is BRNS sponsored symposium and organisers thank BRNS, DAE for its support. We thank IAEA for its cooperation in organising NAC-V. IANCAS is synonymous with the organisation of Symposia related to Nuclear and Radiochemistry and we thank them for coorganising NAC-V.

Support and co-operation of Dr. K.L. Ramakumar, Director, Radiochemistry and Isotope Group, Chairman, NAC-V Organizing Committee is gratefully acknowledged. We thank Dr. B.N. Jagatap, Director, Chemistry Group, BARC for his constant support. Thanks are due to Dr. S.G. Markandeya, Member Secretary, BRNS and Controller, BARC for his keen interest in this symposium. We take this opportunity to thank Prof. A. Chatt, Dalhousie University, Canada and Co-Chairman, Technical Committee for his support and enthusiasm in organising NAC-V in BARC.

We thank all the members of the Advisory Committee, Organizing Committee, Technical Committee and Finance Committee for their valuable support during the formulation of the technical content of the symposium. We are fortunate to have experts in various committees who shared their valuable experience.

We thank Dr. K.K. Swain, Dr. D. Alamelu, Dr. S.K. Thulasidas, Shri K. Venkatesh, Dr. K.V.V. Nair and Shri K.B. Dasari who have contributed immensely in coordinating publication of this book of Abstracts.

We are grateful to the members of Local Organizing Committee (LOC), and Dr. P.K. Pujari, Head, Nuclear Chemistry Section, RCD, BARC who have worked with dedication in organizing this symposium. The efforts made by the conveners of several sub-committees of LOC namely Dr.(Smt.) Suparna Sodaye (Registration), Dr. P.N. Pathak and Dr. D. Alamelu (Souvenir), Shri T.P. Chaturvedi and Dr. A.C. Deb (Accommodation), Dr. Rahul Tripathi and Shri Pranaw Kumar (Transport), Dr. S.K. Thulasidas and Shri M.K. Saxena (Catering), Shri K.C. Jagadeesan and Dr. K.K. Swain (Poster Display), Shri S.Jeyakumar (Exihibition), Shri D.B. Paranjpe and Shri R.G. Dalavi (Hall arrangement) and Dr. Lalit Varshney (Finance). But for the sincere and dedicated efforts of Shri Sharad Nalawade this abstract book would not have been possible. We thank Shri Sharad Nalawade, Shri Vishal N. Koli and Prefect Prints for their effort in printing and publishing the abstract book. Thanks are due to administrative staff of RC&IG, CG, ACD and RCD and special thanks are to Shri Lokesh Joshi, Shri S.R Iyer and Smt. Namrata Kadam. We thank Dr. B.K. Dutta, Head, HRDD and personnel of BARC Training School Hostel for permitting us to hold NAC-V at TSH.

R. Acharya, A. Goswami, A.V.R. Reddy



DALHOUSIE UNIVERSITY
Inspiring Minds

Faculty of Science
2014 January 09

Dear Colleagues,

It is a great honor to welcome you at the Fifth Symposium on Nuclear Analytical Chemistry (NAC-V) being held at the Bhabha Atomic Research Centre (BARC) during 2014 January 20-24. It is being co-sponsored by Board of Research in Nuclear Sciences (BRNS), Department of Atomic Energy (DAE), BARC, Indian Association of Nuclear Chemists and Allied Scientists (IANCAS), and K.C. College in India, and by the International Atomic Energy Agency (IAEA), United Nations.

Some of you may know that I started the NAC series of symposia in Canada with NAC-I at Dalhousie University in Halifax in 1985 June, NAC-II at the University of Toronto in 1992 June to honor Professor Robert E. Jervis, and NAC-III in Halifax in 2001 June to honor several world-famous nuclear analytical chemists. Then I decided that NAC-IV should be held in a country where nuclear analytical chemistry is flourishing and both young scientists and students can attend it. I concluded that BARC will be the best place to hold future NAC symposia. So NAC-IV was held here during 2010 November 15-19. It was a resounding success. It was attended by about 300 delegates from various units of DAE and academic institutes in India along with 27 delegates from foreign countries. The technical program consisted of 30 invited oral and 215 contributed presentations (oral and poster). After an extensive review 85 papers were selected for publication in the Journal of Radiochemical and Nuclear Chemistry (JRNC).

The primary objective of the NAC symposia has been to provide a forum for exchange of information on recent developments in nuclear analytical chemistry. Both fundamental and applied aspects of the subject area have been covered in scientific sessions and informal discussions. A broad range of topics have been covered including: instrumental, preconcentration and radiochemical activation analysis, prompt gamma activation analysis, large sample analysis, nuclear track techniques, nuclear probe and micro-probe techniques, stable and radioisotope tracers, gamma-, alpha- and X-ray spectroscopy, radioactive waste management, speciation, specimen banking, counter terrorism initiatives, and applications of these techniques to atmospheric, biological, biomedical, environmental, epidemiological, forensic, geological, industrial, nuclear, nutritional materials, etc.

NAC-V is set to be as successful as NAC-IV, if not more. I am thankful to the members of many committees, listed in the program, who worked very hard over the last year or so to make NAC-V a very successful symposium. I would like to particularly mention the following persons for their enormous contribution to the organization of NAC-V: Dr. R.K. Sinha, Chairman, Atomic Energy Commission; Dr. S. Basu, Director, BARC; Dr. K.L. Ramakumar, Director, Radiochemistry and Isotope Group; Dr. A.V.R. Reddy, Head, Analytical Chemistry Division; Dr. A. Goswami, Head, Radiochemistry Division; Dr. P.K. Pujari and Dr. R. Acharya, Radiochemistry Division, BARC.

A. Chatt

Amares Chatt, Ph.D., F.C.I.C., F.A.N.S.
Dalhousie University
President, NAC Symposia
President, International Committee on Activation Analysis
Editor, Journal of Radiochemical and Nuclear Chemistry

Department of Chemistry, Dalhousie University, P.O. Box 15000, Halifax, NS B3H 4R2, Canada
Phone: (902) 494-3305, Fax: (902) 494-1310, www.chemistry.dal.ca

NAC-V at a Glance

The Fifth Symposium on Nuclear Analytical Chemistry (NAC-V) is sponsored by Board of Research in Nuclear Sciences (BRNS), Department of Atomic Energy (DAE), India and is organised at the Bhabha Atomic Research Centre (BARC), Mumbai during January 20-24, 2014. The symposium is organised in cooperation with International Atomic Energy Agency (IAEA) and co-organised by Indian Association of Nuclear Chemists and Allied Scientists (IANCAS). A one day special programme of NAC-V is planned at K.C. College on January 22, 2014 as part of its Diamond Jubilee Celebrations and Dr. R.K. Sinha, Chairman, Atomic Energy Commission and Secretary, DAE will be Chief Guest. NAC-V consists of two Plenary Talks, 25 Invited Talks, 10 Invited Orals and 240 contributed paper presentations. Chief Editor, Journal of Radioanalytical and Nuclear Chemistry (JRNC) has agreed to publish 75 full papers after review. The scope wise number of abstracts accepted in NAC-V are given below.

Conventional and prompt gamma-ray activation analysis - 21

Alpha, X-ray and gamma-ray spectrometry - 33

Ion beam analysis techniques -16

Analytical chemistry in nuclear technology -46

Solid state nuclear track techniques - 11

Radioisotope production and applications - 33

Actinide and trace element speciation studies - 09

Environmental radioactivity - 58

Nuclear forensics and safety -05

QA/QC and uncertainty in measurements -08

More than 300 delegates including 18 scientists from abroad (USA, Canada, UK, Japan, Poland, Slovenia, Czech Republic, Mexico, Thailand, South Korea, Russia and Malyasia/Austria) and from institutes like IAEA, NIST, AECL and JAEA are participating in NAC-V. DAE participants are from 11 Units including BARC, IGCAR, NFC, HWB, NPCIL and AMD. More than 100 delegates from 42 academic institutes are participating in NAC-V. NAC-V will be inaugurated by Shri Sekhar Basu, Director, BARC and it will be followed by two plenary talks: (i) Dr. D.B. Mohamad, Deputy Director General, IAEA and (ii) Dr. B. Sur, Director, Nuclear Sciences Division, AECL, Canada. Presentations of Invited Talks, Invited Orals, Posters (209) and Orals (31) will be presented in 15 technical sessions. Senior scientists from India and abroad have agreed to Chair Technical Sessions. About 15 IANCAS awards for the best Poster and Oral presentations will be given. A panel discussion is scheduled on the last day of the symposium to summarise the technical contents under each category (scope) and to chalk out the future directions. NAC-V will conclude with a Valedictory Session. Dr. S. Banerjee, Homi Bhabha Chair Professor and Former Chairman, AEC will be the Chief Guest and Shri S.G. Markandeya, Controller, BARC and Sciencitific Secretary, BRNS, DAE will be the Guest of Honour for the Valedictory Session.

NAC-V

Advisory Committee

Sinha, R.K., Chairman, AEC, India . . Chairman
Basu, S, India
Belgya T., Hungary
Revay Z., Germany
Braun T., Hungary
Bennet John, Australia
Chatt A., Canada
Daud Mohamad, IAEA, Austria
De Corte F., Belgium
De Nadai Fernandes E., Brazil
Ebihara M., Japan
Garg A. N., India
Greenberg R. R., USA
Kailas, S., India
Dr. A.K. Kohli India
Kucera J., Czech Republic
Manchanda V.K., South Korea
Manohar S. B., India
Markandeya, S.G., India
Meera Venkatesh, IAEA, Austria
Modis, B.S., Slovenia
Mukherjee T., India
Nyarko,B., Ghana
Parihar, P.S.,India
Prasad, G.J., India
Raina V. K., India
Ramakumar, K.L., India
Rama Rao P., India
Ramamoorthy N., India
Rao, Raghu, R, Canada
Sarkar, S.K., India
Sai Baba, N., India
Prof. Satya Prakash, India
Sue B Clark, USA
Sood D. D., India
Sharma, D. N., India
Turel Z. R., India
Vasudeva Rao P. R India
Venugopal V., India
Wattal, P.K., India
Purohit, K. C., India
Rajnish Prakash, India
Acharya, D., India
Patra, R. N., India

Finance Committee

Varshney L., BARC . . . . . Chairman
Jeyakumar S., BARC. . . . . Co-Chairman
Pai Rajesh, BARC
Dubey B.P., BARC
Singhal R.K., BARC
Agrawal K.U., BARC

Organizing Committee

Ramakumar, K. L., BARC . . . . . Chairman
Reddy, A.V.R., BARC . . . . . Convener
Aggarwal, S.K., BARC
Bandekar, J.R., BARC
Bagla Hemlata, KC College, Mumbai
Bhanumurthy, K., BARC
Bhatnagar, A., BARC
Chatt, A., Dalhousie Univ., Canada
Datar, V.M., BARC
Desai, Shripal, Gem Inst. India, Mumbai
Goswami, A., BARC
Gurusharan, Singh, BARC
V. D. Puranik, BARC
P.K. Sarkar, BARC
Sunil Jai Kumar, BARC
Lakshman Das N., GITAM University, Vizag
Mangaonkar, K., Mithibai College,
Nagarajan, K., IGCAR
Pillai, M.R.A., BARC
Pujari, P. K., BARC
Rajurkar, N. S., Pune University
Sangeeta, BRNS, BARC
Seshaiah, K., S.V. University, Tirupati
Sharma, A.K., BARC
Pradeep Kumar, BARC
Shukla, D.K., BARC
Srivastava Alok, Panjab University
Tomar, B.S., BARC
Varshney L., BARC
Velmurugan, BARC
Verma, R., BARC
Vitthal, G. K., HWB,
Sharma, R.C., BARC
Singh, P., BARC
Acharya, R., BARC . . . . . Secretary

Technical Committee

Chatt, A., Dalhousie Univ., Canada . . Co-Chairman
Goswami, A., BARC. . . . . Co-Chairman
Acharya, R., BARC
Alamelu, D., BARC
Banerjee, S., BARC
Chowdhury, D.P., VECC, Kolkata
Das, M.K., BRIT, VECC, Kolkata
Das, S.K., VECC, Kolkata
Dash, A., BARC
Jeyakumar, S., BARC
Joshi, A.R., BARC
Kamat, J.V., BARC
Kaushik, C.P., BARC
Lahiri, S., SINP, Kolkata
Mallik, G.K., BARC
Misra, N.L., BARC
Mohapatra, P.K., BARC
Natarajan, V., BARC
Pandey, A.K., BARC
Pathak, P.N., BARC
Pujari, P.K., BARC

Ravi, P.M., BARC
Sangita, D.K., BARC
Sanjeev, Kumar, NCCCM,
Shankaran, K., IGCAR
Sawant, R.M., BARC
Saxena, M.K., BARC
Swain, K.K., BARC
Tripathi, R., BARC
Tripathi, R.M., BARC
Venkatsubramani, C. R., IGCAR
Pant, H J, BARC
Dash, S C, TAPS,
Mukerjee, S.K., BARC

Co-opted Technical Committee Members

Agarwal C., BARC
Anilkumar S., BARC
Bagla H., BARC
Bharadwaj Y.K., BARC
Chakraborty S., BARC
Das Tapas, BARC
Dutta D., BARC
Jha S.K., BARC
Kadam R.M, BARC
Kalsi P.C., BARC
Kannan S., BARC
Mohapatra Manoj, BARC
Murali M.S., BARC
Pranaw Kumar, BARC
Rao D.D., BARC
Rawat Neetika, BARC
Sadaye S., BARC
Sawant Pramila, BARC
Sudarsan K., BARC
Sumit Kumar, ABRC
Thulasidas S.K., BARC
& Others

Local Organizing Committee

Pujari, P.K., BARC . . . . . Chairman

Registration

Sodaye Suparna . . . . . Convener
Venkatesh K. . . . . Co-Convener
Rawat Neetika
Remya Devi, P.S.
Adya V.C.
Vishal N. Koli
Lokesh Joshi
Acharya A.
Manisha V.
Gupta Santosh
Paul Sumana
Biswal J.
Choudhury Sanhita
Naik Apoorva

Accommodation

Chaturvedi T.P.. . . . . Convener
Deb A.C. . . . . Co-convener
Chandrashekar D.
Dutta D.
Kishore Babu D.
Shinde Rakesh N.

Transport

Tripathi R. . . . . Convener
Pranaw Kumar . . . . . Co-Convener
Chandrashekar D.
Kishore Babu D.
Shinde Rakesh N.
Chillar Sumit
Sudarshan K.

Catering

Thulasidas S.K.. . . . . Convener
Hasilkar S.P.
Pradeep Kumar
Nair K Vimalnath

Conference Banquet

Saxena M.K.
Thulasidas S.K.

Hall Management

Paranjpe, D.B. . . . . Convener
Dalavi R.G.. . . . . Co-convener
Pente A.S.
Satpati A.
Koli Chhaya
Soren Sibu
Kadam Namrata

Poster Display

Jagadeesan, K.C. . . . . Convener
Swain K.K. . . . . Co-Convener
Sonar N.L.
Chillar Sumit
Nicy Ajith
Tamilarasu
Mahatre Amol
Shinde Amol D
Brahmaji Rao J.S.

Exhibition

Jeyakumar S. . . . . Convener
Pai Rajesh V

Editors of IANCAS Special Bulletin

Pathak P.N.
Alamelu D.
Acharya R.
Varshney L.
Reddy A.V.R.

Printing, Publication and JRNC full paper

Reddy A V R
Acharya R.
Swain, K. K.
Venkatesh K.
Nair Vimalnath
Nalawade Sharad
Thulasidas S.K.
Alamelu D
Dasari K.B.

Administrative Support

Vishal N. Koli, Joshi Lokesh, Rawat Megha
Susheela Shinde and office staff of
RCD, ACD, CG and RC&IG

Table of Contents

Plenary Talk (PT)

PT-1 **Securing a Better Future for All: Making a Difference with Nuclear Technology 1**
Daud Mohamad

PT-2 **Applications of Nuclear Analytical Techniques for Identifying the Origin and Composition of Found Radioactive Materials 3**
B. Sur, F. Dimayuga, L. Li, G. Li, G. Bentoumi, R. Rogge

Invited Talk (IT)

IT-1 **Development and Applications of k_0-based NAA using Research Reactors at BARC 5**
R. Acharya and A.V.R. Reddy

IT-2 **Applications of Fast Neutron Generators 8**
Amar Sinha

IT-3 **Photon Activation Analysis 10**
H. Naik

IT-4 **Compton Scattering and its Applications: Current Status and Future Prospects 12**
B.L. Ahuja

IT-5 **Synchrotron Radiation based Analytical Techniques (XAS & XRF) 14**
Shambhu Nath Jha

IT-6 **Prediction on the Origin of Ancient Glass Beads by Studying its Potassium content by Compton Suppressed -ray Spectrometry 17**
Kaushik Gangopadhyay, Moumita Maiti, Susanta Lahiri

IT-7 **Application of Analytical Nuclear Techniques to the Heaviest Elements 20**
Y. Nagame, A. Toyoshima, K. Tsukada, M. Asai, T. K. Sato, M. Schäel

IT-8 **Production of ^{261}Rf, ^{262}Db, and ^{265}Sg for Chemical Studies using the Gas-jet Transport System Coupled to GARIS 22**
H. Haba

IT-9 **Nuclear Analytical Techniques in the LMFBR programme 24**
C.R. Venkata Subramani

IT-10 **Studies of Nutritionally and Toxicologically Important Elements in Foods and Diets by Neutron Activation. 26**
A. Chatt

IT-11 **Emerging Applications of Radioisotopes in Nuclear Medicine 28**
Sandip Basu

IT-12 **Half-life Measurement of ^{7}Be in Materials 30**
T. Ohtsuki

IT-13 **Radioactive Sources: Promises, Opportunities, and Challenges to meet the Industrial and Clinical Demands 31**
Ashutosh Dash

IT-14 **Recent Advances in Radiotracer Applications in Industry 34**
H.J. Pant

IT-15 **Optodes for Sensing Metal Ions 38**
Ashok K. Pandey

IT-16 **Recent Trends in Mass Spectrometry for Nuclear Forensics 42**
S.K. Aggarwal

IT-17 **The Potential for Radionuclide and Isotopic Analyses using a Rapid Scanning Magnetic Sector ICP-MS 44**
John Cantle

IT-18 **Assessment of Intakes of Radionuclides : Systems and Methods for Routine and Emergency Scenarios 46**
K.S. Pradeepkumar

IT-19 **Identifying and Correcting Errors in NAA Measurements Using Internal Consistency Checks 49**
Robert R. Greenberg and Richard M. Lindstrom

IT-20 **QA/QC and Uncertainty Assessment in k_0 based NAA 51**
B. Smodiš

IT-21 **Recent Advances in Ratio Primary Reference Measurement Procedures (Definitive Methods) and their Use in Certification of Reference Materials and Controlling Assigned Values in Proficiency Testing 53**
R.S. Dybczyñski, H. Polkowska-Motrenko, E.Chajduk, B. Danko, M. Pyszynska

IT-22 **Deuterium Build up in Moderator Cover Gas System of 540 MWe PHWRS, during Normal Operation and during Reactor Shutdown 55**
S.C. Dash, G. Sriram, R.P.S. Tomer

IT-23 **Effect of Crystal Structure of the Sorbent on the Sorption of Metal Ions 60**
B.S. Tomar

IT-24 **Biosorption study of Radiotoxic Nuclide and toxic Heavy Metals using Green Adsorbent 62**
Hemlata K. Bagla

IT-25 **Development of Particle Induced Gamma-ray Emission methods for low Z Elements and Applications to Materials important for Nuclear Technology 65**
R. Acharya

Invited Oral (IO)

IO-1 **Analysis of Mixture Samples of Uranium Dioxide and Boron Compounds by using Thermal Neutron Prompt Gamma Activation Analysis. 68**
G.M. Sun, E.J. Lee, Hani Baek, Y.W. Lee, G.S. Kim, J.H. Yang

IO-2 **Peptide Receptor Radionuclide Therapy with ^{177}Lu-DOTA-TATE: From Laboratory to Clinics in India. 70**
Tapas Das

IO-3 **Japanese Fir leaves has the Highest Collection Efficiency for ^{137}Cs among Leaves of Six Tree Species in the Ishinomaki Area of Miyagi Prefecture 72**
M. Fukushima, T. Matsutani, T. Nemoto

IO-4 **Production of Radioactive Tracers for Observation of behavior of Radioactive Cesium in Environmental Materials 74**
K. Takamiya, T. Ohtsuki

IO-5 **Applications of Nuclear Analytical Techniques for Impact of Industry to the Environment. 75**
R.K. Dutta, S. Sarkar, R.S. Maharia, M. Sudarshan, R. Acharya, A.V.R. Reddy

IO-6 **X-ray Photoelectron Study on Nitrogen in Explosives: Chemical Fertilizer 77**
P. Dararutana

IO-7 **Radiometric Enzyme Assays: Studies of Fluoxetine Interaction with Thyroid Hormones Metabolism 78**
S. Pavelka

IO-8 **Speciation of Uranium in Solid Matrices 80**
M. Mohapatra and V.Natarajan

IO-9 **Estimation of the Indoor Radon and the Annual Effective Dose from Building Materials 82**
P. Sola, W. Srinuttrakul, S. Laoharojanaphand, N. Suwankot

IO-10 **Mass Spectrometric Determination of Thorium and Uranium in Human Hair and Nails in a High Background Natural Radiation Area of Serbia 84**
S.K. Sahoo

A. Conventional and Prompt Gamma-ray Activation Analysis

A-1 **Improvement of Sensitivities and Detection Limits in Estimation of Rare Earth and Trace Elements in Geological Rock Samples by INAA using DHRUVA Reactor Compared to CIRUS Reactor at BARC, Mumbai 86**
N. Rupa, G.B. Rout, H.B. Shrivastava, V. Koteswara Rao and B.K. Pandey

A-2 **Does Anticoincidence Counting Improve Detection Limits of Short-lived Nuclides by Pseudo-cyclic INAA? 88**
W. Zhang, A. Chatt

A-3 **Determination of Boron in Selected Canadian and Japanese vegetables by Prompt Gamma Activation Analysis 90**
M. Fukushima, H. Matsue, A. Chatt

A-4 **Online Recovery of Radiocesium from Soil, Tissue Paper and Plant Samples by Supercritical Fluid Extraction 92**
A.S. Kanekar, P.N. Pathak, P.K. Mohapatra

A-5 **Analysis of Essential Elements in Medicinal Plants and their Respective Soils by Neutron Activation Analysis 94**
M. Ratna Raju, P.V. Madhusudhana Rao, M.K. Raju, J.S. Brahmaji Rao, D.Vijayalakshmi, N.P. Seshadreesan, C.R. Venkatasubramani

A-6 **The Analysis of Synthesized Copper Bhasma Using Neutron Activation Analysis Technique 96**
Shailesh Kantak, Tanuja Nesari, Nilima Rajurkar

A-7 **Characterization of Kidney Stones using NAA and other Techniques 98**
A Srivastava, K.K. Swain, Nicy Ajith, T. Chavan, S. Bhardwaj, B. Vashisht, D.N. Wagh, U. Mete, R. Acharya and A.V.R. Reddy

A-8 **Determination of Gold in Copper Concentrate using Neutron Activation Analysis 100**
P.S. Remya Devi, Aditi.A. Dalvi, K.K. Swain and R. Verma

A-9 **Evaluation of Soil to Tea Plant Elemental Correlation using k_0 based Internal Monostandard Neutron Activation Analysis 102**
Rupali A. Lagad, D. Alamelu, K.B. Dasari, R. Acharya, Suresh K. Aggarwal

A-10 **Performance of Digital Gamma ray Spectrometer for loss free counting and its Application in NAA for quantification of Aluminum** 104
R. Acharya, K.B. Dasari, D. Chandrasekhar, T.P. Chaturvedi, P.K. Pujari

A-11 **Instrumental NAA for Determination of Trace Elements in Zirconium Oxide and Aluminium Samples** 106
A.D. Shinde, R. Acharya, A.V.R. Reddy

A-12 **Determination of Aluminium content in Foodstuffs by Neutron Activation Analysis utilizing PCF of Dhruva Research Reactor** 108
B.B. Nanda, R.R. Biswal, A. D. Shinde, R. Acharya, P.K. Pujari

A-13 **Inorganic Arsenic Speciation using Membrane Based Separation in Conjunction with HPLC and NAA** 110
Rakesh N. Shinde, A.K. Pandey, R. Acharya, S.A. Ansari, N.S. Rajurkar

A-14 **Utilization of Pneumatic Carrier Facility of Dhruva Reactor for Trace Element Determination by Neutron Activation Analysis** 112
R. Acharya, P.K. Pujari, K.K. Swain, R. Verma, A.V.R. Reddy, N.S. Bhamra, Renuka Patel, K. Chakrabarty, C.G. Karhadkar, Tej Singh, K.P. Singh and Y.S. Rana

A-15 **Elemental Compositional Analysis of Meteorites by Prompt Gamma-ray Neutron Activation Analysis (PGNAA)** 114
Bharat Adur, H.B. Mali, R. Acharya, Z. Revay, T. Belegya, and P.K. Pujari

A-16 **Utilization of AHWR Critical Facility for Research and Development Work on Large Sample NAA** 116
R. Acharya, K.K. Swain, K.B. Dasari, P.K. Pujari, A.V.R. Reddy, S.K. Verma and S.K. De

A-17 **Analysis of Arsenic Accumulation by NAA and its effects on the Mineral Nutrient Profile of Rice (Oryza sativa) Plants** 118
Sudhakar Srivastava, J. J. Akkarakaran, Rakesh N. Shinde, R. Acharya and P. Suprasanna

A-18 **Expanded uncertainties for chlorine, bromine and iodine in Bovine Milk Organohalogens Measured by Neutron Activation** 120
K. Isaac-Olive, A. Chatt1

A-19 **Estimation of Uranium in geological rock samples by Beta-Gamma method and its comparison with Pellet Fluorimetry method** 122
Rita, M.A. Nayeem, Diwakar Gaur, G.B. Rout, B.K. Pandey and A.K. Sarangi

A-20 **Applications of relative and internal monostandard NAA methods for analysis of alloys: as a part of chemical quality control exercise.** 124
A.D. Shinde, R, Acharya, A.V.R. Reddy

A-21 **Neutron Activation Analysis of Minerals from Cuddapah Basin Geological Formations** 126
P.V. Nagendra Kumar, N. Suresh Kumar, R. Acharya, A.V.R. Reddy, L. Krishna Reddy

B. Alpha, X-ray and Gamma-ray Spectrometry

B-1 **Raman and XPS Analyses of the Oxide Formed Over Monel Surfaces Under the Steam Generator Chemistry Conditions in the Presence of Poly(acrylic acid-co-maleic acid) [PAMA]** 128
Akhilesh C. Joshi, A.L.Rufus, S. Velmurugan

B-2 **Studies on Linear Attenuation Coefficient and Total Interaction Cross Sections of Sodium Metal in the Energy Range 0.122-1.330 MeV** 130
Bharat S.Surung and Pravina P. Pawar

B-3 **^{96}Zr(,n) Reaction Cross-section in the End-point Bremsstrahlung Energies of 12-16 and 45-70 MeV . . . 132**
H. Naik, G.N. Kim, R. Schwengner, K. Kim, M. W. Lee, M. Zaman, S.G. Shin, Y. Gey, R. Massavczyh, R. John, A. Junghans, A. Wagner and A. Goswami

B-4 **Determination of Total Interaction Cross section and Mass Energy-absorption Coefficients of Sorbitol using NaI(Tl) Scintillation Detector. . . . 134**
Bibifatima M.Ladhaf, Shaikh Humera. B, Prashant S. Kore and Pravina P. Pawar

B-5 **EDXRF Analysis of Suspended Sediments from Trans Thane Creek Collected by using an in-house Developed Time-Integrated Sediment Sampler. . . . 136**
R. H. Pillay, S. S. Gothankar, S. K. Jha, R. M. Tripathi

B-6 **Measurements of Mass attenuation coefficients and molar extinction coefficients of L-Cystine using gamma ray spectrometer . . . 138**
Prashant S. Kore, Bibifatima M. Ladhaf, Bharat S.Surung, Pravina P. Pawar, Rajkumar M. Lokhande, Umesh S. Rajurkar and Humera B.Shaikh

B-7 **Spatial Distribution Study on Trace Elements in Estuarine Sediment Using EDXRF Technique . . . 140**
P.Y. Ajmal, S.K. Sahu, M. Tiwari, R.C. Bhangare, G.G. Pandit

B-8 **Evaluation of Radiation Dose due to the Use of Fly Ash from Thermal Power Plants as Building Material . . . 142**
R.C. Bhangare, S.K. Sahu, P.Y. Ajmal, M.Tiwari, G.G. Pandit

B-9 **Microanalysis Study on Ancient Lanna-style Decorative Glass Based on XRF Spectroscopy . . . 144**
P. Dararutana, K. Won-in, S. Tancharakorn

B-10 **Compton Scattering Study of Gd Sesquioxide . . . 146**
Jagrati Sahariya, A.M. Ghaleb, F.M. Mohammad and B.L. Ahuja

B-11 **Effect of EXAFS on Total Mass Attenuation Coefficients of some Rare Earth Elements. . . . 148**
N.V. SitaMahalakshmi1, M. Ratnaraju, A. Durgaprasad Rao, P.V.Lakshminarayana and K.Preacmhand

B-12 **Gamma-ray spectrometric analysis of Coastal sediment samples along north east coast of Tamilnadu, India. . . . 150**
M. SureshGandhi , R.Ravisankar, A.Chandrasekaran, B.Venkatakumaran, I.Vijayalakshmi and M.T. Jose

B-13 **Determination of Zirconium and Hafnium in Zirconium Process Stream Solutions from Zirconium Extraction Plant by ED X-Ray Fluorescence Spectrometry (EDXRFS). . . . 152**
B.V. V. Ramana, Y. Balaji Rao and H.R. Ravindra

B-14 **Rapid Identification of Uranium in Various Isotopic Composition by Liquid Scintillation Counting . . . 154**
Sonali P.D. Bhade, S. Anilkumar, P.J. Reddy, A.D. Pant, G.P. Verma, R.V. Kolekar, Rajvir Singh, K.S. Pradeepkumar

B-15 **Application of simulated standard spectra for the analysis of complex sample spectra from NaI(Tl) detectors. . . . 156**
S. Anilkumar, K. Narayani, A.K. Verma, Rajvir Singh and K.S. Pradeepkumar

B-16 **Assessment of Elemental Contamination in Road Dust using EDXRF . . . 158**
I.V. Saradhi, Sandeep P. and G.G. Pandit

B-17 **Measurement of contribution of radioctivity in Liver to Lung . . . 160**
Lokpati Mishra, I.S.Singh, Minal Nadar, G. N. Kalyane and D. D. Rao

B-18 **Experimental Measurement of Mass attenuation Coefficient near L absorption edges by X-ray Spectrometric Technique 162**
Sharanabasappa, B. R. Kerur and Anilkumar S.

B-19 **Gross Alpha and Beta Activities in Potable Waters used by Pharmaceutical Companies in India 164**
Hemalatha.P., Sanu.S. Raj, Madhuparna D., S.K. Jha and R.M. Tripathi

B-20 **Determination of Gamma Ray Mass Attenuation Coefficient Using NaI(Tl) Detector 166**
Vandana A.Tupe , Bibifatima M.Ladhaf , Pravina P. Pawar

B-21 **Characterization of Gasoline and Diesel soot by Energy Dispersive X-ray Spectrometry 168**
P. Kothai, S. Sandeep, S.K. Sahu and G.G. Pandit

B-22 **High Resolution In-Situ Gamma Spectrometry for Determination of Outdoor Terrestrial Gamma Dose Rates at BARC, Mumbai. 170**
Rajesh Sankhla and D.D. Rao

B-23 **Determination of Trace impurities in Uranium Metal using Total Reflection X-ray Fluorescence (TXRF) Spectrometry 172**
Trupti Chavan, D.N. Wagh, V.H. Rupvate and K.N. Hareendran

B-24 **Geochemical Peculiarities of Marine Sediment in Coastal Area. 174**
S.S. Gothankar and S.K. Jha and R.M. Tripathi

B-25 **ESR Spectroscopy Dating of Recently Excavated Archaeological Bone Samples from Kottapuram site using Gamma Irradiation 176**
G. Velraj, R. Hemamalini, S. Tamilarsu, N. Basavaiah

B-26 **Preconcentration of Mercury from Aqueous Samples using Modified XAD Resin 178**
Aditi A. Dalvi, K.K. Swain, Trupti Chavan and D.N. Wagh

B-27 **Application of TXRF for Burn Leach Test of TRISO Coated UO_2 particles of CHTR Fuel 180**
Kaushik Sanyal, S. Sanjay Kumar, Sangita Dhara, N.L. Misra, Rajesh V. Pai, N. Kumar, S.K. Mukerjee and S.K. Aggarwal

B-28 **Non-Destructive EDXRF Determination of Sulphur in Ore Samples 182**
Buddhadev Kanrar,S. Sanjay Kumar, N.L. Misra, S. Mondal, A. K. Singh, R. C. Hubli and S.K. Aggarwal

B-29 **Radiation Effects on Graphene Overlayer on SiO_2 as Probed by Positron Spectroscopy 184**
S. Mukherjee, S.K. Sharma, P. Maheshwari, P.K. Pujari

B-30 **EDXRF Analysis of Medicinal Plants and Spices Grown in the Vicinity of Zinc Smelter. 186**
S. Sarkar, S.S. Ram, M. Sudarshan, R.K. Dutta

B-31 **ED-XRF Analysis of Ancient Potteries of Vellore Dist, Tamilnadu, India with Statistical Approach 188**
R. Ravisankar, A. Naseerutheen. G.Raja Annamalai, A.Chandrasekaran, K.V.Kanagasabapathy, M.V.R. Prasad, K.K. Satpathy

B-32 **Determination of multi-element profiles of soil at Visakhapatnam using EDXRF technique 190**
Sandeep P., Kothai P, C.B. Dusane, S.K. Sahu and G.G. Pandit

B-33 **Measurement of Electron Momentum Density in Sm_2O_3 using Compton Spectroscopy 192**
Sonu Sharma, Alpa Dashora, Jagrati Sahariya, B.L. Ahuja

C. Ion Beam Analysis Techniques

C-1 **A Study of Trace Elemental Distribution in Vegetables by PIXE 194**
Seetharamireddy B., Abdul Sattar S., Madhusudhana Rao P.V., Ramnarayan K.

C-2 **Effect of Ag^{+} Irradiation on Cubic and Tetragonal Yttria Stabilized Zirconia 196**
R. Halder, P. Sengupta, V. Sudarsan, I. Samajdar, P. V. Satyam, G.K.Dey

C-3 **PIXE Analysis of Cancer-Afflicted Human Bladder 198**
G. J. Naga Raju P. Sarita, and S. Bhuloka Reddy

C-4 **Application of $^{52}Cr(p,)^{53}Mn$ Nuclear Resonance Reaction for Depth Profiling Cr in Surface Layers 200**
Pritty Rao, S. Vikram Kumar, Sanjiv Kumar

C-5 **Analysis of Fluorine in Granite Samples using PIGE Technique 202**
A.A. Sukumar, Y. Sunitha, S. Vikram Kumar, Sanjiv Kumar

C-6 **Levels of Trace Elements in Medicinal Plants with Anti-Diabetic Potential 204**
D. K. Ray, S. Jena

C-7 **Optical, Chemical and Thermal Study of Fluoropolymers irradiated with 4 MeV Proton Ion Beam 206**
A. Srivastava, Sarita, A. Singh, P.K. Soni, S.K. Gupta, A. Agarwal

C-8 **Analysis of ancient pottery samples and reference materials by Particle Induced X-ray Emission 208**
K.B. Dasari, R. Acharya, D.K. Ray, A. Behera, N.Lakshmana Das

C-9 **Simultaneous Quantification of Li, Ti and O in Lithium Titanate by Particle Induced Gamma-ray Emission using 8 MeV Proton Beam 210**
Sumit Chhillar, R. Acharya, R. Tripathi, S. Sodaye, K. Sudarshan, P.C. Rout, S.K. Mukherjee, P.K. Pujari

C-10 **R&D Work on Particle Induced Gamma-ray Emission (PIGE) using proton beam at FOTIA, BARC: Present Status and Future Prospects 212**
R. Acharya, S. Chhillar, S. Sodaye, P. K. Pujari, A. Agarwal, S. K. Gupta and P. Singh

C-11 **Studies on Fluoride Contents in Soil Samples from Punjab using Particle Induced Gamma Emission 214**
A. Srivastava, S. Chhillar, Amol D. Shinde, N. Kaur, D. Singh, R. Acharya, P.K. Pujari

C-12 **Characterization of Mercury based Indian Herbomineral drug by Radioisotope Induced EDXRF and Synchtrotron based EXAFS 216**
Daisy Joseph, Rajeeta Joseph, P.Rajput, C.Nayak, A.Saxena, D. Bhattacharya, S.N.Jha, V.Natrajan

C-13 **Changes in Serum Trace Elemental content of Uterine Cervix Cancer Patients using PIXE 218**
P. Sarita, G. J. Naga Raju, and S. Bhuloka Reddy

C-14 **Study of Depth Profile of Hydrogen in Hydrogenated Diamond like Carbon thin Film by Ion Beam Analysis Technique 220**
J. Datta, H.S. Biswas, S. Kumar, D.P. Chowdhury, N.R. Ray, A.V.R. Reddy

C-15 **Depth Profiling of Titanium using a Resonance in $^{48}Ti(p,)^{49}V$ Nuclear Reaction 222**
G. L. N. Reddy, S. Vikram Kumar, J. V. Ramana, Sanjiv Kumar

C-16 **Application of in situ current normalized PIGE method for determination of total boron and its isotopic composition** 224
Sumit Chhillar, R. Acharya, S. Sodaye and P. K. Pujari

D. Analyitcal Chemistry in Nuclear Technology

D-1 **Uranous Generation and its Application to strip Plutonium from Lean Organic in CORAL** 226
A. Chinnusamy, N.K. Pandey, Radha Rani, N. Abirami, C.M. Baghyalakshmi, D. Natarajan, M.C. Devarajan, R.V. Subbarao, V. Vijayakumar and U. Kamachi Mudali

D-2 **Physico-Chemical Investigations of Some Mixed Ligand Complexes of Thorium(IV) Derived from Semicarbazones and Triphenyl Phosphine Oxide** 228
Ram K. Agarwal

D-3 **Electrochemical Approach to Assess Corrosion of Stainless Steel used in PUREX Process** 230
Shagufta Khan, Vivekanand Kain, A.V. R. Reddy

D-4 **Liquid-Liquid Extraction of Praseodymium (III) Using Cyanex 272 in Kerosene** 232
Nandita Panda, Niharbala Devi, Sujata Mishra

D-5 **Ligand Sensitized Fluorescence of Eu^{3+} in Dimethyl Sulphoxide using TTA as a ligand: An Application of Europium Determination in U Matrix** 234
S. Maji, Satendra Kumar, and K.Sankaran

D-6 **Fluorimetric Estimation of U(VI) in the Presence of a Large Excess of Th(IV)** 236
S. Maji, Satendra Kumar and K.Sankaran

D-7 **Light Scattering Studies for Estimation of Hydration Number of Sr(II) and Al(III) ions in Dilute Aqueous Solutions of Nitric Acid** 238
N. Priyadarshini, M. Sampath, Shekhar Kumar and U. Kamachi Mudali

D-8 **Liquid-liquid Extraction of Zr (IV) from HCl Medium using Cyanex921 in Kerosene** 240
B.C.Bhatta, S.K.Sahu and Sujata Mishra

D-9 **Determination of Free Acidity in Nuclear Fuel Reprocessing Streams by Fiber Optic Aided Spectrophotometric Technique** 242
S. Ganesh, P.Velavendan, N.K. Pandey, U. Kamachi Mudali and R. Natarajan

D-10 **Column Chromatographic Method for the Separation of Neodymium from Uranium & Other Elements using poly[dibenzo-18-crown-6]** 244
Shila N. Lad, Baburao S. Mohite

D-11 **Radiochemical Analysis of Strontium-90 in Spent Fuel Storage Bay of a Research Reactor** 246
P.T. Ghare, S.S. Deolekar, V. Pulhani, K.S. Babu, L.K. Vajpyee, R.K.B. Yadav, A.D. Pant, R.K. Gopalakrishnan, K.S. Pradeep Kumar

D-12 **Estimation of ^{55}Fe in Neutron Activated Steel Components** 248
Priya Srinivasan, R.K.Gopalakrishnan, M.S.Murali, A.Goswami

D-13 **Ilmenite Mineral Decomposition using Lithium Metaborate Fusion: ICP-AES Determination of Ti, Fe, Si, Cr, V, Mn, Ca and Mg** 250
A. Premadas

D-14 **An Experimental cum Numerical approach for the Determination of Components in a $UO_{2+x} - U_3O_8$ Admixture** 252
B. Narasimha Murty, G. Brahmananda Reddy and H.R. Ravindra

D-15 **Analysis of Tantalum-10%Tungsten alloy for Fe, Mo, Ni by Flame-AAS Technique 254**
J.R. Jat, Y. Balaji Rao and H.R. Ravindra

D-16 **Inductively Coupled Plasma-Atomic Emission Spectrometric technique for estimation of Ti in D9 Steel 256**
G. Satyanarayana, A.K. Nayak, Y. Balaji Rao and H. R. Ravindra

D-17 **Characterization of Zirconium Alloy by Glow Discharge Optical Emission Spectrometer 258**
A.K. Nayak, Y. Balaji Rao, H.R. Ravindra, B. Prahlad and N. Saibaba

D-18 **Accelerator based Pyrohydrolysis of Sodium Diuranate and Subsequent Determination of F^- and Cl^- by Ion-Chromatography 260**
Shehanaz Bano, Y. Balaji Rao and H. R. Ravindra

D-19 **Development of a Method for Determining the location of Heterogeneous Activity present in 200 litre Waste Drum using USB based MCS System 262**
Sarbjit Singh, Amol Mhatre, Veena Sagar and Nidhi Gupta

D-20 **Spectrophotometric Determination of Zirconium with Chrome Azurol s in Aqueous Streams of Nuclear Fuel Reprocessing 264**
S. Ganesh, P.Velavendan, N.K. Pandey, U. Kamachi Mudali and R. Natarajan

D-21 **Separation of no-carrier –added ^{62}Zn from ^{7}Li Irradiated Cobalt Target Using Calcium Alginate Beads 266**
Kaustab Ghosh, Moumita Maiti, Susanta Lahiri

D-22 **Determination of Boron in ThO_2 Samples. 268**
P.S. Ramanjaneyulu, K.L. Pandey, M.K Saxena, B.S. Tomar and K.L. Ramakumar

D-23 **Effect of Batch size on the Separation of Uranium from Solid (U, Pu, Ag) Oxide Analytical Waste 270**
Nimai Pathak, Mithlesh Kumar, S.K. Thulasidas, V. Natarajan and S.V. Godbole

D-24 **Determination of Microgram Quantities of Common Metals in PVA Films using EDXRF 272**
B.A. Dhawale, Mithlesh Kumar and V. Natarajan

D-25 **Estimation of Boron in Sodium Borosilicate Glass Frit by Fusion at Lower Temperature 274**
D.A. Thakur, N.L. Sonar, T.P Valsala and I.Vishwaraj

D-26 **Effect of Higher Waste Loading on the Properties of Vitrified Waste Product 276**
P.K. Mishra, Y. Raghavendra, Vaishali De, T.P. Valsala and I. Vishwaraj

D-27 **Single Vial Kit Formulation for Preparation of ^{68}Ga-AMBA : A PET Imaging Agent for Prostate Cancers 278**
Usha Pandey, Archana Mukherjee, Naresh Gamre, Haladhar Dev Sarma, Ashutosh Dash

D-28 **Coincidence Summing Corrections for a Clover Detector 280**
Chhavi Agarwal, Laxman S. Danu, A. Goswami and D.C. Biswas

D-29 **Synthesis and Evaluation of a Phenylbenzothiazole-based ^{99m}Tc(CO)$_3$-Radiotracer for Possible Application in imaging -amyloid Plaque. 282**
Drishty Satpati, Aruna Korde, Sharmila Banerjee

D-30 **Quantification and Isotope Ratio Measurement of Boron in U_3Si_2 by Inductively Coupled Plasma Mass Spectrometry. 284**
Abhijit Saha, S.B. Deb, Papu Samanta, B.K. Nagar and M.K. Saxena

D-31 **Microwave Assisted Dissolution Followed by Characterization of XHM-1 alloy by Inductively Coupled Plasma Mass Spectrometry 286**
S.B. Deb, B.K. Nagar, Abhijit Saha and M.K. Saxena

D-32 **Determination of Nitrate in Effluents from Uranium Extraction Plant. 288**
Ayushi Dudwadkar, Sangita D. Kumar and A.V.R. Reddy

D-33 **Spectral Interference of Zirconium on 24 Analyte Elements using CCD based ICP-AES Technique 290**
V.C. Adya, Arijit Sengupta and S.V.Godbole

D-34 **Formulation and Radiochemical Evaluation of a Freeze-dried Mixed Peptide Kit for the Preparation of ^{68}Ga-labeled Peptides for PET Imaging of Somatostatin Receptor Positive Neuroendocrine Cancers 292**
Tapas Das, Mohini Bhadwal, Sharmila Banerjee

D-35 **Installation and Performance Evaluation of an Indigenous Surface Area Analyser 294**
S.N. Pillai, R S Prasad, M.N. Solapurkar, V. Venkatesan, A. Prakash, K.B. Khan and Arun Kumar

D-36 **Characterisation of Dry Tubes in KAMINI reactor 296**
Manish Chand, J.S. Brahmaji Rao, N.P. Seshadreesan and C.R. Venkatasubramani

D-37 **Dose computation of Ti activated products for its qualification as a material for the sample holder in FBTR. 298**
G.V.S. Ashok Kumar, R. Acharya, R. Kumar, C.R. Venkatasubramani and A.V.R. Reddy

D-38 **Cesium Extraction from High Level Waste using Irradiated Calix-Crown-6 Ligands in FS-13 . . . . . 300**
Poonam Jagasia, V.C. Adya, A. Sengupta, P.S. Dhami and P.K. Mohapatra

D-39 **Separation and Determination of Calcium and Iron in Silicon Matrix using Ion Chromatography 302**
M.K. Das, V.V. Raut, S.B. Deb, S. Jeyakumar, M.K. Saxena, B.S.Tomar

D-40 **Membrane based Isotope Dilution Alpha Spectrometry (MEM–IDAS) for Determination of Plutonium concentration 304**
Sumana Paul, R.V. Shah, A.K. Pandey, S.K. Aggarwal

D-41 **Inverse-Frontal Chromatography studies on enrichment of Boron – 10 using quaternery 4- vinylpyridine-divinylbenzene resin 306**
Venki Bejawada, Mohapatra C., Rao A.S., Prasad.K.L., Murthy P.K., Rao A.K., Singh H.P., Vithal G.K., Sangita D. Kumar

D-42 **Development of Carbon and Metallic Nano Particle Composite Materials for the Determination of Uranium and other Heavy Metal Ions 308**
S. Sahoo, M.K. Dey, A.K. Satpati and A.V.R. Reddy

D-43 **Determination of Boron in Graphite, Boron Carbide and Glass by ICP-MS, ICP-OES and Conventional Wet Chemical Methods. 310**
K. Venkatesh, Granthali S. Kamble, Manisha Venkatesh, Sanjukta A. Kumar and A.V.R. Reddy

D-44 **Radioimmunoassay Procedure for Human Insulin Based on magnetizable Particles 312**
R.R. Rasmi, K.B. Shenoy, Jayula Sarnaik, V.B. Kadwad, H.M. Somashekarappa and N. Sivaprasad

D-45 **Attenuation Correction for the Segmented Gamma Ray Assay of Cylindrical Samples 314**
Sabyasachi Patra, Chhavi Agarwal, and A. Goswami

D-46 **On-site Monitoring of Uranium in Low Level Liquid Waste Streams using U-Br-PADAP Strip Indicator Paper Technique 316**
S. Ganesh, P.Velavendan, N.K. Pandey, U. Kamachi Mudali and R. Natarajan

E. Solid State Nuclear Track Techniques

E-1 **Auto-counting of High Density Overlapping Tracks and Neutron Spectrum Measurement Using CR-39 Detectors and in-house Image Analysis Program 318**
Sabyasachi Paul, S.P. Tripathy, G.S. Sahoo, D.S. Joshi, T. Bandyopadhyay

E-2 **Geometrical Parameters of Tracks Registered by Collimated alpha Particles on CR-39 Detector 320**
Pranav M. Joshirao, Chirag K. Vyas, Jae Won Shin, Seung-Woo Hong and Vijay. K. Manchanda

E-3 **Radon, Thoron and their progeny concentration variations in dwellings of Gogi region, Yadgir District of Karnataka, India 322**
Avinash P.R., S. Rajesh, B.R. Kerur, Rosaline Mishra

E-4 **Study on Gamma-ray Energy Absorption in SSNTDs and PTNDs 324**
Vishwanath P. Singh and N.M. Badiger

E-5 **Estimation of Radon exhalation Rate in Gopalpur beach Sand samples Orissa, Eastern India 326**
Ajay Kumar Mahur, Anil Sharma, D. Sengupta R.G. Sonkawade and R. Prasad

E-6 **Thoron Interference in Radon Exhalation Rate Measured by Solid State Nuclear Track Detector based Can Technique 328**
B.K. Sahoo, T.K. Agarwal, B.K. Sapra

E-7 **Distribution of Natural Gamma Radiation and Radon Levels around a Thorium Beach Sand Mining and Processing Facility, Odisha 330**
S. Mohapatra, S.K. Sahoo, J.S. Dubey, Sumesh C.G., S.K. Tripathy, D.V. Sagar, S.V. Godbole, P. M. Ravi and R.M. Tripathi

E-8 **Variation of Radon and its Progeny Levels in Different Types of Floorings and Rooms using LR-115 Solid State Nuclear Track Detectors 332**
Deepak Verma and M Shakir Khan

E-9 **Neutron Dose Estimation for $^{1}H+^{9}Be$ and $^{1}H+^{12}C$ Reactions at 20 MeV Proton Energy via LET Spectrometry using CR-39 Detectors. 334**
G.S. Sahoo, S.P. Tripathy, S. Paul, V. Suman, C. Sunil, D.S. Joshi, T. Bandyopadhyay

E-10 **Measurement of ^{222}Rn and ^{220}Rn Decay Product Deposition Velocities using SSNTD based Passive Detectors 336**
R.P. Rout, R. Mishra, R. Prajith, Jalaluddin S., B.K. Sapra

E-11 **Tetraethyl Ammonium Hydroxide (TEAH) as an Etchant of CR-39 for the Determination of Fluence of Alpha Particles 338**
Pranav M Joshirao, Chirag K. Vyas, K. P. Eappen, Jae Won Shin, Seung- Woo Hong and Vijay. K. Manchanda

F. Radioisotope Production and Applications

F-1 **Effects of Supplemental n-3 Polyunsaturated Fatty Acids in Diet: Studies Performed with Radioanalytical Methods. 340**
S. Pavelka

F-2 **Impact of Gamma Irradiation on Biochemical Parameters of Flacourtia Montana Grahm during different Storage Period 342**
Akshatha, K.R. Chandrashekar

F-3 **Impact of Gamma Irradiation on Biochemical attributes of Jackfruit (Artocarpus heterophyllus L.) seeds during different storage period. 344**
Madhavi Adiga, Madhuri Adiga Akshatha, K.R.Chandrashekar

F-4 **Application of Elovich equation on uptake kinetics of ^{137}Cs by Living Freshwater Macrophytes - A Short Duration Laboratory Study 346**
T.J. Jaison, A.K. Patra, P.M. Ravi and R.M. Tripathi

F-5 **Studies on Transpiration Rate and Tritium Concentration in Transpired Water in Some Plant Species Around Kakrapar Gujarat Site. 348**
Rajkanya. M. Arjune, A.K. Patra, C.P. Joshi, P.M.Ravi and R.M. Tripathi

F-6 **Preparation and Deployment of Indigenous ^{125}I- seeds for the Treatment of Prostate Cancer: Dawn of Prostate brachytherapy in India 350**
Sanjay Kumar Saxena, Yogendra Kumar, Ramu Ram, A.S. Tapase, Vivek J. Anand, Ashutosh Dash

F-7 **Feasibility Studies for the Development of ^{169}Yb-Brachytherapy Seeds: Emerging Radiation Sources for the Management of Cancer 352**
Sanjay Kumar Saxena, Yogendra Kumar, Y.R. Bamankar, Jitendra Nuwad, K.C. Jagadeesan, Ashutosh Dash

F-8 **A Study on Helicobacter pylori infection in different parts of Karnataka using ^{14}C Urea Breath Test 354**
Swaroop K., Jayachandran, Rajashekar K. Patil, K. Bhaskar Shenoy and H. M. Somashekarappa

F-9 **Purification and concentration of ^{68}Ga eluate from SnO_2 based ^{68}Ge/ ^{68}Ga generator 356**
Sankha Chattopadhyay, Md. Nayer Alam, Madhusmita, Luna Barua, Sujata Saha Das, and Malay Kanti Das

F-10 **Evaluation of Photosynthetic Pigments and Protein Content in some Gamma Treated Wheat Varieties Using ^{60}Co as a Source 358**
Sandeep Mishra, Pradeep K Shukla, Pragati Misra, Narayani Shukla, Gayatri Sanghdeep Gautam and P.W. Ramteke

F-11 **Mössbauer Spectroscopic Characterization of Dust Particulates From a Cement Factory and Thermal Power Plant 360**
R. B. Lanjewar and Mamata R. Lanjewar

F-12 **Radiation Pre-Treatment of Seed Imparts Metabolic Stability and Quality Protection during Storage under Accelerated Aging 362**
Sumedha, Bhupinder Singh, R.K. Singhal

F-13 **Seed Quality Preservation Advantage of Gamma Irradiation Seed Pre-Treatment during Long Term Storage in Soybean 363**
Sameer Kumar Guha, Sumedha and Bhupinder Singh

F-14 **$^{14}CO_2$ labeling : A Reliable Technique for Rapid Measurement of Total Root Exudation Capacity and Vascular Sap Flow in Crops 364**
Bhupinder Singh, Sumedha Ahuja, Renu Pandey and R.K. Singhal

F-15 **Screening of High Water Use Efficiency in some Gamma Radiated Cowpea Varieties through Isotopic Ratio Mass Spectrometer (IRMS) 365**
Pradeep K. Shukla, Srikantha G.A., Pragati Misra, Navodita Maurice, M.S. Sheshshayee and P.W. Ramteke

F-16 **Flow Rate Measurements in a Pipeline Using Radiotracer Technique during a Custody Transfer Operation 367**
H.J. Pant, V.K. Sharma, Sunil Goswami, J.S. Samantaray

F-17 **Homogeneity Study in a Glass Manufacturing Unit Using Radiotracer Technique 369**
Sunil Goswami, H.J. Pant, Jayashree Biswal, J.S. Samantray, V.K. Sharma, Sourabh Singhal

F-18 **Application of Radioactive Particle Tracking (RPT) Technique for Quantifying the Liquid Phase Flows in Bubble Columns. 371**
Dinesh V. Kalaga, H.J. Pant, Sunil Goswami, Shantanu Roy, Jyeshtharaj B. Joshi

F-19 **Residence Time Distribution Study in a Pilot-Scale Gas-Solid Fluidized Bed System Using Radiotracer Technique 373**
H.J. Pant, V.K. Sharma, Sunil Goswami, J.S. Samantaray, N.I.G.N. Mohan, Tirupathi Naidu, Gursharan Singh

F-20 **Photon Mass Energy-absorption Coefficients of propionic acid from 122 keV to 1330 keV 375**
Shaikh Humera, Bibifatima M.Ladhaf, B and Pravina P. Pawar

F-21 **Single Vial Kit Formulation for Preparation of PET Radiopharmaceutical: ^{68}Ga-DOTATOC 377**
A. Mukherjee, U. Pandey, R. Chakravarty, H.D. Sarma, G. Samuel, A. Dash

F-22 **Radiotracer Technique in Adsorption Study - Adsorption of Strontium Ions on TiO_2 . . . . . 379**
Shuddhodan P.Mishra and N.Srinivasu

F-23 **Reactor Production of No Carrier Added ^{199}Au for Biomedical Applications 380**
K.V. Vimalnath, Sudipta Chakraborty, Ashutosh Dash

F-24 **Research Trends in Radioisotopes: A Scientometric Analysis 382**
Anil Sagar, B. S. Kademani, K. Bhanumurthy and N. Ramamoorthy

F-25 **Radiotracer Investigation in an Industrial-Scale Oxidizer. 384**
H.J. Pant, V.K. Sharma

F-26 **^{10}Be Dating of Marine Core Sediment from Central Western Bay of Bengal by using Accelerator Mass Spectrometry 386**
P.V.L.Narayana, B.Pankaj Kumar, Rajveer Sharma, Soumya Prakash Dhal, Archna Bohra, S.Chopra, I.N.Rao, A.D.P.Rao

F-27 **Hard and Soft Acid Base Concept of Biosorption - Employing Green Biosorbent by Radiotracer Technique. 388**
Nisha Barot, Roshan Khilnani, Hemlata Bagla

F-28 **Synergistic extraction of Cs(I) using Di-benzo-24-crown-8 and Di-2-ethylhexylphosphoric acid in toluene 390**
T. Bhar, M. Banerjee, S .Basu

F-29 **Effect of Co – Metal Ions Concentration on Iron Metal Ions Adsorption on New Adsorbent Prepared from Cuscuta Powder 392**
Jyotsna Dhanik, Sneha Saurabh, S.K. Tyagi

F-30 **Evaluation of Photosynthetic Efficiency of some Phosphorus Tolerant and Susceptible Rice Varieties using $^{14}C(NaH^{14}CO_3)$ as a Tool 394**
Pradeep K Shukla, Pragati Misra, Narayani Shukla, NavoditaMaurice, Bhupinder Singh and R.C. Pant

F-31 **Investigation of Liquid-Solids Fluidized Bed of Different Particle size through Radioactive Particle Tracking Techniques 396**
Shubham Jain, Priyam Saraswat, Harish J. Pant and Rajesh K. Upadhyay

F-32 **Nanocrystalline Zirconia: A Viable Adsorbent for the Column Chromatography Separation of ^{58}Co from Neutron Irradiated Nickel Targets 398**
K.V. Vimalnath, S. Priyalata, Ramu Ram, S. Chakraborty, Rubel Chakravarty, A. Dash

F-33 **Investigation on the Influence of Metal Ion Impurities on the Complexation behavior of Generator Produced ^{90}Y with bifunctional Chelators 400**
Usha Pandey, Naresh Gamre, Ashutosh Dash

G. Actinide and Trace Element Speciation Studies

G-1 **Sorption of Uranium (VI) by 2-Aminothiazole Functionalized Hydrogels from Aqueous Environment 402**
N. Sivagangi Reddy, K.S.V. Krishna Rao, T.J. Sudha Vani, A.V.R. Reddy, Jayshree Ramkumar, P.V. Nagendra Kumar

G-2 **On the Speciation and Site Symmetry of Uranium in $Sr_2P_2O_7$: A TRFS and Sr K-edge EXAFS Investigation 404**
M. Mohapatra, A.K. Yadav, S.N. Jha, M.J. Kulkarni, D. Bhattacharyya, V. Natarajan and S.V. Godbole

G-3 **Studies on Evaluation of Modified TRUEX Solvent for the Partitioning of Minor Actinides 406**
Arijit Sengupta, M.S. Murali, P.K. Mohapatra

G-4 **Application of a Simple and Rapid Spectrophotometric method for Uranium analysis in Uranium based waste sample 408**
Bholanath Mahanty, C. D. Karekar, D. K. Das, P.G.Behere, Mohd.Afzal

G-5 **Extraction studies on U(VI) using Tri-n-Octyl Phosphine Oxide Dissolved in Room Temperature Ionic Liquids 410**
D.R. Raut, P.K. Mohapatra

G-6 **Assay of Actinide Mixtures by Hybrid K-edge Densitometer 412**
M. Bootharajan, K. Swaminathan and C.R. Venkata Subramani

G-7 **Studies on Actinide Ion Uptake and Transport using Polymer Inclusion Membranes Containing TODGA as the Extractant 414**
B.N. Mahanty, D.R. Raut, D.K. Das, P.G. Behere, Md. Afzal and P.K. Mohapatra

G-8 **N,N,N',N'-Tetraoctyl Diglycolamide Coated Fe_3O_4 Nanoparticles for Americium Preconcentration and Determination with -Spectrometry 416**
V. Chavan, T. Vasudevan, A. Pandey, A. Goswami

G-9 **Separation of Lanthanides and actinides from Simulated High Level Waste using diglycolamide-functionalized calix[4]arene 418**
Arijit Sengupta, P.K.Mohapatra, Mudassir Iqbal, Jurrian Huskens, Willem Verboom

H. Environmental Radioactivity

H-1 **Bioaccumulation of Natural Radionuclides and Dose Transfer to Human Population in the Parangipettai Coastal Ecosystem, Tamil Nadu, India 420**
P. Raja and P. Shahul Hameed

H-2 **Pb Isotopes Induced Bremsstrahlung in Bone Muscle and Teeth 422**
H.C. Manjunatha

H-3 **Dose Assesment of Bremsstrahlung Induced by Beta-Emitter Radioisotopes of Uranium-238 Series in Human Tissues** **424**
H.C. Manjunatha

H-4 **Treatment of Radioactive Liquid Waste Containing Mn^{2+} by Synthetic Hydroxyapatite** **426**
Diganta Gogoi, A.G. Shanmugamani, S.V.S. Rao, T. Kumar, B. Sreekumar, P.K. Sinha

H-5 **Isolation, screening and characterization of Uranium microremediable actinomycetes from fallen leaves of Azadirachta indica in Western Ghats.** **428**
Mrinalini.J.Singh, S.Padmavathy

H-6 **Annual effective dose due to Natural radioactivity in drinking water** **430**
P Padma Savithri, S K Srivastava, A Y Balbudhe, K Vishwa Prasad, P M Ravi and R M Tripathi

H-7 **Natural Radioactivity in Soil and Dose Rate around Hyderabad, India** **432**
A.Y. Balbudhe, K. Vishwa Prasad, S.K. Srivastava, P Padma Savitri, P.M. Ravi and R.M. Tripathi

H-8 **Utilization of Arsenazo-III for Spectrophotometric Determination of Thorium in Soil Samples** **434**
S.K. Srivastava, N. Sreenivasa Rao, A.Y. Balbudhe, K.Vishwa Prasad, P. Padma Savithri, P.M. Ravi and R.M. Tripathi

H-9 **Results of Measurement of the Tritium in the Western Caucasus.** **436**
T. Tsvetkova, I. Nevinsky, V. Nevinsky, B. Suyatin

H-10 **Successful Application of the Nuclear Analytical Chemistry (NAC) Methods in Seismological Researches of Mud Volcanoes and Springs in the Black Sea Zone.** **437**
T. Tsvetkova, I. Nevinsky, B. Suyatin, I. Akkurt, F. Kulali

H-11 **Study of Radon, Thoron and their Progeny levels in Indoor Environment of Firozabad city in U.P., India** **439**
Mukesh Kumar, Anshu Agrawal and Rajesh Kumar

H-12 **Effect of Tsunami on the Natural Radioactivity content in the Beach Sands along the entire East Coast of Tamilnadu State, India** **441**
K.S. Lakshmi, V. Meenakshisundaram, J. Punniyakotti

H-13 **Study on the Spatial Distribution of ^{137}Cs Content in Bottom Sediment and Benthic Species of Mumbai off Coast** **443**
S. Sugandhi, V.M. Joshi, S.K. Jha and R.M. Tripathi

H-14 **Natural Radioactivity Measurement in Soil Samples of Gogi Region, Shahapur, Karnataka** **445**
S. Rajesh, P. Avinash, B. R. Kerur and S. Anilkumar

H-15 **Distribution of Natural Radioactivity in Soil Samples around Tarapur, India** **447**
C. B. Dusane, S. Mishra, S. K. Sahu and G. G. Pandit

H-16 **Environmental Gamma Radiation Monitoring at Visakhapatnam using Thermoluminescence Dosimeters** **449**
M. Swarnkar, S.K. Sahu, P.G. Shetty, R.A. Takale, G.G. Pandit

H-17 **Indoor and Outdoor Gamma Radiation Monitoring at High Background Area of Kerala Using TLDs** **451**
P.G. Shetty, S.K. Sahu, R.A. Takale, M. Swarnkar, G.G. Pandit

H-18 **Optimizations of Teflon Embedded $CaSO_4$: Dy based TLD for Environmental Monitoring Applications** **453**
R.A. Takale, S.K. Sahu, M. Swarnkar, P.G. Shetty, G.G. Pandit

H-19 **Distribution of Uranium & Thorium in Fractionated Sediment Samples Obtained from Different Locations across Thane Creek Area, Mumbai, India 455**
Sukanta Maity, S.K. Sahu and G.G. Pandit

H-20 **Estimation of Sensitivity Factor for Direct Thoron Progeny Sensors in Occupational Environments of a Reprocessing Facility 457**
R. Prajith, S. Jalaluddin, R.P. Rout, R. Mishra, K. Kannan, M.R. Shankaran and B.K. Sapra

H-21 **Environmental Radiation Levels at NARL, Gadanki 459**
Charan Kumar K., Manikiam B., Rajendra Prasad T. and Kamsali Nagaraja

H-22 **Analysis of Cow Dung Samples for Natural Radioactivity. 461**
E. Mahiban Ross and S. Godwin Wesley

H-23 **Estimation of Air to Grass - Dry and Wet Deposition Rates, Velocities, and Mass Interception Factors For Iodine for a Postulated Accidental Scenario 463**
Karunakara N., Ujwal P., Yashodhara I., Sudeep Kumara K., Geetha P.V., Dileep B.N., Joshi P. James and Ravi P.M.

H-24 **Determination of level of radioactivity and Evaluation of Radiation Hazardous in Coastal Sediments of East Coast of Tamilnadu, India. 465**
S. Sivakumar, R. Ravisankar, B. Govardhanan and Prince Prakash Jebakumar

H-25 **Spatial Distribution of Gamma Radiation Levels in Yelagiri Hills, Tamilnadu, India by Gamma Ray Spectrometry. 467**
A. Chandrasekaran, R. Ravisankar, B. Govardhanan, P. Vijayagopal, S.N. Bramha and B. Venkatraman

H-26 **Determination of Uranium in Groundwater using Liquid Scintillation and Cerenkov Counting Techniques 469**
Sonali P.D.Bhade, Ajaykumar, P.J. Reddy, Rupali Karpe-Kamat, R.V. Kolekar, Rajvirsingh, K.S. Pradeepkumar

H-27 **Simultaneous determination of gross alpha and gross activities in water samples using Ultra Low Level Liquid Scintillation Spectrometer 471**
P.J. Reddy, Vandana Pulhani, S.P.D. Bhade, R.V. Kolekar , Rajvir Singh, S.K. Jha and K.S. Pradeepkumar

H-28 **Estimation of Committed Effective Dose due to Tritium in Ground Water in some places of Maharashtra 473**
P.J. Reddy, S.P.D. Bhade, R.V.Kolekar, Rajvir Singh and K.S.Pradeepkumar

H-29 **Studies on Sorption of Uranium on Chitin- A Solid State Microextractant- Application to Preparation of Uranium Free Ground Water 475**
Beena Sunilkumar and G. Chakrapani

H-30 **Estimation of Heavy Metal Pollution in Coringa Mangrove Sediments using PIXE 477**
M. Mahaboob Pacha, P. Anil Kumar

H-31 **Study of Naturally Occurring Radioactive Material (NORM) in Soil using Low Background Gamma ray Spectrometry 479**
A. Srivastava, F. Knolle, F. Hoyler, U.W. Scherer and E.W. Schnug

H-32 **Source Depletion Model for Deposition from a Gaussian Plume 481**
Arun Aravind, H. Seshadri, V. Balasubramaniyan

H-33 **Occurrenceof the Radionuclides in Groundwater of Crystalline Hard Rocks Regions of Central Part Tamil Nadu, India 483**
C. Thivya, S. Chidambaram, K. Tirumalesh, M. V. Prasanna, R. Thilagavathi and M. Nepolian

H-34 **Assessment of Environmental Radioactive Elements (U, ^{222}Rn, ^{3}H) in Groundwater in parts of Nalgonda district, Andhra Pradesh 485**
K.Tirumalesh, H.V. Mohokar, B.K. Sahoo, G. Mallesh

H-35 **Radon and Thoron exhalation measurements in flyash samples collected from dumping area of Panipat Thermal Power Station, India using Smart Radon and Thoron monitor 487**
Lalit Mohan Singh, B.K.Sahoo, B.K. Sapra, Mukesh kumar, Rajendra Prasad, Rajesh Kumar

H-36 **Uranium Leaching from Mining Wastes: Effects of Contact Time, pH and Particle Size 489**
A.C. Patra, P.M. Ravi and R.M. Tripathi

H-37 **Determination of ^{210}Po in Leafy Vegetables and Annual Effective Dose Assessment to the Inhabitants of Mumbai city, India 491**
J.S. Dubey, S. K. Sahoo, A. Nair, S. Mohapatra, A.C. Patra, P. Lenka, P.M. Ravi and R.M. Tripathi

H-38 **^{226}Ra Estimation Using A Continuous Radon Monitor of Semi Conductor Detector Type 493**
C.G. Sumesh, S.K. Sahoo, A. Vinod Kumar, P. M. Ravi, and R.M. Tripathi

H-39 **Estimation of Age Dependent Effective Dose due to intake of ^{226}Ra from Drinking Water in Vizag, India 495**
V.K. Thakur, S.K. Sahoo, S. Mohapatra, N.S. Krishna, P. Lenka, A.V. Kumar, P.M. Ravi and R.M. Tripathi

H-40 **Measurement of Environmental Radon at Mangalore Karnataka, India. 497**
T.K. Agarwal, B.K. Sahoo, B.K. Sapra

H-41 **Spatial Distribution of Tritium in Surface Water and Assessment of Ingestion Dose. 499**
C.K. Rupali, B. Sonali, Priyanka Reddy, S.K. Jha and R.M. Tripathi

H-42 **Role of Lead (Pb^{2+}ion) as modifier as well as former on the properties of Lead-Iron Phosphate and Borosilicate Simulated nuclear waste glasses 501**
G. Hazra, P. Mitra, T. Das, P. P. Malik

H-43 **Active Measurement of Radon and Thoron Exhalation from Soil and Building Materials Samples and Effect of Grain Size 503**
Neetika Chauhan, R.P. Chauhan, B.K. Sahoo, M. Joshi, B.K. Sapra

H-44 **A Correlation Study between Indoor Radon-Thoron Concentration and Soil Exhalation Rates from Indian Dwellings. 505**
Amit Kumar, R. P. Chauhan, Manish Joshi

H-45 **Particle size distribution and Natural Radionuclide's Association in the Mumbai Harbour Bay Bottom Sediment 507**
Hemalatha.P, Madhuparna D, Sanu.S.Raj, S. K Jha and R.M.Tripathi

H-46 **Studies on Concentration of Radionuclides in Medicinal Plants 509**
Chandra Shekara K.,Yashodhara I., Karunakara N. ,Radhakrisna A.P., Somashekarappa H.M.

H-47 **Seasonal Variation of Radioactivity in Ground Water at Trombay. 511**
Vandana Pulhani, Joyeeta Mukherjee, S K Jha and R M Tripathi

H-48 **Radiological Measurement of Phosphate Rock, and Phosphogypsum from Fertilizer Industries in India 513**
S. J. Sartandel, S. V. Bara, S. Chinnaesakki, S. K. Jha and R. M. Tripathi

H-49 **A Simple spectrophotometric method for the determination of Uranium in industrial and environmental samples using 1-(benzo[d]thiazol-2-yl)thiourea 515**
Y. Harinath, K. Seshaiah, A.V.R. Reddy

H-50 **Determination of Effective Vertical Migration Velocity and Residence Times of ^{137}Cs in Sediments of Mumbai Harbor Bay using Compartment Models 517**
Ajay Kumar, Sabyasachi Rout P.M. Ravi and R.M.Tripathi

H-51 **Distribution and Retention of Cs Radioisotopes in Soil Affected by Fukushima Nuclear Plant Accident 519**
S. Mishra, H. Arae, A. Sorimachi, M. Hosoda, S. Tokonami, T. Ishikawa and S.K.Sahoo

H-52 **Tracking of Activity of Major Daughter Products (^{212}Bi , ^{212}Pb & ^{228}Ac) in Thorium Ore with time in a Hermetically Sealed Container 521**
H. Basu, R.K.Singhal, M.V.Pimple, P.K. Sharma and A.V.R.Reddy

H-53 **Determination of ^{134}Cs/^{137}Cs activity in the shore sand and soil samples collected around Fukushima 523**
H. Basu, R.K.Singhal, M.V.Pimple, D.V. Borole, Nobuyoshi Yamashita, A.V.R. Reddy

H-54 **Mobile Radiation Mapping of Indian West Coast by Railway Route 525**
Laxmidhar Sahoo, Anil Otari, Shashank S.Saindane, Suri M.M.K, Rajvir Singh, Pradeepkumar K.S

H-55 **Uranium in Fossils and Palaeosols from Siwaliks 527**
A. Srivastava, R. Patnaik, P.K. Sharma, D.K. Avhad, M.K.T. Bassan, M.V.Pimple and A.V.R.Reddy

H-56 **Radiation Levels and Radionuclide Distributions In Terrestrial, Atmospheric and Aquatic Environs of Gogi Uranium Mining Region of North Karnataka 529**
Yashodhara I., Sudeep Kumara K., Karunakara N. and Tripathi R.M.

H-57 **Radiological Characterization of Drinking Water in Jaduguda Uranium Mining Area and Assessment of Effective Dose to Member of Public. 531**
S.K. Sahoo, S.Mohapatra, J.S. Dubey, V.K. Thakur, P. Lenka, A.C. Patra, V.N. Jha, P.M. Ravi and R.M. Tripathi

H-58 **Comparative Evaluation of Different Extractants towards Cloud Point Extraction of Metal Ions 533**
Neelam Kumari, P.N. Pathak, P.K. Mohapatra

I. Nuclear Forensics and Safety

I-1 **Applicability of Analytical Instrument in Trace Evidence Analysis 535**
Mukesh Sharma and Shailendra Jha

I-2 **Combating Nuclear Terrorism in India: Preventive Nuclear Forensic Perspectives 537**
N.K. Raghav, J.S. Lad, A.V. Deshmukh and S.S.Jagtap

I-3 **A Review on Nuclear Forensic Methodology for Analysis of Nuclear Material of Unknown Origin. 539**
A.V. Deshmukh, N.K Raghav, N.M Fatangare and S.S. Jagtap

I-4 **Thoron Mitigation Using Charcoal Based System 541**
Sudeep Kumara K., Karunakara N., Yashodhara I., Sapra B. K.., Sahoo B. K.., Gaware J. J., Kanse S. D., and Mayya Y. S.

I-5 **Establishing the Lung Counting Facility - An Experience 543**
S. Rajaram, J. Thulasi Brindha, K.R.Sreedevi, P.M. Ravi and R.M. Tripathi

J. QA/QC and Uncertainty in Measurements

J-1 **Performance Evaluation of HPGe detector for Environmental Sample analysis at different Shielding Conditions. 545**
T.J. Jaison, A.K. Patra, P.M. Ravi and R.M. Tripathi

J-2 **Quantification of Measurement Uncertainty in Determination of Uranium in Magnesium Diuranate by Titrimetry 547**
B. Narasimha Murty, G. Brahmananda Reddy and H.R. Ravindra

J-3 **Quantification of Measurement Uncertainty in the Determination of O/U ratio of UO_{2+x} Powders by Titrimetry 549**
B. Narasimha Murty, G. Brahmananda Reddy and H.R. Ravindra

J-4 **Certification of Biological Reference Materials by Instrumental Neutron Activation Analysis 551**
Mamata R. Lanjewar and R.B. Lanjewar

J-5 **Recent Advances in Microwave Heating Assisted Sample Preparation Methodologies in Chemical Quality Control of ThO_2 based MOX Fuels 553**
G. Singh, R.K. Malav, R.B. Bhong, A.B. Name, A. Pandey, D.K. Das, P.G. Behere and Mohd. Afzal

J-6 **Analysis of Titanium in D9 alloy- An Inter Comparison Study and Application to Radioactive Sample 555**
S. Sriram, S. Annapoorani, V. Hemalatha and K. Sankaran

J-7 **Uncertainty Budget in Internal Monostandard NAA for Small and Large Size Samples Analysis 557**
K.B. Dasari, R. Acharya

J-8 **Quantification of Measurement Uncertainty in the Determination of O/U Ratio of Sintered Uranium Dioxide Fuel Pellets by Spectrophotometry 559**
B. Narasimha Murty, U.B. Misra, M. Dutta and H.R. Ravindra

Author Index 561

Securing a Better Future for All: Making a Difference with Nuclear Technology

Daud Mohamad

Deputy Director General, Head of the Department of Nuclear Sciences and Applications, International Atomic Energy Agency (IAEA)

The IAEA is an inter-governmental organization and the world's centre of cooperation in the nuclear field. As per its mandate, the IAEA shall seek to accelerate and enlarge the contribution of atomic energy to peace, health and prosperity throughout the world. The IAEA executes its mandate on the basis of three pillars: nuclear verification and security, safety and technology transfer. Nuclear technologies and techniques can offer vital assistance in fighting disease, improving food security and safety, and studying and sustainably managing water resources and the environment. The IAEA's Department of Nuclear Sciences and Applications works to address these critical developmental needs by helping Member States to apply nuclear science and technology more effectively where they have a comparative advantage and can have substantial socio-economic impact.

The scale of these needs is growing each day as the world's population and life expectancies increase, as global industry and migration multiply the populations of the world's cities and their demands for resources, and as these trends impact human disease, the availability of safe and sufficient supplies of food and water, the health of our terrestrial and marine ecosystems, and the variability of our climate. These are highly complex challenges, and nuclear science and technology, can make impactful contributions in helping Member States to respond to these challenges.

In these areas, the IAEA dedicates a large portion of its resources to human health. Cancer is now a global epidemic with most severe impact on low and medium income (LMI) countries that often lack comprehensive cancer control strategies, access to radiotherapy and the human resources required to administer radiation medicine safely and effectively.

In the Human Health Programme, IAEA experts in radiation medicine, dosimetry and medical physics help Member States to build their capacities in these areas to enable them to establish and operate radiotherapy facilities that provide the safe, effective treatment that patients in LMI countries need. Simultaneously, the IAEA's Programme of Action for Cancer Therapy works closely with the World Health Organization and a coalition of partners in the public and private sector to help Member States mobilize resources and develop comprehensive national cancer control strategies to combat the disease on all fronts.

In addition to its work with cancer, the IAEA also provides support in the use of nuclear imaging techniques for the diagnosis and treatment of cardiovascular diseases, and in the use of stable isotope techniques to develop optimal nutrition regimes for mothers and infants.

With populations, hunger and climate variability on the rise, food and agriculture is another essential area of activity for the IAEA. To maximize the impact of nuclear techniques in this field, the IAEA joined with the Food and Agriculture Organization (FAO) in 1964 to establish the Joint FAO/IAEA Programme on Nuclear Techniques in Food and Agriculture. This programme works to integrate nuclear techniques in all aspects of the agricultural production chain ranging from the farm to the table.

Accordingly, this programme helps Member States to apply nuclear and related techniques to assess and manage the quality of their soils; to optimize the use of fertilizers and water; to develop crop varieties that are resistant to disease and harsh climactic and soil conditions; to maximize the health and productivity of livestock; to control insect pests that damage crops and carry disease, and; to ensure the safety of food products from disease-causing microbes and pests that can prevent access to valuable export markets.

Water resource management represents another great challenge for IAEA Member States, as freshwater sources increasingly stressed by expanding populations and economic activity are suffering the compounding stresses of climate change. Many countries increasingly depend on groundwater resources that can differ vastly in terms of quantity, quality and recharge rates. The first step to developing sustainable management strategies is to understand these characteristics for each resource, and the most effective and economical way to achieve this in many cases is through isotope hydrology. Accordingly, the IAEA's Water Resources Programme assists Member States in building their expertise and capacity in the use of isotope hydrology to enable the development of scientifically based management strategies that can maximize the sustainability of this precious resource.

The sustainability of the earth's natural resources depends heavily on the health of the overall environment on land, in the atmosphere and in our oceans. Understanding the processes and changes that occur in these environments is central to our ability to manage them, and the IAEA's Environment Programme helps Member States to use nuclear techniques to assess these processes, the changes that occur in them, and the impact that these changes may have. This programme places special focus on the marine environment in addressing issues such as ocean

acidification and the impact of radionuclides and organic pollutants on the marine ecosystem.

Underpinning much of the IAEA's work in the above areas is the radiation technology that is necessary to make many of the nuclear applications possible. For example, the diagnosis and treatment of some noncommunicable diseases, among which cancer, requires a variety of radiopharmaceuticals, which themselves require cyclotrons and research reactors for their production. Similarly, the irradiation of food products that reduces spoilage rates and destroys potentially hazardous microbes demands radioactive sources or alternatives such as electron beams. Electron beams have environmental applications as well in the treatment of industrial wastewater and sludge for public health and environmental protection. The IAEA's Radioisotope Production and Radiation Technology Programme assists Member States in the development and application of these technologies to support their efforts in these and other areas.

Even more fundamental to the IAEA's work in the thematic areas above are the laboratory facilities in Vienna, Monaco and Seibersdorf (35km outside Vienna) that support the activities of the Department of Nuclear Sciences and Applications in human health, food and agriculture, water resources and the environment. Unique in the UN system, the IAEA's laboratories are centres for applied R&D, training and education, and the provision of analytical services that support and strengthen the capacities of Member State laboratories.

The laboratories are the backbone of the IAEA's activities in support of Member States' development efforts, and for this reason, the IAEA is now working to modernize and upgrade many of these facilities to ensure their continuing ability to respond to Member States' growing demands and the emerging challenges they face. As with the programmes discussed above, this important undertaking is emblematic of the IAEA's enduring commitment to use nuclear technology to secure a better future for all.



Dr. Daud Mohamad *was appointed Deputy Director General for Nuclear Sciences and Applications, effective 1st January 2011. Prior to joining IAEA Director General Amano's senior management team, Mr Daud held the position of Director General of Malaysian Nuclear Agency (Nuclear Malaysia) since September 2004. He had joined Nuclear Malaysia in 1978 and was one of the pioneer staff of the organization. From 2008 to 2010, Mr Daud served on the IAEA's Standing Advisory Group on Nuclear Applications (SAGNA), and from 2001 to 2010 on the Steering Committee on Training and Education in Radiation Protection and Waste Safety. He had taken up many expert missions to a number of Member States on self-reliance and sustainability programme of nuclear institutions in Asia and the Pacific under the framework of the IAEA. Mr Daud holds a Bachelor of Science degree from Universiti Kebangsaan in Malaysia, a Master of Science degree from McMaster University in Canada, and a PhD in High Level Radioactive Waste Management from University of Glasgow/Scottish Universities Research Reactor Centre in the UK. He has published more than 70 technical papers and was Chief Editor for the book entitled 'Nuclear Science and Technology'.*

Applications of Nuclear Analytical Techniques for Identifying the Origin and Composition of Found Radioactive Materials

B. Sur[1], F. Dimayuga[1], L. Li[1], G. Li[1], G. Bentoumi[1], R. Rogge[2]

1. *Atomic Energy of Canada Limited, Chalk River Laboratories, Chalk River, ON K0J1J0, Canada; E-mail: surb@aecl.ca*
2. *Canadian Neutron Beam Centre, Chalk River Laboratories, Chalk River, ON K0J1J0, Canada*

Radioactive materials and sources have been used worldwide for the last 100 years – for medical diagnosis and therapy, industrial imaging and process monitoring, consumer applications, materials and biological research, and for generating nuclear energy – among other peaceful purposes. Many of the radioactive materials have been produced, and the associated nuclear science and technology developed, at major research sites such as the Chalk River Laboratories in Ontartio, Canada. Sometimes undocumented radioactive materials associated with production, development or use are found, usually in the context of a legacy setting, and their composition and origin needs to be determined in order for these materials to be safely handled and securely dispositioned. The novel applications of nuclear analytical techniques, including mass spectroscopy, gamma and x-ray spectroscopy and neutron beam irradiation techniques, is presented in the context of some recent investigations.

Application of Material Characterization Techniques

An unidentified legacy lead flask containing unknown radioactive materials was found in the Chalk River Laboratory site. Preliminary examination in AECL's hot cells determined that the flask contained several capsules. The initial spectroscopy of the capsules indicated a dominant peak that corresponds to ^{137}Cs, suggesting the contents are irradiated nuclear fuel.

To unambiguously identify the amounts and types of material in the capsules, a number of non-destructive examination techniques are being performed. One such technique is X-ray Fluorescence Spectroscopy analysis to determine the elemental composition of the contents of the capsules.

Due to the high penetration of neutrons in most materials, neutron methods provide the potential to non-destructively provide significant information about the capsule contents. The Canadian Neutron Beam Centre, operating at the NRU Reactor is applying three neutron based methods: (a) transmission-based measurements such as radiography and tomography, (b) diffraction-based measurements, and (c) activation-based measurements, specifically delayed neutron analysis.

Attenuation of the neutron beam transmitted through the sample reveals information about the scattering and absorption properties of the elements within the material, and in some cases offers information on isotopics. A tomograph can be constructed by obtaining a series of radiographs as the sample is rotated through 180°. From these, a computer-generated image can be constructed (i.e. computed tomography). At a minimum, this technique should give a picture of the capsule contents. Also, this technique allows the identification of the canister material and its internal features.

Neutron diffraction reveals information related to the crystal structure. Liquid and amorphous phases lead to a diffraction pattern devoid of sharp peaks, but with structure. Therefore, neutron diffraction will confirm if crystalline material is present and can be used to look for the anticipated phases for known fuels. CNBC have experience using neutrons to study various fuel types of both fresh and irradiated fuels.

Neutron activation analysis (NAA) is a process used to determine elemental concentrations in materials. In essence, when the sample is bombarded with neutrons, the elements form radioactive isotopes which consequently produce radioactive emissions. Using this information, it is possible to study spectra of the emissions of the radioactive sample, and determine the concentrations of the elements within it. In the present case the delayed neutrons are detected to determine the presence of fissile materials. Among the three neutron methods, this is the most speculative. The advantage is that this method has the potential to reveal more information about the isotopes present. It may be possible to combine this with the other two methods to gain greater insight into the contents of the capsules.

It is highly likely that in order to definitively identify the amounts and types of fissile material in the capsules, destructive examination techniques (i.e., chemical/isotopic analysis) would still have to be done. The value of the non-destructive techniques is to reduce the uncertainty in terms of the nature of the hazards involved in the handling of the capsules, particularly in terms of criticality and radiological safety in the facilities involved in the destructive examination.

The destructive examination of the capsules will be conducted in the hot cells, where similar destructive examination is routinely done as part of post-irradiation examination (PIE) activities for experimental and power reactor fuel. Techniques used include ICP-MS

(Inductively Coupled Plasma – Mass Spectrometry), alpha-spectrometry, and beta-counting.

Upon completion of the chemical and isotopic analyses, the remaining contents will be weighed and repackaged into a new appropriate container that will then be sent for disposal. All the characterization results of the contents and the relevant information on the repackaged material will be documented.

It is expected that, following the characterization of the capsules, it will be possible to reconstruct the irradiation history of the material, and to determine the origin, the timeline and the intent of the activities that led to the creation and disposal of the radioactivity.

Cobalt-60 Chronometry

The use of Co-60 for cancer radiation therapy was pioneered by Dr. Harold E. Johns of the University of Saskatchewan in Canada. Co-60 is also commonly used as a radiation source for industrial and agricultural irradiation applications. The occasional discovery of Co-60 sources following the uncontrolled disposal of some irradiators is a well documented occurrence. One factor in the determination of the origin of an undocumented Co-60 source is the age of the source. Since Co-60 decays to Ni-60, in principle the age of the source, or the time elapsed since the Co-60 was created, can be determined by measuring the ratio of Co-60 atoms to that of the daughter Ni-60 atoms present in the material. AECL Chalk River Laboratories has participated in a series of round-robin exercises with five other Canadian and one US laboratory to inter-compare the results of the chemical separation and mass spectroscopy methods developed for such Co-60 chronometry. The optimal separation and measurement conditions yield results that demonstrate the suitability of this method for correctly assessing the age of a Co-60 radioactive source, with age up to 35 years, with a bias of less than a year.

Dr. Bhaskar Sur *graduated with a 5-year Integrated M.Sc. in Physics from Indian Institute of Technology, Kanpur and obtained his Ph.D. in Experimental Nuclear Astrophysics from The Ohio State University, Columbus Ohio. After post-doctoral fellowships at Lawrence Berkeley National Laboratory, Berkeley California and Queen's University, Kingston Ontario, he joined Atomic Energy of Canada Limited at Chalk River Laboratories, Chalk River Ontario in 1992. As Director, Nuclear Science Division in Chalk River Laboratories he oversees R&D in the areas of Applied Physics, Reactor Physics, Nuclear Instrumentation & Control Systems, Radiation Biology and Environmental Technologies. He is the AECL lead for programs in Non-Proliferation & Counter-Terrorism, Tritium & Fusion, and Small Reactors. Dr. Sur is the recipient of the AECL President's Discovery Award in 2007 and the AECL President's Distinguished Merit Award in 2013. He has recently been appointed to the Editorial Board of the AECL Nuclear Review, a peer-reviewed, open access Canadian Nuclear Science and Technology journal.*

Development and Applications of k_0-based NAA using Research Reactors at BARC

R. Acharya[1] and A.V.R. Reddy[2]

1. *Radiochemistry Division, Bhabha Atomic Research Centre, Trombay, Mumbai 400 085, India; Email: racharya@barc.gov.in*
2. *Analytical Chemistry Division, Bhabha Atomic Research Centre, Trombay, Mumbai 400 085, India; Email: avreddy@barc.gov.in*

Neutron activation analysis (NAA) using k_0-based method has been standardized for the analysis of both small and large size samples in diverse matrices. The k_0-based NAA using gold as single comparator was carried out by characterizing irradiation sites of research reactors at BARC and determining the k_0-factors of some analytically important isotopes. The method was validated by analyzing reference materials (RMs) of different origin and applied to geological, environmental and biological samples. The k_0-based Internal Monostandard NAA (IM-NAA) method was developed for the analysis of large size (g-kg scale) and non-standard geometry samples and applied to nuclear reactor structural materials namely zircaloys, stainless steels, nickel alloys and high pure aluminum as well as samples of wheat grains, uranium ore, dross and archaeological and modern clay ceramics. Large sample NAA work was performed for a pottery replica under inter comparison exercise of an IAEA CRP. For large size samples, thermal column at Apasra and graphite reflector position at AHWR Critical facility were characterized and used.

Introduction

Neutron activation analysis (NAA) is a powerful isotope specific nuclear analytical technique for simultaneous determination of multi-elements at major, minor and trace levels in diverse matrices. In routinely used relative method, single or multielement standard is co-irradiated with the sample and the activities formed in both the sample and standard are measured in identical geometry with respect to the detector. On the other hand, single comparator method known as k_0-method, a comparator like Au instead of multi-element standard is co-irradiated with the sample [1-4]. However this method requires characterization of irradiation sites and detection efficiency data. The k_0-NAA method was adapted at RCD, BARC in the year 1995, and later, IM-NAA method was developed to deal with large and non standard geometry samples. Standardization and various applications of k_0-NAA and IM-NAA [6] have been described briefly here and elaborately in our earlier publications starting from 1997 [1-3, 5-20].

Experimental

Irradiation positions of Apsara (core and thermal column, TC), CIRUS (self serve, SS, and pneumatic carrier facility, PCF), and AHWR critical facility (CF) (graphite reflector) were used in our work. Neutron monitors like Au, Zr, In, Mo and Zn were used for neutron spectrum characterization of irradiation positions [17]. The samples were used in the mass ranges of 50 mg to 1 kg. Samples were assayed using a 40% HPGe detector coupled to a multi-channel (8k) analyzer (MCA). The resolution of the detector was 1.9 keV at 1332 keV of ^{60}Co. Peak areas under the characteristic full energy peaks were evaluated by peak-fit method using the PHAST software, developed at BARC. Epithermal neutron shape factor ( ) and sub cadmium to epithermal neutron flux ratio (f) were determined using bare and/or cadmium ratio methods using flux monitors. The f and flux values of the thermal column (TC) and graphite reflector position of CF were obtained using ^{115}In as the monitor. The f, and neutron flux values are given in Table 1.

Results and discussion

k_0-NAA Applications

k_0-NAA method was validated by determining major, minor and trace element concentrations of about 30 elements in many (certified/standard) reference materials (RMs) namely USGS W-1 and NOD-1, IAEA RMs Soil-7 and SL-3 and NIST SRM 1571 [5]. The k_0-NAA method was applied to many samples including gemstones (ruby [1], beryl and emerald [2], sediments, manganese nodules and encrustations, cereals, medicinal and edible leaves. For NAA using short-lived activation products, PCF at CIRUS and Dhruva reactors were extensively used. The IM-NAA using in situ relative efficiency was used for large sample analysis as given below [6-20].

IM-NAA for Small and Large Sample Analysis

For validation of the IM-NAA, SMELS (I-III) and RMs SL-3 and Soil-7 were analyzed using Au and Sc monostandards respectively. Concentrations of 23 elements were determined [7]. The %deviations of determined values were in good agreement (within 8%) with the assigned and certified values of SMELS and RMs respectively. The Z-score values (at 95% CL) for SMELS were within ±1 for most of the elements. IM-NAA method has been applied to a variety of

Table-1: Neutron flux parameters of irradiation positions of reactors

Reactor	Position	-value	$f = {}_{th}/{}_{e}$	$\%n_{th}$	Flux (n cm^{-2} s^{-1})
Apsara	E8	0.035±0.003	50.0±1.5	98.0	$5x10^{11}$
	TC	-	$(6.0±0.4)x10^{3}$	99.98	$1.2x10^{8}$
CIRUS	SS	0.011±0.001	80±3	98.7	$3x10^{13}$
	PCF	0.010±0.001	120±4	99.2	$3x10^{13}$
AHWR CF	GR	-	$(8.6±0.3)x10^{2}$	99.9	$3.4x10^{7}$

samples including meteorite and uranium ores [8,9,12]. The IM-NAA method was applied to analyze uranium ore samples obtained from Jaduguda and Bhatin mines, Jharkhand for multielements including U, Th and rare earth elements (REEs), where, uranium concentrations were found to be about 350-550 mg kg^{-1}[12].

The IM-NAA method was applied for the analysis of many large and non-standard geometry samples of nuclear fuel cladding and structure materials namely zircaloys (zirclaoy 2 and 4), stainless steels (SS 316M, D9 and SS 304L and BCS RMs), 1S grade aluminium, wheat grains, and uranium ores [6,10,11]. Since all the major and/or minor elements in zircaloy and stainless steel samples were amenable to NAA, concentration values were obtained by mass balance approach. One of the best applications of IM-NAA is the analysis of large and non standard geometry ancient potteries for the provenance study. A total of 30 large size and non-standard geometry ancient potteries, obtained from excavated Buddhist sites of Vishakhapatanam and Hyderabad region of AP, India were analyzed [15,16]. Sc, which has good nuclear and geochemical properties, was used as the monostandard. The concentration ratios of key elements Cr, Fe, Co, Ga, Cs, As, La, Ce, Sm, Eu, Lu, Hf and Th with respect to Sc were determined. Values of La/Ce and statistical cluster analysis using concentration ratios of elements were used for grouping/ provenance study.

Recently IM-NAA was used for small and large sample of a pottery replica from Peru under an IAEA CRP and results obtained for 21 elements were used for inter comparison exercise [20].

Conclusions and Future Prospects

The k_0 based IM-NAA method using in-situ relative efficiency is geometry independent and thus was found promising for the analysis of samples of large and non-standard geometry samples. Material characterization using nuclear analytical techniques using NAA methods like PGNAA and fast NAA (FNAA) and ion beam analysis (IBA) approaches like PIXE and PIGE are required to be pursued for complete compositional characterization. Development of methods dealing with analysis of large and not so homogeneous samples is a challenge using LSNAA.

Acknowledgments

Authors are thankful to all contributors and collaborators and personnel of Apsara, Cirus, Dhruva and Critical Facility reactors, BARC for their co-operations.

References

[1] R.N. Acharya, P.P. Burte, A.G.C. Nair, A.V.R. Reddy and S.B. Manohar, J. Radioanal. Nucl. Chem., 220 (1997) 223.

[2] R. Acharya, Ph.D Thesis, University of Mumbai, Mumbai, 2000.

[3] R. Acharya, A.G.C. Nair, K. Sudarshan, A. Goswami and A.V.R. Reddy, J. Radioanal. Nucl. Chem., 278 (2008) 617.

[4] F. De Corte and A. Simonits, Atom. Data Nucl. Data Tables 85 (2003) 47.

[5] R.N. Acharya, A.G.C. Nair, A.V.R. Reddy and S.B. Manohar, Appl. Radiat. Isot., 57 (2002) 391.

[6] A.G.C. Nair, R. Acharya, K. Sudarshan, S. Gangotra, A.V.R. Reddy, S. B. Manohar and A. Goswami, Anal. Chem. 75 (2003) 4868.

[7] R. Acharya, K. K. Swain, Amit Kumar, Nicy Ajith, R. Verma and A. V. R. Reddy J. Radioanal. Nucl. Chem., 286 (2010) 507.

[8] R. Acharya, K. K. Swain and A.V.R. Reddy, Nucl. Instr. Meth. A 622 (2010) 411.

[9] A.G.C. Nair, R. Acharya, A.V.R. Reddy, A. Goswami, B.Adur, H.B. Mali, J. Rathod, R. Patil and K. Vora, Current Science, 87 (2004) 654.

[10] R. Acharya, A.G.C. Nair, A.V.R. Reddy and A. Goswami. J. Nucl. Mat., 326 (2004) 80.

[11] R. Acharya, A.G.C. Nair, A.V.R. Reddy and A. Goswami, Anal. Chim. Acta, 522 (2004) 127.

[12] S. Tiwaria et al., J. Nucl. Radiochem. Sci., 8 (2007) 25.

[13] R. Acharya, A.G.C. Nair, K. Sudarshan A.V.R. Reddy and A. Goswami, Appl. Radiat. Isot., 65 (2007) 164

[14] R. Acharya, K. K. Swain, K. Sudarshan, R. Tripathi, P. K. Pujari and A.V.R. Reddy, Nucl. Instr. and Meth. A, 622 (2010) 460.

[15] K. B. Dasari, R. Acharya, K. K. Swain, N. Lakshmana Das and A. V. R. Reddy, J. Radioanal. Nucl. Chem., 286 (2010) 525.

[16] K.B. Dasari, R. Acharya, N.L. Das and A.V.R. Reddy, J. Radioanal. Nucl. Chem., 294 (2012) 429.

[17] R. Acharya, K.B. Dasari, J.S. Brahmaji Rao, C.R.. Vekatasubramani and A.V.R. Reddy, IEEE Trans. Nucl. Sci. 60 (2013) 3051.

[18] R. Acharya, S. Kolay and A.V.R. Reddy, J. Radioanal. Nucl. Chem., 294 (2012) 309.

[19] K. K. Swain, Nicy Ajith, R. Acharya, R. Verma and A. V. R. Reddy, J. Radioanal. Nucl. Chem., 294 (2012) 319.

[20] R. Acharya, K. K. Swain, K. B. Dasari, A. D. Shinde, P.K. Pujari and A. V. R. Reddy, l., J. Radioanal. Nucl. Chem., 2014 (In press)



Dr. A.V.R. Reddy *joined Nuclear Chemistry Section, Radiochemistry Division, BARC in 1977 after completing one year Orientation course in Chemistry from BARC Training School and is now Head, Analytical Chemistry Division, BARC. His areas of research are nuclear fission, nuclear reactions, nuclear analytical techniques, non-destructive assay methods, electroanalytical chemistry and environmental science. He has more than 500 publications (about 200 journal publications), co-authored four books and edited about 12 compilations in addition to the 9 thematic volumes pertaining to peacefulatom 2009. He has worked on the extension of Periodic Table during 1992-93 in the Institute of Nuclear Chemistry, Mainz, Germany and worked in IAEA during 1999-2000 as a technical officer. He visited many countries in Asia and Europe, delivered lectures and provided advice on QA/QC of nuclear analytical techniques. He was a visiting professor in Mumbai University for 15 years and a professor of HBNI, DAE. Dr. Reddy is member of many scientific associations and fellow of IUPAC. He is vice president of IANCAS and AEACI. He worked as a commission member of International Union of Pure and Applied Chemistry (IUPAC) for three terms. Dr. Reddy is Member Secretary of Basic Science Committee, BRNS and a member of DST PAC.*

Applications of Fast Neutron Generators

Amar Sinha

Neutron and X-ray Physics Division, Bhabha Atomic Research Centre, Mumbai 400 085, India

Fast neutron generators have long been used for onsite applications in activation analysis particularly for checking the quality of cement and coal. However, fast neutron generators can be applied for several new applications. Some of them include use of time of flight and prompt gamma analysis for designing neutron based explosive detection, high sensitivity fissile material detection for nuclear material accounting, portable neutron radiography and testing concepts for advanced reactor systems such as accelerator driven system. We have been developing neutron generators for variety of such applications some of them large systems capable of generating intense neutron source, compact transportable system having moderate neutron source strength for field applications in explosive detection and fissile material detection as well as miniature neutron generators. Simultaneously, we have been developing systems for several applications which include explosive detection system using these generators which utilizes prompt gamma and activation analysis. This system is based on tagged neutron technique. It will use 64 pixel alpha detector which in coincidence with BGO or LaBr prompt gamma detector

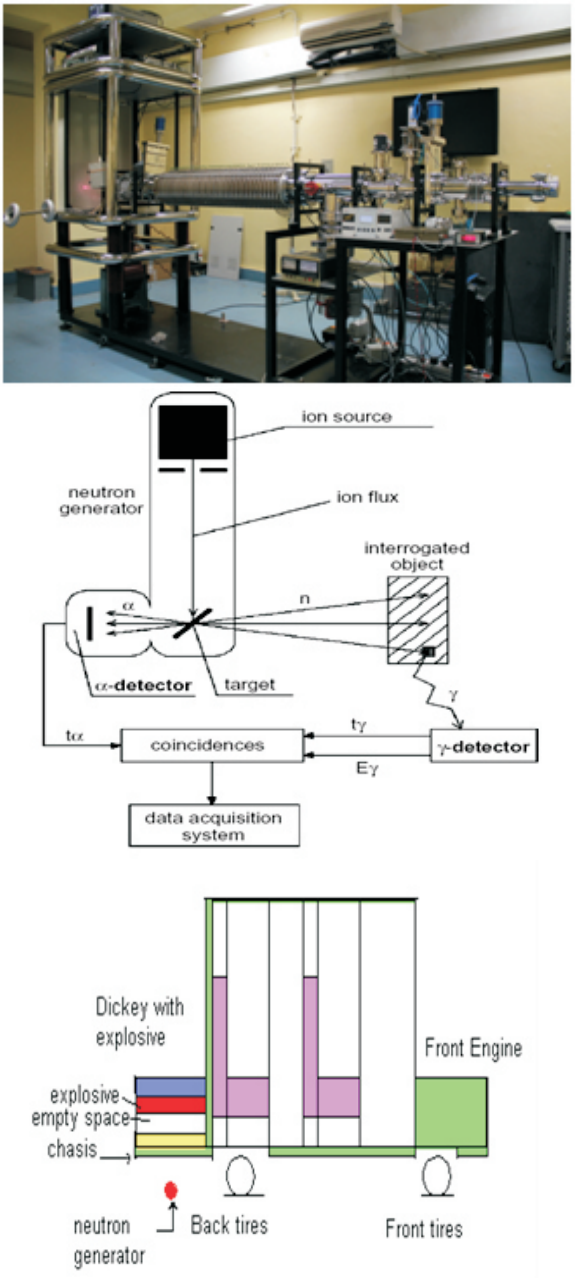


Fig. 1 Transportable neutron generator developed at BARC and schematic of explosive detection

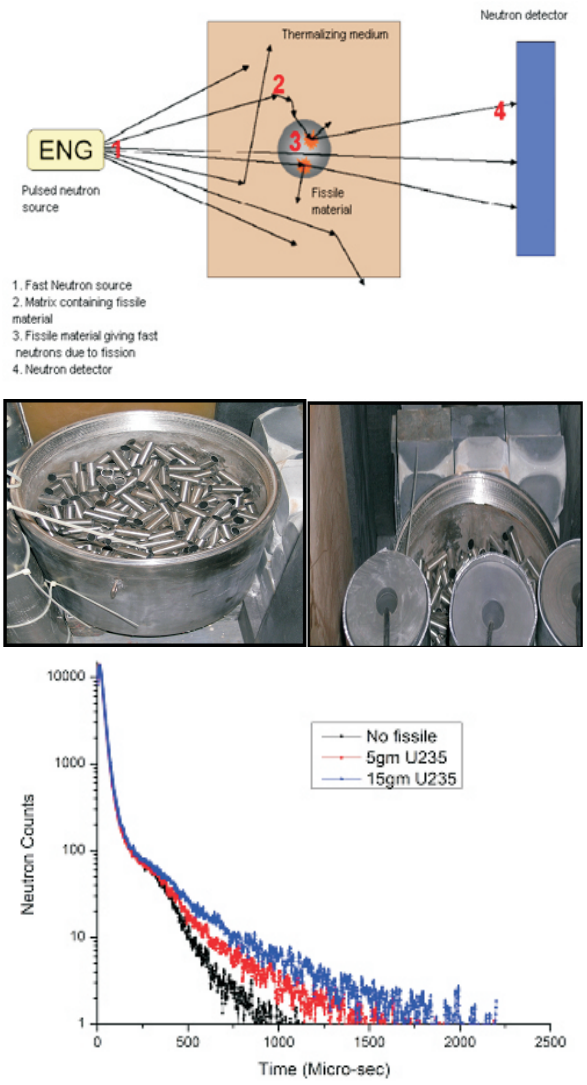


Fig. 2 Fissile material Detection using neutron generator (Differential Die Away Technique)

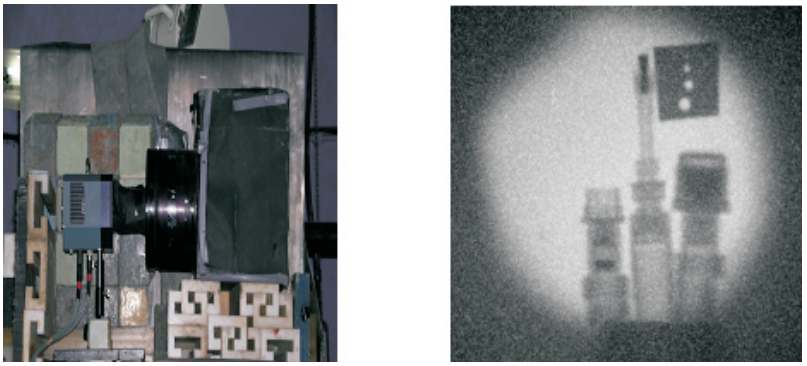


Fig. 3 Testing of Fast neutron radiography for imaging pyro-technique device

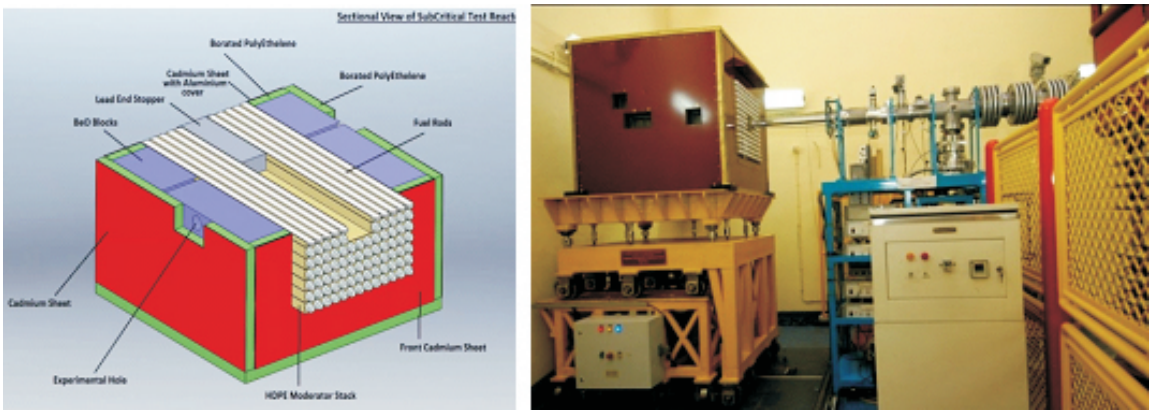


Fig. 4 Developing experimental ADS using neutron generator for studying physics issues of ADS

will determine location of explosive in a vehicle or cargo container.

Another application which we have developed is a highly sensitive method of fissile material detection for nuclear material accounting. The technique used in this system is called differential die away technique and uses external source of pulsed neutron for increasing signal to noise ratio and counting differential signal. This talk will describe the method used for this application.

We will briefly describe two more applications

Onsite Radiography System for Testing of Pyro-technique Devices used in defence or Space Applications

Here neutron generator is being used for developing onsite neutron radiography system.

Use of Neutron Generators for Developing Experimental Accelerator Driven System (ADS)

ADS is merger of accelerator technology with reactor technology which is being developed worldwide for transmuting nuclear waste and utilizing thorium. Before a commercial ADS becomes a reality , there are a number of physics issue which needs to be solved .



Dr. Amar Sinha *is Outstanding Scientist and Head, Neutron and X-ray Physics Division of BARC. He has worked extensively on problems related to neutron physics, Spallation Neutrons, radiation damage, X-ray and neutron imaging applications. He has been responsible for designing and developing first zero power Accelerator Driven system within the country. He has carried out extensive research in Neutron generator development and their applications in explosive detection and fissile material detection. He has developed several techniques of direct relevance to nuclear energy programme such as neutron tomography, two phase visualization using real time neutron imaging, X-ray Phase contrast imaging technique for characterization of CHTR fuel. He helped Mangalore University in the design of microtron based neutron source which is the first such source in a university in India. He is presently developing X-ray Imaging Beamline at INDUS-2 synchrotron for material science and medical applications. He is Professor of Homi Bhabha National Institute. He is Recipient of DAE Technical Excellence Award (2005), Group Achievement Award (2010), Homi Bhabha Science & Technology Award (2011) which is the highest award of Department of Atomic Energy.*

Photon Activation Analysis

H. Naik

Radiochemistry Division, Bhabha Atomic Research Centre, Trombay, Mumbai 400 085, India

The photon induced reaction cross-sections of Zn, Y, Zr, Nb, Mo, Pb, Bi, Th and U within the end-point bremsstrahlung energies of 8-20 and 45-70 MeV have been determined by off-line -ray spectrometric technique and using the microtron and electron linac of four different countries. This has been done to examine the utility of the photo-activation analysis for the estimation of different elements.

The experiment for the measurement of (,n) reaction cross-section of ^{232}Th and ^{238}U within 8-17 MeV have been carried out using the 8 MeV Microtron, Mangalore, India, 10 MeV electron linac, EBC, Kharghar, India [1,2], 20 MeV electron linac, ELBE, Germany and 35 MeV electron linac, SAPHIR, Saclay, France. The (, xn) reaction cross-sections of ^{nat}Zn, ^{89}Y, ^{nat}Zr, ^{93}Nb, ^{nat}Mo, ^{208}Pb and ^{209}Bi with the end-point bremsstrahlung energies of 10-16 and 45-70 MeV have been carried out using the 10 MeV electron linacof EBC, Kharghar, Navi-Mumbai, India [3, 4], 20 MeV electron linac, ELBE of Dresden, Germany [5] and the 100 MeV electron linac of PAL, Pohang, South korea [5,6]. A typical -ray spectrum of photo-activation reaction/fission products of ^{238}U and ^{209}Bi are shown in Fig. 1 and 2. The -ray activities of reaction/ fission products are used for reaction cross-section and fission yield determination using the usual decay equation [1,2].

The (,xn) reaction cross-sections of the above materials for mono-energetic photons have been also calculated using computer code TALYS 1.4, whereas the bremsstrahlung spectrum was obtained from computer code GEANT4 (Fig. 3). Then the calculated flux-weighted reaction cross-sections (e.g. ^{209}Bi(,xn)) were compared with the experimental data (Table 1) and found to be in general agreement. It was also found that the experimental and theoretical (,xn) reaction cross-sections of the above materials (e.g. ^{93}Nb(, xn)) increase very fast from its threshold energy to the threshold energy of the next higher reaction channel (Fig. 4). Then it remains constant up to the energy where the next higher reaction channel reaches maximum. There after it decreases slowly with energy. This indicates the portioned of excitation energy in different degrees of freedom. It was also observed that the increase trend of cross-sections from the threshold energy to its maximum is very sharp for the (, n) and (,2n) reactions channels then the higher reaction channels due to the Giant Dipole Resonance (GDR) effect.

The (,xn) reaction cross-section of structural material such as ^{nat}Zr and ^{93}Nb important for their estimations in Zircaloy-2, zircaloy-4 and Zr-2.5wt% Nb alloy, which are used as cladding material in boiling water reactor (BWR) and pressurized water reactor (PWR) as well as the pressure tubes in pressurized heavy water reactor (PHWR). The (,n) reaction cross-section of ^{100}Mo can be used for the production of ^{99}Mo-^{99}Tc, which is needed for medical application for imaging purpose. The (, pxn) cross-section of ^{nat}Zn is used for the production of ^{67}Cu, which is an important reaction monitor and needed by IAEA. The (,xn)

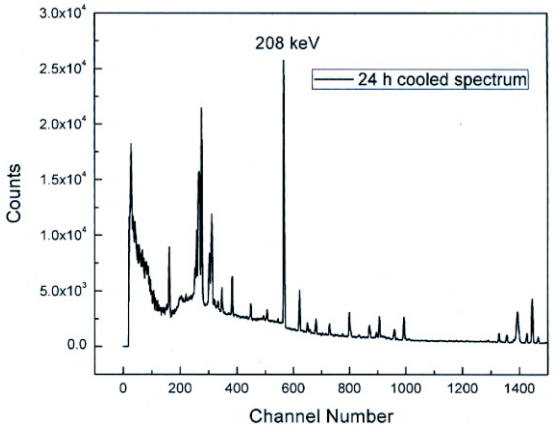


Fig. 1 Gamma-ray spectrum from the activated ^{238}U foil with 10 MeV bremsstrahlung beam

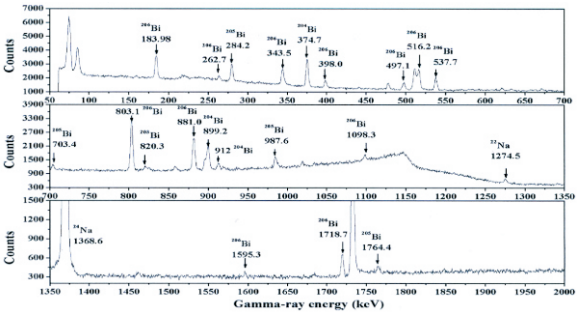


Fig. 2 Gamma-ray spectrum of ^{209}Bi(,xn; x=3-6) reaction products

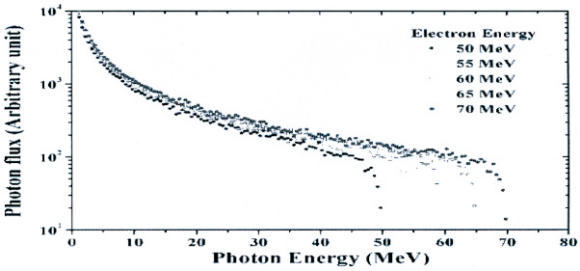


Fig. 3 Plot of Photon flux in arbitrary unit vs. photon energy calculated using GEANT4 code

reaction cross-sections of ^{nat}Pb and ^{209}Bi are needed for the design of accelerated driven sub-critical system (ADSs) based on their application as spallation sources. Similarly, the (,xn) reaction cross-sections of ^{232}Th and ^{238}U are needed for their estimation from the point of the design ADSs and conventional reactors such as BWR, HWR, AHWR and fast reactor based on their application as a spallation source or as breeding fuel materials.

Table-1: The flux-weighted average (,xn) reaction cross-sections of 209Bi

Photo-neutron reaction	Bremsstrahlung energy (MeV)	Photo-neutron cross-section (mb)	
		Experimental	Theoretical
^{209}Bi(,6n)^{203}Bi	50	-	0.00007
	55	-	0.00515
	60	0.023±0.004	0.02728
	65	0.057±0.008	0.06717
	70	0.105±0.022	0.10168
^{209}Bi(,5n)^{204}Bi	50	0.058±0.006	0.04178
	55	0.101±0.022	0.10685
	60	0.149±0.015	0.15030
	65	0.163±0.023	0.17704
	70	0.171±0.019	0.19544
^{209}Bi(,4n)^{205}Bi	50	0.315±0.054	0.26137
	55	0.374±0.035	0.31195
	60	0.389±0.051	0.33912
	65	0.403±0.056	0.36246
	70	0.420±0.055	0.37013
^{209}Bi(,3n)^{206}Bi	50	0.652±0.040	0.65195
	55	0.673±0.065	0.66765
	60	0.701±0.048	0.69432
	65	0.783±0.077	0.71608
	70	0.819±0.088	0.73721

Acknowledgement

The author is thankful to the staff of microtron, at Mangalore, India, electron linac at EBC, Kharghar, Navi-Mumbai, India, ELBE, HZDR, Dresden, Germany, SAPHIR, Saclay, France & PAL, Pohang, Korea for providing the electron beam. The author is also thankful to Dr. A. Goswami, Head, Radiochemistry Division, Dr. S.K. Aggrawal, Associate Director and Dr. K. L. Ramakumar, Director of R & I group for supporting the program and for permitting him to visit, PAL, Korea to carry out this experiment.

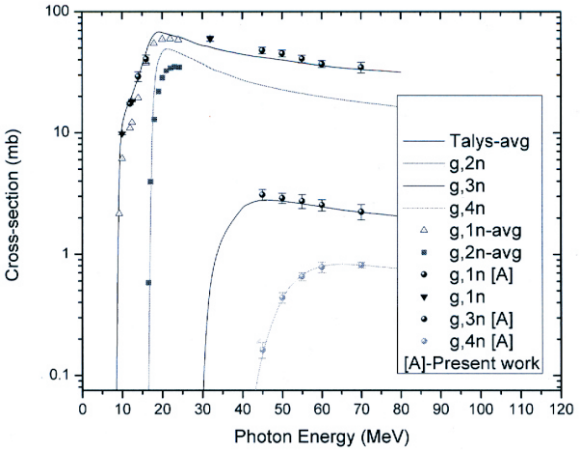


Fig. 4 Plot of experimental and flux-weighted TALYS 93Nb(,xn, x=1-4) reaction

References

[1] H. Naik, Rita Crasta, S.V. Suryanarayana, Ganesh Sanjeev, B. S. Shivashankar, H.G. Raj Prakash, N. Karunakara, H.M. Somashekarappa, M. Kumar, V.T. Nimje, K.C. Mittal and A. Goswami, J. Radioanal. Nucl. Chem. 298, 1065 (2013).

[2] H. Naik, V.T. Nimje, D.Raj, S.V. Suryanarayana, A. Goswami, Sarbjit Singh, S.N. Acharya, K.C. Mttal, S. Ganesan, P. Chandrachoodan, V.K. Manchanda, V. Venugopal, S. Banarjee, Nucl. Phys. A 853, 1 (2011).

[3] R. Crasta, H. Naik, S.V. Suryanarayana, P.M. Prajapati K.C. Jagadisan, S.V. Thakre, S. Ganesh, V.T. Nimje, K.C. Mittal, A. Goswami, J. Radianal. Nucl. Chem. 290, 367 (2011).

[4] R. Crasta, H. Naik, S.V. Suryanarayana, P. M. Prajapati, S.Ganesh, M. Kumar, T .N. Nathaniel, V.T. Nimje, K.C. Mittal and A. Goswami, Radiochim. Acta. 101, 541 (2013).

[5] H. Naik, G.N. Kim, R. Schwengnerc, K. Kim, M. Zaman, M. Tatari, M. Sahid, S.C.Yang, R. John, R. Massavczyk, A. Junghans, S.G. Shin,Y. K A.Wagner, M.W. Lee, A. Goswami, M.-H. Cho, Nucl. Phys. A. 916, 168 (2013).

[6] H. Naik, S. Singh, A. Goswami, V. K. Manchanda, G.N. Kim, K. S. Kim, M.-W.Lee, Md. S. Rahman, D. Raj, S. Ganesan S.V. Suryanarayana, M.–H. Cho, W. Namkung, Nucl. Instr. Meth. Phys. Res. B 269, 1417 (2011).



***Dr. H. Naik**, works in NDA Section, Radio Chemistry Division, BARC, Mumbai. He is a specialist in the field of photon, neutron and charged particle induced reactions and fission of pre-actinides and actinides as well as in the field of non-destructive analysis (NDA). He is chief investigator in the IAEA Research on "Photon, Neutron and Proton Induced Reactions to Produce Medical Isotopes". He is having more than 250 publications. Dr. H. Naik work has been quoted in page 484, 485 and 487 of Chapter 9 (i.e. Fission Fragment Angular Momentum by D. De Frenne) of the Text Book: The Nuclear Fission Process, Boca Raton Ann Arbor Boston, London (1991). His work on determination of thermal neutron fission cross-section of ^{234}Pa i.e. ^{234}Pa(n_{th}, f) has been quoted in the recent nuclide chart in 2013.*

Compton Scattering and its Applications: Current Status and Future Prospects

B.L. Ahuja

Department of Physics, M L Sukhadia University, Udaipur 313001, Rajasthan, India; E-mail: blahuja@yahoo.com

Compton scattering (CS) is an ideal tool to probe the electronic and magnetic properties of materials. The quantity measured in the CS experiment is the double differential scattering cross-section, which enables to determine the electron momentum density. In this talk, I will highlight the applicability of CS technique in determining the electronic structure of explosives like RDX ($C_3H_6N_6O_6$,) and HMX ($C_4H_8N_8O_8$). The applicability of CS in deducing charge transfer in high Z compounds like, $GdAl_2$ will also be presented. In addition, temperature dependent magnetic Compton profiles of rare earth doped cobalt ferrites will also be discussed.

Introduction

Compton scattering (CS) has been proved as a direct probe to study correlated many-body ground states in bulk materials, while avoiding the requirement of surface sensitivity like that in photoemission or electron scattering and long electron mean free path in the case of de Hass-van Alphen experiment [1,2]. The charge Compton profile (CP), $J(p_z)$, is a one dimensional projection of the momentum distribution n(p) of all the electrons (with spin-up plus spin-down). The magnetic Compton profile (MCP), $J_{mag}(p_z)$, corresponds to spin momentum density of unpaired (spin-up minus spin-down) electrons. Mathematically,

$$J(p_z) \quad \sum_i n_{i,\uparrow}(p) \; n_{i,\uparrow}(p)\, dp_x dp_y \qquad (1)$$

$$J_{mag}(p_z) \quad \sum_i n_{i,\uparrow}(p) \; n_{i,\uparrow}(p)\, dp_x dp_y \qquad (2)$$

Methodologies

For the measurement of charge CPs, we have used 20 Ci ^{137}Cs and 100 mCi ^{241}Am Compton spectrometers cited in our laboratory. The details of both the spectrometers are available elsewhere [3,4]. To extract the true CP from raw data, the raw profile is corrected for several systematic corrections like background, instrumental resolution (limited to stripping off the low energy tail), detector efficiency, Compton cross-section, absorption correction, multiple scattering, etc. [1]. Finally, the experimental profile is normalized to the free-atom area (momentum range 0-7 a.u.) [5]. The MCPs are measured using magnetic Compton spectrometer [6] available at SPring-8, Japan.

We have used the linear combination of atomic orbitals (LCAO) [7] and spin-polarized-relativistic-Korringa-Kohn-Rostoker (SPR-KKR) [8] methods to compute the CPs, energy bands, density of states (DOS), Mulliken population (MP) and charge transfer, etc.

Results and Discussion

Ahuja et al. [9] have measured the CPs of secondary explosives like 1,3,5-trinitro-1,3,5-triazinane ($C_3H_6N_6O_6$, also known as RDX) and octahydro-1,3,5,7-tetranitro-1,3,5,7-tetrazocine ($C_4H_8N_8O_8$, also known as HMX). The authors have compared the experimental profiles with the LCAO based calculations. It is found that the CPs deduced from generalized gradient approximation (GGA) give a better agreement with the corresponding experimental profiles than those from other approximations within DFT. In Fig. 1, equally normalized (EN) experimental and DFT-GGA based CPs of RDX and HMX are shown.

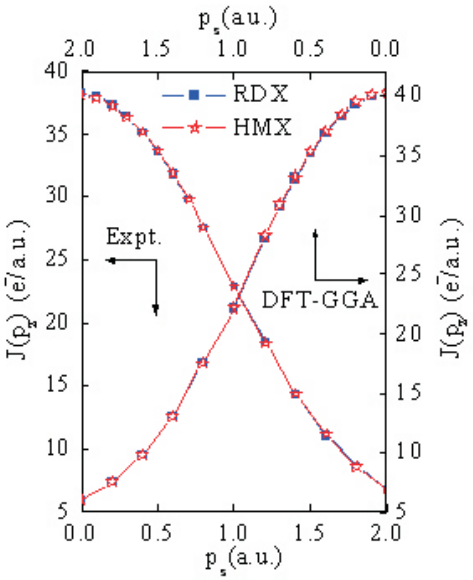


Fig. 1 Experimental and DFT-GGA profiles of RDX and HMX normalized to 55.80 e^- (corresponding to free-atom CP area of RDX). Experimental error is within the size of symbols used

Fig. 1 clearly depicts that EN profiles of RDX and HMX almost overlap on each other. This leads to the similar kind of bonding and thereby electronic behavior of both the materials. From the MP analysis within DFT-GGA calculations, transfer of 0.72e^- from (H_2C-N-) cation to (-NO_2) anion is observed in RDX, while it is 0.77 e^- in HMX. This also validates almost

similar kind of nature of bonding in both the explosives which is in accordance to our CP data.

Sahariya et al. [10] have reported the CPs of $GdAl_2$ and its constituents to establish the role of CS in determining the charge transfer in the high-Z compounds.

Authors have computed the superposition profile $J^{Sup.}$ of $GdAl_2$ compound from the experimental CPs of Gd and Al ($J^{Sup.} = J^{Gd} + 2J^{Al}$). They found significant differences between $J^{Comp.}$ and $J^{Sup.}$ in the vicinity of Compton peak which depicted the failure of the rigid band model and unambiguously confirmed the possibility of charge reorganization on the formation of the compound. The authors have fitted (using least square curve fitting) the experimental valence CPs of the constituents (Gd and Al) to the experimental valence CP of the compound, to determine the charge transfer in $GdAl_2$. Their investigations concluded a charge transfer (average) of 0.31 ± 0.03 e^- from Al Gd on the formation of compound. This result was in very good agreement with the SPR-KKR based calculations, which predicted charge transfer of 0.34 e^- from Al Gd in $GdAl_2$.

Using the magnetic Compton scattering (MCS), Mund et al. [11] have reported the effect of partial substitution of Gd and Dy at Fe site on the spin moment of $CoFe_2O_4$. The temperature dependent MCPs of $CoFe_{1.95}RE_{0.05}O_4$ (RE = Gd, Dy) were decomposed into the constituent profiles to determine their contribution in the total spin moment. The authors found that 5% doping of Dy and Gd at Fe site decrease the total spin moment of the $CoFe_2O_4$ from 3.72 ± 0.03 to 3.50 ± 0.03 $_B$/f.u. and 3.20 ± 0.03 $_B$/f.u., respectively. Further, it was found that this decrease in spin moment corresponds to the decrease in the spin moment at Co site. The authors have attributed this fall to migration of Co^{2+} ions from octahedral site to tetrahedral site on doping of REs in the $CoFe_2O_4$. The authors have also performed the X-ray photoemission spectroscopy (XPS) measurements to determine the occupancy ratio of Co^{2+} ions at octahedral and tetrahedral site. The XPS results were found to be in accordance with the MCP results. In addition, charge and magnetic Compton profile data on $LaFe_{1-x}Ni_xO_3$ (x = 0.4, 0.5) [12] and FeS_2 [13] along with feasibility of MCS in measurement of small spin moments will also be discussed.

Acknowledgements

The Author thanks DST, DRDO, UGC, CSIR, New Delhi, IUC-DAE-CSR, Indore and DAE-BRNS, Mumbai for financial support in form of different research projects.

References

[1] M. J. Cooper, P. E. Mijnarends, N. Shiotani, N. Sakai, A. Bansil, X-ray Compton Scattering, Oxford Univ. Press, Oxford (2004).

[2] B. L. Ahuja (Ed.), Recent Trends in Radiation Physics Research, Himanshu Publications, New Delhi (2010).

[3] B. L. Ahuja, M. Sharma, S. Mathur, Nucl. Instrum. Meth. B 244 (2006) 419: Also B. L. Ahuja, R. Joshi, J. Sahariya, J. Exp. Nanoscience iFirst (2013) In press.

[4] B. L. Ahuja, V. Sharma, A. Rathor, A. R. Jani, B. K. Sharma, Nucl. Instrum. Meth. B 262 (2007) 391: Also V. Raykar, J. Sahariya, B. L. Ahuja, Rad. Phys. Chem. 87 (2013) 35.

[5] F. Biggs, L. B. Mandelsohn, J. B. Mann., Atomic Data Nucl. Data Tables 16 (1975) 201.

[6] Y. Kakutani, Y. Kubo, A. Koizumi, N. Sakai, B. L. Ahuja, B. K. Sharma, J. Phys. Soc. Jpn. 72 (2003) 599.

[7] R. Dovesi, R. Orlando, B. Civalleri, C. Roetti, V. R. Saunders, C. M. Zicovich-Wilson, Z. Kristallogr. 220 (2005) 571.

[8] H. Ebert, D. Kodderitzsch, J. Minar, Rep. Prog. Phys. 74 (2011) 096501.

[9] B. L. Ahuja, P. Jain, J. Sahariya, N. L. Heda, P. Soni, J. Phys. Chem. A. 117 (2013) 5685.

[10] J. Sahariya, H. S. Mund and B. L. Ahuja, J. Phys. Chem. Solids 72 (2011) 1515.

[11] H. S. Mund, J. Sahariya, R. J. Choudhary, D. M. Phase, A. Dashora, M. Itou, Y. Sakurai, B. L. Ahuja, Appl. Phys. Lett. 102 (2013) 232403.

[12] A. Dashora, J. Sahariya, R. J. Choudhary, D. M. Phase, M. Itou, Y. Sakurai, B. L. Ahuja, Appl. Phys. Lett. 102 (2013) 142403

[13] L. Vadkhiya, B. L. Ahuja, J. Alloys Comp. 509 (2011) 3042.



Prof. B.L. Ahuja *is diligently engaged in the field of Compton scattering, environmental physics, X-ray fluorescence, magnetism, engineering of materials for an array of applications (like solar cells, spintronics compounds) and band structure calculations. He was awarded the prestigious BOYSCAST fellowship (1992-93) by DST, New Delhi to work at University of Warwick, U.K. for development of instrumentation for synchrotron radiations. Prof. Ahuja has designed, fabricated and commissioned the first Indian 20 Ci ^{137}Cs Compton spectrometer and the first-ever lowest intensity 100 mCi ^{241}Am Compton spectrometer in M.L. Sukhadia University, Udaipur, Rajasthan. Prof. Ahuja has supervised 22 students for their Ph.D. degree and presently 9 students are working with him for the same. Prof. Ahuja has executed several R&D projects funded by DST, CSIR, UGC, AICTE, UGC-DAE-CSR, BRNS and DRDO, etc. He has also completed his tenure (three years as Head of Physics Department) and Coordinator of DST-FIST (level-2) programme. He has contrived working collaborations with 31 renowned institutes within India and abroad. He has published about 130 papers in very reputed international journals and about 140 publications in conference-proceedings, etc. Prof. Ahuja is also a reviewer of several topmost international journals and is associated with many scientific societies in different capacities. He also holds the distinctive position of Vice-president of Indian Society of Radiation Physics.*

Synchrotron Radiation based Analytical Techniques (XAS & XRF)

Shambhu Nath Jha

Atomic & Molecular Physics Division, Bhabha Atomic Research Centre, Trombay, Mumbai 400 085, India; E-mail: snjha@rrcat.gov.in

A brief description of the principles of X-ray absorption spectroscopy (XAS) and X-ray fluorescence (XRF) techniques is given in this article with emphasis on the advantages of using synchrotron radiation-based instrumentation / beamline. XAS technique is described in more detail to emphasize the strength of the technique as a local structural probe.

Introduction

Synchrotron radiation based analytical techniques such as XAS and XRF offer unique advantages over laboratory-source based techniques. With advent of modern synchrotron sources the field has been further revitalized and paved ways for new techniques such as microprobe XRF and XAS.

XRF spectroscopy

XRF spectroscopy is an analytical technique which involves the detection of emitted characteristic X-rays following excitation of the elements within the sample [1,2]. While electron, particle (protons or alpha particles), or X-ray beams can be employed as the exciting source for this analysis, the use of X-ray beams from a synchrotron source has been instrumental in the advancement of the technique in the area of microprobe XRF imaging and trace level compositional charcaterisation of any sample [3,4]. Synchrotron radiation induced X-ray emission spectroscopy, has become competitive with the earlier microprobe and nanoprobe techniques following the advancements in manipulating and detecting these X-rays. There are two important features that contribute to the superb elemental sensitivities of microprobe SR induced XRF: (i) the absence of the continuum (bremsstrahlung) background radiation that is a feature of spectra obtained from charged particle beams, and (ii) the increased X-ray flux on the sample associated with the use tunable of third generation synchrotron facilities [4]. Detection sensitivities have been reported in the ppb range, with values of 10^{-17}g – 10^{-14} g (depending on the particular element and matrix). Keeping in mind its demand, a microprobe XRF beamline [5] has been setup by RRCAT at Indus-2 synchrotron source facility for trace level compositional characterization of materials.

X-Ray Absorption Spectroscopy

XAS is an important tool for studying most elements of the periodic table and it has been extremely useful for studying transition metals and metalloids. It is specifically useful for studying metals that are otherwise spectroscopically silent; i.e., those that possess filled or empty d-shells and have no spectroscopic signature [6]. XAS is an extremely versatile and highly sensitive technique capable of providing information regarding particular element in many physical states and chemical environments, which find application in wide variety of fields such as bioinorganic chemistry, catalysis, environmental science, nano materials etc. [6].

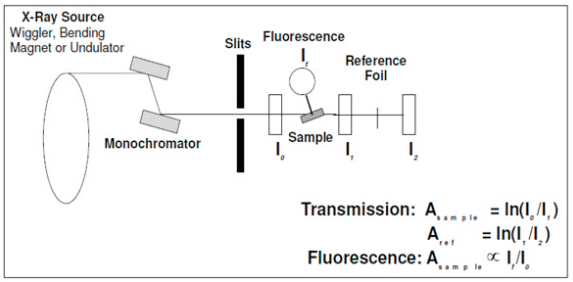


Fig. 1 Schematics of a scanning type EXAFS beamline

XAS, in contrast to XRF spectroscopy, cannot feasibly be performed using a laboratory X-ray source. Instead the highly intense and tunable X-rays generated at a synchrotron are essential for XAS.[7] There are two types of instrumental setups(known as beamline) which are generally employed for XAS measurements using synchrotron radiation: scanning type and dispersive type. At Indus-2 Synchrotron radiation source at RRCAT, Indore, both types of instrumental setups [8,9] have been developed for XAS measurements.

A typical instrumental setup (known as beamline) for XAS is shown in Fig. 1 where it is apparent that XAS data can be collected in two modes: fluorescence mode or transmission mode.

Normally the technique is performed in transmission mode; however, in the case of trace elemental speciation such as those associated with biological samples, doped semiconductor, etc. the technique is often performed in fluorescence mode since it imparts greater sensitivity [7].

In XAS, an X-ray absorption spectrum is generated by subjecting the sample to a tunable X-ray beam produced by a synchrotron source. The X-ray beam energy is swept across an energy range that encompasses the binding energy of the element of interest. When the X-rays have sufficient energy to eject a core electron to an orbital (that is partially filled or empty) or to the continuum, there is an abrupt increase in the absorption coefficient, which gives rise to the dominant feature of the XAS spectrum (Figure2)

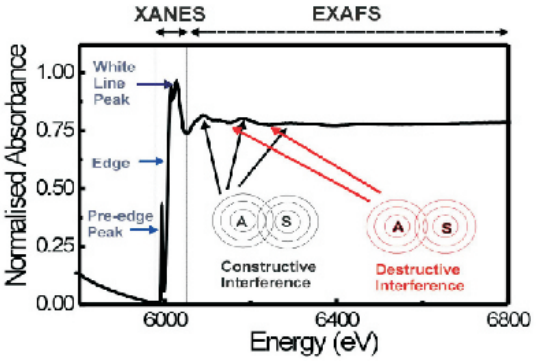


Fig. 2 XAS spectrum defining the XANES and EXAFS regions and showing typical spectral features

known as the "absorption edge" [6]. The XAS spectrum can be divided into two main regions: the X-ray absorption near edge structure (XANES) and extended X-ray absorption fine structure (EXAFS) regions, which contain extremely useful information regarding the local structural environment of the element of interest [6].

The XANES spectrum is typically defined as the region immediately within approximately 50 eV of the edge. Key features of the XANES spectrum include the aforementioned edge, and the white line peak which occurs directly after the edge. The XANES spectrum is sensitive to the oxidation state, the immediate coordinating atoms, and the electronic structure of the absorber atom [6]. It provides information regarding the average coordination environment of the absorber atom and can be used to provide qualitative information [6]. Typically, increases in the oxidation state are associated with increases in the energy associated with the absorption edge, since greater energy is required to eject the core electron [6]. Caution must be used when relying on the spectral edge position to interpret the oxidation state, however, since the coordinating atoms also influence the edge energy. For instance, while the oxidation state does not change, a slight decrease on the local charge of the absorber element brought about by coordination to a less electron withdrawing atom (e.g. S versus O) would result in a lower edge energy [6]. In addition, and complementary to this, the edge energy can be influenced by the metal-ligand bond distance, with the edge energy expected to vary inversely with the square of the metal-ligand distance [6]. Another factor that is observed in the XANES spectrum is that the features become broadened when the coordination environment becomes less symmetric, giving rise to a less intense white line [6]. A typical example of this is the more symmetrical crystalline small-molecule models compared with their protein- or peptide- bound analogues [6]. In some cases a pre-edge peak is also observed. Weak pre-edge peaks for the K edge first row transition metals are observed for the forbidden (dipole selection rules) 1s to 3d transition. They occur for metals that have an unfilled 3d shell and provide an indicator of coordination geometry. For instance, the centrosymmetric octahedral Cr(III) complex exhibits the weakest pre-edge feature, while the loss of centrosymmetry associated with trigonal bipyramidal and tetrahedral complexes is associated with an increase in the intensity of the pre-edge peak [9]. This phenomenon is due to the mixing of the 3d and 4p orbitals and direct quadrupolar coupling [6]. The EXAFS spectrum extends to higher energies and contains more subtle features (Fig. 2). It results from the interaction of the ejected electron with the surrounding atoms and is distinguished by a wavelike structure indicative of the constructive and destructive interference from which it is generated. There are many reviews [6,11,12] in literature regarding detailed information on the principles of EXAFS. Micro-XANES/EXAFS utilises focusing devices (KB mirrors or zone plates) that focus the beam to micron or submicron dimensions, enabling two dimensional elemental /oxidation states mapping.

My talk will cover basic principles of XAS & XRF techniques and will elucidate how the techniques can be used in variety of applications. Also instrumentation involved in setting up such facility around synchrotron radiation source will be discussed.

References

[1] R. Jenkins. X-Ray Fluorescence Spectrometry (J. D. Winefordner) 1999. (John Wiley and Sons: New York).

[2] K. L. Williams. An Introduction to X-Ray Spectrometry 1987 (Allen and Unwin:London)

[3] G. E. Ice, X-Ray Spectrom. 26 (1997) 315.

[4] http://www.lightsources.org

[5] http://www.rrcat.gov.in/technology/accel/srul/beamlines/xrf.html

[6] J. E. Penner-Hahn, Coord. Chem. Rev. 249 (2005) 161.; & INTRODUCTION TO XAFS, A Practical Guide to X-ray Absorption Fine Structure Spectroscopy by GRANT BUNKER, Cambridg Univ. Press.

[7] I. Ascone, W. Meyer-Klaucke, L. Murphy, J. Synch. Rad. 10 (2003) 16.

[8] D.Bhattacharyya, A.K.Poswal, S.N.Jha, Sangeeta and S.C.Sabharwal, Nuclear Instruments and Methods in Physics Research A, 609 (2009) 286.

[9] http://www.cat.gov.in/technology/accel/srul/beamlines/exafs.html

[10] C. Weeks, A. Levina, C. T. Dillon, P. Turner, R. R. Fenton, P. A. Lay, Inorg. Chem. 43 (2004) 7844 J.

[11] B. Aitken, A. Levina, P. A. Lay, Curr. Topics Med. Chem. 11 (2011) 553.

[12] A. Levina, R. S. Armstrong, P. A. Lay, Coord. Chem. Rev. 249 (2005) 14.



Dr. S.N. Jha *completed his M.Sc.(Chem) from Delhi Univ. in the year 1986. He joined Spectroscopy Division, BARC after graduating from 32nd Batch of Training School (1988-1989). He got Ph.D from Mumbai University in the year 1999 in the field of X-ray spectroscopy and instrumentation. Dr. Jha started his career as an analytical spectroscopist and later got involved with synchrotron beamline development project of the Division. Over the years he has contributed significantly towards the development of four beamlines, namely :(i) ARPES beamline at INDUS-1 SRS, (ii) HRVUV beamline at INDUS-1 SRS, (iii) Dispersive EXAFS beamline at INDUS-2 SRS and (iv) Energy scanning EXAFS beamline at INDUS-2 SRS. Presently he is heading a section of Beamline Development and X-ray Application Section of Atomic and Molecular Physics Division, BARC. His current research interest is in the field XAFS and PES spectroscopy using synchrotron radiation source.*

Prediction on the Origin of Ancient Glass Beads by Studying its Potassium content by Compton Suppressed -ray Spectrometry

Kaushik Gangopadhyay[1], Moumita Maiti[2], Susanta Lahiri[3*]

1. *Dept. of Archaeology, University of Calcutta, 1 Reformatory Street, Kolkata 700028, India*
2. *Department of Physics, Indian Institute of Technology Roorkee, Roorkee-247667, India*
3. *Chemical Sciences Division, Saha Institute of Nuclear Physics, 1/AF Bidhannagar, Kolkata-700064, India; E-mail: susanta.lahiri@saha.ac.in*

For the first time, a simple non-destructive technique has been demonstrated to measure the potassium (K) content in the archeological sample like glass beads to trace their origin. K content has been measured in glass beads collected from two sites of Tamilnadu by Compton suppressed -ray spectrometry (CSS).

Introduction

Beads are one of the most important artifacts providing evidence for long distance trade. As portable artifacts they have been used in various types of exchange networks in which ancient societies participated. Beads are found in the South Asian region, from the time of the Indus valley civilization to the late medieval period. Glass beads are made in a variety of methods including winding, dipping, drawing, mould-pressing, cutting and grinding and a combination of all these [1]. The glass beads may be monochrome or of polychrome. Monochrome glass beads are classified as Indo-pacific' glass beads. We will primarily deal with the 'Indo-Pacific' beads from the Bay of Bengal region from where the present samples have been collected. Before 10th and 12th centuries in Northern Europe glass was made using alkali raw materials which were soda-rich, derived either from evaporate deposits or salt-loving plants. The shift to potash rich glasses in the middle ages was considered significant. The composition of glass beads is an important way to know the diffusion routes and transfer of technology.

Chemical analysis shows that translucent dark blue glass beads have elevated amount of manganese in a potassium glass. The analysis presented by Francis [1] shows that certain glass beads from Arikamedu has a high content of potassium. Francis noted that glass beads with colours such as dark blue, purple, violet, black and iron black have potassium as their chief alkali. Glass with high potassium content is virtually non-existent in the West and therefore, the source of the potash rich glasses in antiquity could be India or the South-East Asia.

Therefore, before simple screening of the glass beads from the region for potassium could be a useful exercise, since it has been hypothesized that potassium rich glasses were produced in South India and then traded to South East Asia.

There are numerous methods for K determination including neutron activation analysis (NAA), atomic absorption spectrometry (AAS), inductively coupled plasma optical emission spectroscopy (ICPOES), and mass spectrometry (ICPMS), etc [2-4]. However, the above methods require exhaustive sample treatment or digestion, which are not preferred for precious archaeological samples, especially in the primary screening mode. In this paper, we have demonstrated a new analytical technique to measure the potassium content of the glass bead. The analytical technique is non-destructive in nature, therefore preserving the samples after analysis.

Although numerous literatures are available on the determination of stable potassium as well as determination of ^{40}K by -ray spectrometry [4,5], rarely these two have been combined. The percentage abundance of ^{40}K is fixed in nature; therefore measurement of ^{40}K would give an estimation of total potassium in the sample. This simple relationship has rarely been exploited to measure the potassium content in the sample. One of the reasons is that the presence of ^{40}K in our environment causes huge background of ^{40}K over its content in samples in common gamma detectors (HPGe or NaI(Tl)).

Recently we have demonstrated that the use of Compton suppressor system in combination with huge background shielding would decrease the background of ^{40}K in three to four orders of magnitude. As a result, it has been possible to measure the amount of ^{40}K and eventually the total amount of K in the sample [6]. This non-destructive method has been applied to evaluate the potassium content of the beads collected from different regions.

Experimental

Collection of Sample

Samples were collected from the archaeological sites of Manikorlai and Arikamedu. Both the sites are manufacturing sites of glass beads from the early historic to the medieval period as indicated by the large number of waste materials on the surface.

Measurement

A reverse electrode high purity Ge (HPGe) detector, with a resolution of 2.1 keV at 1.33 MeV, was used as central detector for the Compton Suppressor

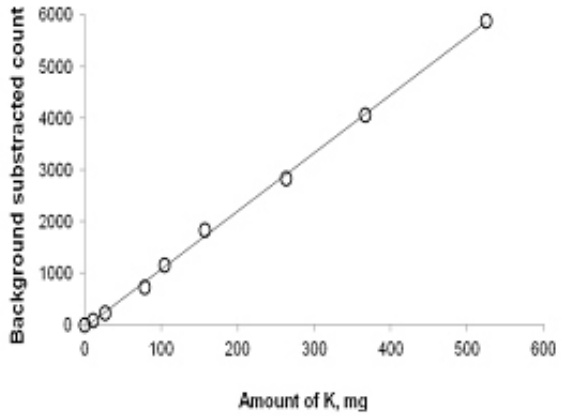


Fig. 1 Calibration showing amount of K vs area count of 1460 keV peak of ^{40}K

System (CSS). The annulus detector system had 9 9 NaI(Tl) crystal with four photomultiplier tubes. A 3 3 NaI(Tl) plug detector was used as cap of the upper section of the annulus. Samples were placed at 1 cm distance from the top of HPGe detector surrounded by the annulus and plug detectors. The entire assembly was shielded by 10 cm thick low background lead as bulk shield with graded lining of 1 mm tin and 1.6 mm copper. The coincidence output was taken to NIM based MCA Multiport II. All the detectors, electronics and Genie 2000 software were procured from CANBERRA. The energy calibration of the CSS system was done with ^{137}Cs, ^{60}Co and ^{133}Ba sources.

The calibration curve (Fig. 1) was drawn by taking the background subtracted area count of 1460.82 keV photo-peak of ^{40}K against the amount of potassium present in each KCl sample. Counts of different amounts of KCl were taken with a preset time of 10^5 s in the CSS. All the KCl samples and beads were taken in a plastic petridis to avoid ^{40}K count from a glass container.

Results and Discussion

The calibration curve describing the total amount of K in KCl vs net ^{40}K peak area shows excellent linearity between 10-600 mg of K (Fig. 1). We have analyzed eight different samples from Tamilnadu. K contents of these samples have been listed in Table 1. All the samples except two showed K content less than 3%. The two samples, one from Arikamedu and another from Manikorlai region showed elevated potassium content ~22% and 15% respectively. The elevated potassium content clearly shows that these glass beads are from different origin and must be subject to further study.

Conclusion

The developed method for determination of potassium in bead samples requires no chemical treatment. The method is therefore a truly non-destructive procedure. This is the first report on the measurement of K content in glass beads, the archaeological samples, by non-destructive method. This paper also reports for the first time an attempt to discriminate glass beads according to their K content and therefore reporting the origin of the glass beads.

Table-1: Measured K content in various glass beads

Sites in Tamilnadu	Object	Weight (g)	Color	K (%)
Manikorlai	Drawn glass bead	2.77	Greenish Grey	1.58
Arikamedu	Drawn glass bead	0.44	Red	22.35
Manikorlai	Drawn glass bead (probably debitegs)	0.94	Red	1.80
Manikorlai	Glass frit	14.81	Black	1.43
Manikorlai	Glass frit	2.66	Blue	14.87
Manikorlai	Drawn glass bead	0.18	Red	3.27
Manikorlai	Drawn glass bead	0.64	Green	0.26
Manikorlai	Drawn glass rod	0.58	Red	1.26

Acknowledgment

This work has been carried out as part of the Saha Institute of Nuclear Physics-Department of Atomic Energy, 12th five year plan project "Trace, Ultratrace Analysis and Isotope Production (TULIP)".

References

[1] Francis, Peter. Asia's Maritime Bead Trade, 300 BC to the Present. Hawai: University of Hawai (2002).

[2] M.A. Shafaei, E. Saion, K. Wood, K. Naghavi, K. Rezaee, J. Radioanal. Nucl. Ch. 288 (2011) 599.

[3] S.M.U. Ali, M.H. Asif, A. Fulati, O. Nur, M. Willander, C. Brannmark, P. Stralfors, U.H. Englund, F. Elinder, B. Danielsson, IEEE T Nanotechnol. 10 (2011) 913.

[4] H. Al-Sulaiti, P.H. Regan, D.A. Bradley, D. Malain, T. Santawamaitre, A. Habib, M. Matthews, S. Bukhari, M. Al-Dosari, Nucl. Instrum. Meth. A 619 (2010) 427.

[5] G. Wallova, K.K. Acharya, G. Walner, J. Radioanal. Nucl. Chem. 283 (2010) 713.

[6] M. Maiti, A. Mandal, S. Lahiri, Appl. Radiat. Isotopes 71 (2013) 37.



***Prof. Susanta Lahiri**, Ph.D, D.Sc is Senior Professor, Saha Institute of Nuclear Physics, Kolkata. He is a Professor of Homi Bhabha National Institute (HBNI), and visiting scientists, CERN. He is specialist in the field of nuclear chemistry, specially isotope production and separation by charged particle activation, radiotracer technique, green chemistry and trace analysis. He is distinguished board member of Journal of Radioanalytical and Nuclear Chemistry. His recent interest includes chemistry of converter targets and the radionuclides produced in converter targets bombarded by GeV range projectiles. He is member of the superheavy element chemistry group at GSI, Germany and also one of the founder members of ECHo collaboration which is dedicated to neutrino mass measurement. He has to his credit about 400 publications out of which 175 are published in reputed international journals.*

Application of Analytical Nuclear Techniques to the Heaviest Elements

Y. Nagame, A. Toyoshima, K. Tsukada, M. Asai, T. K. Sato, M. Schäel

Advanced Science Research Center, Japan Atomic Energy Agency, Tokai, Ibaraki 319-1195, Japan; E-mail: nagame.yuichiro@jaea.go.jp

Chemical studies of the heaviest elements based on an atom-at-a-time scale conducted at JAEA (Japan Atomic Energy Agency) are introduced. Chemical characterization of element 104, rutherfordium (Rf), and element 105, dubnium (Db), in liquid-phases is presented and characteristic behavior of the heaviest elements is discussed in comparison with that of respective homologues in the Periodic Table. An electrochemical approach to the heaviest elements by a flow electrolytic column chromatographic method is also given: successful oxidation of element 102, nobelium (No), with single atoms. Prospects for the future studies on chemical properties of the heaviest elements at JAEA will be briefly considered.

Introduction

Chemical studies of the heaviest elements are extremely interesting and challenging subjects in modern inorganic and nuclear chemistry. A most important and fascinating aspect is to determine the chemical properties of newly-synthesized elements at the uppermost end of the periodic table. The heaviest elements above element 100, fermium (Fm), however, must be produced at accelerators in heavy-ion-induced nuclear reactions and are available as short-lived isotopes only in quantities of a few atoms at a time. In addition, each available atom should be chemically equilibrated rapidly within its life-time. Such restricted experimental conditions make it remarkably difficult to characterize chemical properties of the heaviest elements. Thus, rapid and very efficient analytical nuclear procedures including chemical separation and radiation detection must be devised.

Liquid-phase Chemistry

We have studied liquid chromatographic behavior of the transactinide elements Rf and Db with the rapid chemical separation apparatus AIDA (Automated Ion-exchange apparatus coupled with the Detection system for Alpha spectroscopy) that enables us to perform cyclic column chromatographic separations of short-lived nuclides in aqueous solution and automated detection of -particles within a typical cycle of 1-2 min. For the chromatographic separation, the micro-columns, such as 1.6 mm i.d. 7.0 mm long and 1.0 mm i.d. 3.5 mm long, are employed for the measurement of distribution coefficients (K_d) of the heaviest elements. Chemical reaction should reach equilibrium even in the micro-column experiment.

From the systematic investigation of ion-exchange chromatographic behavior of Rf, it has been found that the properties of Rf are quite similar to those of the group-4 homologues, Zr and Hf, in the formation of chloride, nitrate, and sulfate complexes, although there are some differences in complexation strength between Rf and the lighter homologues [1]. On the contrary, fluoride complex formation of Rf is significantly different from that of the homologues [2-4]. Anionic fluoride complexation of Db, has also been studied. The result clearly demonstrates that the fluoride complex formation of Db is considerably different from that of the group-5 homologue Ta, while the behavior of Db is similar to that of the lighter homologue Nb [5]. For the Db experiment, the newly developed rapid ion-exchange apparatus AIDA-II was introduced; the apparatus is based on continuous sample collection and evaporation of effluents, and successive -particle measurement.

Electrochemistry

Redox studies of the heaviest elements are expected to give valuable information on valence electronic states, such as oxidation states and redox potentials. Well established electrochemical approaches like cyclic voltammetry are, however, not available for the one atom-at-a-time chemistry of the heaviest elements. Thus, one has to investigate redox properties of the heaviest elements based on the partition behavior of single atoms between two phases instead of measurements of electric currents arising from redox reactions.

A new apparatus for the study of electrochemical properties of the heaviest elements has been developed by Toyoshima et al. [6]. The apparatus is based on a flow electrolytic cell combined with column chromatography. The working electrode is made of a bundle of glassy-carbon fibers that is packed in a porous Vycor glass tube (4.8 mm i.d., 7 mm o.d., and 30 mm long) which works as an electrolytic diaphragm. The surface of the carbon fibers was chemically modified with Nafion perfluorinated cation-exchange resin. A platinum-mesh counter electrode was placed in the electrolyte pool to surround the glass tube. The potential on the working electrode was controlled using a potentiostat referring to the 1.0 M LiCl-Ag/AgCl electrode placed in the pool. The apparatus was applied to the oxidation of No^{2+} by controlling the applied potential. We successfully conducted the oxidation of single No^{2+} ions to the trivalent state No^{3+} in á-hydroxyisobutylic acid (á-HiB) solution [7].

In our future program, a reduction experiment of element 106, seaborgium (Sg) will be conducted using the complex system, electrochemistry and rapid extraction, coupled with a recoil separator which serves as a selective pre-separator of the heaviest nuclide. Prospects on this program will be briefly discussed.

References

[1] H. Haba et al., J. Nucl. Radiochem. Sci. 3 (2002) 143.
[2] H. Haba et al., J. Am. Chem. Soc. 126 (2004) 5219.
[3] A. Toyoshima et al., Radiochim. Acta 96 (2008) 125
[4] Y. Ishii et al., Bull. Chem. Soc. Ipan 82 (2011) 903.
[5] Y. Kasamatsu et al., Chem. Lett. 38 (2009) 1084.
[6] A. Toyoshima et al., Radiochim. Acta 96 (2008) 323.
[7] A. Toyoshima et al., J Am Chem Soc 131 (2009) 9180.



Dr. Yuichiro Nagame *is currently Deputy Director General of Advanced Science Research Center (ASRC) in Japan Atomic Energy Agency (JAEA). He received a PhD degree in 1982 with a study of strongly damped collision mechanism in heavy-ion-induced nuclear reactions from Tokyo Metropolitan University. His research interests are chemical and nuclear properties of the heaviest elements, nuclear fission, heavy-ion-induced nuclear reactions, and so on. He is a member of Japan Society of Nuclear and Radiochemical Sciences (JNRS), Chemical Society of Japan, The Physical Society of Japan, and Atomic Energy Society of Japan. He served as a chairman of JNRS during 2010 - 2012. Dr. Nagame was an IUPAC associate member from 2000 to 2001, and is a member/fellow of IUPAC since 2002.*

Production of ^{261}Rf, ^{262}Db, and ^{265}Sg for Chemical Studies using the Gas-jet Transport System Coupled to GARIS

H. Haba

Nishina Center for Accelerator-Based Science, RIKEN, Wako, Saitama 351-0198, Japan; E-mail: haba@riken.jp

The radioisotopes of ^{261}Rf, ^{262}Db, and ^{265}Sg were produced in the reactions of ^{248}Cm(^{18}O,5n)^{261}Rf, ^{248}Cm(^{19}F,5n)^{262}Db, and ^{248}Cm(^{22}Ne,5n)^{265}Sg, respectively, using a gas-jet transport system coupled to the RIKEN gas-filled recoil ion separator, GARIS. Production and decay properties of those nuclides were investigated in detail with a rotating wheel apparatus for and spontaneous fission spectrometry under low background conditions.

Introduction

Recently, chemical characterization of superheavy elements (SHEs) with atomic numbers Z 104 is an extremely interesting and challenging research subject in modern nuclear and radiochemistry [1,2]. A most important and interesting question is to clarify chemical properties and electronic structures of those new elements and to elucidate the influence of relativistic effects on chemical properties of the heaviest elements. In RIKEN, we have been developing a gas-jet transport system coupled to the RIKEN gas-filled recoil ion separator GARIS as a novel technique for the next-generation SHE chemistry [3]. With this method, breakthroughs in SHE chemistry are expected: (i) the background radioactivities originating from unwanted by-products are strongly suppressed, (ii) the intense primary heavy-ion beam is absent in a gas-jet chamber and hence high gas-jet yield is achieved, and (iii) the beam-free conditions also make it possible to investigate new chemical reactions. In this work, we investigated production and decay properties of radioisotopes of ^{261}Rf (Z = 104), ^{262}Db (Z = 105), and ^{265}Sg (Z = 106) available for chemical studies using the GARIS gas-jet system.

Experiment

A schematic of the experimental setup is shown in Fig. 1. Oxygen-18, ^{19}F, and ^{22}Ne beams were extracted from the RIKEN Linear Accelerator, RILAC. The isotopes of ^{261}Rf^{a,b}, ^{262}Db, and ^{265}Sg^{a,b} were produced in the reactions of ^{248}Cm(^{18}O,5n)^{261}Rf, ^{248}Cm(^{19}F,5n)^{262}Db, and ^{248}Cm(^{22}Ne,5n)^{265}Sg, respectively. The evaporation residues of interest were separated in flight from the beam particles and the majority of the nuclear transfer products by GARIS and were guided to a gas-jet chamber at the focal plane of GARIS. The evaporation residues were thermalized in He gas, attached to KCl aerosol particles, and were transported through a Teflon capillary to a chemistry laboratory. Alpha and spontaneous fission (SF) decays of ^{261}Rf^{a,b}, ^{262}Db, and ^{265}Sg^{a,b} were investigated with the rotating wheel apparatus MANON (Measurement system for Alpha-particle and spontaneous fissioN events ON line) under low background conditions.

Results and Discussion

The 1.9-s isomeric state (^{261}Rfb) in ^{261}Rf was directly populated in the ^{248}Cm(^{18}O,5n)^{261}Rf^{b} reaction for the first time [7]. The identification of ^{261}Rf^{b} was based on six - correlations linking decays of ^{261}Rf^{b} and its daughter ^{257}No. The -particle energy of ^{261}Rf^{b} was measured to be E = 8.52 ± 0.05 MeV. The half-life was determined to be $T_{1/2}$ = 1.9 ± 0.4 s based on both 8.52-MeV and SF decay events. The SF branch is b_{SF} = 0.73 ± 0.06. The cross section for the ^{248}Cm(^{18}O,5n)^{261}Rf^{b} reaction is (^{261}Rf^{b}) = 11 ± 2 nb at 95.1 MeV, which gives a cross section ratio of (^{261}Rf^{a})/ (^{261}Rf^{b}) = 1.1 ± 0.2.

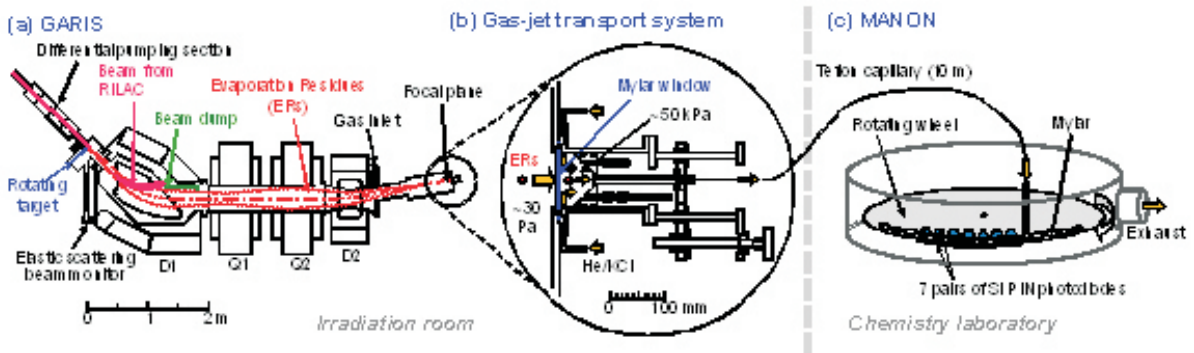


Fig. 1 (a) RIKEN gas-filled recoil ion separator, GARIS, (b) the gas-jet transport system coupled to the focal plane of GARIS, and (c) the rotating wheel apparatus MANON for /SF-spectrometry

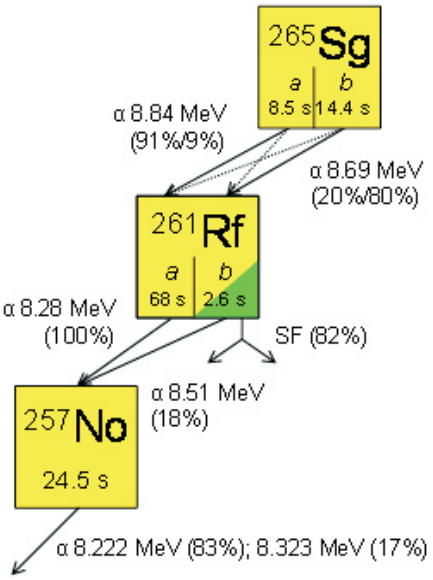


Fig. 2 Decay pattern for the chain $^{265}Sg^{a,b}$ $^{261}Rf^{a,b}$ ^{257}No [8]. The dominant and weak transitions are shown by solid and dashed arrows, respectively, and their intensities are given in parentheses

In the ^{265}Sg experiment [8], eighteen and twenty four decay chains were assigned to ^{265}Sga and ^{265}Sgb, respectively, based on - (-) and -SF correlations. The half-life and -particle energy of $^{265}Sg^{a}$ were measured to be $T_{1/2} = 8.5^{+2.6}_{-1.6}$ s and E = 8.84 ± 0.05 MeV, respectively, and those of $^{265}Sg^{b}$ were $T_{1/2} = 14.4^{+3.7}_{-2.5}$ s and E = 8.69 ± 0.05 MeV. As a daughter product of $^{265}Sg^{a,b}$, the decay properties of $^{261}Rf^{b}$ were derived: $T_{1/2} = 2.6^{+0.7}_{-0.5}$ s, E = 8.51 ± 0.06 MeV, and bSF = 0.82 ± 0.09. These results confirm and refine the complicated decay pattern suggested for the decay chain $^{265}Sg^{a,b}$ $^{261}Rf^{a,b}$ ^{257}No in [9] (see Fig. 2). The production cross sections for $^{265}Sg^{a}$ and $^{265}Sg^{b}$ were determined to be $(^{265}Sg^{a}) = 180^{+80}_{-60}$ pb and $(^{265}Sg^{b}) = 200^{+60}_{-50}$ pb at 117.8 MeV. The total cross section of $(^{265}Sg^{a} + {}^{265}Sg^{b}) = 380^{+90}_{-70}$ pb agrees well with the prediction by the statistical model code HIVAP [10] which takes a prolate deformation of the target nucleus into account to calculate the cross sections in the entrance channel [11,12].

Very recently, decay properties of ^{262}Db and its -decay daughter ^{258}Lr were investigated [13,14]. Based on - and -SF correlations, a total of seventy six chains were assigned to ^{262}Db and ^{258}Lr. The half-lives of ^{262}Db and 258Lr were measured to be $T_{1/2} = 33.8^{+4.4}_{-3.5}$ s and $3.54^{+0.46}_{-0.36}$ s, respectively, and they confirmed the literature data [15]. The -particle energy and intensity of ^{262}Db were revised to E = 8.46 ± 0.04 MeV (I = 70 ± 6%) and E = 8.68 ± 0.04 MeV (I = 30 ± 6%). The SF branch of ^{262}Db was $b_{SF} = 0.52 \pm 0.04$. From an observation of two SF decays which correlated to the decay of ^{262}Db, an electron capture (EC) decay was suggested in ^{258}Lr with bEC = 0.026 ± 0.018. Based on those new decay data of ^{262}Db and ^{258}Lr, the cross section for the ^{248}Cm(^{19}F,5n)^{262}Db reaction in [16,17] was revised to $(^{262}Db) = 2.2 \pm 0.7$ nb at 103 MeV. This new cross section shows a good agreement with a systematic feature of the maximal cross sections of the 5n evaporation channel in the complete fusion reactions of ^{248}Cm target with different projectiles as a function of the compound nucleus atomic number [8].

In the conference, present status and perspectives of the SHE chemistry opened by the GARIS gas-jet system will be also presented.

References

[1] M. Sch el, Angew. Chem. Int. Ed. 45 (2006) 368.

[2] A. T ler and V. Pershina, Chem. Rev. 113 (2013) 1237.

[3] H. Haba et al., J. Nucl. Radiochem. Sci. 8 (2007) 55.

[4] H. Haba et al., Eur. Phys. J. D 45 (2007) 81.

[5] H. Haba et al., J. Nucl. Radiochem. Sci. 9 (2008) 27.

[6] H. Haba et al., Chem. Lett. 38 (2009) 426.

[7] H. Haba et al., Phys. Rev. C 83 (2011) 034602.

[8] H. Haba et al., Phys. Rev. C 85 (2012) 024611.

[9] Ch. E. D lmann and A. T ler, Phys. Rev. C 77 (2008) 064320.

[10] W. Reisdorf and M. Sch el, Z. Phys. A 343 (1992) 47.

[11] K. Nishioet al., Phys. Rev. Lett. 93 (2004) 162701.

[12] K. Nishio et al., Phys. Rev. C 82 (2010) 024611.

[13] H. Haba et al., EuCheMS International Conference on Nuclear and Radiochemistry (NRC8), Sept. 18 (2012), Como, Italy.

[14] H. Haba et al. (to be submitted).

[15] R. B. Firestone and V. S. Shirley, Table of Isotopes, 8th ed., John Wiley & Sons, New York (1996).

[16] Y. Nagame et al., J. Nucl. Radiochem. Sci. 3 (2002) 85.

[17] K. Tsukada et al., Radiochim. Acta 97 (2009) 83.



***Dr. H. Haba** earned his PhD from Kanazawa University, Kanazawa, Japan, in 1999. He worked at Japan Atomic Energy Research Institute (1999–2001) as a postdoc and RIKEN as a postdoc (2002–2004), as a research scientist (2004–2006), and as a senior research scientist (2007–2010). Since 2011, he has led RI Applications Team of Nishina Center for Accelerator-Based Science, RIKEN. His research interests focus on superheavy element chemistry and radioisotope production at the RIKEN RI Beam Factory. He has about 120 publications in reputed international journals and books. He received Young Scientist Award from The Japan Society of Nuclear and Radiochemical Sciences in 2001. He has been a Visiting Associate Professor of Niigata University, Niigata, Japan (2013–present).*

Nuclear Analytical Techniques in the LMFBR programme

C.R. Venkata Subramani

Nuclear and Radioanalytical Chemistry Section, Fuel Chemistry Division, Indira Gandhi Centre for Atomic Research, Kalpakkam 603102, India; E-mail: venkat@igcar.gov.in

This talk describes the use of nuclear analytical techniques to solve various problems in the LMFBR programme at IGCAR as well as at other units at Kalpakkam. The methodology used as well as the results have been discussed in brief.

Introduction

The Radiochemistry Programme was established in the late seventies at IGCAR with a mandate to provide analytical services to the LMFBR programme as well as to other units at Kalpakkam. The preliminary requirements were mainly analytical as many of the laboratories of the centre were under development. With the commissioning and operation of the fast reactor and subsequently of the reprocessing programme, the requirements of nuclear analytical chemistry have gradually increased. This talk details some of the work carried out.

Routine Analytical Services

As per the technical specifications of FBTR, analysis of primary sodium has to be carried out after every shutdown. The sodium is sampled using a bucket sampler and analysed for gamma emitting radionuclides by high resolution gamma spectrometry. The initial results revealed only activation of impurities (^{110m}Ag, ^{124}Sb, ^{203}Hg) in sodium but in recent times traces of activated structural material (^{54}Mn, ^{60}Co) are also being observed. The primary sodium is also assayed annually for plutonium and tritium. The minimum detectable limits for plutonium is about 1 pg Pu/g Na but so far we have not been able to detect any plutonium. Other samples received from the reactor include biological shield cooling water, secondary sodium, etc.

Analytical services are also extended to the Reprocessing Programme as and when requested. The samples include dissolver solution, scrub tanks, high level waste, etc. All samples are assayed mainly by high resolution gamma spectrometry with alpha counting and spectrometry used as and when required.

A number of systems have also been developed for the routine assay of waste packets and drums for fissile material and other gamma emitters (using both gamma and neutron methods), scanning of fuel pins, assay of actinide mixtures using K-edge densitometry, etc.

Non-routine Samples

In addition to the samples described above, a number of samples have been received for various reasons. Some of these samples are discussed in more detail below.

Radioactive Dating of MAPS2 Diffuser Sample

One of the problems encountered in both units of the Madras Atomic Power Station has been the shattering of the diffuser in the moderator circuit and these pieces leaving the calandria vessel and accumulating in the tray positioned just before the moderator pump.

One such piece was received in August 1992 with a request to determine the time of failure. It was informed to the MAPS authorities that it would not be possible to determine the time of failure but upper and lower dates for the failure could be obtained by determining the expected activity of ^{125}Sb formed due to the activation of the tin in zircaloy as a function of time by computation and comparing with the experimentally determined values. Based on this method, it was determined that the earliest possible date of exit of the sample piece from the core of MAPS2 was December 1988 and the latest possible date was July 1990.

Source of Fission Gases in KAMINI water

The Kalpakkam Mini Reactor (KAMINI) is a tank type reactor using ^{233}U-Al alloy fuel encased in Al plates. De-Mineralised water is used as coolant, moderator and biological shield. The reactor commenced operation in the late nineties and it was observed that fission gases were present in the reactor water. The fission source could be due to fuel (^{233}U), fixed contamination on the clad (^{233}U/^{239}Pu – as the fuel had been fabricated in glove boxes which had been used for fabrication of FBTR fuel) or natural uranium impurity in the zircaloy used to cover the reflector (^{235}U). The ratio of the activity of different fission gases is a function of the fissioning system and this was exploited to arrive at a conclusion. The reactor operation history was used to obtain the activity of fission products of interest using the in-house developed code, CHANDY. The experimentally obtained ratios were then compared with the computed ratios. It was seen that the source of fission gases was ^{233}U.

Age of Failed Fuel in FBTR

FBTR is a loop type LMFBR and has a delayed neutron detection (DND) system on each loop. This would help in determining if the subassembly containing the failed fuel element is on the East side or the West side. In addition, we have installed a cover gas

sampling system that is capable of determining the age of the failed fuel. This is obtained by experimentally determining the activity ratio ($^{87}Kr/^{85}Kr$ or $^{88}Kr/^{85}Kr$) and relating this value to the burn up seen by the fuel element.

The cover gas in FBTR is mainly helium with about 12% argon. During reactor operation, the argon would absorb a neutron to give $^{41}Ar(t_{½}$ 109.3 m) while the tramp fuel would undergo fission to release traces of the fission gases. At the time of fuel failure, the accumulated fission gases in the plenum would be released instantaneously resulting in high activity of fission gases in the cover gas and the fission gas monitor would give an alarm. An activated charcoal adsorber column was introduced in the cover gas sampling set up and the cover gas passed flushed through this on receipt of alarm from the fission gases monitoring system. The activated charcoal has different adsorbing capabilities for the inert gases with xenon held longest and argon held least. Using this unit, it was possible to remove the 41Ar from the sample and separate the krypton and xenon isotopes. The separated krypton isotopes were collected in a sample vessel containing activated charcoal at cryogenic temperatures. This vessel was removed to the counting system after collection and monitored continuously to obtain the activities of all the krypton isotopes. Sufficient time (1 day) was allowed to ensure that all the short lived krypton isotopes decayed and it was possible to measure the signal due to 85Kr without large errors. The ratios obtained experimentally were compared with the theoretical data to obtain the burn up (age) of the fuel element .

On 3rd February, 2010 the reactor was operating at 18 MWt and delivering 3 MWe to the grid. At 0505 h, the reactor underwent scram on West DND. The reactor vault was immediately isolated. Using the above described system, a sample of the krypton isotopes was obtained and subject to high resolution gamma spectrometry. The age of the failed fuel was determined by using the activity ratio, $^{87}Kr/^{85}Kr$ or $^{88}Kr/^{85}Kr$. It was seen that the age of the fuel element as given by this ratio was well above 100 GWd/t. Based on the core configuration at the time of fuel failure, it was seen that there were only four subassemblies with burnups above 100. As the West /East ratio was high, the fuel subassembly near the core centre could not be the suspect subassembly. Among the other three, it was possible to identify the suspect subassembly in a single fuel handling operation.



Fig. 1 Expanded view of failure zone

The primary sodium was also analysed by high resolution gamma spectrometry to ensure that the ^{131}I activity was within limits. This measurement also yielded the activity ratio, 135Cs/137Cs. This ratio is also directly related to the age of the failed fuel and since the release of caesium would take place from the failure zone, it is indicative of the position of failure in the fuel pin. This activity ratio indicated that the age of the failed fuel was about 112 GWd/t indicating the failure should have taken place at one of the extremities of the fuel column as this burn up was well below the average burn up of the subassembly (148 GWd/t). It can be seen from Fig. 1 that the area of failure is near the top of the fuel column as predicted.

Cover Gas Purification System for PFBR

The Prototype Fast Breeder Reactor (PFBR) is a 500 MWe pool type LMFBR nearing completion at Kalpakkam. It is permitted to operate with upto four failed fuel pins in the core as gas leakers. However, as dictated by ALARA, it was decided to set up a cover gas purification system to remove the fission gases from the cover gas to ensure that gaseous releases are kept to a minimum. It was decided to use cryogenic cooled adsorber beds of activated charcoal for this purpose. Preliminary experiments to determine the dynamic adsorption coefficient (DAC) for indigenous activated charcoal were carried out using fission gases from MAPS1 reactor. Based on this data, a pilot plant was set up to generate experience in handling of cryogenic systems and to obtain realistic values of DAC at cryogenic temperatures. Based on the pilot plant, the CGPS for PFBR has been designed.

Conclusions

Some typical applications of the use of nuclear analytical techniques to solve problems encountered in the LMFBR fuel cycle have been described.



Shri C.R. Venkata Subramani, *M.Sc, is currently heading the Nuclear and Radioanalytical Chemistry Section of the Fuel Chemistry Division, Chemistry Group at IGCAR, Kalpakkam. He is a specialist in the field of non-destructive assay and on-line monitoring, radio-analytical chemistry and neutron activation analysis. His main interest is in the application of nuclear techniques in reactors and reprocessing plants. He has led the team the designed and operated the pilot plant for LMFBR cover gas purification by adsorption at cryogenic temperatures using activated charcoal which has been installed in PFBR. He has also been responsible for the installation of equipment in FBTR for determining the age of failed fuel. His current interests include development and standardization of procedures for the production of radioisotopes in Fast Reactors and installation of a fast flux facility at FBTR. He was on deputation on Indo-German collaboration and worked at the Nuclear Research Centre, Karlsruhe for one and half years.*

Studies of Nutritionally and Toxicologically Important Elements in Foods and Diets by Neutron Activation

A. Chatt

Trace Analysis Research Centre, Department of Chemistry, Dalhousie University, 6274 Coburg Road, Room 212, PO BOX 15000, Halifax, NS, B3H 4R2, Canada; E-mail: a.chatt@dal.ca

Several neutron activation analysis (NAA) methods in conjunction with conventional and anticoincidence counting have been developed in our laboratory over the years for the quantitative determination of up to 24 elements in foods and diets. Additionally, these methods have been applied to measure bioaccessible, ionic, proteomic, lipidic, and organometallic species of many elements. The overall expanded uncertainties of the methods have also been evaluated.

Introduction

Food has long been known to play a key role not only in the health status of humans but also in their social lives. Relationships between food and physical as well as spiritual well beings have been cited in ancient Indian, Chinese, and Greek literature. Preventive medicine promotes healthy eating and nutritional aspect of food. From the nutritional point of view, the interest is mainly focused on the adequacy of the daily intake of all essential elements through diet by the population at large. Toxicologists, on the other hand, are concerned about the levels of various heavy metals in food. The present knowledge about the dietary requirements for elements is rather poor as evident from the fact that in Canada Recommended Dietary Allowance (RDA) and Adequate Intake (AI) levels have so far been given for only 9 elements (namely Ca, Cu, Fe, I, Mg, Mo, P, Se, Zn), only AI values for 6 elements (namely Cl, Cr, F, K, Mn, Na), and only Tolerable Upper Intake Levels (UL) for B, Ni, and V for healthy persons [1]. The situation is worse for most toxic elements where sufficiently reliable data are not available for setting maximum permissible levels (MPL) to minimize health hazards. It is therefore necessary to monitor diets for as many elements as possible, may they be of nutritional or toxicological importance. One of the main reasons for the inadequacies mentioned above is the lack of appropriate analytical methods.

Diet is the single most important source of all elements for humans in a natural environment, i.e. excluding occupational, accidental or similar exposure to massive amounts of one or more elements. Dietary intake data commonly reported in the literature are largely based on dietary survey methods such as food balance sheets, food records or dietary recalls which rely on food composition table values. Although these techniques have certain advantages, they cannot provide accurate information on the average daily dietary intake (ADDI) of elements; this can only be reliably obtained by analyzing foods actually consumed by a person.

Perhaps equally important is the estimation of the fraction of the total intake that is available for meeting physiological requirements of the body. It is a complex subject to start with, which is made much more difficult by numerous variables that can influence the bioavailability of an element. In vitro enzymolysis of foods and diets offers an attractive alternative to human and animal studies for estimating the bioaccessible/absorbable/soluble fraction of an element. Species of the element is another important variable for assessing toxicity of an element. In the work reported here we have developed various methods for the determination of total, and bioaccessible as well as species-specific fractions of an element in foods and diets.

Methodology

We have developed a combination of instrumental (INAA), epithermal (EINAA), preconcentration (PNAA), and radiochemical (RNAA) neutron activation analysis (NAA) methods for the determination of up to 24 elements in duplicate diets and individual food items. A brief summary of the methods is given below. We have irradiated all samples at the Dalhousie University SLOWPOKE-2 Reactor facility either at a fission neutron flux of 2.5, 5, or 10 $x10^{11}$ cm^{-2} s^{-1} or an epithermal neutron flux of 0.5, 1 or 1.5 $x10^{11}$ cm^{-2} s^{-1}. We have counted the samples using either conventional or Compton suppression gamma-ray spectrometry systems.

The pseudo-cyclic INAA (PC-INAA) and cyclic INAA (CINAA) methods for rapid determinations of low levels of Se through the 17.4-s nuclide of ^{77m}Se consisted of 20-s irradiations, 10-s decays, and 20-s counting using the fast pneumatic transfer cyclic activation system for up to 4 cycles. We analyzed samples containing high levels of interfering elements such as Na, Cl, Al, Mn, etc. by pseudo-cyclic EINAA (PC-EINAA) and cyclic EINAA (CEINAA) and anti-coincidence counting (AC). The absolute detection limits were between 2 and 9 ng. We applied these methods for the routine determination of Se to the composites of 135 food samples with values ranging from as low as 1 g kg^{-1} for tea to 1045 g kg^{-1} for organ meats on fresh weight basis.

We developed an EINAA method for measuring low levels of I in food through the 442.9 keV gamma ray of ^{128}I by irradiating the samples in either a

permanently installed Cd-site or a boron nitride shield for up to 20 min. In order to further improve detection limits, precision, and accuracy we developed an EINAA-AC method. It improved the detection limit by a factor of 2 to 5 and a limit of 3-5 g kg^{-1} was achieved for low-salt foods. The RSD was about ±5% above 200, increasing to ±10% at 20, and then to greater than ±30% at about 5 g kg^{-1} iodine levels. We improved both precision and sensitivity by using a PC-EINAA-AC method for certain types of sample.

We developed an EINAA method for measuring As after 16 h irradiation in the Cd-site. We applied a combination of INAA and EINAA methods for determining the Al content of food by after making correction for P. However, the reliability of results was not that good because of the large correction factor required for the neutron energy spectrum of the reactor used.

We developed an INAA method consisting of irradiation for 10 min, decay for 1 min, and counting for 10 min for the determination of Br, Ca, Cl, K, Mg, Mn, Na and Sn through their medium-lived nuclides. We used 24-h irradiation, 2- or 14-d decay, and 1 or 3 h counting periods for detecting the longer lived nuclides of Co, Cr, Fe, Rb, Sb, Sc and Zn.

We developed a simple RNAA method for the determination of low levels of As, Au, Cu, Fe, Hg, Mo, Sb, Se and Zn in food. The method involved quantitative (>95%) coprecipitation of the above elements with Cu and Zn sulfides at two different pH values.

We developed a PNAA method consisting of coprecipitation of U and Th with calcium phosphate at an alkaline pH followed by irradiation in a boron shield for measuring U content. We then irradiated the precipitate for 12 h in the fission neutron flux, dissolved, and coprecipitated Pa with calcium oxalate. Recoveries were quantitative for both elements.

We evaluated the precision and accuracy of the INAA, INAA-AC, EINAA, EINAA-AC, CINAA, CINAA-AC, CEINAA, CEINAA-AC, PC-INAA, PC-INAA-AC, PC-EINAA, PC-EINAA-AC, PNAA and RNAA methods developed here by analyzing a number of food reference materials. The agreement between our and recommended values is generally good wherever such comparisons can be made. We have also calculated expanded uncertainties of measurement for several elements by the above methods.

It is well known that only a certain fraction of the total element in food is bioavailable. It has been mentioned in the introduction that in vitro enzymolysis can be used for estimating the bioaccessible / absorbable / soluble fraction of an element. We have used this technique for several individual food items as well as duplicate diets.

We have also developed several speciation analysis methods in combination with neutron activation for the separation and quantitative determination of ionic, proteomic, lipidic, and organometallic species of a given element. We have further developed simultaneous speciation NAA (SSNAA) for multielement species.

Conclusions

We have found various forms of NAA to be invaluable for the determination of many trace elements in foods and diets. The technique has unique quality assurance features which can be advantageously used in food studies [2].

References

[1] Health Canada, Dietary Reference Intakes, www.hc-sc.gc.ca/fn-an/nutrition/reference/index-eng.php

[2] R.R. Greenberg, P. Bode, E.A.N. Fernandes, Spectrochimica Acta B, 66 (2011) 193.



***Prof. A. Chatt**, MSc, PhD was Full Professor of Chemistry (1985-2008), Killam Professor of Chemistry (2001-06), Director of SLOWPOKE-2 Reactor facility (1987-2011), and is an Adjunct Professor of Chemistry (2008-) at Dalhousie University. His research fields include nuclear analytical and radiochemistry, gamma-ray spectroscopy, speciation, and nanoparticles. Prof Chatt has published 185 scientific papers in peer-reviewed international scientific journals and 1 book, and presented over 420 invited seminars. He is the Editor of the JRNC. His professional activities include IAEA, OECD/NEA, IDB, and TWAS expert services in numerous countries. He is the President (1995-) of the International Committee on Activation Analysis (ICAA). Prof Chatt is a Fellow of the American Nuclear Society (ANS) and the Chemical Institute of Canada. Hr has received many international awards including the ANS Radiation Science and Technology Award (1996), ANS William D. Ehmann Award (1999), Hevesy Medal Award (2001), and the Ioannes Marcus Marci Medal (2006).*

Emerging Applications of Radioisotopes in Nuclear Medicine

Sandip Basu

Radiation Medicine Centre, Bhabha Atomic Research Centre, Tata Memorial Centre Annexe, Parel, Mumbai 400012, India; E-mail: drsanb@yahoo.com

Introduction

Advances in the domain of radioisotopes and radiopharmaceuticals has been very noteworthy over the past decade and played a major role in enhancing the Nuclear Medicine practice. A number of them have been employed in the day to day clinical practice and have benefitted a large number of patients. For the purpose of systematic discussion, we shall classify into two major heads A. Recent advances in clinical applications of traditional radiotracers B. Newer Radiopharmaceuticals and their applications. The latter could be further subdivided in to the following: (a) Diagnostic (includes i. PET radiopharmaceuticals and ii. Non-PET radiopharmaceuticals for conventional gamma camera imaging) and (b) Therapeutic advances. In the present communication, we shall explore the major developments emphasizing the country perspective.

Lutetium Based Radiopharmaceuticals for Therapeutic Applications

Beyond doubt, ^{177}Lutetium has been the most significant development in the recent times. India has been at the forefront in this area owing to the contributions of radiopharmaceutical research at the BARC [1]. Two clinical areas that have emerged based upon this development:

[a] Peptide Receptor Radionuclide Therapy (PRRT) with ^{177}Lutetium based DOTATATE/DOTANOC targeting the somatostatin receptor positive malignancies. In clinical domain, this has been employed in metastatic neuroendocrine tumors (NET) of various subtypes (primarily gastroenteropancreatic NET) and in certain percentage of dedifferentiated thyroid carcinoma that expresses high somatostatin receptor positivity.

[b] ^{177}Lu-EDTMP: Employed in painful skeletal metastases (e.g. patients with breast cancer and hormone refractory prostate cancer with bone metastases).

Both these radiopharmaceuticals are available for routine patient service from BARC and BRIT.

Indigeneously Formulated ^{99m}Tc-HYNIC-TOC as a valuable substitute for ^{68}Ga-DOTANOC/ DOTATATE for the the pre-treatment evaluation for PRRT

Indigeneously formulated single vial lyophilized ^{99m}Tc-Hynic TOC kit has been an important development that has aided propagation of the PRRT programme across the country (Fig. 1). This would help centres that do not have PET facility or those who do not possess the germanium gallium generator [1].

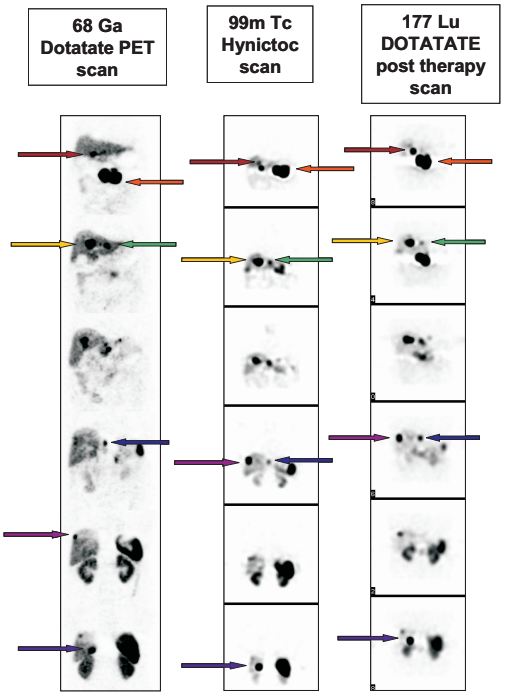


Fig. 1 Single vial lyophilized ^{99m}Tc-Hynic TOC kit

^{68}Ga-DOTANOC and ^{68}Ga-DOTATATE PET/CT

Employing Gallium-68-1,4, 7,10-tetraazacyclododecane-N,N',N'',N'''-tetraacetic acid (gallium-68-DOTA) compounds for positron emission tomography (PET) imaging has significantly improved the quality of imaging NET through improved resolution of PET and higher affinity of the new generation of peptides (DOTANOC and DOTATATE) to SSTR [2]. This has major implications in current and future clinical practice. Multiple Nuclear Medicine centres in India today possess the ^{68}Ge-^{68}Ga generators and use this for routine patient use. A tabulation of the promising PET tracers and their potential clinical applications have been made in Table 1

References

[1] Basu S, Kand P, Mallia M, Korde A, Shimpi H. Gratifying clinical experience with indigeneously formulated single vial lyophilized HYNIC-TOC kit at the Radiopharmaceutical Division of BARC: a pivotal boost for building up a Peptide Receptor Radionuclide Therapy Programme in an Indian setting. Eur J Nucl Med Mol Imaging 2013 Oct;40(10):1622-4. doi: 10.1007/s00259-013-2501-0. Epub 2013 Jul 16.

Table-1: Promising PET Tracers beyond FDG and their potential clinical applications

PET Radiopharmaceuticals beyond FDG	Potential Clinical Applications
^{18}F-Na fluoride (NaF)	Skeletal metastases
11C-Choline, ^{18}F-Choline	Prostate carcinoma
FMISO and FAZA	Hypoxia assessment in tumors
^{68}Ga- OTATOC/ DOTANOC/DOTATATE	Neuroendocrine tumor
^{18}F-Estradiol	Assessing estrogen receptors in tumors
^{18}F-FDOPA	Brain tumors, Movement disorders

[2] Naji M, AL-Nahhas A. Ga-labelled peptides in the management of neuroectodermal tumours. Eur J Nucl Med Mol Imaging. 2012 Feb;39 Suppl 1:S61-7.



Dr S. Basu *is Consultant Nuclear Medicine Physician and the Head, Nuclear Medicine Academic Programme of the Radiation Medicine Centre and actively involved in research and the postgraduate training activities of the center in addition to the routine patient services. He has more than 250 publications in peer-reviewed journals of repute and has authored multiple textbook chapters as well. He serves as the Editorial Board member of the European Journal of Nuclear Medicine and Molecular Imaging, the Nuclear Medicine Communications, Current Molecular Imaging (Associate Editors), the Hellenic journal of Nuclear Medicine and the World Journal of Radiology. He has also served as guest editor of 3 issues of PET Clinics of North America and in the minisymposium of the Indian journal of Cancer. He is the recipient of multiple awards including the Shanti Swarup Bhatnagar Prize 2012 in Medical Sciences and the DAE Scientific and Technical Excellence Award 2007 and the Alavi-Mandell Award from the Education Research Foundation of Society of Nuclear Medicine.*

Half-life Measurement of ^{7}Be in Materials

T. Ohtsuki

Research Center for Electron Photon Science, Kyoto University; E-mail: Ohtsuki@rri.kyoto-u.ac.

The formation of atom-doped C60 and C70 etc. has been investigated by using several types of radionuclides produced by nuclear reactions. From the trace of the radioactivities after high performance liquid chromatography (HPLC), it was found that formation of endohedral fullerenes of Be atom is possible by a recoil process following the nuclear reaction. The decay rate of ^{7}Be electron capture (EC) was measured in C_{70} and Be metal with a reference method. The half-lives of ^{7}Be endohedral C70 and ^{7}Be in Be metal (Be metal(^{7}Be)) were found to be 52.45±0.04 and 53.25±0.04 days, respectively. This amounts to a 1.5% difference in the EC-decay half-life between ^{7}Be@C70 and Be metal (^{7}Be). The results are a reflection of the different electron wave-functions in nuclear site for ^{7}Be inside C70 compared to when ^{7}Be is in a Be metal. The further theoretical interpretation is needed for these experimental results.

Introduction

A long-standing challenge has been to establish the degree to which manipulation of the environmental factors can in practice change nuclear decay rates in experiments to determine the decay rate of ^{7}Be compounds. In addition, there have been several observations of variations in the half-life with host metals, chemical forms, and pressure. From the early data, the half-life of ^{7}Be as a function of different chemical forms and/or host materials have been limited almost to within 0.2%. In recent studies, however, large variations have been observed as a function of different chemical forms and pressures. Therefore, a precise measurement is still needed to obtain the absolute decay rate in different circumstances.

After the discovery of C_{60} and the subsequent successful production of several kinds of fullerenes, endohedral fullerenes which have one or more atoms inside the C_{60}, C_{70}, cages etc. currently have attracted great interest. If their mass production becomes possible, they would have many interesting applications such as stable molecular devices in nano-meter scales and/or as functionalized materials in many fields. We have examined the formation of endohedral fullerenes by a nuclear recoil implantation of several foreign atoms following nuclear reactions [1,2]. We found that the ^{7}Be atom can be endohedrally doped to create the ^{7}Be endohedral fullerenes.

Because of the unique chemical form of fullerenes and/or several factors contributing to give rise to this environment; many -electrons of $C_{60}(C_{70})$, and special dynamic motions inside $C_{60}(C_{70})$ etc., the electron contact density on the ^{7}Be nuclei can be affected significantly by the electron environment of $C_{60}(C_{70})$. Therefore, it is intriguing to measure the half-life of the ^{7}Be inside $C_{60}(C_{70})$; "how does the EC decay rate in ^{7}Be change inside the $C_{60}(C_{70})$ cage relative to other situations?"

So far, we compared the half-life of ^{7}Be when it is encapsulated in a C_{60} cage to that of ^{7}Be in Be metal as a reference. We found a surprisingly shorter half-life of ^{7}Be inside C_{60} [3,4]. This fact implied that the ^{7}Be atoms are located in a unique environment inside C_{60} cage. Furthermore, in order to see the size effect of fullerenes, we demonstrate the change of decay rete of ^{7}Be in ^{7}Be@C_{70} and in Be metal [Be metal(^{7}Be)]. The decay rate of ^{7}Be electron capture (EC) was measured in C_{70} and Be metal with a reference method. The half-lives of ^{7}Be endohedral C_{70} and ^{7}Be in Be metal (Be metal(^{7}Be)) were found to be 52.45±0.04 and 53.25±0.04 days, respectively.

References

[1] T. Ohtsuki et al., Physical Review Letters 77 (1996) 3522.

[2] T. Ohtsuki et al., Physical Review Letters, 81 (1998) 967-970.

[3] T. Ohtsuki et al., Physical Review Letters 93 (2004) 112501.

[4] T. Ohtsuki et al., Physical Review Letters 98 (2007) 252501



***Prof. T. Ohtsuki**, Ph.D, was an Outstanding Scientist of Radio Chemistry and Isotope Production and Application Group at Research Reactor Institute, Kyoto University, Japan (KUR), Kumatori, Osaka, Japan. He is a specialist in the field of nuclear reaction and nuclear fission, environmental radioactivity at KUR. He is an editor of Journal of Nuclear and Radiochemical Sciences in Japan Society, and was an editor of Journal of Radioanalytical Nuclear Chemistry. He has to his credit more than 180 publications in international journals. He has received Award of Nuclear and Radiochemical Sciences (2006). He was Land Collaboration member at GSI, Darmstadt, Germany.*

Radioactive Sources: Promises, Opportunities, and Challenges to meet the Industrial and Clinical Demands

Ashutosh Dash

Isotope Application and Radiopharmaceuticals Division, Bhabha Atomic Research Centre, Trombay, Mumbai 400085, India; E-mail: adash@barc.gov.in

Radioactive source which usually consists of a source core containing a radionuclide, encapsulated in inert metallic capsules, has been the attention, imagination, and close scrutiny of scientists, clinicians, and engineers. Applications of radioactive sources have not only permeated every sector of scientific and technological activities but also form the basis for new technologies as well as driving the evolution of existing ones. This article discusses the preparation and applications of radioactive sources for industrial and clinical applications as well as other applications where it has a role to play.

Introduction

In recent years, there have been unprecedented interests in the use of radioactive sources for a wide range of applications and had a profound influence in the development and growth of science and technology. Such sources have been the attention, imagination, and close scrutiny of scientists, clinicians, and engineers owing to clinical need, technological innovation and conceptual sophistication. Radioactive sources have played a significant role in driving the technological innovations foreword, unfolded numerous unexplored possibilities and permeated virtually every sector of scientific and technological activities. Widespread applications of radioactive sources have not only accelerated the technological progress, but also provided enormous technical and economic benefits. This article discusses the preparation and applications of radioactive sources for industrial and medical applications as well as other applications where it has a role to play.

Radioactive Sources

A radioactive source contains a specific amount of a designated radioisotope that is permanently bonded or fixed in a capsule or matrix designed to prevent release and dispersal of the radioactive material under the most severe conditions which are likely to be encountered in normal use and handling

A radioactive source usually consists of a source core containing a radionuclide which is then encapsulated in inert metallic capsules. With a view to ensuring their utility, these sealed sources are enclosed in various devices that can channel a direct radiation beam at the target material or target tissues while shielding operational personnel from unwanted exposure.

There is a steadily expanding list of radioactive sources with different radioisotopes, which are currently being used or can potentially be used for a wide range of applications. Within the radioactive source, the radionuclide, chemical form, type, physical shape, size and strength will vary widely according to the envisaged applications. The activity of these sources ranges from 10 Bq in sources used for calibration purposes to 100TBq in industrial irradiators and sources used in teletherapy.

Classification of radioactive sources

Application of radioactive sources falls broadly into two categories: medical and industrial procedures.

Medical Sources

Within the framework of medical sources, therapeutic sources are by far the most dominant. Therapeutic intend of radioactive sources is to kill cancerous tissue, reduce the size of a tumor, or reduce pain. They include teletherapy and brachytherapy. In teletherapy, a radiation beam from ^{60}Co source (10-15 kCi) is allowed to focus on the disease site of the patient's body. In order to minimize collateral damage to surrounding tissue, the patient is exposed from several different directions over the course of treatments. In brachytherapy, a sealed radioactive source containing appropriate radionuclide is placed at or near the disease site with the intent of minimizing radiation dose to surrounding healthy tissues. The use of sealed radioactive source in brachytherapy is enticing because it is succinct, tangible, and provides the scope to deliver precise targeted dose of radiation to the malignant cells without significant toxicity to healthy tissue. Since cancer can occur in any location or body system, a wide range of brachytherapy sources containing pertinent radionuclides are required. Brachytherapy is a very successful treatment option for treating a wide range of accessible tumors.

Other major medical application of radioactive sources includes cardiac pacemakers, radiation sterilization of health care products and for blood irradiation.

Industrial Sources

The breadth of applications of radioactive source in industry lies largely on the penetrating power of the radiation emanating from a radionuclide. The ability of the radiation to penetrate through dense materials not only provides a means of determining the state of process materials within the reaction vessels, but also

offers the scope of using this information in a quantitative manner as the basis of instrumentation for control and analysis. Common industrial uses of radioactive sources include non-destructive testing, on-line process control systems, mineral resources evaluation, food irradiation and smoke detection. Industrial radiography widely used in the chemical, petrochemical, and building industries for radiographic inspection of pipes, boilers, and structures where consequences of failure can be severe. Gamma scanning technique is used for diagnosing problems in operating columns like fractional distillation, separation, stripping etc. in petroleum, petrochemical and chemical plants.

In light of the perceived need to monitor industrial production processes, a wide range of industrial gauging sources are used for taking measurements. In order to characterize subsurface properties such as density and moisture percentages, different categories of well-logging sources used. Panoramic irradiators that use gamma radiation from ^{60}Co are used for cross-linking, polymerization, food irradiation and environmental applications such as flue gases, wastewater and sludge treatment.

Calibration Sources

Calibrated sealed sources in the form of disc and rods are fabricated by depositing a measured quantity of activity in the well of plastic discs (=2.5cm) or of a rod [100mm(l) × 10 mm( )]. After drying, the well is filled with an epoxy material and is then sealed with adhesive. These sources were then calibrated with ±5% accuracy using a HPGe detector coupled to a MCA using a NIST traceable standard. Each source is identified by radionuclide, amount of activity, serial number and calibration date.

Radioactive Source Preparation Strategies

While radionuclide source "lives" at the interface between many disciplines, its dependence on the radionuclide is arguably the strongest and *underpin* its success. The inherent determinant for the success of a radionuclide source therefore resides in the selection of a appropriate radionuclide which is based on a number of criteria including half-life, emission type, energy of particulate or gamma emission, purity, specific activity and cost effective production capability. The radioactive source core should have the following properties

Uniform distribution of the radioactivity in the source matrix.

Nonleachability of activity from the source core.

The source matrix should have adequate mechanical, chemical and radiation stability.

Good thermal conductivity to dissipate decay heat during storage.

Usually radioactive source core in metallic forms are preferred as it is possible to irradiate the metal in a reactor to obtain the targeted radionuclide. In situations where it is not possible to obtain the radionuclide of interest or the metallic form is unstable, a source core preparation strategy based on physical or chemical method is used. Typically, choice of a process depends on several parameters which include:

Easy, facile and rapid method involving minimum number of steps.

Ability to deposit requisite quantity of activity.

Process reproducibility

Amenable for operation in a remotely controlled shielded facility.

Generate minimum quantities of radioactive waste.

Process of making source should be economical

The tremendous prospects associated with the radioactive source along with the challenge of preparing source core of requisite quality thus led to a considerable amount of fascinating research and innovative strategies. While the selection of a source core preparation strategy is governed by a number of factors such as appropriateness, scope, prospects, competitive advantages, sustainability, value addition etc., it is primarily aimed at operational simplicity to deposit required quantity of radionuclide on the designated area of the substrate.

Source core preparation techniques that are commonly used include:

(a) Metallic : ^{60}Co, ^{192}Ir, ^{182}Ta, ^{198}Au, ^{103}Pd.

(b) Electrodeposition : ^{63}Ni, ^{57}Co, ^{55}Fe, ^{133}Ba, ^{241}Am.

(c) Chemical deposition : ^{147}Pm, ^{125}I.

(d) Anodization : ^{147}Pm, ^{90}Sr/^{90}Y.

(e) Incorporation into a polymer matrix: ^{60}Co, ^{90}Sr/^{90}Y.

(f) Adsorption : ^{137}Cs.

(g) Vitrification in glass : ^{137}Cs

The selection of radioactive source preparation technology will vary according to the scenarios and depends on the sought application. Each technique with its own specific strengths has the potential to prepare sources with some surmountable restriction. Electrodeposition technique is by far the predominant method used for the preparation of source owing to operational simplicity, flexibility, robustness, high throughput and ability to produce adherent deposit.

Conclusion

Application of radioactive sources in therapy and industries will continue to grow with the ongoing clinical and technological innovations. With the appropriate selection of suitable radionuclide and source preparation strategy, it would be possible to envision a future where the scale and scope of radioactive sources can be tailored to an individual situation. Applications of radioactive sources have passed many milestones but without doubt the end of the road stretches into the distance. Further excitement in this field is awaiting in the foreseeable future.



Dr. Ashutosh Dash *joined the Radiopharmaceuticals Division of BARC in 1983 after graduating from BARC Training school. Dr. Dash obtained his PhD degree from the Bombay University in 1995. He is currently Head, Therapeutic and Reference Sources Section of Radiopharmaceuticals Division, BARC and Professor Homi Bhabha National Institute, Mumbai. He is currently working towards the development and deployment of therapeutic sources in the treatment of cancer. He has worked in Korean Atomic Energy Research Institute (KAERI), Daejon, South Korea as a Visiting Scientist, Cekmece Nuclear Research Centre, Istanbul, Turkey as an International Atomic Energy Agency (IAEA) expert under the Scientist Exchange Program. He has received the Homi Bhabha Science & Technology' Award in the year 2009 in recognition of his outstanding contribution in the field of "Development therapeutic sources for medical applications". He has served as chief scientific investigator and co-investigators in various projects of International Atomic Energy Agency(IAEA). He has published over 95 papers in peer reviewed journals.*

Recent Advances in Radiotracer Applications in Industry

H.J. Pant

Isotope Applications and Radiopharmaceuticals Division, Bhabha Atomic Research Centre, Trombay, Mumbai 400085, India; E-mail: hjpant@barc.gov.in

Radiotracer techniques are well-established and useful tools for troubleshooting and measurement of dynamic parameters in industrial process systems. The economical benefits obtained from the applications of these techniques are considerably high and have been recognized by various end-user industries across the world. There have been some new developments in radiotracer techniques, methodology and applications and the same are briefly discussed in the present paper with a few specific case studies.

Introduction

Radiotracer techniques are widely used for troubleshooting and measurement of process parameters in industrial process systems [1]. The commonly carried out applications of radiotracer techniques in industry include, leak detection in buried pipelines and heat exchangers, flow rate measurement, residence time distribution measurement, sediment transport in Ports, effluent dispersion in water bodies, wear/corrosion rate measurement and various applications in oil fields. During last one decade, there have been some new developments in radiotracer techniques and data analysis methodology that have enabled application of the technique to complex systems and development of some of the new techniques. Some of the recent advances in radiotracer technology include development of multi-input data acquisition systems (MIDAS), radionuclide generators, availability of suitable radiotracers for various phases and improved data analysis methodology. This present paper briefly discusses recent advances and emerging trends in radiotracer applications in industry with a few specific case studies conducted in India.

Radiotracer Technique

Data Acquisition Systems

The monitoring of radiotracer is one of the primary requirements in a radiotracer investigation. In most of the situations, the radiotracer needs to be monitored at a few locations (2-5) with interval more than one minute. NaI(Tl) scintillation detectors based data acquisition system (DAS) have been available for such applications since seventies. However, investigations in fast and complex flow systems require monitoring of radiotracer concentration at 5-50 locations with an interval of 5-10 milliseconds. The availability of high speed microprocessors and high capacity computers made it possible to develop portable multi-input data acquisition system (MIDAS) for radiotracer applications in complex flow systems. Today, MIDAS with inputs varying from 5-48 are commercially available. This has not only increased the scope of the radiotracer techniques but enabled "Tracer Technologists" to measure mean residence times (MRT) of the order of a few seconds and characterize the flows in details. In India, Isotope Applications and Radiopharmaceutical Division, BARC developed a MIDAS with maximum 48 inputs and is being used in various applications.

Radionuclide Generators

The availability of suitable radiotracer in appropriate quantities is primary requirement for a radiotracer investigation. The use of short-lived radioisotopes for industrial applications has several constraints such as need for quick transportation and frequent shipments to the experimental sites located far away from the nuclear establishments. In such situations, "radionuclide generators" are an attractive option to obtain a desired radioisotope and would help in overcoming the difficulties in obtaining readymade radiotracers at remote locations. In addition to this, the availability of radionuclide generators would also enable those countries to conduct radiotracer applications which do not have nuclear reactor for production of radioisotopes and are unable to import short-lived radiotracers because of cost effectiveness and practical reasons. The use of radionuclide generators in healthcare is well established and widely practiced. However, their use in industrial radiotracer applications is limited because of availability of suitable and efficient generators. In recent past, a number of generators such as ^{99}Mo-^{99m}Tc, ^{113}Sn-^{113m}In, ^{140}Ba-^{140}La, ^{137}Cs-^{137}Ba, ^{172}Hf-^{172}Lu, ^{68}Ge-^{68}Ga and ^{83}Rb-^{83m}Kr have been developed and are being used in industrial radiotracer applications [2].

Radiotracer Methodology

Measurement and analysis of RTD is one of the most important and commonly carried out application of radiotracer technique in continuous flow systems. In order to visualize and obtain detailed information of hydrodynamic behavior of the system, the measured RTD needs to be analyzed using suitable hydrodynamic models. Tanks-in-Series and Axial Dispersion Models are most commonly used conventional models for simulation of measured RTD. However, these two are not able to describe flow in complex flow systems. Therefore, complex hydrodynamic flow models need to be developed and numerically solved to simulate the flows in complex systems. During the last decade, commercially available

RTD analysis software with complex flow models have made it possible to analyze RTD data and visualize flows in complex systems. This conventional approach provides only global behavior of the system and do not provide information about local flow patterns inside the systems. This drawback is overcome by modeling the RTD using suitable and validated Computational Fluid Dynamic (CFD) models. Therefore, a new hybrid approach i.e. integration of experimentally measured RTD, results of conventional RTD modeling and results of CFD simulations are used for characterization and visualization of flows in industrial systems. However, the intended CFD models need to be validated before they are used for analysis in conjunction with measured RTD. During last one decade, radiotracer techniques have been used to validate the CFD simulations and subsequently the validated models have been used for flow analysis.

Radiotracer Applications

Fluid Catalyst Cracking Unit (FCCU)

FCCUs are widely used for conversion of heavy oils into gasoline and other lighter products in petroleum refining. The unit consists of various subsystems such as riser reactor, disengager, stripper, regenerator, standpipes and hoppers and involves flow of solid and gas phases at high velocities. A series of radiotracer tests were carried out for tracing solid and gas phases in different sub-systems of an industrial scale FCCU [3]. The schematic diagram of the unit with radiotracer injection and detection locations is shown in Fig. 1. Lanthanum-140 and Krypton-79 are used as radiotracers for tracing the solid (catalyst) and gas phase, respectively. NaI(Tl) scintillation detectors coupled with a MIDAS with 32 inputs were used for monitoring the tracer concentration at an interval of 10 milliseconds. The results of the investigation showed good radial distribution of the two phases in the riser/reactor part of the FCCU. The velocities of gas and solid phase were measured to be 10.5 m/s (MRT=1.4 s) and 7.0 m/s (MRT=2.3 s), respectively. The slip factor was determined to be 1.5. Modelling of the tracer data using Axial Dispersion Model showed plug flow and axially dispersed flow patterns of gas and solid phase, respectively. However, heavy degree of radial maldistribution of catalyst and gas phase was observed in stripper part of the FCCU. Results of model simulation indicated heavy degree of mixing of both the phases in stripper part of the system. The radial distribution of gas phase was poor at the bottom of the regenerator. The gas did not reach the walls and mostly flowed in the centre part of the regenerator. However the radial distribution of gas phase at the top of the regenerator was better. Intermediate degree of axial dispersion of gas phase was observed in regenerator part of the FCCU. The results of the investigation helped plant engineer to modify design of the certain sub-systems and intensify the process.

Glass Production Unit

The schematic diagram of the glass production unit used for production of glass is shown in Fig. 2. The unit consists of a batch mixing and feeding system,

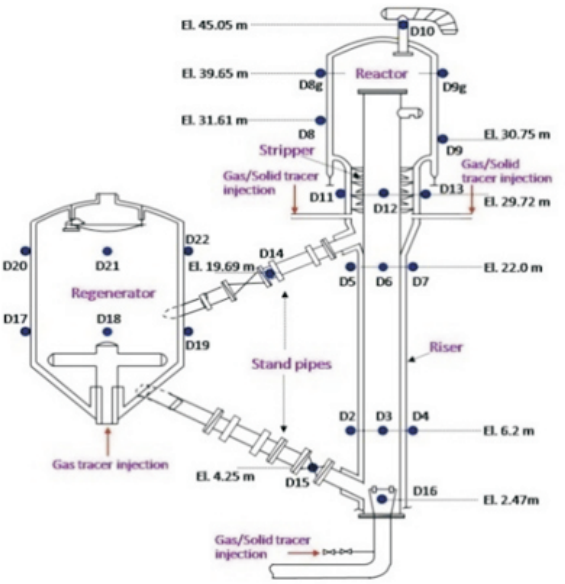


Fig. 1 Schematic diagram of a FCCU and tracer monitoring locations

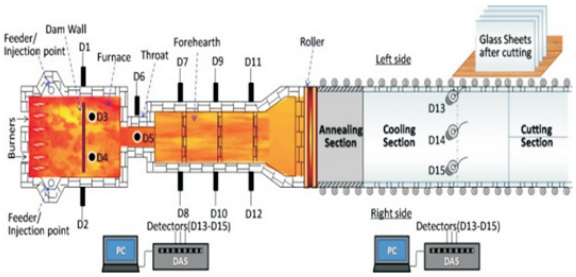


Fig. 2 Schematic diagram of a glass production unit and location of monitoring points

heating system, a tank furnace, forehearth, roller for shaping, and cooling and cutting sections. The mixture of raw materials is fed into the tank furnace (capacity 336 ton) at a rate of 185 ton/day through the two independent feeders connected to right and left side of the furnace. An end fired heating mechanism is used for heating the raw material inside the tank furnace. The feed in the tank melts, reacts, homogenizes and attains a temperature of about 1500°C. After melting, the molten glass flows into the forehearth through a throat, where it is further homogenizes, annealed and attains necessary strength. During the annealing process, the temperature of the molten glass is brought down from 1500°C to 1000°C. After residing inside the forehearth for sufficiently long time, the molten glass is passed through rollers and converted into continuous sheet of desired thickness (0.003 m). The glass sheet is subsequently passed through a long cooling section, where it is cooled to a temperature of about 40°C. At the end of the cooling section, glass sheet is cut into pieces of desired size, (2.1 m x 2.4 m). A radiotracer investigation was carried out in a glass production unit to measure mean residence time of molten glass in different sections of a glass production unit and mixing time of the feed material. In addition to this, the

investigation was also aimed at to investigate homogeneity/uniformity of produced glass and local and global flow patterns. Lanthanum-140 (La-140) as Lanthanum oxide (La_2O_3) was used as radiotracer. Two aliquots of radiotracer each having about 150 mCi activity were simultaneously injected into the furnace through the two independent feeders. The radiotracer was monitored at fifteen different strategically selected locations using collimated and water cooled NaI(Tl) scintillation detectors (D1-D15) connected to two independent MIDAS set to acquire data at an interval of 20 seconds. The acquired data was treated and analyzed.

Based on the analysis, the mean residence times of molten glass within the tank furnace and forehearth were determined to be 31.3 h and 1.8 h, respectively. The dead volume within the furnace of and forehearth were estimated to be about 28.4% and 5.3%, respectively. The mixing time of glass within the entire unit was estimated to be 29 hours. It was found that there were two distinct parallel flow paths followed by the molten glass within the furnace and forehearth of the glass production unit. Poor intermixing has been observed between the two flow streams. In furnace left flow stream showed bypassing, whereas in forehearth right flow stream showed the bypassing. This implies that flow inversion takes place at throat/neck of the furnace. The results of the study could help the plant engineers to control and optimize the production process, and improve the quality of the glass produced.

Radioactive Particle Tracking Technique

Radioactive Particle Tracking Technique (RPTT) is a new technique for flow visualization in pilot-scale industrial process systems [4]. The RPTT involves preparation of a suitable radioactive particle, performing the calibration, introducing the particle into the system, acquiring the data and processing the data. For tracking the fluid, a neutrally buoyant polypropylene bead labeled with a suitable radioisotope is used, whereas for tracing the solid phase, artificially produced solid particles having the same density, shape and diameter are used. After the preparation of the particle, the calibration is performed by mounting the particle at various locations in the system and recording the radiation intensity recorded by each detector at actual operating conditions. After the calibration, the particle is introduced into the operating system and its movement is tracked with time using radiation detectors mounted around the system and connected to a MIDAS. The acquired data in conjunction with the calibration data is used to determine the instantaneous positions of the particle. From the determined positions, the particle trajectories are and velocities are determined. Subsequently, other parameters such as velocity vectors, circulation times, kinetic energy, stress, diffusivities are obtained. Based on these parameters, the complete flow inside the system can be visualized.

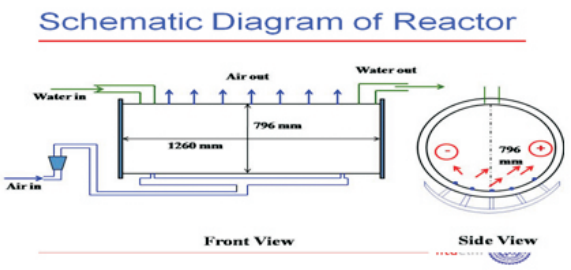


Fig. 3 Application of RPT to a Rotary Fluidized Bioreactor (RFBR)

The technique was developed and successfully implemented in laboratory and pilot-scale systems, including a RFBR designed by an industry for waste water treatment in India (Fig. 3). Based on the results of RPTT, the flow behavior of the media elements was visualized and several flow abnormalities were detected. These flow abnormalities were primarily due to the poor design of the air-distributor system used in the reactor. Based on the results of the investigation, several modifications were suggested to the designer of the reactor. It is expected that the suggested modifications, if implemented, will lead to substantial technological and economical benefits to the industry.

Conclusions

Based on foregoing discussion, it is concluded that the development of multi-input data acquisition systems and availability of suitable radiotracers has enabled tracer technologists to apply the radiotracer techniques to various complex flow systems such as FCCU and also led the development of some of the new techniques such as Radioactive Particle Tracking Technique. The integration of radiotracer data with results of conventional modeling and CFD simulations provide complete information about flow dynamics in industrial systems.

References

[1] J.S.Charlton (Ed), Radioisotope Techniques for problem solving in industrial process plants, Leonard Hill Publications, UK (1986) 320

[2] International Atomic Energy Agency, IAEA Radiation Technology Series No. 5 (2013) 203

[3] Pant, H.J., Sharma, V.K., Nair, A.G.C., Tomar, B.S.,.Nathaniel, T.N., Reddy, A.V.R. and Singh, Gursharan, Appl. Radi. Iso., 67 (2009) 1591.

[4] R.K.Upadhaya, PhD. Thesis, Department of Chemical Engineering, Indian Institute of Technology, Delhi (2010) 464.



Dr. H.J.Pant *obtained his M.Sc Degree in Physics from H.N.Bahuguna Garhwal University, Srinagar Garhwal in 1985 and joined erstwhile Isotope Division, Bhabha Atomic Research Centre, Mumbai in 1988 after graduating from the 31nd Batch of BARC training school. He obtained his Ph.D degree in Physics from Mumbai University in 2000. He is currently serving as the Head, Radiotracer Applications Section in Isotope Applications and radiopharmaceuticals Division of BARC. He is an specialist in Industrial Applications of Radioisotope Techniques and has developed a number of radiotracer techniques and applied them in various industries in India. He was awarded "DAE Scientific and Technical Excellence Award-2010" for his outstanding contribution in the field of "Radiotracer Applications in Industry". He has more than eighty-five publications in international journals and international/national conferences/symposiums. He is a member of International Atomic Energy Agency's expert panel on Industrial Applications of Radioisotopes and was deputed to Thailand, Algeria, Indonesia, Egypt, Republic of Korea and Malaysia as a Technical Cooperation Expert. He is also National Project Coordinator of IAEA/RCA Projects on "Characterizing and Optimizing Process Dynamics in Complex Industrial Systems Using Radiotracer and Sealed Source Techniques".*

Optodes for Sensing Metal Ions

Ashok K. Pandey

Radiochemistry Division, Bhabha Atomic Research Centre, Trombay, Mumbai 400085, India;
E-mail: ashokk@barc.gov.in

The word "optode" or "optrode" is derived from Greek, meaning "the optical way" of generating signal in the sensing layer. The optodes are membrane based optical chemical sensors. These chemical sensors generate an optical response to the chemical reaction that results from the interaction of the analyte with the receptor. The optode designs involve simultaneous preconcentration and determination of the target analyte. In RCD, the color changeable optodes have been developed for Cr(VI), U(VI), Hg(II) ions, and scintillating optodes for alpha-emitting radionuclides and $^{99g}TcO_4^-$. In this talk, an overview of the optodes for metal ions sensors is presented

Introduction

Membrane is the heart of many chemical sensors. The primary function of the membrane is to restrict the accessibility of interfering species to the sensing material. This property of the membrane is extensively utilized in electrochemical sensors like ion-selective electrodes. In some chemical sensor design, a membrane serves as a selective preconcentration layer for the analyte and, therefore, offers a possibility of simultaneous preconcentration and detection of the target analyte. In general, a chemical sensor consists of two basic functional units: (i) receptor, and (ii) transducer. The scheme of a basic design of a chemical sensor is depicted in Fig. 1.

There are different ways to generate optical response proportional to the concentration of analyte in a sensing matrix. The optical response can be based on (a) absorbance, (b) luminescence, (c) reflectance, (d) light scattering and (e) refractive index. In optodes, the membrane, receptor and transducer units are combined into a single sensing matrix as shown in Fig. 2.

In RCD, we are developing two types of membrane based chemical sensors: (i) color changeable optodes, and (ii) scintillating optodes.

Color Changeable Optodes

Most of the optode designs involve simultaneous preconcentration and determination of the target analyte, and are therefore amenable for continuous monitoring of toxic species in aqueous environment. The optodes have been prepared using new indicator dyes, ionophores, chromoionophores and fluoroionophores and highly diversified methods of immobilization [1,2]. A colour changeable optode for Cr (VI) determination has been developed in our laboratory by immobilizing 1,5-diphenylcarbazide (DPC) as the indicator and Aliquat-336 as the carrier in a plasticized cellulose triacetate (CTA) matrix [3]. Poly Vinyl Chloride (PVC) is generally used for preparation of membrane sensors (optodes and electrodes) due to its relatively low cost, good mechanical properties and amenability to plasticization. However, PVC based membranes are known to take up water from aqueous phase and become opaque. The CTA based PIMs do not

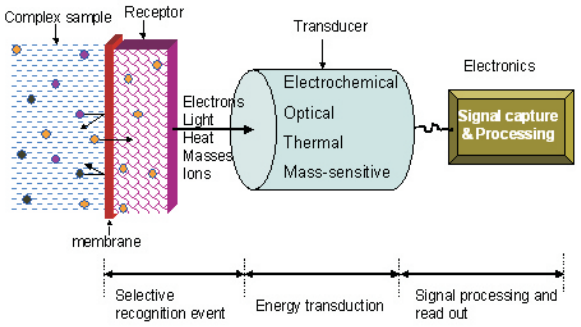


Fig. 1 Schematic representation of a chemical sensor

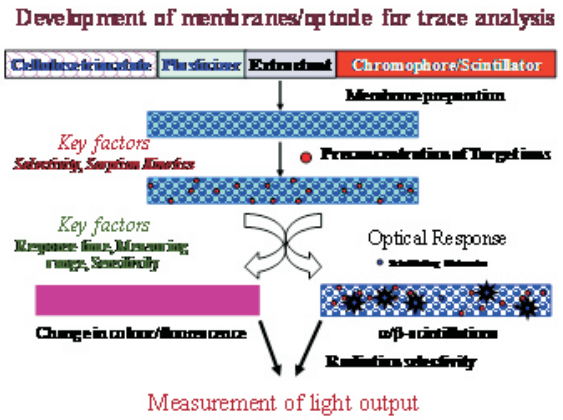


Fig. 2 Scheme showing composition and functioning of the optodes for metal ions sensing

absorb water significantly and have good optical properties. Therefore, CTA was used as the matrix-forming polymer instead of PVC. The optode thus prepared changes colour from transparent to purple and the intensity of purple colour depends on the amount of Cr (VI) preconcentrated in the optode. The optode becomes yellow in colour when higher amount (100 g) of Cr (VI) was present in the equilibrating solution. Using this optode, Cr(VI) even at levels of 13.6 g g^{-1} (in 25 mL of seawater) could be quantitatively detected. This optode for Cr(VI) was found to be stable, cost effective, easy to prepare and

efficient for direct preconcentration and determination of Cr(VI) in a variety of aqueous samples using spectrophotometry. However, it is for one time use only as the reaction of Cr(VI) with DPC is irreversible.

Using the same concept, a color changeable optode for Hg(II) was developed by incorporating a dye 4-(2-pyridylazo)resorcinol (PAR) and a liquid ion-exchanger trioctylmethylammonium chloride (Aliquat-336) in the tri-(2-ethylhexyl) phosphate plasticized cellulose triacetate matrix [4]. Hg(II) and CH_3Hg^+ from aqueous samples could be quantitatively preconcentrated in this transparent optode producing a distinct color change ($_{max}$ = 520 nm) within 5 min of equilibration time in bicarbonate aqueous medium or 30 min in natural water. The uptake of Hg(II) was found to be pH dependant with a maximum (>90%) at pH 7.5. The preconcentration of Hg(II) from a large volume of aqueous solution was used to extend the lower limit of concentration range that can be quantified by the spectrophotometry of optode. It was observed that preconcentration of 11 g Hg(II) in 100 mL (0.11 g/mL) aqueous samples in optode sample changed its color distinctly, and absorbance was above 3 of the blank absorbance.

Optode for UO_2^{2+} ions in the aqueous samples was developed by physical inclusion of a chromophore 2-(5-bromo-2-pyridylazo)-5-diethylamino phenol (Br-PADAP) in a plasticized cellulose triacetate matrix [5]. In order to improve selectivity, a color changeable optode for UO_2^{2+} ions was developed by the immobilization of a chelating agent 8-hydroxyquinaldine (HQ) along with chromophore 4-(2-thiazolylazo)-resorcinol (TAR) in the tri-(2-ethylhexyl) phosphate (TEHP) plasticized cellulose triacetate matrix [6]. On sorption of UO_2^{2+} in the optode matrix, TAR changes color of the optode from yellow to magenta having a maximum absorbance ($_{max}$) at 546 nm as shown in Fig. 3. The optode response, in the form of increase in the absorbance, was found to be linear in the UO_2^{2+} ions concentration range of 0.01 mol L^{-1} - 0.11 mol L^{-1} in tap water as well as aqueous solutions containing 0.1 mol L^{-1} NaCl or $NaNO_3$. The tolerance to the presence of several cations and anions in the determination of UO_2^{2+} ion was studied. It was observed that that 50 ng g^{-1} UO_2^{2+} ions in 100 mL sample can easily be quantified using this optode. The optode was found to be fully reversible, can readily be regenerated by equilibrating it with 0.1 mol L^{-1} HNO_3 and reusable. The applicability of the developed optode in real samples was studied by determining uranium in the ground water samples spiked with a known quantity of UO_2^{2+} ions.

Scintillating PIMs

A radionuclide sensor is a combination of a sensing element, that selectively interacts with a radioactive target, and a transducer that produces a signal generated due to the interaction between the target and the sensing element. The advantage of a radionuclide sensor over the conventional radiation detectors is that it can also provide an efficient preconcentration step integrated with the detection

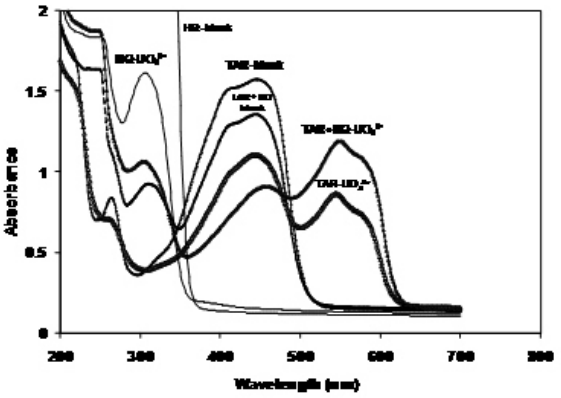


Fig. 3 Absorption spectra of the optodes having different compositions before and after equilibration with solution containing 0.11 mol L^{-1} of U(VI)

process. Generally, organic scintillator molecules are employed for / detection and measurement owing to their fast response time. Grate et al. have reviewed the radionuclide sensors developed for environmental monitoring [7].

We are developing the radionuclide sensor based on scintillating membranes [8,9]. These membranes are similar to PIMs used for the optode except that scintillating molecules are used in place of chromophores. The scintillating membranes have been developed for selective extraction and detection of alpha emitting actinides. These scintillating membranes were prepared by using dioctyl phthalate (DOP) plasticized cellulose triacetate (CTA) membrane containing optimum amounts of extractant bis(2-ethylhexyl)phosphoric acid (HDEHP), scintillator 2,5-diphenyl oxazole (PPO) and wavelength shifter 1,4-bis(2-methylstyryl)benzene (MSB) [8]. The plasticized anion-exchange membranes are highly hydrophobic and have selectivity towards anions depending on their hydration and valence states. The scintillating membrane for $^{99g}TcO_4^-$ anions was prepared by immobilizing liquid anion-exchanger Aliquat-336 along with the scintillators PPO and MSB in a tris-(2-ethylhexyl)phosphate (TEHP) plasticized polystyrene (PS) matrix [10]. The choice of PS as a matrix is based on the fact that it gives better pulse height as compared to other matrix forming polymer like cellulose triacetate (CTA). There is a possibility that other -emitters like $^{131}I^-$ can be distinguished from $^{99g}TcO_4^-$ by their characteristics -rays. The membrane was characterized for its extraction efficiency, scintillation efficiency, pulse height and sorption kinetics. It was found that the membrane sorbed TcO_4^- ions quantitatively (95±5%) from a solution having pH 2, tap water and seawater. The -scintillation pulse height in the membrane was found to be higher than that in the Liquid Scintillation Cocktail, see Fig. 4.

The -counting efficiency of the membrane was found to be 72 % for ^{99g}Tc. The scintillating membrane was found to give a good linear response as a function of

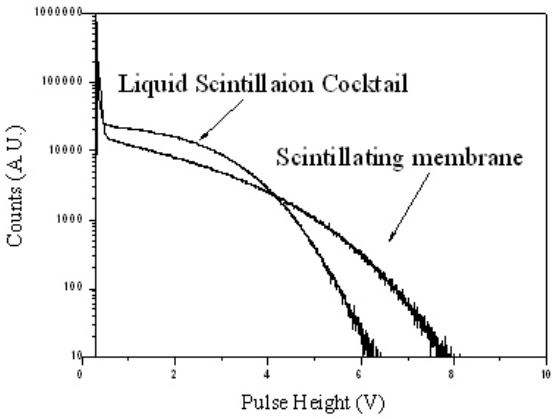


Fig. 4 Comparison of scintillation pulse height of -particles emitted by $^{99g}TcO_4^-$ in liquid scintillation cocktail and scintillating membrane

concentration of TcO_4^- ions transferred to the membrane matrix.Thus, the scintillating membrane developed in our lab can be used for the preconcentration and determination of -emiting anions like $^{99g}TcO_4^-$ ions from the aqueous sample.

Ag Nanoparticles Embedded Nafion-117 Membrane for Sensing Hg^{2+} ions

The standard redox potentials of the systems Hg^{2+}/Hg (+0.85 V) and Ag^+/Ag (+0.80 V) lie close together. It is known that the electrochemical potentials of silver nps are rather electronegative, and galvanic reaction between Ag^0 and Hg^{2+} given below may become possible in the membrane.

$$Ag^0_m \quad (m/2)Hg^2 \qquad mAg \qquad (m/2)Hg^0 \qquad (1)$$

The ^{110m}Ag radiotracer tagged Ag nps were prepared in Nafion-117 membrane by in situ formamide reduction to determine the yield of the galvanic reaction [11]. The membrane samples thus prepared were equilibrated with 0.01 mol L^{-1} $Hg(NO_3)_2$ for subjecting galvanic reaction of Ag^0 with Hg^{2+} ions. After equilibration, the Ag^+ ions formed by the oxidation of Ag nps were removed from the ion-exchange sites of membrane samples by treating these with 0.1 mol L^{-1} $NaNO_3$. It was observed in this study that 97 % of Ag^0 was replaced from the membrane samples. The comparison of Energy Dispersive X-ray Fluorescence (EDXRF) spectra of the membrane samples before and after equilibration with aqueous solution containing Hg^{2+} ions also indicated that the galvanic reaction proceeded quantitatively. The TEM images of the samples subjected to complete galvanic replacement of Ag^0 with the Hg^{2+} ions are shown in Fig. 5.

The radiotracer studies and EDXRF spectra confirmed the complete galvanic replacement of Ag in these samples. The spherical Ag nps are not seen in any TEM image of the sections of the membrane sample subjected to quantitative galvanic reaction with Hg^{2+} ions. Hg^0 thus formed coalesced to bigger size nanostructure that did not have well-defined shape. The

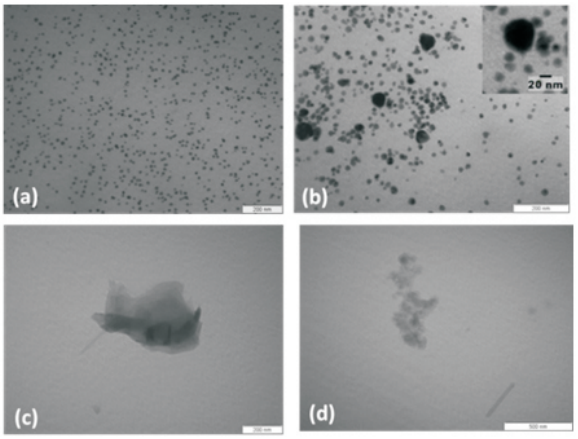


Fig. 5 TEM images of the across sections of the membrane samples subjected to quantitative galvanic replacement of Ag nanoparticles with Hg^{2+} ions. (a) before galvanic reaction, (b) at 50 % of the galvanic reaction, (c) & (d) after completion galvanic reaction

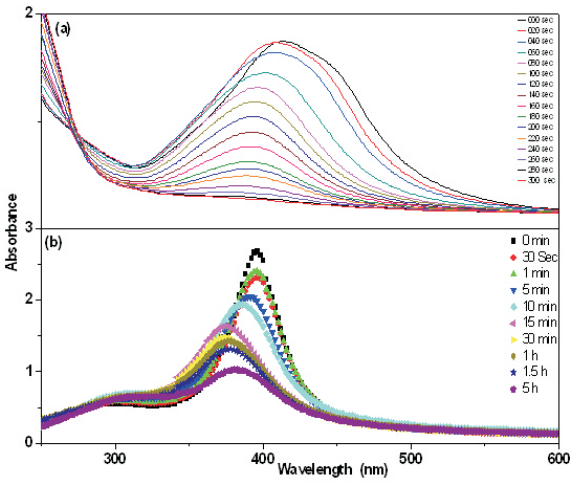


Fig. 6 Surface plasmon absorption of Ag nps embedded Nafion-117 membrane as a function of equilibration time (t) in solution: (a) containing Hg^{2+} ions for complete reduction of Ag^0, (b) containing Hg^{2+} ions less than that required for complete replacement of Ag^0

sorption of Hg^{2+} ions in Ag nps embedded membrane sample was found to be quantitative (95%) from the well-stirred solution. The quantitative uptake of Hg^{2+} ions in cation-exchange membrane could be attributed to the concentration gradient of Hg^{2+} ions between aqueous solution and membrane maintained by the galvanic reaction that changes Hg^{2+} ions to Hg^0. It is important to remove the Hg accumulated in the membrane matrix for its reuse. It was observed that Hg could be re-oxidized and removed from the membrane by its equilibration in 0.5 mol L^{-1} HNO_3 at room temp. UV-Vis spectra of the membrane sample subjected to partial and complete galvanic reaction of Ag nps with Hg^{2+} ions are shown in Fig. 6. It is seen from Fig. 6 that the intensity at $_{max}$, 400 nm decreased continuously

with increase in concentration of mercury in the membrane.

Thus, a chemical sensor for Hg^{2+} ions can be developed using their galvanic reaction with Ag nps in the membrane, which produces optical response in the form of blue shift and decrease in intensity of the SPB of Ag nps.

Conclusions

Ultra trace detection and quantification of toxic metal ions in aqueous samples has important applications in process control and environmental monitoring. Conventional analytical method generally requires a preconcentration step to produce signal above the background noise of the detectors. In view of this, there is a need to develop analytical methods that have superior detection limits. One of the ways is to incorporate a preconcentration step in the methodology. Optical chemical sensors (optodes) are considered to be better suited for on-site monitoring and visual screening of toxic ions/species in the aqueous samples. Optodes are easy to prepare, selective for preconcentration of target analyte in the sensing matrix, and there is no need for separate reference devices. These optodes are based on the preconcentration of the analyte on a solid substrate that produces change in the optical property of the solid substrate which is proportional to the analyte concentration. The measurement of the change in the optical property (absorption, reflectance, fluorescence, scintillation, refractive index etc.) of the solid phase can be used for the detection and quantification of the target analyte. The presence of extractant provides an increase in the selectivity and sensitivity of the optodes as compared to that obtained by solution spectrophotometry using same chromophore.

Acknowledgements

I am thankful to my senior colleagues Dr A. Goswami, Head, Radiochemistry Division and Dr A.V.R. Reddy Head, Analytical Chemistry Division, BARC for their keen interest and contribution to the work described in this manuscript. I am grateful to Dr Y.M. Scindia, Dr Suparna Sodaye, Dr. Y. Kalyan, Dr. Sadanada Das, Mr Rakesh Kumar and Mrs Sumana Paul who were associated with me during their doctoral studies. A major portion of this manuscript is from their Ph.D. research work.

References

[1] E. Bakker, P. Bühlmann, E. Pretsch, Chem. Rev. 97 (1997) 3083.

[2] E. Pretsch, P. Bühlmann, E. Bakker, Chem. Rev., 98 (1998)1593.

[3] Y.M. Scindia, A.K. Pandey, A.V.R. Reddy, S.B. Manohar, Anal. Chimi. Acta, 515 (2004) 311.

[4] Y. Kalyan, A.K. Pandey, P. R. Bhagat, R. Acharya, V. Natarajan, G.R.K. Naidu, A.V.R. Reddy, J. Hazard. Mater. 166 (2009) 377.

[5] J.M. Joshi, P.N. Pathak, A.K. Pandey, V.K. Manchanda, Talanta 76 (2008) 60.

[6] Y. Kalyan, A.K. Pandey, G.R.K. Naidu, A.V.R. Reddy, Spectrochimica Acta Part A 74 (2009) 1235.

[7] J.W. Grate, O.B. Egorov, M.J. O'Hara, T.A. DeVol, Chem. Rev. 108 (2008) 543.

[8] S. Sodaye, R. Tripathi, A.K. Pandey, A.V.R. Reddy, Anal. Chim. Acta 514 (2004) 159.

[9] S. Sodaye, Y.M. Scindia, A.K. Pandey, A.V.R. Reddy, Sensor and Actuator B: Chemical 123 (2007) 50.

[10] S. Das, S, Chakraborty, S. Sodaye, A.K. Pandey, A.V.R. Reddy, Anal. Methods 2 (2010) 728.

[11] R. Kumar, A.K. Pandey, S. Das, S. Dhara, N. L. Misra, R. Shukla, A. K. Tyagi, S.V. Ramagiri, J.R. Bellare, A. Goswami, ChemComm., 46 (2010) 6371.



Dr. Ashok K. Pandey *joined the Radiochemistry Division, Bhabha Atomic Research after completing his M.Sc. in Inorganic Chemistry from Bundelkhand University, Jhansi. He obtained his Ph.D. degree from Mumbai University in 1995. He was Post Doctoral Fellow in Membrane Group at McMaster University, Canada from 1997 to 1999. He has worked in diverse area that includes Solid State Nuclear Track Detectors, analytical methods for actinides, particle induced fission of low Z elements, radiochemistry of neutron induced fission of actinides etc. His current research interest is in the functionalized polymer membranes, nanocomposite membranes, membrane based chemical sensors and separation methods for metal ions. He has to his credit 83 papers published in peer reviewed international journals.*

Recent Trends in Mass Spectrometry for Nuclear Forensics

S.K. Aggarwal

Fuel Chemistry Division, Bhabha Atomic Research Centre, Trombay, Mumbai 400 085, India;
E-mail: skaggr2002@gmail.com

The talk will discuss the various mass spectrometric techniques (TIMS, ICPMS, SIMS, GDMS, GC-MS etc.) which are used to determine isotopic composition of bulk materials and particles; age of the nuclear material since its last chemical purification, impurities and other elements present along with U/Pu, and the usefulness of the isotope ratios of other elements e.g. oxygen and lead for nuclear forensics.

Mass Spectrometry is an important and versatile analytical technique in the field of nuclear forensics which has emerged an area of high concern over the last two decades. The two main objectives of nuclear forensics are to (i) identify the source of illicit trafficking of interdicted nuclear materials mainly uranium (U) and plutonium (Pu), and (ii) search for clandestine activities e.g. ^{235}U enrichment, reprocessing of irradiated U fuel for extracting Pu. Mass spectrometry occupies a unique place in nuclear forensics due to its high sensitivity, capability to perform analysis of bulk materials as well as particles, provide information about the percentage abundances of different isotopes of an element and yield high accuracy data.

The main objectives of the confiscated material are to trace its origin, the intended use, its provenance and the age since last purification. Different mass spectrometric techniques used are thermal ionization mass spectrometry (TIMS), inductively coupled plasma mass spectrometry (ICPMS), secondary ionization mass spectrometry (SIMS) and gas chromatography mass spectrometry (GC-MS). These mass spectrometric techniques are used to determine the isotopic composition, concentration, trace impurities, other elements (e.g Gd, Er, Ga, Li) present along with U and Pu etc. These data are needed to trace the geo-location of U, identify the type of reactor (PWR, BWR, RMBK, Magnox, LMFBR etc.) in which Pu of different grades were produced, the intended use of the material, date of last chemical purification weapon grade etc.

TIMS is regularly used to determine the isotopic composition of U and Pu except for ^{232}U and ^{238}Pu due to the isobaric interferences from ^{232}Th and ^{238}U, respectively. In addition, due to the low abundances of these two isotopes viz. ^{232}U and ^{238}Pu as well as their relatively short half-lives, -spectrometry is preferred to TIMS for routine applications. Isotope dilution TIMS is employed for determining the concentrations of U, Pu, Th, Pa to calculate the age of the material (i.e. U and Pu). There are five different parent daughter couples for Pu viz. ^{238}Pu-^{234}U, ^{239}Pu-^{235}U, ^{240}Pu-^{236}U, ^{241}Pu-^{241}Am, ^{242}Pu-^{238}U. The usefulness of a particular parent-daughter couple depends on many parameters, in particular, on the age of the material since its last purification. For uranium, age determination can be done by using two chronometers viz. ^{234}U-^{230}Th and ^{235}U-^{231}Pa. The concordance in the age obtained by two independent parent-daughter couples enhances the confidence in the data and is recommended for nuclear forensics applications. Isotopic composition of Pb (i.e. radiogenic isotopes ^{206}Pb, ^{207}Pb and ^{208}Pb) can provide information about the geo-location of the material (U,Th).

ICPMS with laser ablation is a useful mass spectrometric technique for the determination of parent/daughter elements and isotopes in the nuclear materials. The availability of high resolution multi-collector ICPMS instruments has provided the analyst with an important analytical toll to determine the ages with high precision. ICPMS is also used for determining other elements present in the interdicted material. The origin of these could be (i) right from their presence in starting materials, (ii) result from the chemicals used during any type of chemical processing done or (iii) purposely added (e.g. Ga, Gd, Dy etc.) to achieve some properties.

SIMS is an important mass spectrometric technique for the analysis of particles and is popular for determining the isotopic composition of U and Pu in micro-samples. This has also been employed to determine the ^{18}O/^{16}O isotope ratio of uranium oxide samples of different origin and thus can be used to distinguish uranium oxide samples of different origins. An interesting study using TIMS, SIMS and glow discharge mass spectrometry (GDMS) was reported in literature demonstrating the useful of ^{18}O/^{16}O isotope ratios in uranium oxide samples.

Among the other mass spectrometric techniques, GC-MS has also been proposed to determine the tracers of chemicals/solvents associated with the nuclear forensic samples. Efforts are going on to develop and employ high sensitivity mass spectrometric techniques like resonance ionisation mass spectrometry (RIMS) and accelerator based mass spectrometry (AMS) to achieve ultra high sensitivity in U and Pu determinations.

Development of isotope correlations using the data on the isotopic composition of U, Pu and Pu/U ratios determined by mass spectrometry are important for nuclear forensics. The isotopic composition of Pu provides useful information about the quality (i.e. weapon grade, reactor grade etc.), the type of reactor in which Pu was produced, neutron spectrum, burn-up etc. These data can be useful to make an important analysis

of the confiscated nuclear material or about the undeclared activity. It is highly desirable to create such data base, for national as well as international security keeping in mind the present worldwide scenario.

There is also a need to have certified and well characterized U and Pu materials of known ages which can be used by various laboratories to validate the methodologies being developed. The present talk will highlight the present status of mass spectrometric techniques being used for forensic applications. A brief summary of some of the work done in our laboratory for understanding the ion source chemistry of Th, U and Pu during their analysis by TIMS will also be given.

References

[1] Klaus Mayer, Maria Wallenius and Zsolt Varga, Chem. Rev. 113 (2013) 884.

[2] Floyd E. Stanley, A.M.Stalcup and H.B.Spitz, J. Radioanal. Nucl. Chem. 295 (2013) 1385.

[3] Rafael C. marin, Jorge E.S.Sarkis and Marcos R. L. Nascimento, J. Radioanal. Nucl. Chem. 295 (2013) 99.

[4] D. Alamelu and S.K.Aggarwal, Int. J. Nucl. Energy Sci. Technol. 6 (2011) 30.

[5] Kenton J. Moody, Ian D. Hutcheon and Patrick M. Grant, Nuclear Forensic Analysis, Taylor & Francis (2005).



Prof. Suresh Kumar Aggarwal *is presently Associate Director of Radiochemistry and Isotope Group (R) and Head of Fuel Chemistry Division (FCD) at Bhabha Atomic Research Center (BARC) at Trombay, Mumbai. He obtained his Ph.D. in 1980 from Mumbai University and had his Post-doctoral Training at University of Virginia at Charlottesville, USA during 1987-89. He joined BARC in 1973 after graduating from 16th batch of BARC Training School (1972-73) with Bhabha Medal Award and has been continuing at BARC in various capacities since 1973. At present, he is serving as a Distinguished Scientist (DS) at BARC. He is nationally and internationally known expert in the field of atomic mass spectrometry. In 1997, he was honored with "EMINENT MASS SPECTROMETRIST" award by the Indian Society for Mass Spectrometry (ISMAS). He is a recognized Ph.D. guide of Mumbai University and Senior Professor of Chemistry at Homi Bhabha National Institute (HBNI) at Mumbai. He has about 700 publications to his credit which includes about 200 papers published in International Journals. He has guided more than 10 PhD students and has served ISMAS in various capacities. He is the Founder President of Indian Society for Electro Analytical Chemistry (ISEAC) and currently, the President of Indian Society for Mass Spectrometry (ISMAS) as well as ISEAC. He has been the Chairperson of many Mass Spectrometry and Electrochemistry Conferences in India organized under the aegis of ISMAS and ISEAC and has edited the Proceedings of these Conferences. He is also a coauthor of the book entitled "Introduction to Mass Spectrometry" published by ISMAS. His other areas of interest include Radiometry, Electrochemistry, X-ray spectroscopy; Laser based Analytical Techniques, Analytical Chemistry for Societal Applications etc.*

The Potential for Radionuclide and Isotopic Analyses using a Rapid Scanning Magnetic Sector ICP-MS

John Cantle

Wrexham, LL13 9XS, UK; E-mail: JC@johncantle.com

Modern high resolution ICP-MS (HR-ICP-MS) instruments offer a number of performance differentiators compared to more widely-used quadrupole ICP-MS instruments. Better sensitivity, superior detection limits and faster scan speeds all offer distinct advantages in addition to the more obvious advantage of higher resolution analysis.

The dynamic range and detector linearity of mass spectrometers of this type can be important for a number of applications. Without a suitably broad dynamic range it is not possible to quantify trace elements in the presence of more abundant (matrix) elements. Typically, an ion counting detector is used for the quantitation of low abundance elements / isotopes, though such detectors are saturated by relatively small ion beams limiting their dynamic range. Additionally, they do not always respond in a linear fashion. This can be especially problematic when measuring isotope ratios, wherein the isotope ratio can vary with the concentration of the element(s) in the sample if the ion counter is not linear.

We report a series of measurements designed to quantify the linearity of the ion counting detector of the Nu Attom HR-ICP-MS, the latest instrument of its kind.

The Nu Attom is a double-focusing, high-resolution magnetic sector mass spectrometer. The instrument is entirely purpose designed and built to provide the best performance and reliability coupled with flexibility and ease-of-use for precise and accurate elemental and isotope ratio analysis. A unique detector system gives the Nu Attom a large dynamic range, and its electrostatic scanning capability has the widest range in its class (40%). Furthermore, the continuously variable high resolution means that sufficient resolution for isobaric separation can be selected with minimum compromise in sensitivity.

The linearity of the Nu Attom's ion counting detector was assessed by analysis of the uranium standard CRM U500 in dry plasma mode. Concentrations of the solutions were selected so that a range of count rates between <1000 cps and >2 Mcps on the different U isotopes were achieved. Total U concentrations used were 50 pg/g, 100 pg/g and 200 pg/g. Four replicates of each concentration were measured in the following sequence 50 pg/g, 200 pg/g and 100 pg/g. All analyses were performed in fast peak jumping mode.

The dwell times for ^{235}U and ^{238}U were 200 s. Dwell time for ^{234}U, ^{236}U, m/z 237 and m/z 239 were 400 s. Peak jumps were made at 20 s. Therefore, the total time for one sweep was around 2 ms. One cycle consisted of 2000 sweeps. Each run consisted of 100 cycles and thus, each run was around 7 minutes long. A deadtime correction of 15.5 ns was applied to signal intensities.

Tailing from ^{238}U was measured at m/z 237 and m/z 239. With the retardation filter on, the tail from ^{238}U onto m/z 237 was around 8 ppm and the tail from ^{238}U onto m/z 239 was around 20 ppm. Due to the equal abundance of ^{235}U and ^{238}U, these were subtracted from ^{234}U and ^{236}U peaks to correct for ^{235}U tailing.

The $^{235}U/^{238}U$ ratio was used for internal mass bias correction using the certified value of the standard of 0.999700 and the exponential correction law. Accuracies of the $^{234}U/^{238}U$ and $^{236}U/^{238}U$ ratios were calculated using the certified values of 0.010422 and 0.001519, respectively. This data can be seen in Table 1.

A second set of samples was also analysed, in this case using wet plasma operation. For this set of analyses, solution concentrations were selected to achieve a range of count rates between <1000 cps and 4.5 Mcps on the different U isotopes. Concentrations used were between 500 pg/g and 8,000 pg/g. Three replicates of each concentration were measured in fast peak jumping mode.

Dwell times for all isotopes were 200 s. Peak jumps were made at 20 s. Therefore, the total time for one sweep was around 2 ms. One cycle consisted of 1000 sweeps. Each run consisted of 70 cycles and thus, each run was around 3 minutes long. Deadtime correction and tailing were accounted for as per the first dataset.

Accuracies of the $^{234}U/^{238}U$ and $^{236}U/^{238}U$ ratios were calculated using the certified values as mentioned above. This data can be seen in Table 2.

The data shown in Table 1 indicates that the Nu Attom produces accurate and precise isotope ratios using its fast peak jumping mode. All ion beams were analysed using the ion counting detector. The isotope ratios do not vary with solution concentration, and the $^{234}U/^{238}U$ and $^{236}U/^{238}U$ values are within 0.15% and 0.04% of the certified values respectively.

Furthermore, the data shown in Table 2 shows that when more concentrated ion beams are used (up to 4.5 Mcps) there is no loss in either accuracy or precision of the measurements. The recommended maximum count rate of the Nu Attom's ion counting detector is 2Mcps. However, these results indicate that linearity is achieved even with more intense ion beams than the specified count rate limit.

Table-1: Count rates and isotope ratios as measured on the Nu Attom using NBS U500 at a variety of concentrations (dry plasma)

^{234}U (cps)	^{235}U (cps)	^{236}U (cps)	^{238}U (cps)	^{234}U/^{238}U	2SE	^{236}U/^{238}U	2SE	Conc. (pg/g)
5345	513867	788	520974	0.010455	3.20E-05	0.001528	1.20E-05	50
20977	2017488	3092	2041056	0.010428	1.60E-05	0.001521	5.10E-06	200
9265	891642	1358	900041	0.010411	2.30E-05	0.001519	8.40E-06	100
5264	506688	768	513215	0.010435	3.00E-05	0.001515	1.20E-05	50
21690	2083790	3173	2105072	0.01044	1.50E-05	0.001521	5.20E-06	200
8971	863373	1317	871612	0.01044	2.30E-05	0.001523	8.90E-06	100
5445	523637	794	529429	0.010439	3.40E-05	0.001519	1.10E-05	50
20762	1995291	3055	2018284	0.010434	1.50E-05	0.001524	5.60E-06	200
9266	890254	1361	901564	0.010435	2.20E-05	0.001521	9.10E-06	100
4615	444921	679	453501	0.010428	3.30E-05	0.001513	1.20E-05	50
16672	1605488	2458	1644452	0.010458	1.70E-05	0.001517	6.40E-06	200
7625	736839	1127	756677	0.010452	2.80E-05	0.001513	9.40E-06	100
			Mean	**0.010438**		**0.00152**		
			SD	1.31E-05		1.56E-06		
			RSD%	**0.125**		**0.3**		
			Accuracy%	**0.15**		**0.04**		

Table-2 : Count rates and isotope ratios as measured on the Nu Attom using NBS U500 at a variety of concentrations (wet plasma)

^{234}U (cps)	^{235}U (cps)	^{236}U (cps)	^{238}U (cps)	^{234}U/^{238}U	2SE	^{236}U/^{238}U	2SE	Conc. (pg/g)
2995	287990	459	290785	0.010376	6.10E-05	0.001532	2.70E-05	500
5968	574920	925	580574	0.01035	6.60E-05	0.001556	2.10E-05	1000
12004	1151781	1835	1162977	0.010397	2.90E-05	0.001538	1.40E-05	2000
23693	2270812	3598	2291426	0.010406	2.60E-05	0.001526	1.20E-05	4000
41979	4033844	6372	4072390	0.010389	2.30E-05	0.001525	7.50E-06	7000
47299	4549946	7170	4592796	0.010371	1.90E-05	0.001524	7.70E-06	8000
2992	284562	459	286898	0.010421	7.30E-05	0.001524	2.70E-05	500
5901	566024	916	571202	0.010382	5.80E-05	0.001549	2.00E-05	1000
11775	1131694	1810	1142594	0.010373	3.40E-05	0.00154	1.40E-05	2000
23609	2265614	3605	2285725	0.01039	3.10E-05	0.001533	1.00E-05	4000
41361	3981371	6347	4019623	0.010364	2.20E-05	0.001543	7.60E-06	7000
46839	4493771	7103	4538556	0.010395	1.80E-05	0.001526	8.40E-06	8000
2937	281150	454	284019	0.010364	7.10E-05	0.001522	3.30E-05	500
5787	554270	897	558926	0.010378	6.20E-05	0.001543	2.10E-05	1000
11667	1120793	1784	1131548	0.010368	3.80E-05	0.001532	1.70E-05	2000
23549	2251992	3560	2272046	0.010436	2.70E-05	0.001526	1.10E-05	4000
40564	3901134	6149	3934048	0.010371	2.10E-05	0.001526	7.70E-06	7000
46879	4503358	7165	4545844	0.010394	2.10E-05	0.001537	7.50E-06	8000
			Mean	**0.010385**		**0.001534**		
			SD	2.13E-05		9.72E-06		
			RSD%	**0.205**		**0.634**		
			Accuracy%	**-0.36**		**0.96**		

The Nu Attom is a high resolution ICP-MS that is ideal for the most demanding ICP-MS requirements in the Nuclear and Radiochemical fields.



Dr. John Cantle *obtained BSc in Chemistry followed by PhD in Analytical Chemistry from Imperial College, London University in 1970 and 1973. Dr Cantle was also awarded Associate of Royal College of Science and Diploma of Imperial College. Following this period Dr Cantle entered the field of Analytical Instrumentation – firstly specialising in Atomic Absorption Spectrometry for trace metals analysis and then since 1979 has been working in Mass Spectrometry with VG Instruments in UK and then followed by Nu Instruments UK. Dr Cantle is an international expert in ICP-MS and has lectured on this topic in many countries at International conferences including MARC in USA and ISMAS in India as well as many others. Dr Cantle also specialises in many other forms of Mass Spectrometry including TIMS, SIMS, GDMS etc*

Assessment of Intakes of Radionuclides : Systems and Methods for Routine and Emergency Scenarios

K.S. Pradeepkumar

Radiation Safety Systems Division, Bhabha Atomic Research Centre, Trombay, Mumbai 400 085, India;
E-mail: pradeep@barc.gov.in

Introduction

Measurements for the detection and evaluation of internal contamination of occupational workers due to intakes of various radionuclides are performed using variety of detector systems and methods. The radionuclides are categorized broadly into gamma emitters (low and high energy) and alpha- beta emitters. The methods adopted for these categories are quite elaborate and also different from each other. Internal body contamination with radionuclides can occur in two different domains. (i) The working areas of nuclear facilities/installations such as nuclear power plants, reprocessing facilities, fuel fabrication plants and nuclear materials mining activities. (ii) The public domain in the event of accidental releases from nuclear facilities or from the explosion of large scale radioactive dispersal devices. The priorities for monitoring in the later scenarios are for use of rapid detection systems and analytical methods to initiate appropriate counter measures. In the prior domain, the normal practices of evaluation with high degree of accuracy and precision are followed.

Intakes of radionuclides into the human body can occur through i) inhalation of particulate matter, ii) ingestion of radionuclides through the consumption of food products, water and beverages and iii) injection through cuts and wounds. Internal Dosimetry Section of Radiation Safety Systems Division (RSSD) is the nodal agency in India, for the development of systems and methods for monitoring and assessment of internal exposures for both occupational workers in nuclear facilities and public in radiological emergencies. Measurements for identification and quantification of internal contamination is an important regulatory requirement to demonstrate the compliance of national radiological limits of protection and for facilitating the control of operations and design of nuclear facilities.

Individual internal contamination monitoring of occupational workers is conducted based on the guidelines of ICRP-78 depending on the nature of work. Namely: i) Routine monitoring - applicable to those workers for whom, the day of intake is assumed to be the mid point of two successive monitoring intervals. ii) Special monitoring- applicable to those workers involved in carrying out special tasks and the time of intake is known as the exposures are planned. This presentation discusses the methods & systems which are in place in RSSD for the assessment of internal contamination in both routine and emergency situations and also highlights the need for improvements in certain areas.

Occupational Monitoring

Occupational workers, the staff working in plants or research laboratories, are likely to get internal contamination primarily through inhalation, much lower than the prescribed limits of radiological protection. The application of personal protective equipments, timely radiological surveys and air activity measurements in working areas ensure that the internal contamination due to various radionuclides lies much below the annual limits. However, Occupational workers are monitored annually or immediately under suspected conditions of exposure, if any, for the assessment of intakes and the committed effective dose (CED). The techniques adopted for the evaluation of internal contamination are briefly described:

High Energy Gamma Emitters (in vivo Monitoring)

In India, shadow shield scanning whole body monitors (SSWBM), employing a 4" (dia) x 3" (thick) NaI(Tl) detector or higher sizes are used for the detection of commonly observed gamma emitters, primarily ^{137}Cs, ^{60}Co and ^{131}I. The systems are calibrated with an industry standard tissue equivalent BOMAB phantom, developed indigenously for Reference Indian Man (RIM) of height :167 cm and weight : 63 kg, using multiple point sources of ^{133}Ba (^{131}I stimulant), ^{137}Cs and ^{60}Co. The detection limits achieved with such systems are lower than 10% of recording level dose of 1 mSv.

Low energy X/gamma Emitters (in vivo Monitoring)

The assessment of internal contamination due to actinides such as ^{241}Am, ^{238}U, ^{235}U and ^{239}Pu are carried out using a phoswich (sandwich of 200 mm dia x 12 mm thick NaI(Tl) and 200 mm dia x 50 mm thick CsI(Tl)) detector and an array of three large area n-type HPGe detectors (3 x 70 mm dia x 25 mm thick) housed in steel rooms. The systems are calibrated with Thorax phantoms (LLNL –Lawrence Livermore National laboratory and JAERI – Japan Atomic Energy Research Institute) containing radionuclides loaded lung sets. The CFs with JAERI phantom were found to be 30% higher compared to those estimated using LLNL phantom at 60 keV for ^{241}Am. JAERI phantom is based on the reference Asian man of height 168 cm and weight 63.5 kg whereas LLNL phantom is based on reference US worker of height 177 cm and 76 kg. The detection limits of are about 5 Bq and 25 Bq for ^{241}Am and ^{238}U respectively. However, the resolution of HPGe detector (FWHM : 0.75 keV) array being far superior to that of

phoswich detectors (FWHM : 10 keV), the identification becomes unambiguous and leads to precise quantification as compared to a Phoswich detector.

Alpha-Beta Emitters (in vitro monitoring)

The intakes due to - and - emitting radionuclides such as ^{239}Pu, ^{234,235,238}U, ^{232}Th, ^{90}Sr and ^{3}H are evaluated using indirect techniques of urine and/or fecal samples analysis. The urinary excretion rates per day are determined and converted to assess the intakes using appropriate bio-kinetic models. Radiochemical analysis for the separation of nuclides and high resolution alpha spectrometry are used for the detection of Pu, U and Th isotopes. Long counting duration of about 4-5 days are adopted to obtain detection limit of 0.2 mBq/d of excretion in urine. This value equates to about 1.3 mSv of CED for soluble ^{239}Pu (type M) for annual monitoring interval and is on par or better with those observed internationally. Methods such as three days pooled urine sample or fission track analysis do exist for further lowering of detection limits, and are contemplated as and when required. The general radiochemical procedure involves, wet oxidation of the urine sample, co-precipitation of Pu along with calcium phosphate, ion exchange separation followed by final activity quantification using alpha spectrometry.

Dose Assessment Methodology

The internal exposure assessment is based on the guidelines outlined by the ICRP in it's publication ICRP-78. The methodology involves experimental measurement for the determination of internal radioactive contamination in the human body and/or excretion rates of radionuclides through urine/feaces. The assessment is carried out in terms of intake and internal dose taking into account of many factors such as the mode of intake, characteristics (physical and chemical) of the radioactive material, the biokinetic behaviour of the contaminant and its decay modes, individual's parameters. The intakes and committed effective doses are also computed using the IAEA/ICRP recommended software IMBA (Integrated Modules for Bioassay Analysis), which contains several features for fitting the measured data and solving biokinetic and dosimetric models.

Internal Contamination Monitoring During Nuclear/Radiological Emergencies

The mechanism of evaluation of internal exposure during nuclear/radiological emergencies is to meet requirement of rapid screening of large numbers of personnel. They could be from members of public or occupational workers from Nuclear facilities. Radiation Safety Systems Division has developed fast scanning type systems and rapid methods for quick assessment and is also on continuous development of systems for further bettering the capabilities. Internationally, it has been observed that the demand for internal contamination monitoring from members of public was very large after the radiological events of Chernobyl, Goiania ^{137}Cs incident, Tokaimora criticality accident and Fukushima accident. Goiania incident was in fact the first incident in which the members of public were administered a de-corporating agent namely Prussian Blue (Radiogardase – a USFDA approved drug) for enhancing the removal of ^{137}Cs from the body. 62 personnel including children were administered with the drug in different doses. Internal doses as high as 5 times ALI or greater were estimated and the efficacy of Prussian Blue was studied in detail. A field whole body counter (2 minutes counting duration) was set up and about 600 individuals were monitored in that area. About 4000 urine samples were analyzed in about 4 months duration to monitor the efficacy of Prussian blue de-corporating agent.

We are equipped with fast screening type whole body monitor (1-2 minutes counting), which can give detection limits equivalent to intakes as low as 0.01 times of ALI for ^{137}Cs and ^{60}Co. A normal working table/chair type monitor based on portable HPGe detector was configured and tested for the assessment of closely spaced multiple gamma emitting radionuclides. A partially shielded chair type Thyroid monitoring system, capable of utilizing multiple detectors such as HPGe, thick NaI(Tl) and thin NaI(Tl) has been developed and commissioned. The system is being used to measure internal contamination due to isotopes of radioiodine (^{125}I, ^{131}I, ^{133}I) on a single platform. Rapid radioanalytical techniques have also been developed for the measurement of ^{90}Sr, Pu/Am/U isoptopes for use during emergencies. The Division has expertise in managing incidental contamination of Pu and Am isotopes through inhalation and also through wound by chelation therapy and wound excision. Similarly, therapeutic procedures for U, I, Sr, Co and other radionuclides exist as part of standard procedures. A mobile radiological laboratory (MRL) equipped with standardized chair type whole body counter, a bulk counting gamma spectrometer and many other portable devices is always under ready to use condition for assessment during emergencies.

References

[1] International Commission on Radiological Protection (1997a). General Principles for the Radiation Protection of the Workers. ICRP Publication 75 Ann. ICRP 27 (1).

[2] International Commission on Radiological Protection (1997c). Individual Monitoring for Internal Exposure of Workers. ICRP Publication 78. Ann. ICRP 27 (3-4).

[3] Pendharkar K. A., Bhati S., Singh I. S., Sawant P. D., Satyabhama N., Nadar M. Y., Vijaygopal P., Patni H. K., Kalyane G. N., Prabhu S. P., Ghare V. P. and Garg S.P., Upgradation of Internal Dosimetry Facilities at BARC Trombay. BARC Newsletter Issue No. 296 (2008) 9.



Dr. K.S. Pradeepkumar *is Head, Radiation Safety Systems Division (RSSD). He joined RSSD after 25th training school. He is member for several association related to radiation safety. His expertise in different filed such as Radiation Safety, Operational Health Physics, Mobile Radiation Mapping techniques, development of Techniques for Radioactive plume tracking, Searching of orphan sources, qualitative & Quantitative assessment of large area radioactive contamination, development of preparedness and response to Radiological emergencies and Nuclear Disasters /emergencies, Establishing Derived Limits of Atmospheric discharges, dose apportionment for nuclear facilities.*

Identifying and Correcting Errors in NAA Measurements Using Internal Consistency Checks

Robert R. Greenberg and Richard M. Lindstrom

Chemical Sciences Division, National Institute of Standards and Technology, 100 Bureau Drive, Stop 8395, Gaithersburg, MD 20899-8395, USA; E-mail: robert.greenberg@nist.gov

Introduction

A wide variety of methods are used to ensure the quality of analytical measurements by all analytical techniques. Typical approaches include (but are not limited to): 1) validating methods prior to use on real samples; 2) verifying the accuracy of the calibration solutions and solid materials intended for use prior to the actual sample measurements; 3) using more than one analytical signal per element to be determined (i.e., with different energies, charge/mass ratios, absorbances, etc.) where practical, evaluating the linearity of calibration curves, and 4) analyzing one or more certified reference materials (CRMs) with similar characteristics to the actual samples under investigation. Analysts employing neutron activation analysis (NAA) can use all of these general methods, however, they have many more tools at their disposal to check for internal inconsistencies within their measurements based on two fundamental differences with most other analytical methods. The first is that the spectrum of each sample changes as a function of time due to radioactive decay, and the second is the simplicity of the physics of NAA, which allows a complete understanding the measurement process [1]. This presentation will focus on demonstrating how the use of multiple counts of the same sample using the same counting geometry but with different decay times, analysis of samples with different sizes, and the use our knowledge of whether a potential bias affects each element in a similar manner or independently, permits identification of a wide variety of measurement errors.

Experimental

Much of the data derives from a re-evaluation of the NIST certification measurements of the content of ion-implanted arsenic in silicon (SRM 2134) [1-3]. In summary, ten approximately 1.1 cm^2 pieces of silicon wafer were irradiated with four prepared calibrators (standards) containing known amounts of arsenic. Each sample was counted at least twice, and each calibrator was counted four times at significantly different decay intervals. A complete uncertainty budget was evaluated looking at about 30 individual uncertainty components. A relative expanded uncertainty of 0.38% was observed.

Results and Discussion

The ability to perform gamma-ray spectrometry on the same sample or calibrator (standard) after different decay times, (using the same counting geometry) often provides the capability of identifying or verifying the absence of many sources of bias such as gamma-ray interferences, erroneous (or no) pileup corrections, erroneous dead-time corrections, use of incorrect half lives, etc. Analysis of one or more replicate samples with significantly different masses can also indicate potential biases due to neutron and gamma-ray self shielding, incorrect blank treatment, as well as count rate effects (since larger samples will have higher dead times at the same geometry). Moreover, many sources of bias affect all elements to the same degree while others do not; so our understanding of how each potential bias affects the different elements in a multielemental analysis can be used to identify which one may be causing inconsistent data. A summary of the characteristics of common sources of bias is given in Table 1.

As an example of how powerful a tool for uncovering problems multiple counts can be, some of the original calibration data from the certification of arsenic in SRM 2134 is discussed below. Fig. 1 shows the original A_0/ g data for one count of each of the four independently pipetted calibrators. The observed agreement seems to be consistent with counting statistics with allowances for uncertainties due to irradiation location and preparation. However, measurements of the same calibrators at different decay intervals indicate that there are serious problems with the measurement, as shown in Fig. 2.

As can readily be seen from Fig. 2, the data is obviously inconsistent among the four counts of each calibrator. Since there is disagreement among the replicate counts of each individual calibrator, any possibility of preparation or irradiation problems is eliminated, and the problem(s) must be dependent on

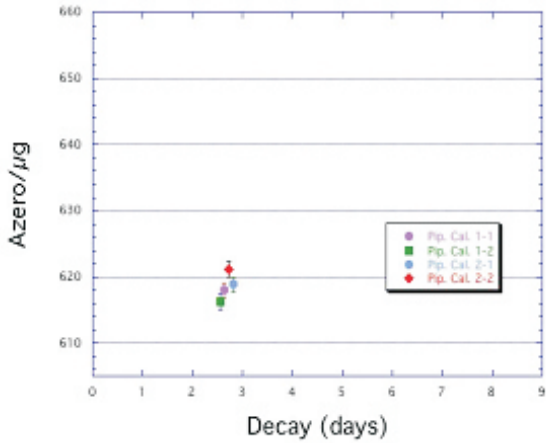


Fig. 1 Original data for 1 count each of 4 arsenic calibrators

Table-1: Some Characteristics of Potential NAA Biases

Potential source of bias	Observable with multiple counts	Observable with different sample sizes	Effects all elements to the same degree
Pulse pile-up	Yes	Yes	Yes
Inadequacy of LT extension	Yes	Yes	No
Gamma-ray interferences	Yes	No	No
Gamma-ray self-shielding	No	Yes	No
Blank	No	Yes	No
Neutron shielding	No	Yes	Yes (thermal)
Basis weight problems	No	No	Yes

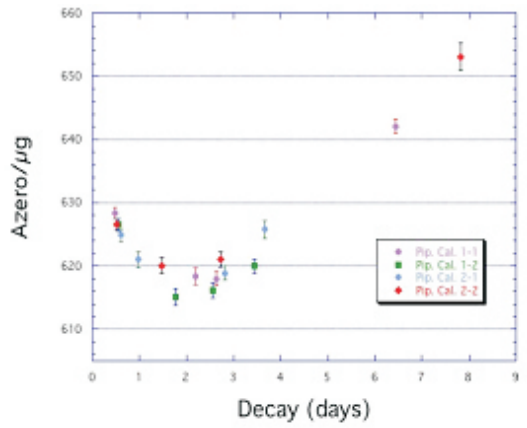


Fig. 2 Original data for all four counts of each of the four individually prepared calibrators

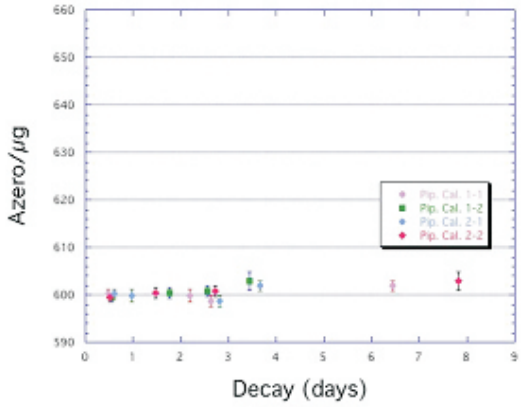


Fig. 3 Corrected data for all four counts of each of the four individually prepared calibrators

gamma spectrometry or decay. Note that the problem(s) are not visible in the data shown in Fig. 1 because the calibrators were counted after very similar decay intervals. In addition the shape of the curve (Fig. 2) is very strange. Most NAA biases tend to result in either a straight line or an exponential, thus the shape of this curve seems to indicate that there are more than one significant bias present.

It tuned out that the ^{76}As half-life listed in the Table of Isotopes, was incorrect, and the hardware pileup correction used overcompensated for pileup events. Substituting the previous ^{76}As half-life, and correcting for pileup overcompensation, the data for all counts (Fig. 3) were consistent with counting statistics (with allowances for irradiation position differences and preparation uncertainties). Note that all figures use the same scale for both X- and Y-axes

In addition to discussing this example, this presentation will describe how to use a few simple tools to maximize the chances of observing significant biases in NAA measurements, and to correct them before the data is finalized.

References

[1] R. R. Greenberg, P. Bode, and E. A. Fernandes, Spectrochimica Acta Part B, 66 (2011) 193.

[2] R. R. Greenberg, R. M. Lindstrom, and D. S. Simons, J. Radioanal. Nucl. Chem., 245 (2000) 57.

[3] D.S. Simons, R.G. Downing, G.P. Lamaze, R.M. Lindstrom, R.R. Greenberg, R.L. Paul, S.B. Schiller, and W.F. Guthrie, Journal of Vacuum Science and Technology B, 25(4) (2007) 1365.



***Dr. Robert R. Greenberg**, Ph. D, is presently a Scientist Emeritus at the (US) National Institute of Standards and Technology, where he formally worked as a Research Chemist/Supervisory Research Chemist for 32 years. He is a specialist in Neutron Activation Analysis (NAA), Chemical Metrology, certification of reference materials and quality assurance for NAA measurements. He was the Group/Team Leader for Nuclear Analytical Methods at NIST for nearly 20 years. He has more than 100 papers in scientific journals, and has presented more than 100 invited talks at scientific conferences. Dr. Greenberg has received numerous awards including the NIST Chemical Science and Technology Laboratory's Technical Achievement Award in 2000, the NIST Judson C. French Award in 2003, the U. S. Department of Commerce Bronze Medal in 2007, and the Georg Hevesy Medal Award, also in 2007. He was elected as a Fellow of the American Nuclear Society in 1998.*

QA/QC and Uncertainty Assessment in k_0 based NAA

B. Smodiš

Department of Environmental Sciences and Reactor Infrastructure Centre, Jožef Stefan Institute, Jamova cesta 39, SI-1000 Ljubljana, Slovenia; E-mail: borut.smodis@ijs.si

Quality aspects of the k_0 based neutron activation analysis are reviewed. In the first part, analytical quality assurance and quality control are defined and systematically presented in more detail. In the second part, the existing approaches and practices for uncertainty assessment are reviewed, emphasizing specific features of the discussed analytical technique. The importance of deriving realistic uncertainty budget for the obtained final measurement result and the need for further improvements in deriving reliable measurement results is emphasized.

Introduction

The k_0 based method of neutron activation analysis (k_0-NAA) can be interpreted either as (1) a single-comparator standardization of NAA which is made versatile with respect to irradiation and counting conditions or (2) an absolute standardization with substitution of the absolute nuclear data by experimentally determined k_0-factors.

In order to demonstrate that a laboratory is producing data of adequate precision, accuracy and sensitivity it is necessary to assess all laboratory procedures at all stages from sampling to reporting. As this is a time consuming and costly process, it is important to ensure that the standards of performance are clearly defined and adhered to.

All analytical measurement results should be accompanied with their respective uncertainties characterizing the dispersion of the values attributed to the measurands. For deriving reliable uncertainty assessment, the analytical process must be well known and understood, and the measurement must be statistically controlled.

QA/QC

Quality assurance (QA) may be defined as all the planned and systematic activities implemented within the quality system and demonstrated as needed, to provide adequate confidence that an entity will fulfil requirements for quality. It refers to the full range of practices employed to ensure that laboratory results are reliable. QA may therefore be defined as the system of documenting and cross referencing the management procedures of the laboratory. The ultimate objective is to ensure that the laboratory functions efficiently and effectively. It is primarily a management system and as such is measurand-independent as it deals with the overall running of the laboratory rather than focusing on individual analyses. The QA program addresses the following issues: management; training; standard operating procedures; laboratory facilities; equipment maintenance and calibration; sampling procedures; sample receipt, storage and disposal; reporting of results. A frequent method of implementing a QA program is to apply for accreditation, which represents the implementation of QA program in conformity with an internationally recognized QA system.

Quality control (QC) refers to operational techniques and activities that are used to fulfil requirements for quality.

Internal QC (IQC) refers to activities conducted within a laboratory for continuous assessment of the quality of measurement results obtained by particular analytical procedures. Whereas QA strives to achieve quality by regulating procedures at laboratory level, IQC focuses on the individual method and tests its performance against mathematically derived quality criteria. It comprises: method validation (e.g., linearity, limit of detection, precision, accuracy); validity checking (e.g., calibration check, use of blanks, recovery checking); precision and accuracy checks (e.g., control by duplicate analysis, precision control using RMs, accuracy control using CRMs); use of control charts.

External QC (EQC) refers to activities leading to comparison with other reference laboratories or consensus results amongst several laboratories. It comprises e.g., participation in inter-laboratory comparison exercises and proficiency tests.

Uncertainty Assessment in k_0-NAA

The use of k_0 – NAA involves many uncertainty sources thus making quantification of uncertainty components rather complex. The relevant measurement equations can be found in [1]. The following topics have to be dealt with:

1. Evaluation or experimental determination of k_0-factors
2. Contribution of epithermal activation, including:
   (a) Experimental determination of f, the subcadmium (thermal)-to-epithermal neutron fluence ratio
   (b) Experimental determination of , the parameter describing the nonideality of the neutron fluence distribution
   (c) Evaluation or experimental determination of E_r, the effective resonance energy

(d) Evaluation or experimental determination of Q_0, the resonance integral to 2200 m s^{-1} cross-section ratio

(e) Evaluation or experimental determination of F_{Cd}, the Cd transmission factor for epithermal neutrons

3. Determination of $_p$, the full-energy peak detection efficiency for the given gamma line
4. Accurate determination of N_p (number of counts in the full energy peak) and its correction for:
   (a) True-coincidence effects
   (b) Burn-up effects
   (c) Nuclear interferences
5. Avoidance or determination of G_{th} and G_e (the correction factors for thermal and epithermal neutron self-shielding, respectively)
6. Application of appropriate convention for non 1/v reactions
7. Constancy of fluence parameters during irradiation; otherwise appropriate correction should be applied.

There are presently four main approaches of assessing measurement uncertainty of k_0-NAA. The first type of assessment is given in [1], yielding to an instructive uncertainty of 3.5% relative regardless of the measurand. The second type of assessment is based on the "Universally applicable spreadsheet technique" founded on numerical calculations [2]. Examples of this approach may be found in [3, 4]. The third approach comprise dedicated computer programs for uncertainty calculations. A Web tool referred to as k_0–GUM Tool complies with the Eurachem approach for the quantification of uncertainty in analytical methods [5]. The program ERON (Error propagation) analytically calculates the relevant partial derivatives obtained from the basic equations, multiplies them with the available standard uncertainties and calculates the combined uncertainty [6, 7].

There are two k_0-NAA programs available on the market: KayWin [8] and k_0-IAEA program [9]. The first one applies a fixed uncertainty (i.e., 3.5%) according to the first type of assessment shown above, for all measurands, combined with the uncertainty of a particular peak area. The second program combines particular uncertainties by solving the linear system of relevant equations in a holistic approach.

Conclusions

The quality assurance and quality control approaches and practices to be applied by k_0-NAA users do not conceptually differ from the procedures used with other analytical techniques. The solely differences might be in details due to the different physical basis of this particular mode of neutron activation analysis when compared to other modes of NAA (e.g., the relative NAA) or non-nuclear analytical techniques.

The uncertainty assessment of the k_0-NAA measurements is a rather complex task that requires profound theoretical and judgment knowledge in applying this method of chemical analysis. There are several parameters where uncertainties should be assessed by judgment knowledge as they cannot be obtained by calculation. However, it is highly recommended to apply nuclide-specific assessments instead of fixed numbers for all measurands as it yields more realistic estimates.

Our laboratory experience and literature surveys reveal that the expanded uncertainties obtained by k_0-NAA measurements are larger than the uncertainties obtained the relative NAA. Therefore, there is continuous challenge to further improve the uncertainty assessment process. This includes upgrading of the existing nuclear database by providing more precise nuclear data needed for k_0-NAA calculations.

References

[1] F. De Corte, Habilitation Thesis, University of Ghent, Belgium (1987).

[2] J. Kragten, Analyst 119 (1994) 2161.

[3] P. Robouch, G. Arana, M. Eguskiza, S. Pommé, N. Etxebarria, J. Radioanal. Nucl. Chem. 245 (2000) 195.

[4] M. Kubešová, J. Kuèera, J. Radioanal. Nucl. Chem. 293 (2012) 87.

[5] N. Younes, P. Robouch, J. Radioanal. Nucl. Chem. 257 (2003) 665.

[6] T. Buèar, B. Smodiš, Nucl. Instrum. Methods A 564 (2006) 683.

[7] T. Buèar, B. Smodiš, Nucl. Instrum. Methods A 595 (2008) 647.

[8] KayWin®, User's Manual, version 2 (2005).

[9] M. Rossbach, M. Blaauw, M. A. Bacchi, X. Lin, J. Radioanal. Nucl. Chem. 274 (2007) 657.



***Prof. B. Smodiš**, is a Scientific Counsellor and Head of the Radioecology Group at the Department of Environmental Sciences, Jožef Stefan Institute (JSI), Ljubljana, Slovenia and Head of the Reactor Infrastructure Centre of the JSI. He is an associate professor of the Jožef Stefan International Postgraduate School. He is a specialist in nuclear analytical chemistry, radioecology, radiochemistry, ecotoxicology, and responsible for the TRIGA Mark II reactor safety and radioactive waste management at JSI. He is the chairman of k_0 Users International Scientific Committee and European Advisory Safety Committee for Research Reactors. He has to his credit more than 340 bibliographic units out of which 90 are published in SCI international journals. Dr. Smodiš is a member of the Presidential Board of International Nuclear Chemistry Society and EURATOM Scientific and Technical Committee. He is also an Associate Editor of the Journal of Radioanalytical and Nuclear Chemistry.*

Recent Advances in Ratio Primary Reference Measurement Procedures (Definitive Methods) and their Use in Certification of Reference Materials and Controlling Assigned Values in Proficiency Testing

R.S. Dybczyñski, H. Polkowska-Motrenko, E.Chajduk, B. Danko, M. Pyszynska

Laboratory of Nuclear Analytical Methods, Institute of Nuclear Chemistry and Technology, 03-195 Warszawa, Dorodna 16, Poland; E-mail: R.Dybczynski@ichtj.waw.pl

The idea of definitive methods based on radiochemical neutron activation analysis (RNAA) [1-5], consists in combination of neutron activation with the highly selective and quantitative post-irradiation isolation of the desired radionuclide by column chromatography followed by -ray spectrometric measurement. The principles of construction of such methods , which were devised in the Institute of Nuclear Chemistry and Technology, are reminded and the significance of these methods for analytical quality assurance is emphasized. According to VIM 3 nomenclature [6] these methods may be called: ratio primary reference measurement procedures (RPRMPs) . RPRMP for the determination of Se is briefly presented and its use for checking the accuracy of "assigned values" established by expert laboratories in some proficiency tests, is demonstrated. Pictorial presentation of RPRMP for As is shown in Fig. 1 and its application to independent confirmation of some of the certified values established in world-wide intercomparisons, in Fig. 2, respectively. The new RPRMP for the determination of Fe in biological materials enabled the detection of negative systematic errors of unknown origin in the case of most laboratories using optical methods which analyzed our recently issued certified reference material (CRM) namely: Oriental Basma Tobacco Leaves (INCT-OBTL-5) [5]. RPRMPs are not intended for routine measurements but rather for checking the accuracy of other methods of inorganic trace analysis, and are used as an assistance in the certification of the candidate materials and assigning values in proficiency tests. Several examples of the use of RPRMPs taken from the recent analytical practice of our Laboratory are presented and discussed in this paper. RPRMPs with their expanded standard uncertainties of 2.7-3.6% are comparable to ID-MS methods and are the only methods of such high metrological quality which can be used for the determination of trace amounts of monoisotopic elements.

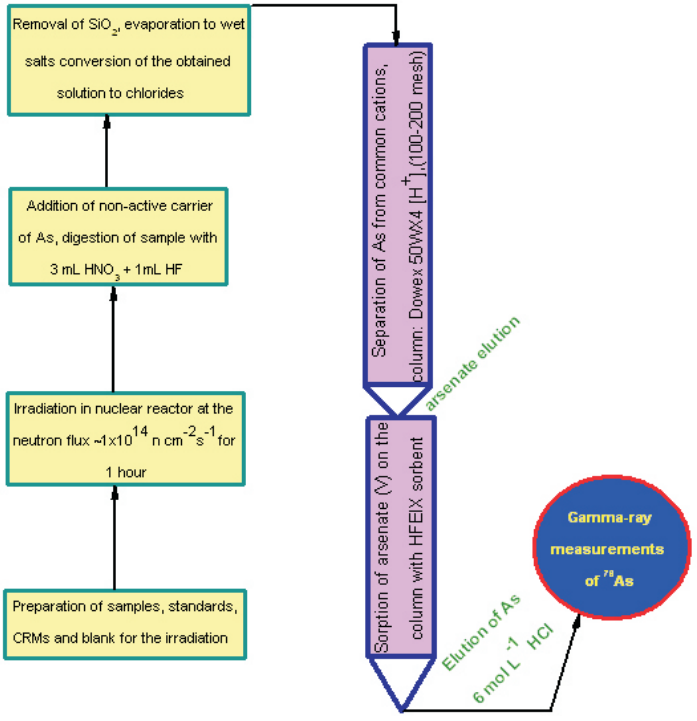


Fig. 1 Analytical scheme for the determination of As by RPRMP in biological materials

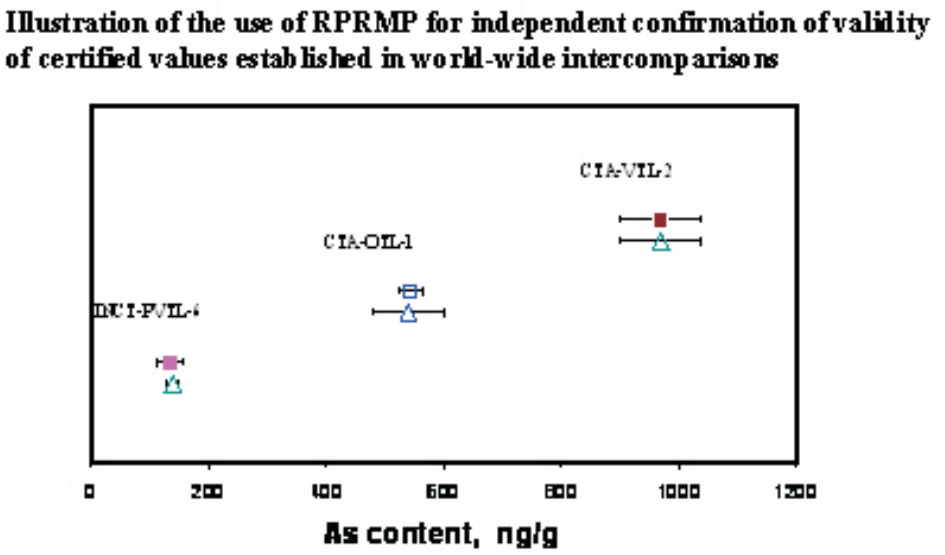


Fig. 2 Confirmation of validity of the certified values for As by RPRMP; Triangles – certified value, Squares – result by RPRMP

References

[1] R.Dybczyñski, Wasek, H.Maleszewska, J.Radioanal.Nucl. Chem., Articles, 130, (1989) 365

[2] R.S.Dybczyñski, B.Danko, H.Polkowska-Motrenko, Z.Samczyñski, Talanta 71, (2007) 529

[3] E. Chajduk, H. Polkowska-Motrenko, R.S. Dybczyñski, Accred.Qual. Assur., 13 (2008) 443

[4] E.Chajduk, R.S.Dybczyñski, Microchim. Acta, 168 (2010) 37

[5] R. S. Dybczyñski, B. Danko, M. Pyszynska, H. Polkowska-Motrenko, Radiochimica Acta 100 (2012) 409

[6] International vocabulary of metrology – Basic and general concepts and associated terms (VIM), ISO/IEC Guide 99, Geneva , (2007)



***Prof. R.S. Dybczyñski** , Ph.D, D.Sc, for nearly the whole scientific carrier was associated with the Institute of Nuclear Research later with the Institute of Nuclear Chemistry and Technology, Warsaw, Poland, serving as a Head of Laboratory of Radiometric Methods and later Head of Department of Analytical Chemistry He is a specialist in ion exchange, radiochemical separations, neutron activation analysis, quality assurance, production and certification of certified reference materials, ion chromatography and rare earth chemistry. In the years 1975-1980 he was managing Analytical Quality Control Service in the International Atomic Energy Agency, Vienna. Prof. Dybczyñski is the author of over 200 scientific papers, 5 books, encyclopedia entries etc. He was the associate editor of the journals Geostandards Newsletter and Chemia Analityczna (Warsaw) and is on the Advisory Board of the Journal of Radioanalytical and Nuclear Chemistry. He is the member of Polish Chemical Society and Committee of Analytical Chemistry of the Polish Acad.Sci., He has been recipient of several awards and medals including W.Kemula medal (2001), A.Waksmundzki medal (2010) and G. Hevesy medal (2013).*

Deuterium Build up in Moderator Cover Gas System of 540 MWe PHWRS, during Normal Operation and during Reactor Shutdown

S.C. Dash, G. Sriram, R.P.S. Tomer

Tarapur Atomic Power Station # 3 & 4, TAPP, NPCIL, Boisar, Thane, Maharashtra, 401504, India;
E-mail: scdash@npcil.co.in

Moderator gets heated up due to neutron moderation and capture, attenuation of gamma radiation as well as due to transfer of heat from other reactor components. The gas space above the moderator is filled with helium. During reactor operation, high neutron flux as well as the gamma radiation causes radiolysis of the moderator heavy water. Even during reactor shutdown radiolysis occurs, depending on flux and water conductivity. The moderator breaks down into deuterium and oxygen and gets released into the helium gas space above moderator. This paper compares the effect on deuterium concentration during normal operation and reactor shutdown.

Introduction

Tarapur Atomic Power Stations 3 & 4 (TAPS # 3 & 4), is a Pressurised Heavy Water Reactor (PHWR) with 540 MWe capacity. In this heavy water is used as moderator. The purpose of heavy water moderator is to maintain criticality in the reactor core, by slowing down the high energy neutrons to a lower energy level, where their probability for fission capture becomes several folds higher. Heavy water used as moderator inside the calandria gets heated up due to neutron moderation and capture, attenuation of gamma radiation as well as due to transfer of heat from other reactor components in contact. Thus heavy water in the calandria also functions as a heat sink in the unlikely event of loss of coolant accident, coincident with the failure of emergency core cooling and in Beyond Design Basis Accident (BDBA). The temperature of moderator at the outlet of calandria is kept at about 76.5^{o}C during normal operation. Thus the total thermal heat to be transferred from moderator to Active Process Water (APW) cooling system is 95 MW.

Moderator cover gas system is used to provide an inert atmosphere over heavy water in calandria (in OPRD lines), in order to avoid downgrading of heavy water due to air ingress. To accommodate changes on moderator volume due to temperature variations & liquid poison injection and to control the pressure in the system, a gas space is provided at the top of calandria free surface of the moderator, in the overpressure relief lines and also above heavy water in calandria head tank. This space is filled with helium, which is an inert gas that does not react chemically with heavy water. Helium is also stable under nuclear radiations. Helium pressure at the calandria top, under cold shutdown condition (30°C) is slightly above atmospheric pressure in order to prevent ingress of air. This pressure increases to 0.6 kg/cm^2 (g) under normal operating condition, due to increase in helium temperature and swelling of heavy water. Under normal operating condition the total helium inventory in cover gas system is approximately 12.5 m^3, when calandria is 100% full. In calandria, during reactor operation, high neutron flux as well as the gamma radiation causes radiolysis of the moderator heavy water. The moderator D_2O breaks down into its constituent elements of deuterium and oxygen. As the moderator D_2O is circulated, these dissolved gases are released into the helium gas space and may eventually reach explosive concentrations. To avoid this, the helium is continuously circulated through recombination units containing 0.5% Palladium coated Alumina catalyst (3 mm dia × 3 mm long pellets) which causes the deuterium and oxygen gas to recombine into heavy water. In this way, the deuterium concentration in the helium is controlled below 4% by volume, which is well below the explosion limit.

The diagram below gives the simplified flowsheet of moderator system

During plant shut down condition, whenever Guaranteed Shutdown State is to be maintained, Gadolinium Nitrate is injected into the moderator system from Shut Down System # 2 (SDS # 2). Even during the unit start up, it is injected, if negative reactivity is to be added, as per reactor physics considerations. The Gadolinium nitrate has the tendency to precipitate as its hydroxide beyond 5.8 pH. Hence the pH is maintained between 5.0-5.5, by addition of nitric acid in moderator. During such conditions the specific conductivity of the moderator D_2O increases, resulting in the increased rate of radiolysis. This increases the deuterium concentration in the moderator cover gas system. When high concentration of D_2, comes in contact with oxygen of higher concentration, explosive mixture results.

Experimental

The explosion hazard is eliminated by keeping D_2 and O_2 levels within operating range. The rate of radiolysis and the rate at which the dissolved gases evolve from the moderator water are affected by a number of factors.

Power Level

The rate of radiolysis increases with increasing radiation. Thus, the higher the power level, the greater the rate at which radiolysis occurs. High conductivity or impurities (ie. nitric acid, resin fines, oils, etc.) in the

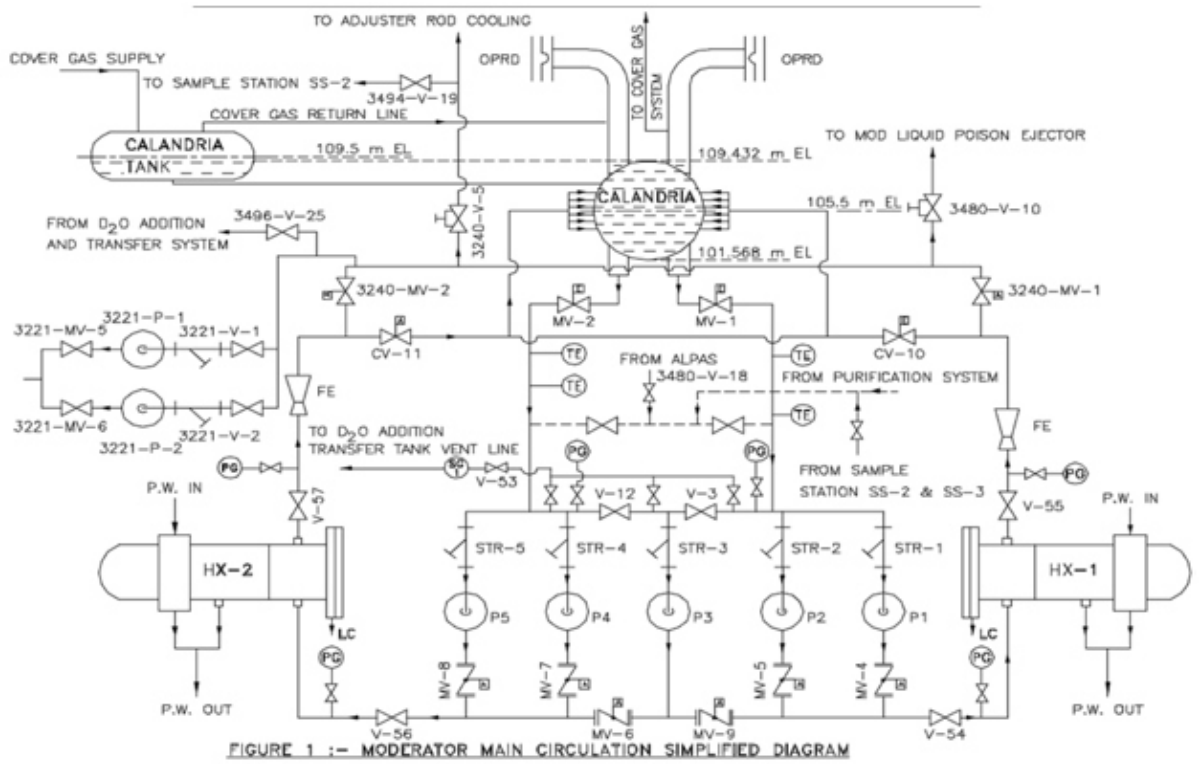


FIGURE 1 :- MODERATOR MAIN CIRCULATION SIMPLIFIED DIAGRAM

moderator D_2O will cause the increase in the radiolysis rate of D_2O, resulting in the evolution of deuterium and oxygen.

Temperature of Moderator

Once these gases are produced, the rate at which they come out of solution also depends on a number of other factors. As the temperature of the moderator increases, the ability of the moderator water to hold these dissolved gases reduces, i.e. solubility decreases. Hence, at higher temperatures the rate at which gases comes out of the water and enter the cover gas is greater than the rate at lower temperatures.

Cover Gas Pressure

As the cover gas pressure of the moderator decreases, the ability of the moderator water to hold the dissolved gases decreases. Again, the gas evolution rate increases as pressure in the cover gas is reduced (i.e. a similar effect can be seen in carbonated drinks, as the container is opened and depressurized, the gases come out of solution).

The level of Moderator

As the moderator level decreases, the D_2 and O_2 concentration in the cover gas increases. This effect is caused by the increased surface area between the moderator and the cover gas, from which the D_2 and O_2 can evolve from the moderator water to the cover gas.

The concentration of D_2 and O_2 in the Moderator

As the concentration of the gases dissolved in the moderator increase, the gases will attempt to reach a new equilibrium state with the cover gas. This will result in the D_2 and O_2 in the moderator evolving from the D_2O at a faster rate (as compared to a lower concentration of D_2 in the moderator) to reach the equilibrium state.

Cover Gas Circulation

All reactor states require the circulation of the cover gas. The reasons for the requirement of continuous circulation are:

High decay gamma fields exist in the core even during shutdowns. This leads to continuous radiolysis of moderator (hence· allowing D_2 and O_2 concentrations to build up). This can be further aggravated by moderator poisons (impurities) which cause a decrease in the natural recombination rate. This is why D_2 concentrations in the cover gas increase during a reactor outage (i.e. radiolysis exceeds the low rate of natural recombination). Continuous circulation also ensures that any samples taken from the cover gas are representative of the cover gas. The circulation also ensures that a flow is maintained to the recombination units, which will recombine the D_2 and O_2 back into D_2O.

Results

Effect of variation in Power Levels on the Deuterium Concentration during Normal Operation

The effect of variation in power level on the moderator cover gas concentration can be understood by correlation provided in the Table 1 below.

The Table 1 below gives the correlation of power levels and deuterium concentration.

Table-1

MONTH	RX POWER	Sp.Cond. s/cm			D_2 %V/V		
		MIN	MAX	AVG	MIN	MAX	AVG
Apr-09	60%	0.18	0.41	0.31	0.4	2.27	1.79
May-09	60%	0.18	0.70	0.34	0.74	2.50	2.03
OCT-09	70%	0.19	0.58	0.32	1.41	2.61	2.09
Mar-10	70%	0.20	0.58	0.33	0.92	2.62	1.87
May-11	82%	0.20	0.45	0.31	2.02	2.91	2.30

Table-2

MODERATOR SYSTEM CHEMISTRY AFTER SDS # 2 ACTUATION							
Unit # 3 Moderator System				Unit # 4 Moderator System			
The no of SDS # 2 actuation	pH	Sp.Cond. s/cm	Gadolinium mg/kg	The no of SDS # 2 actuation	pH	Sp.Cond. s/cm	Gadolinium mg/kg
1	5.12	30.3	16.5	1	5.02	50.7	20.00
2	5.08	41.50	17.45	2	4.09	32.8	11.15
3	5.09	38.20	16.54	3	5.00	42.00	16.94
4	4.95	36.10	14.54	4	4.98	40.10	16.81
5	5.09	41.40	18.45	5	5.03	25.50	12.04
6	5.17	42.70	17.72	6	5.18	31.80	13.16
7	4.90	41.60	17.81	7	4.97	33.00	16.21
8	4.92	40.30	15.69				

The Table-1 clearly indicates that, there is a notable increase in the deuterium concentration, with the increase in the power levels, when conductivity has been of the same order, during normal operation.

Effect of variation of Deuterium Concentration with Specific Conductivity during Shut Down

The Table 2 given below gives the list of SDS # 2 actuations that had taken place at TAPS # 3 & 4 during shutdowns.

Table 2 shows that, during all SDS # 2 actuations the specific conductivity was in the range of 30-50 s/cm, which is much higher than the normal operation levels as indicated in Table-1

Case Study-1

On 30/05/2011, TAPS # 4 reactor was manually shutdown in a planned manner, to carry out Reactor Building Leak Test (RBLT) and other planned jobs. As planned, the SDS # 2 was manually actuated. The moderator water conductivity reached a maximum of 45.6 S/cm during this period. (Please refer Table 3). This was very high compared to the previous two months values. This resulted in increase in deuterium concentration in cover gas due to increased radiolysis of moderator water.

Unlike the previous conditions in this case the SDS # 2 was actuated soon after the reactor was shutdown. The residual neutron flux was existing during this period. In addition to neutron flux, the specific conductivity was also high, owing to the injection of Gd and nitric acid. These two factors combined together, resulted in the increased rate of radiolysis, eventually increasing the rate of deuterium evolution in moderator covergas. During shutdown, the moderator system was depressurised and was in contact with the outside environment. This created a scenario where high concentration of oxygen can come in contact with deuterium, resulting in the formation of explosive mixture.

The data of deuterium concentration of June 2011 clearly shows that when the sp. conductivity increases the deuterium level also increases

Case Study-2

During recent the shut down of TAPS # 4 on 23rd April 2013, the deuterium levels were very low before shut down. Soon after the injection of 16ppm Gd in the moderator the conductivity increased with a proportional increase in the concentration of D_2. The observed values are tabulated in Table-4

Graph- 1

In the Case Study-2, the increase in the deuterium with the increase in the sp. conductivity has been observed as evident from the above Graph-1.

During TAPS # 4 shut down, SDS # 2 was injected in the moderator system. Consequently there was a rise

Table-3

	April 2011			May 2011			June 2011		
	Rx power	Sp . Cond s/cm	D_2% v/v	Rx power	Sp . Cond s/cm	D_2% v/v	Rx power	Sp . Cond s/cm	D_2% v/v
Average	82.%	0.39	2.28	81.%	0.31	2.30	S/D	23.55	0.35*
Minimum	81.%	0.25	0.89	80.%	0.20	2.02	S/D	0.29	<0.01*
Maximum	82.%	0.64	2.72	82.%	0.45	2.91	S/D	45.60	6.25

* - Helium purging was carried out continuously to avoid build up of D_2

Table-4

Date	Power Level	Sp.Cond. s/cm	Time of sampling	D_2% v/v	Remark
20-Apr-13	88%	0.34	12:05	0.83	
			17:25	0.87	
21-Apr-13	90%	0.33	11:00	0.85	
			19:35	0.92	
22-Apr-13	88%	0.32	10:40	0.94	
			19:10	0.96	
23-Apr-13	91%	0.38	10:30	0.90	
	S/D		20:30	1.74	
	S/D	33.00	22:00	2.77	Helium purging initiated
24-Apr-13	S/D	32.70	00:15	3.02	Purging continued
	S/D		02:10	2.14	Purging continued
	S/D		04:20	1.36	Purging continued
	S/D		06:30	1.36	Purging continued
	S/D		08:00	1.17	Purging continued
	S/D		09.00	1.26	Purging continued
24-Apr-13	S/D	31.40	10.30	1.09	Purging continued
			11.30	1.20	Purging continued
			13.30	0.93	Purging stopped

in the specific conductivity and also the concentration of deuterium. The purging was initiated and continued till the deuterium levels were normalised.

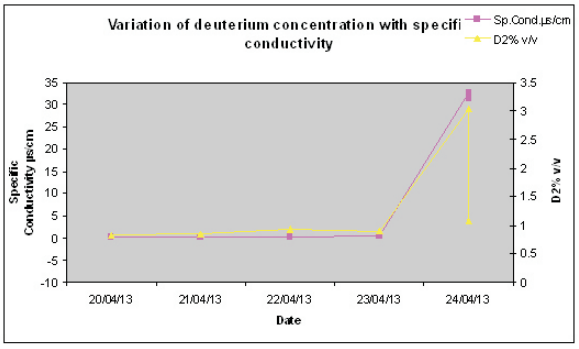
Case Study-3

In TAPS # 3 SDS # 2 was actuated on 28/09/2012. Prior to the actuation the moderator conductivity was in the range of 0.27- 0.29 s/cm. After the SDS # 2 actuation, in this case too there was sharp increase in the specific conductivity and also the deuterium concentration. The Table 5 gives the details of specific conductivity and D_2 concentration just before and after the actuation.

Graph-2 below explains how the deuterium concentration increased with the increase in specific conductivity.

Graph-2

The deuterium concentration was normalised by continuous purging of moderator cover gas with helium.



Such increase in deuterium concentration has been observed during several SDS # 2 actuations. Now when such increase in deuterium is noticed in shutdown, if there is a increase in oxygen concentration in the cover gas, this may give rise to formation of explosive mixture of oxygen & deuterium. Hence during shutdown, when cover gas is de-pressurised or when moderator system components are physically

Table-5

Date	Power Level	Time of sampling	Sp.Cond. s/cm	Time of covergas sampling	D_2% v/v	Remark
27-Sep-12	97.00%			01:30	2.40	
27-Sep-12		10:10	0.29	10:30	2.45	
				19:10	2.42	
28-Sep-12	97.00%	10:15	0.27	02:00	2.46	
				10:40	2.43	
28-Sep-12	S/D			17:45	3.71	Helium purging initiated
28-Sep-12	S/D	20:30	40.30	19:00	3.18	Purging continued
				20:10	2.78	Purging continued
	S/D			21:15	2.49	Purging continued
	S/D			22:35	2.1	Purging continued
29-Sep-12	S/D	3:00	39.60	00:00	1.95	

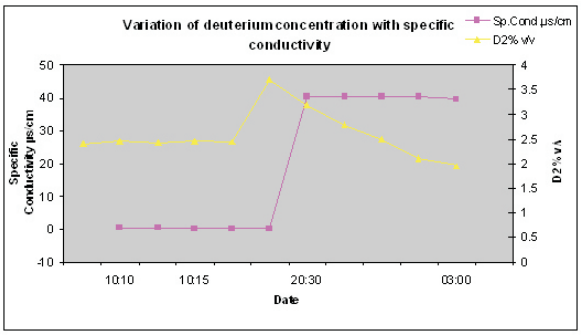
removed from the system, the oxygen ingress takes place. Therefore, the danger of explosion exists.

It is seen from the experience that the deuterium being lighter gets collected at the top most point of cover gas system, viz. OPRD. (Over Pressure Rupture Disc). Hence it is very important to collect the sample from OPRD, where maximum concentration of D_2 exists.

Conclusions

From the case studies presented in this paper it can be concluded that

1. The deuterium concentration in the covergas increases with increase in power levels
2. The deuterium concentration in the covergas increases with increase in specific conductivity.



This emphasises the need to monitor the deuterium concentration under all conditions of normal operation and shutdown of the reactor.



***Dr. S C. Dash**, M.Sc.,Ph.D, is Station Chemist at Tarapur Atomic Power Station # 3&4. He has set up state of art Chemistry Control Laboratory with latest and sophisticated instruments. The laboratory has received appreciation from AEC Chairman, CMD, IIT professors and BARC scientists. He was the first chemist, who commissioned the DM water plant and pioneer in outsourcing the Operation and Maintenance of DM water plant along with some of the activities of the lab. He has designed the Chlorine Dioxide plant and after its erection & commissioning by him, he is operating the same successfully. He is the Management representative for integrated management system. Because of his sincere effort TAPS# 3&4 could get the accredited certificated and could become the first station to get the Accredited IMS certificate at the first go itself. Considering his consistent high quality leadership and contribution he was awarded with NPCIL Special Contribution Award 2011. He is a WANO Tokyo centre lead reviewer in chemistry and carried out two WANO peer reviews in foreign countries.*

Effect of Crystal Structure of the Sorbent on the Sorption of Metal Ions

B.S. Tomar

Radioanalytical Chemistry Division, Bhabha Atomic Research Centre, Trombay, Mumbai 400085, India; E-mail: bstomar@barc.gov.in

Sorption of metal ions by the mineral oxides have been found to be influenced by the crystal structure of the mineral oxide. Investigation of the molecular speciation of the sorbed species helps in understanding the mechanistic aspects of the sorption process and thereby predict the migration of the radionuclide in the geosphere. In the present paper, the literature review of the subject has been carried out followed by some data on Eu(III) sorption by anatase and rutile in absence and presence of citric acid will be presented.

Introduction

Colloidal sized inorganic as well as organic particles present in the ground water have been found to play an important role in the migration of radionuclides in the aquatic environment. Experimental studies are being carried out to investigate the mechanism of metal ion sorption at the solid-water interface [1]. Application of spectroscopic techniques, such as, time resolved laser fluorescence spectroscopy (TRLFS), Extended X-ray absorption fine structure (EXAFS), X-ray near edge absorption spectroscopy (XANES), Attenuated total reflection Fourier transform infra red spectroscopy (ATR-FTIR), etc., reveals molecular level details of the sorbed species, and thereby helps in constraining conclusions drawn from batch level laboratory and modeling exercises. These studies produce a consistent thermodynamic description for the sorption of radioactive contaminants, which is required for predictive transport modeling of contaminants in the geosphere.

One of the interesting aspects of these studies have been to investigate if the sorption behavior of the metal ion is dependent upon the crystal structure of the mineral oxides. Den Auwer et al. carried ouit grazing incidence EXAFS of uranyl ion sorbed on single crystals of rutile (110) and (001) and observed outer sphere uranyl complex formed on (001) plane in contrast to the inner sphere complex formed on (110) plane [2]. Tan et al. investigated sorption of Eu(III) on titania (anatase and rutile, having dominant planes (100) and (110), respectively) using batch experiment, XPS and EXAFS and found difference in the Eu-O coordination number for the two surfaces in presence of humic acid [3].

In our laboratory, sorption of Eu(III) by pure anatase and rutile revealed significant difference in the sorption edge in the two cases as shown in Fig. 1 [4]. Surface complexation modeling of the sorption data showed monodentate as the predominant binding mode of Eu(III) on anatase while on rutile Eu(III) binds preferentially in bidentate binding [5]. This observation is congruent with the formation of multidentate species of Nd(III) on rutile surface observed by Zhang et al. [6]. TRFS measurements showed higher fluorescence life

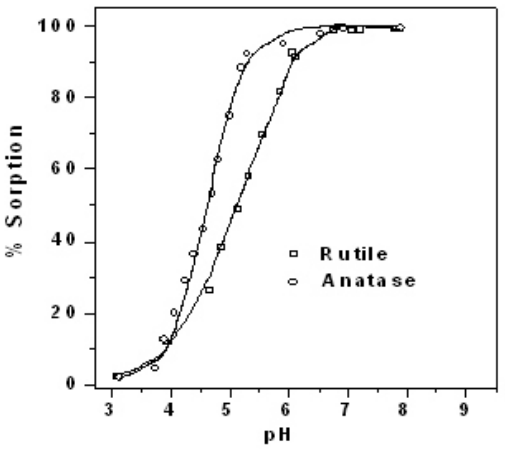


Fig. 1 Sorption of Eu(III) by anatase and rutile at varying pH.

time of the species sorbed onto rutile than that in the case of anatase (Fig. 2.) The life time data are shown in Table 1.

Table-1: Fluorescence data of Eu(III) sorbed onto anatase and rutile

Phase	Asymmetry Ratio	Average Life time pH (s)
Anatase	3.31	210 ± 2
Rutile	2.53	240 ± 2

Organic molecule sorption on different crystalline phases of titania has shown similar difference. In the adsorption of oxalate on anatase (001) and rutile (110) surfaces in aqueous systems, Mendive et al. [7] observed differences between surface complexes on anatase and rutile mainly in the denticity type. In the case of rutile the most stable species consist of bidentate surface complexes while the stability order is opposite (i.e., monodentate) for the anatase surface. Explaining the result on the basis of quantum calculation, the authors conclude the inclusion of surface solvation as crucial for the determination of type of denticity and structure of adsorbed complexes. We have also observed different zeta potential of the anatase and

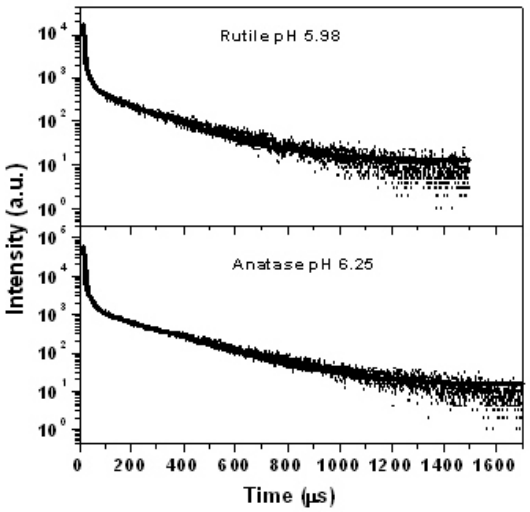


Fig. 2 Fluorescence life time spectra of Eu(III) sorbed onto anatase and rutile

rutile suspensions (point of zero charge: 6.5 and 5.3, respectively) indicating different surface solvation characteristics [5]. Sorption of citrate by anatase and rutile has also been measured by ion chromatography technique. Attempts were also made to investigate the structure of the soprbed species by ATR-FTIR spectroscopy.

In the case of termary metal ion, organic molecule, mineral oxide system, each component may interact with mineral oxide surface. Batch sorption study of Eu(III) by titania in absence as well presence of citrate (with different addition orders of metal ion and ligand) have showed varying sorption behavior in the case of two phases (anatase and rutile). Delineation of structural differences between species formed in dilute systems, such as, sorption of Eu(III) by anatase and rutile, requires stable intense X-ray source like synchrotron facility [8].

Thus the detailed investigations, such as TRLFS, EXAFS and theoretical calculations of surface species are required to understand the reasons behind the differences in the sorption characteristics of the different crystalline phases of the mineral oxides.

Acknowledgements

This work was carried out in association with S.V. Godbole, D. Bhattacharya, S. Jeyakumar, V.V. Raut, Sumit Kumar, Aishwarya Kar and Sharayu Kasar and I thank them for their contribution.

References

[1] H. Geckeis, J. Lutzenkirchen, R. Polly, Th. Rabung, M. Schmidt, Chem. Rev. dx.doi.org/ 10.1021/ cr300370h.

[2] C. D. Auwer, R. Drot, E. Simoni, S. D. Conradson, M. Gaillhanou, J. Mustre de Leon, New J. Chem., 27 (2003) 648.

[3] X. Tan, W. Fan , X. Wang, B. Grambow, Environ. Sci. Technol. 43 (2009) 3115.

[4] Sharayu Kasar, Sumit Kumar, Aishwarya Kar and B.S.Tomar, J. Radioanalyt. Nucl. Chem. 294 (2012) 103.

[5] S. Kasar, S. Kumar, A. S. Kar, S.V. Godbole, B.S. Tomar, Coll. Surf. A. 434 (2013) 72.

[6] Z. Zhang, P. Fenter, Sorption of Nd(III) on rutile-water interface, Langmuir, 20 (2004) 4954.

[7] C. B. Mendive, Th. Bredow, A. Feldhoff, M. A. Blesa, D. Bahnemann, Phys. Chem. Chem. Phys. 11 (2009) 1794.

[8] S. Kumar, A. S. Kar, B. S. Tomar, and D. Bhattacharya, Polyhedron 33 (2012) 33.



Dr. B.S.Tomar *did his M.Sc. in Chemistry from Garhwal University in 1979. He joined Radiochemistry Division in 1982 after graduating from the 25th batch of BARC Training School. He completed his PhD, on Nuclear and Radiochemical studies on fission of actinides, in 1990 from Mumbai University. He worked in Nuclear and Radiochemistry in general and Nuclear Fission, Nuclear Reactions, Perturbed Angular Correlation and Ion beam analysis in particular. His current areas of interest include, Actinide Speciation and Radioanalytical Techniques for study of actinides and fission products. He served as a visiting Professor at Technical University Delft, The Netherlands, during 2007-2008. Currently he is Head, Radio-analytical Chemistry Division at BARC as well as Dean Academic (BARC), Chemical Sciences, of Homi Bhabha National Institute, DAE. He has more than 130 publications in international journals.*

Biosorption study of Radiotoxic Nuclide and toxic Heavy Metals using Green Adsorbent

Hemlata K. Bagla

Department of Nuclear and Radiochemistry, Kishinchand Chellaram College, Churchgate, Mumbai 400 020, India; E-mail: hemabagla@gmail.com

Our research scientifically illuminates the pioneering and successful application of the ancient Indian epitome of energy, Dry Cow Dung Powder, DCP, a combo humiresin, in its naïve 'as it is form' for the bioremediation of toxic pollutants. The potential of DCP to sequester toxic heavy metal ions such as Cr(III), Cr(VI). Cd(II), Hg(II) and radionuclide ^{90}Sr(II) has been successfully demonstrated, employing tracer technique. The Batch equilibration method and all the important parameters such as pH, dose of sorbent, metal ion concentration, contact time, agitation speed, temperature and interference of different salts have been studied and optimized. The study on thermodynamic, kinetic and isotherm modeling of biosorption indicates that it is feasible, eco-friendly and efficient process to employ DCP for the removal of metal ions from aqueous medium. Spectroscopic analysis by FTIR and EDAX effectively explain the mechanism involved in the biosorption by DCP. The adsorption capacity and the pseudo-second order rate constant were also obtained by regression analysis. Thus DCP proves to be Eco-friendly resin for the removal of these toxic pollutants such as Cr(III), Cr(VI), Cd(II), Hg(II) and ^{90}Sr(II) from aqueous medium.

Introduction

In the field of remediation of heavy metal pollutant as well radionuclide, some of the well established processes such as Chemical precipitation, Membrane process, Liquid extraction and Ion exchange [1] have been applied as a tool for the removal of these metal ions. These all methods are not considered to be greener due to some of their shortcomings such as incomplete metal ion removal, high requirement of energy and reagents, generation of toxic sludge or other waste materials which in turn require treatments for their cautious disposal. Eventually it adds on to the cost, time and feasibility of the entire procedure.

The greener and cleaner approach of biosorption is a sure solution to this situation. Bio-sorption phenomenon is acquiring strong footage due to its mechanism based on non-directed physicochemical interactions that occur between metal species and dead biomass. Biosorption deals with both living biomass as well as non-living aggregates of biomaterial. But biosorption by dead biomass is often faster [2], since only passive cell wall based binding transport, into the cell takes place.

DCP, is naturally available bio-organic, complex, polymorphic humified fecal matter of cow and is enriched with minerals, carbohydrates, fats, proteins, bile pigments, aliphatic - aromatic species such as 'Humic acid' (HA), Fulvic acid, Ulmic acid, etc. It also possesses certain dead biomass such as Aerobic heterotrophic bacteria viz. as Acinetobacter sp. and petroleum utilizing bacteria such as Pseudomonas species [3]. The inactive non-living biomass has an inherent property to bind and concentrate heavy metals from aqueous surrounding which facilitates faster as well as easier adsorption. Literature survey for the biosorption of heavy metals on the natural adsorbent material reveals that the adsorbents in current utility is from Biotic and Abiotic as well as from Living and Non-living matrices. But these naturally available materials require some degree of physical and chemical enhancement so as to optimize as an adsorbent, which add on to the economy of entire adsorption process.

In the present study DCP is employed without any pre or post treatment. Being freely and easily available it has an edge over other processed natural adsorbent considering their cost, time and energy efficiency. We have employed radiotracer technique for the quantification of results. In comparison to classical approach of analysis, it offers some unique advantages such as, high sensitivity, non-destructive pattern, freedom from reagent blank etc. [4].

Materials and Methods

Adsorbent

DCP (100 mesh) was provided by Keshav Shrushti, Research centre on Cow product (Thane, India) and due precautions were taken to avoid any contaminations. The integrity of DCP before and after the sorption was studied by measuring the mesh size and was found to be same indicating during biosorption process there were no physical attrition of resin.

Characterization of the DCP

Cow dung powder was dried properly before its utilization, so as to prevent its oxidation by acid due to presence of mixture of alcohols if any. The absence of alcohol is also supported by FTIR analysis of DCP, which is devoid of any characteristic band of alcohol.

The DCP has been characterized using XRF technology for its quantitative as well as qualitative elemental composition. The complete elemental composition, complimentary to XRF technique, C, H,

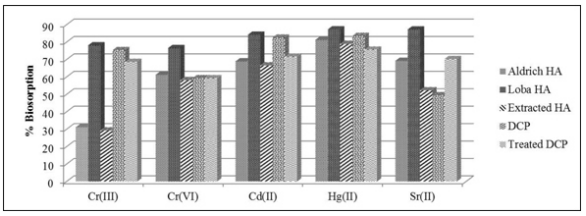


Fig. 1 Biosorption profile of metal ions on various humiresins

N, S, (O), has also been carried out. FTIR analysis proved functionality of DCP as an adsorbent due to the presence of various adsorptive functional groups such as -COOH, -OH, -NH_2, etc. The SEM pattern of DCP clearly revealed the surface texture and porosity of DCP. Many pores and small openings were been found on the surfaces which were responsible for the easier diffusion during adsorption process.

Batch Equilibration Mode

A comparative batch equilibration biosorptive assay has been carried out employing radiotracer technique for uptake of five different metal ions such as Cr(III), Cr(VI), Cd(II), Hg(II) & Sr(II) employing their corresponding radiotracers ^{51}Cr, ^{115m}Cd, ^{203}Hg and ^{90}Sr, which were procured from Board of Radiation & Isotope Technology (BRIT), Mumbai, India.

The effect of different experimental parameters such as pH (from 1-10), metal ion concentration (0.5-20 mg/mL), contact time (0-30 min), agitation speed (0-5000 rpm), amount of adsorbent (50-1000 mg), temperature (273-373 K), adsorption capacity and interference of different salts was studied so as to optimize the parameters for developing efficient adsorption process. Kinetic, thermodynamic and isotherm studies so as to optimize the system for it to be feasible for real application.

Results and Discussion

This study asserts that, 100 mg of DCP removes Cr(III), Cd(II), Hg(II) and Sr(II) at pH 5 to 70% – 80%. Whereas 60% of Cr(VI) is sequestered at pH 1 with 100 mg of DCP. The successful removal of radiotoxic ^{90}Sr from aqueous medium by DCP, has indeed strengthen the scope of remediation of ^{90}Sr from reactor and reprocessing waste. Also, we are constantly progressing in desorption and separation of these radionuclide from DCP with a view of reprocessing the same.

The thermodynamic, kinetic and isotherm modeling of biosorption affirms that biosorption on DCP is feasible, eco-friendly and efficient process to employ DCP for the removal of metal ions from aqueous medium. The negative value of free energy change and enthalpy confirms the feasibility and spontaneous as well as exothermic nature of biosorption process of all the metal ions on DCP. The positive value of entropy change suggests the increase in the randomness at the solid/liquid interface reflecting affinity of DCP for the metal ions.

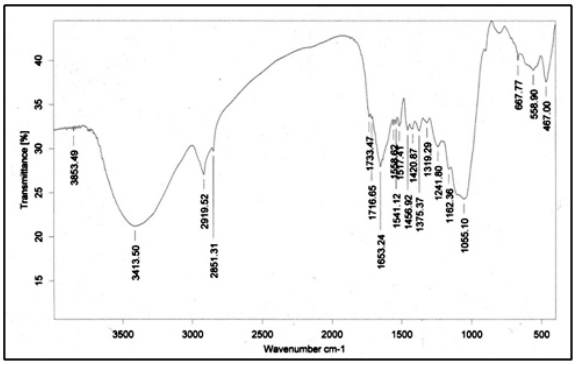


Fig. 2 FTIR Spectra of Dry Cow Dung Powder

The mechanism of biosorption on DCP is well perceived by Desorption and Kinetic studies. It confirms the chemisorption mechanism to be the best fitting, which in turn is supported by meager quantity of back extraction or stripping of metal ions from spent DCP. The best fit of Pseudo-second order Lagergren model of kinetics also supports the chemisorption mechanism. Spectroscopic analysis of DCP before and after biosorption by FTIR and EDAX, effectively explain the mode of chemisorption.

The efficiency of DCP is also compared with 5 different humi resins i.e. Aldrich HA (Germany), Loba HA (India), DCP, Extracted HA from DCP [5] and DCP after removal of HA as described in Fig 1. Results of this study depicts that DCP can effectively remove the different metal ions in considerable manner and is indicative of process feasibility at room temperature, on comparing with its natural as well synthetic contenders, boosting Green Chemistry principle of reaping maximum by minimum.

The HSAB nature of individual ion also contributes in the biosorption process. Our spectral studies indicate DCP being heterogeneous bioresin contains both hard functional group or ligands containing oxygen and soft natured functional groups or ligands containing nitrogen and sulphur. As a rule, presence of HA increases the higher uptake of divalent metal ions and same is practically observed.

Conclusions

Thus DCP is eco-friendly, novel and economically feasible bioresin having great potential in applications in the field of water decontamination, industrial water treatment and in abatement of water pollution. Thus the utility of DCP will surely contribute to convert waste into wealth, refuse into resource and trash into cash, the ultimate aim of waste management strategy. It's rightly said that "The nation which destroys its environment, destroys itself!", hence we need to pursue instant remedies to mitigate our self destruction because healthy environment is the only life line for Survival."

Acknowledgement

We are also thankful to Dr. Raju Apte, Head of Gaushala, Keshav Shrushti, Thane, for providing Dry cow dung powder.

References

[1] Luo H, Dai S, Bonnesen P, Anal. Chem., 76(10) (2004) 2773.

[2] Yu L, Chakraboty S, Basu J, Separ. Purif. Tech., 50(3) 3(2006) 36.

[3] S.B.Akinde, O.Obire, Aerobic heterotrophic bacteria and petroleum-utilising bacteria from cow dung and poultry manure, World J. Microbio & Biotech., 24(9), (2008) 1999.

[4] H.Lieser, Nuclear and Radiochemistry: Fundamentals and Applications, 2nd edition, WILEY-VCH, Germany, (2001).

[5] N. Barot and H. Bagla, European Geosciences Union, Vol. 15, EGU2013-2598, EGU General Assembly, Vienna, Austria, (2013).



Dr. Hemlata Bagla *is currently the vice-Principal at K.C. College, one of the premier institutions of Mumbai. She obtained her Masters in Sciences specializing in Organic chemistry and her Doctorate in Inorganic Chemistry specializing in Radiochemistry from the Institute of Science Mumbai. She is an associate Professor in Chemistry and Head of the department of Nuclear & Radiochemistry. In her twenty- two years of academic experience, she has been a research guide for Masters and PhD students for the last 15 years. Her research interests lie in different thrust areas of Chemical and Biomedical sciences. She has published more than fifty research papers in national and international journals of repute including six being part of NASA's Astrophysical database. She is the recipient of many prestigious awards for her contribution in scientific research, including the Young Associate Award by Maharashtra Academy of Sciences, Dr. Tarun Datta Memorial Award instituted by Indian Association of Nuclear Chemists and Allied Scientists; Young Scientist Award by Indian Council of Chemists and K.C. RATNA award for her outstanding contribution to the development of the Institution and very recently Indo Global Education Award for Excellence in Research by Indus Foundation. She holds many key positions in various scientific associations and professional bodies, including being the Vice-president of Indian Chemical Society (Mumbai Branch).*

Development of Particle Induced Gamma-ray Emission methods for low Z Elements and Applications to Materials important for Nuclear Technology

R. Acharya

Radiochemistry Division, Bhabha Atomic Research Centre, Trombay, Mumbai 400085, India;
E-mail: racharya@barc.gov.in)

Particle induced gamma-ray emission (PIGE) methods using proton beams from tandem accelerators have been standardized for quantification of low Z elements from Li to Ti including B, C, N, O, F Si and Al. Current normalization of count rate was carried out by both Rutherford Backscattering Spectrometry (RBS) and/or in situ method. The PIGE methods have been applied to (i) barium borosilicate glass for its composition and F content, (ii) Lithium or titanium based ceramics including lithium titanate for simultaneous determination of Li, Ti and O and (iii) Boron based compounds including boron carbide for determination of concentration of total boron and its isotopic composition. Details of methods and applications of PIGE are briefly summarized in this article.

Introduction

Ion beam analysis (IBA) is one of the modern analytical techniques for total compositional analysis of materials as well as depth profiling of elements in the near-surface of solids. IBA methods namely particle induced X-ray emission (PIXE), particle induced gamma-ray emission (PIGE), Rutherford backscattering (RBS), elastic recoil detection analysis (ERDA) and nuclear reaction analysis (NRA) are well established and capable of quantification of almost all elements. PIGE is an isotope specific nuclear analytical technique capable of determining low Z elements (Li to even Zn, depending on energy of proton used) and it is complementary to PIXE, XRF and NAA. It involves measurement of prompt gamma rays from nuclear reactions like (p, p'), (p,), (p, n) and (p,) for determination of concentration of an isotope thus element in a sample. The non-destructive nature of PIGE helps for analyzing many complex matrix samples like glass and ceramics as well as sample that are difficult for chemical dissolution. Radiochemistry Division (RCD), BARC has set up PIGE facilities at FOTIA, BARC (Fig 1), IOP, Bhubaneswar (Fig. 2) and BARC-TIFR (Fig. 3). Present paper describes the developmental work in PIGE and its unique applications in materials of glass, lithium based ceramics and boron based compounds, where wet chemical/conventional methods face difficulties. These materials are important in nuclear technology. The elements of interest studied are Li, B, C, N,O,F, Na, Mg, Al, Si, S and Ti. In addition to total elemental concentrations, PIGE method has been standardized for isotopic composition of B and Li.

Experimental

Elemental standards as well as samples in pellet forms (in cellulose or graphite) were irradiated using low energy proton beam (2-4 MeV) at FOTIA and IOP and recently with high energy proton beam (8 MeV) at TIFR with 5-50 nA current in order to get higher gamma-ray yield and improved sensitivity of low Z elements. Prompt gamma rays were measured using HPGe detector based high resolution spectrometers coupled to 8 k MCA. The gamma rays of interest of some elements are shown in Table 1. The concentration of element of interest was calculated by relative method.



Fig. 1 PIGE setup at FOTIA, BARC



Fig. 2 PIGE set-up at IOP, Bhubaneswar

Table-1: Nuclear reactions and gamma-ray energies of some elements used for PIGE work

Element	Reaction	Energy (keV)
Li	^{6}Li(p, n)^{7}Be ^{7}Li(p, p')^{7}Li	429 478
B	^{10}B(p,)^{7}Be ^{10}B(p, p')^{10}B ^{11}B(p, p')^{11}B	429 718 2125
C	^{12}C (p, p') ^{12}C	4439
N	^{14}N (p, p') ^{14}N	2313
O	^{16}O (p, p') ^{16}O	6129
F	^{19}F(p, p')^{19}F	197
Na	^{23}Na(p, p')^{23}Na	440
Al	^{27}Al(p, p')^{27}Al	844, 1014
Si	^{28}Si(p, p')^{28}Si	1273, 1779
Ti	^{48}Ti(p, p')^{48}Ti	983

Since PIGE is an on-line technique, sample and standards are measured separately and thus current monitoring or normalization is important. Two approaches were followed as given below.

(i) RBS Approach: Backscattered ions from thin foils of high Z element Au was placed just before the sample and back scattered proton counts were measured using a Si based surface barrier detector kept at a fixed backward angle with respect to the ion beam. The gamma-ray count rates of the isotope of interest are normalized by the RBS count rate of protons.

(ii) In situ Approach: An element that is not present in the sample and has good sensitivity by PIGE technique (Li or F), is added externally or kept in front of sample (i.e., Al) for in situ current normalization The gamma-ray counts from the isotope of element of interest are normalized by sensitivity of in situ current normalizing element.

Results and discussions

The PIGE spectra of borosilicate glass, lithium titanate and B_4C are shown in Figs. 4-6, respectively. We have used in situ current normalized PIGE method in addition to current RBS approach using thin Au foil. The PIGE method has been successfully applied for quantification of (i) Fluorine in borosilicate glass matrix [1], (ii) Simultaneous quantification of low Z elements in borosilicate glass [2], (iii) Li in lithium based ceramic materials like lithium doped neodymium dititanate [3] and Lithium titanate samples (prepared by sol-gel route) [4,5], (iv) Total boron and boron isotopic composition in boron compounds and boron carbide, (v) Isotopic compositional analysis of B (^{10}B and ^{11}B) and applications to boron carbide and (vi) Soil samples, clay ceramics (archaeological samples) and RMs were analysed.



Fig. 3 PIGE set-up at BARC-TIFR pelletron facility

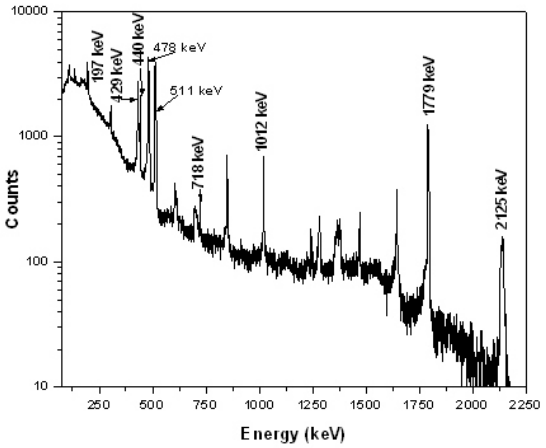


Fig. 4 PIGE spectrum of borosilicate glass sample (Li as in situ current normalizer)

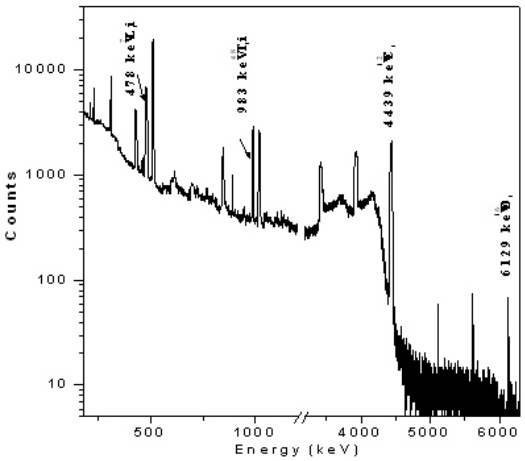


Fig. 5 PIGE spectrum of lithium titanate using 8 MeV proton beam showing Li, Ti and O peaks

Use of high energy proton beam (8 MeV) atTIFR helped us to determine Li, Ti and O simultaneously, which was not possible by using low energy proton (4 MeV) at FOTIA. The thick target gamma ray yield of many isotopes of elements in PIGE are one to two order high from 4 MeV to 8 MeV proton beam, indicating high sensitivity of PIGE for low Z element with a capability of extending its application from S to Zn, in addition to Li to P by low energy proton beam.

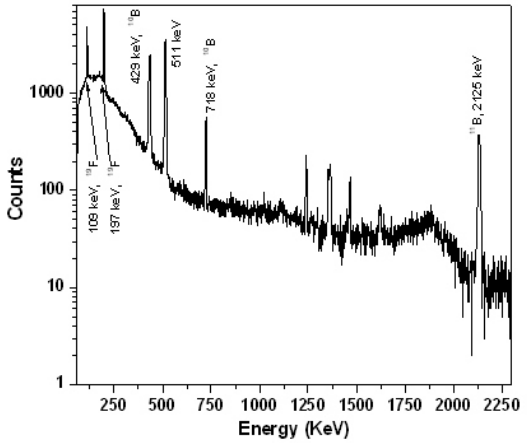


Fig. 6 PIGE spectrum of boron carbide (F as in situ current normalizer)

Future Prospects

In situ current normalized PIGE method is a new approach, which avoids using another experimental set up for RBS. For samples like wax and Pb-Li, mixing of external standard is difficult and here thin aluminium helps for current normalization. . Determination of Be, Li, B and other elements in different matrices (non-powder samples) is being pursued using Al as the in situ current monitor. Isotopic composition analysis of B has been optimized and applied and Li (^{6}Li/^{7}Li) has been standardized. A dedicated external PIXE/PIGE facility is being set up by RCD at FOTIA in addition to present facility. PIGE can be used for simultaneous quantification of Li, Al and O in lithium aluminate and Li, Si and O in lithium silicate and quantification of C, N, O, P, S and Cl in various samples and Be in BeO for chemical quality control.

Acknowledgements

Author thanks all co-workers, collaborators and staff members of FOTIA, IOP and TIFR.

References

[1] S Chhillar, R. Acharya et.al J. Radioanal. Nucl. Chem. 294 (2012) 115.

[2] S Chhillar, R. Acharya et.al., Proc. DAE-BRNS Eleventh biennial symposium on Nuclear and Radiochemistry (NUCAR 2013), Jabalpur.

[3] S Chhillar, R. Acharya et.al. J. Radioanal. Nucl. Chem. 293 (2012) 437.

[4] S Chhillar, R. Acharya et.al, J. Radioanal. Nucl. Chem. 298 (2013) 597.

[5] Sumit Chhillar, R. Acharya et.al, DAE-BRNS Fifth Symposium on Nuclear Analytical Chemistry (NAC-V), 2014, BARC, Mumbai



Dr. Raghunath Acharya *joined Radiochemistry Division, BARC in 1994 and since then he is engaged in R&D work on Nuclear Analytical Chemistry. He has contributed significantly towards k_0 based NAA and prompt gamma-ray NAA (PGNAA) work for multielemental determinations using reactor neutrons and high resolution gamma ray spectrometry. He is instrumental in developing internal monostandard NAA (IM-NAA) method for small and large size sample analysis and applying it for standard-less compositional analysis of nuclear structural materials. He is also engaged in research work trace element speciation studies. Recently, he is working on ion beam analysis (IBA) and standardized an in situ current normalized particle induced gamma ray emission (PIGE) method using proton beam for low Z elements and applied to materials important for nuclear technology. He has 97 journal publications and more than 175 conference presentations to his credit. He received Ph.D. degree in Chemistry from Mumbai University in 2000. He did his postdoctoral studies during 2000-2002 at Dalhousie University, Canada. He is a faculty member and PhD Guide in Homi Bhabha National Institute (HBNI), DAE. He is an elected member of k_0-International Scientific Committee (k_0-ISC) and International Committee on Activation (ICAA). For his significant contributions in Nuclear Analytical Chemistry, Dr. Acharya was awarded Dr. Tarun Datta Memorial Award of IANCAS for the year 2003, Young Scientist Award 2008 (YSA2008) of ICAA and Scientific and Technical Excellence Award of DAE for the year 2009.*

Analysis of Mixture Samples of Uranium Dioxide and Boron Compounds by using Thermal Neutron Prompt Gamma Activation Analysis

G.M. Sun[1], E.J. Lee[1], Hani Baek[1], Y.W. Lee[2], G.S. Kim[2], J.H. Yang[2]

1. *Neutron Utilization Technology Division, Korea Atomic Research Institute, Daejeon 305-353, Korea; E-mail: gmsun@kaeri.re.kr*
2. *Light Water Reactor Technology Division, Korea Atomic Research Institute, Daejeon 305-353, Korea*

The uranium dioxide powder samples were prepared by crushing the fuel pellets and then mixed with adjuvant compounds to improve the combustion characteristics of the nuclear fuel. First adjuvant compound is boron nitride and second adjuvant is hafnium diboride or manganese oxide. The elemental content of the mixture sample was analyzed by thermal neutron prompt gamma activation analysis facility at HANARO research reactor.

Introduction

Uranium dioxide or urania (UO_2) is widely used as fuel for nuclear power plants and its mixture with plutonium oxide is also used in the form of MOX fuel. In order to improve the combustion characteristics, strong absorbers such as Gd, B, Hf and so on are uniformly coated on the fuel pellets and sometimes homogeneously mixed with the powder of uranium dioxide. The contents of the strong absorbers must be evaluated and measured. The prompt gamma activation analysis is one of the most applicable techniques for it. In this study, the elemental content of the strong absorbers mixed with uranium dioxide powder is measured at the thermal neutron-prompt gamma activation analysis (TN-PGAA) facility at the HANARO research reactor.

Experimental

Homogeneous mixture samples of the uranium dioxide and boron compound of UO_2-BN, UO_2-BN-MnO, UO_2-HfB_2, UO_2-HfB_2-MnO were prepared. Table 1 shows the sample form and chemical compositions of the samples and expected elemental contents of B, Hf, Mn relative to the uranium dioxide. UO_2 powder is obtained by crushing the fuel pellets then mixed with adjuvant compounds to improve the combustion characteristics of the nuclear fuel. First adjuvant compound is boron nitride or hafnium diboride and second adjuvant is manganese oxide. The mixtures were annealed in the oven for two or four hours. Weights of B, Hf and Mn are given relative to those of UO_2. The elemental quantification of the prepared samples was carried out at the TN-PGAA (also called SNU-KAERI PGAA) facility at the HANARO research reactor [1]. The facility is located on the ST1 horizontal beam line and its beam characteristics adopting vertically diffracted beam from the horizontal beam line is unique. Fig. 1 shows typical prompt gamma spectrum and analysis windows of HYPERGAM code [2], which was developed by Seoul National University based on the HYPERMET routine [3]. And the Doppler-broadened boron peak with 478 keV was analyzed by DBPA routine [4], which is included in the HYPERGAM code.

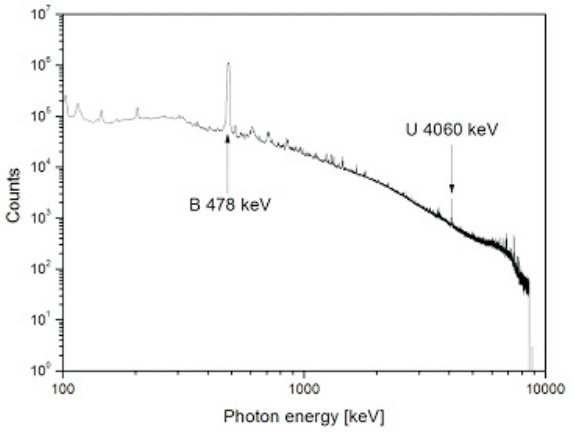


Fig. 1 Typical prompt gamma spectrum for the mixture sample of the uranium dioxide and boron compounds

Results and Discussion

Addition of first adjuvant compounds of boron nitride to the uranium dioxide is expected to improve the combustion characteristics of the nuclear fuel. But the boron nitride is volatile from the mixture during the annealing as shown in Fig. 2. And it is controllable by adding second adjuvant of MnO as shown in Fig. 3. Loss of boron becomes lower due to addition of MnO. More figures and tables will be shown in the presentation and full size paper.

Conclusions

To improve the combustion characteristics of the uranium dioxide fuel, borated compounds of BN or HfB_2 were homogeneously mixed as first adjuvant and annealed. But the boron is likely to loss during processing and shows lower quantity than expected. The second adjuvant of MnO reduced the loss of boron.

Table-1: Sample form and chemical compositions of the samples and measured elemental content relative to the uranium dioxide

No.	Sample ID	Sample Form	Chemical Composition	Expected elemental content [g/mg (UO_2)]			Annealing condition
				B	Hf	Mn	
1	UO_2-1	Crushed pellet	UO_2	-	-	-	1100C, 2h
2	UB1	Crushed pellet	UO_2-0.1wt%BN	0.440	-	-	1100C, 2h
3	UB2	Crushed pellet	UO_2-0.2wt%BN	0.880	-	-	1100C, 2h
4	UB3	Crushed pellet	UO_2-0.5wt%BN	2.200	-	-	1100C, 2h
5	UB4	Crushed pellet	UO_2-1.0wt%BN	4.400	-	-	1100C, 2h
6	UBM1	Crushed pellet	UO_2-0.1wt%BN-0.2wt%MnO	0.440	-	1.548	1100C, 2h
7	UBM2	Crushed pellet	UO_2-0.2wt%BN-0.2wt%MnO	0.880	-	1.548	1100C, 2h
8	UBM3	Crushed pellet	UO_2-0.5wt%BN-0.2wt%MnO	2.200	-	1.548	1100C, 2h
9	UBM4	Crushed pellet	UO_2-1.0wt%BN-0.2wt%MnO	4.400	-	1.548	1100C, 2h
10	UO2-2	Crushed pellet	UO_2	-	-	-	1100C, 4h
11	UH1	Crushed pellet	UO_2-0.1wt%HfB2	0.110	0.890	-	1100C, 4h
12	UH2	Crushed pellet	UO_2-0.2wt%HfB2	0.220	1.780	-	1100C, 4h
13	UH3	Crushed pellet	UO_2-0.5wt%HfB2	0.550	4.450	-	1100C, 4h
14	UH4	Crushed pellet	UO_2-1.0wt%HfB2	1.100	8.900	-	1100C, 4h
15	UHM1	Crushed pellet	UO_2-0.1wt%HfB2-0.2wt%MnO	0.110	0.890	1.548	1100C, 4h
16	UHM2	Crushed pellet	UO_2-0.2wt%HfB2-0.2wt%MnO	0.220	1.780	1.548	1100C, 4h
17	UHM3	Crushed pellet	UO_2-0.5wt%HfB2-0.2wt%MnO	0.550	4.450	1.548	1100C, 4h
18	UHM4	Crushed pellet	UO_2-1.0wt%HfB2-0.2wt%MnO	1.100	8.900	1.548	1100C, 4h

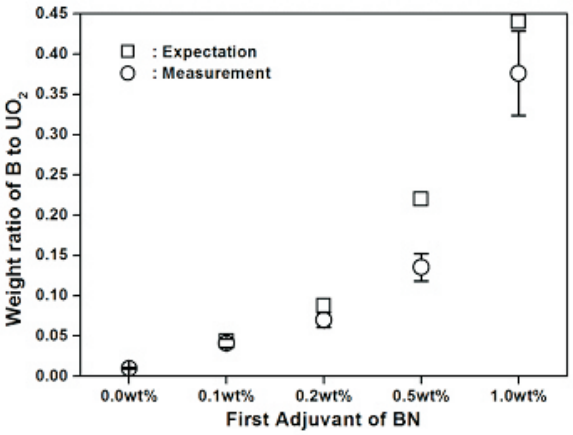


Fig. 2 Weight ratio of B to UO_2 according to the atomic weight fraction of first adjuvant of BN

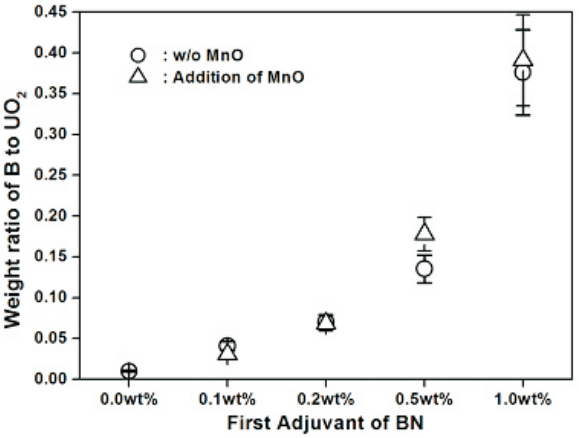


Fig. 3 Weight ratio of B to UO_2 according to the atomic weight fraction of first adjuvant of BN w/o and with a second adjuvant of MnO

The uranium and boron were quantified by using a thermal neutron prompt gamma activation analysis.

References

[1] S.H. Byun, G.M. Sun and H.D. Choi, Nucl. Instr. and Meth., 487 (2002) 521

[2] C.S. Park, H.D. Choi, G.M. Sun and J.H. Whang, Prog. in Nucl. Energ., 50 (2008) 389.

[3] G.W. Phillips and K.W. Marlow, Nucl. Instr. and Meth., 137 (1976) 525.

[4] H.D. Choi, N.S. Jung and B.G. Park, Nucl. Eng. Technol., 41 (2009) 113.

Peptide Receptor Radionuclide Therapy with ^{177}Lu-DOTA-TATE: From Laboratory to Clinics in India

Tapas Das

Isotope Applications and Radiopharmaceuticals Division, Bhabha Atomic Research Centre, Trombay, Mumbai 400085, India; E-mail: tdas@barc.gov.in

Peptide receptor radionuclide therapy (PRRNT) employing ^{177}Lu-DOTA-TATE is the only viable treatment modality for the patients suffering from inoperable and disseminated neuroendocrine cancers over-expressing somatostatin receptors. Although the agent is commercially available from a couple of suppliers, the prohibitively high cost of the agent made it necessary to develop the methodology of preparation of the agent indigenously employing ^{177}Lu produced in our reactor. However, it was quite challenging to prepare the patient dose of the agent as it is required to be prepared with as high specific activity as possible for obtaining the desired therapeutic efficacy. The present article describes the successful development, demonstration and deployment of the agent in India along with the present day status of PRRNT in our country.

Peptide receptor radionuclide therapy (PRRNT) employing radiolabeled somatostatin analogs has emerged as a potential therapeutic modality for the treatment of patients suffering from a wide variety of inoperable and disseminated neuroendocrine cancers in the recent past. Towards this, use of a number of radiolabeled somatostatin analogs has been documented in the literature and amongst these, ^{177}Lu-DOTA-TATE (1,4,7,10-tetraazacyclododecane-1,4,7,10-tetraacetic acid coupled Tyr^3-Octreotate) has undoubtedly become the most popular choice.

The agent is commercially supplied by a limited number of pharmaceutical companies; but the prohibitively high cost made it almost unaffordable to the Indian patients. Therefore, it was necessary to develop the methodologies of its preparation indigenously in our country. However, to successfully develop such an agent, a host of challenges need to be taken care off. The first and foremost one is to produce ^{177}Lu with sufficiently high specific activity using our moderate flux reactors, as the agent needs to be prepared with adequately high specific activity in order to deposit sufficient activity in the cancerous lesions without saturating the limited number of receptors present in the cancerous site. Moreover, ^{177}Lu should be free from any kind of metallic impurities as these impurities are known to drastically affect the radiolabeling efficiency.

No-carrier-added (NCA) ^{177}Lu, which could be obtained through neutron activation of enriched Yb_2O_3 (in ^{176}Yb) target followed by the radiochemical separation of ^{177}Lu from ^{177}Yb, is ideal for the development of such agent. However, complete separation of trace level of ^{177}Lu from the bulk of irradiated Yb target is quite challenging as it involves the separation of two adjacent members of the lanthanide series in a highly radioactive environment. Though we have standardized the procedure of production of NCA ^{177}Lu, the route was found to be not economical as the cross-section of ^{176}Yb(n,)^{177}Yb is quite low (2.4 b) and hence, a majority of the expensive enriched target remains unutilized. Therefore, direct neutron activation route was employed for the production of adequately high specific activity ^{177}Lu. As ^{176}Lu(n,)^{177}Lu has significantly high cross-section (2100 b), it was possible to produce ^{177}Lu with sufficient specific activity in our reactor using this route after the careful adjustment of the irradiation parameters. Presently, ^{177}Lu with a specific activity of 25-40 Ci/mg (925-1480 GBq/mg) is regularly produced in our laboratory on almost weekly basis and supplied to nuclear medicine centers of India for the preparation of ^{177}Lu-DOTA-TATE in their hospital radiopharmacy for human administration. The radiochemical purity of ^{177}Lu produced is ~99.98% at the time of supply. Several process modifications were carried out to reduce the chemical impurities in the radiochemically processed ^{177}Lu and this enabled the percentage of metallic impurities (determined by ICP-AES) to bring down to the desired level.

The specific activity of ^{177}Lu produced by direct neutron irradiation varies significantly from batch to batch due to the variation in the operating conditions of the reactor and irradiation cycles used. The specific activity of ^{177}Lu available at the time of preparation of the agent also varies considerably owing to distance of the nuclear medicine centers from the radionuclide production sites, transportation delay, date and time of actual administration etc. Therefore, preparation of the agent at the hospital radiopharmacy taking into consideration of the available specific activity of ^{177}Lu at the time of preparation is ideal to formulate the agent with best possible specific activity and thus to ensure maximum therapeutic efficacy. Accordingly, a suitable method for the preparation of patient dose of ^{177}Lu-DOTA-TATE (usually, 150-200 mCi i.e. 5.55-7.4 GBq per dose) at the hospital radiopharmacy had been developed in our laboratory. In this method, which is presently followed across our country, the amounts of DOTA-TATE, radio-protecting agent (gentisic acid) and buffer (ammonium acetate) required to be used for the preparation need to be calculated before every single preparation and these varies depending upon the specific activity of ^{177}Lu available at the time of preparation. Therefore, composition of each patient dose is unique, but it ensures the maximum

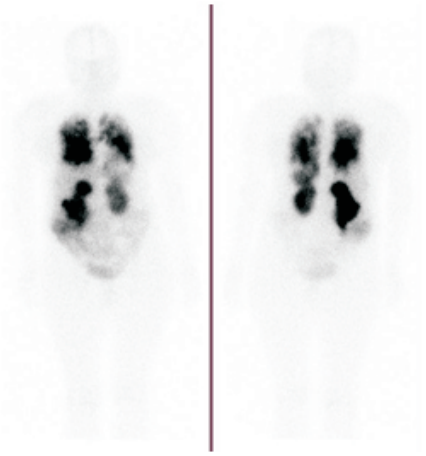


Fig. 1 Whole-body image of a patient treated with 200 mCi (7.4 GBq) of ^{177}Lu-DOTA-TATE

therapeutic efficacy of the agent. This methodology has been successfully adopted and presently practiced in eight hospitals in India and more than 1000 cancer patients have been benefitted from this treatment modality till date. Figure 1 shows the whole-body scintigraphic scan of a neuroendocrine cancer patient treated with 200 mCi (7.4 GBq) of ^{177}Lu-DOTA-TATE prepared using the methodology developed in our laboratory.

Our experience with regularly working with various nuclear medicine centers made us realize that the present methodology is heavily dependent on the working personnel available at the hospitals, as this procedure requires careful adjustment of certain critical reaction parameters. A small deviation from the standard procedure or some miscalculation may lead to the batch failure and consequently loss of expensive peptide and radioactivity. Most importantly, the treatment schedule of the patients gets adversely affected. However, all these problems can be circumvented if a suitable kit is developed, which can be utilized in the hospital radiopharmacy, for a convenient and single-step preparation of the agent. Moreover, the presently used methodology can be adopted in only those centers who have trained radiopharmaceutical chemists at their disposal. Therefore to make this treatment modality more widely available to Indian patients, freeze-dried kits are expected to play a significant role. Working in this direction, recently, we have formulated a freeze-dried kit of DOTA-TATE, comprising a lyophilized mixture of 200 g of DOTA-TATE, 80 mg of gentisic acid and 13.9 mg of ammonium acetate and utilized these kits for the successful preparation of patient doses of ^{177}Lu-DOTA-TATE at the hospital radiopharmacy. Each kit vial could be utilized to prepare a patient dose upto 200 mCi (7.4 GBq) of ^{177}Lu-DOTA-TATE with a radiochemical purity of 99%, provided labeled with ^{177}Lu having a minimum specific activity of 20 Ci/mg (740 GBq/mg). The kits have sufficiently long shelf-life so that they can be stored at the hospital radiopharmacy. The use of such kit is expected to reduce the batch failure and radiation exposure to the working personnel. Necessary work towards obtaining the approval for commercially supplying these kit vials will be initiated in the near future and this is expected to propagate PRRNT to the wider mass of patients in the coming years.

Acknowledgements

The work described in this article is essentially a collective effort of a group of scientists and staff members of the Radiopharmaceuticals Division (presently known as Isotope Applications and Radiopharmaceuticals Division), BARC and their clinical collaborators. The author is one of the major contributors towards the successful applications of ^{177}Lu-DOTA-TATE in India. The author sincerely acknowledges the contributions of all the group members and clinical collaborators toward the success of this program.

Japanese Fir leaves has the Highest Collection Efficiency for ^{137}Cs among Leaves of Six Tree Species in the Ishinomaki Area of Miyagi Prefecture

M. Fukushima[1], T. Matsutani[2], T. Nemoto[2]

1. *Department of Food and Environmental Sciences, Ishinomaki Senshu University, Ishinomaki, Miyagi, Japan; E-mail: fukusima@isenshu-u.ac.jp*
2. *Department of Biological Sciences, Ishinomaki Senshu University, Ishinomaki, Miyagi, Japan*

The leaves of six different naturally occurring tree species growing in Oshika Penninsula were studied to examine their collection efficiency for ^{137}Cs. Japanese Fir leaves were found to have the highest collection efficiency. This trend was found to be consistent over the study period of three years.

Introduction

It is well known that on 2011.03.11 (commonly referred to as 3/11) an earthquake of magnitude 9.0 struck the North East coast, mainly Iwate, Miyagi and Fukushima prefectures, of the Main Island of Japan. This earthquake induced a huge Tsunami which in turn led to the serious accidents at Fukushima Daiichi nuclear power reactors. Our university is located in the Ishinomaki city of Miyagi Prefecture, which is about 99 km NNE of the Fukushima Daiichi nuclear power reactors. Since the nuclear accidents, many scientists around the world have started monitoring radioactivity in soils, plants, and water [1], sediments, foods [2], etc. Thakur recently published a review of it [3].

Although Iwate, Miyagi and Fukushima prefectures are located next to one other from north to south, the contamination was generally not so serious in the first two areas. However, we were aware of some "hot spots" in Oshika Peninsula near our university. We started a program of monitoring ^{137}Cs in tree leaves, plants, soils, sea water, and sediments of Oshika Peninsula in 2012 June. One of the objectives of the present work was to investigate the collection efficiency for ^{137}Cs of the leaves of various naturally occurring tree species growing in that peninsula so that the most efficient one can be selected for further extensive monitoring. A pilot project was initiated for this purpose. The methodology used and some results of this project are presented here.

Experimental

Leaves, soil, seawater, and sediment samples were collected from Higashimatsushima City (around 20 km west of Oshika Peninsula) in 2012 June. Results of only leaves are discussed here. For monitoring ^{137}Cs we selected the leaves of 6 different kinds of evergreen tree in Oshika Peninsula (Fig. 1). These were two species of gymnosperms, namely Japanese Fir (Abies firma) and Japanese Plum Yew (Cephalotaxus harringtonia), and four species of angiosperms, namely Japanese spindle-Tree (Euonymus japonicus), Common Camellia (Camellia japonica), Japanese Eurya (Eurya japonica), and Japanese Aucuba (Aucuba japonica). Several branches were cut from these trees



Fig. 1 Sampling points in Miyagi Prefecture

during 2012 June-2013 April, and leaves and small branches were separated from one another according to the budding year, freeze dried, and pulverized in a mill. The dried leaves powder was doubly sealed in polyethylene bags and placed in polyethylene counting bottles. Some samples needed special treatment. For example, if trees had corn on the branch then the corns were first separated, freeze dried, and pulverized. For Japanese Plum Yew, seeds on branch were separated.

The gamma-ray spectrometry system consisted of a p-type ORTEC Ge detector (GEM40P4-76) with 43% efficiency and a resolution of 1.65 keV at the 1173-keV gamma-ray of ^{60}Co, and an ORTEC digital pulse height analyzer (Easy-MCA) in conjunction with a spectroscopy amplifier 672. The system was calibrated for U8 sample geometry using a multi-isotope standard provided by the Japan Radioisotope Association.

Results and Discussion

It is evident from Fig. 2 that rather high activity levels of ^{137}Cs were found on the dark green leaves of Japanese Fir followed by Japanese Eurya budded in 2010 April and collected in 2013 April.

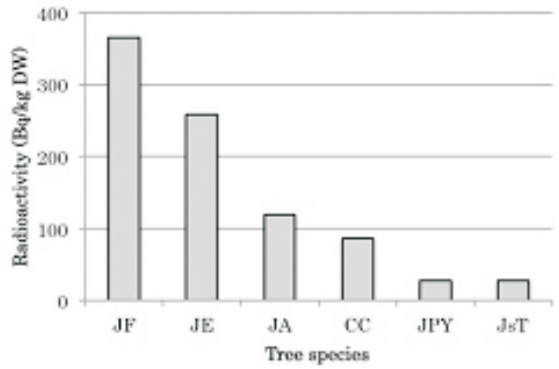


Fig. 2 Activity concentration of ^{137}Cs budded in 2010 April and collected in 2013 April from Oshika Peninsula. Legends: JF: Japanese Fir; JE: Japanese Eurya; JA: Japanese Aucuba; CC:Common Camellia; JPY: Japanese Plum Yew; JsT: Japanese spindle-Tree

Now we need to relate the budding of the leaves of Japanese Fir with time of exposure to ^{137}Cs. It has been reported that swelling bud phase and expanding leaf phase of evergreen trees in Miyagi Prefecture occur every year at the end of April [4]. Freshly expanded leaves have pale green color and can be easily distinguished from old, dark green leaves.

We collected leaves which budded in 2010, 2011 and 2012 April. They had different shades of green from pale to dark. So the dark green colored leaves of the six species that we collected in 2013 April actually budded in 2010 April. Obviously, these leaves were exposed to ^{137}Cs for almost 25 months since the Fukushima Daiichi accident. We observed the same trend of ^{137}Cs accumulation on leaves budded in 2011 April and 2012 April.

Conclusions

We studied leaves of six different tree species in the Oshika Penninsula area which is close to Ishinomaki Senshu University and is known to have some hot spots of ^{137}Cs. We concluded that Japanese Fir leaves have the highest collection efficiency among the six species studied and decided to use it for monitoring ^{137}Cs contamination in this and neighboring areas.

References

[1] T. Yasutaka, T. Kawamoto, Y. Kawabe, T. Sato, M. Sato, Y. Suzuki, K. Nakamura, T. Komai, J Nuclear Sci Tech 50(2013) 674.

[2] T. Itthipoonthanakorn, P. Krisanangkura, S. Udomsomporn, J Radioanal Nucl Chem 297(2013) 419.

[3] P. Thakur, S. Ballard, R. Nelson, Sci Total Environment 458-460 (2013) 577.

[4] Y. Hirabuki, Jap J Ecol 34 (1984) 235.

Production of Radioactive Tracers for Observation of behavior of Radioactive Cesium in Environmental Materials

K. Takamiya, T. Ohtsuki

Research Reactor Institute, Kyoto University, Kumatori, Osaka 5900494, Japan; E-mail: takamiya@rri.kyoto-u.ac.jp

Radioactive materials have been released to the environment from the Fukushima Daiichi Nuclear Power Plant. Observation of behaviors of radioactive isotopes in environmental materials using radioactive tracers is useful. In using the tracer method, producing the same chemical and physical forms of materials is important, however the production of all of the radioactive materials released from the FDNPP is difficult by synthesizing from a commercial radioactive tracers. Production method for various kinds of radioactive cesium tracers using a research reactor has been developed to observe the behaviors of radioactive cesium in the environment.

Introduction

Behavior of the radioactive cesium released from the Fukushima Daiichi Nuclear Power Plant varies depending on its chemical and physical forms, however detailed forms of the radioactive cesium released at the time of the disaster is not clear. For a prediction of the radioactive cesium behavior in the environment in the future, observations for the radioactive cesium with the specific chemical and/or physical forms are required. In the case of radioactive cesium as ion form, it dissolves in water easily and moves in the environment or is adsorbed on materials in the environmental materials, e.g. soils [1,2]. On the other hand, insoluble materials containing radioactive cesium, for example fine grains captured on filter papers, have been found [3]. The detail characteristics of these insoluble cesium has not been clear, however it plays an important role in the environment as time goes by because insoluble cesium in the environment decreases with their physical half-live but soluble cesium does with both physical and environmental half-lives.

Experimental

Radiotracer is useful in observing behavior of trace amount elements, but chemical and physical forms of commercial radiotracers are restricted. However, various kinds of radiotracers, for example insoluble fine gains containing radioactive cesium, can be produced by neutron irradiation of stable cesium using a research reactor. There are various neutron irradiation systems to produce radiotracers in Kyoto University Research Reactor (KUR), e.g. pneumatic tubes, horizontal or slant irradiation holes. In the B-2 irradiation hole that is one of the horizontal irradiation holes of KUR, the new neutron irradiation apparatus has been developed. The overview of the neutron irradiation apparatus installed in the B-2 hole are shown in Fig. 1. The apparatus can transport a larger space

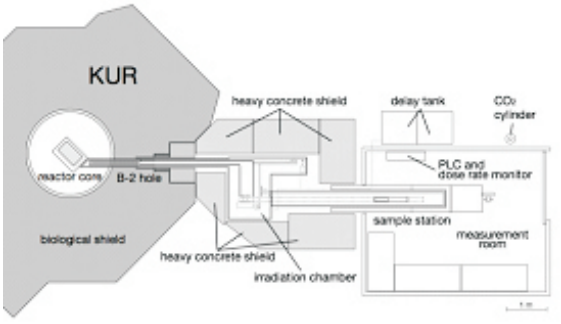


Fig. 1 Overview (horizontal configuration) of the B-2 hole of KUR and the irradiation apparatus

gently to a neutron irradiation field adjacent to the reactor core through the B-2 hole. Therefore, also liquid samples can be irradiated with neutrons. And also the neutron irradiation field can be joined to experimental instruments with tubes that realize irradiation experiments with circulating liquid. In the present report, producing methods of radioactive cesium tracers using KUR and analytical methods for observing the behavior of trace amount of cesium in the environmental materials using the radioactive tracer are suggested.

References

[1] T. Ohno, Y. Muramatsu, Y. Miura, K. Oda, N. Inagawa, H. Ogawa, A. Yamazaki, C. Toyama, M. Sato, Geochem. J. 46 (2012) 287.

[2] N. Kaneyasu, H. Ohashi, F. Suzuki, T. Okuda, F. Ikemori, Environ. Sci. Technol. 46 (2012) 5720.

[3] K. Adachi, M. Kajino, Y. Zaizen, Y. Igarashi, Scientific Reports 3 (2013) 2554.

Applications of Nuclear Analytical Techniques for Impact of Industry to the Environment

R.K. Dutta[1], S. Sarkar[1], R.S. Maharia[1], M. Sudarshan[2], R. Acharya[3], A.V.R. Reddy[4]

1. *Department of Chemistry, Indian Institute of Technology Roorkee, Roorkee 247667, India; E-mail: duttafcy@iitr.ernet.in*
2. *UGC-DAE Consortium for Scientific Research, Kolkata Centre, LB-8, Sector- III, Bidhannagar, Kolkata 700091, India*
3. *Radiochemistry Division, [4]Analytical Chemistry Division, Bhabha Atomic Research Centre, Trombay, Mumbai 400085, India*

Energy dispersive X-ray fluorescence spectrometry was used for analyzing P, S, K, Ca, Mn, Fe, Cu, Zn and Sr in soil, vegetables, cereals and medicinal plants grown in the vicinity of zinc smelter and Zawar mining areas of Rajasthan, India. High Zn accummulation in the food samples (53±6 and 207±17 g g^{-1}) were attributed to Zn levels in soil samples of 1236±86 g g^{-1} (smelter) and 564±76 g g^{-1} (mining). Furthermore, the impact of Khetri Cu mining activity on locally grown medicinal plants was studied by measuring physiological digestion based metal bioaccessibility by Instrumental neutron activation analysis.

Introduction

Environmental pollution is a threat to human system and hence demands assessing pollution index and its remediation. Soil contaminated with metals due to natural and anthropogenic contributions is likely to contaminate vegetables and cereals grown there in, which will consequently impact upon human health via food chain. Globally, smelters and mining areas are recognized as main contributors of metal contamination in soil and are associated with accumulation of abnormally high metal contents in vegetables grown there [1]. Here we present analysis of metal accumulation in vegetables, cereals and medicinal plants grown in Zn and Cu mining areas. Elemental analyses were performed by Energy dispersive X-ray fluorescence spectrometry (EDXRF) and by instrumental neutron activation analysis (INAA). Compared to total concentration of an element, bioavailability or bioaccessibility is a better parameter to assess the impact of metal contents in food samples on human via circulatory system [2]. Bioaccessibility is defined as the fraction of a metal leached due to gastrointestinal digestion, which is available for circulation in human body. We present here a methodology for analyzing physiological gastrointestinal digestion based metal bioaccessibility by INAA.

Experimental

Four leafy vegetable samples, namely, Chenopodium album (CA, wild spinach), Spinacia oleracea (SO, spinach), leaves of Raphanus sativus (RS, radish) and Solanum lycopersicum (SL, tomato) were collected from different locations of zinc smelter site in Birchi, near Udaipur, in India. Vegetable and cereal samples e.g., Carica papaya (CP, Papaya), Lagenaria siceraria (LS, bottle gourd), Triticum aestivum (TA, wheat) and Pennisetum glaucum (PG, corn) were collected from Zawar mata village, adjacent to Zawar zinc mines, near Udaipur, India. Soil samples from both locations were collected. In addition, medicinal plants namely, A. indica (AI, neem), O. sanctum (OS, tulsi) and A. paniculata (AP, kalmegh) were collected from the vicinity of Cu mines in Khetri, Rajasthan, India. All samples were washed repeatedly using deionized water (Millipore), packed separately in pre-cleaned polythene bags and brought to the laboratory. Samples were oven dried at 40°C for 3-5 days, crushed, powdered in agate mortar and sieved through 100 ìm mesh. Elemental analysis of the pelletized samples was performed using Jordan Valley Ex-3600 Energy dispersive X-ray fluorescence (EDXRF) spectrometer, featuring oil-cooled Rh anode X-ray tube. The characteristic X-ray peaks were detected using Si(Li) detector of resolution 150 eV at 5.9 KeV, and analyzed quantitatively by the ExWIN software integrated with the system [3]. A typical EDXRF spectrum of Chenopodium album is given in Fig. 1a and 1b.

For instrumental neutron activation analysis, 100 mg of each powdered sample and Certified Reference Materials (Peach leave, NIST, SRM-1547) were individually packed in aluminum foil and irradiated in a batch for 6h using CIRUS reactor (BARC, Mumbai) with a neutron flux of 10^{13} cm^{-2} s^{-1}. The gamma activities of the activation products of the irradiated samples and reference materials were measured by HPGe detector (40% relative efficiency with 2.0 keV energy resolution at 1330 keV of ^{60}Co), coupled with Compton suppressor and a PC based 8K MCA. The elemental concentrations were determined from the software (PHAST) based spectral analyses. The protocol used for estimating bioaccessible concentration by treating powdered samples in enzyme containing gastric and intestinal fluid of porcine origin is reported in literature [2].

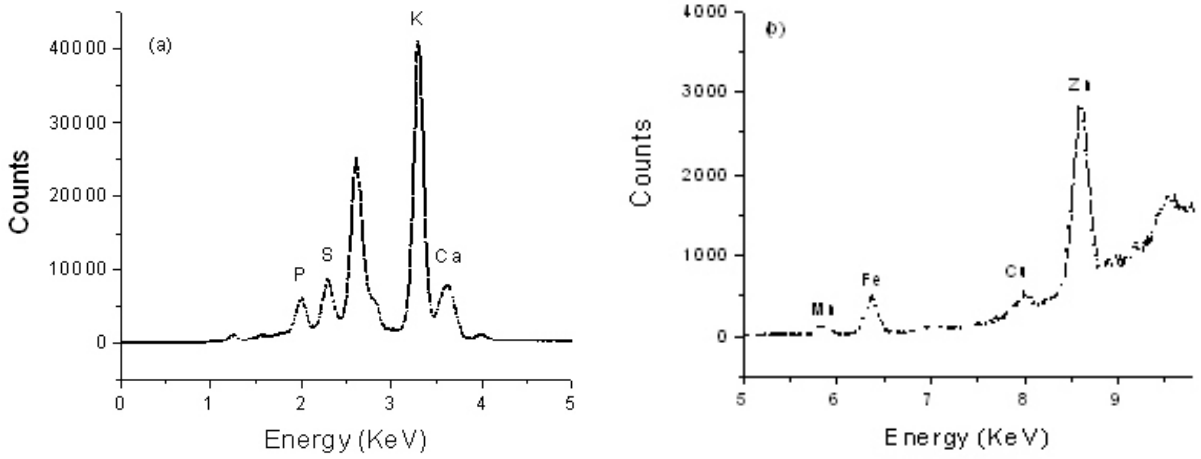


Fig. 1 Typical EDXRF spectra of Chenopodium album recorded with different filters

Results and Discussion

The concentrations of Zn in the samples from smelter site were in the range of 53±6 and 207±17 g g^{-1} (Table 1). Similarly the Zn levels in the samples from zawar mining site are in the range of 54±6 and 82±12 g g^{-1} (Table 2). These concentrations are 3-8 folds higher than normal levels of Zn in vegetable and cereal samples. Such high Zn accumulation in the vegetables and cereals grown in smelter site was attributed to abnormally high Zn levels in local soils (1236±86 g g^{-1}). The concentrations of P, S, K, Ca in the samples from both sites were within normal levels. The concentrations of micronutrients e.g., Fe and Cu were within the normal levels in vegetable samples. However, concentration of Mn in Spinacia oleracea (SO, spinach), leaves of Raphanus sativus (RS, radish) were 4 to 6 fold higher than the normal, while Mn levels in other samples were within normal range.

Table-1: Elemental concentration (mean ± standard deviation, n =3) of samples from smelter site (g g^{-1} unless % is specified) measured by EDXRF.

	CA	SO	RS	SL
P (%)	0.53±0.04	0.42±0.03	0.38±0.05	0.39±0.03
S (%)	0.33±0.02	0.25±0.02	0.33±0.02	0.22±0.02
K (%)	4.19±0.09	2.05±0.06	1.36±0.05	0.03±0.05
Ca(%)	0.83±0.05	0.92±0.04	1.86±0.07	0.69±0.05
Mn	22±3	117±9	78±8	13±3
Fe	84±10	134±11	126±9	65±8
Cu	12 ±3	14±4	11	11±4
Zn	194±22	93±7	207±17	53±6
Sr	418±32	120±9	360±28	20±4

The impact of Khetri Cu mines on medicinal plants were studied by INAA, where the bioaccessibility of Cr, Mn, Fe, Cu and Zn were determined and compared with the same type plants grown in soil without Cu contamination. Though the total concentration of Cu in A. indica (76.5±5.4 g g^{-1}), O. sanctum (38.5±3.2 g g^{-1}) and A. paniculata (31.6±2.6 g g^{-1}) were high, but their bioaccessible concentrations were measured to be 17.2±1.8 g g^{-1}, 7.8 ± 0.8 g g^{-1} and 9.8 ± 0.8 g g^{-1} respectively. Potentially 17.2 g g^{-1} of Cu will be absorbed in human system, which is a high value. Since the amount of intake of medicinal plant is several orders less than food samples, so it is not feasible to compare and comment of the possible adverse effect of such higher bioaccessible concentration of Cu.

Table-2: Elemental concentration (mean ± standard deviation, n =3) of samples from Zawar mines (g g^{-1} unless % is specified) measured by EDXRF.

	TA	LS	CP	PG
P (%)	0.21±0.03	0.56±0.08	0.24±0.04	0.37±0.05
S (%)	0.10±0.02	0.22±0.06	0.24±0.03	0.08±0.02
K (%)	0.32±0.03	2.12±0.18	2.72±0.16	0.43±0.06
Ca(%)	0.05±0.01	0.38±0.04	0.47±0.09	0.06±0.06
Mn	13±3	16±2	ND	10±2
Fe	79±7	72±9	64±8	76±6
Cu	ND	14±6	19±5	ND
Zn	82±12	67±6	54±8	54±6
Sr	9±5	ND	35±6	ND

ND: not detected

Acknowledgement

This work has been carried out under the BRNS project 2011/37C/37/BRNS and authors thank BRNS for the support.

References

[1] A.G. Kachenko, B. Singh, Water, Air, and Soil Pollution 169 (2006) 101

[2] M. Intawongse, J.R. Dean, Trac-Trend Anal. Chem. 25 (2006) 876

[3] S. Majumdar, S.S. Ram, N.K. Jana, S. Santra, A.Chakraborty, M. Sudarsan, X-ray Spectrom. 38 (2009) 469

X-ray Photoelectron Study on Nitrogen in Explosives: Chemical Fertilizer

P. Dararutana

The Royal Thai Army Chemical School at the Royal Thai Army Chemical School, Bangkok 10900 Thailand; E-mail: pisutti@hotmail.com

In this work, chemical fertilizers that are used as explosive stimulants were analyzed using X-ray photoelectron spectroscopy (XPS). It was known that an explosive was defined as a material which contained a large amount of energy stored in chemical bonds. The energetic stability of gaseous products, and hence, their generation came from the formation of strongly bonded like carbon (mono/di)oxide and (di)nitrogen. Consequently, most commercial explosives were contained with $-NO_2$, $-ONO_2$ and $-NHNO_2$ groups which when detonated release gases like the aforementioned ones, e.g., nitroglycerin, TNT, HMX, PETN, nitrocellulose, etc. It was revealed that the elemental compositions, especially N was found in most of the explosive and fertilizer. Scanning electron microscope coupled with energy-dispersive X-ray fluorescence spectroscopy (SEM-EDS) was also carried out to characterize them. XPS spectra showed the nitrogen (N) in the various samples, especially sample #6 and #7. The elemental analysis showed the presence of trace elements. Explosives and fertilizers have differences in specific compositions. It can be concluded that these methods seem to be used as fingerprint to identify the various explosives and fertilizers.

References

[1] Sharma J, et al.: X-ray photoelectron pectroscopy of explosive solids, Online Information of the Defence Community, (1974).

[2] Roy R M, et al.: Propellants, Explosives, yrotechnics 24 (1999) 54.

[3] Gonzalez-Santiago: X-ray photoelectron spectroscopy (XPS) study of hexahydro-1,3,5-trinitro-s-triazine (RDX), M S Thesis, University of Puerto Rico, Puerto Rico, (2007).

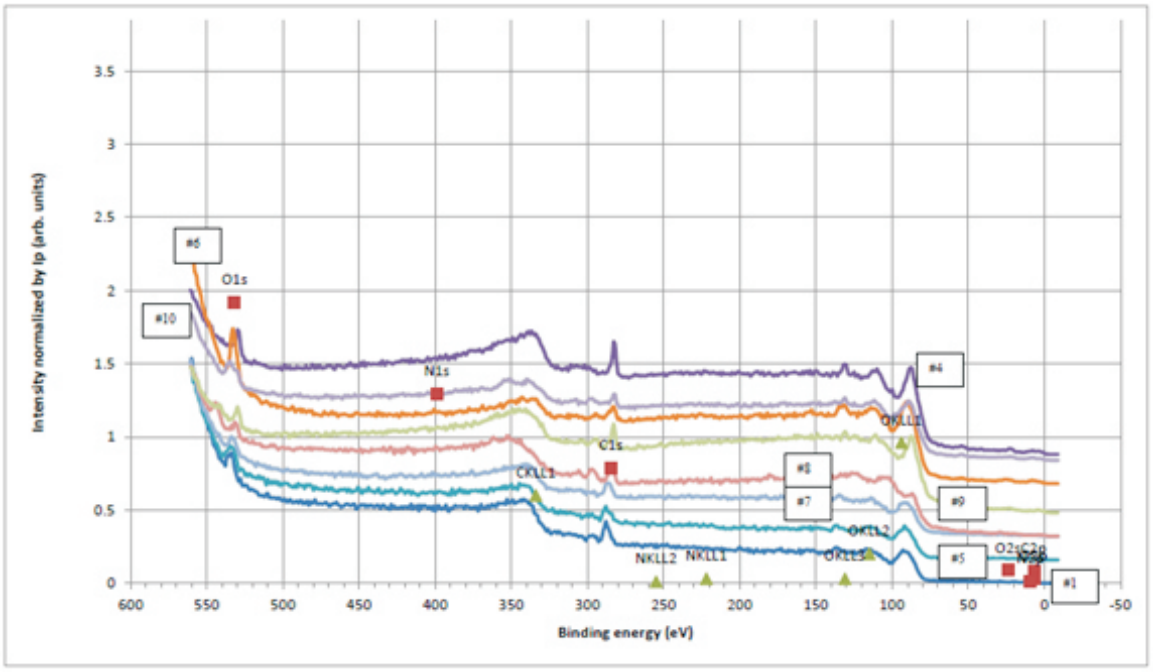


Fig. 1 XPS spectra of fertilizer samples

Radiometric Enzyme Assays: Studies of Fluoxetine Interaction with Thyroid Hormones Metabolism

S. Pavelka[1,2]

1. *Department of Radiometry, Institute of Physiology, Academy of Sciences of the Czech Republic, 142 20 Prague; E-mail: pavelka@biomed.cas.cz or pay@chemi.muni.cz*
2. *Institute of Biochemistry, Faculty of Science, Masaryk University, 611 37 Brno, Czech Republic*

In the present studies, we followed in more details the effects of subchronic administration to Wistar rats of Fluoxetine by itself, or in combination with triiodothyronine, on the metabolism of thyroid hormones in different rat tissues. With the use of our newly elaborated and adapted radiometric enzyme assays, we were able to quantify these effects. Especially, we determined changes in the most important deiodinating and conjugating enzyme activities in the liver, brain, pituitary and several other tissues of the treated rats.

Introduction

Fluoxetine (Fluox) (e.g., Prozac™, Fig. 1) is the most frequently used representative of a group of non-tricyclic antidepressant drugs known as selective serotonin re-uptake inhibitors.

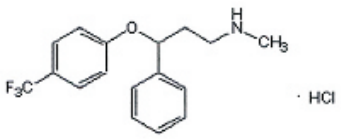


Fig. 1 Fluoxetine hydrochloride (Prozac™)

Thyroid hormones (THs) are supposed to control the activity of some neurotransmitters (e.g., serotonin), which are hypothetically involved in the pathogenesis of depressive illness. On the other hand, many clinical studies indicated that various antidepressant treatments might influence the effects of hormones of hypothalamic-pituitary-thyroid axis in depressed patients [1,2]. It is important that, for example, inadequate activities of brain enzymes iodothyronine deiodinases (IDs) can lead to local insufficient T_3 concentration and might be, therefore, one of the pathogenic factors of depression.

In the presented studies of the interaction of Fluox with the metabolism of THs in the rat, we applied adapted radiometric enzyme assays for iodothyronine sulfotransferases (ST) and uridine 5'-diphospho-glucuronyltransferase (UDP-GT) [3], as well as our newly developed radiometric assays for IDs of types 1, 2 and 3 (D1, D2 and D3, respectively) [4], using [^{125}I]-labeled iodothyronines of as substrates.

Experimental

Pharmacological experiments were performed on 90 young growing male Wistar rats, fed ad libitum a standard pelleted diet. During 25-day experimental period, the rats drank tap water with the addition of various amounts of fluoxetine (Ratiopharm), T_3 (Sigma), or their combinations. After the treatment, rats were killed by decapitation. Serum total and free T_3 and T_4 levels were determined using radioimmunoassay (RIA) kits. The thyroid glands, pituitary, different parts of the brain, liver, kidney and several other tissues were also dissected and used for the preparation of subcellular fractions – microsomes (liver, kidney), sub-mitochondrial supernatants (brain, pituitary, thyroid gland) and cytosols (liver). Samples were used in the following radiometric enzyme assays. Activities of conjugating enzymes UDP-GT and ST, and IDs D1, D2 and D3 were measured in principle as described previously [3, 4], but with some modifications, e.g. of the TLC developing system etc.

Results and Discussion

The elaborated radiometric assay for UDP-GT was usable for the assessment of enzymatic conversion of radiolabeled unconjugated substrate [^{125}I]-rT_3 to conjugated product [^{125}I]-rT_3-glucuronide. About two-fold higher glucuronyltransferase activities were found in liver microsomes of the rats treated with Fluox in comparison with control rats (not shown).

On the contrary, the enzyme activities of iodothyronine sulfotransferases in the liver and kidney cytosolic fractions of the control and treated animals

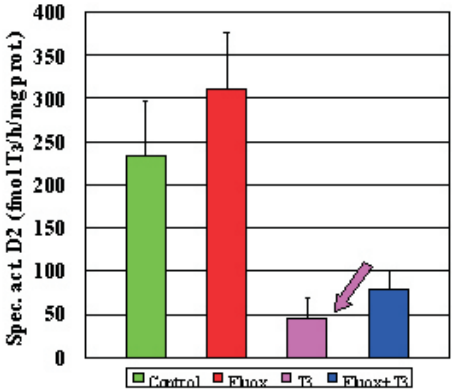


Fig. 2 The influence of fluoxetine, T_3 and their combination on specific enzyme activities of D2 (fmol T_3/h/mg prot.) in rat pituitary

were found to be negligible and not influenced by the treatments.

Subchronic treatment of rats with Fluox by itself caused a moderate increase in D2 and, in turn, a slight decrease in D3 activities in cerebellum and some other regions of the CNS. On the other hand, the administration of T_3 by itself caused, in accordance with our expectation, a substantial decrease in pituitary D2 activity (Fig. 2) and a simultaneous increase in D1 and D3 activities (practically in all tissues studied). In contrast with the effects of T_3 by itself, the treatment of rats with the combination of Fluox plus T_3 caused only non-significant elevation of D1 and D3 activities.

Conclusions

With the use of our newly elaborated and adapted radiometric enzyme assays for IDs and UDP-GT, we were able to quantify the effects of subchronic administration of xenobiotic Fluox, alone or in combination with T_3, on the metabolism of thyroid hormones in the rats.

References

[1] C. Kirkegaard, J. Faber, Eur. J. Endocrinol. 138 (1998) 1

[2] M.F. Sauvage, P. Marquet, A. Rousseau, et al., Toxicol. Appl. Pharmacol. 149 (1998) 127

[3] S. Pavelka, J. Radioanal. Nucl. Chem. 286 (2010) 867

[4] S. Pavelka, J. Radioanal. Nucl. Chem. 286 (2010) 861

Speciation of Uranium in Solid Matrices

M. Mohapatra and V.Natarajan

Radiochemistry Division,Bhabha Atomic Research Centre, Trombay, Mumbai 400 085, India;
E-mail: manojm@barc.gov.in

Owing to the triple resolution of time resolved photoluminescence (TRPLS) technique, speciation of uranium in solids can be carried out in a non invasive manner by this technique. When used in combination with photo acoustic and X-ray absorption (XAS) based non invasive techniques, TRPLS can precisely give information regarding the species under investigation. In the present paper, recent studies on the speciation of uranium carried out at Radiochemistry Division using TRPLS, PAS and XAS will be discussed.

Introduction

The actinide element uranium, along with Am and Cm,shows efficient photoluminescence (PL) properties. Other actinides are known to have closely spaced energy levels, which provide ladder like pathways for the excitation energy to escape through non-radiative modes thus prohibiting the PL. Further, existence of multi valence states of uranium (VI, V, IV and III)in solids are well known [1].The most common species observed in case of U(VI) is the uranyl ion (UO_2^{2+}), wherein uranium ion is in the +6 state and the two oxygen ions in a linear structure. All the electrons in this strongly bonded structure are paired forming the ground electronic level as a singlet. To form higher-energy electronic levels, one of the bonding electrons is transferred to the 5f non-bonding orbital of U. The first excited level is ~ 20,000 cm^{-1} above the ground singlet [2]. PL can occur from this moiety, when photons with energy higher than that of the first excited electronic level are absorbed and the excited uranyl ion relaxes quicklyby non-radiative ways to the first excited electronic level, from which PL originates.The PL spectrum thus is the result of the transitions from the first excited electroniclevel to the ground singlet (often referred to as the zero-phonon (zp, $_g$ $_g^+$ from oxygen to one of the non-bonding uranium orbital) transition and the vibrational levelsassociated with the singlet. UranylPL lines arealways associated with the symmetric and anti-symmetric vibrational modes of the ion in the ground state. The average energy difference of the two modes is about 900 cm^{-1}. Because of this unique feature, the ion has been used as a local structural probe [3]. Apart from this, other forms of U(VI) such as theoctahedral and tetrahedral uranium groups (UO_6^{6-}, UO_4^{2-} and U^{6+}) are also reported to have intense PL [4]. Due to the possible presence of multiple luminescent species, the speciation of uranium in solids presents a challenging task.

Time resolved photoluminescence spectroscopy (TRPLS) is a direct and non-invasive method for speciation studies of metal ions. By virtue of its triple resolution (excitation, emission and life time), it is possible to identify multiple species present simultaneously in a system. When used in combination with other techniques such as Photoacoustic spectroscopy (PAS), EXAFS (Extended X ray absorption fine structure spectroscopy) and XANES (X ray near edge absorption spectroscopy), this challenging task can be carried out smoothly.

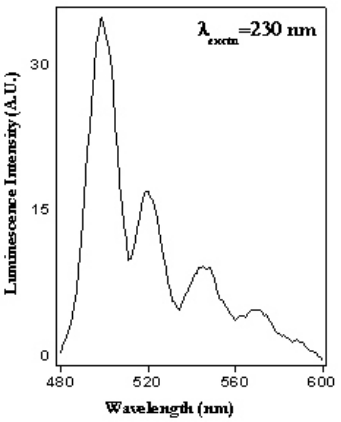


Fig. 1 PL emission spectrum of U:YBO_3

In the present paper, we shall discuss some of our recent investigations on uranium speciation in various solid matrices primarily using TRPLS. Some results obtained from PAS, EXAFS and XANES will also be discussed.

Results and Discussion

Figure 1 shows the emission spectrum of uranium in YBO_3 matrix. It shows emission maxima at 500, 520, 545 and 570nm, which are characteristic of uranium in +6 oxidation state; the peaks at higher wavelengths correspond to the vibrational fine structures. The emission peak at 500 nm is attributed to the zp line of U(VI) as discussed earlier. The observation of zp line at 500 nm and the occurrence of vibrational fine structures ($_1$ ~ 790 cm^{-1}) at room temperature indicated that U(VI) is getting stabilized as uranyl (UO_2^{2+})in the matrix.The predominant PL decay time of the system was found to be 40 sec confirming the presence of uranyl species.

Figure 2 shows the PL emission spectrum of the uranium in another solid matrix namely SrB_4O_7 (SBO) $_{ex}$ = 246 nm. The spectrum shows a strong emission peak at 520 nm with small bands at 500 and 540 nm. This type of spectrum was first reported in

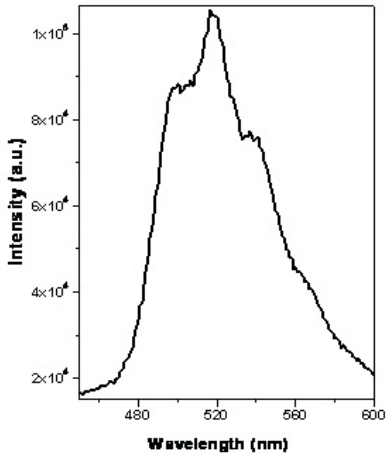


Fig. 2 PL emission spectrum of U:SBO

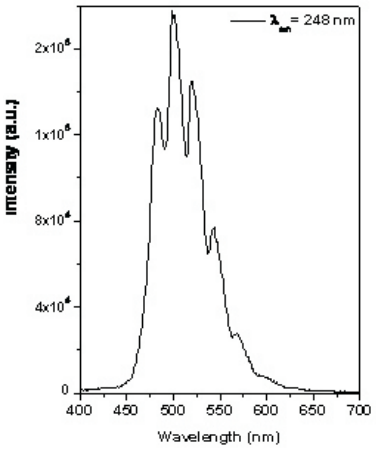


Fig. 3 PL emission spectrum of U:$Sr_2P_2O_7$

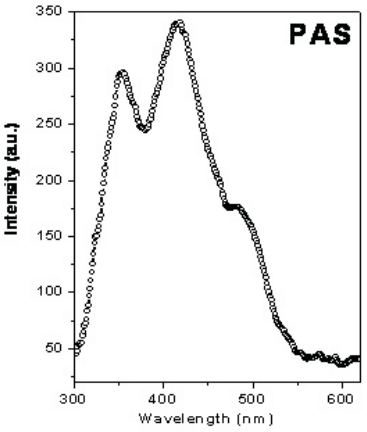


Fig. 4 PAS spectrum of U in nuclear waste glass

SBO by Tanner et al [5] at 77 K. These featureless bands correspond to the transitions from orbitals derived primarily from oxygen (2p) to uranium (6d) orbitals. The transitions are thus parity allowed, but not necessarily electric dipole allowed.

Usually with 4, 5 or 6 equatorial coordination in crystalline materials, the position of the zp line normally varies from 520 to 470 nm. In the present case, the observed band starts at 500 nm. This strongly indicates that the equatorial coordination is in between 4 (as in UO_6^{6-}) and 7 (as in UO_9^{12-}) [1]. It is usually observed that, for uranyl species (UO_2^{2+}), the zp line ($_0$) is strongest peak (as in case of YBO_3), but for uranates, the $_1$ or in some case, the $_2$ is the most intense peak. In this case, as it can be seen, the $_1$ peak is more intense. Further, the vibronic couplings are usually more prominent in case of uranyl as seen in case of YBO_3. But in case of uranates, these are not so prominent. The emission spectrum observed here also closely resembles that of uranates (UO_6^{6-}),which was further confirmed by a decay time value of 200 sec.

Figure 3 shows the emission spectrum of uranium in $Sr_2P_2O_7$matrix. The five line structure as seen in the case of YBO_3 is typical of uranyl ion. The observation of zp line at 485 nm suggested the coordination number of U(VI) is more than 7. The occurrence of vibrational fine structures ($_1 \sim 830$ cm^{-1}) at room temperature also indicated that U(VI) is getting stabilized as uranyl (UO_2^{2+})in the matrix.

PAS spectra closely resemble an excitation spectra except for the fact that, the latter are somewhat better resolved. The PAS spectrum of uranium in Trombay nuclear waste glass (sodium barium borosilicate) is presented in figure 4. U(IV) and U(V) strongly absorbs in the region 600-650 nm and near IR respectively. In the present borosilicate glass system, the nature of the PAS spectrum indicated that uranium mainly exists as U(VI). The observed PAS peaks at 348 and 412 nm are due to the transition between ^{1} $_g^+$ and ^{3} $_u$ states, both spilt into sub-levels by the symmetric stretching of the UO_2 species thus confirming the presence of uranium as uranyl ion.

Conclusion

TRPLS presents a very sensitive technique for speciation of uranium ions in solid matrices. When used in combination with other spectroscopic techniques such as PAS and XAS, it is possible to enhance the information regarding the actinide ion further.

References

[1] G.Blasse, K.C.Bleijenberg, D.M.Krol, J. Lumin 18/19 (1979) 57

[2] A.F. Leung, L. Hayashibara, J. Spadaro, J. Phys. Chem. Solids 60 (1999) 299

[3] P.E. Nielsen, J. Am. Chem. Soc. 114 (1992) 4967

[4] G. Blasse, G. P. M. van den Heuvel, J. J. A. van Hesteren, J. Solid State Chem.21 (1977) 99

[5] P.A.Tanner, P. Z.Wu, L.Jun, L.Yulong,S. Qiang, J. Phys. Chem. Solids 58 (1997)1143

Estimation of the Indoor Radon and the Annual Effective Dose from Building Materials

P. Sola[1], W. Srinuttrakul[1], S. Laoharojanaphand, N. Suwankot[2]

1. *Research and Development Division, Thailand Institute of Nuclear Technology (Public Organization), Ministry of Science and Technology, Ongkharak, Nakhon Nayok, 26120, Thailand; E-mail: ph_solar@hotmail.com*
2. *Nuclear Engineering Division, Electricity Generating Authority of Thailand, Charansanitwong Rd., Bang Kruai, Nonthaburi, 11130 C, Thailand*

Indoor radon and its annual effective dose from the building materials commonly used in Thailand were reported here. Ten granite samples and five other common building materials were bought from the market. Radon emission from each samples were measured using an ionization chamber. The radon concentration in air was then estimated and the radon exhalation rates were calculated. Finally, indoor radon and the annual effective dose were estimated. It has been observed that among the materials selected in this study, granite yields the highest annual effective dose. A good correlation between the radon exhalation rate and the indoor radon concentration was observed. Three samples of granite also showed the annual effective dose higher than the annual exposure limit for the general public of 1 mSv y^{-1} recommended by the International Commission on Radiological Protection (ICRP). By applying appropriate surface coating, the radon emission from some building materials has decreased substantially.

Introduction

Radon, a naturally occurring radionuclide, has been considered as one of a hazardous gas as it may cause lung cancer to human and animal [1]. It is the decay products of natural radioactive materials uranium and thorium. Common building materials usually contain these natural radioactive minerals especially radium-226 and uranium-238. Thus indoor radon is emitted from building materials and can cause health problems especially in the poor ventilate area. Thus radon emitted from the building materials has received substantial interest from several researchers local and abroad [2-4].

Experimental

Building materials of known surface area were placed in a sealed container with the volume of 0.05 cubic meter as shown in Fig. 1. The air inside the container is evacuated then the fresh radon-free air is ventilated into the container. After the equilibrium is reached, the radon emitted is measure by using a pulse-counting ionization chamber at the flow rate of 2 L min^{-1}. The radon measured is the convert to yield relevant information and finally the annual effective dose using the technique derived by Kovler and his team [5].

Results and Discussion

Results of the measured radon concentration from selected material are presented in Table 1. By applying the equations derived by Kovler, the radon exhalation rate and the annual effective dose for each type of building materials were presented in Table 2. From our study it is found that at least 3 samples of granite sheet showed the annual effective dose of 1.1 to 1.2 mSv y^{-1}.



Fig. 1 The sealed-can technique for measuring radon exhaled from building materials and building material samples

These are higher than the annual exposure limit for the general public of 1 mSv y^{-1} recommended by the International Commission on Radiological Protection (ICRP) [6].

Table-1: Range of radon emission concentrations from selected building materials

	Radon emission concentration (Bq m^{-3})
Granite	36-492
Granite with finish coating	180-312
Local marble	12-13
Brick	24-40
Concrete block	119

Table-2: Radon exhalation rate and the annual effective dose from selected building materials

	Radon exhalation rate (Bq m^{-2} h^{-1})	Annual effective dose (mSv y^{-1})
Granite	0.9-11.9	0.3-1.2
Granite with coating	4.4-7.6	0.6-0.7
Local marble	0.5-0.1	0.3-0.3
Brick	0.5-0.8	0.3-0.3
Concrete block	1.37	0.4

Conclusions

In general, radon emission rates are found lowest in marble and highest in un-coating granite. By applying surface finishing materials, the radon emission rate is usually decreased substantially depending on the techniques and materials of coating.

References

[1] International Commission on Radiation Protection [ICRP], England: Pergamon Press. (1994).

[2] A. F. Saady, K. Abdalla, N. A. Hussein, I. S. Elyaseery, Turkish J. Eng. Env. Sci. 34 (2010) , 67

[3] P. Wanabonges, et al., The journal of the Royal Institute of Thailand 32 (2007), 570

[4] T. Srisuwan1, P. Wanabonges, C. Tantasavasdi, JARS 9(2). (2012), 106

[5] K. Kovler, A. Perevalov, V. Steiner, A. Metzger, Journal of Environmental Radioactivity 82, 335–350 (2005).

[6] International Commission on Radiation Protection [ICRP]. Oxford: Pergamon Press. (1990).

Mass Spectrometric Determination of Thorium and Uranium in Human Hair and Nails in a High Background Natural Radiation Area of Serbia

S.K. Sahoo

Project for Environmental Dynamics and Radiation Effects, National Institute of Radiological Sciences, 4-9-1 Anagawa, Inage-ku, Chiba 263-8555, Japan; E-mail: sahoo@nirs.go.jp

The content of elements in human hair and nails can be considered as alternative bio-indicators of public exposure to natural radionuclides and other toxic metals over a long period of months or even years. The level of elements in hair and nails usually reflect their presence in other tissues of body. Hair and nails were collected from a high natural background radiation area in Serbia to analyze the concentration of thorium, uranium and selected trace elements such as Mn, Ni, Cu, Sr, Cd, and Cs using inductively coupled plasma mass spectrometry. Th and U concentrations in hair varied from 0.0002 to 0.0276 g/g and 0.0002 to 0.0771 g/g, respectively. The concentration in nail varied from 0.0023 to 0.0564 g/g and 0.0025 to 0.0447 g/g, for Th and U, respectively. There was a large variation for other metals' concentrations in hair, which may be due to different geological origin and anthropogenic activities.

Introduction

Hair and nails are biomaterials primarily composed of fibrous protein structure, notably keratin [1]. The changes in their appearance and composition are visible signs of deficiency or presence of stored substances in the body. Therefore, they have been recognized as valuable tissues for monitoring human environmental exposure. However, blood and urine tend to show current or recent body status. Bioassay of hair and nails is attractive over other types of clinical specimens like blood and urine as both are natural bio-concentrators, containing relatively higher elemental concentration. Other advantages are painless removal, easy collection and transportation, highly stable at room temperature, easily stored and the concentration reflects an integrated value. It has been reported that some elements including thorium and uranium in hair and nail are higher than in blood. The concentration of uranium in hair is on an average about eight times higher than in urine. Hair may prove a practical dosimeter for metallic environmental pollution [2,3]. Thus, analyzing thorium and uranium content in hair and nails a single time may be a substitute for analyzing several urine samples over a lengthy period in order to estimate the exposure.

Therefore, hair and nails were collected from the same person in most instances to establish, if any, correlation of each element between hair and nails. There are instances of positive correlation between hair and nails, since both are chemically related.

Experimental

Hair and nail samples were collected from 27 informed volunteers living in Niška Banja (Fig. 1), a high natural background radiation area of Serbia [4] by cutting with ceramic equipment and stored in sealed plastic bags to avoid any contamination prior to analysis at National Institute of Radiological Sciences (NIRS), Japan. The samples were washed in the laboratory



Fig. 1 Sampling location of hair and nails

alternately with ultra-pure water and acetone to remove only exogenous contaminants on the samples surface. After the washing procedure, the samples were placed in filter paper for drying at room temperature. Only hair samples were then cut into small fragments using ceramic scissors. Weighed hair samples were transferred to porcelain crucibles and then ashed in a muffle furnace (Denken Co., Ltd., Japan). The ashed samples were transferred to closed PTFE vessels to which was added 6 mL of concentrated HNO_3 and 1 mL of H_2O_2 and digested in a microwave digestion system MLS-1200 (Milestone, Italy). For nail samples, they were open digested in a clean environment using Teflon beakers by adding 6 mL of HNO_3 and 1 mL of H_2O_2.

The contents of thorium, uranium and other selected trace metals in digested hair and nails were measured using inductively coupled plasma mass spectrometry, ICP-MS (Agilent 7500). Calibration curves derived from standard solutions, SPEX multi-element Plasma standard (SPEX CertiPrep Group L.L.C., USA).

Three certified reference materials such as human hair BCR-397 (Institute for Reference Materials and Measurement) sediment JLK-1 (Geological Survey of Japan) and peach leaves SRM 1547 (National Institute of Standards and Technology) were used for validation of analytical procedure and accuracy evaluation.

Results and Discussion

The average range of thorium, uranium and other element concentrations found in hair and nails are summarized in Table 1 and Table 2 respectively. Comparison with world values as well as with other parts of Serbia [5] will be discussed in presentation. A large variation was obtained for metal concentrations, which may be attributed to analytical methodology, data handling, geographical differences or basic population differences that are influenced by diet and environmental factor. Therefore, it is a complicated task to compare the results of hair and nails analyses by different laboratories. However, most of the concentration ranges obtained in the present study could be compared with other populations. The thorium concentration varied widely from 0.0002 to 0.0276 g/g and 0.0023 to 0.0564 g/g for hair and The uranium concentration in the 27 hair samples and the 26 nails varied widely from 0.0002 to 0.0771 g/g and from 0.0025 to 0.0447 g/g, respectively.

Table-1: Metal concentration (g/g) in hair

Element	Present study (Niska Banja)			
	Mean	S.D.	Median	Range
Th	0.006	0.008	0.002	0.0002-0.0276
U	0.017	0.018	0.013	0.0002-0.0771
Cd	0.032	0.048	0.010	0.0016-0.1508
Cs	0.001	0.001	0.001	0-0.0037
Cu	15.560	9.637	17.576	0.468-33.116
Mn	0.678	0.952	0.365	0.035-3.885
Ni	0.437	0.416	0.280	0.037-2.193
Sr	2.406	2.523	1.536	0.110-8.322

Statistical approach to find interrelation between elements in hair and nails will be discussed in detail during presentation.

Table-2: Metal concentration (g/g) in nails

Element	Present study (Niška Banja)			
	Mean	S.D.	Median	range
Th	0.022	0.016	0.017	0.0023-0.0564
U	0.013	0.008	0.010	0.0025-0.0447
Cd	0.180	0.368	0.057	0.012-1.686
Cs	0.057	0.059	0.039	0.009-0.219
Cu	9.544	4.340	7.947	2.967-75.063
Mn	4.244	5.476	2.497	0.600-24.273
Ni	1.547	0.562	1.639	0.398-15.140
Sr	1.099	0.860	0.860	0.373-3.446

Conclusions

Most of elemental concentration ranges, except thorium, were comparable with the data provided by other authors. Only thorium levels were found to be high in both hair and nails from people in this high natural background radiation level area. The elevated levels of trace elements in human body maybe related to environmental exposure.

Acknowledgments

This work has been partially supported by a Grant-in-Aid for scientific research from NIRS President fund and the Project No. 41028 of Ministry for Education and Science of Serbia awarded to Z.S. Zunic. Special thanks goes to Dr. Zora S. Zunic for collecting samples and volunteers of field sites for donation of hair and nail samples.

References

[1] G. Dongarra, M. Lombardo, E. Tamburo, D. Varrica, F. Cibella, G. Cuttita, Environ. Toxic. Pharmaco. 32 (2011) 27.

[2] K. Gellein, S. Lierhagen, P. S. Brevik, M. Teigen, P. Kaur, T. Singh, T. P. Flaten, T. Syversen, Biol. Trace Elem. Res. 123 (2008) 250.

[3] D. I. Hammer, J. F. Finklea, R. H. Hendrics, C. M. Shy, R. J. M. Hortom, Am. J. Epidemiol. 93 (1971) 84.

[4] Z.S. Žunic, I.V. Yarmoshenko, A. Birovljev, F. Bochicchio, M. Quarto, B. Obryk, M. Paszkowski, I. Èelikoviæ, A. Demajo A, P. Ujiœe, J. Environ. Rad. 92 (2007) 165.

[5] Z. S. Žunic, S. Tokonami, S. Mishra, H. Arae, R. Kritsananuwat, S. K. Sahoo, Rad. Protec. Dosim. 152 (2012) 220.

Improvement of Sensitivities and Detection Limits in Estimation of Rare Earth and Trace Elements in Geological Rock Samples by INAA using DHRUVA Reactor Compared to CIRUS Reactor at BARC, Mumbai

N. Rupa, G.B. Rout, H.B. Shrivastava, V. Koteswara Rao and B.K. Pandey

Atomic Minerals Directorate for Exploration and Research, Begumpet, Hyderabad 500 016, India;
E-mail: nrupa.amd@gov.in

Analytical Sensitivities and Detection limits of the La, Ce, Nd, Sm Eu, Tb, Yb, Lu, Sc, Co, Rb, Cs, Ba, Hf, Ta and Th have been estimated in geological rock samples by Instrumental Neutron Activation Analysis after irradiation of the sample with Thermal Neutron flux from CIRUS and DHRUVA reactor at BARC Mumbai. Because of high neutron flux and more irradiation time in DHRUVA reactor the sensitivities of these elements has increased manifold. The detection limits of all the elements improved considerably. REE analysis by INAA technique helps to find the petrogenesis of the rock which indirectly guides the uranium exploration..

Introduction

Instrumental Neutron Activation Analysis is a nondestructive multi-elemental analysis widely used for determination of Rare Earth, and trace elements. This technique has an advantage of being very sensitive for the Rare Earth and trace elements. Neutron Activation is based on irradiation of a sample with neutrons available from different sources [1]. Geological rock samples along with pure elemental standards are irradiated with thermal neutrons from two different nuclear reactors, CIRUS and DHRUVA at BARC Mumbai and induced radioactivity is measured for the determination of concentration of the Rare Earth and trace elements. In this paper comparative study has been carried out for the sensitivities and Detection limits of Rare Earth and trace elements in geological rock samples by using neutron sources from two different reactors.

Experimental Methodology

The geological rock samples are crushed to -200 mesh to ensure homogeneity in the samples. Around 100 mg of each sample is wrapped in high pure Aluminum foil, along with the standards and are irradiated with Thermal neutrons in CIRUS research reactor with a flux of 10^{12} n/cm^2/s for 7 h at BARC Mumbai. After cooling the samples for 2 days these samples are flown to Hyderabad. Analysis is carried out using a p - type (PGC 3018) High Purity Germanium (HPGe) coaxial semiconductor detector (manufactured by DSG detector systems GmbH) with a Resolution of 2.0 keV at 1332 keV of ^{60}Co source and a relative efficiency of 30% coupled to the target dMCA-pro-digital Multi-Channel-Analyser. The sample is kept at a distance of about 10 cm from the detector.

These samples were also irradiated with Thermal neutrons in DHRUVA reactor for 72 h having a flux of 10^{13} n/cm^2/s with a reduced sample weight of around 10 mg. The analysis was carried out with the same detector system mentioned above. The sensitivities and Detection limits were calculated. The INAA technique is carried out by applying relative method. After irradiation of the elemental standards along with the geological rock samples, the activities are measured in identical geometry with respect to detector.

Results and Discussion

Depending on the half life of the elements, the gamma activity is measured in different phases [2]. The concentrations of La, Ce, Nd, Sm Eu, Tb, Yb, Lu, Sc, Co, Rb, Cs, Ba, Hf, Ta and Th have been estimated in geological rock samples by Instrumental Neutron Activation technique using relative method. Sensitivity of an element is defined as counts / sec / g and calculated. Sensitivity depends on cross section, Neutron flux and the gamma ray energy efficiency of the detector, irradiation time, decay time and counting time. Decay time corrections were applied using the formula $e^{-\ t_{d.}}$ where -decay constant of the activation product, t_d is the decay period.

The detection limits are calculated using "Currie Equation"[3].

$$MDL = N_D / \text{Sensitivity of the element} \quad (1)$$

Where $N_D = 4.653 * {}_{NB} + 2.706$

NB is background counts. Counting of samples has been carried out in low background room which is constructed with pure quartz of 2 feet thickness located 3 feet below the ground level. Hence the natural background is low. For the calculation of the background for each peak is as follows:

NB = Gross counts of the peak – Net counts of the peak.

Because of high neutron flux and more irradiation time in DHRUVA reactor the sensitivities and detection limits of these elements has increased manifold.

Table 1: Sensitivities and Minimum Detection limits of elements using CIRUS and DHRUVA reactors

Element	Energy in keV	CIRUS reactor		DHRUVA reactor	
		Sensitivity (Counts/sec/ g)	Detection limits (ng)	Sensitivity (Counts/sec/ g)	Detection limits (ng)
^{139}La ->^{140}La	1596.2	2.2	400	28	50
^{140}Ce ->^{141}Ce	145.4	2.6	500	32	50
^{146}Nd ->^{147}Nd	531.0	0.15	20 g	1	5 g
^{152}Sm ->^{153}Sm	103.2	50	50	425	10
^{151}Eu ->^{152}Eu	1408.0	6.5	10	100	0.5
^{159}Tb ->^{160}Tb	966.2	15	20	270	10
^{174}Yb ->^{175}Yb	396.3	15	70	90	20
^{176}Lu ->^{177}Lu	208.4	140	10	650	2.0
^{45}Sc ->^{46}Sc	889.3	85	10	1685	1.0
^{59}Co ->^{60}Co	1332.5	3.5	200	110	20
^{85}Rb ->^{86}Rb	1077.0	0.13	50 g	2.05	10 g
^{133}Cs ->^{134}Cs	795.9	3	100	100	20
^{130}Ba ->^{131}Ba	496.3	0.016	200 g	0.4	50 g
^{180}Hf ->^{181}Hf	482.2	7	100	90	10
^{181}Ta ->^{182}Ta	1221.4	0.85	100	100	10
^{232}Th ->^{233}Pa	311.9	14	100	130	10

Table 1 below indicates the sensitivity and detection limits with an uncertainty of 10% for Rare Earth and trace elements in geological rock samples using CIRUS and DHRUVA reactors

Conclusions

Rare Earth and trace elements were determined after irradiation of the sample with Thermal Neutron flux from CIRUS and DHRUVA reactor at BARC Mumbai. The sensitivities of La, Ce, Eu, Tb, Sc, Co, Rb, Cs, Ba and Hf improved 10 to 35 times when compared to the sensitivities obtained from CIRUS reactor where as sensitivities of Nd, Sm, Yb, Lu and Th improved 5 to 10 times with Ta showing the maximum improvement by almost 115 times. Due to high thermal neutron flux and more irradiation time in DHRUVA reactor compared to CIRUS reactor, the weight of the sample required is less than 10 mg. The level of activity is high, hence cooling time required after irradiation is 4 to 5 days. The change of reactor from CIRUS to DHRUVA, the improved sensitivities and detection limits in geological rock samples.

References

[1] P.J.Potts, Neutron Activation Analysis, Hand book of silicate rock Analysis Blackie Chapman and Hall New York (1987) 399.

[2] N. Rupa, V. Koteswara Rao, H.K. Sabot, A.A.P.S.R. Acharyulu, G.B. Rout Golden Jubilee Volume, The Indian Mineralogist, J. Min. Soc. India, 45 (2011) 202.

[3] Lloyd A. Currie Analytica Chimica-Acta 391 (1999) 127.

[4] A.V.R. Reddy & R. Acharya, Proc.of DAE-BRNS discussion meet on Current trends and Future perspectives of Neutron Activation Analysis (2006) p.7.

Does Anticoincidence Counting Improve Detection Limits of Short-lived Nuclides by Pseudo-cyclic INAA?

W. Zhang[1,2], A. Chatt[1]

1. *Trace Analysis Research Centre, Department of Chemistry, Dalhousie University, 6274 Coburg Road, Room 212, PO BOX 15000, Halifax, NS, B3H 4R2, Canada; E-mail: a.chatt@dal.ca*
2. *Radiation Protection Bureau of Health Canada, 775 Brookfield Road, AL 6302D1, Ottawa, ON, K1A 1C1, Canada*

A pseudo-cyclic instrumental neutron activation analysis method in conjunction with anticoincidence counting (PC-INAA-AC) has been developed for the determination of up to 9 elements through their short-lived nuclides, namely ^{108}Ag (120 s), ^{110}Ag (24.6 s), ^{165m}Dy (75.4 s), ^{20}F (11.0 s), ^{75m}Ge (48.9 s), ^{179m}Hf (18.7 s), ^{86m}Rb (61.0 s), ^{46m}Sc (18.7 s), ^{77m}Se (17.4 s), and ^{177m}Yb (6.41 s).The method has been applied to several biological and environmental reference materials.

Introduction

Instrumental neutron activation analysis (INAA) is a well-established analytical technique for the simultaneous determination of multielement concentrations in a variety of sample matrices. One of the problems generally encountered in INAA is the high background activity arising from the scattering of photons, a phenomenon known as the Compton Effect. In order to reduce the Compton background events and lower the detection limits, anticoincidence counting (AC) can be employed. The Compton suppression spectrometer (CSS) has been around since the 1950's. The electronic instrumentation and spectrometry systems have been periodically developed over the last 40 years or so. Recently, much more attention has been paid to this technique by nuclear analytical chemists.

The combination of generally high isotopic abundance, large cross section, short time to reach saturation activity, and interference-free gamma-rays indicate that the short-lived nuclides can be produced in high yields and advantageously used for trace element determination within a relatively short total experimental time. For the purpose of the work reported here, the short-lived nuclides are defined as those with half-life less than 120 s. The elements which have a sensitivity ratio of about 1 or <1 for long-to-short-lived nuclides for experimental conditions used here are chosen for the present study [1].

A systematic investigation has been carried out on the merits and limitations of AC counting for short-lived nuclides which are most commonly used in NAA. The list of nuclides of interest include: ^{108}Ag (120 s), ^{110}Ag (24.6 s), ^{165m}Dy (75.4 s), ^{20}F (11.0 s), ^{75m}Ge (48.9 s), ^{179m}Hf (18.7 s), ^{86m}Rb (61.0 s), ^{46m}Sc (18.7 s), ^{77m}Se (17.4 s), and ^{177m}Yb (6.41 s). These nuclides have been studied using both conventional instrumental INAA and pseudo-cyclic INAA (PC-INAA) irradiation procedures. Experiments have been done to calculate the peak efficiency reduction factor (PERF) values of the major gamma-rays of these nuclides. The practical advantages of PC-INAA coupled to anti-coincidence counting (PC-INAA-AC) method have been evaluated.

Experimental

Samples were irradiated in the Dalhousie University SLOWPOKE-2 reactor (DUSR) facility at a fission neutron flux of 5×10^{11} cm^{-2} s^{-1} for 30 s, allowed to decay for 10 s, and counted for 30 s.

An EG&G Ortec HPGe p-type coaxial detector was used as the principal detector in both conventional and anticoincidence gamma-ray spectrometry. This detector had a peak-to-Compton ratio of 93:1, a relative efficiency of 25% with respect to a standard NaI(Tl) detector, and a resolution (FWHM) of 1.72 keV at the 1332.5-keV photopeak of ^{60}Co. The HPGe detector was surrounded with a 10"x10" NaI(Tl) annulus and a 3"x3" NaI(Tl) plug as well as timing electronics for anticoincidence counting; the detector then gave a peak-to-Compton ratio of 582:1 at the 661.6-keV photopeak of ^{137}Cs using the IEEE convention of the number of counts per channel in the Compton plateau (358-382 keV).

Results and Discussion

Several factors that can influence efficiency of the methodology, such as the distance of the sample from the HPGe detector surface and the relative position of the NaI(Tl) annulus with respect to the HPGe detector, were investigated in detail by Zhang [2] and optimized for the short-lived nuclides.

The sensitivities and PERF of the analytically useful gamma-rays of the short-lived nuclides were measured by both conventional and anticoincidence spectrometry. It was evident that the behaviour of short-lived nuclides in anticoincidence counting mode will depend on a given nuclide as well as its photopeaks. For nuclides, such as ^{110}Ag, ^{165m}Dy, ^{20}F, ^{179m}Hf, and ^{177m}Yb, which emit two or more gamma-rays per disintegration, their peak efficiency in anticoincidence counting depends significantly on the individual peak. This means that for the same nuclide, one peak is reduced while the other stays virtually the same or suffers only a small reduction, such as in ^{165m}Dy where the gamma-rays are not in coincidence with each other. The peak efficiency of single gamma-ray emitting nuclides, such as ^{75m}Ge, ^{86m}Rb, ^{46m}Sc, and ^{77m}Se, did not

suffer any reduction in anticoincidence counting; so they can be advantageously measured in an anticoincidence system.

A PC-INAA-AC method and an analytical figure of merit term for the optimization of the best conditions for measuring the activities of the above nuclides were developed [2]. In most cases, 3 to 4 cycles were found to be optimal for their determinations as shown for Se in a previous publication [3]. The methods were applied to a number of biological and environmental materials. The detection limits were significantly lowered to ppb levels using the PC-INAA-AC method. The Rb and Dy content of several NIST reference materials (RM) and Standard Reference Materials (SRM) obtained by the PC-INAA-AC method are presented in Table 1 to demonstrate its usefulness. It is evident that the Dy content of none of the SRMs and RM analyzed here are certified due to the lack of reliable data. In case of Rb, the certified values exist except for two materials. Our values for Rb agree well with the certified values where such comparisons can be made.

Conclusions

The PC-INAA-AC method has been found to be extremely useful for the determination of several elements through their short-lived nuclides which could not have otherwise been done. The detection limits of this method are of the order of ng g^{-1} for all elements analyzed. These limits are at least 2 orders of magnitude lower than those obtained by conventional INAA. So the answer to the question asked in the title is definitely "YES".

Table 1: Rb and Dy content of NIST reference materials by PC-INAA-AC

SRM/RM	Concentration (mg kg^{-1})	
	Rb	Dy
SRM 1515	11.3 ± 0.9	2.32 ± 0.11
NIST value	10.2 ± 1.5	—
SRM 1547	21.3 ± 0.7	0.69 ± 0.05
NIST value	(19.7)	—
SRM 1572	4.47 ± 0.42	0.060 ± 0.007
NIST value	4.84 ± 0.06	—
SRM 1575	10.9 ± 1.1	0.031 ± 0.005
NIST value	11.7 ± 0.1	—
SRM 1577b	13.3 ± 0.7	0.0021±0.0009
NIST value	13.7 ± 1.1	—
RM 8415	2.2 ± 0.3	0.017 ± 0.003
NIST value	—	—

References

[1] R.E. Tout and A. Chatt, Anal. Chimica Acta, 118(1980)341-358.

[2] W. Zhang, Ph.D. Thesis, Dalhousie University, Halifax, NS, Canada (1997).

[3] W. Zhang, A. Chatt, J Radioanal Nucl Chem 282(2009)139-143.

Determination of Boron in Selected Canadian and Japanese vegetables by Prompt Gamma Activation Analysis

M. Fukushima[1], H. Matsue[2], A. Chatt[3]

1. *Department of Basic Sciences, Ishinomaki Senshu University, Ishinomaki, Miyagi, Japan; E-mail: fukusima@isenshu-u.ac.jp*
2. *Analytical Department of Research Reactor and Tandem Accelerator, Japan Atomic Energy Agency, Tokai, Ibaraki, Japan*
3. *Trace Analysis Research Centre, Department of Chemistry, Dalhousie University, Halifax, NS, B3H 4J3, Canada*

A thermal neutron capture prompt-gamma activation analysis (PGAA) method was optimized for the determination of low levels of boron in vegetables using the PGAA facility at the JRR-3 reactor of the Japan Atomic Energy Agency in Tokai. The method is rapid and can be used without any chemical separation. The precision and accuracy of the method are good. The detection limit is around 0.5 mg kg^{-1}.

Introduction

Boron is known to be an essential element for plants. Its deficiency generally leads to reduced growth and lower yield of the plant. Excess boron may cause the death of the whole plant. It has been postulated that boron perhaps is an essential element for both animals and humans but no characteristic biochemical function has yet been proven. Boron has been reported to be nutritionally important and to act as a co-factor for calcium metabolism. It is also toxicologically important as boron can accumulate in certain vegetables as well as in other food items whose consumption may very well constitute a potential hazard. It is therefore necessary to have reliable methods available for the determination of varying levels of boron in foods and diets.

Low levels of boron are rather difficult to measure by almost all analytical techniques. Conventional instrumental neutron activation analysis (INAA) is not particularly suitable either. The ^{10}B isotope has a low abundance (19.7%) and a high thermal neutron capture cross section (4017 b) but produces a stable isotope ^{11}B. The ^{11}B isotope has a high abundance (80.3%) but low cross section (0.005 b) and produces a very short-lived nuclide ^{12}B (20.4 ms). A very fast pneumatic transfer system is required for its detection. The transfer time of the Dalhousie University SLOWPOKE-2 Reactor (DUSR) cyclic system was about 100 ms and therefore not suitable for the analysis of boron by INAA. An indirect INAA method was developed by Moir and Chatt [1] for boron but the detection limit was rather poor.

Two other nuclear analytical techniques are highly suitable for the direct determination of low levels of boron in solid samples, namely neutron activation-mass spectrometry (NA-MS) [2,3] and thermal neutron capture prompt-gamma activation analysis (PGAA) which is also called PGA by some research groups [4,5]. In the work reported here, the PGAA technique was applied to measure boron in selected Canadian and Japanese vegetable samples.

Experimental

The samples consisted of typical Canadian vegetables collected by Health Canada, prepared as-eaten basis, freeze dried and homogenized. The Japanese vegetables were bought from farmers' market in Yamagata Prefecture, washed with tap water, freeze dried, and homogenized.

The PGA facility at the JRR-3 reactor of the Japan Atomic Energy Agency in Tokai was used in this work. The details of the PGAA apparatus have been published by Yonezawa and Wood [6]. About 0.3-0.5 g of each sample was heat sealed in double FEP films of 15 5 mm. Then the sample bag was hung in PTFE frame by PTFE strings. Sample and sample holder were placed in PTFE sample box at an angle 45° to the neutron beam. The thermal neutron flux was 5.7 x 10^{8} cm^{2} s^{-1} when focused. Air was purged from the sample box, and helium gas was allowed to flow through continuously during irradiation. Irradiation time varied between 1000 and 50000 s depending on the boron content of the sample. The gamma-ray spectrum was recorded using a Compton suppression system. The photopeaks were analyzed using the gamma-ray spectrum analysis program by SEIKO EG&G.

Results and Discussion

Boron levels were calculated from the calibration curve using net peak area for the characteristic Doppler-broadened 477-keV photopeak from the ^{10}B(n,)^{7}Li reaction. It is well established that this peak could be interfered with by 472-keV peak of sodium which is known to be present in nutritional materials. The correction method proposed by Anderson et al. [5] was used in this work.

Two control samples were used in this work. Our average value of 66.4±5.0 of three analyses for the NIST SRM 1572 Citrus Leaves agree with the literature values of 63.5±0.2 [5] and 65.8±4.7 [6]. The average value of 34.7±2.7 of three measurements obtained in this work for the NIST SRM 1573 Tomato Leaves agree

with 38.3±0.7 literature [5] and information value of 30. Our detection limit was 0.7 for 1000 s irradiation for both of the SRMs. All values are given in mg kg^{-1}.

The PGAA method was applied to the Canadian and Japanese vegetable samples. A small selection of the results is presented in Tables 1 and 2. These values are similar to those published by Anderson et al. for the U.S. vegetables [7].

Table-1: Mass fractions of boron (mg kg^{-1}) in dry weight and wet weight for Canadian vegetables

Vegetable	Boron mass fraction	
	dry weight	wet weight
Broccoli	31.0 0.9	2.51 0.07
Cauliflower	23.1 0.9	1.39 0.05
Celery	42.4 0.9	2.04 0.04
Lettuce	23.3 0.8	1.58 0.05

Table-2: Mass fractions of boron (mg kg^{-1}) in dry weight and wet weight for Japanese vegetables

Vegetable	Boron mass fraction	
	dry weight	wet weight
Broccoli	24.3 0.6	3.09 0.08
Ginger	11.2 1.2	1.11 0.12
Okra	31.5 0.8	4.61 0.12

Conclusions

The PGAA method was found to be suitable for the determination of low levels of boron in presence of sodium in vegetable samples. The method is applicable to solid samples without any pretreatment. The precision and accuracy of the method are good. The detection limit is around 0.5 mg kg^{-1}.

References

[1] D.L. Moir, A. Chatt, Trans Am Nucl Soc, 73 (1995) 11

[2] W.B. Clarke, M. Koekebakker, R.D. Barr, R.G. Downing, R.F. Fleming, Appl Radiat Isot 38 (1987) 735.

[3] G.V. Iyengar, W.B. Clarke, R.G. Downing, Fresenius J Anal Chem 338 (1990) 562.

[4] M.P. Failey, D.L. Anderson, W.H. Zoller, G.E. Gordon, R.M. Lindstrom, Anal Chem 51 (1979) 2209.

[5] D.L. Anderson, W.C. Cunningham, E.A. Mackey, Fresenius J Anal Chem 338 (1990) 554.

[6] C. Yonezawa, A.K.H. Wood, Anal Chem 67 (1995) 4466.

[7] D.L. Anderson, W.C. Cunningham, T.R. Lindstrom, J Food Composition and Analysis, 7 (1994) 59.

Online Recovery of Radiocesium from Soil, Tissue Paper and Plant Samples by Supercritical Fluid Extraction

A.S. Kanekar, P.N. Pathak, P.K. Mohapatra

Radiochemistry Division, Bhabha Atomic Research Centre, Trombay, Mumbai 400 085, INDIA;
E-mail: ppathak@barc.gov.in

The feasibility of recovery of radio-cesium from soil, tissue papers, and plant samples has been evaluated by supercritical fluid extraction (SFE) route employing calix[4]arene-mono(crown-6) (CC) dissolved in acetonitrile. These studies showed that quantitative recovery of ^{137}Cs from soil samples was difficult under the conditions of these studies. However, experiments performed on tissue papers (cellulose matrix) showed quantitative recovery of ^{137}Cs. On the other hand, ^{137}Cs recovery from plant samples varied between ~50 % (for stems) and ~67.2 % (for leaves) employing 1x10^{-3} M CC + 4 M HNO_3 dissolved in acetonitrile.

Introduction

The production of ^{137}Cs ($t_{1/2}$ = 30.07 years) through man-made fission route (atomic explosions / reactors) and subsequent release during different back-end fuel cycle operations has a profound impact on the Environment. The major contribution to the release started with the testing of nuclear bombs which released about 948 PBq of ^{137}Cs (1 Peta Becquerel = 10^{15} Bq) [1]. 85 PBq ^{137}Cs was released to the environment during the Chernobyl nuclear disaster. In March, 2011, the earthquake and subsequent tsunami resulted in severe damage of the Fukushima-Daiichi Nuclear Power Plant (NPP). This accident led to the release of large quantities of radioactivity mainly the volatile fission products such as ^{133}Xe, ^{85}Kr, ^{131}I, ^{132}I, ^{134}Cs, ^{136}Cs, ^{137}Cs, and ^{132}Te. Therefore, the presence of ^{137}Cs in the natural environment is a radiological concern as it causes significant external and internal radiation exposures of living beings. The measurements of ^{137}Cs in soils give direct clues to the expected external and internal radiation exposure to the humanity. The composition of the soil and the migration behavior of ^{137}Cs can affect its presence and quantity in the food chain. Therefore, the detection and measurements of ^{137}Cs in soils form the basis of backbone of radioecology and radiological protection. The presence of ^{137}Cs in soil samples may often be at a relatively low level which will put a limitation to the conventional direct detection techniques such as gamma ray spectrometry. It, however, requires proper sample preparation involving several pre-concentration steps. In this context, supercritical fluid extraction (SFE) appears attractive option.

An attempt has been made in this paper to evaluate the feasibility of ^{137}Cs recovery from synthetic soil, tissue paper, and plant samples by SFE route employing calix[4]arene-mono(crown-6) (CC, Fig. 1) dissolved in acetonitrile, respectively.

Experimental

The samples (soil: 0.2 g, cellulose: 1'x1' tissue paper, and plant: 1.5 cm x 0.5 cm stem or leaves) were loaded in the extraction vessel and extraction runs were

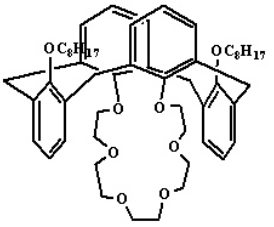


Fig. 1 Calix[4]arene-mono(crown-6) (CC)

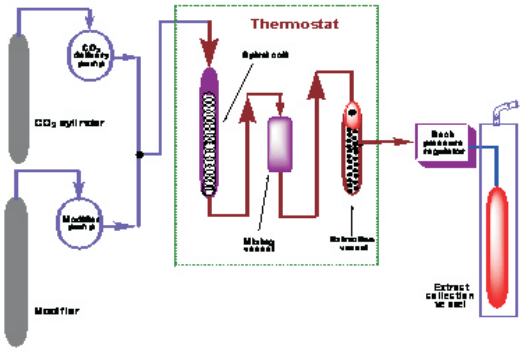


Fig. 2 SFE extraction set-up used in the present study

performed in static mode. 3.0 mL of the modifier solution (containing 1x10^{-5} to 1x10^{-3} M CC + 3-6 M HNO_3 solutions in acetonitrile) was added in the extraction vessel prior to its fixing inside the thermostat (Fig. 2).

CO_2 (>99.99% pure) was delivered to the extraction vessel at a desired flow rate of 3.0 mL/minute using delivery pump. The modifier pump was used to mix a desired percentage of the modifier (0.1 mL/minute, ~3(v/v) % of CO_2 flow rate) to the CO_2 stream. Other parameters such as pressure (P) and temperature (T) were maintained as 200 kg/cm^2 and 40°C, respectively. Independent experiments showed that recovery of ^{137}Cs did not increase beyond that of 30 minutes and therefore this duration was used for equilibration. The extraction vessel was finally flushed with the modifier solution and CO_2 for next 30 minutes. The extracted fractions were collected in glass

collection tubes of 15 mL capacity for 15 minutes containing 1-2 mL acetonitrile as the trap solution. Three fractions were collected during these extraction experiments and after each extraction experiment, a small part from the collected fractions (0.5 mL) was taken for radiometric assay to quantify the recovery of ^{137}Cs (gamma energy: 660 keV) from these samples. Each experiment was repeated at least three times and the reproducibility of the result was within ±10%.

Results and Discussion

Table 1 shows the extraction of Cs from soil matrix using CC dissolved in acetonitrile. Both the nitric acid and CC extractions play an important role in the extraction process as shown below:

$$Cs^{+}_{(aq)} + NO_3^{-}{}_{(aq)} + L_{(org)} + xH_2O_{(org)} \quad CsL^{+}(NO_3)^{-} \cdot x\,H_2O_{(org)}$$

The low extractability of ^{137}Cs from soil matrix is in conformity with the sorption studies reported elsewhere [2]. High sorption properties of the finely dispersed fraction of soils for ^{137}Cs sorption are associated with the capability of certain rock-forming minerals such as phyllosilicates, clays. It is generally recognized that Cs(I) is strongly and selectively sorbed by fraction of soils, sediments and suspended particles.

Table 1: Supercritical fluid extraction ^{137}Cs from soil samples using CC dissolved in acetonitrile; Soil sample size: 0.2 g (25 Bq)

[CC], M	[HNO_3], M	Recovery (%)
$1x10^{-3}$	3.0	25(±2)
$1x10^{-3}$	4.0	47(±2)
$5x10^{-4}$	4.0	17(±2)
$5x10^{-4}$	6.0	35(±3)

However, it was possible to quantitatively recover ^{137}Cs from cellulose matrix of the tissue papers. Table 2 shows (a) an increase in ^{137}Cs recovery with increased CC concentration from 79(±2)% ($1x10^{-6}$ M) to 100(±5)% ($1x10^{-4}$ M) at 4 M HNO_3, and (b) a marginal increase in ^{137}Cs recovery with nitric acid concentration from 90(±2)% (1 M HNO_3) to 100(±5)% (4 M HNO_3) using $1x10^{-4}$ M CC. This observation indicated the influence of matrix on ^{137}Cs recovery.

SFE experiments for ^{137}Cs recovery were also performed on the plant samples (stems and leaves) from Saraca Asoca group, which were prepared in the laboratory by submerging the their roots in 600 mL tap water containing ^{137}Cs activity (~500 Bq/mL). The plant samples were dissected from the portions of stem which was just above the water level so that any external contamination can be avoided. The modifier solution used for these runs was $1x10^{-3}$ M CC + 4 M HNO_3 in acetonitrile. Whereas 49.1(±4.7) % recovery was achieved for stem samples; 67.2(±10.4) % activity could be recovered from the leaf samples (Table 3). SFE experiments after drying and grinding these samples showed no improvement in the recovery of radio-cesium.

Table 2: Supercritical fluid extraction ^{137}Cs from cellulose samples using CC dissolved in acetonitrile; Tissue sample size: 1"x1" (45(±3) Bq)

[CC], M	[HNO_3], M	Recovery (%)
$1x10^{-6}$	4.0	79(±2)
$1x10^{-5}$	4.0	95(±5)
$1x10^{-4}$	1.0	90(±2)
$1x10^{-4}$	2.0	88(±2)
$1x10^{-4}$	3.0	94(±5)
$1x10^{-4}$	4.0	100(±5)

Table 3: Supercritical fluid extraction ^{137}Cs from plant samples (stems and leaves) using $1x10^{-3}$ M CC + 4 M HNO_3 dissolved in acetonitrile

Sample	Initial activity, Bq	Recovery (%)
Samples without drying		
Stem-1	31.25	48.7
Stem-2	36.43	54.0
Stem-3	34.10	44.7
Average:		49.1(±4.7)
Leaf-1	8.8	59.1
Leaf-2	49.2	78.9
Leaf-2	28.7	63.5
Average		67.2(±10.4)
Samples after drying (at 140°C) and crushing as powder		
Leaf-1	9.5	47.1
Stem-1	43.9	56.3
Stem-2	71.6	65.4
Average:		61.0(±6.4)

These studies suggest that SFE method can be used for the recovery and estimation of radio-cesium from different plant samples. However, the recovered activity has to be corrected by a factor for predicting the actual activity.

Conclusions

These studies shows that SFE can be used for the recovery of radio-cesium from different environmental samples. However, extraction from soil samples is relatively difficult.

References

[1] P. Thakur, S. Ballard, R. Nelson. Sci. Total Environ. 458-460 (2013) 577.

[2] S.A. Dmitriev, A.S. Barinov, V.M. Kuptsov, Radiochemistry, 53 (2011) 437.

Analysis of Essential Elements in Medicinal Plants and their Respective Soils by Neutron Activation Analysis

M. Ratna Raju[1], P.V. Madhusudhana Rao[1], M.K. Raju[2], J.S. Brahmaji Rao[3], D.Vijayalakshmi[1], N.P. Seshadreesan[3], C.R. Venkatasubramani[3].

1. *Department of Nuclear Physics, Andhra University, Visakhapatnam 530003, India; E-mail: jessyratnam@gmail.com*
2. *Deaprtment of Physics, Andhra University, Visakhapatnam-530003, India*
3. *Fuel Chemistry Division, Chemistry Group, Indira Gandhi Centre for Atomic Research, Kalpakkam 603 102, India*

In this study, the essential elements for humans in selected medicinal plants and their respective growing soils are measured by Neutron Activation Analysis. The concentrations of Na, K, Fe, Br, Al, Mn, Cl, Ca and Mg were analyzed using 20 kW KAMINI Reactor, Indira Gandhi Centre for Atomic Research (IGCAR), Kalpakkam. Results show that justification for the usage of these medicinal plants in the treatment of various diseases. Moreover, these results can be useful for preparing dosage of the herbal formulations.

Introduction

Medicinal plants are the oldest known health care products in nature. They are rich source of antioxidants and essential inorganic elements [1]. The plant medicines are gaining popularity as alternative and complementary therapies around the world. Therefore, scientific studies of medicinal plants are required to judge their efficacy and medicinal properties. Moreover, medicinal plants have some chemical substances that produce a definite physiological action in a human body. Elements concentrations present in medicinal plants are of great importance to understand their pharmacological actions [2]. Quantification of essential and toxic elements is important for determining the effectiveness of the medicinal plants in treating various diseases.

In the present study, Instrumental Neutron Activation Analysis (INAA) was used for the determination of elemental concentrations of three medicinal plants. This method has been applied, in the past, in the studies of several biological materials including plant samples. Apart from the high sensitivity for many elements, INAA has the advantages such as simultaneous multi elemental analysis, less matrix effects and not influenced by the chemical state of the elements under investigation. Sensitivity of the analytical technique INAA has been exploited to study the elemental content in three Indian medicinal plants, namely Sphaerenthus indicus, Cassia fistula and Murraya koenigii and their respective soils.

Experimental

The scientific names along with the vernacular names of the medicinal plants and their medicinal uses are given in detail in Table 1. In the present investigation samples were collected from the agency regions of Visakhapatnam, Andhra Pradesh. The medicinal plants selected for the study are widely used in treatment of several of diseases. Surface contaminants of the plant samples were removed by washing with tap water twice and then with deionized water.

Table 1: Medicinal plant sample selected for study

Sl. No	Local name	Botanical name	Medicinal use
1	Bodasaramu	Sphaerenthus indicus	It is useful in liver and gastric disorders. Seed and root used as anthelmintic, in chest-pains.
2	Rela	Cassia fistula	It is used in leprosy, jaundice, syphilis and heart diseases.
3	Karivepaku	Murraya koenigii	It is used for diabetes, diahhroea, burns, eye disorder, snake bite

The samples were dried at 70°C for overnight in an oven to reduce moisture content. The samples were powdered using agate mortar and pestle. Two biological reference materials NIST CRM No: 7 (Tea leaves) and IAEA SL-1 (soil sample) were used as a comparator multi-elemental standards for plants and soils respectively.

The samples were weighed in the range 75-150 mg and heat sealed in clean polyethylene. Samples and reference materials were packed in identical geometry and placed in the rabbit (20 mm diameter and 30 mm length) which was tightly screwed. Samples were irradiated for 5 minutes for short lived followed by 6 hours for long lived radionuclides at thermal neutron flux of $6x10^{11} cm^{-2}s^{-1}$ at Pneumatic fast transfer system of KAMINI reactor, IGCAR [3]. After appropriate cooling time, radioactive assay was carried out using High Purity Germanium (HPGe) detector coupled to 8k-channel analyzer.

Results and Discussion

The eleven elements concentrations were determined using relative NAA method. Certified

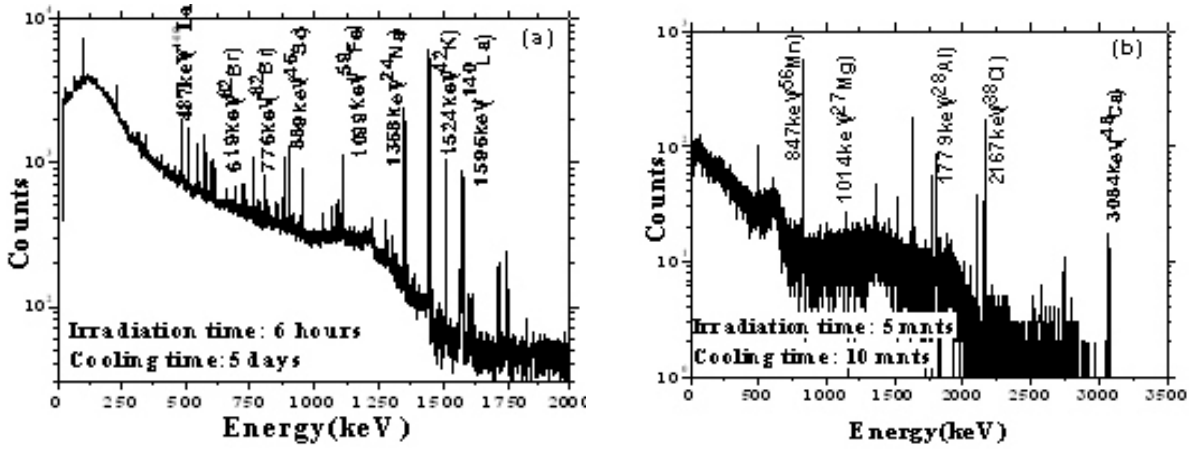


Fig. 1 Gamma ray spectra of sphaerenthus indicus from (a) long and (b) short irradiation of respectively

Reference Materials NIST CRM No: 7 (Tea leaves) and IAEA SL-1 (soil sample) also analysed for validation of the method. Elements Na, K, Fe, Br, La, Sc were determined by long irradiation and Al, Mn, Cl, Ca, Mg were determined by short irradiation. Elements were analyzed in medicinal plants by measuring their characteristic -ray energy as well as half-lives. The typical gamma-ray spectra of sphaerenthus indicus from long and short irradiations are shown in the Fig. 1. Concentrations were determined in reference materials are good agreement with certified values. The uncertainties are due to peak fitting error and counting statistics with in 10%. The observed elemental concentration in medicinal plants at different levels which is mainly attributed to the differences in botanical structure, as well as in the mineral composition of the soil in which the plants are grown.

Among the elements measured in plant samples, K, Al, Fe and Na were found to be present at the major concentration level. Cr, V and Na were found at the minor level, while Br, La and Sc were present at the trace level. The elements Mg, Ca and Hf in plants samples were below detection level which have significant concentration in soil samples. Important factors to consider ambient climatological conditions as well as the mineral composition of the soil in which plant grows.

Conclusions

INAA is very sensitive non-destructive and multi-elemental technique to analyze the biological samples like medicinal plants. The data generated on elemental concentration of the medicinal plants studied will be useful in the preparing different medicines in Ayurveda and other herbal medicine systems of Indian traditional medicine.

References

[1] V. Singh, A.N. Garg, Appl. Radiat. Isot., 48 (1997) 97.

[2] R. Lokhande, P. Singare, M. Andhele, R.Acharya, Natural Science 2 (2010), pp. 26-32.

[3] J.S. Brhamajirao, E. Senthilvadivu, N. P. Seshadreesan, R. Acharya , C. R. Venkatasubramani , A. V. R. Reddy, J Radioanal. Nucl. Chem. 294 (2012)137

The Analysis of Synthesized Copper Bhasma Using Neutron Activation Analysis Technique

Shailesh Kantak[1], Tanuja Nesari[1], Nilima Rajurkar[2*]

1. *Department of Dravyagunavidnyan, Tilak Ayurveda Mahavidyalaya, Pune 411011*
2. *Department of Chemistry, University of Pune, Pune 411 007, India; E-mail: rajurkar@unipune.ac.in*

The present paper deals with Synthesis of copper bhasma by using traditional method of Ayurveda. The Synthesis was carried out in various stages: Samanya Shodhana, Vishesh Shodhana and Marana. The concentration of copper in copper bhasma during each stage of preparation was determined by non-destructive Neutron Activation Analysis technique. For this purpose californium- 252 (flux 10^7 ns^{-1}) spontaneous fission neutron source was used. Activity of Cu-64 was measured using HPGe detector coupled with multichannel analyzer. After vishesh shodhana and Marana resulting copper bhasma showed concentration of copper as 92.89% and 59.79% respectively indicating complete conversion of metal copper into bhasma.

Introduction

The Ayurvedic pharmaceutics includes preparations by using herbs and minerals. The minerals and metal compounds (e.g. gold, iron, copper etc) are converted into non toxic and bio-acceptable, herbo-mineral compound form i.e. Bhasma through complex processes. Bhasmas are easily acceptable, palatable, fast acting and effective in smaller dosages and have longer shelf life without loosing their potency. They are widely and commonly used in various diseases according to their properties. Though bhasmas are superior to herbal products, improperly prepared bhasmas can exhibit potentially severe, toxic and adverse effects on the body, e.g. heavy metal poisoning, hepato-toxicity, renal-toxicity, neuro-toxicity etc and sometimes may lead to death. Hence atmost precaution should be taken during all the stages of preparation of bhasmas. Several processes and preparations like shodhana (purification) and marana (incineration) etc. are performed on original compound or element to convert them into a bio-acceptable form so as to assimilate easily in the body. It was thought in the past that the bhasmas of metal do not contain any traces of basic (original) metal. To support this view it is highly essential to detect the elemental concentration of basic metal in the final product (bhasma). The aggregate view over the above mentioned concept needs detection of the basic element and its concentration to -a) confirm and support the view and -b) also as a step for standardization for proper preparation and quality of final product. Hence it was decided to study elemental content at the outset as a first step of standardization.

Improperly prepared copper bhasma, if consumed, produces number of diseases and may lead to death. Hence, copper is treated with samanya shodhana, (common purification), vishesh shodhana (special purification) and marana (incineration) process. The purpose of shodhana is to remove toxic properties from copper (tamra). Vishesh shodhana is done specifically on particular metal and this process makes the metal suitable for the next process i.e marana. In marana process (incineration) various organic and inorganic substances are added in copper and then incinerated. Copper is reduced to ash (tamra bhasma) after incineration which contains products of organic and inorganic substances. The substances added during marana process helps for proper assimilation of bhasma in human body. During the marana process the non-bioacceptable form is converted into bioacceptable form. Copper bhasma is used in hepatic, gastro-intestinal, cardiac and metabolic disorders.

Metallic bhasmas are highly valued and have their own importance in Ayurvedic formulations. Preparation of bhasmas is very tedious and time consuming procedure. Previously the bhasmas were prepared by the Ayurvedic physicians themselves as per their requirements. Now a days they are manufactured in large scales in pharmaceutical houses. This new approach has created several problems, because the use of new appliances has not been standardized regarding the quality of these bhasma preparations [1]. Bhasmas prepared by different processes show different concentration of copper [2, 3]. Hence it is the need of hour to standardize these bhasmas on the basis of their classical tests as well as advanced analytical techniques. The present work deals with synthesis of copper bhasma using traditional method of Ayurveda and analysis was done by neutron activation analysis technique.

Experimental

Synthesis of Copper Bhasma

AR grade copper sheet of 0.3 mm thickness and 95.55% purity was selected as starting material for synthesis. Schematic diagram of synthesis is shown in Fig. 1.

Analysis of Copper by NAA

Analysis of copper bhasma for its copper content was done after each stage of synthesis using NAA technique. For this purpose, samples were irradiated for 24 hours in ^{252}Cf spontaneous fission neutron source (flux#$10^7 ns^{-1}$) along with standards. After irradiation,

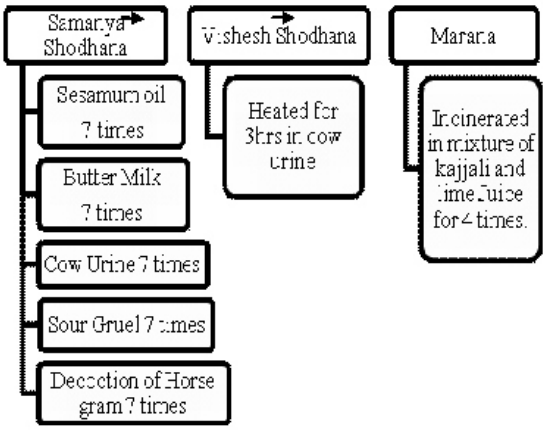


Fig. 1 Schematic diagram of synthesis of copper bhasma

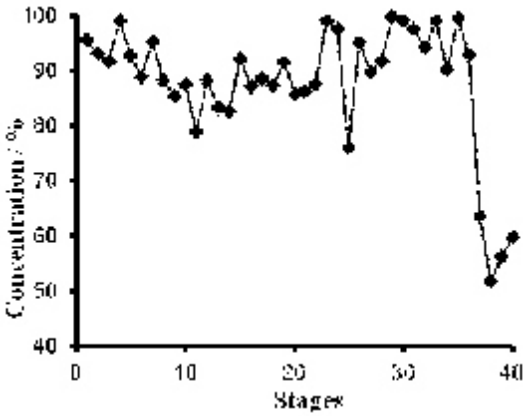


Fig. 2 Variation in concentration of copper after each stage of preparation

the activity of Cu-64 was measured by HPGe detector using 8K multi-channel analyzer. In order to verify the results obtained by NAA, few samples were also analyzed by AAS technique.

Results and Discussions

Synthesis of copper bhasma was carried out in three stages viz. samanya shodhana, vishesh shodhana and marana.

Samanya Shodhana Process

The process consisted of 35 stages. In this process thin copper sheets were heated and immersed in sesamum oil, buttermilk, cow urine, Kanji and decoction of horse gram for seven times, in each medium.

After seven stages of treatment with sesamum oil, the total weight of copper sheets increased by 1.18% while elemental concentration of copper was found to be 95.21%.

The processing with buttermilk (stages 8-14) resulted in gradual decrease in weight of copper sheets 5.59%. The elemental concentration of copper was found to be 82.64%, at the end of this process.

After seven times processing with cow urine(stages 15-21) there was 8.16% loss in weight of copper sheets and elemental concentration was found to be 86.23% indicating removal of impurities from copper sheets.

Further processing with Kanji (Sour gruel) (stages 22-28) resulted in gradual decrease in weight of copper sheets of 6.13% and in elemental concentration of 91.82% of copper.

At the end of 35th stage, seven times processing with decoction of horse gram (Kulath-Kwath) there was further loss in weight of 10.16% of copper sheets and the elemental concentration was found to be 99.59%.

Vishesh Shodhana Process

During this process, copper sheets were heated for 3 hours in cow urine. After the processing, copper concentration was found to be 92.89% indicating initial conversion of process.

Marana Process

Purified copper sheets was smeared with equal quantity of Kajjali (compound of mercury and sulphur) soaked with juice of citrus acida and four gajaputas are given. The gajaputa is an intense heating in an ancient type of furnace consisting of underground cavity measuring 2'x 2'x2' in length, breadth and depth respectively and contains 250 cow-dung cakes of size about 9 inches. The temperature in gajaputa process ranges between 800-1000°C. The crucible containing processed copper sheets was placed at the centre of this furnace and heated continuously for 12 hours. After first gajaputa, the copper concentration was drastically decreased to 63.49% indicating conversion of copper to copper bhasma. After completion of marana process (four gajaputas), the final concentration of copper was found to be 59.79%. A variation of copper concentration after each stage of preparation is shown graphically in Fig. 2.

The synthesized bhasma was examined by classical tests, confirming the formation of copper bhasma.

Conclusion

Study of elemental concentration at each stage of preparation is the first step of standardization which gives an idea about slow conversion of copper into bio-accessible copper bhasma.

References

[1] Y.B. Tripathi. A multidisciplinary approach to standardize Bhasmas (Ayurvedic metallic preparations), Curr Sci. 90 (2006) 897.

[2] A. Kumar, A.C.C. Nair, A.V.R. Reddy, A.N. Goud, Biologically trace element research 109 (2006) 231

[3] M. P. Wadekar, C.V. Rode, Y. N. Bendale, K. R. Patil, A. A. Prabhune, J Pharm. Biomed. Anal. 39(5) (2005) 951.

Characterization of Kidney Stones using NAA and other Techniques

A Srivastava[1], K.K. Swain[2], Nicy Ajith[2], T. Chavan[2], S. Bhardwaj[1], B. Vashisht[1], D.N. Wagh[2], U. Mete[3], R. Acharya[4] and A.V.R. Reddy[2]

1. *Department of Chemistry, Panjab University, Chandigarh 160014, E-mail: alok@pu.ac.in*
2. *Analytical Chemistry Division, Bhabha Atomic Research Centre, Trombay, Mumbai 400085*
3. *Advanced Urology Centre, PG Institute of Medical Education and Research, Chandigarh 160014*
4. *Radiochemistry Division, Bhabha Atomic Research Centre, Trombay, Mumbai 400085*

Six kidney stone samples were collected from patients treated in the Advance Urology Centre of PGIMER, Chandigarh. The samples were characterized using neutron activation analysis (NAA), Energy dispersive X-ray fluorescence (EDXRF), X-ray diffraction (XRD) and Fourier transform infrared spectroscopy (FTIR) techniques. For NAA, samples were irradiated in Tray rod facility of Dhruva reactor, Mumbai. Radioactive assay was carried out using high purity germanium detector coupled to 8k channel analyzer. The elements determined in the samples by NAA are Zn, Sr, Co, Fe, Cr, Sc, Se and Th. ED-XRF was used for quantification of Ca. The concentrations of trace elements like Zn, Sr, Fe and Cr were found to be lower in uric acid composite stones as compared to calcium based stones.

Introduction

Increased incidents of kidney stones have been observed in certain states of India like Punjab, Himachal Pradesh, Haryana, Uttar Pradesh, Rajasthan and Gujarat so much so that the area has been nicknamed Stone Belt of India. Patients having kidney stones suffer from acute pain due to blockage in the track. Kidney stones are generally formed when there is a decrease in urine volume and/or an excess of stone-forming substances in the urine. Some of the factors perhaps responsible for kidney stone formation are metabolic disorder, ion transport within intestinal tract and kidney, diet including fluid intake, genetic factor, geographical location, water quality, climate, occupation, stress, drugs etc. The stone precipitation process is still not properly understood in spite of a number of studies on this subject [1,2] having been carried out using various analytical techniques such as proton induced X-ray emission (PIXE), Energy dispersive X-ray fluorescence (EDXRF), X-ray diffraction (XRD), Rutherford back scattering (RBS) and instrumental neutron activation analysis (INAA). In the present work six kidney stone samples collected from patients being treated in the Advance Urology Centre of Post Graduate Institute of Medicine and Research, Chandigarh were characterized using NAA, EDXRF, XRD and Fourier transform infrared spectroscopy (FTIR) to understand the role of trace elements on the formation of stone.

Experimental

The kidney stones were removed from the patients using extracorporeal shock-wave lithotripsy, endoscopic, laproscopic and various open surgical procedures. The samples were dried for several days in a desiccator followed by grinding using pestle and mortar. Powdered samples were taken for measurements using NAA, EDXRF, FTIR and XRD techniques.

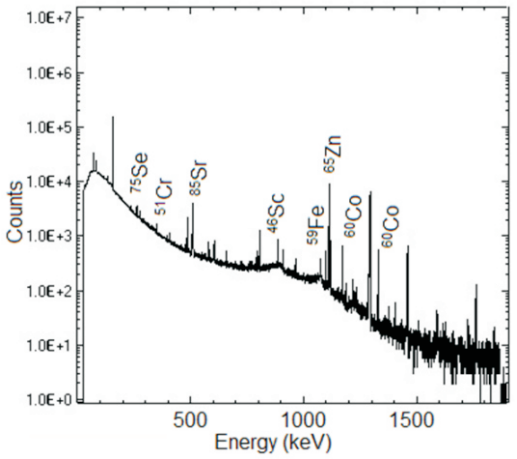


Fig. 1

During NAA, samples (50-100 mg) along with comparators (IAEA Soil-7) were packed in aluminum foils, kept inside Al container and irradiated for 7 days in tray rod facility of Dhruva reactor, BARC at a thermal neutron flux of 10^{13} cm^{-2} s^{-1}. Aliquots of IAEA RM, SL-1 were irradiated for quality control purpose. After irradiation, Al foils were opened and samples were weighed accurately into polyethylene packets for gamma activity measurements. Radioactive assay was carried out using high purity germanium (HPGe) detector coupled to 8k channel analyzer. Gamma ray spectrum of one of the irradiated sample (KS-16) is shown in Fig. 1. Relative method of NAA was used for concentration calculations.

For EDXRF measurements, powdered samples were mixed thoroughly with microcrystalline cellulose powder in agate mortar and pelletized using a hydraulic press. Calibration standards were prepared by mixing known amounts of calcium carbonate with cellulose followed by pelletization. Measurements were made using Jordan Valley, EX-3600 M EDXRF spectrometer

at ACD, BARC. Characteristic K X-rays of Ca (3.69 keV) were used for quantification of Ca. The XRD study was carried out in the Central Instrumentation Laboratory of Panjab University, Chandigarh using X'Pert Pro X-Ray Diffractometer equipped with X'Celerator solid-state detector. The Fourier Transform Infrared (FTIR) studies were carried out in the region of 400-4000 cm^{-1} using Perkin Elmer SPECTRUM BX FTIR. KBr was mixed with powdered samples to prepare pellets for recording the FTIR spectra.

Calculations

In relative method of NAA, mass of element (m) of interest was obtained using the following equation

$$m_s = m_{std} \times (A_s \times D_{std}) / (A_{std} \times D_s) \quad (1)$$

where A is the count rate for sample (s) and standard (std), D (= $e^{- \ td}$) is the decay factor, is decay constant and t_d is decay time. Mass is converted to concentration (mg kg^{-1}) by dividing with the sample mass. The concentration of Ca, using EDXRF technique, was calculated using comparative method.

Result and Discussion

The IAEA RM SL-1 was analyzed along with the samples of interest by INAA technique for quality control. The percentage errors on the measured concentrations of the elements are within ± 8% with respect to the certified / information values.

Table 1: Concentrations (mg kg^{-1}) of elements in Kidney stone samples (N=3)

Element	KS-14	KS-15	KS-16	KS-17	KS-18	KS-19
Sr	84±7	122±8	92±6	17±2	55±3	129±8
Zn	25.4±3.6	18.7±2.6	20.2±2.9	8.7±1.2	18.7±2.6	119±17
Fe	20.4±1.8	12.0±1.0	13.9±1.2	7.2±0.8	12.5±1.7	9.0±0.9
Cr	0.36±0.08	0.23±0.02	0.09±0.01	0.08±0.01	0.11±0.01	0.22±0.02
Th	<0.01	<0.01	<0.01	0.07±0.01	<0.01	<0.01
Se#	32±2	88±5	66±3	131±10	142±5	53±2
Co#	24±1	6±1	22±2	4±1	6±1	123±7
Sc#	1.2±0.3	1.0±0.3	1.4±0.3	1.0±0.3	1.3±0.2	1.2±0.4
Ca (%)*	20.0±1.2	18.5±1.8	22.2±0.4	11.8±0.6	19.8±1.4	21.3±1.4

*by EDXRF (N=4); # indicates g kg^{-1} (ppb)

The results of INAA along with concentrations of Ca (by EDXRF) in the kidney stone samples are given in Table 1. During EDXRF measurements, both samples and standards were mixed thoroughly with about 9 times of cellulose (low Z elements) before pelletization. Therefore major matrix elements in both the cases are similar. Concentrations of Ca in the stones ranged between 11.8% and 22.2%. It is observed that the concentrations of trace elements like Sr and Zn are higher in the stones that have higher concentrations of Ca. Similar positive correlation of these elements with Ca was also observed during our previous studies [2,3].

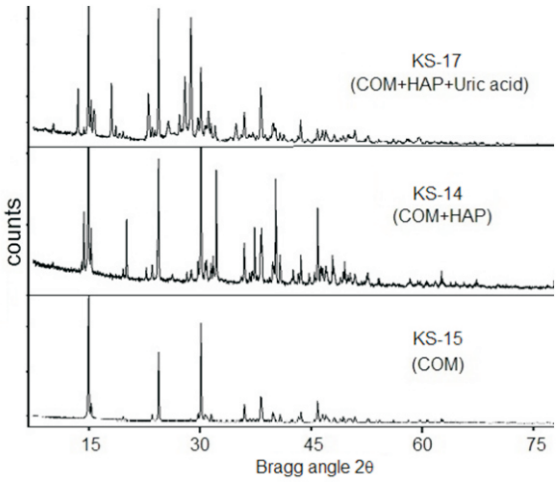


Fig. 2 XRD patterns of three kidney stone samples

The XRD patterns of the kidney stone samples indicated that KS-15, KS-16 and KS-18 are calcium oxalate monohydrate (COM), KS-14 and KS-19 are composite of COM with hydroxy apatite (HAP), and KS-17 is composite of COM, HAP and uric acid. XRD patterns of three representative samples are shown in Fig 2. These observations are supported by the FTIR based data in which characteristic bands at 3020, 1124, 1029 and 786 cm^{-1} were observed in the case of KS-17 which indicates the presence of uric acid along with bands at 1316, 780 and 517 cm^{-1} which are characteristics of COM.

Concentrations of Sr and Zn in KS-17, which is a composite of COM, HAP and uric acid, are lower than those of other samples, but these values are higher than the concentrations reported (Zn: mg kg^{-1} and Sr: < 1 mg kg^{-1}) for uric acid stone [3]. This study indicated the association of higher concentrations of trace elements with Ca based stones compared to uric acid stones. A survey of the diet of thirty five patients suffering from kidney stone disease from the Stone Belt States namely Himachal Pradesh, Punjab and Haryana was carried out. It showed that more than 60 percent of the patients surveyed had diet that was rich in milk and milk products besides spinach, mustard leaves and tea which are good source of Calcium and Oxalate known for facilitating kidney stone formation.

Acknowledgments

Authors thank operating staff of Dhruva reactor, BARC for their cooperation during the sample irradiation for NAA.

References

[1] S. Galassini, N. Q. Liu, G. Moschini, A. Tasca, G. Villi, V. Valkovic, NIM B, 43 (1989) 556.

[2] A. Srivastava, K. K. Swain, N. Ajith, D. N. Wagh, R. Acharya, A. V. R. Reddy and U. Mete; J. Radioanal. Nucl. Chem. 294 (2012) 425.

[3] A. Srivastava, K. K. Swain, B. Vasisth, P. Agrawal, U. Mete, R. Acharya, D. N. Wagh and A. V. R. Reddy, Proceedings of NUCAR (2013) 497-498.

Determination of Gold in Copper Concentrate using Neutron Activation Analysis

P.S. Remya Devi, Aditi.A. Dalvi, K.K. Swain and R. Verma

Analytical Chemistry Division, Bhabha Atomic Research Centre, Trombay, Mumbai 400085, India;
E-mail: rverma@barc.gov.in;

Copper concentrate sample was analyzed by instrumental neutron activation analysis technique for determination of gold. Samples were irradiated at F7 position of Apsara reactor, Trombay. Gamma activity measurements were carried out using high purity germanium detector coupled to 8k channel analyzer. To validate the results, pre as well as post irradiation separation of gold from the matrix was carried out using ion exchange separation method. During post irradiation methodology, ion exchange resins containing gold were irradiated along with suitable resin standards for quantification of the analyte. Apparent detection limit of gold was better in CNAA compared to INAA and RNAA.

Introduction

Copper concentrates are the raw material for copper smelters and contains approximately equal parts of copper, iron and sulfur. Besides these elements, copper concentrates also contain precious metals like gold. From recovery point of view, determination of gold in this matrix is essential.

The determination of gold in copper concentrates presents difficulties because of its low concentrations, heterogeneous distribution and presence of the large amounts of other elements like copper and iron. In order to achieve an interference-free determination at trace levels, it is necessary to separate and/or preconcentrate the gold from a larger amount of the sample.

Methods for the determination of the noble metals have been reviewed by Beamish and Van Loon [1]. The most common method for the determination of the noble metals in geological samples involves a fire-assay pre-concentration step. The fire assay technique is too expensive and also requires special facilities, equipment and a highly skilled assayer to achieve correct gold determinations. This technique is also unsuitable for sulphide minerals [2]. Ion exchange resins have been extensively used for the separation of gold from different matrices [3].

Neutron-activation analysis (NAA) is one of the most sensitive techniques for the determination of noble elements in ores [4]. In the present work, copper concentrate sample was analysed by instrumental neutron activation analysis (INAA). Radiochemical neutron activation analysis (RNAA) and chemical neutron activation analysis (CNAA) were also adopted using ion exchange separation and results were compared

Experimental

All reagents used during this work were of analytical grade. Polythene sheets and glasswares were cleaned with dilute nitric acid. Analytical grade anion exchange resin Dowex 1X8 (50-100 mesh) was used during CNAA and RNAA. Gold standard solution was prepared by dissolving a known quantity of pure gold wire in aqua-regia. The concentration of gold was ascertained by comparing with PlasmaCAL ICP standard. Suitable aliquots (2-5 mL) were evaporated and sealed in polyethylene to be used as comparator.

For INAA and RNAA, 150-200 mg of copper concentrate samples were heat sealed in clean polyethylene sheets. Samples, comparators and polyethylene blanks were triply sealed in polythene for irradiation. All irradiations were carried out for 7 hours at F7 position in APSARA reactor at a thermal neutron flux of about 10^{12} cm^{-2} s^{-1}.

During RNAA, irradiated copper concentrate sample was transferred into Teflon beakers and decomposed on sand bath using hydrofluoric acid (HF) and nitric acid (HNO_3) mixture. During digestion of the sample, small volumes of hydrofluoric acid (HF) and HNO_3 were added repeatedly for complete decomposition. After decomposition, solution was evaporated to dryness; the residue was dissolved in minimum volume of concentrated HCl and evaporated to dryness on water bath. Treatment with HCl was repeated. Finally the residue was taken in 25 mL 0.1M HCl (clear green solution). 200 mg of Dowex 1X8 resin (previously equilibrated with 0.1M HCl and air-dried) was added to sample solution and agitated on mechanical shaker for two hours. The resin was filtered, washed twice with 25 mL of 0.1M HCl; air-dried and packed in polyethylene for radioactive assay. Comparator was processed in a similar manner.

During CNAA, accurately weighed (500 mg to 1 g) samples were taken in a teflon beaker. Sample was decomposed with HF and HNO_3, and ion exchange separation was carried out as described for RNAA. The resin was filtered, washed twice with 25 mL of 0.1M HCl, air dried and packed in polythene. Comparators were prepared by equilibrating resin beads with gold standard solutions. The resin samples containing gold were irradiated in a similar way.

Radioactive assay was carried out using 45% HPGe detector (EURYSIS MESURES) coupled to 8k channel analyzer having resolution of 1.9 keV at 1332 keV of ^{60}Co.

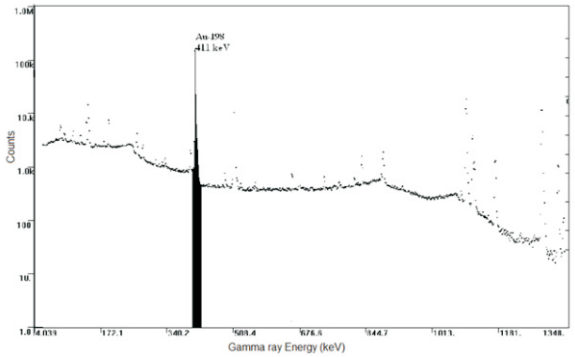


Fig. 1 Gamma ray spectrum of irradiated copper concentrate sample

Calculations

Relative method of NAA was used for determining the concentration of gold. Mass of gold (m_s) was obtained by using the relation

$$m_s = m_{std} \times (A_s \times D_{std}) / (A_{std} \times D_s) \quad (1)$$

where A is the net count rate at gamma ray peak of interest for sample (s) or standard (std), D is the decay factor ($= e^{- \ td}$), is decay constant and t_d is decay time. The mass (m_s) is converted to concentration (mg kg^{-1}) by dividing it with the sample mass.

Results and Discussion

During the work, ^{197}Au (n,) ^{198}Au reaction was used for determination of gold. 411.8 keV gamma ray of ^{198}Au ($T_{1/2}$ = 2.695 d) was used for determination of gold. The sample was allowed to cool for 5 days after irradiation in order to bring down the matrix activity (due to ^{64}Cu) to sufficiently low level. Figure 1 shows a typical gamma ray spectrum of irradiated copper concentrate sample.

The noble elements like gold form anionic complexes, (e.g. $AuCl_4^-$) with chloride ion that are readily retained on anion exchanger. The distribution coefficient values for copper and iron at lower molarities of HCl are low [5]. Therefore ion exchange separation was carried out using 0.1M HCl during RNAA and CNAA.

In ion exchange processes, yield was determined using ^{198}Au radio tracer and yield was found to be >99%.

The measured concentrations of gold in the sample by INAA, RNAA and CNAA are given in Table 1. The uncertainties given in Table 1 are at ±1s confidence limit for n independent sub sample analyses.

Table 1: Concentration of gold in copper concentrate by NAA methods

Method	Gold (mg kg^{-1})
INAA	19.6 ± 2.5 (n = 3)
RNAA	19.9 ± 2.8 (n = 4)
CNAA	18.8 ± 1.0 (n = 3)

From the Table 1, it was observed that results by all the three methodologies are in very good agreement. But the precision obtained by INAA and RNAA are inferior compared to that in the case of CNAA. This may be due to the inhomogeneous distribution of gold in the copper concentrate matrix and sample mass (copper concentrate) is restricted during neutron irradiation. In CNAA, higher masses of samples were processed and resin samples containing gold were irradiated. As matrix activity was negligible in the CNAA, (i) the samples could be counted nearer to the detector thereby increasing the sensitivity and (ii) turn-around time was small. This along with reduction in background resulted in better apparent detection limit of gold compared to INAA and RNAA. Evaluation of blank is important in the CNAA methodologies. Processed blank resins were also analyzed and concentration of gold was below detection limit.

Acknowledgement

Authors are thankful to Dr. A. V. R. Reddy, Head, Analytical Chemistry Division for his suggestions and keen interest.

References

[1] F. E. Beamish, J. C. Van Loon, Recent Advances in the Analytical Chemistry of the Noble Metals, Pergamon Press, Oxford, (1972).

[2] E.L Hoffman, J.R. Clark and J.R. Yeager, Exploration and Mining Geology, 7(1-2) (1998) 155.

[3] A.F. Olteanu, T. Dobre, R. Radulescu, E. Panturu and R. Panturu, UPB Scintific Bulletin, Series B, 72(3) (2010) 233.

[4] S. Kumar, R. Verma and S. Gangadharan, Analyst, 118 (1993) 1085.

[5] K. A. Kraus and F. Nelson, Proc. Intern. Conf. on the Peaceful Uses of Atomic Energy, Vol. VII. Geneva 8–20 August 1955. United Nations, New York, (1955) pp 113.

Evaluation of Soil to Tea Plant Elemental Correlation using k_0 based Internal Monostandard Neutron Activation Analysis

Rupali A. Lagad[1,3], D. Alamelu[1], K.B. Dasari[2], R. Acharya[2], Suresh K. Aggarwal[1]

1. *Fuel Chemistry Division, Bhabha Atomic Research Centre, Trombay, Mumbai 400085*
2. *Radiochemistry Division, Bhabha Atomic Research Centre, Trombay, Mumbai 400085*
3. *Present Address : Geosciences Division, Physical Research Laboratory, Navrangpura, Ahmedabad 380009; India; E-mail: rupali164@gmail.com*

The k_0-based internal monostandard neutron activation analysis (IM-NAA) using Sc as monostandard was employed for the determination of multielemental concentrations in soil and tea plants from tea gardens of Assam, Darjeeling and Kangra, India. A total of 17 tea leaves and corresponding soils of tea plants were analyzed by IM-NAA using neutrons from Dhruva research reactor and high resolution gamma ray spectrometry. Concentrations of nine elements viz. Ce, Co, Cr, Cs, Fe, Rb, Sc, Th and Zn were determined and used to evaluate elemental transfer factors from soil to tea plant and thus for soil-plant elemental correlation studies. High degree of soil to tea plant elemental correlation was observed with Pearson correlation coefficient values (p- value) in the range 0.6-0.9.

Introduction

Indian tea ranks second in world tea production and is one of the main agricultural products on which many tropical and subtropical countries rely for foreign exchange. In India, tea is produced in geographically well differentiated locations such as Assam, Darjeeling (both in the North-East), Nilgiris and Munnar (Southern parts) and Himachal Pradesh (North-West). As these locations are geographically distinct, there could be differences in the elemental content of tea samples originating from these locations depending upon the geochemistry of the soil and other factors. Among North-East tea products, tea grown in Darjeeling has worldwide demand due to its unmatched flavour and taste. Due to its great demand, its market price is very high and so the chances of adulteration and fraud are possible. Therefore, authentication of such valuable food products is essential to protect consumer as well as producer.

Soil is the natural basin for trace elements and, therefore, it plays an important role in element cycle in the environment. The increase in metal content of soil has a great influence on the soil quality and on human health through the plants growing on it [1,2]. Therefore, determination of metal contamination in areas of agricultural activities is important. In the present study, elemental profiling of tea plants and associated soil samples was carried out and corresponding soil-plant element transfer factors were calculated.

Multi-elemental composition pattern of food and soil was employed for authentication study of food stuffs, since, the multielement composition of vegetation is the compositional reflection of the bio-available and mobilised nutrients present in the underlying soils from which they were cultivated.

In the present work, quantitative determinations of nine elements viz. Ce, Co, Cr, Cs, Fe, Rb, Sc, Th & Zn in different tea leaf samples along with corresponding soil samples obtained from different tea plantations (Assam, Darjeeling and Kangra) were carried out using internal monostandard NAA (IM-NAA) employing Sc as monostandard.

Experimental

Total 37 authentic tea leaf buds and corresponding soil samples were collected from different tea producing regions in India. 100 - 150 g of soil samples were collected at a depth of 10 - 20 cm from the ground and from the area near to the root. Tea leaf buds and soil samples were dried and then ground and homogenized to obtain fine powder. Amongst these, 17 representative samples from Assam (8), Darjeeling (6) and Kangra (3) were taken for soil-plant elemental correlation study.

About 100 mg of each tea leaf sample was packed in a clean aluminum foil. The CRM (GSB-7) and IAEA-RM (INCT-TL-1) were also packed in separate Al- foils. For soil samples, about 100 mg of soil sample was packed in duplicate in a clean aluminum foil. The reference materials IAEA-SL-1 and IAEA-SL-3 (Lake sediments) were also packed in separate Al foils. Samples along with the standard reference materials were irradiated together in the tray rod position of Dhruva reactor at Bhabha Atomic Research Centre (BARC), Trombay, Mumbai, for 1 d at a neutron flux of ~$5x10^{13}$ cm^{-2} s^{-1}. After appropriate cooling, the gamma ray activities of the samples were measured by a high-resolution gamma spectrometer consisting of an HPGe detector with a resolution of 2.0 keV at 1332 keV (^{60}Co) and a relative efficiency of 40%. Acquisition of the gamma spectra was performed using a Multi Channel Analyzer coupled to the PHAST software.

Calculations

Elemental concentrations in tea plants and soil were determined by using internal mono standard k_0-NAA method [3]. This approach gives a relative elemental concentration of the element (x) with respect to a suitable mono standard (y) as given below in Equation 1,

$$\frac{m_x}{m_y} = \frac{S.D.C.\ f\ Q_0\ _y\ \frac{P_{Ax}}{P_{Ay}}\ _{,y}^{,x}\ \frac{K_{0,Au}(x)}{K_{0,Au}(y)}}{S.D.C.\ f\ Q_0\ _x} \quad (1)$$

where P_A is the net peak area under the gamma peak of interest, S is the saturation factor, D is the decay factor, C is the counting factor used for correcting the decay during counting period, the $k_{0,Au}$ is the literature k_0-factor with respect to ^{197}Au and is the detection efficiency, f and are neutron flux parameters [3]. Here relative detection efficiency of the detector was used and this in situ relative efficiency was determined using the -rays of activation products generated in the sample due to neutron irradiation.

In the present study, soil-plant concentration ratio was considered as transfer factor (TF) which was calculated using Equation 2.

$$C_{plant} = bc_{soil} \quad (2)$$

Where, 'b' is the transfer factor of an element.

Results and Discussion

Quality control was performed through concurrent analyses of reference materials viz. GSB-7 tea leaves and IAEA- RM-SL-1 lake sediment. The Z score (at 95% confidence limit), which gives a comparison of the determined and the reference values along with the statistical uncertainty of the measurement, were found to be < ±1. Table 1 summarizes the variations in the elemental concentrations of tea plants, soil and transfer factor observed in different regions. The uncertainities reported in the Table reflect the range of the concentrations of the different elements rather than the SD on mean concentrations. The elements Ce, Cr, Cs, Fe and Th were the highest in mean concentrations in Kangra tea leaves, while concentrations of Co and Rb were found highest in Assam and Darjeeling tea plants, respectively. In the case of elemental profiling of soil samples, Kangra region showed the highest mean concentrations of Ce, Cs, Th and Zn. Darjeeling soil samples showed the highest concentrations of Cr and Rb. Concentration of Co was found to be highest in Assam soil samples. In the case of Fe, mean concentration in soil showed order of Darjeeling > Assam > Kangra but a wide variation of concentration in case of Kangra soil samples was observed. Transfer factors were found in the order Zn > Rb > Cs > Co > Ce > Fe > Th > Sc > Cr. Regional variations in the transfer factors were observed.

This variations in the transfer factor of an element may be due to different characteristic parameters of soil e.g. pH of the soil, type of soil etc. A statistical method of correlation showed positive correlations between plant and soil with Pearson correlation coefficient values ranging from 0.55-0.89.

Table-1: Elemental concentration and variation in transfer factors of elements in tea plant and soil from different regions (A: Assam, D: Darjeeling, K: Kangra)

Element	Region	Tea leaves (mg kg^{-1})	Soil (mg kg^{-1})	Transfer factor *(x10^{-4})
Ce	A	0.109±0.024	52.3±20.4	24±10
	D	0.128±0.031	68.5±16.0	19±2
	K	0.808±0.315	108±56	83±29
Co	A	0.122±0.068	42.9±32.0	35±15
	D	0.096±0.014	33.2±11.65	31±9
	K	0.083±0.035	34.3±10.2	24±6
Cr	A	0.127±0.017	270±69	5±2
	D	0.150±0.052	359±112	4±1
	K	0.533±0.166	66±44	111±77
Cs	A	0.095±0.048	43.9±29.9	30±26
	D	0.100±0.026	35.9±15.3	32±15
	K	0.174±0.135	56.8±29.5	29±8
Fe	A	118±5	75001±18004	17±4
	D	120±7	77429±24168	15±5
	K	162±32	58119±6888	28±7
Rb	A	45.7±8.1	1289±1135	550±352
	D	52.8±9.5	1802±927	332±104
	K	47.8±5.9	1495±642	364±153
Sc	A	0.014±0.004	30.6±9.3	5±1
	D	0.012±0.003	27.8±7.3	4±1
	K	0.076±0.013	53.8±24.2	15±4
Th	A	0.004±0.002	3.1±1.5	12±2
	D	0.007±0.004	6.6±2.6	11±4
	K	0.009±0.007	8.8±5.9	10±2
Zn	A	28.8±5.1	576±125	504±21
	D	29.5±24.4	471±286	591±141
	K	29.5±11.6	647±332	473±52

Conclusions

The study of correlation between tea plant and the associated soil elemental concentration using IM-NAA method concluded that there is variation in transfer factor for each element in each region of cultivation. This indicates effect of soil properties on elemental uptake and it also showed there is necessity of a detailed study of soil properties to understand soil-tea plant elemental correlations.

References

[1] K. Loska, D. Wiechula and I. Korus, Environ. Int., 30 (2003) 159.

[2] K. Loska, D. Wiechula, B. Barksa, E. Cebula and A. Chojnecka, Pol. J. Environ. Stud., 12 (2003) 187.

[3] R. Acharya, A.G.C. Nair, K. Sudarshan, A.V.R. Reddy, A. Goswami, Appl. Radi. Isoto. 65 (2007) 164.

Performance of Digital Gamma ray Spectrometer for loss free counting and its Application in NAA for quantification of Aluminum

R. Acharya[1], K.B. Dasari[1], D. Chandrasekhar[2], T.P. Chaturvedi[1], P.K. Pujari[1]

1. *Radiochemistry Division, Bhabha Atomic Research Centre, Trombay, Mumbai 400 085; E-mail: racharya@barc.gov.in*
2. *Product Development Division, Bhabha Atomic Research Centre, Trombay, Mumbai 400 085*

A digital spectrometer loss-free counting system (DSPEC^{PLUS}) based was used for high resolution -ray spectrometry with rapidly varying dead time. This spectrometer is designed for radioactive assay of samples at high dead time and very useful for short lived radionuclides. Performance of the system was tested with both constant as well as varying dead times using ^{57}Co and ^{60}Co (long lived) and ^{28}Al, ^{52}V and ^{128}I(short lived:2 to 25 min.) radionuclides in the dead time ranges of 80- 2%. The DSPEC^{PLUS} was used for counting of short lived activation products obtained in neutron activation analysis (NAA) of a few standards and samples, neutron irradiated at PCF, Dhruva reactor. Aluminum concentrations were determined in two reference materials (RMs) and five samples.

Introduction

All spectroscopy system, whether measuring charged particle, X-rays and gamma rays, exhibit dead time losses during the counting process due to pulse processing in the electronics [1]. Several techniques are employed to reduce the effect of dead time on a spectroscopy system including live time, clock time and loss free counting modes. The electronics in the spectroscopy system utilize some fraction of time, usually in order of 1 to 70 s, to process pulse from the detector. When the incoming pulse count rates are small and constant, there is only a small probability that the first pulse will not be completely processed before the next pulse enters the detector. However, in some applications using short lived nuclides (sec to minutes) the incoming count rates can be high or change rapidly to the point where the processing of one pulse overlaps with the incident time of the subsequent pulse. In these cases the probability for dead time losses becomes much higher [2]. At high count rate, the electronics must compensate for the dead time in order to eliminate the systematic error on quantification of any particular nuclide in a sample.

To solve this problem, numerous methods have been proposed, like loss free counting, zero dead time mode (ZDT) and dead time stabilization. Loss free counting method helps to get actual the number of counts in a multichannel analyzer (MCA) for dead time exhibited during the real time counting period. The period of data acquisition in which electronics are working is called live time (LT). The actual time expired during data collection is called real time (RT). Dead time (DT) is calculated by the following formula.

$$DT = \frac{RT \quad LT}{RT} \quad 100$$

While Westphal introduced loss free counter in 1990's, ORTEC introduced digital spectrometer hardware with dual spectrum correction technique in 2000. DSPEC system has long term stability of gain, calibration and FWHM [3]. Two spectra are collected simultaneously in which one is conventional gamma ray spectrum (live time mode) and another spectrum is corrected by ZDT mode for pulse losses with virtual spectrum [4]. This virtual spectrum fully depends on computer software. Loss free counters are used for (i) long lived constant high dead time (up to 90%) (ii) Rapidly decaying samples counting both short and long lived radionuclides (iii) short lived radionuclides (iv) High dead time due to X-rays.

In the present paper, performance of ORTEC's DSPEC^{puls} digital gamma spectrometry has been used with constant / varying dead time cases. Short lived radionuclides half lives were measured and concentration of aluminum was determined in RMs and samples.

Experimental

The -ray spectrometry system consists of a HPGe detector of 30% relative efficiency and loss free counter model DSPEC^{PLUS} of ORTEC. Both digital and analog spectrometric channels were connected to computer. The experiments were performed using point source of ^{60}Co and ^{57}Co. The ^{60}Co source used as a reference source and ^{57}Co source was used for varying incoming count rate from 900 cps to 40,000 cps by varying their distance from the detector. The dead time varied from 1% to 90% with ^{57}Co source. In each measurement two spectra for LTC and ZDT were collected simultaneously. The peak area of 1332 keV of ^{60}Co was measured from all spectra. The FWHM of 1332 keV was 1.84 keV.

Then Al foil (1.5mg) and vanadium standard (50 g) were sealed in polypropylene. IAEA RMs Soil -7, SL-3 of masses (10 mg), food, ceramic samples were analyses. The samples were irradiated for 1 min in pneumatic carrier facility at Dhruva reactor, BARC at thermal neutron flux of is 5 x 10^{13} $cm^{-2}s^{-1}$. The radioactive assay was carried out using 30% relative efficiency HPGe detector connected to the DSPEC^{PLUS} with 8k MCA.

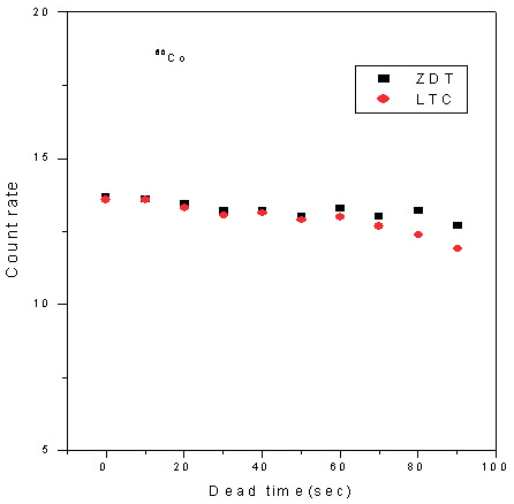


Fig. 1 Variation of ZDT and LTC long lived radionuclide

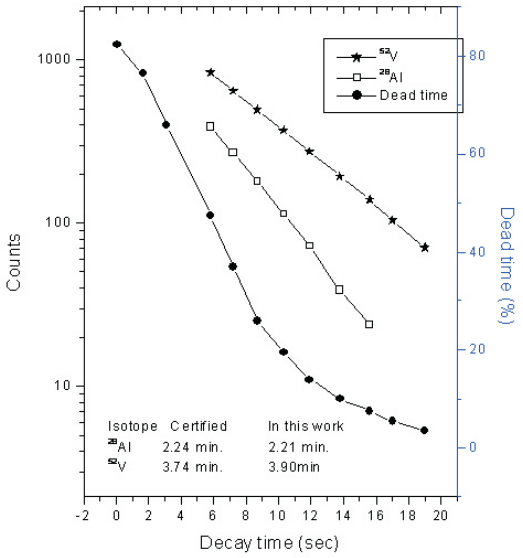


Fig. 2 ^{28}Al and ^{52}V activity decay curve

Results and Discussion

Dead time correction for long-lived nuclides with constant dead time is done by live time counting mode, whereas for varying dead time during counting the live time counting mode does not work properly. ORTEC's digital spectrometer with zero dead time mode is reported to work for both long-lived and short-lived radionuclides. The instrument was tested for its applicability for long-lived radionuclides using ^{60}Co (radionuclides of interest) and ^{57}Co and ^{22}Na (dead time sources). The count rates of 1173 keV and 1332 keV of ^{60}Co were found constant in dead time range of 2-80% is shown in Fig. 1.

To find its applicability to short-lived radionuclides, Al foil was irradiated and measured using lass free counter coupled with HPGe detector in dead time range of 70%-15. The experimental half-lives of ^{28}Al (22.21 min) and ^{52}V were found to be in good agreement with the literature reported half lives and given in Table 1. Short lived radionuclides decay curves were shown in Fig.2. This instrument is helpful for NAA using short-lived nuclides obtained from pneumatic carrier facility (PCF) of Dhruva reactor.

Table 1: Half lives of radionucles determined using loss free counter

Isotope	In this work	Lit. values	% deviation
^{28}Al	2.21 min	2.24 min	1.3
^{52}V	3.90min	3.74 min	-4.1

The half lives of short lived radionuclides in different materials were determined. Al concentrations in different samples are given in Table 2. All half life values are coincidence with certified values with % deviation between 0.42 to 1.3%. Other short lived radionuclides concentrations were determined simultaneously. IAEA Soil-7, SL-3 elemental concentration of Al, V, Ti, Mn, Na, K (2 min to 15 hrs $T_{1/2}$) were determined using PCF-Dhruva reactor. Elemental concentration were determines using live mode peak area and zero dead time mode peak areas. The deviation of values between 30% to 5%, however concentrations in ZDT are in good agreement with certified values with respect to certified values.

Table 2: Aluminum concentration (mg kg^{-1}) in different materials using loss free counter

Matrix	Sample	Al concentration
Sediment	IAEA RM SL-3	24846 ±273 (24500 ± 1200)
Soil	IAEA RM Soil-7	46158±2059 (47000)
Ceramic	Pottery	108816±1305
Ceramic	Brick	132568±1169
Food	Rice	90 ± 4
Food	Turmeric	367 ± 7
Metallic alloy	Nimonic Alloy	84 ± 5

( ) – Recommended value of RM

Acknowledgements

Authors thanks to Dr. A. Goswami, Head, Dr. P.K. Pujari, Head, NCS, Radiochemistry Division, BARC for his support and encouragement.

References

[1] G.F.Knoll, Radiation Detection and Measurement, edition. 7 (1980)

[2] M.Makarewicz, K.Burns, , J. Radioanal. Nucl. Chem, 244 (2000) 649.

[3] Menno Blaauw, Ronald M. Keyser, Appl.Radi. Iso. 67 (2009) 2079.

[4] M. Blaauw, J. Radioanal. Nucl. Chem, 257 (2003) 457

Instrumental NAA for Determination of Trace Elements in Zirconium Oxide and Aluminium Samples

A.D. Shinde[1], R. Acharya[2], A.V.R. Reddy[1]

1. *Analytical Chemistry Division, Bhabha Atomic Research Centre, Trombay, Mumbai 400085, India*
2. *Radiochemistry Division, Bhabha Atomic Research Centre, Trombay, Mumbai 400085, India; E-mail: racharya@barc.gov.in*

For chemical quality control of materials quantification of trace impurities is very important aspect. In view of this instrumental neutron activation analysis using relative and/or internal monostandard method (INAA or IMNAA) was used for the analysis of two ceramic materials namely zirconium oxide and aluminum oxide. The elements determined are as follows: Al, Ti, V, Ni, Mn and Cl in zirconium oxide, Fe, Sc, Cr, Co, Zn, Hf, Ni and Mn in aluminum oxide. The results have been compared with the results obtained by DC-arc-AES (for zirconium oxide) and ICP-MS/GFAAS (for aluminum oxide).

Introduction

Ceramics have historically played an important role in the development of modern science and technology. Owing to its several special properties including high melting point (2750°C), high resistance against acids, low thermal conductivity coefficient and excellent insulation characteristics [1], zirconium dioxide has become an interesting material in various fields of technology. It is used as starting material for production of zircaloys, which is used as structural material in nuclear reactors. High-purity alumina has varied fields of application because of their outstanding mechanical, chemical, optical and thermal characteristics. The properties of these ceramics, however, strongly depend on trace elemental impurities in the ceramic powders as their basic materials [2]. The determination of impurities is essential in order to control their quality and to investigate the synergistic action and correlation of the impurities.

Various analytical techniques such as AAS, ICPMS and ICPAES have been used to determine trace impurities in these oxides. NAA has been scarcely used for the analysis of various ceramic oxides. In this paper instrumental neutron activation analysis using relative and/or IMNAA was used for the analysis of zirconium oxide and aluminum oxide samples.

Experimental

NAA

The irradiation was performed in two sets. In the first one, the samples were irradiated for one minute. In the second, set of samples were irradiated for a longer duration of six hour. The samples were taken in the mass range of 50-100 mg. The standards were prepared from stock standard solution (1000 mg mL^{-1} Merck). The aqueous standard solutions were dried on filter paper and sealed in polythene. The filter paper was also packed for blank correction. The samples and standards were irradiated for 1 min at a neutron flux of 3 x 10^{13} $cm^{-2}s^{-1}$ using PCF, Dhruva for the analysis of short and medium live nuclides. The samples along with the standard were irradiated for 6 h at a neutron flux of 1 x 10^{12} $cm^{-2}s^{-1}$ and 3 x 10^{13} $cm^{-2}s^{-1}$at PFTS, KAMINI and self serve of Cirus respectively for the analysis of long lived nuclides. The radioactive assay was carried out using a 40 % HPGe detector coupled to 8k MCA. Fig 1 gives gamma ray spectrum of the aluminum oxide sample irradiated for six hour. The gamma lines of the activation products namely ^{59}Fe, ^{46}Sc, ^{60}Co and ^{181}Hf were used for in-situ efficiency (133-1332 keV) used in IMNAA method [3].

DC- Arc AES for ZrO_2

A Spectro Arcos direct reader spectrometer coupled with d.c arc and ICP sources was used. A set of standards containing graded amounts of trace analytes in high purity zirconium matrix and 5% AgCl + SrF_2 carrier with 0.003% Pd as an internal standard were prepared using spec-pure compounds. A blank standard was also prepared in a similar manner without addition of analytes. To optimize current settings, the intermediate standard was arced at different current settings.

ICPMS/GFAAS for Al_2O_3

The samples of about 100 mg were dissolved into a mixture of suprapure sulphuric and hydrochloric acid after heating in a microwave for 30 minutes. The resulting solutions were transferred into 100 ml glass beaker and heated upto evaporation. The solutions were diluted upto 100 ml using demineralised water. The calibration standards were prepared from Merck ICPMS standard solutions (1000 mg mL^{-1}). The suprapure nitric acid was added to the flask before dilution to maintain the nitric acid concentration upto 2% in all the samples and standard solutions. ICP-MS measurements were carried out with VG PQ Ex Cell Thermo elemental spectrometer. AAS measurements were carried out on GBC 906 Atomic Absorption Spectrometer.

Results and Discussion

The results obtained for zirconium oxide sample are given in Table 1. The uncertainties expressed on the results are standard deviations of four independent analyses. The % deviation between the results by NAA

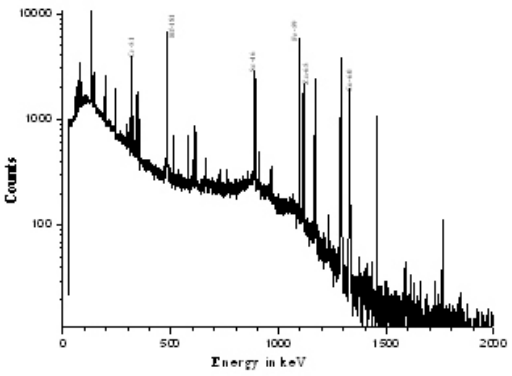


Fig. 1 Gamma ray spectrum of aluminum oxide sample irradiated for 6h

and D.C. Arc AES is lower for Al and Mn while it is higher for V and Ni. The element Ti could not be detected by DC-Arc-AES. The results obtained for aluminum oxide sample are given in Table 2. The elements Hf and Sc could not be detected by ICPMS/GFAAS. The Fe was used as internal monostandard in IMNAA in the case of long lived nuclides. The % deviation between the results obtained by NAA relative method and IMNAA is within ± 4%.The % deviation between the IMNAA and ICP-MS\GFAAS results is within 10%. For Ni, Mn and Cr the % deviation was higher than 5%. The NAA method is found to be more effective for determining elements like Sc and Hf at ppb levels in aluminum oxide matrix, while Ti and Cl in zirconium oxide matrix.

Table-1: Determined concentration of impurity elements in zirconium oxide sample (ZO-1) by NAA and D.C. Arc AES (results are expressed as mg kg^{-1}).

Element	NAA	D.C Arc AES	% Deviations
Al	28.2 ± 0.9	27.1 ± 1.2	3.9
Ti	14.1 ± 0.4	ND	-
V	36.1 ± 1.2	39.1 ± 1.5	8.3
Mn	2.02 ± 0.12	1.95± 0.08	3.4
Ni	11.3 ± 0.6	12.1 ± 0.4	7
Cl	115 ± 4	ND	-

Table-2: Determined concentrations of impurities in aluminium oxide sample ALO-1 by NAA relative method, IMNAA and ICPMS/GFAAS. (Results are expressed as mg kg^{-1}).

Element	NAA relative	IMNAA	GFAAS/ ICP-MS
Fe	1144 ± 24	1134 ± 22	1132 ± 18[a]
Sc*	102 ± 4	101 ± 3	ND
Cr	11.3 ± 0.3	11.2 ± 0.3	12.3 ± 0.3[b]
Co	1.72± 0.05	1.70 ± 0.04	1.70±0.03[b]
Zn	121 ± 2	122 ± 3	121 ± 2[b]
Hf*	98 ± 3	102 ± 4	ND
Ni	42 ± 2	43 ± 1	40 ± 1[b]
Mn	23.1 ± 0.6	22.7 ± 0.4	24.7 ± 0.5[b]

*results are expressed as g kg^{-1}
a = GFAAS value.
b = ICP-MS value.

Conclusion

The NAA technique was applied for the determination of trace impurities in zirconium oxide and aluminum oxide samples. The method is validated by analyzing the samples by DC-arc-AES and GFAAS/ICP-MS. The IMNAA method could determine the trace impurities in aluminum oxide by using Fe as internal monostandard.

Acknowledgement

Author thanks Dr.S. K. Thulasidas, RCD, BARC for their help during DC-arc-AES analysis and Dr. S. A. Kumar, ACD, BARC for her help during ICP-MS/ GFAAS analysis.

References

[1] Kirk-Othmer, Encyclopaedia of Chemical Technology, 2nd edition, Vol. 22, Interscience, New York, 1970, 651.

[2] Broekaert J A C, Graule T, Jenett H, Tolg G, Tschopel P, Fresenius Z Anal Chem 332(1989) 825.

[3] R Acharya, A G C Nair, A V R Reddy, S B Manohar, Appl Radiat Isot, 57 (2002) 391.

[4] N Pathak, V C Adya, A Sengupta, S K Thulasidas, T K Seshagiri, S V Godbole, DAE-BRNS Symposium on Nuclear and Radiochemcitry, 2013 (NUCAR-2013), Feb 19-23, Jabalpur, 395-396.

Determination of Aluminium content in Foodstuffs by Neutron Activation Analysis utilizing PCF of Dhruva Research Reactor

B.B. Nanda[1], R.R. Biswal[1], A. D. Shinde[3], R. Acharya[2], P.K. Pujari[2]

1. *Department of Chemistry, DRIEMS, Biju Patnaik Univ. of Technology, Cuttack, Odisha*
2. *Radiochemistry Division, Bhabha Atomic Research Centre, Trombay, Mumbai 400085, India; E-mail: racharya@barc.gov.in*
3. *PhD student, ACD, BARC, Mumbai*

Aluminium is one of the toxic elements in food and food products are the main sources of aluminium entering the human body. In the present study, Aluminium (Al) content of 25 samples (from market) including rice, rice products, wheat, spices, tea, tea products, and lentitls were determined using instrumental neutron activation analysis (INAA). The concentrations of Al were in the range of 25-500 mg kg^{-1} in general except for tea and one spice sample. Samples were neutron irradiated using PCF of Dhruva reactor and 1779 keV -ray of ^{28}Al was analyzed using HPGe detector based -ray spectrometry. Three RMs was analyzed for method validation. The results obtained by INAA are discussed in this paper.

Introduction

Aluminium is the third most abundant (8.8%) element in the earth's crust. It is found in air, water and soil in different forms such as aluminium, aluminium oxide, sulphide etc. For many years it was not considered as a harmful metal for humans, however, in 1965 animal experiments suggested a possible connection between aluminium and Alzheimer's disease. Oral intake of foodstuff is the most important source of aluminium. Thus aluminium occurs naturally in the environment and is also released due to anthropogenic activities such as mining, industrial uses, in the production of aluminium metals and other aluminium compounds. It is found as a normal constitute of soil, plants and animal tissues. Though, Aluminium has relatively low bioavailability, it is a toxic to human and thus it cause diseases like Alzheimer's disease [2]. The compounds of aluminium are used as antacids, antiperspirants food additives and vaccine adjuvant. Aluminium salts are also widely used in water treatment as Flocculants and it is also present in treated drinking water in the form of reactive spices. The exposures of aluminium are from food, air and water. WHO/FAO limit for tolerable weekly intake value for Aluminium is 1 mg/ kg body weight/ week. According to the agency for toxic substances and disease registry (ATSDR) the minimal risk level (MRL) of aluminium has been established at 2.0 mg/kg/day [3, 4]. From the studies of different foods and medicines, it is observed that Aluminium is the fundamental elements in almost of all food stuffs such as cereal products, lentils, tae, fruits and vegetables and medicines [5, 6].

In view of above aspects, in the present work attempt has been made to quantify the amount of aluminum in selected food stuffs using high sensitive nuclear analytical method namely Instrumnetal Neutron Activation Analysis (INAA) using neutrons from Dhruva research reactor, BARC and high resolution gamma ray spectrometry.

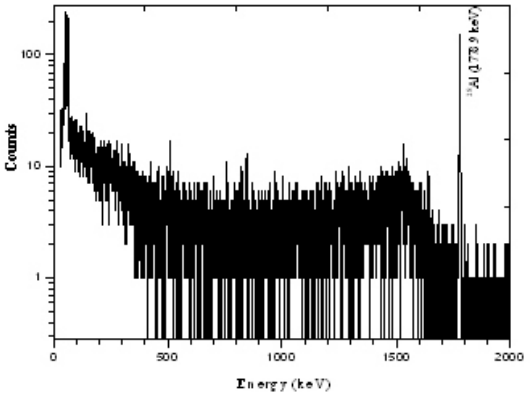


Fig. 1 Gamma ray spectrum of a neutron irradiated rice sample showing 1779 keV OF ^{28}Al

Experimental

More than 100 samples of various food and food products were collected from local markets of Bhubaneswar and Cuttack, Odisha. The samples are rice, wheat, and their products, lentils, and spices. Powdered samples were used for INAA experiment. NAA experiment was carried out at BARC (using Dhruva) 5 x 10^{13} cm^{-2}/s neutron flux. Samples masses were in range 20-30 mg for PCF, Dhruva experiment. Gamma ray energy 1778.9 keV of ^{28}Al ($T_{1/2}$ =2.24 min) was used for Al concentration determination using high resolution gamma ray spectrometry. Radioactive assay was carried out using a 40% relative efficiency HPGe detector at RCD, BARC. Typical gamma spectrum of are shown in Fig. 1 and 2.

Results and Discussion

A total of 25 food samples using PCF, Dhruva reactor were analyzed for aluminium content. Al content was determined by relative NAA. Al concentrations of samples rice (4 No's), lentils (7

Table-1: Determined Al concentration in different food samples

Food products	Name	Concentration in mg kg^{-1}
Rice Products	R1	114 ± 5
	R2	86 ± 2
	R3	33 ± 1
	R4	102 ± 3
Lentils products	L1	462 ± 9
	L2	430 ± 10
	L3	306 ± 8
	L4	283 ± 5
	L5	163 ± 5
	L6	91 ± 4
	L7	66.1 ± 1.1
Wheat products	W1	437 ± 8
	W2	121 ± 2
	W3	116 ± 2
Spices	S1	529 ± 11
	S2	367 ± 7
	S3	269 ± 5
	S4	155 ± 3
Tea	T1	945 ± 21
Glucose	G1	236 ± 4
SRM or RM	NIST SRM 1515 Apple leave	284 ± 8 (286)
	NIST SRM 1573a Tomato leave	609 ± 13 (598)
	IAEA RM SL-3	2.38 ± 0.08 % (2.45 %)

() Certified or information values are given in brackets

No's), Wheat (3 No's), Spices (4 No's), Tea (1 No's), glucose (1 No's) along with 2 NIST SRM and 1 IAEA RMs are given in Table 1. Concentrations of Al ranged from 25- 500 mg kg^{-1} except Tea, spices, and other where it is higher than 500 mg kg^{-1}. Rice and wheat and their products have a low Al concentration.

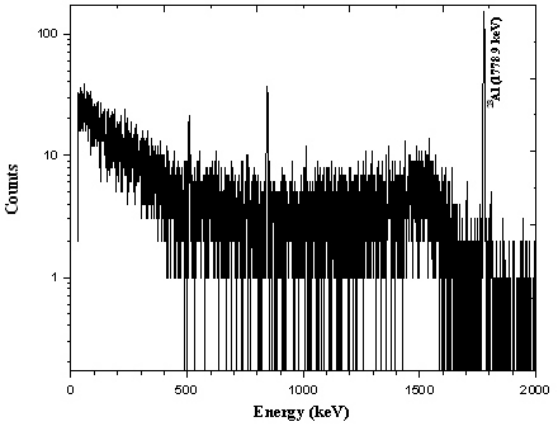


Fig. 2 Gamma ray spectrum of a neutron irradiated spice sample

Uncertainties reported are due to counting statistics. The results are found to be in good agreement with literature values [1-6]. RM/SRM values are in good agreement (1-3%). Effects are being made to collect field samples and soil from field of same variety from different areas. The data on Al will be of help to calculate Al intake by local people by calculating RDA or DDI from find as well as total diet.

Conclusions

PCF Dhruva is suitable for ppm level concentration of Al by INAA. Since ^{28}Al is short lived (2.24 min) the turnaround time is less.

Reference

[1] Scientific Opinion of the Panel on Food Additives, The EFSA Journal, 754 (2008) 1.

[2] Al content in food, Biomed Environ Sci, 6(3) (1993) 19

[3] Al content of selected foods and food products, Env.Sciences Europe 2011, 23-37 doi: 10.1186/2190-4715-23-37.

[4] Food Chem Toxicol,2008 Mar;46 Suppl 1 : S 2-70

[5] Aluminium content is higher in nipple aspirate fluid of breast healthy control. J Appl Toxicol., 31(3) (2011) 262.

[6] Al contents of some foods and food products in the USA, with Al food additives, Food addit Contam, 22(3) (2005) 234.

Inorganic Arsenic Speciation using Membrane Based Separation in Conjunction with HPLC and NAA

Rakesh N. Shinde[1,2], A.K. Pandey[1], R. Acharya[1], S.A. Ansari[1], N.S. Rajurkar[2]

1. *Radiochemistry Division, Bhabha Atomic Research Centre, Trombay, Mumbai 400085, India*
2. *Department of Chemistry, University of Pune, Pune- 411 007, India; E-mail: nsraj@chem.unipune.ac.in*

Functionalized pore filled PHA-Fe and PHA-Ce membranes have been prepared for selective preconcentration of inorganic arsenic species present in water samples and followed by quantification using HPLC and NAA. Precursor Poly(acrylamide) membrane was prepared by UV initiated polymerization of monomer acrylamide (AM) along with crosslinker, methylene-bis-acrylamide (MBA) in the pores of poly(propylene) micropores membrane. Acrylamide functional groups of precursor membrane were converted into hydroxamic acid by subjecting this to a chemical treatment. This membrane was equilibrated with Fe^{3+} and Ce^{4+} ions to form complexes that are selective for preconcentration of inorganic arsenic ions. PHA-Fe membrane selectively takes up As(V) at pH 2 while PHA-Ce membrane takes up both As(III) and As(V) ions at pH 2. Optimized PHA-Fe membrane-NAA method was applied for synthetic samples containing As(V) in the concentration range 10 g L^{-1} to 500 g L^{-1}. The method was validated by ICP-MS.

Introduction

Arsenic contamination in water has posed severe health problems around the world including Bangladesh and West Bengal, India. The WHO set the maximum limit for arsenic in drinking water is 10 g L^{-1}. The toxicity of arsenic to human health ranges from skin lesions to cancer of the brain, liver, kidney, and stomach. A wide range of arsenic toxicity has been determined that depends on its chemical form. Generally inorganic arsenic species are more toxic than organic forms to living organisms, including humans and other animals. Arsenite, As(III) is usually more toxic than arsenate, As(V) due to its high retention time in body. Thus, it is important to know the individual concentration of inorganic arsenic species (As(III) and As(V)) along with total inorganic arsenic concentration in water. Though various methods are used for arsenic speciation there is a need for development of a simple, selective and with better detection limit. Selective preconcentration of a target analyte in solid phase is an effective route not only to enhance detection limit of the conventional analytical method but also for elimination of interfering matrix [1, 2]. Presently, membrane based separation methods are attractive due to (1) enhanced detection limit by preconcentration (2) simple and lower concentration of reagent required (3) can be made as species specific (4) can be used at field site and (5) can be used for remediation purpose. Membrane based preconcentration methods are scarcely reported in literature. Membrane based separation method can be used as an alternative analytical method for arsenic speciation study in various environmental samples.

In the present work, the grafted membranes have been synthesized for arsenic speciation study. Membrane based method was optimized by HPLC. Membrane based separation in conjunction with NAA method was applied for synthetic samples containing As(V) species and validated by ICPMS.

Experimental

Preparation of Membrane

Poly (acrylamide) membrane has been prepared by grafting of monomer, acrylamide (AM) along with a crosslinker methylenebisacrylamide (MBA) in a microporous polypropylene host substrates by photopolymerization method. This poly(acrylamide) grafted membrane was treated with 3M hydroxylamine hydrochloride solution at ambient temperature for 30 minutes followed by pH of the solution was made above 12 by dropwise addition of 4 M NaOH solution and kept for overnight. The membranes were then washed properly and treated with 3M HCl solution for 30 min. and washed again with deionised water repeatedly to remove all the chloride ions. This gave the poly(hydroxamicacid) (PHA) grafted membrane, which was termed as PHA-sorbent. To make a selective for arsenic species these precursor PHA membranes were equilibrated with 0.01M $FeCl_3$ and 0.01M $(NH_4)_2Ce(NO_3)_6$ solution.

Standardization of HPLC Method

Quantification of inorganic arsenic species held in the membrane sample was carried out by HPLC system (Dionex ICS 3000) with Photodiode Array (PDA) detector. Anion exchanger column (PRP-X100) was used for getting clear separation of inorganic arsenic species. Concentration and pH of the mobile phase was optimized for achieve better sensitivity and complete separation of arsenite and arsenate. From 10 M-150 M phosphate buffer was used as mobile phase during optimization step.

Arsenic Sorption-Desorption

HPLC technique was employed to measure arsenic present in aqueous samples before and after equilibration of membrane samples. PHA-Fe and PHA-Ce membrane samples ($2x2cm^2$) were

equilibrated with the mixture of each 15 mg/L of As(V) and As(III) solution for 1hr with a constant stirring. 50 L of the aqueous sample was injected in sample injector of HPLC and absorbance recorded at 200 nm by PDA detector. The % uptake in the membrane sample was calculated by comparing peak area of solution (before and after equilibration of membrane samples with a solution containing arsenic species). The uptake of As(III) and As(V) was studied in different pH (2-9.5) range. The de-loading of arsenic species from the membrane samples was studied by equilibrating the membrane samples in 0.01-0.2 M NaOH solution for overnight.

Application to Synthetic Samples

The optimized PHA-Fe membrane based separation method was applied for 25mL of synthetic samples containing As(V) in the concentration range of 10 g/L to 500 g/L. The pH of the above samples was adjusted to 2. The quantification of As(V) species in the membrane sample was carried out by NAA. Samples and standards of same geometry were irradiated in PCF of Dhruva research reactor facility (neutron flux $5x10^{13}$ cm^{-2} s^{-1}) for 1 min, and 559 keV -ray of ^{76}As (26.3 h) was measured using HPGe -detector coupled to multi-channel analyzer.

Results and Discussion

The amount of monomers grafting in the AM membrane was found to be 152 ± 6 wt. %. 20mM phosphate buffer (pH 9.2) was used as mobile phase for separation of inorganic arsenic species. The presence of Fe and Ce in the membrane samples was confirmed by EDXRF. The uptake profile of As(V) and As(III) in PHA-Fe and PHA-Ce membrane samples as function of pH is shown in Table 1.

Table-1: Percent (%) uptake of As(V) and As(III) in PHA-F and PHA-Ce membranes as a function of pH

Membrane	Species	pH	% Uptake of As in PHA-Fe
PHA-Fe	As(V)	pH=2.0	84 ± 4
PHA-Fe	As(V)	pH=6.5	15 ± 1
PHA-Fe	As(V)	pH=9.5	6 ± 0.4
PHA-Fe	As(III)	pH=2.0	2 ± 0.2
PHA-Fe	As(III)	pH=6.5	5 ± 0.3
PHA-Fe	As(III)	pH=9.5	7 ± 0.4
PHA-Ce	As(V)	pH=2.0	85 ± 3
PHA-Ce	As(V)	pH=6.5	35 ± 3
PHA-Ce	As(V)	pH=9.5	-
PHA-Ce	As(III)	pH=2.0	96 ± 4
PHA-Ce	As(III)	pH=6.5	96 ± 3
PHA-Ce	As(III)	pH=9.5	93 ± 4

In case of PHA-Fe membrane, The uptake of As(V) was maximum and also get clear separation of

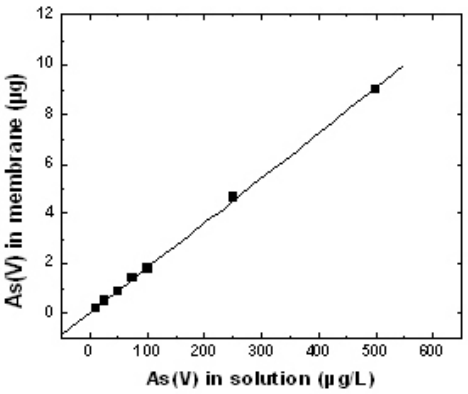


Fig. 3 Calibration curve constructed using synthetic samples containing known concentration of As(V) ions.

As(III) and As(V) achieved in the pH 2. Thus, this PHA-Fe membrane can be used for quantification of As(V) species in aqueous solution. Results of PHA-Ce membranes shows that it sorbs both As(V) as well as As(III). The uptake of As(III) in PHA-Ce was nearly constant (around 95%) in the pH range of 2-9 while in case of As(V), it was maximum (85 %) at pH 2 and after that it decrease. By taking this advantage, PHA-Ce membrane can be used for preconcentration of both As(V) and As(III) species from aqueous samples.

Optimized PHA-Fe membrane based separation in conjunction with NAA method was applied for synthetic samples containing As(V) in the concentration range 10 g/L to 500 g/L. It can be seen from Fig 3. The calibration graph was linear. The membrane based method was validated by ICP-MS method and get results with good agreement.

Conclusion

PHA-Fe and PHA-Ce membranes have been synthesized by UV initiated polymerization method for preconcentration of inorganic arsenic species from aqueous samples. PHA-Fe membranes have shown selective for As(V) while PHA-Ce could be used for both As(V) and As(III) at pH 2. Optimized PHA-Fe membrane in conjunction with NAA method was applied successfully for synthetic samples

Acknowledgements

Authors thank Dr. P. K. Pujari, Head, NCS, RCD and Dr. A. Goswami, Head, RCD for their constant support and encouragement. Authors from Pune University thank BRNS for financial assistance under BARC-PU MoU.

Reference

[1] R.N. Shinde, S. Das, R. Acharya, N.S. Rajurkar, A. K. Pandey, J. of Hazard. Mater. 233–234 (2012) 131.

[2] R.N. Shinde, A. K. Pandey, R. Acharya, R. Guin, S. K. Das N.S. Rajurkar, P. K. Pujari, Wat. Res. 47 (2013) 3551

Utilization of Pneumatic Carrier Facility of Dhruva Reactor for Trace Element Determination by Neutron Activation Analysis

R. Acharya[1], P.K. Pujari[1], K.K. Swain[2], R. Verma[2], A.V.R. Reddy[2], N.S. Bhamra[3], Renuka Patel[3], K. Chakrabarty[3], C.G. Karhadkar[3], Tej Singh[4], K.P. Singh[4] and Y.S. Rana[4]

1. *Radiochemistry Division, Bhabha Atomic Research Centre, Trombay, Mumbai 400085, India; E-mail: racharya@barc.gov.in*
2. *Analytical Chemistry Division, Bhabha Atomic Research Centre, Trombay, Mumbai 400085, India*
3. *Reactor Operations Division, Bhabha Atomic Research Centre, Trombay, Mumbai 400085, India*
4. *Research Reactors Services Division, Bhabha Atomic Research Centre, Trombay, Mumbai 400085, India*

The pneumatic carrier facility (PCF) of Dhruva reactor is being extensively utilized for R&D work and routine sample analysis using Neutron Activation Analysis (NAA). Solid samples and standards are irradiated for 1 minute duration at 50 MW power (neutron flux ~5x10^{13} cm^{-2} s^{-1}) and samples are assayed for gamma radioactivity using HPGe detector coupled to multichannel analyzer. NAA using PCF is very useful for those elements whose activation products are mostly short (seconds to minutes) and medium (minutes to hours) half-lives. Multielements (Al, V, Ti, Ca, Mg, Mn, Cl, I, Na, K etc) and some REEs have been determined in several reference materials and samples of biological, geological, archaeological and environmental matrices as well as nuclear reactor materials.

Introduction

Pneumatic carrier facility (PCF) in a reacor is meant for irradiation of samples for a fixed duration and receiving back through air pressure. The PCF of Dhruva reactor is specially meant for the irradiation of samples. It is suitable for study using short-lived isotopes which require minimum transit time between the completions of irradiation and counting. This facility has provision for shooting the sample into the core for irradiation for short duration (1 min) and receiving back in the same laboratory located outside reactor building. In this facility, the samples are encapsulated in 25mm dia and 38 mm long ethylene propylene capsules and are pneumatically transported to a carrier rod in the reactor from the fume hood located in attached laboratory. Samples are received back in the same fume hood after the fixed period of irradiation. Irradiation of samples is fully automated.

The facility provides a neutron flux of the order of 5 x 10^{13} cm^{-2} s^{-1} at the irradiation location at a reactor power of 50 MW. The facility is mainly used for neutron activation analysis (NAA). A wide variety of samples were irradiated in PCF for application in material sciences, environmental and life sciences, forensic science and archaeology. PCF has also been used for determination of uranium by solid-state nuclear track detector (SSNTD) using fission track analysis (FTA). Photograph of the irradiation facility is given in Fig. 1.

NAA is an isotope specific nuclear analytical technique for simultaneous multielement determination at major to ultra trace concentrations. Use of short-lived activation products (seconds to minutes) reduces the turnaround time of analysis in NAA. The concentration determination of elements is mainly carried out by relative NAA method. The samples that have been analyzed include soil, sediment, clay ceramics (pottery & brick), leaves, cereals, membranes, alloys, nuclear structural materials, graphite, U & Th oxides etc.



Fig. 1 Sample handling from PCF control room

Experimental

Solid samples and standards were sealed in clean polyethylene sheets and were irradiated for 1 minute duration at 50 MW power (neutron flux ~5x10^{13} cm^{-2} s^{-1}). The irradiated samples are assayed for gamma radioactivity using HPGe detector coupled to multichannel analyzer. For short-lived radionuclide measurements, i.e. for varying dead time during counting, loss-free counting system of digital spectrometer was used. Concentrations of the analytes were arrived generally using relative method. Typical gamma ray spectra of irradiated samples are given in Fig. 2 and 3.

Calculations

In relative method of NAA, mass of element (m) of interest was obtained using the following equation

$$m_s = m_{std} \times (A_s \times D_{std}) / (A_{std} \times D_s) \quad (1)$$

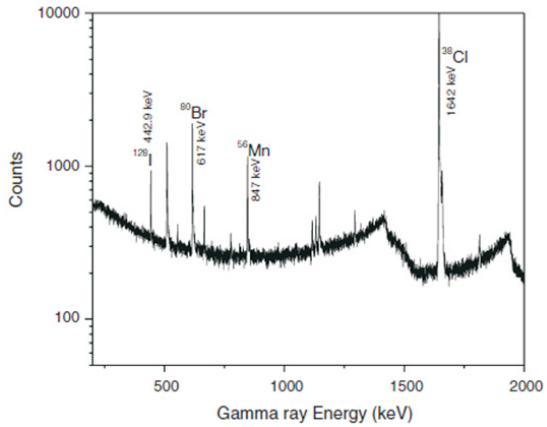


Fig. 2 A typical -ray spectrum of irradiated resin samples after separation of iodine from milk

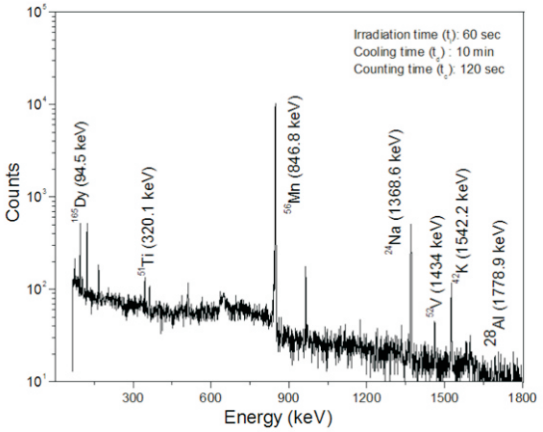


Fig. 3 A typical gamma ray spectrum of irradiated soil

where A is the count rate for sample (s) and standard (std), D (=e ^{t_d}) is the decay factor, is decay constant and t_d is decay time. Mass is converted to concentration (mg kg^{-1}) by dividing with the sample mass.

Various Applications of NAA using PCF

Applications of NAA using PCF are listed here.

Aluminium in food and biological samples as well as soil and reference materials;

Chlorine in zirclaoys, zirconium oxide powders, oil, wax samples and in polyaniline;

Chromium in soil and plant samples from leather tanning industry;

Arsenic in soil, plants (shoot and root of rice plants) and membrane samples;

Iodine in grass, milk and reference materials;

U and Th in their mixed oxides, where samples in diluted powder form with cellulose was used;

Titanium in lithium titanate (tritium breeder) samples;

Compositional analysis of alloys including zirclaoys, nimonic alloy, Ni-alloy and stainless steel;

Multielements in soil and clay samples as well as clay potteries and bricks;

Multilements in soil, plant and tea samples and plant samples from industry area;

Impurities in graphite samples;

Pt in alumina catalysts;

Preparation of ^{76}As tracers for sorption studies;

Analysis of soil and sediment RMs from IAEA (SL-2, SL-1, Soil-7) and Synthetic multielement standards for QA/QC study, for estimating the accuracy of NAA method.

PCF Utilization by BARC, DAE and University personnel

Researchers from different Divisions of BARC namely RCD, ACD, FCD, RPhD and NPD and NPCIL (Mumbai) are utilizing PCF for R&D as well as routine work purposes. The work carried out using PCF of Dhruva has been published in various Journals [1-5] and Symposia and is also part of PhD thesis work of students from BARC and Universities under collaborative work. Universities benefitted from the collaboration work utilizing PCF include, Pune University, IIT Roorkee, GITAM University, Allahabad University, University of Mumbai, Panjab University and NEHU. It has resulted many research publications in journal, symposia and a few reports.

Acknowledgments

Authors thank all the co-workers for their contributions. Authors also thank operating staff of PCF, Dhruva reactor, BARC for their cooperation during the sample irradiation for NAA. Authors also thank Head, RCD; Head, ROD; Head, RRSD and Director, Reactor Group, BARC for their support and encouragement.

References

[1] AV.R. Reddy, T. Newton Nathaniel, A.G.C. Nair, R. Acharya et al., BARC Report, BARC/2007/E/017, 2007.

[2] R. N. Shinde, A.K.Pandey, R. Acharya, R. Guin, S.K. Das, N.S.Rajurkar, P.K. Pujari, Water Research, 47 (2013) 3497.

[3] R. Acharya, Ruma Gupta, P.K. Pujari, J. Radioanal. Nucl. Chem., 294 (2012) 121.

[4] Nicy A, A. Dalvi, K. K. Swain, P. S. Remya Devi, B. B. Kalekar, R. Verma and A. V. R. Reddy, J. Environ. Sci. Health, Part-A, 48 (2013) 422.

[5] S.Badwar, R. Ghosh, B. S. Shivashankar, R. Acharya, S.V. Suryanaraya, J. Basic & Appl. Phys., 1 (2012) 69.

[6] R A. Lagad, D. Alamelu, R. Acharya, S.K. Aggarwal, J. Radioanal. Nucl. Chem., 288 (2011) 613.

[7] R.S. Maharia, R.K. Dutta, R. Acharya, A.V.R. Reddy, J. Env. Sci. and Health, B, 45 (2010) 174.

Elemental Compositional Analysis of Meteorites by Prompt Gamma-ray Neutron Activation Analysis (PGNAA)

Bharat Adur[1], H.B. Mali[1], R. Acharya[2], Z. Revay[3,4], T. Belegya[3], and P.K. Pujari[2]

1. *Akash Ganga Centre for Astronomy, Ambeshiv Khurd, Yeranjad, Badlapur, Thane 421 501, India, E-mail: bharatdur@gmail.com*
2. *Radiochemistry Division, Bhabha Atomic Research Centre, Trombay, Mumbai – 400 085, India; E-mail: racharya@barc.gov.in*
3. *Centre for Energy Research, Hungarian Academy of Sciences, 1525 Budapest 114, P.O. Box 49, Hungary.*
4. *Present address: Technische Universität München, FRM-II,Garching, Germany*

Prompt Gamma ray neutron activation analysis method (PGNAA) is an isotope specific non distractive nuclear analytical method for complete compositional analysis of materials. This technique is being used for determination of various elements such as H,B,Cd,Hg rare earths, alkali metals transition metals in various samples of antiques, geological, biological and meteorites. In this work PGNAA has been used to study three original meteorite samples Dhofar 020 (OMAN), Sikhote Alin (RUSSIA) and North West Africa 2909 (Africa) at Budapest, Hungary and the results are presented in this paper.

Introduction

Meteorites are considered as left materials of the asteroids, which were not able to form the planet between Mars and Jupiter, comets which are placed beyond Pluto. Some meteorites come from Mars and also from the moon. Meteorites have been classified as per their elemental composition, chemical compositions and mineral compositions. In general there are five groups of meteorites (a) Iron meteorites, (b) Stony iron meteorites, (c) Stony meteorites, (d) Chondrites and (e) Achondrites. Meteorite studies can give us valuable information about the origin of our solar system. Why certain elements found in meteorites are more in abundance than the crust of the earth?

Sample Preparation

For the present study three meteorites were taken and their weights noted down as 1) Dhofar 020,weighing approx. 4.299 g, 2) Sikhote Alin, weighing approx. about 4.165 g and 3) North West Africa 2909, weighing approx. about 2.881 g. The following meteorites were commercially made available by Meade Instruments Corporation and Certified by Bert Reynolds.

Before weighing these samples photographs were taken. After weighing the samples 3 pieces of each samples say approx. 0.025 g was cut by a diamond cutter machine (make Meta cut – DCM DRO). Lubricant used while cutting was kerosene. Kerosene was used while cutting as the cutter wheel will not get rusted and also act as a coolant and is rust free. Also to minimize the heat generated while cutting. Since kerosene was used while cutting the samples. It was to be washed with acetone twice to remove the kerosene and also the loose particles attached to the sample. The sample in acetone was held in vibrator containing water. Due to vibration medium it helps in cleaning the samples also loose particles if any will be removed. Each sample was washed twice in this way,then kept for dring in an ovan for 15-20 min. After drying, the samples were kept in a thick polythene bag knowing that very minute quantity of sample was required for analysis.

Methods

Analysis by PGNAA. 1 g approx. was taken and crushed and powdered using an alumina ceramics jaw crusher and agate or alumina mills. PGNAA with cold –neutron beam facility at the Budapest Research Reactor, Hungary. The thermal equivalent neutron flux at this position is 1.2 x 10 $cm^{-2}s^{-1}$. Samples about 0.5g masses were irradiated in vacuum and the prompt -rays were measured for 2-4 h with a Compton suppressed detection system HPGe-BGO detectors). The absolute counting efficiency of the detector was determined using ^{133}Ba and $^{1\ 2}$Eu and prompt gamma rays from ^{1} N(n,)^{1} N and ^{3} Cl (n,)^{3} Cl. The k_0-based PGNAA was used for concentration calculation. Since all major to trace elements were amendable to PGNAA, a standard based approach was used for determining concentrations of elements namely (i) Fe, Si, Ti, Al, Ca, Mg, Na, Mn, V and K (major concentrations 26 – 0.2%) and (ii) Cr, Co, Ni, Cl, Sm and Gd (trace concentrations). The combined uncertainties at 1s obtained were in the range of 0.5-9%. For validation of the k_0-PGNAA method, IAEA RM SL-3 (lake sediment) was analyzed and concentrations of 19 elements were determined. The zeta scores ( ) at about 95% confidence level were found to be 0.1-1, indicating good quality results by k_0-PGNAA.

Discussion

In meteorites brecciated type of structure is important. In stony meteorite numerous angular fragments or granular substance are observed or consisting of small sharp mineral component or fragment is observed. Two types of breccias are observed 1) monomict breccias consisting of same substance and 2) polymict breccias consisting of different types of meteorites. In chondrites of

Table-1: Results of elemental concentrations (%) in Meteorites by PGNAA

Elements	Meteorite-1 Conc (%Unc)	Meteorite-2 Conc (%Unc)	Meteorite-3
H	730 (3) (mg/kg)	170 (8) (mg/kg)	0.224
B	0.90 (4) (mg/kg)	0.83 (4) (mg/kg)	1.17
Na	-	-	0.51
Mg	-	-	12
Al	0.4 (6%)	ND	1.3
Si	0.7 (7)	1.4 (5)	15
Cl	ND	70 (10) ppm	0.2 ppm
K	-	-	0.065
Ca	-	-	0.98
Sc	-	-	6
Ti	-	-	0.059
V	-	-	72 ppm
Cr	-	-	0.38
Mn	-	-	0.2
Fe	61 (1)	92 (1)	23
Co	-	0.44 (4)	0.07
Ni	5.9 (2.7)	5.8 (3.5)	1.55 ppm
Sm	-	-	0.13 ppm
Gd	-	-	0.24 ppm

amphoterites and carboneceous consist of these brecciated structure. Which is observed in ordinary chondrites. In mesosiderites due to the higher iron – nickel phase breccia nature is much more observed. The silicate phase point to polymict breccias. (Vinogradev et al.) In iron meteorites iron being the predominant element with nickel and small amount of cobalt. Iron meteorites showing mineral inclusions are supposed to be from the core of large asteroids. In stony iron meteorites silicates and iron – nickel alloy are in equal proporations. Stony iron consist of two groups 1) is Pallasites and 2) Mesosiderites. Pallasites have olivine crystals placed in an iron – nickel alloy matrix. Where as Mesosiderites are a mixture of metal grains, pyroxenes olivine and plagioclase. Dhofar meteorite consist of impact melt breccia having mineral and lithic clasts embedded in an impact melt rich matrix. Most of it contains anorthositic or highlands materials Sikhote Alin meteorite is composed of Kamasite (cubic FeNI) having small quantity of taenite (cubic NiFe). Silicates as inclusions are rare in these meteorites. The Sikhote Alin has been a massive fall. The meteoroid overall size seems to be estimated to about 9,00,000 kg.(Wikipedia et al.) and the coverage area for this meteorite was about 1.3square km. (Wikipedia et al.) Dhofar 020 it belongs to H4-5 chondrite (J.N. Grossman et al.). The values obtained by PGNAA of elements Fe - 92%, Ni – 5.8%, Co – 0.44% agree well with Sikhote Alin meteorite.

Conclusion

The above results obtained by PGNAA of Dhofar 020, Sikhote Alin and North West Africa 2909 and the chemical composition of the same meteorite done by others confirm that the meteorites are original ones.

Acknowledgements

The work was carried out under AGCA Student Program and Hungarian Academy of Sciences (HAS) International Exchange Program. Authors thank BARC, Mumbai, India and Centre for Energy Research (formerly Institute of Isotopes) and HAS, Hungary for their kind support.

References

[1] G.L. Molnar (Ed), Handbook of Prompt Gamma Activation Analysis with neutron beams, Kluwar Academic Publishers, London (2004).

[2] A.G.C. Nair, R. Acharya, A.V.R. Reddy, A. Goswami, B. Adur, H.B. Mali, J. Rathod, R. Patil, K. Vora, Current Science, 87 (2004)654 .

[3] R. Acharya, B. Adur, H.B. Mali , et al. Composition analysis of basin soil samples from lonar crater by k0-based prompt gamma-ray naa,6th k0 workshop (2013,) 3Energy Research Center, Konkoly-Thege Miklós u. 29-33, 1121 Budapest, Hungary.

[4] Zs. Revay, T. Belgya, Zs. Kasztovszky, J.L. Weil, G.L. Molnar, Nucl. Instr. Meth. B, 213,385 (2004).

[5] Dhofar 020 An Anorthosite impact melt breccia.

[6] Exposition Meteorites: Meteorites Fersman Mineralogical Museum.www.fmm.ru/meteorer.htm

[7] North West Africa 2909 et al. Lunar meteorite. Meteorites.www.wustl.edu/lunar/stones/nwao2909.htm

[8] A.P. Vinogradov – The composition of meteorites: V.I. Vernadsky Institute of Geochemistry and Analytical Chemistry, Academy of Sciences of the U.S.S.R., Moscow, U.S.S.R.

[9] Jeffrey N. Grossman The Meteoritical Bulletin No. 84, 2000 August. Meteoritics & Planetary Science 35, (2000).

[10] Sikhote – Alin meteorite – http://en.wikipedia.org/wiki/Sikhote-Alin_meteorite

[11] Fersman Mineralogical Museum, Russian Academy of Sciences-Moscow,Russia (www.fmm.ru/meteoren.htm)

[12] Meteoritekit.com meteorite classification information. Meade Instruments Corporation.

Utilization of AHWR Critical Facility for Research and Development Work on Large Sample NAA

R. Acharya[1], K.K. Swain[2], K.B. Dasari[1], P.K. Pujari[1], A.V.R. Reddy[2], S K Verma[3] and S K De[3]

1. *Radiochemistry Division, Bhabha Atomic Research Centre, Trombay, Mumbai 400085, India; E-mail: racharya@barc.gov.in*
2. *Analytical Chemistry Division, Bhabha Atomic Research Centre, Trombay, Mumbai 400085, India*
3. *Reactor Operation Division, Bhabha Atomic Research Centre, Trombay, Mumbai 400085, India*

The graphite reflector position of AHWR critical facility (CF) was utilized for analysis of large size (g-kg scale) samples using internal mono standard neutron activation analysis (IM-NAA). The reactor position was characterized by cadmium ratio method using In monitor for total flux and sub cadmium to epithermal flux ratio (f). Large sample neutron activation analysis (LSNAA) work was carried out for samples of stainless steel, ancient and new clay potteries and dross. Large as well as non-standard geometry samples (1 g – 0.5 kg) were irradiated. Radioactive assay was carried out using high resolution gamma ray spectrometry. Concentration ratios obtained by IM-NAA were used for provenance study of 30 clay potteries, obtained from excavated Buddhist sites of AP, India. Concentrations of Au and Ag were determined in not so homogeneous three large size samples of dross. An X-Z rotary scanning unit has been installed for counting large and not so homogeneous samples.

Introduction

The Advanced Heavy Water Reactor Critical Facility (AHWR CF) is a tank type, heavy water moderated reactor with natural uranium metal as fuel. The reactor is designed for a nominal fission power of 100 W and an average neutron flux of 10^8 cm^{-2} s^{-1}. The main objective of this reactor is for conducting experiments and validating the physics design parameters of AHWR [1]. Graphite reflector position of this reactor has facilities for testing neutron detectors and also to irradiate samples (Soil, Geological rock, Biological sample and Metallic alloys) for neutron activation analysis (NAA). NAA is one of the most widely used techniques for trace, minor, major elemental concentration determination in different samples due to properties like simultaneous multielement capability, high sensitivity, high selectivity, negligible matrix effect and non-destructive nature [2]. Large sample analysis is advantageous for obtaining better analytical representativeness instead of replicate sub-sample analysis. A k_0-based internal monostandard NAA (IM-NAA) method using in situ relative detection efficiency [3], developed in BARC, is useful to analyze large and non-standard geometry samples.

The k_0-based IM-NAA method using in situ relative detection efficiency was used to determine elemental concentration ratios with respect to one of the element present in the sample. Insitu relative detection efficiency was obtained using rays of activation products in the required energy range. In the present work, large size pottery, brick, soil and dross samples were analysed using graphite reflector position of AHWR CF reactor for elemental concentration determination using IM-NAA method.

Experimental

Large size samples (1-500g) were packed in polythene. Small samples (100 mg - 500 mg) were also used. Photographs of a few samples are given in Fig. 1. Samples were irradiated in graphite reflector position of AHWR CF (Fig. 2), BARC for 4 h. For neutron flux characterization, indium (10 mg and 0.8 mm thick) was used. Radioactive assay was carried out using high purity germanium (HPGe) detector coupled to 8k channel. Peak areas were determined using peak fit software PHAST. An X-Z scanning unit for gamma ray spectrometry has been installed for counting non homogeneous large size samples.

Calculations

In the IM-NAA using highly thermalized neutrons, the ratio of the mass (m) of an element x to the element y present in the sample is given by the following expression,

$$\frac{m_x}{m_y} \quad \frac{S.D.C._y}{S.D.C._x} \frac{P_{Ax}}{P_{Ay}} \frac{y}{x} \frac{K_{0,Au}(x)}{K_{0,Au}(y)} \qquad (1)$$

where P_A is the net peak area under the gamma peak of interest, S is the saturation factor, D is the decay factor, C is the counting factor used for correcting the decay during counting period, the $k_{0,Au}$ is the literature k_0-factor with respect to ^{197}Au and is the detection efficiency. Here we have used relative detection efficiency of the detector, which is determined using the -rays of activation products produced in the sample. The in-situ relative efficiency is obtained using the following expression.

$$\ln \quad k_j \quad \sum_{i\ 0}^{m} a_i \ln \quad i \qquad (2)$$



Fig. 1 Photographs of some of the samples analyzed

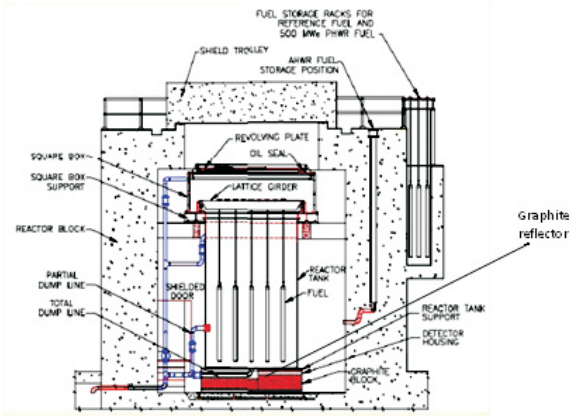


Fig. 2 Graphite reflector position of AHWR CF

where a_i is the coefficients of the polynomial of order m, k_j is a constant characteristic of the jth nuclide. In the calculations a second order polynomial (m = 2) was used. A typical insitu relative detection plot obtained for a large size (38 g) pottery sample is given in Fig. 3, which covers an energy range of 122-2754 keV using ^{152m}Eu, ^{140}La, ^{56}Mn and ^{24}Na.

Results and Discussion

The f-value for CF obtained from the cadmium ratio method was found to be (8.6 0.3) x 10^2. The corresponding thermal equivalent flux is 3.4 x 10^7 n cm^{-2} s^{-1} (> 99.8 % thermal neutron component).

During irradiation of samples in CF, higher masses of the samples were used. This obviates the error due to inhomogeneous distribution of analytes in small sub samples. The overall radiation doses in the irradiated samples after irradiation were less due to low neutron flux in the irradiation position.

Concentrations of Fe, Cr, Ni, Mo, Mn, and As were determined in the austenitic stainless steel CRM, BCS 466 (using a sample of 5 g mass) by standardless approach of IM-NAA using Fe as monostandard. The results obtained are in good agreement (within ±5%) with its certified values.

Ancient potteries, bricks obtained from excavated Buddhist sites of Andhra Pradesh, India were analyzed. The results show promise of IM-NAA in the provenance studies of archaeological artifacts of large and non-standard geometries suggesting that elemental concentration ratios, obtained without using concentration of an external or internal standard, are adequate in such studies.

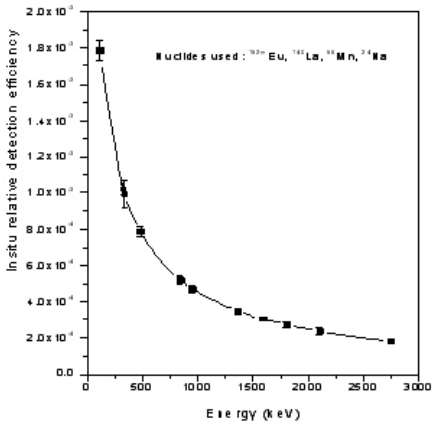


Fig. 3 A typical insitu relative detection efficiency plot of a neutron activated large size pottery sample

Large size (50-100 g) sample neutron activation analysis (LSNAA) of dross from Government Mint, Mumbai was carried out. Analysis of varying masses were used to arrive at representative size for analysis, which indicated representative sample size of 2 g. Concentrations of Au and Ag were found to be in the range of 200-400 mg kg^{-1} and 1200-1700 mg kg^{-1} respectively in the three different samples.

Concentration ratios of elements such as Na, K, Cr, Mn, Fe, Co, Zn, As, Rb, Cs, La, Ce, Sm, Eu, Yb, Lu, Hf and Th with respect to Sc (internal mono standard) were calculated in the IAEA intercomparison sample using IM-NAA. The results are in agreement with small size sample analysis by NAA.

Acknowledgments

Authors thank operating staff of Critical Facility reactor, BARC for their cooperation during the sample irradiation for NAA. This study is a part of the IAEA Coordinated Research Project (CRP Code: F2.30.27) on large sample NAA.

References

[1] R. K. Sinha and A. Kakodkar, Nucl Engg and Design 236 (2006) 683-700.

[2] K. B. Dasari, R. Acharya, K. K. Swain, N. Lakshmana Das and A. V. R. Reddy; J. Radioanal. Nucl. Chem., 286 (2010) 525–531.

[3] A. G. C. Nair , R. Acharya, K. Sudarshan, S. Gangotra, A.V. R. Reddy, S. B. Manohar, A. Goswami, Anal. Chem. 75 (2003) 4868.

Analysis of Arsenic Accumulation by NAA and its effects on the Mineral Nutrient Profile of Rice (Oryza sativa) Plants

Sudhakar Srivastava[1], J. J. Akkarakaran[1], Rakesh N. Shinde[2], R. Acharya[2] and P. Suprasanna[1]

1. *Nuclear Agriculture & Biotechnology Division, Bhabha Atomic Research Centre, Trombay, Mumbai 400094, India*
2. *Radiochemistry Division, Bhabha Atomic Research Centre, Trombay, Mumbai 400094, India; E-mail: sudhakar.srivastava@gmail.com*

This study is aimed at obtaining the impact of As on mineral nutrient profile of rice plants. At 20 M AsIII ($NaAsO_2$), a significant change in Mn, Co, Cu, Fe, Zn, Ni, Se and K levels was observed after 15 days. Neutron Activation Analysis (NAA) using PCF dhruva reactor facility was done for As determination. NAA analysis at increasing AsIII doses showed that As concentration increased progressively, which caused a decline in Mn in roots (beyond 5 M) and shoots (at all concentrations). In case of K, significant increase occurred up to 20 M in roots and shoots followed by a sharp decline at 50 M. The present analyses thus highlight that As induces detrimental impacts on mineral nutrient profile.

Introduction and Experimental

Arsenic (As) contamination of groundwater has emerged as one of the most serious environmental issues in the past decade [1]. The use of As contaminated groundwater for irrigation purposes has led to significant As accumulation in rice plants and seeds [2]. This study was planned to analyze the impact of As accumulation on mineral nutrient profile of rice plants. Rice seeds were grown in kimura nutrient medium in glass beakers in a Plant Growth Chamber (Sanyo, Japan). Then, they were subjected to (3-50 mM; in the form of AsIII; $NaAsO_2$, for 15 days) for phenotypic analyses and 20 M AsIII was selected as LD50 dose from the observed data. At this dose (20 M AsIII) and time (15 days), elemental profile (Mn, Fe, Co, Ni, Cu, Zn, K and Se) was analyzed in roots and shoot of rice using Inductively Coupled Plasma-Mass Spectrometry (ICP-MS). To evaluate the effect of varying AsIII concentrations (3, 5, 10, 20 and 50) on the dynamics of two important nutrient elements (Mn and K), Neutron Activation Analysis (NAA) was carried out using Pneumatic carrier facility (PCF) at Dhruva reactor. Gamma ray of 559 keV of 76As was used for quantification by gamma ray spectrometry using HPGe detector system.

Results, Discussion and Conclusions

ICP-MS analysis various elements showed that As accumulation by rice plants caused a significant decline in Mn (30-41%), Co (23-25%), and Cu (40-75%) level in both shoot and root (Table 1). Fe and Zn levels were increased in roots (29% and 34%, respectively) while declined in shoot (34% and 5%, respectively). The levels of Ni (258% and 40%), Se (166% and 15%) and K (24% and 83%) were increased in roots and shoot (Table 1). These preliminary analyses suggested broad changes on mineral profile of plants under As stress. These changes appear to be due to As induced toxicity on the physiology and growth of plants [3-5]. The competitive effect As on accumulation profile of some mineral elements are known [6-7]. Further, concentration dependent analyses of PGNAA showed that the As concentration in plants increased progressively and was 1205 g g^{-1} in roots and 36 g g^{-1} in shoot at 50 M (Table 2). The increase in As concentration caused a decline in Mn in roots (beyond 5 M) and shoots (at all concentrations). In roots, there was an initial increase in Mn level up to 5 M. In case of K, a significant increase was observed in its concentration up to 20 M in both roots and shoot,

Table-1: Level of mineral nutrients (g g^{-1} DW) in root and shoot of rice seedlings exposed to 20 M AsIII for 15 days

Element	Tissue	Control	Arsenic
As	Root	0	707.8
	Shoot	0	12.65
Mn	Root	254.34	149.03
	Shoot	120.1	91.07
Co	Root	3.71	2.8
	Shoot	0.23	0.18
Cu	Root	135.0	34.61
	Shoot	20.31	12.29
Fe	Root	2328	2993
	Shoot	198.0	130.0
Zn	Root	506.1	678.2
	Shoot	83.2	79.21
Ni	Root	5.1	18.20
	Shoot	0.86	1.21
Se	Root	2.90	7.74
	Shoot	0.91	1.04
K	Root	3.53	4.35
	Shoot	2.59	4.73

which was followed by a sharp decline at 50 M (Table 2). Mn and K are two most important essential elements for the proper functioning of plants. Such major As induced changes in concentration of Mn and K suggest that important pathways like photosynthesis and a number of biochemical reactions will be affected under AsIII stress in rice plants.

Table-2: Level of As, Mn and K (g g^{-1} DW) in root and shoot of rice seedlings exposed to different AsIII concentrations for 15 days

As (M)	Tissue	As	Mn	K
0	Root	0	254.34	3.93
	Shoot	0	125.9	2.66
3	Root	95.7	316.31	4.42
	Shoot	4.25	104.17	3.23
5	Root	191.23	313.03	4.59
	Shoot	4.7	95.56	3.85
10	Root	593.25	237.59	5.91
	Shoot	8.41	87.03	4.48
20	Root	707.8	189.03	4.87
	Shoot	12.65	84.07	4.86
50	Root	1204.87	95.85	1.75
	Shoot	35.64	73.97	2.17

The present analyses thus highlight that As problem in rice may prove harmful not only due to As accumulation but also owing to its detrimental impact on mineral nutrient profile. Further studies of As impact on other essential elements are underway.

References

[1] S. Srivastava, P. Suprasanna, S.F. D'Souza. Int. J. Phytorem. 14 (2012) 506.

[2] R. Tuli, D. Chakrabarty, P.K. Trivedi, R.D. Tripathi. Mol. Breed. 26 (2010) 307.

[3] P.M. Finnegan, W. Chen. Front. Physiol. 6 (2012) 182.

[4] S. Srivastava, A.K. Srivastava, P. Suprasanna, S.F. D'Souza. J. Exp. Bot. 64 (2013) 303.

[5] M. Shri, S. Kumar, D. Chakrabarty, P.K. Trivedi, S. Mallick, P. Misra, et al. Ecotox. Environ. Saf. 72 (2009) 1102.

[6] S. Dwivedi, R.D. Tripathi, P. Tripathi, A. Kumar, R. Dave, S. Mishra, et al. Environ. Sci. Technol. 44 (2010) 9542.

[7] S. Dwivedi, R.D. Tripathi, S. Srivastava, R. Singh, A. Kumar, P. Tripathi, et al. Protoplasma 245 (2010) 113.

Expanded uncertainties for chlorine, bromine and iodine in bovine milk organohalogens measured by neutron activation

K. Isaac-Olive[1,2], A. Chatt[1]

1. *Trace Analysis Research Centre, Department of Chemistry, Dalhousie University, 6274 Coburg Road, Room 212, PO BOX 15000, Halifax, NS, B3H 4R2, Canada; E-mail: kisaaco@uaemex.mix*
2. *Present address: Faculty of Medicine, Universidad Autónoma del Estado de México, Paseo Tollocan s/n esq. Jesús Carranza, Toluca, C.P 50120, Estado de México, Mexico.*

Although milk is of immense importance in nutrition, it may contain toxic pollutants such as organohalogens. In this work a solvent extraction in conjunction with NAA was employed to determine extractable organohalogens in bovine milk lipids with high precision and accuracy. The expanded uncertainty associated with each halogen concentration was calculated. The typical concentrations of iodine, bromine and chlorine were 0.21 0.02, 2.65 0.04 and 32 1 ppm, respectively. The relative expanded uncertainty in all cases was less than 10% under the experimental conditions used.

Introduction

Many organohalogen compounds are known as persistent organic pollutants (POPs) and proven to be highly toxic. Determination of total halogens is not of as much importance as the extractable organohalogen compounds (EOX) in foods and diets. Efficient extraction procedures of these compounds from foods and diets need to be developed as well as the methods for their sensitive determination. Lack of certified reference materials for the validation of analytical methods perhaps makes these measurements less reliable. The objective of this work was to develop a solvent extraction method coupled to neutron activation analysis (NAA) for the determination of EOX present in bovine milk and to calculate the expanded uncertainties associated with the halogen concentrations in the lipid extracts of the milk. NAA is highly suitable for this project because there is no need for chemical digestion after the extraction of the organic compounds; the matrix is composed mainly of C, H, and O whose neutron activation products do not cause interference; and halogens (Cl, Br, I) produce radionuclides which can be used for their sensitive determination.

Experimental

A mixture of hexane and isopropanol was used to separate EOX compounds from bovine milk. For recovery calculation we quantified lipids in milk indirectly by mass balance of total milk with mass of water, proteins, carbohydrates and major minerals in milk. We determined the concentrations of the halogens in the EOX fraction using NAA. We irradiated the samples at the Dalhousie University SLOWPOKE-2 reactor (DUSR) facility in a neutron flux of 2.5×10^{11} $cm^2\ s^{-1}$. The irradiation, decay and counting times were 10, 2, and 10 min, respectively. Counting was carried out in conventional mode using a Ge(Li) detector. The expanded uncertainties in the pre-irradiation, irradiation and post irradiation steps were calculated following recommended procedures and published work [1-5]. A few SRM and RM were employed to carry out external quality control assurance of the NAA method.

Results

Milk lipids represent about 3.29 ± 0.03 % of the total milk mass according to the hexane:isopropanol method used here. Assuming that the lipid content determined indirectly by the mass balance equation is 100% then our method yields about 82% of total milk mass. SRM and RM values determined by NAA were always higher than 91% of the reported value. Table 1 shows each halogen concentration found in the total milk lipid extract calculated by NAA and the expanded uncertainty associated with it. Table 2 shows the expanded uncertainty associated with each analytical step.

Table-1: Mass fractions of halogens (g g^{-1}) in milk lipid extracts and their expanded uncertainties (%).

Element	Total EOX fraction (g g^{-1})	Expanded uncertainty (k=2)(%)
I	0.21 0.02	6.6
Br	2.65 0.04	9.8
Cl	32 1	8.4

Discussion

The NAA method developed is of good precision and accuracy. The higher source of uncertainty in the method is the post-irradiation step where the counting statistics are poor. This source of uncertainty can be improved if longer irradiation and counting times, higher neutron flux and higher detection efficiency are used in the NAA method. Solvent extraction is still a relatively fast and reliable method for separating organic compounds from milk samples. The employed method gave 82% recovery on the average. Fractionation schemes need to be developed to separate phospholipids, glucolipids and neutral lipids in order to isolate the EOX pollutants in the neutral fraction.

Table-2: Relative standard uncertainty (%) associated with each analytical step.

Element	I	Br	Cl
Pre irradiation	0.35	0.20	0.22
Irradiation	0.20	0.19	0.21
Post irradiation	3.32	4.90	4.17
Combined relative standard	3.34	4.91	4.2

Conclusions

The expanded uncertainties in the halogen concentrations determined in milk lipid extract were 8.4, 9.8 and 6.6 for chlorine, bromine and iodine, respectively.

References

[1] EURACHEM/CITAC guide CG 4 "Quantifying uncertainty in analytical measurements", second edition, http://www.measurementuncertainty.org. .

[2] R.R. Greenberg, R.M. Lindstrom, D.S. Simons, J Radioanal Nucl Chem 245 (2000) 57.

[3] P. Bode, E.A. De Nadai Fernandes, R.R. Greenberg, J Radioanal Nucl Chem, 245 (2000) 109.

[4] R.R. Greenberg, P. Bode, E.A. De Nadai Fernandes, Spectrochim Acta B 66 (2011) 193.

[5] R. Acharya, A. Chatt, J Radioanal Nucl Chem 282 (2009) 991.

Estimation of Uranium in geological rock samples by Beta-Gamma method and its comparison with Pellet Fluorimetry method

Rita[1], M.A. Nayeem[1], Diwakar Gaur[2], G.B. Rout[1], B.K. Pandey[1] and A.K. Sarangi[2]

1. *Atomic Minerals Directorate for Exploration and Research, Hyderabad; E-mail: rita.amd@gov.in*
2. *Uranium Corporation of India Limited, Jaduguda*

Geological rock samples collected from Narwapahar Uranium mines, UCIL, Jaduguda were analysed for the estimation of Uranium concentration(U_3O_8) by Beta Gamma method which is a physical technique and same set of samples were analysed by Pellet Flourimetry technique which is a chemical technique. 28 samples were analysed by beta- gamma method and values varied between 240 to 2500 ppm. Samples were analysed by Pellet Fluorimetry and values varied between 260 to 2300 ppm. The results obtained were well comparable by both the techniques.

Introduction

Determination of Uranium concentration in geological rock samples is essential for the Uranium Exploration programme. Uranium concentration in rock samples can be determined by several methods. One of the nuclear techniques is Beta-Gamma method which is a non-destructive and fast method, which is very useful in the Uranium Exploration programme. In this technique, Uranium is estimated irrespective of the disequilibrium in the uranium series and presence of Thorium in the rock sample [1,2].

Geological rock samples collected from Narwapahar Uranium mines, UCIL, Jaduguda were analysed for the estimation of Uranium concentration by Beta Gamma method and also the same set of samples were analysed by Pellet Flourimetry technique.

Experimental Setup for Beta-Gamma Method

The geological rock samples are powdered to -200 mesh in quantities varying from 50 to 150g which is sufficient to ensure good sampling and sufficient counting rates. The beta-gamma technique involves simultaneous measurement of total beta and total gamma radiations emitted by various decay products of Uranium series using pancake GM detector of LND make and NaI(Tl) detector respectively. The size of the NaI(Tl) detector used is 1¾ " x 2". The beta tube is Neon filled and halogen quenched. Here the sample is taken in an aluminum container with diameter 5 cm and height 1.6 cm holding around 50 g of sample. The sample container is placed between the two detectors, thus geometry of the sample obtained is 2 . The U_3O_8 content was determined using the following equation:-

$$U_3O_8 = (1+C)U \quad -CU \qquad (1)$$

Where, U = Beta activity of Uranium, U = gamma activity of Uranium, C = Ra / U , relative contribution of Uranium and Radium groups to total beta activity.

Detection limit of the beta gamma method is 100 ppm.

Pellet Fluorimetry

Here, the geological rock samples are dissolved in acid and obtained in solution form. Uranium from sample solution is extracted to an organic layer and which is in turn stripped back to a platinum crucible and fused with flux of Na_2O_3 and NaF in the ratio of 4:1 at 850°C resulting in a pellet. These pellets are exposed to UV radiation (365 nm) and the resulting fluorescence intensity (= 555 nm) is measured with a pre-calibrated pellet fluorimeter [3]. Detection limit of this technique is 1 ppm.

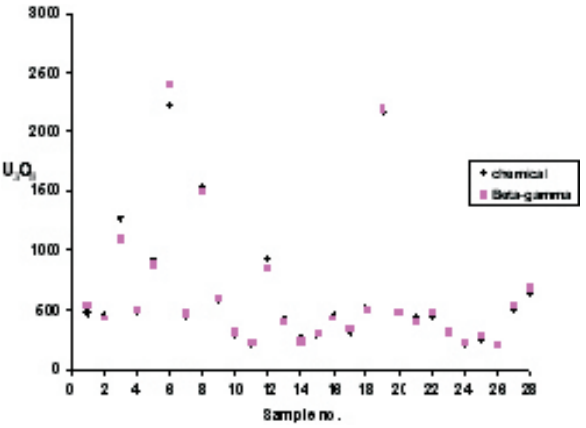


Fig. 1 Comparison of U_3O_8 obtained by Beta Gamma method and Pellet Fluorimetery

The Fig. 1 gives the comparison of U_3O_8 value obtained by Beta-Gamma and Pellet Fluorimetry techniques.

Conclusion

28 samples were analysed for their U_3O_8 content with values ranging from 240 to 2500 ppm by both the methods. It was observed that all the values are comparable and the standard deviation for all the samples is within 10%. The regression coefficient is found to be 0.99. IAEA Uranium standard (assigned value 470 ppm) has also been analysed by the Beta-Gamma method and he obtained value is 463±17 ppm.

Acknowledgement

Authors are thankful to Shri P.S.Parihar, Director AMD and Dr. S. Chandrasekharan, Additional Director (R & D) for extending their support for the study. Also acknowledge the officers and technicians of RSA for their valuable suggestions and cooperation.

References

[1] P.C. Ghosh , Thesis submitted to Indian Institute of Technology, Delhi for Ph.D, (1972)

[2] G.G. Eicholz , J.W. Hilborn, C. McMohan, Canadian J. Phy. 31 (1953) 613.

[3] A. Premadas, G. Sarvanakumar, J. Radioanal. Nucl. Chem., 266(1) (2005) 95.

[4] Uranium Prospecting handbook, Proceeding of a NATO sponsored Advanced study Institute on methods of prospecting for uranium minerals, London, (1971) pp. 157-173.

[5] Radiation detection & measurement by Glenn F. Knoll.

[6] Radioactivity in Geology.E.M. Durance

Applications of relative and internal monostandard NAA methods for analysis of alloys: as a part of chemical quality control exercise.

A.D. Shinde[1], R, Acharya[2], A.V.R. Reddy[1]

1. *Analytical chemistry Division, Bhabha Atomic Research Centre, Trombay, Mumbai 400085, India*
2. *Radiochemistry Division, Bhabha Atomic Research Centre, Trombay, Mumbai 400085, India; E-mail: racharya@barc.gov.in*

INAA using relative as well as internal monostandard methods has been applied for the major, minor and trace element determination of various alloys namely Nimonic alloy, Lead-Bismuth alloy and Zircaloys. The elements determined include, In, Sn, W, Mn Sb and Ag in lead-bismuth alloy, Ni, Ti, Al, V and Mn in Nimonic alloy and In, Sn, Mn, Cl, Hf, Ta, Cr, Fe, Ni and Zr in zircaloys. The results were compared with the results obtained by ICP-AES.

Introduction

Chemical quality control of the materials is required to ensure whether the materials of interest are within the prescribed chemical specifications. Various wet chemical methods are used for the analysis of these materials i.e. ICP-MS, ICP-AES and GFAAS. However such methods requires sample to be dissolved by suitable reagents, which in turn need blank correction to be incorporated in the final result. In the case of metallic alloys, chemical dissolution is a cumbersome process. In such cases, direct instrumental methods such as NAA and XRF can be used for the analysis of these materials. XRF analysis requires a matrix matching standard to obtain reliable results. NAA is a matrix independent technique. NAA method using internal monostandard has been used for the analysis of different matrices [1-4]. In this work Lead-Bismuth alloy, Nimonic alloy and Zircaloy were analyzed by using the IMNAA method. The samples were also analyzed by ICP-AES for method validation. The results obtained are discussed in this paper.

Experimental

Samples in the mass range of 50-100 mg were heat sealed in polyethylene pouches. The standards were prepared form Merck standard solution (1000 mg mL^{-1}). The graded amounts of standard solution were dried on the filter paper and heat sealed in the polythene. The samples were irradiated for 1 minute in Pneumatic Carrier Facility (PCF) at Dhruva reactor, BARC. The neutron flux was 5 x 10^{13} $cm^{-2}s^{-1}$. The long irradiations were performed at research reactor KAMINI, IGCAR, Kalpakkam and self serve of Cirus, BARC. The samples along with standard were irradiated for 2-6 h at a neutron flux of 5 x 10^{12} $cm^{-2}s^{-1}$. The radioactive assay was carried out using a 40% HPGe detector coupled to a 8k MCA. Both NAA relative method and IMNAA were used for the determination of various elements. For ICP-AES analysis, sample solutions were prepared using standard procedures.

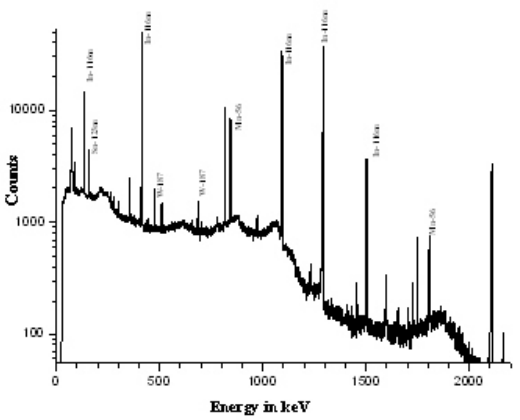


Fig. 1 Gamma ray spectrum of Lead-Bismuth alloy sample irradiated for 1 min at PCF, Dhruva

Results and Discussion

The results obtained for Nimonic, Lead-Bismuth and Zircaloy samples are given in Tables 1, 2 and 3 respectively.

Table-1: Determined concentrations of major, minor and trace elements in Nimonic alloy

Element	NAA relative	IMNAA	ICP-AES
Ni	80.32±1.34	-	80.65±1.98
Ti	0.25±0.01	0.25±0.01	0.24±0.01
Al	56±2	55±1	ND
V	248±10	251±8	ND
Mn	0.98±0.02	0.97±0.01	0.95±0.02
Cr	18.34±0.42	-	18.49±0.55
Fe	0.11±0.01	-	0.11±0.01

The uncertainties expressed on the IMNAA and relative NAA results are standard deviations of four independent measurements. In the case of Nimonic alloy, the elements Al and V were not detected by ICP-AES. The elements Cr and Fe could not be

analyzed by IMNAA method. The % deviation between the ICPAES and NAA relative NAA method was within ± 4%. The % deviation between the IMNAA and relative NAA method was within ± 2%.

Table-2: Determined concentrations of minor and trace elements in Lead-Bismuth alloy.

Element	NAA relative	IMNAA	ICP-AES
In	2.74±0.18	-	2.81±0.12
Cu	35.3±0.8	35.1±0.7	36.2±0.7
Sn	443±11	449±.8	462±12
Mn	49.1±1.8	48.5±1.2	ND
W	83±2	84±2	ND
Zn	10.9±0.2	-	11.4±0.1
Sb	1.62±0.11	-	ND
Ag	22.1±0.9	-	21.5±0.8

Table-3: Determination of trace, minor and major elements in Zircaloy-4 sample.

Element	NAA relative	IMNAA	ICP-AES
Zr (%)	-	98.21±0.88	98.28±0.95
Sn (%)	1.50±0.08	1.49±0.06	1.45±0.05
Cr (%)	0.089±0.004	0.087±0.003	0.090±0.003
Fe (%)	0.190	0.193	0.191
Hf	121±8	119±6	123±5
Mn	3.24±0.18	3.28±0.16	ND
In	0.105±0.09	0.118±0.08	ND
Cl	14.8 ± 0.4	14.1 ± 0.2	ND

In the case of Lead-Bismuth alloy, the elements Sb, W and Mn could not be detected by ICP-AES. The elements Sb, Zn and Ag could not be analyzed by IMNAA. The % deviation between the ICPAES and NAA relative NAA method was within ± 5 %. The % deviation between the IMNAA and NAA relative NAA method was within ± 3%.

In the case of Zircaloy 4 alloy, the element Mn, In and Cl could not be determined by ICP-AES. As all the elements detected in zircaloy 4 sample are amenable to NAA, the actual concentrations are calculated using mass balance approach. The % deviation between the ICPAES and NAA relative NAA method was within ± 3 %. The % deviation between the IMNAA and NAA relative NAA method was within ± 2 %. For method validation BCS CRM 310 (Nimonic alloy was analyzed. The % deviation between results by IMNAA and NAA relative method was less than 3%.

Conclusion

The NAA technique was applied for compositional analysis of Nimonic, lead-bismuth and zircaloy 4 samples. The method was validated by analyzing the samples by ICPAES. The IMNAA method could determine nondestructively the major, minor and trace impurities in these alloys.

Acknowledgement

Author thanks Mrs. M. K.T. Bassan for her help during the ICP-AES analysis. Authors thank Dr. P. K. Pujari and Dr. A. Goswami, RCD for their keen interest and encouragement during the work.

References

[1] A. G. C. Nair, R. Acharya, K. Sudarshan, S. Gangotra, A. V. R. Reddy, S. B. Manohar, A. Goswami, Anal Chem, 75 (2003) 4868.

[2] R. Acharya, A. G. C. Nair, K.Sudarshan, A. V. R. Reddy, A. Goswami, Appl Radiat Isot, 65 (2007) 164.

[3] K. Sudarshan, A. G. C. Nair, A. Goswami, J Radioanal Nucl Chem, 256 (2003) 93.

[4] R. Acharya, A. G. C. Nair, A. V. R. Reddy, A. Goswami, J Nucl Mater, 326 (2004) 80.

Neutron Activation Analysis of Minerals from Cuddapah Basin Geological Formations

P.V. Nagendra Kumar[1], N. Suresh Kumar[2], R. Acharya[3], A.V.R. Reddy[4], L. Krishna Reddy[5]

1. *Department of Chemistry, GITAM University, Hyderabad Campus, Hyderabad, India; E-mail: pv.nagendrakumar@yahoo.com*
2. *Cyclotron Facility, Medical imaging Department, King Fahad specialist hospital, Dhammam*
3. *Radiochemistry Division, Bhabha Atomic Research Centre, Trombay, Mumbai 400085, India*
4. *Analytical Chemistry Division, Bhabha Atomic Research Centre, Trombay, Mumbai 400085, India*
5. *Department of Chemistry, S.V.University, Tirupati*

Green and yellow serpentines along with two associated minerals namely dolomite and intrusive rock dolerite obtained from the asbestos mines of Cuddapah basin, Andhra Pradesh, India were analyzed by k_0-based neutron activation analysis (k_0-NAA) method. Gold (^{197}Au) was used as the single comparator. Two reference materials namely USGS W-1 (geological) and IAEA Soil-7 (environmental) were analyzed as control samples to evaluate the accuracy of the method. A total of 21 elements present at major, minor and trace concentrations were determined in serpentines as well as associated minerals. The elemental concentrations were used for distinguishing and characterizing these minerals, and also to understand the extent of segregation of elements from the associated or host mineral rocks to serpentines.

Introduction

Minerals like Serpentines, dolomites etc were analysed by Neutron activation analysis for multi elemental profile including rare earths. Serpentines are a class of secondary minerals derived by alterations in magnesium rich silicate minerals. They have a formula of $[Mg_3Si_2O_5(OH)_4]_2$ with varying concentrations of other elements [1]. It can be found in igneous rock, but it is more often a secondary mineral, usually resulting from the alteration of minerals or rocks containing magnesium. Serpentines mainly occur as fibrous chrysotile (an asbestos) or as a lamellar or platy antigorite and are found as discontinuous bands along the bedding planes separated by serpentinised dolomitic limestone.

The formation of serpentine and asbestos in Vempalle area, Cuddapah basin has been discussed by several workers. Coulson [2] suggested that serpentine and associated asbestos were formed due to hydrothermal solutions accompanying the dolerite intrusive. It was also reported that hydrothermal solutions accompanying the igneous sills have rendered serpentinisation in the magnesium rich limestone by supplying silica, magnesium and water [3]. The carbonate rock may be metamorphosed into dolomitic marble. Most dolomites probably originate from the partial replacement of the calcium in limestone by magnesium.

Experimental

Sampling and Sample Preparation

Two varieties of serpentines viz. serpentine black and serpentine yellow along with the altered and unaltered dolomites and intrusive dolerite were systematically collected in the asbestos mines of Brahmanapalle village of Pullivendla Taluq in Cuddapah basin, Cuddapah district, Andhra Pradesh, India. The samples were sun-dried, powdered and heated in an air oven at 105°C for about 24 hours. The powdered samples together with an accurately weighed gold standard (about 5 g), aliquoted from gold standard solution, were doubly sealed in polythene. The control samples (USGS W-1 and IAEA CRM Soil-7) were also sealed in the similar way to that of samples.

Irradiations

Samples, gold standard and control samples were irradiated at the E8 position of APSARA reactor at BARC, Trombay, Mumbai. The duration of irradiation was varied between 5 minutes and 7 hours depending on the half-lives of radionuclides of interest. The neutron flux at E8 position of APSARA reactor is ~ 10^{12} $cm^{-2}.s^{-1}$.

Measurement of Radioactivity

After appropriate cooling period, the samples were mounted on standard Perspex plates and assayed for gamma activity using a 16% relative efficiency HPGe detector coupled to a PC based 4K channel analyzer in an efficiency calibrated position with reproducible sample-to-detector geometry. The peak areas were evaluated using a peak fit software called PHAST, developed at BARC.

Calculations

The concentration of an element, C_i, was calculated using following equation,

$$C_i \quad g\ g^{-1} \quad \frac{N_p / LT}{S.D.C.W} \Big/ \frac{N_p / LT}{S.D.C.w}^{*} \quad \frac{1}{k_0} \quad \frac{f \quad Q_0(\ )^{*}}{f \quad Q_0(\ )} \quad ^{*}$$

Table-1: Elemental Concentrations of dolerite, serpentines and dolomites (in mg.kg^{-1} unless % or g. kg^{-1} is indicated)

Element	Dolerite	Black Serpentine	Yellow serpentine	Altereddolomite	Unaltered dolomite
Na	1325±79	162.4±7.5	93.3±5.0	86.9±5.9	654.7±18
Mg%	9.2±0.5	22.7±1.8	18.1±0.6	8.3±0.2	12.9±1.4
Al%	1.9±0.1	4.0±0.2	0.110±0.005	0.110±0.005	0.17±0.0
Cl	ND	400±11	255±3	289±9	132.3±5.2
Ca%	8.75±1.15	ND	0.55±0.02	18.1±1.3	25.5±1.8
Sc	27.1±1.1	25.3±1.1	0.16±0.01	0.50±0.02	0.22±0.01
Ti %	0.48±0.03	0.70±0.04	ND	ND	ND
V	209.5±14.1	172.4±8.5	ND	ND	ND
Cr	70.1±4.1	53.7±3.2	ND	ND	ND
Mn	2921±160	2722±54	28.7±.0.1	144.0±9.5	145.3±3.6
Fe%	7.94±0.20	5.00±0.38	0.22±0.01	ND	ND
Co	30.5± 1.8	37.3±2.3	4.4±0.2	5.6±0.3	4.7±0.3
As	ND	4.99±0.18	13.4±1.2	6.2±0.1	0.76±0.05
Ba	ND	ND	545±53	222±17	158.6±9.2
La	13.7±1.0	10.9±0.7	1.82±0.04	3.07±0.06	1.28±0.08
Ce	41.3±2.2	24.3±1.5	ND	ND	8.32±0.67
Sm	2.97±0.15	1.77±0.08	0.48±0.03	0.23±0.01	0.22±0.02
Eu#	990±60	350±20	100±5	50±2	20.1±1.1
Dy	ND	9.19±0.57	0.27±0.01	ND	ND
Yb	2.99±0.13	2.22±0.10	ND	ND	ND
Au#	ND	13.20±1.01	ND	20.3±1.5	10.1±0.8

ND- not detected, (info) – information value

where N_p is the net counts under the peak, S is the saturation factor $1 - e^{-t_{irr}}$, D is the decay factor e^{-t_C}, C is the counting factor for correcting the decay during counting period and is given by ((1 - e^{-LT}/ LT) and t_{irr}, t_c and LT are time durations for irradiation, cooling and counting of the sample respectively, W is the mass of the sample, w is the mass of the comparator, k_0 is the literature recommended k_0-factor, $Q_o(\ )$ is the ratio of cross sections and is equal to $I_o(\ ) / {}_0$, where, $I_o(\ )$ is infinitely dilute resonance integral corrected for , ${}_0$ is the thermal neutron capture cross section, is the detection efficiency of the detector for the gamma-ray energy used and the symbol * refers to the corresponding parameters of the comparator.

Results and Discussion

Concentrations of 20 elements including 6 rare earth elements (REEs) have been determined along with certified reference materials, USGS W-1 and IAEA Soil-7, by the k_0-based INAA are measured. The elemental concentrations of the two serpentines as well as the associated minerals obtained are given in Table 1. A total of 21 elements have been determined in these minerals.

Conclusions

The k_0-INAA method was used for the determination of major, minor and trace elements. The concentrations of elements namely Sc, Cr and Co were found to be higher for black serpentine than the yellow serpentine, which are in good agreement with the literature. The concentrations of elements Na, Sc, V, Cr, Fe and REEs are found to be in the same order from dolerite to black serpentine to yellow serpentine.

Present study indicated that both dolomite and dolerite contribute elements during serpentine formations, with the contribution of dolerite higher than that of dolomite for many macro and trace elements.

References

[1] B. Mason, L. G. Berry, Elements of Mineralogy, W.H. Freeman and Company, San Francisco, USA (1968) pp. 443-444.

[2] The Columbia Electronic Encyclopedia, 6th ed. Copyright © 2003, Columbia University Press., http://www.infoplease.com/ce6/sci/A0844507.html..

[3] A. L. Coulson, Mem. G.S.I., Vol. 64, Part 2 (1934).

Raman and XPS Analyses of the Oxide Formed Over Monel Surfaces Under the Steam Generator Chemistry Conditions in the Presence of Poly(acrylic acid-co-maleic acid) [PAMA]

Akhilesh C. Joshi, A.L.Rufus, S. Velmurugan

Water and Steam Chemistry Division, Bhabha Atomic Research Centre Facilities, Kalpakkam 603 102; E-mail: svelu@igcar.gov.in; Fax: +91-44-27480097

Use of polymeric dispersants in steam generators (SG) is expected to reduce fouling. This paper presents Raman and XPS analyses in characterising the oxide formed on monel under SG chemistry conditions in presence of Poly(acrylic acid-co-maleic acid) [PAMA], a polymeric dispersant. The results showed that PAMA affects the transportation and redeposition of metal ions. Further, PAMA interacts with metals by adsorbing onto their surfaces.

Introduction

Polymer dispersants are being explored to control fouling [1-2] in Steam Generators (SG) of nuclear reactors. Fouling in SG causes decreased heat transfer efficiency, SG tube failure, thermal hydraulic disturbances and associated problems [3]. The wide range of possible applications of polymer dispersants [1-2] encouraged to study the effect of Poly(acrylic acid-co-maleic acid) [PAMA] on the formation of oxide on SG structural materials under secondary side water chemistry conditions. In this context, static autoclave experiments were carried out and the results pertaining to monel surfaces (SG tube material in old generation Indian PHWRs), are discussed in this paper.

Experimental

Monel coupons were exposed in a static autoclave to secondary side water chemistry conditions in the absence and presence of 175 ppb of PAMA for 10 days at 200°C and 250°C. Coupons of carbon steel and incoloy-800 were also exposed along with monel to mimic the real system conditions. Oxides formed over monel surfaces were characterised by XRD, X-ray photoelectron spectroscopy (XPS) and Raman spectroscopy. Analysis of autoclave solution was done using inductively coupled plasma atomic emission spectroscopy (ICP-AES).

Results and Discussion

Analysis of the autoclave solution for iron, nickel and copper at the end of exposure was found to be below detection limit in ML (monel exposed in the absence of PAMA) and ML+PM (monel exposed in the presence of PAMA) experiments. The Raman spectra of ML (Fig. 1b) showed the oxide phase to be a nickel based spinel, while in ML+PM (Fig. 1a) the oxide phase was corresponding to simple copper and nickel oxides. Besides, optical microscope showed small triangular crystals scattered all over the surface. Raman analysis of these triangular crystals was corresponding to magnetite phase. Thus, the oxide formed in the presence of PAMA is simple oxides of copper and nickel super imposed by triangular crystals of scanty magnetite phase.

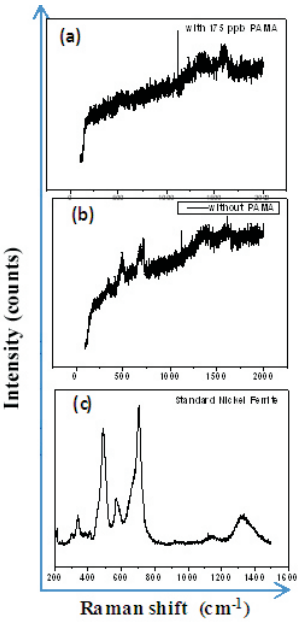


Fig. 1 Raman spectra of monel-400 (a) with PAMA (b) without PAMA (c) standard nickel ferrite

In the XPS analysis, since PAMA is an organic compound, carbon and oxygen peaks were analyzed in detail. Both C 1s and O 1s peaks for ML+PM were broad compared to ML as shown in Fig. 2(a) & 2(b). Both the broad peaks were deconvulated to find out the possible compounds on ML+PM surface. C 1s and O 1s deconvulated peaks are presented in the Table 1. Deconvulation of C 1s indicates adsorption of PAMA on the monel surface. This is also supported by O 1s deconvulation. Surprisingly, though PAMA does not contain nitrogen, the ML+PM showed a peak for nitrogen (Fig. 2c), which was absent in the case of ML. The source of nitrogen would have been either ethanolamine (NH_2-CH_2-CH_2-OH) or hydrazine (N_2H_4) that are secondary side additives to maintain required pH and dissolved oxygen respectively. This is supported by the deconvulation of O 1s peak, which indicated the presence of organic hydroxyl group on the surface.

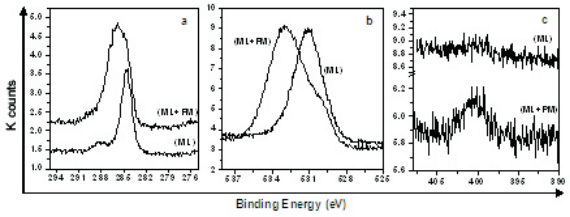


Fig. 2 (a) Carbon 1s peak (b) Oxygen 1s peak (c) Nitrogen 1s peak

Table 1: Deconvulated peaks of C 1s and O 1s for PAMA exposed monel surface

Peak	Peak centre (eV)	FWHM (eV)	Remarks
C 1s	284.8	1.6	*PMA , Graphite
	285.9	1.6	PMA , $MeCH_2OH$
	287.0	1.6	PMA
	288.5	1.6	PMA
O 1s	530.2	1.8	Oxide
	531.4	1.8	Hydroxide
	532.2	1.8	moisture , PMA
	532.9	1.8	-C-OH
	533.9	1.8	PMA

*PMA – Poly methacrylic acid

The source of hydroxyl group should be from ethanolamine. Though, both these additives were present in the autoclave during the exposure of ML and ML+PM, the nitrogen peak was seen only in the case of ML+PM. Thus, apart from the adsorption on the monel surface, PAMA also reacts with hydroxyl (-OH) or $-NH_2$ group of ethanolamine and/or hydrazine.

Monel is an alloy of mainly Cu (~32%) and Ni (~66%) with minor amounts of Cr and Fe. XPS analysis of these elements were recorded for both ML and ML+PM. Apart from the strong peaks for Cu and Ni, weak signals were obtained for Fe while the Cr peak was below detection limit. Relative concentrations of Cu, Ni and O are shown in Table 2. Oxygen concentration was higher in the case of ML+PM owing the presence of PAMA. Ni concentration was comparable in both ML and ML+PM, while copper was 4 times less in the case of ML+PM when compared to ML.

Raman spectrum of ML showed nickel based spinel. The iron for the formation of spinel should have come from carbon steel or/and incoloy-800 coupons that were exposed along with monel-400 coupons. In the case of ML+PM, the Raman shift corresponds to copper and nickel oxide phase that constitute the major phase. In some locations peaks corresponding to magnetite were also observed. Though, PAMA prevents the transportation and deposition of metal ions (iron), it is not 100% effective. In the presence of PAMA, the atomic percentage of copper and nickel in the oxide is nearly similar to that of monel-400. This substantiates the Raman results, which showed that copper oxide and nickel oxides were formed over the monel surfaces in the presence of PAMA. In the absence of PAMA, the ratio of copper and nickel on the surface is different from that of the base alloy. This may be due to dissolution, transportation and redeposition of metal ions, which is possible in the absence of dispersants.

Table 2: Relative concentrations of Cu, Ni and oxygen for monel surfaces exposed in the presence and absence of PAMA

Sample	Cu (%)	Ni (%)	O (%)
ML	20.6	20.4	59.0
ML+PM	5.4	22.5	72.1

Conclusions

Raman and XPS analyses helped to understand the phenomena of transportation and redeposition of metal ions in the presence of PAMA, a polymeric dispersant. XPS analysis also showed that PAMA interacts with the metal by adsorbing onto its surface.

Acknowledgements

The authors thank Vinit K. Mittal and Dr. P. Chandramohan of WSCD for experimental support and discussion on XPS & Raman techniques.

References

[1] Polymeric Dispersants, A Review of the Literature, EPRI, Palo Alto, CA, (1999) TE-114159.

[2] P. V. Balakrishnan, S. J. Klimas, L. Lepine and C. W. Turner, AECL-11975, (1999) COG-99-165-I.

[3] M. Bohnet, Fouling of Heat Transfer Surfaces. Chem. Eng. Tech. (1987) 113.

Studies on Linear Attenuation Coefficient and Total Interaction Cross Sections of Sodium Metal in the Energy Range 0.122-1.330 MeV

Bharat S.Surung and Pravina P. Pawar

Department of Physics, Dr.Babasaheb Ambedkar Marathwada University, Aurangabad 431004, India;
E-mail: pravina.pawar@yahoo.com

Mass attenuation coefficients and total interaction cross sections of Sodium metal were measured at 122, 356, 511, 662, 1170, 1275 and 1330 keV photon energies using a well collimated narrow beam good geometry set up. The gamma-rays were detected using NaI (Tl) scintillation detection system with a resolution of 10.2% at 662 keV. The mass attenuation coefficients at different energies were calculated using XCOM programme. The mass attenuation coefficient data were then used to obtain the linear attenuation coefficients and total interaction cross sections of Sodium metal. It was observed that the linear attenuation coefficient and total interaction cross sections goes on decreasing with increase of gamma-ray energy. The results show that, the experimentally obtained values are in good agreement with the theoretical values calculated based on XCOM data up to 2 % error.

Introduction

Linear attenuation coefficients and total interaction cross sections are two quantities widely used in the study of interaction of -rays with matter [1]. Accurate values of photo electric cross section from photon radiation in several materials are needed in solving various problem in radiation physics and radiation dosimetry. It is necessary to ensure that the theoretically predicated values do indeed agree with experimental results [3]. Extensive studies have been carried out to determination gamma ray attenuation coefficients for various elements and photon energy [2-7].

Gamma radiations in the energy region above 200 keV up to about 1500 keV interact with matter predominantly by photoelectric effect, Compton effect, and pair production processes .The photon interaction cross-section can be expressed as a function of the photon energy and the atomic number Z. At a given photon energy, the interaction cross section is proportional to Z^n where n is expected to be between 4 and 5 for the photoelectric effect, 1 for the Compton effect, and 2 for pair production [8]. From the mass attenuation coefficient, related parameters can be derived, such as the linear attenuation coefficients and total interaction cross-section [9].

The nature of interaction of metals such as Sodium is desirable over this energy region. Theoretical values for the mass attenuation coefficients can be found in the tabulation [10]. In this work, we have measured the mass attenuation coefficients and total interaction cross sections of Sodium metal .in the energy range 122 to 1330 keV and then compared these experimentally evaluated parameters with theory using XCOM program [11].

Experimental

The five radioactive sources ^{57}Co,^{133}Ba , ^{137}Cs and ^{60}Co and ^{22}Na were used in the present investigation. Gamma rays of energy from 122 - 1330 keV emitted by the above radioactive sources, (procured from Bhaba Atomic Research Centre, Mumbai) were collimated and detected by NaI(Tl) detector having energy resolution of 10.2% at 662 keV. The signals from the detector were amplified and analyzed with 8K multichannel analyzer. By using the diameter of the pellet and mean value of the mass of the pellet, the mass per unit area was determined in each case. The sample thicknesses were selected in order to satisfy the following ideal condition as far as possible [12].

2 ln (I_0 /I) 4

Table 1: Linear attenuation coefficients (cm^{-1}) of Sodium metal from 122 to 1330keV.

Energy keV	exp.	theo.	% deviation
122	0.14356	0.14259	-0.68027
356	0.09312	0.09215	-1.05263
511	0.07857	0.07760	-1.25000
662	0.06984	0.06887	-1.40845
1170	0.05529	0.05626	1.72414
1275	0.04947	0.05044	1..92308
1330	0.04947	0.04850	-2.00000

Equations

This attenuation of the beam is described by the following equation:

$$I = I_0 e^{\quad t} \qquad (1)$$

where I_0 and I are the unattenuated and attenuated photon intensities, respectively, and (cm^{-1}) is the linear attenuation coefficient of the material. A coefficient more accurately characterizing a given

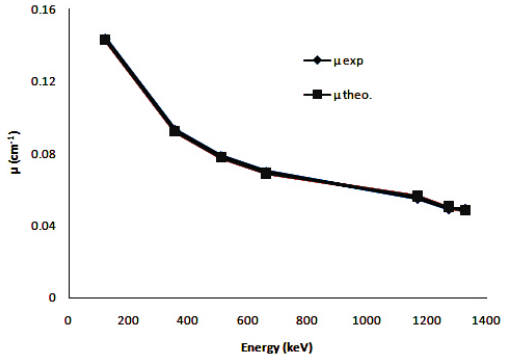


Fig. 1 The typical plots of versus E for sodium metal

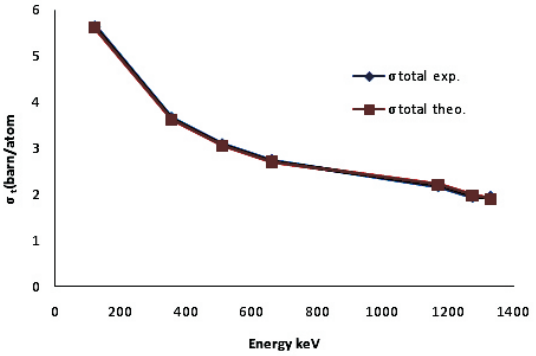


Fig. 2 The typical plots of $_t$ versus E for sodium metal

Table 2: Total interaction cross sections $_t$ (in barn /atom) of Sodium metal from 122 to 1330 keV.

Energy keV	$_t$ exp.	$_t$. theo.	% deviation
122	5.647411	5.609253	-0.68027
356	3.663185	3.625027	-1.05263
511	3.090813	3.052655	-1.25000
662	2.747389	2.709231	-1.40845
1170	2.175016	2.213175	1.72414
1275	1.946067	1.984225	1.92308
1330	1.946067	1.907909	-2.00000

material is the, density-independent ,mass attenuation coefficient / (cm^2 gm^{-1}).Rearrangement of Eq.(1) yields the following equation for the linear attenuation coefficient:

$$= 1 \ln(I_0/I) \quad (2)$$

t In Eq. (2), t (cm) is the sample thickness. The mass attenuation coefficients / (cm^2gm^{-1}) for the samples were obtained from Eq. (3) by using the density of the corresponding samples:

$$_m = / \ (cm^2\ gm^{-1}) = \frac{1}{t} 1 \ln(I_0/I) \quad (3)$$

where (g/cm^3) is a measured density of the corresponding sample, and I_0 and I are the unattenuated and attenuated photon intensities respectively. The values of the mass attenuation coefficients were then used to determine the linear attenuation coefficients ( ) by dividing these values with its density and to determine the total attenuation cross sections ($_t$) by using following equation

$$_t = / \ (A/N_A) *10^{24} \quad (4)$$

where A is the atomic mass and N_A is Avogadro's Number .N_A=6.02486*10^{23}

Results and Discussion

The values of linear attenuation coefficients (cm^{-1}) and total interaction cross sections $_t$ (in barn /atom)of Sodium metal from 122 to 1330keV are displayed in Table 1and Table 2 . and the typical plots of versus E and $_t$ versus E for sodium metal is displayed in Fig. 1 and Fig. 2 It is seen from Fig.1 and Fig. 2 that the values for linear attenuation coefficients and total interaction cross sections goes on decreasing with increase of gamma-ray energy. The results show that, the experimentally obtained values are in good agreement with the theoretical values calculated based on XCOM data up to 2% error.

Conclusions

The present experimental study has been undertaken to get information on mass attenuation coefficient / values and related parameters like linear attenuation coefficient ( ) and total interaction cross sections for sodium metal. It has been found that the / is useful and sensitive physical quantity to determine and $_t$ for sodium metal. In the interaction of photon with matter, / and $_t$ values are dependent on the physical and chemical environments of the samples.

References

[1] Terra F S MOD .Phys. Lett .B8 28 (1997) 1781.
[2] C.M.Davinson ,Evans R D phys Rev .81 (1951) 404
[3] Goswani B, Chaudhari N, phys Rev A7 (1973) 539
[4] Pawar P P,J.chem.pharm .Res.,3(4) (2011) 899.
[5] PawarP P ,Bichile G K J.chem.pharm .Res., 3(5) (2011) 267.
[6] Pawar P P, Bichile G K J.chem.pharm .Res., 3(6) (2011) 693.
[7] Pawar P P, Bichile G K Archives of Physics Research, 3(1) (2012) 60.
[8] Murthy, R.C.,. Nature 207 (1965) 398.
[9] Pawar P.P., Bichile G.K., Radiation Physics and Chemistry, article in press(accepted 4th July, 2013).
[10] Hubbell J. H. and Berger M.J., Photon attenuation. In : Jaerger,R.G.(Ed.),Engineering compendium on radiation shielding.1. 91AEA,Vienna, Austria. (1968) p. 198.(4).
[11] Hubbell J H. Seltzer S M National Institute of Standards and Technology (IR) Report, No, (1995); 5632.
[12] Creagh, D C., Nucl.Instrum.and Meth. A 255, (1987), 1-16.

^{96}Zr(,n) Reaction Cross-section in the End-point Bremsstrahlung Energies of 12-16 and 45-70 MeV

H. Naik[1], G.N. Kim[1], R. Schwengner[3], K. Kim[2], M. W. Lee[2], M. Zaman[2], S.G. Shin[4], Y. Gey[4], R. Massavczyh[3], R. John[3], A. Junghans[3], A. Wagner[3] and A. Goswami[1]

1. *Radiochemistry Division, Bhabha Atomic Research Centre, Mumbai 400085, India*
2. *Department of Physics, Kyungpook National University, Daegu702-701, Republic of Korea*
3. *Institut for Strahlenphysik, Helmholtz-Zentrum Dresden-Rossendorf (HZDR), Dressden, Germany*
4. *Division of Advanced Nuclear Engineering, POSTEC, Pohang 790-784, Republic of Korea*

The ^{96}Zr(,n)^{95}Zr reaction cross-section was determined at end-point bremsstrahlung energies of 12, 14, 16, 45, 50, 55, 60 and 70 MeV by activation and off-line -ray spectrometric technique. The same reaction cross-sections were also calculated theoretically using TALYS code and arefound to be in good agreement with present data. It was also found that the experimental and the flux-weighted theoretical values increase from the threshold value to 14.32 MeV, where (,2n) reaction channel opens. Thereafter it decreases slightly with energy due to the opening of higher reaction channels. This indicates the role of excitation energy and its partition in different reaction channels.

Introduction

Zr metal and its alloy have low neutron absorption cross section [1] for low energy neutrons. Thus they have major application in nuclear power industry as the structural and cladding materials in most of the conventional water reactors and ADSs. Therefore it is important to estimate the amount of Zr in structural and cladding materials using method other than neutron activation. One among different method is the photo-activation technique, which is yet to be developed. However, the photons beam available is in the form of bremsstrahlung from the electron linac. In view of this, in the present work the ^{96}Zr(, n) reaction cross-section in the end-point bremsstrahlung energies of 12-16 and 45-70 MeV has been determined using activation and off-line -ray spectrometric technique.

Experimental

About 32.6-41.6 mg ^{nat}Zr metal (size = 0.56 - 1 cm^{2}x0.1 mm) and 55-75 mg of Au metal (size=0.48 cm^{2}x 0.1 mm) wrapped with 0.025 mm thick Al were irradiated for 8.5-10.5 h with end-point bremsstrahlung energies of 12-16 MeV using the 20 MeV electron linac ELBE at HZDR, Dresden, Germanay using the rabbit facility. The bremsstrahlung radiation was generated by impinging the electron beam on a solid graphite beam dump. During the experiments, the electron LINAC was operated with a pulse repetition rate (PRR) of 13 MHz, a pulse width of 10 ps and an average beam current of 550 A. Similar samples were also irradiated for 0.5-3 h with end-point bremsstrahlung energies of 45-70 MeV using the 100 MeV electron linac at PAL, Pohang, Korea. The bremsstrahlungwas generated when a pulsed electron beam hit a thin tungsten(W) metal foil with a size of 100 cm^2 x 0.1 mm. The current of the electron beam during irradiation was 10-35 mA at 3.75 Hz with a beam width of 1.5 s. The -ray counting of the irradiated targets of Zr and Au along with an aluminum catcher was done by using energy and efficiency-calibrated 90% HPGe detector coupled to a PC based 16K channel analyzer. The resolution of the detector system was 2.0 keV at 1332.0 keV of ^{60}Co.

Calculation and Results

The net peak area (A_{net}) corresponding to the photo-peak was calculated by summing the counts under the full energy peak and subtracting the linear Compton background. $A_{net}$of^{196}Au and^{95}Zr are related to the photon flux ( ), target atom (N) and cross-section ( ) as,

$$A_{net} = N\langle\ \rangle\ a\ (1- e^{-\ t})\ e^{-\ T}(1- e^{-\ CL})/$$

Where 'a' and are the -rayabundance of the analyzed and its detection efficiency.*t, T, CL,* and *LT* are the irradiation, cooling, live and counting time, respectively.

The photo-peak activities of 333, 356 and 426 keV -lines of ^{196}Au from the ^{197}Au(, n) reaction were used as the flux monitor [2]. The nuclear spectroscopic data were taken from ref. [3]. The flux-weighted average cross-section $\langle\ \rangle$ for ^{197}Au(, n)^{196}Au reaction used in the calculation of bremsstrahlung flux was obtained as $\langle\ \rangle$ = / . The bremsstrahlung spectrum was obtained using computer code GEANT4 [4]. Then the average $\langle\ \rangle$ for the ^{96}Zr(, n)^{95}Zr reaction was calculated from the 724 and 756 keV photo-peak activities. The ^{96}Zr(, n)^{95}Zr reaction cross-section at the end-point bremsstrahlung energies of 12, 14, 16, 45, 50, 55, 60 and 70 MeV from the present work and at 10 and 12.5 MeV from our earlier work [5,6] were plotted in Fig. 1. In the same figure, the flux-weighted values from the literature data [7] and theoretical value from TALYS [8] were also plotted for comparison.

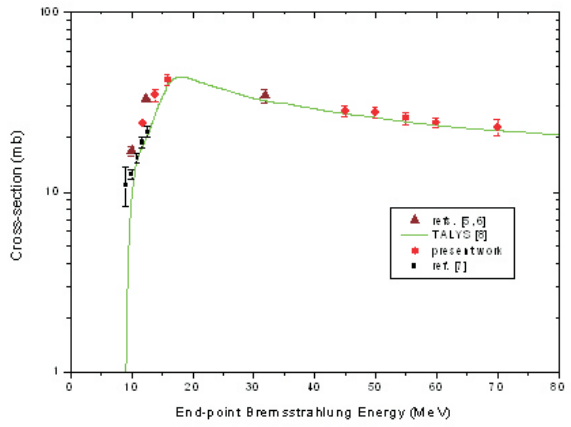


Fig. 1

Discussion and Conclusion

It can be seen from Fig. 1 that the experimental ^{96}Zr(,n)^{95}Zr reaction cross-section are in good agreement with the theoretical values of TALYS [8]. From Fig. 1, it is also clear that the experimental and theoretical values increasefrom the threshold value of 7.86 MeV to the end-point bremsstrahlung energy of 14.32 MeV. This is because the ^{96}Zr(,2n) reaction has the threshold value of 14.32 MeV. When ^{96}Zr(,2n) reaction cross-section start increasing, the ^{96}Zr(,n) reaction cross-section remains constant up to 22.5 MeV. Thereafter when ^{96}Zr(,3n) reaction starts opening, the cross-section for ^{96}Zr(,n) reaction decreases slowly. This indicates that the shearing of excitation energy in different reactions channels. Further, it can be seen from Fig. 1 that the increase of ^{96}Zr(,n) reaction cross-section is very sharp from 7.86 MeV to 15-20 MeV, which is the region of GDR. Thus in the beginning the sharp increase trend is due to the GDR effect besides the role of excitation energy.

Acknowledgement

The authors are thankful to the staff of electron linac ELBE at HZDR, Dresden, Germany and at PAL, Pohang, Korea for providing the electron beam. Dr. H. Naik thankful to Dr. K. L. Ramakumar, director of RC & I group for supporting the program and for permitting him to visit, PAL, Korea to carry out this experiment.

References

[1] IAEA-EXFOR, Experimental Nuclear Reaction Data, [http://www-ndsw.iaea.org.exfor].

[2] V.V. Varlamov et al. Izv.Rossiiskoi Akademii Nauk, Ser.Fiz., 74 (2010) 884.

[3] R. B. Firestone and L. P. Ekstrom, (2004):[http://ie.lbl.gov/toi/index.asp].

[4] S. Agostinelli et al., Nucl. Instr. Meth. A 506 (2005) 250.

[5] R.Crasta et al. Radiochim.Acta (accepted).

[6] A.K. Md. L. Rahman et al. J. Nucl. Sci. Tech. 47 (2010) 618.

[7] A. Lepretre et al. Nucl.Phys.Al75 (1971) 609.

[8] A.J. Koning et al. AIP Conf.Proc.769 (2005) 1154.

Determination of Total Interaction Cross section and Mass Energy-absorption Coefficients of Sorbitol using NaI(Tl) Scintillation Detector

Bibifatima M.Ladhaf, Shaikh Humera. B, Prashant S. Kore and Pravina P. Pawar

Department of Physics, Dr. Babasaheb Ambedkar Marathwada University, Aurangabad 431004, India;
E-mail: pravana.pawar@yahoo.com

Mass attenuation coefficients of Sorbitol ($C_6H_{14}0_6$) were measured at 122, 356, 511, 662, 1170, 1275 and 1330 keV photon energies using a well collimated narrow beam good geometry set up. The gamma-rays were detected using NaI(Tl) scintillation detection system with a resolution of 10.2% at 662 keV. The mass attenuation coefficients at different energies were calculated using XCOM programme. The mass attenuation coefficient data were then used to obtain the total attenuation cross-sections and mass energy-absorption coefficients of Sorbitol. It was observed that the total attenuation cross-sections and mass energy-absorption coefficients goes on decreasing with increase of gamma-ray energy. The results show that, the experimentally obtained values are in good agreement with the theoretical values calculated based on XCOM data up to 2% error.

Introduction

Data on the transmission and absorption of gamma rays in biological, shielding and dosimetric materials assume great significance by virtue of their diverse applications in the field of medical physics and radiation biology, as well as in many other areas of human enterprise [1] Photons of energy from 1500 keV down to about 5 keV are widely used in medical and biological application [2] especially during diagnosis and therapy. In recent years, several investigators have studied nature of interaction of bilogically important molecules with photons in this energy range [3-5]. The mass attenuation coefficient / and mass energy-absorption coefficient $_{en}$/ are basic quantities used in calculations of the penetration and the energy deposition by energetic photons in biological, shielding, and other materials. They are widely used as reference data in radiation shielding and dosimetry [6].

A variety of physiological functions inside living systems are performed by complex molecules such as carbohydrates, proteins, fats and oils composed of H, C, N and O elements. Carbohydrates are the most abundant class of biological molecules found in all living organisms. Carbohydrates include sugars, starches, cellulose and many other compounds found in living organisms. A thorough knowledge of the nature of interaction of these biologically important complex molecules such as carbohydrates is desirable over this energy region.

In this work, we have measured the total interaction cross-sections and mass energy-absorption coefficients $_{en}$/ of Sorbitol ($C_6H_{14}0_6$) in the energy range 122 to 1330 keV.

Experimental

The five radioactive sources ^{57}Co,^{133}Ba , ^{137}Cs and ^{60}Co and ^{22}Na were used in the present investigation. Gamma rays of energy from 122 - 1330 keV emitted by the above radioactive sources, (procured from Bhaba Atomic Research Centre, Mumbai) were collimated and detected by NaI(Tl) detector having energy resolution of 10.2% at 662 keV. The signals from the detector were amplified and analyzed with 8K multichannel analyzer. The diameters of the samples were determined with the help of a traveling microscope. It was observed that the attenuation of photons of the empty containers were negligible. Each sample pellet was weighed in a sensitive digital balance having an accuracy 0.001 mg .The weighing was repeated several times to obtain consistent value of the mass. The mean of this set of values was taken to be the mass of the sample. By using the diameter of the pellet and mean value of the mass of the pellet, the mass per unit area was determined in each case. The sample thicknesses were selected in order to satisfy the following ideal condition as far as possible [7].

2 ln (I_0 /I) 4

Table1: Total interaction cross-sections ($_{tot}$) barn/molecule) of Sorbitol from 122 to 1330keV.

Energy keV	$_{tot}$ exp.	$_{tot}$ theo.	% deviation
122	47.47129	47.16892	-0.641030
356	32.05068	32.35304	0.934579
511	27.51521	27.21284	-1.111110
662	24.49156	24.18919	-1.250000
1170	20.25845	19.95608	-1.515150
1275	18.14189	18.44429	1.639344
1330	17.83953	17.83953	0.000000

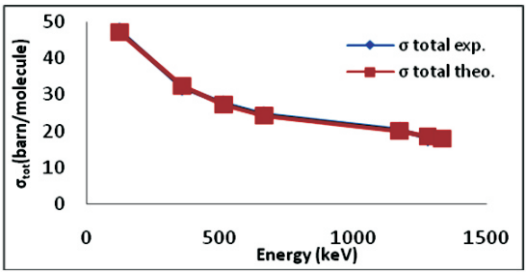


Fig. 1 The typical plots of $_{tot}$ versus E for Sorbitol ($C_6H_{14}0_6$)

Table2: Mass energy-absorption coefficient $_{en}/$ (cm^2 /g) of Sorbitol from 122 to 1330keV.

Energy keV	$_{en}/$ exp.(10^{24})	$_{en}/$ theo.(10^{24})
122	0.0421	0.0418
356	0.0284	0.0287
511	0.0244	0.0241
662	0.0217	0.0215
1170	0.018	0.0177
1275	0.0161	0.0163
1330	0.0158	0.0158

Equations

The attenuation of the beam is described by the following equation:

$$I=I_0e^{-\ t} \qquad (1)$$

where I_0 and I are the unattenuated and attenuated photon intensities, respectively, and (cm^{-1}) is the linear attenuation coefficient of the material. Rearrangement of Eq.(1) yields the following equation for the linear attenuation coefficient:

$$=\frac{1}{t}\ln(I_0/I) \qquad (2)$$

In Eq. (2), t (cm) is the sample thickness. The mass attenuation coefficients / (cm^2gm^{-1}) for the samples were obtained from Eq. (3) as:

$$_m= \ / \ (cm^2\ gm^{-1}) = \frac{1}{t}1\ \ln(I_0/I) \qquad (3)$$

where (gm/cm^3) is a measured density of the corresponding sample. The values of the mass attenuation coefficients were then used to determine the total interaction cross-section ($_{tot}$) by the following relation :

$$(\ _{t,ot}) = \ _m(M/N_A) \qquad (4)$$

The values of mass energy-absorption coefficient, $_{en}/$ in Table 2, following the definition in paragraph B.4.of [8] and in section 4.1 [9-10] were computed as,

$$_{en}/ \ = \ _{m,en}\,(N_A/A_r) \qquad (5)$$

in which, N_A is Avagadro's number (6.02486 * 10^{23} mol^{-1}) and A_r is the relative atomic mass (atomic weight) and, $_{m,en,}$ is the total molecular energy-absorption cross section,

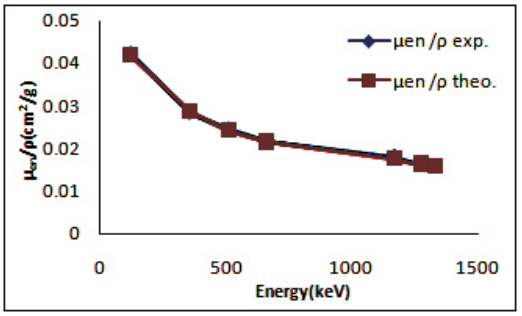


Fig. 2 The typical plots of $_{en}/$ versus E for Sorbitol($C_6H_{14}0_6$)

Results and Discussion

The values of the total interaction cross-sections ($_{tot}$) (barn/molecule) and mass energy-absorption coefficients $_{en}/$ of Sorbitol from 122 keV to 1330 keV are displayed in Table 1and Table 2 resp. In Fig.1. the typical plots of $_{tot}$ versus E is displayed. The typical plots of $_{en}/$ versus E is given in Fig.2. It is seen from Fig.1 and Fig.2 that the values for total interaction cross-sections and the mass energy-absorption coefficient goes on decreasing with increase of gamma-ray energy. The results show that, the experimentally obtained values are in good agreement with the theoretical values.

Conclusions

The present experimental study has been undertaken to get information on the total attenuation cross-sections($_{t,ot}$) and mass energy-absorption coefficient ($_{en}/$) of Sorbitol sample. It has been found that the $_m$ is useful and sensitive physical quantity to determine $_{t,ot}$ and $_{en}/$ for H,C, and O based biological compounds In the interaction of photon with matter, both values are dependent on the physical and chemical environments of the samples

References

[1] Manjunathguru V.,Umesh T.K., J.Phys.B At.Mol.Opt.Phys: 40 (2007) 3707.

[2] Jackson D.F.,Hawkes D.J., Phys.Rep.70 (1981) 169.

[3] Kirby B.J.,Davis J.R., Grant J.A, Morgan M.J., Phys. Med. Biol. 48(2003) 3389.

[4] Midgley S.M. Phys.Med.Biol.49 (2004) 307.

[5] Midgley S.M. Phys.Med.Biol.50(2005) 4139.

[6] Hubbell J H.and Seltzer S M National Institute of Standards and Technology (IR) Report No, (1995) 5632.

[7] Creagh, D C., Nucl.Instrum.and Meth. A 255 (1987) 1.

[8] ICRU Report 33, Washingaton, DC (1980).

[9] Berger R.T.,Radiat.Res., 15 (1961) 1.

[10] R.Manohara and S.M.Hanagodimath, Med.Phys. 35(1) (2008) 388.

EDXRF Analysis of Suspended Sediments from Trans Thane Creek Collected by using an in-house Developed Time-Integrated Sediment Sampler

R. H. Pillay, S. S. Gothankar, S. K. Jha, R. M. Tripathi

Health Physics Division, Bhabha Atomic Research Centre, Trombay, Mumbai 400085, India;
E-mail: rekhahp@barc.gov.in

The capacity of the sediment to concentrate most of the trace and toxic elements, makes them useful indicators for monitoring purposes and for predicting sources of pollution in the aquatic system. To collect the suspended sediment, a cylindrical time-integrated sampler was developed, wherein the flow velocity was reduced by a factor in excess of 600 relative to the ambient flow which induced sedimentation of the suspended sediment particles as the water moved through the cylinder towards the outlet tube. Suspended sediment collected was dried, weighed and pellets were made to analyse for trace and toxic elements using Energy Dispersive X-Ray Fluorescence (EDXRF) Technique.

Introduction

Trace elements are intrinsic, natural constituents of our environment. The natural aquatic ecosystem has been continuously disturbed by human activities. Toxic elements are dispersed in the environment through industrial effluents; organic wastes refuse burning and power generation. They can undergo long distance displacement from the source depending upon whether they are in the gaseous or particulate form. Wastes from various industries get dispersed on land and are carried to hydrosphere by rain water movement. The study of trace elements in the environment is more important in comparison to other pollutants due to their non bio-degradable nature, accumulative properties and long biological half lives. The capacity of the sediment to concentrate trace levels of most of the elements makes them useful indicators for monitoring purposes and for detecting sources of pollution in the aquatic system. The shallow-funnel shaped thane creek is a semi enclosed water body opened to Arabian sea at its south west approach and is also connected to its northern extremity to the ulhas river through a narrow channel. The Thane creek is receiving industrial as well as domestic effluent from point and non-point sources.

Experimental

To collect the suspended sediment, a cylindrical time-integrated sampler was developed. This sampler was fixed to a boat in a horizontal position in the Thane creek. The measurement of water quality parameters like temperature and salinity was carried out using standard methods. The suspended load was determined using the grab sampling method.

The suspended sediment collected was dried and weighed. Pellets (3 cm in dia and 2mm thick) were prepared by pressing 1 gram of sediment with 1 gram of binding material (cellulose powder) under 10 metric ton hydraulic pressure. The samples were analysed by ED-XRF Model 3600 (Jorden Valley Make) using suitable transmission filters to remove primary–beam continuum and provide a substantially monochromatic target–line excitation source [2]. To obtain optimum excitation of the low Z element, Cu filter was used. As the atoms of the elements of interest return to their initial stable state, they emit X-ray photons which are detected by Si(Li) detector coupled with PC based 2K MCA. Acquired spectrum was analysed and the concentration of each elements were evaluated by comparing net counts of respective elements in sample with those obtained from IAEA certified reference standard 356 in the same operative condition.

Results and discussion

During the course of tidal activity in a creek, a variation in the distribution of sediments in the water was observed. Once submerged, water continuously enters through the inlet tube of the sediment sampler at a velocity proportional to the ambient flow velocity. Within the cylindrical sampler, the flow velocity is reduced by a factor in excess of 600, relative to the ambient flow [1]. This reduced inflow velocity induces sedimentation of the suspended sediment particles as the water moves through the cylinder towards the outlet tube. Sample representing the average concentration of various trace elements in the sediment for a pre-determined duration was collected using the integrated sampler. The amount of suspended sediment collected during the total period of deployment is given in Table.1. Fig 1 shows the trapped suspended sediment in the sampler. The temperature of water varied from 16 to 35°C. Salinity of water ranged from 33.4 to 33.7psu. The concentration of suspended sediment in the water varied from 100 to 900 mg/L. Trace element concentrations of Ti, V, Cr and Mn were found to be between 4000 to 7000 ppm, 100 to 300 ppm, 70 to 200 ppm and 700 to 1200 ppm (Table 2). Natural crustal concentration gives a ratio of Mn (950 ppm) to V (135 ppm) as 7. In our study at different locations, the Mn to V ratio gives a variation from 2.4 to 9 (graph 1). Auto emission of Mn and the relative abundance of heavy ferrous and nonferrous industry which are the major sources of Mn may be its contributors to the creek ecosystem in Mumbai and could be the possible reason

for the higher ratio. The lower ratio can be attributed to input of V from the industries producing steel.

Table 1: Total suspended sediment Collected with time of deployment

S. No.	Time of deployment (in hours)	Total suspended sediment (in grams)
1.	3	4.0
2.	6	6.7
3.	12	9.8

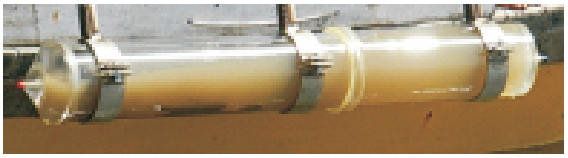
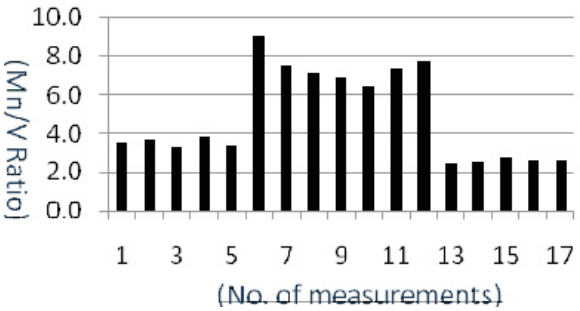


Fig. 1



Graph 1 Variation in Mn/V ratio

Conclusion

The amount of suspended sediment collected fulfills the requirement of a sample size to generate trace element data using Nuclear Analytical techniques like XRF and INAA. The samples were collected from near centroid of the creek which provided the representative samples. The obtained sample size gave an opportunity to understand the geochemistry of suspended sediment. The difference in the Mn/V ratios in the suspended sediments can be attributed to the relative abundance of heavy ferrous and nonferrous industry which are the major sources of Mn in Mumbai, the auto emission of Mn, and the input of V from the industries producing steel.

Table 2: Result of analysis of different elements in suspended samples along with Standard Reference Material

IAEA- 356 marine ediment Elements	Ti	V	Cr	Mn
Reference value (ppm)	2190	55.5	69.8	312
Our value (ppm)	2200	50	64	305
Observed value(ppm) Location 1	4969 6171 6534 6293	270 169 283 296	170 191 158 152 152.39	1197 1169 1122 710 710.46
Mean	5992	255	168	1050
Standard deviation ( )	±698	±57	±17	±228
Observed value (ppm) Location 2	6720 6652 6580 6020	268 145 147 268	185 177 149 143	1199 1160 1093 1078
Mean	6493	207	163	1133
Standard deviation ( )	±320	±71	±20	±57

Reference

[1] M.A.Russell, D.E. Walling, R.A. Hodgkin son: Proc. of symposium at Waterloo,Ontario, Canada, (2000), pp 119-127, editor:M. Stone

[2] S. K. Jha, S. B. Chavan, G. G. Pandit, B. S. Negi And S. Sadasivan; Environmental monitoring and assessment, volume 76(2) (2002).

Measurements of Mass attenuation coefficients and molar extinction coefficients of L-Cystine using gamma ray spectrometer

Prashant S. Kore, Bibifatima M. Ladhaf, Bharat S.Surung, Pravina P. Pawar, Rajkumar M. Lokhande, Umesh S. Rajurkar and Humera B.Shaikh[7]

Department of Physics, Dr.Babasaheb Ambedkar Marathwada University, Aurangabad 431004, India;
E-mail: koreprashant33@gmail.com

The mass attenuation coefficients of gamma rays in L-Cystine ($C_6H_{12}N_2O_4S_2$)has been measured at the photon energies, 511, 662, 1170, 1275 and 1330 keV .Experimental values for the molar extinction coefficient have been derived using mass attenuation coefficients and compared with therotical calculations There is good agreement between experiment and theory.

Introduction

Interaction cross sections and mass attenuation coefficients of amino acids, the buildings blocks of proteins, have been published by [1-3].

At a given photon energy, the interaction cross section is proportional to Z^n where n is expected to be between 4 and 5 for the photoelectric effect, 1 for the Compton effect, and 2 for pair production [4]. From the mass attenuation coefficient, related parameters can be derived, such as the total interaction cross- section and the molar extinction coefficient [5].

A variety of physiological functions inside living systems are performed by complex molecules such as carbohydrates, proteins, fats and oils composed of H,C,N and O elements. Sugars and amino acids are the building blocks of carbohydrates and proteins. Photons of energy from 1500 keV down to about 5 keV are widely used in medical and biological applications [6] especially during diagnosis and therapy. A thorough knowledge of the nature of interaction of these biologically important complex molecules such as carbohydrates is desirable over this energy region. Theoretical values for the mass attenuation coefficients can be found in the tabulation [7]. In this work, we have measured the mass attenuation coefficients and the molar extinction coefficients of L-Cystine ($C_6H_{12}N_2O_4S_2$) in the energy range 122 to 1330 keV and then compared these experimentally evaluated parameters with theory using XCOM program [8].

Experimental

The five radioactive sources ^{57}Co,^{133}Ba , ^{137}Cs and ^{60}Co and ^{22}Na were used in the present investigation. Gamma rays of energy from 122 - 1330 keV emitted by the above radioactive sources,(procured from Bhaba Atomic Research Centre, Mumbai) were collimated and detected by NaI(Tl) detector having energy resolution of 10.2 % at 662 keV. The signals from the detector were amplified and analyzed with 8K multichannel analyzer. The diameters of the samples were determined with the help of a traveling microscope. It was observed that the attenuation of photons of the empty containers were negligible. Each sample pellet was weighed in a sensitive digital balance having an accuracy 0.001 mg. The weighing was repeated several times to obtain consistent value of the mass. The mean of this set of values was taken to be the mass of the sample. By using the diameter of the pellet and mean value of the mass of the pellet, the mass per unit area was determined in each case. The sample thicknesses were selected in order to satisfy the following ideal condition as far as possible [9].

2 $\ln(I_0/I)$ 4

Table-1: Molar extinction coefficients (cm^2mol^{-1}) of L-Cystine from 122 to 1330 keV

Energy keV	exp.	theo.	% deviation
122	16.6942	16.7985	0.6211
356	11.0599	10.9556	-0.9524
511	9.2861	9.1818	-1.1364
662	8.1384	8.1384	0
1170	6.7820	6.6777	-1.5625
1275	6.1560	6.052	-1.7241
1330	6.05164	5.9473	-1.7544

Equations

This attenuation of the beam is described by the following equation:

$$I=I_0e^{-\ t} \qquad (1)$$

where I_0 and I are the unattenuated and attenuated photon intensities, respectively, and (cm^{-1}) is the linear attenuation coefficient of the material. A coefficient more accurately characterizing a given material is the density-independent, mass attenuation coefficient / (cm^2 gm^{-1}). Rearrangement of Eq.(1) yields the following equation for the linear attenuation coefficient:

$$= \frac{1}{t}\ln(I_0/I) \qquad (2)$$

t In Eq. (2), t (cm) is the sample thickness .The mass attenuation coefficients / (cm^2gm^{-1}) for the samples

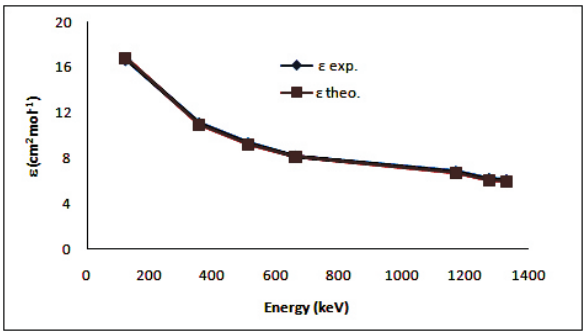


Fig. 1 The typical plots of versus E for L-Cystine($C_6H_{12}N_2O_4S_2$)

were obtained from Eq. (3) by using the density of the corresponding samples:

$$_m = / \ (cm^2\ gm^{-1}) = \frac{1}{t} \ln(I_0/I) \qquad (3)$$

where (gm/cm^3) is a measured density of the corresponding sample, and I_0 and I are the unattenuated and attenuated photon intensities, respectively.

The values of the mass attenuation coefficients were then used to determine the total molecular cross-section ($_{tot}$) by the following relation :

$$(\ _{t,ot}) = \ _m(M/N_A) \qquad (4)$$

where $M = \ _i\ n_i\ A_i$ is the molecular weight of the compound, N_A is the Avogadro's number, n_i is the total number of atoms (with respect to mass number) in the molecule and A_i is the atomic weight of the ith element in a molecule.

The values of molar extinction coefficients were determined using the following relation :

$$= 0.4343\ N_A\ _{tot} \qquad (5)$$

Results and Discussion

The values of molar extinction coefficients (cm^2mol^{-1}) of L-Cystine from 122 to 1330keVare displayed inTable 1. In Fig.1.the typical plots of versus E for L-Cystine ($C_6H_{12}N_2O_4S_2$) is given. The typical plots of / versus E for L-Cystine ($C_6H_{12}N_2O_4S_2$) is given in Fig.2. The typical Gamma ray spectra for all sources is displayed in Fig. 3. It is seen from Fig.1 and Fig 2 that the values for the molar extinction coefficient and mass attenuation coefficients goes on decreasing with increase of gamma-ray energy. The results show that, the experimentally obtained values are in good agreement with the theoretical values calculated based on XCOM data up to 2% error.

Conclusions

The present experimental study has been undertaken to get information on mass attenuation coefficient $_m$ values and related parameters ($_{tot}$ and) for L-Cystine sample. It has been found that the $_m$ is useful and sensitive physical quantity to determine for H,C, and O based biological compounds.In the interaction of photon with matter, $_m$ values are dependent on the physical and chemical environments of the samples.

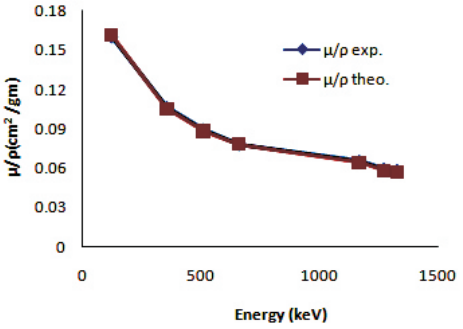


Fig. 2 The typical plots of / versus E for L-Cystine ($C_6H_{12}N_2O_4S_2$)

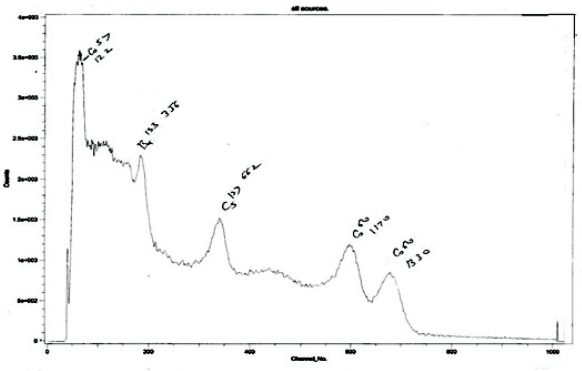


Fig. 3 Gamma ray spectra for all sources

References

[1] Gopinathan Nair,K.P. Gowda C.,Shylaja Kumari J., Anasuya S.J, Umesh T.K., Gowda R. Radiat. Phys. Chem. 43 (1994) 581.

[2] Gopinathan Nair,K.P., Umesh T.K., Gowda R. R. Radiat. Phys. Chem. 45 (1995) 231.

[3] Sandhu G.K, Kulwant Singh, Lark B.S,Gerward L 65 (2002) 211

[4] Murthy, R.C.,. Nature 207 (1965) 398.

[5] Pawar P.P., Bichile G.K., Radiation Physics and Chemistry, article in press(accepted 4th July, 2013).

[6] Hubbell J H Phys.Med.Biol.44 (1999) R1-R22.

[7] Hubbell J. H. and Berger M.J., Photon attenuation. In : Jaerger,R.G.(Ed.),Engineering compendium on radiation shielding.1. 91AEA,Vienna, Austria. (4) (1968) p. 198..

[8] Hubbell J H. Seltzer S M National Institute of Standards and Technology (IR) Report, No, (1995) 5632.

[9] Creagh, D C., Nucl.Instrum.and Meth. A 255 (1987) 1

Spatial Distribution Study on Trace Elements in Estuarine Sediment Using EDXRF Technique

P.Y. Ajmal, S.K. Sahu, M. Tiwari, R.C. Bhangare, G.G. Pandit

Environmental Monitoring & Assessment Section, Health Safety & Environment Group, Bhabha Atomic Research Centre, Trombay, Mumbai 400085; E-mail: sksahu@barc.gov.in

Distribution of trace elements in surface sediment is influenced by its texture, mineralogical composition and physical transport. The spatial concentration profile of eleven elements in surface sediment samples, namely V, Cr, Mn, Co, Ni, Cu, Zn, As, Br, Sr, and Pb were measured using Energy dispersive X-ray fluorescence (EDXRF) technique. To check the anthropogenic input, various indices (enrichment factor, contamination factor, index of geoaccumulation and pollution load index) were calculated and compared.

Introduction

With the rapid industrialization and economic development in coastal region, heavy metals are continuing to be introduced to estuarine and coastal environment around the world [1, 2]. Sediments are important carriers of trace metals in the hydrological cycle and because metals are partitioned with the surrounding waters, they reflect the quality of an aquatic system. Coastal and estuarine regions are the important sinks for many persistent pollutants as they accumulate in organisms and bottom sediments [3]. Sediments play a major role in the determining pollution pattern of aquatic systems and reflecting the history of pollutants deposition [4,5]. Elements such as Fe, Ni, Cu, Co, Mn, As, Cr, Pb and Zn etc. are used in contamination studies in marine systems due to their relationship with anthropogenic activities. These elements participate in various biogeochemical mechanisms that have significant mobility, which affects the ecosystems through bioaccumulation and biomagnifications process and are potentially toxic for environment and human beings [6,7]. Studying the distribution of metals in sediments adjacent to settlement and industrial areas can provide information to researchers with evidence of the anthropogenic impact on ecosystems and, therefore, aid in assessing the risks associated with discharged human waste. The aim of this study was to determine concentrations of heavy metals in the marine creek system which are considered to be toxic to the aquatic environment. Heavy metals considered in this study were Cr, Zn Cu, Mn, Co. A few so called "toxic" elements such as As, Pb, Sr and Br were also studied. Three main aspects of present study are: (1) Spatial distribution of the elements in the sediment samples (2) calculations of various indices to investigate contamination levels and anthropogenic contribution of elements.

Materials and Methods

Sediment samples were collected at four locations from the Thane creek as shown in Fig. 1 represented as S1, S2, S3 and S4. One gram of freeze dried and fine sieved (<63 m) sediment core sample was homogeneously mixed with 1g cellulose powder



Fig. 1 Sampling locations at thane creek

(Sigma Aldrich). Then homogenized mixture was converted in pellets under a hydraulic pressure of 25 tones for three minutes. All measurements were carried out under vacuum, using a Xenemetrix EX-6600 EDXRF spectrometer. This consists of an X-ray tube with a Rh anode as the source of X-rays with a HVPS 60kV, 6.6 mA power supply, a LN_2 cooled Si(Li) detector with a resolution of 131 eV at, Mn K (5.9 keV) X-ray and a 8-sample turret that enables mounting and analyzing 8 samples at a time.

Standard reference materials (SRMs) IAEA-405 (trace element and methylmercury in estuarine sediment) and IAEA-433 (marine sediment) were used for calibration. Elements of interest analyzed in both SRMs showed good agreement with certified reference values. To check the anthropogenic input various indices (enrichment factor, contamination factor, index of geoaccumulation and pollution load index) were calculated and compared. Standard equations to calculate those indices were taken from the literature.

Table-1: Combinations of the parameters and X-ray filters used in the EDXRF setup to find the different elements

Elements	Voltage (kV)	Current A	Secondary target	Preset time (s)	Range (keV)
V, Cr, Mn, Co, Ni, Cu, Zn	40	4000	Ge	300	0-40
As, Br, Sr, Pb	50	4800	Zr	500	0-40

Results and Discussion

Organic carbon (%) and pH of sediment core samples were measured for all four sampling sites. The organic carbon was analysed by a high temperature catalytic combustion based TOC analyser. Mean values obtained for organic carbon content in sediment core sediments sample were found to be 2.1±0.4% by weight. Organic carbon contents in sediment core samples were not significantly found to change with vertical depth and with location. For pH evaluation 5g of dried and grinded sediment core samples were dissolved in 25 ml $CaCl_2$ dilute solution and left in ultrasonic bath for 2 to 3 minute. pH values of the samples were measured using a digital pH meter (Eutech Instruments CyberScan PC510). The pH values ranged from 7.2 to 8.2 in tested sediment core samples.

The concentration of Zn, V, Cr, Mn, Co, Ni and Cu were found to be 109.4±8.4, 234±13.6, 200.4±10.5, 662.3±47.1, 23.02±5.6, 59.6±2.1, and 46.3±2.3 mg/kg respectively in the surface sediment samples. Concentration of As, Pb, Sr and Br in samples were found to be 14.1±1.3, 46.4±4.4, 118.3±10.2 and 72±8.1 mg/kg respectively. Fe concentration was additionally measured for all locations to calculate enrichment factor according to (8) and found to be 65±3.4 mg/g.

The values of enrichment factor are represented in figure 2 for S1, S2, S3 and S4 locations. Zn, V, Cr, Co, Ni, Cu, and Pb showed moderate EF values (2 EF 5) indicating its contamination in sediments. Arsenic was found to be significantly enriched (EF 5) in all sediment core samples under investigation, S1 location was found slightly more contaminated by As than other locations (S2, S3 and S4). Vanadium showed slightly increasing trend from S1 to S4 locations. Arsenic showed considerable contamination levels at S1 and S3 location while at S2 and S4 with moderate contamination levels. The Igeo values of Pb, Cu, Cr, V, and Zn fall in the range 0-1 (class '2'), indicating unpolluted to moderately polluted levels in sediment core samples. Igeo values of As in sediment core samples were found in class '3' reveals moderately polluted levels. Co had Igeo <0 at S1 S2 and S3 location while it was found at S4 with unpolluted to moderately

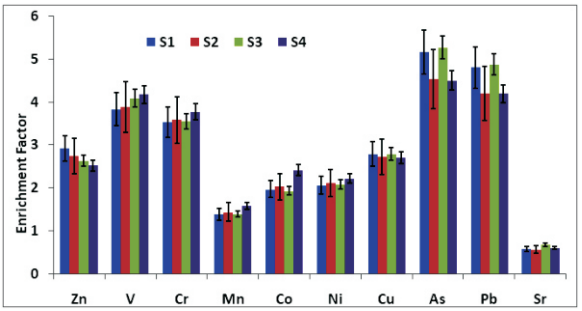


Fig. 2 Enrichment factor values for elements in sediment samples collected from four different locations of Trans Thane creek

polluted level. Values of Pollution Load Index (PLI) were 1.19, 1.18, 1.17 and 1.22 respectively for the sampling locations S1, S2, S3 and S4. The pollution load index did not show much fluctuation with location wise. The values of PLI were greater than 1 showing that there is also significant anthropogenic contribution to the sediment core.

Conclusions

Present study shows that the spatial concentration of elements in sediments is not varying remarkably. This indicates that there is continuous and same source of the elements. Thane creek is an active and commercial harbor surrounded by several industries like Oil refinery plant, Fertilizer, Fossil plant. Pollution Load Index (PLI) Values indicates order of anthropogenic contributions for measured sites is S4>S1>S2>S3. Arsenic shows considerable contamination levels at S1 and S3 location while at S2 and S4 with moderate contamination levels.

References

[1] Feng, H., Han, X., Zhang, W., Yu, L., Marine Pollution Bulletin. 49 (2004) 910.

[2] Santos, I. R., Silva-Filho, E.V., Schaefer, C.E., Albuquerque-Filho, M.R., Campos, L.S., Marine Pollution Bulletin. 50 (2005) 85.

[3] Szefer, P., Glassby, G.P., Pempkowiak, J., Kaliszan, R., Chem. Geol.120 (1995) 111.

[4] Casas, J.M., Rosas, H., Solé, M., Lao, C., Environmental Geology. 44 (2003) 325.

[5] Singh, K.P., Mohan, D., Singh, V.K., Malik, A., J. Hydrolog. 312 (2005) 14.

[6] Ip, C.C.M., Xi, X.D., Zhang, G., Wai, O.W.H., Li, Y.S., Environ. Pollut. 147 (2) (2007) 311.

[7] MuZoz, P., Lange, C.B., Gutierrez, D., Hebbeln, D., Salamanca, M.A., Dezileau, L., Reyss, J.L., Benninger. L.K., 2004. Deep-Sea Res. (2004) 2523.

[8] Bhangare R.C., Ajmal P.Y., Sahu S.K., Pandit G.G., Puranik V.D. Int. J. Coal Geol. 86 (2011) 349.

Evaluation of Radiation Dose due to the Use of Fly Ash from Thermal Power Plants as Building Material

R.C. Bhangare, S.K. Sahu, P.Y. Ajmal, M.Tiwari, G.G. Pandit

Environmental Monitoring & Assessment Section, Health Safety & Environment Group, Bhabha Atomic Research Centre, Trombay, Mumbai 400085, India; E-mail: sksahu@barc.gov.in

The fly ash from coal fired thermal power plants has cementitious properties. Use of the same in construction is growing recently. It also is well known that the fly ash contains elevated levels of naturally occurring radionuclides. The use of fly ash in building material thus exposes the occupants to radiation doses from these radionuclides. An attempt was made to evaluate the radiation doses arising from a dwelling built using fly ash as one of the components of the concrete at different proportions. The radioactivity concentrations were determined gamma spectrometrically. The doses were calculated assuming different scenarios of construction.

Introduction

The use of materials containing naturally occurring radionuclides for house construction may enhance the natural radiation background to which some population groups are exposed. Living in a house built with materials containing naturally occurring radionuclides in excess, could be one of the practices of radiological concern. The monitoring of radiation doses arising due to use of such materials is thus very important. Provided that the concentration activities of the radionuclides in these materials are known, the absorbed dose and inhalation dose in air inside a room can be calculated using a mathematical formulation. External exposure results from gamma emitter radionuclides existing in the walls, floor and ceiling while internal exposure is mainly from the emanated radon from all these faces of the room. Mathematical models can be used to predict external and internal dose rates inside a room, provided the compartment geometry and the radionuclide concentration activities are known [1].

This paper presents a methodology and theoretical evaluation of indoor external gamma and internal radon doses in the air of a hypothetical room. Doses were evaluated taking into account different variations in the construction material and type of the dwelling. Calculations were performed for observed radioactivities of ^{40}K, ^{226}Ra and ^{232}Th in fly ash samples from different power plants.

Materials and Methods

Fly ash samples were collected from 6 different thermal power plants (about 15 Nos. from each) across India. The samples were dried for 24h in an air-circulation oven at 110°C, powdered, homogenized and about 100g of each sample was filled in plastic containers and sealed to make them airtight for 1 month to ascertain establishment of secular equilibrium between ^{226}Ra and ^{228}Th with their daughters and to prevent radon loss. After attainment of secular equilibrium the samples were subjected to gamma-ray spectrometric analysis.

Gamma Spectrometric Analysis

The gamma-spectrometry system having an n-type coaxial HPGe detector (DSG, Germany) shielded with 7.5cm thick lead having 50% relative efficiency and a resolution of 2.1keV at 1.33MeV gamma energy of ^{60}Co was used. The gamma spectra acquired for 60,000s were analyzed using an 8K PC based multichannel analyzer (PHAST, Electronics Division, BARC).

Internal and External doses

To assess the radiological hazard of fly ash and bottom ash used as building materials, the radium equivalent activity (Ra_{eq}) is used. Ra_{eq} can be calculated as

$$Ra_{eq} = A_{Ra} + 1.43A_{Th} + 0.077A_K \quad (1)$$

Where A_{Ra}, A_{Th} and A_K are the activity concentrations of ^{226}Ra, ^{232}Th and ^{40}K in Bq kg^{-1} respectively. Ra_{eq} is related to the external -dose and internal dose due to radon and its daughters. The maximum value of Ra_{eq} in building materials must be less than 370 Bq kg^{-1} for safe use as recommended by UNSCEAR [2].

The dwelling was geometrically defined as a single room consisting of a set of three pairs of rectangular slabs of finite thickness. The dimensions of the hypothetical room were 4m x 5m x 2.8m. Doors and windows were not considered in the present study. The specific dose rates in nGy h^{-1} per Bq kg^{-1} for the radionuclides ^{226}Ra, ^{232}Th and ^{40}K were taken from [1] as 0.7, 0.92 and 0.072 respectively. The external dose can be estimated using a simple linear function given by

$$D = Q_i C_i \quad (2)$$

where D is the absorbed dose rate in air (Gy s^{-1}), Q_i is the dose conversion factor for the radionuclide precursor of the decay series i (Gy s^{-1} per Bq kg^{-1}), and C_i is the activity concentration of the radionuclide precursor of the decay series i (Bq kg^{-1}). The external dose is thus given by

External Dose = dose rate x exposure time (3)

The internal dose is received due to radon emanation in the air from the building material. In order to calculate the radon production rate of a concrete sample, the radium specific activity of all concrete constituents must be known. The Radon exhalation rate is given by [3] as

$$Jf = Q \quad f l_o \tan h (d/l_o) (Bq\ m^{-2}\ S^{-1}) \qquad (4)$$

Where, Q is the concrete specific activity (Bq kg^{-1}), Jf is the radon exhalation rate (Bq m^{-2} S^{-1}), is the decay constant of radon, is the density of concrete, f is the radon emanating fraction, l_o is the diffusion length in concrete, d is the half thickness of the building element. Indoor radon concentration and associated alpha exposures are thus given by

$$Css = J_f A/ \quad V \quad (Bq\ m^{-3}) \qquad (5)$$

Where, A=area of concrete surface, V=volume of room, =Air exchange rate and thus dose is given as

$$\text{Internal Dose} = Css \times IR \times DCF \times IOF \qquad (6)$$

Where, IR=Inhalation rate, DCF=Dose conversion factor, IOF=Indoor occupancy factor.

Results and Discussion

The gamma spectrommetrically determined activity concentrations of the fly ashes from different thermal power plants alongwith their calculated radium equivalent activities (Ra_{eq}) are shown in Table 1. The fly ash from plant 2 showed highest activity concentration of all the radionuclides, while the fly ash from plant 1 showed the minimum. It is noteworthy that the Ra_{eq} values for none of the samples exceeded the prescribed limit of 370Bq/kg.

Table 1: Activity Concentrations of the radionuclides in fly ash

Fly ash	226Ra (Bq/kg)	232Th (Bq/kg)	40K (Bq/kg)	Averag e Raeq (Bq/kg)
Plant 1	48.3-71.1	34.3-54.2	38.4-60.1	121.7
Plant 2	83.1-115.2	94.3-142.6	172.3-223.6	299.9
Plant 3	62.3-93.4	33.6-51.4	36.3-56.7	139.8
Plant 4	73.2-107.5	29.7-44.3	72.1-96.3	148.9
Plant 5	50.7-72.6	72.4-101.5	61.4-82.4	189.7
Plant 6	71.5-96.3	98.4-138.7	105.4-156.7	261.8

The internal and external doses in room were calculated considering two scenarios i.e. office and home. The exposure time in office was taken as 8 hours a day and 5 days a week, whereas for home the exposure time was considered to be whole year with occupancy factor of 0.8. The yearly internal dose due to use of 100% fly ash (extreme condition) as the construction material in the room is shown in Fig. 1. The internal dose at office varied from 0.028 to 0.049mSv/year while at home it varied between 0.099 to 0.17mSv/year for different fly ashes.

The yearly external doses due to use of 100% fly ash from different plants are shown in Fig.2.

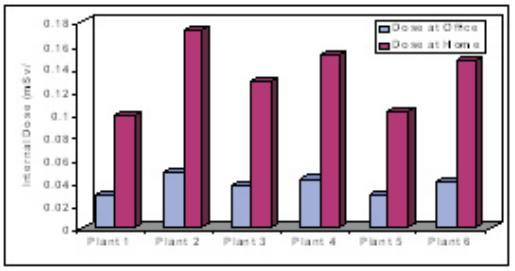


Fig. 1 Yearly internal dose to the occupants due to use of fly ash as construction material

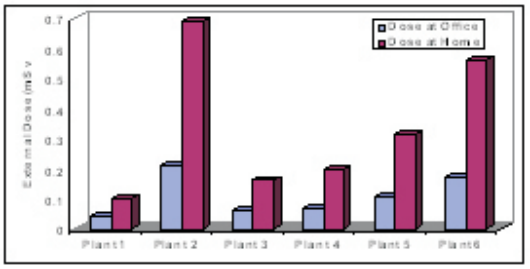


Fig. 2 Yearly external dose to the occupants due to use of fly ash as construction material

The external doses ranged between 0.046 to 0.21 mSv/year at office and 0.1 to 0.69 mSv/year at home. The cumulative dose (i.e. internal + external) from the use of 100% fly ash as the building material ranged from 0.074 to 0.26mSv/year at office and 0.2 to 0.86mSv/year at the home. None of the doses exceeded the value of 1mSv/year.

Table 2 shows the average (average of all 5 plants) doses due to varying amounts of fly ash as building material.

Table 2: Dose with varying %age of fly ash

Assumed %age of fly ash*	Internal Dose (mSv/year)		External Dose (mSv/year)	
	Office	Home	Office	Home
25% Fly ash	0.027	0.095	0.028	0.039
50% Fly ash	0.031	0.108	0.057	0.138
75% Fly ash	0.034	0.121	0.085	0.238
100% Fly ash	0.038	0.134	0.114	0.338

*Remaining %age is the cement

It was assumed that the building materials were different combinations of fly ash and cement. It can be observed that the dose increases with increase in percentage of fly ash.

References

[1] M. F. MaÂduar, G.Hiromoto. Rad. Prot. Dosimetry (2004) Vol. 111, No. 2, pp. 221-228

[2] UNSCEAR (1988), Sources, effects and risk of ionizing radiation. United Nations, New York

[3] American Concrete Institute. ACI Manual of concrete practice, code section ACI 211.1e91. Detroit, Mich: American Concrete Institute; 2009

Microanalysis Study on Ancient Lanna-style Decorative Glass Based on XRF Spectroscopy

P. Dararutana[1], K. Won-in[2], S. Tancharakorn[3]

1. *The Royal Thai Army Chemical School at the Royal Thai Army Chemical Department, Bangkok 10900 Thailand*
2. *Faculty of Science, Kasetsart University, Bangkok 10900 Thailand*
3. *Synchrotron Light Research Institute, Nakhon Ratchasima 30000 Thailand; E-mail: pisutti@hotmail.com*

Differences of archaeological objects found in Thailand, especially glass. Due to the complex nature of materials, extremely sensitive, spatially resolved, multi-elemental and versatile analytical instruments were needed. The techniques employed should be as a noninvasive as possible and able to give complementary information from macroscopic to nanometer scales. In this work, X-ray based spectroscopy including -XRF, EDXRF and PIXE were used to analyze chemical composition of the Lanna-style glass. Chemical distribution and microstructure were also studied. It can be concluded that these techniques in combination are powerful for the investigation of heterogeneous glassy materials and to answer the archaeology's questions.

Introduction

Due to the complex nature of materials and objects of cultural heritage, analytical instruments employed should be very sensitive, spatially resolved, multi-elemental and versatile. Moreover, they should be as noninvasive as possible and capable of giving complementary information at different scales ranging from macroscopic to nanometer levels. Quantitative analysis of major, minor and trace elements of archaeological materials is crucial to answer questions associated with manufacturing technology, raw materials, origin, restoration and protective conservation. X-ray based techniques have been used to analyze the archaeological glass including XRF, XRD, PIXE, XPS and XAS [1-8].

Lanna-style decorative glass which called ACG/ABG is one of decorative glasses which are found throughout Thailand in special places, such as, Buddhist temples, which, for centuries, have served as community centers for the locals [9-11]. It is found mostly in the northern and northeastern Thailand, as shown in Fig. 1, and some parts of Laos, Burma and China [12-14]. As the glasses have kept deteriorating over time, restorations must be performed routinely to preserve these cultural crafts for later generations to appreciate.

Experimental

ACG/ABG samples which collected from the fragments that broken with deterioration over time and fall down to ground from the Buddhist temples at Wat Phra Singh Woramahaviharn, Chiang Mai (northern Thailand), were characterized with the aim of obtaining information that would lead to identification of the samples by mean of -XRF, PIXE and SEM-EDS.

-XRF, PIXE and EDS were used to analyze the chemical composition, while -XRF and SEM were also used to study the elemental distribution and microstructure, respectively.



Fig. 1 Lanna-style decorative glass

Results and Discussion

Compositional analysis showed that the main contents were SiO_2 and PbO. K_2O and CaO were as minor contents. The differences in color were affected from the addition of iron, copper and manganese.

Cross-sectional SEM observations of ACG/ABG showed three different layers including metal substrate, binder and coated glass. The glasses were mostly transparency with plenty and bubbles.

Conclusion

Lanna-style decorative glass fragments were successfully analyzed by -XRF, PIXE and SEM-EDS, to characterize the materials used and obtained the information of their manufacturing technology. It is mostly lead-silica based glasses. Their colors resulted from metal ions. It can be suggested that the considerable content of the fluxing Pb, as well as the presence of Fe and Cu, can be mostly observed in the samples.

Non-destructive techniques based on X-ray fluorescence spectroscopy proved to be very useful. It

was the first time in Thailand that these were used to analyze the ancient decorative glasses, especially -XRF. They offer opportunities for novel applications and prospects for new directions in archaeological science research in Thailand.

Acknowledgements

The research was partly funded by the Faculty of Science at Kasetsart University. The Plasma and Beam Physics Facility at the Faculty of Science of Chiang Mai University, Maejo University and Thailand Synchrotron Light Research Institute (Public Organization) were thanked for providing PIXE, SEM/EDS and -XRF, respectively. The Glass and Glass Products Research and Development Laboratory of Chiang Mai University provided property measurements and team expertise.

References

[1] I. Nakai, M. Mutsunaga, M. Adachi, J. Phys. France. 2 (1997) 1033.

[2] S. Quartieri, et al., Eur. J. Mineral. 14 (2002) 749.

[3] S. Padovani, et al., Applied Physics A. 79 (2004) 223.

[4] P. Arletti, et al., Applied Physics A. 83 (2006) 239.

[5] D. Barilaro, et al., Vibrational Spectroscopy. 42 (2006) 381.

[6] W. klysubun, et al., Analytical and Bioanalytical Chemistry. 399 (2011) 3033.

[7] K. Won-in, et al., Spectrochimica Acta A. 83 (2011) 231.

[8] K. Won-in, et al., Journal of Radioanalytical and Nuclear Chemistry, 294 (2012) 247.

[9] K. Chotichutrakul, Thai Art and Culture Vol.6: Ratanakosin Art: Glass Mosaic (Fine Arts Department, Thailand 1982).

[10] N. Punjabhan and S. Na Nakhonphanom, The Art of Thai Wood Carving: Sukhothai, Ayutthaya, Ratanakosin (Rerngrom Publishing Co., Ltd., Thailand 1992).

[11] N. Punjabhan, et al., The Charm of Lanna Wood Carving (Rerngrom Publishing Co.,Ltd., Thailand 1994).

[12] P. Dararutana, Journal of Electron Microscopy Society of Thailand. 12 (1998) 38.

[13] P. Dararutana, N. Sirikulrat, T. Tunkasiri, in Abstracts Book of the 16th International Conference on X-ray Optics and Microanalysis (Vienna), 2001.

[14] P. Dararutana, N. Sirikulrat, in Microscopy Book Series No. 3 Vol. 2: Modern Research and Education Topics in Microscopy, (Formatex, Spain 2007).

Compton Scattering Study of Gd Sesquioxide

Jagrati Sahariya[1], A.M. Ghaleb[2], F.M. Mohammad[3] and B.L. Ahuja[4]

1. *Department of Physics, Manipal University, Jaipur-303007, Rajasthan, India; E-mail: jagrati.sahariya@gmail.com*
2. *Department of Physics, College of Science, University of Kirkuk, Kirkuk, Iraq*
3. *Department of Physics, College of Science, University of Tikreet, Tikreet, Iraq*
4. *Department of Physics, M L Sukhadia University, Udaipur-313001, Rajasthan, India*

We present the experimental and theoretical Compton profiles of Gd_2O_3. The measurement has been made at an intermediate resolution of 0.34 a.u. using an indigenous 20 Ci ^{137}Cs Compton spectrometer. The measured profile is compared with the theoretical Compton profiles deduced from the linear combination of atomic orbitals (LCAO) method with density functional theory (DFT). In addition, we also report the energy bands and density of states in Gd_2O_3 using LCAO-DFT method. It is seen that generalized gradient approximation within DFT gives a better agreement with the experimental profile than other schemes of DFT.

Introduction

Rare earth sesquioxides (Ln_2O_3, Ln = rare earth metal) are generally wide band gap semiconductors. Gadolinium sesquioxide (Gd_2O_3), a middle rare earth sesquioxide, has been extensively used in ceramic capacitors, color TV tubes, high temperature glazes, coloring glasses, carbon-arc-light electrodes, vacuum deposition and also in microwave industry [1,2].

The Compton scattering (CS), an inelastic scattering, is a well known tool to probe the electronic properties of variety of materials [3]. In the CS, one measures the double differential scattering cross-section which is also proportional to the Compton profile (CP) $J(p_z)$. Mathematically,

$$\frac{d^2}{d\ dE_2} \quad J\ p_z \qquad (1)$$

Here E_2 is the energy of scattered photons and p_z is the z-component of the linear momentum of an electron. Conventionally, z axis is taken along the scattering vector. Further, the $J(p_z)$ which is projection of the electron momentum density (p) along the scattering vector (z-axis) is given by,

$$J\ p_z \qquad p\ dp_x\ dp_y \qquad (2)$$

Experiment and Theory

We have measured the CP of Gd_2O_3 using 740 GBq (20 Ci) ^{137}Cs Compton spectrometer [4]. To extract the true CP, the raw data were corrected for several systematic corrections like background, instrumental resolution (limited to stripping off the low energy tail), detector efficiency, Compton cross-section, absorption correction, multiple scattering, etc. [3]. Finally, the experimental profile was normalized to the free atom area (momentum range 0-7 a.u.) viz. 60.30 e^- [5]. To compare our experimental Compton data, we have computed CPs, energy bands and density of states (DOS) of Gd_2O_3 using linear combination of atomic orbitals (LCAO) using CRYSTAL09 code [6]. We have employed local density approximation (LDA), generalized gradient approximation (GGA) and second order generalized gradient approximation (SOGGA). We have considered the quasi relativistic pseudopotential (PP) basis sets for Gd taken from http://www,theochem.uni-stuttgrat.de and all electron basis sets for O. Following the default tolerances in the CRYSTAL09 code, the SCF calculations have been performed for 120 k points in the irreducible BZ. For the valence electrons, the momentum density function was calculated from the sum of squared modulii of the occupied momentum space pseudo-wave functions.

Results and Discussion

Energy bands obtained from PP-DFT-GGA for Gd_2O_3 along the high symmetry directions are shown in Fig. 1(a). The energy bands depict large band gap semiconducting nature of Gd_2O_3. From our PP-DFT-GGA based computation the band gap is found to be 3.85 eV, while for PP-DFT-SOGGA(LDA) it is 3.90(4.00) eV. The band gap computed from our LCAO calculations is close to that deduced from the DFT calculations (3.60 eV) [1]. Total and partial DOS of Gd_2O_3 are presented in Fig. 1(b). The energy bands of Gd_2O_3 can be divided into two groups. Bands below the Fermi level (E_F) are denser than those in conduction region and are mainly due to O atoms with a small contribution from Gd. The bands above the E_F are dominated by the Gd (5d and 6s states, not shown here). Further, except fine structures and eigen values, overall shapes of energy bands computed using PP-DFT-LDA/SOGGA are similar to those deduced from PP-DFT-GGA. Therefore, we have not shown the bands and DOS from PP-DFT-LDA/SOGGA scheme.

The differences between the experimental and convoluted theoretical CPs are presented in Fig. 2. Before taking the differences, all the theoretical profiles were convoluted on the experimental resolution (0.34 a.u.) and then were normalized to the free atom Compton profile area [5]. Fig. 2 depicts that in the low momentum region (p_z<0.8 a.u.), PP-DFT-GGA based

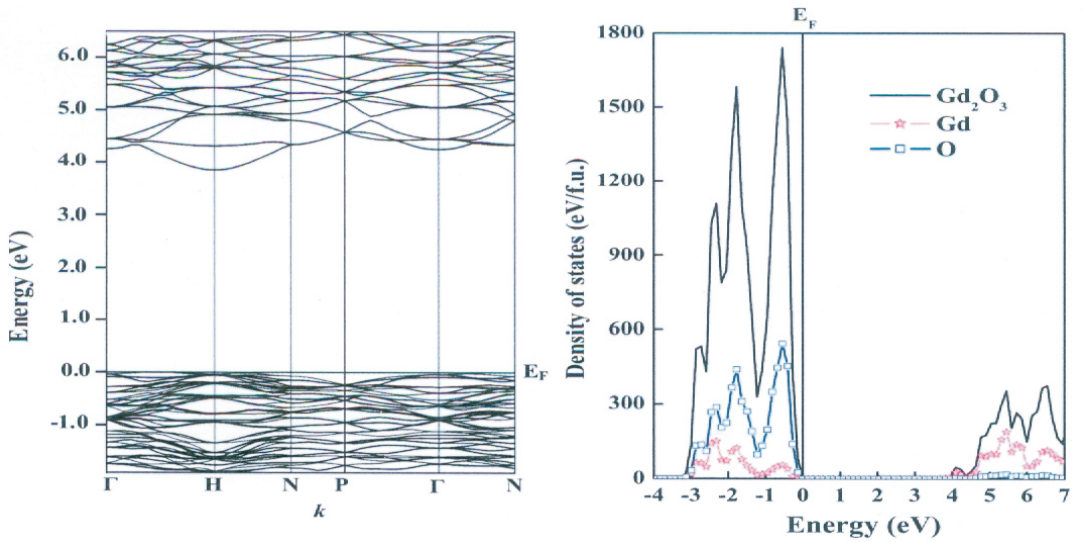


Fig. 1 (a) Energy bands of cubic Gd_2O_3 along the high symmetry directions and (b) total and partial density of states using PP-DFT-GGA scheme

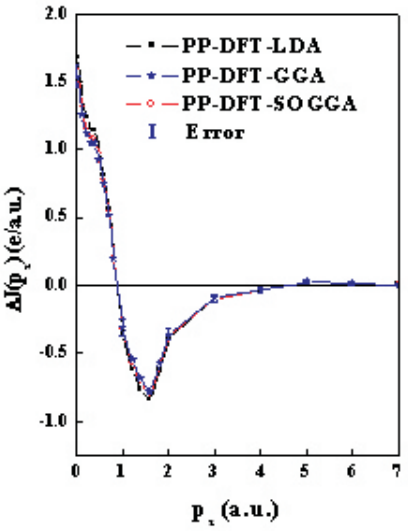


Fig. 2 Difference between convoluted theoretical and experimental Compton profiles. Experimental errors (±) are within the size of the symbols used

CP shows relatively better agreement with the experimental profile as compared to other DFT approximations.

We have also confirmed it on the basis of ^{2} fitting (which determines how well a particular model fits the observed data).

The difference between the experimental and theoretical CPs at low momentum values may be due to the poor quality of the basis sets for Gd. In the present LCAO based computations, Lam-Platzman correction [3] and relativistic effects are ignored which may lead to an overestimation of CP in low momentum region. Since the shape of CP in high momentum (p_z 4 a.u.) is governed by core contribution, the differences between experimental and theoretical profiles are negligible in this region.

Acknowledgement

We are thankful to DAE-BRNS, Mumbai for providing the financial support in form of a research project (grant No. 2012/37P/43/BRNS).

References

[1] F. X. Zhang, M. Lang, J. W. Wang, U. Becker, R. C. Ewing, Phys. Rev. B 78 (2008) 064114.

[2] A. M. Pires, M. R. Davolos, C. O. Paiva-Santos, E. B. Stucchi, J. Flor, J. Solid State Chem. 171 (2003) 420.

[3] M. J. Cooper, P. E. Mijnarends, N. Shiotani, N. Sakai, A. Bansil, X-ray Compton Scattering, Oxford Univ. Press, Oxford (2004).

[4] B. L. Ahuja, M. Sharma, S. Mathur, Nucl. Instrum. Meth. B 244 (2006) 419.

[5] F. Biggs, L. B. Mandelsohn, J. B. Mann., Atomic Data Nucl. Data Tables 16 (1975) 201.

[6] R. Dovesi, R. Orlando, B. Civalleri, C. Roetti, V. R. Saunders, C. M. Zicovich-Wilson, Z. Kristallogr. 220 (2005) 571.

Effect of EXAFS on Total Mass Attenuation Coefficients of some Rare Earth Elements

N.V. SitaMahalakshmi1, M. Ratnaraju, A. Durgaprasad Rao, P.V.Lakshminarayana and K.Preacmhand

Department of Nuclear Physics, Andhra University, Visakhapatnam 530 003, India; E-mail: sitaphd@gmail.cm

The total mass attenuation coefficients for rare earth compounds La_2O_3, Nd_2O_3, Sm_2O_3, Gd_2O_3 and Dy_2O_3 were measured at different energies between 30 and 53 keV using a modified narrow beam geometry employing selective excitation method. La_2O_3, Nd_2O_3, Sm_2O_3, Gd_2O_3 and Dy_2O_3 were choosen as secondary exciters. The secondary exciters were excited by 59.5 keV -ray from 100 mCi ^{241}Am radioactive source and the K X-ray lines emitted by the secondary exciters were counted by a Hyper pure Germanium detector. The present experimental results were compared with the theoretical values estimated using XCOM. It was observed that mixture rule method is not valid for the determination of the mass attenuation coefficients of compounds, especially at pre and post edge regions of K absorption edge.

Introduction

Accurate measurement of total mass attenuation coefficients are of great importance for basic studies of atomic, nuclear, molecular, radiation and medical physics. The accurate knowledge of attenuation coefficients is also useful for radiation shielding calculations. The impact of computerized tomography (CT) in diagnostic medicine is another interesting area that demands accurate knowledge of attenuation coefficients in biological matrices so that the differentiation of tissues in the reconstruction of images by the axial homographic technique can be improved.

A through survey of the literature [1,2] showed that the total mass attenuation coefficients are determined in the rare earth compounds only at certain limited energies. In the present work by employing selective excitation method the total mass attenuation coefficients of rare earth compounds were measured at several energies where no earlier experimental data is available.

Experimental Details

The experimental setup used in the present investigations is based on the narrow – beam geometry reported Premachand et.al [3]. The slit after exciter has a central hole of 3 mm diameter. The slit before the absorber has a central hole of 6 mm diameter and the slit before the detector has a central hole of 8 mm diameter. The geometry is so designed such that the exciter was inclined at an angle of 45 degrees to the source. The experimental arrangement consists of an HPGe detector (Canberra model GX 1018), whose FWHM is 700 eV at 22keV energy. The signal from detector was amplified and processed in a PC-based multichannel pulse height analyzer.

After ascertaining the suitability of the experimental setup, the K X- ray spectra of different compounds selected in the present work were recorded at different energies. These spectra were recorded for sufficient long time such that 10^4 to 10^5 counts were recorded under the photo peak to obtain good statistical accuracy with and without absorbers.

The X-ray mass attenuation coefficient, / , for any material are usually estimated from Bragg's additive law or more commonly called mixture rule. Thus / for any chemical compound or material is given by

$$— \quad {}_i w_i \; — \qquad (1)$$
$$\quad i$$

Where w_i is the proportion by weight, (/)$_i$ (cm^2/g) is the mass attenuation coefficient of the constituent element i of the compound or mixture.

The overall error in the measured mass attenuation coefficients is less than3%. The measured total mass attenuation coefficients along with theoretical values estimated from XCOM are tabulated in tables 1-5 for the oxides of Lanthanum, Neodymium, Samarium, Gadolinium and Dysprosium respectively.(The remaining tables will be present in the full paper) Deviations observed in all elements very near to K absorption edge. The total mass attenuation coefficients at nine energies for, La_2O_3, six energies for Nd_2O_3, five energies for Sm_2O_3,four energies for $Gd_2O_3$and five energies for Dy_2O_3. The percentage difference (PD) between experimental and theoretical values were given in the last column of each table they were calculated using the below equation (2) and fifth column represents difference, (Ex–Ek) between the incident photon energy Ex, and K shell binding energy Ek of the elemnet.

$$PD = \frac{— \quad — }{— \quad} \; 100\% \qquad (2)$$
$$\quad \text{theory}$$

Results and Discussions

The total mass attenuation coefficients thus obtained for each compound at different energies are

compared with their theoretical total mass attenuation coefficients of the different compounds in the present work were estimated using sum rule or mixture rule from XCOM [4].

In the present study there is a good agreement between present experimental and theoretical values, but the deviations observed in all elements at near the k absorption edges of rare earth elements. In Lanthanum Oxide there is a deviation at 39.906keV which is 998eV above the K absorption edge. In Neodymium Oxide deviation observed at 42.75keV which is 809eV below the absorption edge by -8.29%. In Samarium Oxide the experimental value is smaller than theoretical value by 0.84% at 45.714 keV.In Gadolinium Oxide there is a deviation at 48.918 keV by 4.76% which is 1.3 keV below the absorption edge. In Dysprosium Oxide deviation observed at 52.352 keV by 12.1% which is 1.47keV below the K absorption edge. All other experimental values are in agreement with the theoretical values of XCOM within the experimental error.

The deviations of the present experimental mass attenuation coefficients from theoretical values may possible be due to the invalidity of mixture rule at energies very near to the K edges. Also the deviation at energies above edge support EXAFS (Extended X-ray Absorption Fine Structure) effect and below K edge support RRS (Resonance Raman Scattering) effects.

Conclusions

In the present investigation the total mass attenuation coefficients for different rare earth compounds in the energy region 30-53 keV was estimated and the experimental values are in good agreement with theoretical values at energies away from the K edge. However, at energies near to K- edge the experimental values are deviated from theoretical values. The present results indicate that mixture rule is valid only at energies away by 1.5keV below the K edge and 2keV above the K edge. Below the K edge the deviation ranges from 4% to 12% and is more as the energy decreases. Hence on the basis of the present results we can state that the sum rule is valid only, away by 1.7 keV below the edge and is valid away by 2 keV above the K edge. The deviations at energies above K edge of the heavy element in the compound may be due to EXAFS (Extended X-ray Absorption Fine Structure) effect and below K edge may be due to RRS (Resonance Raman Scattering) effects.

Table-1: Experimental mass attenuation coefficients of Lanthanum oxide

Energy in keV	Attenuation coefficient (/) of La_2O_3 in cm^2/g	Theory XCOM (/) in cm^2/g	P.D %	E =Ex -Ek
30.85	8.36	8.38	-0.24	-8.058
35.131	5.92	5.93	-0.17	-3.777
37.179	5.23	5.11	-2.35	-1.729
39.906	23.00	22.2	-3.6	0.998
42.75	18.30	18.5	-1.08	3.842
45.622	15.49	15.7	-1.34	6.714
45.714	15.48	15.6	-0.77	6.806
48.916	12.93	13.1	-1.29	10.008
52.352	10.76	11.0	-2.18	13.444

References

[1] B.R Kerur, M.T Lagare, R. Nathuram, Rad. Phys. and Chem. 75 (2006) 7.

[2] H.A. Jahagirdar, B. Hanumaiah, S.R. Thantadarya, Rad. Phys. and Chem. 47 (1996) 801.

[3] K. Premachand, D.K.S.Reddy, V.RadhakrishnaMurty, J.Phy B. 9 (1976) 177.

[4] L Gerward, N Guilbert, K.B Jensen, Rad. Phys. and Chem. 60 (2001) 23.

Gamma-ray spectrometric analysis of Coastal sediment samples along north east coast of Tamilnadu,India.

M. SureshGandhi [1], R.Ravisankar[2], A.Chandrasekaran[3], B.Venkatakumaran[2], I.Vijayalakshmi[4] and M.T.Jose[4]

1. *Department of Geology University of Madras Guindy Campus, Chennai -600 025,Tamilnadu,India*
2. *Post Graduate and Research Department of Physics, Government Arts College, Tiruvannamalai 606603, Tamilnadu, India; E-mail: ravisankarphysics@gmail.com*
3. *Department of Physics, Global Institute of Engineering &Technology, Vellore-632509, Tamilnadu, India*
4. *Radiological Safety Division. Indira Gandhi Centre for Atomic Research, Kalpakkam 603102, Tamilnadu, India.*

The concentration of natural gamma emitting ^{238}U, ^{232}Th and ^{40}K radionuclides in beach sediments along north east coast of Tamilnadu India have been carried out using a NaI(Tl) gamma ray spectrometric technique with an aim of evaluating radiation hazards to mankind. To assess the radiological hazards of coastal sediments, the absorbed and annual effective dose equivalence are calculated. The results of this study can be used as a baseline for future research.

Introduction

Natural radioactivity is wide spread in the earth's environment and it exists in various geological formations like soils, rocks, plants, sand, water and air. Hence, humans should be aware of their natural environment with regard to the radiation health effects. Sediment is a naturally occurring material that is broken down by processes of weathering and erosion, and is subsequently transported by the action of wind, water, or ice, and/or by the force of gravity acting on the particle itself. Sediments are most often transported by water (fluvial processes), wind (Aeolian processes) and glaciers. Radiological studies have been made in sediment beach locations, mainly in India, because along its coastline there are quite a few monazite sand bearing placer deposits causing natural high background radiation areas[1]. The main objective of this study was to determine natural radionuclide activity concentrations in sediment samples and to evaluate the absorbed dose rate due to natural radioactivity associated with beach sediments.

Materials and Methods

Sample Collection

The present study area covers from Besant nagar, Chennai to Aliyakuppam of Pondicherry city covering about 165 km stretch in north east coast of Tamil Nadu. Fig. 1 shows the collected sample locations. The collected locations are named as Besant Nagar (BN), Thiruvanmiyur (TM), Payanurkuppam (PK) , Kovalam Creek (KC), Nemilikuppam (NK), Mahabalipuram (MB), Kalpakkam (KP), Periyakuppam (PV), Perumthuravu (PT), Marakanam (MK). Sediment samples were collected using Peterson grab at all the designated locations during low tide. The sediment samples were collected from a depth of 5 cm from the surface. Each sample has the weight of about 3 kg. The collected samples were air dried at room temperature in open air. The samples were placed in plastic pouches and transported to the laboratory.



Fig. 1 Sample collected locations of north east coast of Tamil nadu

Gamma ray Spectrometric Analysis

All samples were subjected to gamma spectral analysis with a counting time of 10,000 seconds. A 3" x 3" NaI (Tl) detector was employed with adequate lead shielding which reduced the background by a factor of about 95%. The concentrations of various radionuclides of interest were determined in Bq kg^{-1} using the count spectra. The gamma-ray photo peaks corresponding to 1.46 MeV (^{40}K), 1.76 MeV (^{214}Bi) and 2.614 MeV (^{208}Tl) were considered in arriving at the activity of ^{40}K, ^{238}U and ^{232}Th in the samples. The detection limit of NaI(Tl) detector system for ^{40}K, ^{238}U and ^{232}Th are 8.5, 2.21 and 2.11 Bq kg^{-1}, respectively for a counting time of 10, 000 secs.

Results and Discussions

Activity concentrations of ^{238}U, ^{232}Th and ^{40}K in the Sediments

The activity concentrations of ^{238}U, ^{232}Th and ^{40}K sediment samples are given in Table 1. All values are

given in Bq kg^{-1} of dry weight. The activities range and mean values (in brackets) for ^{238}U, ^{232}Th and ^{40}K are 2.21 – 104.6 (35.12), 24.35 – 2856.82 (713.16) and 250.9 – 560.4 (349.60) Bq kg^{-1}, respectively. The wide variations of the activity concentration values are due to their presence in the marine environment and their physical, chemical and geo-chemical properties [2]. The results show that the mean activity concentration of ^{232}Th is higher when compared with worldwide average value 30 Bq kg^{-1} [1].

Table-1: Activty concentration Absorbed dose rate(D_R), Annual effective dose rate (H_R)

Sl. No	Sample Id	Activity Concentration			D_R (nGy/h)	H_R (mSv /y)
		^{238}U	^{232}Th	^{40}K		
1	BN	33.58	259.14	260.5	197.97	0.244
2	TM	15.89	113.26	299.57	94.85	0.117
3	PK	30.24	461.57	317.03	333.72	0.410
4	KC	BDL	106.74	393.04	87.60	0.108
5	NK	104.6	2139.57	306.03	1482.78	1.824
6	MB	96.83	2856.82	560.43	1967.82	2.420
7	KP	33.29	519.41	396.28	376.89	0.464
8	PV	BDL	24.35	318.38	29.59	0.036
9	PT	17.83	494.47	393.95	353.53	0.435
10	MK	18.99	156.27	250.87	122.78	0.151
Average		35.125	713.16	349.608	504.75	0.621

BDL=2.21Bq/kg

The highest activity concentration of ^{238}U, ^{232}Th & ^{40}K was observed in Mahabalipuram. Fig. 2 shows the variation of activity concentration at different sampling locations.

Absorbed dose rate (D_R)

The absorbed gamma dose rates due to gamma radiations in air at 1m above the ground surface for the uniform distribution of the naturally occurring radionuclides (^{238}U, ^{232}Th and ^{40}K) were calculated based on guidelines provided by UNSCEAR[1]. The conversion factors used to compute absorbed gamma dose rate (D_R) in air per unit activity concentration in Bq kg^{-1} (dry weight) corresponds to 0.462 nGy/h for ^{238}U, 0.604 nGy/h for ^{232}Th and 0.042 nGy/h for ^{40}K. Therefore D_R can be calculated as follows [1]:

$$D_R\,(nGy\ h^{-1}) = 0.462A_U + 0.604\ A_{Th} + 0.0.42A_K \quad (1)$$

where A_U, A_{Th} and A_K are the activity concentrations of ^{238}U, ^{232}Th and ^{40}K in Bq kg^{-1}, respectively. The absorbed dose rate values ranged between 29.59 and 1967.82, with a mean value of 504.75 nGy h^{-1}. The estimated mean value of D_R in the studied samples is higher than the world average (populated-weighted) absorbed gamma dose rate of 84 nGy h^{-1}. This may be due to monazite deposits and heavy minerals present in the study area. Fig.3 shows the variation of absorbed gamma dose rate with different locations.

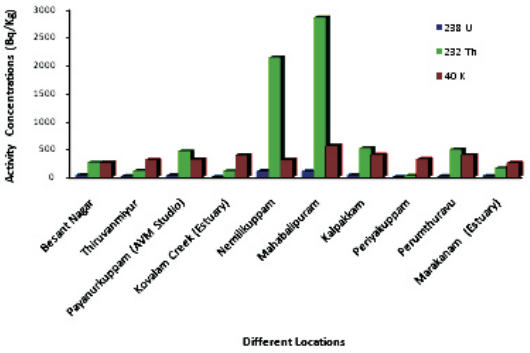


Fig. 2

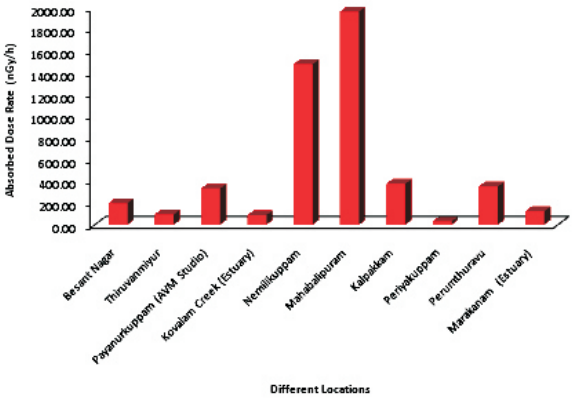


Fig. 3 Variation of absorbed gamma dose rate with different locations

Conclusion

The activity concentrations of ^{238}U, ^{232}Th and ^{40}K in sediments collected at different locations along the north east coast of Tamilnadu have been determined. The highest activity concentrations of ^{232}Th, ^{238}U and ^{40}K were observed in sediments from Mahabalipuram. The results of this study can be used as a baseline for future research and the data obtained in this study may be useful for radiological mapping of the study area.

References

[1] UNSCEAR,United Nations Scientific Committee on the effects of Atomic Radiation, United Nations, New York (2000).

[2] R.Ravisankar, K.Vanasundari, A.Chandrasekaran, A.,Rajalakshmi,M.Suganya, Vijayagopal, V. Meenakshisundaram, V.App.Radi and Iso.70 ,(2012) 699.

Determination of Zirconium and Hafnium in Zirconium Process Stream Solutions from Zirconium Extraction Plant by ED X-Ray Fluorescence Spectrometry (EDXRFS)

B.V. V. Ramana, Y. Balaji Rao and H.R. Ravindra

Control Laboratory, Nuclear Fuel Complex, ECIL Post, Hyderabad 500062; E-mail: ybr4793@gmail.com

Energy dispersive X-Ray fluorescence (EDXRFS) method is developed and standardized for the determination of Zr and Hf contents on routine basis in various process stream solutions covering a wide range of concentrations from Zirconium Extraction Plant at Nuclear Fuel Complex. From the results Zirconium Oxide (ZrO_2) and Hafnium oxide (HfO_2) were calculated for reporting purpose. The method has been applied to aqueous stream samples. Except for dilution, not much sample preparation was involved in the analysis and accordingly the experimental parameters were optimized. The results from EDXRFS method are compared with gravimetric (phallic acid precipitation) method and WDXRFS method and are found to be in good agreement. A RSD 2% has been achieved in both the cases.

Introduction

Nuclear Fuel complex is engaged in manufacturing and supply of Fuel Assemblies, core structural components and sub-assemblies on regular basis to Nuclear Power Reactors operating in India. Core Structural components include coolent tubes, fuel tubes, garter springs and other reactivity mechanism. These components are fabricated from Reactor Grade (RG) Zirconium metal (also called as RG Zirconium Sponge) following a well established melting and fabrication process at NFC. The Reactor Grade Zirconium metal is prepared from ZrO_2 which in turn is produced from washed & dry frit (WDF) powder after a series of wet chemical processes at zirconium extraction plant. WDF is obtained from Alkali fusion of Zircon sand which results into a mixture of Sodium Zirconate & Sodium Silicate and the mixture is leached with water to remove sodium silicate. Sodium Zirconate is dissolved in Nitric Acid. Crude zirconium nitrate thus obtained is subjected to Solvent Extraction with 35% TBP in Kerosene after adjustment of free acidity. Pure Zirconium Nitrate solution obtained thereafter is precipitated with NH_4OH to obtain $Zr(OH)_4$ which is dried and calcined to get pure Zirconium Oxide Powder. During these conversions, several process stream solutions of both aqueous and organic are generated. They include aqueous solutions of Raffinate, Scrub Raffinate (SR), Pure Solution (PS), Instant Raffinate and organic solutions of Extract, Extract pure, Lean Solvent. Measurement of concentration of Zirconium in these process stream solutions at different stages of processing becomes essential for effective process monitoring. Zirconium in dissolution slurry, dry powder etc. is for knowing the material input, in scrub raffinate, extract for solvent extraction efficiency, in Pure solution and lean solvent for efficiency of stripping etc. The determination of Zirconium in these process streams over a wide range of concentrations and in the presence of impurities which finds way during the dissolution of the ore and also picked up during the process stream on regular basis by a single technique assumes importance. The technique becomes desirable especially for large analytical load, when it has got advantages of simplicity, rapidity, sensitivity, adequate accuracy and precision along with cost effectiveness. Various techniques are available in the literature for the determination of Zirconium from very low to very high concentrations. They include gravimetry, Wavelength Dispersive X-ray Fluorescence Spectrometry (WDXRFS), Spectrophotometer etc. However each of these techniques is limited with inherent difficulties and hence cannot be applied to all streams without any difficulty. In view of the above present EDXRF method is developed.

Instrumentation and parameters

A hand held and portable Innov-X systems ALPHA-4000 series EDXRF Spectrometer, equipped with a Ta-anode miniature X-ray tube having a range of 10–40 kV and 10–80 A and Si PiN diode detector was employed for measurements. Fixed standard filter of 2 mm Al is used in the instrument. The system can be operated on AC or with Li-ion rechargeable battery. A high speed data acquisition circuitry and a HP iPAQ integrated pocket PC hand held computer for calculations, results and operator interface is included in the system. The pocket PC has got internal rechargeable battery and works on Windows CE operating system with proprietary Innov-X Software application. The system is pistol shape designed for difficult testing locations and has got auto compensation for irregular or small samples. It has got fundamental parameters (FP) for no standard analyses and has got stored grade libraries for rapid grade identification/stored finger print libraries for rapid material identification. The sample solutions were exposed to X-rays in a specially designed titanium liquid sample cell of 10 mL capacity with a Mylar film window of 6 micron thickness. The sample cell along with Mylar window is placed in an aluminium sample holder for measurements. K (15.67keV) line of Zr and

L (8.98 keV) line of Hf were used for the measurements.

Preparation of ZrO_2 & HfO_2 Standards

As the certified reference for Zirconium and Hafnium are not readily available, stock solutions for ZrO_2 and HfO_2 are prepared separately. Dissolve 4 gm of 99.9% pure ZrO_2 powder in 5mL of HF+HNO_3 mixture followed by addition of 10 mL H_2SO_4 & fuming. Precipitate it with NH_4OH and dissolve precipitate in 10 HNO_3 and make up to 100 ml to get 40mg/ml stock solution. Similarly HfO_2 standard is prepared by taking 99.9% pure HfO_2 powder. Stock solutions are diluted as per the requirement. A set of 26 standards are taken each containing different quantities of ZrO_2 (0.1 to 12 g/l) and HfO_2 (0.1 to 3.5 g/l).

Preparation of Sample Solutions

The concentration of ZrO_2 in different process stream solutions varies with the type of process stream. The ZrO_2 content in raffinate & instant raffinates is low while in scrub raffinate (SR), pure solutions (PS) is high. Therefore it is essential to bring the concentrations of ZrO_2 and HfO_2 in all these streams to a dynamic range by suitable dilution so that they should lie in the range of standard solutions. Samples which do not require any dilutions are taken as such for measurements.

Results and Discussions

Initially Zr and Hf contents were measured and from the results Zirconium Oxide (ZrO_2) and Hafnium oxide (HfO_2) contents were calculated for reporting purpose. Owing to the dilutions carried out on process stream solutions, it appears to involve a dilution error, especially in the case of SR/PS samples. However, the final results have revealed that the errors are not very significant. This makes EDXRF analyzer as an attractive technique apart from being non-destructive in nature. These factors are very important for an industrial laboratory where high analytical load is expected for clearing the process samples to take a decision on downstream processing. The results from EDXRFS method are compared with other methods and are found to be in good agreement. The EDXRFS measurements carried over a range of 0.1–90 g L^{-1} of ZrO_2 and 0.1- 10gL^{-1} of HfO_2. A RSD 2% has been achieved in both the cases. The Table 1 shows the values of concentration of ZrO_2 and HfO_2 measured directly by EDXRF analyzer and through calibration graph drawn manually using synthetic standards with concentration range of 0.1–12 g L-1 and 0.18 – 3.5 g L-1 respectively. When these standards were measured 10 times a standard deviation of ± 0.066 for ZrO_2 and ±0.047 for HfO_2 at 3 g/l, ±0.099 for ZrO_2 and ±0.042 for HfO_2 at 6 g/l, ±0.095 for ZrO_2 and ±0.103 for HfO_2 at 9 g/l and ±0.022 for ZrO_2 and ±0.084 for HfO_2 at 12 g/l has been achieved. Table: 2 shows the comparison of ZrO_2 + HfO_2 concentrations in a typical PS, SR and Monitor Buffer (MB) measured by different techniques and it seen there is a good agreement between the techniques. A Philips PW1404 WDXRFS analyzer was employed for the purpose. A De Jongh's model has been applied for correction to take care of non-linearity observed at higher concentrations due to self absorption. In gravimetric method suitable aliquot of the sample (~60mgZrO_2+HfO_2) is precipitated with ammonium hydroxide after fuming with H_2SO_4. The precipitate is dissolved in HNO_3 and again precipitated with phallic acid. The resultant precipitate is ignited at 900°C and weighed as ZrO_2+HfO_2.

Table-1: Comparison of concentration of ZrO_2 and HfO_2 values obtained by EDXRF analyzer and through calibration graph

ZrO_2 (g/l)			HfO_2 (g/l)		
STD	Through analyzer	Through graph	STD	Through analyzer	Through graph
0.5	0.51	0.26	0.18	0.16	0.27
1	0.97	0.85	0.2	0.19	0.29
2	1.91	2.01	0.25	0.19	0.29
2.5	2.4	2.6	0.3	0.23	0.32
3	2.78	3.04	0.35	0.25	0.34
3.5	3.27	3.6	0.5	0.46	0.50
4	3.77	4.1	0.6	0.57	0.60
4.5	4.22	4.6	0.7	0.64	0.65
5	4.71	5.1	0.8	0.74	0.73
5.5	5.32	5.7	0.9	0.91	0.87
6	5.66	6.1	1	1.02	0.96
6.5	6.15	6.6	1.25	1.3	1.2
7	6.59	7.02	1.5	1.65	1.48
7.5	6.97	7.4	1.75	1.91	1.7
8	7.44	7.8	2	2.33	1.98
8.5	7.94	8.2	2.25	2.71	2.29
9	8.54	8.7	2.5	2.99	2.51
9.5	9.15	9.2	3	3.63	3.01
10	11.1	10.6	3.25	3.97	3.28
12	13.7	12.1	3.5	4.25	3.50

Table-2: Comparison of concentration of ZrO_2 & HfO_2 values measured by different techniques

Samples	WDXRF (g/l)	EDXRF (g/l)	Gravimetric method (g/l)
	ZrO_2+HfO_2	ZrO_2+HfO_2	ZrO_2+HfO_2
PS-560	87.4±0.23	87.5±1.2	86.8±0.1
PS-227	80±0.23	78.1±1.2	79.4±0.1
SR-560	35.8±0.24	36±0.8	35.5±0.1
MB	6±0.4	6.4±0.14	6.2±0.1
SR-227	42±0.24	41.5±0.8	41.7±0.1

Acknowledgements

The authors are grateful to Shri N. Saibaba, DS and CE, NFC and Shri B. Prahlad, DCE (QA, TS, HRD & Library) for permitting to publish the paper. Also Smt P. Prameela Devi, SA/E is thanked for her help during the course of the work.

Rapid Identification of Uranium in Various Isotopic Composition by Liquid Scintillation Counting

Sonali P.D. Bhade, S. Anilkumar, P.J. Reddy, A.D. Pant, G.P. Verma, R.V. Kolekar, Rajvir Singh, K.S. Pradeepkumar.

Radiation Safety Systems Division, Bhabha Atomic Research Centre, Trombay, Mumbai 400085, India; E-mail: sonali@barc.gov.in

Because of various fuel cycle operations, it is likely to observe uranium in various isotopic compositions. It is essential to identify and assess the uranium concentration in effluents and other environmental matrices as a part of environmental monitoring and in emergency scenarios. Studies have been carried out to apply alpha Liquid Scintillation Counting (LSC) technique based on Pulse Shape Analysis (PSA), for the determination of uranium concentration and its isotopic composition. The results obtained were compared with that of alpha spectrometry and were found to be in good agreement. This technique offers a fast and reliable analysis for uranium in liquid medium.

Introduction

Since the beginning of nuclear age, there has been widespread use of uranium involving the mining of uranium ore, enrichment and nuclear fuel fabrication. Uranium is a naturally occurring, ubiquitous metal found in various chemical forms in soils, rocks, seas, and oceans [1]. Uranium may result in different isotopic forms: natural, enriched and depleted. For Natural Uranium (NU), usually there exists equilibrium between ^{238}U and ^{234}U. On the contrary, for depleted (or enriched) uranium, the secular equilibrium is disturbed because of the extraction procedures. In particular, the weight percentage of ^{234}U tends to be proportional to the percentage of ^{235}U because of similar sensitivity to the enrichment procedure [2]. During the manufacture of nuclear fuel, the concentration of ^{235}U is commonly increased from about 0.72% to about 3-4%. The residue, depleted uranium contains about 0.2% ^{235}U. Depleted Uranium (DU) is a by-product from uranium enrichment and reprocessing. Table1 illustrate the proportion (%) of uranium isotopes by weight and activity in natural and depleted uranium.

Table.1: Percentages of uranium isotopes by weight and activity in natural and depleted uranium

Isotope	Relative Isotopic Abundance (%)			
	Natural by weight	Uranium by activity	Depleted by weight	Uranium by activity
^{238}U	99.28	48.8	99.8	83.7
^{235}U	0.72	2.4	0.2	1.1
^{234}U	0.0057	48.8	0.001	15.2

Numerous methods such as mass spectrometry, neutron activation analysis, voltammetry and alpha spectroscopy are available for the determination of uranium, depending on experimental objectives and the type of analysis [3-5]. In the present work studies have been carried out to check the possibility of using Liquid scintillation counting (LSC) technique for the determination of uranium and its isotopic composition. Liquid Scintillation Counting (LSC) for alpha activity measurement is rapid yet reliable technique based on Pulse Shape Analysis (PSA).

Experimental

Quantulus 1220 LSC is equipped with Pulse Shape Analyzer (PSA) that can simultaneously discriminate and accumulate alpha and beta spectra separately. However alpha spectra collected are of poor resolution and the peaks are shifted to lower energies, at higher quench levels. Quench level has been optimized for better resolution using ^{241}Am alpha spectrum. Energy resolution of about 400 keV has been achieved for the optimized quench level. With this resolution it is very difficult to do alpha spectrometry of complex nuclides. But with the use of analytical peak fitting procedure it is possible to do alpha spectrometry for samples containing radionuclides of wide alpha energies. Analytical peak fitting of alpha spectra from LSS was carried out using InterWinner software. This software performs a simultaneous fit to all the statistically significant peaks appearing in the spectrum and de-convolutes the multiplets based on the peak shape calibration.

In order to maximize the light output from alpha decays, extractive scintillation cocktail was used that was prepared by adding di (2-ethyl-hexyl)-phosphoric acid (HDEHP-60 g/L) to Optiphase Hisafe-3 scintillation cocktail. All the measurements were carried out in High Density polyethylene (HDPE) vials to facilitate the maximum light output. Natural uranium standard sources of different activity levels and depleted uranium source were counted in Quantulus LSC at corresponding optimized PSA setting [6]. The present LSC system has two dual programmable Multi channel Analyzers (MCA). By setting the optimized PSA level, it is possible to route events in MCA and events in MCA. The alpha counting data stored in alpha MCA of LSC was then used as the input data for the de-convolution of spectral peaks using InterWinner program. The measured alpha spectra of NU sample and separated ^{238}U and ^{234}U spectral peaks are shown in Fig.1. The measured alpha spectra of DU and deconvoluted ^{238}U and ^{234}U spectral peaks are shown in Fig. 2. It is clearly seen that the peak due to ^{234}U has been separated even though the trace of ^{235}U is masked

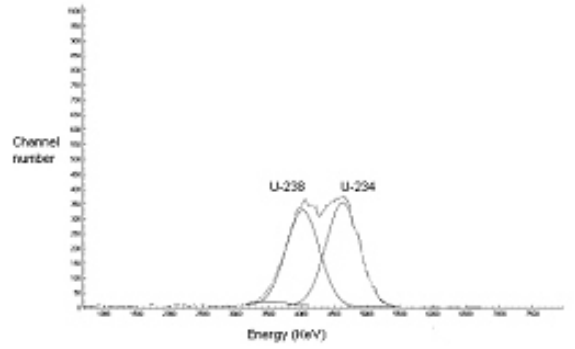


Fig. 1 LSC alpha spectrum of natural uranium

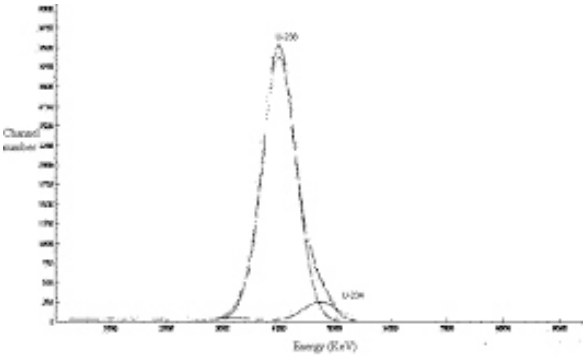


Fig. 2 LSC alpha spectrum of depleted uranium

completely. Two distinct peaks of ^{238}U and ^{234}U characterize natural uranium while a major ^{238}U peak and a minor one for ^{234}U characterize depleted uranium as illustrated in Figs. 1 and 2 respectively.

Result and Discussion

Now a days LSC is emerging as one of the most widely used techniques because of easy and fast sample preparation. However the energy resolution of alpha particles is poor with liquid scintillators. Energy resolution is proportional to the number of photons created in the decay event. Alpha particles lose their kinetic energy in short distance inside the scintillation medium, producing a small number of photons, compared to the photons produced by beta particles. Due to the excellent alpha-beta separation, Quantulus enables sensitive and precise measurements of emitting nuclides even in the presence of -emitting nuclides. Pulse shape discrimination reduces the backgrounds by rejecting beta and gamma pulses with 99.95% efficiency, with energy resolution being substantially improved over typical LSS equipment. High efficiency (nearly 100%) offered by the LSS technique is very useful in achieving improved minimum detectable activity suitable for the determination of environmental contamination with natural actinide isotopes and evaluation of their source. Optiphase Hisafe-3 scintillation cocktail show about 10% resolution at 5MeV alpha energy in HDPE vials which is not sufficient to de-convolute the composite

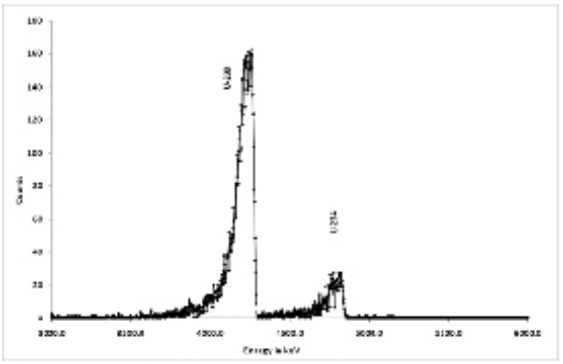


Fig. 3 Alpha spectrum of depleted uranium from PIPS detector

spectra of uranium shown in figure 1. The alpha spectrum of depleted uranium sample taken using PIPS detector based spectrometry system is shown in Fig.3.

Table-2: Results of activity measurement of depleted and natural Uranium by LSS and alpha spectrometry

Techniques used	Countiing time	Able to detect and quantify			Activity ratio $^{234}U/^{238}U$
		^{238}U	^{234}U	^{235}U	
Alpha spectro-metry	20000 s	Yes	Yes	Yes	0.13 (DU) 1.03 (NU)
LSC	12000 s	Yes	Yes	No	0.12 (DU) 1.09 (NU)

Conclusion

Alpha LSC based on PSA technique, coupled with spectral analysis fitting technique has proved to be precise and rapid technique to study the uranium contamination of liquid samples. It allows determining the isotopic ratio $^{234}U/^{238}U$ which is an indirect tool to determine the type of uranium isotopic forms. It would be interesting to apply the present technique to environmental matrices such as ground water, well water and soils.

References

[1] Greenwood, N.N., Earnshaw, A.: Chemistry of the Elements. London: Pergamon Press, (1984) pp 1542

[2] D.Binachi, P.Cortese, G. Dellacasa and I. Merlano, Nucl. Inst. Meth. Phy. Res.. A 553 (2005) 543

[3] D.W. Boomer, M.J. Powell, Anal. Chem. 59 (1987) 2810.

[4] N. Dacheux, J. Aupiais, Anal. Chem., 69 (1997) 2275

[5] C.M.G. van den Berg, M. Nimmo, Anal. Chem., 59 (1987) 924

[6] Sonali Bhade, P.J. Reddy, A. Narayanan, K.K. Narayan, D. A. R. Babu and D.N. Sharma, J. Radioanal. Nucl. Chem. 284 (2010), 367 .

Application of simulated standard spectra for the analysis of complex sample spectra from NaI(Tl) detectors

S. Anilkumar, K. Narayani, A.K. Verma, Rajvir Singh and K.S. Pradeepkumar

Radiation Safety Systems Division, Bhabha Atomic Research Centre, Trombay, Mumbai 400085, India; E-mail: anilk@barc.gov.in

Scintillation detector based Gamma ray spectrometry is one of the prominent analytical techniques used for the assay of radionuclides. High efficiency, low cost and ease of operation attracts many analysts for using scintillation detectors. But these detectors offer poor energy resolution making it difficult the analysis of complex gamma ray spectra. A number of spectrum analysis methods are available and the least squares method is regarded as the most accurate one. The main disadvantage of this method is the requirement of standard sources for all nuclides expected in the complex spectrum. For some applications it is not possible and feasible to have standard radionuclides in the geometry of the measurement. In this present work an approach of using simulated standard spectrum of the radionuclides for the least squares analysis is studied. The paper describes the methodology used for the generation of simulated spectrum and validation of results using standard sources in the NaI(Tl) based gamma ray spectrometer.

Introduction

Gamma ray spectrometry is the science dealing with the use of a gamma ray spectrometer and the subsequent analysis of the spectral data obtained from the spectrometer. High efficiency, low cost and ease of operation attracts many analysts for using scintillation detectors for the gamma ray spectrometry work. NaI(Tl) scintillation detector is commonly used for the gamma spectrometry analysis in laboratories. But these detectors are very popular for radiation surveys of large areas for the estimation of the local concentrations of uranium, thorium and potassium, or for the estimation of fall out nuclides in environmental samples [1,2].

Unlike the HPGe detectors, where photo peak analysis is employed, the analysis of gamma spectra from scintillation detector demands full spectrum analysis for unfolding the complex spectrum. The method of spectrum analysis depends on the complexity of the gamma ray spectrum, ie., the number of nuclides present in the sample. A number of analysis methods are available and the least squares method is regarded as the most accurate one. The least squares theory and its application for the analysis of complex NaI(Tl) gamma ray spectra from mixture of nuclides has been explained elsewhere [3]. In least squares procedure gamma ray spectrum (counts Vs channel) obtained from a multichannel analyser is the main input data. In the sample spectrum, the net counts recorded in any channel are a function of the activity of each nuclide in the sample. The least squares procedure requires the response function library or the Compton fraction library of all radio nuclides in the same geometry. The response function for each radionuclides expected in the sample are obtained by using standard sources of these radionuclides in the same geometry. This requirement is a major limitation to handle radionuclides for which standards are not available due to shorter half lives such as ^{41}Ar, ^{131}I etc.

Many authors have used Monte Carlo (MC) simulations to develop the response functions of NaI(Tl) detectors for a wide energy range (up to 20 MeV) [4]. In the present work, the use of simulated spectrum obtained by Monte Carlo methods for generating Compton fraction library was studied. Response functions for various nuclides can be simulated using the nuclear data and detector parameters. The results obtained using the Compton fraction library of individual radionuclides generated from simulation in the least squares analysis is compared with that of results obtained using physical standards. The details of simulation and the results obtained for a mixture of three radionuclides in the aqueous solution is discussed in this paper.

Experimental

The experimental set up involves a 3"x3" NaI(Tl) scintillation detector coupled with a 1k multichannel analyser. The geometry selected for the measurement is water in cylindrical container of 7 cm dia and 7.5 cm height. The radionuclides selected for the study are ^{133}Ba, ^{137}Cs and ^{60}Co considering its importance in the fuel cycle operations. The standard sources of ^{133}Ba, ^{137}Cs and ^{60}Co were prepared using known activity in water in the above container. Individual spectra were acquired for these sources and the response function or Compton fraction library was created. Set of five samples with known combinations of ^{133}Ba, ^{137}Cs and ^{60}Co were prepared to study the effectiveness of the analysis procedure. These samples are counted for a period of 5000 seconds and the complex spectra was analysed using least squares method based on the Compton fraction library generated experimentally.

Based on the detector parameters and the geometry of the source, individual nuclide spectra have been simulated using Monte Carlo methods. The detector and geometry model used for simulation was validated using standard source of ^{137}Cs in similar

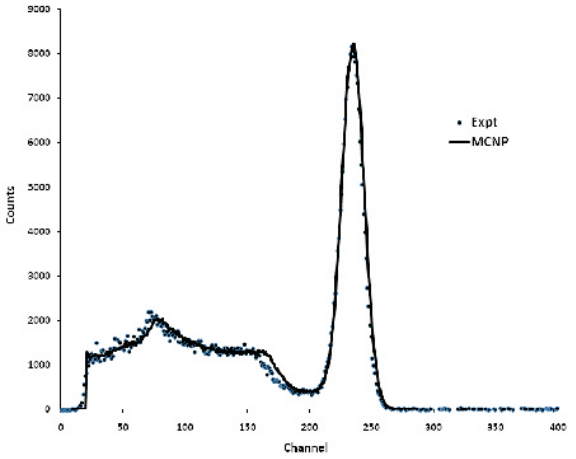


Fig. 1 Experimental and simulated spectrum of Cs-137 in geometry

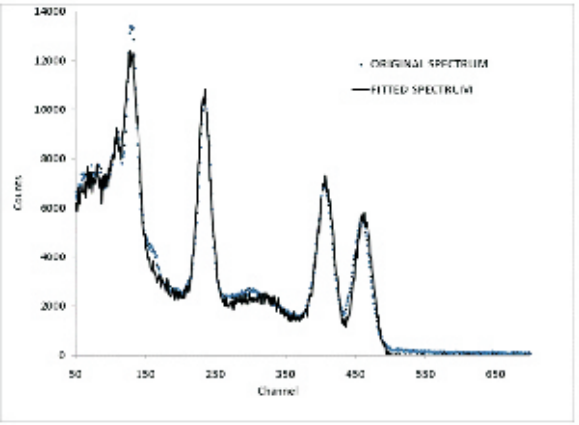


Fig. 2 Original and fitted spectrum using Least Squares program

geometry and found satisfactory. The comparison of experimental and simulated spectra of ^{137}Cs in the cylindrical container is shown in Fig.1. It was observed that the count rate obtained in peak region was in agreement with experimental spectrum within 5.5%. Similar way the spectra for ^{133}Ba and ^{60}Co in the geometry were simulated. From the simulated spectra of all the nuclides the Compton fraction library was created as per the requirement of least squares program. The experimental complex spectra obtained from a set of five samples have been analysed using the simulated Compton library and the results are compared with that of the results obtained using experimental Compton library. The results are shown in Table.1.

Table 1: Activity estimated using experimental Compton fraction and simulated Compton fraction by least squares method in mixed sources.

Sl. No	Nuclide	Original activity (Bq)	Estimated activity (Bq)	
			Using Experimental Compton Fraction	Using Simulated Compton Fraction
1	Ba-133	969.8	997.28	983.28
	Cs-137	570.97	541.46	645.83
	Co-60	1459.8	1383.69	1439.25
2	Ba-133	673.72	682.6	679.66
	Cs-137	1569.36	1538.35	1614.58
	Co-60	660.24	599.7	630.84
3	Ba-133	1352.3	1383.97	1342.62
	Cs-137	854.76	818.29	911.76
	Co-60	660.24	584.02	616.82
4	Ba-133	673.72	691.36	710.30
	Cs-137	1139.68	1118.29	1234.68
	Co-60	1162.03	1099.65	1107.47
5	Ba-133	673.72	688.7	701.94
	Cs-137	1575.6	1558.42	1639.91
	Co-60	660.24	615.07	621.5

Results and Discussion

Least squares method has been widely used for the analysis of complex gamma spectra obtained from scintillation detector based gamma spectrometer. The FORTRAN based Least Squares analysis code developed in our group has been used for the study. Monte Carlo techniques for the creation of simulated spectrum have been discussed by many authors for calculating the response of various photon energies in the detector. The accuracy of the simulation depends on many factors like detector modeling and geometry. From the present study it is seen that Monte Carlo technique can be very well be used for the creation of Compton library or the response function of radionuclides for the analysis based on least squares method. The results obtained from the analysis of mixed sources shows that the technique of using simulated spectrum in place of original spectrum for the creation of Compton fraction is working very well. The estimated activity values by both the methods are within ±10% of the original activity. The original and the fitted spectrum using the Compton fraction (simulated) by the least squares program is shown in Fig.2.

References

[1] Hendriks. P.H.G.M, Limburg. J and De Meijer. R.J, Journal of Enviromental Radioactivity 84(2001).

[2] Muminov, I.T., Muhamedov. A.K., Osmanov. B.S., Safarov. A.A. and Safarov. A.N. (2005), Journal of Enviromental Radioactivity 84(2005) 321-331.

[3] Rangarajan. C, Mishra. U.C., Gopalakrishnan. S and Sadasivan. S,(1973), BARC Report, 686.

[4] Hu-Xia Shi, Bo-Xian Chen, Ti-Zhu Li, Di Yun, Applied Radiation and Isotopes 57 (2002) 517–524

Assessment of Elemental Contamination in Road Dust using EDXRF

I.V. Saradhi, Sandeep P. and G.G. Pandit

Environmental Monitoring and Assessment Section, Bhabha Atomic Research Centre, Mumbai 400085, India; E-mail: ivs@barc.gov.in

Several studies have revealed significant contribution of vehicular emissions to air pollution problems in urban areas. To study the effect of vehicular emissions, road dust samples were collected from different locations in Mumbai and analyzed for the elemental concentrations using Energy Dispersive X-Ray Fluorescence (EDXRF) technique. Fourteen elements were analyzed (viz., Fe, Ca, Al, Mg, Ti, K, Mn, V, Cr, Zn, Cu, Ni, Co and Pb) and significant contribution from crustal related elements was observed in road dust samples. Enrichment Factor analysis showed enrichment of V, Zn, Ni, Pb and Ca. Factor analysis identified natural crust (soil), brake wear, tyre wear and industrial sources contributing to the road dust.

Introduction

Trace elements concentrate on urban surfaces e.g. roads, as dust particles. The health implications of inhalation and/or ingestion of these dust particles are significant. The aim of this study is to characterize trace and toxic elements present in the road dust samples collected at various locations in Mumbai and to identify the sources contributing to the road dust.

Materials and Methods

Road dust samples were collected in areas of very high traffic (Vikhroli, Ghatkopar (W), Phoenix Mall-Kurla, Sion, Suman Nagar), medium traffic (Shivaji Nagar, Mankhurd), express way (on Eastern Expressway) and on roads near industrial area (Tata Power, HPCL Refinery). 200 g of road dust was collected in self sealed polythene bags during January, 2013 (17 samples). Homogenous sample passed through 75 m sieve was used for making pellets of 2.5cm dia (1 g road dust and 1 g binder) using hydraulic press applying a load of 20 tons. Elemental concentrations were measured using Xenemetrix make EDXRF system having 400 W Rh anode X-Ray tube as an excitation source (measurement conditions are presented in Table 1). The detector is cryogenic cooled Lithium drifted Si with a resolution of 131 eV at Mn K . The concentrations of 14 elements viz. Fe, Ca, Al, Mg, Ti, K, Mn, V, Cr, Zn, Cu, Ni, Co and Pb were quantified using built in software. IAEA SL-3 and IAEA 405 reference materials were used for calibration. Typical spectrum of road dust sample obtained using Ti target is presented in Fig. 1.

Table-1 : Measurement conditions used in EDXRF setup for analysis of different elements

Element	Voltage (kV)	Current (A)	Sec. Target	Count Time (s)	Atm.
Mg, Al, K	27	4500	Ti	900	Vacuum
Ca, Ti, V, Cr, Mn, Fe, Co, Ni, Cu, Zn	40	1500	Ge	600	Air
Pb	50	800	Mo	600	Air

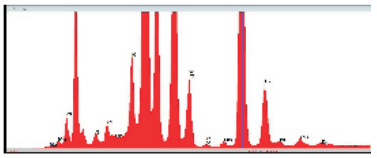


Fig. 1 Spectrum of Road Dust Sample (RD1) obtained using Ti Secondary Target

Enrichment factor analysis was used to differentiate between elements originating from anthropogenic activities and those of natural activities. The Enrichment Factor of element X (EF_x) in the sample with respect to natural abundance (in soil) is calculated using the formula

$$EF_x = \frac{X_s / E_{s(ref)}}{X_c / E_{c(ref)}}_{roaddust} \Big/ {}_{soil}$$

Where X_s and X_c are concentrations of the element of interest in road dust sample and soil respectively. $E_{s(ref)}$ and $E_{c(ref)}$ are the concentrations of reference element in road dust sample and soil respectively. The elemental concentrations of Mumbai soil [1] are used as reference for estimation of enrichment factor. Factor analysis (FA) technique is commonly used for identification of sources in air borne particulate matter, soil and road dust. In the present study this technique has been used to identify the sources contributing to road dust. The details of the FA methodology are discussed elsewhere [2].

Results and Discussion

The average concentrations of elements in road dust are presented in Table 2. The results show high concentrations of crustal related elements in road dust. Trends of average elemental concentrations (for few elements) in each traffic category are presented in

Fig. 2. As shown the average Fe concentration was highest in industrial area, where roads are not well maintained, and lowest in heavy traffic area. Similar trends are observed for other crustal related elements. As shown in Fig. 2 the K levels are higher in heavy traffic and medium traffic areas compared to industrial area and express way. The high K levels in medium traffic area could be due to presence of municipal solid waste landfill near the sampling point. In landfill, biomass is burnt to reduce its volume resulting in high K levels in air particulate matter [3]. Zn and Pb are high in heavy traffic area due to contribution from break wear and fuel combustion. Also V and Ni are higher in industrial area where oil refineries are located.

Table-2: Average Elemental Composition of Road Dust Samples collected in Mumbai

Element	Mean (mg/kg)	S.D. (mg/kg)	Enrichment Factor
Fe	63524	7543	2.99
Ca	43857	6179	13.6
Al	29502	4047	-
Mg	20263	2239	-
Ti	11033	1725	-
K	3879	654	2.37
Mn	1050	99	2.51
V	201	25	7.99
Cr	239	58	2.51
Zn	235	51	20.81
Cu	106	27	2.22
Ni	47	10	4.66
Co	22	4	-
Pb	70	32	6.04

Table 2 also presents enrichment factors (EF) estimated using the trace elemental data generated. The values of EF for Fe, K, Mn and Cr are all below 3 indicating their crustal origin. However, Ca being crustal element was enriched, which could be due to presence of cement particles in road dust. V, Zn, Ni and Pb are enriched indicating contribution of anthropogenic sources. The highest enrichment factor was recorded for Zn at Vikhroli which is a heavy traffic congested area.

The elemental data generated was subjected to factor analysis to determine the profile of contributing sources. Four factors were generated which accounted for cumulative variance of 88 %. Table 3 presents the varimax rotated components of each factor. Factor 1, which gave highest percentage of variance (40.2 %), with high factor loadings of Fe, Ca, Al, Mg, Mn indicating crustal source. Factor 2 explained 31.8 % variance with high loadings of Cr, Zn, Cu, Co and Pb. This factor with high loadings of Zn signifies tyre wear. The third factor with high loadings of V and Ni signifies oil combustion source which could be a mix of vehicular exhaust emissions and emissions from nearby industrial sources. The fourth source with high loadings of Ti, K and Pb indicates the brake wear as titanium [4] is used in brake lining.

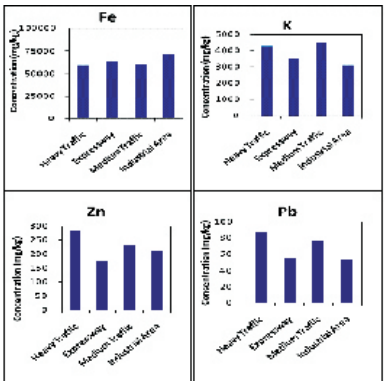


Fig. 2 Elemental distribution of road dust in different traffic categories

Table-3: Varimax Rotated Factor Loadings of Road dust samples

Element	Factor 1 (Crustal)	Factor 2 (Tyre wear)	Factor 3 (Indust-trial)	Factor 4 (Brake wear)
Fe	0.91	-0.05	0.29	0.10
Ca	0.83	-0.27	0.04	0.25
Al	0.92	0.09	0.13	0.09
Mg	0.69	0.03	0.62	0.03
Ti	-0.60	0.28	0.14	0.68
K	-0.21	0.30	-0.53	0.67
Mn	0.86	0.01	0.24	0.09
V	0.28	0.16	0.86	0.14
Cr	0.03	0.88	0.26	0.11
Zn	-0.24	0.83	0.11	0.39
Cu	-0.22	0.86	-0.01	0.40
Ni	0.17	0.34	0.78	0.28
Co	0.04	0.91	0.10	0.06
Pb	0.17	0.63	-0.05	0.65

Conclusion

The present study investigated elemental composition of road dust at selected locations in Mumbai. Enrichment factor and factor analysis were used to ascertain the contribution of natural and anthropogenic sources. The results of factor analysis showed contribution from crustal, vehicular and industrial sources apart from tyre wear and brake wear. Further, the study successfully demonstrates the use of EDXRF technique for determination of elemental composition of road dust.

References

[1] T.N. Mahadevan, Ph.D Thesis, University of Mumbai, (1986) 321.

[2] P. Kothai, I.V. Saradhi, P. Prathibha, P.K. Hopke, G.G. Pandit, V.D. Puranik, 8 (2008), 423.

[3] M.A.K. Khalila, R.A. Rasmussen, Atmospheric Environment 33 (2003), 1211.

[4] S. M. Atiemo, F. G. Ofosu, I. J. K. Aboh, O. C. Oppon, X-Ray Spectrometry, 41 (2012) 105.

Measurement of contribution of radioctivity in Liver to Lung

Lokpati Mishra, I.S.Singh, Minal Nadar, G. N. Kalyane and D. D. Rao

Radiation Safety Systems Division, Bhabha Atomic Research Centre, Trombay, Mumbai 400 085, India;
E-mail: lokpati@barc.gov.in

Contribution factors (CFs) (from liver to lungs) for in vivo assessment of ^{241}Am using an array of HPGe detectors have been estimated. Measurements were carried out in standard geometry using an array of three 70mm dia. and 25mm thick HPGe detectors inside totally shielded steel room for various chest overlay plates of the LLNL realistic thorax phantom loaded with liver set having uniformly distributed ^{241}Am activity. Results of this study will be useful in the assessment of Pu/Am in case of old exposure of radiation workers.

Introduction

In nuclear fuel cycle operations, plutonium plays a pivotal role. The measurement of plutonium burden in radiation workers by direct method, at the desired detection level is rendered difficult due to low yield of their photons and their significant attenuation / absorption in the lungs and the chest overlay tissues [1]. In-vivo assessment of plutonium is carried out using ^{241}Am as a tracer. The gamma photons of 59.5 keV emitted from ^{241}Am are used for its detection and quantification and by using Pu:Am ratio , plutonium lung burden is evaluated. For this purpose, specialized radiation detectors with large area, good energy resolution and very low background are required. In order to reduce detector background, measurements are carried out inside totally shielded steel room.

The actinide monitoring system, consisting of an array of three HPGe detectors inside totally shielded steel room, is calibrated using realistic thorax phantoms such as Lawrence Livermore National Laboratory (LLNL) phantom or Japan Atomic Energy Research centre (JAERI) phantom having known amount of radioactivity uniformly distributed in the lungs. This calibration is true with the assumption that activity is only in the lungs and there is no contribution from other parts of the body. Biokinetic behavior of ^{241}Am is such that a major fraction of it is transferred to liver and skeleton from blood [2]. In old exposure cases of ^{241}Am in radiation workers, estimation of internal contamination of ^{241}Am in lungs becomes difficult due to contribution of ^{241}Am from liver and skeleton (bone in thorax regions). In this study, measurements have been carried out to estimate CFs for the actinide monitoring system (from liver to the lungs) for ^{241}Am using LLNL phantom. Estimated CFs have been used to estimate contribution in count rate for lungs due to the activity present in liver at different time intervals post exposure.

Materials and Methods

Detector System

The actinide lung monitoring system consisting of an array of three 70 mm dia. and 25 mm thick n-type HPGe detectors inside totally shielded steel room was used in this study. The signal from each detector can be analyzed separately through three multi channel analyzer (MCA) cards as well as in any combination with other detectors [3]. Interwinner and Winnerdose softwares were used for analyzing spectras. The actinide lung monitor is provided with a bed which has been specially designed and fabricated to move in all the three directions while the detector has the facility of vertical movement. Figure 1 shows the Actinide Lung Monitor mounted inside the steel room.



Fig. 1 The Actinide Lung Monitor showing array of HPGe detector with LLNL phantom

LLNL Phantom

LLNL is the physical thorax phantom based on Caucasian man with mass 76 kg and height 177 cm [4]. LLNL torso phantom has a simulated rib cage and removable lungs, liver and lymph nodes. Chest overlay plates provide representation of individuals with different chest wall thicknesses (cwt) [5].

LLNL phantom was loaded with liver containing known amount of uniformly distributed ^{241}Am activity and measurements were carried out with lungs as target organ in supine geometry. In this geometry detector centre is kept on the phantom midline and one end of the detector is kept tangential to the supra-sternal notch of the phantom. CFs are defined as net count rate (cpm) per unit activity (kBq) present in liver. CFs have been estimated for different layers of chest overlay plates of LLNL phantom using the measured data.

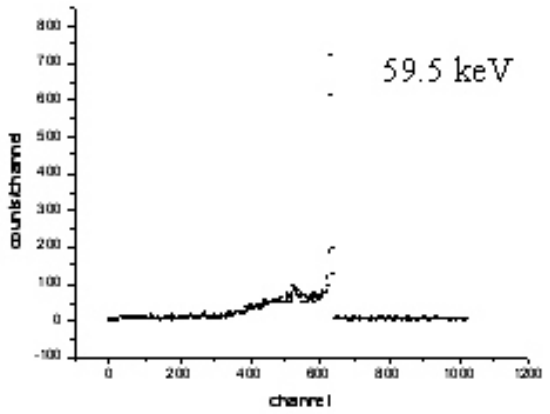


Fig. 2 Pulse height spectra of an array of HPGe detectors for ^{241}Am distributed in liver of the LLNL phantom

Results and Discussion

Estimated contribution factors (from liver to lungs) for various chest overlay of LLNL phantom are given in Table 1. Figure 2 shows pulse height spectra of an array of HPGe detectors for lungs as target organ when activity is distributed in liver of the phantom. Contribution of 43.57 cpm/kBq has been evaluated for chest overlay thickness of 1.76 cm which is an average cwt of Indian radiation workers. The contribution decreases with increase in chest overlay thickness due to increased attenuation of photons of 59.5 keV.

Table-1: Liver to lungs contribution factors (CFs) for ^{241}Am activity present in liver of LLNL phantom using an array of HPGe detectors.

Chest over lay thickness (cm)	Liver to lungs CFs [net count rate normalized with activity present in liver] (cpm/kBq)
1.76	43.57
2.84	37.19
3.49	34.39
4.31	26.88
6.18	18.49

Bio-kinetic model of ^{241}Am has been solved to estimate retained activity in lungs and liver at different time post exposure [6] and it has been found that for Type M compounds, maximum activity in liver is at 300 days post exposure while for type S compounds the maximum activity in liver is at about 1000 days post exposure. It must be noted here that ^{241}Am is behaving as Type S only when it is embedded in Pu matrix. Table 2 gives amount of ^{241}Am retained in lungs and liver at different time post exposure. The values presented here are for acute inhalation intake equivalent to annual limit of intake.

Table-2: Retained activity of ^{241} Am in lungs and liver at different times post exposure for acute inhalation of activity equivalent to 20 mSv CED

Days(Post exposure)	Retained ^{241}Am (Bq) Type S		Retained ^{241}Am (Bq) Type M	
	lung	liver	lung	liver
1	153.60	0.51	42.62	9.25
100	87.36	1.13	14.73	16.28
300	67.20	1.73	4.21	18.13
1000	36.00	2.45	0.07	12.21
1112	33.12	2.46	0.04	11.47
10000	2.04	0.76	3.0E-22	1.61

Using Table 1 and Table 2 contribution of liver activity to lungs has been estimated. For a radiation worker with chest wall thickness of 1.76 cm having acute intake of 1 ALI of Type M ^{241}Am, the contribution from liver to lungs is 0.4 counts per minute at 1 day post exposure. This value increases with time and reaches to maximum of 0.8 counts per minute at 300 days post exposure. For type S ^{241}Am compounds maximum contribution is found to be about 0.1cpm. Using this methodology the contribution of ^{241}Am retained in liver to lung activity estimation at different time intervals can be calculated for different amount of initial intake.

Conclusion

Contribution factors (from liver to lungs) for in vivo assessment of ^{241}Am using an array of HPGe detectors have been estimated. The result shows that these factors depend on time elapsed post exposure as well as on solubility of radionuclide. Using this methodology, contribution factors for other detection systems can also be evaluated. This study will be helpful in measurement of Pu/Am in lungs in presence of Pu/Am deposited in liver from previous intake.

References

[1] Lokpati Mishra, M.Tech. Thesis, (RSE) HBNI (2010) p.8.

[2] ICRP 78, Annals of the ICRP, ICRP Publication, (1997) p. 78

[3] Pendharkar K. A., et al BARC Newsletter. 296, pp.9- 23 (2008).

[4] IAEA, Safety Series No. 114, IAEA, Vienna (1996).

[5] Newton D., et.al (Proc. Sym. Paris, 1984), IAEA, Vienaa (1985) 183-199.

[6] Garg, S.P., Singh, I.S., Harikumar, M. and Sharma, R.C. Radiation Protection and Environment. 24(1-2) (2001) 135.

Experimental Measurement of Mass attenuation Coefficient near L absorption edges by X-ray Spectrometric Technique

Sharanabasappa[1], B. R. Kerur[2] and Anilkumar.S[3]

1. *Department of Physics, JSSATE, Bangalore 560060, India; E-mail:sharanphy@gmail.com*
2. *Department of Physics, Gulbarga University, Gulbarga 585105, India.*
3. *Radiation Safety System Division, BARC, Mumbai 400085, India.*

Total mass attenuation coefficients (MAC) of various compounds such as Barium chloride, Lanthanum sulfate at different X-ray energies were measured. The X-ray energy ranges from 5.895 to 17.864 keV. Here HPGe detector measures MAC. The results compared with theoretical values, agreement found to be good when the incident photon energy is far below and away from the L edge. In some cases disagreement is observed between measured and theoretical MAC values near L absorption edges. In the present work, the non validity of mixture rule and discrepancies of obtained values with theory near L absorption edge are discussed.

Keywords: Mass attenuation coefficient, L absorption edge, Resonance Raman Scattering, EXAFS

Introduction

The study of X-ray and gamma ray interactions with matter has greater impact in all discipline of Science and Technology. The property of gamma rays highest penetration power compared to all other radiations and the neutral charge has found many applications in industry, agriculture, radiography, spectrometry, medicine and dosimetry. The study of interaction of radiations with matter gives details about nature of the interactions of the photons with the physical objects. Thus it explains the exponential reduction of the intensity with the thickness of the material. But when the incident photon energy approaches the absorption edge of the elements present in the sample, then the exponential reduction of incident photon intensity is not linear. Hence under such circumstances the photon interaction study is very important.

The mass attenuation co-efficient for a compound is computed using the mixture rule, which is given by

$$/ = {}_i (/)_i \quad (1)$$

Where $_i$ is the proportion by weight if the ith element present in the compound and $(/)_i$ is the mass attenuation co-efficient of the ith constituent element of the compound. For a chemical compound $_i$ can be written as,

$$_i = a_i A_i / (a_j A_j) \quad (2)$$

A_i is the atomic weight of the ith element and a_j is the number of formula units in compound.

Experimental Procedure

The total attenuation coefficient was determined by measuring the transmission intensity of the X-rays through good geometrical arrangement and is shown in Fig. 1.

The geometrical arrangement adopted is a good geometry and is arranged vertically over the window of the HPGe X-ray detector system.

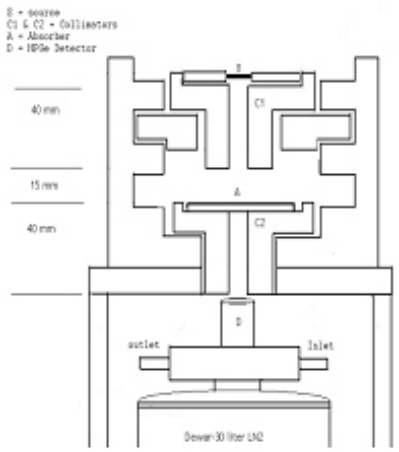


Fig. 1

The X-ray spectrometer consist of an n-type detector of area 500 mm^2 and 100 mm thick high purity Germanium connected to DSA-1000 16K MCA. The spectrometer is operated by Genie 2000 software. The detector is directly coupled to a preamplifier through a cool FET device and mounted over a rigid cryostat with an accompanying Dewar for liquid Nitrogen. In the present case live time of the MCA is selected. Radioisotopes of ^{109}Cd, ^{241}Am, ^{55}Fe and ^{57}Co each of 25 Ci procured from BRIT Mumbai were used as X-ray sources in the present work. Compounds such as Barium chloride, Lanthanum sulfate and Lanthanum oxide purchased from Himedia.

Results and Discussion

The experimental / value along with their associated error were calculated by the least-squares fit which are given in Table 1. The theoretical values were calculated by WinXCom programme which is the successor of XCOM. The uncertainty involved in the

theoretical value is about 1-2%. Since the reproducibility of our experimental value is within 2% and from counting statistics, areal density thickness measurement which contributes an experimental error of about 1-2 %. Hence an overall experimental error i.e., PD of about 4% was treated as agreement between experimental and theoretical value. On the other hand PD greater than 4% should be considered as disagreement between experimental and theoretical value.

Table-1: Comparison between theory and experimental mass attenuation coefficients in Lanthanum Sulfate for different energies.

X-ray energy in keV, E_x	E_{Li}	$E= E_x - E_{Li}$ in keV	Experimental cm^2/g	Theoretical value cm^2/g	P.D
5.895 K Fe	6.266 5.891 5.483	-0.371 -0.004 +0.412	314.4 4.5	292.1	+7.6
6.404 K Co	6.266 5.891 5.483	+0.224 +0.599 +1.007	239.9 4.9	269.3	-10.9
6.490 K Fe	6.266 5.891 5.483	+0.138 +0.513 +0.921	226.2 5.6	260.2	-13.1
7.05 K Co	6.266 5.891 5.483	+0.784 +1.159 +1.567	226.8 1.9	210.6	+7.6
8.041 K Cu	6.266 5.891 5.483	+1.775 +2.150 +2.558	159.6 3.4	150.4	+6.1
8.900 K Cu	6.266 5.891 5.483	+2.639 +3.014 +3.422	117.3 2.1	114.8	+2.1
14.390 Co	6.266 5.891 5.483	8.124 8.499 8.907	30.82 0.64	31.92	-3.4

In the Table there is a good agreement between theoretical and experimental results for the energies between 8.041 to 14.39 keV for Lanthanum compound. Since the incident photon energy is far away from the L absorption edge, as discussed in the introduction there is good agreement between experiments with theory within 4%.

On the other hand the mixture rule is not in agreement for the compound Lanthanum Sulfate with $E= (E_x - E_{Li})$ from 0.415 to 1.061 for L_I, L_{II} and L_{III} edges. It is observed that in some compounds the incident X-ray energy is sufficient to knock out L_{II} and L_{III} edge electrons only but not L_I edge electron and in some cases only L_{III} edge electron knock out but not L_{II} and L_{III} edge electrons as it can be seen from all the tables particularly at 5.895 keV X-rays.

Hence the experimental value deviates from the theoretical value by +7.6, -10.9, -13.1 and +7.6 in case of Lanthanum sulfate. Thus mixture rule cannot be applicable near Lanthanum L absorption edges. These deviations are due to the addition of the two or three L_I, L_{II} and L_{III} edges and contribute to the mass attenuation coefficient. In the present investigation the contribution coming from all the L edges can't be resolved to get only one edge effect on the mass attenuation coefficient value. This is the inherent property of the element even it can't be done with the synchrotron radiation. Since the edge effect on the mass attenuation coefficient arises from L_I, L_{II} and L_{III} edges as the photon energy increased step by step, so the contribution coming from each edge increases one by one as the energy is increased. In the present case, at incident photon energy 5.895 keV the deviation between experimental and theoretical mass attenuation coefficient is found out to be about 7.6% due to L_{II} and L_{III} edge only and not from L_I, since L_I edge is far away from the incident photon energy. Whereas in case of 6.404 keV X-rays the deviation found to be about -10.9% for the same compound, it is addition of the three edge viz., L_I, L_{II} and L_{III} edges.

Conclusion

The observed deviation between the experimental and theoretical / values may be attributed to the effects of the resonance scattering of X-rays near absorption edges, extended X-ray absorption fine structure, chemical, molecular and thermal environments. Hence this leads to the deviation of the experimental / value from that of the theoretical value. The observed deviation can be attributed to the fact that the calculation of theoretical value has been done by considering single atomic wave functions. The experimental value deviates from the theory which shows that the above effects have to be taken into consideration while calculating the theoretical / value near the absorption edges. In the present case it is verified for the L edges that the Bragg's addivity law does not holds well near absorption edges. Our results clearly call for the theoretical recalculations of mass attenuation coefficient near absorption edge of K and L edges and also by considering experimental data.

References

[1] J. H. Hubbell, X-ray cross-section and crossroads (The International Radiation Physics Society)-Richard Pratt's contributions to both, Radiat. Phys. Chem. 59 (2000), 113.

[2] B. R. Kerur, S. R. Thontadarya and B. Hanumaiah, Anomalous X-ray attenuation Coefficients around the absorption edges using Mn K x-rays. Appl.Radiat. Isot. 45 (1994), 159.

Gross Alpha and Beta Activities in Potable Waters used by Pharmaceutical Companies in India

Hemalatha.P., Sanu.S. Raj, Madhuparna D., S.K. Jha and R.M. Tripathi

Environmental Radiation Monitoring Section, Health Physics Division, Bhabha Atomic Research Centre, Mumbai 400 085, India; E-mail: hemlathap@gmail.com

This paper presents the gross alpha and gross beta radioactivity present in potable waters used by pharmaceutical firms from different states of India. A three year analysis in more than 90 water samples indicated that the gross alpha activity was observed to be in the range of <1 to42.9±2.5mBq/l while gross beta activity was in the range of <20 to 67.6±2 mBq/l. Higher level of activity was observed in Goa waters. However the activities were observed to be within the limits of drinking water regulations as per USEPA 40CFR.141and WHO regulations.

Introduction

Radioactivity in drinking water is principally derived from two sources: a) The leaching of radionuclides from rocks and soils b) The deposition of radionuclides from the atmosphere. Natural uranium and its progenies are found in all types of rocks and soil in varied concentration. It leaches out from rocks and minerals, mixes with water and eventually contributes in the drinking water sources. If the bedrock contains considerable amounts of natural uranium, its corresponding daughter radionuclides radium, polonium and lead may be present in potable water obtained from these sources. Apart from this, the development of nuclear technology has produced an increase of the radioactive content in environmental matrices. Measurement of Gross alpha and gross beta in any environmental samples will give an overall estimation of the radioactivity present due to natural and anthropogenic activities. Hence, Gross alpha and gross beta -particle activity measurements are generally carried out in drinking water mostly for screening purposes [1]. The main radionuclide contributing radiological effects in the uranium series are, produced by radium and its daughter products. Radium, and radioactive anthropogenic strontium being chemically similar to Calcium, follows the biological pathway and gets deposited in bone surfaces. When bore well water is being utilized for consumable purposes, these waters are generally treated for conventional pollutants to comply with drinking water quality. Water treatment such as demineralising ion exchange processes can only reduce the activity to some extent, but cannot remove it totally. Assessment of natural radioactivity is being regulated by international recommendations through WHO, [2]. This paper gives a three years study of gross alpha and beta activities in potable waters used by pharmaceutical firms for their preparations.

Materials and Methods

Potable water samples from different Pharmaceutical firms such as CIPLA Units, Mediorals Ltd, Meditab Ltd, Alembic Pharmaceuticals etc. from different parts of India such as Maharashtra. Goa, Himachal Pradesh,, Madhya Pradesh etc. were received and analysed for Radioactivty content. The nature of the water samples were from bore well and municipal water supply units. Gross alpha and beta activities were estimated by chemical treatment followed by radioactivity measurement.

Gross Alpha Activity Measurement

One liter of water sample was filtered through 0.22 m Millipore filter and acidified with conc. HCl to pH-2. Barium and Iron carrier were added in the sample. Then by addition of 50% Ammonium Sulphate solution and 1:1 NH_3 solution at pH–7, $Fe(OH)_3$ and $BaSO_4$ were precipitated. The precipitate was quantitatively transferred into a planchet and Estimated the alpha activity by counting in a ZnS(Ag) gross alphadetector.

Gross Beta Estimation in Potable water

Similarly one liter of water sample was filtered through 0.22 m Millipore filter, acidified with conc. HCl. Then Ca and Cs carrier were added and heated on a hot plate to 60°C. Then by adjusting the pH to 4 Calcium Oxalate, was precipitated by adding Sulkowich reagent. Then the solution was allowed to cool to room temperature and 2 to 3 mg of Ammonium Phospho Molybdate was added. The precipitate was then transferred into a 25 mm dia aluminium planchet and estimated the beta activity by counting in a low background Gas flow beta detector .

Results and Discussion

International regulations on water intended for human consumption have specified radioactivity limits suitable for drinking water for gross alpha activity as 0.1 Bq/Land for beta activity as 1Bq/L [3]. The three year analysis results of the water samples for gross activities revealed that the amount of gross alpha levels in potable water was observed to be in the range of <1 to42.9±2.5mBq/L with a overall mean of 33.27 and gross beta activity was in the range of <20 to 67.6±2mBq/L. Since these water sources are from different places, due to the rocks and groundwater source, radioactivity may buildup from natural Uranium and Th. Hence radium isotopes were

estimated by co-precipitation of radium with Pb, Ba Sulphate followed by Beta counting. The paper further discusses the details of ^{226}Ra and ^{228}Ra concentration in the water samples compared with the gross activity observed. The values were compared with different locations. Higher values were observed in the waters from Goa and Karnataka. It was observed that bore well waters showed higher activity levels compared to municipal water supply.

References

[1] Environmental Protection Agency, 1997. National primary drinking water regulations. 40 CFR part 141. U.S. Federal.

[2] WHO, Guidelines for Drinking-Water Quality, Recommendations, 3rd Edition., Vol. 1. Geneva, 2008.International Atomic Energy Agency, International Basic Safety Standards for Protection against Ionizing Radiation and for the Safety of Radiation Sources, No. 115 IAEA, Vienna, (1995).

[3] USEPA, Final Draft for the Drinking Water Criteria Document on Radium, USEPA, Washington, DC, (1991), TR-1241-85.

Table-1: Mean gross alpha and gross beta activity levels in potable water Samples received from Pharmaceutical firms from different states of India

Year	Location	Gross alpha (mBq/L)	Gross beta (mBq/L)
2010	Maharashtra	1.05	22.99
	Madhya Pradesh	1	21.65
	Karnataka	10.56	14.69
	Himachal Pradesh	1	20.17
	Andhra pradesh	4.13	26.47
	Goa	17.12	66.81
2011	Maharashtra	1	20
	Madhya Pradesh	1	20
	Karnataka	6.71	26.25
	Himachal Pradesh	8.73	20
	Goa	11.56	30.79
2012	Maharashtra	1.02	25.32
	Madhya Pradesh	1	27.34
	Karnataka	33.27	30.75
	Goa	7.66	20.66

Determination of Gamma Ray Mass Attenuation Coefficient Using NaI(Tl) Detector

Vandana A.Tupe [1], Bibifatima M.Ladhaf [2], Pravina P. Pawar [2]

1. *Dept. of Physics, Gajanan junior college Rajuri Navgon Dist Beed.431 122(M.S.) India; E-mail: pravina.pawar@yahoo.com*
2. *Department of Physics, Dr.Babasaheb Ambedkar Marathwada University, Aurangabad: 431004.India.*

Photon mass attenuation coefficients of Manganese metal were determined in the energy range 122-1500 keV in a well-collimated narrow beam good geometry set-up using a NaI (Tl) scintillation detector. The gamma-rays were detected with a resolution of 10.2% at 662 keV. The mass attenuation coefficient (/) data were then used to obtain the molar extinction coefficients ( ) for Manganese metal. It was observed that molar extinction coefficients goes on decreasing with increase of gamma-ray energy. The results show that, the experimental values of molar extinction coefficients are in good agreement with the theoretical values upto 2% error.

Introduction

This work concerns determination of photon attenuation or absorption properties of material using the application of Lambert-Beer's law with standard transmission method by adopting narrow beam geometry. Accurate values of mass attenuation coefficient for photon radiations of Manganese metal in several energies are needed in solving various problems in radiation physics and radiation dosimetry. Due to the damaging effects of high-energy photons, it is necessary to know how much energy is deposited in tissue during diagnostic treatments involving such radiation. In addition, gamma radiation is used in cancer treatments where it is important to know how much energy will be deposited in healthy and in tumorous tissue.

Eating a small amount of manganese each day is important in maintaining health. The amount of manganese in a normal diet (about 2,000-9,000 (g/day) seems to be enough to meet daily need, and no cases of illness from eating too little manganese have been reported in humans. In animals eating too little manganese can interfere with normal growth, bone formation, and reproduction. Too much manganese, however, can cause serious illness [1]. The mass attenuation coefficients for high purity elemental material (Mn) was measured in the gamma-ray energy obtained by a variable-energy gamma-ray source range from 10 keV to 1500 keV using a Sodium Iodide detector [2].

Manganese is used principally in the manufacture of iron and steel alloys and manganese compounds and as an ingredient in various products. Manganese dioxide and other manganese compounds are used in products such as batteries, glass and fireworks. Potassium permanganate is used as an oxidant for cleaning, bleaching and disinfection purposes. Manganese greensands are used in some locations for potable water treatment. An organic manganese compound, methylcyclopentadienyl manganese tricarbonyl (MMT), is used as an octane-enhancing agent in unleaded petrol in Canada, the United States of America (USA), Europe, Asia and South America. Other manganese compounds are used in fertilizers, varnish and fungicides and as livestock feeding supplements.

The photon mass attenuation coefficient data which are most often used are the compilation of the National Bureau of Standards. A significant number of photon attenuation coefficient measurements, calculations and compilations has been published. [3]. Appreciable discrepancies between some of the experimental and theoretical values indicate the need for additional, accurate and consistent measurements of mass attenuation coefficients.

Experimental

The five standard gamma sources ^{57}Co, ^{133}Ba, ^{137}Cs, ^{60}Co and ^{22}Na are used. Gamma rays of energy 122, 360, 511, 662, 1170, 1275 and 1330 keV emitted by the above radioactive sources (procured from Bhaba Atomic Research Centre, Mumbai) were collimated and detected by NaI(Tl) detector having energy resolution of 10.2% at 662 keV. The Sodium Iodide detector [0.75"x2"] was connected to PC based 8k-MCA. The signals from the detector were amplified and analysed with 8 K multichannel analyzer.

The Manganese metal samples under investigation were confined in cylindrical plastic containers of inner diameter 5 cm. It was found that the attenuation of the photon beam by the material of the empty containers was negligible. The sample thus prepared was weighed in an electrical balance exactly to the third decimal place. The weighing was repeated a number of times to obtain concordant values of the mass. A mean of this set of concordant values was taken to be the mass of the sample. Using the mean values of the mass and the inner diameter, the mass per unit area of each sample was determined. The thickness of the samples (mass per unit area) was chosen such that a $t <$ 0.6 criterion was satisfied at each energy, in order to minimize the effects due to multiple scattering.

Table-1: Molar extinction coefficients (cm^2mol^{-1}) of Manganese from 122 to 1330 keV

Energy keV	exp.	theo.	% deviation
122	6.465943	6.442083	-0.37037
356	2.290518	2.314378	1.030928
511	1.837187	1.861046	1.282051
662	1.622451	1.646310	1.449275
1170	1.407714	1.431574	1.666667
1275	1.240697	1.216838	-1.960780
1330	1.169119	1.169119	0.000000

Equations

This attenuation of the beam is described by the following equation:

$$I = I_0 e^{-x} \quad (1)$$

Where I_0 and I are the unattenuated and attenuated photon intensities respectively and the is the linear attenuation coefficient (cm^{-1}). A coefficient more accurately characterizing a given material is the density-independent, mass attenuation coefficient / (cm^2 gm^{-1}). Rearrangement of Eq.(1) yields the following equation for the linear attenuation coefficient:

$$= \frac{1}{t} \ln (I_0/I) \quad (2)$$

In Eq. (2), t(cm) is the sample thickness. The mass attenuation coefficients / (cm^2 gm^{-1}) for the samples were obtained from Eq. (3) by using the density of the corresponding samples:

$$_m = / (cm^2gm^{-1}) = \frac{1}{t} \ln (I_0/I) \quad (3)$$

where, (gm/cm^3) is a measured density of the corresponding sample.

The values of the mass attenuation coefficients were then used to determine the total molecular cross-section ($_{tot}$) by the following relation :

$$(_{tot}) = _m(A/N_A), \quad (4)$$

where, A is the atomic weight of the compound, N_A is the Avogadro's number.

The values of molar extinction coefficients were determined using the following relation [4] :

$$= (1/\ln 10)*N_A* _{tot} = 0.4343* N_A * _{tot} \quad (5)$$

Results and Discussion

The values of molar extinction coefficients (cm^2mol^{-1}) of Manganese from 122 to 1330keVare displayed in Table 1. In Fig.1 the typical plots of versus E for Manganese is given. The block diagram of Sodium Iodide detector is displayed in Fig 2. It is seen from Fig. 1 that the values for the molar extinction coefficient goes on decreasing with increase of gamma-ray energy. The results show that, the experimentally obtained values are in good agreement with the theoretical values calculated based on XCOM data up to 2% error.

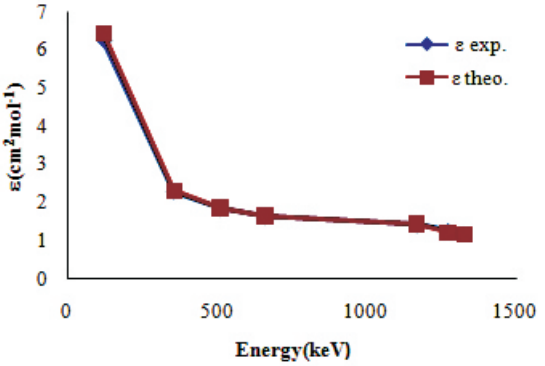


Fig. 1 Variation of Molar extinction coefficients with energy for Manganese from 122 keV to 1330 keV

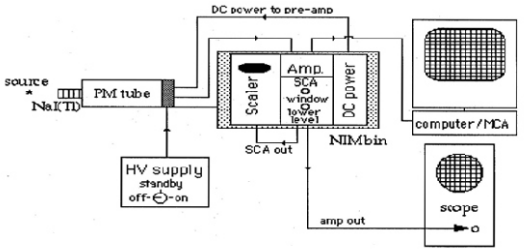


Fig. 2 Block diagram of Sodium Iodide detector

Conclusions

In the present work, linear attenuation coefficient and total attenuation cross-sections for Manganese metal were obtained using the measured values of their mass attenuation coefficients in the photon energy range 122 to 1330 keV. The attenuation coefficient data were then used to obtain the molar extinction coefficients, (cm^2 mol^{-1}). It was observed that as energy increases the molar extinction coefficients goes on decreasing and for higher energies it nearly remains constant as a function of gamma-ray energy. The results show that, the experimental values of molar extinction coefficients of Manganese are in good agreement with the theoretical values upto 2 % error calculated using the XCOM programme [5].

References

[1] Kaçal M. R., Han I., and Akman F., Nuclear Science and Technology ISBN : 978-81-7895-546-9, 59-69, (2012).

[2] Gerward, L., Guilbert, N., Jensen, K.B., Levring, H, Radiat. Phys. Chem. 60 (2001) 23.

[3] Hubell J.H. and Berger M., (Springer-Verlag,Berlin,), (1967).

[4] G.K.Sandhu, Kulwant Singh, B.S.Lark, L.Gerward, Radiation Physics and Chemistry,65 (2002) 211.

[5] Hubbell,J.H.,.Int.J.Appl.Radiat.Isot. 33 (1982) 1269.

Characterization of Gasoline and Diesel soot by Energy Dispersive X-ray Spectrometry

P. Kothai, S. Sandeep, S.K. Sahu and G.G. Pandit

Environmental Monitoring and Assessment Section, Bhabha Atomic Research Centre, Trombay, Mumbai 400 0085

Carbon soot emitted due to the combustion of gasoline and diesel fuel in the vehicular exhaust were characterized for trace and toxic elements by EDXRF, a key Nuclear Analytical Technique. About 16 trace elements were determined in the soot particles using various secondary targets after optimizing the analyzing parameters. As the crustal origin of fossil fuels suggest high concentrations mineral elements, Ca, Fe, Mg, Al found to be in higher levels in both the types of soot particles. Interestingly higher concentrations of Zn was observed in petrol soot. In general, most of the elements showed comparatively higher concentrations in gasoline soot than diesel soot.

Introduction

Air pollution is one of the serious environmental concern of the urban Asian cities including India where majority of the population is exposed to poor air quality. The health related problems such as respiratory diseases, risk of developing cancers and other serious ailments etc. due to poor air quality are known and well documented [1]. Particularly, in India, there is a high influx of population to urban areas, which has led to growing cities, sharp increase in traffic, trajectory growth, rapid economic development and industrialization, and higher levels of energy consumption. Two decades ago, most of the air pollution was due to industrial emissions and burning of fuel. But today, the ever increasing proliferation of automobiles would indicate that, if uncontrolled, pollutants emitted from the vehicular exhaust could increase without limit. It is also observed that in India 45-70% of the total air pollution in urban areas is contributed by auto exhaust pollution [2]. Statistics given by society of Indian automobile Manufacturers during 2012 indicates, in 2005-06 there were 8.9M vehicles sold and in five years this number has scaled to 15M (in 2010-11) increasing the number of vehicles especially in the metropolitan cities to 32 percentages.

The major air pollutants emitted by the motor vehicles include substantial quantity of Carbon di oxide, Carbon monoxide, Hydro carbons, oxides of Nitrogen, Suspended Particulate Matter and other air toxins. Apart from the increasing number of vehicles, other reasons for increasing vehicular pollution are the types of engines used, types of fuel used, and age of vehicles resulting into higher idling emissions and congested road traffic. As per the present scenario diesel and gasoline engines are the main contributors of vehicular pollution. Particulate matter, one of the criteria pollutants is emitted directly in to the atmosphere from the tail pipes of vehicles in the size fraction of 2.5 m whereas particles of 10 m size were introduced by means of brake and tire wear. Among the diesel and petrol engine particulate emissions, diesel exhaust emission is considered as about ten times higher than those by non catalyst gasoline engine particulate emissions.

The effect of particulate emissions on health has been of great interest for many decades. Adverse health effects of particulate matter in the size fraction 2.5 m are proven by several epidemiological studies. In recent years, it has been recognized that a large proportion of particles emitted from vehicles lie in the ultra fine region (<100nm) and vehicle emissions may contribute upto 85% of particle number in urban areas. Over 30 epidemiological studies link diesel exhaust to lung cancer [3]. This explains the necessary of analysis of composition of particles emitted from vehicular exhaust. In the present study diesel and petrol soots were collected and analysed for trace and toxic elements using one of the key Nuclear Analytical technique Energy Dispersive X-ray Fluorescence (EDXRF). The simplicity, speed of operation, minimum sample preparation and fairly low detection limits made the EDXRF technique as an efficient tool to analyze about 16 trace elements in the soot particles.

Experimental

Representative samples of soot particles deposited inside the tail pipes were collected from diesel and petrol engine based vehicles. Dried samples were made into pellets of size 25 mm. The soot pellets were analyzed using EDXRF system of Xenemetrix 3600 model provided with the Si(Li) detector of 20 mm^2 with 150 eV energy resolution at 5.9 keV Mn x-rays. The system was calibrated with suitable pellets made up of similar matrix and quality control was studies were performed by analyzing IAEA reference materials such as IAEA 405, 433, SL1 and SL 3.

Results and Discussion

The soot pellets were analyzed for trace and toxic elements in three steps using EDXRF technique. Suitable secondary targets were used in each step and the operating parameters such as current, voltage and time of counting were optimized for minimum counting error and the dead time during the analysis was maintained within 20% throughout the analysis. The parameters used for the study are presented in table 1and a typical spectrum of petrol soot analysed using Ti target is presented in Fig.1.

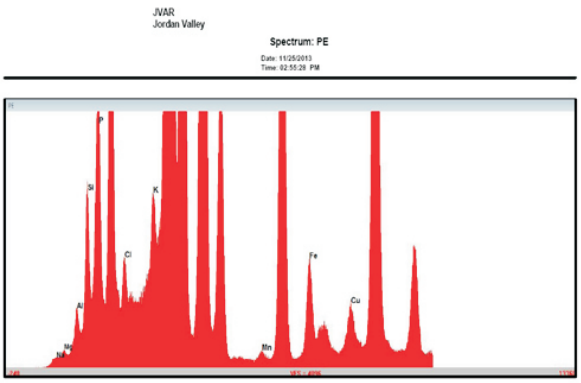


Fig. 1 Spectrum of Petrol soot analysed using Ti target under vaccum

Table-1: Parameters and conditions of Analysis using EDXRF

Secondary Target	Voltage (kV)	Current (A)	Atmosphere	Elements
Ti	25	4800	Vaccum	Na, Mg, Al, K, Ca
Ge	40	800	Air	Ti, V, Cr, Mn, Fe, Ni, Cu, Zn
Mo	40	1000	Air	As, Pb, Br

Concentration levels of trace elements in the gasoline and diesel soots are depicted in Fig.2. The results showed very high concentrations of Ca and Fe in both the soot samples, which are the indicators of the crustal origin of fossil fuel products. Following the high mineral concentrations Zinc, Aluminium, Sodium and Magnesium were found to be higher in petrol soot. Particularly, very high concentration of Zn was observed in petrol soot. Zinc Dialkyl Dithio Phosphate (ZDDP) is added as an anti wear additive for gasoline and diesel engine oils. In diesel engine oils additive is used only as primary ZDDP and in the gasoline oil primary as well as secondary ZDDP are used because in the petrol engines there is a requirement for cold starts i.e. operation at lower temperature. Therefore, Concentration of Zinc additive added is more in gasoline motor oils and this could be the reason for the high Zn concentrations of gasoline soot. On the other hand, in diesel soot Zinc concentration was observed to be lesser than the levels of other minerals such as Mg, Al, K and Ti. Lead levels in the gasoline and diesel soots found to be similar and were about 300 g/gm. Arsenic and Bromine were observed as the least contributing elements to the particulates of exhaust emission. The

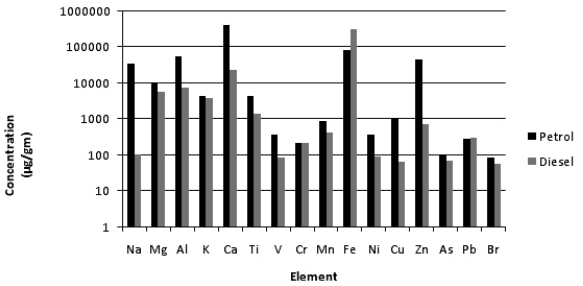


Fig. 2 Concentration of trace elements in gasoline and diesel soot

results as a whole showed higher concentrations of trace elements in the petrol soot than the diesel emissions. Studies conducted by Cheung et al [4] also showed comparatively higher emission factors for gasoline engine vehicles than diesel based vehicles for most of the elements. Only few studies were noticed based on the elemental composition analysis of particulates emitted from the exhaust and most of the studies were focused mainly on gaseous pollutants emitted by the exhaust. The present study gives an insight of elemental constitution of soot emitted by the gasoline and diesel emissions and further detailed studies based on collection of particles through impaction and filtration on filter papers will definitely provide better knowledge on the elemental composition of soot.

Conclusion

Elemental composition of soot emitted from the exhaust of gasoline and diesel based engines were determined. Results showed higher mineral element contributions in both the samples. Zinc found to be comparatively higher in petrol soot than the diesel soot. The entire result showed comparatively higher concentrations of trace elements in the gasoline soot.

References

[1] CPCB, Status of the Vehicular pollution control programme in India (2010) p. 1

[2] T. Subramani, Int. Jour. Eng. Res. And App.2(3) (2012) 1753.

[3] E.L. Avol, W.J. Gauderman, S.M. Tan, S.J. London, Am. J Respir. Crit. Care Med.164 (2001) 2067.

[4] K.L Cheung, L. Ntziachristos, T. Tzamkiozis, J.J. Schauer, Z. Samaras, K.F. Moore, C. Sioutas, Aerosol Sci. Technol. 44 (2010) 500.

High Resolution In-Situ Gamma Spectrometry for Determination of Outdoor Terrestrial Gamma Dose Rates at BARC, Mumbai.

Rajesh Sankhla and D.D. Rao

Radiation Safety Systems Division,Bhabha Atomic Research Centre, BARC Hospital, Anushaktinagar, Mumbai 400094, India; E-mail: rsankhla@barc.gov.in

In-situ, high-resolution, gamma-ray spectrometry measurements were performed at six pre selected locations of BARC, Mumbai. Calibration factors for the portable HPGe detector for field spectrometry were evaluated based on detector physical parameters. Specific Activities and gamma absorbed dose rates in air due to naturally occurring radionuclides ^{238}U and ^{232}Th series and ^{40}K are determined. The observed total ambient -absorbed dose rates due to primordial radio nuclides in BARC premises area ranged between 13.6 and 32.1 nGy h^{-1} with a mean of 21.6 ±2.0 nGy h^{-1}.

Introduction

In-situ gamma spectrometry means the direct measurement of radioactivity in open terrain. This method will yield the same information as soil samples analysed in lab., in a much shorter time and in more economical manner. The principal advantage of in-situ monitoring is that the detector samples the photon flux from a large volume of soil which averages out inhomogenities. This method was first developed by Beck et al [1].

One of the main external sources of irradiation to the human body is terrestrial gamma radiation emitted by naturally occurring radioisotopes. The most prominent primordial radionuclides are ^{238}U, ^{232}Th and their progenies and ^{40}K, which are exist in trace levels in all ground formations. A portable HPGe detector coupled with 4K MCA was employed in this study. The present study provides natural background data of BARC premises using in-situ gamma spectrometry.

Study Area

BARC is situated in north east of Mumbai. It is a premier multi directional nuclear research establishment having research facilities comprising complete nuclear fuel cycle. The complex lies stretched out alongside five suburbs-Chembur, Govandi, Mankhurd, Mandala and Trombay. This study area is chosen as large population resides adjacent to the complex.

Materials and Methods

Selection of Sites for measurements

A total of 6 locations were selected for measurement across BARC premises. Efforts were made to ensure that the sites were as evenly spaced as possible. In order to exclude the contributions from structures and road coatings, measurements were made at the center of empty spaces with areas of at least 20 m x 20m.

Field Measurements

In-situ gamma measurements were conducted using a portable, Canberra make High-Purity Germanium (HPGe) detector (coaxial cylinder of 52.5 mm in diameter and 43.9 mm in length) with a relative efficiency of 20% and an energy resolution (FWHM) of 1.8 KeV at the 1.33 MeV ^{60}Co peak. The detector was operated by MCA-166, a stand-alone portable multichannel analyzer. Spectra of 4K channels were collected and analyzed by the win TMCA32 software in a notebook PC.



Fig. 1 In-situ gamma spectrometry setup in the field

In order to evaluate the concentration of ^{238}U and ^{232}Th, their decay product namely, 1.765 MeV (^{214}Bi) and 2.614 MeV (^{208}Tl) were used where as for ^{40}K concentration, peak at 1.461MeV was used. At each measurement site, the detector was placed on a wooden stand (Tripod) at a height of 1m with the detector facing downward and its axis vertical, the gamma ray flux, both direct and scattered from the radionuclides in the soil were counted for a preset time of 1800 seconds.

Calibration Factors for field Spectrometry

Detector calibration factor C_f (cpm/ Bq kg^{-1}) is expressed as a product of three different factors that can be determined separately i.e.,

$$C_f = (N_f/A_s) = (N_f/N_0)\ (N_0/\ )\ (\ /A_s) \qquad (1)$$

Where, N_f/A_s is radionuclide peak count rate per unit concentration (cpm/Bq kg^{-1}). N_f/N_0 is Angular Correction Factor required to account for detector angular response. $N_0/$ is Peak count rate(cpm) per photon fluence rate for photon beam incident on the

detector along the detector axis (normal to the detector face) whereas /A_s is the total unscattered photon fluence rate at the detector location per unit inventory.

Helfer and Miller [2] conducted experiments using HPGe detectors of different volumes and developed empirical formulae along with tabulated data which were utilized to determine calibration factor (C_f) for different radionuclides for above said HPGe detector.

Table-1: Detector calibration factor C_f for three important radionuclides

Radio nuclides	Energy (MeV)	Calibration Factor (C_f) (cpm/Bq kg^{-1})
^{40}K	1.460	0.09844
^{214}Bi (^{238}U Series)	1.765	0.13206
^{208}Tl (^{232}Th Series)	2.615	0.26602

Reliability of these factors has been established [3]through laboratory gamma-ray spectrometric measurements of activity concentration of the natural radionuclides of soil samples collected at the same sites where in-situ measurements were made.

Evaluation of Dose Rate

The methodology given by Beck [1] is used to evaluate dose rate in air per unit activity concentration in soil. These factors (nGy.h $^{-1}$per Bq. Kg $^{-1}$) are independent of detector type and were calculated for ^{40}K and ^{238}U and ^{232}Th series. A uniform profile of soil distribution is assumed and admitting that series are in equilibrium. The total absorbed dose rate (nGy/h) due to terrestrial radionuclides is derived by

$$D = 0.0424\ A_k + 0.450\ A_U + 0.668\ A_{Th} \quad (2)$$

Where, D is the total absorbed dose rate in nGy h^{-1}, A_K, A_U and A_{Th} are the activity concentrations of ^{40}K, ^{238}U and ^{232}Th in Bq /kg respectively.

Results and Discussion

The activity concentrations of the primordial radionuclides have been detected and measured at 6 important locations. The range and average values of the activity concentration of the primordial radionuclides and total gamma absorbed dose at all the locations across the BARC premises are presented in Table 2.

The activity concentration of ^{40}K across the BARC premises ranged between 99.6 and 194.4 Bq kg^{-1} with a mean of 137 Bqkg^{-1}; ^{238}U was between 4.0 and 11.4 Bq kg^{-1} with a mean of 7.8 Bqkg^{-1}while that of ^{232}Th ranged between 7.1 and 28.2Bq kg^{-1} with a mean of 18.6 Bqkg^{-1}. The total -absorbed dose rates in air in the area ranged between 13.6 and 32.1 nGy h^{-1} with a mean of 21.6 nGy h^{-1}.

The average gamma absorbed dose rates represents about 39% of the indian average of 56 nGy h^{-1} of outdoor terrestrial gamma radiation exposure. (UNSCEAR, 2000).

Conclusion

The high resolution, in-situ gamma-ray spectrometric method has been employed in the determination of the natural gamma radiation dose levels across BARC premises. These results are expected to provide the background data for the evaluation of any future contamination in the environment due to local accidental releases or large scale international scale accident.

Acknowledgement

Authors are grateful to Dr K.S.Pradeepkumar, Head, Radiation safety Systems Division for keen interest and constant encouragement. Special thanks are also due to Shri D.Toppo for his help in spectrometry setup preparation at all the aforesaid locations.

References

[1] Beck. H.L, De Campo.J.A and Gogolak.C.V, (1972), USAEC Report HASL-258.

[2] Helfer. I. K and Miller. K. M, (1988), Health Physics, Vol. 55, pp. 15-29.

[3] Vijayagopal. P, Singh I.S. Garg. S.P, Pendharkar K.A. Fourteenth National Symposium on Environment (NSE-14).

Table-2: Activity concentration and absorbed dose rate due to ^{40}K, ^{238}U and ^{232}Th at different locations

Location	Activity ^{40}K Bq/Kg	Activity ^{238}U Bq/Kg	Activity ^{232}Th Bq/Kg	Total Dose Rate nGy/hr
Location-1	99.6±7.1	9.3±2.0	28.2±2.0	27.2±2.3
Location-2	179.5±8.5	5.8±1.8	7.1±0.9	15.0±1.4
Location-3	108.4±7.4	9.8±2.5	18.5±1.6	21.4±2.3
Location-4	194.4±9.1	11.4±3.3	28.2±2.0	32.1±2.7
Location-5	126±7.1	4.0±1.5	20.3±1.8	20.7±1.5
Location-6	114.1±7.1	6.3±1.5	9.0±1.5	13.6±1.6
Mean	137.0±7.7	7.8±2.2	18.6±1.6	21.6±2.0

Determination of Trace impurities in Uranium Metal using Total Reflection X-ray Fluorescence (TXRF) Spectrometry

Trupti Chavan[1], D.N. Wagh[1], V.H. Rupvate[2] and K.N. Hareendran[2]

1. *Analytical Chemistry Division, Bhabha Atomic Research Centre, Trombay, Mumbai 400085, India; Email:dnwagh@barc.gov.in*
2. *Uranium Extraction Division, Bhabha Atomic Research Centre, Trombay, Mumbai 400085*

Cr, Mn, Fe, Co, Ni, Cu, Zn and Pb were determined in uranium metal by Total Reflection X-ray Fluorescence (TXRF) Spectrometry. The method was validated using MERCK ICP multi elemental standard solution. Impurities were separated by extracting uranium with 30% tri-n-butyl phosphate in CCl_4 from 4N HNO_3 followed by extraction with 0.2 M tri-n-octyl phosphine oxide (TOPO) in CCl_4. After extraction, aqueous phase was spiked with Ga as internal standard and analyzed by TXRF spectrometer using Mo K excitation source. The values obtained by TXRF were compared with values obtained by ICP-AES. Relative standard deviation (n=7) was about 5% (1s) while limit of detection ranged from 20-40 ng mL^{-1}.

Introduction

The determination of impurities in the uranium at various stages of the nuclear fuel cycle plays an important role in quality control and the achievement of chemical and metallurgical requirements. Because the performance of nuclear fuel in reactors depends mainly on the chemical composition of its impurities and their concentration in nuclear fuel has to be maintained below certain limits[1]. Therefore, sensitive, accurate, precise, and rapid methods for the determination of impurities in uranium matrices are necessary.

A Number of analytical techniques have been used for the elemental characterization of uranium metal, depending upon the elements to be analysed, concentration range of impurities in the uranium matrices, required precision and accuracy, sample throughput and time of analysis. The various methods used include [2-3] ICP-MS, ICP-AES, AAS, GFAAS, NAA and HPLC-ICP-MS. Recently Total Reflection X-ray Fluorescence (TXRF) has also been used for characterisation of Uranium Oxide [4-5]. TXRF has become very competitive for trace element analysis of nuclear materials due to its simultaneous multi elemental nature, high sensitivity down to ng g^{-1} level, requirement of very small amount of sample, large dynamic range and use of single comparator.

In the present work, uranium metal produced by magnesiothermic reduction at uranium extraction division (UED) was analysed using TXRF. The results obtained using TXRF were validated by carrying out analysis using ICP-AES at UED.

Experimental

TXRF spectrometer (model No. TX-2000) from G.N.R. Analytical Instruments group, Italy having a W-Mo dual anode X-ray tube for excitation of characteristic X-rays and W-C multilayer for monochromatisation of source line was used. A SDD droplet type detector having active area of 30 mm^2 and resolution of 124 eV at 5.9 keV Mn K X-rays, coupled to a 8K channel analyser was used to acquire TXRF spectra. The characteristic K X-rays of Cr, Mn, Fe, Co, Ni, Cu, Zn and L X-rays of Pb of the analytes were excited using Mo K X-rays from X-ray tube operated at 40 kV and 30 mA. The data acquisition was carried out for 500 seconds. The data acquisition and processing was done using SCX_SCAN and SinerX software respectively, provided with the instrument. The quantification was done using Ga as internal standard and measuring the area under the peak. The instrument was calibrated using 1 g mL^{-1} multi-elemental standard solution prepared by diluting MERCK ICP Multi elemental standard solution.

ICP-OES: JY-238, Ultrace resolution 0.005 nm (first order) was used for ICP-AES measurements.

Preparation of Sample

The reagents tri-n-butyl phosphate (TBP), tri-n-octyl phosphine oxide (TOPO), Carbon tetra chloride (CCl_4), Triton X-100, Silicon Solution of AR grade and supra pure HNO_3 were used. Milli-Q deionised water was used for dilution. All the solution analysed were spiked with 0.02% V/V Triton X-100 solution prior to analysis.

For the calibration of TXRF spectrometer, calculating the relative sensitivities and validation of the method of analysis, three working standards STD-A, STD-B and STD-C having elemental concentrations of 500 ng mL^{-1}, 1 g mL^{-1} and 10 g mL^{-1} respectively, were prepared by diluting MERCK ICP multi elemental standard solution (1mg mL^{-1}). The Ga present in the standards was used as internal standard. Working standard solution STD-B (1 g mL^{-1}) was used for the calibration of the instrument and the relative sensitivities were calculated using all the three working standard solutions. Sample process blank as well as acid blanks were also used for blank correction. A 10 L aliquot of solution to be analysed was pipetted at the centre of the quartz sample support previously treated with 10 L silicon solution and dried

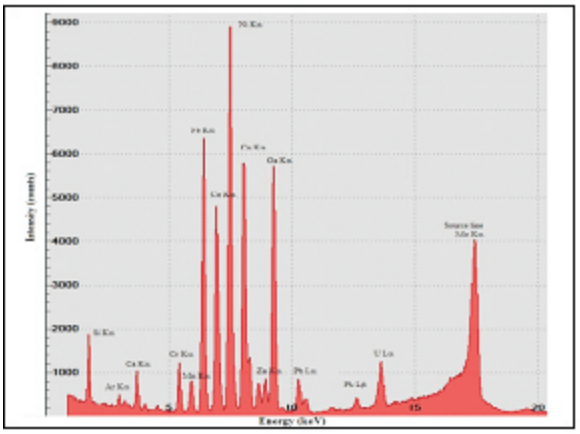


Fig. 1 TXRF Spectra of Uranium Sample 880

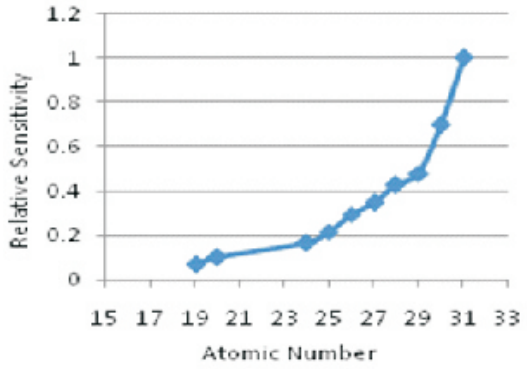


Fig. 2 Relative sensitivity for K series lines

under IR lamp. Concentrations of the elements were computed using the relative sensitivity curve.

About 5 gms of accurately weighed uranium metal sample was dissolved in 5 mL conc. HNO_3, evaporated to dryness and made up to 25 mL with 4 M HNO_3. Uranium was extracted by equilibrating the solution with 30% TBP in CCl_4 and extraction was carried out thrice. This was followed by another extraction with 0.2 M TOPO in CCl_4. The aqueous phase was made up to 25 mL with deionised water. Both samples 880 and 881 were taken in duplicate.

1 mL of the above solution was spiked with 20 g of Ga (1 mg mL^{-1} Ga MERCK ICP Standard Traceable to SRM from NIST) as internal standard and made up to 2 mL with deionised water. 10 L aliquots of each sample solution to be analysed was pipetted at the centre of the quartz sample support and analysed using TXRF. Three aliquots of each sample were pipette out separately and analysed using TXRF.

Results and Discussion

Figure 1 shows the TXRF spectra of uranium sample 880 and Fig. 2 shows the relative sensitivity for K series lines with respect to Ga. The results obtained on trace metal impurities in uranium metal samples using TXRF and ICP-AES are given in Table 1. Recovery studies were also carried out by spiking the aliquots of the original sample solutions with known concentrations of the multi elemental standards prior to uranium separation. The % recovery for all the elements analysed was in the range of 81 to 119%. The detection limits were in the range of 20-40 ng mL^{-1}.

Table-1: Results of analysis of uranium metal

Sample No.	880		881	
	TXRF	ICP-AES	TXRF	ICP-AES
Element	Concentration (g/g)			
Cr	56.75± 1.59	57.70 ±0.59	29.12± 0.92	31.86± 0.56
Mn	24.65± 1.12	22.57± 0.11	25.6± 2.28	21.97± 0.11
Fe	182.93± 12.00	164.67± 1.99	136.28± 4.89	140.08± 1.29
Co	<0.70	<1.2	<0.70	<1.2
Ni	215.82± 10.90	220.00± 2.56	113.35± 9.19	114.15± 2.42
Cu	114.33± 6.82	ND	93.13± 3.36	ND
Zn	7.2± 1.97	ND	3.93± 0.45	ND
Pb	11.07± 1.24	ND	10.65± 0.97	ND

ND- not determined

Table 1 shows that the analysis result obtained by TXRF are in very good agreement with the values obtained using ICP-AES. The sensitivities using TXRF can be further improved by optimising the experimental and instrumental parameters.

Conclusion

The results obtained on uranium metal samples indicate that the TXRF technique can be used for trace elemental analysis of nuclear materials.

Acknowledgement

The authors are thankful to Dr. A. V. R. Reddy, Head Analytical Chemistry Division and Dr. R. Verma, Head Nuclear Analytical Methods Section, Analytical Chemistry Division for their interest in this work.

References

[1] S. Bürger, L. R. Riciputi, D. A. Bostick, Journal of Radioanalytical and Nuclear Chemistry, Vol. 274, No.3 (2007) 491

[2] A. L. De Souza, M. E. B. Cotrim and M. P. F. Pires Microchemical Journal 106 (2013) 194

[3] R. K. Malhotra and K. Satyanarayana, Talanta 50 Issue 3 (1999) 601

[4] N.L. Misra, k.K. D. Sing Mudher,, V. C. Adya, B. Rajeshwari and V. Venugopal, Spectrochemica Acta part B 60 (2005) 834

[5] S.M. Simabuko, C. Vazquez, S. Boeykens, and R. C. Barroso X-ray Specrom. 31(2002)167.

Geochemical Peculiarities of Marine Sediment in Coastal Area

S.S. Gothankar and S.K. Jha and R.M. Tripathi

Health Physics Division, Bhabha Atomic Research Centre, Mumbai 400085, India; E-mail: sujatasg@barc.gov.in

To understand the impact of anthropogenic activity on coastal marine environment, sediment samples were collected covering the west and east coastal line of India. The elemental concentrations of K, Ca, Ti, Mn, Fe, Ni, Cu, Zn, Pb, Rb and Sr were determined using Energy Dispersive X-ray Fluorescence Technique (EDXRF). The concentration of Pb was found to be higher at Rameshwaram, whereas sediment collected from Okha gives highest concentration of Ni. The result indicates the impact of land based source of pollutant in the few locations due to the anthropogenic activities.

Introduction

The study of sediment in coastal area has great importance in understanding the interaction between human activities and marine system. The fate and disposal of most trace and toxic elements is much affected by the extent of their uptake and release from the suspended particles, along with the sinking, horizontal transport and accumulation of particles in the sediments. The sediments at the bottom of coastal marine environment contains large inventory of toxic elements released due to land based activity. Pollutant concentration in sediments provides a more stable means of obtaining an indication of the state of associated water. Sediments can also serve as sorbants or concentrators for various inorganic and organic chemicals [1,2]. The study was carried out to understand the present status of toxic metal contaminants in coastal marine environment of east and west coast of India, which is ultimate receiptants of point and non point sources.

Experimental

India has an extensive coastline comprising of a variety of coastal and near shore ecosystems of very high diversity. This coastline is about 6000 kilometers in length comprising of the Arabian Sea, the Bay of Bengal and the Indian Ocean in west, east and south respectively with a continental shelf of 0.5 million square kilometers including an exclusive economic zone of 2.02 million square kilometers. The sediment sample collection was carried out using grab sampler along east and west coast of India. The sampling location covers Okha, Diu, Daman and Porbandar area of Gujarat coast, Tarapur, Ratnagiri and Murud of Maharashtra coast. In the east coast, the samples were collected from Chennai, Pondicherry, Karaikkal, Rameshwarm, Tuticorin, Kanyakumari and Nagarcoil. All the samples were homogenized, freeze dried, ground and stored in polythene bottles. Adequate precaution was taken during sampling and handling to prevent cross contamination of the sample. For quantative measurements of trace and toxic elements using EDXRF technique (EDXRF Model 3600 -Jordan Valley Make) pellets were prepared by mixing 1 gram of sample and 1 gram of binding material (cellulose powder) under 10 metric ton hydraulic pressure. The samples were analysed along with Reference standards IAEA- 405 and elemental concentration in the sample was estimated by comparative method. All the elements (K, Ca, Ti, Mn, Fe, Ni, Cu, Zn, Rb and Sr) were determined through their K X-rays except Pb, which was determined through L X-rays using X-ray generated at the Rh anode of the X-ray tube. Suitable transmission filters were used to remove primary beam continuum in order to provide substantially monochromatic excitation line.

Result and Discussion

Table 1 gives the sampling location and trace elemental concentration at respective location. The concentration of K, Ca, Ti, and Fe ranged between 0.1% to 1.6 %, 0.4% to 12.5%, 0.03% to 2.7% and 0.3 % to 6.5% respectively. High concentration of Fe in the Murud region can be due to the high concentration of trace elements in the lethogenic flux. All along the east and west coast line of India, the variation in the concentration of Mn was from 70.2 to 674.2 mg kg^{-1}. The concentration of Ni varies from 1.0 to 105 mg kg^{-1} and the highest concentration was observed at Okha reflecting the impact of land based source in this region. The concentration of Pb varies from 2.0 to 56.6 mg kg^{-1} and the highest concentration was observed at Rameshwaram. Zn concentration varies from 13.7 mg kg^{-1} at Chennai to 97.2 mg kg^{-1} at Okha, whereas Cu concentration varies from 18.0 mg kg^{-1} at Kanyakumari to 107 mg kg^{-1} at Pondicherry. The Rb and Sr concentration in the sediment collected at different location varies in the range of 7.5 to 97.3 and 78.1 to 2406 mg kg^{-1} respectively.

Conclusion

The study carried out in the east and west coast of India to understand the existing distribution of trace and toxic elements concentration in the coastal sediments. The data indicates an elevated level of Pb in the Rameshwaram region, whereas Okha shows the higher Ni concentration compare to other locations, reflecting the characteristic impact of land based anthropogenic sources in the area.

Reference

[1] U. Forstner, Inorganic pollutants particularly heavy metals in estuaries: Chemistry and bio chemistry of estuaries. Eds. E. Olaussan and F. Cato, John Wiley and Sons Ltd., 307-340.

[2] S. K. Jha, S. B. Chavan, G. G. Pandit, B. S. Negi and S. Sadasivan, Env. Monitoring and Assess. 76 (2002) 249.

Table-1: Elemental concentration (mg kg^{-1}) in sediment samples collected from east and west coast of India

Location	K (%)	Ca (%)	Ti (%)	Fe (%)	Mn	Ni	Cu	Zn	Pb	Rb	Sr
Okha	1.6± 0.1	6.3± 0.4	0.3± 0.1	3.7± 0.2	436±26	105±9	70±6	97±8	2.0±0.1	97±10	1093±55
Diu	0.5± 0.1	6.3± 0.4	0.5± 0.1	4.3± 0.3	489±40	52±5	34±3	51±3	2.0±0.1	41±5	600±35
Porbandar	1.3± 0.2	4.2± 0.3	0.4± 0.1	4.6± 0.3	541±13	41±5	98±8	93±5	16.8±0.9	83±9	360±22
Daman	0.6± 0.1	1.2± 0.2	0.5± 0.1	5.5± 0.2	674±36	23±3	64±5	49±5	33.3±2	70±8	147±10
Tarapur	0.5± 0.1	2.1± 0.3	0.6± 0.1	4.9± 0.3	514±42	29±3	63±5	53±4	21.9±1	31±3	198±13
Ratnagiri	0.2± 0.1	1.0± 0.2	1.3± 0.1	2.7± 0.2	125±11	21±2	30±3	36±3	12.2±1	15±2	78±6
Murud	0.6± 0.1	3.5± 0.2	0.7± 0.1	6.5± 0.3	501±42	21±2	88±8	38±3	29.4±2	79±9	505±37
Chennai	0.6± 0.1	0.4± 0.1	0.03± 0.01	0.3± 0.02	149±10	28±2	50±4	13±1	31±2	19±2	239±14
Pondicherry	0.6± 0.1	0.7± 0.2	0.3± 0.1	0.9± 0.1	260±17	7±2	107±9	14±2	51.3±3	40±4	371±20
Karaikkal	0.4± 0.1	1.1± 0.2	1.1± 0.1	2.6± 0.2	624±32	39±1	34±3	53±3	4.4±2	10±1	224±18
Rameshwaram	0.7± 0.1	10.4± 0.2	0.7± 0.1	0.8± 0.1	270±25	63±4	36±3	18±1	56.6±3	54±5	2406±41
Tuticorin	0.9± 0.1	12.5± 0.3	0.03± 0.01	0.4± 0.02	143±10	1±0.3	65±6	15±1	40.2±2	53±6	1642±28
Kanyakumari	0.1± 0.1	6.6± 0.2	2.7± 0.2	2.7± 0.1	396±22	33±2	18±1	22±2	16.4±1	7±1	580±20
Nagarcoil	0.1± 0.1	6.7± 0.3	0.2± 0.1	0.4± 0.03	70±7	29±2	35±3	14±1	10.5±0.7	15±2	447±19

ESR Spectroscopy Dating of Recently Excavated Archaeological Bone Samples from Kottapuram site using Gamma Irradiation

G. Velraj[1], R. Hemamalini[2], S. Tamilarsu[1], N. Basavaiah[3]

1. *Department of Physics, Periyar University, Salem-11, Tamilnadu, India; E-mail: gvelraj@yahoo.co.uk*
2. *Sri Sarada College for Women (Autonomous), Salem-16, Tamilnadu, India*
3. *Indian Institute of Geomagnetism, New Panvel (W), Navi Mumbai, 410218, India*

The study of radiation defects created in biomaterials such as bones can be used in dating with importance to paleontology and archaeology. Electron Spin Resonance Specroscopy is applied to estimate the age of bones excavated from the archaeological site at kottapuram in Kerala state south India. Gamma irradiated samples were analyzed by ESR spectrometry in order to obtain the growth curve and showed ESR behavior. The age of the bone samples were determined.

Keywords: ESR spectroscopy, gamma irradiation, horse bone.

Introduction

Ancient cultures and societies which leave no written history can be traced back by archaeological studies. Physical and chemical phenomena have been involved in solving archaeological and geological problems and also act as clocks for elapsed time and record it. Natural radiation in the environment produces lattice defects or fills traps in geological and archaeological materials with electrons or holes. The total dose of the natural radiations, termed the archaeological dose (AD), is proportional to the age and may be determined by measuring the concentration of the defects or radicals in the material [1]. Radiation damage occurs in materials as a result of uranium uptake, and external effects. This damage is usually repaired in living tissue, but accumulates in dead tissue. Electron spin resonance (ESR) dating is an absolute dating method suitable for the Quaternary studies which can be applied to a wide range of materials. It is based on determining the natural radiation dose to which a sample has been exposed during its burial period [2]. The ESR measurement is relatively simple, requires a small quantity of material, and this technique has a wide range of age applicability (from a few hundreds to million years) [3]. The amount of material to be dated can be an impediment for the use of others conventional techniques. Response to the introduction of this method to the field of archaeology and anthropology has been favorable since it may date beyond the limit of radiocarbon (~ 50,000 years) [4].

Materials and Method

Three fossil bone samples as goat were collected from archaeological site at Kottapuram in Kerala South India. The samples are obtained from kottapuram in sites at which we can also determine the local annual radiation dose. Enamel is irradiated to different doses using ^{60}Co -rays, and the ESR spectrometer is used to measure the increase in signal with dose, which is plotted as a function of dose. The past dose is estimated from the equivalent dose (D_E), which is given by the dose intercept of the line showing the incremental growth of the signal as a function of dose.

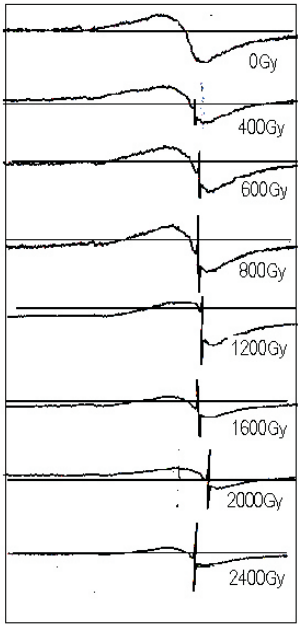


Fig. 1 ESR Spectra for KHB sample

Result and Discussion

A fossil bone is composed of an organic part called "collagen" and an inorganic part called "hydroxyapatite" $Ca_{10}(PO_4)_6(OH)_2$. The signal of CO_2^- produced from CO_3^- impurity ions in hydroxyapatite were used for the ESR dating of fossil bones. Dating using ESR method is analytical tool to explicate recent methods and analysis. It is the best choice to calculate the age of bone sample. The gamma radiation is used to trap the electron from the surface of the bone and on counting the amount of the bone electrons trapped in the bone samples used to calculate the age of fossil samples [5-7]. The fossil bone sample, goat were collected from archaeological site at Kottapuram in Kerala South India and are name as KHB. The esr spectra were recorded for all eight irradiated samples and graphs are shown in Fig. 1.

The samples divided into eight sets and seven are given additive dose (AD) of 400 Gy, 600 Gy,

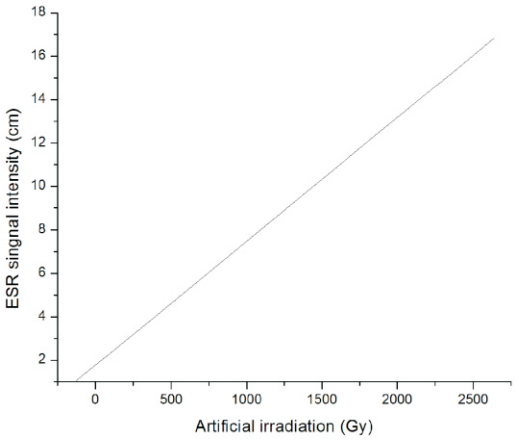


Fig. 2 Artificial dose Vs ESR intensirty of the Sample KHB

800 Gy.1200 Gy, 1600 Gy, 2000 Gy and 2400 Gy respectively. The 0Gy represents the spectra recorded without irradiation and the spectrum was recorded at room temperature for all the eight irradiation sample of KHB and the graphs are shown in Fig. 2. The g values for each irradiated graps are calculated. The average g values

Found to be 1.9868 the graphs are plotted in polynominal fit and alone in linear fit. The intensity values for the samples are given in Table 1. The equivalent dose (ED) for a particular intensity versus the artificial dose plot is towards the negative X-axis. The negative value of the dose is ED of the sample and this value is substitute in this equation.

T_{age}=ED (GY)/D (GY) ka

Table-1: The intensity values for corresponding artificial dose for the KHB sample

Artificial dose(Gy)	Esr.int (cm) khb
0	3.7
400	2.5
600	3.1
800	4.9
1200	7.1
1600	11.3
2000	12.5
2400	16

The values equivalent dose (ED) and dose rate (D) of the archaeological samples constitute the main part of the EPR dating and the ages in years for the bone samples to be found 23 ± 02 Ka years are tabulated in (1.2). The ages obtained by ESR suggest that these bone samples had lived in the upper (tarantian) stage of the Pleistocene epoch[8].

Table-2: The estimated ages of the sample

Sample code	Equivalent Dose (Gy)	Ages in year By ESR	Geological period in Pleistocene epoch
KHB	156.5506	2302.2	Upper (Tarantian) stages

Conclusion

By using spectroscopic techniques such as ESR an attempt has been made to date the archaeological bone collected from archaeological site which are recently excavated in Kerala, India. The obtained results are good agreement with the data. The maximum error in determining the age of the sample in this method is due to the residuals in the extrapolating the graph.

Acknowledgement

The authors acknowledge with thank to DAE-BRNS for funding through major research project.

Reference

[1] Ikeya, M. New Applications of Electron Spin Resonance Dating, Dosimetry and Microscopy, Singapore, World Scientific publication (1993).

[2] Mortin Jonas Concepts and methods of ESR dating, Radiat. Meas., 27 (1977) 943.

[3] L.C. Oliveira, A. Kinoshita1, A.M.F. Barreto, A.M. Figueiredo, J.L. Silva and O. Baffa, ESR dating of teeth from Brazilianmegafauna, Journal of Physics: Conference Series 249 012062 (2010).

[4] Ikeya M., Electron spin resonance as a method of dating: Archaeometry, 20 (1978) 147.

[5] Madras District Gazetter-Sout Arcot district Gazetter, G.Elangovan district Gazetters, Madras record office, Egmore p.167.

[6] Brennan, B.J., McGuirl, E.L., Schwarcz,H.P. and Prestwich, W.V., Beta Doses in Tooth Enamel by "One-Group " Theory and the ROSY ESR Dating software. Radiation meas, 27 (1997) 307.

[7] Ikeya M, Nature 48 (1975) 255.

[8] Rahndhawa, H., "Modern Molecular Spectroscopy", Macmillan India Ltd. (2003) 20-523 .

Preconcentration of Mercury from Aqueous Samples using Modified XAD Resin

Aditi A. Dalvi, K.K. Swain, Trupti Chavan and D.N. Wagh

Analytical Chemistry Division, Bhabha Atomic Research Centre, Trombay, Mumbai 400085, India;
E-mail: aadalvi@barc.gov.in

XAD-4 resin was coated with dithizone in ethylene diammine medium. The modified XAD resin was used for the preconcentration of mercury from aqueous samples by batch method and experimental conditions were optimized for the maximum uptake. The polymeric support was characterized. Energy dispersive X-ray fluorescence spectrometry (EDXRF) was used for the quantification of mercury. Linear calibration was obtained in the concentration range of 0.4 to 20 g L^{-1} for mercury. Interferences of Cu, Pb, Zn, Fe, Ni, Pt, Pd and Au on the sorption of mercury were studied.

Introduction

Mercury is highly toxic element and effects of mercury poisoning include paralysis, blindness or insanity, chromosome damage, birth defects and neurological, gastrointestinal and renal damages. The most common example of acute mercury poisoning is the "Minamata disease" which causes mental disturbance; difWculty in swallowing; loss of balance, speech, sight and hearing; degeneration of brain and finally leading to death [1]. Inorganic mercury has high affinity for the sulfur containing groups of proteins and thereby gets accumulated in the body. Determination of mercury (Hg) in environmental samples including water is essential due to its high toxicity. The World Health Organization (WHO) recommended water quality guidelines of less than 6 g L^{-1} for inorganic mercury [2]. Suitable analytical methodologies are required for accurate determination of mercury at ultra-trace levels in environmental samples. Several analytical techniques [3] have been applied for the determination of mercury, which include atomic absorption spectrometry (AAS), inductively coupled plasma optical emission spectrometry (ICPOES), inductively coupled plasma mass spectrometry (ICPMS) and neutron activation analysis (NAA).

Mercury usually exists in the environmental matrices at ppb (g L^{-1}) level with complex matrix. Therefore, separation and preconcentration methodologies are often required prior to the determination.

Dithizone (1, 5 diphenylthiocarbazone) is an organic colorimetric reagent which is used for the determination of elements like mercury because of its affinity towards the metal. Dithizone anchored polymers have been reported for the separation of mercury [4]. In this work, XAD-4 resin was modified with dithizone and used for preconcentration of mercury from aqueous samples.

Experimental

A 25 mL stock solution (4 g L^{-1}) of mercury (II) was prepared by dissolving 0.1374 g of analytical reagent grade $HgCl_2$ (Merck) in 2 mL concentrated nitric acid diluting with deionized water. A working standard of 400 g L^{-1} was obtained by step wise dilution of the stock solution with deionized water.

Dithizone (Merck) solution (0.03M) was prepared by dissolving appropriate amount in ethylenediammine (Merck).

30 g of XAD-4 resin was weighed and transferred in a beaker containing the dithizone solution. It was kept for 15 minutes with occasional stirring. The color of the resin beads changed from white to brown. The beads were washed thoroughly with deionized water and were stored in water for further use. Dried beads were used for characterization.

For calibration, 4 to 200 ng of mercury in solutions were taken and diluted to 10 mL. The sulphuric acid concentration in the solutions was maintained at 0.05M. Dithizone modified resin beads (~200 mg) were then added and the solutions were equilibrated for 1 h on a mechanical shaker. After equilibration, the resin beads were separated using Whatman 541 filter paper, washed with deionized water and air dried. The air-dried samples were directly analyzed using EDXRF (Jordan Valley, EX-3600 M EDXRF spectrometer at ACD, BARC). A SLP series LEO Si(Li) detector having an active area of 30 mm^2 and 3.5mm thickness was used to measure the intensity of X-rays. The detector has a resolution of 140 eV at 5.9 keV of Mn K X ray. The intensities of fluorescent X-rays were measured using a PC-based 2k channel analyzer and nEXt software. Characteristic L X-rays of Hg (L : 9.98 keV and L : 11.82 keV) were used for quantification of the analyte.

For studying the interferences of various metal ions on the sorption of mercury, elemental standard solutions of Cu, Ni, Cd, Zn, Pb, Fe (10 to 100 mg L^{-1}), Pd, Au (0.5 to 10 mg L^{-1}) and Pt (7 to 70 mg L^{-1}) were added to 10 g L^{-1} of Hg standard solutions and equilibrated with 200 mg of modified resin for 1 hour on a mechanical shaker. Then the resins were separated, washed and dried followed by determination using EDXRF. Synthetic water samples containing 10 g L^{-1} of Hg were also analyzed. A typical EDXRF spectrum

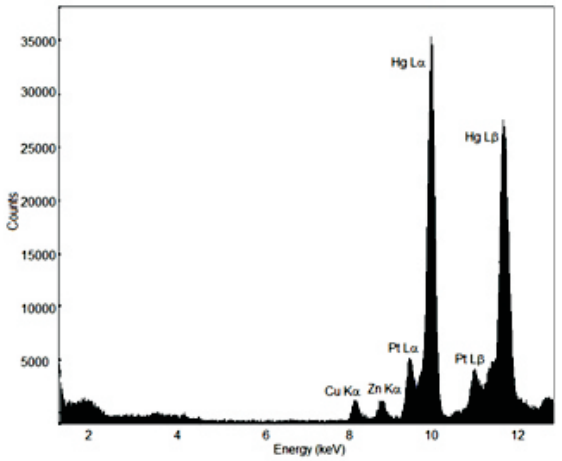


Fig. 1 EDXRF spectrum of mercury (10 g L^{-1}) sorbed on dithizone modified XAD-4 in presence of Cu, Pb, Zn, Fe, Ni, Cd (each 10 mg L^{-1}) , Pt(7 mg L^{-1}) and Au, Pd (each 1 mg L^{-1})

of the modified resin containing mercury after the separation is given in Fig. 1.

Calculations

The concentration of mercury was calculated using comparative method during EDXRF.

Results and Discussion

Dithizone is one of the most popular reagent employed for the spectrophotometric determination of Hg(II) because of its high sensitivity and selectivity. It forms stable complex with Hg(II) under slightly acidic conditions. As the solubilities of dithizone and its mercury complex in water are low, dithizone coated XAD beads are suitable for preconcentration of mercury from water. Preconcentration of mercury on dithizone modified XAD beads was carried out from 0.05M sulfuric acid medium. EDXRF measurements revealed that the response was linear in the concentration range of 0.4 to 20 g L^{-1} for mercury as seen in the calibration plot (Fig. 2).

Detection limit of mercury using this methodology was found to be 0.1 g L^{-1} for aqueous samples which is well below the WHO limit. Recovery

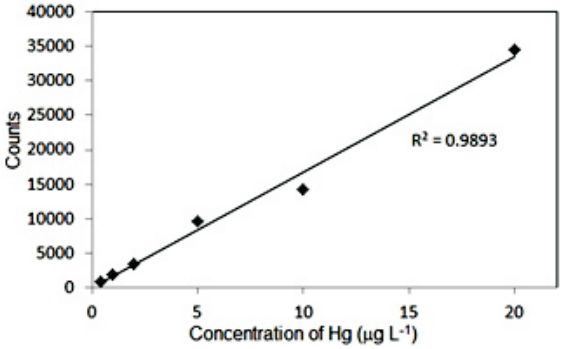


Fig. 2 Calibration graph of mercury using EDXRF

of Hg from synthetic water samples was found to be > 98 %.

Determination as well as recovery of mercury was not affected in the presence of Cu, Pb, Zn, Fe, Ni and Cd. Though Pd and Pt were slightly adsorbed on the resin, they do not interfere in the determination of Hg in the concentration range studied. Gold at concentrations above 1 mg L^{-1} was found to interfere in the EDXRF measurements of Hg (10 g L^{-1}). Such high concentrations of Au, Pt and Pd are rarely found in water samples. Dithizone coated resin beads can therefore be employed for preconcentration and determination of Hg from drinking water as well as other aqueous samples.

Acknowledgement

Authors are thankful to Dr. A. V. R. Reddy, Head, Analytical Chemistry Division and Dr. R. Verma, Head, NAMS, ACD for their suggestions and keen interest.

References

[1] M. J. Ahmed and M. S. Alam, Spectroscopy 17, 45 (2003).

[2] Guideline for drinking water quality, World Health Organization, Geneva, Switzerland, 2nd edn, 1993, vol. 1.

[3] C. Yin, J. Iqbal, H. Hu, B. Liu, L. Zhang, B. Zhu and Y. Du, J Haz Mater 233-234, 207 (2012).

[4] R. Shah and S. Devi, Reactive & Functional Polymers, 31, 9 (1996).

Application of TXRF for Burn Leach Test of TRISO Coated UO_2 particles of CHTR Fuel

Kaushik Sanyal, S. Sanjay Kumar, Sangita Dhara, N.L. Misra, Rajesh V. Pai, N. Kumar, S.K. Mukerjee and S.K. Aggarwal

Fuel Chemistry Division, Bhabha Atomic Research Centre, Trombay, Mumbai 400085, India;
E-mail: nlmisra@barc.gov.in

A simple TXRF method to assess the quality of SiC coating in UO_2 tristructural isotropic (TRISO) coated particles was developed. The method consists of heating the TRISO coated particles at 850°C for about 96 hours to constant weight and then boiling the residue obtained in suprapure concentrated nitric acid for about one hour. Presence of any uranium in the supernatant nitric acid is indicative of cracked SiC layers. No uranium could be found in the supernatant suprapure nitric acid, analysed by TXRF, used for such burn leach test in our experiment using UO_2 TRISO coated particles prepared in BARC. The study indicates that the coated particles have strong SiC coating free from any cracks.

Introduction

In order to utilize its vast thorium resources and to provide electricity in remote areas, India proposes to utilize Compact High Temperature Reactors (CHTRs). These reactors are proposed to be ^{233}Uranium-thorium fuel based reactors to be operated in remote areas not connected to electrical grid. In addition, these reactors would provide process heat of 1000°C temperature which will facilitate production of hydrogen by water splitting process [1,2]. The CHTR fuel is based on Tri-isotropic (TRISO) coated particle consisting of ^{233}U-Th core, coated with low density pyrolytic carbon, inner high density pyrolytic carbon, silicon carbide interlayer and outer high density pyrolytic carbon. TRISO coated particle can withstand high temperature (1600°C). SiC layer in the fuel particles of these reactors is very important as it serves as cladding of the fuel and containment for the fission products. It should be free from any cracks. One of the essential characterization techniques for quality assurance of the SiC layer is burn leach test. In this test, the coated particles are burnt in air down to SiC layer until the weight remains constant. The residual ash and particles are treated with nitric acid at 100°C. If any uranium is found in the acid solution, it is due to defective SiC layer. Analysis of this solution with TXRF can give an idea of the quality of SiC layer in coated particles with minimum amount of the sample as TXRF is multielemental analytical technique for trace element analysis requiring samples in ng level [3,4]. This shall be beneficial in terms of waste management as well as in terms of radiation dose to the operator when this test shall be made using ^{233}U based fuel [5]. The present study was conducted to assess the quality of Triso coated UO_2 particles having natural uranium and prepared in BARC.

Experimental

Sample Preparation

About 100 mg of TRISO coated natural UO_2 particles prepared using fuel coating facility at BARC were calcined at 850°C for 96 hrs inside a furnace to constant weight. For leaching studies, 10 mL of Conc. Suprapure HNO_3 was taken in a cleaned quartz beaker and 60 mg of the calcined particles were put in the beaker. The beaker was heated on a water bath for 1 hr on a hot plate. An aliquot of 1 mL was taken from this (heated and then cooled), nitric acid and an internal standard (Ga, 10 g/mL) was added to this solution. For blank measurements nitric acid was boiled without any coated particle and Ga internal standard was mixed in similar way. These solutions were used for TXRF measurements after depositing 10 L of the sample on quartz TXRF sample supports.

Instrumentation

An ITAL Structures TXRF spectrometer TX 2000 having Mo K as excitation source was used for TXRF measurements. The X-ray generator was operated at 40 kV and 20 mA. A W-C multilayer was used for getting the monochromatic X-rays. The instrument is equipped to measure twelve samples sequentially. The X-rays were detected and measured using a Si(Li) detector having a resolution of 139 eV (FWHM) at Mn K (5.9 keV). For TXRF measurements, a live time of 1000s was used.

Results and Discussion

For Burn Leach Test, TXRF has an advantage that the consumption of the sample for such study shall be very less as TXRF measurements require samples in microlitres (10-50 L) with detection limits of the elements in ng/mL level. For this study, natural uranium coated particles prepared at BARC, Mumbai were used. The TRISO coated particles were heated to 850°C in air atmosphere for 96 hours so that the outer pyrolytic carbon layer is burnt off and SiC layer is exposed. The weight loss observed was 6.9%. A part of these calcined particles (about 36 number containing 32.26 mg of uranium) was immersed in 10 mL of suprapure nitric acid in a clean beaker and heated on a water bath for one hour. The volume reduction if any was made up with nitric acid. Finally 1 mL of the nitric acid was taken out

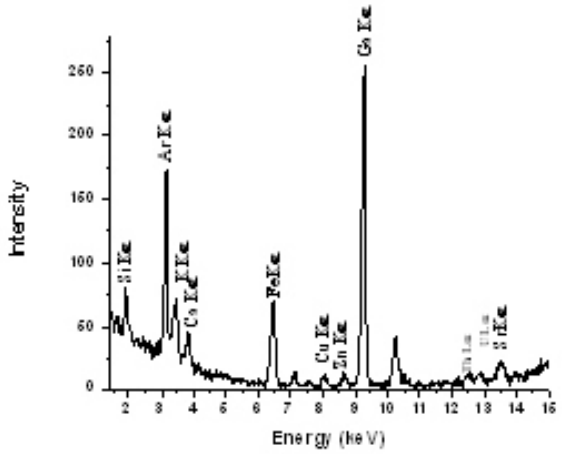


Fig.1 TXRF spectrum of nitric acid obtained after heating TRISO-coated UO_2 particles immersed in it

and mixed with 100 microlitres of Ga internal standard solution having 10 g/mL Ga concentration. An aliquot of 30 L was deposited on quartz TXRF sample supports and the TXRF spectra recorded using a live time of 1000 s. The TXRF spectrum of this specimen is shown in Fig. 1. The concentration of uranium in this nitric acid, determined by TXRF, was found to be equal to the blank value (30 ng/mL) as ultra trace levels of uranium and thorium are always present in suprapure nitric acid. If SiC layer of any of the coated particles would have cracked, it would have given appreciable uranium concentration in the supernatant nitric acid after heating with it due to diffusion of concentrated nitric acid to the uranium oxide particles and its dissolution. This uranium would have been certainly detected by TXRF as its detection limits for uranium are in ng/mL level [4]. The observation that no uranium is being leached in nitric acid from the UO_2 TRISO-coated particles indicates that the SiC layer is defect free.

Conclusion

TXRF could be successfully applied for burn leach test of TRISO-coated UO_2 particles to detect the integrity of SiC layer. The method when extended to ^{233}U based fuel shall be beneficial with respect to requirement of small amount of sample and thereby production of less radioactive waste as well as low radiation dose to the analyst. In addition, this method is fast and can detect other impurities simultaneously.

Acknowledgements

The authors are thankful to Shri Arun Kumar, Director, Nuclear Fuels Group, BARC and Dr. D. Sathiyamoorthy, ex-Head Powder Metallurgy Division BARC and their colleagues for their invaluable support for this work.

References

[1] Compact High Temperature Reactor (CHTR), I.V. Dulera, A. Basak, P.P. Kelkar and R.K. Sinha Reactor Engineering Division, Bhabha Atomic Research Centre www.barc.gov.in/publications/nl/2006/200610-22.pdf

[2] High temperature reactors, I.V. Dulera, R.K. Sinha, J. Nucl. Mater. 383 (2008) 183.

[3] R. Klockenkaemper, Total Reflection X-ray Fluorescence Analysis, Chemical Analysis Vol.140, John Wiley & Sons, New York (1996).

[4] Total reflection X-ray fluorescence and energy-dispersive X-ray fluorescence characterizations of nuclear materials, N. L. Misra, Pramana- 76 (2011) 201.

[5] An EDXRF method for determination of uranium and thorium in AHWR fuel after dissolution, Sangita Dhara, S. Sanjay Kumar, N.L. Misra and Suresh K. Aggarwal, X-ray Spectrom. 38 (2009) 112-116.

Non-Destructive EDXRF Determination of Sulphur in Ore Samples

Buddhadev Kanrar[1], S. Sanjay Kumar[1], N.L. Misra[1], S. Mondal[2], A. K. Singh[2], R. C. Hubli[2] and S.K. Aggarwal[1]

1. *Fuel Chemistry Division, Bhabha Atomic Research Centre, Trombay, Mumbai 400085, India; E-mail: nlmisra@barc.gov.in, nlmisra@yahoo.com*
2. *Materials Processing Division, Bhabha Atomic Research Centre, Trombay, Mumbai 400085, India*

A non-destructive method for determination of sulphur in solid samples has been developed. The method consists of making thin specimens of solid samples using their paste with collodion on Mylar films, drying them and measuring their EDXRF spectra. A calibration plot was made by plotting intensity ratio of S K and scattered excitation source intensity against % S in solid samples. Determinations of sulphur in solid samples were made by recording their EDXRF spectra in similar way and using this calibration plot. The method was tested using the certified standards with different thickness. Later the method was extended to analyse sulphur in some processed ore samples with satisfactory results.

Introduction

Sulphur is present as pyrite in different ore samples. During metal recovery from ores it gets oxidised. The kinetics and mechanisms of pyrite oxidation are important in order to understand and control the reactions in ore processing [1]. When Pyrite is present in uranium ore, it gets dissolved during alkaline leaching of uranium used for uranium metallurgical process. This dissolution of pyrite increases the temperature of the solution and dissolves some undesirable materials also in the alkaline leachants. These undesired materials hinder the recovery of uranium from the ore. In addition, some uranium is adsorbed with the pyrite ore making recovery of uranium difficult. In order to know at which stage of uranium recovery, using alkaline leach method, pyrite dissolution takes place, it is essential to know sulphur content in the residue left at different stages of such leaching [1]. This shall be beneficial in adopting an efficient method for uranium recovery. Though EDXRF can be used for such determinations [2,3], it requires matrix matched standards which are rarely available. However, if a thin sample specimen of such residue can be made, the sulphur can be determined easily as this specimen shall be free from the matrix effect. Even if some matrix effect is present in this specimen, it can be counterchecked by making a slightly thick specimen and using a calibration plot between intensity ratio of S K and exciting scattered radiation against the sulphur percentage. Since S K analytical line energy is low (2.31 keV), it shall see mainly absorption effect while coming out from a specimen and this absorption effect can be counterchecked by making a calibration plot between intensity ratio of S K and exciting scattered radiation against the sulphur percentage as the scattered exciting radiation shall also undergo only absorption effect. Using this assumption, a study to develop EDXRF method for sulphur determination in solid samples was taken up.

Experimental

Sample Preparation

For making calibration plots, three "Geostats, Asutralia" ore standards containing 0.5, 1 and 2% of Sulphur and a blank sample were used. About 100 mg of finely ground solid standards were mixed with collodion solution to make uniform pastes in separate cleaned pestle mortars. Thin film specimens of the pastes were made on 4 micron thin Mylar films stretched uniformly over PVC rings with the help of pestles. These films were dried and presented for XRF measurements.

Instrumentation

For EDXRF measurements, a Jordan Valley EX-3600TEC EDXRF spectrometer having Rh target was used. The instrument is equipped with a ten position sample chamber and can measure ten samples sequentially. There is a provision of different filters to reduce the background in a particular energy region and also secondary targets to excite certain elemental X-ray lines efficiently. The tube was operated at 20 kV and 2000 A. In order to excite S K efficiently and reduce the background, a Ge secondary target was used. All measurements were made in air atmosphere.

Results and Discussion

The EDXRF spectrum of a standard sample specimen containing 2% S is shown in Fig.1. The detection limit calculated using this spectrum was found to be 0.3%. The intensity of S K X-ray line in EDXRF spectrum of the specimen prepared for 0.5% of S was negligible and hence this was not used for calibration. For making the calibration plot, the intensity ratio of S K and Ge K line was plotted against S % in the standards and this was linear as shown in Fig. 2. Another set of similar specimens of these standards with varying amounts of sample film were made in similar way and their EDXRF spectra were measured in similar way. These specimens were analysed using the above calibration plot and the results obtained are shown in Table 1.

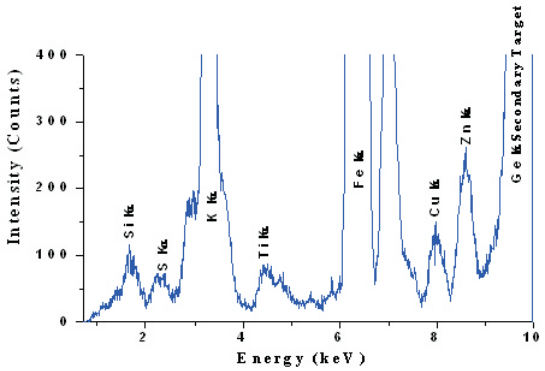


Fig. 1 EDXRF spectrum of the ore sample

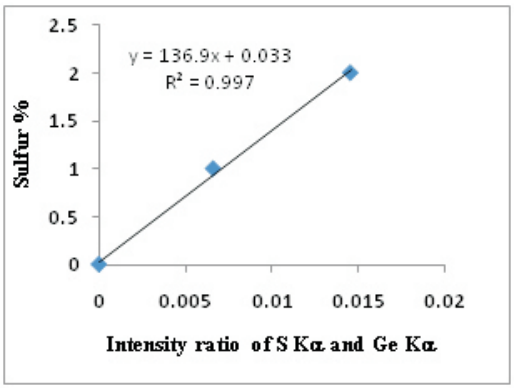


Fig. 2 Calibration plot obtained for sulphur determination

Table-1: Certified and EDXRF determined sulphur concentrations in ore standards

Standard	Certified S % ± 1	EDXRF determined S ± 1	EDXRF / Certified
GS305-10	0.51 ± 0.04	Not detected	-
GS302-3	1.03 ± 0.09	1.10 ± 0.05	1.07
GS307-3	1.98 ± 0.10	1.9 ± 0.1	0.96

The deviation of EDXRF determined sulphur concentrations from the certified values was below 7% and the relative standard deviation was below 5% (1 ,n=3). This good agreement in EDXRF determined sulphur concentrations and certified values despite different sample thickness shows the effectiveness of this method for sulphur analysis in ore samples. Later the method was extended to some processed ore samples at different stages of processing and the results are shown in Table 2.

Conclusion

A non-destructive method for sulphur determination in solid samples was developed. The method involves making a calibration plot by plotting intensity ratio of S K and exciting scattered radiation (in this case Ge K) against the sulphur % in the standards. The method gives satisfactory results for the analysis of sulphur in ore standards containing sulphur as well as ore samples. The detection limit can be further improved using monochromatic high intensity excitation source. A comparison of analytical results using some other technique shall be useful in counterchecking the EDXRF analysis results.

References

[1] Cláudia Lima Caldeira, PhD thesis entitled "Investigation of pyrite oxidation in alkaline solutions by thermodynamic modeling and analyses by X–ray diffraction, infrared and Raman spectroscopy", UNIVERSIDADE FEDERAL DE MINAS GERAIS, France (2005).

[2] R.E. Van Griken and A. Markowicz, Handbook of X-ray spectrometry, Marcel and Dekker Inc. 1993.

[3] N.L. Misra and S.K. Aggarwal, Spectrochim. Acta Part – B 63 (2008) 1395.

Table-2: EDXRF determined concentration of sulphur

Sample*	Leaching Stage	EDXRF determined Sulphur %	Standard Deviation (1)	Relative Standard Deviation (%)
Feed	Ground ore	0.64	0.05	7.4
1T1	Before reaching temperature and pressure	0.7	0.1	14.1
2T1	Before reaching temperature and pressure	0.7	0.1	19.1
1T9	6hrs of leaching, 4kg/cm^2 O_2 pressure,130^{0}C	0.72	0.05	6.5
2T9	6hrs of leaching, 6kg/cm^2 O_2 pressure,130^{0}C	0.47	0.07	15.4
3T9	6hrs of leaching, 10kg/cm^2 O_2 pressure,130^{0}C	0.5	0.1	22.5

Radiation Effects on Graphene Overlayer on SiO_2 as Probed by Positron Spectroscopy

S. Mukherjee, S.K. Sharma, P. Maheshwari, P.K. Pujari

Radiochemistry Division, Bhabha Atomic Research Centre, Trombay, Mumbai 400085, India;
E-mail: pujari@barc.gov.in

Alpha radiation damage of graphene layers on SiO_2/Si substrate has been studied using positron and Raman spectroscopy. Graphene was transferred on the oxide layer via dip casting method. Radiation damage has been mostly in the surface and the SiO_2 layer even though the range of alpha in Si is ~ micro meter. Positron data can clearly separate the damage in graphene, SiO_2 and the SiO_2-Si interface. The damage in graphene layer shows a linear relationship with alpha fluence suggesting that the graphene/SiO_2/Si system can be used to monitor low level radiation.

Introduction

Graphene has been described as the material for next generation field effect transistors and various nanosensors [1] A novel application will be for radiation detection of alpha particles replacing the conventional proportional counter devices which have limited application for online radiation detection of radiation. Since such applications are in environments with intense radiation, it is important to understand the change in device properties with radiation damage. Various damages, leading to radiation hardening can significantly alter device performance. Here we have probed the damage caused by alpha particles in the surface and near-surface region of graphene-SiO_2-Si multi-layer, which is the building block of graphene based devices. Such devices can be installed at critical locations like fuel reprocessing or waste management plants where any accidental leak can be detected at early stages.

Experimental

Large-area graphene layers were synthesized by Chemical vapor deposition of methane gas on Cu foils at 1000°C and following the Cu etch, were transferred onto the SiO_2/Si substrate and dried in an oven at 60°C. Radiation was carried out using a ^{241}Am source which is incorporated into the surface of an anodized Al foil of 0.3 mm thickness. The source emits 331 alpha particles per second in the forward hemisphere. Samples were placed at varying distance and varying time from the source to obtain different exposure (Table 1). The radiation conditions are described in detail in Ref 2.

Table-1: Alpha irradiation condition for different graphene/Sio2/Si samples. The range of alpha particles from ^{241}Am source is ~50 mm in air [2]

Sample	Distance (mm)	Time (h)
1	10	1
2	20	1
3	50	1
4	10	2
5	10	4

Depth dependent Doppler broadening of annihilation radiation (DBAR) have been carried out on graphene samples using a monoenergetic positron beam of ~ 200 eV. The positron implantation energy was varied by biasing the sample increasing more negative. The resultant gamma spectrum was recorded using high purity Ge detector of 1.2 keV resolution at 514 keV. The monitoring parameter here is called "S-parameter" which is defined by the ratio of area of central region (510.3-511.7 keV) to the total peak area (508- 514 keV). The positron implantation depth (d) in nm can be related to the positron energy (E, keV) by, $d \frac{40}{} E^{1.6}$, where is the material density in gm/cc.

Thus one can tune the positron beam energy to specifically probe surface, near surface or buried interfaces. To elucidate the number of graphene layers and extent of damage by alpha particles, Raman spectra for the samples have been carried out using 532 nm line. The number of layers in graphene sheet has been measured using the 2D peak at the wavelength of 2680 cm^{-1}. The damage of the graphene layer was monitored using the ratio of the D peak (1340 cm^{-1}) and the G peak (1570 cm^{-1})[3] .

Result and Discussion

The 2D Raman peak was used to ascertain the number of graphene layers [3]. Based on the Gaussian fit, all the samples contain less than 2 graphene layers. It was further confirmed by the ratio of I(G, ~1570 cm-1)/I(2D) being in the range of 0.2-0.32 suggesting that the samples contain single graphene layer.

The change in S- parameter ($S= S_{sample}-S_{3rdsample}$) is shown in Fig. 2 and is compared to the Raman data as well. The change is S-parameter is highest in the surface region, corresponding to positron energy range 0- 1.5 keV. The SiO_2-Si region corresponds to positron energy 3 keV – 6 keV. As can be seen from the positron data, we can separate out the damages to the graphene and the buried SiO_2-Si interface. The ratio I(D)/I(G), based on the D and G peak area from the Raman spectrum, is indicative of the damage in the sample and is plotted as function of time/distance^2 (Fig. 2). In this plot the abscissa is proportional to the dose of alpha

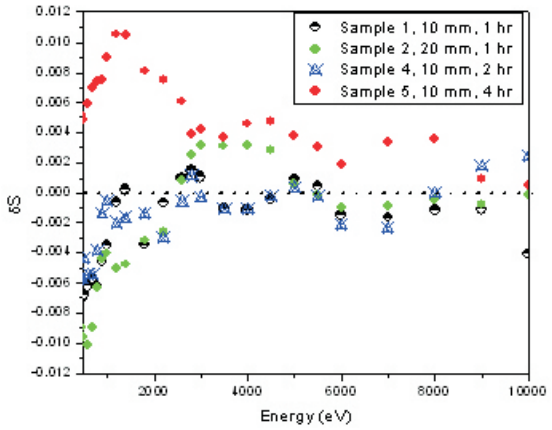


Fig. 1 *The change in S parameter (S = Ssample-$S_{3rdsample}$). Significant changes in S at lower positron energy (< 3 keV) corresponding to low implantation depth is observed*

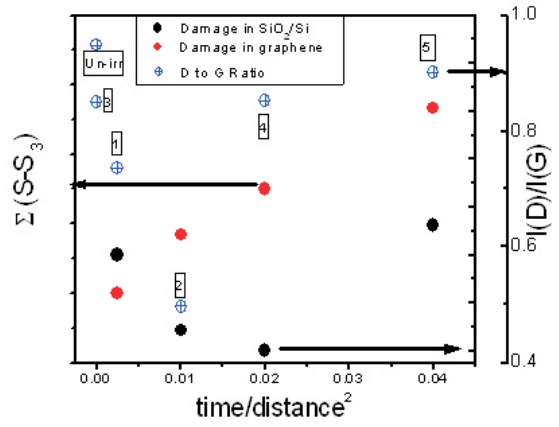


Fig. 2 *The aggregate $S_{E_1}^{E_2}$ S S_3 is shown with E_1= 0(3) keV and E_2 = 1.5(6) keV corresponding to damage in graphene (SiO_2/Si). The I(D)/I(G) from the Raman data does not show marked variation with the alpha fluence. For comparison with Table1, the sample numbers are marked next to the Raman data. The ratio for an unirradiated sample is shown as well*

particle. The damage for sample 3 as well as an unirradiated sample is shown as well. It is to be pointed that, for Sample 3, the alpha particle range in air is less than the source-sample distance [2]. As can be clearly seen, the variation is not related to the fluence, since the I(D)/I(G) for highest dose (Sample 5) is similar to the unirradiated samples (Sample 3). We think the variation is more due to the damage introduced while synthesizing the graphene layer or while transferring it. No change in the Raman peak corresponding to silicon was observed either when compared to the unirradiated ones.

Conclusion

Alpha particle induced damage in graphene-SiO_2-Si system has been analyzed using depth dependent Doppler broadening of annihilation radiation and Raman spectroscopy. With the positron data, we can separate out the damage to the graphene layer as well as the SiO_2-Si interface. On the other hand, Raman data shows no systematic variation with the alpha fluence.

Ackowledement

We would like to acknowledge V. K. Manchanda and Atul Kulkarni for providing the samples.

References

[1] Isaac Childres, Luis A. Jauregui, Michael Foxe, Jifa Tian, Romaneh Jalilian, Igor Jovanovic and Yong P. Chen, Appl. Phys. Lett. 97(2010), 173109

[2] Pranav M. Joshirao, Jae Won Shin, Chirag K Vyas, Atul D. Kulkarni, Hojoong Kim, Taesung Kim, Seung-Woo Hong, Vijay K. Manchanda, Appl Radiat Isot. 81(2013),184.

[3] A. C. Ferrari1, J. C. Meyer, V. Scardaci, C. Casiraghi, M. Lazzeri, F. Mauri, S. Piscanec, D. Jiang, K. S. Novoselov, S. Roth, and A. K. Geim, Phys. Rev. Lett. 97 (2006), 187401

EDXRF Analysis of Medicinal Plants and Spices Grown in the Vicinity of Zinc Smelter

S. Sarkar[1], S.S. Ram[2], M. Sudarshan[2], R.K. Dutta[1]

1. *Department of Chemistry, Indian Institute of Technology Roorkee, Roorkee 247667, India; E-mail: duttafcy@iitr.ernet.in*
2. *UGC-DAE Consortium for Scientific Research, Kolkata Centre, LB-8, Sector- III, Bidhannagar, Kolkata 700091, India*

Energy dispersive X-ray fluorescence spectrometry was used for analyzing P, S, K, Ca, Mn, Fe, Cu, Zn and Sr in soil medicinal plants and spices grown near zinc smelter site in Rajasthan, India. The mobility of these elements from soil to plant species was studied by determining their bioaccumulation factors. The zinc level was measured as 628±34 g g^{-1} in neem leaves, 34±3 g g^{-1} in aloe vera, 120±8 g g^{-1} in mustard seeds and 63±5 g g^{-1} in fenugreek. Methodology is being developed to study physiological gastrointestinal digestion based bioaccessibility of Zn and other elements by EDXRF.

Introduction

Medicinal plants and spices are routinely used in India, China, Arab and Europe due to their traditional culture and knowledge about the herbs and spices, and are considered to be important sources of essential micronutrients for proper functioning of human body. However industrialization and more importantly, improper waste management policies could lead to contamination of air, water and soil around the industrial site. The inorganic contaminates like heavy metals might be accumulated in plants and plant products grown around industrial sites, which subsequently pose threat to human health via food chain. Smelters around the world are identified as one of the contributors of environmental pollutions. Un-planned waste discharge from smelters could affect physic-chemical properties of soil and contaminate soil with abnormally high concentrations of heavy metals [1]. This induces bioaccumulation of heavy metals in plants and plant products [2].

Here we present elemental analysis of soil, medicinal plants (Neem and Aloe vera), and spices (Mustard seeds and Fenugreek seeds) grown in the vicinity of a zinc smelter in Rajasthan. Elemental analyses were performed by energy dispersive X-ray fluorescence spectrometry (EDXRF). Elemental concentration is not a suitable indicator to assess the adversary health effects of heavy metal contaminated food samples. Bioavailability or bioaccessibility, which is the fraction of a metal leached from food materials during gastrointestinal digestion, is accounted as a better parameter to assess the impact of metal contents in food samples on human health via circulatory system [3]. We are developing a methodology for analyzing physiological gastrointestinal digestion based metal bioaccessibility by EDXRF.

Experimental

Leaves of Neem, stems of Aloe vera, Mustard and Fenugreek seeds, and soil samples were collected from eight different locations in a village named Birchi in Rajasthan (India) which is 0.5 km from a zinc smelter. All samples (except soil) were washed repeatedly with de-ionized water (Millipore) to removed dust particles and were packed and labeled separately (including soil samples) in pre-cleaned polythene bags brought to the laboratory. All samples were oven dried at 40 ^{o}C for 3 – 5 days, crushed, powdered in agate mortar and sieved through 100 m mesh. Elemental analysis of the pelletized samples and certified reference material (Peach leaves: NIST, SRM-1547) was performed using Jordan Valley Ex-3600 Energy dispersive X-ray fluorescence (EDXRF) spectrometer, which featured oil-cooled Rh anode X-ray tube. The characteristic X-ray peaks were detected using Si(Li) detector of resolution 150 eV at 5.9 keV, and analyzed quantitatively by the ExWIN software integrated with the system [4].

Results and Discussion

The EDXRF measurements of NIST standard Peach leaves (SRM-1547) were in good agreement with the certified values (Table 1). The concentrations of the elements measured in the NIST standard esturine sediment (SRM 1646a) were also in close agreement with the certified values, thus establishing the validation of EDXRF analysis of plants materials and soil samples. A typical EDXRF spectrum of Neem leaves from smelter site is given in Fig 1a and 1b. The concentrations of major elements namely P, S, K, Ca were within normal levels with respect to plant based food materials. Among trace elements, Mn content was 2-3 folds higher in the mustard seeds (110±8 g g^{-1}) compared to the other samples. The Zn level was abnormally high (628±34 g g^{-1}) in Neem leaves. The Zn levels were also high in Mustard (120±8 g g^{-1}) and Fenugreek (63±5 g g^{-1}). Such high concentrations of Zn in these samples were attributable to very high Zn levels in the soil samples 1236±86 g g^{-1}. Notably, the concentrations of trace elements (especially Fe and Zn) and sulphur in Aloe vera were significantly lower than the other samples, which were attributed to poor bioaccumulation factors of these elements in Aloe vera.

Table-1: EDXRF measurement of NIST Peach leaves (SRM-1547), given as mean ±2 standard deviation (g g^{-1} unless % is specified, n =3)

	Experimental	Certified
P	1295 ± 86	1370±70
S	1910 ± 94	(2000)
K (%)	2.32 ± 0.12	2.43±0.03
Ca (%)	1.49± 0.09	1.56±0.02
Mn	91 ± 14	98±3
Fe	202 ± 32	218±14
Cu	3.4 ± 0.6	3.7±0.4
Zn	17.1 ± 1.4	17.9±0.4
Sr	48 ± 10	53±4

( ) information only

Table-2: Elemental concentration of dried samples from Zn smelter measured by EDXRF, given as mean ± standard deviation (g g^{-1} unless % is specified, n =3)

	Neem	Aloe vera	Mustard	Fenugreek
P (%)	0.08±0.02	0.14±0.02	0.25±0.03	0.36±0.08
S (%)	0.19±0.06	0.04±0.01	0.59±0.05	0.38±0.08
K (%)	1.12±0.10	1.82±0.12	2.02±0.11	1.92±0.14
Ca(%)	2.13±0.24	1.58±0.10	1.93±0.09	0.96±0.08
Mn	24±3	28±3	110±8	39±3
Fe	218±16	76±6	213±15	140±12
Cu	12±4	ND	8±3	9±3
Zn	628±34	34±3	120±8	63±5
Sr	448±28	166±14	290±18	96±9

ND: not detected

Acknowledgement

This work has been carried out under the BRNS project 2011/37C/37/BRNS and authors thank BRNS for the support.

References

[1] A.G. Kachenko, B. Singh, Water, Air, and Soil Pollution 169 (2006) 101

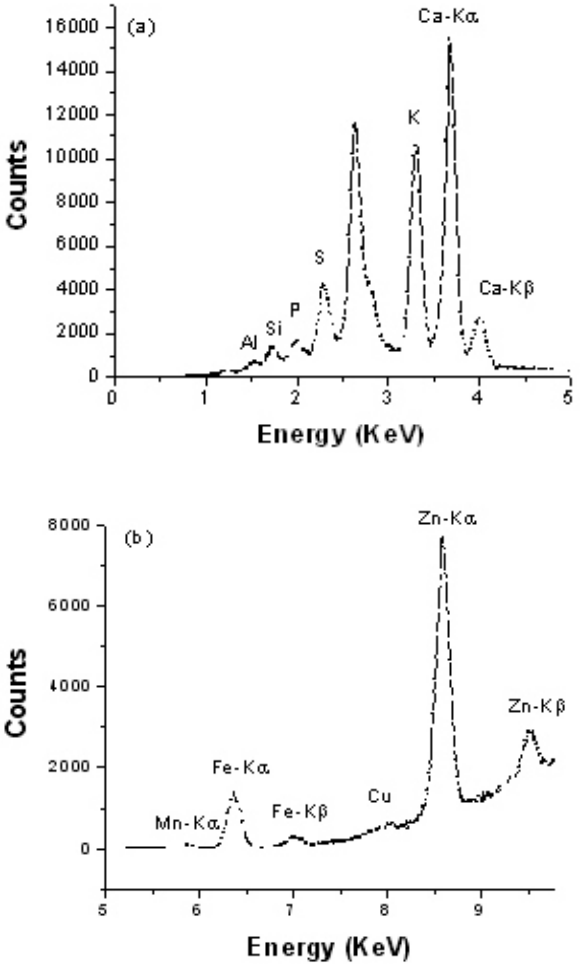


Fig. 1 Typical EDXRF spectrum of Neem leaves from smelter site

[2] M. Intawongse, J.R. Dean, Trac-Trend Anal. Chem. 25 (2006) 876

[3] R.S. Maharia, R.K. Dutta, R. Acharya, A.V.R. Reddy, J. Environ. Sci. Heal. B. 45 (2010) 174

[4] S. Majumdar, S.S. Ram, N.K. Jana, S. Santra, A.Chakraborty, M. Sudarsan, X-ray Spectrom. 38 (2009) 469

ED-XRF Analysis of Ancient Potteries of Vellore Dist, Tamilnadu, India with Statistical Approach

R. Ravisankar[1], A. Naseerutheen[2]. G.Raja Annamalai[3], A.Chandrasekaran[4], K.V.Kanagasabapathy[5], M.V.R. Prasad[5], K.K. Satpathy[5]

1. *Post Graduate and Research Department of Physics, Government Arts College, Tiruvanamalai 606 601, India; E-mail: ravisankarphysics@gmail.com*
2. *Department of Physics, C.Abdul Hakeem College, Melvisharam 632 509, Tamilnadu, India*
3. *Department of Physics, Shri Krishnaa College of Engineering Technology, Mannadipet,Puducherry-605501, India*
4. *Department of Physics, Global Institute of Engineering & Technology, Vellore 632 509, Tamilnadu, India.*
5. *Environment and Safety Division, RSEG, EIRSG, Indira Gandhi Centre for Atomic Research, Kalpakkam 603 102, India*

Energy dispersive X-ray fluorescence (EDXRF) was used to determine the major and trace element composition of ancient potteries recovered in and around Arcot, City, Vellore Dist, Tamilnadu. Fourteen chemical elements were determined. From the analysis, it was found that pottery samples were non-calcareous and also low refractory in nature. Multivariate statistical analysis on the results indicated similarities and correlation between the samples based on their elemental composition. The methodology successfully distinguished the samples where five chemical groups were discerned.

Introduction

Potteries are among the oldest and most significant technological innovations in the history of human achievement, and first truly synthetic material. Chemical analysis and technical examination of art works play an essential role in providing historical, artistic and technical information. Among the various analytical methods employed in artworks studies, X-ray fluorescence spectrometry has been widely used since the 1960s. In this work, fourteen chemical elements have been detected in ancient pottery recovered from the Vellore dist, Tamilnadu using the EDXRF technique. The obtained data is processed by factor analysis to identify the grouping between the potteries.

Materials and Methods

Sample Collection

Ten potsherds were recovered from the ancient settlement in and around Vellore dist. Fig. 1 shows the collected pottery samples. The samples were taken at depth from soil surface to about 6m. After removal of the surface deposit, pottery samples were ground into a fine powder using an agate motor. All powdered samples were dried at 110°C for 24 hrs and stored in desiccators until they were measured.

ED-XRF Technique

One gram of the fine ground sample and 0.5g of the boric acid (H_3PO_3) were mixed. The mixture was thoroughly ground and pressed to firm a pellet of 25 mm diameter using a hydraulic press. The prepared samples were analyzed using the EDXRF available at Environment and Safety Division, RSEG, EIRSG, Indira Gandhi Centre for Atomic Research, Kalpakkam,Tamilnadu.



Fig. 1 Shows the collected ancient potteries of Vellore dist

The instrument used for this study was a PW 4025 Minipal supplied by M/s Philips, Netherlands. The standard stream sediment (GBW 7305) was used as reference material for standardizing the instrument.

Results and Discussion

ED-XRF Analysis

The chemical analysis of ten analyzed potsherds (MP, PP, TM, KV, AT, VM, KP, APM, and WH & UD) is shown in Table 1. Si, Al, Ca, Fe, K and Ti were traced in abundance where as Cu, Zn, Pb, La, Co, V, Cd and Cr was founded to be minor constituents. The nature of clay minerals whether they are calcareous or non calcareous can be identified from the percentage of Calcium Oxide (CaO) in the clay. According to Maniatis [1] the clays that contain more than 6% of CaO, are known as Calcareous clays and less than 6% CaO are known as non-Calcareous clays. If the fluxes concentration (K_2O, Fe_2O_3, CaO, MgO and TiO_2) are more than 9%, the clays are classified as low refractory and classified as high refractory if the fluxes in the sample are less than 9%.

In our analysis, the CaO was less than 6% in all the samples which showed that the clays were non-Calcareous and the fluxes concentration were

Table-1: Elemental composition of ancient potteries of Vellore dist

Sample ID	MP	PP	TM	KV	AT	VM	KP	PM	WH	UD
SiO_2	37.4	41.9	43	39.4	35.08	39.4	38.3	38.9	42.4	37.9
Al_2O_3	6.61	7.75	7.18	6.24	7.54	6.8	6.42	7.37	6.99	8.31
*CaO	1.54	2.24	1.54	1.24	1.48	1.24	1.82	1.4	2.38	1.24
Fe_2O_3	5.15	6.43	6.72	5.44	5.58	5.44	6	7.15	6.58	6.72
K_2O	0.94	1.2	1.81	1.33	1.57	1.69	1.45	2.05	2.17	2.77
TiO_2	0.47	0.83	0.47	0.83	0.47	0.7	0.48	0.58	0.5	0.58
Cu	38.2	52.7	69.16	84.9	42.03	83	53.5	65.7	54.3	41.9
Zn	131	131	131.2	153	152.93	141	127	107	127	139
Pb	19.8	25.1	21.29	21.8	18.75	19.2	25.6	24.4	23	22.5
La	23.4	25.4	24.34	33.5	28.09	31.7	24	24.8	22.3	22.1
Co	15.5	21.7	22.27	31.2	18.5	30.4	20	24.4	21.1	21.5
V	35.7	34.8	39.02	699	44.87	44.8	24.2	96.3	53.5	45.6
Cd	0.21	0.41	0.43	0.71	0.58	0.55	0.49	0.77	0.53	1.09
Cr	88.1	95.6	98.7	107	91.5	106	93.5	91.2	84.6	91

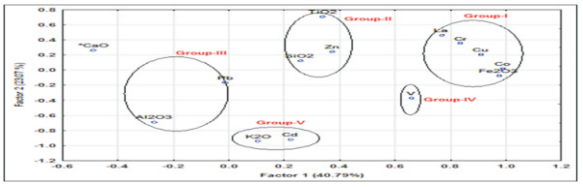


Fig. 2 Shows the factor-1 Vs factor-2

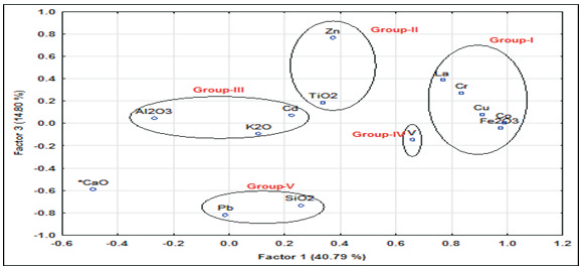


Fig. 3 Shows the factor-1 Vs factor-3

greater than 9% indicating that the clays were low refractory in nature

Statistical Analysis

PCA was performed using the software STATISTICA (version10.0).Table 2 shows the factor loading for the three extracted factors. The three factors extracted in this study explain 78.67% of the total variance of the data set [2]. From the factor analysis, the ten potsherds are classified into five groups. Figures 2 and 3 present plots of factor score 1 against factor scores 2 and 3, respectively. Group-I (MP, UD, PP, KP, TM) consisted of five potsherds which were characterized by positive values of Factor-1 and Factor-2 taking into account a more relevant contribution of Fe_2O_3, Co, Cu and La in the factor loadings. Group-II(WH) had moderate contribution of Zn, TiO_2 and SiO_2 and which were most likely to be made of local clay in South India. Group-III (AT) characterized by positive values of Factor-3 which had high concentration of Cd, K_2O and Al_2O_3. Hence, these potteries were made from slightly different local clay. Group-IV (VM,KV) and V (PM) is characterized by concentration of V and Pb respectively.

Table-2: Factor Loading Matrix for the samples

Element	Factor-1	Factor-2	Factor-3
SiO_2	0.2569	0.1268	-0.7319
Al_2O_3	-0.2683	-0.6877	0.0476
CaO	-0.4880	0.2657	-0.5919
Fe_2O_3	0.9738	-0.0765	-0.0411
K_2O	0.1052	-0.9441	-0.0923
TiO_2	0.3366	0.7094	0.1858
Cu	0.9081	0.2040	0.0786
Zn	0.3722	0.2464	0.7664
Pb	-0.0135	-0.1642	-0.8189
La	0.7681	0.4632	0.3887
Co	0.9868	0.0219	0.0092
V	0.6581	-0.3706	-0.1455
Cd	0.2223	-0.9192	0.0733
Cr	0.8345	0.3537	0.2708
% of Variance	40.79	23.07	14.80

Conclusion

Using ED-XRF the elemental composition of potteries was determined. From the analysis, used clay are non-Calcareous and low refractory in nature The elemental composition values loaded to identify the grouping of potteries. The results confirm the existence one major group in addition to four small groups.

References

[1] Maniatis,Y., Tite,M.S., Journal of Archaeol. Sci. 8 (1981) 59.

[2] Ravisankar,R., Raja Annamalai,G., Naseerutheen,A., Chandrasekaran,A., Prasad,M.V.R., Satpathy,K.K., Maheswaran,C Spectrochimica Acta Part A: Mol. Biomol. Spect.115 (2013) 845.

Determination of multi-element profiles of soil at Visakhapatnam using EDXRF technique

Sandeep P., Kothai P, C.B. Dusane, S.K. Sahu and G.G. Pandit

Environmental Monitoring and Assessment Section, Bhabha Atomic Research Centre, Trombay, Mumbai 400085, India; E-mail: ggp@barc.gov.in

Source profile database are reported for major sources of particulate matter pollution, at Visakhapatnam. Representative soil samples were collected from these source areas and analyzed in EDXR. Analysis results indicated that V and Ni are predominant at Petroleum refineries (PR) and Zn was found to be dominating at complex road and ore industry. Higher concentration of As was observed at TPP as compared to all other sites. In the case of major elements, at all sources Al was the dominating except at PR. Further Ca was found to be high at the PR site as compared to other sites.

Introduction

The particulate matter (PM) suspended in the atmosphere can have its origin in natural or anthropogenic sources. Understanding potential sources of the particulate matter in the urban atmosphere is important for air quality management. The identification of a given source and the quantification of its contribution for the local air pollution depend on a comparison between the measured elemental concentration at the sampling site and the relative concentration of the chemical elements at the source (i.e., source profile). These profiles differ with sources, process operating conditions, geology, and geographic seasonality. Location specific source profiles are therefore needed for source apportionment studies.

Over the years, there has been a tremendous increase in human population, road transports, vehicular traffic and industries in Visakhapatnam region. This has led to increase in the concentration of particulate pollutants in the ambient air. The present study was part of an effort towards developing a database of air pollution source profiles specific to Visakhapatnam, Andhra Pradesh, India. Sources were selected based on their respective prominence for the PM sampling site.

The attractiveness of nuclear analytical techniques viz. neutron activation analysis (NAA), X-ray fluorescence (XRF) and particle-induced X-ray emission (PIXE) for their non-destructive nature and the ability to perform a simultaneous multi-elemental determination has led to their extensive application in industrial and research laboratories for different types of materials. For the analysis of Environmental samples, XRF has the advantage of being a rapid and inexpensive method with a simple sample preparation [1]. Hence in the present study EDXRF is used for the sample analysis.

Experimental

Sampling

Representative soil and road dust samples were collected from locations near the receptor site in city. These samples were dried, sieved to particle size less than 75 laboratory. Total eight sampling sites were selected in the study area.1) Steel plant (SP), 2) Thermal power plant (TPP), 3) Petroleum refineries (PR), 4) Complex road (CR), 5) southern biotech industry (SB), 6) Granite industry (GI), 7) Ore industry (AO), 8) Alloy industry (IO)

Sample Preparation and Analysis

500mg each of sample and cellulose were taken to make the pellets by applying a pressure. A 25 mm diameter die was used to make the pellets. All measurements were carried out using a Xenemetrix make, EX-3600 EDXRF spectrometer. This consists of an X-ray tube with Rh anode as the source of X-rays and Si(Li) detector with a resolution of 150 eV at 5.9 keV Mn X-ray. Secondary targets are used to modify the Rh spectrum from the X-ray tube. The concentrations of 15 elements, namely major (i.e. Mg, Al, K, Ca, Ti, Mn, Fe) and trace (i.e. V, Cr, Cu, Ni, Zn, As, Br and Pb) were measured using different secondary targets (Ti, Ge, Mo).

Table-1: Optimized EDXRF parameters for elemental analysis

Secondary Target	Elements	Voltage (KV)	Current (A)	Analysis Time (S)
Ti	Mg, Al, K, Ca	25	4800	600
Ge	Ti, V, Cr, Mn, Fe, Ni, Cu, Zn	40	800	600
Mo	Pb, Br	40	1000	600

Quality Assurance

The procedures adopted for elemental analysis was established by analyzing the standard certified reference material namely IAEA SL1, IAEA SL3, IAEA 405, IAEA 433. The results of the standard analysis showed good agreement with the certified values.

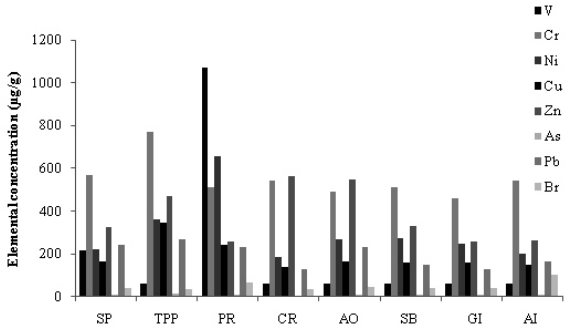


Fig. 1 Source profiling of trace elements

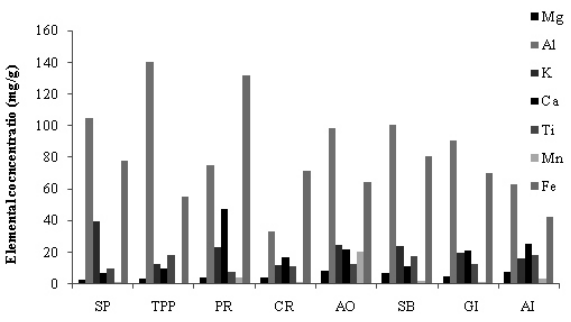


Fig. 2 Source profiling of major elements

Results and Discussion

PR

Chemical profiling of the PR soil sample shows that V and Ni are predominant at this site followed by Cr, Zn etc. In the case of major elements, Fe is dominating followed by Al, Ca, K. It is interesting to observe that Ca was found to have highest concentration at PR as compared to all other sites.

Thermal power plant and Steel plant

Chemical profiling of Fly ash sample from thermal power plant indicates that it has high Arsenic concentration as compared to all other sites. Among the trace metals, Cr is the predominant element followed by Zn, Ni, Pb etc. at both sites. It is also observed that no vanadium is found at TPP, whereas V is observed at steel plant. In the case of Cu, TPP sample is found to have large concentration as compared to steel plant sample. Among the major elements, Al is the dominating at both the sites followed by Fe, Ti, K and Ca.

Complex road and ore Industry

Zn is the dominating element at both sites followed by Cr, Ni, Cu, Pb etc. Among major elements Fe is dominating at CR, whereas Al is major element at ore industry followed by Ca, K etc. It is interesting to observe that Mn is found to have high value at AO as compared to CR.

Alloy Industry, GI and Southern biotech

Sample analysis shows that Cr is the predominant element at these sites followed by Zn, Ni, Pb, Cu, Br and As, whereas among major elements Al is the dominating followed by Fe. At SB and GI, Mn levels are nearly similar, whereas its value is high at AI. Similarly Ca is observed to have least value at SB as compared to GI and AI.

Conclusion

Source profiles developed in the present study are comparable with the profiles reported in literature. For example V and Ni are marker elements of petroleum industries, similar profiles are observed in present study. As and Zn are the marker elements of the TPP and Vehicular (tyre wear) emissions; similar is observed in our study. Further studied need to be continued to get the full picture the source profiles at the study site, Visakhapatnam. Use of the EDXRF method for multi-elemental profiling of particulate matter source has proved to be helpful, as the method is relatively simple, inexpensive and has a short turnaround time as compared to other nuclear analytical techniques. The technique also offers the opportunity to get data on Pb and Cu, which are important elements in many environmental studies; Pb cannot be determined by INAA and Cu is troublesome as well [2].

References

[1] V. Cojocaru, A. Pantelica, E. Pincovschi, I.I. Georgescu, Rom. J,. Phys. 55 (7-8) (2010) 815

[2] IAEA-TECDOC-1215 Use of research reactors for NAA, Appendix II. IAEA, Vienna, (2001).

Measurement of Electron Momentum Density in Sm_2O_3 using Compton Spectroscopy

Sonu Sharma[1], Alpa Dashora[2], Jagrati Sahariya[1], B.L. Ahuja[1]

1. *Department of Physics, University College of Science, M.L. Sukhadia University, Udaipur 313 001, India*
2. *Department of Physics, University of Mumbai, Vidyanagari, Mumbai 400 098, India; E-mail: dashoralpa@gmail.com*

Electron momentum density in Sm_2O_3 has been measured using a 20 Ci ^{137}Cs Compton spectrometer at a momentum resolution of 0.34 a.u. To support our experimental investigation, theoretical isotropic Compton profiles have been computed using linear combination of atomic orbitals method with various electron exchange and correlation approximations. The Compton profile computed using the parameterization of Wu-Cohen within the generalized gradient approximation is found to be in good agreement with the present measurement.

Introduction

The study of electron momentum density distribution through the Compton scattering depends on the impulse approximation, which allows the target electrons to be treated as free electrons. Moreover, if the interaction is truly impulsive, the electron does not move appreciably during the interaction and therefore sees the same potential just before and after collision with the photon. If the target consists of electrons with a distribution of momenta n(p), the Doppler broadening of the spectrum of the scattered radiation known as Compton profile, $J(p_z)$, is defined as [1]:

$$J(p_z) = \int n(p)\, dp_x\, dp_y \qquad (1)$$

The Compton spectroscopy is a well recognized probe to study the electron momentum density of materials and hence their electronic properties [2].

Within last decade, rare earth oxides have been extensively investigated due to their high resistivities, high dielectric constants, and large band gap characteristics for wide range of technological applications including memory devices, switching mechanism for logic devices, and optoelectronic devices [3]. These oxides are also found as potential candidates of metal oxide semiconductor devices [4]. Specially, Sm_2O_3 is attractive to substitute SiO_2 in the CMOS devices because of its dielectric constant and high chemical and thermal stability with Si.

In this paper, we present the first ever experimental Compton profile of Sm_2O_3 using 661.65 keV -rays emitted by 20 Ci ^{137}Cs source. The Compton line shape is compared with theoretical Compton profiles computed using *ab-initio* calculations.

Experiment

The Compton profile of Sm_2O_3 is measured using a 20 Ci ^{137}Cs Compton spectrometer [5]. The high purity (99.95%) polycrystalline sample of Sm_2O_3 was kept in a perspex ampoule having very thin Mylar sheets on both sides. The ampoule was pressed to form a pellet (0.33 cm thickness and 2.52 cm dia.). The bulk density of the sample was found to be 2.46 g/cm^3. The incident beam of 661.65 keV -rays was scattered by the sample through a mean angle of 160±0.5^o. The energy spectrum of the scattered radiation was measured using a high purity Ge detector (Canberra, USA) with the associated electronics like pre-amplifier, spectroscopy amplifier, analog to digital converter and 4096-channel analyser.

The raw data was accumulated over a total period of 323.12 h to get reasonable statistics in Compton region. The background contribution was determined from an independent measurement without keeping the sample in the sample holder. The measurement was performed at ambient temperature and normal pressure. To extract the true Compton profile, the raw data was corrected for several corrections like background, instrumental resolution, detector efficiency, sample absorption, Compton cross-section and multiple scattering, etc. Finally, the Compton profile was normalised to the free atom profile area [6] of 59.07 e^- in the momentum range 0-7 a.u.

Theory

To compare our experimental momentum densities, we have computed the Compton profiles using the *ab-initio* linear combination of atomic orbitals (LCAO) employing the CRYSTAL09 code of Dovesi group [7]. A variety of schemes of exchange and correlation within density functional theory (DFT) namely local density approximation (LDA) [8] and generalized gradient approximation (GGA) with different exchange and correlation functions like revised Perdew-Becke-Ernzehof (PBE-sol) [9], second-order GGA (SO-GGA) [10] and Wu-Cohen (WC-GGA) [11] have been considered. In the present computation, pseudopotential (PP) approach has been employed. In PP-HF scheme, the one electron Hamiltonian operator is given as [7],

$$\hat{h}_{PP} \quad \hat{t} \quad \hat{c} \quad \hat{X}_{HF} \quad \hat{e}_{PP} \qquad (2)$$

where $\hat{t}, \hat{c}, \hat{X}_{HF}$ and $\hat{e}_{PP}$ are kinetic, Coulomb, exchange and effective core pseudopotential (ECP) operators, respectively. The ECP was used to describe the core part of Sm [12] while the all electron basis sets

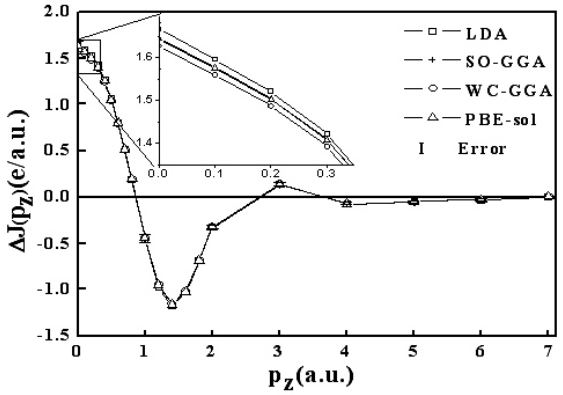


Fig. 1 Difference between experimental and theoretical Compton profiles. Inset shows the deviations within limited region

were taken for O [13]. The lattice parameter for cubic Sm_2O_3 was taken as a=10.921 [14].

Results and Discussion

In Fig. 1, we have plotted the difference between the present convoluted theoretical profiles (spherical averaged) and the measured experimental profile of Sm_2O_3. In order to account for the experimental resolution in the theoretical data, we have convoluted the theory with the experimental resolution function. Fig. 1 depicts that in the high momentum region (p_z 4 a.u.), the theoretical profiles are nearly equal to the experimental data. It was expected since the free atom Compton profiles reasonably describe core contribution, which dominates in the high momentum region. In contrast, significant differences between theory and experiment are seen near p_z = 0 a.u. Within the framework of PP, a very small difference is seen between various exchange and correlation functionals of DFT scheme.

To clearly see the role of different exchange and correlation functionals, we have magnified the low momentum region in the inset of Fig. 1. It is seen that the WC-GGA functional shows minimum deviation from the experimental data, while the LDA depicts the largest deviations. The fitting shows a marginally better agreement of DFT-GGA-WC based profiles with the experimental profile than other schemes. Differences between theory and experiment may be due to non-inclusion of relativistic effects and Lam-Platzman correlation [2] in the LCAO calculations. Quality of PP basis sets used in the present LCAO calculations may also governs the value of $J(p_z)$.

Conclusions

We have presented the first ever experimental and theoretical (LCAO based) Compton profiles of Sm_2O_3. It is seen that the LCAO-DFT-GGA (WC) gives a marginally better agreement with the experiment than other LDA/GGA schemes. To compare the experiment in a more accurate way, relativistic Compton profiles with Lam-Platzman correlation corrections are required.

Acknowledgements

Authors are thankful to BRNS-DAE, Mumbai for financial assistance. AD thanks SERB, New Delhi for Fast Track YS Project.

References

[1] Compton Scattering, B. Williams, McGraw-Hill, London (1977).

[2] X-ray Compton Scattering, M.J. Cooper, P.E. Mijnarends, N. Shiotani, N. Sakai and A. Bansil Oxford Science Publications, New York (2004).

[3] H. Yang, H. Wang, H. M. Luo, D. M. Feldmann, P. C. Dowden, R. F. DePaula, Q. X. Jia, Appl. Phys. Lett. 92 (2008) 062905.

[4] K. Shalini, S. A. Shivashankar, Bull. Mater. Sci. 28 (2005) 49.

[5] B. L. Ahuja, M. Sharma, S. Mathur, Nucl. Instrum. Meth. B 244 (2006) 419.

[6] F. Biggs, L. B. Mendelson, J. B. Mann, At. Nucl. Data Tables 60 (1975) 201.

[7] R. Dovesi, V. R. Saunders, C. Roetti, R. Orlando, .M. Zicovich-Wilson, F. Pascale, B. Civalleri, K. Doll, N. M. Harrison, I. J. Bush, Ph. D'Arco, M. Llunell, 2009 CRYSTAL09 Users' Manual, University of Torino, Torino (2009).

[8] M. D. Towler, A. Zupan, and M. Causa, Phys. Commun. 98 (1996) 181.

[9] J. P. Perdew, A. Ruzsinszky, G. I. Csonka, O. A. Vydrov, G. E. Scuseria, L. A. Constantin, X. Zhou, K. Burke, Phys. Rev. Lett. 100 (2008) 136406.

[10] Y. Zhao, D. G. Truhlar, J. Chem. Phys 128 (2008) 184109.

[11] Z. Wu, R. E. Cohen, Phys. Rev. B 73 (2006) 235116.

[12] http://www.theochem.uni-stutgart.de/_Hlt367955434 Hlt367955435BM 1 BM 2 pseudopoten-tials/index.en.html.

[13] http://w_Hlt236129925w_Hlt236129925w.tcm.phy.cam.ac.uk/mdt26/basis_Hlt236197530_Hlt236197531 BM 3 BM 4 sets/O basis.txt

[14] D. D. Johnson, Phys. Rev. B. 38 (1998)12807.

A Study of Trace Elemental Distribution in Vegetables by PIXE

Seetharamireddy B., Abdul Sattar S., Madhusudhana Rao P.V., Ramnarayan K.

Nuclear Physics Department, Andhra University, Visakhapatnam 530003, India;
E-mail: seetharam.byreddy@gmail.com

Vegetables form a part of staple diet in almost all the households in developing countries like India. The present study is carried out to measure and analyze the trace elemental concentrations in eight vegetables commonly consumed in the Indian sub-continent and to determine their contribution to RDA and also to check whether any of them are present in concentrations above accepted levels. In this work Proton Induced X-ray Emission (PIXE) technique has been employed and a 3MeV proton beam was used to excite the samples. The spectra were recorded using an Si (Li) detector and data analysis was done using the Gupix Software. The elements Cl, K, Ca, Ti,V, Mn, Fe, Co, Cu, Zn,Br, Rb and Sr were detected and their concentrations determined.

Introduction

In developing countries like India, vegetables form a part of staple diet in almost all the households. While the required amount of vegetables in our daily diet must be 300 to 350 gm per person [1] Butt & Haq [2] have estimated , that only 80-90 gm of vegetables per person is being used in daily diet. Assuming that an individual consumes one of the vegetables like Brinjal, Potato or gourd per day it would be interesting to see what portion of Recommended Dietary Allowance (RDA) of important elements like Zn, Mn, Se, etc. are met from this source. In the present study trace elemental analysis of eight vegetables was undertaken.

Materials & Methods

One twenty samples of eight vegetable species were collected from around Amalapuram town, East Godavari District, Andhra Pradesh, India. These samples were washed in tap water and rinsed thoroughly with double distilled water in order to remove surface contamination. Each plant sample was then dried, ground and homogenized in an agate mortar. A quantity of 120 mg of each powder sample was mixed with high purity graphite powder (99.999%) in 3:2 ratio. The purpose of mixing graphite powder is to monitor the beam current. The resultant mixture was compressed using a 10 ton hydraulic press into pellets of 13 mm diameter and about 2 mm thickness. These pellets were then used as targets for the PIXE experiment.

Experimental Details & Analysis

The experimental work was carried out at the Institute of Physics, Bhubaneswar, with a 3 MeV Pelletron accelerator. The samples were mounted on a target ladder and were kept in the scattering chamber evacuated to a high degree of vacuum (10^{-6} torr). A proton beam of 3 MeV energy was employed to excite the samples. The beam current was kept at about 20 nA. The targets were positioned at an angle of 45^0 to the beam direction. The proton beam was collimated to a diameter of 4mm and was made to fall on the target. The detector was kept at an angle of 45^0 to the target position and at an angle of 90^0 to the proton beam direction. The characteristic X-rays emitted from each sample were recorded with a high-resolution Si(Li) detector (FWHM 160 eV at 5.9 keV energy), which has a sensitive area of 30 mm^2 and provided with a thin beryllium window of 8- m thickness. The spectra were collected for a sufficiently long time so that good statistical accuracies were maintained. For each sample; the total charge collected and the average beam current were noted. The obtained PIXE spectra corresponding to different vegetables were analyzed using GUPIX software package. This package has provision to convert the X-ray intensities into elemental concentrations using a standardization technique involving fundamental parameters, predetermined instrument constants and input parameters such as solid angle, charge collected, etc. Using this software package different elements present in each medicinal plant were identified and their concentrations determined. To ensure the reliability of this technique in reproducing concentration of low Z-elements, the accuracy of the technique was checked by analyzing NIST-apple leaves sample (1515).

Results and Discussion

The average concentrations of different major, minor and trace elements present in each of these eight vegetables and the corresponding standard deviations are furnished in Table 1. The typical PIXE spectrum is shown in Fig. 1. The RDA of various trace elements [3,4] are as follows: Fe-10-15 mg, Cu-1-3 mg, Ca-800-1200 mg, Zn-12-15 mg, Mn-11 mg. Iron is present in all the vegetables with maximum in Potato. Iron is an important element in human body metabolism which acts as a catalyst and is present in greater amount than any other trace element. Copper is found in small amounts in five of the presently analyzed vegetables with maximum in Brinjal (6 ppm). Copper is an essential trace element necessary for normal biological activities of amino acids and tyrosinase enzymes. Manganese is present in six of the vegetables analyzed with maximum in Beet root. Manganese is essential for normal growth, skeletal formation and normal reproductive function.

Table-1: Concentrations (ppm) of trace elements in the vegetables under study

Element	Tomato	Little Gourd	Ridge Gourd	Potato	Brinjal	Carrot	Beet root	Bitter gourd
Cl	3200 ± 100	1100 ± 60	1000 ± 110	2000 ± 180	1600 ± 60	2000 ± 175	6350 ± 850	800 ± 160
K	10500 ± 150	7500 ± 800	6300 ± 750	7400 ± 680	7800 ± 650	12800 ± 770	9800 ± 950	6100 ± 950
Ca	1300 ± 50	1950 ± 50	2250 ± 210	400 ± 40	1250 ± 140	3450 ± 480	2200 ± 250	1550 ± 150
Ti	60 ± 10	31.5 ± 5.7	44.1 ± 9.3	42.6 ± 7.6	52.3 ± 6.8	43.2 ± 8.1	40.8 ± 8.8	41.2 ± 7.7
V	14.2 ± 6.1	6.3 ± 3.5	BDL*	BDL*	BDL*	BDL*	4.2 ± 1.1	BDL*
Mn	BDL*	3.9 ± 1.9	6.0 ± 1.8	BDL*	11.2 ± 2.3	8.5 ± 3.0	30.3 ± 3.8	7.3 ± 2.5
Fe	48 ± 5	37.5±2.8	45±4	66.7±3.8	46.5±3.5	52.7 ± 5.1	42.5 ± 5.2	41.9 ± 3.1
Cu	BDL*	2.3±1.0	BDL*	1.8±0.7	6.0±1.4	BDL*	1.5 ± 0.6	BDL*
Zn	10.9±2.7	5.1±1.4	10.5±2.4	9.6±2.0	6.4±1.6	7.8 ± 1.9	13.3 ± 2.4	12.3 ± 2.1
Se	3.0±1.0	1.5±0.9	BDL*	2.6±1.1	BDL*	BDL*	4.0 ± 2.7	BDL*
Br	10.1±4.6	BDL*	BDL*	BDL*	BDL*	BDL*	BDL*	BDL*
Rb	12.9±4.2	BDL*	BDL*	BDL*	9.3±4.7	BDL*	BDL*	BDL*
Sr	BDL*	BDL*	BDL*	BDL*	10.5±4.8	10.0 ± 5.9	BDL*	BDL*

*Below detection limit

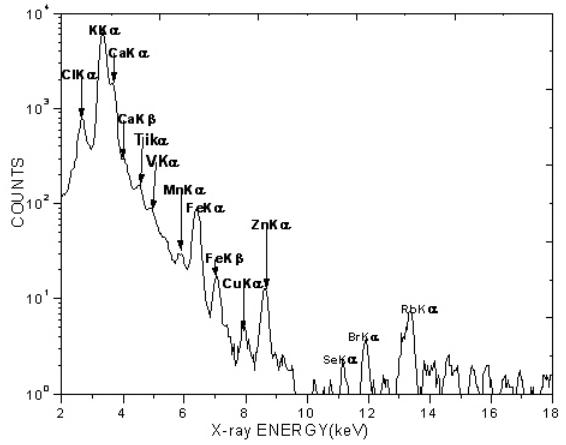


Fig. 1 PIXE spectrum of Tomato

Zinc is the second abundant trace element in the human body. It is essential for the normal functioning of the cell including protein synthesis, carbohydrate metabolism, cell growth and cell division. The RDA for Zinc is 12-15 mg.[3]. Zinc was found in all vegetables analyzed except Cabbage and Cucumber.

The concentration of zinc in these vegetables is found to be 5.1 ppm (Little Gourd) to 13.3 (Beet root).

Calcium is needed for formation and maintenance of bones, the development of teeth and healthy gums. It is necessary for blood clotting, stabilizing many body functions and is thought to assist in preventing bowel cancer. The RDA for calcium is 800 -1200 mg. [4]. In all the vegetables analyzed in the present study, calcium was found in appreciable amounts. The maximum was found in Lady Finger (3650 ppm) and minimum in Potato (400 ppm). Thus all the vegetables analyzed contain some beneficial trace elements in varying quantities and all of them in safe levels.

Conclusions

Eight vegetables, commonly consumed in Asian countries are analyzed for determination of trace elemental concentrations. All the vegetables contain beneficial elements Ca, K, Cu, Zinc and Iron in various quantities and none of them exceed acceptable levels. All are free from toxic elements like As, Cd, Pb and Hg.

References

[1] Anonymous. Health Guideline for the use of Wastewater in Agriculture and Aquaculture. Tech. Rep. Sci. 778, 10, Report of WHO Science Group, World Health Organization, Geneva, Switzerland (1998).

[2] S. J. Butt, M. Imran-Al-Haq, Vegetable Cultivation – Secret of Manifold Prosperity's Science, Technology and Development, 12(3) (1993) 46.

[3] L. A. Kaplan, J Pesca, S C Kazmierczak 4th Ed. Published by Mosby, (1993) pp. 707.

[4] Recommended dietary allowances the National Academy of Sciences, National Academy Press, Washington D.C. (1989)

Effect of Ag^+ Irradiation on Cubic and Tetragonal Yttria Stabilized Zirconia

R. Halder[1], P. Sengupta[1], V. Sudarsan[2], I. Samajdar[3], P. V. Satyam[4], G.K.Dey[1]

1. *Materials Science Division, Bhabha Atomic Research Centre, Trombay, Mumbai 400085, India; E-mail: rumuhalder24feb@gmail.com*
2. *Chemistry Division, Bhabha Atomic Research Centre, Trombay, Mumbai 400085, India*
3. *Department of Metallurgical Engineering and Material Science, Indian Institute of Technology Mumbai, Mumbai 400076, India*
4. *Institute of Physics, Bhubaneswar 751005, India*

Cubic and tetragonal zirconia pellets, doped with 8 mol% and 3 mol% yttrium oxide respectively, synthesized by powder metallurgy route were subjected to 1.5 MeV Ag^+ ion irradiation in the fluence range 10^{11}-10^{15} ions/cm^2. The initially white samples were colored after irradiation at higher doses due to formation of F centers. EBSD characterization of cubic zirconia sample irradiated at 10^{14} ions/cm^2 show circular spots over the matrix in image quality (IQ) map. This could be attributed to the formation of silver oxide particles or other small defect clusters such as vacancy aggregates produced by displacement process leading to mis-indexing. Photoluminescence spectroscopy of tetragonal zirconia irradiated at highest doses indicates quenching of the PL intensity due to formation of irradiation induced killer centers while there is no appreciable change in case of cubic zirconia.

Introduction

Cubic yttria stabilized zirconia (8YSZ), a highly radiation resistant refractory ceramic is one of the promising inert matrix candidate for Pu incineration and actinide transmutation in Accelerator Driven Sub-Critical Systems [1-3] as well as host matrix for TRU waste immobilization. Hence the study of the response of 8YSZ to ion irradiation is an essential requirement to evaluate its applicability in harsh service conditions. Similar study was carried out with tetragonal yttria stabilized zirconia (3YSZ) for comparison and studying the effect of crystal structure on radiation induced changes.

Experimental

7 mm diameter pellets of 8YSZ and 3YSZ were synthesized by powder metallurgy route- cold compaction at 28 MPa and sintering in air at 1500°C and 1425°C respectively with three hours holding time followed by furnace cooling. Irradiation using 1.5 MeV Ag^+ ion beam was done at room temperature using a -15° ion beam implanter in vacuum of 10^{-7} mbar, with fluence in range 10^{11}-10^{15} ions/cm^2. Bulk characterization was done by EPMA (electron probe micro analyser) and study of optical properties of irradiated samples was carried out by photolumunescence spectroscopy using Xe source using excitation wavelength of 350 nm.

Results and Discussion

Microstructural characterization of as prepared pellets by EPMA using a steady electron beam accelerated at 20 kV show homogeneous distribution of elements and equi-axed grain for both 3 YSZ and 8 YSZ and xrd peaks conform to both the crystal structures. EBSD color coded map for cubic zirconia show that there is no preferential direction of orientation of the grains and the mis-orientation between the neighboring grains remained mostly <5°.

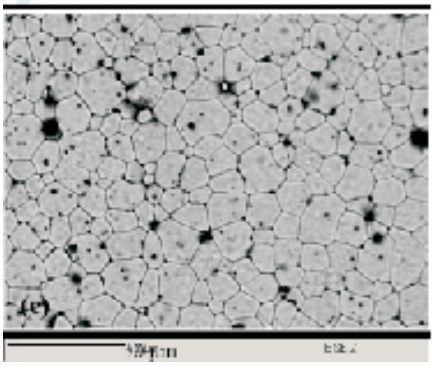


Fig. 1 BSE image of representative as prepared 8 YSZ pellet

The projected range and straggling in the matrix caused by Ag ion was calculated using SRIM (Stopping Range of Ions in Matter) computer code (Version SRIM 2008.04).The results are summarized in Table 1.

Table 1: Results of SRIM calculation taking angle of incidence as 0° since the pellets were polycrystalline

Parameter	3YSZ	8YSZ
dE/dx elec	1.615E+02	1.618E+02
dE/dx nuclear	2.311E+02	2.321E+02
Range	3561	3724
Lateral Straggling	997	1043
Longitudinal straggling	742	776

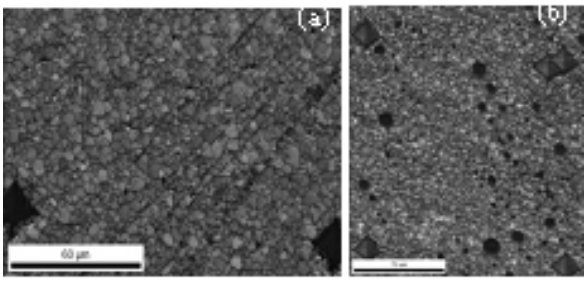


Fig. 2 (a) IQ map of as prepared 8 YSZ pellet from EBSD and (b) IQ map of as Ag^+ irradiated 8 YSZ pellet with fluence 3 x 10^{14} ions/cm^2 showing circular spots at surface resulted from mis-indexing

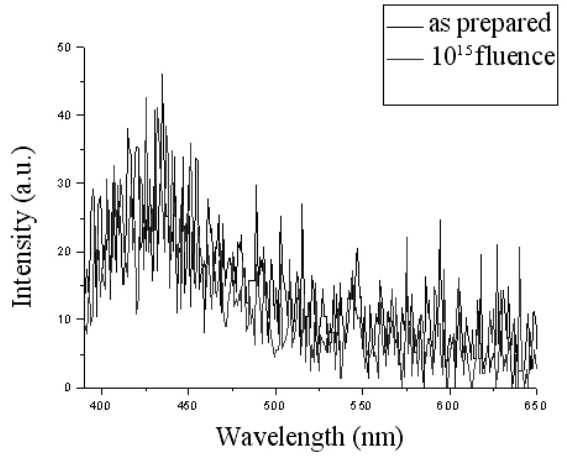


Fig. 3 Emission spectra of 8 YSZ – as prepared and irradiated with 1.5 MeV Ag^+ ion beam to dose 10^{15} ions/cm^2.

The initially white samples became purple colored when irradiated above doses 10^{14} ions/cm^2 indicating the formation of F-centres, which is a well known effect of ion-irradiation on YSZ documented in literature [4]. EBSD characterization of ion irradiated cubic zirconia sample does not show any detectable change in grain size or orientation. However circular spots were seen in image quality (IQ) map of Ag^+ irradiated sample owing to mis-indexing.

Photoluminescence spectroscopy of the cubic and tetragonal zirconia both as prepared and irradiated to highest doses show that there is a broad emission peak centered at ~420 nm corresponding to excitation of 350 nm in all cases. Since no shift in peak position was observed, it can be predicted that the bulk crystal structure of the material remained same and no new defect states were generated. Quenching of PL intensity after irradiation occurs only in case of 3YSZ but not in case of 8 YSZ. This could be due to ability of cubic zirconia to accommodate large number of vacancies into its structure.

Summary

Cubic and tetragonal zirconia when irradiated with Ag ion upto different fluences forms color centers. Because of the observed purple coloration only the presence of F centers is anticipated. The PL intensity did not change much in case of 8YSZ owing to stability of cubic phase while the decrease in case of 3YSZ could be attributable to formation of killer centers.

References

[1] L.M. Wang, S.X. Wang, S. Zhu, R.C. Ewing, J. Nuc. Mater, 348 (2006) 223

[2] A. Debelle, B. Decamps, A. Declemy, L. Thome, G. Sattonay, F. Garrido, I. Jozwik, J. Jagielsky, Scripta Mater, 63 (2003) 665

[3] C.Degueldre, P.Heimgartner, M.A.Pouchon, U. Kasemeyer, Prog. Nucl. Mate, 38 (2001) 301

[4] J.M. Costantini, F. Beuneu, K. Schwartz, C. Trautmann, J. Phys. Condens Matter. 22 (34) (2010) 115

PIXE Analysis of Cancer-Afflicted Human Bladder

G. J. Naga Raju[1] P. Sarita[2], and S. Bhuloka Reddy[3]

1. *Department of Physics, UCEV, JNTUK, Vizianagaram-535 003, India; E-mail: gjnraju@yahoo.com*
2. *Department of Physics, GIT, GITAM University, Visakhapatnam-530 045, India*
3. *Swami Jnanananda Laboratories for Nuclear Research, Andhra University, Visakahpatnam-530 003, India*

Particle induced x-ray emission (PIXE) technique was used for analysis of trace elements in normal and cancer-afflicted human bladder tissues. The samples were irradiated with a proton beam of 3 MeV energy generated by 3 MV Pelletron Accelerator at the Institute of Physics, Bhubaneswar, India. The elements Cl, K, Ca, Ti, Cr, Mn, Fe, Ni, Cu, Zn, and Se were identified and their concentrations were estimated. The deficiency or excess of different trace elements observed in the cancer tissues relative to the normal tissues of bladder are correlated to the pathology of cancer.

Introduction

Trace elements are undoubtedly important for the vital processes of life but, even more important is the fact that their functional forms and their characteristic concentrations must be maintained within narrow limits. Trace element imbalance is surfacing as potentially instrumental in explaining carcinogenesis. Since trace elements markedly influence several key biological events - including cell cycle regulation, processes involved in replication or transcription, immune competence, maintenance of free radical levels, and factors involved with apoptosis – they could participate either in the initiation or even in the later stages observed during tumour progression. Trace elemental analysis of tumours could become a powerful diagnostic and prognostic tool and moreover, subsequent interruption or alteration of the trace element supply of tumours could be developed into an effective cancer treatment strategy. With this objective, our group has undertaken a series of studies on trace elemental analysis of various cancer-afflicted human organs. As a part of these investigations we have analyzed the tissues of bladder cancer (which accounts for approximately 90% of cancers of the urinary tract) for their trace elemental content using particle induced X-ray emission technique (PIXE).

Materials and Methods

Tissue samples were surgically removed from 18 patients of bladder cancer (with ages ranging from 37 to 73, mean age 55.17 years) together with small amount of non-cancer or normal tissues surrounding the malignant part. Estimation of trace elemental concentrations in the paired samples avoid many variations attributed to age, sex, diet, medication, genetics, hormonal status, and environmental factors [1]. These samples were collected from the Pathology Department of Andhra Medical College, Visakhapatnam. Fresh tissue samples were lyophilized and then ground into a fine powder. A known quantity of yttrium and graphite was added to the sample and resulting mixture was pressed into a pellet, and then used as target. The PIXE measurements were carried out using a 3 MeV collimated proton beam from the 3 MV Tandem Pelletron Accelerator at Institute of Physics, Bhubaneswar, India. The detailed experimental procedure, method of validation and data analysis of the PIXE spectra can be found in one of our earlier papers [2].

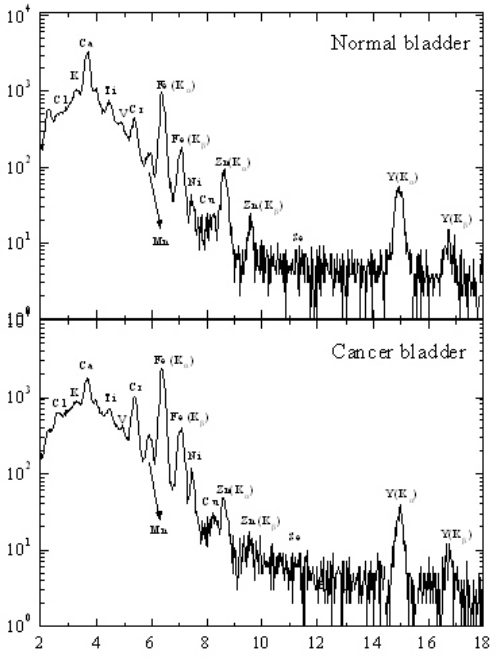


Fig. 1 PIXE spectra of normal and carcinoma tissues of bladder

Results and Discussion

The PIXE spectra recorded with normal and carcinoma tissues of bladder are depicted in Fig. 1.

The concentration data is averaged for the different samples of normal and cancerous tissues of bladder. The average concentrations, the corresponding standard deviations, and the significant value (p value) for each element are shown in Table 1. From Table 1, it can be seen that the elements Cl, K, Ca, Ti, V, Cr, Mn, Fe, Co, Ni, Cu, Zn, and Se are identified and their

Table-1: Comparison of elemental concentrations (ppm) in normal and cancerous tissues of bladder.

Elements	Normal Bladder	Cancerous Bladder	Level of significance (p value)
Cl	451.1 132.9	662.2 154.6	<0.001
K	113.1 17.1	29.7 11.8	<0.0005
Ca	669.0 142.0	199.5 55.5	<0.0005
Ti	74.0 13.5	41.9 13.1	<0.0005
V	5.2 1.7	6.9 2.5	<0.05
Cr	52.6 12.4	135.1 18.2	<0.0005
Mn	4.5 2.2	10.1 3.4	$<1x10^{-5}$
Fe	185.9 34.8	365.8 65.5	<0.0005
Ni	6.8 2.2	16.6 3.7	<0.0005
Cu	1.19 0.7	3.57 1.2	<0.001
Zn	82.27 15.9	61.32 10.6	<0.005
Se	2.1 0.7	1.6 0.7	>0.05

concentrations are estimated. In the cancerous tissues of bladder, the concentrations of Cr, Mn, Fe, Ni, and Cu are higher while the concentrations of K, Ca, and Ti are lower when compared to those in normal tissues of bladder. The concentrations of Cl, V, Zn, and Se in cancerous and normal tissues of bladder are in agreement within standard deviations.

Higher levels of Cr are observed in the analyzed cancerous tissues of bladder ($p<0.0005$) compared to the normal tissues. Various mechanisms have been suggested till date regarding chromate carcinogenicity [3,4].

In the present work, the concentrations of Fe are found to be higher in the cancerous tissues of bladder ($p<0.0005$) when compared to the normal tissues. The elevated levels of Fe observed in the present work may either be the cause or the consequence of cancer. The involvement of Fe in tumour development and progression can be understood in terms of oxidative DNA damage [5].

Nickel content is found to be significantly higher in the cancerous tissues of bladder ($p<0.0005$) when compared with the normal tissues. Nickel is a major environmental contaminant. Human exposure to Ni occurs primarily via inhalation, ingestion, and dermal absorption and is a function of bioavailability. Exposure to Ni compounds can have adverse effects on human health [6]. The most significant toxicological effect of Ni is its ability to cause human cancer.

Copper levels are observed to be elevated in the cancerous tissues of bladder ($p<0.001$) relative to the normal tissues. The fact that Cu is involved in the initiation and promotion of carcinogenesis by the generation of free radicals [7] and in the progression of tumour growth through angiogenesis [8] correlates with the present findings.

Conclusions

Once it is established that, excess or deficient levels of a particular trace element are responsible for initiating and promoting cancer, suitable measures can be adopted to achieve optimal concentrations of that element. It is plausible to think that better understanding of the mechanisms by which trace elements initiate, promote or inhibit bladder cancer might be used in slowing the progression and onset of bladder cancer.

References

[1] K. Geraki, M.J. Farquharson, D.A. Bradley, Phys. Med. Biol. 47 (2002) 2327.

[2] G. J. Naga Raju, P. Sarita, et al., Eur. J. of Cancer Prev. 16 (2007) 108.

[3] S. De Flora S, K.E. Wetterhahn Life Chem. Rep. 7 (1989) 169.

[4] J. Ye, S. Wang, et al., J. Biol. Chem. 274 (1999) 34974.

[5] V. Abalea, J. Cillard, et al., Carcinogenesis 19 (1998) 1053.

[6] E. Denkhaus, K. Salnikow, Crit. Rev. Onclo. Hemat. 42 (2002) 35.

[7] A.D. Armendariz, C.D. Vulpe, Am. Soc. Nutr. Sci. J. Nutr. 133 (2003) 203E.

[8] G. J. Brewer, R. D. Dick, et al., Clin. Cancer Res. 6 (2000) 1.

Application of ^{52}Cr(p,)^{53}Mn Nuclear Resonance Reaction for Depth Profiling Cr in Surface Layers

Pritty Rao, S. Vikram Kumar, Sanjiv Kumar*

National Centre for Compositional Characterization of Materials, BARC, ECIL Post, Hyderabad, India;
E-mail: sanjivcccm@rediffmail.com

A method for depth profiling of chromium in the surface and near surface regions of materials using the resonance at 1005 keV in ^{52}Cr(p,)^{53}Mn nuclear reaction is presented. The detection limit, depth resolution and probing depth of the resonance in Si are determined to be about 3 at.%, 25 nm and ~ 2 m respectively form the excitation function of the reaction constructed in 0.90 1.1 MeV proton energy region by measuring 378 keV prompt -rays from ^{53}Mn nuclei. The reaction is interference free and provides an approach for profiling chromium in mid as well as high Z matrices.

Introduction

Chromium is an important constituent of several structural materials. Its determination and depth distribution in the surface and near surface regions are of interest from the point of view of investigating corrosion and interfacial reactions. Amongst the surface analytical techniques, nuclear resonance reaction analysis (NRRA) is the technique of choice for depth profile measurements as it is not only non-destructive but is also isotope specific. It, therefore, facilitates interference free and unambiguous analysis. However NRRA has often been used in the analysis of low Z (16) elements. So far as its application to higher Z elements is concerned, Gossett has demonstrated the applicability of resonances in (p,) reaction for profiling transition elements including Cr in steels [1]. But the study did not provide details of the experimental conditions and the analytical features of the resonances. In this paper, we report the results of our investigations on depth profiling of Cr in films and in the surface regions of materials using the resonance at 1005 keV in ^{52}Cr(p,)^{53}Mn nuclear reaction. Detection sensitivity, depth resolution and probing depth of the resonance which are important considerations for depth profile measurements, have been probed.

Experimental

The excitation function of ^{52}Cr(p,)^{53}Mn reaction was constructed in 0.9-1.1 MeV proton energy region in steps of 0.5 keV. It involved the bombardment of a CrN target (containing isotopes in natural abundance) at normal incidence with a collimated proton beam (=2mm, current = 500 700 nA) and the measurement of 378 keV prompt -rays emanating from the reaction by a high purity germanium (HPGe) detector (efficiency 40%; FWHM 1.8 keV at 1332.5 keV) at 0 or 90 with the direction of the projectiles. The data was acquired for a charge of 200 C at each incident energy by a PC based multichannel analyser. The experiments were conducted using 3 MV tandem accelerator at NCCCM, Hyderabad.

Results and Discussion

CrN/Si films used as targets for the construction of excitation function for determining the analytical features of the resonance were prepared by DC magnetron sputtering technique. The atomic composition (N_{Cr}:N_N = 1:1, error ~ ±5%) and the phase purity of the films were established by Rutherford backscattering spectrometry (RBS) and X-ray diffraction respectively. The choice of CrN films over elemental Cr films as targets is based on account of its superior chemical stability.

^{52}Cr(p,)^{53}Mn nuclear reaction exhibits resonances at 918 keV, 952.6 keV, 986.9 keV and 1005 keV [2]. Amongst these, the resonance at 1005 keV is the strongest and is suitable for analytical applications. 378 keV -rays result from the transition involving the first excited state (J= 5/2) and ground state (J= 7/2) of ^{53}Mn nucleus. The other transitions yield low intensity -rays. The excitation function of the reaction in the vicinity of the resonance is shown in Fig. 1. The variation in the yield around 1007 keV is probably due to the non-uniformity of the target and or the presence of an impurity such as oxygen. As can be judged from the yield curve, the resonance is very sharp. The

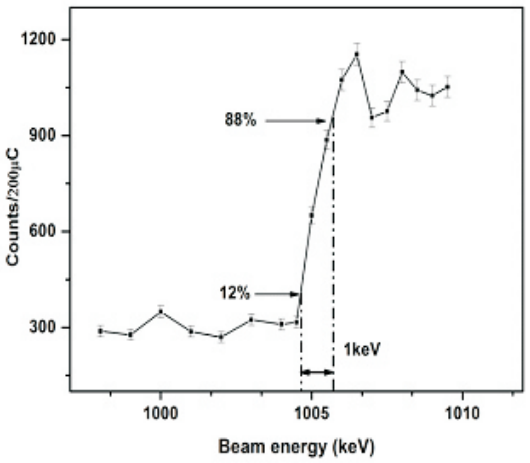


Fig. 1 Excitation curve of ^{52}Cr(p,)^{53}Mn nuclear reaction

inherent width of the resonance is about 50 eV which is difficult to determine under the present experimental conditions. The curve is, in fact, a convolution of the natural width of the resonance and extraneous factors contributing to the broadening of the beam energy. The depth resolution of the reaction, under this condition, is about 25 nm which is estimated by the energy difference (~1000 eV) between 12% and 88% of the yield, assuming the excitation curve to be overwhelmingly Gaussian. The detection limit of reaction is measured to be about 3 at.% while its probing depth in Si is about 2 microns. A survey of prompt -rays from (p,), (p,p) and (p,) nuclear reactions for low as well as high Z elements shows the absence of any interference to the 378 keV -rays, though the presence of such elements as Na, Al can give rise to higher background in the energy region. These results suggest that the resonance reaction is eminently suitable for depth profiling Cr in the surface regions of materials. The efficacy of the method was further verified by analyzing samples of diverse nature.

Conclusion

The applicability of ^{52}Cr(p,)^{53}Mn resonance reaction for depth profiling Cr in material surfaces is demonstrated. Due to the absence of any interfering reaction, the method is well suited for analyzing Cr in ferrous materials as well. It is a major advantage over Rutherford backscattering spectrometry wherein such an analysis in difficult due to kinematic reasons.

References

[1] C.R. Gossett, Nucl. Instr. and Meth. 168 (1980) 217.

[2] R. L. Schulte, J. D. King, H.W. Taylor, Nucl. Phys. A 243 (1975) 201.

Analysis of Fluorine in Granite Samples using PIGE Technique

A.A. Sukumar, Y. Sunitha, S. Vikram Kumar, Sanjiv Kumar

National Centre for Compositional Characterization of Materials, Bhabha Atomic Research Centre, ECIL Post, Hyderabad, India; E-mail: sanjivcccm@rediffmail.com

Fluorosis and osteoselerosis are widespread in Nalgonda and adjoining areas in Andhra Pradesh due to abnormally high levels of fluorine in water sources and soil. To trace the origin of such an occurrence, granites from the region were analysed for their fluorine content by proton induced -ray emission (PIGE) technique employing $^{19}F(p,p')^{19}F$ nuclear reaction. Several other light elements such as Na, Al, Mg and Si were also determined by means of the respective (p,) or (p, p) nuclear reactions. The samples contained 50-500 ppm fluorine which, by weathering or other geological processes might have contributed to the fluorine content of water and soil.

Introduction

The prevalence of fluorine above permissible levels in water sources and soil in Nalgonda and surrounding areas in Andhra Pradesh has been a cause of concern for long due to its ill effects on human health. While remedial measures are the need of the hour, identification of sources responsible for the elevated levels of fluorine is equally important. Geographically, the area is a plateau region with fairly large abundance of granites. In an attempt to fathom out contributing sources, granites from different parts of the region were analysed for their fluorine content. Proton induced -ray emission (PIGE), an ion beam analysis (IBA) technique, was chosen for the analysis in view of its high sensitivity to fluorine and minimal sample preparation. The simultaneous multielement detection capability of the technique was exploited to detect and determine other light elements present in the rock samples. The principles of the technique are described in detail in elsewhere [1]. Briefly, it involves the high resolution -ray spectrometry of prompt -rays emanating from (p, p), (p,) and (p,) reactions induced by a proton beam in a thick target. It is a simple, rapid and non-destructive method. For quantification, comparator method is usually employed and is performed by invoking the concepts of thick target yield and stopping power.

Experimental

Granite samples collected from different regions were powdered and homogeneously mixed with 15% high purity graphite. The respective powders, each weighing about 0.5 gm were subsequently mixed with 250 L of 1w/v% polyvinyl alcohol solution and pressed into 20 mm diameter pellets which served as targets for the PIGE experiments. These experiments involved irradiation of the targets with a 2.5 MeV proton beam in a scattering chamber in 5 x 10^{-6} torr vacuum. The -rays were detected by a high purity Ge (HPGe) detector (Canberra: Model GC4019, relative efficiency: 40%, resolution: 1.9 keV at 1.33 MeV). The data was acquired by a PC based multichannel analyzer for charges sufficient to produce good statistics. A USGs Granite standard, G-2, was used for quantification.

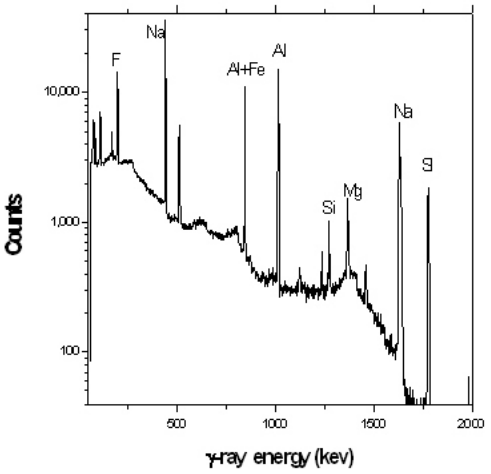


Fig. 1 PIGE spectrum of granite rock sample

Results and Discussion

Fig.1 shows a typical -ray spectrum of a granite sample. Elements such as F, Na, Mg, Al, Si etc. are present in the samples. The elements have been identified on the basis of their characteristic -rays.

The concentration of elements along with their respective reactions and -rays are listed in Table 1. It can be seen that Na, Mg, Al and Si are present in percentage levels while the content of F varies in 50-500 ppm range. The typical value of uncertainty in the measurement was <7%. Investigations revealed that ground water samples from the regions having granite rich in fluoride, contain 10-25 mg/L (ppm) fluorine. It is to be noted that the concentration of fluorine in surface water generally ranges from 0.01 to 0.3 mg/L. The high content of fluorine can result due to the leaching of fluoride from the granitic rocks.

Conclusion

PIGE measurements show that granite rocks in Nalgonda region have high content of fluorine and probably contribute to the fluorine contamination of water bodies.

References

[1] R.B. Boulton, G.T. Ewan, Anal. Chem. 49(1977) 1297.

Table-1: Concentration of F, Na, Mg, Al and Si in rock samples of different regions.

Element	-ray reactions	Location				
		Nalgonda-1	Nalgonda-3	Keesara-1	Keesara-2	Keesara-3
Na	23Na(p,p')23Na (E =440 keV)	3.07%	3.22%	2.80%	3.07%	4.73%
Mg	24Mg(p,p')24Mg (E =1369)	0.48%	0.53%	0.51%	0.54%	0.55%
Al	27Al(p,p')27Al (E =1014keV)	8.81%	9.65%	9.20%	9.96%	9.85%
Si	29Si(p,p')29Si (E =1274keV)	39.83%	33.78%	36.15%	37.57%	34.35%
F	19F(p,p')19F (E =197keV)	195 ppm	394 ppm	519 ppm	469 ppm	55 ppm

Levels of Trace Elements in Medicinal Plants with Anti-Diabetic Potential

D. K. Ray[1, 2], S. Jena[1]

1. *Department of Chemistry, Utkal University, Vani Vihar, Bhubaneswar-751004, Odisha, India; E-mail: dkray2006@gmail.com*
2. *Institute of Physics, Bhubaneswar 751005, Odisha, India*

Medicinal plants with anti-diabetic potential have been characterized by Particle-Induced X-ray Emission (PIXE) technique. Trace elements such as Ti, V, Cr, Mn, Fe, Co, Ni, Cu, Zn, Rb, Sr and Pb are found to be present in these studied medicinal plant samples. The concentrations of elements like K and Ca are quantified in percentage level whereas other elements are found to be in parts per million levels. Elemental analysis of ten different medicinal plant samples commonly used for management and cure of diabetes, shows variation in concentrations. These elements either directly or indirectly may play some role to control diabetes.

Introduction

Prevalence of all the leading chronic diseases is increasing worldwide at an alarming rate, with the majority taking place in developing countries. In India chronic diseases have surpassed communicable diseases as the leading cause of death and disability [1,2]. Diabetes mellitus is the world's largest chronic metabolic disease. According to the International Diabetes Federation, 61.3 million people in India had diabetes in 2011. That figure is projected to rise to 101.2 million by 2030 [3,4]. Various anti-diabetic drugs are available commercially for the management and control of diabetes. The oral anti-diabetic agents have varying effects on diabetes and they are not free from adverse side effects [5]. In India, many indigenous plants and plant parts are used to manage and control diabetes. The therapeutic properties exhibited by the medicinal plants are due to pharmacologically active compounds and some essential trace elements, which can be available to the human body from consumption of these medicinal plants. Although present in minute quantities, trace elements perform variety of functions. For many chemical elements (trace elements), there is a narrow range of suitability for the human body [6]. Hence it is of particular importance to determine their concentrations in medicinal plants with anti-diabetic potential.

Experimental

Medicinal plant samples commonly used for control and management of diabetes in eastern India were collected from Bhubaneswar, Odisha. The samples were dried in an oven at about 80°C for overnight and subsequently powdered. The powdered samples were mixed with pure graphite in the ratio 1:1 by mass. The mixture was thoroughly homogenized and thick targets of 13 mm diameter were prepared. Similarly, thick targets of certified reference materials (CRMs) of tomato leaves (NIST-1573) and apple leaves (NIST-1515), from National Institute of Standards and Technology (NIST, USA) were also prepared

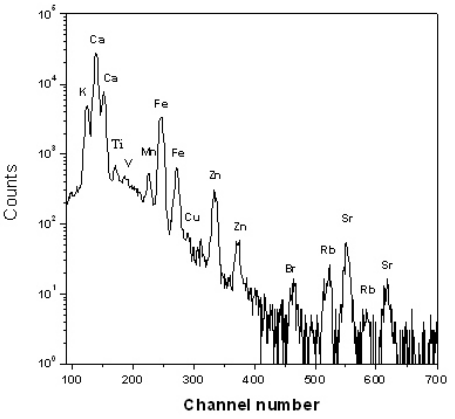


Fig. 1 PIXE spectrum of Aegle marmelos sample

Elemental analysis was carried out by using Particle induced X-ray Emission (PIXE) technique. The prepared thick targets of samples and CRMs were irradiated with 3 MeV proton beam from a 3MV-pelletron accelerator at Institute of Physics, Bhubaneswar (India) [7]. The characteristic X-rays of the elements present in all the samples were measured by using Si (Li) detector with a resolution of 160 eV at 5.9 keV. A PC based multi-channel analyzer (MCA), calibrated with ^{55}Fe X-ray source was used to record the spectra. The spectra were analyzed by using GUPIXWIN software [8]. Pellets of CRMs were irradiated with 3 MeV proton beam for quantification and verification of the results.

Results and Discussion

The PIXE spectrum of Aegle marmelos sample is presented in Fig. 1. Elements like K, Ca, Ti, V, Cr, Mn, Fe, Co, Ni, Cu, Zn, Rb, Sr, Pb etc. have been quantified in the medicinal plants. These elements are found to be present in different proportions in the studied medicinal plant samples. Elemental concentrations of these 14 elements of three medicinal plants are given in Table 1. These elements either directly or indirectly play some role to control diabetes. The variation of these elements

may be the cause of the pathological condition. The obtained result of elemental concentration shows a large variation that may be useful for evaluating the importance of certain elements in curing the disease (diabetes) delicately. PIXE is a good technique for the multi elemental analysis of medicinal plant samples.

Table-1: Elemental concentrations of three medicinal plant samples analyzed by PIXE

Elements	Aegle marmelos (Wood Apple)	Murraya koenigii (Curry Leaf tree)	Moringa oleifera (Moringa)
K (%)	0.9 ± 0.1	1.6 ± 0.2	2.1 ± 0.1
Ca (%)	0.9 ± 0.1	5.6 ± 0.1	3.7 ± 0.1
Ti	38.6 1.7	41.2 2.1	56.5 3.5
V	7.6 1.5	3.1 0.7	5.4 1.1
Cr	1.9 ± 0.7	2.5 ± 0.7	ND
Mn	31.7± 3.1	46.7 ± 2.5	20.9 ± 2.8
Fe	83.1 ± 3.6	101.8 ± 3.8	106.8 ± 4.1
Co	3.7 0.6	ND	ND
Ni	4.6 0.4	ND	5.7 0.8
Cu	9.3 ± 0.4	11.6 ± 0.4	10.5 ± 0.4
Zn	4.6 ± 0.7	33.9 ± 1.3	7.4 ± 0.7
Rb	14.3 ± 1.5	18.7 ± 1.6	34.6 ± 1.9
Sr	159.3 ± 2.7	92.3 ± 2.2	81.2 ± 2.1
Pb	19.1± 2.5	11.2± 2.0	13.5± 2.2

ND- not detected, (Common Names)

Acknowledgements

The staffs of Ion Beam Laboratory, Institute of Physics, Bhubaneswar, are acknowledged for their help during PIXE experiments.

References

[1] R. Gupta, P. Joshi, V. Mohan, K. S. Reddy, S. Yusuf, Heart, 94 (2008) 16.

[2] R. Joshi, M. Cardona, S. Iyengar, Int. J. Epidemiol. 35 (2006) 1522.

[3] Global status report on non-communicable diseases 2010. Geneva, World Health Organization, 2011

[4] N. Unwin, D. Whiting, L. Guariguata, G. Ghyoot, D. Gan, Eds.,Diabetes Atlas, International Diabetes Federation, Brussels, Belgium, 5th edition, 2011

[5] N. V. Chu, A. P. S. Kong, D. D. Kim, D. Armstrong, S. Baxi, R. Deutsch, M. Caulfield, S. R. Mudaliar, R. Reitz, R. R. Henry, P. D. Reaven, Diabet. Care, 25 (3) (2002) 542

[6] D. K. Ray, P. K. Nayak, T. R. Rautray, V. Vijayan, S. Jena, Ind. J. Physics 78B, (2004) 103

[7] P. K. Nayak, D. Das, V.Vijayan, P. Singh, V. Chakravortty, Nucl. Instr. and Meth. B 215 (2004) 251

[8] K.B. Dasari, R. Acharya, D. Joseph, N. L. Das, Proc. of the DAE Symp. on Nucl. Phys. 56 (2011) 1150

Optical, Chemical and Thermal Study of Fluoropolymers irradiated with 4 MeV Proton Ion Beam

A. Srivastava[1], Sarita[1], A. Singh[1,2], P.K. Soni[2], S.K. Gupta[3], A. Agarwal[3]

1. *Department of Chemistry, Panjab University, Chandigarh 160014, India; E-mail: alok@pu.ac.in*
2. *Terminal Ballastic Research Laboratory, Sector-30, Chandigarh 160030, India*
3. *Applied Accelerator Physics Division, Bhabha Atomic Research Centre, Trombay, Mumbai 400085, India*
4. *Radiochemistry Division, Bhabha Atomic Research Centre, Trombay, Mumbai 400085, India*

Fluoropolymers in the form of copolymer of Chlorotrifluoro Ethylene and Vinyledene Trifluoride in the ratio 2.6: 1 to 3:1 were exposed to 4 MeV proton ion beam with total ion fluence ranging from 2.2 x 10^{13} to 5.2 x 10^{14} ions at the Folding Tandem Ion Accelerator (FOTIA) Facility of Bhabha Atomic Research Centre, Mumbai. Significant changes in optical, chemical and thermal properties were observed in the irradiated copolymer when compared to its pristine counterpart.

Introduction

Fluorinated polymers are in great demand as binding materials for preparation of composites as these polymers are not only chemically and thermally stable but are also inflammable, resistant to attack of acid, alkali and oil besides ageing and oxidation [1]. They are widely used in many industrial applications such as gaskets, seals, and O-rings in aerospace, petrochemical, automotive, medical and electrical industries [2]. They are also used as a polymeric binder in high energy materials (HEMs) composites such as plastic bonded explosives (PBXs) and propellants [3,4]. Although, fluoropolymers exhibit outstanding resistance on exposure to non ionizing radiations like UV-VIS and IR radiation, their stability has been found to decrease when exposed to ionizing radiation like X-rays, Gamma rays, electrons etc. Parada et al [5] and Muntele et al [6] have studied the role of radiation effect on fluoropolymers like tetra fluoroethylene hexa fluoropropylene (FEP) and Trifluoroethylene perfluoro methoxylene (PFA) and observed some physicochemical change. In the present work the role of radiation dose on the physicochemical properties of copolymer of chlrotrifluoro ethylene with vinidylene fluoride is studied by exposing it to different ion fluence using 4 MeV proton ion beam with a view to understand the role of radiation effect vis a vis chemical composition and structure as well as applicability of the radiation modified fluoropolymer as binding material.

Experimental

The samples of copolymers of CTFE and VDF in the form of film of size 1.5 cm x 1.5 cm and having thickness of nearly 100 microns were placed on a ladder which was kept in an irradiation chamber which was evacuated to 10^{-6} Torr. The irradiation of polymers was carried out using 4 MeV collimated proton beam having diameter ranging between 8 to 12 mm. The irradiated samples were then characterized for chemical modification using Fourier Transform Infrared (FTIR) Spectroscopy and for thermal modification using Differential Scanning Calorimetry (DSC) method. The Fourier Transform Infrared (FTIR) studies were carried out in the region of 400-4000 cm^{-1} using Perkin Elmer SPECTRUM Spectrophotometer. The DSC thermograms were recorded by using Mettler Toledo 823^e differential scanning calorimeter instrument. The weight of samples studied was in the range of 4.5 1.0 mg. The scanning was carried out from room temperature to 600°C at the rate of 10°C/min using dry nitrogen gas flowing at the rate of 50 cc/min. The temperature calibration was achieved by using indium–zinc standard and that of heat flow by using indium standard.

The optical study was carried out by recording the optical micrograph of pristine and irradiated PET films by using optical microscope (Leitz DIALUX 20 EB). The maximum 200X magnification was used to study the colour and surface of the polymers. The images were clicked with the help of attached camera. The measurements were carried out two weeks after the irradiation of the foils hence the reported results represent the stationary state of the irradiated foils where the meta stable defects (if any) would have got annealed and the radiation enhanced oxidation (if any) would have got completed

Result and Discussion

The comparison of pristine film with irradiated ones showed that the studied copolymer changed its colour from light to dark brown even at ion fluence as low as 2.2 x 10^{13}. This could perhaps be due conjugation as a result of release of degradation products like HCl, HF etc due to the breaking of C-H, C-Cl and C-F bonds arising as a result of energy deposited in the polymeric system by the swift light ions of proton. Table 1 shows the percentage reflectance of absorption bands namely 2915 cm^{-1} (C-H), 1426 cm^{-1} (C-F) and 740 cm^{-1} (C-Cl) of pristine film along with that of irradiated ones.It can be observed from the above staed table that there is significant decrease in the intensity of absorption bands with the increase in total ion fluence.

The thermogram depicted in Fig. 1 shows the thermal decomposition behavior of pristine and irridiated fluoropolymer films. The weight loss of the

Table-1: Reflectance (%), wavenumber of bands (cm^{-1}) of interest and total number of ions to which CTFE-VDF copolymer films were exposed.

Bands	Pristine	4.53×10^{13}	5.29×10^{14}
C-Cl Stretching	78.82(740)	77.43(740)	67.35(740)
C-F Stretching	88.90(1426)	88.98(1426)	80.21(1426)
C-H Stretching	89.81(2915)	89.19(2915)	84.81(2915)

pristine as well as that of the film irradiated with total ion fluence of 4.5 x 10^{13} (low dose) is observed to be confined to a single-step degradation pattern. The T_{onset}, T_{endset} and T_{max} temperature in centigrade for pristine film exposed was found to be 423.9, 467.9 and 458.6 respectively where as that of the film exposed to lower dose was found to be 419.9, 463.5 and 455.3 respectively. The thermal degradation temperature of pristine and irridiated fluoropolymer showed a slight change. The TG data indicated that the thermal decomposition for fluoropolymer irradiated with total ion flunce of 2.2 x 10^{14} (high dose) occurred in the lower temperature range i.e 370-450°C whereas the thermal decomposition for pristine occurred at higher temperature range i.e 420-465°C. The irridiated samples which were stable up to about 370°C underwent a weight loss of less than 0.5-1.8 % below temperature 400°C. as a result of radiation induced degradation of the polymer. The pristine however did not show any significant decomposition till 420°C, indicating that it possessed the necessary thermal stability for subsequent applications such as polymeric binders. The study further shows that beyond certain radiation dose i.e total ion fluence the copolymer CTFE-VDF too degrades like PFA and FEP therefore making it unfit as binding material.

Acknowledgments

Authors thank operating staff of Folding Tandem Ion Accelerator, BARC, Mumbai for their cooperation during the sample irradiation. The help rendered by Mr.Sandeep of Central Instruments Laboratory of Chemistry Department, Panjab University is also acknowledged.

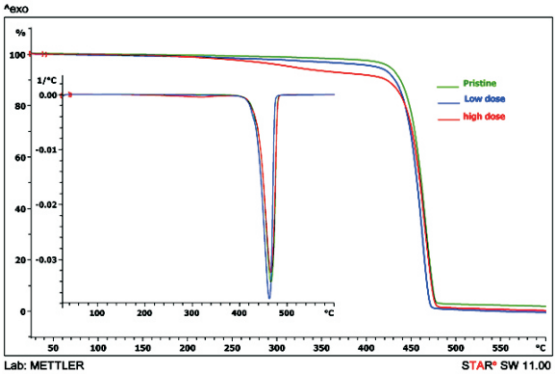


Fig. 1 TG/DTG curves CTFE-VDF copolymer films exposed to different total ion fluence of protons (a) pristine, (b) 2.16 x 10^{13} and (c) 2.16 x 10^{14}

References

[1] G. Moggi, P. Bonardelli and J.C Bart, J. Polym Bull 7, 115 (1982).

[2] G. Ajroldi, M. Pianca, M. Fumagalliand, G.Moggi, Polymer 30, 2180 (1989).

[3] A. Singh, P. K. Soni, M. Singh and A. Srivastava, Thermochimica Acta 548, 88 (2012).

[4] A. Singh, P. K. Soni, T. Shekhram and A. Srivastava, Jour. of Applied Polymer Science 127, 1251 (2013)

[5] M. A. Parada, R. A. Minamisawa and R. A. Almeida, Brazillian Jour. Physics 34, 948 (2004)

[6] C.I. Muntelle, S.R. Allavarov, I.C. Montele and D.Ila NIMB 261, 694 (2006)

Analysis of ancient pottery samples and reference materials by Particle Induced X-ray Emission

K.B. Dasari[1,2], R. Acharya[1*], D.K. Ray[3], A. Behera[3], N.Lakshmana Das[2*]

1. *Radiochemistry Division, Bhabha Atomic Research Centre, Trombay, Mumbai 400 085; E-mail: racharya@barc.gov.in*
2. *GITAM Institute of Science, GITAM University, Visakhapatnam 530 045; E-mail: nldas9@gmail.com*
3. *Ion Beam Laboratory, Institute of Physics, Bhubaneswar 751 005*

Particle Induced X-ray Emission using proton beam (1.5 and 3 MeV) from 3MV tandem accelerator at IOP was applied to ancient pottery samples for determination of major to trace element concentrations. Thick targets in graphite matrix were irradiated at about 10 nA current and characteristic X-rays were measured using a Si(Li) detector coupled to MCA. Concentrations of thirteen elements K, Ca, Ti, V, Cr, Mn, Fe, Cu, Zn, Ni, Rb, Sr and Zr were determined. The results of all elements including transition elements were used for grouping (same or different) the ancient potteries. IAEA RMs SL-1 and SL-3 were analyzed by PIXE as part of application and validation of method.

Introduction

Provenance studies of archaeological ceramic artifacts are best done by their chemical composition. Among the ceramics artifacts of potteries bricks and tiles [1], potteries are most studied due to their strong correlation to the source clay and recipe of the making. Trace elements are finger prints of source clay and thus provide authentic information for the grouping study of artifacts i.e. to establish they are from same or different origin / source. The elements having non-volatile and immobile nature or similar geochemical properties (transition elements or rare earth elements (REEs)) are chosen for grouping study. Analytical techniques such as instrumental neutron activation analysis (INAA), prompt gamma ray NAA (PGNAA), particle induced X-ray emission (PIXE) and particle induced gamma ray emission (PIGE) and energy dispersive X-ray fluorescence (EDXRF) are used for obtaining elemental concentrations. We have used INAA for analysis of small samples of ancient potteries [1,2]. PIXE is an alternate analytical tool to INAA. PIXE is a high sensitive surface analytical technique and is capable of determination of major, minor and trace elemental concentrations depending on energy and intensity of proton beam [3].

In the present study, about 30 ancient pottery samples collected from ancinet Buddhist sites of Andhra Pradesh were analysed using PIXE technique. Along with pottey samples, IAEA reference materials were analysed for validation method. All elements including transition elements were used for grouping study.

Experimental

Authenticated pottery samples were collected with help of Dept. of archaeology and Museums, Visakhapatnam. About 2 g pottery samples grounded and 400 mg weighed samples was taken for study. Samples were mixed with high purity graphite powder in 3:1 ratio. The purpose of mixing graphite powder as a binder, it is high pure and it acts as monitor the beam current from the sample during irradiation. The resultant mixture was compressed using a 2 ton hydraulic press into pellets of 13 mm diameter and about 1 mm thickness. The experiment was carried out using 3 MV tandem accelerator at Institute of Physics (IOP), Bhubaneswar with 1.5 and 3 MeV proton energies (current ~10 nA) were used. Pellets were placed on an aluminum ladder in the PIXE chamber at 0° to the beam direction and X-rays were analyzed using a LN_2 cooled Si(Li) detector of resolution 150 eV at 5.9 keV X-ray of Mn coupled with MCA 1 software. Typical spectra obtained for irradiated pottery sample are given in Fig. 1.

GUPIX software was used for analysis of PIXE spectra to get net peak area and also for concentration calculation. Elements detected with 1.5 MeV proton beam were Cl, K, Ca, Sc, Ti, V, Cr, Mn and Fe and with 3 MeV proton beam were Ni, Cu, Rb, Sr and Zr. While using 3 MeV proton beam, 60 ìm thick Al filter was used to cut the low energy X-rays from major elements like Si and Al.

Results and Discussion

Elemental concentrations namely K, Ca, Ti, V, Cr, Mn, Fe Ni, Cu, Zn, Rb, Sr and Zr were determined in ancient potteries as well as IAEA RMs SL-1and SL-3. Results of two IAEA RMs and two ancient pottery samples are given in Tables 1 and 2 respectively. The uncertainties quoted are due to peak fitting and counting statistics at ±1s confidence limit and they are in the range of 3-12%. The % deviation of elements determined with respect to recommended values are within ±10% indicating good quality of results.

Results of thirteen elements in three different potteries are given in Table 2. Elemental concentrations including transition elements like Fe, Mn, V, Cr, Cu and Ni are used for grouping the objects under study. As seen in the Table 2, potteries 1 and 2 are comparatively similar pottery 3, which was collected faraway place than earlier two samples. The results were used in statistical cluster analysis, which revealed that the

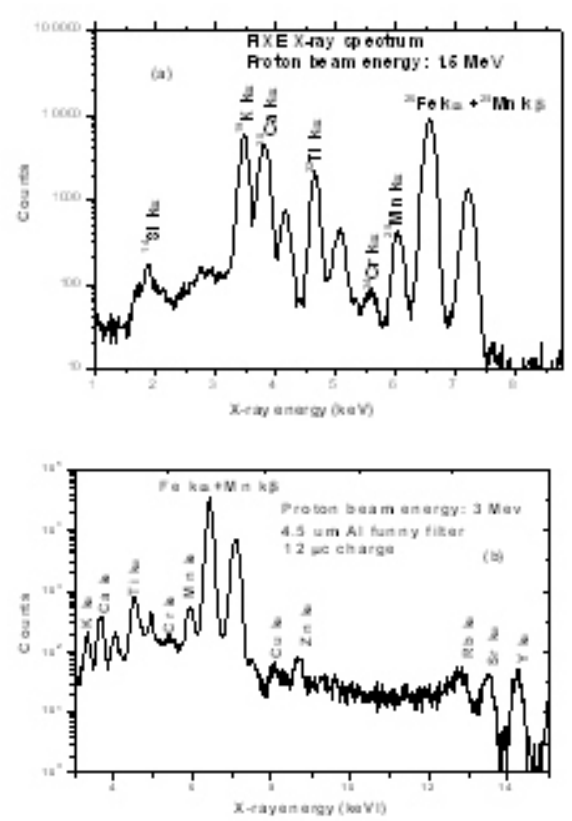


Fig. 1 Typical X-ray spectra of ancient pottery sample using (a) 1.5 MeV and (b) 3 MeV proton energies

Table-1 Determined concentrations (mg kg^{-1}) of IAEA RM SL-1 and SL-3 analysed by PIXE

Element	IAEA SL-1		IAEA SL-3	
	Thiswork	Recom. /info.	Thiswork	Recom. /info.
Cl	11.12±1.3	(10)	1.81±0.5	NA
K	16667±86	(15000)	7933±23	8740±786
Ca	2581±36	(2500)	95844±293	111100±4444
Ti	4984±52	(5170)	2580±321	2610±313
V	182±16	170±15.3	NA	17.3
Cr	98 ±21	(104)	38±21	(42.7)
Mn	3418±12	(3460)	415±11	390±35
Fe	66053±31	(67400)	12012±21	(10300)
Ni	39.6±22.9	44.9±8.08	14.6±3.2	NA
Zn	213±20.6	223± 8.92	40.6±6.5	36.1±2.5
Rb	119±18	113±11.3	33.1±1.9	38.8±0.7

NA: not available

Table-2: Results of two ancient pottery samples analysed by PIXE

Element	Pottery 1	Pottery 2	Pottery 3
K %	1.08±0.07	1.15±0.04	1.33±0.05
Ca %	0.44±0.02	0.38±0.02	0.56±0.04
Ti %	0.77±0.04	0.69±0.03	0.55±0.02
V	116±8	106±6	86±5
Cr	143±11	134±6	104±6
Mn	892±32	1765±59	2768±98
Fe %	5.53±0.06	4.99±0.05	4.46±0.08
Cu	77±5	56±6	98±4
Zn	144±13	121±7	129±11
Ni	76.6±4	88±5	109±8
Rb	109±7	126±9	256±17
Sr	1514±46	1326±35	1106±11
Zr	121±8	ND	156±8

samples under study fell into broadly tow groups. Thus PIXE can be used as an alternate method to NAA and other techniques, for ceramic samples and RM analysis.

Acknowledgements: Authors from GITAM University thank Dr. P.K. Pujari, Head, NCS, RCD and Dr. A. Goswami, Head, RCD, BARC for the support and encouragement. Authors thankfully acknowledge UGC-DAE CSR, Mumbai for the project and financial assistance and Dr. P. Gayatri, Director, Department of Archaeology and Museum, Govt. of Andhra Pradesh, Hyderabad for providing authentic samples.

References

[1] K.B. Dasari,et al., J. Radianal. Nucl. Chem. 294(2012) 339.

[2] K.B. Dasari, et al., J. Radioanal. Nucl. Chem. 286(2010) 525.

[3] A. Adraens Spectrochimica Act Part B 60(2005) 1503.

Simultaneous Quantification of Li, Ti and O in Lithium Titanate by Particle Induced Gamma-ray Emission using 8 MeV Proton Beam

Sumit Chhillar[1], R. Acharya[1], R. Tripathi[1], S. Sodaye[1], K. Sudarshan[1], P.C. Rout[2], S.K. Mukherjee[3], P.K. Pujari[1]

1. *Radiochemistry Division, Bhabha Atomic Research Centre, Trombay, Mumbai 400085, India; E-mail: racharya@barc.gov.in*
2. *Nuclear Physics Division, Bhabha Atomic Research Centre, Trombay, Mumbai 400085, India*
3. *Fuel Chemistry Division, Bhabha Atomic Research Centre, Trombay, Mumbai 400085, India*

Simultaneous quantification of Li, Ti and O in lithium titanate (Li_2TiO_3) is difficult by particle induced gamma-ray emission (PIGE) using low energy (~4 MeV) proton beam. PIGE method using 8 MeV proton beam at BARC-TIFR pelletron facility was standardized for compositional characterization of sol-gel synthesized Li_2TiO_3 by determining concentrations of Li, Ti and O simultaneously. Thick targets of samples, synthetic samples and standards were prepared in graphite matrix. Beam current variation was normalized by Rutherford Backscattering Spectrometry (RBS) using a thin gold foil. The gamma-rays of 478, 981 and 6129 keV were measured from $^{7}Li(p, p')^{7}Li$, $^{48}Ti(p, p')^{48}Ti$ and $^{16}O(p, p')^{16}O$ nuclear reactions for quantification of Li, Ti and O, respectively. The method was validated by determining concentrations of Li, TI and O in a synthetic sample.

Introduction

Lithium titanate is an important candidate for tritium breeding material. Synthetically this ceramic material can be prepared either by wet-chemical methods or through solid sate reaction synthesis. Lithium titanate (Li_2TiO_3) is considered as one of the suitable candidates for blanket material because of tritium recovery at low temperature and its good chemical stability. Compositional characterization of this ceramic is important because any non-stoichiometry in this material will affect its thermo-chemical properties and tritium release behavior other than synthetic route optimization. This material is analytically difficult to analyze by conventional analytical methods as it is difficult to dissolve the sintered material. Non-destructive nuclear/radio-analytical methods like neutron activation analysis (NAA), particle induced X-ray emission (PIXE) and XRF are not suitable for compositional characterization of Li_2TiO_3 except for Ti. PIGE using proton beam, capable of determining low Z elements, is a suitable nuclear analytical method for Li, Ti and O, however, at low proton energy it can determine Li but at higher proton energy it is feasible to determine all three elements simultaneously. We have standardized PIGE method using 4 MeV protons beams at folded tandem ion accelerator (FOTIA) facility at BARC, Mumbai, for Li and NAA for Ti [1,2]. In the present work, we report for the first time to the best our knowledge, simultaneous quantification of Li, O and Ti in this sol-gel synthesized ceramic material by PIGE using high energy (8 MeV) proton beam from BARC-TIFR pelletron facility.

Experimental

The targets for irradiation were prepared in graphite matrix. Standard was prepared by homogenously mixing Li_2CO_3 (~ 50 mg) and TiO_2 (~ 50 mg) in graphite matrix. In order to validate the method, synthetic sample for Li, Ti and O was prepared by mixing TiO_2 (~ 60 mg) and Li_2CO_3 (~60 mg) in graphite matrix. Targets of sintered lithium titanate samples were prepared by mixing ~100 mg of samples with graphite matrix. The target pellets were mounted on Al ladder and irradiated with 8 MeV proton beam (beam current ~10-15 nA) from pelletron facility of BARC-TIFR, Mumbai. The respective gamma-rays from the targets were measured by using 30% HPGe detector, placed perpendicular to the direction of the beam, coupled with 8k MCA. In order to normalize the beam current fluctuations during the irradiations the count rate of targets were normalized by RBS count rate of Au thin foil fixed just before the target pellet. The determination of Li, Ti and O is based on the measurement of 478 keV, 981 keV and 6129 keV of gamma-ray from $^{7}Li(p, p')^{7}Li$, $^{48}Ti(p, p')^{48}Ti$ and $^{16}O(p, p')^{16}O$ nuclear reactions, respectively. The RBS normalized sensitivities of Li, Ti and O were used for calculating the concentrations (in wt%) of Li, Ti and O in Li_2TiO_3 samples as given below:

$$C(x)=(CPS_x/CPS_{RBS})/(CPS_{std}/(CPS_{RBS}*(Mass_x)_{std})$$

Results and Discussion

The PIGE spectrum of lithium titanate sample is shown in Fig. 1, which clearly shows the gamma rays of Li, Ti and O. Fig. 2 shows the comparison plot of expected and obtained concentrations of Li, Ti and O one synthetic sample and the results of determined concentrations are in good agreement (within 3% for Li, 1% for Ti and 2% for O) with the expected values of Li, O and Ti. Results for two sintered samples of lithium titanate are shown in Table 1. For oxygen, it is necessary to acquire the spectrum for longer time as the detection efficiency HPGe detector is low for this high energy (6.129 MeV) gamma-ray. The uncertainties reported in the results are the propagated ones which are due to the mass of sample and standard (< 0.2%),

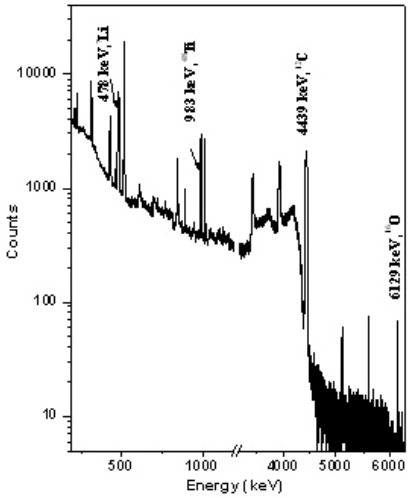


Fig. 1 PIGE spectrum of lithium titanate sample showing the gamma-lines of Li, Ti and O when irradiated with 8 MeV proton beam

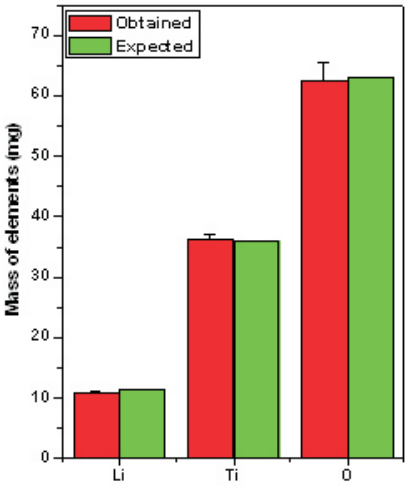


Fig. 2 Comparison between the expected and obtained values of Li, Ti and O in a synthetic sample analyzed by PIGE

counting statistics and peak fitting (< 3% for Li and Ti and < 6 % for O) errors. PIGE method could determine Li, Ti and O due to higher excitation function responses of isotopes at higher energy.

Table-1: PIGE results showing the weight % of constituent elements of Li_2TiO_3 samples prepared by sol-gel synthetic route

Element	Sam- Id.	Sample 1	Sample 2
Li	Expected (wt%)	12.67	12.67
	Obtained (wt%)	12.0 ± 0.3	12.3 ± 0.4
Ti	Expected (wt%)	43.5	43.5
	Obtained (wt%)	43.7 ± 1.2	43.9 ± 1.3
O	Expected (wt%)	43.8	43.8
	Obtained (wt%)	44.3± 2.5	43.8 ± 2.5

Conclusions

PIGE with 8 MeV proton beam was used for simultaneous determination of Li, Ti and O. The method reported here is non-destructive, simple and sensitive in nature for this ceramic material.

Acknowledgements

The authors thank Dr. A. Goswami, Head, RCD and Dr. S. K. Aggarwal, Associate Director, RC&I Group and Head, FCD, BARC for their support and encouragements. Authors thank Shri T.V. Vittal Rao and Shri Y. R. Bamankar, FCD, BARC for providing samples. Authors thank Dr. Suresh Kumar, NPD for valuable suggestion for PIGE experiment at TIFR.. Authors thank BARC-TIFR pelletron staff for help during experiment. One of the authors (Sumit Chhillar) thanks HBNI-DAE for the financial assistance.

References

[1] Sumit Chhillar R. Acharya T. V. Vittal Rao, Y. R. Bamankar, S. K. Mukerjee, P. K. Pujari and S. K. Aggarwal, J. Radioanal. Nucl. Chem., 298 (2013) 597.

[2] Sumit Chhillar, R. Acharya, R. V. Pai,,S. Sodaye, S. K. Mukerjee, P. K. Pujari J Radioanal. Nucl. Chem. 293 (2012) 437.

[3] Pritty Rao, G. L. N. Reddy, J. V. Ramana, S. K. Mukherjee, S. Vikram Kumar, Y. Sunitha, Sanjiv Kumar, 11th Biennial DAE-BRNS Symposium on Nuclear and Radiochemistry.

R&D Work on Particle Induced Gamma-ray Emission (PIGE) using proton beam at FOTIA, BARC: Present Status and Future Prospects

R. Acharya[1], S. Chhillar[1], S. Sodaye[1], P. K. Pujari[1], A. Agarwal[2], S. K. Gupta[2] and P. Singh[2]

1. *Radiochemistry Division, Bhabha Atomic Research Centre, Mumbai 400085, India; racharya@barc.gov.in*
2. *Ion Accelerator Development Division, Bhabha Atomic Research Centre, Mumbai 400085, India*

Particle induced gamma-ray emission (PIGE) is an isotope specific nuclear analytical capable of determining concentration of low Z elements (like Li, Be, B, F, Na, Mg, Al, Si, P and S) in diverse matrices. PIGE is complementary to NAA, PIXE and XRF. It involves measurement of prompt gamma-rays from inelastic scattering (p, p) and nuclear reactions like (p, n), (p,) and (p,). Radiochemistry Division has set-upped a PIGE facility at FOTIA (folded tandem ion accelerator facility), with the help of IADD, BARC. PIGE method has been applied to various type of samples like borosilicate glass, lithium based ceramics, boron based compounds, solid samples and ceramic reference materials.

Introduction

Ion beam analysis (IBA) is an important analytical technique involving the use of MeV ion beams to probe the composition and obtain elemental depth profiles in the near-surface layer of solids. All IBA methods like RBS (Rutherford backscattering), ERDA (elastic recoil detection analysis), PIGE (particle induced gamma-ray emission), PIXE (particle induced X-ray emission), NRA (nuclear reaction analysis) and EBS (elastic backscattering spectrometry which is non-Rutherford in nature) are highly sensitive and allow the detection and hence quantification of almost all elements. In the present paper we will detail briefly the setting-up of PIGE facility at folded tandem ion accelerator (FOTIA, 6MV), IADD, BARC, Mumbai, used for quantification of light elements.

PIGE is an important nuclear analytical technique used for determination of light elements (Z 20) in diverse matrices. In this technique, beam of charged particles fall on sample surface and nuclear reactions like (p, p'), (p,), (p, n) and (p,) and gamma-rays emitted in this process are the signature of a specific isotopes. The number of gamma-ray counts is directly proportional to the concentration of an isotope in the sample.

PIGE uses gamma-rays, thus experiences less matrix effect. This property helps in applying PIGE for thick samples. Due to its non-destructive nature, capability to analyze low Z elements simultaneously due to its high sensitive towards some of the light elements like Li, B, F, Al and Si.

Experimental

FOTIA has the five opening ports after analyzing magnet. Out of the five ports, PIGE facility was set-up in 25°S beam line. The beam is taken in the reaction chamber kept at vacuum of 10^{-6} torr. The sample and HPGe detector is generally kept at an angle of 90° with respect to the beam direction in order to avoid Doppler broadening in the measurements of -rays in PIGE experiments.



Fig. 1 PIGE setup at FOTIA BARC



Fig. 2 Optical photograph of typical PIGE pellets in cellulose matrix fixed on target ladder

The standard and sample targets for irradiation were prepared in pellet form (dia. 2 cm thickness 2 mm) using either cellulose or graphite as binder and matrix. Optical photographs of PIGE facility setup (Fig. 1) and targets mounted on stainless steel ladder (Fig. 2). The targets were irradiated with 4 MeV proton beam (10-20 nA) depending on the concentration of analyte in the target. The gamma-ray corresponding to different isotopes of elements was measured by high resolution gamma-ray spectrometry. The gamma-lines used for the quantification of Li (429 keV for ^{6}Li and 478 keV for ^{7}Li), B (429 keV for ^{10}B, 718 keV and 2125 keV for $^{(10, 11)}$B), F (110 keV and 197 keV for ^{19}F), Na (440 keV for ^{23}Na), Si (1779 for ^{28}Si) and Al (844 and 1014 keV for ^{27}Al) in different samples of lithium titanate,

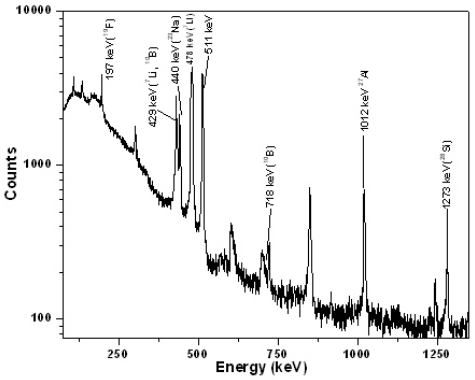


Fig. 3 PIGE spectrum of lithium titanate showing peaks of Li and F

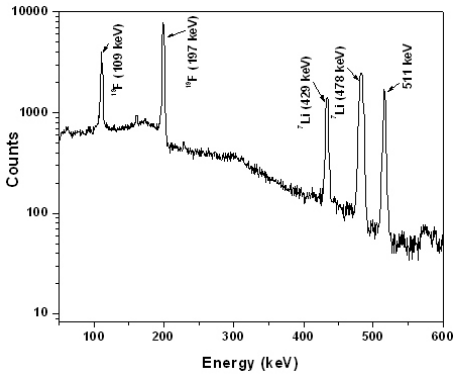


Fig. 4 PIGE spectrum of lithium titanate showing peaks of Li and F

borosilicate glass boron carbide, ceramic reference materials (soil and sediments). The gamma-lines were measured by using 30% HPGe detector, placed in a direction perpendicular with respect to the incident beam, coupled with 8k MCA. The concentration of isotope of an element of interest was calculated by using relative method. The PIGE method was validated by using synthetic samples.

Results and Discussions

We have developed in situ current normalized PIGE method in addition to RBS approach using thin Au foil. The samples of interest are glass, ceramics (Li and Ti based) reference materials and soil. The PIGE method has been successfully applied for quantification of:

1. Fluorine in borosilicate glass matrix [1].
2. Simultaneous quantification of low Z elements in borosilicate glass [2]
3. Li in lithium based ceramic materials like titanate samples (prepared by sol-gel route) and lithium doped neodymium dititanate [3, 4].
4. Total boron and boron isotopic composition in boron compounds and boron carbide

The PIGE spectra of borosilicate glass, lithium titanate are shown in Figs. 3 and 4, respectively. In case of F quantification in borosilicate glass [1], we use both RBS and in situ (using Li) current normalizing approach. F is used as in situ current normalizing element in Li based ceramic materials [2,3] and boron based compound. Since PIGE is isotope specific, it is applied for ^{10}B and ^{11}B quantification for enriched and natural B_4C. Details are given in this abstract book elsewhere by S. Chhillar et.al.

Future Prospects

RCD has developed in situ current normalized PIGE method using low energy proton beam for light elements. The non-destructive nature and simultaneous determination of light elements makes PIGE as an attractive nuclear analytical. The gamma-ray spectra of different low Z elements are free from interference and experience negligible of no matrix effect. Isotopic composition analysis of B has been optimized and Li ($^6Li/^7Li$) is in progress. Determination of Be, Li, B and other elements in different matrices (non-powder samples) is being pursued using Al as the in situ current monitor. A dedicated external PIXE/PIGE facility is being set up by RCD at FOTIA in addition to present facility for development and application work for low Z elements.

Acknowledgement

Authors thank Dr. A. Goswami, Head RCD, BARC for his constructive and encouraging suggestion and discussions during the work, Authors also thank FOTIA staff members for their support during the experimental work at IADD, BARC.

References

[1] Sumit Chhillar, R. Acharya, S. Sodaye, K. Sudarshan, S. Santra, R. K. Mishra, C. P. Kaushik R. K. Choudhury, P. K. Pujari, J. Radioanal. Nucl. Chem. 294 (2012) 115

[2] Sumit Chhillar, R. Acharya, R. V. Pai,,S. Sodaye, S. K. Mukerjee, P. K. Pujari, J. Radioanal. Nucl. Chem. 293 (2012) 437

[3] Sumit Chhillar R. Acharya T. V. Vittal Rao, Y. R. Bamankar, S. K. Mukerjee, P. K. Pujari and S. K. Aggarwal, J. Radioanal. Nucl. Chem. DOI 10.1007/s10967-013-2609-5.

[4] Sumit Chhillar, R. Acharya, R. K. Mishra, C. P. Kaushik and P. K. Pujari, Proceedings Eleventh biennial symposium on Nuclear and Radiochemistry 2013.

Studies on Fluoride Contents in Soil Samples from Punjab using Particle Induced Gamma Emission

A. Srivastava[1], S. Chhillar[2], Amol D. Shinde[3], N. Kaur[1], D. Singh[4], R. Acharya[2], P.K. Pujari[2]

1. *Department of Chemistry, Panjab University, Chandigarh 160014, India; E-mail: alok@pu.ac.in*
2. *Radiochemistry Division, Bhabha Atomic Research Centre, Trombay, Mumbai 400085*
3. *Analytical Chemistry Division, Bhabha Atomic Research Centre, Trombay, Mumbai 400085*
4. *Department of Soil, Punjab Agricultural University, Ludhiana 141027*

A particle induced gamma-ray emission (PIGE) methodology has been standardized for quantification of fluorine in soil samples of different regions of Punjab, using 4 MeV proton beam from folded tandem ion accelerator (FOTIA) at BARC, Mumbai. The standards, reference material standard (NIST SRM 1645a) and soil samples were prepared by mixing in cellulose matrix with constant amount of lithium carbonate. Li was used as in situ current normalizing element for normalizing beam current variations during the experiments. The gamma-rays of energies 197 keV and 478 keV were measured from $^{19}F(p,p')^{19}F$ and $^{7}Li(p,p')^{7}Li$ nuclear reactions by using high resolution gamma-ray spectrometry.

Introduction

It is a well-established fact that long exposure to fluoride could be harmful to bones and teeth. It has been estimated that in India close to 62 million people are affected by water contaminated with fluoride [1]. Rajni Sharma [2] has reported that the concentration of fluoride in drinking water from Amritsar, Bhatinda, Faridkot, Fatehgarh Sahib, Firozepur, Gurdaspur, Mansa, Moga, Muktsar, Patiala and Sangrur Districts of Panjab is higher than the permissible level of 1.5 ppm recommended by World Health Organization. The main sources of fluoride in water are minerals like fluorite, fluoraptatite and cryolite which are present deep in earth's crust at concentration level of 600-700 ppm. Fluorine is also known to be present significantly in products of coal combustion besides pesticides and fertilizer. Punjab being the foremost State in agriculture production during the green revolution has been a site for indiscriminate application of pesticides and fertilizers in its soil. Therefore, it should not be surprising if soil itself could be an important source leading to the contamination of drinking water by fluoride. Rajbir Kaur et al. [3] have recently reported the concentration of fluoride in soil samples collected from locations in and around Chandigarh the capital city of Punjab State which are not affected by fluoride rich water.

In the present work, the concentration of soil from locations possibly having elevated level of fluoride in water have been analyzed for fluoride content using PIGE method, a well established nuclear analytical technique highly sensitive for low Z elements (Z<17) especially for F and Li.

Experimental

Soil samples were collected from different locations of Punjab, where fluoride contamination has been reported previously. The samples were collected at a depth ranging 5 to 30 cm by using normal auger method. The samples were dried below 60 degrees centigrade for 12 hours. In order to normalize the affect

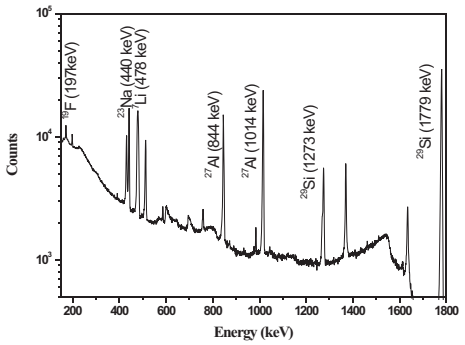


Fig. 1 Particle induced gamma-ray emission spectrum of one of the soil samples

of beam current fluctuations an in situ current normalizing element (Li) was added in constant amount to every target. The count rate of gamma-line of interest (197 keV for F) are normalized by the count rate of gamma-ray from in situ element (478 keV Li) counts.

Sample pellets were prepared by mixing homogenously soil samples (~300 mg) with Li_2CO_3 (~20 mg) in cellulose matrix. Standards were prepared by mixing homogenously about 30-50 mg of CaF_2 and 20 mg of Li_2CO_3 and about 550 mg of cellulose. The pellets were irradiated, under high vacuum (10^{-6} torr) conditions, with 4 MeV proton beam (beam current 5 – 10 nA) from FOTIA, BARC, Mumbai. The duration of irradiation time was varied between 10 – 60 minutes depending on the F amount in the targets. The 197 keV prompt gamma-rays of F from the $^{19}F(p,p')^{19}F$ reaction were measured using a 30% HPGe detector placed perpendicularly to the beam axis at a distance of 5 cm from the target ladder. For method validation, a control sample pellet was prepared using NIST SRM 1645a. Typical gamma ray spectrum of a soil sample is shown in Fig. 1. The gamma ray spectra were analyzed using peak fitting software (PHAST) [4] to determine the peak areas under the gamma ray peaks of 197 keV from

the ^{19}F (p, p') ^{19}F and 478 keV from the ^{7}Li (p,p') ^{7}Li reactions respectively. Lithium normalized sensitivity of 197 keV gamma-ray of F was used for quantification of F in various soil samples.

Results and Discussion

Figure 1 shows the gamma-ray spectrum of a representative soil sample. Table 1 gives the amount of fluorine present in different soil samples. And the results obtained for NIST SRM 1645a. It can be observed that the concentration of fluoride in the locations studied ranged between 414 and 5746 mg/kg. The minimum was observed at Nabha [Sam-8] in Patiala District and the maximum at Talwandi Sabo [Sam-3] in Bhatinda District. The uncertainties in the results reported are mainly due to the counting statistics and peak fitting errors. The mean fluoride concentration was obtained as 1398 ± 94 mg/kg.

Table-1: Concentrations (mg/kg) of Fluorine in different locations of Punjab

Sl. No.	Sample	F Conc (mg/kg)
1	Sam-1	1440 ± 22
2	Sam-2	1348 ± 21
3	Sam-3	5746 ± 77
4	Sam-4	1398 ± 21
5	Sam-5	952 ± 14
6	Sam-6	689 ± 11
7	Sam-7	719 ± 13
8	Sam-8	414 ± 6
9	Sam-9	1680 ± 23
10	Sam-10	676 ± 8
11	Sam-11	816 ± 11
12	Sam-12	755 ± 16

A comparison of the data obtained in the present work from region affected by fluoride with that obtained by Kaur et al [2] from region unaffected by fluoride contamination of water shows that the minimum and maximum concentration of fluoride in soil ranged between 275 and 869 mg/kg with a mean of 522 ± 58 mg/kg. The mean soil concentration in the affected region seemed to be nearly three times more than that observed in the unaffected region.

Conclusion

The concentration of fluoride in soil in region affected by fluoride contaminated water is significantly high. It can be further stated that the nuclear analytical technique PIGE can be successfully used for such type of studies. It would be interesting to carry out further work in this direction to make more concrete conclusion as the body of data is still scanty.

Acknowledgement

Authors thanks sincerely to Dr. A.V.R. Reddy, Head, ACD, and Dr. A. Goswami, Head, RCD, BARC, Mumbai for their suggestions and support during the experiment. Authors also thanks to Mr. S. K. Gupta, Mr. A. Agarwal and entire FOTIA staff, IADD, BARC Mumbai for their keen interest and extending their help during the experiments.

Figure 1: Particle induced gamma-ray emission spectrum of one of the soil samples

References

[1] N.Arlappa, Q.I. Aatif and R. Srinivas, Int J Res Dev Health. 1 (2013) 97

[2] R.Sharma, Asian Jour. of Adv.Sci. and Eng. Research 1 (2012) 1

[3] R.Kaur, M.Oswal, A.Singh, N.Kaur, K.P.Singh, B.R.Behra, G.Singh and A. Kumar, Proc. DAE Symposium on Nucl. Phys. 55 (2010) 778

[4] Mukhopadhyay PK, Proceedings of the symposium on intelligent nuclear instrumentation (INIT-2001), Bhabha Atomic Research Centre, Mumbai, p 313 (2001)

Characterization of Mercury based Indian Herbomineral drug by Radioisotope Induced EDXRF and Synchtrotron based EXAFS

Daisy Joseph[1], Rajeeta Joseph[2], P.Rajput[3], C.Nayak[3], A.Saxena[1], D.Bhattacharya[3], S.N.Jha[3]V.Natrajan[4]

1. *Nuclear Physics Division, Bhabha Atomic Research Centre, Trombay, Mumbai 400 085*
2. *Bharati Vidyapeeth Dental College, Pune*
3. *Atomic and Molecular Physics Division, Bhabha Atomic Research Centre, Trombay, Mumbai 400 085*
4. *Radiochemistry Division, Bhabha Atomic Research Centre, Trombay, Mumbai 400 085*

An Indian herbomineral drug was characterized for its trace elements by radioisotope induced EDXRF.The drug contains minerals like mercury, sulfur and arsenic disulfide, along with herbs such as dhaturra, bhrami, vacha etc. All the above ingredients were processed together in a step wise manner (6 steps), Hence the motive was to expect some change in the drug molecule at every step of processing it. The 6 samples are the samples collected at every step of drug preparation. These 6 samples which are collected as intermediatary samples would be then evaluated for its role in various neuropsychological (psychosis, depression etc) disorders in experimental animals such as rats/mice. Hence it was required to find the elements/ trace elements composition, details of chemical components present in the drug samples,. It was seen that using EDXRF it was possible to determine As and Hg .The EXAFS results also showed the presence of As in their sulphide form

Introduction

Ayurveda makes use of herbal preparations for their curative effects. Use of metallic herbal preparations (bhasma), in which a process termed bhasmikarana used to prepare the drug is unique to the Ayurveda. It is believed that the bhasmikarana process converts the metal into its specially desired chemical compound, which eliminates the toxicity of the metal and has the necessary medicinal benefits [1]. Ayurvedic texts provide a list of tests for the efficacy of the bhasmikarana process. The tests which are essentially qualitative ensure that the resulting drug is very fine (small grains), has no metallic shine and does not ally with silver even at higher temperature to which it is subjected [2]. However, these qualitative tests do not provide any quantitative information about the composition and the structure of the final drug. For any drug containing heavy metals (for example mercury), such structural information is an absolute necessity [3]. The present herbomineral drug mercury based bhasma is prescribed for certain diseases, viz. Psychosis, depression The combination of sulphur is believed to have neutralized the pharmaco-kinetics and bio-distribution of Kajjali (a sulphur and mercury preparation). Several others have also worked on the efficacy and safety aspects of mercurial preparations in such traditional drugs. None of the work presents the elemental and structural characterization of the drug, which is essential requirement to discuss the non toxicity and therapeutic value of the mercurial preparations. Various techniques, viz. XRD, TEM, XPS, IFIR, FTIR, DTA, TGA, EDAX and AAS can be used for characterisation of this drug. In this report, the composition of the present herbomineral drug has been analyzed using EDXRF and its structure has been investigated using synchrotron based EXAFS.

Experimental

The 6 samples were as follows Sample 4: Hg + S,Sample 5: Hg+S+AsS,Sample 6 : Hg+S+AsS + dhattur(plant) ,Sample 7: Hg+S+AsS + Vacha(plant) Sample 8: Hg+S+AsS +Agast(plant) ,Sample 9: Hg+S+AsS + Brahmi(plant) These samples were collected at every step of drug preparation.The samples were powdered finely and mixed with cellulose as a binding material to make self-supporting pellets weighing 300 mg. The samples were then placed in front of an XRF spectrometer, consisting of Cd^{109} radioactive source,a Si (Li) detector cooled at liquid nitrogen temperature (77 K), along with required electronics. The reverse bias of 800 V was applied across the semiconductor junction of Si (Li) detector and the resolution of the detector was 150 eV at 5.9 keV. The X-ray spectra were recorded for a counting time of 2000 seconds and stored in a PC based multi-channel analyzer for further offline analysis.

Results and Discussion

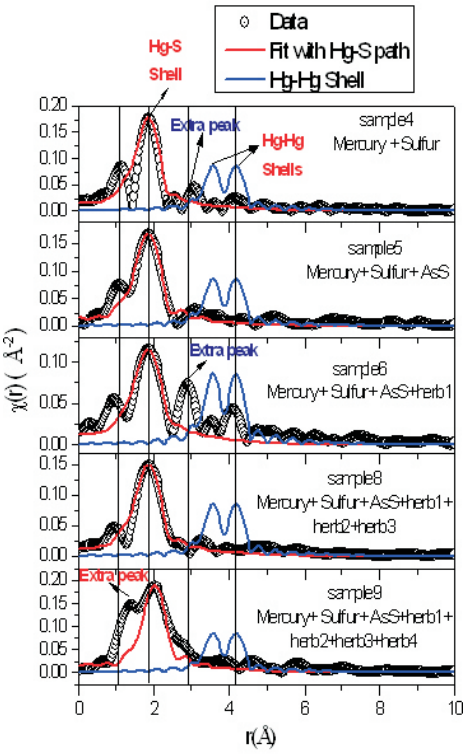
The XRF results for the herbomineral samples are as follows:

Sample No	Major analyte	Trace
Sample 4	Hg	Y
Sample 5	Hg and As	Fe
Sample 6	Hg and As	Fe
Sample 7	Hg and As	Fe
Sample 8	Hg and As	Fe and Ca
Sample 9	Hg and As	Fe and Cu

The EXAFS results for Hg and As edge is as follows

Conclusions:

By XRF As, Hg, Fe, Ca were detected. S was not detected as S X-rays get absorbed in the detector window. However AsS and HgS was seen in EXAFS spectra. There is no peak in the experimental data corresponding to the 2nd shell of HgS viz.., the Hg-Hg shell (corresponding to the blue lines).It may happen that Hg is not present in the form of HgS in the samples, instead Hg forms bonds with S, C or O present in the herbs. The peaks near 3Å for samples 4 & 6 and near 1.5 Å of sample 9 might be due to bond formation of Hg with C or O atoms of the herbs. Sample 6 shows maximum disorder and the Hg-S bond length shows an increasing trend from sample 4 to sample 9. A more comprehensive report is underway regarding its structure after a complete analysis of EXAFS.spectra.



References

[1] Wadekar, Bendale YN, Patil KR & Prabhune AA, J Pharm Biomed, Anal, 39 (2005) 951.

[2] Kulkarni-Dudhgaonkar SB, Rasaratna Samuchyaya, (Shivaji,University Publication, Kolhapur), (1970), 158.

[3] Patel NG, Folk Medicine: The Art and the Science, In: RP Steiner (Eds), (American Chemical Society, Washington), (1986), 41.

Changes in Serum Trace Elemental content of Uterine Cervix Cancer Patients using PIXE

P. Sarita[1], G. J. Naga Raju[2], and S. Bhuloka Reddy[3]

1. *Department of Physics, GIT, GITAM University, Visakhapatnam-530 045, India; E-mail: sarita0309@yahoo.co.in*
2. *Department of Physics, UCEV, JNTUK, Vizianagaram-535 003, India*
3. *Swami Jnanananda Laboratories for Nuclear Research, Andhra University, Visakahpatnam-530 003, India*

The objective of this study was to evaluate the levels of trace elements in blood sera of uterine cervix cancer patients, analyze their alteration with respect to healthy controls and identify the best predictors amongst these for disease occurrence and progression. Particle induced X-ray emission (PIXE) technique was used in this work to identify and quantify trace elements Ti, V, Cr, Mn, Fe, Co, Ni, Cu, Zn, As, Se, Br in the blood sera of uterine cervix cancer subjects and healthy control subjects. The observed alterations are discussed with respect to the possible mechanisms by which these elements might influence the carcinogenic process.

Introduction

Cancer of the cervix is the second most common cancer in women worldwide and is a leading cause of cancer-related deaths in women in underdeveloped countries. Worldwide, approximately 500,000 cases of cervical cancer are diagnosed each year. In recent years, numerous studies were carried out to understand the etiology of uterine cervix cancer, but the molecular mechanisms involved in initiation and progression of cervical cancer are still not well understood.

This study was undertaken with an aim to evaluate the levels of trace elements in blood sera of cervical cancer patients, analyze the alteration with respect to healthy controls and establish the role played by them in the initiation, promotion and inhibition of cancer. Here an attempt is also made to correlate the occurrence of trace elements to the clinical stage of tumour and thereby identify the best predictors amongst these for disease occurrence and progression. Particle induced X-ray emission (PIXE) technique, a relatively simple yet powerful analytical technique was used for the multi-elemental analysis of the blood serum samples.

Materials and Methods

Forty nine newly diagnosed, histologically proven, uterine cervix cancer patients (mean age = 47 10 years) were inducted in this study. These uterine cervix cancer patients were further classified as having limited disease (stage I: 9 patients and stage II: 12 patients) or advanced disease (stage III: 28 patients). Thirty age-matched, apparently healthy female volunteers who had not had any medication served as controls (mean age 45 10 years).

The blood samples of cervix cancer patients were collected from Lion's Cancer Treatment and Research Centre, Visakhapatnam. The PIXE measurements were carried out using a 2.5 MeV collimated proton beam from the 3 MV Tandem Pelletron Accelerator at Institute of Physics, Bhubaneswar, India. The detailed experimental procedure and data analysis of the PIXE spectra can be found in our earlier papers [1].

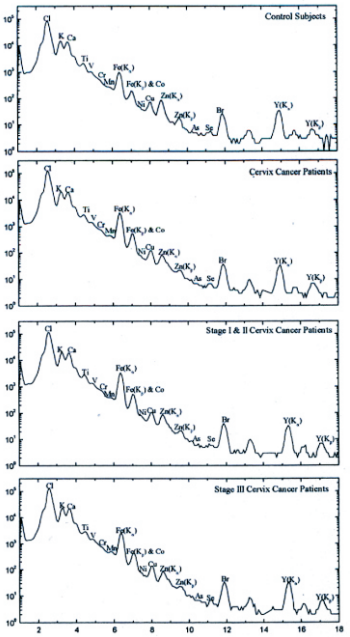


Fig. 1 PIXE spectra of different studied groups

Results and Discussion

Blood serum samples of the cervix cancer patients were analyzed for their trace elemental content. Figure 1 depicts the PIXE spectra recorded for the different studied groups.

The average concentrations for the different studied groups along with the corresponding standard deviations and the p values are given in Table 1. From this table, it is observed that the elemental profiles in blood serum of cervix cancer patients displayed increased concentrations of Cr, Mn, Fe, Ni, Cu, As and lowered concentrations of V, Co, Zn, Se, and Br in comparison with control subjects.

Table-1: Concentrations (in g/g) of trace elements in the blood sera of control subjects and cervix cancer, Stage I & II, Stage III patients.

Trace Elements	Control subjects C_{CS} SD (ppm)	Cervix cancer patients		Stage I & II cervix cancer patients		Stage III cervix cancer patients	
		C_{CP} SD (ppm)	$p_{CP,CS}$ [a]	$C_{I\&II}$ SD (ppm)	$p_{I\&II,CS}$ [b]	C_{III} SD (ppm)	$p_{III,CS}$ [c]
Ti	415 17	420 15	>0.05	395 15	<0.05	439 16	>0.05
V	32.0 12.5	28.9 11.0	>0.05	28.2 10.1	>0.05	29.5 11.6	>0.05
Cr	18.6 7.8	26.6 6.7	<0.05	33 6.4	<0.05	21.9 7	>0.05
Mn	29.8 5.7	39.0 5.1	>0.05	26.5 4.8	<0.05	48.4 5.3	<0.0005
Fe	291 7	555 7	<0.005	633 7.8	<0.01	497 7	<0.05
Co	2.9 1.1	1.7 0.5	>0.05	3.7 0.5	>0.05	0.2 0.5	>0.05
Ni	7.2 3.2	9.6 2.9	<0.05	11.5 3.1	<0.05	8.2 2.9	>0.05
Cu	24.6 3.4	34.8 3.2	<0.0001	29.6 3.1	<0.05	38.7 3.2	<0.00005
Zn	38.5 3.9	22.8 3.2	<0.00001	23.5 3.2	<0.0005	22.2 3.2	<0.0005
As	0.9 0.5	1.1 0.9	>0.05	0.4 0.6	>0.05	1.7 1.2	>0.05
Se	2.5 2.5	1.3 1.7	<0.005	2.1 1.9	<0.05	1.7 1.5	<0.005
Br	46.1 7.1	40.5 5.8	>0.05	48.6 6.3	>0.05	34.4 5.4	<0.05

C_{CS}, C_{CP}, $C_{I\&II}$, C_{III}: Concentration of trace elements in control subjects, newly diagnosed cervix cancer patients, Stage-I&II cervix cancer patients, and Stage-III cervix cancer patients, SD: Standard Deviation
[a] $p_{CP,CS}$: p value between newly diagnosed cervix cancer patients and Control subjects.
[b] $p_{I\&II,CS}$: p value between Stage-I&II cervix cancer patients and Control subjects.
[c] $p_{III,CS}$: p value between Stage-III cervix cancer patients and Control subjects.

When considered by stage of disease, it can be observed from Table 1, that the levels of serum Ti, Mn, Cu, and As were higher while those of serum Cr, Fe, Co, Ni, Se, and Br were lower in Stage III patients than in Stage I and Stage II patients. There was a trend to elevation in serum Cu levels and depression in serum Se levels as the disease progresses. The serum Zn levels were found to significantly low in both the patients groups with respect to control subjects. However, no significant alteration in the serum Zn content was found among the cervix cancer patients with limited disease (Stage I and II) and advanced disease (Stage III).

The present findings of elevated copper levels in the serum of cervix cancer patients suggest that excess copper might have led to the initiation and promotion of cancer in these patients by causing oxidative DNA damage [2] and by creating zinc deficiency [3]. The observed low levels of zinc in the sera of cervix cancer patients included in this study lend support to the hypothesis that a low zinc status enhances the risk of developing cancer through the increase in oxidative stress and DNA damage [4] along with an inability to adequately signal DNA repair mechanisms [4].

Selenium is found to exhibit antioxidant effects via glutathione peroxidase (GSH-Px), act as an inhibitor of angiogenesis [5], enhance immune response [6], and control unnecessary proliferation of cells by inducing cell cycle arrest at the G_2-M transition phase [7]. This apparent diversity in the effects of selenium on cancer cells explains how its deficiency might lead to the initiation and promotion of cancer.

The serum Cu/Zn ratio was significantly higher for cervix cancer patients than for the control group (1.91 0.46 vs. 1.47 0.41). Patients with advanced stages of the disease had more elevated Cu/Zn ratios than patients with Stages I and II combined (2.09±0.49 versus 1.68±0.43).

Conclusions

The results obtained in this study have helped in elucidating the effects of altered homeostasis of trace elements copper, zinc, and selenium in the etiology of cervix cancer. This study has also led to a better understanding of the mechanisms involved in carcinogenesis.

References

[1] P. Sarita, G. J. Naga Raju, et al., J. of Radioanal. Nuc. Chem. 294 (3) (2012) 355.

[2] A.D. Armendariz, C.D. Vulpe, Am. Soc. Nutr. Sci. J. Nutr. 133 (2003) 203E.

[3] E.J. Gyorffy, H. Chan, Am. J. Gastroenterol. 87 (1992) 1054.

[4] E. Ho, C. Courtemanche, B.N. Ames, J. Nutr.133 (2003) 2543.

[5] G.F. Combs, L.C. Clark, B.W. Turnbull, BioFactors 14 (2001) 153.

[6] M.K. Baum, M.J. Miguez-Burbano, et al., J. Infect. Dis. 182 (2000) S69.

[7] AV Gasparian, YJ Yao, et al., Mol. Cancer Therapeutics 1(2002) 1079.

Study of Depth Profile of Hydrogen in Hydrogenated Diamond like Carbon thin Film by Ion Beam Analysis Technique

J. Datta[1], H.S. Biswas[2], S. Kumar[3], D.P. Chowdhury[1], N.R. Ray[4], A.V.R. Reddy[5]

1. *Analytical Chemistry Division, BARC, Variable Energy Cyclotron Centre, Kolkata 700064, India; E-mail: jdatta@vecc.gov.in*
2. *Dept. of Chemistry, Surendranath College, Kolkata-700009, India*
3. *National Centre for Compositional Characterization of Materials, BARC, Hyderabad 500062, India*
4. *Surface Physics Material Science Division, Saha Institute of Nuclear Physics, Kolkata 700064, India*
5. *Analytical Chemistry Division, Bhabha Atomic Research Centre, Trombay, Mumbai 400085, India*

The depth profiling of hydrogen has been carried out in as-prepared and annealed Hydrogenated Diamond Like Carbon (HDLC) thin films by Nuclear Reaction Analysis technique using resonance reaction $^{1}H(^{19}F, \ )^{16}O$ with $^{19}F^{3+}$ ion beam. The hydrogen concentration at different depth of the films was determined by measuring the yield of 6.1 MeV promt -ray from the resonance reaction. The observed variation of depth profile of hydrogen of the as-prepared and annealed HDLC films at different temperatures are reported here. It has been found that our experimental observations corroborate the theoretical model of diamond/graphite/Si (100) interfaces of HDLC films. The desorption of hydrogen due to ion beam irradiation of the film is also studied.

Introduction

The structural investigation of Hydrogenated Diamond Like Carbon (HDLC) films, by confocal micro Raman spectroscopy shows that coherency of sp^3 C-H and sp^2 C=C carbons in the HDLC can produce a continuous nonporous thin film (thickness 168 nm) having atomically smooth surface [1-2]. The Raman spectra do not tell us about why and how the interlayer disorder region is created in the HDLC film. The main effect of hydrogen in HDLC films is to modify its C-C network at different depth of the film. How these modifications occur at various depth of the HDLC film during its synthesis onto Si substrate cannot be studied by Raman spectroscopy, because the skin depth in Raman measurements is ~6 m and using this technique we get information for the whole material rather than at different depth of the thin film having thickness ~168 nm. Therefore the aim of this work was to explore the depth profile of hydrogen in the HDLC film by ion beam analysis techniques, viz., nuclear reaction analysis (NRA) technique, in order to know how hydrogen modify C-C network in the HDLC film.

Experimental

The HDLC thin films [1-2] were deposited on mirror-polished Si (100) substrate at room temperature using asymmetric capacitively coupled Rf 13.56 MHz plasma system for 30 min at a pressure of 0.7 mbar with a flow rate of helium at 1500 SCCM (SCCM denotes cubic centimeter per minute at STP), hydrogen at 500 SCCM, and varying the flow rate of methane. Four samples, for which the CH_4 flow rates are 20, 30, 40 and 70 SCCM, were represented as samples A–D. The samples A-D, annealed at high temperatures 750°C and 1050°C in high vacuum (~ 1 10^{-7} torr) furnace, to study removal of hydrogen from the samples. Nuclear reaction analysis (NRA) [3], a non-destructive technique, using $^{1}H(^{19}F, \ )^{16}O$ resonance reaction at 6.4 MeV with $^{19}F^{3+}$ ion beam from 3 MV Tandetron accelerator at NCCCM, Hyderabad, India, was used to determine the depth profile of the as-prepared and annealed samples A-D. The hydrogen content at different depth of the film was obtained from the measured yield of 6.1 MeV -ray during the bombardment with $^{19}F^{3+}$ ion beam. The incident energy of the beam was increased in steps of 20/40 keV above the 6.4 MeV resonance energy.

Results and Discussion

The atomic fraction of hydrogen in the HDLC film (considering as a binary film, C_xH_y) was estimated by the following equation [4]

$$f^{H}_{HDLC} \quad \frac{f^{H}_{Std.} \quad {}^{C}_{HDLC}}{Y_{Std.} \quad f^{H}_{Std.} \quad {}^{C}_{HDLC} \quad {}^{H}_{HDLC}} \qquad (1)$$

Where Y ratio of gamma yields for standard and sample, f atomic fraction of hydrogen in the film material given in subscript, $_{Std}$ and ^{i} stands for the stopping cross section for the standard and the ith element having in the superscript, respectively. The Y is obtained from the gamma-ray yields recorded in a PC-based multichannel analyzer. The stopping power data is calculation using SRIM-2008.04 [5]. The depth χ_R is estimated from the range-energy relationship and the stopping power is estimated using Bragg's law of linear additivity.

The typical -ray yield showed that when the incident energy (E_{in}) was less than the resonance energy (E_R), the -ray yield corresponds to 'background yield' and for $E_{in} = E_R$ the -ray yield corresponds to the presence of hydrogen atoms onto the surface of HDLC sample. With the increase of energy of the beam penetrating into the sample, the -ray yield starts

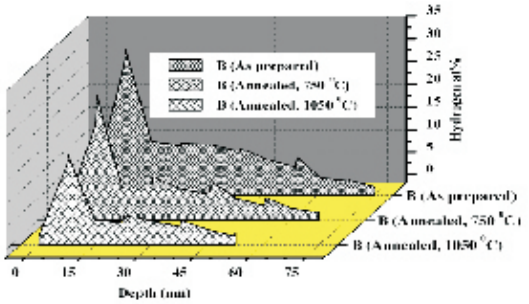


Fig. 1 Depth profile of HDLC thin films onto Si(100) substrate. Flow rate of CH_4 is 30 SCCM

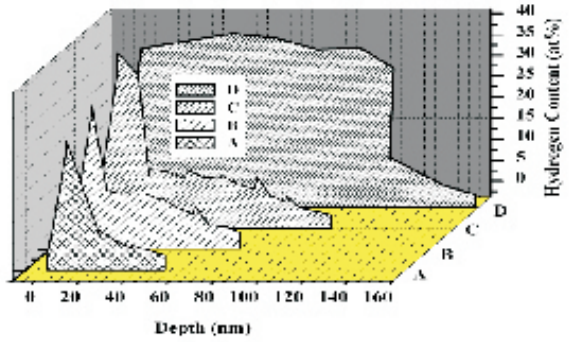


Fig. 2 Depth profile of as-prepared HDLC films, A – D, deposited with different CH_4 flow rate.

decreasing from the surface of the target. The typical behavior for -ray yield at different depth of as prepared and annealed HDLC sample was observed to be similar. The hydrogen content of the annealed films, in all cases, was lower than that of the as-prepared samples as shown in Fig. 1. The variation of hydrogen with depth was faster in as-prepared sample than that for annealed one. The decreasing trend of hydrogen content with increase of annealing temperature, as expected, is shown in Fig. 1 indicating significant loss of bonded hydrogen atoms from the HDLC sample due to annealing effect. The maximum depth at which the yields of hydrogen content was more or less equal to the background counts depends upon the annealing temperature; these depths are 83 nm for as prepared, 68 nm at 750, 59 nm at 1050°C for sample B. Therefore decreasing of depth of hydrogen content in the HDLC sample with increasing annealing temperature, may be attributed to conversion of sp^3 C-H (diamond like) to sp^2 C=C (graphite like) structure in the HDLC sample.

The maximum depths of hydrogen content observed in the HDLC film depend upon flow rate of CH_4 as shown in Fig. 2. The migration of hydrogen towards surface from the interface, as reflected from these depths, might be due to heat transfer from the sample holder to the backing silicon material and then into the sample during the annealing process. The atomic fraction of Hydrogen in the as prepared HDLC film, estimated using equation (1) based upon NRA measurements. are presented in Table 1.

Table-1: Error on the data?)Atomic fraction of hydrogen in the HDLC film as a function of flow rate of methane

Sample	CH_4 flow (SCCM)	Hydrogen content At%
A	20	27.1
B	30	30.5
C	40	32.9
D	70	34.1

In some hydrogenous carbon materials loss of hydrogen under ion irradiation is reported [6]. In such cases, the concentration of hydrogen should be measured as a function of ion dose and the initial hydrogen content can be obtained by extrapolation to the zero dose condition. This desorption is maximum for the as-prepared films compared to annealed films.

Conclusions

We conclude that HDLC is composed of sp^3C-H and sp^2C=C carbons. The hydrogen content is maximum at the surface of the films. This hydrogen terminates the unsaturated bonds of carbon in the film surface at the end of their deposition. The hydrogen content increases with the increase of flow rate of CH_4 at a constant flow rate of hydrogen and helium. The hydrogen content decreases with the depth of the films are matches with the Robertson model [7] of diamond/graphite/Si (100) interface which minimizes the lattice mismatch and interfacial energy.

References

[1] J. Datta, N. R. Ray, P. Sen, H. S. Biswas, E. A. Vogler, Materials Lett. 71 (2012) 131.

[2] N. R. Ray, J. Datta, H. S. Biswas, S. Datta, IEEE Transactions on Plasma Science 40 (7) (2012) 1789.

[3] D. A. Liech, T. A. Tombrello, Nucl. Inst. and Meth. 108 (1973) 67.

[4] S. Kumar, J. V. Ramana, C. David, V. S. Raju, Nucl. Inst. and Meth. in Phys. Res. B 179 (2001) 113.

[5] J. F. Ziegler, M. D .Ziegler, J. P. Biersack The Stopping and Range of Ions in Matter, 2008 SRIM – Version 2008.04 www.SRIM.org

[6] V. D. Vankar, N. Dilawar, Vacuum 47 (11) (1996) 1275.

[7] J. Robertson, J. Gerber, S. Sattel, M. Weiler, K. Jung, H. Ehrhardt, Appl. Phys. Lett. 66 (1995) 3287.

Depth Profiling of Titanium using a Resonance in $^{48}Ti(p,)^{49}V$ Nuclear Reaction

G. L. N. Reddy, S. Vikram Kumar, J. V. Ramana, Sanjiv Kumar*

National Centre for Compositional Characterization of Materials, BARC, ECIL Post, Hyderabad, India;
E-mail: sanjivcccm@rediffmail.com

Titanium is an important constituent of several technologically important materials. Its depth profile in the surface regions is desirable for standardizing the manufacturing process and assessment of functionality of materials. The resonance at 1.362 MeV in $^{48}Ti(p,)^{49}V$ reaction (E = 7.9 MeV) has been used for depth profiling Ti in Ti based films. The -rays are measured by a bismuth germanate detector. The method has a detection sensitivity of about 6.5×10^{20} at.cm^{-3} and can provide determinations with a depth resolution of about 25 nm up to a depth of about 800 nm in Si. Selectivity is another important feature of this non-destructive method of depth profiling.

Introduction

Depth profiling is an important aspect of surface science. Selectivity, sensitivity and high depth resolution capability are the major criteria of a depth profiling technique which, preferably, should be non-destructive in nature as well. Narrow resonance profiling (NRP), a variant of nuclear reaction analysis (NRA), is endowed with these features and is a technique of choice for high resolution depth profiling [1]. It exploits narrow resonances in the excitation function of a nuclear reaction and invokes the concept of stopping power for non destructive depth profile measurements. The technique has been extensively used in the analysis of low Z elements; however, its potential for medium or high Z elements has not been explored. In the present study, we have extended its application to Ti by means of the resonance at 1362 keV in $^{48}Ti(p,)^{49}V$ reaction and report its analytical capabilities. Ti has found wide ranging applications in several fields as a metal, an implant, thin films or an alloying element. Analysis in the surface regions has important implications in the preparation and functional assessment of these materials.

Experimental

The excitation function of $^{48}Ti(p,)^{49}V$ reaction was constructed in the 1.3-1.4 MeV proton energy region in steps of 0.5 keV. It involved the bombardment of a Ti metal film (containing isotopes in natural abundance) on Si at normal incidence with a collimated proton beam (=2mm, current = 500 700 nA) and the measurement of 7.9 MeV prompt -rays emanating from the reaction by a bismuth germanate (BGO) detector at 90 with the direction of the projectiles. The data was acquired for a charge of 200 C at each incident energy by a PC based multichannel analyser. The experiments were carried out using 3 MV tandem accelerator at NCCCM, Hyderabad.

Ti based films used as targets for the construction of excitation function for determining the analytical features of the resonance were prepared by electron beam evaporation technique. The films did not contain any impurity in measurable levels. It was ascertained by analyzing the films by 2.4 MeV -Rutherford backscattering spectrometry (RBS).

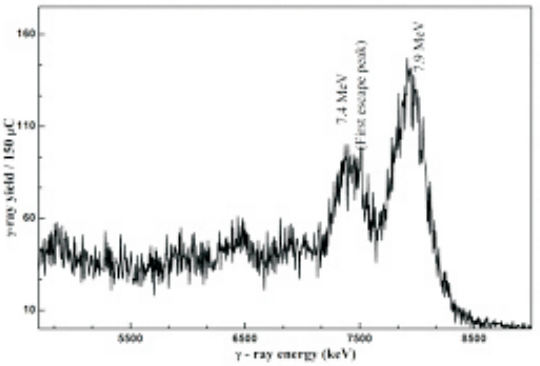


Fig. 1 -ray spectrum from $^{48}Ti(p,)^{49}V$ nuclear resonance reaction recorded using BGO detector

Results and Discussion

The resonance at 1362 keV has a strength of 4.9 eV while the other resonances have strengths 3.5 eV. Furthermore, the former resonance has a natural width of about 50 eV. Therefore amongst the four, it is the most well suited resonance for high resolution depth profile measurements [2]. A typical -ray spectra recorded for a Ti film at 1362 keV proton beam energy is shown in Fig. 1. It consists of a well pronounced photopeak at 7.9 MeV and the corresponding first escape peak at 7.4 MeV while the second escape peak is barely discernible. The detection limit and depth resolution of the resonance under the present experimental conditions were derived from the excitation function depicted in Fig. 2. The detection limit of the reaction was estimated to be about 6.5×10^{20} at. cm^{-3} while its depth resolution in Si was about 25 nm in the surface regions. Its probing depth is limited to about 800 nm in Si due to the resonance at 1388 MeV which is also produces 7.9 MeV -rays. It is to be noted

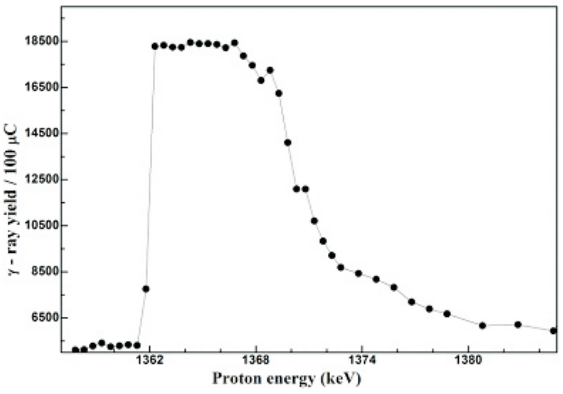


Fig. 2 *Excitation function of $^{48}Ti(p,)^{49}V$ nuclear resonance reaction*

that in the case of thick targets, the interferences due to resonances at 1007 keV and 1013 keV can be easily discerned, as the related states in V^{49} nuclei decay predominantly through the emission of 7.4 MeV -rays.

The method has been applied for depth profiling Ti in TiO_2 and TiN films on Si. There was no interference due to Si in the depth profile measurements of Ti. For a wider applicability, interferences arising from Fe, Ni and Cr were also studied.

Conclusions

A nuclear resonance reaction analysis based method for high resolution depth profiling of Ti is described. This method can also be used for the analysis of ultrathin Ti bearing films.

References

[1] B. Maurel, G. Amsel, Nucl. Instr. and Meth. 197 (1982) 1.

[2] Th. Lenz, H. Baumann and F. Rauch, Nucl. Instr. and Meth. B 8 (1987) 280.

Application of in situ current normalized PIGE method for determination of total boron and its isotopic composition

Sumit Chhillar, R. Acharya, S. Sodaye and P. K. Pujari

Radiochemistry Division, Bhabha Atomic Research Centre, Trombay, Mumbai 400085, India;
E-mail: racharya@barc.gov.in

A particle induced gamma-ray emission (PIGE) method using proton beam has been standardized for determination of isotopic composition of natural boron and enriched boron samples. Target pellets of boron standard and samples were prepared in cellulose matrix. The prompt gamma rays of 429 keV, 718 keV and 2125 keV were measured from $^{10}B(p,\ )^{7}Be$, $^{10}B(p,p')^{10}B$ and $^{11}B(p,p')^{11}B$ nuclear reactions, respectively. For normalizing the beam current variations in situ current normalization method was used. Validation of method was carried out using synthetic samples of boron carbide, borax, borazine and lithium metaborate in cellulose matrix.

Introduction

Boron and its compounds are important in nuclear technology due to its high neutron absorption cross section (764 b for ^{11}B and 3837 b for ^{10}B). The neutron absorption property of boron is advantageously used in various applications in nuclear reactors such as control rod applications, burnable poison (boron carbide, boric acid, bocarsil, boral, polyboron, borated wood and borated steel), reactivity control, nuclear material storage and neutron shielding (boral, borated paraffin wax). For chemical quality control, it is necessary to quantify accurately the boron content and $^{10}B/^{11}B$ isotopic ratio in the final/finished product in various borated materials and compounds of boron.

Routine analysis of boron is carried out by wet chemical methods (UV-VIS spectrometry, IC, ICP-AES and MS). Wet chemical methods are sensitive for boron analysis but are destructive in nature. Amongst the nuclear analytical methods, prompt gamma ray NAA (PGNAA) [1] and particle induced gamma ray emission are suitable for total boron and its isotopic composition determination. In absence of PGNAA, PIGE method can be used for quantification of total boron and determination of its isotopic composition in the samples like boron carbide, boric acid, carborane and borazine. PIGE is highly sensitive and suitable for quantification of low Z elements in various matrices.

PIGE utilizes measurement of prompt gamma rays due to inelastic scattering or nuclear reactions like (p,), (p, p'), (p, n) and (p,) of projectile with targets. Since PIGE is an isotope specific technique, it can easily quantify the isotopic composition of boron ($^{10}B/^{11}B$) and lithium ($^{6}Li/^{7}Li$). PIGE using proton and deuteron beams is capable of determining light elements like Li, Be, B, C, N, O, F, Na, Mg, Al, Si, P, S, Cl, K, Ca and Ti [2].

In the case of boron (element of interest), PIGE utilizes measurement of prompt gamma rays of 429 keV, 718 keV and 2125 keV from $^{10}B(p,\ )^{7}Be$, $^{10}B(p,p')^{10}B$ and $^{11}B(p,p')^{11}B$ reactions, respectively, by using high resolution gamma-ray spectrometry. Since both ^{10}B and ^{11}B have different gamma rays, thus total boron quantification and its isotopic composition can be determined by PIGE method.

In the present work, we have standardized a PIGE method for non-destructive quantification of boron and its isotopic composition in different samples of boron compounds using F and Al for in situ current normalization.

Experimental

Standard pellets of boron were prepared by homogenously mixing varying amount of H_3BO_3 in cellulose with fixed amount of CaF_2 (~ 25 mg). For method validation, known amount of lithium metaborate and borax and borazine were mixed with cellulose and CaF_2 in constant amount (~ 25 mg). The isotopic composition of boron ($^{10}B/^{11}B$) was varied by mixing natural B_4C with 67% (^{10}B) enriched B_4C in different proportion. Boron carbide samples were prepared by homogenously mixing B_4C (~75 mg having different $^{10}B/^{11}B$ ratio) with cellulose and CaF_2 (~25 mg). For normalizing the beam current fluctuations during the irradiation every target was covered with thin Al foil (~7.6 m). The targets were irradiated with 4 MeV proton beam (beam current ~5-10 nA) from folded tandem ion accelerator (FOTIA) IADD, BARC. Prompt -rays of energies 429 keV and 718 keV of ^{10}B and 2125 keV of ^{11}B, 197 keV of fluorine and 1014 keV of aluminum were measured in the standards and synthetic samples which were irradiated and counted in reproducible geometry. The gamma-rays were measured using high resolution gamma-ray spectrometry. Fig 1 and 2 show the -ray spectra of natural and enriched B_4C samples.

Results and Discussion

In situ current normalized PIGE method (using F and Al) has been standardized and validated by using synthetic samples of boron carbide, lithium metaborate, borax and borazine for total boron and boron isotopic composition. The total boron in these samples was in the range of 30.71 to 59.34 mg. A plot of the validation results is shown in fig 3.The total boron amounts in the

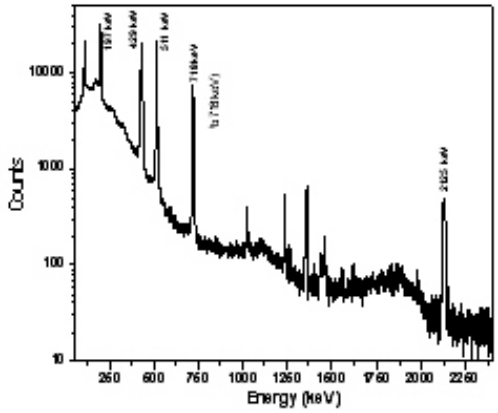


Fig. 1 PIGE spectrum of natural B_4C containing F as in situ current normalizing element

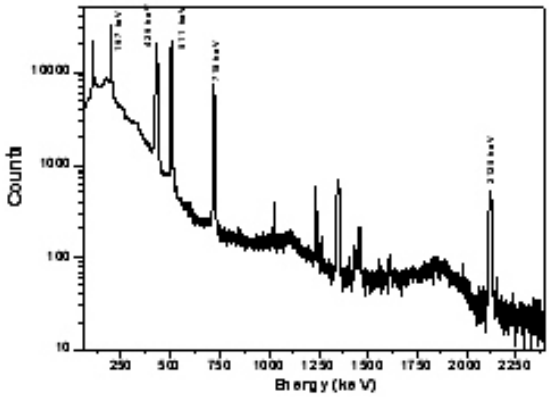


Fig. 2 PIGE spectrum of enriched B_4C containing F as in situ current normalizing element

synthetic samples are in good agreement with the expected values (within 2%). The uncertainties quoted are in the range of 1-3 % which is due to the counting statistics and peak fitting errors. For isotopic composition of boron, a calibration plot was obtained by plotting ratio of fluorine normalized CPS (429 keV/2125 keV) and (718 keV/2125 keV) against $^{10}B/^{11}B$ ratio (Fig. 3) in samples with different ^{10}B enrichment. The slope of calibration curve was used for determining $^{10}B/^{11}B$ ratio and the results the given in Table 1.

Table-1: PIGE results for isotopic composition and total boron in different samples of boron

Sam-Id	$^{10}B/^{11}B$ (Exp.)	$^{10}B/^{11}B$ (Obt.)	Enrich (%)
B-1	0.46	0.44	31.0
B-2	1.20	1.15	55.0
B-3	2.03	1.99	67.0
B-4	0.25	0.26	20.0
Borazine	-	0.24	20.0

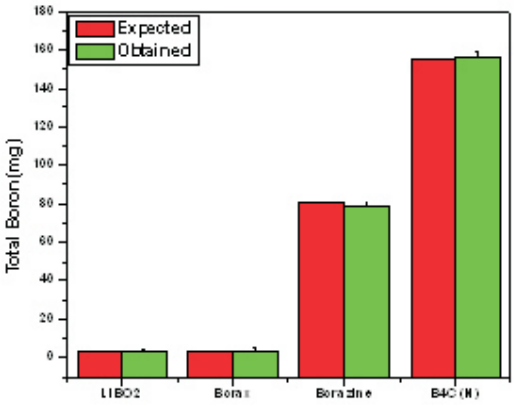


Fig. 3 Results of boron content (in wt %) in synthetic samples obtained by PIGE

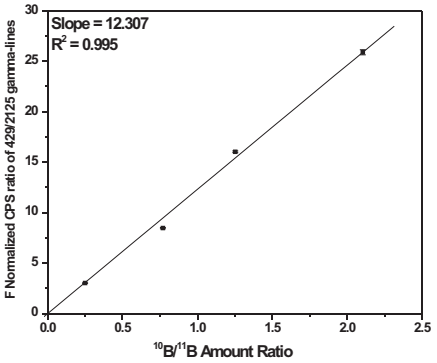


Fig. 4 Calibration plot: Ratio of CPS of $^{10}B/^{11}B$ vs $^{10}B/^{11}B$ mass ratios

Conclusions

In situ current normalized PIGE methods using F and Al foil were standardized for total boron and its isotopic composition determination in various samples containing boron. The separate gamma-lines of ^{10}B and ^{11}B make it possible to quantify total boron as well as determination of its isotopic compositions.

Acknowledgements

Authors thank Dr. A. Goswami, Head, RCD for his constant encouragement during the work. Authors thank Dr. P. Singh, Head, IADD and Mr. S.K. Gupta, Mr. A. Agarwal and FOTIA operating staff of IADD, BARC for extending their help during the experiment.

References

[1] R. Acharya, J. Radional. Nucl. Chem., 281 (2009) 291.

[2] S. Chhillar, R. Acharya, S. Sodaye, K. Sudarshan, S. Santra, R. K. Mishra, C. P. Kaushik R. K. Choudhury, P. K. Pujari, J Radioanal. Nucl. Chem., 294 (2012) 115

Uranous Generation and its Application to strip Plutonium from Lean Organic in CORAL

A. Chinnusamy[1], N.K. Pandey[1], Radha Rani[2], N. Abirami[2], C.M. Baghyalakshmi[2], D. Natarajan[2], M.C. Devarajan[2], R.V. Subbarao[2], V. Vijayakumar[2] and U. Kamachi mudali[1]

1. *Reprocessing Research & Development Division, Reprocessing Group, Indira Gandhi Centre for Atomic Research, Kalpakkam 603102, India; E-mail: chinu@igcar.gov.in*
2. *Reprocessing Plant Operation Division, Reprocessing Group, Indira Gandhi Centre for Atomic Research, Kalpakkam 603102, India*

The lean organic containing plutonium (200 mg/L -1.2 g/L)after the first cycle extraction , is stripped back by introducing single and multiple point in the strip section from the externally added uranous stabilized with hydrazine which is generated electrolytically from uranyl nitrate solution made of dissolving U_3O_8. This paper deals with preparation of uranyl by fumeless dissolution of U_3O_8,experimental runs of generation of uranous from uranyl by electrolytic method and dilution of uranous to the stoichiometric amount to strip the plutonium from lean organic. Pu^{4+} in the lean organic is reduced to Pu^{3+} by U^{4+} and stripped to aqueous phase.

Introduction

Reprocessing of FBTR spent fuel in IGCAR, India is a challenging task due to high burn up, high specific activity and high content of plutonium with short cooled and it is being reprocessed in CORAL (COmpact Reprocessing of Advanced fuels in Lead cells), having burn up of 25, 50,100 and 155 GWd/te by a modified PUREX process [1] and the chemistry of PUREX process [2] is very well reviewed. In the spent fast reactor carbide fuel reprocessing by modified PUREX process, U(VI) & Pu(IV) are co-extracted from nitric acid by a solution containing 30% TBP in NPH leaving the bulk of the fission products in the aqueous stream. The uranium and plutonium are recovered in the 1st cycle itself in which both are extracted and stripped back by dual stripping with 0.01 N and 4 N nitric acid followed by partitioning via oxalate precipitation. Even though low residence time contactor such as centrifugal extractors are used for extraction, the solvent undergoes degradation and the damage of solvent TBP due to radiolysis and hydrolysis is high and the retention of plutonium in lean organic is around 200ppm -1.2 g/L with the specific activity of 2- 50 mCi/L due to degradation of TBP into DBP, MBP which form complex with Pu, Ru and Zr, which are not easily removed. To reduce the radiation damage and in the waste volume reduction of the solvent, recovery of the retained plutonium from the lean organic stream before recycling is an important step and it is achieved by the reduction of Pu(IV) to Pu(III) by U(IV) and the consequent stripping of the inextractable Pu(III) from the solvent phase to the aqueous nitric acid phase. During the reprocessing campaigns in CORAL, the plutonium from the lean organic phase is recovered [3] based on the single and multiple point addition of uranous solution stabilized with hydrazine. To generate U(IV), electrochemical reduction methods of U(VI) to U(IV) is carried out externally and used to strip the retained plutonium from the lean organic, because of its simplicity, high efficiency, clean and safe method. The uranous in presence of hydrazine as stabilizer is introduced in the stripping section since U(IV) with hydrazine stabilizer is salt free reagent and no non volatile impurities are added and it is considered as better reagent for Pu (IV) reduction . There are large number of experimental methods [4] used to generate uranous and strip the plutonium from the organic phase have been described elsewhere. This paper describes the routine work of dissolution of U_3O_8, experimental runs to generate U^{4+} and carried out dilution of U^{4+} solution in makeup area and send to HCW to strip Pu from the lean organic phase.

Experimental

The stock solution of 300-600g/L of uranium is prepared by dissolving U_3O_8 powder using conc. nitric acid and the uranium is analyzed by modified Davies-Gray method [5] and it is used for electrolysis after suitable dilution for preparing 50-100 g/L uranium and added into the electrolytic solution to run the routine experiments. The free acidity of uranyl stock solution is analyzed by Bromothymol Blue indicator method after complexing with potassium oxalate. Uranous in uranyl (in-between the experimental runs) is determined by ferroin indicator method and free acidity of the solution and hydrazine concentration is simultaneously determined by pH metric method during experimental runs. The schematic diagram of the electrolyzer for the experimental runs is shown in Fig.1 and conc. of reagents used for experimental runs and diluted uranous conc. for stripping are in Tables 1 and 2.

Current: 9-10 amps Voltage: 4-5 volts

Current efficiency: 50-60% Current density: 7.5mA / sq.cm

Electrochemical reactions:

At anode:

$$2\,H_2O \quad O_2 + 4H^+ + 4\,e^-\ E^o = -\,1.23\ V \qquad (1)$$

$$N_2H_5^+ \quad N_2 + 5H^+ + 4e^-\ E^o = -\,0.23\ V \qquad (2)$$

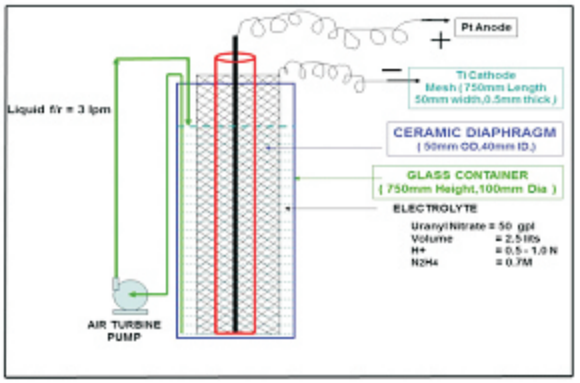


Fig. 1 Electrolytic set up used for uranous generation

Table 1: Routine experimental runs for generation of uranous 50-100 g/L(N_2H_4=0.4-0.8M) from various stock solution of 400-600 g/L

Sl. No	U^{4+}g/L	$[H^+]$	Sl. No	U^{4+}g/L	$[H^+]$
1	72.01	0.33	13	96.8	0.48
2	49.40	0.88	14	96.2	0.63
3	96.80	0.48	15	49.48	0.56
4	96.12	0.63	16	99.32	0.52
5	75.26	0.62	17	76.69	0.53
6	75.20	0.58	18	74.01	0.12
7	49.78	1.59	19	48.90	0.08
8	74.82.	0.55	20	50.00	0.67
9	74.38	0.72	21	71.76	1.11
10	73.90	0.53	22	70.60	0.98
11	72.02	0.37	23	28.20	1.29
12	49.40	0.88	24	28.02	1.07

Table 2: Diluted U^{4+}solution used for Pu stripping (N_2H_4=0.5-0.7M)

Sl. No	U^{4+}g/L	$[H^+]$	Sl. No	U^{4+} g/L	$[H^+]$
1	13.33	0.09	13	11.80	0.48
2	9.50	0.10	14	9.94	0.34
3	9.52	0.54	15	10.60	0.42
4	9.53	0.38	16	9.97	0.33
5	9.51	0.11	17	9.10	0.24
6	8.30	0.26	18	9.28	0.22
7	8.21	2.98	19	7.60	0.24
8	8.15	2.91	20	7.48	0.25
9	10.90	0.08	21	9.95	0.28
10	9.82	0.39	22	9.96	0.30
11	9.40	0.40	23	8.45	0.39
12	11.12	0.36	24	8.15	2.97

At cathode:

$$UO_2^{2+} + 4H^+ + 2\,e^- \quad U^{4+} + 2H_2O \; E^o = 0.33\ V \quad (3)$$

$$NO_3^- + 3H^+ + 2e^- \quad HNO_2 + H_2O \; E^0 = 0.94V \quad (4)$$

$$HNO_2 + H^+ + e^- \quad NO \; + H_2O \; E^o = 0.99V \quad (5)$$

Chemical reactions:

$$U^{4+} + 2Pu^{4+} + 2H_2O \quad UO_2^{2+} + 2Pu^{3+} + 4H^+ \quad (6)$$

$$N_2H_4 + 2HNO_2 \quad N_2 \; + N_2O + 3H_2O \quad (7)$$

Results and Discussion

The lean organic which contains Pu with varying concentration of 200 mg/l -1.2 g/L is stripped back by uranous of 10 g/L is used which is higher than the stoichiometric quantity should be enough to reduce Pu^{4+} quantitatively to Pu^{3+} and back extracted to aqueous .Actually the stoichiometric concentration of U(IV) should reduce Pu (IV) to Pu $^{3+}$. However

1. The competing side reaction of acid destruction prominently takes place in aqueous phase
2. Larger difference in the potentials of UO_2^{2+} /U^{4+} (0.33) and Pu^{4+} /Pu^{3+} (0.94) redox system.
3. Hydrazine is partially extracted into the organic and the auto catalytic reaction of nitrous acid with extracted U^{4+} and reduced Pu $^{3+}$ in the organic as well as aqueous and the destruction of N_2H_4 at anode.
4. The redox potential of Pu^{4+}/Pu^{3+} and NO_3^- /NO_2^- are nearly equal.

It shows that the current density in the experimental runs are only 50-60% can be sacrificed at the cost of rapidity of experimental runs to generate U^{4+} for routine campaigns to strip Pu from the lean organic phase .

Conclusion

In the large scale electrolytic reduction of U(VI) to U(IV) and its application of stripping of plutonium from lean organic in CORAL, 100-600 g/L of uranyl nitrate batches could be reduced to 80-90% of uranous in 4 to 12 hours.The number of experimental parameters in the reduction process are tabulated and the experimental runs are continued . Recoveries of more than 99.8% for plutonium and 99.9% for uranium are routinely obtained from lean organic in various campaigns.

References

[1] R.Natarajan, IANCAS Bull. 14,2 (1998) 27

[2] D.D. Sood, S.K. Patil, J. Radioanal. Nucl. Chem. 203(2) (1996) 547

[3] R. Natarajan, IGCARBENCHMARKS (2009-10)134

[4] N.K. Pandey, IGC NEWS LETTER,85 (2010) 9-10

[5] W. Davies and W. Gray, Talanta, 11 (1964) 1203

Physico-Chemical Investigations of Some Mixed Ligand Complexes of Thorium(IV) Derived from Semicarbazones and Triphenyl Phosphine Oxide

Ram K. Agarwal

Department of Chemistry, Lajpat Rai Postgraduate College, Sahibabad-201 005 (Ghaziabad), India;
E-mail: ram_agarwal54@yahoo.com

In present studies, the synthesis of some mixed ligand complexes of thorium(IV) derived from 4[N-(4'-ethylbenzalidene)amino]antipyrine semicarbazone (EBAAPS) and 4[N-(2',4'-dimethyl benzalidene)amino]antipyrine semicarbazone (DMBAAPS) as primary ligand and triphenyl phosphine oxide (TPPO) as secondary ligand with the general composition $ThX_4 \cdot n(L)TPPO$ (n = 1, X = Cl, Br, NCS or NO_3; n = 2 X = I or ClO_4; L = EBAAPS or DMBAAPS). All the coordination compounds were characterized through elemental analyses, molar conductance, molecular weight, infrared, data and thermogravimetric analysis. The infrared studies reveal that the semicarbazones behave as neutral tridentate (N,N,O) and TPPO coordinates through its lone oxygen atom. The nitrates are bicovalently bonded, while thiocyanates are N-coordinated in these compounds. Thermal stabilities of these coordination compounds have been investigated through thermogravimetric analyses. In conclusion, the coordination number of the central metal ion displays coordination number 7, 8, 9 or 12 depending on the nature of the anionic ligands.

Introduction

The first and most remarkable peculiarity of the actinide elements is the great variety of known oxidation states. The coordination polyhedra of the actinide ions have been extensively investigated [1-5]. The metal ion size and charge offer two other parameters to be considered in the type of the obtainable complexes. According to the Ahrland and Pearson, thorium(IV) belong to class-A metal (hard acid) group, in which the coordinating ability of ligands decreases along the series N > P > As; O > S > Se and F > Cl > Br. In view of high coordination compound formed by Th^{4+}, it is considered to isocate some high coordination compounds of two new semicarbazones, i.e., 4[N-(4'-ethylbenzalidene)amino] antipyrine semicarbazone (EBAAPS) and 4[N-(2',4'-dimethylbenzalidene)amino]antipyrine semicarbazone (DMBAAPS) as primary ligand and triphenyl phosphine oxide (TPPO) as secondary ligand.

Experimental

Thorium(IV) salts either procured commercially or prepared by known method [5]. Both semicarbazones EBAAPS and DMBAAPS were synthesized in this laboratory using 4-aminoantipyrine as starting material [5,6]. Triphenyl phosphine oxide was purchased from Aldrich.

All the complexes were synthesized by following general method. The reaction mixture containing equal volumes (20 mL) of solutions of corresponding thorium(IV) salt, semicarbazone and TPPO in acetone in required molar bath for ~ 2-3 hrs. the resulting yellow to brown coloured solid complexes separated out on cooling in ice bath. It has filtered, washed with acetone and finally dried over P_4O_{10}.

Results and Discussions

The isolated thorium(IV) complexes have the general composition $ThX_4 \cdot n(L)TPPO$ (n = 1, X = Cl, Br, NCS or NO_3; n = 2, X = I or ClO_4, L = EBAAPS or DMBAAPS). All the thorium(IV) complexes are stable and can be stored for long periods except thorium(IV) iodide complexes which decompose slowly at room temperature with evolution of iodine vapours.The molar conductance values in $PhNO_2$ suggest that chloro, bromo, nitrato and thiocyanato complexes are non-electrolytes, whereas the iodo and perchlorato complexes whereas the iodo and perchlorato complexes dissociate in this solvent. The iodo complexes appear to be a 1:2, while the perchlorato complexes behave as 1:4 electrolyte.

In infrared spectra as expected (NH_2) band of the hydrazine nitrogen of semicarbazide (1622 cm^{-1}) is absent in the infrared spectra of semicarbazones [7]. It has also been observed that the amide-II band is shifted towards the lower energy side compared to that of semicarbazone. The effect is due to the electron density drift from the hydrazinic nitrogen [8]. The characteristic absorption of the carbonyl group in EBAAPS or DMBAAPS is observed in 1700-1680 cm^{-1} region [9,10]. In these complexes this band is shifted towards lower energy in the 1650-1640 cm^{-1} region. The amide-II band in the free ligands has been observed at ~ 1565 cm^{-1}. In all the present complexes this band is also shifted towards lower wave number by ~30 cm^{-1}. This observation suggests coordination through the carbonyl oxygen atom. The strong bands ~ 1600 cm^{-1} in these semicarbazones apparently has a large contribution from the (C=N) mode of semicarbazone moiety. This has been observed as a blue shift in the position of the (C=N) band in all complexes as compared to the free ligands. Another

strong band was observed at ~1610 cm^{-1} due to azomethine (C=N) absorption. On complexation this band is shifted towards the lower frequency region clearly indicating the coordination through the azomethine-N atom [10,11]. In secondary ligand TPPO, the strong (P=O) stretching frequency in free TPPO appears as a strong absorption at 1195 cm^{-1}, which appears in the region 1110-1095 cm^{-1} showing coordination of TPPO to Th(IV) metal ion through its lone oxygen atom [12]. In far infrared spectra the bands due to (Th-N)/(Th-O) are also observed. In perchlorato complexes, the presence of bands at 1090 and 620 cm^{-1} attributed to $_3$ and $_4$ vibrations of ionic perchlorate ions [3,4]. The bidentate nature of the nitrato groups is indicated by the presence of bands at 1520 ($_4$), 1285 ($_1$), 1040 ($_2$), 820 ($_6$) and 730 ($_3$/ $_5$) cm^{-1}. In thiocyanato complexes the presence of bands at 2050 (C N), 830 (CS) and 465 cm^{-1} (NCS) show that the terminal isothiocyanate is N-bonded to the Th^{4+} ion [3,4].

The thermogravimetric curves of Th(IV) complexes do not show the presence of aquo ligands either in or out of the coordination sphere. The TG curves of $[ThX_4(EBAAPS)\cdot TPPO]$ (X = Cl, Br, NCS or NO_3) indicate that in 150-165ºC temperature range, one molecule of TPPO has been evaporated off, while in 200-280ºC the weight is corresponds to loss of EBAAPS molecule. Finally at 610-620ºC oxohalide and oxothiocyanato formation have been observed. In case of nitrato complexes the final product is ThO_2 [3,4].

Stereochemistry

In thorium(IV) chloro, bromo and thiocyanato complexes, the conductance and molecular weight determination suggest that the complexes are non-ionic in nature. The infrared data suggest that EBAAPS and DMBAAPS behaves as neutral (N,N,O) donors, while TPPO is a neutral oxygen donor. Thus the coordination number of Th(IV) is found to be eight in these complexes. In case of iodo complexes, the 1:2 electrolytic nature suggests that two iodine atoms are present outside the coordination sphere and hence the coordination number of thorium(IV) in iodo complexes is found to be 9. In nitrato complexes, a coordination number 12 is suggested, while in perchlorato complexes thorium(IV) is surrounded by 7 donor ligands and thus produce a coordination number 7 [1,2].

References

[1] K.W. Bagnall, Coord. Chem. Rev., 2 (1967) 145.

[2] R.K. Agarwal, H. Agarwal and K. Arora, Rev. Inorg. Chem., 20 (2000) 1.

[3] R.K.Agarwal, K. Arora and P. Dutt, Polyhedron, 13, (1994) 957.

[4] R.K.Agarwal, S.Prasad and V.Chand, Int.Chem., 1 (2012) 576.

[5] R.K. Agarwal, I. Chakraborti and H. Agarwal, Synth. React. Inorg. Met.-Org. Chem., 34 (2004) 1453.

[6] R.K. Agarwal, I. Chakraborti and H. Agarwal, Synth. React. Inorg. Met.-Org. Chem., 34 (2004) 1431.

[7] G. Reed and M. Cohn, J. Biol. Chem., 255 (1970) 662.

[8] H. Leavnon, J. Chem. Phys., 49 (1968) 2031.

[9] M.J. Campbell and R. Grzeskowiak, J. Inorg. Nucl. Chem., 30 (1968) 1865.

[10] Ram K.Agarwal,S.Prasad and Upma Singh, Int.J.Chem., 1 (2012) 264.

[11] J.F. Dyer, Application of Absorption Spectroscopy of Organic Compounds, Prentice-Hall, New Delhi, India (1984).

[12] R.K. Agarwal, A.K. Srivastava and T.N. Srivastava, Indian J.Chem., 18A (1979) 459

Electrochemical Approach to Assess Corrosion of Stainless Steel used in PUREX Process

Shagufta Khan[1,2], Vivekanand Kain[2], A.V. R. Reddy[1]

1. *Analytical Chemistry Division, Bhabha Atomic Research Centre, Mumbai 400085, India, E-mail: shagufta@barc.gov.in*
2. *Materials Science Division, Bhabha Atomic Research Centre, Mumbai 400085*

In present study, type 304L and 304 L NAG (nitric acid grade) were subjected to a heat treatment to simulate the worst microstructure in the HAZ (heat affected zone) of the weldment. Corrosion behavior of heat treated types 304L and 304 L NAG was investigated in nitric acid using potentiodynamic and potentiostatic technique and mode of corrosion attained using surface morphological technique. The investigation focuses on influence of nitric acid concentration and operating temperature on corrosion of type 304L and type 304 L NAG at transpassive potential.

Introduction

Nuclear spent fuel reprocessing plants require corrosion resistant materials for uninterrupted operation. Major equipments of the plants are made up of types 304 L and 304 L NAG. These plants use Plutonium - URanium Extraction (PUREX) process which requires highly acidic condition to extract uranium and plutonium into the organic phase. Highly acidic condition, high temperature and presence of oxidizing ions such as fission and corrosion product increase operating potential to transpassive potential regime. Stainless steels are prone to intergranular corrosion (IGC) in transpassive potential regime. This paper focuses on the IGC of type 304L at transpassive potential regime. The study aims to investigate how change in acid concentration and process temperature modify the transpassive potential thus affecting corrosion rates and form of corrosion.

Experimental

The materials chosen for this study were austenitic stainless steels types 304L (commercial purity) and 304 L NAG. The chemical composition of type 304L in wt % is 18.05 Cr, 7.95 Ni, 0.034 P, 0.003 S, 1.47 Mn, 0.024 C, 0.04 N and the rest is Fe. It should be noted that the Ni content is 7.95 wt% against the specified limits of 8 to 12 wt%. The chemical composition of type 304 L NAG in wt % is 18.72 Cr, 10.19 Ni, 0.024 P, 0.004 S, 1.58 Mn, 0.014 C, 0.018 N and the rest is Fe. Test specimens having the ratio of total cross-sectional area to the total surface area of 14% were cut from the as-received materials and given heat treatment of 675 °C for 1 h. A 2 mm diameter hole was drilled on one side of the heat treated specimen. The specimens were ground on successively finer grit of emery papers till 600 grit was reached. The edges and corners were smoothened. Finally specimens were cleaned with soap solution and dried with acetone. These specimens were used for polarization and potentiostatic studies.

The microstructure of the as received and heat treated specimens were revealed using practice A of ASTM A262 [1]. Degree of sensitization (DOS) of specimens were measured using double loop potentiokinetic reactivation technique [2]. The experimental set up used for polarization study was the same as reported in the previous study [3]. Streicher used a similar set up for electrode potential measurements in boiling acid [4]. An acid bridge provided electrical connectivity while avoiding direct immersion of calomel electrode in near boiling nitric acid. Calomel electrode, platinum plate and test specimens were used as reference electrode, counter electrode and working electrode respectively. Polarization experiments were done in 3M, 6M and 9M nitric acid at 95°C. For potentiostatic experiments the setup used was the same as described for polarization experiments [3]. The values of the potential to be applied were determined from the result of polarization experiments and ranged from passive to transpassive potentials. The test solution was 3 M, 6 M and 9 M nitric acid in three sets of test at 95°C for the potentiostatic tests. To study role of temperature a set of potentiostatic tests were carried out in 6 M nitric acid at 55°C, 7°C, 85°C and 95°C. Each potentiostic test was conducted for 48 h. After the exposure weight loss of the specimen was measured and corrosion rate was calculated as per equation 1 [1]:

$$r = (7290 \times W) \quad (A \times t \times d) \qquad (1)$$

where r is corrosion rate (mm/month), A is total exposed surface area (cm^2), W is weight loss (g) of specimen after exposure to 6 M near boiling nitric acid for 48 h and d is density of the specimen (g/cm^3).

The morphology of attack was studied using optical and scanning electron microscopy.

Results and Discussion

The microstructure of as-received and heat treated specimens were “step” and “dual” respectively. The value for DOS of type 304L in as received condition was 0.07%. DOS increased to 0.7% after heat-treatment of 675°C for 1 h. It indicates that these alloys were not sensitized by the chosen heat treatment. Fig. 1 shows the potentiodynamic polarisation curves of type 304L heat treated at 675°C for 1 h in near boiling nitric acid of concentrations 3M, 6M and 9M. The E_{corr} moved from

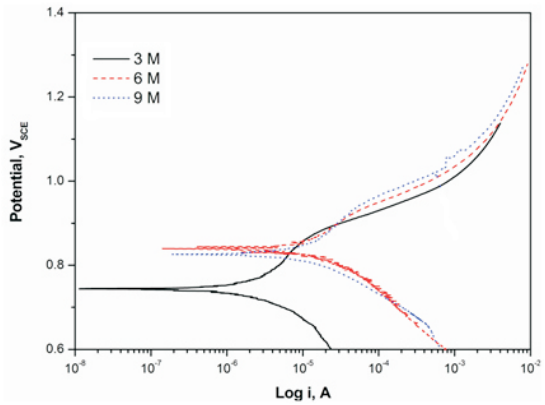


Fig. 1 Polarization curve of type 304L in nitric acid of various concentration at 95°C

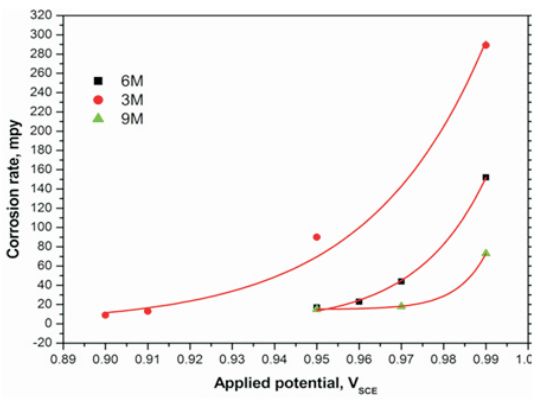


Fig. 2 Corrosion rate as a function of potential at different concentration of HNO_3 at 95°C

0.74 V_{SCE} in 3M nitric acid to 0.839 V_{SCE} in 6M nitric acid. However the E_{corr} in 9M nitric acid is slightly lower compared to 6M nitric acid. Transpassive potentials are the least in 3M and highest in 9M nitric acid. This shows that kinetics of transpassive dissolution of type 304L has increased with decreasing concentration of nitric acid.

The relationship between corrosion rates of type 304L measured after 48 h exposure in near boiling nitric acid of various comcentration and applied potentials is shown in Fig. 2. The corrosion rate increased at each potential with decreasing concentration of nitric acid. A threshold potential corresponding to corrosion rate of 24 mpy was established below which uniform corrosion occurred and above which IGC was observesd. The threshold potential for type 304L in 3M, 6M and 9M nitric acid were 0.92 V_{SCE}, 0.96 V_{SCE} and 0.98 V_{SCE} respectively. Surface morphological studies revealed no grain dropping below threshold potential and severe grain dropping above threshold potential.

Arrhenius plot for corrosion of type 304L NAG in 6M nitric acid at 0.99 V_{SCE} of applied potential is shown in Fig.3. The activation energy for corrosion of type 304L NAG in 6M nitric acid at 0.99V_{SCE} applied potential calculated using equation 2 was 72.56 kJ/mole.

$$\text{Logr} = -(\text{Ea} \quad 2.303\ \text{RT}) + A_2 \qquad (2)$$

where E_a is activation energy, A is Pre-exponential factor R is Universal gas constant and T is temperature in Kelvin.

Activation energy for corrosion of type 304 in various HNO_3/HF systems ranged from 22.6 to 58.8 kJ/mole [5]. Activation energy for corrosion of type 304L NAG was higher compared to type 304. This can be due to: (1) corrosion systems in the present investigation and in Covino et al. study are not same, (2) Type 304L NAG is an improved grade over type 304 thus exhibits superior corrosion resistance compared to type 304 SS in nitric acid.

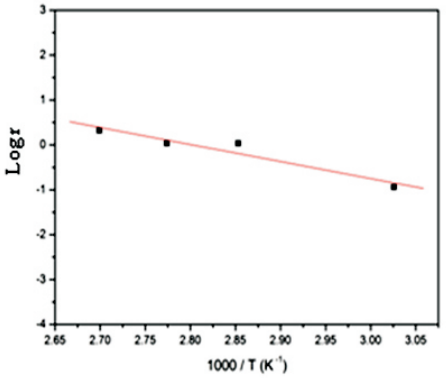


Fig. 3 Arrhenius plot of log r versus 1 / T with slopes equal to – Ea / 2.303 R for type 304L (NAG)

Conclusions

Type 304L even in non sensitized condition showed severe IGC at transpassive potential in nitric acid at all the three concentrations (3M-9M).

Polarization studies revealed that transpassive potential of type 304L at 95 decreased with lowering of acid concentration.

Threshold potential of type 304 L in various concentrations of nitric acid were in the order: 3M < 6 M < 9M.

The activation energy for corrosion of type 304L NAG in 6 M nitric acid at 0.99V_{SCE} was 72.56 kJ/mole.

References

[1] "ASTM A 262 – 02a", Annual book of ASTM standards, ASTM International, PA 19428-2959, United States, 2002.

[2] P. Majidi, M. A. Streicher, Corrosion, 40 (1984) 584.

[3] S. Bhise, V. Kain, Corros. Eng. Sci.Techn., 47(2011) 61.

[4] M. A. Striecher, J. Electrochem. soc., 106 (1959) 161.

[5] B. S. Covino et al., Met. Trans. A, 17A (1986) 137.

Liquid-Liquid Extraction of Praseodymium (III) Using Cyanex 272 in Kerosene

Nandita Panda, Niharbala Devi, Sujata Mishra

Department of Chemistry, Institute of Technical Education and Research, Siksha'O'Anusandhan deemed to be University, Bhubaneswarm 751030, E-mail:drsujatamishra97@gmail.com

The extraction of Pr(III) from nitric acid medium using Cyanex 272(HA) in kerosene was studied. The effect of various parameters like equilibration time, nitric acid concentration, extractant concentration, temperature, nature of diluents on the extraction of Pr (III) has been investigated. The extraction of metal decreased with increase in acid concentration. The extraction of Pr (III) was 70% from the aqueous phase of 0.001M HNO_3 using 1M Cyanex 272. On the basis of slope analysis, the composition of the extracted species is proposed to be $Pr(NO_3)_2.A(HA)$. Kerosene was found to be effective diluent for the extraction of Pr (III) from nitric acid medium using Cyanex272.

Introduction

The rare earth elements are vastly used in the production of electronics, magnets, catalyst, etc. Solvent extraction represents one of the best separation technique for rare earth extraction separation due to its simplicity, rapidity in micro as well as macro scale level. The organophosphorous extractants are widely used for the extraction and separation of lanthanides because of their selectivity [1,2]. Acidic organophosphorous extractants like Cyanex 272, DEHPA and PC88A are widely used for the extraction and separation of rare earth ions from various aqueous media [3,4]. The authors have already reported the extraction of Nd (III) from nitric acid medium using Cyanex 272 in kerosene [5]. The present study involving the extraction of Pr (III) from nitric acid medium using Cyanex 272 in kerosene may provide pathway to achieve an optimum extraction condition for Pr (III) and explore possibilities for the separation of these two metals.

Experimental

Reagents

Stock solution of Pr (III) (Merck, AR grade) was prepared by dissolving the required amount of oxide in concentrated nitric acid solution and evaporating excess of acid, then diluting to the required concentration. Distilled kerosene was used as the organic phase diluent. The commercial extractant, Cyanex 272 obtained from Cytec, Canada Inc. was used without further purification. All other reagents used were of analytical reagent grade.

Procedure

Equal volumes (10mL) of aqueous phase containing Pr (III) ion (0.001 M) in HNO_3 and organic phase with Cyanex 272 in kerosene were shaken for thirty minutes in a separatory funnel. Complete equilibrium was achieved only in thirty minutes. The Pr (III) concentration in the aqueous phase before and after the extraction was determined by using an ELICO UV-Visible Spectrophotometer by Arsenazo (III) method [6].The distribution coefficient (D) was calculated by taking the ratio of equilibrium concentration of Pr (III) in organic phase and that in the aqueous phase. From D values, the percentage of extraction was calculated (%E= 100(D/D+1)).

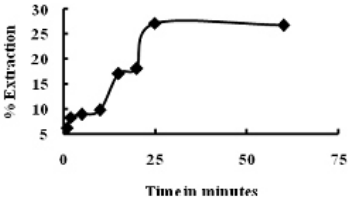


Fig. 1 Plot of %E versus Equilibration time for the extraction of 0.001 M Pr (III) from 0.001 M HNO_3 using 0.4 M Cyanex 272 in kerosene

Results and Discussion

Effect of Equilibration Time

The effect of equilibration time on the extraction of 0.001 M Pr (III) from 0.001 M HNO_3 using 0.4 M Cyanex 272 was studied within the range from 1 minute to 60 minutes. The metal ion extraction increased from 2% to 50% when the contact time increased from 1 minute to 30 minutes and then it remained constant with further increase in the contact time (Fig.1).

Effect of Nitric Acid Concentration

Being a cation exchanger, Cyanex 272 has the ability to extract Pr (III) from low acid medium. The effect of varying nitric acid concentration from 0.001 M to 0.05 M on the extraction of 0.001 M Pr (III) using 0.1 M Cyanex 272 was studied. The results showed that the extraction of 0.001 M Pr (III) decreased from 27% to 2% with increase in acid concentration from 0.001 M to 0.05 M. The plot of log D versus log [HNO_3] yields a straight line with a slope of -0.57, nearly equal to -1. It indicates the release of one H^+ ion in the extraction process [Fig.2].

Effect of Cyanex 272 Concentration

Extraction of 0.001 M Pr (III) from 0.001 M HNO_3 was carried out by varying the extractant

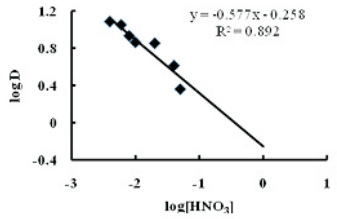


Fig. 2 Plot of log D vs log [HNO_3] for the extraction of 0.001 M Pr (III) using 0.1 M Cyanex 272

concentration in kerosene. The extraction was found to increase from 2% to 70% with increase in Cyanex 272 concentration from 0.1 M–1 M. To know the involvement of Cyanex 272 in the extracted complex, the plot was drawn taking log D versus log [Cyanex 272]. The slope value approximately equal to one indicates the involvement of one molecule of extractant in the extracted complex (Fig.3).

Diluent Variation

The effect of diluents (kerosene, benzene, toluene, xylene and chloroform) on the extraction of 0.001 M Pr (III) with Cyanex 272 from 0.001 M HNO_3 was studied. The results confirmed that the extraction of Pr (III) was maximum when kerosene was used as diluent (Table 1). Though benzene, xylene have high dielectric constant than kerosene, but are less efficient for extraction of Pr(III). This is probably due to the lower solubility of the extracted species in these diluents as compared with kerosene and also because of the different intermolecular diluent- diluent and extractant- diluent interactions that occur in aromatic and non- aromatic diluents [7].

Table1: Effect of diluents on extraction of 0.001 M Pr(III) from 0.001 M HNO_3 using 0.4 M Cyanex 272.

Diluents	D
Kerosene	1.027
Benzene	0.03
Chloroform	0.525
Toluene	0.124
Xylene	0.3867

Extraction Equilibrium

Trivalent lanthanides in the aqueous phase form a number of complexes in the presence of nitrate ions [8] and as Cyanex 272 extracts the metal ions by cation exchange mechanism, the species like $Pr(NO_3)^{2+}$ may get extracted into the organic phase. Cyanex 272 exists as dimer in organic non-polar diluents [9]. Based on the above results, the following extraction equilibrium can be established.

$$Pr(NO_3)_2^{+}{}_{(aq)} + (HA)_{2(org)} \quad Pr(NO_3)_2 . A(HA)_{(org)} + H^{+}{}_{(aq)}$$

Effect of Temperature

The effect of temperature on the extraction of 0.001 M Pr(III) from 0.001 M HNO_3 with 0.4 M Cyanex 272 was studied by varying the temperature from 298K-338K. It was observed that the extraction decreased with increase in temperature. The enthalpy

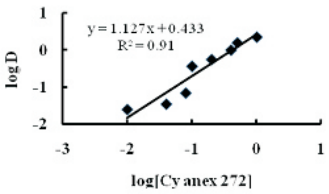


Fig. 3 Plot of log D vs log[Cyanex 272] for the extraction of 0.001 M Pr(III) from 0.001 M HNO_3.

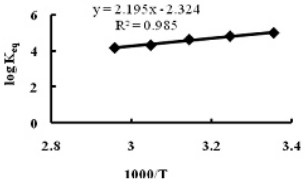


Fig. 4 Plot of log K_{eq} versus 1000/T for the extraction of 0.001 M Pr (III) from 0.001 M HNO_3 using 0.4 M Cyanex 272

change (H) and entropy change (S) were calculated by using Van't Hoff equation, which is given as:

$$\log K_{eq} = - \Delta H/2.303RT + \Delta S/2.303R$$

From Fig.4, the H was found to be -42.0kJmol^{-1} and S to be - 44.5JK^{-1}mol^{-1} which indicates that the extraction was exothermic owing to the formation of a stable complex.

Conclusions

In this study, it has been found that the extraction of Pr(III) decreased with increase in acid concentration. The extraction decreased with increase in temperature. Maximum extraction of 70% was achieved from 0.001 M HNO_3 using 1 M Cyanex 272 in kerosene.

Acknowledgements

The authors are grateful to Cytec Canada for providing Cyanex 272 and also thankful to authorities of Siksha 'O' Anusandhan deemed to be University for the encouragement to carry out this research work.

References

[1] Q Jia, Z Li, W Zhou, S Tong, H Li, S Meng, Sep Purif Technol. 64 (2009) 345.

[2] Q Jia, Z Li, W Zhou, H Li,, J Chem Technol Biotechnol. 84 (2009) 565.

[3] T K Ioannou, M Smutz, R G Baustia, Metall Trans. 3 (1972) 2639.

[4] S N Bhattacharya, K M Ganguly, Hydrometallurgy. 32 (1993) 201.

[5] N Panda, N B Devi, S Mishra, J. Radioanal. Nucl. Chem.295 (2013) 1205.

[6] S B Savvin, Talanta.3 (1961) 673.

[7] O.Abd EL-Naby Desouky, Ph.D.thesis,2006.

[8] M L P Reddy, J R Bosco Bharathi, S Peter, T R Ramamohan,Talanta, 50 (1999) 79.

[9] J M Zhao, X Y Shen, F L Deng, F C Wang, Y Wu, H Z Liu, Sep Purif Technol. 78 (2011) 345.

Ligand Sensitized Fluorescence of Eu^{3+} in Dimethyl Sulphoxide using TTA as a ligand: An Application of Europium Determination in U Matrix

S. Maji, Satendra Kumar, and K.Sankaran

Analytical Chemistry and Spectroscopy Section, Materials Chemistry Division, Chemistry Group, Indira Gandhi Centre for Atomic Research, Kalpakkam 603 102; E-mail: siuli@igcar.gov.in

Ligand sensitized fluorescence of Eu^{3+} using thenoyltrifluoroacetone (TTA) as a sensitizing ligand is studied in dimethyl sulphoxide (DMSO) medium. TTA ligand enhances the fluorescence of Eu^{3+} by a factor of 40000 in DMSO. The quenching of Eu^{3+}-TTA fluorescence by uranium is found to be less in DMSO solvent which leads the trace determination of europium in uranium matrix without any matrix removal.

Introduction

Uranium oxide is used as a nuclear fuel material in nuclear reactors for power production [1]. Presence of some of the lanthanides like Sm, Eu, Gd and Dy beyond a specified limit (Eu: 3ppm) in uranium oxide is found to affect the performance of the nuclear reactor [2-4]. Conventional Analytical techniques like ICP-OES and Mass spectrometry require chemical separation or extraction and pre-concentration of traces of lanthanides from the matrix to minimize the effect of matrix on the estimation.

In aqueous medium, Eu^{3+} gives strong fluorescence when it forms a ternary complex with TTA and certain other neutral ligands [5-6]. Fluorescence of Eu^{3+} in this ternary complex in aqueous medium is quenched strongly by the presence of uranium. In this work, several other solvents are tried to see the extent of quenching of Eu^{3+} fluorescence in presence of uranium. Quenching effect of uranium on Eu^{3+} fluorescence is found to be different in different solvents with a minimum in dimethyl sulphoxide (DMSO). Consequently, TTA sensitized fluorescence of Eu^{3+} in DMSO provides a method for the estimation of Eu^{3+} in a Uranium matrix.

Experimental

Fluorescence spectra were recorded using an Edinburgh FLS920 spectrofluorimeter with 450W xenon lamp as excitation source. Solutions were taken in a 2 mm path length cell. The band-pass for the excitation and emission monohromators were set at 3nm for both. Standard aqueous stock solution of Eu^{3+} was prepared by dissolving the required amount of Eu_2O_3 (99.9%, Indian Rare Earths) in distilled nitric acid and evaporated to dryness. The residue was then dissolved by adding water to get the required concentration of 15.2 mg/mL of Eu^{3+}. From this stock, solutions of different concentrations of Eu^{3+} were prepared for further use. Stock solution of 500 mg/mL of uranium was prepared by dissolving the uranium oxide in nitric acid and evaporated to dryness. The residue was then dissolved in 0.5 M nitric acid. Stock solution of TTA (Aldrich) was prepared by dissolving the required amount of the reagent in ethanol (Hayman, 99.9%).

For conducting the fluorescence studies, Eu^{3+}-TTA complex was prepared by mixing required amount of TTA. (typically 2-10 L) and Eu^{3+} (2.5-5 L) in 0.5 mL of DMSO.

Results and Discussions

Figs. 1&2 shows the emission and excitation spectrum of Eu^{3+} in DMSO respectively. These figures clearly show that the ligand TTA enhances the fluorescence of Eu^{3+} by about 40000 times relative to the fluorescence of Eu^{3+} without the ligand in dimethyl sulphoxide medium.

The effect of uranium on the fluorescence intensity of Eu^{3+}-TTA complex is shown in Fig. 3. Strong quenching was observed in aqueous medium with the addition of uranium. About 97 % intensity was reduced with the addition of just 25 g/mL of uranium. For the same concentration of uranium in DMSO, the decrease in intensity of fluorescence is about four times less indicating that quenching is less in the case of DMSO.

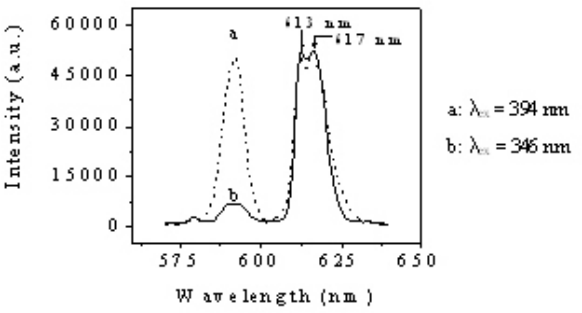


Fig. 1 Emission spectra of (a) Eu^{3+} [152 g/mL] without TTA and (b) Eu^{3+} [3.8 ng/mL] complexed with TTA in DMSO; [TTA] = $2x10^{-4}$ M

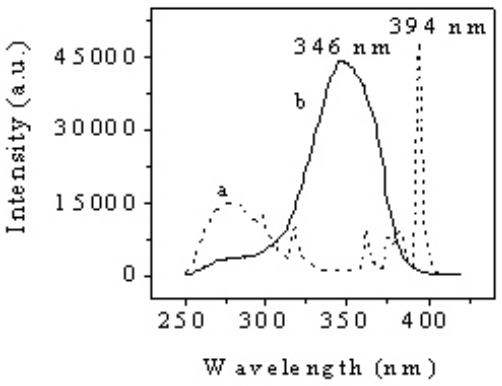


Fig. 2 Excitation spectra of (a) Eu^{3+} [152 g/mL] without TTA and (b) Eu^{3+} [3.8 ng/mL] complexed with TTA in DMSO; [TTA] = $2x10^{-4}$ M; $_{em}$ = 544 nm.

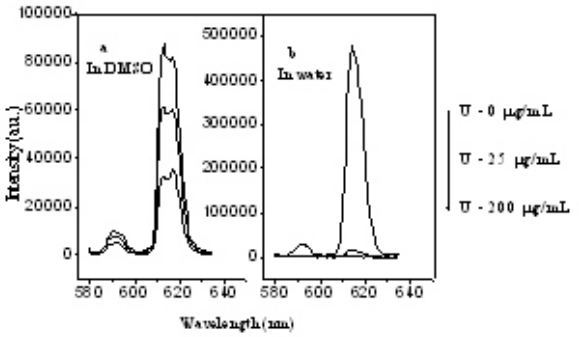


Fig. 3 Emission spectra of a) Eu^{3+}-TTA in DMSO and b) Eu^{3+}-TTA-TOPO/TritonX-100 in water for different concentration of uranium; [Eu^{3+}] = 7.6 ng/mL, [TTA] = $2x10^{-4}$ M, [TOPO] = $1x10^{-4}$ M and $_{ex}$ = 346 nm

Four synthetic solutions of uranium (500 mg/ml) were prepared, containing Eu^{3+} in the range of 0.3 – 2.4 g/ml. Fluorescence spectra were recorded after diluting to 1000 times in DMSO. Standard addition method was used to estimate the Eu^{3+} concentration in these solutions. The results are presented in Table 1. The estimated values are within 10 % of the actual values. The relative standard deviation for fluorescence intensity of the sample containing 0.3 g/mL europium in 500 mg/mL of uranium is 5%.

Conclusion

Ligand sensitized fluorescence using TTA as a sensitizing ligand in dimethy sulphoxide is presented for trace level determination of Eu^{3+} in uranium matrix. The use of DMSO as a solvent is advantageous over water as the quenching effect exerted by uranium on the fluorescence of Eu^{3+} is drastically less which makes it attractive for application in nuclear industry. Europium in the range of 0.6 to 4.8 g/g in U matrix is estimated with good precision and accuracy in synthetic samples.

Table-1 Estimations of Eu^{3+} in synthetic samples

Sample No.	Eu^{3+} as prepared (g/mL)	Eu^{3+} as estimated (g/mL)	Deviations (%)
1	0.31	0.34	9.7
2	1.22	1.20	2
3	1.82	1.67	8.2
4	2.43	2.17	10.7

References

[1] H. Stehle, H. Assmann, F. wunderlich, Nucl. Eng.and Design 33(2) (1975) 230.

[2] R.K. Malhotra, K. Satyanarayana, Talanta 50 (1999) 601.

[3] Ki-Soo Cho, In-Suck Suh, J. Korean Nucl. Soc. 15(2) (1983) 142.

[4] PFBR/31100/SP/1028

[5] Y.-Xiang Ci, Z.-Hua Lan, Analyst 113 (1988) 1453.

[6] N. Arnaud, J. Georges, Analyst 122 (1997) 14

Fluorimetric Estimation of U(VI) in the Presence of a Large Excess of Th(IV)

S. Maji, Satendra Kumar and K.Sankaran

Analytical Chemistry and Spectroscopy Section, Materials Chemistry Division, Chemistry Group, Indira Gandhi Centre for Atomic Research, Kalpakkam 603 102; E-mail: siuli@igcar.gov.in

Spectrofluorimetric determination of U(VI) in the presence of a large excess of Th(IV) has been carried out in a solution containing 1M H_3PO_4 and 1M H_2SO_4 . U(VI) when present to an extent of 0.001% of Th(IV) (Th:U = 100,000:1) can be analysed by this method. Synthetic samples are prepared mimicking the components of ThO_2 fuel and the concentration of U(VI) was estimated by standard addition method and slope method.

Introduction

Estimation of uranium in thorium matrix is important as thoria is used as blanket in the fast breeder test reactor (FBTR) [1] and planned to be used as blanket in PFBR (prototype fast breeder reactor). Numerous spectrophotometric methods [2,3] have been reported for trace analysis of uranium in Th matrix.

Fluorescence Spectroscopy is an excellent analytical tool for the estimation of uranium. But the fluorescence of uranyl (UO_2^{2+}) is known to be weak in aqueous solution due to quenching by water. In order to overcome this problem, fluorescence enhancing reagents such as H_3PO_4, H_2SO_4, $HClO_4$, fluran etc. have been used [4,5]. The most widely used enhancing reagent is H_3PO_4. In 1M of H_3PO_4 solution, the fluorescence of uranium is enhanced by more than three orders of magnitude as compared to aqueous uranium fluorescence without any complexing agent.

The H_3PO_4 solution can not be used for the estimation of uranium when it is present in a large excess of thorium as thorium forms thorium phosphate precipitate which is highly insoluble. One can use H_2SO_4 solution as sulphate of Th is soluble in water but the sensitivity of uranium fluorescence in this medium is much poorer than H_3PO_4. In the present work, an attempt has been made to determine U in excess of Th using a mixture of 1M H_3PO_4 and 1M H_2SO_4 solution (referred hereafter as 'acid mixture'). The results are presented in this paper.

Experimental

Fluorescence spectra were recorded using an Edinburgh FLS920 spectrofluorimeter with 450W Xenon lamp as excitation source. Solutions were taken in a 10 mm path length cell. The band-pass for the excitation and emission monohromators were set at 7 and 4 nm respectively. The fluorescence of the samples was recorded using an excitation at 255 nm. The emission spectrum was recorded over the range 460-600 nm. The intensity of the uranium emission at 515 nm was used for fluorimetric estimation.

The stock solutions of different elements were prepared by dissolving the corresponding oxide or nitrate salts. The H_3PO_4 and H_2SO_4 used were of analytical grade. Millipore water was used for sample preparation. Different synthetic solutions were prepared containing U, Th and other ions which are usually present as impurities in thoria [6]. The concentrations of all these ions used in these synthetic solutions are given in Table 1. All these ions altogether are referred as 'other ions' in the text.

Table-1: Typical composition of the 'other ions' mimicking the impurities ThO_2

Concentration used in synthetic samples (ppm)	Concentration (Expected) in ThO_2 (ppm)	Elements
6.5	65	Al
58.6	586	Ca
1.1	11	Ce
1.3	13	Cr
11	110	Cu
13.4	134	Fe
7.4	74	Mg
0.7	7	Mn
4.5	45	Mo
5.7	57	Ni

Total = 110.2 ppm

Results and Discussions

The fluorescence of U at different concentrations are recorded in 1M H_3PO_4, 1M H_2SO_4 and in 'acid mixture'. The calibration curves obtained for U in different solutions are given in Fig. 1. It is clear from the Fig.1 that sensitivity of U in the 'acid mixture' is slightly less than the sensitivity in 1 M H_3PO_4 but much more than the sensitivity in 1 M H_2SO_4.

The effect of Th on the fluorescence of uranyl was examined and is shown in Fig. 2. About 40 % drop in intensity of uranyl fluorescence is found when Th is about 10,000 ppm. Hence to estimate the concentration of U in excess of Th a correction procedure should be applied. The correction procedure (slope method)

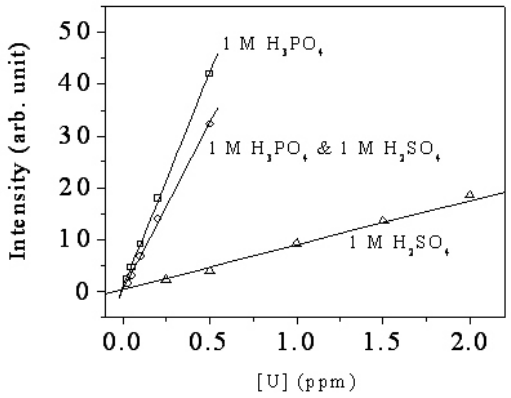


Fig. 1 Calibration curve of U in different medium

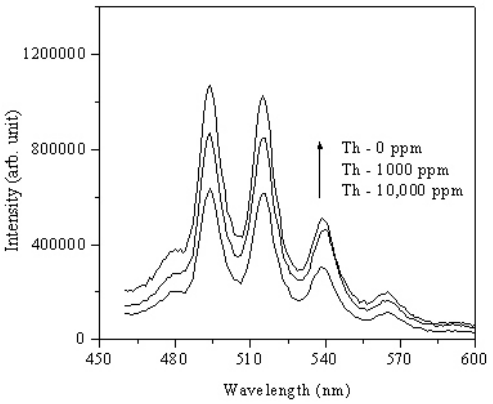


Fig. 2 Effect of Th on the fluorescence of U [0.1 ppm]

Table-2: Comparisons of the estimated concentrations of U in the synthetic solutions obtained by slope method and standard addition method. Deviations are given in the parenthesis.

Sample ID	Concentration as prepared (ppm)			Concentration of U as measured (ppm)	
	'other ions'	[Th]	[U]	[U] std. addition method	[U] slope-method
Syn I	0	5,000	0.1	0.12 (20 %)	0.11 (10 %)
Syn II	110.2	100,000	1	1.42 (42 %)	1.15 (15 %)
Syn III	,,	,,	2	2.22 (11 %)	2.16 (8 %)
Syn IV	1102	,,	10	11.5 (15 %)	10.7 (7 %)

outlined in Ref. [7] is applied here for the estimates of U. The same estimates are also obtained using standard addition method.

Synthetic solutions containing different concentrations of U, Th and 'other ions' are prepared and their concentrations are given in Table 2. These solutions are suitably diluted in 'acid mixture' and fluorescence is measured. Corrections based on slope method are made to arrive at the concentration of U and the estimates are compared with standard addition method.

Conclusion

The 'acid mixture' (1 M H_3PO_4 and 1 M H_2SO_4) has been demonstrated as a good solvent for the estimation of U in a large excess of Th. Limit of detection has been calculated to be 100 ppb in the presence of 10,000 ppm of Th. This makes it attractive for application in nuclear industry.

References

[1] G. Srinivasan, K.V. Suresh Kumar, B. Rajendran and P.V. Ramalingam; Nuc. Eng. & Design, 236 (2006) 796.

[2] Shui-Chieh Hung, Chang-ling Qu, and Shui-Sheng Wu; Talanta 29 (1982) 629.

[3] A. Suresh, Dinesh K. Patre, T.G. Srinivasan and P.R. Vasudeva Rao; Specchim. Acta A 58 (2002) 341.

[4] C. Moulin, P. Decambox, and L. Trecani; Anal. Chim. Acta, 321 (1996) 121.

[5] G. Meinrath, Y. Kato and Z. Yoshida; J. Radio. Nucl. Chem., 174(2) (1993) 299.

[6] A. Sarkar, D. Alamelu, and S.K. Aggarwal, J. Nucl. Materials, 384 (2009) 158.

[7] S. Maji, K. Sundararajan, and K. S. Viswanathan; Spec. Acta A 56 (2000) 1251.

Light Scattering Studies for Estimation of Hydration Number of Sr(II) and Al(III) ions in Dilute Aqueous Solutions of Nitric Acid

N. Priyadarshini, M. Sampath, Shekhar Kumar and U. Kamachi Mudali

Process Development and Equipment Section, Reprocessing R&D Division, Reprocessing Group, Indira Gandhi centre for Atomic Research, Kalpakkam 603102, India; E-mail: shekhar@igcar.gov.in

Light scattering technique was used to probe the hydration of Sr(II) and Al(III) cations in aqueous nitric acid medium at 298±2K. Dynamic Light Scattering method was used to arrive at the diameter of the hydrated ion of Al(III). It has been determined as 0.95 nm which was in well agreement with the reported values. In case of Sr(II) ion, it was difficult to predict due to limitation in the detection range of the instrument (0.8nm to 6.54ìm). Refractive index measurements were done at 298.15 K. The molecular weight of the hydrated ion was determined from the Debye plot. At high acidity with OH/Al ratio of 0 i.e pure $Al(NO_3)_3$ solution without the addition of base, the number of solvating molecules was observed to be 5. Similarly for strontium, 9 water molecules were in the primary hydration sphere possibly existing in the form of $Sr(H_2O)_9^{2+}$. Second virial coefficient shows negative values in both the cases. The molecular weight of hydrated ion of Al(III) is 113Da and that of Sr(II) is 253Da.

Introduction

Hydrolysis and hydration of the Aluminum (III) ion in aqueous solution play a fundamental role in the reactivity and mobility of the Al(III) hydrolysis species that are important in materials chemistry, environmental science and medicine. The initial hydrolysis of Al can be understood from the following equation

$$Al(H_2O)_6^{3+} + H_2O \quad Al(H_2O)_5(OH)^{2+} + H_3O^+$$

In aqueous systems, at pH<3 it exists as octahedral $Al(H_2O)_6^{3+}$ [1]. The first hydrolysis product $Al(OH)^{2+}$ was hexacoordinate. But Car–Parrinello simulations and ab initio methods predicted that pentacoordinate structure was stable [2]. Meanwhile, density functional theory (DFT), also suggests five-coordinate geometry as stable form. In the present investigation light scattering has been used as an analytical tool to study hydration of Al^{3+} in aqueous environment.

Strontium has an associated coordination number ranging from 7-10. Recent studies by Quantum mechanical molecular dynamic simulation and AXD studies show that Sr has coordination number of 9 with highest probability [3]. The ambiguity in the coordination number of Sr has been clearly clarified by the present investigation.

Experimental

$Al(NO_3)_3.9H_2O$ (M/S Across organics assay of >99.0%) was used for preparing the solutions. It is of analytical grade and used as such. Anhydrous $Sr(NO_3)_2$ (M/S Alfa Aesar, minimum assay of 99.0%) was used for preparing Sr^{2+} solutions. Both the salts were dissolved in 1M nitric acid (AR-Fisher, assay of 69-71%) to a concentration of 0.1 to 0.3 M of Al and 0.025 to 0.125 M of Sr. All the solutions were prepared at room temperature. Water used for making the solutions was ASTM grade I water with a resistivity of 18.2 M .cm^{-1} at 298.15K and TOC < 15ppb obtained from a Millipore simplicity system.

Results and Discussion

Particle Size Distribution

Particle size measurements were carried out at 298 K using Microtrac (Nanotrac ULTRA) particle size analyser. It was based on a 3mW laser diode operating at a wavelength of 780 nm and used controlled reference method to generate wide spectrum of heterodyne difference frequencies. The scattered light was measured at an angle of 180°. The hydrodynamic particle radius R_h can be derived using Stokes-Einstein relation (1).

$$R_h \quad \frac{k_B T}{6 \quad D} \qquad (1)$$

where k_B is Boltzmann's constant, T is the temperature, is viscosity of the solvent and D is the diffusion coefficient. The performance of the instrument was checked with the reference material (100 nm polystyrene microsphere suspended in water) prior to particle size measurements. The uncertainty in the measurement was ±1 nm. The ionic diameter of hydrated Al^{3+} ion was estimated as 0.95 nm which can be validated with the earlier reported values predicted by various methods like diffusion studies [3], individual ion activity method. The diameter of the hydrated ion includes only the primary hydration sphere. The diameter of hydrated ion of Sr(II) was determined as 0.5nm by diffusion studies [3]. It was difficult to predict by this method due to the limitation in the detection range of the instrument (0.8 nm to 6.54 ìm).

Refractive Index Increment

Refractive index (n) of solutions of different concentration of Sr^{2+} and Al^{3+} was measured on Anton Paar RXA 156 refractometer equipped with integrated

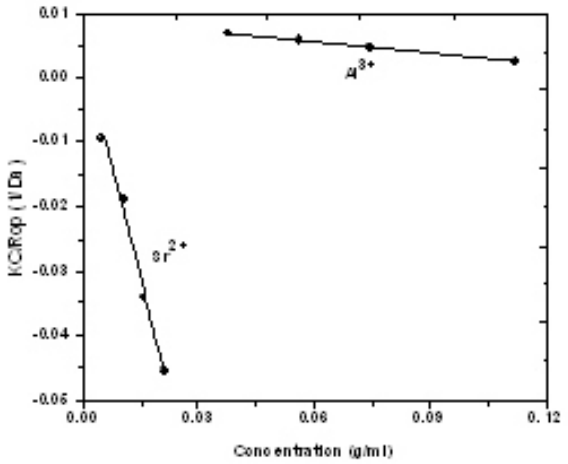


Fig. 1 Debye plot for various concentrations of Sr^{2+} and Al^{3+} hydrated ions

peltier thermostat with standard deviation of 2 x 10^{-5} n_D at 298 K. As the concentration increases refractive index also increases. These values were used for generating the Debye plot.

Molecular Weight of Hydrolyzed Sr(II) and Al(III) Ions

The molecular weight of a polymer can be obtained using Rayleigh equation given in equation (2)

$$\frac{KC}{R} \quad \frac{1}{M_W} + 2A_2C \qquad (2)$$

Where the optical constant $K = [2\ n(dn/dC)]^2/N_A\ ^4{}_o$, R is the excess Rayleigh ratio, M_w is the weight average molecular weight of the solute, C is the concentration (in g/ml), A_2 is the second virial coefficient, $_o$ is the wavelength of light used, N_A is Avogadro's number and dn/dC is the refractive index increment due to the solute under a given set of solution conditions. The Debye plot is KC/R vs. Concentration in g/ml. The intercept of the plot gives $1/M_W$ and the slope is used to calculate the second virial coefficient [4].

The molecular weight of the hydrated ion obtained from the Debye plot clearly shows that there is a possibility of Aluminium ion penta-coordinated by water molecules. The molecular weight of the hydrated Sr^{2+} was determined as 253 Da. This shows that Sr is solvated by 9 water molecules. The second virial coefficient from the slope of the plot has a negative value in both the cases showing high solute-solute interatction. Figure 1 shows the Debye plot for hydrated ions of Sr^{2+} and Al^{3+}. The calculated parameters from the Debye plot are given in Table 1.

Table-1: Calculated parameters from the Debye plot for hydrated Al^{3+} and Sr^{2+} ion.

Substance	Measured at = 780 nm	
	M_w Da	Second virial coefficient A_2 (ml g^{-1} Da)
Al^{3+}(hydrated)	113	-5.48E-02
Sr^{2+}(hydrated)	253	-2.35

Conclusions

Light scattering technique has provided a new approach to understand the nature of ion solvent interaction and its possibility to arrive at hydration number of metal cation under study. Debye plot was used to estimate the molecular weight of hydrated ion. The second virial coefficient has also been determined.

References

[1] A. Fratiello, R. E. Lee, V. M. Nishida, R. E. Schuster, J. Chem. Phys. 48 (1968) 3705.

[2] T. W. Swaddle, Rosenqvist, P. Yu, E. Bylaska, B. L. Philiips, W. H. Casey, Science, 308 (2005) 1450.

[3] A.G. Volkov, S. Paula, D. W. Deamer, Bioelectrochem. Bioenergetics, 42 (1997) 153.

[4] J. B. Bruce, Robert Pecora, "Dynamic light scattering with application in physics, chemistry and biology", Wiley-New York, (1976)

Liquid-liquid Extraction of Zr (IV) from HCl Medium using Cyanex921 in Kerosene

B.C.Bhatta[1], S.K.Sahu and Sujata Mishra[2]

1. *Department of Chemistry, College of Engineering and Technology, Bhubaneswar 751003, Odisha*
2. *Department of Chemistry, Institute of Technical Education and Research, Siksha'O'Anusandhan deemed to be University, Bhubaneswar 751030; E-mail: drsujatamishra97@gmail.com*

The liquid – liquid extraction of Zr (IV) from acidic chloride solutions was carried out with Cyanex 921 as an extractant diluted in kerosene. The extraction of Zr(IV) from 5M HCl increases with increase in chloride ion concentration using ammonium chloride or potassium chloride in the aqueous phase. The positive enthalpy change and positive entropy change using 0.01M Cyanex921 shows endothermic process with increase in randomness. The percentage of extraction of Zr (IV) increased with increase in concentration of metal ion concentration up to 0.01M and thereafter remains constant. Study on effect of diluents revealed that extraction of Zr (IV) using kerosene as diluent was maximum.

Introduction

Zirconium is as a used construction material of nuclear reactors.Zirconium is used as a shielding material in the nuclear industry, catalyst in organic reactions, dye pigments, ceramic industry etc. Literature study shows that a limited no. of extractants have been used for the extraction of zirconium. With respect to the importance of zirconium in nuclear technology, the solvent extraction of Zr(IV) has been studied by several authors.Organophosphorus compounds such as TBP and Cyanex-272 bis(2,4,4-trimethylpentyl)phosphinic acid., D2EHPA (di(2-ethylhexyl phosphoric acid) have been extensively employed as extractants for zirconium [1-4].Thermodynamics of solvent extraction of Zr(IV) has been studied from different aqueous media using secondary amine Amberlite LA-2,the neutral organo-phosphorus donor TBP and the liquid organophosphorus cation exchanger, HDEHP [5]. Cyanex-921(Trioctyl phosphine oxide) is a well known extractant. The present study reports the extraction behaviour of Zr(IV) from concentrated acidic chloride solution with Cyanex 921 in kerosene. Various experimental variables such as the effect of chloride ion conc., effect of temperature, the nature of diluents, and concentration of metal on the extraction have been investigated.

Experimental

Reagents

Cyanex 921 supplied by Cytec, canada was used without purification. As a source of Zr(IV), Zr $OCl_2.8H_2O$ (MERCK) was used. Distilled kerosene was used as a diluent. Freshly prepared solutions of Zr(IV) were used for extraction experiments. All other reagents used were of analytical reagent grade

Procedure

Equal aliquots (10ml) of the aqueous phase containing 0.001M $ZrOCl_2.8H_2O$ in HCl and the organic phase with the extractant in kerosene were shaken for twenty five minutes in a separating funnel. Complete equilibrium was achieved in twenty five minutes. The Zr(IV) concentration in aqueous phase before and after the extraction was determined by Arsenazo(III) method using ELICO UV-Visible spectrophotometer. From D values, the percentage of extraction was calculated (%E= 100(D/D+1)).

Results and Discussion

Effect of Chloride Ion Concentration

The effect of chloride ion concentration in 5M HCl of 0.001M Zr(IV) using 0.01M Cyanex 921 was studied. It was found that the percentage of extraction of of Zr(IV) increases with increase in concentration of NH4Cl and KCl varying chloride ion concentration (0.01M-0.1M) in 5M HCl of 0.001M Zr(IV) using 0.01M Cyanex921.

Effect of Temperature

The effect of temperature on the extraction of 0.001M Zr (IV) from aqueous solution containing 4M HCl with 0.01M Cyanex 921 was studied in the temperature range 298K-339K.It was observed that an increase in temperature, of the extracting solution, the extraction of Zr(IV) increases. The results showed in (Fig. 1) the plot of $\log K_{eq}$ versus 1000/T gives a linear relation with a negative slope. Applying Van't Hoffs equation, the thermodynamic parameters, change in enthalpy and change in entropy were calculated to be 13.6 kJ mol^{-1} and 71.2 $JK^{-1}mol^{-1}$.It ensures the extraction process to be endothermic accompanying with an increase in the randomness using 0.01M Cyanex921.

Effect of Diluents

Effect of diluents (kerosene, Benzene, Toluene, xylene, chloroform) on the extraction of Zr(IV) from 4M HCl using 0.01M Cyanex921 was carried out. The results obtained confirmed that the percentage of extraction was maximum when kerosene was as diluent.

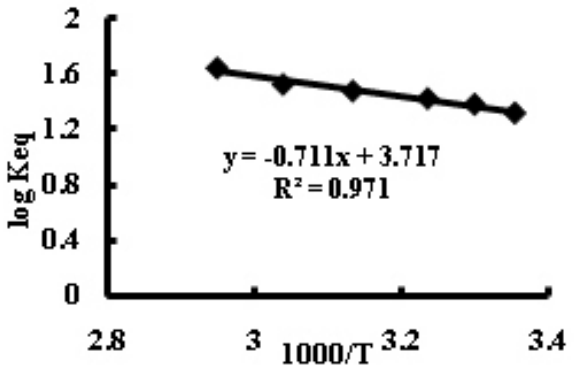


Fig. 1 Plot of log K vs 1000/T in the extraction of 0.001 M Zr (IV) from4M HCl

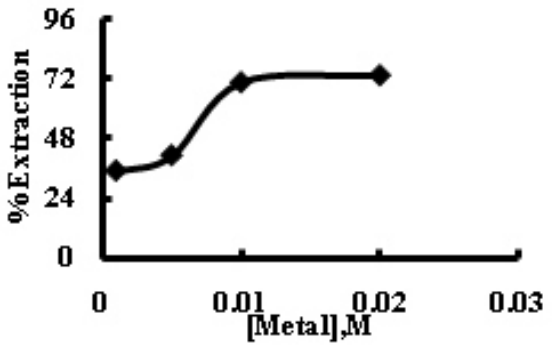


Fig. 2 Plot of %E vs [Metal],M in the extraction of 0.001 M Zr (IV) from 4M HCl

Table-1: Effect of Diluents on the extraction of 0.001 M Zr(IV) from 4 M HCl

Diluents	D	%E
Kerosene	0.538	35
Benzene	0.24	19
Toluene	0.199	17
Xylene	0.165	14
Chloroform	0.075	7

Effect of Metal Ion Concentration

The extraction of 0.001M Zr(IV) from 5M HCl was studied by increasing the concentration of the zirconium metal from 0.001M to 0.02M (Fig. 1) . The percentage of extraction (E) was increases from 35% to 74% with the increase in concentration of metal and thereafter remains constant.

Conclusions

The extraction of Zr(IV) increases with increase in concentration of metal ion concentration, temperature and chloride ion.

Acknowledgements

The authors are grateful to Cytec Canada for providing the gift sample of Cyanex 921 and they are also thankful to authorities of Siksha 'O' Anusandhan deemed to be University for the encouragement to carry out this research work.

References

[1] R.K. Biswas, M.A. Hayat. Hydrometallurgy,63 (2002) 149.

[2] B Ramachandra Reddy, J Rajesh Kumar and AVarada Reddy, Analytical Sciences, 20 (2004) 20.

[3] M.Taghizadeh,R.Ghasemzadeh,S.N.Ashrafizadeh,M. Ghannadi, Hydrometallurgy, 96 (2009) 77.

[4] S Biswas S.Basu, J.Radioanal.and Nucl. Chem. 242 (1999) 253.

[5] A.A.Abdel,Fattah,S.M.Ali,F.H.ElSweify,J.Radioanal. and Nucl. Chemistry, 253(3) (2002) 465.

Determination of Free Acidity in Nuclear Fuel Reprocessing Streams by Fiber Optic Aided Spectrophotometric Technique

S. Ganesh, P.Velavendan, N.K. Pandey, U. Kamachi Mudali and R. Natarajan

Reprocessing Research Development Division, Indira Gandhi centre for atomic research, Kalpakkam 603102; E-mail: velp@igcar.gov.in

A fiber optic aided spectrophotometric technique has been developed for the determination of free acidity in nuclear fuel reprocessing streams. The developed method is simple, accurate and applicable to all ranges of nitric acid and heavy metal concentrations relevant to the purex process. The method is based on the formation of yellow colour with an acid-sensitive indicator such as chrome azurol s, the intensity of yellow colour is proportional to the acid concentration. The system obeys Lambert-Beer's law at 455 nm in the range of acidity 1-10 M of nitric acid. The results obtained are reproducible with standard deviation 2% and relative error is less than 3%. The results obtained by the developed technique are in good agreement with those obtained by the standard procedure. This method is adaptable for remote operation and on-line monitoring.

Introduction

Nuclear fuel reprocessing requires a real-time monitoring of free acid concentration should be accurately and rapidly controlled in order to optimize liquid-liquid extraction, stripping, purification steps and process efficiency [1]. The reprocessing of actinides required to maintain nitric acid concentration at a constant level which various from 1 to 10 M. The acidity measurements are usually performed via the classical titrimetric methods which are destructive and time-consuming. In addition, they produce analytical wastes and sometimes are not sufficiently reliable due to the interfering species, especially the heavy-metal cations which need prior separation. A first spectrophotometric approach to monitor nitric acid concentrations up to about 10 M was developed and reported [2-3]. Thus, the development of a fiber optic aided spectrophotometric method allows remote operation in harsh environments and essential for fast and accurate determination of free acidity.

Experimental

Fiber optic aided spectrophotometery with 1 cm path length probe is used for measuring absorbance. All reagents used were of analytical reagent grade. Standard solutions of nitric acid were prepared by dilution of concentrated nitric acid. 0.025% of Chrome azurol s was prepared in distilled water.

Results and Discussion

Fiber optic aided spectrophotometric method for the determination of free acid in nuclear fuel reprocessing stream was standardized using an acid-sensitive indicator such as Chrome azurol. Absorbance for each samples were measured at the wavelength of the maximum absorption at 455 nm and made the calibration graph. Fig. 1 shows a typical calibration graph made for the standard nitric acid concentration ranges from 1 to 10 M with RSD 0.81%. The concentration of nitric acid in the unknown sample was determined by comparing absorbance with standard calibration graph. Tables 1 indicate the results obtained by the present method are in good agreement with those obtained by the standard method [4].

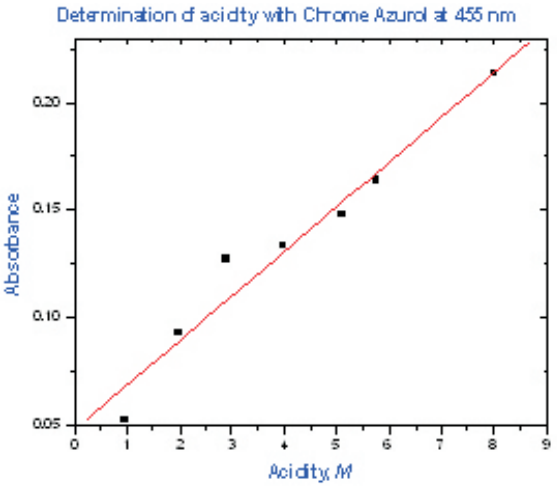


Fig. 1 A typical calibration graph for determination of free acidity with chrome azurol s at 455 nm

Table 1: Comparison of two different analytical techniques for the determination of free acidity.

Sl. No	Determination of acidity (M)	
	Present Method	Titrimetry [4]
1	0.949	0.962
2	5.210	5.234
3	4.018	3.991
4	1.894	1.908

References

[1] W.P. Carey, M.D. DeGrandpre, B.S. Jorgensen, Anal.Chem. 61, 15 (1989) 1674.

[2] W.P. Carey, M.D. DeGrandepre, Appl.Spectr. 45 (1991) 834

[3] A.A. Garrison, M.Z. Martin, AT-process, J.Process Anal.Chem 1 (1995) 95 & 127.

[4] S. Ganesh, F. Khan, M.K. Ahmed, S.K. Pandey, Talanta 85 (2011) 958.

Column Chromatographic Method for the Separation of Neodymium from Uranium & Other Elements using poly[dibenzo-18-crown-6]

Shila N. Lad[1], Baburao S. Mohite[*1]

Analytical and Environmental Research Lab, Department of Chemistry, Shivaji University, Kolhapur 416004 (MS) India; E-mail: lad.sheela@rediffmail.com, bsmohite@hotmail.com

A simple and efficient column chromatographic method has been developed for the separation of U (VI), Nd (III) and other metals using poly [dibenzo-18-crown-6] as stationary phase and hippuric acid as a counter ion. The various eluting agents were found efficient eluents for Nd (III). The capacity of crown polymer for Nd (III) was found to be 0.55±0.01mmol/g. The tolerance limits of various cations and anions for Nd (III) were determined. Nd (III) was quantitatively separated from other metal ions in binary as well as multicomponent mixtures. The good separation yields were obtained and had good reproducibility (±2%). The method was simple, rapid and selective.

Introduction

Main constituents in nuclear spent fuels are actinides like uranium, thorium and various fission products. Neodymium (III) is used in burn up measurements which are essential for fuel development studies and evaluation of power reactor operation [1]. Crown ethers are widely used as extractants for lanthanides and actinides, sorbents and chromatographic techniques [2]. The polymeric crown ethers are stable to radiolysis, organic solvents and to temperatures. All extractions with crown ethers and cryptands are governed by the nature of counter anion. The amino acids form complexes with metal ions due to formation of zwitter ion, hence poly[dibenzo-18-crown- 6] was used as a stationary phase in our study. No attempts were made on the sorption study of Nd(III) using poly[dibenzo-18-crown-6] in hippuric acid medium. The study was extended for the separation of Nd(III) from U(VI) and other metal ions. The method is simple and developed without having sophisticated instruments.

Apparatus and Reagents

A digital visible spectrophotometer (215D, Thermo Electron LLS, India), a digital pH meter (Model LI-120,Elico, India) with glass and calomel electrodes and a digital flame photometer (PI, Model No. 041, India) were used. Nd(III) stock solution was prepared by dissolving 1.243 g of neodymium chloride hexahydrate (AR, Fuka, Switzerland) in 100 ml distilled deionised water. The solution was standardized gravimetrically. The standard (100 g / ml) solution was prepared by appropriate dilution of the stock solution. Hippuric acid solution was prepared by dissolving 0.1791 g of hippuric acid in distilled deionised water and solution was diluted to 100 ml poly[dibenzo-18-crown-6] (Darmstadt, Germany) was used after screening to 100-200 mesh. 0.5 g of polymer was slurred with distilled, deionised water and poured into a pyrex glass chromatographic column (20× 0.8 cm i.d.). The column was used after preconditioning with hippuric acid solution.

General Procedure

An aliquot of solution containing 40 g/mL Nd (III) was mixed with hippuric acid solution in concentration range 1×10^{-2} to 1×10^{-6} M in a total volume of 10 ml. The solution was then passed through a poly[dibenzo-18-crown-6] column preconditioned with the same concentration of hippuric acid as that of the sample solution at flow rate of 0.5 mL / min. The column was washed with same concentration of hippuric acid. The adsorbed metal ion was then eluted with different eluting agents. 5 ml fractions were collected and the Nd (III) content was determined spectrophotometrically with Arsenazo-III at 650 nm [3,4]. The concentration of metal ion was calculated from calibration graph.

Result and Discussion

Adsorption of Nd(III) on poly[dibenzo-18-crown-6] as a function of hippuric acid concentration.

Concentration of hippuric acid was varied from 1×10^{-2} to 1×10^{-10} M. It was found that there was quantitative (100%) adsorption from 1×10^{-2} to 1×10^{-8}M. For further studies 1×10^{-3} M concentration of hippuric acid was selected.

Elution studies of Nd(III) with various eluting agents

Quantitative desorption of Nd(III) was performed with various eluting agents. 40 g /ml Nd (III) was adsorbed on the poly[dibenzo-18-crown-6] at 1×10^{-3} M hippuric acid concentration. HCl, HBr, $HClO_4$, H_2SO_4 and CH_3COOH were used as eluting agents. The results showed that 0.1 to 8 M HCl, 1 to 8 M HBr, 0.1 to 8 M H_2SO_4, 1 to 8 M $HClO_4$ were found to be efficient eluents for the elution of Nd(III). Further elution studies

Table-1: Multicomponent Separation

Sl. No.	Mixture	Taken (g)	Recovery	SD	Eluent
1	Li	50	98.2	±0.23	NAPC
	U	50	98.4	±0.25	0.2 M A.C.
	Nd	50	99.0	±0.30	4.0 M HCl
2	Ca	50	98.4	±0.01	NAPC
	U	50	98.8	±0.25	0.2 M A.C.
	Nd	50	98.9	±0.42	4.0 M HCl
3	Li	50	98.5	±0.23	NAPC
	U	50	98.0	±0.37	0.2 M A.C.
	Ni	50	99.1	±0.41	4 M A.A.
	Nd	50	97.9	±0.52	4 M HCl
4	Ca	50	98.6	±0.29	NAPC
	U	50	99.2	±0.34	0.2 M A.C.
	Co	50	98.1	±0.61	4 M A.A.
	Nd	50	97.9	±0.40	4.0 M HCl

NAPC – No sorption passing through column, A.C. - Ammonium carbonate, A.A.- Acetic acid

of Nd(III) in this work were carried out by using 4 M HCl.

Effect of varying concentration of Nd(III)

Capacity of poly[dibenzo-18-crown-6]

In order to find the capacity of Nd(III), the concentration of Nd(III) was varied from 50 to 600 g /ml. The results showed that, the adsorption of Nd(III) was quantitative (100%) upto 400 g /mL. With increase in concentration of Nd(III), there was decrease in the percentage adsorption. From this study, it was found that the capacity of 1.0 gm of poly[dibenzo-18-crown-6] for Nd(III) is 0.55±0.01 m mol/g.

Separation of Nd(III) from binary mixture (diverse ion effect)

Nd(III) was extracted in the presence of wide range of foreign ions. The tolerance limit was set such that the amount of foreign ions required to cause a ±2% error in the recovery of Nd(III). The tolerance limits (mg) of various cations and anions are shown in the parenthesis.

Li^{+}(35), Na^{+}(5), K^{+}(4), Cs^{+}(40), Be^{+2}(0.08), Mg^{+2}(0.1), Ca^{+2}(5), Sr^{+2}(0.01), Ba^{+2}(0.5), Co^{+2}(1), Ni^{+2}(1), Mn^{+2}(3), Zn^{+2}(2), Cd^{+2}(3), Pb^{+2}(10), Sb^{+3}(3), Fe^{+3}(0.3), Tl^{+3}(0.7), V^{+5}(0.1), Cr^{3+}(<0.01), U^{6+}(0.1), Al^{3+}(0.04), Ce^{3+}(0.1), La^{+3}(0.1), Mo^{+6}(<0.01), W^{+6}(2), Cl^{-}(2), Br^{-}(1), SCN^{-}(4), ClO_4^{-}(4), CH_3COO^{-}(4), SO_4^{-2}(4), tartarate(5), oxalate(4), citrate(0.5), ascorbate (4), I^{-}(5), NH_4^{+}(10)

Separation of Nd(III) from multicomponent mixtures

In ternary mixture separation, we found good recovery of analytes hence the study was extended to separate quaternary mixtures. The mixture containing Li^{+}, U(VI) and Nd(III) in 1×10^{-3} M hippuric acid was separated. Li^{+} and Ca^{2+} were not sorbed on the column and hence collected in the effluent (aq. phase). Nd(III) showed 0% recovery by 0.2M A.C. and U(VI) showed 100% recovery by 0.2M A.C. Hence at first, U(VI) was eluted by 0.2 M A.C. and then Nd(III) was eluted by 4 M HCl. Nd(III) showed 0% recovery by 4M acetic acid and Ni(II)/Co(II) showed 100% recovery by 4M acetic acid. Similarly by using corresponding conditions of eluents further mixtures were separated.

Conclusion

Using column chromatographic method and poly[dibenzo-18-crown-6] as a stationary phase, the separation of U(VI), Nd(III) and other metals in hippuric acid medium has been achieved. The concentration of hippuric acid required is very low. In addition to adopting a simple method, our study incorporates the separation of Nd(III) from Li(I), Ca(II), Ni(II) and U(VI) with good reproducibility (approximately ±2%) in binary as well as in multicomponent mixtures.

References

[1] Ch. S. K. Raju, M. S.Subramanian, J. Hazard. Mat. 145 (2007) 315.

[2] Yoshio, H. Noguchi crown ethers for chemical analysis, Anal. Lett., 15(15) (1982) 1197.

[3] Z. Marczenco, Spectrophotometric Determination of Elements, Chichester, Ellis Horword Limited, (1976) 199.

[4] S B.Savvin, Organic reagents of Arsenazo III group, Moscow: Atomizdat, (1971).

Radiochemical Analysis of Strontium-90 in Spent Fuel Storage Bay of a Research Reactor

P.T. Ghare[1], S.S. Deolekar[2], V. Pulhani[3], K.S. Babu[1], L.K. Vajpyee[1], R.K.B. Yadav[1], A.D. Pant[1], R.K. Gopalakrishnan[1], K.S. Pradeep Kumar[1]

1. *Radiation Safety Systems Division, Bhabha Atomic Research Cetnre, Trombay, Mumbai 400085, India; E-mail: ptghare@barc.gov.in*
2. *BARC Safety Council Secretariat, Bhabha Atomic Research Cetnre, Trombay, Mumbai 400085, India*
3. *Health Physics Division, Bhabha Atomic Research Cetnre, Trombay, Mumbai 400085, India*

Abstract

A study on estimation of Sr-90 activity present in the spent fuel storage bay water of a research reactor was carried out. Sr-90, a pure beta emitter with a half life of 29 years exhibits biochemical similarity with calcium present in human bones and hence is important from internal exposure point of view. The work was taken up for effective internal exposure control of the personnel involved in various activities carried out in bays where potential for Sr-90 getting airborne is significant. The method involves selective precipitation of Sr-90 using suitable carrier and thereafter counting it in gross beta counting system. The total activity obtained by gross beta measurement agrees well with sum of the activities obtained by the individual measurements of Cs-137 by gamma spectrometry and Sr-90 by beta counting after radiochemical separation.

Introduction

In this research reactor, the spent fuel storage bay was used for storage of trisected irradiated spent fuel sections. Gamma spectrometry of spent fuel storage bay water indicated presence of Cs-137 as the most prominent gamma emitting radionuclide. Sr-90, being a pure beta emitter, a radiochemical method was used for its estimation. Daughter product of Sr-90 is Y-90 which is a high energy beta emitter with half life of 64 hrs. Sr-90 and Y-90 present in the spent fuel bay water are in secular equilibrium. Efficiency of end window GM counter obtained using Cs-137 and Sr-90 source in equal proportions was used for calculation of gross beta activity of spent fuel bay water samples. Estimation of Sr-90 is important during various bay cleanup activities, handling of spent fuel material and from management of radioactive waste point of view.

Methods and Materials

Part I – Precipitation of Strontium-90 as Strontium Carbonate and its counting

10 ml of representative bay water sample was taken for analysis of Sr-90. After its acidification with concentrated nitric acid and addition of Strontium and Barium carriers, pH was adjusted to 8 with 1:1 ammonium hydroxide. Saturated ammonium carbonate was used as precipitating agent and Sr-90 was precipitated as Strontium Carbonate. The precipitate was then dried under infrared lamp, weighed and counted for gross beta activity in a low background beta counting system. The aluminum planchette containing Strontium carbonate precipitate was covered properly and was kept for 15 days for ingrowth of Y-90 and to attain equilibrium between Sr-90 and Y-90.

Part II – Precipitation of Yttrium-90 as Yttrium Oxalate and its counting

After 15 days (for attaining secular equilibrium between Sr-90 and Y-90), the planchette was dried again under infrared lamp and counted for gross beta activity. On acidification and addition of Yttrium carrier, 1:1 ammonium hydroxide was added to get a precipitate of Yttrium hydroxide. It was dissolved in nitric acid. Oxalic acid was added to get a precipitate of Yttrium oxalate. The precipitate was collected on an aluminum planchette, dried and counted for gross beta activity in a low background beta counter.

Part III – Activity Calculation :

Sr-90 activity in Bq/mL was calculated as follows;

$$\text{Activity (Bq/mL)} = \frac{C \quad 10^6}{R_{Sr} \; R_Y \; V} \qquad (1)$$

Where

C – Count rate

– % Efficiency of the gross beta counting system

R_{Sr} - % recovery of Strontium-90

R_Y - % recovery of Yttrium-90

V – Volume of sample taken for analysis in mL

Results and Discussion

The activity results obtained are tabulated in Table 1. In the table, percentage Sr-90 activity is shown with respect to gross beta activity. It was observed that the average activity of Sr-90 in water sample was 7.55 Bq/mL and the percentage of Sr-90 activity in water samples from spent fuel storage bay varied from 4.99 to 14.51%.

Table 1: Activity Results of Water Samples

Sl. No	Activity (Bq/mL)				% of Sr-90 in gross activity (d)
	Gross using GM counter (a)	Cs-137 by gamma Spectro-metry (b)	Sr-90 by Radiochemical Analysis (c)	Total (b+c)	
1	148.86 ± 2.99	122.60 ± 28.96	7.43 ± 0.29	130.03 ± 28.96	4.99
2	86.33 ± 2.28	80.29 ± 23.44	12.53 ± 0.35	92.82 ± 23.44	14.51
3	63.80 ± 1.95	57.42 ± 19.82	5.76 ± 0.24	63.18 ± 19.82	9.03
4	34.00 ± 1.43	24.25 ± 12.88	3.29 ± 0.21	27.54 ± 12.88	9.68
5	76.07 ± 2.14	62.55 ± 20.69	5.10 ± 0.24	67.65 ± 20.69	6.70
6	75.40 ± 2.13	64.84 ± 21.06	8.90 ± 0.38	73.74 ± 21.06	11.80
7	82.27± 2.22	69.93 ± 21.87	9.78 ± 0.43	79.71 ± 21.87	11.89
8	69.00 ± 2.03	45.23 ± 17.59	7.10 ± 0.27	52.33 ± 17.59	10.29

Conclusion

Sr-90 activity in Spent Fuel Storage Bay water was estimated by radiochemical analysis. Estimation of Sr-90 in spent fuel storage bay is important in the point of view for evaluation of the Derived Air Concentration (DAC). The total activity obtained by gross beta measurement agrees well with sum of the activities obtained by the individual measurements of Cs-137 by gamma spectrometry and Sr-90 by beta counting after radiochemical separation.

References

[1] N. Vajda, C.K. Kim, Appl. Rad. Isot., 68 (2010) 2306.

[2] Tables of radionuclides, Nuclear Data Centre, Korea Atomic Energy Research Institute (2000).

[3] IAEA, Radiological characterization of shut down nuclear reactors for decommissioning purpose, IAEA technical reports Sr no 389, IAEA, Vienna, Austria, (1998).

[4] ICRP Publication 89

[5] International Atomic Energy Agency (IAEA), 'Reference Methods for marine radioactivity studies. Tech Rep Ser 118, IAEA' (1970) p 129.

[6] International Atomic Energy Agency (IAEA) Measurement of radionuclides in food and the environment, Technical Report Series No. 295 (1989) p.70.

[7] F. Goutelard, R. Nazard, C. Bocquet, N. Coquenlorge, P. Letessier and D. Calmet, Appl. Rad. Isot., 53(1-2) (2000) 145.

Estimation of ^{55}Fe in Neutron Activated Steel Components

Priya Srinivasan[1], R.K.Gopalakrishnan[1], M.S.Murali[2], A.Goswami[2]

1. *Radiation Safety Systems Division, Bhabha Atomic Research Centre, Trombay, Mumbai 400 085, India*
2. *Radiochemistry Division, Bhabha Atomic Research Centre, Trombay, Mumbai 400 085, India; E-mail: agoswami@barc.gov.in*

^{55}Fe is one of the important radionuclide during characterisation of reactor wastes. Owing to its very low energy emission it can be conveniently called as Hard-to-detect (HTD) radionuclide. Separation of ^{55}Fe from activation products in standard steel was achieved using Anion exchange process. ^{55}Fe activity was evaluated based on the cross section data and compared with experimental value determined using Liquid Scintillation Spectroscopy and an excellent agreement was found (within 2% deviation). This methodology was adopted for separation and analysis of ^{55}Fe in a specimen steel sample collected from shutdown research reactor APSARA.

Introduction

In reactor facilities, the system and structural components made up of stainless steel undergo neutron activation resulting in production of various activation products. ^{55}Fe is produced in steel predominantly by ^{54}Fe (n,) ^{55}Fe in the 5.9% abundant ^{54}Fe isotope with a thermal neutron absorption cross section of 2.25± 0.18 b. The other production modes include ^{56}Fe (n,2n) ^{55}Fe (E_{th}=11.4 MeV), ^{56}Fe (,n) ^{55}Fe (E_{th}= 11.2 MeV), ^{58}Ni (n,)^{55}Fe (E_{th}= 3.1 MeV). ^{55}Fe ($t_{1/2}$ = 2.73 y) decays to stable ^{55}Mn via electron capture emitting Auger electrons and X-rays with energies of 5.88 keV, 6.49 keV. The low energy emission hinders direct determination by gamma spectrometry, which makes ^{55}Fe one of hard-to-detect (HTD) radionuclide [1] in waste characterisation. This work aims to evaluate the ^{55}Fe activity in neutron activated steel system components of reactor facilities. The chemical separation and counting procedure was validated by the measurement of ^{55}Fe in neutron activated ASTM SS316M steel sample. The methodology was also applied to a specimen sample from the steel structural component of shutdown research reactor APSARA.

Materials and Methods

Tricarb 2910TR LSC with QuantaSmartTM (Perkinelmer Inc. USA) software for data acquisition and processing was used for measurement of ^{55}Fe. ^{55}Fe standard solution procured from Eckert and Ziegler, Germany (specific activity of 415.1kBqg^{-1} at reference date March 2010, with an expanded uncertainty of ±3.2%) was used for quench measurements. Optiphase Hisafe-III Perkinelmer Inc. (USA) was used as scintillation cocktail. Bio-rad anion exchange resin from Bio-rad Laboratory (USA) was used.

Two standard ASTM SS316M (37.9, 43.8mg) steel samples were subjected to neutron activation at a flux of 10^{12} ncm^{-2} s^{-1} for a period of 7 days. Two years post irradiation, radiochemical separation of Fe [2] from steel was carried out. The steel samples were dissolved in 9M HCl and gently evaporated to dryness and the residue dissolved in 10 ml of 9M HCl. From this, 1ml of dissolved steel solution was taken for radiochemical separation and 2mg each of Ni, Fe, Co and Cr carriers were added and evaporated to dryness and collected in 1ml of 9M HCl. This solution was passed through an anion exchange resin column (Dowex 1 x 8 of 100-200 mesh) preconditioned in 9M HCl medium. The column was first washed with 10ml of 9M HCl and Ni and Cr was eluted and Co and Fe was retained in the column. 4M HCl was added to elute Co and finally, Fe was eluted using 0.5M HCl. The Fe eluate was quantitatively collected. The chemical yield of iron was determined using ICP-AES. Samples were prepared for estimation of ^{55}Fe using LSC taking 0.5ml of aliquot in 5ml of scintillator. The same procedure for estimating ^{55}Fe was applied for a sample collected from SS pool liner of shutdown research reactor APSARA.

Quench Measurement using ^{55}Fe Standard

Counting efficiency in LSC can be affected by the degree of quenching in the sample. Presence of colour in a medium can cause color quenching. For determining the absolute sample activity it is necessary to measure the level of quench of the samples first, and then make the corrections for the measured reduction in counting efficiencies [3]. A Quench curve which represents the relationship between tSIE (quench indicating parameter) and the counting efficiency was constructed using standard ^{55}Fe in 0-7 keV region. The effect of color quench on efficiency was determined preparing solutions of different concentrations of $FeCl_3$ (Fe=0.2 to 11.2 mg) in 0.5 mL of 0.5M HCl. Each sample was spiked with equal amounts of ^{55}Fe standard and 5 mL of Optiphase Hisafe-III scintillator were added. The samples were counted in LSC for a counting time of 5 min.

Results and Discussion

Table 1 presents the results of quench study carried out to find the effect of colour quenching on efficiency. The quench indicating parameter tSIE and the efficiency values determined using ^{55}Fe standard activity with increasing stable Fe content is shown. The colour quench measurements indicate that the counting efficiency is fairly constant over the stable Fe

concentration studied, with an average counting efficiency of 24%.

Table 1: Effect of Colour Quenching - Variation in Stable iron content

Stable Fe(mg)	^{55}Fe activity (Bq)	tSIE	Counting efficiency
0.21	175.55 ± 5.6	372.76	(2.43 ± 0.02)x10^{-1}
0.55	174.52 ± 5.6	370.01	(2.41 ± 0.02)x10^{-1}
3.05	176.46 ± 5.6	369.48	(2.41 ± 0.02)x10^{-1}
5.83	171.78 ± 5.5	362.71	(2.39 ± 0.02)x10^{-1}
11.83	191.18 ± 6.1	361.91	(2.27 ± 0.02)x10^{-1}

Gamma spectrometry of the irradiated standard steel samples conducted in an earlier study [4] revealed ^{59}Fe, ^{60}Co, ^{58}Co, ^{51}Cr and ^{54}Mn to be the major gamma emitters and the decontamination factors achieved for these interfering radionuclides in the radiochemical separation procedure were also found to be high (DF for Fe : 7.3x10^4, Cr:2.5x10^5; Co: 5.1 x 10^4). After an adequate cooling period of 2 years post irradiation, the interference of ^{59}Fe ($t_{1/2}$= 44 days) could be completely avoided in the LSC analysis for ^{55}Fe. Figure 1 shows a set of LSC spectrum of ^{55}Fe from the separated aqueous fraction containing only iron after chemical separation. Spectrum of standard ^{55}Fe (A), spectrum obtained from the irradiated steel after chemical separation (B), ^{55}Fe separated from APSARA steel (C) along with the background spectrum (D are given.

The chemical recovery of stable Fe determined by ICP-AES in all the experiments was found to about 90%. ^{55}Fe activity in steel was computed using the relation: $A(Bq/g) = \frac{cps}{EWTX'}$, where 'E' is the fractional efficiency, 'W' weight of steel analysed for ^{55}Fe, 'T' is time of counting and X is the chemical yield. The activity of ^{55}Fe determined in the two irradiated standard ASTM 316M steel samples were 1.39 x 10^7 Bq/g and 1.38x10^7 Bq/g. Activity calculated using the neutron flux at the irradiation position and the neutron activation cross section data after accounting for the cooling period was 1.41x10^7 Bq/g which is in good agreement with the experimentally determined value (within 2% deviation). This chemical separation method was adopted for the APSARA sample and the specific activity of ^{55}Fe was estimated to 1.3x10^3 Bq/g.

Conclusion

The chemical separation method was successfully applied for the analysis of ^{55}Fe in standard steel samples and reactor structural steel samples. This study will provide valuable data during reactor decommissioning.

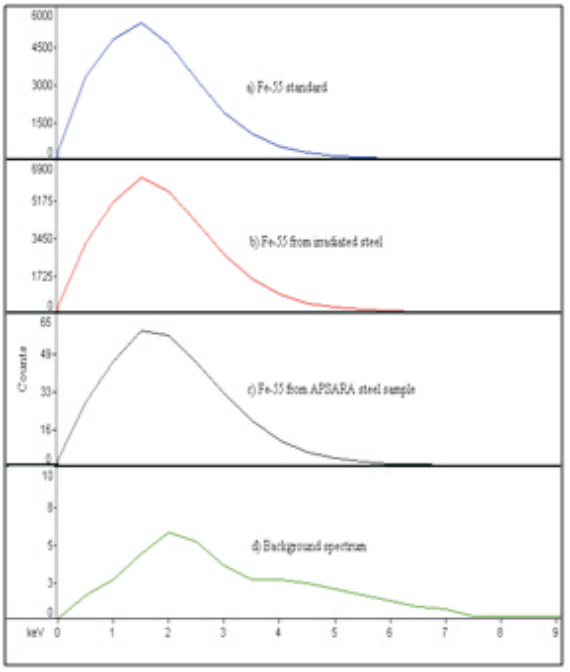


Fig. 1 LSC spectrum of Fe-55

Acknowledgments

The authors express their sincere gratitude to Dr. D.N. Sharma, Director, Health Safety and Environment Group (HS&EG) for the keen interest and valuable suggestions provided during the course of this work. The co-operation and technical support extended by Dr. K.S. Pradeepkumar, Head, RSSD is gratefully acknowledged.

Reference

[1] IAEA Technical Reports Series No.389 (1998)

[2] D.F. Williams, G.D.O'Kelly, Radiochim. Acta 64 (1994) 49.

[3] Michael F. L'Annunziata, Handbook of radioactivity analysis, 2nd Edition, Academic Press, (1998).

[4] Priya.S, Murali M.S, et.al ., J Radioanal Nucl DOI 10.1007/s10967-013-2591-y

Ilmenite Mineral Decomposition using Lithium Metaborate Fusion: ICP-AES Determination of Ti, Fe, Si, Cr, V, Mn, Ca and Mg

A. Premadas

Chemistry Laboratory, Atomic Minerals Directorate for Exploration and Research, AMD Complex, Begumpet, Hyderabad 500 016, India; E-mail: apremadas@yahoo.co.in

A simple and effective ilmenite mineral decomposition procedure using $LiBO_2$ fusion is reported. After the fusion, sample solution is prepared in oxalic acid-hydrochloric acid media which is used for the direct estimation of Ti, Fe, Si, Cr, V, Mn, Ca and Mg after suitable dilution using ICPAES. A Matrix matching calibration standards was used for Si, Cr, V, Mn, Ca and Mg determination. Accuracy of the analytical results are established by analyzing certified reference material Ilmenite-Dillinger SX 6704, and ilmenite samples from Manavalakuruchi area in Tamil Nadu.

Introduction

Ilmenite mineral is one of the main sources of Ti metal, and it is refractory in nature represented by the chemical formula $FeOTiO_2$. It is available in plenty in the eastern and western sea coasts of India. Titanium metal is used for the production of high-tech alloys used in air craft industries, surgical implants due to its corrosion resistance, light weight and good strength [1]. Since Ti is a high field strength element, and ilmenite being a refractory mineral an effective decomposition and preparation of a stable sample solution for elemental analysis in dilute mineral acid is a difficult task. A complete Ilmenite sample decomposition (100 to 250 mg) is achieved normally by fusion with large quantity of fluxes (10 to 20 times or more) like $KHSO_4$ [2] Na_2HPO_4 and NaH_2PO_4, [3] Na_2O_2 [3] etc., but it introduces lot of salt contents. Sample digestion (50 to 100 mg) with phosphoric acid is also reported [4]. ICP-AES is a multi-elemental instrumental analysis technique having good dynamic range and very good sensitivity for refractory elements, and widely used for the analysis of the refractory minerals like columbite-tantalite, Ilmenite and rutile [2], monazite [5].

The lithium meta-borate fusion technique is used for the decomposition of rock samples and certain refractory minerals. Its utility as a flux for the decomposition of ilmenite mineral is studied [6] during the mineral beneficiation study, however, elemental characterization using ICP-AES is lacking. It was observed that less quantity of lithium meta-borate flux (2 g. flux for 0.400 g sample) is sufficient for the complete decomposition of the mineral, and it reduces the salt content in the aspirated solution for instrumental elemental analysis. The fusion bead is dissolved in a mixture of hydrochloric acid, oxalic acid and hydrogen peroxide, and the sample solution is stable up to one month period of time studied. The solution after suitable dilution is used for the analysis of Ti, Fe, Si, Cr, V, Mn, Ca and Mg.

Experimental

A Jobin Yvon model 2000(2) sequential ICP-AES from M/S Jobin Yvon, France was used. The instrumental parameters used are same as reported earlier [7]. The emission lines (in nm) used are Ti-334.0941, Fe-238.204, Si-251.611, Cr- 205.552, V-292.402, Mn- 257.610, Ca- 393.366, and Mg-285.213. A stock solution of 1000 g mL^{-1} each was prepared from high purity (>99.9%) oxides/salts of TiO_2, Fe_2O_3, SiO_2, Cr_2O_3, V_2O_5, MnO_2, $CaCO_3$ and MgO, using recommended procedure. Working standard solutions for instrumental calibration were prepared by dilution in 5% HCl and 0.2% oxalic acid containing (a) 10 to 70 g mL^{-1} each Ti and Fe, and (b) matrix matching 0.5-5 g mL^{-1} each for Si, Cr, V, Mn, Ca and Mg was used.

Lithium Metaborate Fusion

A 0.400 g. powdered (-200 mesh size) ilmenite mineral was mixed with 2 gram lithium meta-borate powder in a Pt-Au (95:5) alloy crucible and fused over a burner to red hot condition for about one hour with occasional swirling. The crucible was cooled, and transferred into a beaker containing 2g oxalic acid, 10 ml concentrated HCl and around 150 ml water. To this 2 ml of H_2O_2 solution was added and then placed on a hot-plate (~100°C) with occasional swirling and the crucible was taken out. The resulting clear solution was diluted to 250 ml with distilled water. A suitably diluted solution (20 fold for Ti and Fe; and 5 fold for Si, Cr, V, Mn, Ca and Mg) was used for the elemental analysis.

Results and Discussion

The commonly used $KHSO_4$ fusion [2] needs more quantity of the flux (7-10g for 0.100 to 0.250 g sample) for the fusion. It increases the salt content leading to frequent clogging in concentric nebulizer of the ICP-AES instrument beside the plasma fluttering. The ortho-phosphoric acid decomposition procedure [4] needs around 15 ml phosphoric acid, and up to only 100 mg sample could only be taken up for the decomposition. A mixture of NaH_2PO_4 and Na_2HPO_4 [3] needs 5g. flux for the complete decomposition of 0.5g sample. In most of the above procedures the element silicon in the sample cannot be determined because the flux does not bring Si completely in to solution. The lithium meta-borate fusion has the following advantages (i) more quantity of the sample

Table-1: Analytical results of Ti, Fe, Si, Cr, V, Mn, Ca and Mg in Ilmenite reference material Dillinger SX6704, and in two natural Ilmenite samples by the proposed and reported method [3]

Element (%)	Ilmenite-Dillinger SX67 04		Manavalakuruchi ilmenite-1		Manavalakuruchi ilmenite-2	
	Recommended (%)	Found (%)	Present method (%)	Reported method (%)	Present method (%))	Reported method (%)
TiO_2	31.925	31.60± 0.21				
Fe_2O_3(t)	51.80	51.63 ± 0.25	42.80	42.13	42.88	42.32
SiO_2	7.93	7.60 ± 0.30	1.08	0.95	2.01	1.85
Cr_2O_3	0.109	0.11 ± 0.01	0.13	0.12	0.10	0.10
V_2O_5	0.286	0.28 ± 0.02	0.21	0.20	0.21	0.22
MnO_2	0.154	0.16 ± 0.01	0.45	0.44	0.44	0.45
CaO	1.30	1.35 ± 0.02	0.08	0.10	0.03	<0.05
MgO	2.81	2.95 ± 0.01	0.77	0.75	0.68	0.70

Values shown in parenthesis for Dillinger SX6704 are the uncertainty associated

can be taken (0.400 g) for fusion (2g flux), (ii) it does not produce any harmful fumes and (iii) silicon can also be determined in the same solution.

Effect of Ti and Fe on the ICP-AES determination of trace level Si, Cr, V, Mn, Ca and Mg

The effect of 100 to 1000 g mL^{-1} of Ti and Fe was studied independently on the emission lines intensity of 1 g ml^{-1} of Si, Cr, V, Mn, Mg, and Ca. It was observed that, the presence of 500 g mL^{-1} Ti, the emission signal of the analyte was suppressed around 6-8% and 10 to 14%, due to the presence of 300 and 500 g mL^{-1} Ti respectively. Therefore, the robustness of the plasma was evaluated comparing the ionic (280.270 nm) and atomic lines (285.213 nm) intensity ratio using Mg (5 g mL^{-1}). The lines intensity ratio was 9 for solution in 5% HCl alone, and it decreased to 8.2 and 7.8 in the presence of 500 and 1000 Ti g mL^{-1} respectively using 1000W plasma power. Decrease in the intensity ratio (up to 8 to 13%) in the presence of titanium could be due to the possible high energy required for the decomposition of the refractory oxides of Ti formed. The intensity ratio was also estimated by increasing the forward power to 1200W. But no significant improvement was noticed. However no appreciable change in the Mg lines intensity ratio was noticed in the presence of up to 1000 g ml^{-1} Fe, 4 mg mL^{-1} each of $LiBO_2$ or oxalic acid, when studied independently. However, in the presence of $LiBO_2$ and oxalic acid (4mg ml^{-1}each) together, the emission signal of the analyte was reduced. Therefore, to overcome the combined suppression effect of Ti, $LiBO_2$ and oxalic acid, an approximate matrix matched (with respect to Ti, Fe , oxalic acid and $LiBO_2$) calibration standards (on the basis of sample dilution described above) for Si, Cr, V, Mn, Ca and Mg was used to get more accurate value.

Accuracy and Reproducibility

One international certified ilmenite mineral and two natural Ilmenite samples were fused with the $LiBO_2$ as given in the experimental section. The stock solution after the suitable dilution was analysed for Ti, Fe, Si, Cr, V, Mn, Ca and Mg, and they are in good agreement with the recommended values for reference material confirming the accuracy of the method as shown in Table 1. The analytical data of the Ilmenite samples (Manavalakuruchi area of Tamil Nadu) by the proposed method is also agreed well with the reported method of ilmenite analysis [3]. The uncertainty factor associated with the estimated values for each element in the reference Ilmenite sample is also given in table 1. The determination limits for Ca, Cr, V, Si is 0.03% each and for Mg it is 0.02% under the sample dilution given in the experimental section.

Acknowledgements

Author is thankful to Dr. G. Chakrapani, Head, Chemistry Group, Shri S. Chandrasekharan, Additional Director (R&D), AMD, Hyderabad, for support and encouragement and Shri P. S. Parihar, Director, AMD, for approving the manuscript for presentation/ publication in the seminar proceedings.

References

[1] A.Stanley , J. J. Burke and R. H. Hiltz Jr. " Titanium in Industry, Technology and Structural Titanium", D Van Nostrand Company Inc, New York (1955).

[2] W.R. Scholler, and A. R. Powell, "The Analysis of Minerals and Ores of Rarer Elements", Charles Griffin and Co. London (1955), p. 119-131.

[3] R. Radhamani, P. Murugessan, A. Premadas, and P.K. Srivastava,. Talanta, 71 (2007) 1932.

[4] D.S.R. Murty, B. Gomathy, Roopa Bose and R. Rangaswamy, At.Spectrosc, 19 (1998) 17.

[5] A. Premadas and C.R. Korge, At.Spectrosc, 27 (2006) 170.

[6] R. Venugopal "International Seminar on Mineral Procesasing Technology, Jan 6-8 (2005).

[7] A. Premadas. At. Spectrosc, 33 (2012) 14.

An Experimental cum Numerical approach for the Determination of Components in a UO_{2+x} – U_3O_8 Admixture

B. Narasimha Murty, G. Brahmananda Reddy and H.R. Ravindra

Control Laboratory, Nuclear Fuel Complex, Hyderabad 500 062, India; E-mail: ravindra@nfrc.gov.in

The present paper describes how to calculate the content of triuranium octaoxide still to be reduced in case of hyperstoichiometric uranium dioxide obtained by the reduction of triuranium octaoxide and to estimate the extent of optimum reworking to be done to achieve the desired product.

Introduction

Ammonium diuranate(ADU) precipitation route has been one of the important routes of production of uranium dioxide nuclear fuel and has extensively been investigated by various researchers [1,2] with variety of objectives. In this route of production, it is essential to convert the ADU to This paper describes an analytical methodology to determine individual components of a binary admixture of a hyper stoichiometric uranium dioxide and triuranium octaoxide. The calculated compositions based on the experimentally determined O/U ratio are correlated with the respective composition values of synthetically prepared mixtures and expression for composition is deduced. The derived expression find its use in evaluating the efficiency of the reduction process in the conversion of UO_{2+x} U_3O_8 in a production plant.

Derivation of the Mathematical Expression

Let the binary mixture of hyperstoichiometric uranium dioxide (UO_{2+x}) and triuranium octaoxide (U_3O_8) contain p% of hyperstoichiometric uranium dioxide and (100 – p)% triuranium octaoxide, on weight basis. It is now possible to calculate the content of U(VI) and total uranium present in such a mixture.

U(VI) = A + B (1) where

$$A \quad \frac{W \quad M_U \quad p \quad x}{100 \quad M_{UO_2} \quad xM_O}$$

$$B \quad \frac{2 \quad (100-p) \quad M_U \quad W}{100 \quad M_{U_3O_8}}$$

Total uranium = C + D (2) where

$$C \quad \frac{W \quad M_U \quad p}{100 \quad M_{UO_2} \quad xM_O}$$

$$D \quad \frac{3 \quad (100-p) \quad M_U \quad W}{100 \quad M_{U_3O_8}}$$

Where M_O, M_U, M_{UO_2}, $M_{U_3O_8}$ and W respectively are atomic mass of oxygen, atomic mass of uranium, molar mass of uranium dioxide, molar mass of triuranium octaoxide and weight of the mixture.

From (1) and (2), it is easy to calculate the oxygen to uranium atomic ratio of the mixture as $\frac{O}{U}$ ratio is nothing but 2 plus ratio of contents of U(VI) and total uranium in the mixture. Thus, $\frac{O}{U}$ ratio of mixture =

$$2 \quad \frac{E \quad F}{G \quad H} \quad (3)$$

$$E \quad x \quad M_{U_3O_8} \quad p$$

$$F \quad 2 \quad (100 \quad p) \quad M_{UO_2} \quad xM_O$$

$$G \quad M_{U_3O_8} \quad p$$

$$H \quad 3 \quad (100 \quad p) \quad M_{UO_2} \quad xM_O$$

If we determine the excess oxygen of synthetic sample mixture experimentally ($x_{exp\,t}$), then,

$$p \quad \frac{100 \quad I \quad J}{K \quad J \quad L} \quad (4) \text{ where}$$

$$I = 3 \quad x_{exp\,t} - 2$$

$$J = M_{UO_2} + xM_O$$

$$K = M_{U_3O_8} \quad (x \quad e_{exp\,t})$$

$$L = 3 \quad x_{exp\,t} + 2$$

From the equation (4) values of "p" were calculated (p_{cal}) using x = 0.15 for various synthetic mixtures.

Experimental

Accurately weighed quantities of hyperstoichiometric uranium dioxide and triuranium octaoxide powders so that the weight of the total the mixture is 10.0 g were taken in a mortar and homogenized thoroughly with a pestle. The synthetic mixtures containing various percentages of hyperstoichiometric uranium dioxide namely 0, 10, 20, 30, 40, 50, 60, 70, 80, 90 and 100 % triuranium octaoxide were prepared. ratio $\frac{O}{U}$ in the synthetic mixtures were determined experimentally by titrimetry.

Results and Discussion

The calculated value (p_{cal}) and the actual "p" were correlated and the best fit was obtained as %p = -0.013 x

Table-1: Experimentally determined $\frac{O}{U}$ ratios of synthetic mixtures and the correspondingly deduced $x_{exp\ t}$ values for the synthetic mixtures

Sample Code	Synthetic composition		$\frac{O}{U}$ ratio	$x_{exp\ t}$
	$\%U_3O_8$	$\%UO_{2+x}$		
SA	0	100	2.046	0.046
SB	10	90	2.104	0.104
SC	20	80	2.167	0.167
SD	30	70	2.224	0.224
SE	40	60	2.295	0.295
SF	50	50	2.346	0.346
SG	60	40	2.416	0.416
SH	70	30	2.472	0.472
SI	80	20	2.542	0.542
SJ	90	10	2.607	0.607
SK	100	0	2.671	0.671

$a^2 + 2.01 \times a + 6.4$; $R^2 = 0.997$ for an admixture of $UO_{2.15}$-U_3O_8. Thus, triuranium octaoxide in the sample is given by (100 – p)% and hence the composition of sample mixture can be calculated in terms of the experimentally determined parameter "$x_{exp\ t}$". The "$x_{exp\ t}$" determined for synthetic mixtures of $UO_{2.046}$ and U_3O_8 are shown in Table.

Conclusions

It is concluded that it is possible to quantitatively calculate the content of triuranium octaoxide still to be reduced in case of hyperstoichiometric uranium dioxide obtained by the reduction of triuranium octaoxide and showing positive deviation with respect to the critical excess oxygen content. This helps also to estimate the extent of optimum reworking to be done to achieve the desired product.

Acknowledgements

The authors express their deep sense of gratitude to Sri N. Saibaba, Chief Executive, NFC and to Sri B. Prahlad, DCE(QA, TS, HRD & Lib) for their encouragement and support in the present investigation.

A partially reduced UO_{2+X} sample was analyzed for O/U ratio and accordingly the $x_{exp\ t}$ obtained as 0.312 and was substituted to calculate p i.e. $\%UO_{2.15}$ and finally the $\%U_3O_8$ still to be reduced was determined to be as 43.4%.

References

[1] B. Narasimha Murty, P. Balakrishna, R.B. Yadav and C. Ganguly, Powder Technology, 115 (2001) 167.

[2] Z. Xiangwen, M. Jingtao, H. Shaochang, Z. Xingyu, W. Yang, D.C. Sheng, L.T. Xiang, G. Wenli, T. Yaping and T. Chunhe, Nuclear Engineering and Design, 250 (2012) 192.

Analysis of Tantalum-10%Tungsten alloy for Fe, Mo, Ni by Flame-AAS Technique

J.R. Jat, Y. Balaji Rao and H.R. Ravindra

Control Laboratory, Nuclear Fuel Complex, ECIL Post, Hyderabad 500062; E-mail: ybr4793@gmail.com

The paper deals with analysis of Tantalum-10% Tungsten alloy for Fe, Mo, Ni by Flame-Atomic Absorption Spectrometry (Flame-AAS). The results have been compared with Inductively Coupled Plasma Atomic Emission Spectrometry (ICP-AES) method. Experimental conditions employed in the measurements by both the instruments are given in the paper.

Introduction

Industrial applications of Tantalum-10% Tungsten alloy, known commercially as Tantalloy, are of strategic importance owing to the specially superior mechanical properties such as improved tensile yield and creep properties especially in the temperature range of 1100 to 1700°C. Besides this, Tantalloy is applied in aerospace industry for making hot-gas valves, rocket engine skirts and also as corrosion resistant valves and liners in chemical industry. It has got excellent corrosion resistance to most acids (other than hydrofluoric) and to liquid metals. Further, Tantalum-10%Tungsten is being used for high temperature applications, electronics industry, vacuum furnace heat element, heat insulation, capacitor etc. The alloy is being marketed by in the form of bar ingot, ribbon, wire sheet and also as ultra high purity metal powder. Nuclear Fuel Complex (NFC) at Hyderabad presently enjoys the pride of being the first and probably the sole manufacturer of pure Tantalloy in India. Production and purification trials are being undertaken by the Special Material Plant (SMP) in NFC. The chemical composition of this alloy is (Content max weight%): Fe:0.010, Mo:0.020, Ni:0.010, C:0.010, O:0.015, N:0.010, H:0.0015, Nb:0.100, Si: 0.005, Ti: 0.010, W: 9.0-11.0% and remainder tantalum. Hence, it is important to characterize this alloy with respect to these impurities. Therefore, a systematic study was made in our laboratory for optimizing a method for the analysis Fe, Mo and Ni in Tantalloy by Flame-AAS. Also comparison has been made by ICP-AES and found to be in good agreement.

Experimental Details

Chemicals and Reagents

All chemicals and reagents like HNO_3, HF, H_3BO_3 etc. used for the preparation of sample and standards are of AR grade. Pure metals (99.999%) for Fe and Ni have been used for making standard solutions of these elements. Spectroscopy grade pure MoO_3 (99.9995%) obtained from Johnson-Matthey (UK) was used for making Mo standard solution. Millipore (18M resistivity) water has been employed for all dilutions.

Procedure for sample and standards preparations

4 mL of conc. nitric acid and 2 mL of conc. hydrofluoric acid have been added slowly to one gram sample taken in 100 mL teflon beaker and heated on water bath for one hour followed by half an hour on hot plate for complete dissolution. Subsequently, 10 mL of 5% oxalic acid and 20 mL of 5% boric acid were added and made made up to 100 mL. Similarly a reagent blank was prepared. Initially, a stock standard solution of 100 g/mL of each Fe, Mo and Ni were prepared separately. Further, sample solutions containing standards in the range of 0.8, 1.6, 2.4 g/mL for Fe, Ni, and 2, 4, 6 g/mL of Mo also prepared for calibrating the AAS instrument. These same solutions are also used for ICP-AES calibration.

Instrumental Conditions

Flame-AAS: Flame Atomic Absorption Spectrometer (Model: Analtik Jena Vario6, Germany and GBC Savanta, Australia) with back ground correction in double beam operation have been used for the present work.

Operating conditions

AAS

Iron: Analytical line of 248.3 nm, hollow cathode lamp current of 8.0 mA, slit width of 0.2 nm and 5cm burner has been used. Nitrous Oxide-acetylene flame with fuel flow of 190 L/hr and 400 L/hr of total oxidant was used. The nebulizer flow rate of 3.0 mL/min was maintained for aspirating the sample solution.

Molybdenum: Analytical line of 313.3 nm, hollow cathode lamp current of 7.0 mA, slit width of 0.2 nm and 5 cm burner has been used. Nitrous Oxide-acetylene flame with fuel flow of 190 L/hr and 400 L/hr of total oxidant was used. The nebulizer flow rate of 3.0 mL/min was maintained for aspirating the sample solution.

For Nickel: Analytical line of 232.0 nm, hollow cathode lamp current of 4.0 mA, slit width of 0.2 nm and 10 cm burner has been used. Air-acetylene (C_2H_2) flame with fuel flow of 55 L/hr and 400 L/hr of total oxidant was used. The nebulizer flow rate of 5.0 mL/min was maintained for aspiration of sample solution.

Deuterium arc lamp was used for background correction in AAS measurements.

ICP-AES

Inductively Coupled Plasma Atomic Emission Spectrometer (Model: Ultima 2C HR Horiba ICP-AES: Inductively Jobin Yvon, France) was used for the analysis with the following conditions: Grating: 4320 Grooves/mm, holographic diffraction grating, Focal length of monochromator : 1 Meter, Mount :Czerny Turner; RF Generator frequency: 40.68 MHz, Forward power: 1.0 KW; Plasma Gas: Ar (12 L/min), Sheathing Gas: Ar (0.2 to 0.3 L/min), Aerosol Gas: 0.4 L/min ; Observation zone: 15 mm above working coil; HF Resistant plastic high salt nebulizer and Teflon spray chamber, polypropylene sheath gas system, alumina injector tube, peristaltic pump. Wavelengths for Fe-238.207 nm, Mo-202.030 nm and Ni-231.604 nm have been chosen for ICP-AES measurements.

Results and Discussion

Calibration graphs obtained for iron, molybdenum and nickel using Flame-AAS technique have shown the regression coefficients of R^2=0.999 for iron, R^2=0.997 for molybdenum and R^2=0.999 for nickel. This shows that calibration graphs are linear and method is suitable for analysis of these elements in tanatalum-10% tungsten alloy in the required specifications range. A Relative Standard Deviation (RSD) of ±8.11% (at 137 ppm) for Fe, of ±6.56% (at 160 ppm) for Mo and for Ni ±6.19% (at 56ppm) have been obtained.Table 1 shows the comparison between results obtained by Flame-AAS and ICP-AES.

Conclusions

The Flame-AAS procedure described in this work is simple, sensitive, cost effective and reproducible and can be used for measurements of iron, molybdenum and nickel in Tantalum-10%Tungsten alloy on regular basis.

Table-1: Comparison between Flame-AAS and ICP-AES

Element	Sample ID	Flame-AAS (ppm)	ICP-AES (ppm)
Fe	SMP/EB-762	137	140
	SMP/EB-764	215	205
Mo	SMP/EB-762	160	<200
	SMP/EB-764	200	200
Ni	SMP/EB-762	56	<50
	SMP/EB-764	<50	<50

Acknowledgements

The authors are grateful to Shri N.Sai Baba, Chief Executive, NFC, Hyderabad and Shri B.Prahlad, DCE (QA, TS, HRD & LIS) for permitting to publish the present paper. Authors wish to acknowledge given by Sri. G.Satyanarayana, SO/D Control Laboratory for his technical support.

References

[1] G. Svehla, Vogel's Qualitative Inorganic Analysis (7th Edition), Pearson Education, India, (2004) 304.

[2] N.H.Furman, Stanadard methods of chemical analysis of the elements (6th Edition), D. Van Nostrand Company, Inc, USA, (1962) 1158

[3] Paul Greenberg, Anal. Chem., 9(6) (1957) 899.

Inductively Coupled Plasma-Atomic Emission Spectrometric technique for estimation of Ti in D9 Steel

G. Satyanarayana, A.K. Nayak, Y. Balaji Rao and H. R. Ravindra

Control Laboratory, Nuclear Fuel Complex, ECIL Post, Hyderabad 500 062; E-mail: ybr4793@gmail.com

The present paper describes a new methodology for estimation of Titanium in D9 steel by Inductively Coupled Plasma Atomic Emission Spectrometer (ICP-AES). The procedure involves dissolution of D9 alloy in a mixture of Hydrochloric Acid, Nitric Acid and Hydrofluoric acid followed by determination of Titanium by ICP-AES (Model: JY Ultima 2CHR). A Relative Standard Deviation of less than ±5% has been achieved in this method.

Introduction

Fast Breeder Reactor (FBR) plays an important role in Indian nuclear power program [1]. Zirconium alloys, which are being used for structural components in light water reactors (LWR) and pressurized water reactors (PWR), are not desirable as structural materials in Fast Breeder Reactors due to their unfavorable high temperature mechanical properties like creep strength. Earlier SS 316 was used as structural for FBR. However the problem of void swelling of the clad (SS316) with increasing burn-up necessitated the development of D9 alloy for structural material of Prototype Fast Breeder Reactor (PFBR). D9 is a titanium modified SS316 steel containing Cr (13.5-14.5%), Ni (14.5-15.5%), Mn (1.65-2.35%) as alloying elements. Ti/C ratio in this alloy is very important as it controls tensile and creep properties of the material which makes 0.26% Ti (5-7.5 times of C) desirable [2-3]. A method was developed for determination of Ti content in D9 alloy by Inductively Coupled Plasma Atomic Emission Spectrometer (ICP-AES). Several methods have been cited in literature estimation of Ti content in steels such as XRFS, Spark based OES etc. However requirement of suitable Standard Reference Materials (SRM) for quantification purpose limits the application of XRFS and Spark based OES though these are solid based techniques. Thus, ICP-AES technique was chosen for present study.

Experiment

Instrumentation and Parameters

ICP-AES: Inductively Coupled Plasma Atomic Emission Spectrometer (Model: Ultima 2C HR Horiba Jobin Yvon, France) Grating: 4320 Grooves/mm, holographic diffraction grating, Focal length of monochromator : 1 Meter, Mount :Czerny Turner; RF Generator frequency: 40.68MHz, Forward power: 1.0 KW; Plasma Gas: Argon (12L/min), Sheathing Gas: Argon (0.2 to 0.3 L/min), Aerosol Gas: 0.4 L/min ; Observation zone: 15 mm above working coil; HF Resistant plastic high salt nebulizer and Teflon spray chamber, polypropylene sheath gas system, alumina injector tube, peristaltic pump and other accessories are employed.

Standard Preparation

A stock standard solution containing 1 mg/ml of Ti is prepared from spectroscopy grade Titanium Oxide (TiO_2) powder.

Sample Preparation

Around 1 gram of sample was taken in a Teflon beaker. 12 mL of aqua regia was added to this followed by heating on water bath. After complete dissolution 2 mL of HF was added and made up to 100 mL with distilled water.

Preparation of Calibration Standards

Calibration standards containing 0 g/mL, 10 g/mL, 20 g/mL and 40 g/mL of Ti in 10 mg/mL of sample solution were prepared.

Measurement of Standards and Samples

All the measurements were carried-out in sequential mode. Profiling was carried out at 323.452 nm, 334.941 nm, 336.121 nm, 338.376 nm, 368.520 nm by superimposing spectral lines of Ti obtained by aspirating solutions of blank, blank with 40 g/mL of Ti, sample, sample with 40 g/mL of Ti into plasma. Standard addition method was followed for calibration and 338.376 nm line of Ti is used for calibration and measurement purpose.

Results and Discussion

Experimental studies were carried out to know the matrix and probable inter-element spectral interferences, background intensity and signal intensity suppression for some sensitive lines of analyte element by recording line profiles with and without matrix in solution. Since D9 is an alloy of Fe, Cr and Ni, so spectral interferences due to these elements on above spectral lines of Ti were studied. It was observed that 323.452 nm, 334.941 nm, 336.121 nm lines of Ti have interference with Fe, Cr, Ni and were not selected even though they are more sensitive than 338.376 nm, 368.520 nm lines of Ti. Among these two lines since 338.376 nm is more sensitive than 368.520 nm so it was used for calibration and measurement purpose. Also it is observed that there is suppression (~10%) in the intensity of 338.376 nm line due to matrix (Fe). However, as calibration was done in presence of matrix

(standard addition method), matrix effect could be normalized. Also, as Ti in D9 is estimated at percentage level the reduction in intensity due to matrix merely affect the regular analysis. Obtained calibration curve for Ti is found to be linear with a correlation coefficient (R^2) value of 0.9998. An SRM was analyzed by this method to validate its suitability and the result is tabulated in Table 1. To know the repeatability and reproducibility in measurement of Ti by this technique, multiple measurements (11 times) were carried out in two different laboratories (NFC and MIDHANI) and RSD was calculated to be less than ±5% (Table 2). Also $F_{calculated}$ (2.78) is less than $F_{tabulated}$ (2.98) for ten degrees of freedom at 95% confidence level. This shows that there is no significant variation in the precision of measurements. Six real time samples were analyzed at MIDHANI and NFC and the results were tabulated in Table 3.

Table-1: % Ti in SRM Standards

SRM	Certified value	ICP-AES value
BCS/SS465	0.30	0.33
NIST 364	0.24	0.23

Table-2: Eleven samples collected from OE-10033-1 D9 alloy are measured for Ti content at MIDHANI and NFC using ICP-AES Technique

Sl. No	Ti%(OE-10033-1)	
	NFC	MIDHANI
1	0.26	0.23
2	0.26	0.23
3	0.25	0.24
4	0.24	0.24
5	0.26	0.23
6	0.24	0.23
7	0.23	0.22
8	0.23	0.24
9	0.23	0.24
10	0.23	0.24
11	0.23	0.25
Mean	0.2445	0.23545
Std Dev	0.013685	0.008202
$F_{calculated} = 2.78$ & $F_{tabulated} = 2.98$		

Table-3: Real time sample analysis result

Sample Code	MIDHANI	NFC
	Ti (%)	
494M	0.28	0.29
524G	0.33	0.32
494N	0.29	0.29
524L	0.28	0.29
524E	0.27	0.27
524	0.32	0.32

Acknowledgement

The authors are thankful to Shri N. Saibaba, DS & Chief Executive, NFC for his kind permission to publish the paper. Also the authors wish to thank Shri B.Prahlad, DCE (QA, TS, HRD & LIS) for keen interest and constant encouragement during the course of present work. They also wish to thank Shri E. Prabhatha Reddy, SA/C for his technical assistance.

References

[1] Baldev Raj, S L Mannan, P.R. Vasudeva Rao and M.D. Mathew, Sadhan 27(5) (2002) 527.

[2] S. Latha, M.D. Mathew, P. Parameswaran, K. Bhanu Sankara Rao, S.L. Mannan, Int. J. Press. Vess. and Piping 85 (2008) 866.

[3] C. David, B.K. Panigrahi, S. Balaji, A.K. Balamuragan, K.G.M. Nair, G. Amarendra, C.S. Sundar, Baldev Raj. J. Nucl. Mat., 383(1-2) (2008) 132.

Characterization of Zirconium Alloy by Glow Discharge Optical Emission Spectrometer

A.K. Nayak, Y. Balaji Rao, H.R. Ravindra, B. Prahlad and N. Saibaba

Control Laboratory, Nuclear Fuel Complex, Hyderabd 62, E-mail: ybr4793@gmail.com

The present paper discusses about a new method developed for determination alloying elements as well as impurities in Zirconium alloy using Glow Discharge Optical Emission Spectrometer (GD-OES).The method was validated with the help of available CRMs and other techniques like AAS and ICP-AES. Statistical studies like F-test, Z-test have been carried out and it is observed that the developed method is very accurate and there is no bias in the precision between GD-OES and AAS with respect to alloying elements and between GD-OES and ICP-AES with respect to impurity elements in Zircaloys.

Introduction

Zirconium alloys are widely employed in the for manufacturing manufacture of various reactor core components such as fuel clad, pressure tubes, calandria tubes etc. used in water cooled nuclear power reactors like BWRs and PHWRs due to their optimum mechanical properties, corrosion resistance to high temperature aqueous environments, low neutron absorption cross section and resistance to radiation damage. Series of Zirconium alloys (also known as Zircaloys) viz; Zr-Sn, Zr-Nb; Zr-Sn-Nb have been developed for this purpose. Among them Zr-2 (Zr-1.2-1.7%Sn, 0.07-0.2%Fe, 0.05-0.15%Cr, 0.03-0.08% Ni) and Zr-4 (Zr-1.2-1.7%Sn, 0.18-0.24%Fe, 0.07-0.13%Cr) and Zr-Nb (2.5-2.8% Nb) are three important alloys of Zr-Sn and Zr-Nb series. In order to get the optimum behavior of Zircaloy products under the reactor conditions, it is essential to monitor the content of alloying elements as well as some critical impurities in the alloy as a part of QA program. An attempt was made to evaluate the concentration of alloying elements such as Sn, Fe, Cr, and Ni and impurities like Al, Cu, Mn, Mo, Nb, Si and Ti in Zircaloys by using Glow Discharge Optical Emission Spectrometer (GD-OES). Since As cumbersome sample preparation steps as in AAS and ICP-AES can be avoided by using GD source for the analysis of solid samples, GD-OES plays a very important role in sharing qualifying very high analytical load of quality assurance of process intermediates and final products which are generally encountered in an industrial laboratory.

Instrument Details

Instrument: Glow Discharge Optical Emission Spectrometer (GD-OES), Make: HORIBA JOBIN YVON, France Model: GD- PROFILER HR, Wavelength range: 120 nm- 600 nm, RF generator frequency: 13.56 MHz, Detectors: High Dynamic Detectors (HDD), Monochromator: Grating: 3600 grooves/mm, Focal length: 0.64m, Polychromator: Grating: 2400 lines/mm, Focal length: 1m, No. of channels: 47

Experiment

A CRM (NBS 1239) was analyzed using GD-OES and the result was validated using ICP-AES and AAS analyses results. This practice was carried out to optimize standardize the procedure for characterization of Zircaloys by using GD-OES and to validate the results with the help of other techniques and CRMs.

Sample Preparation

All reference materials and samples were are polished to obtain a mirror finished surface. As the sample chamber in GD-OES is designed for vertical mounting of the samples, surface finish plays a significant role in analysis. Rough and uneven surface of the samples can lead to leakage of atmospheric air in to GD Plasma chamber where Argon atmosphere is maintained resulting in into extinction of plasma.

Instrumental Conditions

Argon gas pressure inside plasma chamber and input power to RF source were optimized to get the maximum intensity for spectral lines of elements of our interest in the given matrix. Flush time of 5s was optimized to clean GD lamp and sample surface with Argon gas flow at high pressure prior to starting the measurement. Pre-integration time of 90s was fixed in order to reach a steady state in instrument output before starting the measurement. The pre-integration helps in removing oxides, surface defects etc. prior to starting a bulk measurement. Ar gas pressure 900Pa, Power to RF source 100W, Bulk acquisition time 10s were maintained during experiment.

Calibration

Suitable wavelengths which are free from interference (as given in Table 1) were selected for elements of interest. The instrument was calibrated with Certified Reference Materials i.e. NBS 1237, NBS 1238, NBS 1239, WC 867, WC 868, WC 869. The calibration curves for all the elements are found to be linear with a co-relation coefficient (R^2) 0.99 (Table 1).

Test of accuracy

To ascertain the accuracy of the technique one of the CRMs (NBS 1239) was analyzed 11 times using

GD-OES for the different elements and the data is given as shown in Table 2.

Table-1: Elements of interest with selected wavelengths and co-relation coefficients

Element	(nm)	R^2	Element	(nm)	R^2
Al	394.408	0.996	Nb	316.345	0.999
Cr	425.439	0.999	Ni	349.301	0.992
Cu	324.759	0.994	Si	251.615	0.998
Fe	373.492	0.998	Sn	284.003	0.996
Mn	403.455	0.992	Ti	365.355	0.995
Mo	390.301	0.996			

Table-2: t-tests to check the accuracy of GD-OES

Element	Conc. (%) in NBS 1239	Avg. conc. (%) obtained	s	RSD (%)	t-score
Al	0.0050	0.0049	0.0001	2.48	0.027
Cr	0.1055	0.1058	0.0006	0.54	1.57
Cu	0.0030	0.0031	0.0001	3.00	0.358
Fe	0.2300	0.2295	0.0016	0.76	0.99
Mn	0.0050	0.0054	0.0001	1.47	0.1658
Mo	0.0045	0.0048	0.0001	1.45	0.132
Nb	0.0220	0.0245	0.0003	1.07	0.311
Ni	0.0045	0.0047	0.0001	2.86	0.046
Si	0.0095	0.0085	0.0002	2.81	0.185
Sn	1.61	1.60	0.0190	3.28	2.12
Ti	0.0040	0.0043	0.0001	0.88	0.663

Discussion

(1) From Table 2, it is evident that $t_{calculated}$ for all elements of interest are less than $t_{tabulated}$ (2.228 for 10 numbers of degrees of freedom) at 95% confidence level. Hence it can be concluded that the mean concentration of elements obtained by GD-OES technique are comparable with the true value/ certified value. (2) $F_{calculated}$ for Cr, Fe, Ni and Sn analyzed by GD-OES and AAS (Table 3), $F_{calculated}$ for Al, Cu, Mn, Nb, Ni, Si and Ti analyzed by GD-OES and ICP-AES (shown in table-4) are less than $F_{tabulated}$ (2.98 for 10 numbers of degrees of freedom) at 95% confidence level. This shows that there is no bias in the precision of GD-OES and AAS techniques w.r.t. Cr, Fe, Ni, Sn and of GD-OES and ICP-AES w.r.t. Al, Cu, Mn, Nb, Ni, Si and Ti. However $F_{calculated}$ for Mo is greater than $F_{tabulated}$ which may be attributed to high value of standard deviation (s) obtained for Mo by ICP-AES. (3) Z-score for all elements lies between the mean concentrations of Cr, Fe, Ni, Sn obtained by GD-OES and AAS, mean concentrations of Al, Cu, Mn, Mo, Nb, Ni, Si and Ti obtained by GD-OES and ICP-AES techniques are comparable. Except for surface polishing, no much sample preparation is required for GDOES measurements, making it an attractive tool for any industrial laboratory like ours where very high analytical load is encountered for QC clearance.

Table-3: Conc. of Cr, Fe, Ni and Sn in NBS 1239 obtained by GD-OES and AAS techniques.

Parameters		Mean conc.	s	% RSD	$F_{cal.}$	Z-score
Cr (%)	GD-OES	0.1058	0.006	0.51	2.77	-1.9
	AAS	0.1078	0.001	0.92		
Fe (%)	GD-OES	0.2295	0.0016	0.69	2.44	1.07
	AAS	0.2318	0.0025	0.81		
Ni (ppm)	GD-OES	47.45	1.36	2.86	1.67	-0.255
	AAS	47.90	1.76	3.67		
Sn (%)	GD-OES	1.6	0.019	0.73	2.13	1.61
	AAS	1.584	0.014	0.88		

Table-4: Conc. of Al, Cu, Mn, Mo, Nb, Ni, Si and Ti in NBS 1239 obtained by GD-OES and ICP-AES techniques

Parameters		Mean conc.	s	% RSD	$F_{cal.}$	Z-score
Al (ppm)	GD-OES	49.10	1.22	2.48	2.59	-1.16
	ICP-AES	50.0	0.77	1.54		
Cu (ppm)	GD-OES	30.63	0.92	3.0	1.2	1.66
	ICP-AES	29.3	0.8	2.73		
Mn (ppm)	GD-OES	54.3	0.8	1.47	1.31	-0.64
	ICP-AES	54.9	0.94	1.71		
Mo (ppm)	GD-OES	48.1	0.7	1.45	5.48	1.03
	AAS	46.4	1.64	3.53		
Nb (ppm)	GD-OES	245.7	2.64	1.01	2.79	0.69
	ICP-AES	243	3.91	1.61		
Ni (ppm)	GD-OES	47.45	1.36	2.86	1.78	-0.18
	ICP-AES	47.63	1.01	2.14		
Si (ppm)	GD-OES	85	2.31	2.71	1.37	0.18
	ICP-AES	84.63	2.06	2.40		
Ti (ppm)	GD-OES	43.5	1.43	3.28	2.32	0.94
	ICP-AES	42.63	0.92	2.15		

Conclusion

The present method using GD-OES can be employed as a reliable analytical tool for the estimation of elements such as like Al, Cr, Cu, Fe, Mn, Mo, Nb, Ni, Si, Sn and Ti in Zircaloys.

Acknowledgements

The authors wish to express their thanks to staff members of AAS, ICP-AES lab for their support.

References

[1] R. Kenneth Marcus and Jose A.C. Broekaert; Glow Discharge Plasma in Analytical Spectroscopy, Wiley Publications.

Accelerator based Pyrohydrolysis of Sodium Diuranate and Subsequent Determination of F^- and Cl^- by Ion-Chromatography

Shehanaz Bano, Y. Balaji Rao and H. R. Ravindra

Control Laboratory, Nuclear Fuel Complex, Hyderabad 500062, India; E-mail: ybr4793@gmail.com

In the present paper we report a method for the extraction of F^- and Cl^- from sodium diuranate (SDU) using accelerator U_3O_8 by pyrohydrolysis technique and their simultaneous determination by ion chromatography. The effect of temperature, extraction time, sample size and accelerators MoO_3, WO_3 and U_3O_8 on the recovery of F^- and Cl^- from SDU has been studied and pyrohydrolysis conditions were optimized. The average recoveries obtained for F^- and Cl^- in spiked samples were more than 90%.

Introduction

A new alkaline leaching route for processing of Uranium ore from Tummalapalle has been employed that involves initial oxidation of U(1V) to U(V1) and then subsequently dissolution in Na_2CO_3 to obtain sodium diuranate (SDU) and in this process other minerals present in the ore also undergo dissolution forming sodium product [1]. Impurities F^- and Cl^- present in SDU is also expected to be majorly present in sodium form which are slowly hydrolysable group [2]. The present investigations explore the effect of different accelerators MoO_3, WO_3 and U_3O_8 for the quantitative extraction of F^- and Cl^- from SDU followed by their determination by Ion-Chromatography.

Experimental

Instrumentation

Pyrohydrolysis of SDU obtained from Tummallapalle and SDU mixed with accelerators were carried out in a quartz make pyrohydrolysis set up. IC with suppressed conductivity detector was employed. Metrosep A Supp 5 250/4.0 anion column with guard column Metrosep A Supp 4/5 were used and sample was introduced through six port rheodyne injector fitted with 20 L loop.

Reagents

All solutions were prepared using Ultra High Quality water (18.2 M). A mixture of 3.2 mM Na_2CO_3 and 1 mM $NaHCO_3$ solution was used as eluent. Stock solution of 1 mg/mL standards of F^- and Cl^- were prepared by dissolving 0.2210 g of NaF and 0.1648 g of NaCl and making up to 100 mL with water in 100 mL volumetric flask. From the stock solution, standards of F^- and Cl^- of the range 2-10 g/mL were prepared in 10 ml volumetric flask with appropriate dilutions.

Procedure

SDU powder and SDU powder mixed with accelerators were homogenized and subjected to pyrohydrolysis. During pyrohydrolysis oxygen carrier gas was bubbled through water at 30-50 mL/min flow rate and moist gas was allowed to pass through the sample. The tip of the quartz tube outlet was dipped in collecting flask (10 mL volumetric flask) containing water (absorbing liquid) to collect Cl^- and F^- evolving out during pyrohydrolysis from the sample in the form of HCl and HF. The collected solutions were then injected into IC system for simultaneous determination.

Results and Discussion

Optimization of Pyrohydrolysis Conditions for the Complete Extraction of Fluoride and Chloride

For optimizing the pyrohydrolysis conditions, initially the extraction of F^- and Cl^- from SDU powder at different temperatures from 900 to 1100°C for constant extraction time of 60 minutes was studied. It was seen that extraction has increased with increase in temp. and is maximum at 1100°C. Similarly, pyrohydrolysis extraction was carried out at two different sample sizes of 0.25 g and 0.5 g and extraction was observed to be maximum with the smaller sample size. This may be attributed to effective distribution of heat throughout the sample bed. The effect of different accelerators like MoO_3, WO_3 and U_3O_8 on extraction efficiency was also studied by carrying out pyrohydrolysis at 900°C for 60 min. using SDU mixed with accelerators in the ratio of 1:1. From the Fig. 1 it is seen that extraction efficiency has increased in the presence of accelerators and also it is seen that all the accelerators are equally effective in expelling F^- and Cl^- from the sample. Further to this, extraction temp. was increased to 1100°C from 900°C for 60 min. using U_3O_8 accelerator and it was observed that there was a slight increase in quantity of extraction by 15% of F^- and 8% of Cl^- at 1100°C. However, similar experiment could not be carried out with MoO_3 and WO_3 accelerators as the respective reaction products with SDU were volatile in nature at 900°C and above.

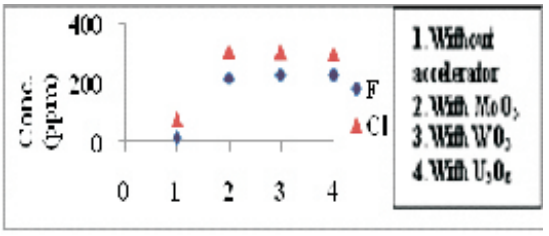


Fig. 1 Effect of accelerators on extraction at 900°C, time 60 min., sample size 0.25 g, 1:1 ratio of sample: accelerator

Effect of quantity of accelerator at different ratio of SDU and U_3O_8 (1:1, 1:2 and 1:3) was also studied and it was observed that quantity of expulsion of F^- and Cl^- remained same. Expulsion of F^- and Cl^- at different extraction times of 60, 80 and 100 min. was also studied and there was no significant increase in quantity of expulsion with time. Based on these observations, the pyrohydrolyitc conditions were optimized as shown in Table 1. The collected solutions after pyrohydrolysis was injected into Ion Chromatography sytem, F^- peak was obtained at 6.5 min and Cl^- peak at 9.7 min. with eluent flow of 0.6 mL/min., prior to injection of sample, linear calibration graph was obtained with R^2 value of greater than 0.99 by injecting standards and recording peak area of the respective ions.

Table-1: Optimized pyro-hydrolysis conditions for Extraction of F- and Cl- from SDU

Parameters	Optimum Condition
Sample size	0.25 g
Wt. of U_3O_8	0.25 g
Extraction time	60 min.
Pyrohydrolysis temp.	1100°C
Oxygen flow rate	30-50 ml/min

Mechanism and Recovery Studies

As no specific reason could be given for release of trapped halides, if any in SDU lattice, an assumption can be made that the halides are present as NaF and NaCl due to nature of preparation of SDU. Further XRD studies are being conducted to see the phase transformation of SDU during the pyrohydrolysis at different temperatures [3]. The study will help us in knowing the release of trapped halides, if any, during phase conversions of SDU. As known alkali halides especially alkali fluorides are slowly hydrolysable group but with U_3O_8 it can be easily hydrolyzable with the following possible reaction [2]:

$$6\ NaX + 2U_3O_8 + O_2 + 3H_2O = 3Na_2U_2O_7 + 6HX$$

In order to substantiate this, NaF and NaCl were mixed with U_3O_8 separately and subjected to pyrohydrolysis. The XRD pattern of the two reactions products as shown in Fig.2 clearly indicating the presence of $Na_2U_2O_7$ peaks. Thus, the presence of U_3O_8 accelerator is helping in the fast expulsion of F^- and Cl^- by reacting with the slowly hydrolyzable halides.

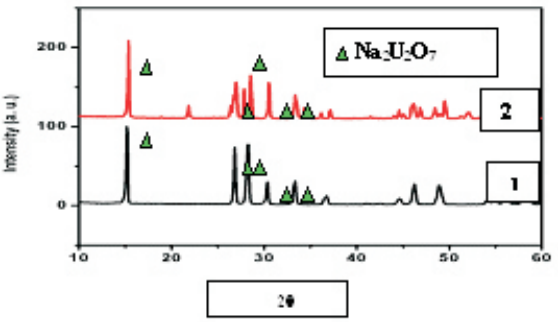


Fig. 2 XRD pattern of pyrohydrolyzed sample of NaF and U_3O_8 (1); NaCl and U_3O_8 (2)

Quantitative extraction of F^- and Cl^- was confirmed by carrying out recovery studies. 50 g and 100 g of F^- and Cl^- were added in solution form by taking 0.05 ml and 0.1 ml respectively using micropipette as NaCl and NaF from 1 mg/mL stock solution in pre-pyrohydrolyzed and preanalyzed sample. The average recoveries obtained were more than 90% for both F^- and Cl^-.

Conclusion

The present method deve loped for the estimation of F^- and Cl^- in SDU using pyrohydrolysis-ion chromatography (PH-IC) technique with U_3O_8 as accelerator can be successfully employed for the said purpose on regular basis.

Acknowledgements

The authors are grateful to Shri N. Saibaba, DS and CE, NFC for permitting to publish the paper and authors also acknowledge the encouragement given by Shri B. Prahlad, DCE (QA, TS, HRD & Library) during the course of the work.

References

[1] A.K Suri, Barc Newsletter, 317, Nov-Dec.(2010)

[2] D. E. Harrington and R. S. Dorsett, AEC Research and Development report, Savannah River Laboratory, Aiken, South Caroline, 46th Ed. Dec (1965).

[3] E.H.P. Cordfunke, R.P. Muis, W. Ouweltjes, H.E. Flotow, P.A.G. O'Hare, The J. Chem. Thermodyanamics, 14, 4 (1982) 313

Development of a Method for Determining the location of Heterogeneous Activity present in 200 litre Waste Drum using USB based MCS System

Sarbjit Singh[1], Amol Mhatre[1], Veena Sagar[2] and Nidhi Gupta[3]

1. *Radiochemistry Division, Bhabha Atomic Research Centre, Mumbai 400085, India, E-mail: sarbjitsingh@yahoo.com*
2. *Radioanalytical Chemistry Division, Bhabha Atomic Research Centre, Mumbai 400085, India*
3. *Electronics Division, Bhabha Atomic Research Centre, Mumbai 400085, India*

A method was developed for determining the location of activity present in 200 litre waste drum using USB based MCS system coupled to a segmented gamma ray scanner. ^{137}Cs source was kept at various distances from centre of the drum along the axis of the detector. Drum was rotated and the activity profiles were determined as a function of angle of rotation. The plot of the count rate as a function of angle of rotation was found to have two peaks. The experimental and calculated data were found to match well at all angles. Present studies have shown that the ratio of height and width of the profile at angles of 0 and 180 can be used to determine the location of the activity in the drum.

Introduction

The segmented gamma ray scanning system based on HPGe detector was setup [1] to monitor alpha active waste drums which can measure as low as 50 mg of ^{239}Pu present in the 200 litre drum. Though enough compensation is achieved by rotation, but still there is change in efficiency depending upon the distance of the activity from the centre of the drum [2]. Hence, results can be erroneous if the activity present is heterogeneous or lumps of plutonium are present in the drum. Heterogeneous drums can be monitored using involved technique of passive and active tomography [3]. In order to monitor waste drums with a reasonable accuracy and in a reasonable time, a combination of segmented gamma ray scanner and USB based MCS system were developed. Present work describes the system for the determination of the location of activity by measuring the activity profile. The activity profile as a function of angle of rotation can be used to monitor the location of the heterogeneous activity present in the drum.

Experimental

The segmented gamma ray scanning system consists of a drum manipulator which can rotate as well as move up and down the 200 litre waste drum kept on its platform. An USB based MCS system coupled with this scanning system was setup to determine the location of the heterogeneous activity present in the drum. Using the angle of rotation and vertical displacement, position of the drum in front of the collimator can be determined. The gamma ray counting as a function of time will help in deciding the distribution of activity present in the drum. The amount of radioactivity due to various radio nuclides can be determined by separate experiment using HPGe detector system in the PHA mode. Gamma ray counting was carried out using a well collimated and shielded NaI(Tl) detector system. A 10 Ci source of ^{137}Cs was fixed on the inner wall of the drum along central axis of the detector and collimator. In order to compare the performance of USB based MCS system, an experiment was carried out to determine the activity profile as a function of angle using manual mode of the drum manipulator system.

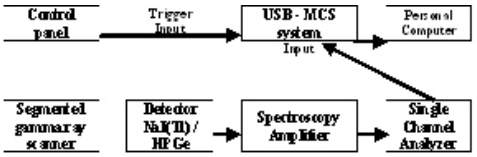


Fig. 1 USB based MCS scanner system coupled to segmented gamma ray scanning system

USB based MCS Scanner System

Fig. 1 shows the block diagram of the USB based MCS system. The system was used in multi group mode, in which the 8192 channels can be split into 64 groups with each group having 128 channels. Whenever there is a trigger from the limit switch, counting starts in the next group. Hence, the data collected in any particular channel of all the groups will correspond to same angle of rotation from the zero position of the drum.

Similar experiments were carried out by changing the distance of the source from centre of the drum (d = 0 mm) to the end of the drum (d=295 mm). The activity profile was measured by rotating the drum in front of the collimated NaI(Tl) detector. In each multi group counting set, the data collected in all 64 groups were added to improve the counting statistics. The average background counts were subtracted from each channel counts to arrive at the corrected count rates.

Results and Discussion

The plot of the count rate of ^{137}Cs source as a function of angle of rotation in the manual mode was

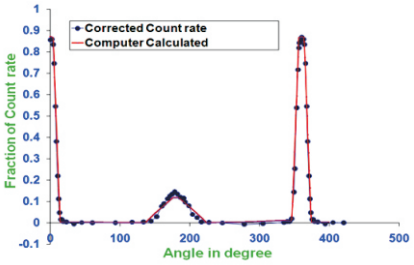


Fig. 2 Plot for the corrected count rate and computer calculated count rate (Manual Mode)

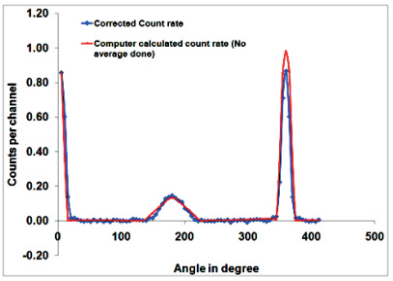


Fig. 3 Plot for the corrected count rate and computer calculated count rate (USB-MCS)

found to have two peaks (Fig. 2). The intensity profile of the activity near 0 was found to be much larger and sharper as compared to the one at 180 . A computer program was developed in FORTRAN to calculate the variation in intensity of the gamma rays as a function of angle of rotation. The experimental and calculated data were found to match well at all angles of rotation.

USB based MCS System in Multi Group Mode

The plot of combined data acquired in all 64 groups for the count rate of ^{137}Cs source as a function of angle of rotation was found to have two peaks (Fig.3). The activity profile obtained using manual mode (Fig.2) and USB-MCS mode (Fig.3) were found to agree well. The only difference in data collection using these two modes is that the data points in case of Manual Mode are at particular angle, whereas in case of MCS Mode, the data points are for mean average angle during the rotation within one channel.

The activity profile data were fitted to two Gaussian peaks to determine their width, height and area at 0 and 180 . The activity profile was found to become broader and broader as the source moved from the end of the drum to the centre of the drum. The width of the peak was small for 0 when the source was at the end of the drum. As the source was moved nearer to the centre of drum, the width of profile for 0 was found to increase till it became flat at the centre of the drum. When the source was at the end of the drum, width of the peak was about 2.9 times more at 180 than at 0 . Also as the source was moved nearer to the centre, the width of profile at 180 was also found to increase till it became flat at the centre of drum.

The ratios of peak widths at 0 and 180 were found to increase from 0.37 to 1 as the source moved from end of the drum to the centre of drum (Fig.4). Therefore, the ratios of peak widths can be used to determine the location of the source in the drum. The angular span of both the peaks at 0 and 180 were found to increase continuously as the source was moved from the end of the drum to the centre of the drum. Therefore the ratios of the peak areas cannot be used to determine the location of the source.

The height of the peak was more at 0 when the source was at the end of drum. As the source was moved to the centre of drum, height of the profile at 0 was found to decrease till there was a flat profile. When the source was at the end of drum, peak height was about

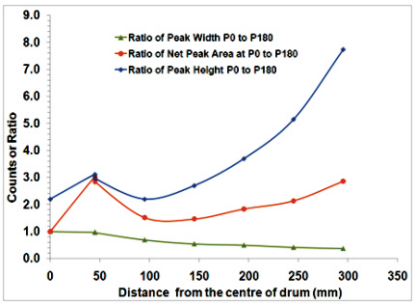


Fig. 4 Plot for the ratios of width, area and height of the peak profile as a function of the distance of the source from the centre of the drum at 0 and 180 angles (USB-MCS)

7.7 times more at 0 than at 180 . Also as the source was moved to the centre of drum, the height of profile at 180 was found to decrease till it was a flat profile. Ratio of peak heights at angle 0 to that at angle 180 was found to decrease from 7.7 to the lowest value as the source was moved from the end of drum to the centre of drum (Fig.4). Therefore the ratio of peak heights can also be used to determine the location of the source in the drum with respect to the angle of rotation.

Conclusion

These studies have shown that the ratio of height and width of profile at angles of 0 and 180 can be used to determine the location of source in the drum. The ratio of peak areas can also be used as a secondary confirmation for the determination of the location of source in the drum.

Acknowledgment

We are thankful to Electronics Division for developing the USB based MCS system and also thankful to Centre for Design & Manufacture for the development of the drum manipulator system.

References

[1] S. Singh, V. B. Sagar, A. Mhatre, A. Ramaswami, Report BARC/2006/I/015, B.A.R.C., Mumbai, India.

[2] S. Singh, A.Mhatre, NUCAR Mumbai, India, January 7-10, (2009), NUCAR-2009. Page E1

[3] Office of Environ Management, Office of Sci. and Technol, U.S. Dept. of Energy, Sept (1999), Report DOE/EM-0470.

Spectrophotometric Determination of Zirconium with Chrome Azurol s in Aqueous Streams of Nuclear Fuel Reprocessing

S. Ganesh, P.Velavendan, N.K. Pandey, U. Kamachi Mudali and R. Natarajan

Reprocessing Research and Development Division, Indira Gandhi Centre for Atomic Research, Kalpakkam 603102, India; E-mail: velp@igcar.gov.in

A sensitive and reproducible spectrophotometric method for the determination of zirconium is developed. The method is based on the formation of stable bluish violet colour complex with Chrome Azurol S (CAS) with maximum absorption at 598 nm. The complex formed obeys Beer's law in the range of 1-7 g/mL. Under optimum conditions, the sensitivity of the proposed method, (i.e. the detection limit), molar absorptivity and Sandell's sensitivity values are 2.42 g/mL, 3.93 x 10^3 L.Mol^{-1}.cm^{-1} and 2.54 x 10^{-4} g/cm^2 respectively. Relative standard deviation is less than 2% and correlation coefficient is 0.997. The present method is highly sensitive, selective, rapid and simple. It can be applied for the direct determination of zirconium in environmental, industrial, water and nuclear reprocessing samples.

Introduction

In the reprocessing of Fast Breeder Reactor (FBR) fuels, zirconium is of particular importance because it is one of the most readily extractable fission products and contaminates uranium and plutonium products. The fission yield of Zr is 7-7.5%. ^{95}Zr has a half-life of 65 days and in transient equilibrium with ^{95}Nb with half-life of 35 days. ^{95}Zr is to be considered while designing the solvent extraction flow sheet for the reprocessing of nuclear fuels with a cooling period of around two years or less. The ^{95}Zr - ^{95}Nb pair is responsible for the majority of gamma activity of dissolver solution of short cooled fuels and it contributes to around 1% of the total activity for a typical FBR fuel with 6 month's cooling [1]. Determination of trace amounts of zirconium in environmental and industrial samples is interesting because of the high toxicity of its compounds. There are numerous analytical methods for the quantitative determination of zirconium reported in the literature. In the present paper, a sensitive spectrophotometric method for the quantitative determination of zirconium, based on its complex formation with chrome azurol S is described.

Experimental

All absorbance measurements were recorded by indigenously developed fiber optic aided spectrophotometer with dip type probe. All the reagents used were of analytical grade and all solutions were prepared using distilled water. A standard zirconium solutions (100 g/mL) were prepared by dissolving $ZrO(NO_3)_2 \cdot 2H_2O$, (Lobal Chemie) in distilled water. The solution was standardized as per the standard procedure [2]. Working solutions were prepared by appropriate dilution of standard solutions. Buffer solutions was prepared from sodium acetate (0.1M) and acetic acid (0.1 M) and pH was adjusted to 4. 2 with 0.05M acetic acid by using a pH meter. Stock solution of Chrome Azurol S was prepared by dissolving 0.05 g in 100 mL distilled water.

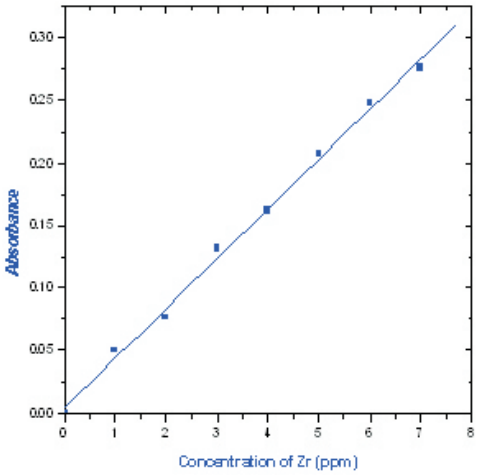


Fig. 1 Calibration graph for the determination of zirconium at 598 nm

A suitable aliquot of Zr (IV) solution was transferred quantitatively into 10 mL capacity standard flasks. 1 mL of sodium acetate /acetic acid buffer, 0.3 mL of 0.05% Chrome Azurol S solution was added. The mixture was then made up to the mark with distilled water and 1M nitric acid. Absorbance was measured against a reagent blank prepared under identical conditions at 598 nm.

Results and Discussion

The spectrophotometric method for the determination of zirconium was standardized using Chrome Azurol S as a complexing agent. The calibration graph is linear for the zirconium concentration in the range of 1-7 g/mL with correlation coefficient of 0.997. Figure 1 shows the calibration graph obtained with maximum absorbance at 598 nm for standard zirconium solution. In the present study, chrome azurol S is a preferred chromogenic reagent on account of its high sensitivity and selectivity. The Zr-CAS complex formed is stable.

Typical absorption spectra of chrome azurol s and zirconium at pH 4.2 at 598 nm are shown in Fig. 2. The reaction conditions, as well as the various experimental parameters affecting the formation and stability of the bluish violet coloured complex of Zr-CAS, were carefully investigated and optimized. The results obtained in the present method are in good agreement with those obtained by using BrPADAP [3] as a chromogenic reagent and represented in Table. 1.

Table-1: Comparison of results with Br-PADAP

Sl. No	Spectrophhotometric techniques (g/mL)	
	Present method	Br-PADAP
1	27.51	26.89
2	18.02	17.76
3	10.15	9.63
4	2.78	2.12
5	11.7	10.10

Conclusions

A spectrophotometric method for the determination of zirconium using CAS has been developed. CAS forms a very stable complex with zirconium at pH 4.2. The proposed method is simple, rapid, reliable and accurate. The method posse's distinct advantages over the existing methods in terms of cost, simplicity, sensitivity, ease of operation and potential for application for the determination of zirconium in environmental, industrial and nuclear reprocessing samples.

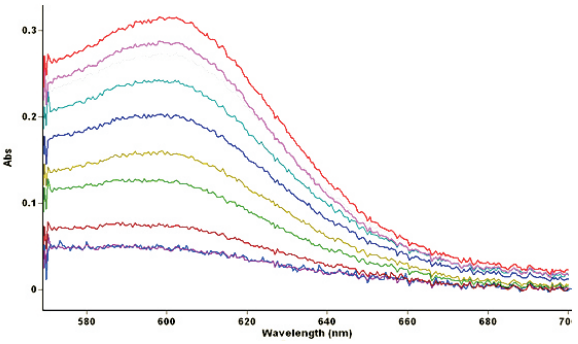


Fig. 2 Typical absorption spectrum of zirconium with Chrome Azurol S at 598 nm

References

[1] J. B. Hedrick, "Zirconium and hafnium", US Geological Survey Minerals Year book, (2000) pp. 87-104.

[2] J. Mendham, R. C. Denney, J. D. Barnes and M. Thomas, Vogel's Textbook of quantitative chemical analysis, (6th Edition) Prentice Hall, New York, (2000) pp.473.

[3] G. V. Rathaiah and M. C. Eshwar, Talanta, 36 (1988) 502.

Separation of no-carrier –added ^{62}Zn from ^{7}Li Irradiated Cobalt Target Using Calcium Alginate Beads

Kaustab Ghosh[1], Moumita Maiti[2*], Susanta Lahiri[1]

1. *Chemical Sciences Division, Saha Institute of Nuclear Physics, 1/AF Bidhannagar, Kolkata-700064, India*
2. *Department of Physics, Indian Institute of Technology Roorkee, Roorkee-247667, India; E-mail: moumifph@iitr.ernet.in*

A ^{59}Co target was irradiated with 47 MeV ^{7}Li, which produced NCA ^{62}Zn in the target matrix. NCA ^{62}Zn was separated from the target matrix by adsorption on calcium alginate beads kept in HNO_3 solutions of different pH values (1-6). The optimum separation condition was achieved at pH 5, where ~83% NCA ^{62}Zn was adsorbed on the alginate beads along with some contamination from the bulk Co. The complete separation of ^{62}Zn from the bulk was achieved on desorbing Co from the beads with 0.1 M $NaNO_2$. The remaining ^{62}Zn was separated on re-adsorption under the same condition.

Introduction

The present era demands chemical processes that are greener, eco friendly and non hazardous. In this aspect, biopolymers such as alginate play an important role. Alginate is a natural polymer composed of varying compositions of -1,4 linked D-mannuronic and L-guluronic acids [1]. The presence of carboxy groups in the alginate structure mediates the adsorption of the metal ions. The adsorption property of the alginate has already been investigated for Cu^{2+}, Co^{2+}, Zn^{2+}, Cd^{2+}, La^{3+} etc, earlier [2, 3]. Thus alginate has the potential to adsorb ions of natural and radioactive origin and can be used as an effective medium in the field of separation chemistry.

The importance of zinc in many processes of metabolisms in living cells is well known. No-carrier-added (NCA) ^{62}Zn (9.26 h) is a PET radioisotope mostly used in the preparation of ^{62}Zn/^{62}Cu (9.74 min) generators [4, 5].

The production of tracer packet consisting of radioisotopes of micro nutrient elements such as Mn, Cu, Zn, Ga, Ge, As and Se by successive bombardment of ^{16}O, ^{7}Li and ^{12}C was first explored by Lahiri and Nayak [6,7]. The radioisotopes of the micronutrient elements were separated from the bulk Co target by liquid-liquid extraction with 25% NH_3 and a mixture of 1% di-(2-ethylhexyl) phosphoric acid (HDEHP) and 10% tributylphosphate (TBP) in cyclohexane followed by sequential separation of the NCA products employing trioctylamine (TOA) as extractant [7].

The ^{7}Li bombardment on ^{59}Co target produces NCA ^{62}Zn in the target matrix. This alternate production method is rarely explored and very few reports are available on the separation of ^{62}Zn from the Co target. We therefore made an attempt for the first time to separate NCA ^{62}Zn from Co target using calcium alginate beads.

Experimental

A ^{59}Co target of thickness 19.6 mg/cm^2 was irradiated with 47 MeV ^{7}Li with a total dose of 2320 C for 10.4 h at BARC-TIFR Pelletron, Mumbai, India. The total charge of irradiation was measured with the help of a current integrator. After irradiation, the target was cooled for 20 hours for the decay of short lived products. The target was dissolved in 5 M HNO_3 and spiked with ^{60}Co (5.27 yr). The active solution was evaporated to dryness twice and finally kept at 10^{-2} M HNO_3. Thus a 10 mL active stock solution containing NCA ^{62}Zn and ^{60}Co for monitoring of the bulk was prepared for radiochemical separations.

The calcium alginate beads were prepared as described by Nayak and Lahiri, 2006 [1]. A 3% (w/v) slurry of sodium alginate was prepared in hot (60°C) deionized water and cooled and was added drop wise into a solution of 20% $CaCl_2.2H_2O$ (w/v) with constant stirring maintaining a temperature of 4-7°C. By doing so, the water soluble sodium alginate was converted into water insoluble calcium alginate beads. Before use, the beads were collected by filtration and the excess water on the bead surface was adsorbed on tissue paper.

Six different pH (1-6) solutions were prepared in HNO_3 medium. For the adsorption study, 30 numbers of beads were equilibrated in 3 mL of the respective pH solution for 1 hour before exposing to the radionuclide solution. After equilibration, 0.2 mL of the stock activity was added to each of the solutions and was shaken for 15 minutes. The adsorption systems were allowed to settle for 10 minutes. Once the equilibrium is reached, 2 mL aliquot was collected from each pH in different plastic vials for -spectrometric studies.

Desorption study of the radionuclides from the beads was carried out with 0.1 M $NaNO_2$ and 0.1 M HNO_3 respectively. For the removal of bulk Co, after adsorption, the beads were removed from the supernatant liquid and 3.2 mL of 0.1 M $NaNO_2$ was added to the beads and incubated for 30 minutes. After incubation, the mixture was shaken for 15 minutes and settled for 10 minutes and 2 mL aliquot was collected for -spectrometric analysis. After the complete removal of the bulk Co from the beads, the beads were treated with 3.2 mL of 0.1 M HNO_3 to carry out desorption study of NCA ^{62}Zn from the alginate beads.

Results and Discussion

The -spectroscopic analysis of the ^{7}Li irradiated ^{59}Co target confirmed the production of NCA ^{62}Zn, ^{63}Zn (38.47 min), ^{61}Cu (3.33 h) and ^{56}Mn (2.6 h) in the target matrix. The yield of NCA ^{62}Zn after 1.4 hour of the end of bombardment (EOB) was 680 kBq/ Ah.

The adsorption profile of NCA ^{62}Zn and bulk Co on the calcium alginate beads at different pH (1-6) solutions is shown in Fig. 1. It is evident from the figure that there is an increasing tendency in adsorption of NCA ^{62}Zn with the increase in pH of HNO_3 solution and a maximum adsorption of 83% is achieved at pH 5. The adsorption of bulk Co on the calcium alginate beads is also steadily increasing from 4% at pH 1 to 57% at pH 6. The optimum condition was achieved at pH 5, where 83% NCA ^{62}Zn was adsorbed on the calcium alginate beads along with 47% bulk Co. The remaining 17% NCA ^{62}Zn in the pH 5 solution was separated on re-adsorption with calcium alginate beads under the same condition.

The bulk Co was removed from the beads on desorbing with 0.1 M $NaNO_2$ twice, without any loss of NCA ^{62}Zn. After the removal of bulk Co, the NCA ^{62}Zn came to the solution on desorbing the beads with 0.1 M HNO_3. Distribution coefficient of Zn and Co was calculated with respect to retention of Zn and Co in beads and their original amount in the feed solution. The separation factor was 3.3×10^{4}.

At pH 5, both NCA ^{62}Zn and bulk Co exists as cationic species such as Zn^{2+}, Co^{2+}, etc, respectively [8], which leads to the adsorption of the metal ions to the anionic carboxyl part of the alginate polymer. However, the binding stability of Zn ions is much greater than that of Co [2], and this helps in the higher adsorption of NCA ^{62}Zn over bulk Co and removal of bulk Co with 0.1 M $NaNO_2$ from the alginate beads during desorption studies. At lower pH, the effective maximum binding capacity of the alginate for the metal ions is much reduced and this leads to lower adsorption of the metal ions with the bio-polymer [2].

Conclusion

The advantage of using alginate polymer includes biodegradability, hydrophilicity and natural origin. In this respect, the method is green and offers an effective platform for the separation of NCA ^{62}Zn from the bulk cobalt. This efficient method leads to the high separation factor of 10^{4}.

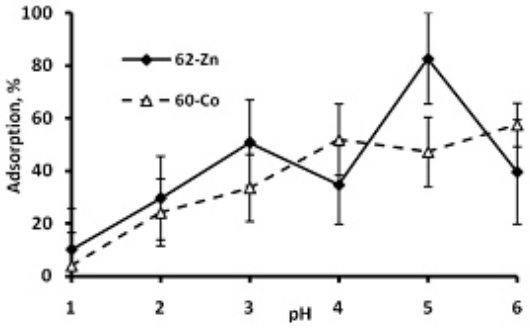


Fig. 1 Adsorption profile of NCA ^{62}Zn and bulk Co with different pH solutions

Acknowledgment

We thank BARC-TIFR Pelletron staff for their help. This work has been carried out as part of the SINP-DAE-12 five year plan project "Trace Ultratrace Analysis and Isotope Production (TULIP)". KG is thankful to Council of Scientific & Industrial Research (CSIR) India for financial support.

References

[1] D. Nayak, S. Lahiri, J. Radioanal. Nucl. Chem. 267 (2006) 59.

[2] L. K. Jang, D. Nguyen, G. G. Geesey, Wat. Res. 33 (1999) 2817.

[3] L. K. Jang, S. L. Lopez, S. L. Eastman, P. Pryfogle, Biotechnol. Bioeng. 37 (1991) 266.

[4] M. A. Green, C. J. Mathias, M. J. Welch, A. H. McGuire, D. Perry, F. Fernandez-Rubio, J. S. Perlmutter, M. E. Raichle, R. B. Bergmann, J. Nucl. Med. 31 (1990) 1989.

[5] A. R. Jalilian, B. Fateh, M. Ghergherehchi, A. Karimian, M. Matlloobi, S. Moradkhani, M. Kamalidehghan, F. Tabeie, Iran. J. Radiat. Res. 1 (2003) 37.

[6] D. Nayak, S. Lahiri, J. Radioanal. Nucl. Chem. 254 (2002) 619.

[7] D. Nayak, S. Lahiri, J. Nucl. Radiochem. Sci. 4 (2003) 1.

[8] W. Verweij, CHEAQS PRO: A computer program for calculating CHemical Equilibria in Aquatic Systems, (2013), http://home.telfort.nl/cheaqs/index.html.

Determination of Boron in ThO_2 Samples

P.S. Ramanjaneyulu[1], K.L. Pandey[2], M.K Saxena[1], B.S. Tomar[1] and K.L. Ramakumar[1]

1. *Radioanalytical Chemistry Division, Bhabha Atomic Research Centre, Mumbai 400 085, India; E-mail: psr@barc.gov.in*
2. *Integrated Fuel Fabrication Facility, Bhabha Atomic Research Centre, Mumbai 400 085, India*

Studies on the determination of boron in ThO_2 employing spectrophotometry with curcumin as complexing agent are described here. In this methodology, sample was dissolved in concentrated ortho phosphoric acid. Boron was separated with 10% 2-ethyl hexane 1,3 diol in $CHCl_3$ from dissolved solution and then colour was developed with curcumin in acetic acid in the presence of H_2SO_4. Absolute detection limit of the methodology is 30 ng. Precision and accuracy of the methodology is 4% and 2% respectively.

Introduction

In comparison to the limited uranium reserves, India has abundant resources of thorium. Importance of thorium oxide (ThO_2) in Indian nuclear technology is poised to grow with the induction of advanced heavy water reactors (AHWRs) into the third stage of India's nuclear power programme. Boron is a stringent specification in all the nuclear materials including ThO_2 due to its high thermal neutron absorption cross section. Boron has to be determined in these materials. The most commonly employed methodologies in characterization of nuclear fuels like ThO_2 are inductively coupled plasma atomic emission spectroscopy (ICP-AES) [1,2] and carrier distillation DC arc atomic emission spectroscopy (DC arc-AES) [3]. Even though these techniques are highly sensitive and capable of multi elements determination in a single aliquot but suffer from poor precision for the determination boron in refractory materials like ThO_2. Moreover, these techniques also require matrix matched reference materials for each analysis. Employing these techniques, DAE, India, ILCE reference materials of ThO_2 for several elements including boron were prepared [4]. The certified boron values in these reference materials show large variation of about 50% to 100%. Hence it is necessary to develop an alternative methodology with good precision and accuracy.

Because of simplicity, comparable sensitivity with other methods, non-requirement of sophisticated equipment and less operating cost, spectrophotometic methods are preferred over other methods. Moreover, in spectrophotometric method matrix matched standards are not a necessary requirement once the method is validated for the determination of boron from any matrix [5,6]. In this methodology, sample has to be dissolved with suitable acid media without using HF and then boron has to be separated prior to the colour development with curcumin to avoid interference from other impurities and water.

The present paper describes the development of the methodology for the determination of boron in ThO_2 and its validation.

Experimental

Sample Dissolution

A weighed aliquot of ThO_2 sample (0.4 g) was taken in a100 mL quartz round bottom flask. 5 mL of ortho phosphoric acid was added and then connected to a water-cooled condenser. The outlet end of condenser was dipped in de-ionized water to trap the gaseous products. The flask containing the sample and acid was heated with the help of heating mantel until clear solution was formed. After cooling the solution to room temperature, the solution in the flask and the condensate were transferred quantitatively to a pre-weighed polypropylene 25 mL flask with de-ionised water. A reagent blank solution was also prepared in the same way by adding all the reagents without sample.

Separation of Boron

A weighed aliquot of the sample solution (about 13.5 g) was taken in a 20 mL quartz beaker. 2.0 mL of 10% 2- ethyl hexane 1,3 diol (EHD) in $CHCl_3$ was added to the above solution. The mixture was stirred for three minutes using a magnetic stirrer, to facilitate the extraction of boron into the organic phase. The two phases were allowed to settle and the organic phase was separated by suction using a polypropylene weight burette. This process was repeated five times (five batch extractions) for quantitative separation of boron. The organic phase separated in each extraction was collected and pooled in another 10 mL quartz beaker.

Colour Development and Absorbance Measurement

The $CHCl_3$ was evaporated from the entire organic phase, by keeping overnight in a fume hood. To the leftover residue, 1.0 mL of 0.4% curcumin in CH_3COOH and 0.5 mL of concentrated H_2SO_4 were added. After about 80 minutes, this mixture was quantitatively transferred into a 10 mL standard quartz volumetric flask and diluted with N, N-dimethyl formamide (DMF). The blank solution was also subjected to color development as mentioned above. The absorbance of the colored complex with reference to blank solution was measured at 560 nm by using quartz cell having 1 cm path length. For calibration

purpose, standard boric acid aliquots were taken in the place of sample and subjected to above mentioned procedure. Calibration plot was constructed between blank corrected absorbance and amount of boron (g) present in the aliquot.

Results and Discussion

Quantitative Extraction and Complexation

Preliminary studies on standard boric acid aliquot solutions showed that four batch extractions with 10% EHD in $CHCl_3$ were adequate for quantitative recovery of boron. Hence, in all further experiments, extraction was carried out five times. It was found that 40 minutes was required for quantitative complex formation between curcumin and boron in EHD. Detailed investigations carried out previously in our laboratory indicated that there was no interference from other ions (Al, Cr, Mg, Ca, Fe, Mn, Mo, F^-, W) even if these are present at a level of 1000 times more to the amount of boron present in aliquot [5].

Calibration Plot, Precision and Detection Limit of the Method

A linear regression equation obtained for calibration is given below

$$A = 0.870 \times m + 0.019 \qquad (1)$$

Where, A = Absorbance, m = Amount of boron present aliquot in g.

The linear correlation coefficient is 0.998 over the linear range of 0.25 – 1.3 g with seven data points. Relative standard deviation (%RSD) and mean recovery of boron in ten independent standard boric acid aliquots were found to be 4.2 % (at 1 level) and 98% respectively. From a given sample, five independent solid aliquots were taken, dissolved and boron was determined in each of the dissolved solid aliquots in duplicate (total 10 determinations.) A relative standard deviation of 5.7% was obtained. In order to determine the limit of detection, ten independent blank solutions were prepared and absorbance was measured with respect to water. The absolute limit of detection of this method was evaluated at 3 level of blank and found to be 0.03 g.

Validation of the Method

The method has been validated, by analysing boron concentration in DAE, India, Inter Laboratory Comparision Experiments (ILCE) standards of boron in ThO_2 matrix. The results are presented in Table 1. As can be seen, by applying statistical treatment of the data (t test), there is no significant difference (95% confidence interval) between the results obtained in the present work and the recommended values.

Table-1: Validation of methodology.

Standard ID	Conc.of Boron (g g^{-1})	
	Certified Values	Present Method*
ThO_2 – B	0.77 0.51	0.25 0.02
ThO_2 – S	1.20 0.60	0.77 0.11
ThO_2 – D	0.80 0.40	0.71 0.07

*Mean of four determinations

Conclusion

A simple, precise and accurate method based on spectrophotometry has been developed for the determination of boron in ThO_2. ThO_2 has been dissolved in ortho H_3PO_4 without loss of boron. The developed method has been validated using DAE, India ILCE ThO_2 reference materials. Possibility of assigning new values for DAE ILCE standards could be explored.

References

[1] M. Gopalkishnan, K. Radhakrishnan, P.S. Dhami V.T. Kulkarn, M.V. Joshi , A.B. Patwardhan , A. Ramanujam, J.N. Mathur, Talanta 44 (1997) 169.

[2] .J. Kulkarni, A.A. Argekar, J.N. Mathur, A.G. Page, Analytica Chimica Acta 370 (1998) 163.

[3] N. K. Porwal, A. A. Argekar, P. J. Pnrohit, A. G. Page, and M. D. Sastry, Fresenius J Anal Chem., 338 (1990) 255.

[4] DAE Inter-laboratory Comparison (ILCE) for the Determination of Trace Metals in Thorium Oxide, Compiled by Radiochemistry Division BARC and Control Laboratory NFC, Hyderabad, Internal Report, June (2006).

[5] P.S. Ramanjaneyulu, Y.S. Sayi, V.A. Raman and K.L. Ramakumar, J. of Radioanal. and Nucl. Chem. 274 (2007) 109.

[6] P.S. Ramanjaneyulu, Y.S. Sayi, K.L. Ramakumar, J. of Nucl. Mat., 378 (2008) 139.

Effect of Batch size on the Separation of Uranium from Solid (U, Pu, Ag) Oxide Analytical Waste

Nimai Pathak, Mithlesh Kumar, S.K. Thulasidas, V. Natarajan and S.V. Godbole

Radiochemistry Division, Bhabha Atomic Research Centre, Mumbai 400 085, India; E-mail: vnatra@barc.gov.in

Earlier we had studied the effect of leaching a solid analytical waste of (U,Pu)O_2 and AgCl with nitric acid of different molarities and for identical as well as varying time intervals. In the present work, the effect of leaching of this waste with nitric acid was studied as a function of batch size. Three different lots of the waste having different amounts were subjected to multiple leaching with 8 M nitric acid for 15 minutes each time. The results are discussed in this report.

Introduction

Recovery of plutonium from nuclear waste is an important activity of any nuclear program in view of its strategic importance. In Radiochemistry Division, the trace metal analysis of Pu bearing fuel materials such as PuO_2, (U,Pu)O_2 and (U,Pu)C are being carried out using the DC arc-Carrier Distillation technique. During this process, solid analytical waste containing Pu and ^{241}Am is generated. This comprises of left-over of samples and prepared charges. The main constituents of this waste are uranium oxide, plutonium oxide and silver chloride. Earlier anion exchange separation was used extensively to separate gram quantities of Pu from large amounts of U and mg quantities of ^{241}Am, which was time consuming. Further the quantitative dissolution of the (U,Pu,Ag) oxide waste will be difficult due to the presence of AgCl used as carrier for the DC arc-AES analysis. Fast alternate methods are desirable for separating bulk uranium from such type of analytical solid waste [1,2]. In this context, we have studied the effect of simple leaching with nitric acid on the bulk separation of uranium from analytical waste, wherein the leaching time, number of leaching steps and concentration of nitric acid were varied so as to achieve maximum separation of uranium from the solid waste [3]. It was demonstrated that from 5g batch of the waste by simple leaching with 8M /16 M HNO_3 in four 15 minutes steps, entire uranium can be separated from the waste along with 1-2% Pu. This work is an extension of the earlier work. Here we have investigated the effect of batch size on the separation of uranium using multi-step room temperature leaching with 8 M HNO_3.

Experimental

Three lots weighing 5, 10 and 20 grams were weighed form the analytical waste containing U, Pu oxides and Ag. The homogeneity of the different aliquots was checked by determining U and Pu content and isotopic composition of Pu by gamma ray spectroscopic measurements. Initially leaching of 5 g aliquot was carried out using 20 mL of concentrated nitric acid. Multiple leaching for 15 minutes each was done to make sure of removal of total uranium. Similar investigations were carried out with 10 and 20 g aliquots also. The number of steps were decided such that the final leachate is colourless. The U and Pu contents of the leachates after each step of leaching were determined by ICP-AES method using an Ultima ICP-AES spectrometer and appropriate U and Pu standards. The leachate solutions were diluted suitably so that the uranium concentration in the final solutions were in the concentration range 1-500 g/ml. Silver was also analysed along with U and Pu. Further two leachate solutions were also analysed for uranium using biamperometry in order to cross check the results obtained by ICP-AES.

Results and Discussion

The isotopic composition of three lots were determined by gamma spectrometry. The values were found to be nearly the same (^{238}Pu-0.078 0.002%, ^{239}Pu-80.2 0.1%, ^{240}Pu -17.9 0.1 %, ^{241}Pu-1.42 0.01%, ^{242}Pu -0.40 0.01%). This suggested that the near homogeneity of the different lots. We have chosen 8 M HNO_3 as the leachate in this work, as our earlier studies showed that by leaching with 8 M as well as 16 M HNO_3 for 15 minutes in four steps, entire uranium can be separated from 5 g batch of (U,Pu,Ag) (O,Cl) waste.

The results of leaching of 5, 10 and 15 g lots with 8 M HNO_3 are shown in Tables 1, 2 and 3 respectively. In the case of leaching of the 5 g solid waste with 8 M HNO_3, it was observed that the amount of U leached in the first step was maximum, while in the subsequent steps this went on decreasing. After the fourth step of leaching, the leachate turned colorless. Still one more leaching was done to ensure complete separation of uranium. In case of Pu, the amount leached was in the 3-7 mg/mL range. The total amount of Pu leached was about 23 mg, which corresponds to 2.1% of the Pu amount before dissolution. In case of uranium, the major amount (2.7 g out of 5g) could be leached in 5 steps as seen from Table 1. In case of 10g batch, once again nearly entire uranium (5.4g) could be removed after 6 leaching steps. The plutonium removed in this case was 81.6 mg, which is about 3.1% of the initial Pu content. In the case of 20 g batch, even after 6 steps of leaching, the entire uranium could not be removed. The U amount leached was about 9 g, which is about 83% of the initial content. The Pu amount leached along with uranium was 125 mg, which is 2.4% of the initial Pu

Table 1: Amount of U/Pu leached with 20 mL 8 M HNO_3 (15 min., ICP-AES)- 5g lot

Step	U (g)	Pu (mg)	Ag (mg)
1	1.82 0.03	7.4 0.02	1.0 0.02
2.	0.59 0.01	2.1 0.01	0.2 0.004
3	0.13 0.01	11.6 0.03	0.7 0.01
4	0.04 0.01	4.2 0.01	0.1 0.002
5	0.01 0.002	2.6 0.01	—
Total	2.59 ± 0.05	27.9± 0.06	2.0± 0.04

*U conc. by biamperometry -2.65±0.03 g

Table 2: Amount of U/Pu leached with 20 ml 8 M HNO_3 (15 min. ICP-AES)- 10g lot

Step	U (g)	Pu (mg)	Ag (mg)
1	2.80 0.03	15 0.03	1.8 0.02
2.	1.76 0.02	10 0.05	1 0.01
3	0.42 0.005	28.8 0.04	2.6 0.02
4	0.33 0.004	17.8 0.04	1.3 0.01
5	0.06 0.001	5.4. 0.01	0.2 0.002
6	0.03 0.001	4.6. 0.02	0.1 0.002
Total	5.4± 0.1	81.6± 0.1	7.0± 0.07

Table 3: Amount of U/Pu leached with 20 ml 8 M HNO_3 (15 min. ICP-AES)- 20g lot

Step	U (g)	Pu (mg)	Ag (mg)
1	4.83 0.03	20.8 0.04	6.0 0.04
2.	1.87 0.01	7.8 0.02	1.0 0.01
3	0.98 0.002	45.6 0.10	5.9 0.04
4	0.83 0.01	23.9 0.05	2.5 0.02
5	0.32 0.003	15.3 0.03	1.0 0.02
6	0.21 0.002	11.6 0.03	0.2 0.005
Total	9.04± 0.1	125± 0.15	16.6± 0.02

*U conc. by biamperometry -8.4 ± 0.1 g.

content. As far as silver is concerned, the amount leached in the three aliquots after multistep leaching was in the range 2-17 mg, which is negligible as compared to its content in the original lot. The U concentration determined by biamperometric values for leached U in 5 and 20g lots support our conclusions regarding U. The residue left in both 5 and 10g lot after leaching process is mainly gram amounts of plutonium along with silver in nitrate form. This needs to be dissolved in conc.HNO_3-HF mixture followed by evaporation and repeated leaching with 4M HNO_3, as per the established procedure.

Conclusion

In the present work, the effect of batch size on the separation of uranium by simple multi-step leaching with 8 M HNO_3 at room temperature was investigated. It was found that for 5 and 10 g batch of the solid waste, this procedure results in complete separation of uranium from the waste. From the leachate containing gram amounts of uranium along with milligram amounts of plutonium, the latter can be separated by TBP/dedecane extraction. For lots of bigger size, larger volume of 8 M HNO_3 may help in faster removal of uranium. This needs to be investigated further.

References

[1] V.A. Raman, Dipti Shah, U.K. Thakur, M.A. Mahajan, D.M. Naronha, Keshav Chander, R.M. Sawant and K.L. Ramakumar, NUCAR 2005, Guru Nanak Dev University, Amritsar, India (2005).

[2] K.M. Micahel, C. Janardanan, K. Kumaraguru, P.R. Rakshe, M. Rathinam, G.R. Dharampurkar, B.S. Thite, K.K.Gupta, S.D. Chaudhari, N. Sinalkar, Manisha Lokhande, R.T. Ajithlal, K. Vijayan, U. Jambunthan, S.K. Munshi, P.K. Dey and G.C. Jain, BARC Founder's day issue (2005) 83.

[3] M.J. Kulkarni, V. Natarajan, N.S. Hon, S.K. Thulasidas, Newton Nathaniel, Chaavi Agarwal, Amol Mhatre and S.V. Godbole, Proc. NUCAR 2013 Jabalpur, (2013).

Determination of Microgram Quantities of Common Metals in PVA Films using EDXRF

B.A. Dhawale, Mithlesh Kumar and V. Natarajan

Radiochemistry Division, Bhabha Atomic Research Centre, Mumbai 400085, India; E-mail: vnatra@barc.gov.in

With a view to examine the capability of EDXRF based method for determination of microgram amounts of five common analytesin film form, different concentrations of these analytes (2-50 g/g) were incorporated into polyvinyl alcohol matrix. Linear calibration for the analytes could be obtained in the concentration range 5-50 g/g. The limits of detection for the analytes were found to be of the order of 2-4 g/g. Effect of uranium on the intensity of analyte X-rays was studied in the PVA films containing fixed amount of the uranium and varying concentrations of the analytes.

Introduction

DC arc – Atomic Emission Spectrometry is currently used in our laboratory for the determination of about 20 common impurities in uranium oxides and carbides in the 0.1-10/10-1000 g/g range. X-ray spectrometric methods such as EDXRF are conventionally used for the determination of major matrix elements such as U and Pu at different stages of nuclear fuel cycle. We have demonstrated the application of EDXRF for the determination of common impurities in U_3O_8 and ThO_2 in pellet form [1,2]. The detection limits for common and rare earth analytes in the aqueous solutions were determined by us to be about 10-15 g/mL. By EDXRF analysis of polyvinyl alcohol (PVA) films loaded with rare earth analytes, we have achieved lower detection limits for Eu, Gd, Dy and Sm (5 g/g) as compared to those obtained in aqueous medium [3]. In our recent work on the determination of process pick up impurities such as Cr, Cu, Ni, Fe and Mn in PVA films, we could achieve detection limits of about 5-6 g/g [4]. In the present work, attempts were made prepare smaller PVA films loaded with these analytes in the concentration range 2-50 g/g with a view to improve the detection limit. Further the effect of uranium (1 mg/mL) on the intensities of the analyte X-rays was investigated. This work was done to use EDXRF technique for the selected analytes in U based samples.

Experimental

A Jordan Valley EX-3600M EDXRF spectrometer, equipped with a Rh source, 6 filters, Ge secondary target and a Si(Li) detector was used for the present work. A master solution standard containing the analyte elements of interest, was prepared by mixing appropriate quantities of their spec-pure oxides and dissolving them in dilute nitric acid. A set of synthetic solution standards with Cr, Cu, Ni, Fe and Mn in the range 2-50 g/ml was prepared. PVA films (dia. 28-30 mm) containing the five analytes in graded amounts (2-50 g/g) were prepared to serve as working standards as follows: Solutions of the selected analytes were added to 1 gm of PVA powder. This was later dissolved in 5 ml of quartz doubly distilled water. This mixture was heated at 340 K with constant stirring for about 20 minutes. Then this was poured on a flat glass surface. After 1-2 days, dry films of PVA containing varying amount of the analytes were obtained. These films were cut into circular pieces (25mm dia.) and used in standardizing the determination the analytes. One film without the analytes was prepared and used as the blank. A second set of films were prepared from solutions containing 1 mg/mL of uranium and 0, 5, 10 and 20 g/g of these analytes to study the effect of uranium on the determination of these analytes. Lastly two PVA films with 5/15 g/g (along with 1 mg/g of uranium) were prepared separately to serve as synthetic samples. The instrumental parameters were optimized (for both sets) with secondary Ge target using the highest standard to obtain maximum counts for the analytes. The optimized conditions for the simultaneous determination of the five analytes in PVA films were 25kV /1200 A / 10keV /100sec./air. The films were counted under identical geometry. The K x-rays of the analytes were used for quantification.

Results and Discussion

The calibration plots for the determination of analytes dispersed in PVA matrix, were found to be linear in the range 5-50 g with a precision of about 10%, while the detection limits were found to be about 2-4 g. In case of Mn and Cr, 2 g could be detected with a precision of about 20-25%. Therefore it is clear that in PVA, the analytical range of determination for Cr, Fe, Ni and Mn is 5-50 g/g. The sensitivity was found to be maximum for Nickel. The low precision obtained is understood as due to slight differences in the thickness/area of the prepared PVA films. Though the sensitivity of PVA film was found to be lower than those for aqueous solutions in our earlier work, the detection limits of have been improved down to 2-4 g/g.

The effect of fixed concentration of uranium (1 mg/mL) on the analyte x-ray intensities was studied by counting the U loaded analyte films. The purpose of this exercise was to directly determine the analytes in uranium based samples after dissolution. The variation of intensity as a function of concentration of the

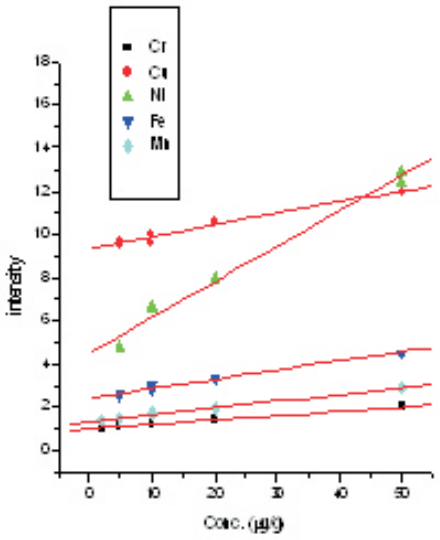


Fig. 1 Calibration plots for Cr, Cu, Ni, Fe, Mn in PVA (2-50 g/g)

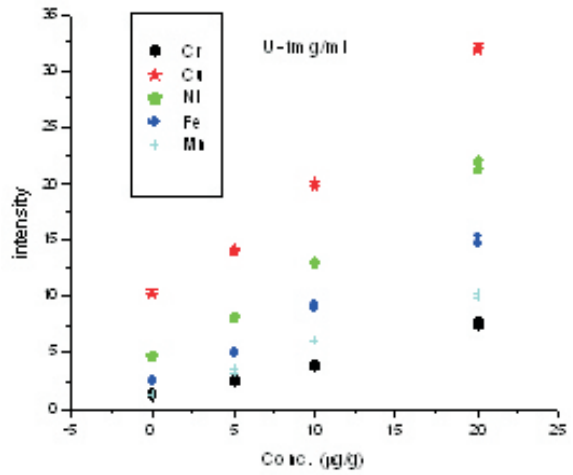


Fig. 2 Calibration plots for Cr, Cu, Ni, Fe, Mn (5-50 g/g) in PVA containing 1mg/g of uranium

individual analytes in this case was studied. This is shown in Fig. 2. Linear calibration plots could be obtained in this case also. However the intensity (counts per second) was higher for all the analytes as compared to those films without uranium. This can be understood as due to the higher density of uranium containing films, which leads to higher absorption of source X-rays.

Using the present method, the concentration of the analytes were determined in two PVA film samples containing 5 and 15 g/mL of the analytes along with 1 mg/mL of uranium The results are shown in Table 1. It can be seen that the results obtained are in good agreement with the added concentration values of the analytes.

Table 1: Results of analysis of synthetic PVasamples containing uranium (1 mg/g)

Anal.	Sample 1 Added Deter. Amount (g/g)		Sample 2 Added Deter. Amount (g/g)	
Cr	5	6.1 ± 0.7	15	14.5± 0.8
Cu	5	5.6± 0.5	15	15.2± 0.5
Ni	5	4.3 ± 0.6	15	16.0± 0.6
Fe	5	5.7± 0.5	15	14.4± 0.8
Mn	5	5.2± 0.6	15	15.8± 0.7

Conclusion

An EDXRF method for the determination of microgram quantites of five common process pick up impurities in polyvinyl alcohol matrix was developed. In the presence of 1 mg/g of uranium, the analyte intensities increased due to increased density of the film. However the calibration for the analytes was still linear. Using this calibration, two synthetic samples containing uranium along with two different concentrations of analytes were analysed. The agreement between the added and determined analyte concentration values were good.

References

[1] V.Natarajan, B. Rajeswari, B.A. Dhawale, N.S.Hon, S.V. Godbole and V.K.Manchanda, J. Radioanal. Nucl. Chem. 280 (2009) 27.

[2] V.Natarajan, B.A.Dhawale, B.Rajeswari, N.S.Hon, S.K.Thulasidas, N.K. Porwal, S.V.Godbole and V.K. Manchanda, Spectrochim. Acta B 63 (2008) 817.

[3] N K Porwal, V Natarajan, Mithlesh Kumar, B Rajeswari, M J Kulkarni, M K Bhide, B A Dhawale and S V Godbole, Ind. J.Chem. 49A (2010) 1055.

[4] B.A.Dhawale, Mithlesh Kumar, Nimai Pathak, M.J.Kulkarni, V.Natarajan and S.V.Godbole, Proc. NUCAR 2013, Jabalpur, Feb.(2013).

Estimation of Boron in Sodium Borosilicate Glass Frit by Fusion at Lower Temperature

D.A. Thakur, N.L. Sonar, T.P Valsala and I.Vishwaraj

Tarapur Waste Management Plant, Nuclear Recycle Board, Bhabha Atomic Research Centre, Tarapur, India; E-mail: tpvalsala@barctara.gov.in

In India High level radioactive liquid waste is immobilized in sodium borosilicate glass matrix. Chemical characterisation of the glass frit is essential to decide the waste to glass frit ratio for vitrification operation. Dissolution of glass sample for its characterization is done by fusion with Sodium carbonate at high temperatures. The error in the estimation of Boron in this fused glass is high due to volatalisation of boron at high temperature. Present paper details the use of sodium hydroxide as flux for fusion of glass sample at lower temperature. The boron is estimated by alkalimetric titration in presence of glycols like glycerol. The effect of presence of other glass components was also studied. Estimation of only boric acid with out fusion has shown recovery of 99.0 %. The boron recovery after fusion with NaOH pellets was found to be 97 – 98 %.. The recovery of boron in presence of glass components like Fe_2O_3, TiO_2 and SiO_2 together has indicated recovery of about 97 -98 %. Further for the sodium borosilicate glass samples the recovery obtained is 92-94%. The lower value is due to the volatilization of boron during glass preparation.

Introduction

High level radioactive liquid waste (HLW) is generated during reprocessing of the spent fuel at PREFRE. Sodium borosilicate glass has been adopted as a solid matrix for immobilization of the HLW world wide [1]. In the joule heated ceramic melter at AVS Tarapur [2] the base glass in the form of preformed glass nodules is used instead of slurry containing raw glass forming chemicals. Chemical characterisation of the preformed glass frit is an essential requirement for deciding waste to glass frit ratio for vitrification operation. Estimation of boron in glass involve alkalimetry titration of boron as hydrated borate complex ion with polyhydroxy compounds like glycerol, mannitol, sorbitol etc [3, 4] at phenolphthalein end point. The common method of decomposition of glass sample using sodium carbonate requires fusion at high temperature (around 900°C). However due to the high volatility of boron during fusion at high temperature the error in the boron estimation will be high here. Hence a method based on fusion of glass samples at lower temperature (around 350°C) using sodium hydroxide pellets [5] has been adopted for the present study. The paper describes the standardization of estimation of boron in presence of other glass components by fusion with sodium hydroxide pellets at lower temperature.

Experimental

All the chemicals used for the experiment were of AR grade and used without further purification. All experiments were carried out in triplicate and the average values are presented.

Initially titrations were carried out with standard boric acid solution. Then solutions prepared from fusion of boric acid with NaOH pellets were for titration. Further to see the effect of other glass components, fusion and estimation of boron was carried out in presence of components like Fe_2O_3, TiO_2 and SiO_2 in combination. The concentrations of these chemicals were taken as per the quantity present in the base glass nodules used for vitrification of HLW. Sodium borosilicate glass samples having two known composition were prepared using raw chemicals as given in Table 1 in Pt crucible for standardizing the procedure for estimation of boron in glass samples.

Table-1: Five and three component glass compositions

Component	Weight %	Chemical	Weight
SiO_2	48.0	SiO_2	47.0
B_2O_3	26.2	H_3BO_3	25.6
Na_2O	11.7	Na_2CO_3	27.4
TiO_2	9.5		
Fe_2O_3	4.6		

Finely crushed powder of chemicals was used for the study. Fusion and dissolution were carried out in Pt crucible as per the procedure described below.

Procedure

Take 3 gm of NaOH pellets in Nickel crucible and heat slowly to melt. Cool the melt in desicator. Transfer accurately 0.3-0.5 gm of finely powdered sample into the above crucible. Heat the crucible with lid in place gently till it melts and further till red hot. Cool the crucible and then extract the fused content with distilled water into a polypropylene beaker. Wash the crucible and lid with minimum water and then finally with 5-6 ml of 1M HCl. Keep the total volume within 60-70 ml, add few drops of phenolphthalein indicator and neutralize the content with dilute HCl. Transfer the content in volumetric flask and digest on boiling water

bath for 10-15 min. Make up the volume to 100 ml. Take suitable aliquot of the solution and neutralize it to phenolphthalein end point. To this add 10 ml of the pre-neutralised glycerol. Wait for few minutes and titrate against standard NaOH (0.1M) at phenolphthalein end point.

The boron content is calculated using the equation:

1mL 0.1M NaOH = 1.083 mg of B (1)

Result and Discussion

Boric acid being a weak monoprotic acid ($K_a = 6.4 \times 10^{-10}$) cannot be titrated accurately with standard alkali. However, by the addition of certain organic polyhydroxy compounds, such as mannitol, glucose, sorbitol or glycerol, it acts as a much stronger acid and can be titrated to a phenolphthalein end point [3]. 1:1 and 1:3 mol ratio complexes are formed between the hydrated borate ion and 1,2- or 1,3-diols and acts as much stronger acid.

The percentage recovery of 99 was obtained for boric acid when titrated directly (Table 2). In the case of boric acid fused with NaOH, 97.5 percentage recoveries were obtained. Also the recovery of boron in presence of glass components like Fe_2O_3, TiO_2 and SiO_2 is 97.2 %. The lower value in these two cases may be due to minor volatilization of boron during fusion and extraction steps. Further for the sodium borosilicate glass samples the recovery obtained is 92-94%. Here the H_3BO_3 content in the sample is the amount of boric acid in the raw mix taken for glass preparation. During glass preparation there is volatilization of boron from the glass mixture. Hence the actual H_3BO_3 content in the glass sample will be less. Considering about 3-4% loss of boric acid during glass preparation the recovery will become 96-97%.

In comparison with the nuclear techniques which are non-destructive and high sensitive, this method is less sensitive. However considering accuracy required for analysis of vitrified waste product this method is suitable.

Table-2: Analysis of boric acid in different samples

Sample	H_3BO_3 content in sample, g	H_3BO_3 estimated, g	Recovery, %
H_3BO_3 solution	0.5	0.495	99.0
H_3BO_3 fused	0.4	0.390	97.5
H_3BO_3+ Fe_2O_3 + TiO_2 + SiO_2 fused	0.4	0.389	97.2
3 component glass	0.228	0.214	93.8
5 component glass	0.233	0.216	92.7

Conclusion

Use of NaOH as flux for fusion is reducing the boron losses during the dissolution of glass samples due to lower fusion temperature. The estimation of boron in the fused mass can be carried out effectively by making use of poly hydroxyl compound like glycerol within 2-3% error. Presence of other component of the glass has negligible effect on estimation of boron in these samples.

Acknowledgement

Authors are thankful to Shri. Y. Kulkarni, Chief Supdt. TNRPO, NRB Tarapur, for his guidance and support.

References

[1] M. I. Ojovan and O. K. Karlina, Radiochim. Acta 34 (1992) 97.

[2] Raj K, Prasad KK., Bansal NK., Nucl. Engg. Design. 236 (2006) 914.

[3] Ball G.R. and Fajans E.W, J. Soc. Glass technology 35 (1951).

[4] Jeffery G.H, Bassett J., Mendham J., Denney R.C, "Vogel's Quantitative Chemical Analysis" 5th Edition, (1989).

[5] B. Mitra and B.C. Sinha, Transactions of the Indian Ceramic Society, Vol.46(3), (1987).

Effect of Higher Waste Loading on the Properties of Vitrified Waste Product

P.K. Mishra, Y. Raghavendra, Vaishali De, T.P. Valsala and I. Vishwaraj

Tarapur Waste Management Plant, Nuclear Recycle Board, Bhabha Atomic Research Centre, Tarapur, India; E-mail: tpvalsala@barctara.gov.in

Joule heated ceramic melter is used for the vitrification of high level waste at Advanced vitrification system at TWMP Tarapur. In joule heated ceramic melter base glass in the form of glass nodules is used instead of slurry containing raw glass forming chemicals. Sodium oxide acts as modifier in glass matrix and small variation in its concentration may vary the properties of the glass and hence the melter parameters. As the composition of the base glass is fixed the concentration of Na in the HLW is one of the limiting factors for the waste loading for the vitrification process. Different product glass samples having varying concentrations of sodium oxide were prepared and characterized with respect to pouring temperature, glass transition temperature, homogeneity, density and chemical durability.

Introduction

Sodium borosilicate glass matrix has been adopted by India for immobilization of High Level radioactive Waste (HLW) [1]. Vitrification process using induction heated metallic melter and joule heated ceramic melter are being adopted at Trombay and Tarapur respectively [2]. In joule heated ceramic melter the base glass in the form of glass nodules is used instead of slurry containing raw glass forming chemicals. A five component base glass composition based on SiO_2-B_2O_3-Na_2O-Fe_2O_3-TiO_2 system was studied and being used at AVS at Tarapur.

The properties and structure of the glass are strongly dependent on the composition, mainly on the SiO_2/Na_2O mole ratio. Composition of the presently selected vitrified waste product has SiO_2/Na_2O ratio 1.85 to 2.0. Since the glass forming chemicals are added in the form of preformed glass nodules, there is no scope for changing the base glass composition when the HLW composition changes. This restricts the waste loading and hence the through put of the melter whenever there is high sodium content in the waste. This calls for selection of product glass composition having lower SiO_2/Na_2O ratio based on acceptable glass properties and melter parameters. Keeping this in mind a study was conducted to see the effect higher sodium content on the properties of vitrified product.

Experimental

Glass Preparation

Preparation of the glass samples were carried out as per the procedure given in our earlier publication [3]. Glass samples with varying mole ratios of SiO_2/Na_2O were prepared using base glass nodules and sodium carbonate in siliminite crucibles in silicon carbide muffle furnace. The SiO_2/Na_2O and Na_2O/B_2O_3 ratios of the product glass samples are given in Table 1.

Characterisation

Fusion and pouring temperatures of the glass samples were noted during preparation. The refined glass sample was used for thermal and chemical characterization.

Table 1: Composition of the product glass samples

Glass Code	Mole ratios	
	SiO_2/Na_2O	Na_2O/B_2O_3
G-1	4.30	0.50
G-2	3.46	0.63
G-3	2.58	0.82
G-4	2.06	1.03
G-5	1.69	1.26
G-6	1.41	1.50

To ascertain the amorphous nature of the glass product, XRD analysis was carried out using Siemen's Make, KRISTALLOFLEX D-500 instrument. Density of the glass samples from different areas of the product glass was determined by water displacement method [4] to see the homogeneity in the product. Glass transition temperature (Tg) was measured using differential thermal analyser, DT-30, make Schimadzu. The chemical durability of glass was measured by standard leach method in which glass is crushed in to powder of -16 to +25 ASTM mesh size and packed in SS mesh [5].

Results and Discussion

According to the literature [6] when the Na_2O concentration in the borosilicate glass is such that the value of R (Na_2O/B_2O_3 mole ratio) is R*(=0.5+0.0625K, where K=SiO_2/B_2O_3 mole ratio) there the Na^+ cations interact as charge compensators for the four coordinated boron atoms. For R > R* the additional Na^+ cations causes depolymerisation of the glass net work by forming non bridging oxygen (NBO)

ions in the silica net work. At higher Na contents (R 0.5 + 0.25 K) NBO's are formed in the borate units also.

From Table 2 it can be seen that the pouring temperature is decreasing with increase in Na content. The decrease is higher for samples whose R value is more than 1.03 (G5 & G6). Similarly the glass transition temperature (Tg) values are also decreasing drastically when R > 1.03. This may be due to the formation of NBO's in both silicate and borate units rather than only in silicate unit when R is less than 1.03. Density values obtained for samples from different areas of the glass were comparable and show the homogeneity in the product glass. Also the XRD scans of the samples were showing amorphous nature in all cases. The stabilized leach rates obtained after 3 months leaching period was comparable in all cases and are with in the acceptable limits.

Table 2: Properties of the product glass samples

Glass Code	Pouring Temp. ^{o}C	Density (gm/cc)	Tg, ^{o}C	Leach rate, $g.cm^{-2}.d^{-1}$
G -1	1000	2.50	552.6	1.66E-04
G -2	980	2.54	557.0	1.27E-04
G -3	980	2.56	559.0	1.75E-04
G -4	950	2.58	555.0	1.43E-04
G -5	900	2.60	532.0	1.36E-04
G -6	875	2.61	511.5	6.63E-05

Conclusion

Increase in the sodium content in the product glass decreases the pouring and glass transition temperatures. However upto SiO_2/Na_2O mole ratio 1.70 the decrease is not very drastic. Also the density and the leach rates are not much affected by the higher Na content. Hence product glass with SiO_2/Na_2O mole ratio 1.75 can be considered for vitrification operation so as to increase the waste loading.

Acknowledgement

The authors are grateful to Dr. J.G Shah, NRG BARC Mumbai for XRD scans of the samples. Authors are thankful to Shri. Y. Kulkarni, Chief Supdt. TNRPO, NRB Tarapur, for his guidance and support.

References

[1] M. I. Ojovan and O. K. Karlina, Radiochim. Acta 34 (1992) 97.

[2] K.Raj, K.K.Prasad, N.K.Bansal, Nucl. Engg. Design, 236 (2006).

[3] De Vaishali, Sah R.K, Mishra P.K., Sonar N.L., Valsala T.P. and Sonavane M.S, THERMANS-2008, (2008), 398.

[4] G. H. Jeffery, J. Bassett, J. Mendham, R. C. Denney, "Vogel's Text book of quantitative chemical analysis", Fifth edition.

[5] Hanawalt et al., Anal. Chem., 10, (1938) 475 (PDF # 01-0927).

[6] W.J.Dell, P.J. Bray, S.Z.Xiao, Journal of non crystalline solids, 58 (1983) 1.

Single Vial Kit Formulation for Preparation of ^{68}Ga-AMBA : A PET Imaging Agent for Prostate Cancers

Usha Pandey[1], Archana Mukherjee[1], Naresh Gamre[1], Haladhar Dev Sarma[2], Ashutosh Dash[1,*]

1. *Isotope Applications & Radiopharmaceuticals Division, Bhabha Atomic Research Centre, Mumbai 400085, India*
2. *Radiation Biology and Health Sciences Division, Bhabha Atomic Research Centre, Mumbai 400085, India; E-mail: adash@barc.gov.in*

This work was aimed at the kit formulation of a bombesin analog, AMBA, for potential use in imaging of prostate cancers after ^{68}Ga labeling. Towards this aim, a kit was formulated in acetate buffer under aseptic conditions for labeling with ^{68}Ga eluted from the nanoceria-PAN based ^{68}Ge/^{68}Ga BARC generator. All the reaction parameters for optimum radiolabeling were standardized and the radiometal complexes were characterized by chromatography techniques. The kit formulations gave >95% radiolabeling yields consistently when tested up to two months. Pharmacokinetics of the radiolabeled peptide was studied in Swiss mice, which showed fast clearance of activity via renal route.

Introduction

Gallium-68, a positron emitter has gained significant attention from research and clinical communities in recent times due to its advantages such as availability from ^{68}Ge/^{68}Ga generator system and a convenient half life of 68 minutes. The availability from a generator system completely eliminates the need for an on-site cyclotron while the short half matches excellently with the pharmacokinetics of many peptides used clinically for imaging. $^{68}Ga^{+3}$ can form complexes with ligands having oxygen and nitrogen as donor atoms thereby making it possible to radiolabel biomolecules conjugated with suitable chelating ligands. Currently, automated modules are commercially available for routine preparation of ^{68}Ga labeled peptides for imaging purposes. However, for wider application of ^{68}Ga radiopharmaceuticals, it would be preferable to formulate the peptides in ready to use kit form to be used with ^{68}Ga eluted from generator systems.

Cancers of the prostate express receptors for the peptide bombesin. A bombesin analog AMBA (DOTA-glycyl-4 aminobenzoyl BN [7-14]) has shown promising results in clinical trials for prostate cancer imaging [1]. The objective of this work was to formulate lyophilized, ready to use AMBA kits to be used with ^{68}Ga eluted from the novel ^{68}Ge/^{68}Ga BARC generator which uses nanoceria-PAN as adsorbent [2].

Experimental

Prior to kit formulation, experiments were carried out for optimization of radiolabeling with the generator eluted ^{68}Ga by varying the reaction conditions such as concentration of peptide, ^{68}Ga activity, temperature and time. Subsequently, the peptide AMBA was formulated as a ready to use kit in sodium acetate buffer employing aseptic conditions, freeze dried and was tested for sterility and absence of pyrogens. Dilute HCl (0.1 N) for elution of ^{68}Ga from the generator was also prepared aseptically and provided along with the kit. For radiolabeling, ^{68}Ga (in 0.1 N HCl) from the in-house ^{68}Ge/^{68}Ga BARC generator was eluted directly into kit vial containing 50 g of the peptide. The reaction was allowed to proceed at 90°C for 10 minutes. Percentage radiochemical yield was estimated by HPLC (C18 Reverse phase column using a gradient elution of water and aceotonitrile containing 0.1% trifluoro acetic acid) and paper chromatography in 50% acetonitrile in water.

Stability of ^{68}Ga-AMBA was studied both in human serum as well as in saline. Long term stability of the kits was tested by radiolabeling with ^{68}Ga at periodic intervals up to two months. Biodistribution studies were carried out in normal Swiss mice to determine the pharmacokinetic pattern of ^{68}Ga-AMBA in small animals.

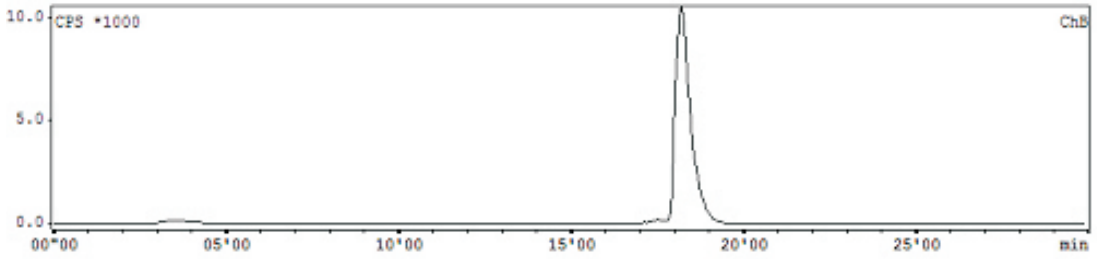


Fig. 1 HPLC radiochromatograph of ^{68}Ga-AMBA conjugate

Results and Discussion

Greater than 95% radiochemical yields of ^{68}Ga-AMBA could be obtained under optimized conditions using ^{68}Ga eluted from the ^{68}Ge/^{68}Ga BARC generator. The radiolabeled peptide had a retention time of 18.1 minutes in the standardized HPLC system while free gallium under the same conditions had a retention time of 3.3 minutes. The formulated peptide kits passed sterility and apyrogenicity tests as per pharmacopeia. The radiolabeled peptide was stable in saline and human serum up to 2 h (period of study). The kit vials exhibited consistently good ^{68}Ga radiolabeling yields (>95%) when tested up to two months. Biodistribution studies in Swiss mice revealed fast clearance of activity via renal route.

Table 1: Biodistribution data of ^{68}Ga-AMBA conjugate in Swiss mice

Organ/Tissues	30min	1h
Blood	4.91 (1.1)	1.25 (0.5)
Liver	3.51 (0.5)	1.37 (0.9)
Int+ GB	5.13 (1.1)	3.36 (1.1)
Stomach	2.42 (2.2)	0.86 (0.7)
Heart	1.32 (0.2	0.0
Lungs	4.58 (0.3)	0.12 (0.1)
Spleen	0.0	0.0
bone	0.0	0.0
Muscle	0.41 (0.2)	0.3 (0.1)
Kidneys	41.96 (15.0)	10.43 (5.4)
Excreta	35.75 (5.3)	82.30 (6.0)

Conclusions

Single vial kit of the peptide AMBA could be successfully formulated for the preparation of ^{68}Ga-AMBA for possible use in molecular imaging of prostate cancers. The availability of such ready to use kit formulations along with the ^{68}Ge/^{68}Ga generator systems would pave way for wider clinical utilization of the radioisotope ^{68}Ga.

Acknowledgements

The authors are thankful to Dr. Gursharan Singh, Associate Director (I) and Head, IA&RPhD, RC&I group, BARC for his support. Thanks are also due to Dr. (Smt.) Grace Samuel, Head, RPES, IA&RPhD for the help provided for the work.

References

[1] D. L. Smith, W. A. P. Breeman, J. Sims-Mourtada. Appl. Radiat. Isot. 76 (2013) 14.

[2] R. Chakravarty, R. Shukla, R. Ram, M. Venkatesh, A. Dash, A. K. Tyagi. ACS Appl. Mater. Interfaces. 2 (2010) 2069.

Coincidence Summing Corrections for a Clover Detector

Chhavi Agarwal[1], Laxman S. Danu[2], A. Goswami[1] and D.C. Biswas[2]

1. *Radiochemistry Division, Bhabha Atomic Research Centre, Trombay, Mumbai 400085, India; E-mail: agoswami|@barc.gov.in*
2. *Nuclear Physics Division, Bhabha Atomic Research Centre, Trombay, Mumbai 400085, India*

The true coincidence summing effect on the full energy peak efficiency calibration of a clover detector has been determined using mono-energetic and multi-energetic gamma ray sources. The effect has been studied as a function of sample to detector distance for point sources. At distances, d=3.2 cm and 10.2 cm, significant deviation of the efficiencies corresponding to gamma rays of coincident sources (^{60}Co, ^{152}Eu and ^{133}Ba) from the extrapolated efficiencies of mono-energetic sources (^{109}Cd, ^{57}Co, ^{203}Hg, ^{51}Cr, ^{137}Cs, ^{65}Zn) at the respective energies was observed, indicating the effect of coincidence summing. The coincidence summing factors (k_{TCS}) at these energies have been experimentally obtained by taking the ratio of corresponding mono-energetic extrapolated efficiencies to multi-energetic efficiencies. Coincidence correction factors as high as 1.25 has been obtained.

Introduction

In gamma ray spectrometry, true coincidence summing takes place when two or more cascade gamma rays (or a gamma ray and an X-ray) which are emitted in cascade with each other, are detected within the resolving time of the detector. This will lead to inaccurate peak areas leading to erroneous results in quantitative estimation of activity of radionuclides. The extent of coincidence summing depends upon the probability that two gamma rays emitted simultaneously will be detected simultaneously [1, 2]. Therefore, these effects are independent of count rate of the source and depend solely on the emission probabilities and detection efficiencies of the cascade gamma rays. The magnitudes of these corrections become significant at close sample-to-detector distances owing to a greater probability of two gamma rays reaching the detector simultaneously. These corrections become particularly important for environmental or other low activity samples where one needs to count the sample as close as possible to the detector.

In our earlier work, coincidence summing factors were obtained experimentally and theoretically for a co-axial HPGe detector [3]. The coincidence summing effect also becomes a serious problem for high efficiency detectors such as Clover and well type detectors. In the present work, the effect of coincidence summing on the full energy peak (FEP) efficiency of a clover detector has been studied at different sample-to-detector distances (d=3.2, 10.2 cm). A set of standard point sources of ^{60}Co, ^{109}Cd, ^{57}Co, ^{203}Hg, ^{51}Cr, ^{137}Cs, ^{65}Zn, ^{152}Eu and ^{133}Ba have been used for the study. The experimental coincidence correction factors have been obtained by taking the ratio of the corresponding extrapolated mono-energetic efficiency to the multi-energetic efficiency.

Experimental

In this study, a clover detector consisting of four co-axial n-type Ge diodes of 50 mm diameter and 60 mm length mounted in a common cryostat was used. The total active volume of the detector was 470 cm^3 and corresponds to 89% of the original Ge volume [4]. The detector was first calibrated for its efficiency by counting point sources of standard ^{133}Ba and ^{152}Eu at 25.4 cm from the detector end cap. Such a large distance was chosen for efficiency calibration with these multi gamma sources so as to avoid any uncertainty in the efficiency curve due to coincidence summing. The Eu-Ba efficiencies were fitted into a fourth order log-log polynomial curve by non linear least square fitting. The efficiencies at d = 25.4 cm were then used to obtain disintegration rates (dps) of point sources of ^{109}Cd, ^{57}Co, ^{203}Hg, ^{51}Cr, ^{137}Cs, ^{65}Zn and ^{60}Co prepared from the activities procured from Board of Radiation and Isotope Technology, Mumbai. Once calibrated, the mono-energetic sources were then counted at closer distances (d = 3.2 and 10.2 cm) to obtain FEP efficiencies ( ) as given by:

$$\frac{cps}{I \; x\, dps} \qquad (1)$$

where cps is the count rate at the energy of interest and I is the gamma ray emission probabilities taken from Table of Isotopes [5].

Results and Discussion

Figure 1 and 2 shows the experimental efficiencies of ^{152}Eu, ^{133}Ba, ^{60}Co, ^{109}Cd, ^{57}Co, ^{203}Hg, ^{51}Cr, ^{137}Cs and ^{65}Zn at d = 10.2 cm and 3.2 cm respectively. The efficiencies determined from noncoincident sources like ^{137}Cs, ^{109}Cd, ^{57}Co, ^{203}Hg, ^{51}Cr, ^{65}Zn have been fitted to a fourth order log-log polynomial at both the distances to obtain efficiency curve which is free of coincidence summing. In absence of any coincidence summing of gamma rays, efficiencies of mono-energetic and multi-energetic sources are expected to fall on a single curve. As seen from Fig. 1, at 10.2 cm distance, the efficiencies obtained from the multi-gamma ray sources show slight deviation from the mono-energetic efficiency curve.

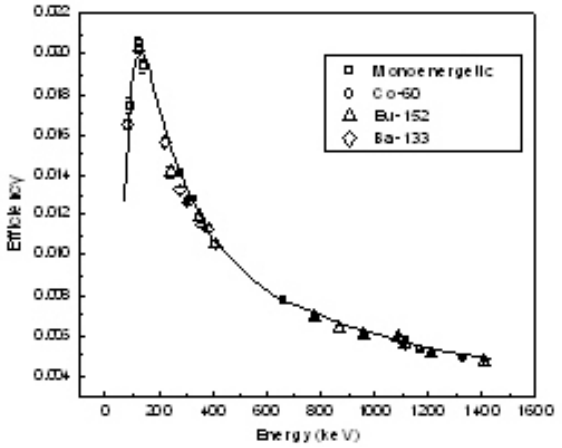


Fig. 1 Efficiencies as a function of gamma ray energy for point source geometry at sample to detector distance of 10.2 cm

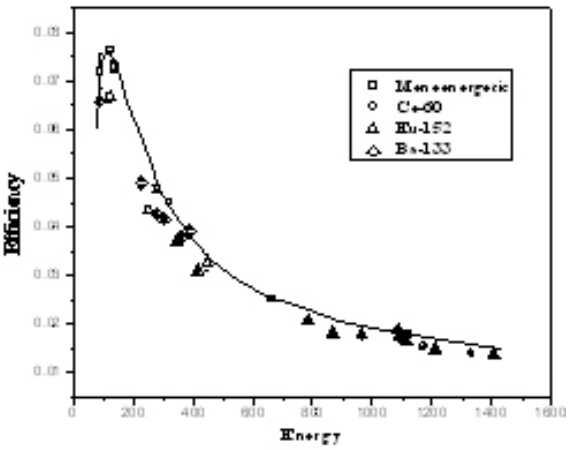


Fig. 2 Efficiencies as a function of gamma ray energy for point source geometry at sample to detector distance of 3.2 cm

This shows, that at this distance, the coincidence summing corrections are small.

However, at d=3.2 cm, significant deviation between the multi-energetic source efficiency and the monoenergetic efficiency curve is seen (Fig. 2). This shows the true coincidence summing corrections are very important at this distance. The true coincidence summing factors ($k_{TCS}(E)$) were experimentally obtained using the ratio of extrapolated mono-energetic efficiency at the respective energy to the corresponding multi-energetic efficiency, as given by:

$$k_{TCS}(E) \quad \frac{\text{Monoenergetic efficiency (E)}}{\text{Multienergetic efficiency (E)}} \qquad (2)$$

where, E represents the energy at which coincidence summing correction factor is determined. The experimental correction factors as high as 1.25 at d = 3.2 cm and 1.10 at d = 10.2 cm were obtained showing the importance of coincidence summing corrections to get reliable results from clover detector.

Conclusion

The present study shows that coincidence summing correction can be very important for high efficiency detectors such as clover detectors when the sample is counted even at 10 cm distance from the detector.

References

[1] K. Debertin, R.G.Helmer, Gamma and X-ray spectrometry with semiconductor detectors, North Holland (1998).

[2] G. Gilmore and J.D. Hemingway, Practical Gamma Ray Spectrometry, John Wiley & Sons, ISBN 0471 951 501 (1995),

[3] C. Agarwal, S. Chaudhury, A. Goswami and M. Gathibandhe, Journal of Radioanalytical and Nuclear Chemistry 289(2011) 773.

[4] G. Duchene, F.A. Beck, P.J.Twin, G. de France, D. Curien, L. Han, C.W. Beausang, M.A. Bentley, P.J. Nolan and J. Simpson, Nuclear Instruments and Methods in Physics Research A 432 (1999)90.

[5] R.B. Firestone Table of Isotopes, Wiley-Interscience Publishing, Eighth Edition (1996).

Synthesis and Evaluation of a Phenylbenzothiazole-based $^{99m}Tc(CO)_3$- Radiotracer for Possible Application in imaging -amyloid Plaque

Drishty Satpati, Aruna Korde, Sharmila Banerjee

Isotope Applications & Radiopharmaceuticals Division, Bhabha Atomic Research Centre, Trombay, Mumbai 400085, India; E-mail: sharmila@barc.gov.in

Radiopharmaceuticals targeting amyloid beta (A) deposits in brain are useful in early diagnosis of Alzheimer's disease and monitoring the effectiveness of therapeutic treatments. Hence benzothiazole known to have high affinity for A has been derivatized in order to introduce pyridine and amino acetic acid moiety for radiolabeling with $[^{99m}Tc(CO)_3(H_2O)_3]^+$ precursor. The radiotracer, $^{99m}Tc(CO)_3$-BTPAMA was tested for in vitro stability, serum stability and stability towards exchange with other ligands (histidine and cysteine). In vivo biodistribution studies to determine the pharmacokinetics and ability of the radiotracer to cross the blood brain barrier were carried out in normal Swiss mice. The radiotracer prepared in >95% radiochemical yield was found to be stable in vitro for 6 hours as well as in serum and in presence of other ligands as determined by HPLC. Biodistribution studies in normal Swiss mice showed brain uptake of 0.25±0.04% ID/g at 2 min p.i, indicating the ability of the radiotracer to cross the blood brain barrier.

Introduction

The formation of -amyloid (A) plaques in brain is a characteristic feature of Alzheimer's disease (AD) [1,2]. In vivo visualization of A plaques using radiolabeled molecular probes can help in early diagnosis of AD and monitor the efficacy of anti-amyloid therapy [3]. In the present report, 2-(4′-aminophenyl)-1,3-benzothiazole has been synthesized and subsequently derivatized to introduce a suitable chelating agent for complexation with $[^{99m}Tc(CO)_3(H_2O)_3]^+$ precursor. The in vitro stability of the radiotracer, $^{99m}Tc(CO)_3$-BTPAMA as well as its potential for possible application in amyloid imaging of patients suffering from Alzheimer's disease has been evaluated in vivo. The results demonstrate its ability to cross the blood brain barrier.

Experimental

2-(4′-aminophenyl)-1,3-benzothiazole (BT) was synthesized in one step and further derivatized in order to introduce the picolylamine monoacetic acid (PAMA) chelator in three steps as shown in Fig. 1. The ligand was characterized by NMR and mass spectrometry.

For radiolabeling, BTPAMA (100 g) was added to $[^{99m}Tc(CO)_3(H_2O)_3]^+$ precursor (prepared using Isolink® kit) and incubated at pH 7, 70ºC for 20 min. The lipophilicity of the complex was studied using solvent extraction in octanol and saline. In vitro stability of the complex was assessed by incubation in phosphate buffer saline (PBS) at 37<C, pH 7.0 for 6 hours and monitoring the HPLC elution profile. Serum stability studies were carried out by incubation of the radiolabeled complex (0.2 mL) with human serum (1 mL) at 37 C for 1 h. Proteins were precipitated by addition of acetonitrile (1 mL) and the supernatant was injected in HPLC to determine the serum stability of the complex. Stability towards exchange with other ligands was studied by incubation of the complex (0.1 mL) with histidine and cysteine solution (10 L, 0.5 M) in distilled water at 37°C for 1 h. The mixture was analyzed by HPLC to determine the extent of exchange, if any. In vivo biodistribution studies of $^{99m}Tc(CO)_3$-complex were carried out in normal Swiss mice at 2 min, 60 min and 120 min p.i. to assess the pharmacokinetics and ability to cross the blood brain barrier.

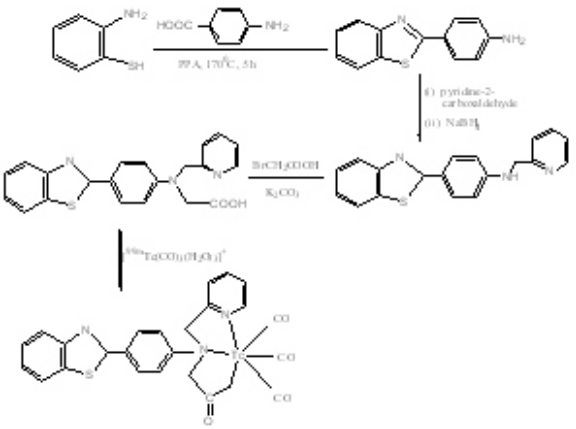


Fig. 1 Synthesis of 2-(4′-aminophenyl)-1,3-benzothiazole derivative

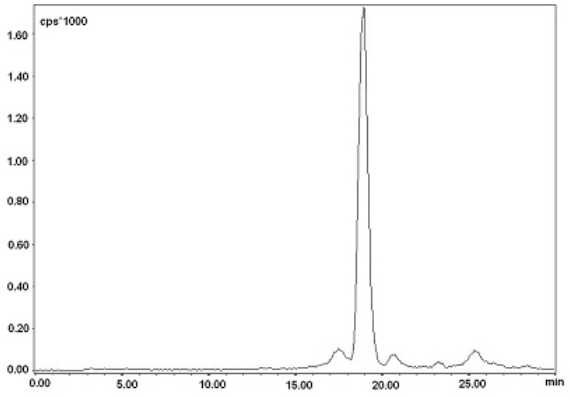


Fig. 2 HPLC pattern of $^{99m}Tc(CO)_3$-BTPAMA complex

Results and Discussion

The picolylamine monoacetic acid derivative of 2-(4´-aminophenyl)-1,3-benzothiazole (BTPAMA), containing NNO as coordinating atoms was synthesized for complexation with $[^{99m}Tc(CO)_3(H_2O)_3]^+$ precursor. The radiotracer, $^{99m}Tc(CO)_3$-BTPAMA was prepared in >95% radiochemical yield (RCY), as determined by HPLC. Retention time of $[^{99m}Tc(CO)_3(H_2O)_3]^+$ precursor in HPLC was 13.7 min whereas that of the radiolabeled complex was 19 min. (Fig. 2) Log $P_{o/w}$ was found to be 1.03±0.01 which is within the optimal range (log P = 1-3) of agents known to exhibit passive diffusion through the blood brain barrier (BBB). Incubation of $^{99m}Tc(CO)_3$-complex with PBS, human serum or excess amount of histidine and cysteine did not lead to alterations in the retention time and pattern of the peak obtained in HPLC system. The results indicate stability of the complex in reaction mixture for at least 6 hours, kinetic inertness and stability towards transchelation respectively. In vivo distribution studies in normal Swiss mice (Table 1) with no amyloid deposits showed brain uptake of 0.25±0.04% ID/g at 2 min p.i. that reduced to 0.11±0.01% ID/g at 1 h p.i. The lower uptake in brain may be attributed to high molecular weight of the radiotracer (555 g/mol). The radioactivity was excreted via renal as well as hepatobiliary route. Brain uptake in normal mice was low but there is a possibility of increase in the retention of radioactivity in AD mice brain where binding with amyloid plaques is anticipated.

Conclusion

The current radiotracer has shown the ability to cross the blood brain barrier. However, the pharmacokinetic properties were not favorable with low brain uptake and high retention of radioactivity in blood, liver and kidneys, thereby limiting its applicability in imaging studies. A possible reason which could be considered is that introduction of the bulky chelating moiety may have adversely affected the pharmacokinetics of the radiotracer. The results provide insight towards designing a radiotracer with a smaller chelating group and intercepted by a suitable spacer from the phenylbenzothiazole pharmacophore.

Table-1: Biodistribution studies of $^{99m}Tc(CO)_3$-BTPAMA complex in Swiss mice (%ID/g) (n=4)

Organ	2 min	1 h	2 h
Blood	10.1±1.5	8.5±1.2	4.2±0.2
Liver	20.9±3.6	23.2±0.8	21.3±1.0
Kidney	29±1.2	39.6±2.6	28.1±4.5
Intestine	6.1±1.8	9.7±1.5	9.8±1.2
Stomach	0.8±0.0	1.2±0.9	1.2±0.3
Heart	3.8±0.07	2.8±0.3	3.0±0.2
Lungs	1.9±0.8	0.5±0.1	0.3±0.05
Brain	0.25±0.0	0.11±0.0	0.19±0.0

Acknowledgements

Authors are thankful to Dr. Gursharan Singh, Associate Director (I), Radiochemistry and Isotope Group for his constant support and encouragement.

References

[1] C. A. Mathis, Y. Wang, W. E. Klunk, Curr. Pharm. Des. 10 (2004) 1469.

[2] J. Hardy, D. J. Selkoe, Science 297 (2002) 353.

[3] N. Okamura, S. Furumoto, H. Arai, R. Iwata, K. Yanai, Y. Kudo, Curr. Medical Imaging Rev. 4 (2008) 56.

[4] K. S. Lin, M. L. Debnath, C. A. Mathis, W. E. Klunk, Bioorg. Med. Chem. Lett. 19 (2009) 2258.

Quantification and Isotope Ratio Measurement of Boron in U_3Si_2 by Inductively Coupled Plasma Mass Spectrometry

Abhijit Saha[1], S.B. Deb[1], Papu Samanta[2], B.K. Nagar[1] and M.K. Saxena[1]

1. *Radioanalytical Chemistry Division, Bhabha Atomic Research Centre, Trombay, Mumbai 400 085, India; E-mail: saxenamk@barc.gov.in*
2. *Integral Fuel Fabrication Facility, Bhabha Atomic Research Centre, Trombay, Mumbai 400 085, India*

An analytical methodology was developed for precise quantification and isotope ratio measurement of boron in U_3Si_2 matrix by using ICP-MS after matrix separation. The analytical technique was validated by recovery studies employing standard addition method and the accuracy in isotope ratio measurement was improved by correcting the bias factor after analyzing NIST SRM951. The quantification of B in the three U_3Si_2 samples was found in the range of 2.32-3.90 g g^{-1} with a maximum standard deviation of 3%. The $^{10}B/^{11}B$ value in the three samples was found to be 0.2455±0.0042, 0.2451±0.0036 and 0.2452±0.0041.

Introduction

Internationally there has been a trend to convert the highly enriched uranium (HEU) based research reactors to low enriched uranium (LEU) one, owing to the concern about the proliferation associated with HEU. A direct consequence of this conversion process is the requirement of higher uranium density in the fuel core. For this the most widely accepted technical solution is the use of uranium silicide type fuels, especially U_3Si_2 dispersed in aluminum matrix [1]. U_3Si_2, performed extremely well under irradiation tests, even with uranium densities up to 5.0 Mg m^{-3} [2]. U_3Si_2 has 92.3 wt% U_{total} and 7.7% wt% Si. In India programs have been initiated to load the modified APSARA core with U_3Si_2 fuel dispersed in alumina matrix. Their use as nuclear fuel is subject to the conditions of strict conformation of the established specifications of trace impurities. The concentration of elements possessing high thermal neutron absorption cross section in U_3Si_2 is important from the stand point of neutron economy. The high neutron cross sections of boron make essential the determination of even traces of this element. Since the isotopic composition (IC) of natural boron varies by -30 to +60‰ [3] depending on the geological source, it becomes essential to determine its concentration along with IC in each fuel lot to arrive at total neutron poisoning effect of boron. There are numerous techniques [3-5] available for the quantification of trace amounts of boron but the use of highly sensitive ICP-MS has the advantage that in addition to the amount it has the capability to determine the IC of the elements. It is however necessary to dilute the dissolved solutions appropriately or separate the matrix prior to ICP-MS analysis for the accurate and precise quantification of trace impurities. Here we have developed an analytical technique to quantify traces of boron along with its IC in U_3Si_2, after matrix separation, by employing ICP-MS. The developed analytical technique was validated, for boron quantification, by standard addition method. The IC of boron was also determined in the solutions by ICP-MS. A NIST SRM951 certified reference material was used to correct for the bias factor to obtain the accurate value of $^{10}B/^{11}B$ ratio by ICP-MS.

Experimental

Instrumentation

An inductively coupled plasma orthogonal accelaration time of flight mass spectrometer (ICP-oa-TOF-MS), (GBC, Australia), was used for the determination and IC measurement of trace B in U_3Si_2 matrix. The mass analyser was calibrated for the mass range of 7-209 amu. The instrumental operating parameters of ICP-MS are the same as reported earlier [6].

Matrix Dissolution and Separation

The precise quantification of low Z elements like boron in uranium matrix by ICP-MS requires quantitative separation of matrices to minimize the matrix effect. In this work the matrix separation was carried out in two steps due to the presence of the diverse major elements. Firstly Si was removed during dissolution of the sample in concentrated HNO_3 under the IR lamp, by dropwise addition of HF till the solution becomes clear of SiF_4 fumes. The removal of Si as SiF_4 (b.p. -65°C) during the dissolution process also causes the loss of B as BF_3 (b.p. -101°C). Since it was reported that boron can be quantitatively retained in solution during HF addition as boron-manitol complex [7], a similar technique was employed in our case. A 1mL manitol solution of 100 mg L^{-1} was added to the sample solution prior to the HF addition. The resulting clear solution was then evaporated near to dryness and the process was repeated for 3-4 times by adding conc. HNO_3. Finally the sample was made upto an appropriate volume in 4M HNO_3. The purpose of this repeated evaporation process was to keep uranium as $UO_2(NO_3)_2$ and not as UO_2F_2. Thereafter U was separated by the conventional solvent extraction technique using three contacts with 30% TBP in CCl_4. The raffinate was then evaporated near to dryness and made up to an appropriate volume in a Nalgene

volumetric flask with 1% (v/v) HNO_3 and finally analysed by ICP-MS. In order to compensate the sensitivity variations under the plasma operating conditions Lithium (Li) was used as an internal standard.

Recovery Studies by Standard Addition Technique

In order to validate the adopted analytical technique standard addition was carried out in the vicinity of the matrix blank value. A 1000 mg L^{-1} standard solution of B was used for standard addition after appropriate dilution. The addition was carried out prior to the addition of HF and the process repeated in a similar way as discussed above.

Results and Discussion

The proposed matrix separation method is successful in complete removal of Si and lowers the Uranium concentration in the raffinate to < 5 g g^{-1}.The quantification of the boron was done by monitoring the ^{11}B isotope in mass spectrometer. The calibration plot was made by analyzing a range of boron standard solutions with a fixed Li concentration. The linear regression fit of $^{11}B/^{7}Lie$ intensity ratio vs. concentration of B results in r^2 = 0.999. Using this calibration plot the obtained recoveries of 96%, as given in Table 1, validates the adopted methodology. The effect of uranium, at <5 g g^{-1}, on boron quantification in the separated solutions were negligible as is demonstrated in the recoveries as given in Table 1, where the amount added and amount found were within the experimental uncertainties of ICP-MS at such trace level of analyis. For accurate IC measurements, a NIST SRM, with certified $^{10}B/^{11}B$ value of 0.2473 0.0002, was analysed on a daily basis to determine the bias factor on IC measurements. This factor was then applied to the IC value obtained for B in the sample. Three real U_3Si_2 samples were analysed for their boron concentration as well as IC and the results are presented in Table 2.

Conclusion

A simple and novel method was developed for the precise quantification as well as isotopic ratio measurement of B in U_3Si_2 by ICP-MS after matrix separation. Reproducible recoveries of 96% by standard addition validate the separation technique. Three real U_3Si_2 samples were analysed by the proposed method with an instrumental precision of 2-3%. The instrument and method detection limits were found to be 700 ng L^{-1} and 140 g kg^{-1}.

Table-1: Results of recovery studies employing ICP-MS (n=5)

Amount of B added (g g^{-1})	Amount of B found (g g^{-1})	Percentage recovery
0	2.55±0.07	-
0.5	3.03±0.06	96±2
1	3.52±0.08	97±2
2.5	5.00±0.12	98±2

Table-2: Results of analysis of three real U_3Si_2 sample (n=5)

Serial no.	Amount of B found (g g^{-1})	$^{10}B/^{11}B$
1	2.32±0.05	0.2455±0.0042
2	3.34±0.09	0.2451±0.0036
3	3.90±0.11	0.2452±0.0041

Acknowledgment

We are indebted to Dr. B.S.Tomar, Head, RACD, BARC and Dr. K.L. Ramakumar, Director, RC & IG, BARC for their support and encouragement.

References

[1] Y.S. Kim, J. Nucl. Mater., 410 (2011)1-9.

[2] F. Muhammad, Prog. in Nucl. Energy, 51 (2009) 141.

[3] E. Zolfonoun, Spectrochim. Acta Part B, 81 (2013) 64.

[4] R.N. Sah, Biol. Trace Elem. Res., 66 (1998) 39.

[5] A. Al-Ammar, Spectrochim. Acta Part B, 55 (2000) 1861.

[6] A. Saha, Atom. Spectrosc., 34 (4) (2013) 125.

[7] T. Ishikawa, Anal. Chem., 62 (1990) 2612.

Microwave Assisted Dissolution Followed by Characterization of XHM-1 alloy by Inductively Coupled Plasma Mass Spectrometry

S.B. Deb, B.K. Nagar, Abhijit Saha and M.K. Saxena*

Radioanalytical Chemistry Division, Bhabha Atomic Research Centre, Trombay, Mumbai 400 085, India; E-mail: saxenamk@barc.gov.in

XHM-1 alloy is considered to be a promising structural material for water cooled reactors. An analytical methodology was developed for its characterization of both the alloying and trace elements to support its Chemical Quality Control upon fabrication. A microwave digestion procedure was developed and optimized for its quantitative dissolution followed by chemical characterization employing ICP-MS. The alloying elements viz., Al, Cr, Ni, Ti, V and Fe were found to be within the expected range as reported in literature. Nine trace elements viz., Ce, Co, Cu, Mg, Mn, Mo, Pb, Ta, W and Zn were detected in the alloy and quantified.

Introduction

The XHM-1 alloy (Cr-Ni base alloy containing Mo additions) has been found to be a better structural material for water cooled nuclear power reactors compared to austenitic stainless steel because of the high irradiation and corrosion resistance of the former [1,2]. XHM-1 alloy is used as a spacer strip in Compact Light Water Reactor (CLWR) and is a promising cladding material for advanced reactors. With a view to fabricate it indigenously it is desirable to develop methodology for its characterization so as to account for the alloying as well as the trace metallic elements after its fabrication. Although direct solid multielemental analytical techniques like LAICP-MS [3], XRF [4], GDMS [5], etc are available for direct quantification of major, minor and trace elements in refractory solids but they are limited in this case by the absence of matrix matched certified reference materials (CRMs). Consequently it becomes essential to dissolve the matrix and bring the constituents into solution form for their accurate and precise quantification. Initial attempts to dissolve the refractory alloy by conventional acid mixtures were not successful and subsequently a microwave dissolution procedure was developed and optimized for its quantitative dissolution. The alloying as well as the trace metallic elements in the matrix were then quantified by an inductively coupled plasma orthogonal acceleration mass spectrometer (ICP-oa-TOF-MS).

Experimental

An Anton Par Multiwave 3000 microwave digestion system with 8x rotor was used for dissolution of XHM-1 alloy material. Various operating parameters of microwave digestion system were optimized for quantitative dissolution of the alloy. The digestion was carried out by taking about 100 mg of the alloy, 6 mL HNO_3, 2 mL HF and 2 mL of $HClO_4$ with 800W power, 5 min. ramp and 45 min. hold time. The solution was then evaporated near to dryness and then diluted on weight basis to the desired volume with 1% HNO_3. The resulting final solution was then analysed by ICP-oa-TOF-MS (GBC, 8000R). The mass analyser was calibrated for the mass range of 7-209 amu. The instrumental operating parameters of ICP-MS are the same as reported earlier [6].

Results and Discussion

The refractory nature of XHM-1 makes its dissolution difficult, and till date there is no report dealing with such work. We had used the microwave digestion system for this purpose. The refractory nature of the alloy could be due to the passive layer of Cr_2O_3, which requires a corrosive combination of acids for its dissolution. A mixture of HNO_3, HF and $HClO_4$ were consequently used and the optimized quantity of the acids were arrived at by taking different combinations of each as given in Table 1 keeping the hold time, power and ramp constant at 60 mins, 800 W, and 5 mins respectively. Thereafter the time of digestion was optimized as shown in Table 2. There was a need to dilute the resulting solutions to different extents for the quantification of alloying and trace elements by ICP-MS. In order to compensate for the sensitivity variations, known amounts of internal standard were deliberately added to the samples prior to their dissolution. The instrument has an inbuilt smartgate [7] which was utilized for blanking the mass peaks of matrix while quantifying trace elements.

The elements were subdivided into two categories according to their atomic masses for selecting the appropriate internal standard. Scandium was chosen as an internal standard for the first category which includes the low Z elements viz., Al, Cr, Co, Cu, Fe, Mg, Mn Ni, Ti, V and Zn and indium for the second category which includes the high Z elements viz., Ce, Mo, Pb, Ta and W. Such categorization of elements results in the exact quantification by correcting the sensitivity variations of the analytes in the plasma. Finally the concentrations of the interested analytes in the solution were calculated using the following formula:

$$C_{A\,(actual)} = C_{A(found)} \times (C_{IS(expected)}/C_{IS(found)})$$

where C_A and C_{IS} are analyte and internal standard concentrations respectively.

The analyte and internal standard concentrations were obtained from the individual calibration plots with r^2 0.999. The results of the mass spectrometric analysis for alloying and trace elements are represented in Table 3 and 4. The composition of the alloy, as determined by this method, with respect to alloying elements was within the expected range as reported in literature [1].

Table-1: Optimization of acid combination for microwave digestion of XHM-1 alloy (Power = 800W, Ramp = 5 min, Hold time = 60 min)

Sample amount	Amount of acids (mL)			Completely dissolved
	HNO_3	$HClO_4$	HF	
~ 100 mg	8	1	1	No
	7	1.5	1.5	No
	6	2	2	Yes

Table-2: Optimization of hold time for microwave digestion of XHM-1 alloy (Sample amount ~ 100 mg)

Amount of acids	Power (W)	Ramp (min)	Hold time (min)	Completely dissolved
6 mL HNO_3 + 2mL HF + 2 ml $HClO_4$	800	5	60	Yes
			45	Yes
			30	No

Table-3: Analysis of alloying elements in XHM-1 alloy (n=10)

Element	Expected range (in %)	Amount found (in %)
Ni	Balance	56.8 1.1
Cr	40-44[a]	40.6±0.8
Mo	1-1.5[a]	1.05±0.02
Fe	0.3[b]	0.22±0.01
V	——	0.16±0.01
Al	0.2[b]	0.12±0.01
Ti	0.25[b]	0.11±0.01

[a]reported in literature (Ref. 1), [b] not reported in literature but expected values are given

Table-4: Analysis of trace elements in XHM-1alloy (n=10)

Element	Amount found (g g^{-1})
Ce	20±2
Co	590±20
Cu	45±4
Mg	160±10
Mn	65±5
Pb	270 0
Ta	450 0
W	90
Zn	710 0

Conclusion

An optimized microwave digestion procedure, for the dissolution of highly refractory XHM-1 alloy, was developed for the first time. The six alloying elements and nine trace metallic elements were precisely quantified by internal standard method using ICP-MS. The standard deviations (1) in the measurement of alloying and trace elements were found to lie in the range of 2-9% and 3-10% respectively.

Acknowledgment

We are indebted to Dr. B.S.Tomar, Head, RACD, BARC and Dr. K.L. Ramakumar, Director, RC & IG, BARC for their support and encouragement.

References

[1] M.I. Solonin, J. Nucl. Mater., 258-263 (1998) 1762.

[2] M.I. Solonin, J. Nucl. Mater., 233-237 (1996) 586.

[3] Y. Zhu, J. Anal. At. Spectrom., 28(2) (2013) 310.

[4] C. Degueldre Talanta, 115 (2013) 986.

[5] Robertson-Honecker, J. Anal. At. Spectrom., 23(11), (2008) 1508.

[6] A. Saha, Atom. Spectrosc., 34 (4) (2013) 125.

[7] R.E. Sturgeon, J. Anal. Atom. Spectrom., 15 (2000) 607.

Determination of Nitrate in Effluents from Uranium Extraction Plant

Ayushi Dudwadkar, Sangita D. Kumar and A.V.R. Reddy

Analytical Chemistry Division, Bhabha Atomic Research Centre, Mumbai 400085, India;
E-mail: ayushi@barc.gov.in

Determination of nitrate concentration in the effluent samples from Uranium Extraction Plant is required before its safe discharge. As the different streams are diluted with sea water these samples contain high concentration of chloride. The large concentration of chloride poses a challenge in the determination of nitrate; hence, matrix elimination is accomplished by adopting a sample pretreatment technique. The present study was carried out to develop a simple, accurate and rapid analytical methodology for the determination of nitrate in the above matrices. The quantitative determination of nitrate was accomplished using anion exchange chromatography with conductometric detection.

Introduction

During uranium metal production; large quantity of effluent is generated which contains high concentration of ammonium nitrate (45-50 g L^{-1}). These effluents need to be monitored for nitrate before their safe discharge. The maximum limit for nitrate concentration in drinking waters is 50 g mL^{-1} and 45 g mL^{-1} recommended by WHO and Bureau of Indian standards respectively [1,2]. Hence determination of nitrate concentration level in water is important.

Several analytical methods like colorimetry, ion selective electrode (ISE) and ion chromatography are used for the analysis of nitrate in various samples [3,4]. Ion chromatography is useful for separation and quantitative determination of trace quantities of the ions in the presence of large amounts of similar ions or matrix [5]. A simple, accurate and rapid analytical methodology for the determination of nitrate has been developed.

Experimental

Reagents

All reagents were of analytical grade and obtained from Sarabhai M. Chemicals, Baroda, India. The working standard and spiking solutions were prepared by dissolving sodium salt in 18 M demonized water (Barnstead, Boston, MA, USA).

Instrumentation

The ion chromatographic instrument Dionex 5000 system consisting of a Pump unit SP-5, IC Separation Centre, ASRS300 Suppressor with IC conductivity detector DC-5 was used for the analysis. Anion separation was carried out in suppressor mode on AS11-HC anion exchange analytical column (4 mm X 250 mm) connected in series with a AG11-HC guard column (4 mm x 20 mm). The mobile phase was a solution of 35 mM NaOH with a flow rate of 1.0 mL min^{-1}. The column temperature was 30°C and suppressor current was 112 mA. The optimum resolution and elution time for different anions were found under these conditions. The volume of the sample injection loop was 25 L.

Experimental

All samples were diluted using deionised water (18 M , Barnstead, Boston, MA, USA). The sample solutions were filtered using a Millipore filter assembly.

Pretreatment Procedure

Diluted sample solutions (50 fold) were passed through Dionex OnGuard-Ag and OnGuard-H columns connected in series. H-guard cartridges have exchange capacity of 2.0 to 2.5 meq /cartridge on water swollen basis while Ag-cartridge can be used for treating 9 mL of 1% sodium chloride solution. Both the columns are stable over pH range of 0-14.

Results and Discussion

The effluent samples were collected from the discharge point in sea, at south site, BARC. Direct determination of nitrate using ion selective electrode could not be done because of sea water chloride content in these samples was about 20 x 10^3 mgL^{-1}. Hence there was a high interference from matrix in the determination of nitrate using ISE. In the present work an ion chromatographic method was developed for the determination of nitrate in effluent. A single step sample pretreatment procedure was adopted to eliminate the chloride and cations, interference. For this the commercially available OnGuard-Ag cartridge was used. The cartridge contains a high capacity, strong acid cation exchange resin in silver form. It removes chloride anions by precipitation. When an aliquot of effluent solution was passed through the OnGuard-Ag cartridge the sodium ions exchange with Ag ions and remain in the column while the chloride was precipitated within the cartridge as AgCl by the following reaction:

R-Ag + NaCl R-Na+ AgCl

This solution emerging out of the cartridge is passed through OnGuard-H cartridge to remove the

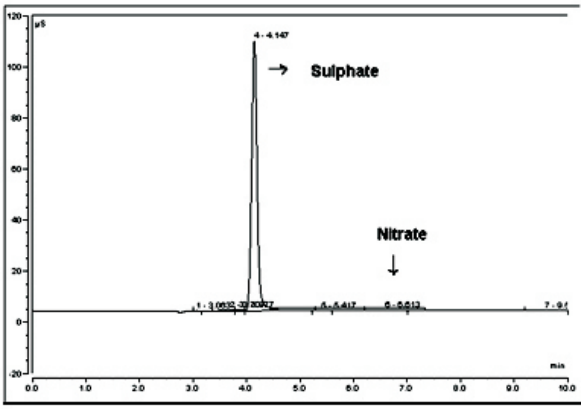


Fig 1a Chromatogram showing sulphate and nitrate peaks in the effluent sample

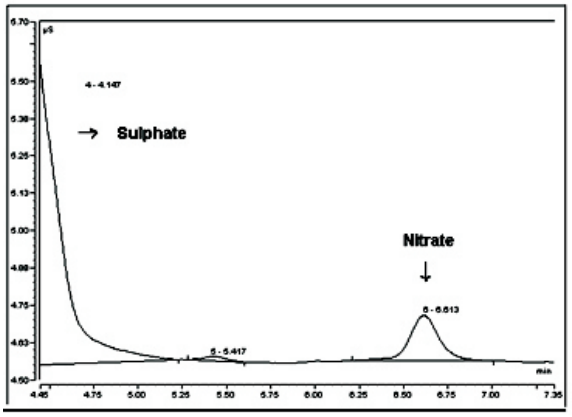


Fig. 1b Chromatogram showing zoom nitrate peak in the effluent sample

transition metal ions/ uranium from the effluent by the following reaction:

$$R–SO_3H^+ + M^{+n}(NO_3)_n \quad (R–SO_3)_{nM}^{+n} + nHNO$$

Thus the cartridge was useful to remove the heavy metal ions quantitatively provided that the concentrations of the ions were below the total capacity of the packing material of the cartridge. The anion identified in the treated samples was nitrate based on comparisons with that of standard anion mixture (Fig.1)

A linear calibration plot was obtained for standard nitrate solutions in the range of 06-2.0 g mL^{-1}. The limit of detection LOD and the limit of quantification LOQ were 0.02 and 0.06 g mL^{-1} respectively for nitrate anions. The relative standard deviation was 5% for the overall method. The nitrate content in the nitrate bearing effluent is as given in Table 1.

Table 1: Nitrate concentration in various samples

Sample	Nitrate mgL^{-1}
Effluent 1	12.5 0.6
Effluent 2	22.4 1.1
Effluent 3	12.3 0.6

Conclusion

The ion chromatography technique was applied to determine nitrate in the presence of high concentration of chloride in effluent generated during uranyl nitrate production. The studies established that the concentration of nitrate is below the safe discharge limit.

Acknowledgement

Effluents solutions were received from Uranium Extraction Division, BARC. Authors are thankful to Ms Niyoti Shenoy, Analytical chemistry Division, Bhabha Atomic Research Centre, for the ISE studies.

References

[1] World Health Organisation Guidelines for Drinking-Water Quality, Nitrates and nitrites in drinking water (2004) WHO/SDE/WSH/04.08/56.

[2] Bureau of Indian Standards (BIS) Draft Indian Standard drinking water specification (Second Revision of IS 10500), (2009) Doc: FAD 25(2047) C.

[3] A. Dudwadkar, N. Shenoy, J. M. Joshi, S. D. Kumar, H. Rao and A.V.R.Reddy, Sep. Sci.Technol 48 (2013) 1.

[4] Ayushi D., Arijit Sengupta, Sangita D. Kumar, A.G. Kumbhar and G. Venkateswaran, Int. J. Anal. Chem. (2011) Article ID 813061.

[5] Ayushi, Sangita D. Kumar and A.V.R.Reddy, J. Chromatogr. Sci., 50 (2012) 81.

Spectral Interference of Zirconium on 24 Analyte Elements using CCD based ICP-AES Technique

V.C. Adya, Arijit Sengupta and S.V.Godbole

Radiochemistry Division, Bhabha Atomic Research Centre, Trombay, Mumbai 400085, India;
E-mail: vcadya@barc.tgov.in

In the present studies, the spectral interference of zirconium on different analytical lines of 24 critical analytes using CCD based ICP-AES technique is described. Suitable analytical lines for zirconium were identified along with their detection limits. The sensitivity and the detection limits of analytical channels for different elements in presence of Zr matrix were calculated. Subsequently analytical lines with least interference from Zr and better detection limits were selected for their determinations.

Introduction

Trace metallic impurity analysis is one of the prime steps of chemical quality control of nuclear fuels and associated materials. To achieve the desired burn-up, successful life span of the fuel in the reactor and successful running of the reactor, it is required to have stringent physical and chemical quality control and quality assurance measures of nuclear fuels and associated materials. Atomic emission spectroscopic technique being simultaneous, multi-elemental one, has acceptable analytical performance viz. detection limits, sensitivity, linear dynamic range etc., is regularly used for determination of trace metallic analytes in nuclear fuels and associated materials. Zirconium is world-wide accepted as cladding material in nuclear industry due to its low thermal neutron absorption cross section. U-Zr, U-Pu-Zr, Zr-Nb etc binary and ternary alloy materials are also gaining importance as nuclear fuels and associated materials in nuclear industries. So there is a need of developing a method for the determination of trace constituents in Zr matrix. Due to its line rich emission spectra, presence of Zr even at trace levels, can lead to the over estimation of analytes due to the spectral interferences. For the determination of trace metallic constituents, either it has to be separated physically from the trace metals using d.c. arc carrier distillation technique or chemical separation followed by ICP-AES analysis of the raffinate . In our previous studies, we have reported the spectral interference of Am, Pu and U on other analytes using ICP-AES technique [1, 2, 3, 4]. In the present study, a method was developed for the determination of Ag, Al B, Cd, Ca, Co, Cr, Cu, Dy, Eu, Fe, Ga, Gd, In, Mg, Mn, Na, Ni, Pb, Si Sm, V and Zn using charged coupled device (CCD) based detector without any physical or chemical separation. CCD based detector has option of choosing additional analytical lines free from Zr interference. A suitable analytical method was also developed for the determination of Zr which involved identification of suitable analytical lines of Zr i.e. 339.198 nm, 343.823 nm, 257.139 nm and

272.262 nm, investigation of analytical performances (detection limits, sensitivity etc.) of these identified lines etc.

Experimental

Standard solutions for rare earth and other common impurity elements were prepared from CertiPUR ICP multi-elemental standard solutions (E-Merck, Darmstadt, Germany) by proper dilution with 0.5 M HNO_3. Supra- pure HNO_3 (E-Merck, Darmstadt, Germany) and quartz double distilled water were used for making 0.5 M HNO_3. Multi-point standardization was carried out using 0.5M HNO_3 as lower standard and 0.05-1000 /mL of the corresponding elemental standard as higher standards for each line after proper peak search. To understand the spectral interference of Zr on other analytes, pure Zr solution of different concentrations were used and contributions at each analytical channel were monitored. The analytical experiments were carried out using computer controlled, high resolution, simultaneous atomic emission spectrometer (Spectro Arcos, Germany) with ICP and DC Arc as excitation sources and a charged coupled device (CCD) as detector, the details for which are given elsewhere [3].

Results and Discussions

Determination of Zirconium by ICP-AES

Zr is a multi electronic system, having line rich emission spectra. Due to the availability of more number of emission lines, the sensitivity of the lines was found to be less and the detection limits were found to be poorer compared with PMT based detection system. For exploring the superior analytical performance of CCD based detector system, an analytical method was developed for the determination of zirconium by ICP-AES. The study included identification of suitable analytical lines of Zr namely, 339.198nm, 343.823 nm, 257.139 nm and 272.262 nm. The calibration curves were established and are shown in Fig. 1. It was found that 343.823 nm, 257.139 nm and 272.262 nm lines can be used for the determination of Zr upto 1000 g/mL with less than 5% RSD while for 339.198 nm line, 200 g/mL is the upper limit of detection for Zr. The sensitivity and detection limits of zirconium using the above mentioned analytical lines were evaluated using the slopes of the calibration curves and the concentration equivalent to the intensity equal to the

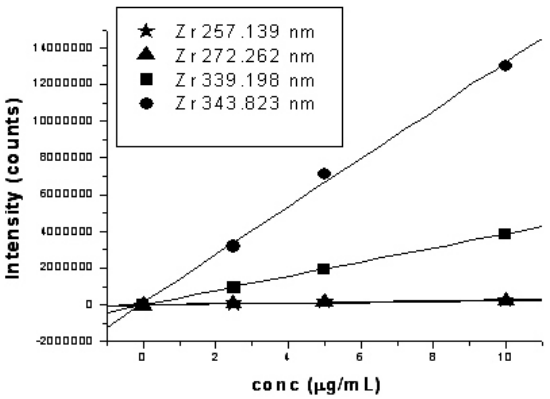


Fig. 1 Calibration curves for Zr

average of the blank value + three times of the standard deviation of the above measurement i.e. x + 3 . According to the analytical performance, 343.823 nm emission line with detection limit 0.09 g/mL, is the best analytical line for Zr amongst the four lines mentioned.

Spectral interference of zirconium on different analytes

In the present case, due to the advancement of detector system i.e. array of pixels of CCD detector, option of choosing analytical line for avoiding spectral interference is more. A detailed study was carried out to study the spectral interference of Zr on 24 different analytes and to choose appropriate emission lines for the trace determinations of these elements in presence of Zr matrix. For each of the analyte (24 nos.), more than four analytical lines were selected, studied and the best analytical line for each of the analyte which were free from Zr interference having superior detection limits, sensitivity were finalized and are shown in Table-1. The range of estimation for these analytes were found lie between 10-3265 ppm based on 1 g ZrO_2, which necessitates the chemical separation of Zr matrix to meet the specification limits. The contribution of Zr at ppm levels observed during d.c. arc AES and ICP-AES techniques for analytes can be calculated from the values shown in Table 1 using finalized analytical lines.

Conclusion

A systematic study was carried out to understand the spectral interference of zirconium on the analytical channels of 24 critical elements. The detection limits, sensitivity and correction factors of the analytes were calculated in presence of zirconium matrix. An analytical method was developed for the determination of zirconium by ICP-AES, which included the identification of the emission lines, establishing the calibration curves and evaluating the sensitivity and detection limits of zirconium. The method developed is useful in arriving at correct determinations for analytes carried out using ICP-AES technique after chemical separation of Zr matrix rcontaining residual Zr at ppm levels.

Table-1: Determination of spectral interference of Zr on analytes, detection limits, sensitivity

Element	Wave-length (nm)	Contribu-tion* (g/mL)	D.L. (g/mL)	Sensitivity (Counts/ /mL)
Ag	338.202	0.06	0.0004	$1.2x10^{-5}$
Al	308.215	0.113	0.008	$4.1x10^{-5}$
B	249.773	0.032	0.001	$2.1x10^{-5}$
Cd	28.802	0.021	0.0006	$8.1x10^{-5}$
Ca	396.847	0.147	0.0004	$2.1x10^{-7}$
Co	238.892	0.036	0.0008	$1.5x10^{-5}$
Cr	267.716	0.13	0.0005	$2.7x10^{-5}$
Cu	324.754	0.04	0.0001	$4.5x10^{-6}$
Dy	353.17	0.026	0.001	$4.5x10^{-6}$
Eu	420.505	0.01	0.0006	$2.9x10^{-6}$
Fe	373.486	0.449	0.0081	0.0001
Ga	294.364	0.237	0.004383	$7.0x10^{-5}$
Gd	342.247	0.12	0.001	$1.5x10^{-5}$
In	303.936	3.265	0.0071	0.0001
Mg	280.27	< 0.05	0.0005	$9.1x10^{-7}$
Mn	257.611	0.016	$8.6X10^{-5}$	$2.1X10^{-6}$
Na	589.592	0.05	0.002	$2.2x10^{-5}$
Ni	231.604	0.064	0.001	$2.8x10^{-5}$
Pb	220.353	0.19	0.009	0.00015
Si	288.158	0.132	0.0007	5.3x10-5
Sm	428.079	0.064	0.007	3.9x10-5
V	292.402	< 0.05	0.0005	8.3x10-6
Zn	213.856	0.028	0.001	6.0x10-6

* In presence of 1 mg/mL of Zr

References

[1] A.Sengupta, V.C.Adya, M.Kumar, S.K.Thulasidas, S.V.Godbole and V.K.Manchanda. Atomic Spectroscopy 32 (2011) 49.

[2] Thulasidas S.K., Adya V.C., Kumar M., Seshagiri T.K., Godbole S.V.Atomic Spectroscopy, 32 (6) (2011) 228.

[3] A.Sengupta, V.C.Adya, T.K.Seshagiri and S.V.Godbole Atomic Spectroscopy, 34 (2) (2013) 53.

[4] A.Sengupta, V.C.Adya, and S.V.Godbole, JRNC, DOI:10.1007/s10967-013-2520-0

Formulation and Radiochemical Evaluation of a Freeze-dried Mixed Peptide Kit for the Preparation of ^{68}Ga-labeled Peptides for PET Imaging of Somatostatin Receptor Positive Neuroendocrine Cancers

Tapas Das, Mohini Bhadwal, Sharmila Banerjee

Isotope Applications and Radiopharmaceuticals Division, Bhabha Atomic Research Centre, Trombay, Mumbai 400085, India; E-mail: tdas@barc.gov.in

Ga-68 labeled DOTA-coupled somatostatin analogue peptides are regularly used for the PET imaging of patients suspected to be suffering from various types of neuroendocrine cancers over-expressing somatostatin receptors. The radiopeptides have different degree of affinities towards different somatostatin receptor subtypes, which are expressed with dissimilar concentrations in cancerous lesions. The article describes development of a freeze-dried kit containing equal amount of DOTA-TATE and DOTA-NOC and use of the kit for the easy and convenient preparation of ^{68}Ga-labeled mixed peptides. The simultaneous use of two different peptides in the kit is expected to pick up more cancerous lesions and would have a wider applicability in diagnosis of neuroendocrine cancers.

Introduction

Scintigraphic imaging of patients suspected to be suffering from various kinds of neuroendocrine cancers is presently a routine clinical practise in nuclear medicine facilities across the globe. Neuroendocrine cancers represent a heterogeneous group of tumors, which over-express various kinds of receptors [1]. It is well documented that majority of such cancers over-express somatostatin receptors (SSTR) and therefore, radiolabeled somatostatin (SST) analogues have found pivotal importance in the detection and treatment of patients suffering from neuroendocrine cancers [1].

The use of a few radiolabeled SST analogues, such as, ^{111}In-Octreotide, ^{99m}Tc-Hynic-TOC (hydroxynicotinamide coupled Tyr^3-Octreotide), ^{68}Ga-DOTA-TOC, ^{68}Ga-DOTA-NOC (Nal^3-Octreotide) have been reported for the regular detection of neuroendocrine cancers [1]. Amongst these, ^{68}Ga-labeled SST analogues scores over the other agents as ^{68}Ga, being a PET radioisotope, provides superior quality images with a much better resolution. Moreover, the availability of ^{68}Ga from a ^{68}Ge/^{68}Ga radionuclide generator, which excludes the necessity of medical cyclotron at the hospital premises, has made these agents quite popular [2].

It is well known that SSTRs have five main receptor subtypes which have been identified as SSTR1, SSTR2, SSTR3, SSTR4 and SSTR5. Moreover, it is well documented in the contemporary literatures that these SSTR subtypes are over-expressed to different extents in different tumors as well as in the tumors of the same kind [3]. Ga-68 labeled DOTA-TATE is primarily taken up by SSTR2 receptor subtypes but have poor affinity towards SSTR3 and SSTR5 subtypes. On the other hand, ^{68}Ga-DOTA-NOC is reported to exhibit higher affinity towards SSTR2, SSTR3 and SSTR5, though it's affinity towards SSTR2 is much lower than that exhibited by ^{68}Ga-DOTA-TATE [1]. Therefore, the use of both these radiopeptides together while imaging the patients is expected to pick up more cancerous lesions compared to an imaging procedure involving use of either of the two radiopeptides (^{68}Ga-DOTA-TATE and ^{68}Ga-DOTA-NOC). The envisaged modality would presumably have a wider spectrum of application in diagnosis of a variety of neuroendocrine tumors with SSTR over-expression.

In the present work, we report the formulation of a freeze-dried kit comprising equal amount of DOTA-TATE and DOTA-NOC. The methodology of using this kit for the convenient and single step preparation of ^{68}Ga-labeled mixed peptides with high radiochemical purity has been standardized. Herein we report our initial experience of developing a novel freeze-dried mixed peptide kit which may be more useful for detecting the cancerous lesions of neuroendocrine origin.

Experimental

Freeze-dried mixed peptide kits were prepared (10 kit vials in each batch) following the protocol mentioned below. DOTA-TATE (procured from PiChem, Austria) and DOTA-NOC (procured from ABX Advanced Biochemical Compounds, Germany), solutions were prepared by dissolving the DOTA-coupled peptides in high purity supra-pure water (obtained from Merck, Germany) with a concentration of 1 g/ L. Sodium acetate buffer (1 M, pH 4) was prepared by mixing 2.9 mL of aqueous sodium acetate solution with 7.1 mL of glacial acetic acid. For the preparation of kits, 200 L of DOTA-TATE solution and equal volume of DOTA-NOC solution were added with 9.6 mL of the buffer. The pH of the resulting mixture was found to be ~4. The solution was subsequently subjected to Millipore (0.22) filtration and aliquoted into 10 thoroughly cleaned and autoclaved pharmaceutical borosilicate glass vials. All these operations were carried out under aseptic conditions. The vials were

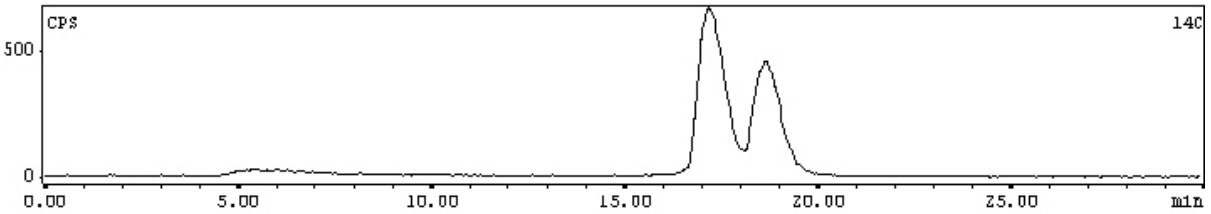


Fig. 1 Typical HPLC profile of 68Ga-labeled DOTA-TATE and DOTA-NOC, prepared using the mixed peptide kit

incubated for a period of 24 h at -4 °C followed by another 24 h at -40°C. Finally, the vials were freeze-dried in a lyophilizer (Labocene Coolsafe™ 55-4 freeze-drier, Denmark) for ~8 h, whereby mixed peptide kits were obtained. The kits were stored at -4°C temperature.

Ga-68, used for the present study, was eluted from a 1.11 GBq (30 mCi) SnO_2-based $^{68}Ga/^{68}Ge$ radionuclide generator system (obtained from iThemba Labs, South Africa). The generator was eluted with 0.1 N HCl and $^{68}GaCl_3$, thus obtained, was further purified by using a cation exchange column (Strata™ X-C, Phenomenex, India) prior to radiolabeling. Final elution of ^{68}Ga from the cation exchange column was carried out using 2.4% 0.05 N HCl in acetone as the eluting solvent.

Ga-68-labeled mixed radiopeptide was prepared by dissolving the contents of the lyophilized kit material in 400 L of supra-pure water followed by the addition of 100 L $GaCl_3$ and subsequently incubating the reaction mixture in a boiling water bath (100°C) for a period of 15 min. The radiolabeled mixed peptide, thus prepared, was characterized by both paper chromatography (PC) and high performance liquid chromatography (HPLC). PC was carried out in Whatman 3 MM chromatography paper (UK) using acetonitrile : water (1 : 1, v/v) as the eluting solvent. HPLC was carried out using a dual pump HPLC unit (Jasco, Japan) with a C-18 reverse phase HiQ-Sil (25 cm 0.46 cm) column employing water (A) and acetonitrile (B) mixtures with 0.1% trifluoroacetic acid as the mobile phase (0-4 min 95% A, 4-15 min 95% A to 5% A, 15-20 min 5% A, 20-25 min 5% A to 95% A, 25-30 min 95% A).

Further purification of ^{68}Ga-labeled mixed peptide was carried out using C-18 reverse phase Sep-Pak® cartridges (Waters, India). The purification procedure involved pre-conditioning of the column using 4 mL of ethanol and 2 mL of distilled water followed by loading of the radiolabeled preparation onto the column. Free $GaCl_3$ was eluted using 4 mL of distilled water and subsequently radiolabeled peptide was eluted using 1 mL of 60% ethanol in saline.

Results

In a batch, 10 freeze-dried mixed peptide kits, each comprising 20 g of DOTA-TATE, 20 g of DOTA-NOC and 22.8 mg of sodium acetate, were formulated. In PC, it was observed that the activity corresponding to ^{68}Ga-labeled peptides moved towards the solvent front (R_f = 0.5 - 1.0), while uncomplexed ^{68}Ga remained at the point of spotting (R_f = 0 - 0.1) under identical conditions. In HPLC, ^{68}Ga-labeled peptides exhibited retention times of ~17 min (corresponding to ^{68}Ga-DOTA-TATE) and ~19 min (corresponding to ^{68}Ga-DOTA-NOC), while uncomplexed ^{68}Ga was eluted from the column at 3.5 min. Radiochemical purity of ^{68}Ga-labeled peptides was determined by employing both these techniques and was found to be 98%. A typical HPLC profile of ^{68}Ga-labeled peptides, prepared using the developed kit, is shown in Fig. 1. After purification through Sep-Pak column, the radiolabeled preparation was obtained with 99% radiochemical purity, which is suitable for human administration.

Conclusion

A lyophilized mixed peptide kit, comprising equal amount of DOTA-TATE and DOTA-NOC was developed. The kit can be utilized for the easy and convenient preparation of a mixture of ^{68}Ga-labeled DOTA-TATE and DOTA-NOC with high radiochemical purity. The use of this kit may have the advantage of being able to detect more cancerous lesions when used for the scintigraphy of SSTR-positive neuroendocrine cancer patients.

References

[1] D. Wild, J. B. Bomanji, P. Benkert, H. Maecke, P. J. Ell, J. C. Reubi, M. E. Caplin, J Nucl. Med. 54 (2013) 364.

[2] F. Rosch, Recent Res. Cancer 194 (2012) 3.

[3] W. W. de Herder, L. J. Hofland, A. J. van der Lely, S.W.J. Lamberts, Endocr-Relat. Cancer 10 (2003) 451.

Installation and Performance Evaluation of an Indigenous Surface Area Analyser

S.N. Pillai[1], R S Prasad[2], M.N. Solapurkar[1], V. Venkatesan[1], A. Prakash[1], K.B. Khan[1] and Arun Kumar[1]

1. *Radiometallurgy Division, Bhabha Atomic Research Centre, Trombay, Mumbai 400 085, India; E-mail: amritp@barc.gov.in*
2. *Engineering Design and Development Division, Bhabha Atomic Research Centre, Trombay, Mumbai 400 085, India*

An indigenously available surface area analyser was installed inside glove box and checked for its performance by analyzing uranium oxide and thorium oxide powders at RMD. The unit has been made ready for analysis of Plutonium oxide powders after incorporating several important features.

Introduction

Radiometallurgy Division is involved in the fabrication of Mixed Carbide fuels for FBTR. Similarly other units of DAE are involved in the fabrication of natural UO_2 based fuels, mixed oxide fuels where UO_2 powder is being used with varying amount of PuO_2. Similarly, forthcoming reactors such as AHWR (Advanced Heavy Water Reactors) are based on fuels like ThO_2 and UO_2/PuO_2. The fabrication of these fuels with the desired specifications depend very well on the characteristics of feed materials viz. UO_2, PuO_2, ThO_2 powder. Surface area of these powders is one of the very important specification which determines the behavior of the powder during fabrication like pre compaction, compaction, sintering etc. The specific surface area of UO_{2+x} powders is a key guiding parameter for sintering of oxide powders to get sintered UO_2 pellets of consistent density to be used in Nuclear Power Reactors [1,2]. It has also been reported that plutonium oxide powder surface area data are of great importance to the community using nuclear materials. Plutonium oxide particles readily adsorb water vapor from the surrounding atmosphere and the amount they can adsorb is dependent on the oxide's specific surface area. The greater the surface area, the greater the amount of adsorbed water. It is very important to anticipate the moisture content of plutonium oxide powders because, in the presence of plutonium, water can likely be transformed into highly reactive and potentially explosive hydrogen (H_2) gas due to radiolysis [3]. Apart from these, the deviation in specification will also lead to rejection /recycling of the material which is highly undesirable in any fuel fabrication facility. RMD had a surface area analyzer of Quantasorb Make which was regularly being used for surface area characterization of feed materials. Due to continuous use for several years, the parts of the unit deteriorated and could not be used further.

Experimental

As determination of surface area in feed materials is mandatory in a fuel production facility, a new indigenously available surface area analyser was procured for this purpose from M/s S.P.Consultants, Mumbai. The equipment works on BET principle and can be used for both multipoint and single point measurement. There is a dynamic flow of He-N_2 gas mixture through the sample cell containing the sample and over a thermal conductivity bridge. The sample cell is immersed in liquid nitrogen bath and at equilibrium we get an adsorption signal by measuring the change in thermal conductivity of the gas mixture. The liquid nitrogen bath is removed from the sample cell and the sample is brought to room temperature using water bath and we obtain a desorption signal. The desorption signal is calibrated by injecting a known amount of N_2 gas. Surface area of the sample is calculated using BET equation. As a routine process we are using single point BET method with He – 30% N_2 gas mixture as it is rapid and yields reliable results.

Glove Box Adaptation

In RMD surface area of radioactive materials like PuO_2, UO_2, ThO_2, (Pu,U)C powders are measured. These materials are radiotoxic and are handled in alpha tight glove boxes. Apart from being radiotoxic, (Pu,U)C powders are highly pyrophoric also. Therefore, the glove boxes are purged with high purity inert N_2 gas on a once through basis. The glove boxes are maintained at a pressure of -1"WG. Surface area is measured at liquid nitrogen temperature. Liquid nitrogen is pumped into the glove box using N_2 gas at high pressure using an indigenously designed liquid N_2 transfer system. Handling liquid nitrogen in a radioactive glove box of fixed volume of one cubic meter maintained at -1"WG pressure is extremely risky as there is a hazard of radiotoxic contamination of personnel and laboratory in case of accidental liquid nitrogen spillage inside the glove box. The severity of such an accident is enormous because liquid to gas expansion ratio of nitrogen is 1:694 at 20°C. All safety features were incorporated to rule out such an accident. The SS flooring of the glove box was covered by 1" thick ceramic fibre boards which absorb liquid nitrogen spilled on it preventing instantaneous expansion of liquid nitrogen. The glove box was connected to a -10"WG pressure header line through two parallely connected solenoid valves which gets actuated when the glove box pressure increases to -0.5"WG. Hence in case of accidental liquid nitrogen spillage, it first gets absorbed by the ceramic fibre boards and as the glove

box pressure increases slowly the solenoid valves take care of the expansion gas not allowing the neoprene gauntlets to be thrown off or the breaking of the glass panels, thus preventing any possible accident involving hazardous radioactive materials.

Results and Discussion

Using the above equipment in the glove box set up described above, surface area of UO_2 and ThO_2 powder materials were measured by single point BET method. The surface area measurement involves sample preparation by degassing any adsorbed gas on the adsorbent surface by heating the sample in N_2 atmosphere at approximately 120°C for half an hour. After cooling to room temperature, the sample weight was measured. Adsorption, desorption, and calibration runs were carried out automatically using computer interfacing and software provided. It can be carried out manually as well. The results are mentioned below with an overall R.S.D of 5%.

Table-1

Sample	Results of surface area
ThO_2	8.38 m^2/gm
$DDUO_2$	2.30 m^2/gm
$LiTiO_3$	21.51 m^2/gm
ThO_2-30%UO_2	3.16 m^2/gm

Conclusion

Results obtained from the newly installed unit compares well with results obtained from the earlier imported unit. The surface area value of standard sample obtained from the equipment is also satisfactory. The unit can very well be used for Pu containing samples.

References

[1] J.K.Dawson and R G Sowden, Chemical Aspects of Nuclear Reactors, Vol.1Gas Cooled Reactors, Butter Worths, London, PP122-124

[2] Uranium Oxide, Properties and Nuclear Applications, Ed. J Bele, Naval Reactors Division of Reactor Development,USAEC, (1961)

[3] David Wayne and Carl Mrtinee, Plutonium manufacturing and Technology Division

Characterisation of Dry Tubes in KAMINI reactor

Manish Chand, J.S. Brahmaji Rao, N.P. Seshadreesan and C.R. Venkatasubramani

Fuel Chemistry Division, Chemistry Group, Indira Gandhi Centre for Atomic Research, Kalpakkam 603 102, India; E-mail: venkat@igcar.gov.in

Two aluminum dry tubes (DT1 and DT2) have been introduced in the reactor tank of KAMINI for testing the various neutron detectors. These locations can be used for large sample activation analysis and characterization studies were conducted to obtain the vertical neutron flux profile, the sub-cadmium to epithermal neutron flux ratio (f) and the epicadmium neutron flux shape factor ( ).

Introduction

KAMINI reactor has one high flux pneumatic fast transfer system (PFTS), two thimbles and one west beam port for carrying out neutron activation analysis. Characterization of the PFTS has been reported [1] earlier. Two new aluminum dry tubes (DT1 & DT2) have been introduced just outside BeO reflector blocks in the reactor tank of KAMINI for testing neutron detectors. Since these can be used as additional irradiation positions, the flux characterization work was taken up. In view of their convenient dimensions, DT1 ~75mm ID and DT2 ~103mm ID, this study will enable carrying out Large Sample Neutron Activation analysis (LSNAA)[2,3] using these locations.

DT1 is located close to the core at a distance of 35cm from its centre, while DT2 is located adjacent to the south beam port at a distance of 90 cm from core centre [3]. The paper details the vertical flux profiles in these tubes, determination of the the sub-cadmium to epithermal neutron flux ratio (f) at DT1 and DT2 and epicadmium neutron flux shape factor ( ) at DT1.

Experimental

Gold standards were prepared by drying about 100 to 250 g Au from a std solution on filter paper. These were doubly sealed in polythene bags. A set of 17 such Au standards were fixed at regular intervals on a thin strong thread carrying an empty plastic bottle at the bottom. This was placed inside the DT1 tube and it was ensured that the plastic bottle with one Au standard fixed in the middle was at the bottom of the tube. The distance of this standard from the bottom was 37mm. Likewise, in the next run, Au standards around 0.5 to 2mg level were placed inside DT2 in a similar fashion. The first standard inside the bottle was at a distance of 67 mm from the bottom. Irradiations were carried out for 2h at 20kW. For the determination of f and , Au and Zr standards with and without cadmium cover of 1mm thickness and width to length ratio as 1:2 were irradiated for 2h and 6h respectively at DT1 at the 37mm position. For the determination of f, cadmium covered gold standard was irradiated at the peak position of DT1 and bottom position of DT2. The relevant nuclear data used in calculations were taken from the literature[4].

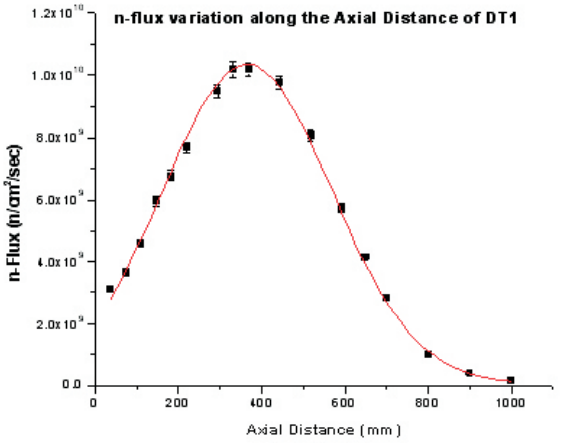


Fig. 1 Variation of n-flux as a function of axial distance from the bottom

Results and Discussion

Figure 1 shows the vertical profile of the neutron flux obtained in DT1 starting from a distance of 37mm from the bottom of the tube and for DT2 starting from 67 mm from the bottom. The curves were fitted to a Gaussian and Lorentzian respectively as shown by the line. Table 1 presents the values of f and obtained.

Table-1: Results of f and -Determination at DT1 and DT2

f	DT1		DT2
	@3.7cm	@36.8cm	@6.7cm
	348 ± 9 330 ± 9 362 ± 12	143 ± 5	121 ± 6 111 ± 6
	-0.2376#	-	-
	-0.3082*		

#Dual ratio method
*Cd-cover triple monitor method

As expected, due to its closer location to the core, the flux in DT1(1.02E+10) is two orders of magnitude higher than the flux in DT2 (1.0E+08). However, the f value for DT2 is considerably lower than expected near the bottom of the dry tube and this could be due to contribution from the neutrons leaking from the south

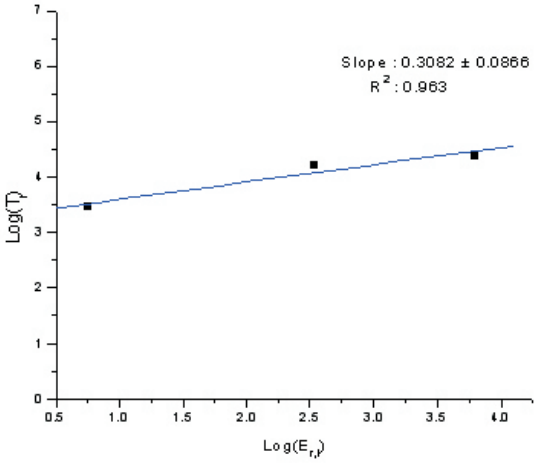


Fig. 2 Log(T_i) versus Log($\overline{E}_{r,i}$)

beam tube as these neutrons have a considerable epithermal component.

The average value at center of the sample container i.e. at 3.7cm from the bottom of DT1 tube using dual ratio method was -0.2376 ± 0.0167. The value obtained using Cd-cover triple monitor method was -0.3082 ± 0.0866. The final iteration plot of Log(T_i) versus Log($\overline{E}_{r,i}$) by Cd-cover method using triple monitors (^{197}Au, ^{96}Zr, ^{94}Zr) is shown in Fig. 2.

Conclusions

Two new irradiation locations at KAMINI reactor that can be used for large sample activation analysis have been characterized. The flux in DT1 is adequate and this position can accommodate samples with a volume of about 500 mL. Design and development of mechanical arrangements for loading and unloading of samples is in progress.

References

[1] J.S. Brahmaji Rao, E. Senthilvadivu, N. P. Seshadreesan, R. Acharya, C. R. Venkatasubramani, A. V. R. Reddy, J Radioanal. Nucl. Chem. 294 (2012) 137.

[2] P.Bode and R.M.W Overwater, J.Radioanal. Nucl. Chem. 167 (1993) 169.

[3] K.Sudharshan ,A.G.C.Nair, A.Goswami, Jr.Radioanal Nucl. Chem. 256 (2003) 93

[4] E. Radha, V. Sathiamoorthy and R.S. Keshavamurthy, Design Note ROD/KAMINI/KTN-79 (2013)

[5] F. De Corte, A. Simonits, Atomic Data Nuclear Data Tables, 85 (2003) 47.

Dose computation of Ti activated products for its qualification as a material for the sample holder in FBTR

G.V.S. Ashok Kumar[1], R. Acharya[2], R. Kumar[1], C.R. Venkatasubramani[1] and A.V.R. Reddy[3]

1. *Fuel Chemistry Division, Indira Gandhi Centre for Atomic Research, Kalpakkam 603102, India, E-mail: venkat@igcar.gov.in*
2. *Radiochemistry Division, Bhabha Atomic Research Centre, Trombay, Mumbai 400085, India*
3. *Analytical Chemistry Division, Bhabha Atomic Research Centre, Trombay, Mumbai 400085, India*

Development of a Fast flux experimental facility with a sample holder facility in FBTR has been envisaged to carry out the studies on i) fast neutron activation analysis and ii) fission studies. This paper describes the facility in detail and dose computations that are to be generated due to long irradiation of the material of the sample holder i.e. titanium.

Introduction

FBTR is sodium cooled, mixed-carbide fuelled reactor. Its main aim is to generate experience in the operation of sodium cooled fast reactor and serve as an irradiation facility for the development of fuels and structural materials for future fast reactors [1]. The temperature of the sodium that emerges from each fuel subassembly is monitored using thermocouples. Four thermocouples are provided as an integral part of central canal plug (CCP) to monitor the outlet temperature of central subassembly in the control plug of the reactor. There is a cavity which extends from top of CCP to just above the fuel subassemblies (FSA) (bottom of CCP). The cavity was envisaged as a potential irradiation location above the core. The cavity is closed by a small auxiliary shield plug. The shielding provided by CCP and its shield plug ensures that the dose due to neutron and gamma streaming is within regulatory limits at the top of the plug.

In order to enable the experiments to be carried out at FBTR, auxiliary shield plug of CCP has to be modified by attaching a long rod with a sample holder at its end. Insertion and removal of samples is from the top of the reactor. Even though the samples are not in contact with sodium, it has to be stable at the temperature of sodium during reactor operation.

Titanium is a strong, lustrous, corrosion resistant metal with a high strength to weight ratio. It has a melting point of 1680°C and a boiling point of 3300°C. It is slow to react with water and air due to the formation of an oxide protective coating. It reacts readily with oxygen in air at 1200°C and pure oxygen at 610°C to form titanium dioxide [2]. In view of the high temperature requirement for the reaction of titanium with air and also the formation of a protective coating, it can be a suitable candidate material for the fabrication of the modified CCP as maximum temperature expected to be seen is around 550°C in this location. In addition titanium produces only short lived neutron activation product (^{51}Ti-5.5 min) which does not add to the activities and dose after the irradiation. This paper computes the activation of the Ti rod and the resultant dose due to prolonged irradiation.

Experimental: Dose Computations

The rod attached to the bottom of the central canal plug undergoes all possible nuclear reactions and hence it is necessary to compute the dose due to this rod under various conditions. The two major source of activation reactions are the nuclear reactions that occur in the matrix material or in its impurities. Dose computations were carried out using titanium as the matrix material and the details are described below. It was assumed that the location of the sample holder is 28.5cm above the central subassembly with the associated flux of 1.16 x 10^{13} n/cm^2/sec.

Table-1: Isotopic composition of titanium (Average atomic weight: 47.9 and density: 4.54 g/cc)

Isotope	Abundance (%)
^{46}Ti	8.25
^{47}Ti	7.44
^{48}Ti	73.72
^{49}Ti	5.42
^{50}Ti	5.15

The isotopic composition of Ti is shown in table 1. Trace elemental impurities in Ti were determined using both relative and internal mono-standard (IM)NAA methods. The Ti sample was irradiated for 7 h in self serve position of CIRUS reactor, BARC at a neutron flux of 3 x 10^{13} n.cm^{-2}.s^{-1} for long and medium lived activation products like As, Na, K, Sb, La, Ta, Fe, Co, Sm, Cr and Sc. Mn and Cl were estimated by carrying out a short irradiation of 1 min duration at pneumatic carrier facility of Dhruva reactor with a neutron flux of 5 x 10^{13} n.cm^{-2}.s^{-1}[3]. The impurities present are shown in Table 2.

As the reaction rates vary considerably with distance from the bottom, the rod was divided into three portions each having a length of about 1 m for the purpose of this work. The reaction rates were computed at three locations of the titanium rod i.e. bottom, middle and top. The microscopic reaction rates for the various possible reactions with Ti and for the impurities present in Ti are presented in Table 3 and Table 4 respectively.

Table-2: Impurities present in titanium

Element	Concentration (ppm)
As	9.2 0.1
Na	10 1
W	8.14 0.04
Sb	1.52 0.01
La	0.13 0.004
Ta	6.9 0.1
Fe	483 6
Co	3.94 0.03
Sm	0.15 0.01
K	32.7 1.3
Cr	147 4
Mn	21.5 3
Cl	36.0 1.7
Sc	0.368 0.002

In view of their low concentrations, neutron capture reaction only was considered for these impurities.

Table-3: Microscopic reaction rates for titanium.

Reaction	$t_{1/2}$ of product	Microscopic Reaction Rate		
		Bottom	Middle	Top
$^{46}Ti(n,2n)^{45}Ti$	3.08 h	2.64E+05	7.85E+02	9.70E-02
$^{46}Ti(n,p)^{46}Sc$	83.79 d	5.43E+08	1.07E+06	2.00E+02
$^{47}Ti(n,p)^{47}Sc$	3.35 d	1.25E+09	1.95E+06	1.77E+02
$^{48}Ti(n,p)^{48}Sc$	1.82 d	1.29E+07	2.72E+04	4.84E+00
$^{49}Ti(n,p)^{49}Sc$	0.96 h	3.48E+07	6.35E+04	8.76E+00
$^{50}Ti(n,p)^{50}Sc$	0.028 h	3.24E+05	7.43E+02	1.00E-01
$^{50}Ti(n,\ )^{51}Sc$	0.096 h	3.25E+10	1.67E+09	1.96E+02
$^{48}Ti(n,\ )^{45}Ca$	162.6 d	1.49E+04	4.11E+01	5.51E-03
$^{50}Ti(n,\ )^{47}Ca$	4.536 d	2.55E+03	7.74E+00	9.62E-04

Taking into account the operation cycle of FBTR, it was assumed that a continuous irradiation period of 10 days followed by 1 hour cooling was typical for the experiments planned and computations were carried out to obtain the activity induced per unit volume under these conditions. Assuming a length of 1.1 m and a diameter of 14 mm, the total activities and the gamma emission rates were calculated. The source is essentially a line source and the dose due to this line source has been computed and is presented in Table 5.

Results and Discussion

The use of titanium is preferred as the dose obtained after 10 days of irradiation at 400kW power is about 125 mR/h at a distance of 2 cm and reduces to about 0.8 mR/h at a distance of 1m. The above computations assumed that the reaction rates at the bottom of the titanium rod i.e. 28.5 cm above FSA head

Table-4: Microscopic reaction rates of the impurities in Ti.

Reaction	$t_{1/2}$ of product	Microscopic Reaction Rate		
		Bottom	Middle	Top
$^{75}As(n,\ )^{76}As$	1.08 d	4.81E+13	1.5E+12	5.74E+5
$^{37}Cl(n,\ )^{38}Cl$	37.2 m	6.79E+10	4.0E+09	4.29E+2
$^{59}Co(n,\ )^{60}Co$	5.27 a	5.26E+13	1.9E+12	7.00E+5
$^{50}Cr(n,\ )^{51}Cr$	27.7 d	2.27E+12	1.4E+11	1.63E+4
$^{58}Fe(n,\ )^{59}Fe$	44.4 d	1.34E+12	2.9E+10	1.42E+4
$^{139}La(n,\ )^{140}La$	1.68 d	6.08E+12	2.8E+11	7.47E+4
$^{55}Mn(n,\ )^{56}Mn$	2.58 h	8.45E+12	2.4E+11	8.89E+4
$^{23}Na(n,\ )^{24}Na$	15.0 h	8.73E+10	5.1E+09	1.42E+3
$^{121}Sb(n,\ )^{122}Sb$	2.72 d	7.40E+13	4.7E+12	5.71E+5
$^{45}Sc(n,\ )^{46}Sc$	83.7 d	3.38E+12	2.4E+11	2.01E+4
$^{152}Sm(n,\ )^{153}Sm$	46.2 h	7.72E+14	6.7E+13	3.24E+6
$^{181}Ta(n,\ )^{182}Ta$	114.4d	2.48E+14	1.5E+13	1.88E+6
$^{186}W(n,\ )^{187}W$	23.72 h	2.03E+14	1.3E+13	1.84E+6

Table-5: Dose computations for titanium rod.

Sl. No	Distance from rod(cm)	Dose (R/h)
		400 kW
1	2.0	0.125
2	100.0	0.819E-03

is applicable to entire 1.1 m length of the bottom portion. It can be seen from tables 3 and 4 that the fall in reaction rates between the bottom portion and the middle portion varies between approximately ten to about three orders of magnitude. Hence, it is expected that the actual dose would be lower than the computed values and the dose rates mentioned in the table 5 are on the conservative side. Dose computations had been carried out earlier for both SS316 and pure nickel as the material of construction for the extension rod and the dose obtained using these materials was unacceptably high for unshielded handling operations. Hence, Ti can be considered as a suitable material for the sample holder in FBTR as it leads to only a low radiation dose on its activation.

References

[1] K.V.Suresh Kumar, A. Babu, B. Anandapadmanaban& G. Srinivasan, Energy Procedia7 (2011) 323.

[2] "Titanium"http://www.britannica.com/eb/article-9072643/titanium, Columbia Encylopedia (6th ed.). New York: Columbia University Press 2000-2006. ISBN 0-7876-5015-3.

[3] R. Acharya, K.B. Dasari, S. Sodaye, P.K. Pujari, C.R. VenkataSubramani, Proc. Nucl. Radiochem. symp, (Ed) R.M. Sawant, S.K. Sali, Meera Venkatesh & V. Venugopal, BRNS, Visakhapatnam (2011) p.170.

Cesium Extraction from High Level Waste using Irradiated Calix-Crown-6 Ligands in FS-13

Poonam Jagasia[1], V.C. Adya[2], A. Sengupta[2], P.S. Dhami[3] and P. K. Mohapatra[2,*]

1. *Process Development Division, Bhabha Atomic Research Centre, Trombay, Mumbai-400 085, India*
2. *Radiochemistry Division, Bhabha Atomic Research Centre, Trombay, Mumbai-400 085, India; E-mail: mpatra@barc.gov.in*
3. *Fuel Reprocessing Division, Bhabha Atomic Research Centre, Trombay, Mumbai-400 085, India*

We have evaluated four calix-crown-6 ligands, viz. CC, CBC, CNC and CMC in FS-13 for the recovery of radio-cesium from high level waste after exposing the extractants to 100 MRad gamma ray dose. The nature of the extracted species with the irradiated ligands by slope analysis method and was found to change significantly as compared to unirradiated ligands. Studies have also been carried out using simulated high level waste with both irradiated and unirradiated ligand solutions. The solvent system containing CBC in FS-13 was actual high level waste using 100 times diluted feed.

Introduction

One of the major sources of radioactivity of the high level waste (HLW) is ^{137}Cs, which needs to be separated efficiently to solve the MANREM problem. Furthermore, the recovered radio-cesium can be used in irradiators for sludge treatment, brachy therapy, blood irradiators, gamma camera, etc [1]. Macrocyclic ligands such as crown ethers have been suggested to be size selective complexing agents, though not many studies with actual wastes are reported. On the other hand, calix-crown-6 extractants have been reported for radio-cesium recovery from alkaline wastes by what is now famously known as the Caustic Side Solvent Extraction (CSSX) process [2]. However, the calix-crown extractant used in this process which is the well known BOBCalixC6 (bis-octylbenzo-calix-crown-6) has limited application in recovery studies involving acidic waste solutions. Other calix-crown-6 ligands (Fig. 1) were used for the separation of ^{137}Cs from nitric acid medium while using nitrobenzene as the diluent [3,4]. However, in view of unacceptability of nitrobenzene as a diluent alternative diluents were evaluated and we have reported much improved radio-cesium recovery with phenyltrifluoromethyl sulfone (PTMS, which is also known as FS-13) with several commercial ligands like calix[4]arene-bis-crown-6 (CC), calix[4]arene-benzo-bis-crown-6 (CBC), calix[4]arene-naphtho-bis-crown-6 (CNC) suggested effective separation of ^{137}Cs from simulated high level waste [4].

The objectives of the present study were to understand the radiolytic degradation behaviour of the calix-crown-6 ligands in FS-13 as the solvents. The evaluation of the irradiated solvents included studies such as Cs(I) extraction, nature of the extracted species, studies with simulated HLW, etc. We have also carried out studies on the relative extraction of other metal ions present in SHLW by ICP-AES.

Experimental

Calix[4]arene-bis-crown-6 (CC), calix[4]arene-benzo-bis-crown-6 (CBC), calix[4]arene-naphtho-bis-crown-6 (CNC) were obtained from Across Organics, Belgium while bis-octyloxy)calix [4] arene-mono-crown-6 (CMC) was obtained from Orion Chemicals, Mumbai as a gift sample. FS-13 was synthesized as reported earlier [5]. Simulated HLW solutions were prepared by dissolving AR grade salts of the respective metal nitrates as reported earlier [6].

Solvent extraction experiments were carried out by equilibrating equal volumes of organic and aqueous phases in stopperred glass tubes in a thermostated bath at 25 1°C. The estimation of the elements in the simulated HLW solution was carried out by ICP-AES methods. Radiolysis studies were carried out using a ^{60}Co irradiator (0.16 MRad/h).

Results and Discussions

Studies with Irradiated Solvents

We have previously reported a systematic study on the radiolytic degradation of the calix-crown-6

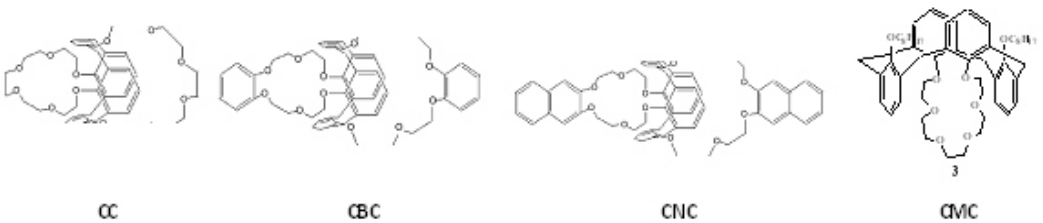


Fig. 1 Structural formulae of the calix-crown extractants used in the present study

Table-1: Results of ligand variation experiments with 3 M HNO_3 using unirradiated and irradiated calix-crown-6 ligands

Ligand	Unirradiated ligand		Irradiated ligand (100 MRad)		Instability index: ($D_{unirradiated}/D_{irradiated}$)
	Slope	R^2	Slope	R^2	
CC	1.22±0.22	0.953	0.74±0.04	0.995	4.0
CBC	0.93±0.02	0.999	1.08±0.14	0.976	4.2
CNC	0.94±0.06	0.994	1.45±0.19	0.974	8.2
CMC	1.17±0.15	0.977	0.56±0.73	0.978	10

solvents. A careful analysis of the data (Table 1) obtained with solvents exposed to 100 MRad dose of gamma radiation suggested reasonably good stability of CC and CBC with an instability index (I.I. defined as the ratio of the D_{Cs} values of unirradiated and irradiated solvents) of ~4 as compared to CNC (I.I. of 8.2) and CMC (I.I. of 10) suggesting that CNC and CMC can not be used for process application. This is also evident from the slope analysis results which indicate drastic variations in the slopes of the log D vs log [Extractant] plots (Table 1) for CC, CNC and CMC while insignificant change was seen with CBC. Similarly, in view of the low partition coefficient of CC (Table 2), it can not be used for plant scale applications implying CBC is the best choice out of the four calix-crown-6 ligands being evaluated.

Table-2: Partition coefficient data for the ligands in 3 M HNO_3 using $1.0x10^{-3}$ M calix-crown-6 ligands in PTMS

Ligand	Partition coefficient
CC	91
CBC	3663
CNC	2227
CMC	102

Extraction from SHLW

Results of the studies on the extraction of Cs(I) from simulated high level waste using irradiated calix-crown-6 solvents are listed in Table 3. These studies indicated partial extraction of Ba, La and Mo suggested that the irradiated solvent is not very suitable for the extraction of other elements present in the HLW which meant high selectivity factors. However, the selectivity factors have definitely become inferior as compared to the unirradited solvents as reported previously [6].

Extraction from actual HLW

Studies have been carried out using actual HLW in a glove box using 100 times diluted feed solutions. The results are included in Table 4 which indicated near quantitative extraction of ^{137}Cs from the HLW with almost no extraction of the other radionuclides. It may be mentioned here that in view of large concentrations of U and significant amount of Pu in the HLW, the feed was contacted with TBP 2 times prior to the extraction with the calix-crown-6 ligand solution.

Table-3: Extraction of metal ions in SHLW using irradiated solutions of calix-crown ligands ($1.0x10^{-3}$ M) in FS-13

M	Amount (mg/L)	Amount remained in aqueous phase after extraction			
		CC	CBC	CNC	CMC
Ba	57±6	14±2	30±3	38±4	50±5
Ce	2.8±0.3	2.8±0.3	2.7±0.3	2.7±0.3	2.8±0.2
Cr	11.0±1	10.2+1	10.6±1	10.1±1	10.2±1
Fe	93±9	88±8	85±9	84±8	88±0.9
La	3.4±0.3	1.7±0.2	1.9±0.2	2.2±0.2	2.7±0.3
Mn	52±5	47±0.5	45±0.5	44±4	45±4
Mo	19.2±2	14.1±1	14.9±1.5	15.6±1.6	17.4±2
Nd	7.6±0.8	7.2±0.7	7.0±0.7	7.0±0.7	7.1±0.7
Ni	8.6±0.8	9.0±0.9	8.5±0.9	8.1±0.8	8.2±0.8
Sm	12.2±1.2	12.2±1	12.5±1.2	12.0±1.2	11.8±1.1
Sr	2.5±0.3	2.6±0.3	2.4±0.2	2.3±0.23	2.4±0.2
Y	11.2±1.1	11.9±1	11.2±1.1	10.8±1.1	10.8±1
Zr	4.8±0.5	4.4±0.4	4.2±0.4	4.3±0.4	4.3±0.4

Table-4: Extraction data with 100 times diluted actual HLW with 1mM CBC. Phase ratio: 1:1, Contact time: 10 min.

Radionuclide	O1	O2	O3	O4	Raffinate
^{144}Ce, Ci/L	ND	ND	ND	ND	0.108
^{106}Ru, Ci/L	0.18	0.20	0.16	0.17	67.2
^{137}Cs, Ci/L	31.4	16.1	2.5	0.5	<0.1
^{95}Zr, Ci/L	ND	ND	ND	ND	0.019
^{95}Nb, Ci/L	ND	ND	ND	ND	0.256

ND: Not detected

Conclusions

Studies on the irradiated solvents indicated that CBC in FS-13 can be used for the recovery of Cs from actual HLW. Studies with SHLW indicated minor coextraction of Ba, La and Mo. Studies with actual HLW suggested good possibility of application of the CBC based solvent though undiluted HLW can be treated employing higher concentrations of the extractant.

References

[1] W.W. Schulz, L.A. Bray, Sep. Sci. Tech. 22 (1987) 191.
[2] R.A. Leonard, et al., Sep. Sci. Technol., 36 (2001) 743.
[3] D.R. Raut, et al.Sep. Sci. Technol., 44, 3664 (2009).
[4] D.R. Raut, et al., J. Membr. Sci., 429 (2013) 197.
[5] P.K. Mohapatra et al., J. Hazard. Mater., 181(2010)679.
[6] P. Jagasia, et al. Proceedings of NUCAR 2013.

Separation and Determination of Calcium and Iron in Silicon Matrix using Ion Chromatography

M.K. Das, V.V. Raut, S.B. Deb, S. Jeyakumar, M.K. Saxena, B.S.Tomar

Radioanalytical Chemistry Division, Bhabha Atomic Research Centre, Trombay, Mumbai 400085, India; E-mal: sjkumar@barc.gov.in

Ion chromatographic (IC) methods for the determination of Ca and Fe in silicon matrix were developed. The methods involve the removal of Si as SiF_4 by the addition of calculated amount of HF. The IC separation of Ca from other metal ions was carried out on a cation exchange column using 0.02 N H_2SO_4 as eluent with suppressed conductivity detection. The developed method was calibrated in the concentration range between 0.05 and 5 ppm and the linear correlation coefficient was found to be 0.998. Iron determination was carried out on a RP column dynamically modified with 5 mM camphor-10-sulphonic acid and 0.2 M mandelic acid at pH 3.8 as eluent. A linear calibration was obtained in the concentration range between 0.5 and 25 ppm of Fe (R^2 = 0.9998).

Introduction

Silicon is an important nuclear material as it is used in the fabrication of silicon based nuclear fuels such as U_3Si_2 etc. For the preparation of such fuels, elemental silicon is being used and hence, it is necessary to know the purity of silicon that is to be used in the fabrication. In view of this, the chemical characterization of silicon play a key role in assessing the purity of the silicon which in turn controls the chemical specifications of the finished fuel material.

In general, metallic impurity analyses in silicon and its uranium compounds are carried out using inductively coupled plasma mass spectrometry (ICP-MS) [1]. In the case of ICP-MS with quadrupole mass analyser, the determination of Ca and Fe become difficult due to isobaric interference from some plasma species. Since Ca and Fe are the common impurities and they have specification limits in the final fuel materials, it is essential to know the concentrations of Ca and Fe in silicon prior to its use with the fabrication of the fuel material. Therefore, there is a need for an alternate analytical method for the determination of Ca and Fe in Silicon.

Spectrophotometry methods are available for the determination of Ca and Fe, however, the methods demand the complete separation of these elements from the possible interfering metals such as Mg, Ba, Sr etc. for calcium and Bi, Mo etc. for Fe [2]. Since IC provides separation and detection (determination) simultaneously, it would be appropriate to use IC for this purpose. The present work deals with the development of two independent IC methods for the determination of Ca and Fe, respectively.

Experimental

Instrumentation

A commercial ion chromatograph (IC) was used in the present study which consisted of a solvent delivery pump (ICS-3000), a conductivity detector (ED 50A), Absorbance detector (AD-20) and a Cation Self-Regenerant Suppressor (CSRS-II). The samples were injected through a 20 L loop fitted to a Rheodyne six port injector. The separator columns used were IonPac CS12A(250 mm x 4 mm) with its guard column CG12 (50 mm x 4 mm) for Ca and Hypersil, ODS-2 (250 mm x 4 mm) for Fe.

Reagents

All reagents were prepared from analytical grade (AR) chemicals. The standard stock solutions of metal ions were prepared by dissolving from their respective high purity salts. Working standards were prepared by appropriate dilution of the stock solutions. High purity water (18.2 M) obtained from a MilliQ water system used for the preparation of all solutions.

Sample Preparation

Accurately weighed quantity of Si powder (~100mg) was taken in a teflon beaker and dissolved in Conc. HNO_3. Further, calculated amount of Conc. HF was added and heated under IR lamp to remove Si as SiF_4. Finally the solution was made with 1% HNO_3 medium after giving Conc. HNO_3 treatment. Prior to the IC analyses, the samples were appropriately diluted.

Results and Discussion

IC Separation and determination of Ca

IC separation of Ca from alkali, alkaline and other metals was carried out on a cation exchange column. Since IC methods with methanesulfonic acid (MSA) as eluent were known [3], eluents with varying concentrations of MSA (15-25 mM) were attempted. It was observed that with MSA, the elution of Ca resulted in broad peaks not suitable for quantification. The sluggish elution of Ca may be attributed to the high acidity of the sample medium which can suppress the dissociation of MSA, which is a weak electrolyte. Hence, H_2SO_4 was taken as an alternate eluent. Eluents with varying concentrations of H_2SO_4 were used and 0.02 N H_2SO_4 was found to be the optimum eluent composition for the separation of Ca from other metals. The method was calibrated over a concentration range of 0.05 ppm to 0.5 ppm and the R^2 was found to be

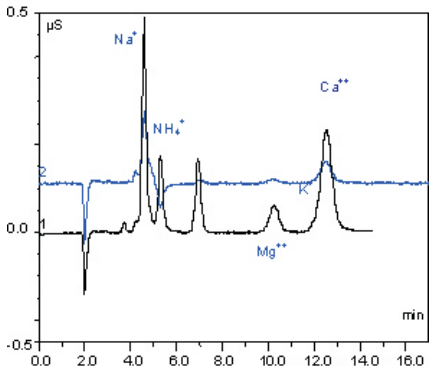


Fig. 1 Chromatogram (1) Standard solution consisting of Na^+, NH_4^+, K^+, Mg^{++} and Ca^{++}; & (2). Si-sample. Column: CS12A along with CG12; Mobile phase: 0.02N H_2SO_4; CSRS used; SRS: 100mA; Detection: Conductivity detector

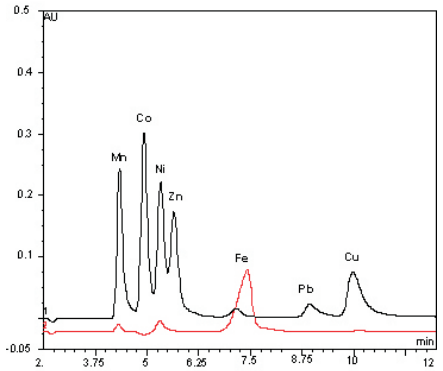


Fig. 2 Chromatogram (1) Standard solution consisting of Mn, Co, Ni, Zn, Fe, Pb and Cu; & (2). Si-sample; ODS-2-column; Eluent: 5mM CSA + 0.2M MA; pH 3.8; FR: 1.5ml/min; Absorbance Detection; PCR: PAR; 520nm

0.998. Based on the calculation using S/N=3, the LOD for Ca was 15 ppb. Figure.1 shows an overlay of typical chromatograms obtained for a standard mixture of metal ions and Si-sample solution.

IC Separation and Determination of Fe

Separation of Fe(III) along with other transition metal impurities was carried out on a reversed phase column using ion interaction chromatography mode. The column was dynamically modified with 5 mM Camphor-10-sulphonic acid (CSA), an ion interaction reagent (IIR) (modified cation exchanger). 0.2 M mandelic acid (MA) at pH 3.8 was used as eluent. Although simple aliphatic acids like tartaric, oxalic acids etc. are well known complexing agents used in the liquid chromatography separations of divalent and trivalent metal ions, mandelic acid was chosen in the present case because the tartrate and oxalate complexes of Fe(III) were stable and therefore, Fe elutes very close to the excluded peak, which causes its quantification difficult. The mandelate-Fe(III) complex exhibited significant retention and it was well separated from the other transition metals. A post column reagent of 5 x 10^{-5} M PAR was used at a flow rate of 0.8 mL/min for the detection of metal ions at 520 nm. The method was calibrated over the concentration range 1 to 25 ppm and the R^2 obtained as 0.9998 and the LOD was 0.5 ppm. For this separation, it is necessary to maintain the sample pH between 1.5 and 2 (adjusted with liq. NH_3).

Figure 2 shows an overlay of the chromatograms obtained for the standard as well as for the sample. Table 1 shows the results obtained for the samples.

Table-1: Results obtained for the samples

Samples	Concentration of Ca (%)*	Concentration of Fe (%)*
S-1	0.12 0.006	0.97 0.048
S-2	0.13 0.006	0.95 0.047
S-3	0.15 0.007	0.92 0.045

(*mean of three values)

Conclusions

Ion chromatography methods were developed for the interference free determination of Ca and Fe in Silicon and successfully applied for the real samples.

References

[1] Peter Herzner, and Klaus G. Heumann, Anal. Chem. 64 (1992) 2942.

[2] Z. Marczenko, and M. Balcerzak, Separation, Preconcentration and spectrophotometry in Inorganic Analysis, Elsevier (2000).

[3] Vaibhavi V. Raut, M. K. Das, S. Jeyakumar, and K.L. Ramakumar, DAE-BRNS Biennial Symposium on Emerging Trends in Separation Science and Technology, Delhi (2008).

Membrane based Isotope Dilution Alpha Spectrometry (MEM–IDAS) for Determination of Plutonium concentration

Sumana Paul[1], R.V. Shah[1], A.K. Pandey[2], S.K. Aggarwal[1]

1. *Fuel Chemistry Division, Bhabha Atomic Research Centre, Trombay, Mumbai 400085, India, E-mail: skaggr2002@rediffmail.com*
2. *Radiochemistry Division, Bhabha Atomic Research Centre, Trombay, Mumbai 400085, India*

Membrane based isotope dilution alpha spectrometry ((MEM-IDAS) was developed for the determination of plutonium concentration in complex aqueous matrices. A bi-functionalized polyethersulfone membrane was prepared by photo-induced free radical grafting process. The membrane was used for preconcentration of Pu from 3M HNO_3 medium followed by direct quantification of the preconcentrated Pu by IDAS, using ^{238}Pu spike. Pu concentrations in two unknown samples were determined and the results obtained were in good agreement with the biamperometric data.

Introduction

Determination of concentration of plutonium in various matrices e.g. dissolver solution of irradiated fuel, nuclear waste stream, environmental and biological samples is essential due to its strategic importance as well as associated radio-toxicity. Isotope Dilution (ID) technique is ideally suited for the determination of Pu concentration in a complex matrix like the dissolver solution of irradiated fuel which contains various fission products in different proportions, in addition to other actinide elements like U, Am etc. [1]. Isotope dilution provides highly precise and accurate results since the technique is independent of non-quantitative chemical recovery and matrix interferences. In ID–alpha spectrometry (IDAS), Pu concentration in a given sample is determined from the change in ^{238}Pu/(^{239}Pu+^{240}Pu) alpha activity ratio of the sample with respect to the same in a mixture of the sample and the spike solution. IDAS using ^{238}Pu as spike has been reported for determination of Pu concentration [2]. However, in order to produce good quality alpha source for IDAS, electrochemical deposition of Pu has to be carried out which is laborious and time consuming.

The present work involves the development of a thin, bifunctionalized grafted membrane suitable for selective preconcentration of Pu from complex matrices followed by quantification by direct measurement of the alpha activity in the membrane. Two monomers, 2-hydroxyethyl methacrylate phosphoric acid ester (HEMP) and 2-acrylamido-2-methyl-1-propanesulphonic acid (AMPS) were surface grafted on polyethersulfone (PES) membrane by photo–induced free radical process. Since phosphoric acid functional group has strong coordinating property towards actinides [3], the grafted membrane was found suitable for the quantitative extraction of various actinides depending on the acidity of the aqueous medium. The sulphonic acid functional groups in the polymer facilitate the ion transfer mechanism as well as help in charge neutralization. The HEMP-co-AMPS grafted PES membrane was used for preconcentration of Pu from 3M HNO_3 medium, followed by quantification of Pu by direct alpha spectrometry of the membrane.

Experimental

The monomers were grafted by irradiating 2x1 cm pieces of PES membrane, dipped in an equimolar mixture of HEMP and AMPS dissolved in 1:1 water-ethanol mixture, in a UV-photoreactor (= 365 nm) for 15 min. The PES membrane undergoes UV-induced photolysis to form free radicals, which in turn can initiate graft polymerization of the monomers on the surface of the host membrane. After grafting the membranes were washed with water-ethanol mixture to remove any unpolymerized component and were dried in oven at 70-80 .

For determination of Pu concentration by IDAS, weighed amount of ^{238}Pu spike solution was added to weighed amount of the sample. The mixture was treated with 3M HNO_3 and 20% H_2O_2 to convert all the Pu into Pu(IV) and equilibrated with HEMP-co-AMPS grafted PES membrane in 5 mL of 3M HNO_3 medium to get optimum extraction. After equilibration, the membrane was washed thoroughly with water, dried and placed directly in front of an ion–implanted alpha detector [PIPS Canberra, PD-300-16-100AM; resolution = 15 keV (FWHM) at 5.486 MeV alpha energy of ^{241}Am] with 300 mm^2 surface area to record the alpha spectrum.

Results and Discussion

The SEM–EDS analysis confirmed the homogeneous distribution of phosphoric acid and sulphonic acid groups on the surface of the grafted PES membrane. The sulphur to phosphorus (S/P) ratio was found to be 2.22 0.04, which is higher than the S/P ratio in the monomer mixture. This was attributed to the presence of S atoms on PES membrane. The physical structure of PES membrane did not change as grafting yield was 3-5 wt. %.

Figure 1 shows a comparison of the alpha spectra acquired from Pu loaded PES membrane with that of Pu

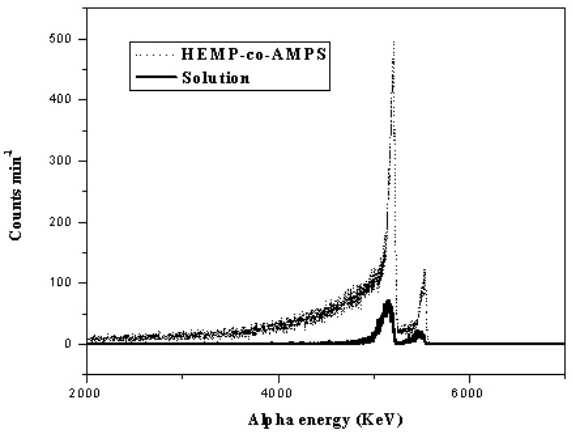


Fig. 1 Peak shapes of Pu loaded HEMP-co-AMPS grafted PES membrane & Pu deposited on steel planchet

solution (10 L) deposited on stainless steel planchet. Though, degradation of alpha energy is slightly higher in case of PES membrane compared to the planchetted source, count rate is higher for the membrane due to preconcentration of Pu from equilibrating solution, which in turn provides higher sensitivity.

In the present study, Pu concentrations in two unknown samples were determined by IDAS. Different amounts of PHWR grade Pu solution were added to two aqueous samples and Pu concentrations in these two samples were determined by biamperometry. A ^{238}Pu spike was used for isotope dilution. The isotopic compositions of the spike and the sample are given in Table 1. The ^{238}Pu/(^{239}Pu+^{240}Pu) alpha activity ratios for the spike and the sample were found to be 3808 and 0.2614, respectively.

Table-1: Isotopic composition of Pu in the sample and spike used for MEM–IDAS

Isotope	Atom fraction	
	Spike	Sample
^{238}Pu	0.9388	0.0016
^{239}Pu	0.0584	0.6879
^{240}Pu	0.0025	0.2694
^{241}Pu	0.0002	0.0209
^{2428}Pu	-	0.0201

A known amount of spike W_{sp} was added to a known amount of sample W_{sa} and alpha spectra of the sample, spike and the spiked mixture were recorded after preconcentration of Pu on grafted PES membrane. Concentration of Pu in the sample (C_{sa}) was determined using Eq. 1 [2]:

$$C_{sa} \frac{C_{sp}W_{sp}}{W_{sa}} \frac{^{238}A.F._{.238\ sp}}{^{239}A.F._{.239\ sa}} \frac{^{240}A.F._{.240\ sa}}{} \frac{R_{sp} - R_m}{R_{sp}\ R_m - R_{sa}} \frac{\langle At.Wt.\rangle_{sa}}{\langle At.Wt.\rangle_{sp}} \quad (1)$$

where, C_{sp} is the concentration of Pu in the spike solution, R_{sa}, R_{sp} and R_m are the alpha activity ratios in sample, spike and mixture respectively, AF is atom fraction and At.Wt. is average atomic weight of Pu. Pu concentrations in two unknown samples were determined by MEM-IDAS method and the results are given in Table 2. The results obtained by MEM-IDAS method agreed within ~5% with the biamperometric data.

Table-2: Concentration of Pu determined by MEM-IDAS using ^{238}Pu/(^{239}Pu+^{240}Pu) alpha activity ratio

Sample No.	Alpha activity ratio	Concentration (g/g)	
		M-IDAS	Biamperometry
1	0.55	2.40 0.09*	2.57
2	0.64	5.21 0.16*	5.14

*Average of three aliquots

Conclusions

Membrane based isotope dilution alpha spectrometry (MEM–IDAS) method was developed for the determination of Pu in complex aqueous matrices. A bi–functionalized polyethersulfone membrane was prepared by photo–induced free radical grafting process. The membrane was used for preconcentration of Pu from 3M HNO_3 medium followed by direct quantification of the preconcentrated Pu by IDAS using ^{238}Pu enriched spike. The method eliminates separate purification and alpha source preparation steps required for traditional IDAS method, thereby reducing analysis time and secondary waste generated. The M-IDAS method provided good precision and accuracy for determination of Pu at low levels in environmental and biological matrices.

References

[1] S. Paul, A. Sarkar, D. Alamelu, R.V. Shah, S.K. Aggarwal, Radiochim. Acta 100 (2012) 291.

[2] M.V. Ramaniah, H.C. Jain, S.K. Aggarwal, S.A. Chitambar, V.D. Kavimandan, A.I. Almaula, P.M. Shah, A.R.Parab, V.L. Sant, Nucl. Technol. 49 (1980) 121.

[3] Sumana Paul, Pranaw Kumar, A.K. Pandey, S.K. Aggarwal; Proceedings of 11th biennial DAE-BRNS Nuclear and Radiochemistry Symposium (NUCAR 2013), Paper No. B-17, p. 211.

Inverse-Frontal Chromatography studies on enrichment of Boron – 10 using quaternery 4- vinylpyridine-divinylbenzene resin

Venki Bejawada[1], Mohapatra.C[1], Rao A.S[1], Prasad.K.L[1], Murthy P.K[1], Rao A.K[1], Singh H.P[1], Vithal G.K[2], Sangita D Kumar[3]

1. *Process Control & Analytical Laboratory, Heavy Water Plant (Manuguru) , Manuguru, Andhrapradesh, 507116, India, E-mail: bejawadaanji@gmail.com, venkat@man.hwb.gov.in*
2. *Heavy Water Board, V.S.Bhavan, Mumbai 400085, India*
3. *Analytical Chemistry Division, Bhabha Atomic Research Centre, Trombay, Mumbai 400085, India*

In order to enrich ^{10}B, band migration of boric acid-mannitol with hydrochloric acid solution was performed by inverse frontal chromatography on a porous, 25% corsslinked, 38% quaternized 4-vinylpyridine-divinylbenzene resin (py-resin). The work was initiated to replace the existing strong base anion exchange resin type-II (SBA-II) which is used in Boron Enrichment Plant (BEP) of heavy water plant Manuguru. Before its application in BEP, it is mandatory to evaluate py-resin for its performance. The studies showed that maximum of 40% ^{10}B enrichment observed after 13 m band movement and there was no further improvement , hence profile sampling carried out after 28 m.

Introduction

Boron is known to have two stable isotopes, ^{10}B and ^{11}B with thermal neutron absorption cross-sections of ^{10}B and ^{11}B are 3837 and 0.005 barn respectively. The natural abundance of ^{10}B is 19.85%. Boron enriched in ^{10}B is used in the nuclear industry as control/shutoff rods in nuclear reactors, sensors for neutron counting, materials for neutron shielding etc [1].Ion-exchange chromatography is one of the most promising processes for boron isotope separation, and it has been used for the separation of boron on plant scale [2].

Boron isotope fractionation using porous, 20% cross-linked resin made from 4-vinylpyridine-divinylbenzene (4-VP/DVB) was earlier reported [12]. A good isotope separation was observed with the quaternized (4-VP/DVB) resin by inverse-frontal chromatography of boric acid-mannitol with hydrochloric acid solution. Inverse-frontal chromatography is an operational mode of chromatography in which an ion-exchange column is first saturated with the feed solution (of the isotopes to be separated), and the loaded material is then developed with a suitable developing agent. The selectivity of the developing agent for the resin should be higher than that of the components in the feed material to ensure "total refluxing." Initially boric acid-mannitol complex loaded to the resin packed in three columns up to saturation, then it was developed with hydrochloric acid solution which has more affinity to resin than boric acid-mannitol complex. During this process ^{10}B enriches at the rear end and ^{11}B enriches in the front end.

Experimental

Chemicals: NaOH, HCl, H_3BO_3, mannitol, py-resin.

Synthesis of Quaternized (4-VP/DVB) Resin

An experimental pyridine based resin was synthesized by co-polymerizing 4-vinylpyridine and divinylbenzene monomers in the presence of pore-forming agents by suspension polymerization. The purity of the commercial divinylbenzene was about 60%. The crosslinkage of the polymer was 25%. The polymer beads were white in colour. The polymer thus obtained was quaternized with dimethyl sulfate at 60 C for 165 minutes.

Preparation of Chromatographic Columns and Operation Procedure

Columns C_1 to C_6 were regenerated with 1 M NaOH and thoroughly washed with deionized water. Peristaltic pump was used for feeding of different solutions. Column C_1 loaded with feed solution containing 0.1 M H_3BO_3 (0.1985 atom % ^{10}B) and 0.2 M mannitol until saturation was reached. Boric acid concentration was monitored by titrating against standard NaOH using phenolphthalein indicator after addition of mannitol to the boric acid sample. Once C_1 is saturated the outlet of C_1 is connected to C_2 and then C_3. All these three columns i.e., C_1 to C_3 were loaded with boric acid till saturation. All these effluents are collected in a carbyl to determine the loading capacity of the resin. After the saturation of three columns initially C_1 was connected to the eluting agent (0.1 M HCl) line and C_3 outlet was connected to C_4 and the continuous monitoring of C4 outlet was carried out for boric acid concentration from. The elution process continued with a flow rate of 20 mL/minute (5cm/hour band moment). Once boric acid appeared in C_4 outlet, then it is connected to C_5. Like wise the operation continued in cyclic manner to move a migration of 28 meters of band moments. After completion of 28 meters of band moment profile sampling was done from C_2 outlet. These samples were analyzed using Inductively Coupled Mass Spectrometer for the determination of ^{10}B%.

Calculations

Mannitol-boric acid loading calculations

Inlet concentration of Mannito Boric Acid = 0.104 M (55.0L)

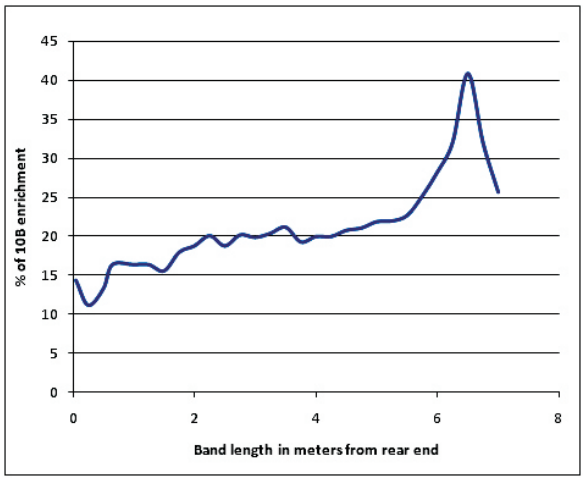
Outlet concentration of Mannito Boric Acid = 0.018 M (55.0L)

Boric Acid Loaded in columns = 288.91 g /9.0L of resin or 32.1 g/L of resin.

Amount of Enriched Boric Acid Collected at the end of experiment (Isotopic purity 22.0%) recovered from the resin after completion of the experiment = 52.3 g

Plot of percentage of enrichment Vs Band length

The plot of % of enrichment of ^{10}B against the band length from the rear end of the boric acid on resin phase is follows.



Conclusions

Boric acid enrichment is significantly more compared to the strong base anion exchange resin-II after a band moment of 13 m, whereas amount of boric acid loaded is less compared to the later one. Also it was observed that pressure built up in the columns during the operation, which could be due to the fines of the resin.

Future planning:

Since the expansion of Boric acid band, it is planned to conduct an experiment with decreased band length and decreased band movement and as there is no significant increase in enrichment of ^{10}B after a band movement of 12 or 13 m, to conduct the experiment by cut and feed method after 12 or 13m of migration.

References

[1] BARC news letter, Issue number 313, MAR-APR. (2010).

[2] P. Desrnoulins. in Stable Isotopes. Applicotion-Production, Gif-Sur-Yvette, France, (1994) 117.

[3] Y. Yoneda, T. Uchijirna, and M. Makishirna J. Phys. Chern., 63 (1959) 2057.

[4] M. M. Urgell. J. Iglesias. J. Casas, J. M. Saviron. and M. Quintanilla, Third CJN Int. Conf. Peaceful Uses of Atomic Energy, Spain, May (1964) 491.

[5] R. Rosset. H. Fould. M. Chemla. H. Labrousse. and J . Hure. Bull. Soc. Chitn. Fv., 3 (1964) 607.

[6] G. Christoph, J. Heybey. and H. Scutze. Isotopenpraxis, 12 (1976) 17.

[7] T. Hirao, M. Kotaka. and H. Kakihana. Nippon Nagaku Kaishi. (1973) 1477

[8] S. Itch. M. Ada, M. Okarnoto, M. Nomura, and Y. Fujii, fsotopenpraxis, 21 (1985) 204.

[9] Y. Sakuma, M. Aida. M. Okarnoto. and H. Kakihana, Bull. Chern. Soc. Jpn., 53 (1980) 1860.

[10] M. Aida, Y. Fujii, and M. Okarnoto, Sep. Sci. Techno/., 21 (1986) 643.

[11] Y. Fujii, M. Aida, and M. Okamoto, fbid.. 20 (1985) 377.

[12] A Mardan, Nucl. Sci. J., (In Press)

[13] M. Marhol, fon Exchange in Anulyticul Chemistry. Their Properties and Use in Inorganic Chemistry, Elsevier Science. Amsterdam (1982).

[14] S. Braman, in Trearise on Analytical Chemistry. 2nd ed. (I. M. Kolthoff and P. J. Elving. Eds.), Wiley. New York, NY (1978) 1.

[15] B. K. Sharma and R. Subramanian, Indian J. Chern. 30A (1991) 531.

Development of Carbon and Metallic Nano Particle Composite Materials for the Determination of Uranium and other Heavy Metal Ions

S. Sahoo, M.K. Dey, A.K. Satpati and A.V.R. Reddy

Analytical Chemistry Division, Bhabha Atomic Research Centre, Trombay, Mumbai, India; E-mail: asatpati@barc.gov.in

Carbon and metallic nano particle based composite materials were developed and characterised for the determination of heavy metal ions and uranium in trace concentration levels. Composite material were electrodeposited on the substrate electrode and applied for the electrochemical determination of metal ions. Electrodeposition parameters to synthesise the composite material and the analytical parameters for determination were optimised.

Introduction

Heavy metallic trace elements have been one of the most detrimental sources of pollution to the environments. They also have devastation effect on the ecological balance. Toxic heavy metals have been consistently increasing in the environment due to many human activities over time. Rapid diffusion of these metal ions in the environments and their deposition in almost all matrices of the food materials is a major concern. Heavy metals also constitute a human body in minor to trace levels. Their concentrations in the human system are so important that at marginally different concentrations they behave like nutrients or toxins. Other than presence in some marine diatoms Cd is generally considered as toxic and a human carcinogenic [1, 2]. In plants, Cd causes inhibition of photosynthesis, respiration, nitrogen metabolism and decreases water and mineral uptake [3]. Electrochemical methods based on the anodic stripping voltammetry using either mercury drop or the mercury film as the working electrode provides excellent method of the determination of heavy metal ions. However, use of mercury as the working electrode material is a debatable issue considering the toxicity of mercury [4]. Graphitic carbon in the form of paste called carbon paste electrode (CPE) is good alternative to mercury. However, CPE on its own could not preconcentrate any heavy metal ions on the surface. Bi-film and Sb-film modified CPE were introduced as an alternate electrode material in stripping voltammetry [5-11]. Electrochemical method based modified solid electrode has the advantage for the determination of toxic heavy metal ions due to its low cost and easy miniaturization, necessary in the field application.

Experimental

Electrochemical studies were carried out using the cell assembly with a three-electrode configuration consisting of the modified CPE as the working electrode and saturated calomel electrode (SCE) as the reference electrode. The potentials applied, measured and reported in this study were with respect to the SCE reference electrode at room temperature (298 K). A platinum rod served as the counter electrode.

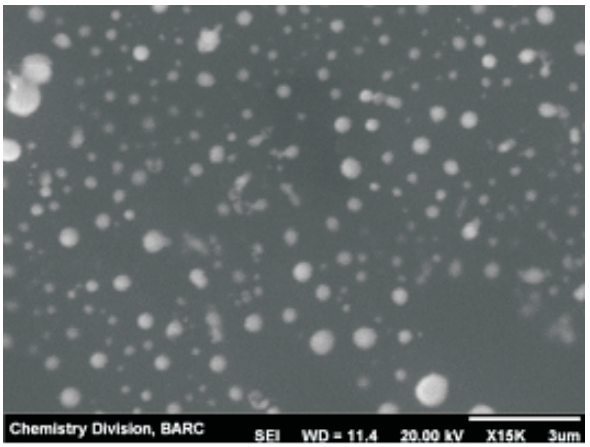


Fig. 1 SEM image of Hg nano droplets deposited over CPE

Electrochemical measurements were performed using an Eco Chemie Potentiostat/Galvanostat, Autolab-302N; the data acquisition and analysis were carried out by GPES 4.9 software. Prior to electrochemical scan, voltammetric solution was purged with high purity nitrogen for 10 min. Samples were not required to digest for the determination of heavy metal ions using the modified electrode.

Results and Discussion

Composite material of graphitic, multiwall carbon nano tube (MWCNT) and gold nano particles were prepared as electrode material for the determination of heavy metal ions. The CPE modified with Bi and gold nano particle composite material was abbreviated as CPE/Bi/AuNPs. For the determination of uranium composite material was modified with mercury nano droplets and adsorptive stripping voltammetry was employed. Nano composite materials were characterized using SEM, AFM, XRF and impedance measurements. SEM image of mercury nano droplet modified CPE applied for the determination of U was shown in Fig. 1. Metal ions like, Zn, Cd, Pb, Cu and Hg were determined using differential pulse anodic stripping voltammetry. Effect of electrochemical

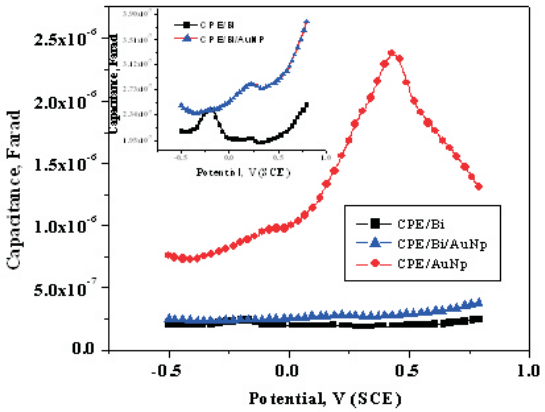


Fig. 2 Impedance plots of different deposits in 0.1 M acetate buffer solution of pH 4.5

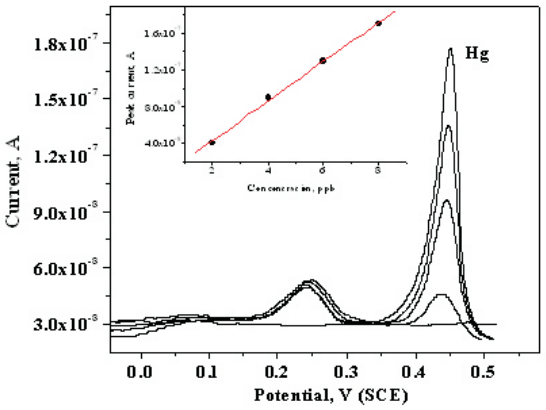


Fig. 3 Voltammetric response of Hg with 2 g L^{-1} of Hg^{2+} every time, Inset: corresponding linear calibration plot with the fitted line

parameters for the deposition and stripping were investigated and a deposition potential of -1.2 V for 300 s was optimised for simultaneous determination of these metal ions. However, to increase the sensitivity of Hg determination, separate calibration plot was constructed by increasing the amount of gold content in the composite material. A higher gold content was detrimental to the determination of other heavy metal ions due to the enhanced hydrogen evolution problems.

Electrochemical characterization of the Bismuth Bi/AuNp composite film modified carbon paste electrode (CPE/Bi/AuNPs) was carried out using electrochemical impedance measurements. Electrochemical impedance measurements were carried out at single frequency of 100 Hz with varying potentials shown in Fig. 2. For the comparison, carbon paste electrode modified with gold nano particles (CPE/Au) and carbon paste electrode modified with Bi film (CPE/Bi) were also shown. The capacitance of the Bi film modified carbon paste electrode was lowest. Inset of Fig. 2 shown some features of the change of capacitance with potentials. At around -0.2 V the increased capacitance was due to the oxidation of Bi-film. In the case CPE/Bi/AuNPs electrode, oxidation of metallic Bi was shifted to around 0.2 V. With incorporation of AuNPs into the Bi-film the capacitance has marginally increased due to the enhanced active surface area and also due to high activities of the AuNPs to electrochemical processes in blank solutions. CPE/Au electrode has shown very high capacitance way higher than the other two electrodes. The lower capacitance of the CPE/Bi/AuNps electrode is beneficial to have lower background in stripping analysis, in other words the film exhibits better conductivity. AuNPs modified CPE was applied for the determination of Hg and corresponding voltammograms are shown in Fig. 3. Corresponding calibration plot is shown in the inset of Fig. 3. The calibration plot was linear with the limit of detection of 0.14 gL^{-1} was obtained.

Conclusions

Carbon based composite materials were deposited and characterised. Composite materials were applied for the determination of heavy metal ions and also on Uranium. A few results on the analytical performance of the materials were shown.

References

[1] T. Lane, M. Saito, G. N. George, I. J. Pickering, R. C. Prince, F. M. M. Morel, Nature, 42 (2005) 435.

[2] M. P. Waalkes, S. Rehm, M. G. Cherian, Toxicol. Sci., 54 (2000) 11.

[3] L. S. di Toppi, R. Gabbrielli, Env. Exp. Bot., 41 (1999)105.

[4] J. Wang, Acc. Chem. Res., 35 (2002) 811.

[5] J. Wang, J. Lu, S. B. Hocevar, P. A. M. Farias, B. Ogorevc, Anal. Chem., 72 (2000) 3218.

[6] J. Wang, J. M. Lu, U. A. Kirgoz, S. B. Hocevar, B. Ogorevc, Anal. Chim. Acta, 434 (2001) 29.

[7] J. Wang, Electroanalysis, 17(2005)1341.

[8] O. Abollino, A. Giacomino, M. Malandrino, S. Marro and E. Mentasti, J. Appl. Electrochem., 39 (2009) 2209.

[9] E. Bernalte, C. Marín Sánchez, E. P. Gil, Sens. and Actu. B, 161 (2012) 669.

[10] E. Bernalte , C. Mar2n Sanchez and E. P. Gil, Talanta, 97 (2012) 187.

[11] G. O. Buica C. Bucher, J. C. Moutet, G. Royal, E. S. Aman, E. M. Ungureanu, Electroanalysis, 21(2009) 77.

Determination of Boron in Graphite, Boron Carbide and Glass by ICP-MS, ICP-OES and Conventional Wet Chemical Methods

K. Venkatesh, Granthali S. Kamble, Manisha Venkatesh, Sanjukta A. Kumar and A.V.R. Reddy

Analytical Chemistry Division, Bhabha Atomic Research Centre, Trombay, Mumbai 400085, E-mail: vkvenki@barc.gov.in

Boron is an important element of interest in nuclear reactor materials due to its high neutron absorption cross section ($_0$ =3837 barns for ^{10}B). In the present paper, R & D work and routinely used methods have been described for the analysis of case samples (1) Graphite where boron is present at trace levels, (2) Boron Carbide having boron concentration of about 80% and (3) Glass containing 4-6 % boron.

Introduction

Boron has a high neutron absorption cross section and monitoring boron content becomes imperative in nuclear fuel and nuclear structural materials like graphite which is used as a reflector and moderator in nuclear reactors. The boron concentration in the finished nuclear products must be determined with high accuracy and precision to be fit for its intended use. On the other hand, the high neutron absorption cross section makes it suitable as control rods for controlling the rate of nuclear reaction in research reactors. Borated paraffin is used as neutron moderator and absorber of neutrons. Boron is a major constituent in glass used for vitrification of nuclear waste. Boron is helpful in the vitrification process for reducing melting point and increasing breakage index and heat resistance. Additionally, boron increases chemical resistance of glasses. In all these materials boron concentration needs to be quantified reliably. The methods described in this article have been developed and documented. This article gives a summary of the work carried out in Analytical Chemistry Division, BARC over the past 2 decades, along with the recent developments [1,2]. To validate the method and for Quality Assurance purpose, samples have been analysed by nuclear analytical methods like Nuclear Reaction Analysis (graphite samples), at NCCM, Hyderabad and Particle Induced Gamma-ray Emission (for glass samples).

Experimental

Determination of Boron Content in Graphite

A method has been standardized in Analytical Chemistry Division, BARC for determining trace amounts of boron, which is a marker element for certifying the quality of graphite used in nuclear reactors. The method [1] involves dry ashing of graphite after fixing boron using barium hydroxide and determination by Inductively Coupled Plasma Mass Spectrometer (ICP-MS) using matrix matched standards.

Determination of Boron in Boron Carbide

An accurately weighed sample (about 0.1 g) is taken in a platinum crucible and is fused with 1.0 g of Na_2CO_3 for about 1h. The fused mass is cooled and leached using hot water. Interfering metal ions (if any), are separated by precipitation as carbonate by addition of AR grade $CaCO_3$. The sample is digested and filtered. The filtrate is made up to 250 mL. A 50 mL aliquot is taken in a 400 mL beaker; the solution is acidified and boiled for 2 min to expel CO_2. The solution is cooled and neutralized using methyl red indicator, followed by the addition of 2 g mannitol. The mannito-boric acid complex thus formed is then titrated against standard NaOH using phenolphthalein indicator.



Fig. 1 3 MV Tandetron at NCCCM, Hyderabad

Determination of Boron in Glass

The glass samples were dissolved by fusing them with Na_2CO_3 in a platinum crucible. The fused mass was leached with water and the boron content in the sample was determined using ICP-AES. Analytical parameters were optimized for quantitative recovery of boron from the sample matrix.

Results and Discussion

The use of ICP-MS allows the detection of boron in graphite at trace concentrations of 1 g g^{-1} with a method RSD of 5%. The method was verified by spike recovery experiments. Recoveries were found to be 100±2% in the concentration range of 1 to 100 g g^{-1}. A few samples were also measured by Ion Beam Analysis (IBA) carried out using the 3 MV Tandetron (Fig. 1) at Surface and Profile Measurement Laboratory, CCCM, Hyderabad, to validate the present method. Values were found to be in very good agreement [2].

The Na_2CO_3 method allows the determination of boron in boron carbide samlpes in the range of 1% to 100% with a method RSD of 0.5%.

The co-efficient of variation in glass samples, over triplicate analyses, was found to be 6%. The method was validated by comparing the results of the analysis with those obtained using a classical alkalimetric titration method (Table 1).

Table-1: Comparative study of boron contents using Titrimetry and ICP-OES

Sl. No.	Glass	% Boron (ICP-OES)	% Boron (Titrimetry)
1	GM-33 MOX-II	6.3± 0.4	6.3± 0.1
2	GM-44-WG	5.2± 0.3	5.4±0.1
3	PRTRF- 181	4.8± 0.3	5.6±0.1
4	FGS- 0.8	5.5± 0.3	6.1±0.1

Boron content of three samples (2,3 and 4) listed in Table 1 were analyzed by PIGE and the results are in good agreement. Work on determination of boron in various matrices using PIGE is being pursued in collaboration with Radio Chemistry Division, BARC.

Acknowledgements

The authors thank Dr. R. Acharya Radiochemistry Division, BARC, for his support and cooperation in preparation of this abstract and boron determination using PIGE. The authors also thank Dr. Sanjiv Kumar, NCCCM, BARC, Hyderabad, for his continued support in validating our results by Ion Beam Analysis.

References

[1] A. Tambe, K. Venkatesh and P. V. Ravindran; Exploration and Research for Atomic Minerals; 19 (2009) 191.

[2] K.Venkatesh, Sanjukta A. Kumar, Granthali S. Tambe, Shailaja P.Pandey; BARC Report (External) (2013) 004.

Radioimmunoassay Procedure for Human Insulin Based on magnetizable Particles

R.R. Rasmi[1], K.B. Shenoy[1], Jayula Sarnaik[2], V.B. Kadwad[2], H.M. Somashekarappa[1] and N. Sivaprasad[2]

1. *Centre for Application of Radioisotopes and Radiation Technology (CARRT), Mangalore University, Mangalagangothri 574199, India ; E-mail : bshenoyk@gmail.com*
2. *Radiopharmaceuticals Programme, Board of Radiation and Isotope Technology (BRIT), Vashi Complex, Sector 20, Vashi, Navi Mumbai 400705, India*

Introduction

Insulin is a 51 amino acid hormone secreted in the pancreas by the islets of Langerhans. It is an anabolic polypeptide that regulates carbohydrate metabolism.

We describe a user-friendly solid phase RIA for insulin based on antibody coupled magnetizable cellulose particles. The developed technique offers greater convenience by eliminating the need for precipitation and centrifugation to separate the antigen-antibody complex from free antigen with minimal errors.

Materials

Anti-insulin antibody was procured from Fitzgerald, USA. Patented Magnetizable cellulose particles were from BRIT. ^{125}I used for labeling was from Radiopharmaceuticals Division, BARC, India. Bovine serum for preparation of insulin standards was purchased from Himedia, India. Porcine insulin (100% cross reactivity with human insulin) used for the preparation of kit standards and 1,1 carbonyldiimidazole (CDI) were procured from Sigma Chemical Company, USA. All other reagents were of AR or GR grade. Single well manual gamma counter from ECIL, India and a multi-well gamma counter from STRATEC, Germany were used for counting the radioactivity associated with bound immune complex.

Experimental

Buffers Used

0.1M Sodium Bicarbonate buffer, pH 8.6
0.1M Sodium Acetate buffer, pH 4

Assay Buffer

0.05M Phosphate buffer, pH 7.4 containing 0.2% BSA and 0.1% Tween 20

Wash buffer

0.05M Phosphate buffer, pH 7.4 containing 0.5% Tween-20 and 0.9% Sodium Chloride

Magnetizable cellulose particles (average particle size of ~1.8 m) were covalently linked to anti-insulin antibody using carbonyldiimidazole (CDI) activation method [1]. Magnetizable cellulose particles have been preferred over similar other polymer coated magnetizable particles as they offer stable solid supports with reduced NSB [2-4]. Anti-insulin antibody was precipitated using sodium sulfate precipitation method prior to coupling with CDI activated magnetizable cellulose particles. Briefly, 1 g of particles in acetone were activated by carbonyldiimidazole. The activated particles were sequentially washed with acetone, double distilled water and bicarbonate buffer. The antibody in bicarbonate buffer was added to the activated magnetizable cellulose particles and incubated for 24 h on a shaker at 300 rpm. The antibody coupled particles were alternatively washed with bicarbonate buffer and acetate buffer and finally suspended in assay buffer.

Insulin tracer of a specific activity 150 Ci/ g was prepared by conventional chloramine-T method [5].

The standard curve using anti-insulin antibody coupled to magnetizable cellulose particles was established for serum insulin standards ranging from 7.5 to 200 IU/mL in hormone free serum.

The optimized protocol uses 200 L of standard/sample, 100 L of anti-insulin antibody coupled to magnetizable cellulose particles incubated overnight on shaker at a speed of 300 rpm, followed by addition of 100 L tracer with an incubation of 4h on shaker. The separation of the bound and free components of magnetizable particles was carried out using magnetic rack. The supernatant was decanted gently and all tubes were washed twice with wash buffer. Tubes were counted for radioactivity using I-125 counter for one minute.

Results

By using in-house prepared magnetizable cellulose particles, it was possible to economize on the amount of the antibody required for the assay. The magnetizable cellulose particle-antibody titre was found to be 1:4000, this corresponds to three times increase in consumption of antibody as compared with corresponding assay based on liquid phase separation system (1:12,000 titre). Generally, other solid phase assays like coated tube assays or coated beads do consume 5-12 times more antibody [2]. Non specific binding (NSB) checked by indirect method was found to be less than 1%. Anti-insulin antibody coupled to magnetizable cellulose particles was found to be stable for not less than 1 year when stored at 4°C. Intra-assay variations were between 5% to 10% whereas inter-assay variations were between 8% and 12%. Recovery of added insulin standards in serum samples were between 92% to 112%. The sensitivity of the assay

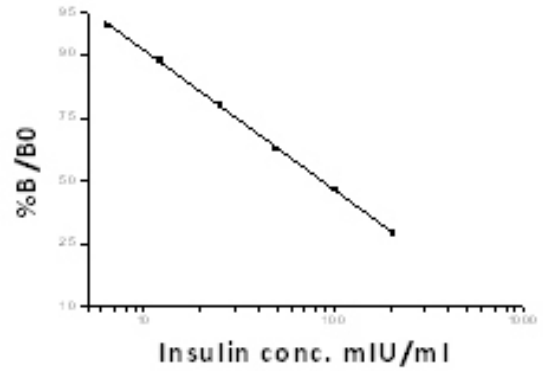


Fig. 1 A typical insulin RIA standard curve

was 5.5 IU/mL. No significant cross reactivity was observed with Somatostatin, Proinsulin, Pancreatic Polypeptide, C-peptide and glucagon. A typical standard curve is given in Fig. 1.

The sample values obtained by the present method correlated well with the values obtained in the existing BRIT Insulin RIA kit.

Discussion

Basically, success of most immunoassay procedures mostly lies in the efficient separation of the Ag-Ab complex from free Ag. Earlier methods employed cumbersome procedures like charcoal separation [6] and double antibody technique using anti-guinea pig -globulin [7]. The developed magnetizable particle separation for the insulin assay employs simple, one-step efficient and complete separation thereby providing more sensitive and accurate quantification of insulin levels.

Porcine insulin is the choice for the preparation of kit standards as well as for the preparation of tracer by the majority of the insulin immunoassay kit manufacturers as cross reactivity of porcine insulin with human insulin is 100% and widely available commercially in purified form [8].

Conclusion

The developed assay procedure can be adopted for large-scale production of Insulin RIA kits. Ready to use standards along with minimal pipetting steps make this assay protocol very attractive and can be compared with assays based on antibody coated tubes available from overseas suppliers, with an added advantage of economy in antibody consumption. Continuous large-scale production and supply of these kits over the years is possible due to local production of almost all reagents.

The sensitivity (5.5 IU/ml) and the range 7.5-200 IU/ml offered by the developed assay was comparable with the existing RIA kit for insulin based on liquid phase separation system supplied by BRIT (Product code: RIAK-1, sensitivity: 10 IU/ml, standard range: 12.5-200 IU/ml) with the added advantage of convenience and simplicity.

References

[1] Magnetizable Cellulose/iron Oxide Particle Activation and Coupling to Antibody (1.1'-Carbonyldiimidazole: CDI), SCIPAC Document No. 253051 (1996) 104.

[2] V. B. Kadwad, N. Jyotsna, N. Sivaprasad, P. K. Sinha, J. Radioanal. Nucl. Chem. 210 (1996) 27.

[3] U. V. Prasad, R. Krishna Mohan, G. Samuel, C. V. Harinarayan, N. Sivaprasad, M. Venkatesh, J. Radioanal. Nucl. Chem. 136:6 (2012) 963.

[4] R.K Mohan , V Kadwad, G Samuel, M Venkatesh, N Sivaprasad, J. Radioanal. Nucl. Chem.268 (2006) 461.

[5] F. C. Greenwood, W. M. Hunter, A. Klopper, British Medical Journal 5374 (1964) 22.

[6] J. D. M. Albano, R. P. Ekins, G. Maritz, C. Turner, Acta Endocrinol 1:70 (1972) 487.

[7] M. Dalpé-Scott, H. M. Heick, N. Bégin-Heick, Can J Biochem. 60:10 (1982) 962.

[8] T. J. Reimers, R. G. Cowan, J. P. McCann, M. W. Ross, American Journal of Veterinary Research, 43:7 (1982) 1274.

Attenuation Correction for the Segmented Gamma Ray Assay of Cylindrical Samples

Sabyasachi Patra, Chhavi Agarwal, and A. Goswami

Radiochemistry Division, Bhabha Atomic Research Centre, Mumbai 400-085, India; E-mail: agoswami@barc.gov.in

The Hybrid Monte Carlo (HMC) approach proposed earlier for self-attenuation correction, has been extended to the segmented gamma ray assay of the cylindrical samples. The lead acetate solutions in the concentration range of 100-450 mg/mL were chosen as the attenuating matrix. The attenuation correction factors were obtained at the gamma ray energies of ^{75}Se. The linear attenuation coefficient required as an input in the calculations, were obtained experimentally using ^{75}Se as the transmittance source. The HMC method has been validated by comparing the results with the experimental, far-field, near-field and MCNP calculated attenuation correction factors.

Introduction

Nondestructive assay (NDA) technique based on passive gamma ray spectrometry is generally used for the assay of special nuclear materials (SNM) in their existing form. Although these techniques are less accurate than conventional chemical and electrochemical techniques, but they are direct, fast and do not generate any radioactive waste. For the assay of an inhomogeneous sample, the NDA of the bulk material is superior to other solution analytical techniques based on physical sampling, because the finite number of samples may not be representative of the bulk nuclear material. The self-attenuation is an important factor to be carefully taken care during gamma-spectrometry based NDA. Different analytical formula and numerical methods are available in literature for attenuation correction [1]. A Hybrid Monte Carlo (HMC) method for attenuation correction has been developed in our previous work [2] and also validated experimentally using cylindrical, box and disc geometry [3].

For the NDA of an inhomogeneous sample, simple gamma spectrometric assay is inadequate because it cannot take into account the vertical variations in source distribution and matrix densities inherently present in this type of samples. Radial inhomogeneities are usually less pronounced, and their effects are substantially reduced by sample rotation. The Segmented Gamma ray Assay (SGA) is the most commonly employed technique for the assay of such heterogeneous samples. The basic principle of the SGA is to divide the sample into thin vertical segments and assay each segment independently using the transmission corrected passive assay technique. After all the segments have been measured, the results are summed to give the total assay for the sample. The SGA is usually employed to measure waste drums, typically 200 litre or smaller cylindrical waste containers. Most SGA systems employ a single shielded HPGe detector and single transmission source. In front of the detector, an open ended collimator is placed, so that the detector sees only one segment in height but the width of the drum.

In the present work, the HMC method has been extended to the SGA of 500 mL cylindrical samples. A prototype SGA system was designed in our laboratory to study the attenuation correction during segmented gamma-ray assay of 500 mL cylindrical samples. The lead acetate solutions in the concentration range of 100-450 mg/mL were chosen as the attenuating matrix, owing to the high Z of lead and high solubility of lead acetate. The attenuation correction factors were obtained at the gamma ray energies of ^{75}Se. The linear attenuation coefficient required as an input in the calculations, were obtained experimentally using ^{75}Se as the transmittance source. The method has been validated by comparing the results with the experimental, far-field, near-field and MCNP calculated attenuation correction factors.

Experimental

The lead acetate solutions in the concentration range of 100 - 450 mg/mL were prepared by dissolving required amount of lead acetate in water. The volume of these solutions was kept as 500 mL. The linear attenuation coefficients, (cm^{-1}) were obtained for four lead acetate samples at the gamma ray energies of ^{75}Se by transmission measurement of a collimated beam of ^{75}Se. For this, the transmission source was counted with and without the sample. Here, the unattenuated count rate was obtained by replacing the sample with water.

To get experimental attenuation correction factors, known amount of ^{75}Se activity was added to the lead acetate samples and to a water sample (blank). These samples were then counted in a 20% HPGe with a resolution of 2.2 keV at 1332 keV , collimated by an open-ended collimator with a width of 1.2 cm and length of 5.08 cm. The counting was done at d = 10.3 cm and 20.4 cm.

Results and Discussion

Figure 1 shows the experimental count rate per gram for ^{75}Se activity at 136 keV as a function of lead acetate concentration. The straight line in the figure shows the expected count rate per gram of ^{75}Se if there would have been no attenuation. However, in reality, it can be seen from the figure that due to gamma ray

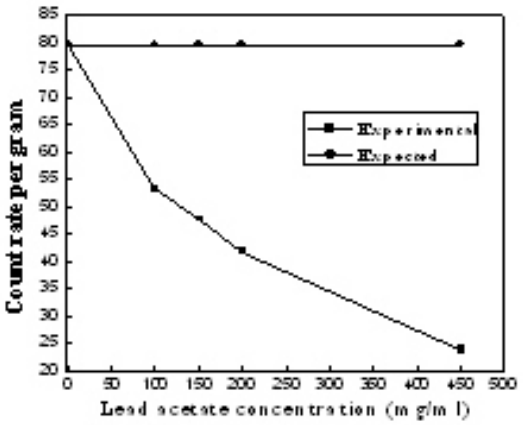


Fig. 1 *Count rate per gram of ^{75}Se activity at 136 keV as a function of lead acetate concentration*

attenuation, there is increasing deviation from linearity with increasing lead acetate concentration increases.

Experimental k_{att} were determined by taking the ratio of count rate per gram of blank to the count rate per gram of the sample. Figure 2 gives the Comparison of k_{att} obtained using different methods for segmented gamma ray assay system as a function of transmittance for two sample-to-detector distances (d) (a) d = 10.3 cm (b) d = 20.4 cm.

It can be seen that the experimental and HMC results are within 2-3% over the whole transmittance range at d = 10.3 cm and within 4-5 % at d = 20.4 cm. The MCNP k_{att} values matches within 5-10% with the HMC method k_{att} at both the distances. At d=20.4 cm, the far-field results are within 1% of the HMC and experimental values upto a transmittance of ~10%. Below this transmittance, the far-field value deviates by about 6%. Whereas at d= 10.3 cm, this deviation of far-field formula starts below the transmittance of ~ 60%. In this case, at lower transmittance, the far-field formula deviates from HMC and experimental attenuation correction factors by about 15-16%. This indicates that although far-field formula for segmented gamma ray scanning can be used successfully for samples with higher transmittance even at close sample-to-detector distance, however, it cannot be used for samples with lower transmittance even at far distance. The near-field values match reasonably well with the MCNP and experimental k_{att} values at d = 20.4 cm. But at d = 10.3 cm, as seen from the figure, the near-field formula values deviates by about 10% at lower transmittance.

This implies that the near-field formula although said to be valid at close sample-detector geometry over all transmittance range, starts working only after certain sample-to-detector distance, whereas the HMC approach is found to be applicable at all sample-to-detector distance.

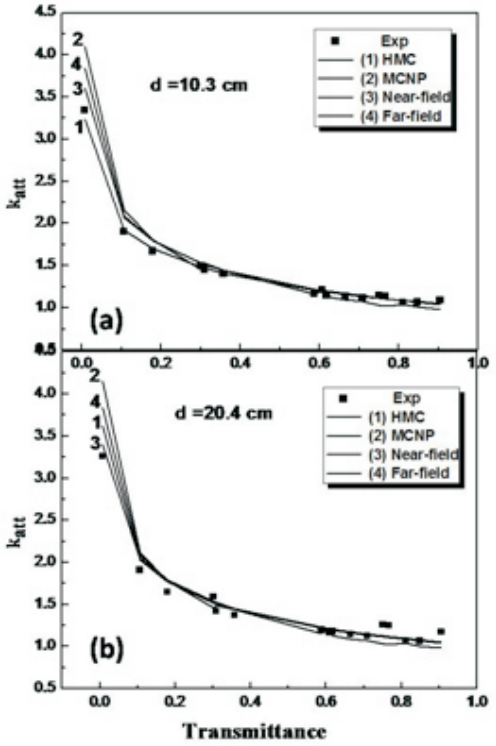


Fig. 2 Comparison of attenuation correction factors obtained using different methods for segmented gamma ray assay system as a function of transmittance for two sample-to-detector distances (d) (a) d = 10.3 cm (b) d = 20.4 cm

Conclusions

The HMC method has been theoretically and experimentally validated. It was observed that the near-field formulas available in literature are applicable only after certain sample-to-detector distance. The results of the present calculation show the possibility of using a simplified common approach to calculate the k_{att} for the segmented gamma ray assay system without bothering about the sample-to-detector distance, over wide range of transmittance.

References

[1] D. Reilly, N. Ensslin, H. Jr. Smith and S. Kreiner, Passive non-destructive assay of nuclear materials, Los Alamos National Laboratory, United States, (1991).

[2] C. Agarwal, S. Poi, A. Goswami, M. Gathibandhe and R.A. Agrawal, Nucl. Instr. And Meth. A 597 (2008) 198.

[3] C. Agarwal, S. Poi, A. Mhatre, A. Goswami and M. Gathibandhe, Nucl. Instr. And Meth. A 607 (2009) 439.

On-site Monitoring of Uranium in Low Level Liquid Waste Streams using U-Br-PADAP Strip Indicator Paper Technique

S. Ganesh, P.Velavendan, N.K. Pandey, U. Kamachi Mudali and R. Natarajan

Reprocessing Research Development Division, Indira Gandhi centre for atomic research, Kalpakkam 603102, India; E-mail: velp@igcar.gov.in

A simple, rapid and selective colorimetric technique for the determination of low level concentration of uranium in nuclear waste streams is described. The proposed method is based on the intensity of U-BrPADAP (Uranium-2-(5-Bromo-2-pyridylazo)-5-diethyl-aminophenol) colour formed on strip indicator paper. The effect of pH, concentration of chromogenic reagent, stability of the colour, volume of buffer solution and interference of metal ions were studied. The method is inexpensive, applicable for determination of uranium in water streams in nuclear reactor/polluted water samples. The detection limit is 1mg/L. Various uranium samples have been tested for the validation of the proposed method. The results obtained are reproducible and good agreement with those obtained by the standard technique.

Introduction

Analysis of uranium in ore extracts, low level liquid waste streams from nuclear fuel reprocessing and in natural waters (underground waters, mineral, well waters and water from areas with potential pollutants) needs simple and rapid methods for quantification of uranium. Determination of uranium content in samples associated with the low level liquid waste disposal or for safeguard inspection activities required fast, reliable and cheap analytical methods at trace level concentration. Because of the increased usage of uranium for nuclear power generation and also the risks associated with low level liquid waste disposal from uranium-handling plants [1]. A number of analytical methods have been reported for the determination of trace level concentration of uranium in environmental samples [2]. The present method is simple, fast and reliable based on colorimetric technique.

Experimental

All reagents used were of analytical reagent grade. Stock solution of uranium were prepared and standardized [3] by potentiometric method. 0.05% of 2-(5-Bromo-2-pyridylazo)-5-diethyl-aminophenol) were prepared in ethanol with buffer solution (TEA) and Cyclohexanediamine tetra acetic acid (CyDTA). Buffer solution of pH 11.2 was prepared by dissolving 13.5 mL of triethanolamine (TEA) in 100 mL distilled water. Complexing solution was prepared by dissolving 5 g of CyDTA and 1g of NaF in distilled water, adjusting the pH to 11.2 with sodium hydroxide and diluted to 100 mL. Whatmann filter paper no.1 is washed with double distilled water and allowed to dry in air. 100 mL of of Br-PADAP solution was prepared and the filter paper was immersed for 24 to 36 hours to impregnate BrPADAP on filter paper and dried at room temperature.

Uranium standard solution of different concentration was prepared in 10 mL standard flask. Suitable aliquot of uranium standard solution was added on the BrPADAP strip indicator paper and dried at room temperature. The intensity of the developed colour was observed and found to be in the increasing order with respect to uranium concentrations. Using this standardized colorimetric technique uranium present in the unknown samples at trace level concentration was determined rapidly by comparing the standard strip chart.

Results and Discussion

The reaction between uranium and Br-PADAP is a well established process. Br-PADAP form pyridyl azo chelate red complex with uranium in ethanolic medium. These properties results from strong interaction of the lone pair of the alkylated amino group in the para position towards the azo group with the aromatic ring. TEA may serve as suitable masking agent for interference of metal ions such as Th, Zr, and Ce. The effect of buffer solution, variation of BrPADAP concentration, stability of strip indicator paper was also studied. A standard U-BrPADAP strip indicator chart is represented photographically in Fig.1. Comparisons of results of simulated uranium solution with unknown samples are shown in Fig.2.

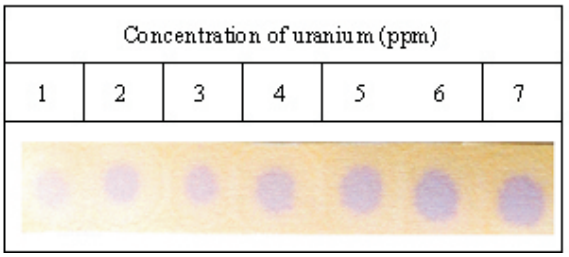


Fig. 1 Standard U-BrPADAP strip indicator chart

Conclusions

The developed method is simple, fast and reliable for the routine analysis of various streams contains low level concentration of uranium.

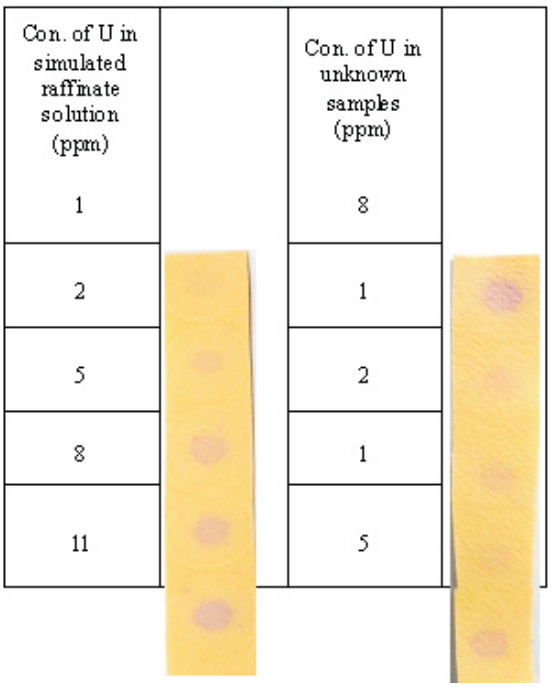


Fig. 2 Comparisons of results of simulated uranium solution with unknown samples

References

[1] Z.Tosheva, K.Stoyanova, L.Nikolchev, J.Enviorn. Radioact., 72 (2004) 47.

[2] S.Ganesh, F.Khan, M.K.Ahmed, P.Velavendan, N.K.Pandey, U.Kamachi Mudali, S.K. Pandey, J Radianal Nucl Chem 292 (2012) 331.

[3] W. Davies, W.Gray, Talanta 11 (1964) 1203.

Auto-counting of High Density Overlapping Tracks and Neutron Spectrum Measurement Using CR-39 Detectors and in-house Image Analysis Program

Sabyasachi Paul, S.P. Tripathy, G.S. Sahoo, D.S. Joshi, T. Bandyopadhyay

Health Physics Division, Bhabha Atomic Research Centre, Trombay, Mumbai 400085, India;
E-mail; spaul@barc.gov.in

An effort is made in this work to overcome the difficulty of counting highly dense and overlapping tracks in solid polymeric track detectors (SPTD) such as CR-39. A program is developed to automatically count the track density which is found to be faster and more precise compared to other commonly used image analysing software. The results obtained by the present methodology are compared with those obtained using other software.

Introduction

Solid polymeric track detectors such as CR-39 ($C_{12}H_{18}O_7$) are extensively used for routine monitoring of environmental radioactivity and neutron measurements around reactor and accelerator facilities. Since the neutron field around particle accelerators is often pulsed and mixed [1], CR-39 detectors are found to be more suitable due to their permanent and integral mode of signal registration, insensitivity to low LET radiations and ease of accessibility (smaller size and no supporting instrumentation) during irradiation and simplicity in etching procedure [2]. Nevertheless, the processing and counting of the registered tracks are tedious and time consuming which can be overcome with rapid etching techniques [3] and automatic counting [4,5]. Several image analysing software such as AxioVision from Carl Zeiss, ImageJ, etc. are available for automatic counting of the tracks which somehow are not up to the mark due to failure in automatic separation of the actual tracks and track-like defects in the detector and counting of highly dense overlapping tracks. Some of the software are capable of segregating the overlapping tracks before counting, which is not done perfectly thus introducing errors in the measurement and affecting the computational time.

In this aspect, a new program (autoTRAK_n) is developed in this work to count the high density overlapping tracks without applying the segregation procedure. The accuracy of the method is tested by exposing CR-39 detectors with D-T neutron source and the comparison with other available software are presented in the paper. The program is based on the analysis of greylevel variation within each track and is already applied to generate standard neutron spectra which are reported earlier [5]. However, the effect of bin-width on the generated neutron spectra is investigated in this work.

Materials and Methods

Irradiation, Etching and Imaging

A set of CR-39 detectors of dimension 10×20×1.5 mm^3 are irradiated with 14 MeV D-T neutrons at 6 cm distance for 250 s at the Institute of Plasma Research, India. After irradiation, the neutron induced recoil tracks are developed using chemical etching (6.25 N NaOH, 70°C, 9h) and track images are captured by a 5 MP Carl Zeiss camera at a magnification of 100x. Similar procedure is followed for a pristine CR-39 detector for background correction.

Image Analysis

The 2D-greyscale images are processed using autoTRAK_n program [5] by correlating the variation in grey values within each track with depth (in terms of range of the particle, obtained from SRIM [6]). The quantitative estimation of greyscale variation is done with an 8-bit color coding to distinguish color ranges varying between 0 (black) and 255 (white) [4]. The images are taken in transmission mode of the microscope and the variation in light intensity due to attenuation of light inside the detector material is determined by the program. From this variation in the track depth, the distribution of the depth and hence the energy of recoil particle can be calculated. Then recoil particle energy (E_R) is converted to neutron energy (E_n) using the scattering angle ( ) of the particle with respect to the surface of the detector, using the relation (1),

$$E_R \quad \frac{4A}{1 \quad A^2}\cos^2 \quad E_n \qquad (1)$$

where, A the mass of the recoil particle. Finally the track depth distribution (tracks cm^{-2}) is folded back with track to detector response function (tracks n^{-1}) to obtain the incident neutron fluence (n cm^{-2}) and their energy distribution. Along with this, the effect of bin width on the spectrum is also studied.

Results and Discussion

A track image having high density overlapping tracks due to neutron-induced secondary charged particles along with the counting of track density by the present program (autoTRAK_n) and by 2 other available image analysing softwares (AxioVision, ImageJ) is shown in Fig.1. As can be seen in the figure, the identification and contour recognition of tracks are found to be better in case of autoTRAK_n. Most of the

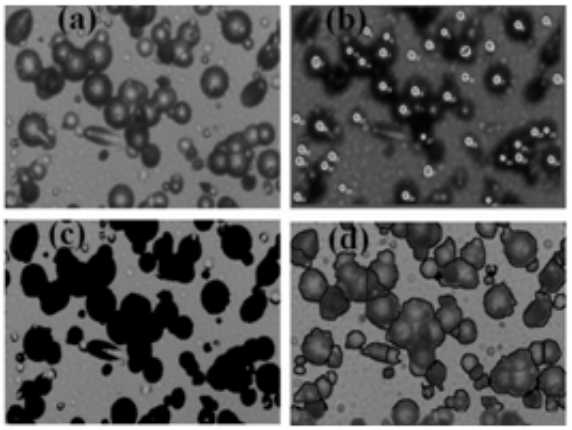


Fig. 1 Microphotograph of recoil tracks due to D-T (14 MeV) neutrons in CR-39 detector. (a) Original track image (42 m×27 m), and the tracks detected with (b) autoTRAK_n, (c) AxioVision and (d) ImageJ

overlapping tracks are counted as single track by AxioVision and ImageJ thus affecting the overall track density. Since the track recognition by the present method is based on the grey value analysis of each pixel, it is possible to distinguish almost all the overlapping tracks because of the separation of most intense pixel within the tracks. The track recognition by autoTRAK_n is based on inside out approach, i.e., the track centre is chosen first for detection purpose and then the boundary of that track is searched [4]. Once the track boundary is obtained, the track is registered and patched with a single color to avoid repeated counting of the same track. The track density and other relevant parameters as obtained using 3 different analysing methods are given in Table 1. As shown in Table 1, neutron fluence obtained by autoTRAK_n is found to be about 2 and 3 times higher compared to ImageJ and AxioVision respectively.

Table 1: Estimation of the neutron fluence with different software

Software	Average no. of tracks per frame	Track density (track cm^{-2})	Fluence (n cm^{-2})
autoTRAK_n	631	2.65×10^{5}	1.43×10^{9}
AxioVision	245	1.03×10^{5}	0.55×10^{9}
ImageJ	337	1.42×10^{5}	0.76×10^{9}

The program autoTRAK_n is already applied to generate standard neutron spectra and is reported earlier [5]. However, an attempt is made in this work is to study the effect of bin-width on the neutron spectrum. The analysis is carried out with three different bin sizes viz., 0.1, 0.5 and 1 MeV and the unit spectra for each bin-width are presented in Fig. 2. All three spectra are found to be Gaussian in nature around 14 MeV. The

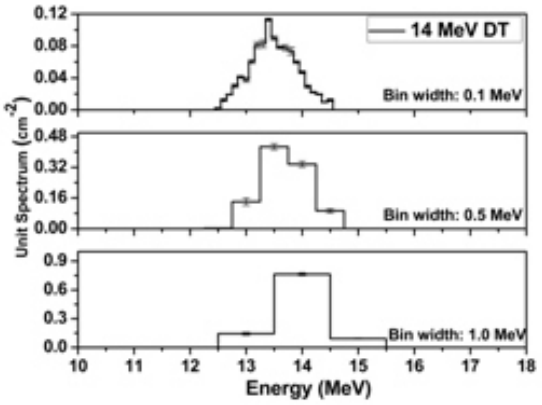


Fig. 2 Effect of bin-width on D-T neutron spectra obtained using CR-39 and autoTRAK_n program

amplitudes of the unit spectra are different due to different number of bins within the energy range and the individual spectra are given as in Fig. 2.

As can be seen from Fig. 2 and as expected, the peak position is not affected by bin size variations, particularly when statistically significant number of tracks are analyzed (~20,000) and the error bar is found to be within 5%. However, 1 MeV bin-width seems more acceptable in producing a smooth spectrum.

Conclusions

In this work, a simple and effective program (autoTRAK_n) is applied for automatic counting of high density overlapping tracks without involving any segregation procedure as usually done by other available image analysing software. The code is found to be more accurate in estimating the track density compared to other software due to its inside out approach in detecting tracks. This track detection algorithm (without individual track processing for spectrum generation) can be used separately as a subroutine for faster computing and precise estimation of track density and/or neutron fluence for routine measurements. For spectrum measurement, even though the bin size does not affect the peak position, 1 MeV bin-width is found to be more acceptable in generating a smooth spectrum.

References

[1] P.K. Sarkar, Radiat. Meas. 45 (2010) 1476.

[2] G. S. Sahoo, S. P. Tripathy, C. Sunil, P. K. Sarkar, Nucl. Ins. Meth. A, 708 (2013) 46.

[3] S.P. Tripathy et al, Nucl. Ins. Meth. A 612 (2010) 421.

[4] S. Paul, S.P. Tripathy, P.K. Sarkar, Nucl. Ins. Meth. A 690 (2012) 58

[5] S. Paul, S.P. Tripathy, G. S. Sahoo, T. Bandyopadhyay, P.K. Sarkar, Nucl. Ins. Meth. A (In Press).

[6] J. F. Ziegler, M. D. Ziegler, J. P. Biersack, Nucl. Ins. Meth. B 268 (2010) 1818.

Geometrical Parameters of Tracks Registered by Collimated alpha Particles on CR-39 Detector

Pranav M. Joshirao[1], Chirag K. Vyas[1], Jae Won Shin[2], Seung-Woo Hong[1,2] and Vijay. K. Manchanda[1]

1. *Department of Energy Science, Sungkyunkwan University, Suwon, South Korea 440746, E-mail: vkm49@skku.edu or vkm25749@gmail.com*
2. *Department of Physics, Sungkyunkwan University, Suwon, South Korea 440746*

The track characteristics of CR-39 exposed to alpha radiations depend on various factors like a) angle of incidence, b) energy of incidence c) nature of chemical etchant and d) etching conditions. The characteristics of tracks were studied as a function of angle of incidence of alpha particles emanating from a collimated ^{241}Am source. GEANT 4 simulation was carried out to obtain the angular distribution and energy distribution of the alpha particles incident on CR-39 detector placed at a distance of 1.5 cm. An attempt was made to correlate the experimental track density as well as geometrical parameters of the tracks with the simulation parameters.

Introduction

Solid state nuclear track detectors (SSNTDs) are passive but ultrasensitive to charged particle radiations. CR-39 (polyallyl diglycol carbonate) has been used for a variety of applications including radon monitoring in environment, uranium prospecting and basic nuclear radiation studies. Latent tracks formed on exposure to radiations are developed using chemicals which etch tracks preferentially over bulk material followed by their inspection using an optical microscope. The geometry of the tracks depends on the energy and incident angle of the charged particles. 2D images of the tracks are either circular (for normal incidence) or elliptical (for acute angle incidence).The aspect ratio value (ratio of major axis to minor axis) is a parameter which can be determined experimentally. GEANT4 simulation studies can help understand the energy / angular distribution of the alpha particles incident on the CR-39 detector. An attempt has been made in the present work to correlate the aspect ratio of the tracks with the incident angle obtained by GEANT4 simulation.

Experimental

Schematic of the experimental setup is given in Fig.1. The alpha source was a planar, electroplated ^{241}Am (main alpha energy 5.49 MeV) having activity 3.585 kBq (4 geometry), and surface emission rate of 106500 /min in 2 geometry. It was procured from Eckert & Ziegler – Isotope Products, USA. The active area of the source was covered with an SS sheet of 0.6 cm thickness with a circular slit of 0.3cm diameter at the centre (for reducing the divergence of alpha particles). The CR-39 film was of dimension 0.5 cm x 1 cm. The breadth was divided into regions of 1 mm width and each region was further divided into square sub regions of 1mm x 1mm. The regions were referred to as A-E and the sub regions were referred to as A1-A5, B1-B5. The regions A, B and B` are aligned with the 3 mm aperture of the source. The alpha fluence and angular distribution in each region was computed by GEANT 4 simulation (version 9.4.p02). A detailed description

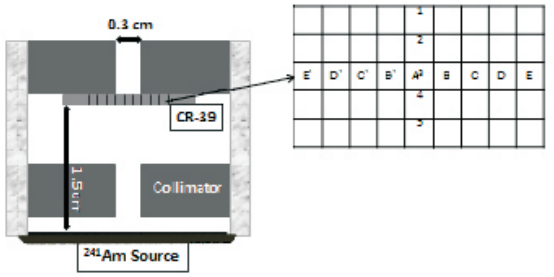


Fig. 1 Schematic of experimental set up

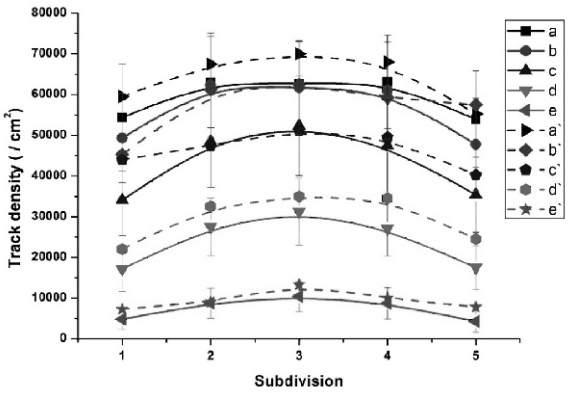


Fig. 2 Simulated and experimental track density values (a – e: simulated; a`– e`: experimental)

and validation of the code can be found at the GEANT4 website [1]. Track development was done using 6M NaOH at 60°C as etchant in a sonicator for 4 hours.

Results and Discussion

The experimentally obtained track density values for different regions and sub regions were compared with simulated values. Fig. 2 shows that there is reasonable agreement between the two sets. It is observed that the farther we go from the aligned region, the track density value decreases. This is because alphas are cut off by the collimator, thereby reducing the

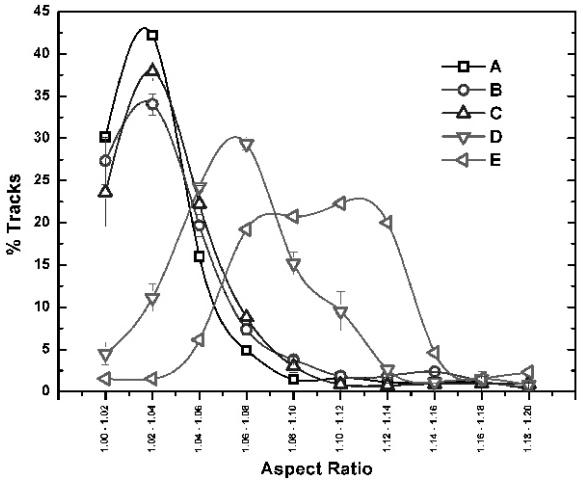


Fig. 3 % tracks distribution for different regions

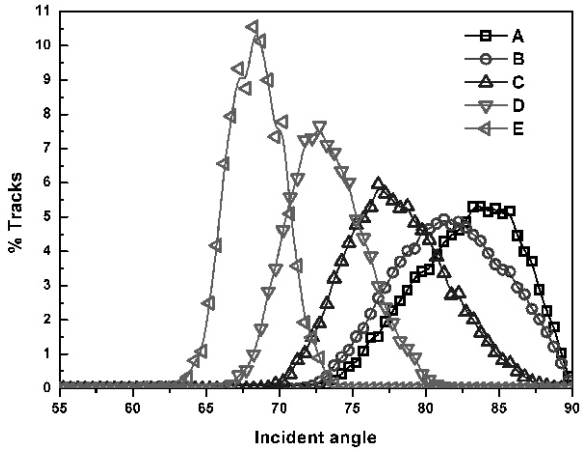


Fig. 4 *Simulated angular distribution for different regions*

number of impinging alphas on the detector. The angle of incidence of alphas defines the track geometry. Fig.3 shows the experimentally obtained distribution of tracks for specified aspect ratio range for different regions. It is observed that the peak shifts towards lower aspect ratio for regions having higher incidence angles. For lower angle of incidence, aspect ratio shifts farther away from unity. Also, for regions which are not in alignment with the radiation source, a broad peak is observed. Fig. 4 gives the simulated angular distribution for different regions. The aligned regions have tracks registered at incident angles starting from 90°. As we move farther from the aligned regions, the angular distribution deviates from 90°. Table 1 summarizes the angular distribution of different regions as obtained by GEANT 4 simulation. This is reflected in the aspect ratio values for these regions as well

Table 1: Range of incident alpha for different regions.

Region	Simulated incidence angle range	Aspect ratio (maxima)
A	73° – 90°	1.01-1.03
B	72°– 90°	1.02-1.04
C	70°– 90°	1.02-1.04
D	67°– 82°	1.06-1.08
E	63°– 74°	1.12-1.14

Acknowledgement

This research was supported by World Class University (WCU) Program to V.K.M.and S.W.H. through the National Research Foundation of Korea (NRF) funded by Ministry of Education, Science and Technology (R31-2008-10029).

References

[1] Geant4: A toolkit for the simulation of the passage of particles through matter, available online at <http://geant4.web.cern.ch/geant4/>.

Radon, Thoron and their progeny concentration variations in dwellings of Gogi region, Yadgir District of Karnataka, India

Avinash P.R.[1], S. Rajesh[1], B.R. Kerur[1], Rosaline Mishra[2]

1. *Department of Physics, Gulbarga University, Gulbarga 585 106, India; E-mail: kerbrk@yahoo.com*
2. *Radiological Protection and Advisory Division, BARC, Mumbai 400 085, India.*

The radiation dose due to inhalation of radon, thoron and their progenies constitute a major part (50%) of the total natural background dose received by a man. Thus measurement of indoor radon in dwellings is very important. In the present study, radon, thoron and their decay product measurements were carried out using passive detector systems, namely the pinhole dosimeters and Direct Radon (Thoron) progeny sensors. These measurements were carried out in indoor environments (different dwelling types) during January-April 2013, in the Gogi region. The long time averaged radon, thoron and decay product concentrations were found to be within the permissible UNSCEAR limits.

Introduction

^{222}Rn (radon) and ^{220}Rn (thoron) belong to ^{238}U and ^{232}Th naturally occurring decay series and their inhalation contributes to about half of the natural radiation dose [1]. The energetic alpha particles emitted from ^{222}Rn and two of its daughter elements viz. ^{214}Po and ^{218}Po are highly effective in damaging the tissue and are considered to be a causative agent for lung cancer in human beings [2]. In a lifetime a living house is at the action level of 200 Bq/m^3 carries a 3-5% risk of fatal cancer [5,6]. This has been an increasing awareness regarding the measurement of radon, Thoron and decay products simultaneously. A lot of work has been carried out towards this.

The study area covers Gogi region of Yadgir district belonging to northern part of Karnataka situated between 16°11'- 16°50' N Latitudes and 76°17'-77°28' E Longitudes, with a geographical area of 5234.4 Sq.km. The northern part of the district represents a plateau, typical of Deccan Trap terrain and the soil types in the district are deep black, medium black soil, shallow soil and lateritic soil. In the present work, simultaneous measurement of radon and thoron gas along with their decay product concentrations measurements has been carried out in the indoor environments.

Materials and Methods

Selection of Indoor Environments

Different types of houses were selected for deployment like Reinforced Concrete Construction (RCC), Mud, Rockwood, and Tin. In this region, the Gogi(K), Gogi Peth, Singanahalli, Karkalli, Rabanalli and Kanchinakavi villages were covered, and 32, 30, 09, 10, 15, 04 houses were selected respectively. So, a total of 100 houses were selected. The measurements were carried out during Jan-April 2013.

Detectors used

For radon and thoron gas measurements pinhole dosimeters have been used. The dimension of the pinhole dosimeters is 2 mm length and 1 mm diameter are made in this circular disc, consist of 2 compartments, a) only radon chamber, b) radon+thoron chamber. In each chamber 3 x 3 cm size LR115 type SSNTD is installed. For Radon and Thoron decay products, DTPS-DRPS dosimeters were used [3]. It consists of aluminized mylar mounted LR115 detector for separately measuring the radon progeny and thoron progeny. For measuring only the attached fraction of the progeny concentration wire-mesh capped DTPS/DRPS were used [4].

Deployment details

The pinhole dosimeters along with DTPS-DRPS dosimeters are deployed in January in the dwellings with 50cm distance from the wall at a height of more than 2m above the ground level and about 50 cm below the ceilings and away from the walls.

Analysis

After the exposure for 3 months the detectors were retrieved and etched using 2.5 N NaOH solution at 60°C for 90 min. Subsequently, the tracks were counted using a spark counter and these counted tracks are converted into the radionuclide concentrations by the use of appropriate calibration factors. The annual inhalation dose of the present study region is calculated using the following relation

$$\text{Dose} = (\text{CRn} \times 0.17 + \text{CTn} \times 0.11 + \text{EECRn} \times 9 + \text{EECTn} \times 40) \times 8760 \times 0.8 \times 10^{-6}\ \text{mSv}$$

where, C_{Rn} and C_{Tn} are the concentration of radon and thoron in Bq/m^3, EEC_{Rn} and EEC_{Tn} are the respective radon and thoron progeny concentrations. 0.17 and 0.11 (nSv/Bq/m^3/h) are the dose conversion factors for radon and thoron gas, 9 and 40 (nSv/Bq/m^3/h) are the dose conversion factors for radon and thoron progenies, 8760 h/y is the indoor occupancy time, 0.8 is the Indoor occupancy factor.

Results and Discussion

In the present work, ^{222}Rn and ^{220}Rn and their progeny concentrations were measured for the month Jan-April, 2013. These results support studies, showing

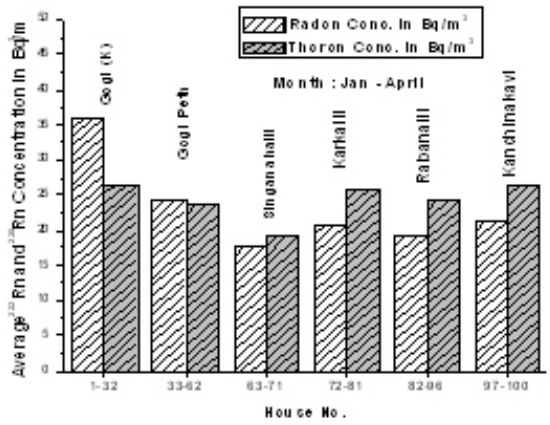


Fig. 1 The ^{222}Rn and ^{220}Rn concentration of the Gogi region

equal concentration of thoron in comparison with radon in certain cases (Table 1).

The ^{222}Rn and ^{220}Rn and their progeny concentrations have been measured in different type of dwellings located in the Gogi region and the values were found to be within the permissible UNSCEAR limits [7]. The attached fraction of progeny concentration marked as EEC_{WRn} and EEC_{WTn} in Table 1 was also found to be very close to the total progeny concentration. This indicates very low unattached fraction. Further the studies on the seasonal variation in Gogi and other villages will be carried out.

Conclusion

The 1st set of simultaneous long time averaged radon, thoron and progeny concentration measurements were carried out in around 100 dwellings of Gogi region. The thoron concentrations were observed to be almost equal to radon gas concentrations. The progeny concentrations were found to be in the same range as reported in other regions. The analyses of the successive sets are in progress.

Acknowledgement

The authors express their deep sense of gratitude to Board of Research in Nuclear Science (BRNS) for providing the financial support to carry out this work successfully. The authors are also thankful to the members of Radon/Thoron Progeny Research Laboratory, RP&AD, BARC, Mumbai for their help in carrying out intercomparison exercises. The cooperation extended by all the residents of Gogi region is highly appreciated.

References

[1] T. S. Shashikumar, M. S. Chandrashekara, N. Nagaiah and L. Paramesh; Radiation Protection Dosimetry, 133(1) (2009) 44.

[2] Rohit Mehra and Pankaj Bala; Advances in Applied Science Research. 4(1) (2013) 212.

[3] Rosaline Mishra, Y.S. Mayya; Radiation Measurements 43 (2008) 1408 .

[4] Y.S. Mayya, Rosaline Mishra, Rama Prajith, B.K. Sapra, H.S. Kushwaha; Science of the Total Environment 409 (2010) 378.

[5] ICRP; Protection against radon-222 at home and at work; ICRP Publication 65 (1993).

[6] NRPB; Health Risks from Radon Faculty of Public Health Medicine, Chilton: NRPB (2000)

[7] UNSCEAR; Sources and effects of ionizing radiations United Nations, New York (2000).

Table 1: The average radon, thoron and their progeny concentrations (Total EEC_{Rn} EEC_{Tn} and Attached fraction EEC_{WRn} EEC_{WTn}) of Gogi region.

Sl. No.	Sample Location	House No.	Average ^{222}Rn Conc. (C_{Rn}) in Bq/m^3	Average ^{220}Rn Conc. (C_{Tn}) in Bq/m^3	Average EEC_{Rn} in Bq/m^3	Average EEC_{Tn} in Bq/m^3	Average EEC_{WRn} in Bq/m^3	Average EEC_{WTn} in Bq/m^3	Average Annual inhalation dose in mSv/y
1	Gogi (K)	1-32	36.01±15.71	26.59±12.35	15.61±7.21	1.31±0.50	15.31±5.41	1.34±0.48	1.41±0.57
2	Gogi Peth	33-62	24.18±7.19	23.68±4.37	10.28±4.08	1.02±0.31	9.68±3.46	1.21±0.35	0.98±0.33
3	Singanahalli	63-71	17.69±2.79	19.01±4.92	10.66±1.40	0.98±0.12	8.22±0.89	0.91±0.15	0.98±0.12
4	Karakalli	72-81	20.76±1.89	25.63±2.82	11.83±1.62	1.17±0.11	11.29±1.56	1.16±0.12	1.12±0.14
5	Rabanalli	82-96	19.03±2.67	24.21±2.54	11.23±1.19	1.10±0.11	10.68±1.25	1.06±0.14	1.06±0.11
6	Kanchinakavi	97-100	21.27±7.28	26.11±4.06	11.57±2.48	1.14±0.28	11.98±2.29	1.21±0.30	1.10±0.24

Study on Gamma-ray Energy Absorption in SSNTDs and PTNDs

Vishwanath P. Singh[1] and N.M. Badiger[2]

1. *Department of Physics, Karnatak University, Dharwad, 580003, India; E-mail: kudphyvps@rediffmail.com*
2. *Health Physics Section, Kaiga Atomic Power Station-3&4, NPCIL, Karwar, 581400, India*

Abstract

The gamma-ray energy absorption in solid state nuclear track detectors and plastic nuclear track detector has been computed in the present study. Energy absorption buildup factors were calculated for photon energy 0.015 to 15 MeV by Geometrical Progression (G-P) method. An appreciable variation in energy absorption buildup factors was observed for investigated detectors. The energy absorption buildup factors were small in low- and high photon energy was observed in intermediate-energy region. This study is vital in the field of neutron dosimetry by solid state and plastic nuclear track detectors for gamma dose measurements.

Keywords: energy absorption, G-P fitting, nuclear track detectors

Introduction

Nuclear track detectors have potential applications in various areas such as nuclear physics, space physics, material science, geophysics, bio-medical sciences, dosimetry and environmental science. Possibilities of gamma radiation measurement by solid state nuclear track detectors (SSNTDs) and plastic nuclear track detectors (PTNDs) have been reported [1, 2, 3]. SSNTDs are being used for neutron personnel monitoring in nuclear reactors and accelerators in presence of gamma-ray. In track detectors, for gamma-ray measurement as well as interactions requires in-depth knowledge of energy loss in the detector materials.

Harima et al. [4] developed a fitting formula, called Geometrical Progression (G-P) which gives buildup factors of the good agreement with the ANS-6.4.3 [5]. Harima reviewed historical and reported the current gamma photon buildup factors [6]. Various researchers investigated gamma-ray buildup factors in neutron shielding and concrete materials [7, 8] which show that the G-P fitting is very useful and accurate method for estimation of energy absorption buildup factors.

Materials and Methods

We have taken Olovine, Quartz, Sodalime, PC (Makrofol, Lexan, Millar), CN (Daicell, LR-115) soild state and plastic nuclear track detectros for computation of gamma energy absorption buildup factors. These deterors are common in use for measurement of neutron and gamma radiation. The energy absorption buildup factors (EABFs) were computed by G-P fitting method [6]. The computational work was done in three steps (a) calculation of equivalent atomic number, Z_{eq} (b) calculation of G-P fitting parameters and (c) calculation of buildup factors. The detailed description for computation EABFs can be found elsewhere [8].

Result and Discussion

The variation of EABF values of the selected detectors for photon energy 0.015 to 15 MeV at 0.5 and 40 mfp is shown in Fig. 1. It was noted that the EABF values of the detectors were minimum for low- and high-energy photon whereas highest in the intermediate-energies. The buildup factors in low-energy are small because the photon are completely removed during the photo-electric absorption, gradually increase with the photon energy due to multiple scattering by Compton scattering in the intermediate-energy and finally reduce in high-energy region due to pair-production process. The analysis showed that the EABF values increase with penetration depths. It is to be noted that the PC is having highest and olivine lowest EABF values for entire energy region of interest at low penetration depth whereas the pattern changes for large penetration depth above 3 MeV. The reason for reversal behavior may be due to that beyond 3 MeV, the pair-production dominant on the Compton scattering and produces the electron-positron pairs. These pair particles may escape from the detector medium of lower penetration depth whereas will multiple scatter in large penetration depths as well as start off the secondary gamma photons (0.511 MeV) by annihilation to increase the gamma photon intensities. Analysis signifies that the EABF values for PC detector are minimum at large penetration depths for photon energy region above 3 MeV whereas Olivine detector is observed to be with largest EABF value.

Conclusion

The gamma-ray energy absorption buildup factors solid state and plastic nuclear track detectors were calculated by Geometrical Progression method. The results shows that energy absorption buildup factors of the selected detectors are highest in medium energy range whereas minimum in low- and high- photon energies. These buildup factors increase with penetration depths. The study should be useful for neutron dosimetric purposes by nuclear track detectors.

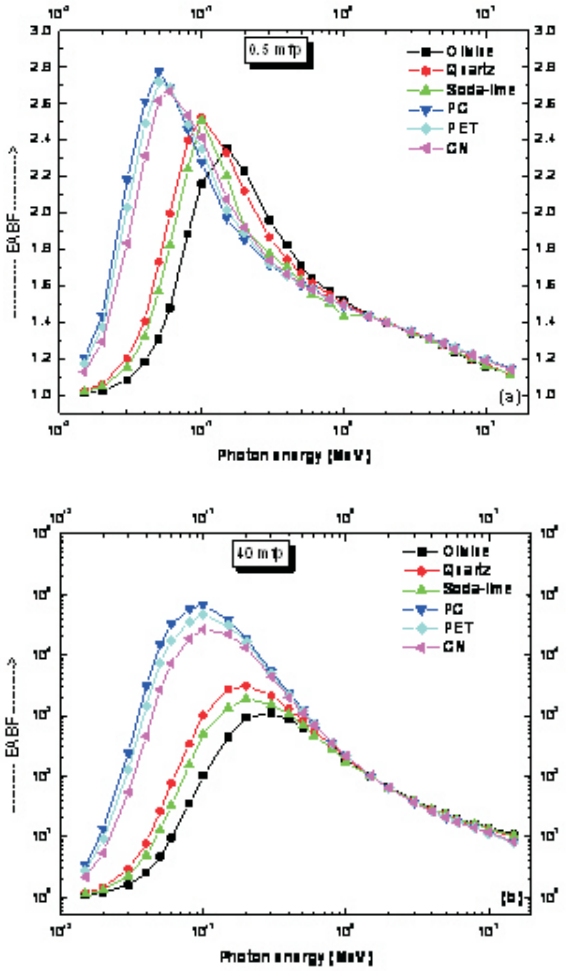


Fig. 1 Energy absorption buildup factors of solid state and plastic nuclear tract detectors

References

[1] P. C. Kalsi, Indian J. Phys. 83 (6) (2009) 799.

[2] B. Milenkoviae, D. Nikeziae, N. Stevanoviae, Radia. Measur. 45, (2010)1338.

[3] N. A. Khan, H. A. Khan, K. Gul, M. Anwar, G. Hussain, R. A. Akbar, A. Waheed, M. S. Shaikh, Nucl. Instrum. Methods. 173 (1980) 163.

[4] Y. Harima, Y. Sakamoto, S. Tanka, M. Kawai, Nucl. Sci. Engg. 94 (1986) 24.

[5] ANSI/ANS-6.4.3, American Nuclear Society, La Grange Park, Illinois (1991).

[6] Y. Harima, Nucl. Sci. and Eng. 83, (1983) 299.

[7] M. Kurudirek, D. Sardari, N. Khaledi, C. Çak2r, K. S. Mann, Ann. Nucl. Ener. 53 (2013) p.485.

[8] V. P. Singh, N. M. Badiger, Nucl. Ener. Scien. Tech. 7 1 (2012) 75.

Estimation of Radon exhalation Rate in Gopalpur beach Sand samples Orissa, Eastern India

Ajay Kumar Mahur[1*], Anil Sharma[2,3], D. Sengupta[4] R.G. Sonkawade[5] and R. Prasad[1]

1. *Department of Applied Science, Viveakanada College of Technology and Management Aligarh-202001 India; E-mail: ajaymahur345@rediffmail.com*
2. *B B A University Vidya Vihar, Rai Bareilly Road Lucknow 226 025, India*
3. *University School of Basic & Applied Sciences, G G S I P University, New Delhi 110403, India*
4. *Department of Geology and Geophysics, I.I.T., Kharaghpur, West Bengal 721302, India*
5. *Inter- University Accelerator Centre, Aruna Asaf Ali Marg New Delhi- 110067, India*

In the present studies radon exhalation rates in sand samples collected from Gopalpur beach placer deposit in Orissa are measured by using "Sealed can technique" using type LR 115-II nuclear track detectors. Radon activities are found to vary from 371.4 ± 23.0 to 800.0 ± 33.8 Bqm^{-3} with an average value of 549.2 ±27.8 Bqm^{-3}. Surface exhalation rates in these samples are found to vary from 133.4 ± 8.3 to 287.7 ±12.1 mBqm^{-2}h^{-1}with an average value of 197.2 ± 9.9 mBqm^{-2}h^{-1}, whereas, mass exhalation rates vary from 5.1 ± 0.3 to 11.1 ± 0.5 mBqkg^{-1}h^{-1} with an average of 7.6 ± 0.4 mBqkg^{-1}h^{-1}.

Introduction

Radon exhaling properties of porous materials are of prime importance for the estimation of radiation risk and have been the subject of several investigations [1,2]. The correlation between the uranium concentration and the radon emanation potential of the source material is required for radon risk.

The sand is the basic ingredient used in construction materials in India. By mixing it with cement, sand is commonly used as a binding material for fired clay and fly ash bricks for the construction of walls and also as a plastering material. It is also used in the preparation of concrete. Thus it is quite important to find its radon emanation potential to have an estimation of radiation risk to the habitants.

Study area: Gopalpur is located at 19°16'N 84°55'E / 19.27°N 84.92°E / 19.27; 84.92 on the coast of Bay of Bengal, around 160 km south of Paradip and 260 km north of Visakhapatnam. It is a natural, deep sea port on the east coast of India. Gopalpur lies on a 4 km stretch of barren coast line, with no mangrove or tropical forests. The coast line falls in the rain-shadow of the region.

Materials and Methods

Radon Exhalation Rate

For the measurement of radon exhalation rate, "sealed can technique" was used. Equal amount of samples (100 g) were placed in the cans (diameter 7.0 cm and height 7.5 cm) similar to those used in the calibration experiment [3]. LR-115 type II solid state nuclear track detector (2 cm × 2 cm) was fixed on the top inside the cylindrical can. The cans are sealed for 90 days and thus the sensitive lower surface of the detector is freely exposed to the emergent radon so that it could record the tracks of alpha particles resulting from the decay of radon in the remaining volume of can. Radon and its daughters reach an equilibrium concentration after 4 hours and hence the equilibrium activity of emergent radon can be obtained from the geometry of can and the time of exposure. After the exposure for 95 days the detectors were taken out and etched in 2.5 N NaOH at 60^0 C for a period of 90 min in a constant temperature water bath. The resultant alpha-particle tracks were counted using an optical microscope at a magnification of 400 ×. From the track density the radon activity was calculated using a calibration factor of 0.056 track cm^{-2} d^{-1} (Bq m^{-3})$^{-1}$, obtained from an earlier calibration experiment [3] and recalibration afterwards.

Surface exhalation rate is obtained from the following expression [4-8].

$$E_A = \frac{CV}{A\,T + \frac{1}{-}\,e^{\;T}\;1} \qquad (1)$$

This formula is also modified to calculate the mass exhalation rate

$$E_M = \frac{CV}{M\,T + \frac{1}{-}\,e^{\;T}\;1} \qquad (2)$$

where, E_A is radon surface exhalation rate (Bq m^{-2} h^{-1}) ; E_M is radon mass exhalation rate (Bq kg^{-1}h^{-1}) ; C is a radon exposure as measured by LR -115 type II solid state nuclear track detector (Bq m^{-3} h) ;V is the effective volume of can (m^3); is the decay constant for radon (h^{-1}); T is the exposure time (h); A is the area of the can (m^2) and M is mass of the sample.

Results and Discussion

The values of radon activities, mass exhalation rates and surface exhalation rates in the sand samples collected from the Gopalpur beach Sand samples Orissa, Eastern India are measured. Values of radon activities are found to vary from 371.4 ± 23.0 to 800.0 ± 33.8 Bqm^{-3} with an average value of 549.2 ±27.8 Bqm^{-3}. Surface exhalation rates in these samples are found to

vary from 133.4 ± 8.3 to 287.7 ±12.1 $mBqm^{-2}h^{-1}$ with an average value of 197.2 ± 9.9 $mBqm^{-2}h^{-1}$, whereas, mass exhalation rates vary from 5.1 ± 0.3 to 11.1 ± 0.5 $mBqkg^{-1}h^{-1}$ with an average of 7.6 ± 0.4 $mBqkg^{-1}h^{-1}$.

References

[1] Jonassen, N. Health Phys. 45(1983) 369.

[2] Karmadoost,et al., Nucl. Tracks Radiat. Meas. 15(1988) 647.

[3] Singh, et al., Radiat. Prot. Environ. 3(1997) 129.

[4] Mahur, et al., Nucl. Instr. and Meth. in Physics Research B 266 (2008a) 1591.

[5] Mahur, et al., J. Environ. Radioact. 99(2008b) 1289.

[6] Mahur, et al, Appl. Radiat. Isot. 66(2008c) 401.

[7] Mahur, et al., Indian Journal of Pure & Applied Physics. 48 (2010) 486.

[8] Mahur, et al., Radiation Measurements 50 (2013) 130.

Thoron Interference in Radon Exhalation Rate Measured by Solid State Nuclear Track Detector based Can Technique

B.K. Sahoo, T.K. Agarwal, B.K. Sapra

Radiological Physics and Advisory Division, Bhabha Atomic Research Centre, Mumbai- 400 085, India;
E-mail: bijay@barc.gov.in

The objective of this study was to establish the possible thoron (^{220}Rn) interference in the radon (^{222}Rn) exhalation rate, commonly measured by Solid State Nuclear Track Detector (SSNTD) based Can technique. The investigation was carried out using nine samples, of which 3 samples were enriched in ^{226}Ra (uranium tailings), 3 samples were enriched in ^{232}Th (Mixture of soil and Thorium Oxide) and remaining 3 samples were enriched with both ^{226}Ra and ^{232}Th (Monazite Sand). Experiments were carried out following the standard procedure of 'Can' technique as well as active techniques as a reference method for ^{222}Rn and ^{220}Rn exhalation measurements. It was found that there is a significant deviation between the results obtained by can technique and active technique. This arises mainly due to unwanted track registration in SSNTD (LR-115 Kodak Type II) because of ^{220}Rn emission from sample. Calculation shows that this ^{220}Rn interference may lead to overestimation of ^{222}Rn exhalation by a significant factor which can be as high as 12 depending upon the rate of ^{220}Rn exhalation from samples. It was also observed that the recommendation of maintaining a gap of 7 cm between surface of the sample and SSNTD in the conventional 'Can' technique is not adequate enough to ignore the ^{220}Rn interference

Introduction

Radon (^{222}Rn) and thoron (^{220}Rn) exhalation from soil and building materials are the major source of indoor radon concentration which is responsible for contributing half of the natural radiation dose to humans. Solid State Nuclear Track Detector (SSNTD) based 'Can' technique has been widely used to measure ^{222}Rn exhalation from samples of these materials. This technique was proposed by Abujarad [1] aiming to quantify the ^{222}Rn exhalation from samples of building materials using a track detector (CR-39 or LR-115). Since soil and building materials contain some amount of ^{232}Th, it is expected that they will also emit ^{220}Rn in addition to ^{222}Rn. The present study has been carried to investigate the possible interference of ^{220}Rn on measured ^{222}Rn exhalation rate.

Materials and Methods

Experiments were carried out following the standard procedure of 'Can' technique [1] as well as active techniques [2] for ^{222}Rn and ^{220}Rn exhalation measurements. Total of nine samples were analyzed, of which 3 samples were enriched in ^{226}Ra (uranium tailings), 3 samples were enriched in ^{232}Th (Mixture of soil and Thorium Oxide) and remaining 3 samples were enriched with both ^{226}Ra and ^{232}Th (Monazite Sand). In the case of 'Can' technique, Sample (~100 g) was placed at the bottom of a cylindrical sealed can of 10 cm height and 7cm diameter. The mouth of the cylindrical 'Can' was sealed with a cover and fitted with LR-115 type-II plastic track detectors at the top inner surface.

The same 'Can' has been utilized to measure ^{222}Rn and ^{220}Rn exhalation by using continuous ^{222}Rn and ^{220}Rn monitor respectively. The experimental set up is shown in Fig. 1. The ^{222}Rn mass exhalation rate (J_m) of the sample was extracted by least square fitting of



Fig. 1 Active measurement of radon exhalation using the Can connected to Smart Radon Monitor

Eq.(1) [2] to the measured buildup data of radon concentration in the can while ^{220}Rn surface exhalation rate (J_T) of the sample was obtained from the Eq. (2) [3] using the measured equilibrium concentration of ^{220}Rn (C_T) and other input parameters.

$$C_R(t) = \frac{J_R M}{V \lambda_e}\left(1 - e^{-\lambda_e t}\right) + C_0 e^{-\lambda_e t} \quad (1)$$

$$J_T = \frac{C_T V \lambda_T}{A} \quad (2)$$

where, $C_R(t)$ is the radon concentration measured by radon monitor at time t, V is effective volume of the set up i.e. sum of detector volume of radon monitor and air volume inside the can, λ_e is the effective decay constant which is sum of radon decay constant, radon back diffusion constant and leakage rate of chamber, if any, M is mass of sample and C_0 is initial radon concentration inside the chamber at t=0, λ_T is the decay

Table 1: Results of measured radon and thoron exhalation from analyzed samples using active and 'Can' techniques

Sample type	Sample Code	Radon mass exhalation rate ($Bq\ kg^{-1}\ h^{-1}$)		Thoron surface exhalation rate by active technique ($Bq\ m^{-2}\ s^{-1}$)
		Active technique	Can technique	
U tailings	UT-1	4.32 ± 0.41	4.95 ± 0.45	0.62± 0.08
	UT-2	4.63 ± 0.61	5.87 ± 0.38	0.85± 0.12
	UT-3	5.25± 0.52	6.12 ± 0.48	0.75± 0.11
Mixture of soil and ThO_2	Th-1	0.024 ± 0.005	0.28±0.03	67.35± 6.34
	Th-2	0.034± 0.006	0.32± 0.04	68.58± 8.20
	Th-3	0.037± 0.003	0.29± 0.02	68.08± 8.56
Monazite sand	MS-1	1.55 ± 0.22	4.56 ± 0.42	18.34 ± 2.52
	MS-2	1.39 ± 0.18	4.22 ± 0.34	16.51 ± 3.23
	MS-3	1.45 ± 0.21	5.16 ± 0.52	21.36 ± 3.12

constant of ^{220}Rn, A is the surface area of ^{220}Rn exhalation (i.e area of the Can).

Results and Discussion

The results of ^{222}Rn and ^{220}Rn exhalation obtained by SSNTD based can technique as well as active technique are given in Table 1. It may be observed that ^{222}Rn exhalation rate measured by Can technique was close to the value that measured by active technique only in the case of ^{226}Ra enrich samples. In other cases, there is a significant deviation between the results obtained by can technique and active technique, which is mainly due to ^{220}Rn interference in the SSNTD (LR-115) based Can technique. LR-115 detector present in the Can registers track due to alpha particle emission from decay of ^{222}Rn as well as ^{220}Rn in the volume of the Can and thus overestimate the ^{222}Rn exhalation value in the process of calculation. Though, LR-115 film is normally kept 7 cm away from the surface of the sample inside the Can, but this distance may not be adequate enough to ignore the track contribution due to ^{220}Rn emission from samples. Calculation shows that this ^{220}Rn interference may lead to overestimation of ^{222}Rn exhalation by a significant factor which can be as high as 12 depending upon the rate of ^{220}Rn exhalation from samples.

Conclusion

It is found that ^{220}Rn can interfere in ^{222}Rn exhalation measurement made by Can technique. This leads to overestimation of ^{222}Rn exhalation by a significant factor which can be as high as 12 depending upon the thorium content of the samples and size of Can. The recommendation of maintaining a gap of 7 cm between surface of the sample and SSNTD in the conventional 'Can' technique is not adequate enough to ignore the ^{220}Rn interference. Thus, time has come to relook at the 'Can' technique and redesign it to minimize the interference of ^{220}Rn.

Acknowledgements

Authors would like to thank Shri DAR Babu, Head, RP&AD BARC for his encouragement and support.

Reference

[1] Abu-jarad, F. A., Nucl. Tracks Radiat. Meas., 15 (1-4) (1988) 525.

[2] Sahoo BK, Nathwani D, Eappen KP, Ramachandran TV, Gaware JJ, Mayya YS. Rad. Meas., 42 (2007) 1422.

[3] Sahoo B.K., Mayya Y.S., Agric. and Forest Meteorol, 150 (2010) 1211.

Distribution of Natural Gamma Radiation and Radon Levels around a Thorium Beach Sand Mining and Processing Facility, Odisha

S. Mohapatra[1], S.K. Sahoo[1], J.S. Dubey[1], Sumesh C.G.[1], S.K. Tripathy[1], D.V. Sagar[1], S.V. Godbole[2], P. M. Ravi[1] and R.M. Tripathi[1]

1. *Health Physics Division, Bhabha Atomic Research Centre, Trombay, Mumbai 400 085, E-mail: jbsmohapatra@gmail.com*
2. *Radiochemistry Division, Bhabha Atomic Research Centre, Trombay, Mumbai-400 085*

Present work deals with the study of the distribution of natural gamma radiation and radon levels around a thorium beach sand mining and processing facility, Odisha, called as Orissa Sand Complex (OSCOM). The study area is a Natural High background Radiation Area (NHBRA) and the external gamma radiation levels vary from 40-1800 with an average of 226 nSv/h. The observed gamma radiation levels, 86 % are more than 100 nSv/h. The average outdoor and indoor radon levels were found to be 21 and 30 which ranged between 6-41 and 18-65 Bq/m$^{3.}$

Introduction

Natural background radiation contributes significantly (80 %) to the annual effective dose received by the general population [1,2]. Natural background radiation arises due to radionuclides ^{238}U, ^{232}Th, ^{40}K, ^{222}Rn and ^{220}Rn present in indoor and outdoor environment [3]. Radiation exposures vary as a result of human activities and practices and geological distribution. The greatest fraction of the natural radiation exposure (nearly 50 %) to humans results from inhalation of the short-lived decay products of radon (^{222}Rn) and thoron (^{220}Rn), from the indoor air and outdoor atmosphere [4]. It is well known that inhalation of the short-lived decay products of ^{222}Rn, and their subsequent deposition along the walls of the various airways of the bronchial tree provides the main pathway for radiation exposure of the lungs. This exposure is mostly produced by the alpha particles emitted by these radionuclides. However some areas in the world map are called as natural high background radiation areas (NHBRA) due to local geology, and due to the presence of radiogenic heavy minerals [1,5]. The inhabitants of these areas are exposed to external radiation levels higher than the global average background values. Orissa Sands Complex (OSCOM) located in Chhatrapur district of Odisha, is coming under such HBRA due to the high monazite placer deposit. Mohanty et. al. dissussed about the details of the geology of this region and other HBRA areas worldwide [6]. The Objective of the present study is to establish existing gamma radiation and radon levels around a thorium beach sand mining and processing facility, OSCOM, Odisha.

Experimental

The surrounding environment upto 15 Km around OSCOM, Indian Rare Earth Ltd. is divides into three zones and surveyed for gamma radiation and radon activity concentration. The study area is situated around the monazite rich natural high background area in Chatrapur, Ganjam district (19°15$^{'}$ - 19°21$^{'}$ N, 84°3$^{'}$ - 84°55$^{'}$ E) of Odisha state in eastern India. India Rare Earth Limited (IREL) operates here to recover heavy minerals from the beach sand. People residing around the area are subjected to higher levels of natural background radiation due to presence of naturally enhanced radionuclide levels in the environment [7, 8].

Four hundred and ninety two locations were surveyed for natural gamma radiation using radiation survey meter. Seventy six outdoor and ten indoor locations were surveyed for radon concentration measurement by scintillation cell radon monitor. Details of the sampling are given elsewhere [7,9].

Results and Discussion

The external gamma radiation levels in villages around the thorium mining facility vary from 40-1800 nSv/h with an average of 226 nSv/h. The large variation can be attributed to the natural heterogeneous distribution of monazite sands in the region. The average gamma radiation level is higher than the global and national values which is obvious due to the high background status of the area [1]. From the frequency distribution graph (fig.1) it is clear that, 86 % of the gamma radiation level are more than 100 nSv/h. External gamma radiation levels higher than 500 nSv/h is observed in some locations (31 out of 492). This may be due to some localized placer deposit of monazite. The summary statistics of the gamma radiation observed is shown in Table 1.

The average outdoor and indoor radon levels were found to be 21 and 30 Bq/m^3 which ranged between 6-41 and 18-65 Bq/m^3, respectively. The measured outdoor radon concentration is within the global reported value of 1-100 Bq/m^3 [1]. However, the average outdoor radon level is relatively higher than the global average value of 10 Bq/m^3. Measured average indoor radon concentration is comparable with the global average value of 40 Bq/m^3. As the external gamma radiation level in the study area is elevated due to thorium and uranium content in monazite sand, a higher concentration of radon is also anticipated. However due to strong winds in the coastal area and open house concept due to tropical climate, the outdoor

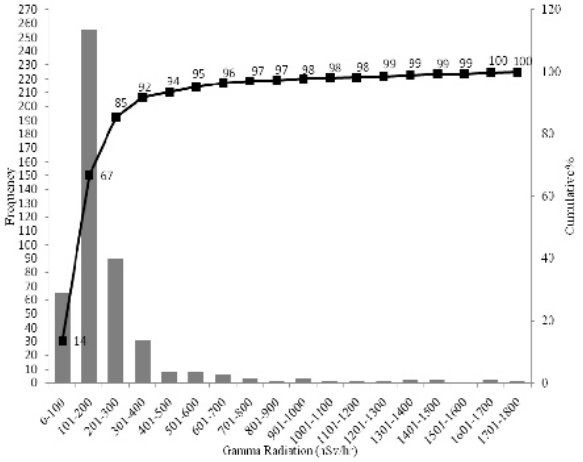


Fig. 1 Frequency distribution of external gamma radiation around OSCOM, Odisha

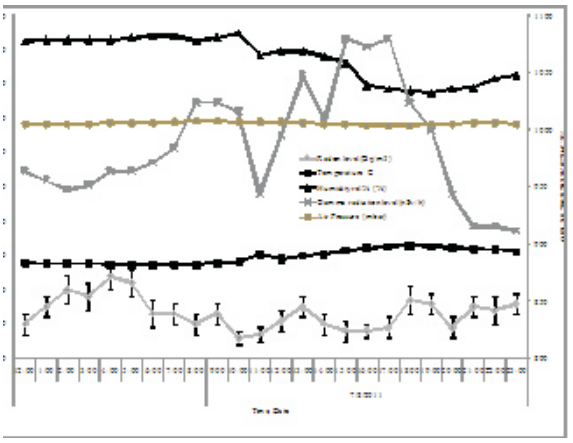


Fig. 2 Radon and Gamma radiation levels around OSCOM, Odisha

and indoor radon levels are comparable. Variation of radon and gamma radiation levels is plotted in Fig. 2 along with the temperature, relative humidity and atmospheric pressure. A typical diurnal variation of indoor radon concentration along with atmospheric humidity and temperature is observed. Radon concentration is higher in early morning hours and lower in early afternoon hours. The radon concentration is showing an inverse relation for the temperature. The concentration decreases with decreasing humidity level and vice versa. Similar results are obtained for radon concentration in south west coast of India (10).

Table 1: Summary statistics of external gamma radiation

Statistical parameters	External gamma radiation (nSv/h)
Mean	225.9
Standard Error	10.3
Median	155.0
Mode	150.0
Standard Deviation	226.3
Sample Variance	51229.1

Conclusion

Precise and accurate estimation of natural radioactivity is of utmost importance in order to assess the radiation dose received by members of the public. The external gamma radiation levels in villages around the beach sand mining and thorium processing facility, Odisha vary from 40-1800 nSv/h with an average of 226 nSv/h. The observed gamma radiation levels, 86 % are more than 100 nSv/h. The average gamma radiation level is higher than the global and national values which is obvious due to the high background status of the area The average outdoor and indoor radon levels were found to be 21 and 30 which ranged between 6-41 and 18-65 Bq/m^3. The outdoor radon level is higher than the global average values.

References

[1] UNSCEAR, Sources and Effects of Ionising Radiation, United Nations, New York, (2008).

[2] K. K. Narayan, D. K. Krishna, M. C. Subbaramu. ISRP (K) (1991) BR-3.

[3] M. Sreenath Reddy, Ch Gopal Reddy, P Yadagiri Reddy, K. Rama Reddy. Indian Journal of Pure and Applied Phys. 48, (2010) 778.

[4] J. Porstendorfer. J Aerosol Sci. 25(2) (1994) 219.

[5] B.G. Bennett, Fourth International Conference on High Levels of Natural Radiation: Radiation Doses and Health Effects, Beijing, China, Elsevier, Tokyo, (1996) 15.

[6] A.K. Mohanty, D. Sengupta, S.K. Das, S.K. Saha, K.V. Van. J. Environ Radioact., 75 (2004) 15.

[7] S.K. Sahoo, S. Mohapatra, A.C. Patra, D.V. Sagar, S.K. Tripathi, P. Patra, R.M. Tripathi and V.D. Puranik. International conferences on Recent Advances in Environmental Protection, RAEP Agra, (2009) 21.

[8] P. Lenka, S. K. Sahoo, S. Mohapatra, A. C. Patra, J. S. Dubey, D. Vidyasagar, R. M. Tripathi and V. D. Puranik. Radioprotect and Dosim, (2012), doi:10.1093/rpd/ncs115.

[9] A. V. Kumar, S. K. Sahoo, C. G. Sumesh, N. S. Krishna, R.M. Tripathi, V.D. Puranik and H.S. Kushwaha, (2010), BARC Report BARC/2010/I/003.

[10] N. Karunakara, H.M. Somashekarappa, K.M. Rajashekara, K. Siddappa, International Congress Series. 1276 (2005) 341.

Variation of Radon and its Progeny Levels in Different Types of Floorings and Rooms using LR-115 Solid State Nuclear Track Detectors

Deepak Verma and M Shakir Khan

Department of Applied Physics, Z. H. College of Engineering & Technology, Aligarh Muslim University, Aligarh-202002, Uttar Pradesh, India; E-mail: dpkapad@gmail.com

We have measured the concentration of radon and its progeny in dwellings of Nasik city based on the variation of rooms and floors by using LR-115 solid state nuclear track detectors. Radon and its progeny concentration were found higher in kitchen followed by bathroom and living room. Also the dwellings with granite floor show higher concentration of radon as compared to cement and plastic sheet floor. In all the dwellings, radon and its progeny levels were found below action limit giving an annual effective dose under the safety limits set by ICRP.

Introduction

The health hazard linked to radon and its progeny have become a matter of public concern. The principal health effect attributed to inhalation of radon and its daughters is lung cancer. When the resulting atoms, called radon progeny, are formed, they are electrically charged and can attach themselves to tiny dust particles in indoor air. These dust particles can easily be inhaled into the lung and can adhere to the lining of the lung. The deposited atoms decay by emitting alpha radiation, which damages cells in the lung. Alpha radiations can disrupt DNA of these lung cells. This DNA damage has the potential to be one step in a chain of events that can lead to cancer [1]. In the present paper, we reported radon and its progeny levels in different dwellings based on the variation of rooms and floors in Nashik city (Maharashtra, India) by using LR-115 solid state nuclear track detectors (SSNTDs).

Materials and Methods

The SSNTDs of size 1.5 cm×1.5 cm fixed on a thick plastic card in bare mode were suspended at about 2 m above the ground surface in the different rooms of a dwelling (i.e. kitchen, bathroom and living room) for the exposure of about three months. After the exposure, detectors were removed and etched in 2.5 NaOH for 1.5 h in a constant temperature water bath at 60°C. Then these detectors were washed, dried and scanned for track density measurements using the binocular optical microscope at a magnification of 100X. The track densities converted into Potential Alpha Energy Concentration (PAEC) for radon progeny by using the following equation:

$$C_p\,(\text{mWL}) \quad \frac{}{K \quad t} \qquad (1)$$

Where is the track density in tracks/cm^2, t is the exposure time in days and K is the calibration factor.

Radon concentration can be calculated by using the following expression:

$$C_{Rn}\,(\text{Bq}/\text{m}^3) \quad \frac{3700 \quad \text{WL}_{\text{conc.}}}{F} \qquad (2)$$

Where F is the equilibrium factor having the value of 0.4. A conversion factor of 3.88 mSv/WLM was used to estimate the annual effective dose.

Results and Discussion

The values of radon and its progeny (i.e. PAEC) concentration in different rooms (i.e. kitchen, bathroom and living room) of all dwellings (Table 1) vary from 37.0 to 169.2 Bq/m^3 and 4.0 to 18.3 mWL with an effective dose varies from 0.6 to 2.9 mSv/y. The variation of radon levels in different room shown in Fig. 1. From Fig. 1 it is clear that the maximum level of radon and its progeny was observed in kitchens while minimum was found in living room. The reason for this increased radon in kitchen may be the burning of fuel (i.e. cooking gas etc.) and the use of tap water. The cooking gas contains so many radioactive elements which help to increase the radon level [2]. Also the domestic water with high concentrations of radon can

Table 1: Values of PAEC, Radon concentration and Effective dose in different parts of dwellings

Types of room	PAEC (mWL)			Radon conc. (Bq/m^3)			Effective dose (mSv/y)		
	Min.	Max.	Average	Min.	Max.	Average	Min.	Max.	Average
Kitchen	12.0	18.3	14.9	111.0	169.2	138.4	1.9	2.9	2.3
Bathroom	7.6	16.0	11.9	70.3	148.0	110.6	1.2	2.5	1.8
Living room	4.0	10.2	7.2	37.0	94.30	67.12	0.6	1.6	1.1

Table 2: Values of PAEC, Radon concentration and Effective dose in different types of floor

Types of floor	PAEC (mWL)			Radon conc. (Bq/m^3)			Effective dose (mSv/y)		
	Min.	Max.	Average	Min.	Max.	Average	Min.	Max.	Average
Granite	8.8	14.8	11.9	81.4	136.6	110.1	1.3	2.3	1.8
Cement	4.9	10.2	7.4	45.3	94.3	69.2	0.7	1.6	1.1
Plastic (Vinyl)	3.7	8.6	6.3	34.2	79.5	58.23	0.5	1.3	0.9

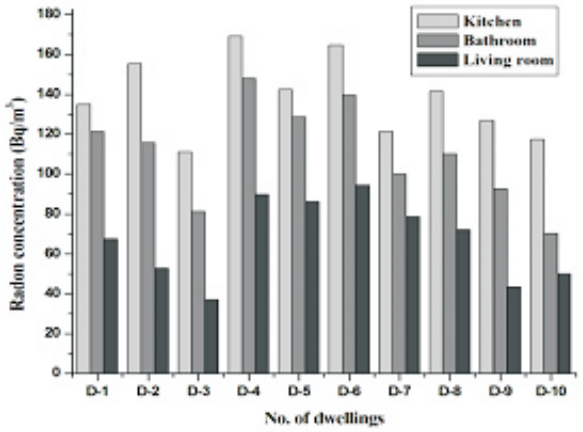


Fig. 1 Room wise variation of radon levels

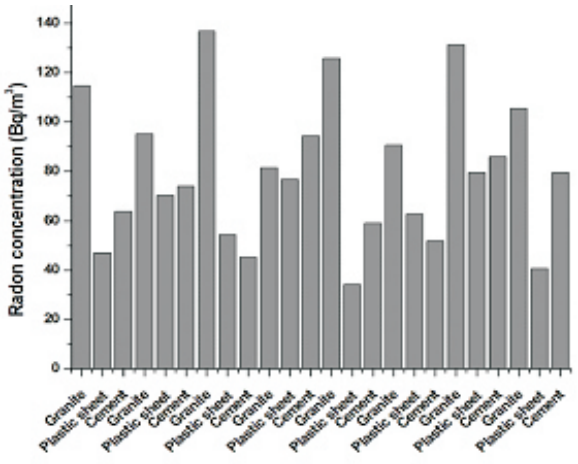


Fig. 2 Floor-wise variation of radon levels

make contributions to the indoor radon [3]. The indoor radon and its progeny i.e. PAEC concentration in all dwellings having different types of floor (i.e. granite, cemented and plastic floor) varies from 34.2 to 136.6 Bq/m^3 and 3.7 to 14.8 mWL. The estimated annual effective dose received by the residents of the studied areas varies from 0.5 mSv to 2.3 mSv. Figure 2 show the concentrations of radon with respect to the different types of floor, which reveal that the dwellings with granite flooring have relatively higher concentrations of radon and its progeny compared to the other type of floorings.

This higher value observed in granite floor dwellings is due to the high abundances of U, Th, and K found in granite [4]. These elements might have contributed to high radon levels. As the cement has low permeability and it impedes the flow of radon [5] so the dwellings having the cemented floor show lower radon level compared to granite. The radon concentrations for dwellings using plastic sheets as floor covering materials have the lower values than other types of floors (Fig. 2). It is due to the good inhibition property of plastic [6] compared to cement.

Conclusion

In the present study an attempt has been made to know the concentration levels of radon and its progeny in different dwellings based on room-wise and floor-wise variation. The results obtained in this systematic study are summarised as below:

The measurements indicate the higher radon concentration in kitchen followed by bathroom and living room. In kitchen the radon levels found higher than the WHO reference level of 100 Bq/m^3 but less than the ICRP recommended action level of 200-600 Bq/m^3.

The overall average indoor radon concentration in kitchen is about twice that found in living room.

Dwelling with granite floor show maximum radon levels due to the presence of natural radioactive nuclide U, Th and K.

Due to the good inhibition property of plastic sheet, the lower values of radon found in the dwellings having floor covered with plastic covering material.

The average indoor radon levels in all rooms found more than the world average values of 40 Bq/m^3. However these values were lower than the values recommended by Health Protection Agency, UK (200 Bq/m^3 limits).

Results obtained have shown that the average effective dose in most of the dwellings was higher than the average national and world recommended value of 1.0 mSv/y, but under the lower action limit of 3 mSv/y suggested by ICRP.

References

[1] E. A. Nekolla, A. M. Kellerer, M. Kuse-Isingschulte, Radiat. Res. 152 (1999) S3.

[2] Mamta Gupta, A. K. Mahur and K. D. Verma, Adv. App. Sci. Res. 3(3) (2012) 1262.

[3] K. J. Kearfott, Health Phys. 56 (1989) 169.

[4] N. Kochhar, Indian Minerals, 43(3-4) (1989) 339.

[5] R. P. Chauhan and S. K. Chakarvarti, Nucl. Sci. J, 38(6) (2001) 415.

[6] K. N. Yu, E. C. M. Young, M. J. Stokes, Health Phys. 73(2) (1997) 373.

Neutron Dose Estimation for $^{1}H+^{9}Be$ and $^{1}H+^{12}C$ Reactions at 20 MeV Proton Energy via LET Spectrometry using CR-39 Detectors

G.S. Sahoo, S.P. Tripathy, S. Paul, V. Suman, C. Sunil, D.S. Joshi, T. Bandyopadhyay

Health Physics Division, Bhabha Atomic Research Centre, Mumbai-400 085, India;
E-mail: sahoo.gouri232@gmail.com

In this work, the neutron dose is estimated by LET spectrometry method for two reactions, viz. $^{1}H+^{9}Be$ and $^{1}H+^{12}C$ at 20 MeV proton energy using CR-39 track detectors, which is useful for radiation protection of occupational workers. The LET spectrum is generated from the major, minor radii of each track and thickness of removed surface from each side of the detector due to chemical etching. The absorbed dose and dose equivalent per incident proton obtained from the LET spectrum are found to be about 12.5 and 8 times higher in $^{1}H+^{9}Be$ reaction than $^{1}H+^{12}C$ reaction.

Introduction

In a positive ion accelerator, neutron is the dominant radiation [1] produced during the interaction of ion with the target. The energy and yield of the emitted neutrons depend on the type and energy of the projectile and type of the target. It is worthful to measure or estimate neutron dose for different combination of projectiles and targets to have the knowledge on the dose delivered to the person working in the accelerator radiation environment. Though neutron dose can be measured by various available active detectors, however some passive detectors such as CR-39 is preferred in order to overcome the limitations of the use of active systems when radiation field is pulsed and mixed in nature [2].

In this work, neutron dose equivalent is estimated by LET (Linear Energy Transfer) spectrometry method [3] for $^{1}H+^{9}Be$ and $^{1}H+^{12}C$ reactions at 20 MeV proton energy using CR-39 track detectors. LET spectrum is crucial for determining the energy deposition in microscopic level to estimate the absorbed dose (D_{LET}) and dose equivalent (H_{LET}). In our previous work [4], we have used LET spectrometry method for estimation of dose due to mono-energetic neutrons. However, the main objective of this work is to study and compare the LET spectrum and dose due to neutrons produced from $^{1}H+^{9}Be$ and $^{1}H+^{12}C$ reactions at 20 MeV proton energy.

Experimental

Irradiation

CR-39 detectors are irradiated to neutrons at distance of 7.5 cm and 90^{0} with respect to beam direction in BARC-TIFR Pelletron facility. The neutrons are produced from the interaction of 20 MeV protons with 3mm thick ^{9}Be and ^{12}C targets. Since the range values of 20 MeV protons in ^{9}Be and ^{12}C are 2.78 and 2.1 mm respectively, 3 mm thick targets are found to be sufficient to stop the protons completely. The total accumulated charges on the target are obtained by a current integrator attached to it. The total charges on the ^{9}Be and ^{12}C targets are determined to be 23.4 C and 50.1 C respectively. From the total charges, numbers of protons hitting the ^{9}Be and ^{12}C targets are found to be $1.46x10^{14}$ and $3.12x10^{14}$ respectively.

Track Development and Image Analysis

After irradiation, the initial thickness of the detectors is measured using a precision thickness gauge (Hanatek made) with resolution of 0.1ìm. Then the neutron induced latent tracks produced in CR-39 detectors are developed by chemical etching (6.25N NaOH 70^{0}C, 9h). After etching the final thickness of the detectors are also taken. The images of developed tracks are taken using an optical microscope (Carl Zeiss) at a magnification of 200x. The captured images are analysed using an image analyzing software Axiovision 4.8. All the relevant track parameters are automatically obtained by the software, out of which the major and minor radii of all the counted tracks are considered for getting etch rate ratio, V which is the ratio of track etch rate (V_t) to bulk etch rate (V_b).

Generation of V Spectrum and LET Spectrum

The etch rate ratio (V) is calculated from the major and minor radii using the formulation [5] as given below

$$\tan \quad \frac{T}{2a} \quad 1 \quad \frac{b^2}{T^2} \qquad (1)$$

$$V \quad \frac{V_t}{t_b} \quad \frac{1}{\sin} \qquad (2)$$

where is the cone angle of the track, a and b are major and minor entrance radii of tracks, T is the thickness of removed surface from each side of the detector during etching. From the distribution of V, the V spectra are obtained for neutrons emitted from $^{1}H+^{9}Be$ and $^{1}H+^{12}C$ reactions. The V spectra are then converted to LET spectra using the calibration curve reported in the literature [3]. From the LET spectra, absorbed dose (D_{LET}) and dose equivalent (H_{LET}) are obtained for both the reactions.

Results and Discussions

Fig.1. shows the V spectra obtained by plotting the track density per proton versus the etch rate ratio

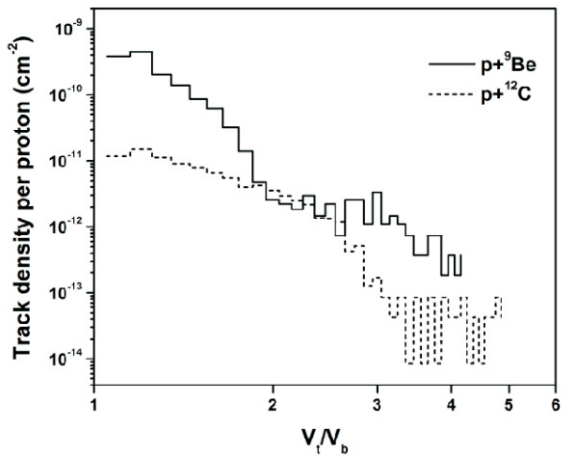


Fig. 1 V spectra obtained from track parameters for $^{1}H+^{9}Be$ and $^{1}H+^{12}C$ reactions

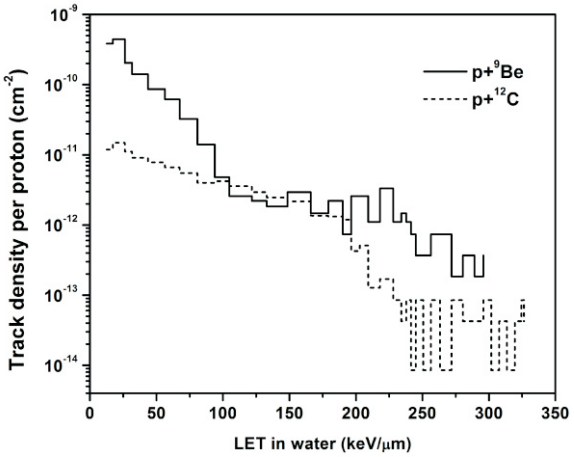


Fig. 2 LET spectra for $^{1}H+^{9}Be$ and $^{1}H+^{12}C$ reactions

(V_t/V_b). The V values are observed to extend up to 4.15 and 4.85 in case of $^{1}H+^{9}Be$ and $^{1}H+^{12}C$ reactions respectively. The LET spectra obtained from the V spectra using the calibration curve [3] are shown in Fig.2. From fig. 2 it is observed that the LET spectra extend upto 295 keV/ m in case of $^{1}H+^{9}Be$ reaction which is comparably lesser than $^{1}H+^{12}C$ reaction where it goes upto 325 keV/ m which is due to larger ellipticity of tracks in case of ^{12}C. The track density per proton as shown in Table.1 is found to be about 15 times more in $^{1}H+^{9}Be$ reaction than that of $^{1}H+^{12}C$ reaction indicating more neutron yield in case of ^{9}Be target. It can be seen in Fig.2 that the neutron yield form ^{9}Be target is higher than ^{12}C target particularly below100 keV/ m and above 200 keV/ m of LET. The statistical fluctuations at higher LET values are due to low counts of large size tracks.

The dose characteristics (D_{LET}, H_{LET}) of secondary particles due to neutrons emitted from both the reactions are determined from the measured LET spectra. From the LET spectra, D_{LET} and H_{LET} are calculated using the formulations [3]

$$D_{LET} = \frac{dN}{dL} LdL \quad (3)$$

$$H_{LET} = \frac{dN}{dL} LQ\ L\ dL \quad (4)$$

where dN/dL is the number of tracks per unit area in a LET interval and L is the value of LET. Q(L) is the quality factor given in ICRP 60 [6]. The microdosimetric distributions of D_{LET} and H_{LET} as a function of LET are also obtained. D_{LET} and H_{LET} values for both $^{1}H+^{9}Be$ and $^{1}H+^{12}C$ reactions are shown in Table.1 and is found to be more in $^{1}H+^{9}Be$ reaction compared to $^{1}H+^{12}C$ reaction. It can be concluded that, for a single proton, more dose is delivered if neutrons are produced from a composite system formed by beryllium nucleus compared to carbon, for the same proton energy.

Table-1: Track density, absorbed dose (D_{LET}) and dose equivalent (H_{LET}) for $^{1}H+^{9}Be$ and $^{1}H+^{12}C$ reactions at 20 MeV ^{1}H.

Reactions	Track density per proton (cm^{-2})	D_{LET} per proton (mGy)	H_{LET} per proton (mSv)
$^{1}H+^{9}Be$	1.4×10^{-9}	2.1×10^{-14}	2.7×10^{-13}
$^{1}H+^{12}C$	9.2×10^{-11}	1.7×10^{-15}	3.3×10^{-14}

Conclusion

Neutron dose is estimated for 20 MeV $^{1}H+^{9}Be$ and 20 MeV $^{1}H+^{12}C$ reactions using CR-39 detectors via LET spectrometry method. From the LET spectrum, it is found that neutron yield is more in $^{1}H+^{9}Be$ reaction compared to $^{1}H+^{12}C$ reaction for single proton incidence. Also similar observation is found for absorbed dose and dose equivalent. This method is found to be simple for estimation of dose when energy distribution and/or radiation components are not known and is useful while employing CR-39 as personal dosemeters. The dose values obtained in this study can be useful for personal neutron dosimetry and radiation protection of occupational workers involved in the accelerator environment.

References

[1] P.K. Sarkar, Radiat. Meas. 45 (2010) 1476.

[2] S. Agosteo, Radiat. Meas. 45 (2010) 1171.

[3] F.Spurny, A.G. Molokanov, V.P. Bamblevski, Radiat. Prot. Dosim. 110 (2004) 675.

[4] G.S. Sahoo, S.P. Tripathy, C. Sunil, P.K. Sarkar, Nucl. Instr. Meth. Phys. Res. A708 (2013) 46.

[5] J. Charvat, F.Spurny, Radiat. Meas. 14 (1988) 447.

[6] ICRP Publication 60, Annals of the ICRP 21 (1991).

Measurement of ^{222}Rn and ^{220}Rn Decay Product Deposition Velocities using SSNTD based Passive Detectors

R.P. Rout, R. Mishra, R. Prajith, Jalaluddin S., B.K. Sapra

Radiological Physics and Advisory Division, Bhabha Atomic Research Centre, Trombay, Mumbai 400085, India; E-mail: rprout@barc.gov.in

Direct Radon Progeny Sensor (DRPS) and Direct Thoron Progeny Sensor (DTPS) are SSNTD based passive detectors used for the measurement of inhalation dose based on the deposition velocities of ^{222}Rn/^{220}Rn decay products on these sensors. In the present study, the deposition velocities were experimentally measured in indoor environment and also compared with the model calculations. Measured deposition velocities of both ^{222}Rn and ^{220}Rn decay products were found to be lognormally distributed with GM and GSD of (0.12 m, 1.85) for radon decay products and (0.07 m, 1.75) for thoron decay products, which were found to agree well with the model calculation.

Introduction

Short lived decay products of radon (^{222}Rn) and thoron (^{220}Rn) are the major contributors to natural dose to humans [1]. Deposition velocity (V_e) is the parameter which is a measure of the rate at which these decay products will be deposited on the surfaces and thus removed from indoor air. It is defined as,

$$V_e \quad \frac{\text{Deposited atom flux } \frac{\text{Atoms / cm}^2}{\text{s}} \text{ on the surface}}{\text{Atom concentration (Atoms / cm}^3\text{) in atmosphere}} \qquad (1)$$

V_e is also an important parameter for the deposition based detectors which were used for the estimation of inhalation dose. V_e depends on many environmental factors such as aerosol concentration (Z), activity size distribution of the decay products (d), ventilation rate ($_v$) and turbulence parameter (u*) [2, 3]. In the present study, V_e of both radon and thoron were measured experimentally in indoor environment and the results were compared with theoretical modeling. This is a part of the program 'updation of deposition velocities of ^{222}Rn and ^{220}Rn in indoors'.

Measurement of Deposition Velocity

Measurements of deposition velocities for radon and thoron were carried out in 20 houses of Mumbai using the passive detectors, Direct Radon progeny Sensor (DRPS) and Direct Thoron progeny Sensor (DTPS) and the active integrated sampler [3]. These detectors basically consist of SSNTD films with suitable absorbers mounted on them. It was observed that, V_e for radon and thoron have log-normal distributions with Geometric mean (GM) and Geometric Standard Deviation (GSD) of (0.12, 1.85) for radon and (0.07, 1.75) for thoron (Fig. 1).

Model Calculation of Deposition Velocity

The environmental parameters (Z, d, $_v$ and u*), on which deposition velocity depends, have log-normal distributions with GM and GSD shown in Table 1.

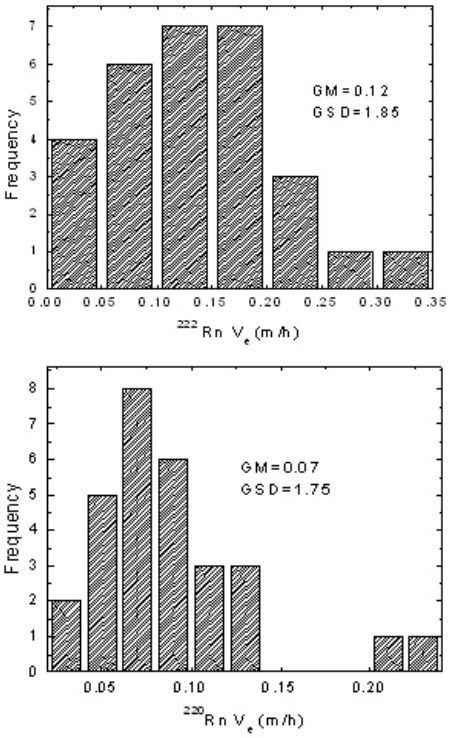


Fig. 1 Frequency distributions of deposition velocities of radon (^{222}Rn) and thoron (^{220}Rn) measured in indoor

Table 1: GM and GSD values of the input parameters (Z, d, $_v$ and u*) used in the present study [2-5]

Parameters	GM	GSD
Z	$3x10^4$ p/cc	2.5
d	0.12 m	2.2
$_v$	1 h^{-1}	2.5
u*	2 cm/s	2.5

A Monte-Carlo simulation was carried out for estimation of deposition velocities of radon and thoron

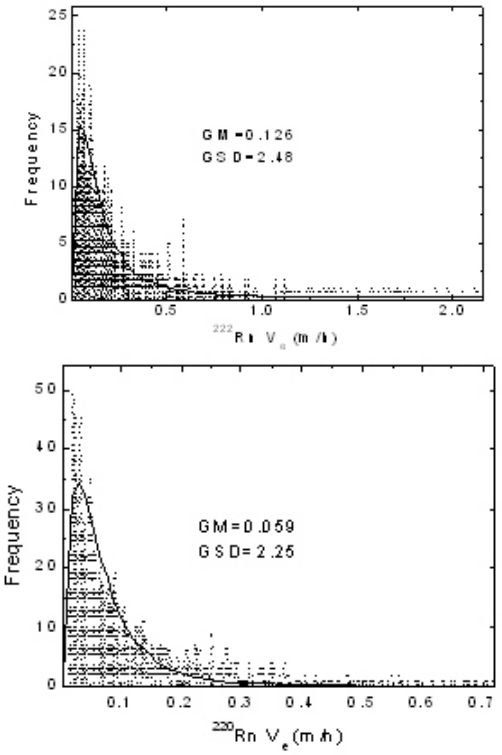


Fig. 2 Frequency distributions of deposition velocity of radon and thoron from Monte-Carlo simulation

decay products using Lai-Nazaroff model [5] and Jacobi model [6] for ideal room dimensions. The sample space was 1000 in each case. The simulated deposition velocities were observed to be log-normally distributed with GMs and GSDs of (0.126, 2.48) in case of radon and (0.059, 2.25) in case of thoron (Fig. 2).

Results and Discussion

It was observed that,

1. Deposition velocities of ^{222}Rn and ^{220}Rn measured in the houses were consistent with the earlier studies carried out in test house condition [3]
2. Both ^{222}Rn and ^{220}Rn deposition velocities showed log-normal distributions.
3. The GM and GSD obtained using Monte Carlo simulation were in agreement with the experiments.

Conclusion

The measured and model calculated deposition velocities of radon and thoron decay products were found to be lognormally distributed and good agreement were observed in their GM and GSD values.

References

[1] UNSCEAR, Report to General Assembly with Annexes, United Nations. Sources and Effects of Ionizing Radiation (2000).

[2] J. Porstendorfer, Radiation Protection Dosimetry 7 (1984) 107.

[3] R. Mishra, Y. S. Mayya, H. S. Kushwaha, ` J. Aerosol Sc. 40 (2009) 1

[4] USEPA, 2011

[5] A. C. K. Lai and W. Nazaroff, J. Aerosol Sc. 31 (2009) 463.

[6] W. Jacobi, Health Physics 22 (1972) 441.

Tetraethyl Ammonium Hydroxide (TEAH) as an Etchant of CR-39 for the Determination of Fluence of Alpha Particles

Pranav M Joshirao[1], Chirag K. Vyas[1], K. P. Eappen[1], Jae Won Shin[2], Seung- Woo Hong[1,2] and Vijay. K. Manchanda[1]

1. *Department of Energy Science, Sungkyunkwan University, Suwon, South Korea 440746; E-mail: vkm49@skku.edu or vkm25749@gmail.com*
2. *Department of Physics,Sungkyunkwan University, Suwon, South Korea 440746*

Choice of chemical etchant and temperature are pivotal to the successful employment of solid state nuclear track detectors for determining the fluence of charged particles. An attempt has been made in the present work to investigate a mixture (20%:80% (v/v) of 2.7M tetraethylammonium hydroxide and 6M NaOH (TEAH-NaOH) at varying temperature as an alternate etchant.. It was found that bulk / track etch rate increased and etching time decreased significantly when the mixture was used at 80° C. Improved efficiency of TEAH-NaOH was attributed to its lower etching activation energy as compared to NaOH. The reduction in etching time can enhance the sample throughput of radioanalytical labs where CR-39 is used for radon monitoring and uranium prospecting.

Introduction

There is a need to work on chemical etchants which are more efficient and can facilitate the development of latent tracks in shorter periods. Etchant efficiency to reveal a latent track in a polymer exposed to charged radiations depends on the ratio of track etch rate and bulk etch rate. In turn, it depends on several factors like a) composition of polymer; b) etchant capability to dissolve etched products; c) stirring to displace etched products from the track site; d) temperature; e) rate of energy loss of the charged particle in the track trajectory. The nature of chemical etchant and the etching conditions (like concentration and temperature) play an important role in determining the efficiency of etchant [1]. Tetraethyl ammonium hydroxide (TEAH) and its mixture with NaOH in varying proportion was studied as an etchant of CR-39 exposed to 6.1MeV alpha particles from ^{252}Cf by Kobayashi and Fujii [2]. In the present work, we have studied the etching behaviour of CR-39 in a mixture of 20%: 80% (v/v) of 2.7M tetraethylammonium hydroxide and 6M NaOH (TEAH-NaOH) at different temperatures. The efficiency of the new etchant was studied by measuring the track density as a function of etching time and temperature. Role of etched products in facilitating the etching was investigated. Activation energy for bulk etching as well as track etching were determined.

Experimental

Set up for the exposure of CR-39 is shown in Fig.1. The CR-39 detector used in the present study was purchased from PPG coatings (Hong Kong) Co., Ltd. The dimensions of the detectors used were 0.5 cm (L) x0.5cm (B) x 0.1 cm (T). The alpha source employed in the present study was a planar, electroplated ^{241}Am (main alpha energy 5.49 MeV) having activity 3.585 kBq (4 geometry) and surface emission rate of 106500 /min in 2 geometry. It was procured from Eckert & Ziegler - Isotope Products, USA and was certified by

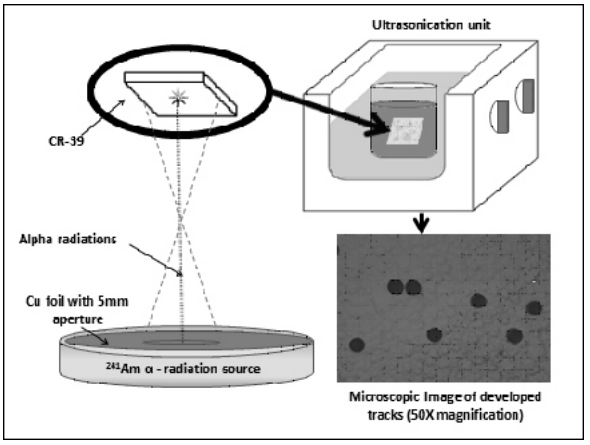


Fig. 1 Schematic of exposure set up

Industrial gauging laboratory, California. It is an electrodeposited and diffusion bonded oxide, with active area diameter of 45 mm. In the present work, the active area of the source was covered with a copper foil of 25 m thickness with a circular slit of ~6 mm diameter at the centre for collimation (to reduce the divergence) of alpha particles.Alpha track images were taken by an optical microscope (Olympus BX51M-N35MF) at 50X magnification using Tomoroscope eye 3.5 software with least count of 0.01 micrometer.

Covered source was counted for alpha activity using Berthold LB770, 10 channel low level gas proportional counter and the fluence of alpha particles was computed at the position of CR-39 detector. The alpha activity obtained was 68 Bq (4 geometry) and the fluence at a distance of 0.95 cm away from the source, where CR-39 detector was placed was obtained as follows:

Alpha fluence = S / 4 D^2 /sec

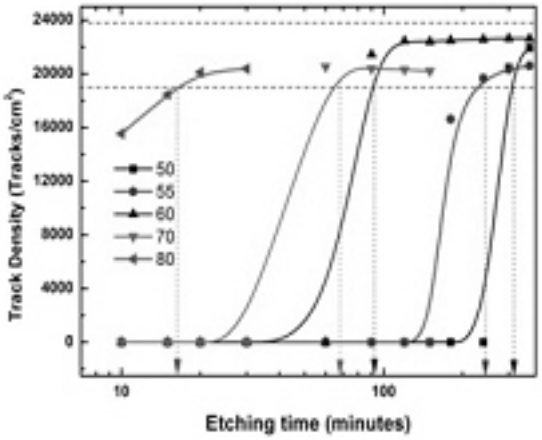


Fig. 2 Track density profile as a function of etching time for varying temperatures

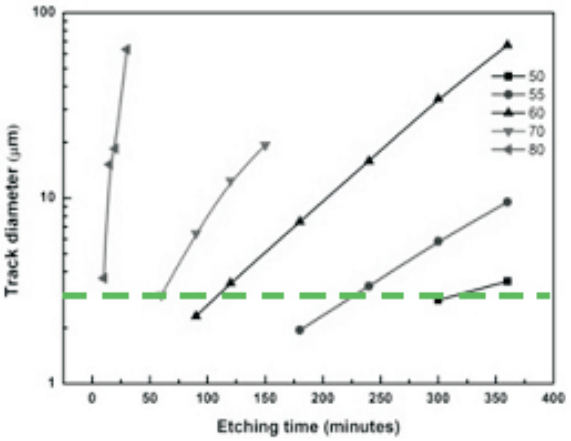


Fig. 3 Track diameter as a function of etching time for varying temperatures.

where S = alpha activity; D = distance between the source and sample. Expected fluence of alpha radiation is 5.99 /sec or 21564 / hour. cm^{-2}.

Results and Discussion

Fig. 2 shows the observed track density profile as a function of etching time for TEAH-NaOH in the temperature range 50°C-80°C. Considering standard deviation of ±10% in track density , it appears that 17 minutes of etching time is sufficient to arrive at the expected track density at 80°C. Fig. 3 shows that diameter of the track increases vary sharply with time at 70°C and 80°C. At other temperatures also, there is linear increase in track diameter as a function of etching time, and the slope increases with temperature. Threshold diameter for the track registration was 3 micron in the present work.

In comparison to the conventional etchant (6M NaOH), the etching time required is ten times less to attain the expected track density values. The etching efficiency is influenced by the ratio of bulk etch rate to track etch rate . % efficiency of TEAH – NaOH at 80 °C was 58% while that for conventional etchant (6M NaOH, 60°C) was only 48%. The activation energy value for TEAH-NaOH was 0.87 ± 0.02 eV, which is less than the reported value of 0.981 ± 0.001 eV for 6M NaOH [3].

Conclusions

1. Using TEAH-NaOH at 60°C, etching time for the development of latent tracks is reduced to 90 minutes from 4 hours (needed with 6M NaOH at 60°C). Etching time is further reduced to 17 minutes if the temperature is maintained at 80°C.
2. Bulk etch rate as well as track etch rates are larger by 40% with TEAH-NaOH as compared to NaOH at 60°C. However the bulk etch rate and track etch rate increase further 4 folds by increasing temperature to 80°C. The activation energy value for TEAH - NaOH is lower as compared to that of NaOH

Acknowledgement

This research was supported by World Class University (WCU) Program to V.K.M.and S.W.H. through the National Research Foundation of Korea (NRF) funded by Ministry of Education, Science and Technology (R31-2008-10029).

References

[1] D. Hermsdorf, M. Hunger, S. Starke, F. Weickert, Radiat. Meas., 42 (2007) 1.

[2] T. Kobayashi and M. Fujii, Nucl. Tracks Radiat. Meas., 15(1 - 4) (1988) 175.

[3] Puran C. Kalsi, Chhavi Agarwal, J Mater. Sci., 43 (2008) 2865.

Effects of Supplemental n-3 Polyunsaturated Fatty Acids in Diet: Studies Performed with Radioanalytical Methods

S. Pavelka[1,2]

1. *Department of Radiometry, Institute of Physiology, Academy of Sciences of the Czech Republic, 142 20 Prague*
2. *Institute of Biochemistry, Faculty of Science, Masaryk University, 611 37 Brno, Czech Republic; E-mail: pavelka@biomed.cas.cz or pav@chemi.muni.cz*

The aim of our present study was to test whether and in what way n-3 polyunsaturated fatty acids (n-3 PUFA) supplementation can affect changes of lipid metabolism induced in rats by alteration of their thyroid status. In spite of the fact that several biochemical parameters, analyzed with the use of radioanalytical methods, such as total T_3 serum levels, activity of liver mitochondrial glycerol-3-phosphate dehydrogenase, blood glucose and plasma lipids, amongst different thyroid states (EU vs. TH vs. HY) were shown to be distinct, we found no significant effect of 6-week-supplementation of n-3 PUFA on the above mentioned parameters.

Introduction

N-3 polyunsaturated fatty acids (n-3 PUFA), mostly of marine fish origin, that are rich in eicosapentaenoic acid (EPA, 20:5 n-3) and docosahexaenoic acid (DHA, 22:6 n-3) are well known food components recommended for the prevention of cardiovascular diseases, atherosclerosis and management of hyperlipidemia, as shown in numerous clinical trials and animal experimental studies [see 1 for references].

Thyroid hormones (THs) L-thyroxine (T_4) and 3,3',5-triiodo-L-thyronine (T_3) represent one of the major endocrine regulators exerting a variety of effects on cellular development, growth and differentiation, and on metabolic processes practically in all tissues. It is well known that thyroid hormones play important roles in lipid metabolism because alteration of the thyroid status is associated with changes in serum lipid and lipoprotein concentrations. In human studies, hypothyroidism was usually associated with increased levels of serum triglycerides, total cholesterol and very low density lipoprotein (LDL) cholesterol. In contrast, hyper-thyroidism was associated with decreased levels of serum triglycerides, cholesterol and LDL cholesterol.

The hypolipidemic effect of n-3 PUFA is not completely understood and can be explained by several mechanisms. For example, there are some indications of a potential cross-talk between n-3 PUFA and THs in the liver [2]. In the present study, therefore, we tried to test whether and in what way n-3 PUFA supplementation can affect changes of lipid metabolism induced in rats by alteration of their thyroid status.

Experimental

Pharmacological experiments were performed on 36 growing male inbred Lewis rats, fed ad libitum a standard pelleted diet. At the age of 4 weeks, rats weighing 65±5 g were randomly divided into three groups: 1) euthyroid (EU), 2) hypothyroid (HY), and 3) hyperthyroid (TH). The HY status was induced and maintained with a 0.05 % solution of methimazole in drinking water. The TH status was induced and maintained by intraperitoneal injection of T_3 (0.15 mg/kg body weight) 3 times a week. The EU rats were age-matched littermates of the experimental animals. From the 13th week of age, n-3 PUFA were administered intragastrically (200 mg/kg b.w./day) to a half of the rats in each experimental group for 6 weeks. After 6 weeks of n-3 PUFA supplementation, the animals were sacrificed, blood samples were obtained and sera were prepared by a standard procedure and stored at -80°C until used for measuring thyroid hormone concentrations and lipid parameters. Livers from each rat were quickly excised and immediately processed for mitochondria isolation. Serum concentrations of total triiodothyronine (tT_3) and total thyroxine (tT_4) were assayed radioimmunologically using RIA kits. Postprandial concentrations of triglycerides, total cholesterol, high-density lipoprotein (HDL) and LDL cholesterol in serum samples were measured using commercial kits. The enzyme activity of liver mitochondrial glycerol-3-phosphate dehydrogenase (GPDH) was measured spectrophotometrically [3].

Results and Discussion

The administration of T_3 or methimazole induced TH or HY status in the experimental rats, respectively. In comparison with control (EU) rats, tT_3 concentrations were significantly increased (nearly 6-fold) in the TH rats and decreased (to one third) in the HY rats. The mean activity of GPDH was significantly increased (ca. 6-fold) in the TH rats and decreased (to 75 %) in the HY rats, what corresponded well with the altered thyroid status. None of the thyroid hormone levels were significantly altered by supplementation of n-3 PUFA.

Figure 1 depicts concentrations of postprandial (nonfasting) plasma lipids according to the thyroid state and n-3 PUFA treatment. Significant elevation of

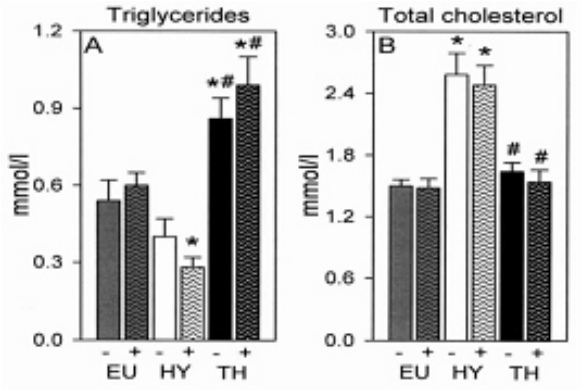


Fig. 1 Non-fasting levels of plasma lipids in the euthyroid (EU), hypothyroid (HY) and hyper-thyroid (TH) rats without (!) and with (+) n-3 PUFA supplementation. Data are presented as means ± SEM (n = 6 animals per group). Signifi-cantly different: $^{*}p \# 0.05$ vs. EU status; $^{\#}p \# 0.05$ vs. HY status.

plasma triglycerides was observed in the TH rats compared to the EU and HY rats (Fig. 1A).

Hypothyroidism was associated with hyperchole-sterolemia. The levels of total cholesterol (Fig. 1B) were significantly higher in the HY rats than in the EU and TH rats.

Treatment with n-3 PUFA did not significantly modify either serum triglyceride levels or serum cholesterol levels in any analyzed group.

Conclusions

We found no significant effect of 6-week-supplementation of n-3 PUFA on several biochemical parameters analyzed with the use of radioanalytical methods, in spite of the fact that these parameters were shown to be distinct amongst rats maintained in different thyroid states (EU vs. TH vs. HY). N-3 PUFA thus did not ameliorate changes induced by altered thyroid states.

References

[1] H. Rauchová, M. Vokurková, S. Pavelka, et al., Horm. Metab. Res. 45 (2013) 507.

[2] Y.Y. Liu, G.A. Brent, Trends Endocrinol. Metab. 21 (2010) 166.

[3] H. Rauchová, T. Mráèek, P. Novák, et al., Horm. Metab. Res. 43 (2011) 43.

Impact of Gamma Irradiation on Biochemical Parameters of Flacourtia Montana Grahm during different Storage Period

Akshatha, K.R. Chandrashekar

Department of Applied Botany, Mangalore University, Mangalagangothri, 574199, Karnataka, India; E-mail: konambi@yahoo.com

Biochemical attributes such as ascorbic acid content, anthocyanin content, PAL activity, phenolics content and antioxidant activity of the irradiated (0-2 kGy) F. montana Grahm. fruits were determined during 4 weeks of cold storage. Doses of 1.5 to 2 kGy enhanced the ascorbic acid content where as total anthocyanin was maintained at 1.5 kGy. Increase in PAL activity was observed with radiation treatment which may count for increased phenolics. A significant increase in the DPPH radical scavenging and reducing power was observed at 0.5 kGy, 1 kGy & 2 kGy.

Introduction

F. montana Grahm is one of the endemic species of the Western Ghats belongs to the family Flacourtiaceae which produces red color edible fruits. The fruits are used to relive nausea, fever, diarrhea, piles, weakness of limbs, bleeding gum and also useful in digestion.

Cold pasteurization is one of the commercial application of gamma rays in the food industry and many researches revealed that gamma irradiation can successfully extend the shelf life of vegetables and fruits [1, 2]. Even though, irradiation enhances the shelf life it also acts as one of the stress factor which stimulates the activity of enzymes such as phenylalanine ammonia-lyase (PAL) leading to enhanced production of phenolics and also development of browning pigments and membrane damage [3] To date, there is a lack of information about the effect of gamma radiation on F.montana Grahm. The present study was performed to evaluate the impact of different doses of gamma irradiation and subsequent storage at 4°C on the biochemical attributes of the fruits where there is a severe post harvest contamination by fungus.

Experimental

Mature fruits of F.montana Grahm were obtained from Charmadi region (Altitude $13^0 03' 32.04'' N$, Latitude $75^0 25' 51.91' E$, Elevation 151 ft) during the month of April 2012 and packed in bi-axially oriented polypropylene bags (BOPP, 25 , 12 x 12 cm) and subjected to different doses (0 kGy, 0.5 k Gy, 1 kGy, 1.5 kGy and 2 kGy) of gamma radiation using ^{60}Co gamma source with a dose rate of 8.9 kGy/hr at CARRT (Center for Application of Radiation and Radioisotope Technology) Mangalore University.

Fruit samples were stored at 4^0C for four weeks and observed for the biochemical variation during each week spectrophotometrically. Ascorbic acid content was determined by using DNPH method [4]. Total anthocyanin content was determined by differential pH method [5]. PAL activity is determined by enzyme assay [6]. Phenolics content was determined by Folin–Ciocalteu method [7]. Antioxidant activity was measured using DPPH radical scavenging activity [8] and reducing power using potassium ferricyanide [9]. The data were analyzed using SPSS20 statistical software at P#0.05 significance level.

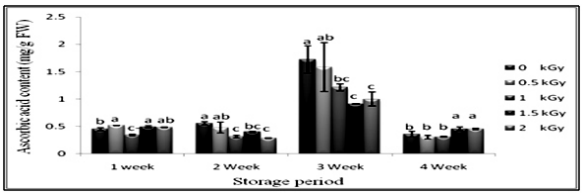


Fig. 1 Gamma impact on ascorbic acid content

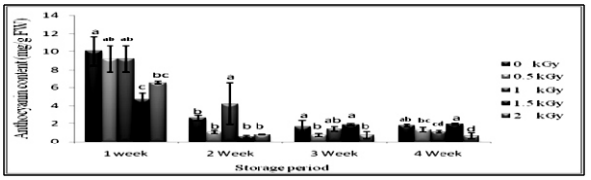


Fig. 2 Gamma impact on Anthocyanin content

Results and Discussion

There was a slight decrease in the ascorbic acid content above 1 kGy till 3weeks but on 4th week of storage there was an increase (Fig.1). Irradiation did not alter the anthocyanin content at lower doses of radiation but a significant decrease was observed in the fruits irradiated with higher dose of 2 kGy and 1.5 kGy (Fig.2). There was no significant difference in the PAL(Phenyl alanine ammonia lyase) activity in the first week but the activity enhanced above 1kGy and reached its maximum at 2 kGy at the 4th week (Fig.3). Similar to PAL activity, highest phenolic content was observed with increased dose at 4 th week of storage (Fig.4). Enhanced radical scavenging activity was observed at 1 kGy irradiation dose which was significantly higher compared to other treatments (Fig.5). Similarly there was a significant increase in the reducing power with increased dose during fourth week of storage (Fig.6). Earlier works on most of the horticultural crops revealed that irradiation up to 1 kGy

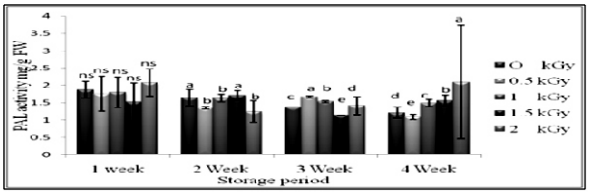


Fig. 3 Gamma impact on PAL activity

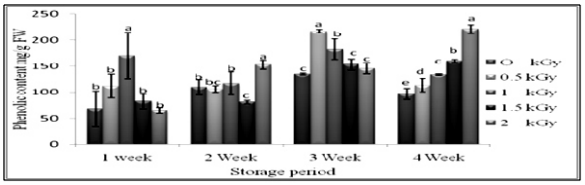


Fig. 4 Gamma impact on Phenolic content

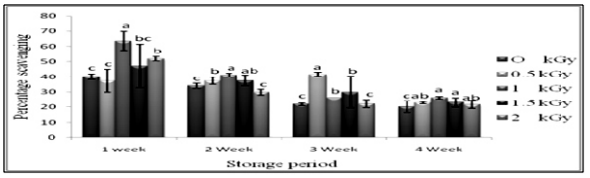


Fig. 5 Gamma impact on DPPH scavenging

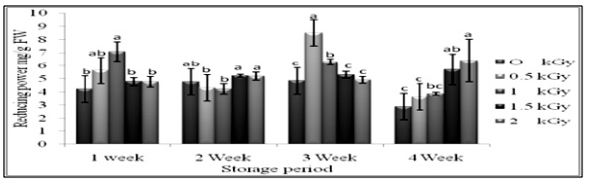


Fig. 6 Gamma impact on reducing power

or lower had no significant impact on ascorbic acid content.

Figs. 1-6. Effect of gamma irradiation on biochemical attributes of F.montana Grahm fruits during 4 weeks of cold storage.

In Citrus clementina irradiation enhanced phenolic synthesis was correlated with phenylalanine ammonia-lyase activity (PAL) during storage. Similarly in the present study irradiation enhanced phenolics may be counted for enhanced antioxidant activity.

Conclusion

Gamma irradiation was effective in maintaining quality of the F.monatna Grahm fruits without sacrificing its biochemical attributes.

References

[1] IAEA. Irradiation Technology and Techniques, 2nd ed.; Technical Report Series 80; Vienna, Austria, (1982) 114.

[2] Josephson, E. S.; Peterson, M. S. Preservation of Food by Ionizing Radiation; CRC Press: Boca Raton, FL, (1982) Vol. I-III.

[3] Oufedjikh, H., Mahrouz, M., Joseph,M., Amiot, Lacroix, M., J. Agric. Food Chem. 48 (2000) 559.

[4] Nino HV and Shah W., Vitamins. In: Tietz NW. Editor. Fundamentals of Clinical Chemistry. 2nd edition. WB Saunders, Philadelphia, (1986) pp. 547-550.

[5] Giusti, M.M., Wrolstad, R.E., Unit F1.2: anthocyanins: In: Wrolstad, R.E., Schwartz, S.J. (Eds.), Current Protocols in Food Analytical Chemistry. John Wiley & Sons, New York, USA, (2001) pp.1-13.

[6] Brueske, C.H., Physiol.Plant pathol 16 (1980) 409.

[7] Taga, M.S., Miller, E.E., Pratt, D.E., J. Am. Oil Chem. Soc. 61 (1984) 928.

[8] Mensor, L.I., Menezes, F.S., Leitao, G.G., Reis, A.S., Dos Santos, T., Coube, C.S., Leitao, S.G., Phytother. Res. 15 (2001) 127.

[9] Oyaizu M, Japanese Journal of Nutrition 44 (1986) 307.

Impact of Gamma Irradiation on Biochemical attributes of Jackfruit (Artocarpus heterophyllus L.) seeds during different storage period.

Madhavi Adiga, Madhuri Adiga Akshatha, K.R.Chandrashekar

Department of Applied Botany, Mangalore University, Mangalagangothri, 574199, Karnataka, India;.
E-mail: konambi@yahoo.com

Seeds of A. heterophyllus Lam. were exposed to different (0.5- 2.5 kGy) doses of gamma radiation and stored for 3 weeks under ambient condition for observation of biochemical changes. The significant increase in phenolic content was observed at 2.5 kGy compared to control. Increase in protein content was observed at 1.5 and 2kGy at the end of 3rd week. Increased total soluble sugar content was observed with increased dose. Enhancement in antioxidant activity at 2kGy may be due to the increased phenolic content.

Introduction

Artocarpus heterophyllus L. belongs to family Moraceae is indigenous to the rainforests of the Western Ghats of India. It is one of the economical, fruit and timber yielding plant which produces recalcitrant seeds with good source of starch and dietary fibres [1,2].

Presence of high moisture content makes the storage difficult. Irradiation of food items is a powerful tool against microbial contamination and sprouting during long term storage. Ionizing radiations have also been proved effective in improving the overall nutritional attributes, including some desired changes in functional properties of seed flours besides reducing microbial contamination [3,4]. Therefore, our objective was to study the impact of gamma irradiation on biochemical attributes of Jackfruit seeds during different storage period.

Experimental

A.hirsutus L. seeds were irradiated with 0.5,1, 1.5, 2, and 2.5 kGy doses of gamma radiation using ^{60}Co source and observed for biochemical changes. Protein content was determined using Lowry's method, phenolic content using Folin-Ciocalteu's reagent. Total soluble sugar using refractometery and antioxidant activity by DPPH radical scavenging activity and reducing power assay.

Results and Discussion

Increased protein content was observed in the first week of storage at 0.5 kGy and at the end of 3rd week a considerable enhancement of protein content was observed at 1.5 and 2 k Gy (Fig.1). As illustrated in the Fig.2. in all the three weeks at 2.5 kGy highest quantity of total soluble sugar was observed which was substantially higher compared to control. Irradiation of Mucuna seeds was effective in enhancing the protein content and maintaining the nutritional quality of the seeds [5]. In the present study nutritional parameters of the A. heterohyllus L. seeds were maintained even at 2.5 kGy dose.

Increased phenolics production was observed in A.heterophyllus L. seeds with dose from second week

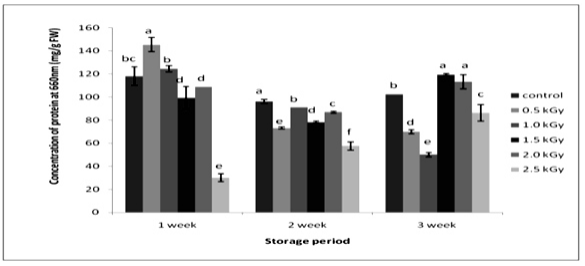


Fig. 1 Effect of Gamma Radiation on Protein content.

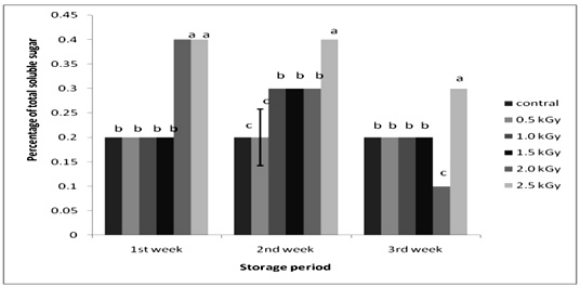


Fig. 2 Effect of Gamma Radiation on Total Soluble Sugar

of storage (Fig. 3). At the end of third week, significant increase in the phenolics was observed at 2 kGy and 2.5 kGy. Similar to phenolic content considerable increase in DPPH radical scavenging activity was observed at higher dose of 2.5 kGy during third week of storage (Fig. 4). A substantial increase was observed only in the first week of storage which was on par during second and thiFrd week (Fig.5). In Soya bean seeds gamma irradiation significantly enhanced the phenolic content and DPPH radical scavenging activity which could be compared with our results on A.heterophyllus Lam [6]. Although, phenolics are considered as one of the major antinutrients, considerable interest has been recently shown in their possible antioxidant activities and potential health benefits by consumption of plants produce with high phenolics to reduce cardio-cerebrovascular diseases and cancer mortality [7,8].

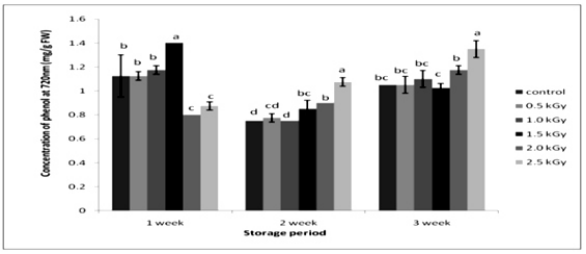


Fig. 3 Effect of Gamma Radiation on Phenol content

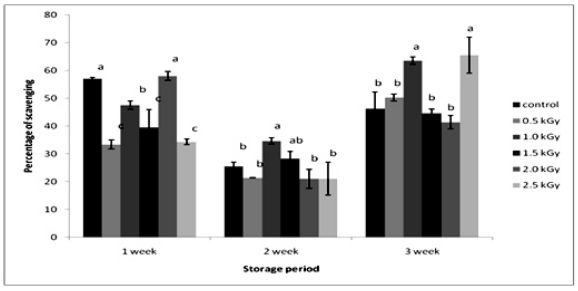


Fig. 4 Effect of Gamma Radiation on DPPH radical Scavenging Activity

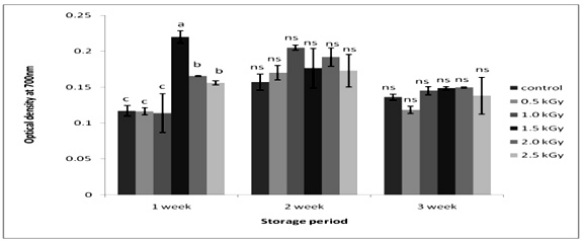


Fig. 5 Effect of Gamma Radiation on reducing power

Conclusion

Significant increase in the protein content and total soluble sugar by gamma irradiation during storage may be helpful in maintaining the nutritive quality of the seeds. Enhancement in radical scavenging activity may be due to enhanced phenolics production which may help in the protection of seeds from radiation stress.

Reference

[1] Ferrao, J. E. M. Tropical Fruits; species with edible fruits Vol. 1 Corporate author, Institute of Scientific. Tropical fruit growing (1999) Research and tropical, Lisbon

[2] U.P. Hettiaratchi, S. Ekanayake, J. Welihinda, Ceylon Med. J. 56(2) (2011) 54.

[3] M.K. Dogbevi, C Vachon, M. Lacroix, Radiat Phys Chem 57(2000) 265.

[4] A. B. Hassan., G. A.M. Osman, M. A.H. Rushdi, M. M. Eltayeb, E.E. Diab, Pakistan Journal of Nutrition 8 (2) (2009) 167.

[5] R. Bhat, R. Kandikere Sridhar, Yokotani –Tomita Kaori, Food Chem. 103 (2006) 860.

[6] D. Stajner, M. Milosevic, B.M. Popovic, Int. J. Mol. Sci., 8 (2007) 618.

[7] M.G.L. Hertog, P.M. Sweetnam, A.M. Fehily, P.C. Elwood, D. Kromhout, American Journal of Clinical Nutrition, 65(1997) 1489.

Application of Elovich equation on uptake kinetics of ^{137}Cs by Living Freshwater Macrophytes - A Short Duration Laboratory Study

T.J. Jaison[1], A.K. Patra[1], P.M. Ravi[2] and R.M. Tripathi[2]

1. *ESL (ESS, Health Physics Division, BARC), Kakrapar Atomic Power Station, Gujarat 394651; E-mail: jaisontjohn@npcil.co.in*
2. *Health Physics Division, Bhabha Atomic Research Centre, Mumbai 400 085*

Application of Elovich equation on uptake kinetics of ^{137}Cs by two living macrophytes during controlled experiments on short duration exposure is studied. Compliance to 2nd order kinetics indicates the mechanism could be chemi-sorption, involving polar functional groups present on the extracelluar surface of the macrophytes. Data analysis suggests that Myriophyllum s. exhibits faster adsorption rate than Hydrilla v. As Myriophyllum s. exhibits better kinetics than Hydrilla v., former could be a better natural adsorbing media for ^{137}Cs.

Introduction

Most studies on pollutant bioaccumulation in macrophytes are aimed at assessing removal efficiency or toxic effects without taking into account the metal bioaccumulation process by macrophytes. It has been reported that biosorption may be classified as being: extra-cellular accumulation/precipitation, cell surface sorption/precipitation, and intracellular accumulation [1]. This paper presents application of Elovich equation on the uptake of ^{137}Cs by predominant submerged macrophytes (Myriophyllum spicatum and Hydrilla verticillata) present in Moticher Lake, during a controlled study on short duration exposure. The lake is the recipient water body of low level liquid effluent from Kakrapar Atomic Power Station, Surat, Gujarat and fed by river Tapi and further used for agricultural purpose.

Material and Methods

The uptake experiments were conducted using individual clean and healthy fresh macrophytes samples obtained from upstream area, of comparable weights. Particular plant species of about 10 g fresh weight (W) were introduced into the water column of upstream water (V) with a known quantity of added ^{137}Cs activity in one liter glass vessels. Water samples were taken at different exposure periods (t minutes), analyzed and estimated ^{137}Cs activity as C_t (Bq/L) by Gamma Spectrometry (HPGe of 100% relative efficiency) calibrated using liquid standards traceable to NIST. Individual sets of experiments were conducted at room temperature for different durations of exposure at different initial concentrations of ^{137}Cs (C_0 in Bq/L). Experiments with Myriophyllum s. were with C_0 of 180.5, 503.1, 2059.1 & 2555.3 and with Hydrilla v. were of 200.4, 800.3, 2000.3 & 2555.3respectively. The amount of Cs uptake by macrophyte (q_t in Bq/g) at respective time interval was estimated.

Results and Discussion

Reduction in ^{137}Cs concentration in water column for studied durations of exposure against respective initial concentration was estimated from C_0 and C_t in terms of percentage. The results (Fig. 1) indicate that the percentage reduction at lower initial concentration of ^{137}Cs in water column is comparatively higher than that of higher initial concentration in the case of both submerged species.

The plots of uptake from water column show fast and immediate uptake pattern by both the species. Similar fast initial uptake followed by movement to reach an equilibrium state was observed by Hornik et al., [2] for Cs^+ in Bacopa monnieri and Egeria densa. Hence it is assumed that the observed biouptake during short term experiments are predominantly extra-cellular and depends on contaminant concentration in water column and availability of extra-cellular adsorption sites on the plant surface. The adsorption data on Myriophyllum spicatum and Hydrilla verticillata are therefore subjected to Elovich model and pseudo second order.

Experimental data are applied to the linear form of pseudo-second order kinetic model equation by linear regression of (t/q_t) vs. t as shown in Table 1. The

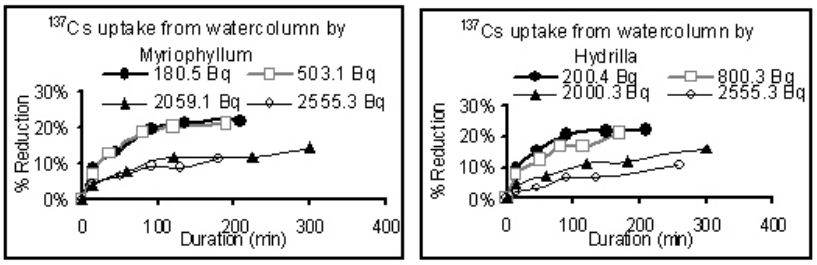


Fig. 1 ^{137}Cs uptake by macrophytes in terms of % reduction in water column.

Table-1: Pseudo-second order & Elovich kinetic model

Macrophyte species	C_0 (Bq/L)	Pseudo-second order kinetic model					Elovich kinetic model				
		k_2 (gm/Bq/min)	q_e (Bq/gm)	h (Bq/gm/min)	R^2	p	(Bq/g/min)	(g/Bq)	R^2	p	R_E factor
Myriophyllum s.	180.5	6.6E-03	4.65	0.14	0.994	2.0E-04	0.31	1.00	0.97	2.7E-03	0.32
	503.1	2.4E-03	12.61	0.38	0.997	8.7E-05	0.41	0.54	0.97	2.0E-03	0.30
	2059.1	7.6E-04	28.53	0.62	0.964	2.9E-03	1.51	0.15	0.95	5.4E-03	0.21
	2555.3	6.2E-04	32.79	0.66	0.955	4.1E-03	2.33	0.14	0.93	8.9E-03	0.20
Hydrilla v.	200.4	7.9E-03	5.07	0.20	0.999	2.3E-05	0.48	0.98	0.97	1.8E-03	0.25
	800.3	1.2E-03	20.16	0.47	0.964	2.9E-03	0.90	0.24	0.94	6.3E-03	0.23
	2000.3	6.8E-04	27.21	0.50	0.947	5.2E-03	1.38	0.14	0.92	9.0E-03	0.22
	2555.3	4.1E-04	36.58	0.55	0.897	1.5E-02	1.51	0.13	0.91	1.3E-02	0.21

regression coefficient R^2 and p values of the results favored second order kinetic model. This indicates an active sorption process between $^{137}Cs^+$ ions and polar functional groups present on the extracelluar surface of the macrophytes which can be involved in chemical bonding, as chemi-sorption processes show good compliance with the pseudo-second order kinetic model [3]. The rate constant k_2 (g/Bq/min) as well as initial adsorption rate h (Bq/g/min) are higher for Myriophyllum s. (6.2×10^{-4} & 0.664) than that of Hydrilla v. (4.1×10^{-4} & 0.552) at a given contaminant concentration (C_0 : 2555.3 Bq/L). This indicates that former could be better natural adsorbing media for ^{137}Cs than the latter, at least during the early period of exposure. This may be due to the structure and shape of the species, especially the leaves offers more surface area in case of Myriophyllum s. than that of Hydrilla v.

Elovich kinetic model

One of the most useful models for describing chemical adsorption is the Elovich equation [4].

$$q_t = (1/\ ) \ln \quad + 1/\ \ln t \qquad (1)$$

where q_t (Bq/g), (Bq/g/min) is the initial adsorption rate and (g/Bq) is the desorption constant related to the extent of the surface coverage and activation energy for chemisorption. The adsorption data were tested for Elovich kinetic model by linear regression of q_t vs ln t and results are summarized in Table 1. The results show that the initial adsorption rate increases with the increase in contaminant concentration in water column while desorption constant decreases. The results also indicate that Myriophyllum s. exhibits higher and values for a given contaminant concentration than Hydrilla v. This is also an indication of a better role played by Myriophyllum s. in initial adsorption of ^{137}Cs compared to Hydrilla v.

The adsorption data were also tested against the dimensionless Elovich equation [5] to derive R_E, the approaching equilibrium factor.

$$q_t/q_{ref} = R_E \ln (t/t_{ref}) + 1 \qquad (2)$$

For an adsorption system, let t_{ref} (min) be the longest time in adsorption process, q_{ref} (Bq/g) the solid phase concentration at time $t = t_{ref}$ and qt (Bq/g) is the adsorbed quantity at time t. The value of R_E is > 0.3 means slow adsorption process, if $0.3 > R_E < 0.1$ for mild adsorption and if $0.1 > R_E < 0.02$ rapid adsorption process. The adsorption process exhibited by the living macrophytes on this study could be classified as mild adsorption process since the derived R_E values are between 0.30 and 0.10. It is observed that at the same initial contaminant concentration Myriophyllum s. performs a rapid process than Hydrilla v.

Conclusion

Uptake kinetics of ^{137}Cs by two living freshwater submerged macrophytes (Myriophyllum s.& Hydrilla v.) were studied using pseudo second order kinetics and Elovich model for short duration exposures with varying ^{137}Cs concentration. Compliance to 2nd order kinetics indicates the mechanism could be chemi-sorption. Since Myriophyllum s. exhibits better kinetics than Hydrilla v., former could be better natural adsorbing media for ^{137}Cs due to its physiological advantage over the other.

Acknowledgments

The authors would like to thank Dr. D.N. Sharma, Director, Health, Safety and Environment Group, BARC and Shri. L. K. Jain, Site Director, KAPS for their keen interest and encouragement.

References

[1] F.Veglio and F. Beolchini., Hydrometallurgy. 44 (1997) 301.

[2] M. Hornik, M. Pipiska, J. Augustin, Nova Biotech. 8-1 (2008) 55.

[3] Ho Y.S., Journal of Haz. Mat., 136, (2006) 681.

[4] Elovich S.Yu., O.G Larionov, Bulletin of the Academy of Sciences of the USSR Division of Chem. Sci. 11 (2), (1962) 191.

[5] Wu F., Tseng R., Juang R., Chem. Eng. Journal 150, (2009) 366.

Studies on Transpiration Rate and Tritium Concentration in Transpired Water in Some Plant Species Around Kakrapar Gujarat Site

Rajkanya. M. Arjune.[1], A.K. Patra[1], C.P. Joshi[1], P.M.Ravi[2] and R.M. Tripathi[2]

1. *Environmental Survey Laboratory (ESS, Health Physics Division, Bhabha Atomic Research Centre), Kakrapar Atomic Power Station, Gujarat-394651, India; E-mail: rajkanya@npcil.co.in*
2. *Health Physics Division, Bhabha Atomic Research Centre, Mumbai 400 085, India*

Introduction

At Kakrapar Gujarat site, two PHWRs each are having a capacity of 220 MWe have been operational since 1994 and two more units are under construction (700 MWe PHWRs). Tritiated water (HTO) is one of the constituents of gaseous effluents released from a PHWR type nuclear reactor. The released HTO undergoes dilution and dispersion depending on the meteorological conditions and follow the ecological path of water molecules present in the environment. Water is continuously being released from the plant through the process of transpiration and fresh water is taken up from soil and atmosphere. The transpiration takes place through stomata opening in the leaf and the rate depends upon several conditions such as type of plant, temperature, humidity, etc. It is estimated that less than 5% of the water absorbed is used in metabolic reactions by an average plant and the remaining 95% water is released in the atmosphere as water vapors (Bendre, et al, 1995) [1].

Transpiration depends upon type of the plant and meteorological conditions of the site. Site-specific Transpiration rate is essential to understand the tritium cycling in the environment. No such data for Kakrapar Gujarat site is available. This paper presents the site-specific transpiration rate of some commonly available plants at Kakrapar Gujarat site.

Materials and Methods

Measurement of Tritium in Transpired Water from Leaf and Air Moisture Samples

The transpiration rate is measured by the standard method of collecting and weighing transpired water vapor (Anderson et. al, 1952) [2]. Air moisture was collected by using moisture condensation method. 10 mL of the sample was transferred to 20 mL vial and 10 mL scintillation cocktail was added to that vial. These samples were counted for ^{3}H using Ultra low level Liquid Scintillation Spectrometer (LSS) system, Model: TRICARB-3170 TR/SL).

Results and Discussions

Tritium activity in air moisture and plant transpired water

^{3}H activity in air moisture and plant leaf transpired water sample was observed to be in the range of 0.17-4.77 Bq/m^3 and 38-3733 Bq/L respectively. Maximum activity in air and plant leaf transpired water was found to be in Solid waste Management facility (SWMF) and watch tower-3 respectively. The site specific ratio of activity of tritium in transpired water to air moisture (Ri) was estimated and found to be in the range of 0.01-0.41 with GM: 0.12. Selvi et al., 2005 [3], reported the site specific ratio of activity of tritium in transpired water to air moisture as 0.1-0.2. Kornada and Martin (1973) [4] reported the vegetation to atmospheric tritium ratio as 0.17-0.49.

Estimation of Site Specific Transpiration Rate

Site specific Transpiration rate was estimated in 42 nos. of different leaf samples (10 varieties of plant) around Kakrapar Gujarat site within exclusion boundary and was found to be in the range of 0.05-2.96 g/g fresh wt. per hour. Minimum and maximum transpiration rate was observed to be in Leucaena leucocephala (Local name: Subabul) and Mangifera indica (Local name: Mango) respectively. Mango leaf showed maximum transpiration during March while Madhuca longifolia (Local name: Mahua) leaf showed maximum transpiration during April.

Factors affecting Transpiration rate

The transpiration rate of a plant is related to its age, canopy area and climatic factors like temperature, rainfall, humidity, soil water and wind velocity. It is observed that the transpiration rate was positively correlated to atmospheric temperature and the correlation coefficient was found to be 0.67. Variation transpiration rate with surface area in two different plant species (Gauva and Mango) was studied. It is observed that the transpiration rate is significant and positively correlated with leaf surface area as shown in Fig. 1. The correlation coefficient was found to be 0.72 and 0.61 in guava and mango leaf respectively.

Acknowledgements

The authors would like to thank Dr. D.N. Sharma, Director, Health, Safety and Environment Group (HS&E group), BARC for his keen interest and encouragement. The authors are grateful to Shri L. K. Jain, Site Director, Kakrapar site and Shri. Lokesh Kumar, Project Director, Kakrapar Atomic Power Project-3&4 for their continuous support during this study. The assistance rendered by Shri M. K Chaudhary, Smt. Padma Chaudhary, Shri. Mityabhai Chaudhary and all other ESL staff is thankfully acknowledged.

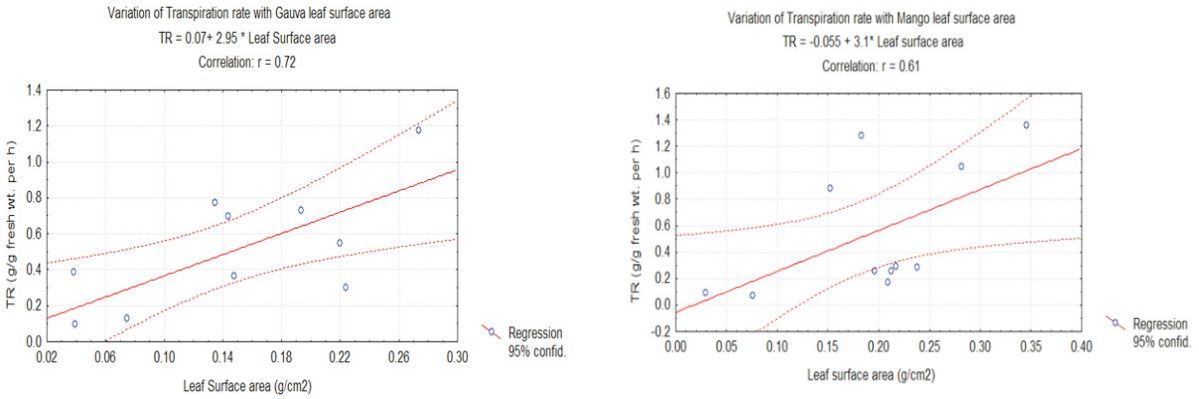


Fig. 1 Variation Transpiration rate with leaf surface area

References

[1] Asol Bendre, Pande, P. C. C. Introductory Botany, First Edition, (1995).

[2] Anderson, D. B., Meye , B. S, Plant Physiology, Second Edition, (1952) p.123.

[3] Selvi, S. B., Ravi, P. M., Hegde, A. G., Studies on Transpiration Rate and Tritium concentration in Transpired Water in Some Plant at Kaiga site, IARP-2005, (2005).

[4] Koranda, J. J, Martin, J. R., The movement of tritium in ecological systems. In: Moghissi, A. A, Carter, M.W.Eds. Tritium Phoenix, (1973) p.341.

Preparation and Deployment of Indigenous ^{125}I- seeds for the Treatment of Prostate Cancer: Dawn of Prostate brachytherapy in India

Sanjay Kumar Saxena[1], Yogendra Kumar[1], Ramu Ram[1], A.S. Tapase[1], Vivek J. Anand[2], Ashutosh Dash[1]

1. *Isotope Applications & Radiopharmaceuticals Division Bhabha Atomic Research Centre, Trombay, Mumbai 400085, India; E-mail: adash@barc.gov.in*
2. *P.D. Hinduja National Hospital & Medical Research Centre, Mumbai, India*

'Permanent seed implantation' using ^{125}I- seeds represents an effective treatment modality for prostate cancer. An innovative strategy to prepare and deploy ^{125}I- seeds for treatment of prostate cancer has been evolved. Seeds prepared by chemisorptions of ^{125}I on palladium coated silver wires were characterized and encased in titanium tubes by ND:YAG laser.Several batches of critically evaluated seeds exhibiting release of < 185 Bq of ^{125}I were supplied to P.D. Hinduja Hospital,Mumbai for treatment of prostate cancer patients. Successful deployment of indigenous seeds in prostate brachytherapy has opened a new window for making prostate brachytherapy affordable to needy cancer patients.

Keywords: ^{125}I, prostate brachytherapy, EDS, uniformity

Introduction

Brachytherapy is a treatment modality that is widely used in management of early stage prostate cancer. Permanently embedding an assembly of radioactive seeds consisting of low energy emitting radionuclides (20-35 keV X or) and high dose rate treatments with Linacs or afterloading machines using radioactive sources of very high strength (8- 10 Ci of Ir-192) are generally used for treatment of prostate cancer. On account of favorable radiation characteristics of ^{125}I , radioactive seeds containing 15-25 MBq of ^{125}I are effectively used in permanent seed implantation [1]. Due to commercial concerns, source preparation strategies are not revealed by overseas suppliers and exorbitant cost of imported seeds deprive needy cancer patients to garner the benefits of this treatment modality. BARC has previously developed and deployed indigenous ^{125}I-seeds for the treatment of eye cancer in India [2]. This achievement opened an avenue for deployment of seeds in relatively more challenging domain for the treatment of prostate cancer. This paper describes the optimization of process for chemisorptions of ^{125}I on palladium coated silver wires, characterization, laser encapsulation, quality assurance and supply of sources to a collaborating cancer treatment hospital.

Experimental

Preparation of ^{125}I-Seeds

The process parameters were optimized for quantitative chemisorptions of in-house produced ^{125}I on palladium coated silver wires of 3 mm (l) × 0.5 mm ( ) with slight modifications of our earlier reported procedure [2]. Under optimized conditions, seeds containing 11-15 MBq of ^{125}I were prepared by suitably adjusting the amount of ^{125}I in feed solution. Sources were encapsulated in titanium tubes of 4.75 mm (l) × 0.8 mm ( ) by Nd: YAG laser. Source strength of ^{125}I seeds was measured with pre-calibrated re-entrant ion chamber.

Characterization of Base Matrix

SEM-EDS analyses of palladium coated silver rods were carried out for studying the surface morphology and elemental distribution.

Quality Assurance and Supply of ^{125}I Seeds

Leachability of radioactive seed in water was determined at ambient temperature over a period of 48 h and uniformity check was carried out by standard autoradiography technique. Radioactive seeds were tested for classification performance tests for impact, thermal shock, pressure and vacuum endurance tests in accordance with AERB stipulated norms. Several batches of radioactive seeds were processed and prior to use in therapy, seeds were tested for absence of leakage (hot water immersion test at 50 C for 5h) and surface contamination. Samples of leakage and surface contamination tests were measured with the help of NaI(Tl) counter. All approved seeds were passed through MICK surgical needles for ensuring their dimensional accuracy within the tolerances accepted in clinical practice.

Results and Discussion

Chemisorption of ^{125}I on palladium coated silver wires could be proficiently achieved with more than 82% yield with addition of ~ 5 g of carrier iodide. Table 1 represents the effect of carrier concentration on iodide uptake. SEM micrograph of source base matrix taken under 5000 times magnification indicated agglomerated clusters with excellent homogeneity.

EDS pattern as shown in Fig.1, indicated presence of iodine peaks on various points of source matrix with uniformity within ± 3.8%.

Table 1: Effect of carrier on chemisorptions of ^{125}I

Sl. No.	Amount of carrier iodide (g)	% Chemisorption of ^{125}I (Mean ± SD)
1.	0.50	16 ± 6.3
2.	1.0	29± 4.7
3.	1.5	39± 2.8
4.	2.0	53± 4.9
5.	3.0	61± 3.5
6.	4.0	73± 5.2
7.	5.0	82± 3.4
8.	5.5	81 ± 2.7

n=3,temp. 60-70 C, reaction time- 6 h,^{125}I- 3.7 MBq

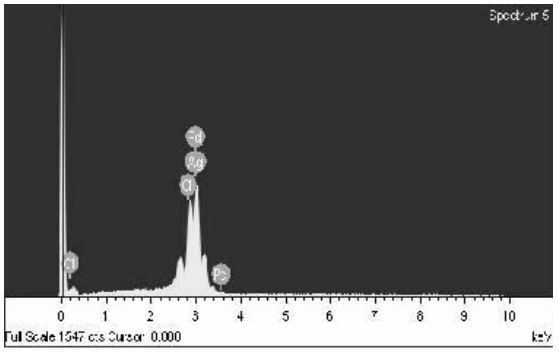


Fig. 1 EDS spectra of non radioactive source

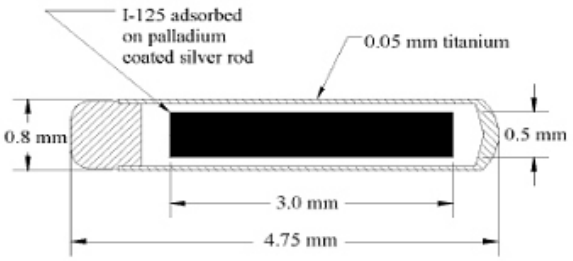


Fig. 2 Schematic of encapsulated ^{125} I seed

Laser encapsulation of radioactive seeds could be successfully achieved with negligible distortion of external surface of titanium tubes. Fig. 2 represents the schematic of laser encapsulated ^{125} I seed.

Variations in values of optical density of x-ray films exposed with radioactive seeds were found to be within ±5.9%. An average of these two values was considered to exhibit a maximum variation of radioactivity within ±4.9%. The leachability of ^{125}I from radioactive seed was found to be < 0.007%, well within the maximum allowed limit of 0.01%. Prototype seeds qualified all the regulatory tests w.r.t. impact, high temperature resistance, thermal shock, pressure and vacuum resistance etc. and removable surface contamination after performing all the stipulated tests was found to be < 185 Bq, the maximum limit set by AERB, India. Table 2 summarizes the data for quality control of various batches of ^{125}I-seeds, which could be processed and supplied on the requests received from P.D. Hinduja Hospital, Mumbai for performing permanent seed implantation in five prostate cancer patients.

Table 2: Quality control of ^{125}I seeds

No. of Seeds (MBq)	Uniformity (± %)	Max. Leakage (Bq)	Max. Surface contamination (Bq)
50 (14.4)	3.7	155	27
70 (15.5)	5.2	129	51
90 (14.8)	5.9	164	116
60 (14.8)	4.8	168	121
100 (14.5)	5.7	122	67

Conclusion

Strategies could be evolved to carry out large scale fabrication of ^{125}I seeds and seeds produced at BARC could be successfully deployed for prostate brachytherapy at P.D. Hinduja Hospital, Mumbai. The present work has opened a new avenue to medical fraternity to offer an effective treatment modality to needy cancer patients. The development of indigenous seeds for prostate brachytherapy has immense potential in future to reduce the import burdens of medical centres.

Acknowledgements

Authors are grateful to Dr. K.L. Ramakumar, Director, RC&IG for his encouragement and support. The authors express their thanks to Dr. Gursharan Singh, Associate Director, RC&IG for his encouragement. The help rendered by Shri. K.P. Muthe of TPD, BARC for SEM-EDS analysis is also gratefully acknowledged.

References

[1] Bowens P., Flynn A., J. Radiotherapy practice, 4 (2004) 85.

[2] Shah P.K., Narendran V., Selvaraj U., Guhan P., Saxena S.K., Dash A., Astraham M., I.J. Opthalmology, 60(4) (2012) 289.

Feasibility Studies for the Development of ^{169}Yb-Brachytherapy Seeds: Emerging Radiation Sources for the Management of Cancer

Sanjay Kumar Saxena[1], Yogendra Kumar[1], Y.R. Bamankar[2], Jitendra Nuwad[3], K.C. Jagadeesan[1], Ashutosh Dash[1]

1. *Isotope Applications & Radiopharmaceuticals Division, Bhabha Atomic Research Centre, Trombay, Mumbai 400085, India; E-mail: adash@barc.gov.in*
2. *Fuel Chemistry Division, Bhabha Atomic Research Centre, Trombay, Mumbai 400085, India*
3. *Chemistry Division, Bhabha Atomic Research Centre, Trombay, Mumbai 400085, India*

This paper describes studies for preparation of ^{169}Yb - brachytherapy seeds by encapsulating six 0.65 mm ( ) Yb_2O_3 microspheres in titanium capsules. Microspheres synthesized by sol-gel route were characterized by XRD, SEM, and EDS & ICP-AES. Crystalline microspheres exhibited uniformity of ytterbium with < 0.1 % leachability. Optimization of neutron irradiation was accomplished by conducting irradiations in DHRUVA. Newly developed LDR ^{169}Yb - seed is promising for its potential use in prostate brachytherapy. As an alternative to existing ^{192}Ir - HDR sources, protocol to prepare radiologically safer ^{169}Y-source (~10 Ci) by using ~15 % enriched targets was also formulated.

Keywords: ^{169}Yb, sol-gel, microspheres, brachytherapy, SEM, EDS, leachability

Introduction

Sealed sources incorporating various radionuclides find extensive use in the treatment of cancer by delivering radiation dose to the tumor. Brachytherapy seeds incorporating ^{125}I , ^{103}Pd etc. are in demand for the treatment of eye, prostate and brain cancers [1]. ^{169}Yb (half-life 32.02 days; mean gamma emission 93 keV) is known to be superior to some currently available brachytherapy nuclides[2] and hence there is a renewed interest in considering ^{169}Yb seeds as a substitute for higher-energy HDR ^{192}Ir seeds in temporary interstitial brachytherapy applications [3]. ^{169}Yb (0.5 to 2 mCi seed) is also an alternate to commonly used ^{125}I /^{103}Pd seeds in prostate brachytherapy as ^{169}Yb provides a higher initial dose rate for permanent implants compared to ^{125}I or ^{103}Pd. Natural Yb contains 0.13% of ^{168}Yb that on account of large thermal neutron capture cross-section of 2300 barns can be conveniently converted to ^{169}Yb in a nuclear reactor. In the present communication, we describe the studies that have been carried out to develop a new design of ^{169}Yb - seed, consisting of six microspheres ~ 0.6-0.65 mm ( ) arranged within a titanium capsule to serve as a brachytherapy seed after neutron irradiation.

Experimental

Preparation of Microspheres

Yb_2O_3 microspheres were prepared by Internal Gelation Process (IGP) of Sol-Gel technique. Briefly, a solution containing 1.0 mole of Yb $(NO_3)_3$ and 0.13 mole of HMTA was mixed well. Droplets of the feed solution were allowed to pass through a column containing hot silicon oil. Gel spheres could be prepared from the solution having 0.85 M of Yb and 2.125 M of [HMTA, Urea]. These were degreased with CCl_4 and washed with NH_4OH solution for 3 h. The spheres so formed were dried, heated to 1000 C for 2h and were finally sieved to 0.6- 0.65 mm ( ) size.

Characterization of Microspheres

Determination of surface area and porosity of microspheres was carried out by N_2 gas with the help of 'SORPTOMATIC 1990' analyzer by studying adsorption- desorption isotherms using multi point BET Method. Density of microspheres was determined by gas displacement method. SEM-EDS analyses of gold coated microspheres were carried out for studying the surface morphology and elemental distribution. XRD pattern of microspheres was obtained by powder diffraction method. Leachability of non radioactive Yb_2O_3 microspheres in water was determined at ambient temperature over a period of 48 h and concentration of Yb^{3+} and Si^{4+} metal ions was determined by ICP-AES.

Neutron Irradiation

Neutron irradiations of Yb_2O_3 targets was carried out in DHRUVA for a maximum up to two weeks. The irradiated targets after irradiations were dissolved in Conc. HNO_3 and were finally reconstituted in 0.5M HNO_3. Gamma spectrum of a diluted aliquot was taken with the help of HPGe - 4K MCA system pre calibrated with a standard ^{133}Ba source of ~ 0.1 Ci strength. Theoretical estimation of radioactivity of ^{169}Yb and ^{175}Yb at different time intervals was carried out and values were compared with experimental results. Based on these observations, irradiation of pre-assembled Yb_2O_3 - seeds (i.e., six microspheres encapsulated in titanium capsule) was also carried out over a period of 7-14 days at an average thermal neutron flux of 5 x 10^{13} n/cm^2/sec. Irradiated sealed assembly was decayed over different durations to bring the levels of co-product ^{175}Yb to less than 0.5%. Based on these experiments, irradiation calculations for irradiating natural as well as

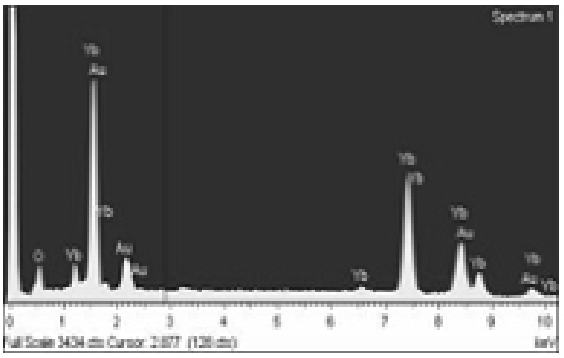


Fig. 1 EDS spectra of Yb_2O_3 microsphere

enriched Yb_2O_3 microspheres were carried out to optimize the irradiation and decay times to bring the levels of ^{175}Yb below < 0.5%.

Quality Assurance

The uniformity of activity in $^{169}Yb_2O_3$ - seed was assessed by standard autoradiography and optical density variation of exposed X-ray film was used as a measure of uniformity of radioactivity. Surface contamination and leakage of radioactivity from sources was checked by assaying the released radioactivity with the help of NaI (Tl) counter.

Results and Discussion

Sol-gel synthesis of microspheres facilitated formation of nearly spherical beads of 0.6-0.65mm ( ). The BET surface area and pore volume of heat treated samples were found to be 22.3 m^2/g and 0.10 cc/g respectively. Pore size distribution indicated that the pores in microspheres are in 30 A to 150 A range. The density of the microspheres was found to be 8.1 g/cc. EDS spectra as shown in Fig. 1 represents presence of peaks attributed to various elements available on the surface of microsphere.

XRD pattern showed presence of peaks of cubic phase crystalline Yb_2O_3. It was observed that the ytterbium microspheres were having no impurities of silicon and release of Yb^{+3} ions was ~ 0.09 % of ytterbium content. Fig. 2 represents the indigenous design of prototype ^{169}Yb-brachytherapy seed for its possible use in LDR as well as HDR brachytherapy applications.

It was observed that irradiation of titanium encased microspheres for a period of 7 days at an average neutron flux of 5×10^{13} $n/cm^2/sec$ and its post irradiation cooling for 90 days is adequate to produce ^{169}Yb- seed (up to 74 MBq strength) for low dose rate applications. The leakage and surface contamination from sealed source assembly were found to be less than the maximum allowable limit of 185 Bq. Fabrication of ^{169}Yb - brachytherapy seeds for HDR applications need use of enriched targets, which could produce seeds containing 296-370 GBq of ^{169}Yb . Owing to exorbitant cost of enriched targets, the calculations for making high dose rate sources were carried out theoretically. It is seen that with an enrichment factor of ~ 15%, the microspheres irradiated for a period of 120 days and cooling of 7-10 days can produce the HDR seeds of desired level i.e., 296-370 GBq (~ 8-10 Ci) of ^{169}Yb activity with specific activity ~ 53 GBq/mg w.r.t Yb.

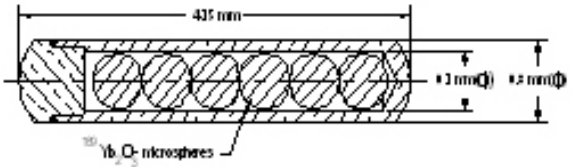


Fig. 2 Design of ^{169}Yb- brachytherapy seed

Conclusion

The feasibility study has demonstrated the utility of ytterbium oxide microspheres to prepare ^{169}Yb brachytherapy seed for their possible use in brachytherapy.The present work would be useful in fabrication of ^{169}Yb-brchytherapy seeds for assessing the potential of alternate brachytherapy seeds for their applications in various brachytherapy procedures.

Acknowledgements

Authors are grateful to Dr. K.L. Ramakumar, Director, RC&IG for his encouragement and support. The authors express their thanks to Dr. Gursharan Singh, Associate Director, RC&IG for his encouragement. We sincerely acknowledge the help provided by Dr. A.V.R. Reddy, Head, Analytical Chemistry Division, BARC for providing the support for trace metal analysis.

References

[1] Finger, P.T, Surv. Opthalmol. 42 (1997) 215.

[2] S.M. Loft, I.P. Coles and R.G. Dale, The British Journal of Radiology, 65, 771, 252.

[3] R K Das, V Mishra, H Perera, A S Meigooni and Jeffrey F Williamson, Phys. Med. Bid. 40 (1995) 741.

A Study on Helicobacter pylori infection in different parts of Karnataka using ^{14}C Urea Breath Test

Swaroop K.[1], Jayachandran[2], Rajashekar K. Patil[3], K. Bhaskar Shenoy[3] and H. M. Somashekarappa[1]

1. *Centre for Application of Radioisotopes and Radiation Technology (CARRT), USIC, Mangalore University, Mangalagangotri 574 199, Karnataka, India*
2. *Board of Radiation & Isotope Technology, BRIT, Vashi Complex, Sector 20, Vashi, Navi Mumbai 400 705, India*
3. *Department of Applied Zoology, Mangalore University, Mangalagangotri 574 199, Karnataka, India; E-mail: carrtmu@gmail.com*

A non-invasive ^{14}C Urea Breath Test (^{14}C UBT) technique was used for the diagnosis of Helicobacter pylori (H pylori) infection in symptomatic and asymptomatic individuals. The test utilises $^{14}CO_2$ released due to the action of urease produced by H pylori. ^{14}C UBT is found to be a simple alternative for endoscopic examinations for diagnosing H pylori infection. The test was performed on 664 subjects from various parts of Karnataka. Among them 34.9% of the subjects were found to be H pylori positive, and the infection rate varied from 16.9% to 38.6%.

Introduction

Helicobacter pylori (H pylori) is extremely widespread in humans and is now regarded as one of the commonest infections. According to a report by the World Gastroenterology Organization (WGO) developing countries generally have a much higher overall prevalence (up to 95 % of the population are infected in some countries) compared to the Western world (30–50 % infection rates) [1]. The incidence of H Pylori infection is estimated to be approximately 0.5% per year in adults of developed countries. This incidence has been decreasing over time. However, the incidence of H Pylori infection continues to be high in developing countries (3% to 10% per year) [2].

The accurate diagnosis of the status of H pylori in a subject is important for correct therapy and this also helps in designing and executing eradication programs. As Carbon–14 urea breath test (^{14}C UBT) is a simple, innocuous, economical, and one of the most accurate methods available for assessing H pylori status, it is recommended as the gold standard, a non-invasive method for diagnosing H pylori infection [3].

Methodology

^{14}C-Urea Breath Test (^{14}C-UBT):

To do the test, the patient is administered a ^{14}C labelled urea capsule. If the patient has the H pylori infection, the ^{14}C urea will react with the urease produced by the H pylori bacteria and break down into ^{14}C labelled bicarbonate ($H^{14}CO_3^-$) ions and ammonium (NH_4^+). The ^{14}C labelled bicarbonate ions will reach the blood stream, get transported to the lungs and be subsequently exhaled as ^{14}C labelled carbon dioxide ($^{14}CO_2$). The exhaled $^{14}CO_2$ is then absorbed in a trapping solution. After adding the scintillation cocktail the collected sample is quantified for radioactivity using liquid scintillation counter (LSC). The pictorial representation of ^{14}C UBT is given in Fig. 1.

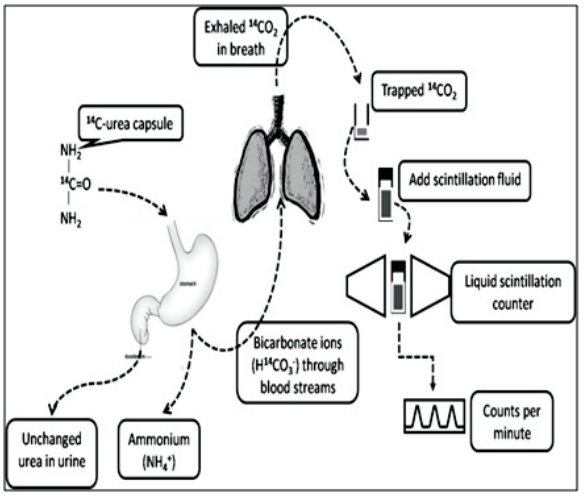


Fig. 1 Principle of ^{14}C-Urea Breath Test [3]

The study was carried out in Dakshina Kannada, Chikmagalur, and Gadag districts of Karnataka state, India. The subjects were explained the purpose of the study and their consent was taken. All subjects were interviewed by means of a questionnaire which covered their family history, age, educational background, lifestyle related items such as urban or rural lifestyle, hygienic lifestyle, food habits, and alcohol consumption.

Result and Discussion

Randomly selected samples of 664 persons aged 15 years and above were surveyed from various parts of Karnataka. Collections of breath sample from the general public as well as from gastric symptomatic patients was carried out in Dakshina Kannada (400 subjects), Chikmagalur (157 subjects) and Gadag (106 subjects). All the collected breath samples were analyzed for H pylori infections with different conditions. Since environmental condition, lifestyle

and socio-economic status of people differ from each other, the subjects of each district were analyzed individually based on their lifestyle, gender, food habits, and alcohol consumption.

The survey carried out for the prevalence of H pylori infection using ^{14}C UBT as a diagnostic tool reveals the infection rate to be 38.5 %, 38.6%, and 16.9% in Dakshina Kannada, Chikmagalur, and Gadag districts, respectively.

The infection rate of the rural and urban populations of all three districts was analyzed. It is found that the infection rate of the rural population (39.7%) is relatively higher than the urban population (36.1%) in Dakshina Kannada district. Whereas in Chikmagalur and Gadag districts, the infection rate is higher in the urban population - 44.8% and 17.6%, respectively, than the rural population - 32.5% and 13.5%, respectively.

The infection rate in the female population of Dakshina Kannada (40.9%), Chikmagalur (41.6%), and Gadag (24%) is relatively higher than the respective male population (37.1%, 36% and 13.1%).

The subjects were analyzed by means of their food habits. They were categorized as vegetarian and non-vegetarian. In Dakshina Kannada and Chikmagalur, the infection rate is significantly more in non-vegetarians - 42.4% and 68%, respectively compared to the vegetarian population - 28.3% and 33.5%, respectively. But, the difference between the infection rate in vegetarian (15.2%) and non-vegetarian (14.2%) is only 1% in the population of Gadag district.

The alcoholic male population of Dakshina Kannada, Chikmagalur and Gadag have shown infection rate of 46.3%, 67%, and 31.2%, respectively, which is much higher than the total infection rate of 37.1%, 36%, and 13.1% of the corresponding male population.

Conclusion

The survey carried out for the prevalence of H pylori infection using ^{14}C UBT as a diagnostic tool shows variation in the infection rate from 16.9% to 38.6% in Dakshina Kannada, Chikmagalur and Gadag districts of the Karnataka. The overall infection rate of all the three districts (34.34%) is much less compared to the reported range of Asian and African countries (70% to >90%) by the World Gastroenterology Organization (WGO). However, it compares well and within the reported range of Europe and North American countries (30% to 50%) [1].

The prevalence of H pylori infection in the rural population of Chikmagalur and Gadag district is less compared to the urban population. Whereas, the difference in H pylori infection among the urban population (36.1%) is very narrow (3.6%) in comparison to the rural population (39.7%) of Dakshina Kannada district. The gender specific studies of all the three districts shows slightly higher infection rate in the female population. The non-vegetarian and alcoholic population of all the three districts shows higher H pylori infection rate when compared to vegetarian and non-alcoholic population.

The studies show greater prevalence of H pylori in Dakshina Kannada and Chikmagalur compared to Gadag. The reason for this finding may be the dietary habits, environmental conditions, and lifestyles. As per the data more than 75% of population of Dakshina Kannada are non-vegetarians. But in Gadag we found more than 80% of the populations are vegetarians. The data also shows that alcoholic subjects are more prone to the infection.

Acknowledgement

The authors are thankful to Dr. N. Sivaprasad, former SGM, BRIT, Mumbai for his guidance and help in carrying out this study. The authors are grateful to the Board of Research in Nuclear Science for funding this research work.

References

[1] World Gastroenterology Organisation Global Guidelines, (2010) 1.

[2] Tat-Kin Tsang and Manish Prasad Shrestha, www.intechopen.com, p 39.

[3] Swaroop K., Jayachandran, Shrikanth L. Patil and H. M. Somashekarappa, Radiat. Prot. and Environ., 34 (2011) 206.

Purification and concentration of ^{68}Ga eluate from SnO_2 based $^{68}Ge/^{68}Ga$ generator

Sankha Chattopadhyay, Md. Nayer Alam, Madhusmita, Luna Barua, Sujata Saha Das, and Malay Kanti Das

Radiopharmaceuticals Lab., Regional Centre, BRIT, VECC, Kolkata, India

The ^{68}Ga radioisotope is an excellent source in clinical PET application due to its ease of availability from $^{68}Ge/^{68}Ga$ generator having a shelf life of 1 year. Eluates from most of the commercially available generators have low concentration of ^{68}Ga radioactivity, high acid concentration and traces of various metal contaminants and thus it is not suitable for labelling work. Therefore ,pre-concentration and purification of the initial generator eluate is required.

Introduction

^{68}Ga has immense potential in PET imaging for several reasons: (a) Long shelf life of the generator (potentially up to 1 year or even longer), (b) its 68 min half life matches with the pharmacokinetics of many peptides and other small molecules owing to rapid diffusion, localisation at the target and fast blood clearance, (c) ^{68}Ga forms stable complexes with various types of chelating agents with its +3 oxidation state. The most commonly available commercial $^{68}Ge/^{68}Ga$ generator systems used are based on TiO_2 or SnO_2 as sorbents. In this study tin dioxide (SnO_2, prepared in our laboratory from metallic tin) has been employed as sorbent material to retain ^{68}Ge in the column and Ga-68 was eluted periodically from the column generator in 1N HCl. Post-elution purification of primary ^{68}Ga eluate obtained from the generator was achieved by using a combine cation and anion exchange column in series.

Experimental

^{68}Ge has been produced in VECC through the nuclear reaction: ^{nat}Zn (,2n)^{68}Ge. Irradiated target was dissolved in 1N HCl was loaded on to the SnO_2 column (i.d 8mm). The column was prepared with 0.5-0.7 gm SnO_2 (150-200 mesh size) preconditioned with dil. HCL. The column was then thoroughly washed with 600ml of 1N HCl to remove the traces of Zn that may come from the target. ^{68}Ga was then eluted routinely with 4 ml 1 N HCl. The purification of the initial generator eluate was carried out on a cation exchange resin followed by a small anion exchange column. The whole operation was a closed process using manually operated two and three way valves connected to a vaccum pump. The purification process steps are shown in Fig. 1. The activity of ^{68}Ga before and after purification was measured using a calibrated dose calibrator (ISOMED 50, Hans Walischmiller GmbH, Dresden, Germany). The radionuclidic purity of the purified ^{68}Ga was determined by gamma spectrometry using HPGe detector. Trace level of the metal ion contamination in the ^{68}Ga eluate may be due to the presence of tin ions which might come from the column matrix. This was determined by ICP-OES technique using iCAP 6500 ICP spectrometer (Thermo Scientific) in the decayed sample.

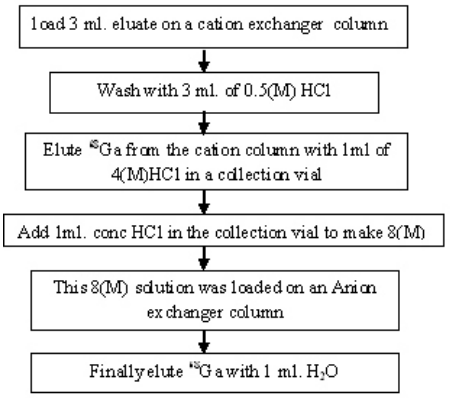


Fig. 1 Flowchart of purification of primary eluate from the $^{68}Ge/^{68}Ga$ generator

Results and Discussion

Elution efficiency of Ga-68 from the generator was about 65 %. The recovery yield of purified ^{68}Ga was over 85% (n=40). The pH of the final solution was 7.0. Possible ^{68}Ge break-through was assessed following a decay period (post EOI) of at least two days to allow for decay of unsupported ^{68}Ga. ^{68}Ge and ^{65}Zn removal by the purification processes were determined by gamma spectrometry monitoring 1077 keV -peak and 1115 keV -peak respectively. Quality of Ga-68: In the ^{68}Ga eluate ^{68}Ge concentration before and after purification was 0 .008% and 0.00015% respectively (Fig. 2) and that of ^{65}Zn was 0.00005%. and 0.000009% , respectively (Fig. 3). Sn concentration in the primary ^{68}Ge eluate was 0.03 ppm

Conclusions

The purification and concentration of ^{68}Ga thus developed with Dowex resin as per our knowledge is a new attempt, and recurring ^{68}Ga concentration of primary eluate from the SnO_2 based $^{68}Ge/^{68}Ga$ generator resulting in high radioactive concentration. This will ensure high radiochemical labelling yield of somatostatin analogue peptide with ^{68}Ga.

References

[1] Nelson, F., Murase, T., Kraus, K.A., J.Chromatogr. 13 (1963) 503.

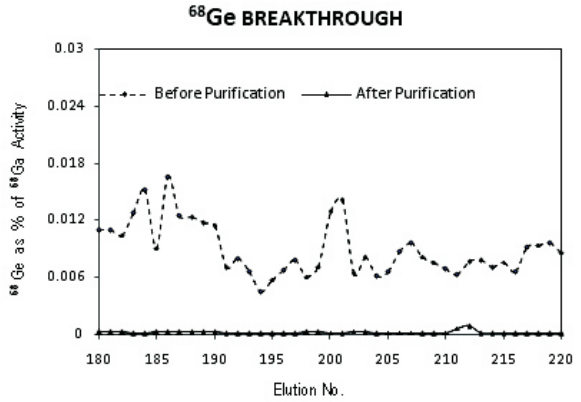


Fig. 2 *^{68}Ge breakthrough in the eluate before and after purification*

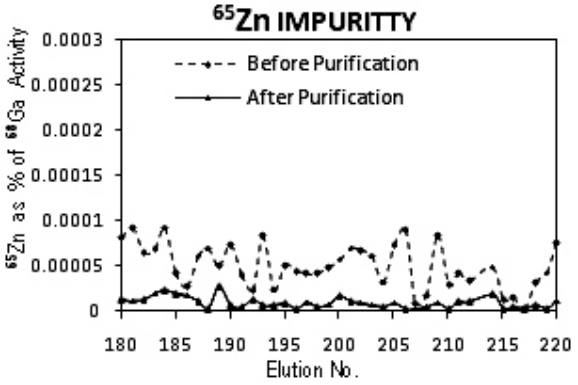


Fig. 3 *^{65}Zn impurity in the eluate before and after purification.*

[2] Zhernosekov, K.P., Filosofov, D.V., Baum, R.P., Aschoff, P., Adrian, H.J., Bihl, H., Razbash, A.A., Jahn, M., Jennewein, M., Rosch, F., J. Nucl. Med. 48, (2007) 1741.

[3] Gebhardt P., Opfermann Th., Saluz H. P., Appl. Radiat. Isot. 68 , (2010) 1057.

[4] Saha Das Sujata, Chattopadhyay Sankha, Alam Md. Nayer, Madhusmita, Barua Luna, Das Malay Kanti, Appl. Radiat. Isot. 79 , (2013) 42.

Evaluation of Photosynthetic Pigments and Protein Content in some Gamma Treated Wheat Varieties Using ^{60}Co as a Source

Sandeep Mishra[1], Pradeep K Shukla[1], Pragati Misra[2], Narayani Shukla[3], Gayatri[5] Sanghdeep Gautam[4] and P.W. Ramteke[1]

1. *Department of Biological Sciences, School of Basic Sciences, Sam Higginbottom Institute of Agriculture, Technology and Sciences (Deemed to be University), Allahabad, Uttar Pradesh, India; E-mail: pragatimisra3@rediffmail.com*
2. *Department of Tissue Engineering, Jacob School ofBiotechnology and Bioengineering, Sam Higginbottom Institute of Agriculture, Technology and Sciences (Deemed to be University), Allahabad, Uttar Pradesh, India*
3. *Department of Biochemistry and Biochemical Engineering, Jacob School ofBiotechnology and Bioengineering, Sam Higginbottom Institute of Agriculture, Technology and Sciences (Deemed to be University), Allahabad, Uttar Pradesh, India*
4. *Department of Molecular and cellular engineering, Jacob School ofBiotechnology and Bioengineering, Sam Higginbottom Institute of Agriculture, Technology and Sciences (Deemed to be University), Allahabad, Uttar Pradesh, India*

Introduction

Wheat (TriticumaestivumL.) is world's most widely cultivated food crop. In India, it is the second important staple cereal food playing a vital role in stabilizing the food grain production in the country [8]. Nutritive value of wheat is also high as compare to other cereals. It contains more protein than other cereals. Gamma rays are also very important in mutation breeding and in vitro mutagenesis in order to develop required features of plants and increase the genetic variability. The many mutant varieties, which are resistant to diseases, cold salt and with high quality, have been developed [1]. In plant improvement, the irradiation of seeds may cause genetic variability that enable plant breeders to select new genotypes with improved qualitative and quantitative characteristics [2]. Gamma rays belong to ionizing radiation and are the most energetic form of such electromagnetic radiation, having the energy level from around 10 kilo electron volts (keV) to several hundred keV. Therefore, they are more penetrating than any other types of radiation such as alpha and beta rays [4]. Gamma radiation can be useful for the alteration of physiological characters. The biological effect of gamma-rays is based on the interaction with atoms or molecules in the cell, particularly water, to produce free radicals. These radicals can damage or modify important components of plant cells and have also been reported to modulate differentially the morphological, anatomical and biochemical characters of the cell and the organism therein. Gamma rays are often used on plants in developing varieties that are agriculturally and economically important and have high productivity potential [1,3,5].

Material and Methods

Seeds of four wheat varieties (namely LOK-1, HUW-234, PBW-154, and HD-2733) were treated by different doses of Gamma radiation (10 Gy, 20 Gy, 30 Gy, 40 Gy) using ^{60}Co as source in National Botanical Institute (NBRI) research institute of CSIR at Lucknow. Estimation of chlorophyll was done by using dimethyl sulphoxide (DMSO) extraction procedure. The chlorophyll a, chlorophyll b and total chlorophyll content were calculated according to the method of Hiscox and Israelsham[6].

Chlorophyll a (mg/g fresh weight)

$$= (12.7 \times A_{663} - 2.63 \times A_{645}) \times (v/1000 \times W)$$

Chlorophyll b(mg/g fresh weight)

$$= (22.9 \times A_{645} - 4.45 \times A_{663}) \times (v/1000 \times W)$$

Total Chlorophyll (mg/g fresh weight)

$$= (20.2 \times A_{663} - 8.02 \times A_{645}) \times (v/1000 \times W)$$

Total carotenoids (-carotene + xanthophylls) estimation requires simultaneous estimation of chlorophyll-b. The assay is based on the various equations for the determination of pigments based on their absorption in organic solvents at various wavelength as described by Lichtenthaler and Wellburn [7].

Carotenoid(mg/g fresh weight)

$$= A_{470} \times (3.27 \times \text{chl. a} + 140 \times \text{chl.b}) \times (v/1000 \times w)$$

The SPAD meter was also used to analyze the chlorophyll status of a plant. The SPAD meter measures chlorophyll content (SPAD Chlorophyll meter reading SCMR) per unit leaf area.Fluorescence steady state value (Ft) and quantum yield (Qy) values were recorded by using plant fluoropen device.

Experimental Result

The results showed that there was a significant difference in chlorophyll 'a' (mg/g fresh weight) content among all the varieties under different treatments. The maximum chlorophyll acontent was observed in PBW-154 in T_0 (1.84 mg/g fresh weight), whereas the minimum was observed in variety HUW-234 in T_4 (0.25 mg/g fresh weight) at 40 Gy of gamma radiation, under all the treatments.The data showed that there was a significant difference in chlorophyll 'b' (mg/g fresh weight) content in all the varieties under different treatments. The maximum chlorophyll content was observed in PBW-154 in T_0

(0.84 mg/g fresh weight), whereas the minimum was observed in variety HD-2733 in T_4 (0.17 mg/g fresh weight) at 40 Gy of gamma radiation, under all the treatments. Result showed that there was a significant difference in SCMR readings (mg/g fresh weight) content in all the varieties under different treatments. The maximum SCMR readings was observed in variety PB-154 in control T_0 (64.20 mg/g), whereas the minimum was observed in variety LOK-1 in T_4 (22.76 mg/g fresh weight) at 40 Gy of gamma radiation, under all the treatments.The results showed that there was significant difference in total carotenoid (mg/g fresh weight) content in all the varieties under different treatments. The maximum carotenoid was observed in variety PBW-154 in control T_0 (7.10 mg/g fresh weight), whereas the minimum was observed in variety HUE-234 in T_4 (5.65 mg/g fresh weight) at 40 Gy of gamma radiation, under all the treatments. The Result showed that there was a significant difference in QY (%) in all the varieties under different treatments. The maximum QY (%) was observed in variety PBW- 154 in control T_0 (0.62%), whereas the minimum was observed in variety HD-2733 in T_4 (0.44%) at 40 Gyof Gamma radiation, under all the treatments.The data showed that there was a significant difference in Ft in all the varieties under different treatments. The maximum ft was recorded in variety PBW-154 in control T_0 (2116), whereas the minimum was observed in the variety LOK-1 in T_4 (1434) at 40 Gy of gamma radiations.The data showed that there was a significant difference in soluble protein content (mg/g fresh wt.) among all the varieties under different treatments. The maximum soluble protein was observed in variety PBW-154 in control (32.52 mg/g fresh wt.), whereas the minimum was observed in variety HD-2733 (25.64 mg/g fresh wt.) in T_4 at 40 Gy of Gamma radiation.

Summary

The results showed that variety PBW-154 was relatively tolerant to gamma radiation among all the verities, whereas, HD-2733 and LOK-1 were sensitive to gamma radiation varieties. The biochemical parameters in all wheat varieties, chlorophyll content and protein content, showed a significant decrease with the increase in treatment of gamma radiation stress.

References

[1] S.M. Jain, B. S. Ahloowalia and R. E. Veilleux, In: Crop Improvement. Kluwer Academic Publishers, 12 (1998) 203.

[2] G. S. Murty, and A. Austin, Indian J. Agron. (1963). 225.

[3] C. Artk, and E. Peksen Ondokuz-Mays- University, -Ziraat-Fakultesi-Dergisi, (2006) 95.

[4] E. Kovacs and A. Keresztes, Micron, 33 (2002) 199.

[5] A. Kiong, S. H. L. Pick, G. Lai and A. R. Harun, Am-Eurasian J. Sustain. Agric., 2 (2008) 135.

[6] J.D. Hiscox and G.F. Israelstam, GF, Canadian Journal of Botany, 57 (1979) 1332.

[7] H. K. Lichtenthaler and A. R. Wellburn, Biochemical Society Transactions, 11 (1983) 591.

[8] Dubcovsky, J., Luo, M. C. and Dvorak, J., Theor. Appl. Genet. 91 (1995) 795.

Mössbauer Spectroscopic Characterization of Dust Particulates From a Cement Factory and Thermal Power Plant

R. B. Lanjewar[1.] and Mamata R. Lanjewar[2]

1. *Department of Chemistry, Dharampeth M.P.Deo Memorial Science College, Nagpur, (M.S.) India; E-mail: rb_lanjewar@rediffmail.com*
2. *Department of Chemistry, Shivaji Science College, Congress Nagar, Nagpur, (M.S.), India*

In this paper we present the study of dust particulates collected from six different location in the areas surrounding cement factory in central India and Thermal Power Plant. It is analyzed by Mössbauer spectroscopy that the iron exists in the chemical state of structural iron (Fe^{2+}, Fe^{3+}).The analysis of the ^{57}Fe Mössbauer Spectra recorded at room and liquid nitrogen temperatures, showed that iron species in all samples consisted of Fe_2O_3, Fe_3O_4, $Fe_2(SO_4)_3$ and Fe^{2+} high spin state but their proportions were different in different sites, dependent of each environmental condition. Mössbauer spectra recorded at both 300K and 78 K show the differences in the phase composition of iron containing ambient air dust particulates from cement factory. In addition, the transformation of iron compound in air was discussed.

Introduction

Iron is the major constituent of the whole earth (35.0 %) and the fourth major constituent of the earth's crust (4.5 %). The atmosphere contains less than 0.0001 % by mass of iron, however, airborne particulate matter is composed of 1.0 to 5.0 % by mass of iron [1]. Since large amounts of iron are mobilized in the earth's crust, atmospheric Fe is generally assumed to be soil derived [2,3]. It is clear that anthropogenic emissions may also account for iron emissions into the atmosphere, however, models of identification of air pollution sources are lacking of consistency to explain the origin and occurrence of iron. Various industrial operations of the civilized world emit dust, gases, vapours and mist. The air inside a factory building can be polluted by released of contaminants from industrial processes to the air of the workroom [4]. Air pollution is persistent upon strongly nowadays because of its adverse effects on human health. With increasing industrialization, many inorganic pollutants are continuously loading the atmosphere causing serious health hazards. Mossbauer spectroscopy can used to study that information from Fe. Mössbauer spectroscopy is particularly useful for studying the iron content and provide information regarding the structural and chemical aspects of the iron atoms in iron containing compounds.

In order to know the source of pollutants and quality of atmospheric environment around an industrial area, it is essential to have an accurate analysis of various components. The identify the various pollutants and their amounts is important to evaluate its health effects and toxic stresses. The aim of the present work was study the Mössbauer Spectroscopy of ambient air dust particulate samples and to know their phase composition.

Materials and Methods

Samples

Ambient air dust particulates were collected from six different locations around the cement factory and thermal power plant located in Central India, by NEERI, Nagpur. Samples were collected using High Volume Sampler with preweighed glass fiber filter paper of size 20cm x 25cm with a average flow rate of 1.5m^3/min. The samples were dried in a desiccator. A fine powder of the dust particulate was scratched using a Teflon coated spatula to avoid the metal contamination.

The Mössbauer spectra were recorded on transducer driven M sbauer spectrometer in constant acceleration mode (ELCENT) at room temperature. A ~5 mCi ^{57}Co(Rh) source was used. The spectrometer was calibrated using a natural iron foil. The isomer shift values were reported with respect to metallic iron. The spectra were fitted with Lorentzian line shapes by using least square fitting procedure.

Result and Discussion

Mössbauer Spectra recorded at room temperature and 78K spectra of the samples collected from Cochin city and nearby industrial area are shown in Fig.1. In the spectrum at room temperature, there are two components with quadrupole splitting doublet besides small contribution from the background (Fig.1A). In the spectrum at 78K there is a component with magnetic hyperfine splitting sextet besides the component already appearing at RT. This result indicates that the iron particles in the particulates are very small, showing a superparamagnetic behavior at RT and partly ferromagnetic at 78K. Such behavior of the particles shown in Mossbauer spectra typically belongs to ultrafine ferromagnetic or antiferromagnetic particles due to magnetic spin relaxation. The result showed that iron compounds in all samples consists of Fe_2O_3, Fe_3O_4 and Fe^{2+} high spin state but their proportions were different at different sampling sites, depending on environmental condition. The relative concentration of iron oxide in sample is higher than the one in commercial and suburban districts. In order to study the transformation of iron compound the samples collected from different locations were taken M sbauer spectra.

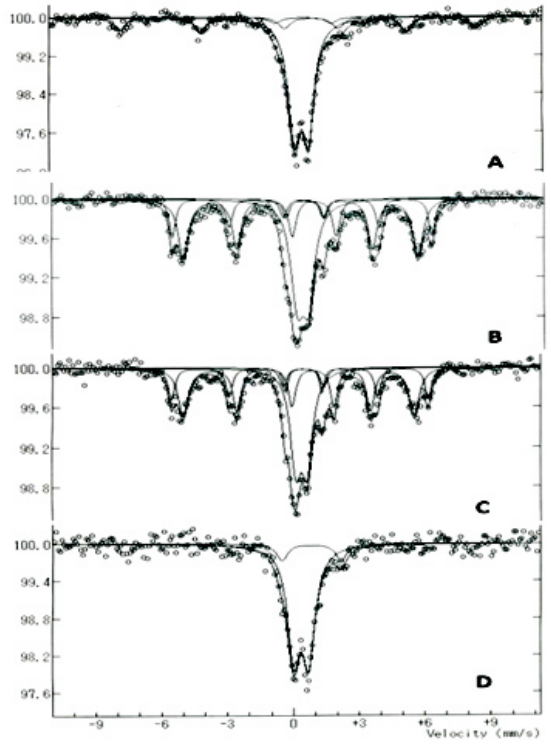


Fig. 1 Mossbauer spectra of Ambient dust particulate matter at (A) and (D) room temperature and (B) and (C) at 78K

The transformation of Fe_3O_4 to Fe_2O_3 was found. The spectra at 78 K appear much stronger magnetic hyperfine splitting sextet than the one at 293K. It means that the iron particles contained in air particulates are small, showing a supermagnetic behaviour at room temperature and ferromagnetic partly at 78K.

Such behaviour of the air particulates particles appearing in a Mössbauer spectrum typically belongs to ultrafine ferromagnetic or antiferromagnetic particles due to magnetic spin relaxation. The Mössbauer spectra were fitted by two doublets and two magnetic sextets at room temperature, and one more sextet was added at 78K. From it is found that the intensity of doublet and sextets components do not change with sites and temperature. All samples shows two doublets with large small quadrupole splitting and multiple sextets. Based on the hyperfine parameters, i.e., isomer shift ( ), quadrupole splitting (E_Q), the doublet with larger quadrupole splitting was assigned to paramagnetic ferrous iron. Also, the doublet with small quadrupole splitting was assigned to paramagnetic ferric iron. Since the magnetic field H_{eff} of the magnetic hyperfine sextet was 515 kOe at room temperature, the sextet was attributed to kind of iron oxides like hematite. Assuming the same Debye- Waller factors for all iron compounds and neglecting saturation effects, the relative intensities of the compounds in the same samples were measured using area method. The relative area of Fe_3O_4 in the sample AKT-1 is higher than the sample AKT-2 while the relative area of -Fe_2O_3 in the sample AKT-2 is higher than the sample AKT-1

Conclusion

In order to control air pollution effectively, it is necessary to understand in detail its physical and chemical processes that govern its formation and transport. The Mössbauer spectroscopy is a very useful technique for identification of iron-containing phases in environmental samples.

References

[1] B. Mahieu, J. Ladriere and G. Desafdeleer, J. of Phys (1976) C6-837.

[2] G. Chang, Hyperfine Interaction, 151/152 (2003) 299.

[3] T.E.Gradel, C.J. Weschler and M.L.Mandich, Nature 317 (1985) 240.

[4] B. Kopcewicz and M. Kopcewicz, Struct. Chem., 2 (1995) 303.

Radiation Pre-Treatment of Seed Imparts Metabolic Stability and Quality Protection during Storage under Accelerated Aging

Sumedha[1], Bhupinder Singh[1], R.K. Singhal[2]

1. *Nuclear Research laboratory, Indian Agricultural Research Institute, New Delhi 110012, India; E-mail: bhupindersinghiari@yahoo.com*
2. *Analytical Chemistry Division, Bhabha Atomic Research Centre, Mumbai 400085*

Quality of seed is known to deteriorate due to unfavoured temperature and relative humidity during accelerated aging. Protecting the seed quality during storage is thus a priority challenge for the seed industry till the seeds end up with the end user. Gamma radiation treatment has been shown to improve source to sink transport of photosynthates during terminal heat stress in cereals. An experiment was conducted to measure seed irradiation induced biochemical changes in groundnut cultivar TG-37A stored under accelerated aging at 45±2 ^{o}C and 95-100 % humidity for 0, 5, 10, 15, 20 and 40 days to aging. The gamma irradiation doses were control (0), 0.005, 0.025, 0.1, 0.5 and 1.0 kGy. Seed samples were periodically evaluated for oil and fatty acid profile by the soxhlet extraction method and gas chromatography mass spectroscopy respectively. Here alike earlier studies variation in fatty acid profile of seed was used as an indicator of seed health under harsh storage conditions of accelerated aging. In the majority of plant species having oil rich seeds, the lipids that are at risk of auto-oxidation contain oleic (18:1), linoleic (18:2) and linolenic (18:3) fatty acid chain. Degree of unsaturation has a significant influence on degree of degradation. Decreased total lipid content in aged sunflower seeds have been reported. Auto-oxidation of unsaturated fatty acids was noticed, especially for linoleic acid in seed of oil crop after seven years of storage. Our results showed radiation treatment did not cause any significant change in oleic (C18:1), linoleic acids (C18:2) and linolenic (C18:3) acid content of seeds. This shows that gamma radiation essentially slows down the lipid peroxidation which essentially protects membrane permeability and reduces the rate of seed deterioration at high temperature and RH. Radiation treatment imparts metabolic stability in seeds during storage under accelerated aging conditions.

Seed Quality Preservation Advantage of Gamma Irradiation Seed Pre-Treatment during Long Term Storage in Soybean

Sameer Kumar Guha, Sumedha and Bhupinder Singh

Nuclear Research laboratory, Indian Agricultural Research Institute, New Delhi, 110012, India;
E-mail: bhupindersinghiari@yahoo.com

The experiment was conducted to analyse the effect of gamma irradiation seed pre-treatment on insect damage and quality preservation of soybean seeds during long term storage at ambient temperature (27-42°C) and relative humidity (50-95%). Freshly harvested seeds of soybean (cv. Pusa-9814) were treated with control (0), 0.01, 0.05, 0.5, 1.0, 3.0, 5.0 kGy gamma radiation on a Gamma irradiator (Gamma Chamber 5000, Co-60 source, activity 12000 Ci, BRIT, Mumbai, India) at the Nuclear Research Laboratory, IARI, New Delhi and were stored over one year in cotton cloth bags under ambient conditions. Protein and oil per cent and fatty acid profile was measured in freshly harvested zero time unirradiated control, aged unirradiated control and other treatments of ionizing radiation. Seed oil was extracted through the soxhlet extraction method and oil profiling was done by gas chromatography. Change in saturated and unsaturated fatty acids like palmitic, stearic, oleic, linolic , linolenic acid and oleic to linoleic ratio was measured. Oil content of unirradiated stored seeds compared to that of the freshly harvested control was lower. However, radiation in general, helped in maintaining a higher seed oil during storage when compared with that of the aged unirradiated control and was insignificantly reduced over the fresh unirrradiated control. Further, gamma irradiation treatment did not yield any adverse affect on the seed protein even after prolonged storage. The results reveal a reduced rate of lipid degradation and improved seed hardness over untreated control with no significant change in fatty acid profile of the irradiated and the unirradiated seeds over a long term storage period.

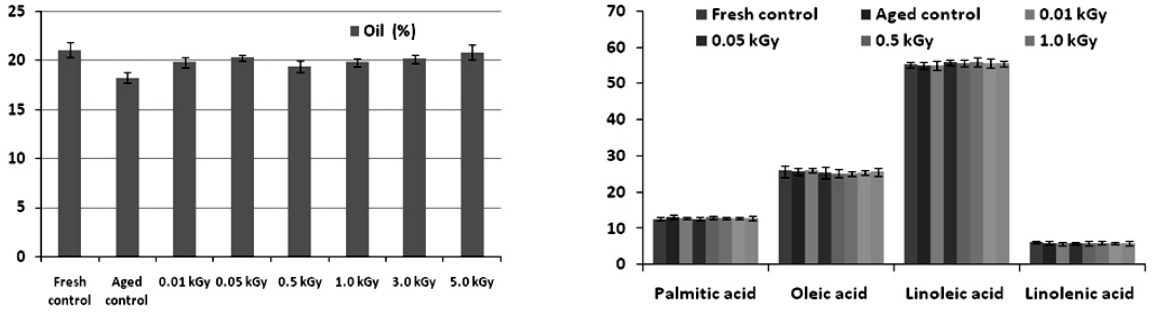


Fig. 1 Effect of gamma irradiation on oil percent and oil profiling of soybean (cv. Pusa-9814) on storage

$^{14}CO_2$ labeling : A Reliable Technique for Rapid Measurement Of Total Root Exudation Capacity and Vascular Sap Flow in Crops

Bhupinder Singh[1], Sumedha Ahuja[1], Renu Pandey[2] and R.K. Singhal[3]

1. *Nuclear Research Laboratory, Indian Agricultural Research Institute, New Delhi, India; E-mail: bhupindersinghiari@yahoo.com*
2. *Division of Plant Physiology, Indian Agricultural Research Institute, New Delhi*
3. *Analytical Chemistry Division, Bhabha Atomic Research Centre, Mumbai 400 085*

Ability of roots to release organic compounds in its rhizosphere is known to improve plant available nutrients and reduces heavy metal toxicity by immobilization. It is regarded as an important determinant of micro nutrient deficiency tolerance in plants. Uptake of nutrients and tranlocation of photoassimilates, on the other hand are governed by the strength of the transpiration stream and sink demand respectively. Measurement of vascular sap flow, thus, is critical for understanding of the translocation efficiency and consequently the sink demand that keeps changing during the crop growth cycle. Measurement of the root exudation capacity and the vascular sap flow is cumbersome and time consuming. Since, the exudates released by the roots and the photosynthates translocated between the source and the sink are essentially carbon compounds, use of labeled carbon as tag could potentially be exploited for a rapid and reliable measurement of exudation and vascular sap flow in crop plants. We report here the experimental results involving ^{14}C labeling of groundnut, a legume crop. as $^{14}CO_2$ generated by acidification of sodium bicarbonate. An additional factor of seed gamma irradiation was used to generate variability in in the root exudation and the sap flow. The ^{14}C release by the roots was compared against the ^{14}C transport in the vascular sap. An experimental hypothesis that a higher ^{14}C level in the vascular sap would indicate a higher root release of carbon by the roots into the rhizosphere was verified.
Key words: root exudation capacity, vascular sap flow, groundnut, $^{14}CO_2$ labeling

Screening of High Water Use Efficiency in some Gamma Radiated Cowpea Varieties through Isotopic Ratio Mass Spectrometer (IRMS)

Pradeep K. Shukla[1], Srikantha G.A.[1], Pragati Misra[2], Navodita Maurice[1], M.S. Sheshshayee[3] and P.W. Ramteke[1]

1. *Department of Biological Sciences, School of Basic Sciences, Sam Higginbottom Institute of Agriculture, Technology and Sciences (Deemed to be University), Allahabad,Uttar Pradesh, India; E-mail: pradeepshukla@yahoo.co.in*
2. *Department of Tissue Engineering, Jacob School of Biotechnology and Bioengineering, Sam Higginbottom Institute of Agriculture, Technology and Sciences (Deemed to be University), Allahabad, Uttar Pradesh, India*
3. *Department of Crop Physiology, GKVK, Bangalore*

An experiment was conducted to screen high water use efficient cowpea variety using different doses of gamma radiation using ^{60}Co as source. Seeds of four cowpea varieties (namely HR-1, BG-12, AnkurGomti, KhashiKanchan) were treated by different doses of Gamma radiation (T_1=10 Gy, T_2=20Gy, T_3=30 Gy, T_4=40 Gy) and were subjected for relative water content (RWC), carbon isotope Discrimination (^{13}C) and number of flowers at 30 and 45 DAS analysis. Results showed that RWC was found to be the maximum in the variety HR-1 in control T_0 (0.63%), whereas the minimum was observed in variety Khashikanchan in T_4 (0.26%). ^{13}C discrimination was found to be the maximum in the variety Ankur Gomati and the minimum in the variety BG-12.. maximum number of flowers was observed in variety KhasiKanchan in control T_0 at 30 and 45 DAS respectively.

Introduction

Cowpea (Vignaunguiculata L. Walp), a leguminous food crops, is one of a major food crop of millions of people in developing countries. Cowpea grain contains about 25% protein and 64% carbohydrate. It is highly sensitive to water stress during flowering and pod-filling stages [1,2]. The exploitable fresh water resources globally reached a plateau and there is an increasing demand for water conservation in all the sectors including agriculture. In fact water will be the single most limitation to achieve or to improve crop productivity in future. Therefore, water harvesting, moisture conservation and increasing water use efficiency of crop plants assume the greatest significance [8]. Gamma rays are often used for developing plants varieties that are agriculturally and economically important and have high productivity potential with the minimum input. Gamma irradiation can be useful for the alteration of one or a few physiological characters Mutagenesis by means of gamma rays has played an important role in the producing new mutants with improved properties which can produce higher amounts of commercially [3-5].

Materials and Methods

Seeds of four cowpea varieties (namely HR-1, BG-12, AnkurGomti, KhashiKanchan) were treated by different doses of Gamma radiation (T_1=10 Gy, T_2=20Gy, T_3=30 Gy, T_4=40 Gy) using ^{60}Co as source at National Botanical Institute (NBRI) research institute of CSIR at Lucknow.

From each variety, plants were selected randomly for counting number of flowers on 30 and 45 days after sowing (DAS). Each observation was recorded.For the estimation of relative water content (RWC) 0.5 g of leaf (FW) was taken and soaked in distilled water overnight to get them saturated. Then the leaf samples were weighed again to get the turgid weight (TW). The samples were then dried in an oven at 80°C for 24 h and weighed (DW). The relative water contents were measured as following:

$$RWC = (FW-DW)/ (TW-DW) \times 100$$

The carbon isotope Discrimination (^{13}C) was determined by using isotopic ratio mass spectrometer (IRMS) at Department of Crop physiology, University of Agricultural Sciences, GKVK, Bangalore, with an objective to study how far ^{13}C is associated with the observed genetic variability in WUE in few crop species. Third fully expanded leaves that were developed during the experimental period were collected (5-6 for each genotype) dried at 80^0C for 3 days. Dried samples were powdered in a motar and pestle. Care was taken to prevent any mixing of different samples by washing the pestle and mortar with alcohol after grinding each sample. One gram of powdered leaf sample was put in glass vial and used for ^{13}C analysis. Based on the fractionation (isotopic composition with respect to PDB), the ^{13}C discrimination (^{13}C) in the plant samples was computed as follows:

$$^{13}C\ (\%) = \frac{^{a}{}^{13}C \quad {}_{p}{}^{13}C}{1 \quad {}_{p}{}^{13}C / 1000}$$

Result and Discussion

The results obtained from IRMS analysis showed that amongst the varieties, ^{13}C discrimination was the maximum in the variety Ankur Gomati and the minimum in the variety BG-12. The ^{13}C discrimination found to be decreasing with the increasing dose of gamma radiation i.e. it was the maximum in control and the minimum in T_4 (40 Gy).

The result showed a significant difference in number of flowers among all the treatments in all the varieties. At 30 DAS, the maximum number of flowers was observed in variety KhasiKanchan in control T_0 (5.00), whereas the minimum was observed in variety HR-1 in T_4 (1.00) at 40 Gy gamma radiation, whereas, at 45 DAS, the result showed that there was a significant difference in number of flowers in all the varieties under different treatments. The maximum number of flowers was observed in variety Khasikanchan in control T_0 (9.00), whereas the minimum was observed in BG-12 in T_4(2.00) at 40 Gy of gamma radiation, under all the treatments.

Relative water content decreased due to gamma radiation. Result showed significantly decrease in relative water content with increased gamma radiation. The maximum Relative water content was observed in variety HR-1 in control T_0 (0.63%), whereas the minimum was observed in variety Khashikanchan in T_4 (0.26%) at 40 Gy of gamma radiation.

Maximizing the efficiency of biomass production per unit amount of water transpired (WUE) had been a major research focus of plant scientists especially under tropical conditions [7]. Though this is an important water conserving strategy evolved by plants, due to strong relationship between water loss and biomass production, selecting for high WUE often resulted in low biomass production [6].

The gamma ray had adverse effect on traits of plants and this depended on plant species or varieties and dose of irradiation [10]. Gamma irradiation was found to increase plant growth and development by inducing cytological changes. Irradiation also been successfully used for mutation in breeding of various crops and ornamental plants [9].

Conclusion

From the present studyand on the basis of observation it can be concluded that the varieties HR-1, Aankur Gomati and Khashikanchan showed the maximum responses for relative water content (RWC), carbon isotope Discrimination (^{13}C) and number of flowers, respectively From the agricultural point of view, the use of novel approaches like genetic, physiological, biochemical, and molecular techniques should be combined to develop or screen a higher water use efficient cowpea varieties in the near future.

References

[1] N. Ahmed, Zaki and Rashed, International Journal of Computational Engineering & Management, (2011) 1.

[2] H. Watanabe, H. Kondo, K. Abe, I. Nishimura, Y. Emori and S. Arai, J Biol Chem. (1990) 15832.

[3] S. Y. Awale, A. Tezuka, H. Banskota and S. Kadota, Bioorganic and Medicinal Chemistry, (2002) 31.

[4] A.K. Dubey, J.R. Yadav and B. Singh, Progressive Agric, (2007) 46.

[5] M.N. Mishra, Hina-Qadri and S. Mishra, Int. J. Plant Sci.Muzaffarnagar, (2007) 44.

[6] Udaya Kumar, R. C. N. Rao, G. D. Farquhar, H. S. Talwar, and T. G. Prasad, Aust. J. of Plant Physiology 22 (1995) 185.

[7] Passioura, J. B., Aust. J. Plant Physiol. 13(1986) 1191.

[8] G. Shankar, B. T. Krishna Prasad, M. S. Sheshshayee, K. N. Natarj, Udaya Kumar, M. and T. G. Prasad, Current Sci. (1996). 675.

[9] S. K. Thimmaiah, P. Mahadevu, K. N. Srinivasappa and A. N. Shankra, J. Nuclear Agric. and Biol., (1998) 142.

[10] C. Artk, C. and E. Peksen, Ondokuz-Mays-University,-Ziraat-Fakultesi-Dergisi, (2006) 95.

Flow Rate Measurements in a Pipeline Using Radiotracer Technique during a Custody Transfer Operation

H.J. Pant, V.K. Sharma, Sunil Goswami, J.S. Samantaray

Isotope Applications and Radiopharmaceutical Division, Bhabha Atomic Research centre, Mumbai 400085, India; E-mail: hjpant@barc.gov.in

Flow rate measurements were carried out in a pipeline transporting Lube Oil from a tanker-ship, anchored at a jetty in a Port, to an onshore storage facility using radiotracer technique. Bromine-82 as para-dibromobenzene was used as a radiotracer. Three tracer tests were carried out at different pumping pressure and the mean flow rate was estimated to be 130 m^3/h. The total quantity of Lube Oil pumped was estimated to be 360 m^3 during pumping operation of 2.77 hours. The measured flow rate or total quantity pumped helped Port Authorities to verify the quantity received at onshore storage facility during custody transfer operation.

Introduction

Various chemicals, petroleum products, petrochemicals are often pumped through pipelines from tanker-ships, anchored at Jetties in Ports, to an onshore storage facilities during custody transfer operations. The pipelines and storage facilities are owned by a distribution agency whereas the tanker-ships belong to different companies. The Jetties are maintained and owned by the Ports. In a custody transfer operation, the distribution agency receiving the product has to pay revenue to the Port depending upon the quantity of the product pumped. The pipelines meant for transporting the products during the custody transfer operations do not have flow meters installed as different products are pumped through the same pipeline one after another, and thus a single conventional flow meter cannot be used for flow rate measurements of different products. Therefore Port Authorities has to depend upon the Receiving Agency to know the total quantity of the product pumped. There is often difference between the actual quantity pumped by the tanker-ship and the quantity received by the agency either due to loss of material during handling operation or wrong information provided by the Agency, causing loss of revenue to the Port. Therefore, at the request of a Port Authorities, a radiotracer technique was applied to measure flow rates in a pipeline transporting Lube Oil during a custody transfer operation [1,2]. The main objective of the flow rate measurement was to demonstrate applicability of radiotracer technique for flow rate measurements during custody transfer operations and verify claim of the Receiving Agency about the total quantity pumped.

Experimental

Radiotracer Technique

The radiotracer technique based on transit time method is commonly used for flow rate measurement in pipelines or closed conduits where the volume of the test section is known [1,2]. The technique involves instantaneous injection of a gamma-emitting radiotracer at a selected location in the pipeline and monitoring its passage at two or more than two downstream locations using externally mounted radiation detectors as shown in Fig. 1. The first detector is mounted at sufficiently downstream location from the injection point to allow complete lateral mixing of the radiotracer. The first moment of a tracer distribution curve is given as (1):

$$\bar{t}_i \quad \frac{\int_0^t t\,C\,t}{\int_0^t C\,t} \qquad (1)$$

where, i: 1 and 2 for first and second detection point, respectively. The mean transit time ($\bar{t}$) of the tracer pulse between the two detectors is determined from the difference of first moments (centroids) of the tracer concentration curves recorded at two locations. The geometric volume (V) between the two monitoring locations is determined from the distance (L) and the cross-sectional area (A) of the pipeline. Knowing the geometric volume and mean transit time, the volumetric flow rate (Q) is calculated from the following simple relation:

$$Q = L\,A/\bar{t} = V/\bar{t} \qquad (2)$$

The accuracy of the measurements depends mainly upon (i) complete or sufficient lateral mixing of tracer between the injection point and first detection point (iii) accuracy in measurement of volume of the test section. The technique is suitable for pipelines of known cross-section and bore flow i.e. completely filled pipeline. Accuracy of the order of 1-2% can be achieved in practice [1,2]. If the pumping time is known, the quantity of lube oil pumped can be estimated.

Radiotracer Experiment

The schematic diagram of the experimental setup is shown in Fig. 1. It was desired to measure the flow rate of the Lube Oil (density: 860 kg/m^3) being transferred from a tanker-ship, anchored at a Jetty in a Port, to a storage facility located at an onshore location during one of the custody transfer operations. Bromine-82 as para-dibromobenzene was used as

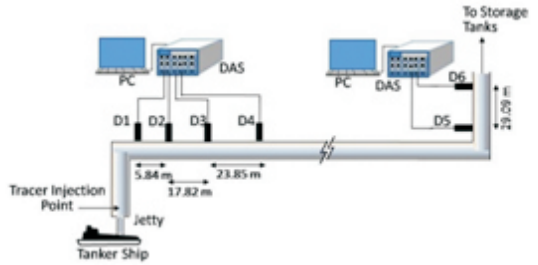


Fig. 1 Schematic diagram of experimental setup

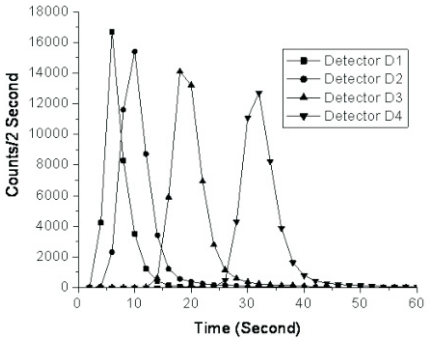


Fig. 2 Response of detector D1, D2, D3, D4

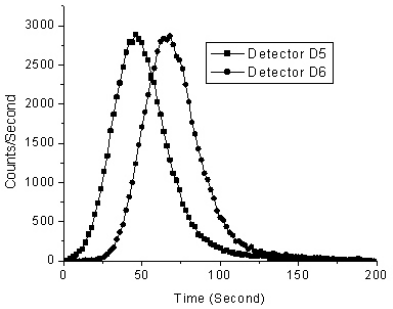


Fig. 3 Response of detector D5 and D6

radiotracer. Three tracer tests were conducted at three different pumping pressure and about 37 MBq (1 mCi) activity was used in each test. The radiotracer was instantaneously injected into the pipeline at a location near Jetty as shown in Fig.1 and monitored at six downstream axial locations using collimated NaI(Tl) scintillation detectors (D1, D2, D3, D4, D5, D6). The detectors were separated by known distances as shown in Fig. 1. The detectors were connected to two independent data acquisition systems programmed and synchronized to record data at an interval of 500 ms. The recorded data was saved in the connected laptops for analysis.

Results and Discussion

The tracer concentration data recorded by the detectors were corrected for background and the typical curves are shown in Fig. 2 and Fig.3. The first moment (centroid) of each tracer concentration curve was determined using Equation 1. The differences between the moments of the detectors provide transit time between the detectors and are given in Table 1. The volume of test section between different detector pairs i.e. D1D2, D2D3, D3D4 and D5D6 was determined to be 0.139, 0.426, 0.570, 0.696 m^3, respectively. Knowing the transit times and volume between the detectors, the flow rates were determined using Equation 2 and are given in Table 1. Three tracer tests were conducted at three different pumping pressure and mean flow rate ($\overline{Q}$) was estimated to be 130 m^3/h. The total time of pumping was 2.77 hours. Thus the total quantity of Lube Oil pumped during the transfer operation was estimated to be 360 m^3 (310 metric tonne). However, the Receiving Agency reported that only a quantity of about 288 metric tonne was received during the transfer operation. This indicated either loss of oil during handling or the receiving Agency did not disclose the actual quantity received.

Conclusion

The radiotracer technique was successfully applied to measure the flow rate in a pipeline and estimate total quantity of Lube Oil pumped during a custody transfer operation. The mean flow rate and total quantity pumped were estimated to be to be 130 m^3/h and 360 m^3, respectively. The measured flow rate and total quantity pumped were used by the Port authority to verify the data claimed by the receiving agency and take appropriate measures during the custody transfer operations.

References

[1] International Atomic Energy Agency: Technical Report Series No. 316. Guidebook on radioisotope tracers in industry. IAEA, Vienna (1990).

[2] International Standards Organization, Measurement of Water Flow in Closed Conduits-Tracer Methods-Part VII: Transit Time Method Using Radioactive Tracers, ISO Report No. 2975/VII (1977b).

Table1: Results of flow rate measurements

Test No	T_{Inj} (h)	P (kg/cm^2)	$\bar{t}_{12}$ (s)	$\bar{t}_{23}$ (s)	$\bar{t}_{34}$ (s)	$\bar{t}_{56}$ (s)	Q_{12} (m^3/h)	Q_{23} (m^3/h)	Q_{34} (m^3/h)	Q_{56} (m^3/h)	(m^3/h)
1	13:14	1.5	3.5	9.3	12.7	19.5	122	165	162	129	130
2	13:28	3.5	4.2	10.9	14.5	18.3	119	140	141	137	
3	14:51	4.7	5.0	13.7	19.1	—	100	112	105	—	

T_{Inj}.: Time of injection, P=Pressure, t:Mean residence time, Q: Flow rate, Numbers in subscript indicates detector number

Homogeneity Study in a Glass Manufacturing Unit Using Radiotracer Technique

Sunil Goswami[1], H.J. Pant[1], Jayashree Biswal[1], J.S. Samantray[1], V.K. Sharma[1], Sourabh Singhal[2]

1. *Isotope Applications and Radiopharmaceutical Division, Bhabha Atomic Research centre, Mumbai-400085, India; E-mail: hjpant@barc.gov.in*
2. *Gujarat Borosil Limited, Bharuch, Gujarat, India*

Homogeneity of glass is a key factor determining their physical and chemical properties and overall quality. However, quantification of the homogeneity of a glass is still a challenge for glass technologists. A radiotracer technique was employed to investigate homogeneity of glass produced in a glass production unit using Lanthanum-140 as radiotracer. Results of the study showed that the homogenization time of glass within the unit was 29 hours.

Introduction

The quality of glass produced in a glass manufacturing unit depends upon a number of parameters such as melting of raw materials, homogenization of the melts, glass stream velocity, mass flow pattern, bypass flow and stream circulation. Therefore, glass technologists have made great effort in developing different types of technologies for improving the glass quality. Homogenization of glass melts is one of the important parameters that govern the overall quality of the glass products. Existing methods to investigate homogeneity in glass include visual inspection, optical measurements and compositional measurements. However, these methods have certain drawbacks such as low sensitivity to compositional fluctuation, complexity of the measurements, time consuming and lack of required accuracy. All these drawbacks can be overcome by employing radiotracer technique [1-3]. Present paper describes application of a radiotracer technique for investigation of homogeneity of glass and estimation of the homogenization time in a glass manufacturing unit.

Experimental

The schematic diagram of glass manufacturing unit for production of glass sheets is shown in Fig. 1. The unit consists of a tank furnace, a forehearth, a shaping roller, an annealing chamber, a cooling and cutting section. The mixture of raw materials is fed into to the furnace through the two independent feeders connected to right and left side of the furnace. The raw material melts in the furnace, homogenized in the forehearth, and rolled into sheets of desired thickness by the shaping roller. Subsequently, the continuous glass sheet is annealed in annealing chamber, cooled in the cooling section and cut into desired size in the cutting section.

Lanthanum-140 (^{140}La) as lanthanum oxide (La_2O_3) was used as a radiotracer in the investigation. The radiotracer was mixed with silica oxide as carrier. Two aliquots of radiotracer each having activity about 7.5 GBq were simultaneously injected into the furnace through the two independent feeders.

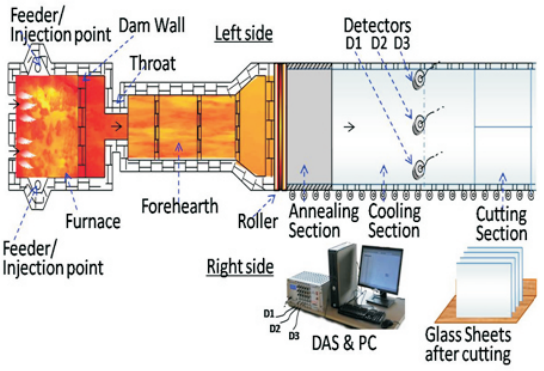


Fig. 1 Schematic diagram of the glass furnace

The radiotracer was monitored at three different points at an axial location at the end of the cooling section as shown in Fig. 1. Three independent collimated NaI(Tl) scintillation detectors connected to a data acquisition system (DAS) were used for online monitoring of tracer concentration in glass sheet. The continuous rolling glass sheet of thickness 0.003 m was cut into a size of 2.1 m length and 2.4 m width. A sheet was collected at an interval of 30 minutes after breakthrough of tracer at three monitoring locations, and stored for off line homogeneity measurements. The separated glass sheets were subsequently cut into two equal halves (size: 2.1 m x 1.2 m) and used for measurement of radiotracer concentration. Each half of the sheet was superimposed on a wooden sheet of the same size (2.1 m x 1.2 m) and marked with nine equidistant points as shown in Fig. 2. A collimated NaI(Tl) scintillation detector connected to an independent data acquisition system was placed on the marked points and radiotracer concentration (counts/5 second) was recorded at each marked location.

Results and Discussion

The measured counts were corrected for background radiation level and decay of radiotracer. Five repeat readings were taken at each location. The mean tracer concentration of three axial points along each transects i.e. L-1, L-2, L-3, R-1, R-2 and R-3 were plotted as a function of time for each sheet and the plot is

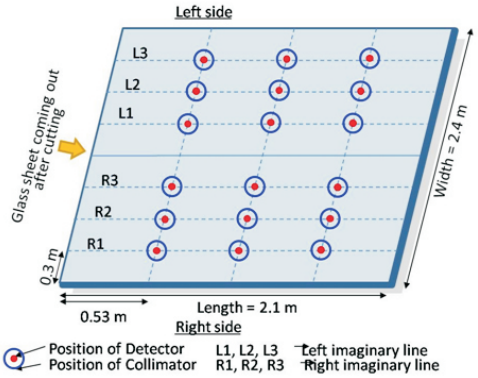


Fig. 2 Methodology used for measurement of tracer concentration in glass sheet

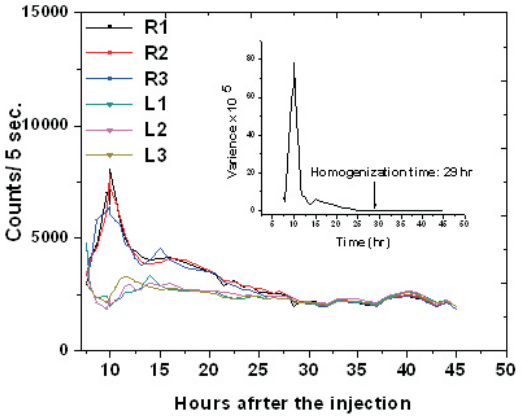


Fig. 3 Variation of tracer concentration along six axial transects (L1, L2, L3, R1, R2 and R3) of the glass sheet with respect to time. Inset: Variance vs. time plot

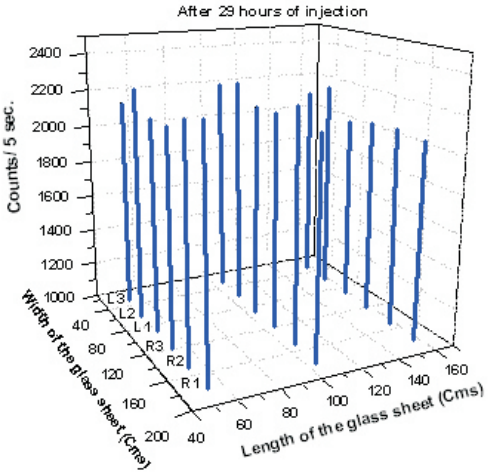


Fig. 4 Variation of tracer concentration in a glass sheet at glass homogenization time

shown in Fig. 3. It has been observed that there are two distinct groups of graphs corresponding to two halves of the glass sheet. The tracer concentration along three left hand side transacts (L1, L2, L3) of left-half of the sheet is almost the same. Similarly, the tracer concentration along right hand side transacts (R1, R2, R3) of right-half of the sheet are similar. The tracer concentration in the two halves of the glass sheets is initially different but gradually becomes equal. This implies that the two injected aliquots of radiotracer flows along two parallel flow streams i.e. left hand side and right hand side stream. This indicates that the raw material fed from the two sides do not immediately mix within the tank furnace causing inhomogeneity in glass production process. In order to quantify the homogenization time, the variance (^{2}) of the radiotracer data was plotted as function of time the homogenization time was estimated to be 29 hours. A typical bar-chart showing the radiotracer concentrations at eighteen different points within the glass sheet (both the halves) collected after 29 hours of injection is shown in Fig. 4. This implies that the radiotracer takes 29 hours to mix homogeneously within the molten glass in the glass manufacturing unit.

Conclusion

Radiotracer technique was successfully applied to measure homogenization time of glass melt in a glass manufacturing unit. It was found that there were two distinct parallel flow paths followed by the molten glass within the glass production unit. From the result of the radiotracer investigation, the homogenization time of the molten glass within the unit was estimated to be 29 hours. This implies that the feed takes 29 hours to melt, completely mix and uniformly distributed within the glass matrix. The results of the study helped plant engineers to control and optimize the production process, improve the quality of the glass and assess the health of the glass furnace of the manufacturing unit.

References

[1] H.J. Pant, A. Kundu, K.D.P Nigam; Reviews in Chemical Engineering 17 (2001) 165.

[2] J. Palige, A.G. Chmielewiski, Z.R. Dziewonski, H.Rahimi, A.Naimpour, A.Amini, A. Abedinzadeh, E. Khalilipour, Nukleonika 40 (1995) 67.

[3] J. St. Michalik, K. G. Kruszewski; Isotopenraxis 22 (1986) 232.

Application of Radioactive Particle Tracking (RPT) Technique for Quantifying the Liquid Phase Flows in Bubble Columns

Dinesh V. Kalaga[1], H.J. Pant[2], Sunil Goswami[2], Shantanu Roy[3], Jyeshtharaj B. Joshi[4]

1. *Department of Chemical Engineering, Indian Institute of Technology, Gandhinagar 382424, India*
2. *Isotope Applications and Radiopharmaceuticals Division, BARC, Trombay, Mumbai 400085, India; E-mail: hjpant@barc.gov.in*
3. *Department of Chemical Engineering, Indian Institute of Technology-Delhi, New Delhi 110016, India.*
4. *Homi Bhabha National Institute, Anushaktinagar, Mumbai 400094, India.*

Liquid phase hydrodynamics were quantified in 0.12 m diameter cylindrical bubble column for air-water system using a non-invasive radioactive particle tracking (RPT) technique. An array of twelve NaI scintillation detectors was used to track the motion of a neutrally buoyant radioactive tracer particle (Sc-46). In the present work, experiments were performed to study the effect of superficial gas velocity on liquid phase hydrodynamics for three superficial gas velocities to cover both homogenous and heterogeneous flow regimes. The experimental results shows that, the time averaged axial mean liquid velocity profiles were found to be positive near the center and negative near the walls, indicating the liquid phase circulations. An attempt has also been made to understand the errors associated with tracer particle size and activity on the accuracy of RPT technique.

Introduction

Bubble columns are gas-liquid contactors are widely used in industry because of their simple construction and operation. Important applications include oxidation, hydrogenation, hydrohalogenation, ammonolysis, hydroformylation, Fischer-Trospch reaction, ozonolysis, carbonylation, carboxylation, alkylation, fermentation, hydrometallurgical operations, waste water treatment, steel ladle stirring, column flotation, etc [1]. The performance of the bubble column reactors are strongly affected by the regime of operation, which in turn depends on the superficial gas velocity. Therefore, in the present work it was thought desirable to employ a non-invasive RPT technique to quantify the liquid hydrodynamics in bubble column. Further, an attempt has been made to assess the errors associated with tracer particle size and strength on the accuracy of the RPT technique.

Principle and Operation of RPT

RPT uses the -radiation emitted by a single radioactive tracer particle to track its motion in the multiphase reactor. The -rays emitted by the tracer particle were recorded by the array of strategically placed twelve NaI Scintillation detectors. The counts (intensity of radiation) recorded by the detector is inversely proportional to the distance between the detector and tracer particle. A distance-count relationship was established using a prior calibration of all detectors was performed by keeping the particle at several known locations (approx. 300). During the actual RPT experiment the tracer particle is introduced to move freely inside the vessel for each flow condition. Its position is monitored by the array of detectors with a sampling rate of 50 Hz using an online acquisition system for the duration of 14 to 16 hrs. The counts recorded by the each detector are converted into the corresponding instantaneous distance between the tracer and detector using the pre-established distance-count relationship. Instantaneous position of the tracer particle was calculated from the instantaneous distances obtained for all the detectors using a algorithm that models the emission, transmission and detection of the gamma-ray photons [2]. The time differencing of the instantaneous positions yields instantaneous velocities and the corresponding ensemble average gives you mean velocities. The turbulent parameters were calculated from the mean and instantaneous velocities. The more details related to hardware and data analysis of RPT can found elsewhere [3].

Experimental set-up

RPT experiments were performed in bubble column of height 1.2 m and internal diameter 120 mm using air as gas phase and tap water as liquid phase. Figure 1 shows the schematic diagram of the bubble

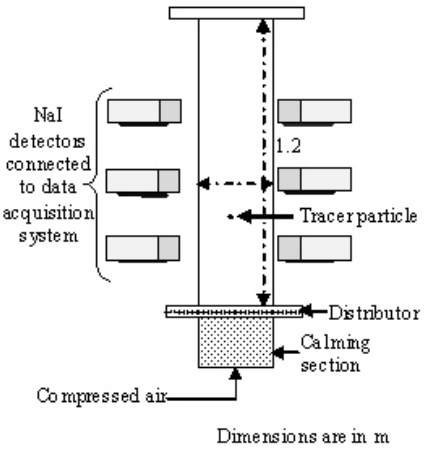


Fig. 1 Schematic diagram of the experimental set-up

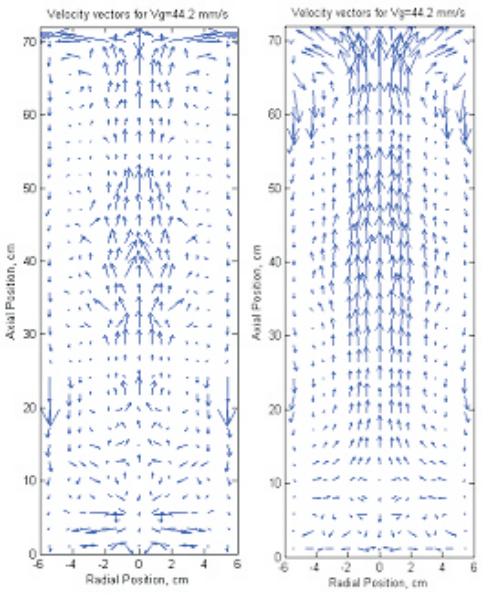


Fig. 2 Overall liquid flow patterns for superficial gas velocity of 0.442 m/s: (A) Particle 1 (B) Particle 2

column experimental set-up. The compressed air was passed through air and moisture filters to remove dust and oil droplets. The air to the column was sparged through distributor and the flow rate was measured using a series of calibrated rotameters. The gas distributor was having 30 apertures, the diameter of each aperture is 2 mm and pitch between two apertures is 10 mm. To study the effect of superficial gas velocity, tracer particle size and activity, three superficial gas velocities (0.044, 0.132 and 0.221 m/s) and two different tracer particles (particle1: size=2.5 mm, activity = 100 Ci; particle2: size = 1.2 mm, activity = 400 Ci) were chosen. The static liquid head is kept constant at 0.65 m for all the experiments.

Results and Discussion

Figure 2 shows the time averaged axial velocity vector plots obtained using both the tracer particles for a superficial gas velocity of 0.044 m/s.

It is clear that, for both the particles two circulation cells were observed with liquid ascending along the centre of the column and descending near the column wall. Despite of acquiring data of 14 hrs the

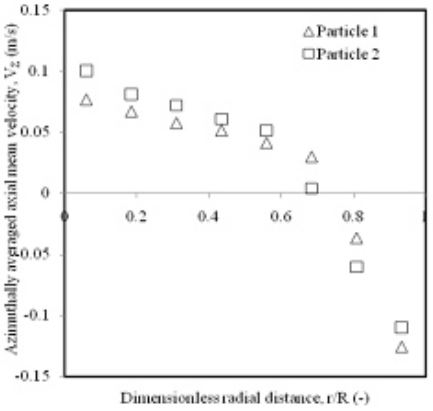


Fig. 3 Variation of axial mean liquid velocity along the dimensionless radial distance for superficial gas velocity of 0.442 m/s

vector plots for particle 1 is not smooth which implies the inability of the tracer particle to track the liquid phase due to its large size. For particle 2 however (smaller size), the vector plots are significantly smoother. Figure 3 shows the azimuthally averaged axial mean liquid velocity at an axial location of 0.23 m above the distributor for the superficial gas velocity of 0.044 m/s. Mean liquid velocity near center (r/R=0) of the column is positive and at the wall (r/R=1) is negative. Which shows that the liquid moving in the upward direction along with the bubble plume and going down along the walls of the column. From figure 3, It is also evident that particle 1 under predicting the ascending mean liquid velocity and over predicting the descending liquid velocity.

Conclusions

It is found that the liquid phase hydrodynamics strongly depends on the superficial gas velocity. Physical properties of the tracer particle significantly affect the accuracy of the RPT experiments.

References

[1] J. B. Joshi, Chem. Eng. Sci. 56 (2001) 5893.

[2] F. Larachi, G. Kennedy, J. Chaouki, Nucl. Instrum. Methods Phys. Res., Sect. A, 338 (2-3), (1994) 568.

[3] R. K. Upadhyay, H. J. Pant, Shantanu Roy, Chem. Eng. Sci. 96 (2013) 152.

Residence Time Distribution Study in a Pilot-Scale Gas-Solid Fluidized Bed System Using Radiotracer Technique

H.J. Pant[1], V.K. Sharma[1], Sunil Goswami[1], J.S. Samantaray[1], N.I.G.N. Mohan[2], Tirupathi Naidu[2], Gursharan Singh[1]

1. *Isotope Applications and Radiopharmaceuticals Division, Bhabha Atomic Research centre, Mumbai 400085, India; E-mail: hjpant@barc.gov.in*
2. *Corporate Research & Development Division, Bharta Heavy Electricals Limited, Vikas Nagar, Hyderabad-500093, India*

Residence time distributions (RTD) of coal particles were measured in a pilot-scale gas-solid fluidized bed system (FBS) using radiotracer technique. The main objectives of the study were to measure the mean residence times (MRTs) of the particles within the system and evaluate mixing of the gas and solid phases. Gold-198 labeled on coal particles were used as radiotracer. The MRTs were determined from the measured RTDs. A two-parameter Tanks-in-Series Model was used to simulate the measured RTDs and characterize the mixing. The results of the study indicated that the FBS behaved as a continuously stirred-tank reactor with a small fraction of the coal particles bypassing from the system.

Introduction

Fluidization is a process in which solid particles are suspended by an upward flow of air or liquid. The system in which the fluidization is carried out is usually called as Fluidized Bed System (FBS). The efficiency of the fluidization process depends upon mixing between gas and solids phases and residence times of the phases that in turn depends upon type and design of the gas distributor used in the system. Measurement and analysis of residence time distribution (RTD) is one of the best approaches to characterize mixing of the phases in continuous industrial flow system and evaluate the performance of the distributor [1]. Radiotracer techniques are widely used to measure RTD of process material in industrial flow systems because of their high detection sensitivity, "in-situ" detection, physicochemical compatibility, availability of wide range of suitable tracers, limited memory effect and utility in harsh industrial environment [1].This paper describes the measurement and analysis of RTD of solid phase in a pilot-scale fluidized bed system fitted with a conical distributor.

Experimental

Fluidized Bed System

The schematic diagram of the pilot-scale fluidized bed system is shown in Fig. 1. Coal particles (0.4-4 mm) and air were used as solid and gas phase respectively. The system consists of various subsystems such as a fluidizer fitted with a conical distributor, a freeboard section, a cyclone, a feed transport system, an air supply system and an ash extraction system. A compressor supplies air for fluidization and to the feed transportation system. The fluidizer consists of a metal cylinder of 5 mm thick, 650 mm internal diameter and 1500 mm height. An air plenum of internal diameter of 880 mm is fitted with the bottom section by a flange. A conical distributor with a stand pipe is mounted between air plenum and the fluidizer. The top section of

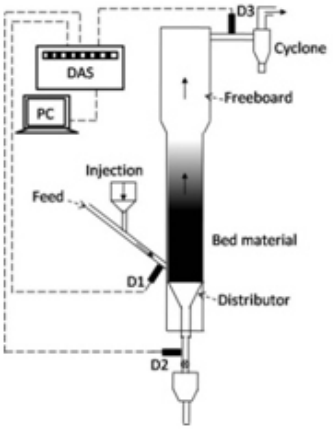


Fig. 1 Schematic diagram of experimental setup

the system is called as freeboard and is made of a Perspex cylinder of internal diameter of 880 mm and height of 1095 mm. The freeboard section is connected to a cyclone where fine coal particles and air are separated. The fines captured in the cyclone are at the bottom of the cyclone, whereas air escapes to the atmosphere through a filter. The coal particles are fed to the bed at a level of 275 mm from the top of the distributor using a continuous rotary feeder. The bulk of the coal particles are continuously removed from bottom using a rotary extractor. However, a fraction of fines exit from the top of the system. The feed and extraction rates can be measured and controlled independently as per experimental requirements.

RTD Experiments

A series of four experiments was carried out at different operating and process conditions given in Table 1. Gold-198 (gamma energy: 400 keV, half-life: 65 hours) labeled coal particles (weight: 25 gms, activity:100 MBq) was used as radiotracer in each experiment. The radiotracer was instantaneously injected into the feed pipe using a specially fabricated

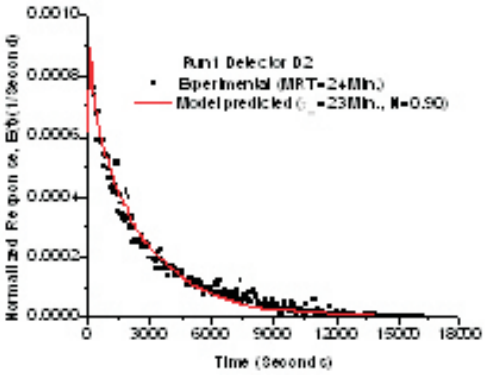


Fig. 2 Experimental and model predicted RTD curves

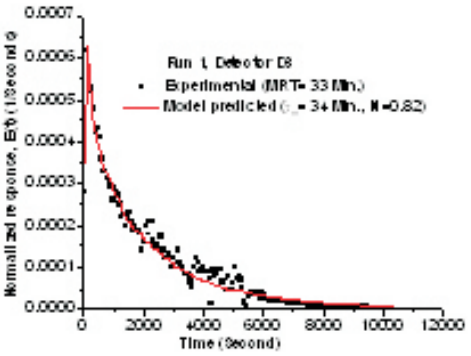


Fig. 3 Experimental and model predicted RTD curves

injection arraignment and monitored at three locations (D1, D2 and D3) as shown in Fig. 1. All the detectors were connected to a data acquisition system (DAS) set to record tracer concentration data at an interval of every 30 seconds. The tracer concentration data acquired as a function of time was saved and analyzed.

Data Analysis and Results

The theoretical MRT ($_t$) of coal particles within the system is estimated by dividing mean of initial and final bed weights by mean of feed and extraction rates; and are given in Table 1 for different operating conditions. The measured tracer concentration curves were treated and normalized and MRTs were obtained. The first moment of the RTD curve is the experimental MRT ($_e$) and is given as (1):

$$ _m \quad \frac{\int_0^t t\, C_i \, dt}{\int_0^t C_i \, t \, dt} \qquad (1) $$

where i = 1, 2…n. The experimentally determined MRTs are given in Table 1. It is observed that experimental MRTs are lower than the theoretical MRTS indicating presence of void volume within the fluidized and bypassing of solids. Tanks-in-series model was used to characterize mixing and solution of model to an impulse injection of tracer into the system is given as (2):

$$ E(t) = \frac{N^N t^{N-1} e^{Nt/\bar{t}_m}}{N\, \bar{t}_m^N} \qquad (2) $$

where, $_m$: model MRT, (N): gamma function, N: tank number. The value N less than unity corresponds to bypassing or short-circuiting of some of the coal particles but lacks a physical interpretation, except when it is an integer. The results of RTD simulation are given in Table 1. Similar results were obtained in case of fine particles exiting from top of the system. Two representative curves showing comparison of experimental and model simulated RTD are shown in Fig 2 and Fig 3.

Conclusions

The MRTs of coarser as well fine coal particles were determined. The analysis of RTD curve using tanks-in-series model indicated that the FBS behaves as a well-mixed system with a small fraction of bypassing of fine as well as coarser coal particles. The design of the gas distributor was found to be adequate for good mixing of the two phases but needs minor design modifications to prevent bypassing. The performance of the distributor needs to be compared with other types of distributors such as flat-plate distributor.

References

[1] Pant, H.J., Kundu, A. and Nigam, K.D.P., Reviews in Chemical Engineering, 17 (2001) 165.

[2] Nauman, E.B., and Buffham, B.A., Mixing in Contineous Flow Systems, Jhon Wiley & Sons, New York, (1983) p.271.

Table 1: Operating conditions and results of RTD analysis of bulk flow

Run No.	P (kg/cm^2)	H (mm)	Q_a (kg/h)	W_i (kg)	Q_{feed} (kg/h)	Q_b (kg/h)	Q_t (kg/h)	W_f (kg)	$_t$ (Min)	$_e$ (Min)	Parameters	
											$_m$ (Min)	N
1	0.73	650	1431	256	353	328	20	353	44	33	34	0.82
2	0.83	650	1457	256	248	200	23	236	69	39	47	0.95
3	0.65	975	1471	360	342	341	21	462	60	23	22	0.92
4	0.69	975	1457	360	571	490	30	528	42	34	33	0.78

P: Pressure, H: Static bed height, Q_a: Air flow rate, W_i:Initial bed weight, W_f:Final bed weight, Q_b: Bottom extraction rate, Q_t: Top extraction rate

Photon Mass Energy-absorption Coefficients of propionic acid from 122 keV to 1330 keV

Shaikh Humera, Bibifatima M.Ladhaf, B and Pravina P. Pawar

Department of Physics, Dr.Babasaheb Ambedkar Marathwada University, Aurangabad: 431004.India, E-mail: pravina.pawar@yahoo.com

Mass energy-absorption coefficients $_{en}/$ are tabulated in units of cm^2/g for energies 122 keV to 1330 keV for Propionic acid ($C_3H_6O_2$) The gamma-rays were detected using NaI (Tl) scintillation detection system with a resolution of 10.2% at 662 keV. The mass attenuation coefficients at different energies were calculated using XCOM programme. The mass attenuation coefficient data were then used to obtain the total attenuation cross-sections and molecular energy-absorption cross section of Propionic acid. It was observed that the mass energy-absorption coefficients $_{n}/$ goes on decreasing with increase of gamma-ray energy. The results show that, the experimentally obtained values are in good agreement with the theoretical values.

Introduction

The mass attenuation coefficient / and mass energy-absorption coefficient $_{en}/$ are basic quantities used in calculations of the penetration and the energy deposition by energetic photons in biological, shielding, and other materials. They are widely used as reference data in radiation shielding and dosimetry [1]. The mass energy-absorption coefficient $_{en}/$, takes into account the fraction of the kinetic energy that is subsequently lost in radiative energy loss processes (Bremsstrahlung) as the charged particles slow to rest in the absorbing medium. The net charged particles energy is, in turn, a morea or less valid approximately to the amount of photon energy made available for the production of biological, chemical and other effects associated with exposure of ionizing radiation. Therefore, has an essential role in estimating the absorbed dose in medical and health physics [2].

A variety of physiological functions inside living systems are performed by complex molecules such as carbohydrates, proteins, fats and oils composed of H,C,N and O elements In chemistry, and especially in biochemistry, a fatty acid is a carboxylic acid with a long aliphatic tail (chain), which is either saturated or unsaturated. Most naturally occurring fatty acids have a chain of an even number of carbon atoms, from 4 to 28. Fatty acids are usually derived from triglycerides or phospholipids. When they are not attached to other molecules, they are known as “free” fatty acids. Fatty acids are important sources of fuel because, when metabolized, they yield large quantities of ATP. Many cell types can use either glucose or fatty acids for this purpose. In particular, heart and skeletal muscle prefer fatty acids. Despite long-standing assertions to the contrary, the brain can use fatty acids as a source of fuel in addition to glucose and ketone bodies. Functions of Fatty Acids is Source of energy in stored forms also it is Solubilize vitamins like A, D, E, and K, Building units of majority of lipids and Constituent of phospholipids [3].

In this work, we have measured the mass energy-absorption coefficients $_{en}/$ of Propionic acid ($C_3H_6O_2$)in the energy range 122 to 1330 keV.

Experimental

The five radioactive sources ^{57}Co,^{133}Ba , ^{137}Cs and ^{60}Co and ^{22}Na were used in the present investigation. Gamma rays of energy from 122-1330 keV emitted by the above radioactive sources,(procured from Bhaba Atomic Research Centre, Mumbai) were collimated and detected by NaI(Tl) detector having energy resolution of 10.2% at 662keV. The signals from the detector were amplified and analyzed with 8K multichannel analyzer. The diameters of the samples were determined with the help of a traveling microscope. It was observed that the attenuation of photons of the empty containers were negligible. Each sample pellet was weighed in a sensitive digital balance having an accuracy 0.001 mg .The weighing was repeated several times to obtain consistent value of the mass. The mean of this set of values was taken to be the mass of the sample. By using the diameter of the pellet and mean value of the mass of the pellet, the mass per unit area was determined in each case. The sample thicknesses were selected in order to satisfy the following ideal condition as far as possible [4].

$$2 \quad \ln (I_0 / I) \quad 4$$

Results and Discussion

The values of mass energy-absorption coefficient $_{en}/$ (cm^2gm^{-1}) of Propionic acid from 122 keV to 1330 keVare displayed in Table 1. In Fig.1.the typical plots of $_{en}/$ versus E for Propionic acid ($C_3H_6O_2$) is given. Schematic view of Scintillation counter is displayed in Fig. 2. It is seen from Fig.1 that the values for the mass energy-absorption coefficient goes on increasing with increase of gamma-ray energy. The results show that, the experimentally obtained values are in good agreement with the theoretical values.

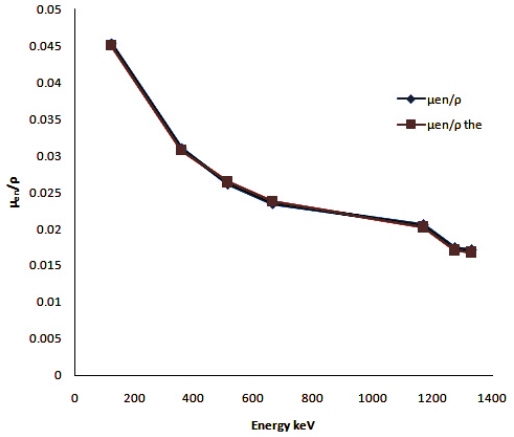


Fig. 1 The typical plots of $_{en}/$ versus E for Propionic acid ($C_3H_6O_2$)

Conclusions

The present experimental study has been undertaken to get information on mass energy-absorption coefficient $_{en}/$ of Propionic acid sample. In the interaction of photon with matter, $_{en}/$ values are dependent on the physical and chemical environments of the samples.

Table-1: Mass energy-absorption coefficient $_{en}/$ (cm^2 /g) of Propionic acid from 122 to 1330 keV.

Energy keV	$_{en}/$ exp.(10^{24})	$_{en}/$ theo.(10^{24})
122	0.0453355	0.0450449
356	0.0310259	0.0307360
511	0.0260747	0.0263644
662	0.0234594	0.0237490
1170	0.0205345	0.0202453
1275	0.0173468	0.0170577
1330	0.0170567	0.0167676

Equations

This attenuation of the beam is described by the following equation:

$$I = I_0 e^{-\ t} \qquad (1)$$

where I_0 and I are the unattenuated and attenuated photon intensities, respectively, and (cm^{-1}) is the linear attenuation coefficient of the material. A coefficient more accurately characterizing a given material is the, density-independent ,mass attenuation coefficient / $(cm^2\ g^{-1})$.Rearrangement of Eq.(1) yields the following equation for the linear attenuation coefficient:

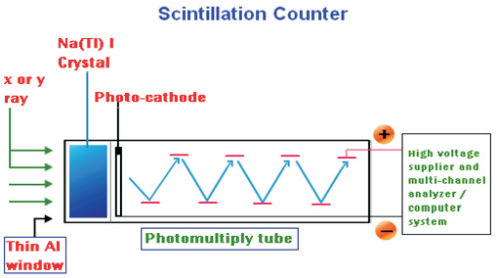


Fig. 2 The schematic view of Scintillation counter

$$= (1/t)\ \ln(I_0/I) \qquad (2)$$

In Eq. (2), t (cm) is the sample thickness .The mass attenuation coefficients / (cm^2gm^{-1}) for the samples were obtained from Eq. (3) by using the density of the corresponding samples:

$$_m = / \ (cm^2\ gm^{-1}) = (1/\ t\ )\ \ln(I_0/I) \qquad (3)$$

where (gm/cm^3) is a measured density of the corresponding sample, and I_0 and I are the unattenuated and attenuated photon intensities, respectively. The values of the mass attenuation coefficients were then used to determine the total interaction cross-section ($_{tot}$) by the following relation :

$$(\ _{t,ot}) = \ _m(M/N_A) \qquad (4)$$

The mass energy-absorption coefficient, $_{en}/$, is a measure of the average fractional amount of incident photon energy transferred to kinetic energy of charged particles as a result of these interactions.Values of $_{en}/$ in table 1,following the definition in paragraph B.4.of [5] and in section 4.1 [6,7] were computed as,

$$_{en}/ \ = \ _{m,en}\ (N_A/A_r) \qquad (5)$$

in which , N_A is Avagadro's number (6.02486 x 10^{23} mol^{-1}) and A_r is the relative atomic mass (atomic weight) and, $_{m,en,}$ is the total molecular energy-absorption cross section,

References

[1] Hubbell J H.and Seltzer S M National Institute of Standards and Technology (IR) Report, No, (1995) 5632.

[2] Hubbell J H., Int. J. Appl. Radiat. Isot. 33 (1982) 1269.

[3] D.Voet and J.G.Voet, Biochemistry, 2nd ed. Wiley, London (1995).

[4] Creagh, D C., Nucl.Instrum.and Meth. A 255 (1987) 1.

[5] ICRU Report 33, Washingaton, DC (1980).

[6] Berger R.T.,Radiat.Res., 15 (1961) 1.

[7] S.R.Manohara and S.M.Hanagodimath, Med. Phys. 35/1 (2008) 388.

Single Vial Kit Formulation for Preparation of PET Radiopharmaceutical: ^{68}Ga-DOTATOC

A. Mukherjee[1], U. Pandey[1], R. Chakravarty[1], H.D. Sarma[2], G. Samuel[1], A. Dash[1]

1. *Isotope Applications & Radiopharmaceuticals Division, Bhabha Atomic Research Centre, Mumbai 400085, India; E-mail: adash@barc.gov.in*
2. *Radiation Biology and Health Sciences Division, Bhabha Atomic Research Centre, Mumbai 400085, India.*

The aim of the study was to establish a cost effective and facile method for preparation of clinical grade ^{68}Ga-DOTATOC for PET imaging of neuroendocrine tumors. Kit for peptide conjugate, DOTATOC was formulated under sterile conditions. Radiolabeling with ^{68}Ga eluted from novel ^{68}Ge/^{68}Ga BARC generator was optimized and complex was characterized by PC and HPLC. Consistency in ^{68}Ga labeling using kit vials was achieved when tested up to three months. Pharmacokinetics of ^{68}Ga-DOTATOC was studied in small animals. Fast clearance of activity via renal route as reported for ^{68}Ga-DOTATOC peptide was observed. Clinical application of ^{68}Ga-DOTATOC was also demonstrated.

Introduction

Gallium-68 is a positron emitting radioisotope available from ^{68}Ge/^{68}Ga generator system. It is widely used for preparation of ^{68}Ga radiopharmaceuticals for PET imaging. Gallium-68 labeled DOTA conjugated somatostatin analogues are widely used for detection of neuroendocrine tumors (NET), treatment planning prior to ^{177}Lu or ^{90}Y-DOTA-peptide therapy and also for predicting response to treatment after radionuclide therapy [1]. Automated modules for preparation of ^{68}Ga radiopharmaceuticals such as ^{68}Ga-DOTATOC are commercially available. However, they have a maximum lifespan of one year and are expensive for countries like India.

Availability of peptide formulations in kit form for easy radiolabeling with generator eluted ^{68}Ga is desired for wider applications of ^{68}Ga radiopharmaceuticals. A novel ^{68}Ge/^{68}Ga generator using nanoceria as adsorbent was developed indigenously at BARC [2]. Lyophilized DOTATOC kits were formulated for preparation of ^{68}Ga-DOTATOC using ^{68}Ga eluted from the ^{68}Ge/^{68}Ga BARC generator. Patient doses of ^{68}Ga-DOTATOC using ^{68}Ga eluted from ^{68}Ge/^{68}Ga BARC generator were prepared and imaging studies were carried out in collaboration with Tata Memorial Hospital, Parel, Mumbai.

Experimental

Single vial kit of somatostatin analogue, DOTA-Tyr^3-Octreotide (DOTATOC) was formulated in sodium acetate buffer under sterile conditions, freeze dried and tested for sterility and endotoxin content. 0.1 N HCl was also prepared and dispensed under sterile conditions and provided along with the kit for elution of ^{68}Ga from ^{68}Ge/^{68}Ga BARC generator. 92.5-148 MBq (2.5-4.0 mCi) ^{68}Ga from the novel ^{68}Ge/^{68}Ga BARC generator was eluted directly into the kit vial containing 50 g DOTATOC using sterile 0.1 N HCl. Incubation was carried out at 90 C for 10 min. Radiochemical yield of preparation was estimated by HPLC and paper chromatography in 50 % acetonitrile in water.

Optimization of radiolabeling with generator eluted ^{68}Ga was carried out by varying the reaction conditions such as temperature, time, concentration of peptide and different activities of ^{68}Ga. Stability of the radiolabeled peptide in serum and saline was studied. Long term stability of kits was tested by radiolabeling with ^{68}Ga at periodic intervals up to three months. Biodistribution studies were carried out in normal Swiss mice to determine the pharmacokinetic pattern of ^{68}Ga-DOTATOC in small animals.

Preparation of patient doses of ^{68}Ga-DOTATOC involved radiolabeling of DOTATOC with 92.5- 48 MBq (2.5-4.0 mCi) ^{68}Ga followed by addition of 10 mM EDTA to the complex. The preparation was filtered through sterile 0.22 filter. Sterile ^{68}Ga-DOTATOC was injected into patients for detection of neuroendocrine tumors. Imaging was carried out 1 h p.i of ^{68}Ga-DOTATOC using Philips Gemini TF PET/CT machine.

Results and Discussion

DOTATOC kits formulated under sterile conditions passed sterility and BET tests as per IP. Greater than 95 % radiochemical yield was observed when radiolabeling was carried out with ^{68}Ga eluted in 0.1 N HCl from a ^{68}Ge/^{68}Ga BARC generator as depicted in Fig.1. The ^{68}Ga-DOTATOC complex was stable in saline and human serum when studied up to 2 h. Consistency in ^{68}Ga labeling using kit vials was achieved when tested up to three months. Biodistribution studies in Swiss mice revealed fast clearance of activity via renal route as reported for ^{68}Ga-DOTATOC peptide. Patient doses 55.5-92.5 MBq (1.5-2.5 mCi) were prepared and injected into patients for imaging studies. Clinical information on number of lesions and extent of metastasis of NETs was obtained from ^{68}Ga-DOTATOC PET scans.

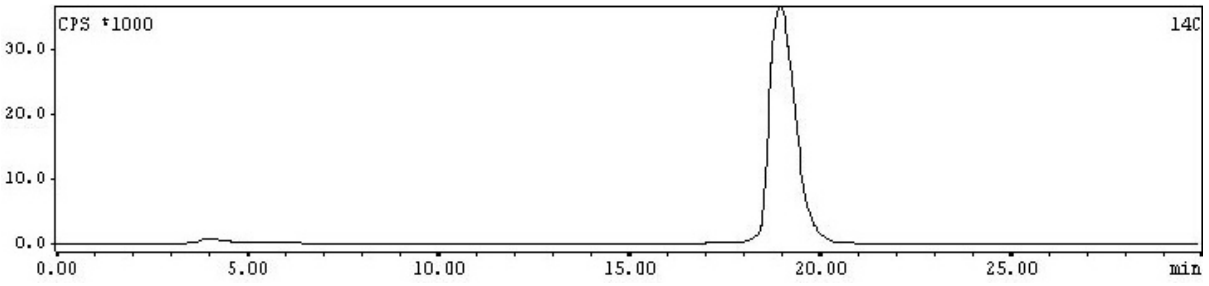


Fig. 1 HPLC radiochromatograph of ^{68}Ga-DOTATOC complex

Table-1: Biodistribution data of ^{68}Ga-DOTATOC complex in Swiss mice at 1 h p.i.

Organ/Tissue	%ID/gm
Blood	1.22 (0.34)
Liver	1.27(0.37)
Int +GB	1.01(0.04)
Stomach	1.17(0.42)
Heart	0.51 (0.19)
Lung	1.80 (0.28)
Spleen	0.89 (0.54)
Bone	1.62 (1.52)
Muscle	5.74 (0.47)
Kidneys	11.96 (6.67)
Excreta	72.33 (5.72)

(n=4, figures in the parenthesis represent standard deviations)

Conclusions

Development of single vial DOTATOC kit for preparation of ^{68}Ga-DOTATOC was demonstrated. Successful preparation of patient doses of ^{68}Ga-DOTATOC using ^{68}Ga eluted from ^{68}Ge/^{68}Ga BARC generator was achieved. Preparation of ^{68}Ga radiopharmaceuticals using kit based formulations is a cost effective and efficient method compared to costly modules for preparation of PET radiopharmaceuticals. Deployment of kits for preparation of current peptide based PET radiopharmaceuticals is expected to expand the clinical applications of newly developed molecular imaging agents.

Acknowledgements

The authors are thankful to Dr. Gursharan Singh, Associate Director (I) and Head, IA&RPhD, RC&I group BARC for his support. The authors are also thankful to Dr. M.R.A. Pillai, Former Head, RPhD for initiating the work.

References

[1] W. A. Breeman, E. de Blois, H. Sze Chan, M. Konijnenberg, D. J. Kwekkeboom, E. P. Krenning, Semin. Nucl. Med. 41 (2011) 314.

[2] R. Chakravarty, R. Shukla, R. Ram, M. Venkatesh, A. Dash, A. K. Tyagi, ACS Appl. Mater. Interfaces. 2 (2010) 2069.

Radiotracer Technique in Adsorption Study - Adsorption of Strontium Ions on TiO_2

Shuddhodan P.Mishra[1] and N.Srinivasu[1,2]

1. *Nuclear and Radiochemistry Laboratory, Department of Chemistry, Banaras Hindu University, Varanasi 221 005*
2. *Department of Science and Humanities, Vignan University, Vadlamudi, Gumtur. A.P*

The adsorption of strontium ions on titanium dioxide has been studied as a function of concentration (10^{-7} to 10^{-2}M), temperature (303 to 333 K) and pH values (6.8 to 11.4) of the adsorptive solution using radiotracer technique. The kinetics of adsorption was found to follow first order rate law with respective adsorptive concentration. The adsorption of strontium ions were not significantly affected by the exposure of titanium (IV) oxide adsorbent to neutrons and -radiations from a (Ra-Be) neutron source having an integral flux of 3.85×10^6 neutrons/cm^2/S.

Reactor Production of No Carrier Added ^{199}Au for Biomedical Applications

K.V. Vimalnath, Sudipta Chakraborty, Ashutosh Dash

Isotope Application and Radiopharmaceuticals Division, Bhabha Atomic Research Centre, Trombay, Mumbai 400085, India; E-mail: adash@barc.gov.in

This paper described the reactor production of no-carrier-added (NCA) ^{199}Au by neutron activation of ^{198}Pt and the radiochemical separation of ^{199}Au from Pt targets following liquid–liquid extraction (LLX) using ethyl acetate as an extractant. The effect of experimental parameters for the selective extraction of ^{199}Au were investigated and optimized. An optimized chemical processing procedure of providing NCA ^{199}Au of requisite purity in high yields has been the positive outcome.

Introduction

Owing to its favourable decay characteristics ^{199}Au [$T_{½}$ = 3.15 d, E_{max} = 0.474 MeV] is an attractive radionuclide for therapeutic applications. It also emits photons of 494 keV (97%) and 158 keV(36.9%). It is a radioisotope having very good potential for use in radioimmunotherapy, because of its favourable decay characteristics [1].

Production of ^{199}Au is performed by indirect methods, such as neutron capture of ^{198}Pt followed by decay of the ^{199}Pt ($T_{1/2}$ = 30.80 m) to generate ^{199}Au. The reaction cross-section is moderate 3.6 barns.

^{198}Pt (n,) ^{199}Pt ^{199}Au (1)

Natural ^{198}Pt has an isotopic abundance of 7.163% and activation cross section of 3.31b for (n,) reaction at thermal neutron energy. In order to tap the potential of ^{199}Au for therapy, development of an indigenous technology to undertake large scale production is not only an interesting proposition but also may be viewed as a necessity. The tremendous therapeutic prospects associated with this radionuclide along with the challenge of providing clinical grade ^{199}Au have thus generated a number of separation strategies [2-4] among which liquid–liquid extraction (LLX) received most attention. Within the framework of LLX, the scope of using ethyl acetate seemed to be an interesting prospect and motivated us to pursue further.

In this paper, we described the experimental findings, an overview of overall separation procedure and assessment of the quality of the ^{199}Au for medical application.

Experimental

Materials

Reagents of analytical grade were procured from reputed manufacturers and used during the course of this work. ^{199}Au and ^{197}Pt radiotracer used in this investigation were available in-house. NaI(Tl) scintillation counter, HPGe-MCA detector coupled with a multichannel analyser (MCA) were used for radioactivity determination in various experiments. Distribution ratios (D) of Pt and Au at different pH were determined following standard radiometric procedures.

Neutron Irradiation of Pt Target

20 mg Platinum sponge of natural isotopic composition was weighed into an aluminum container, sealed by cold press welding and irradiated in Dhruva research reactor at a thermal neutron flux of 2.3×10^{13} $n.cm^{-2}.s^{-1}$ for 7 days.

Radiochemical Processing and Separation of ^{199}Au

Radiochemical processing of neutron irradiated Pt target was carried out in a 100 mm thick lead shielded isotope processing facility with remote handling accessories. Irradiated Pt target was retrieved into a dissolution flask and dissolved in 4 mL aqua regia by gentle heating to enable complete dissolution. The solution obtained was evaporated to dryness, heated in excess of conc. HCl to expel nitric acid. The residue left after evaporation to dryness was reconstituted with 10 mL of 5 M HCl. A measured aliquot from this stock was taken and subjected to high resolution gamma ray spectrometry not only to ascertain total ^{199}Au radioactivity produced but also to characterize co-produced radionuclide impurities (Fig. 1). The solution is then transferred to a 50 mL separating funnel containing 10 mL ethyl acetate to extract ^{199}Au into the organic phase. ethyl acetate. Ethyl acetate fraction was separated and washed with 5 M HCl, transferred to a round bottom flask, heated gently to near dryness and the residue was treated with 1 mL concentrated HNO_3 to destroy any organic matter. Excess nitric acid was destroyed by treatment with 1 mL of conc HCl. The solution is evaporated to near dryness and reconstituted in 5 mL of 0.1 M HCl. Its radioactivity content as well as radionuclide purity was ascertained by gamma ray spectrometric measurement of suitably diluted aliquots for appropriate time at a suitable geometry in a HPGe detector coupled to MCA system (Fig. 2).

Results and Discussion

In order to dissolve the neutron irradiated platinum sponge target, the scope of using aqua-regia seemed attractive owing to the formation of soluble chloroplatinic acid.

Pt 6 HCl 4 HNO_3 = H_2PtCl_6 + 4 NO_2 + 4 H_2O

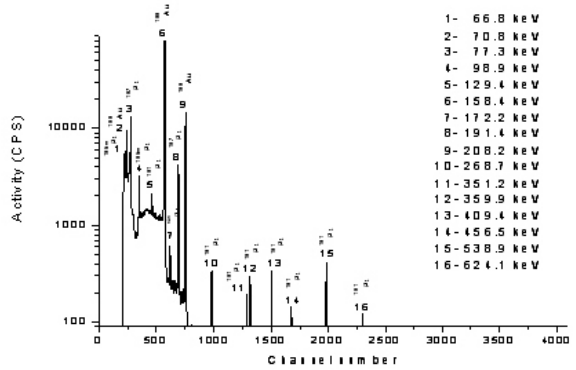


Fig. 1 Gamma spectra of the feed solution

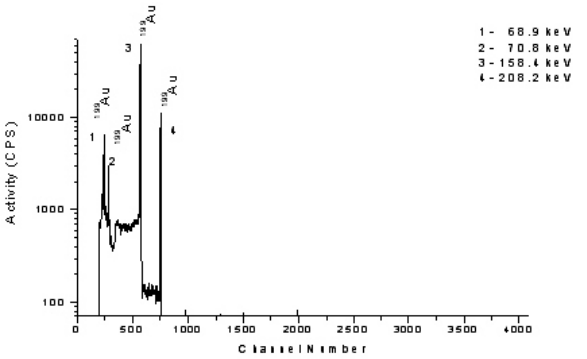


Fig. 2 Gamma spectra of separated ^{199}Au

An orange-brown solution of H_2PtCl_6 was obtained on complete dissolution. Fig. 1 displayed the gamma ray spectra of feed solution recorded before commencing the radiochemical separation which shows gamma peaks pertaining to only Pt and Au radionuclides. This indicated that the target is free from metallic impurities.

In the light of the implicit need to arrive at the optimum separation conditions for the extraction of microscopic amount of ^{199}Au from macroscopic quantity of Pt, distribution ratio (D) at various acid concentration of aqueous phase were determined and results obtained are summarized in Table 1. A careful scrutiny of the results indicated that at 5 M HCl, the D value of ^{199}Au is maximum. However, equally important is the negligible D values for Pt at this acidity which provide the option for quantitative transfer of microscopic amount of ^{199}Au into the organic phase.

Table 1: Distribution ratio (D) of ^{199}Au and ^{197}Pt

HCl concentration (M)	D	
	^{199}Au	^{197}Pt
1	5.3 ± 0.1	0.06 ± 0.01
2	7.0 ± 0.1	0.06 ± 0.01
3	10.3 ± 0.2	0.07 ± 0.02
4	11.6 ± 0.4	0.05 ± 0.01
5	20.0 ± 0.5	0.07 ± 0.02
6	7.7 ± 0.6	0.08 ± 0.01
7	6.1 ± 0.8	0.01 ± 0.01
8	6.1 ± 0.1	0.08 ± 0.02
9	4.2 ± 0.3	0.07 ± 0.01
10	1.2 ± 0.1	0.11 ± 0.03

This approach has been simplified in our work and directed towards the development of a radiochemical procedure for the selective extraction of microscopic amount of 'no-carrier added' (NCA) ^{199}Au into the organic phase. The developed procedure was validated using neutron irradiated sample as per the details described above to evaluate the efficacy of the ethyl acetate in the presence of intense radiation environment with the radiolytic products generated for propitious outcome.

While it is possible to extract >75 % of ^{199}Au in a single extraction, multiple extractions (3 times) constitute an effective proposition to extract >95% of ^{199}Au from aqueous phase. A reproducible separation efficiency of 94-97% was achieved. In a typical batch, about 290 MBq (7.84 mCi) ^{199}Au could be produced by irradiating 20 mg platinum target. The radionuclide purity of separated ^{199}Au is crucial and need to be assured not only to justify the technological success of this approach but also ascertain their usefulness in therapy. The gamma ray spectrum of the separated product is depicted in Fig. 2 which shows peaks corresponding to ^{199}Au only.

The separated NCA ^{199}Au could be used for the formulation of radiopharmaceuticals for therapeutic applications

Conclusion

The objective of arriving at a simple, robust production method for NCA ^{199}Au has been achieved. It is envisaged that the reported technique would serve in good stead for the routine production of ^{199}Au for therapeutic applications.

References

[1] A.T. Vaughan, N. R. Varley, Nucl. Med. Biol.15(1988) 293.

[2] K.L. Kolsky, L.F. Mausner, Appl Radiat Isot.44 (1993) 553.

[3] M. Bonardi, M. Gallorini, F. Groppi, C. Birattari, L. Gin, J. Lab. Compd. Radiopharm. 44 (2001) S767.

[4] N.R. Das, K. Banerjee, K. Chatterjee, S. Lahiri, Appl. Radiat. Isot. 50 (1999) 643.

Research Trends in Radioisotopes: A Scientometric Analysis

Anil Sagar[1], B. S. Kademani[1], K. Bhanumurthy[1] and N. Ramamoorthy[2]

1. *Scientific Information Resource Division, Bhabha Atomic Research Centre, Mumbai, India, E-mail: bsk@barc.gov.in*
2. *Office of Director, Bhabha Atomic Research Centre, Mumbai, India*

Radioisotopes or radionuclides are radioactive forms of elements and are usually produced in research reactors and accelerators. They have wide ranging applications in healthcare, industry, food and agriculture, and environmental monitoring. Following over five decades of vast experience accumulated, radioisotope technology has developed to a high degree of sophistication and it is estimated that about 200 radioisotopes are in regular use. This paper attempts to highlight the publication status and growth of radioisotope research across the world and make quantitative and qualitative assessment by way of analyzing the following features of research output based on Web of Science database during the period 1993-2012.

Year-wise Growth of Publications and Citations

A total of 31488 publications were published on radioisotopes during 1993-2012 and these publications received 482549 citations. Year-wise distribution of publications and citations is given in Fig. 1. The highest number of publications 2036 (6.47%) was published in 2012. The highest number of citations 33316 (6.90%) was received in 1999. The highest average citations per publication was 24.77 in 1993. There were 4421 (14.04%) publications with no citations during the period under study. Overall Collaboration Coefficient (CR) was very high (0.91) as 28729 (91.21%) publications of the total documents were multi-authored and the highest collaboration rate (0.94) was in 2010 and 2011. An exponential growth of publications was observed in this study.



Fig. 1 Year-wise distribution of publications

Continent-wise Share of Publications

The percent-wise share of radioisotope research in six continents of the world during 1993-2012 is depicted in Fig-2. It was observed that Europe is the most productive continent with 18267 (46.75%) publications and 296158 (46.70%) citations followed by North America with 10444 (26.73%) publications and 236167 (37.24%) citations and Asia with 8202 (20.99%) publications and 71044 (11.20%) citations.

Publications from Australia/Oceania received the highest average number of citations (24.36) per publication followed by North America with 22.61 average citations per publication, Europe with 16.21 average citations per publication, South America with 10.05, Asia with 8.66 average citations per publication and Africa with 7.64 average citations per publication.

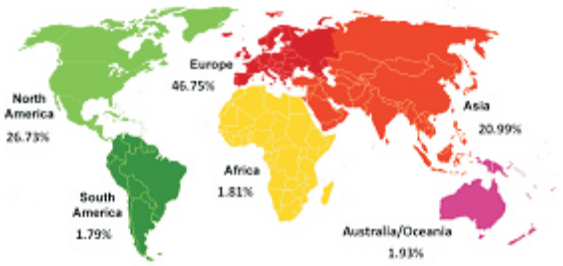


Fig. 2 Continents-wise distribution of share of publications

Highly Productive Countries in Radioisotope Research

In all, there were 134 countries involved in research in radioisotope research and which published at least one publication. The USA topped the list with highest share (29.31%) of publications. Germany ranked second with 8.16% share of publications followed by England with 7.44% share of publications, Japan with 6.97% share of publications, France with 6.38% share of publications, Italy with 4.75% share of publications, Russia with 4.73% share of publications, Canada with 3.3% share of publications, Spain with 3.17% share of publications, Sweden with 3.07% share of publications, Netherlands with 3.03% share of publications, Switzerland with 2.72% share of publications and India with 2.63% share of publications.

Country-wise Publication Efficiency Index (PEI)

Publication Efficiency Index (PEI) is a measure of research quality [1], it indicates whether the impact of publications in a country in a research field is compatible with the research efforts. The value of PEI >1 for a country indicates that the impact of

publications is more than the research effort devoted to it for that particular country and vice versa. The Netherlands had the highest PEI (1.93%) followed by Switzerland with 1.68%, USA with 1.52%, Scotland with 1.47%, Australia with 1.4%, England with 1.23% and Canada with 1.23.

International Collaborative Index (ICI) for Top Productive Countries

Among the top productive countries it was observed that out of 30 countries, 27 countries have very high values (100) of ICI. Hungary obtained the highest (109.02%) international collaborative index followed by Brazil with 107.46%, Peoples Republic of China with 107.3%, South Korea with 107.12%, Taiwan with 106.71% and India with 105.81% [2].

Subject-wise Distribution of Publications and Citations

Based on the classification of subject-categories in Journal Citation Report (JCR-2012) of Thomson Reuters, the publication output data of radioisotope research was classified into 9 broad subjects. Medical Sciences accounts for the largest share 12094 (38.14%) of publications in the total worldwide output which received 263672 (54.64%) citations followed by Earth & Environmental Sciences with 6515 (20.69%) publications and 77382 (16.04%) citations, Chemical Sciences with 4967 (15.77%) publications and 43612 (9.04%) citations, Engineering Sciences with 2393 (7.6%) publications and 23913 (4.96%) citations, Biological Sciences with 2227 (7.07%) publications and 39594 (8.21%) citations, Nuclear Science & Technology with 1238 (3.93%) publications and 4449 (0.92%) citations, Physical Sciences with 1182 (3.75%) publications and 15875 (3.29%) citations, Food & Agriculture Sciences with 541 (1.72%) publications and 6919 (1.43%) citations and Multidisciplinary Sciences with 331 (1.05%) publications and 7133 (1.48%) citations.

Quality of Research Output

Around 90.90% (28624) of the total publications were published in the journals with impact factors (IF) ranging from 00.01 to 153.46 and received 92.32% (445480) citations, and 9.10% (2864) publications were published in journals having without impact factor. The highest number of publications (9553, 30.34%) appeared in 764 journals having impact factor range from 1.01to #2.00 and received 80204 (16.62%) citations with 8.40 average citation per publication.

Journals Preferred for Publication by the Scientists

The scientific research in radioisotopes is spread over 3391 different journals. More than 60% of the publications were published in only 173 key-journals. The highly productive journals are: J Environ Radioactiv (IF-2.119) With 1220 (3.87%) publications, J Radioanal Nucl Ch (IF-1.467) With 1218 (3.87%) publications, Appl Radiat Isotopes (IF-1.179) With 1128 (3.58%) publications, Radiat Prot Dosim (IF-0.909) With 784 (2.49%) publications, J Nucl Med (IF-5.774) With 777 (2.47%) publications, Health Phys (IF-1.017) With 662 (2.1%) publications, Radiochim Acta (IF-1.373) With 487 (1.55%) publications, Nucl Instrum Meth A (IF-1.142) With 436 (1.38%) publications, Sci Total Environ (IF-3.258) With 411 (1.31%) publications, Nucl Med Commun (IF-1.379) With 391 (1.24%) publications, Nucl Instrum Meth B (IF-1.266) With 368 (1.17%) publications, Clin Nucl Med (IF-2.955) With 333 (1.06%) publications, Eur J Nucl Med Mol I (IF-5.114) With 302 (0.96%) publications and Nucl Med Biol (IF-2.517) With 244 (0.77%) publications.

References

[1] J. Guan, M. Ma, Scientometrics. 70 (2007), 107.

[2] P. S. Nagpaul, Scientometrics. 46 (1999) 109.

Radiotracer Investigation in an Industrial-Scale Oxidizer

H.J. Pant, V.K. Sharma

Isotope Applications and Radiopharmaceuticals Division, Bhabha Atomic Research centre, Trombay, Mumbai 400085, India; E-mail: hjpant@barc.gov.in

A radiotracer investigation was carried out in an industrial-scale oxidizer. The main objectives of the investigation were to measure residence time distribution (RTD) of the process fluid and determine mean residence time (MRT) and degree of mixing. Bromine-82 as p-dibromo biphenyl was used as radiotracer for measuring RTD of the organic process fluid. The MRT of the fluid was determined to be 328.5 minute. Tank-in-series model was used to simulate the measured RTD and results of the simulation showed that high degree of mixing occurred within the oxidizer and the oxidizer behaved as a well-mixed reactor. The results of the investigation were used to design an indigenous oxidizer.

Introduction

Dimethyl Terephthalate (DMT) is produced by oxidation of p-xylene (PX) and Methyl p-toluate (MPT) and esterification of the oxidation product with methanol. The oxidation reaction takes place in presence of a catalyst and is an exothermic reaction. This process is carried out in a reactor called oxidizer. Knowledge of residence time distribution, mean residence time and degree of mixing of process fluid are three important parameters of a chemical reactor and have direct bearing on quality of the product and efficiency of the process. In addition to this, these parameters are also required for process intensification and design and scale-up of new reactors. Various conventional tracer techniques are used for measurement of laboratory-scale reactors but the same cannot be used in industrial-scale reactors. Radiotracer techniques are ideal tools for measurement of above-mentioned hydrodynamic parameters because of their many advantages and often do not have any alternatives [1,2]. A private company near Mumbai operates a DMT plant having an oxidation reactor. The plant was built and setup with the help of a foreign company and was more than 25 year old. A need was felt by the company to increase production capability of DMT and thus wanted to indigenously design and setup another plant. Therefore, information about residence time and degree of mixing was required. The present paper describes a radiotracer investigation carried out in the above mentioned industrial-scale oxidation reactor to measure residence time and degree of mixing.

Experimental

The schematic diagram of the oxidation reactor and experimental setup is shown in Fig. 1. The oxidizer is a bubble column reactor consisting of a vertical stainless steel cylindrical vessel of height of 27 m and diameter of 4.45 m. The operating volume of the reactor is 315 m^3 including volume of the vapor phase. During operation, about 20% of the volume is occupied by vapor phase and remaining 80% is occupied by liquid. The liquid reactants (p-xylene + methyl p-toluate + catalyst) are fed into the reactor from the top section while the air is fed to the reactor from bottom at a flow rate of 28500 N m^3/hr through a sparger. The oxidation

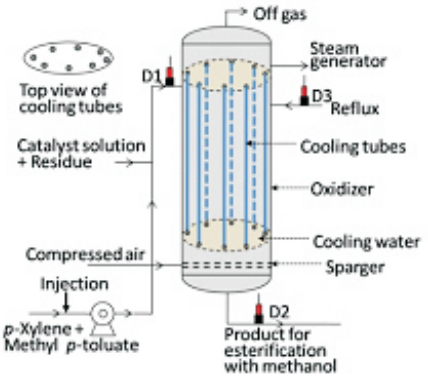


Fig. 1 Schematic diagram and experimental setup

reaction is an exothermic reaction and significant amount of heat is generated during the reaction. In order to remove the excess heat, cooling water is continuously fed through the cooling tubes, provided in peripheral part of the oxidizer. The water is subsequently converted into steam. The reactor operates at 165-170°C and 7.0-7.3 bars.

Two repeat tracer tests were carried out at identical process and operating conditions. Bromoine-82 (half- life: 36 h, gamma energies: 0.55 (70%), 1.32 (27%)) as p-dibromo biphenyl was used as a tracer. In first test about 2.6 GBq (70 mCi) activity was used while in second test about 1.5GBq (40 mCi) activity was used. The tracer was instantaneously injected into p-xylene feed line and monitored at three different locations i.e. near the injection point, inlet and outlet of the reactor using collimated scintillation detectors. The detectors were connected to a computer controlled data acquisition system. The data acquisition system was set to record tracer concentration at an interval of one minute.

Data Analysis and Results

The measured tracer concentration curves were corrected for background, background rise due to recycle, radioactive decay, tailing effect and residence time distribution curve was obtained by dividing each

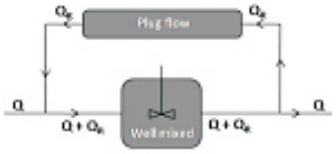


Fig. 2 Block diagram of proposed mode

tracer concentration data by area of the measured C(t)-t curve. Thus

$$E(t) = C_i(t) / \int_0^t t\, C_i(t) \qquad (1)$$

The first moment of the RTD curve is the experimental MRT ( ) and is given as (2):

$$t = \int_0^t t\, C_i\, dt / \int_0^t C_i(t)\, dt \qquad (2)$$

where i = 1, 2…n. The experimentally determined MRTs are given in Table 1. In present case, theoretical MRT ( ) is given as:

$$V/Q_T \quad V/(Q+Q_R) \qquad (3)$$

Where, V and Q_T are effective liquid volume inside the reactor and total liquid flow rate through the reactor, respectively. Since the recirculation flow rate was not known, the theoretical MRT could not be determined.

Tanks-in-series model with plug flow component in recirculation was proposed and used to characterize mixing of fluid in the reactor. The block diagram of the proposed model is given in Fig. 2.

The analytical solution of the model for an impulse injection of tracer at the inlet of the reactor is given by (4):

$$E_m(t) \quad \frac{N^N t^{N-1} e^{-N\frac{t}{\tau_m}}}{\tau_m^N \; N-1\,!} \qquad (4)$$

where, τ_m is model predicted mean residence time and N is number of tank. In the case of two extreme ideal flow patterns, N=1 for perfect mixing and N for plug flow (minimum mixing). The least squares curve-fitting technique is used to fit the two curves and obtain the values of model parameters, corresponding to the minimum root mean square (RMS) value [3]. The results of RTD simulation are given in Table 1. A typical plot showing comparison of experimental and model simulated RTD curves is shown in Fig. 3.

Table 1: Results of RTD measurements

Run No.	V_L (m^3)	QL (m^3/h)	(Min)	QR (m^3/h)	$_R$ (Min)	$_O$ (Min)	N
1	252	40	385	4	373	325	1
2	252	40	422	4	390	332	1

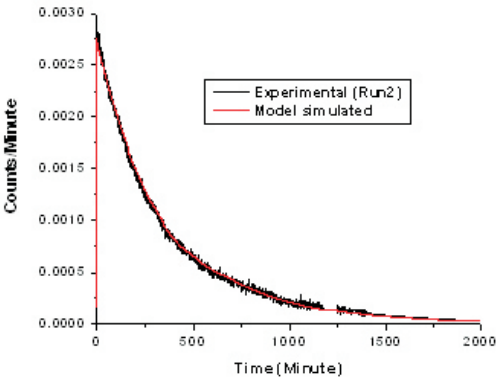


Fig. 3 Comparison of experimental and model simulated RTD curves (Run 2)

The experimental MRT of fluid within the reactor with recirculation was determined to be inside the oxidizer was found to be 403.5 minutes. The results of the model simulation showed that the proposed model fits very well to the experimental data and the reactor behaved as a well-mixed reactor. Based on model simulation, the parameters i.e. recirculation flow rate (Q_R), MRT ($_R$) in recirculation stream (Plug flow component), MRT in oxidizer ($_O$) and degree of mixing (N) were obtained. Q_R was estimated to be 10% of initial feed rate i.e 4 m^3/h. The MRTs within the oxidizer and recirculating stream were found to be 381.5 and 328.5 min, respectively.

Conclusions

No malfunctioning and abnormality was observed in flow during operation of the reactor. The MRT of liquid phase in the reactor was found to be 328.5 minutes. The tank-in-series model with plug flow component in recirculation stream was found suitable to describe the flow in the oxidizer. Results of model simulation indicated that the reactor behaves as an ideal well-mixed reactor. The obtained results were used for validating the theoretical calculations/correlations and design a new oxidizer.

References

[1] J.S.Charlton, Radioisotope Techniques for problem solving in industrial process plants, Leonard Hill Publications, UK (1986).

[2] International Atomic Energy Agency, Computer Manual Series, No. 11. IAEA, Vienna, Austria (1996).

[3] M.L.Michelsen, Chem. Eng. Sci. 4 (1972) 171.

^{10}Be Dating of Marine Core Sediment from Central Western Bay of Bengal by using Accelerator Mass Spectrometry

P.V.L.Narayana[1], B.Pankaj Kumar[2], Rajveer Sharma[2], Soumya Prakash Dhal[3], Archna Bohra[2], S.Chopra[2], I.N.Rao[4], A.D.P.Rao[1]

1. *Swami Jnanananda Laboratories for Nuclear Research, Nuclear Chemistry & Chemical Oceanography, Andhra University, Visakhapatnam 530 003, India; E-mail: pvl.nuclearphysics@andhrauniversity.edu.in*
2. *Inter University Accelerator Centre, Aruna Asaf Ali Marg, New Delhi 110067 India*
3. *Department of Physics, Pondicherry University, Pondicherry 605014, India*
4. *Department of Physical, Nuclear Chemistry & Chemical Oceanography, Andhra University, Visakhapatnam 530 003, India*

A 4.12 m long marine sediment gravity core was collected during 157 cruise of ORV Sagar Kanya (October 2000) from the marginal coastal waters of central western Bay of Bengal. Sediment samples were taken for every 50cm interval; i.e 7 samples are studied for dating purpose. Rate of sedimentation and age of the core was determined with the cosmogenic radionuclide ^{10}Be by using Accelerator Mass Spectrometry (AMS). ^{9}Be was determined using ICPMS. The data is in good agreement with literature values.

Introduction

Sediment is any particulate matter that can be transported by fluid flow, which eventually deposited at the bottom of a water body. They are the important carriers of metals in major and minor quantities in the hydrological cycle Coastal and estuarine regions are the important sinks for many persistent metal pollutants those accumulate with organisms by forming in the bottom sediments. Thus, geochemical characteristics of the sediments can be used to infer the weathering trends and the sources of elements and its pollution in the sediments. They can also be used for understanding historical incidents that were happened. The central western Bay of Bengal coastal waters receives more sediment terrigenous inputs from the rivers Godavari and Krishna forming huge deltaic area. So far number of geochemical studies was performed by different researchers with different objectives. Geochemical studies on core sediments of the continental slopes of the Bay of Bengal are few. But very few reports are available on the dating of core sediment by using different stable isotopes (ex. C,O). No studies are available dating of core sediments by using 'Be' radio isotopes in the continental shelf areas of the Bay of Bengal sediments. ^{10}Be is a long lived cosmogenic radioactive isotope is used to calculate age and accumulation rate of sedimentation in the marginal sediments of central western Bay of Bengal. Therefore the author has undertaken the present investigation with the following objective. The aim of the present study is to understand the age and rate of sedimentation of the core sediment near to Nizampatnam Bay by using AMS system through ^{10}Be isotope method.

Experimental

The core was sub sampled to each with 2 cm interval. The samples were dried at 60°C, ground to fine powder using agate mortar and sieved through 230 mesh size. For Be dating purpose every 50cm interval, total 7 samples are studied. Approximately 1 gram weight of each sample was taken and then leaching process was carried to extract the maximum possibility of Be isotopes. The leachate was processed to separate out the beryllium isotopes. Collected Be was placed on hot plate at 120°C temperature and dried until the remaining amount was equal to1 ml. Be samples were shifted into separate centrifuge tubes and equivalent amount of (NH_3) was added to get precipitation. After getting precipitation, these centrifuge tubes were put into centrifuge machine at 4500 RPM to remove liquid from the precipitation. The precipitated one is beryllium hydroxide Be $(OH)_2$. The liquid part was separated from the precipitation and put into a furnace in a quartz vials and maintained temperature at 90°C for 4 hours, 400°C for 6 hours and 900°C for 8 hours. Hydroxides of Be were converted into oxides form. The powdered BeO was loaded to the cathode tube with Nb powder [1] and analyzed for ^{10}Be/^{9}Be using AMS. Beryllium-10 was measured on the Tandem Accelerator Mass Spectrometer at the IUAC, New Delhi. Stable ^{9}Be concentration was determined by using inductively coupled plasma mass spectrometry (ICPMS).

Results and Discussions

Dating studies of the core sediments are useful to delineate possible Holocene/Pleistocene boundary. The details of the dating, rate of sedimentation and their interpretation are given in Table 1. Seven sections of core samples i.e., from 50 to 350 cm by having 50 cm intervals (7 samples) are used for dating studies that carried out by using cosmogenic ^{10}Be/^{9}Be radio isotopes.

The rate of sedimentation in the upper part (0-150 cm) of this core is 0.009 cm/yr (or) 9 cm/kyr, while it is in the range 150-350 cm of the core is 0.00425 cm/yr or 4.25 cm/kyr. The total rate of sedimentation in the entire core up to 350 cm is 0.0062 cm/yr or 6.2 cm/kyr. In the

Table-1: Age and sedimentation rates of the sediment core in the Nizampatnam Bay (Bay of Bengal)

Depth (cm)	Age (year)	Sedimentation rate (cm/year)
50	1300±169	0.013
100	4902±637	0.008
150	11120±1446	0.006
200	19879±2584	0.004
250	31212±4958	0.004
300	45161±5871	0.003
350	61786±8032	0.006

core, low sedimentation rate obtained at depth 300 cm is 0.003 cm/yr or 3cm/kyr that belong to the Pleistocene period and high rate of sedimentation at depth 50 cm is 0.013 cm/yr or 13 cm/kyr observed, which belongs to Holocene period. Based on the ages and rate of sedimentation of the present core, its range 0 to 150 cm belongs to Holocene period and below 150 cm it considered to be the Middle Pleistocene period. Similar age and sedimentation rates of the core from the continental margin of the south western Bay of Bengal was reported by Sri Rama Krishna [2] (2006), in the Nizampatnam Bay by Venkateswara Rao [3] (2008).

Conclusions

Based on the ages and rate of sedimentation of the present core, the depth range from 0 to 150 cm belongs to Holocene period and after 150 cm it considered to be the Middle Pleistocene period. This is also corroborated by the obtained data of $CaCO_3$ and magnetic susceptibility.

Acknowledgments

Thanks to the Dr.Amit Roy, Director IUAC, Accelerator user Committee for allotting AMS beam time.

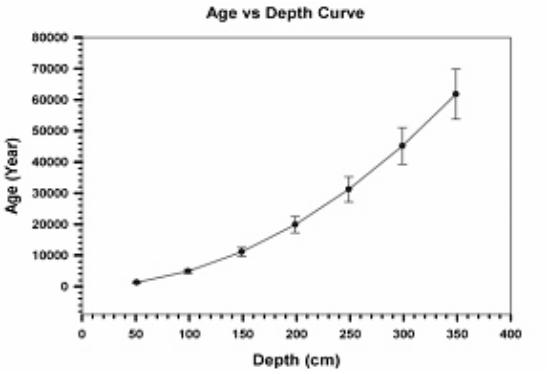


Fig. 1 Age vs Depth curve

References

[1] Pankaj Kumar., Pattanaik, J.K., Ojha, S., Gargari, S., Joshi, R., Roonwal, G.S., Balakrishnan, S., Chopra, S., Kanjilal, D., 2011. J. Raad Nucl Chem DOI 10.1007/s10967-011-1184-x.

[2] Sri Ramakrishna, M., 2006. A Study of some stratigraphic tool for the Indian Ocean sediments. Ph.D Thesis, Andhra University, Visakhapatnam (unpublished).

[3] Venkateswara Rao, M., 2008. Textural, geochemical and palynological studies of sediment cores from Bay of Benagal, India. Ph.D Thesis, Andhra University, Visakhapatnam (unpublished).

Hard and Soft Acid Base Concept of Biosorption - Employing Green Biosorbent by Radiotracer Technique

Nisha Barot, Roshan Khilnani, Hemlata Bagla

Department of Nuclear and Radiochemistry, Kishinchand Chellaram College, Churchgate, Mumbai 400 020, India; E-mail: hemabagla@gmail.com

This explicit investigation aims to explore a green and clean alternative for the waste water treatment and to justify one of the most prevailing mechanisms of biosorption based on Hard and Soft Acid Base (HSAB) theory successfully. The potential of Dry cow dung powder (DCP) to sequester toxic heavy metal ions such as Cr(III), Cr(VI), Cd(II), Hg(II) and radiotoxic ^{90}Sr(II) has been productively established, employing radiotracer technique. We have carried out batch equilibration method and all the important parameters have been optimized. The investigation of biosorptive interference of various ligands have been demonstrated by employing twenty –three, different organic as well as inorganic salts or ligands with varying proportions. Today, the field of biosorption has acquired new vistas by embracing the concept of 'Waste is the Commodity', so as, DCP, the eco-friendly combo humiresin, advantageously emboss its efficiency in the same regards.

Introduction

Biosorption is a metabolism-independent, passive process with physico-chemical binding of metal ions involving non-living biomass [1]. The knowledge of mechanism is essential also for understanding the biosorption process and it serves as a basis for quantitative stoichiometric considerations which in turn constitutes the foundation for mathematical modeling of the process [2]. When the chemical or physiological reactions occurring during biosorption are known, the rate, quantity and specificity of the metal uptake can be manipulated through the specification and control of process parameters.

The obvious biosorptive behavior of DCP has been explained by Hard & Soft Acid Base concept, HSAB theory, given by Pearson [3], which elucidates the crucial role of HSAB characteristics of both pollutants as well as the aqueous milieu, which helps in governing the success of process. The various metal ionic species exhibit a preference for the ligand binding on the biomass based on its chemical coordination characteristics.

The key factors such as relative size of solute, solute-solute interaction, their solubility, stability, ionic character, relative affinity, speciation and most important their concentration, plays a vital role in the adsorption process. All these factors can either result in mutual inhibition of competing adsorbate, which decrease the efficiency of adsorption or their mutual complex can enhance the adsorption rate. The variation in the concentration of one component influences the concentration of other component. In case of metal–metal interaction it has positive impact whereas the metal-ligand interaction exhibits a negative impact. The free ion concentration of a metal decreases with an increase in the ligand concentration [4]. The higher concentration of ligands reduces the percentage adsorption due to readily forming stable metal-ligand complex or due to competition between metal ions and ligands for the sorption sites on the adsorbent. Some ligands with optimum concentration increase the adsorption of concerned metal ion due to co-adsorptive effect on the adsorbent. These biosorptive phenomenons are aptly proved by our present study on DCP. Hence, the interference of various salts has been studied so as to demonstrate the direct application of DCP on industrial effluent with many dissolved salts. The radiotracer technique, in comparison to classical approach, offers some unique advantages of high sensitivity, non-destructive pattern, freedom from reagent blank etc.

Experimental

A comparative batch equilibration biosorptive assay has been carried out employing radiotracer technique for uptake of Cr(III), Cr(VI), Cd(II), Hg(II) & Sr(II) employing their corresponding radiotracers ^{51}Cr, ^{115m}Cd, ^{203}Hg and ^{90}Sr which were procured from Board of Radiation & Isotope Technology (BRIT), Mumbai. The effect of different experimental parameters such as pH (from 1-10), metal ion concentration (0.5-20 mg/mL), contact time (0-30 min), agitation speed (0-5000 rpm), amount of adsorbent (50-1000 mg) and temperature (273-373K), adsorption capacity and interference of organic as well as inorganic salts have been studied so as to optimize the parameters. We have also carried out kinetic studies so as to optimize the system for it to be feasible for real application.

Results and Discussion

To study the effect of interference of different salts on the percentage biosorption of metal ions on DCP, different organic as well as inorganic salts have been studied with varying proportion of 10 mg, 25 mg, 50 mg and 100 mg. It is observed that some salts were proved to be non-interfering with concentration as high as 100 mg, whereas some were profoundly suppressing the adsorption process even with concentration of 10

Table-1: The non-interfering and interfering ligands with optimized biosorption process parameters.

Common constant parameters: Contact time = 10 min; Speed of rotation = 4000 rpm; Room temperature 30 ± 2^{0}C Initial metal ion concentration = 1 mg/mL Amount of DCP = 100 mg; pH = 5					
Varying parameter	Cr (III)	Cr (VI)	Cd (II)	Hg (II)	Sr (II)
% Biosorption	70 -80	30 - 40	70 -80	70 -80	70 -80
Oxidation state	+3	+6	+2	+2	+2
HSAB nature	Hard Acid	Hard Acid	Hard Base	Hard Base	Hard Acid
Ligands Non-Interfering					
at 10 mg	SA, TC, CI, SI, EA, AC, DC	CI, SI, EA, MA, HY	CI, EA, AC, DC, CM	CI, SI, CH, ID, NI	EA, CM, NI, BC, TS, CA
at 100 mg	CB, BR, ID, NA	ID, NA	NA	NA, MA, HY	MA, PH, CI
Ligands Interfering					
at 10 mg	TU, PH, TS, OX, MA TR	NI, OX, TS, TC, CM, TR, TU,	TR, TU, OX, TC, NI, HY, TS	EA , TC, TS, SA TU, OX, TR	CH, NA , TR, CB, HY, TU
KEY: Sulphate (SA), Thiocynate (TC), Citrate (CI), Sulphite (SI), EDTA (EA), Acetate (AC), Tartrate (TR), Dichromate (DC), Mangnate (MA), Hydroxide (HY), Chromate (CM), Chloride (CH), Iodide(ID), Nitrite (NI), Bicarbonate (BC), Thiosulphate (TS), Chlorate (CA), Carbonate (CB), Bromide (BR), Nitrate (NA), Phosphate (PH), Thiourea (TU), Oxalate (OX).					

mg. According to this theory, metal ions act as Lewis acid and ligands act as Lewis base. Hard acids tend to form a strong bond with hard base and soft acid with soft base. Heavy metals are considered as soft ions and thus they form very strong bond with soft base such as CN^-, RS^-, SH^- etc., nitrogen or sulphur containing ligands, which decreases the adsorption of metal ions. [5].

In regular practice of bioremediation, the interfering ligands are chemically treated or masked with appropriate reagents to suppress the decrease in biosorption. Even on addition of these foreign chemicals or masking agents in the system in small concentration, it not only burdens the economy and feasibility of reaction but also it questions the green and clean phenomenon of process [6].

This dilemma is solved by DCP, an eco friendly humiresin, enriched with minerals, carbohydrates, fats, proteins, bile pigments, aliphatic - aromatic species such as 'Humic acid', Fulvic acid and many naturally present functional group such as carboxyl, phenols, quinols, amide etc. of both hard and soft nature, making it 'combo' in nature which sorbs both concerned metal ions as well as ligands present in the system. Thus the ligands which were masking the biosorption process of heavy metal ions in this study were treated by mere increase in the dose of DCP, which successfully solves the problem without affecting efficiency of the process. This is exemplified by three very basic interactions happening in multicomponent system [7] i.e. (i) Synergism: Mutual enhancement, (ii) Antagonism: Mutual decrement and (iii) Non-interaction: Neutral effect.

Conclusions

Thus we conclude that DCP has a great potential in the field of water decontamination, industrial water treatment and in abatement of water pollution. Our results convey that the nature of ligands and their concentration present in the effluent should be known so to get optimum biosorption with in-situ conditions. The selection of any process should be considered in the terms of its feasibility and it should also contest the 3A's concept of affordability, acceptability and adaptability. On this background, our research with DCP proves its affordability by being free and naturally available, its acceptability by HSAB concept and its adaptability by its Combo nature.

References

[1] Yu, L.J., Chakraboty, S., Basu, J.K, Separ. Purif. Tech. (2006), 50(3), 336-341.

[2] B. Volesky, J. Yang, Envir. Sci. Technol. (1990), 33, 4, 4079-4085.

[3] Pearson R. G., Surv. Prog. Chem., (1969), 5, 1.

[4] Morel F., McDuff R. E., Morgan J. J., Trace metals and Metal-Organic interactions in Natural Waters, Singer, P.C., Ed., Ann Arbor Science, Ann Arbor MI, (1973),157.

[5] Williams D. R., The Metals of Life: The solution Chemistry of Metal ions in Biological Systems, Van Nostrand Reinhold, London (1971).

[6] G. Naja, V. Murphy, B. Volesky, Biosorption and Meatls, Wiley Encyclopedia of Industrial Biotechnology, 2t-S-1Ed-D-P.

[7] Tsezos, M., E. Remoudaki, and A. Hatzikioseyian. SWEMP'98, (1998). Ankara, Turkey.

Synergistic extraction of Cs(I) using Di-benzo-24-crown-8 and Di-2-ethylhexylphosphoric acid in toluene

T. Bhar, M. Banerjee, S .Basu

Department of Chemistry, The University of Burdwan, Burdwan 713104, W.B., India

Nuclear and analytical laboratory, Department of Chemistry, The University of Burdwan, Burdwan – 713104, W.B., India, E-mail:tania.bhar1@gmail.com.

The liquid-liquid extraction of cesium from aqueous chloride medium by a mixture of Di-benzo-24-crown-8 and 2-ethylhexylphosphoric acid (D2EHPA) into toluene is reported. Synergism was observed in the mixed extraction of labeled Cs(I) into toluene. Thermodynamic parameters controlling the nature of the extraction were also evaluated from the distribution ratio values obtained at different temperatures. Such results are important in order to explain the extraction mechanism.

Introduction

The removal of cesium from radioactive wastes resulting from the reprocessing of nuclear fuels continues to be an important technological problem [1]. A variety of different separation methods have been studied, including solvent extraction, ion exchange, and precipitation. Among the solvent extraction systems studied, the use of crown ethers as ion-selective complexants has received significant attention [2-4]. In the present work, we report the use of Di-benzo-24-crown-8 (CE) (ligand) in the liquid-liquid extraction of Cs(I) from aqueous medium and the effect of D2EHPA (donor) on such extraction system.

Experimental

In the general extraction procedure, an aqueous solution containing~100 g mL^{-1} of Cs(I) spiked with ^{137}Cs (supplied by BRIT, India) was adjusted to pH 1.0 by a Sambros model 335 digital pH-meter and equilibrated for 15 minutes with an equal volume of organic phase containing CE in toluene and to keep the ionic strength fixed, aqueous solution was always added with 0.1M $NaClO_4$ before extraction . For synergistic studies, the organic phase was a mixture of CE and D2EHPA (M/S Sigma) in desired ratio. After equilibrium, the radio activities of both of the aqueous and organic phases were measured by a S.C. -ray spectrometer (Nucleonix India make) with NaI(Tl) detector and from the data obtained, distribution coefficient was calculated. For the study of the temperature effect, equilibrations were carried out in a temperature controlled mechanical shaker, after which distribution coefficient were determined in usual way.

Result and Discussion

Several parameters for the extraction of Cs(I) with CE were optimised by preliminary experiments which show that extraction equilibrium was attained within 15 min, at an aqueous pH_{eq} 1.00 and toluene was found to have maximum extraction efficiency among a series of organic solvents. The optimum concentration of the extractant was determined by extracting the labelled solution at pH 1.0 and slope value found ~ 1 (Fig. 1).

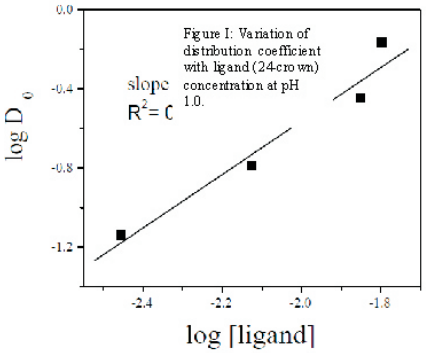


Fig. 1 Variation of distribution coefficient with ligand (24-crown) concentration at pH 1.0.

Conc. Of Crown ether(mol lit^{-1})	Distribution coefficient
0.003	0.073
0.008	0.163
0.011	0.276
0.014	0.356
0.018	0.689

Extraction of Cs (I) from aqueous chloride medium by pure D2EHPA (HR) in toluene was also investigated. Composition of extractable species is 1: 1.

Thus, when the ligand is mixed with donors a marked enhancement in the extent of Cs (I) extraction takes place. As Dmix is always greater than D_0, mixed extraction definitely leads to synergism (s.c. = synergistic coefficient [4]).

The plot of log ($D_{mix} – D_0 – D_s$) against both log [ligand] and log[donor] shows straight lines of slope values ~1 (Fig. 2) and ~1 (Fig. 3) respectively. Thus, ternary species could be assigned as $[Cs (CE) (HR)]_{org}$.

Fig. 3. Variation of distribution coefficient against D2EHPA concentration at different fixed 24-crown concentration (B 0.002 mol dm^{-3}, C 0.004 mol dm^{-3}, D 0.006 mol dm^{-3}) at pH = 1.0.

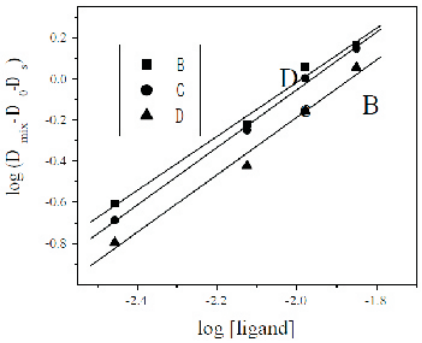


Fig. 2 Variation of distribution coefficient against 24-crown concentration at different fixed D2EHPA concentration (B .0035 mol dm^{-3}, C .0075 mol dm^{-3}, D .0105 mol dm^{-3}) at pH= 1.0

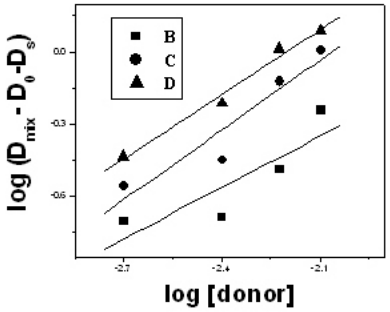


Fig. 3 Variation of distribution coefficient against D2EHPA concentration at different fixed 24-crown concentration (B 0.002 mol dm^{-3}, C 0.004 mol dm^{-3}, D 0.006 mol dm^{-3}) at pH = 1.0

Table-1: Results of synergistic extraction of Cs (I) (due to very much poor values D_s are neglected)

[24-crown] (mol dm^{-3})	[D2EHPA] (mol dm^{-3})	D_{mix}	D_0	S.C
0.002	0.0035	0.289	0.104	0.351
	0.0075	0.596	0.221	0.434
	0.0105	1.031	0.311	0.492
	0.0141	1.542	0.407	0.574
0.004	0.0035	0.312	0.117	0.465
	0.0075	0.760	0.224	0.586
	0.0105	1.317	0.342	0.628
	0.0141	1.796	0.419	0.651
0.006	0.0035	0.354	0.123	0.573
	0.0075	0.781	0.245	0.637
	0.0105	1.434	0.355	0.639
	0.0141	1.842	0.427	0.694

Temperature effects on the extraction of cesium (I) by individual ligand and mixture of ligand and donor have also been studied.

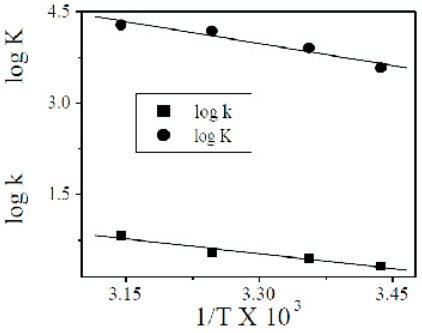


Fig. 4 Temperature variation of equilibrium constant of Cs (I) extraction (k and K for binary and ternary extractions)

From the values of equilibrium extraction constant at the temperature range investigated, the Vant Hoff equation was used to calculate the enthalpy change.

$$\log K = - \Delta H / 2.303 RT + \Delta S / 2.303R$$

The plot of log K against 1/T is a straight line (Fig. IV) where the slope gives the enthalpy of reaction (H^0) and the intercepts corresponds to entropy (S^0) value. The values of G^0, H^0, S^0 are shown in (Table 2).

Table-2: Thermodynamic parameters

System	G^0 kJ mol-1	H^0 kJ mol-1	S^0 J K-1 mol-1
Metal ion + ligand	-2.11±0.10	31.12±.02	111.82±.02
Metal ion+ ligand + donor	21.62±0.15	46.15±0.10	227.66±0.10

Conclusion

Poor extractions in binary system indicate association of water molecules in inner sphere of metal ion. In the mixed extraction water molecules associated in inner sphere of metal ion are replaced by donor molecules. Postulation of such reaction pathways are supported by the endothermic nature of ternary extraction with subsequent positive values of entropy changes. This is clearly indicative of formation of inner sphere complex by the present combination of ligand and donor.

References

[1] L. Cecille ed.,"Radioactive Waste Management and Disposal", Elsevier, London Chemistry Division Annual Progress Report, U.S.D.O.E., ORNL-6756, 199 (1993) 109.

[2] W. W. Schulz., L. A. Bray, Sep.Sci.Techol.2 (1987) 191.

[3] Blasius,E., Nilles,K.-H., Radiochimica Acta, 35 (1984) 173

[4] R. A. Sachlaben, Y. Deng, D. K. Bailey, B. A. Moyer, Sol. Ext. Ion. Exch, 14 (1996) 995.

Effect of Co – Metal Ions Concentration on Iron Metal Ions Adsorption on New Adsorbent Prepared from Cuscuta Powder

Jyotsna Dhanik[1], Sneha Saurabh[1], S.K. Tyagi[2]

1. *Department of Chemistry, G.B.Pant University of Agriculture & Technology, Pantnagar, Pin-263145, Uttarakhand*
2. *Radiations and Isotopic Tracers Laboratory, G.B.Pant University of Agriculture & Technology, Pantnagar, Pin-263145, Uttarakhand; E-mail: sk_tyagi@rediff.com*

In the present study a new adsorbent prepared from natural problematic weed plant was evaluated for the % adsorption of Fe(II) ions and effect of co-metal ions of Cu(II), Mn(II), Zn(II) and Ca(II) on adsorption of Fe(II) ions. The experimental results indicated that in the absence of any co-metal ions the percentage adsorption of Fe^{2+} ions on Cuscuta powder was 91.0%. The percentage adsorption of Fe^{2+} ions was found to be decreased in presence of co-metal ions in the solution.

Introduction

Adsorption of heavy metals, which is the passive uptake of the metals by dead / inactive biological materials or by materials derived from biological sources, has attracted significant attention during the past few decades as an alternative to the conventional methods of heavy metals removal from aquatic systems [1-5]. Initial incentives of the process include low cost of the biosorbents, great efficiency for metal's removal at low concentration, potential for biosorbent regeneration and metal recovery, high velocity of sorption and desorption, limited generation of secondary residues and more environmentally friendly (e.g. easy to eliminate compared to conventional resins) [4,6]. Adsorption process has advantages over the other methods because of simple design with a sludge free environment and can involve low investment in term of both initial cost and level required. Iron is an essential micro-nutrient for the plants, animals and humen. Its role in plants is either as a metal component of enzymes or as a functional co-factor of enzymes reactions. Its requirement to the plants in the early stages of growth is critical to ensure good yields and quality of the produce. The excess of iron in the drinking water creates bad odours and yellowish colour which makes it unfit for drinking. Iron overload in the human body may results in the damage to the heart, liver and other organs [7]. In view of its importance, these experiments were planned and done to evaluate Cuscuta powder as adsorbent for the adsorption of ferrous ions from aqueous solutions in presence of co- metal ions. Different factors affect the adsorption process are; characteristics of the adsorbent, concentration of the adsorbate, contact time, temperature, pH of solution and concentration of co-ions in the adsorbate solution. In the present study the adsorbent was prepared from zero value weed plants of Cuscuta (Cassytha filiformis) and effect of concentration of co-metal ions in the adsorbate solution was studied using Fe-59 radiotracer.

Experimental

The adsorbent used in this study was Cuscuta powder prepared form Cuscuta plants (Cassytha filiformis) by drying & milling processes. The Cuscuta powder was activated by 0.1N NH_4Cl solution at 110ºC followed by X-rays irradiation using 500 mA rotating anode X-Rays machine in Surgery & Radiology department of university. X-rays irradiation of adsorbent was done for the activation of adsorbent.The studies of adsorption of Fe^{2+} ions on Cuscuta powder were done using Fe-59 radiotracer to understand the effect of co- metal ions on adsorption of Fe^{2+} ions. The adsorption study of Fe^{2+} ions on Cuscuta powder was carried out by batch method. The initial concentration of Fe^{2+} ions in the adsorbate solutions was 10 ppm.The removal percentage or percent adsorption was calculated using the following expression; Percent Adsorption = $(C_i - C_t)\times 100 \div C_i$, Where C_i is initial concentration (ppm) of the adsorbate solution & C_t is final concentration (ppm). The adsorption of Fe^{2+} ions were studied in the presence of Cu^{2+}, Mn^{2+}, Ca^{2+} and Zn^{2+} ions separately at different concentrations in the range of 0 – 15 ppm of Co- metal ions, using 1 g of adsorbent powder for 10 mL adsorbate solution. The radioactivity was measured by Gamma ray spectrometer with NaI (Tl) based well type detector. For the radioactivity measurement 1 mL of solution before and after adsorption was taken in glass counting tubes.

Results and Discussion

Fig. 1 shows the effect of concentration of Cu^{2+} ions on percentage adsorption of Fe^{2+} ions on Cuscuta powder from aqueous solution. The data reveals that in presence of Cu^{2+} ions the percentage adsorption of Fe^{2+} ions decreases with the increase of the concentration of Cu^{2+} ions & adsorption capacity also decreases in the same manner. Percentage adsorption of Fe^{2+} ions decreased sharply upto 3 ppm Cu^{2+} ions concentration and after it there was an increase in percentage

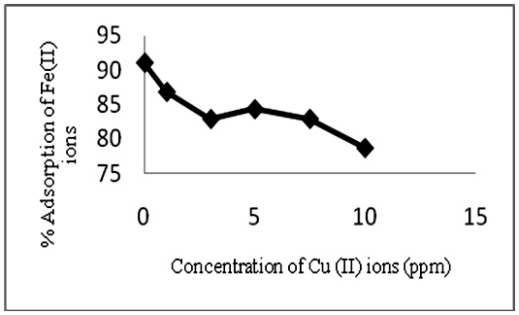


Fig. 1 Effect of Cu^{2+} ions on % adsorption of Fe^{2+} ions

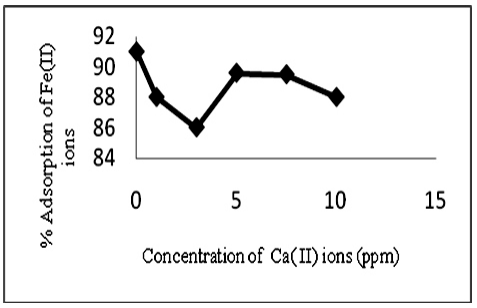


Fig. 3 Effect of Ca^{2+} ions on % adsorption of Fe^{2+} ions

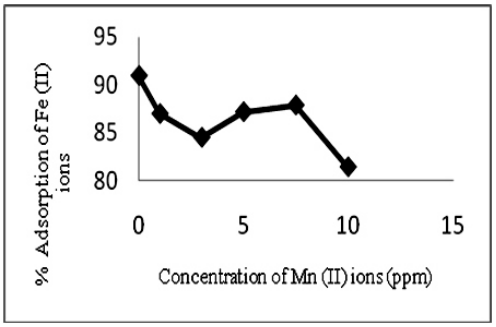


Fig. 2 Effect of Mn^{2+} ions on % adsorption of Fe^{2+} ions

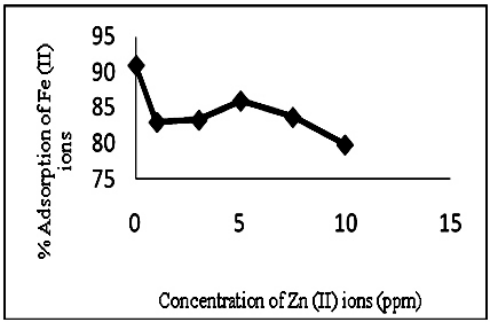


Fig. 4 Effect of Zn^{2+} ions on % adsorption of Fe^{2+} ions

adsorption of Fe^{2+} ions at 5 ppm of Cu^{2+} ions concentration. Fig.2 depicts effect of concentration of Mn^{2+} ions on percentage adsorption of Fe^{2+} ions. Initially at 1 ppm of Mn^{2+} ions concentration the percentage adsorption was observed 87% and after this concentration, percentage adsorption was observed to slightly decrease at 3 ppm concentration of Mn^{2+} ions. Again it increases from 5 ppm to 7.5 ppm concentration of Mn^{2+} ions. After 7.5 ppm concentration of Mn^{2+} ions percentage adsorption was rapidly decreased. The results depicted in Fig. 3 reveals the effect of concentration of Ca^{2+} ions on percentage adsorption of Fe^{2+} ions on Cuscuta powder from aqueous solution. It indicates that initially the percentage adsorption of Fe^{2+} ions was observed 91.0% which decreased with the increase of concentration of Ca^{2+} ions in upto 4.0 ppm. Thereafter Fe^{2+} ions adsorption increases up to 5 ppm concentration of Ca^{2+} ions. Fig. 4 depicts the effect of concentration of Zn^{2+} ions on percentage adsorption of Fe^{2+} ions on Cuscuta powder from aqueous solution. The experimental results indicated that in the absence of any co-metal ions the percentage adsorption of Fe^{2+} ions on Cuscuta powder was 91.0% for 10 ppm Fe^{2+} ions concentration and 1g adsorbent dose. It may change for lower concentration of adsorbate solution. The effect of Zn^{2+} ions concentration on the percentage adsorption of Fe^{2+} ions was found that % adsorption of Fe^{2+} ions was decreased from 91.0% to 83% with the increase of Zn^{2+} ions concentration from 0 to 4 ppm in adsorbate solution.

Conclusion

All these co- metal ions which were studied have affected the adsorption of Fe^{2+} ions differently. In binary systems, the metal ions affected the adsorption of Fe^{2+} ions on Cuscuta powder in the following order; $Cu^{2+} > Zn^{2+} > Mn^{2+} > Ca^{2+}$.

Refrences

[1] U. Farooq, J. A. Kozinski, M. A. Khan and M. Athar, Bioresource Technology, 101(14) (2010) 5043.

[2] N. Das, Hydrometallurgy, 103(1-4) (2010) 180.

[3] T. A. Davis, B. Volesky and A. Mucci, Water Research, 37(18) (2003) 4311.

[4] G. Crini, Progress in Polymer Science, 30(1) (2005) 38.

[5] D. Kratochvil and B. Volesky, Water Research, 34(12) (2000) 3186.

[6] B. Volesky, Hydrometallurgy, 59(2-3) (2001) 203.

[7] Burke, A., Elvan, Y. and Nesrin, H.; Turk J. Med. Sci. 30 (2000) 341.

Evaluation of Photosynthetic Efficiency of some Phosphorus Tolerant and Susceptible Rice Varieties using $^{14}C(NaH^{14}CO_3)$ as a Tool

Pradeep K Shukla[1], Pragati Misra[1,2], Narayani Shukla[3], NavoditaMaurice[4], Bhupinder Singh[5] and R.C. Pant[6]

1. *Department of Biological Sciences, School of Basic Sciences, Sam Higginbottom Institute of Agriculture, Technology and Sciences (Deemed to be University), Allahabad, Uttar Pradesh, India; E-mail: narayanshukla00@gmail.com*
2. *Department of Tissue Engineering, Jacob School of Biotechnology and Bioengineering, Sam Higginbottom Institute of Agriculture, Technology and Sciences (Deemed to be University), Allahabad, Uttar Pradesh, India*
3. *Department of Biochemistry and Biochemical Engineering, Jacob School of Biotechnology and Bioengineering, Sam Higginbottom Institute of Agriculture, Technology and Sciences (Deemed to be University), Allahabad, Uttar Pradesh, India*
5. *Nuclear Research Laboratory, I.A.R.I., Pusa, New Delhi*
6. *Kumaon University, Nainital, Uttaranchal*

Introduction

"The most precious things are not jades and pearls but the five grains". The five referred to in this Chinese saying are most likely to be rice, wheat, millet, sorghum and maize.Rice is grown on all continents except Antarctica. Demand for rice is expected to grow faster than production in most countries. Approaches to bridging the gap between projected demand and the current level of production include expanding the rice area (horizontal expansion), increasing yield (vertical expansion), bridging the yield gap and reducing the losses [4,10]. Rice culture is thus the cornerstone of cultural, social and economic development in Asia[5].Rice like any other cereal requires considerable quantity of phosphorus for vigorous growth and high grain yield. Rice like many other grass plants does not readily exhibit the distinct purple (anthocyanin formation) associated with phosphorus deficiency. Phosphorus has a stimulatory effect on crop growth yield and uptake [8]. Phosphorus deficiency is associated with the nucleic acid, physiological processes such as photosynthesis and respiration and biozyme. Phosphate (Pi) plays a central role as reactant and effector molecule in plant cell metabolism. In plants, phosphate plays a pivotal structural and regulatory role at the nexus of photosynthesis, energy conservation and carbon metabolism. However, Pi is the least accessible macronutrient in most of the ecosystems and its low availability has profound consequences for plant growth and physiology [2]. Phosphorus deficiency is a widespread nutritional problem greatly affecting crop production. It is estimated that 5-7 billion hectares of land (equivalent to about 67% of total farmland used worldwide) contains too low level of plant available phosphorus which is limiting crop production in many world regions [3].Genotypic differences in nutrient acquisition are important determinants of nutrient supply [9]. Cultivar improvement for tolerant nutrient use can complement agronomic approaches. Improved screening techniques related to specific mechanisms of nutrient efficiency will facilitate genetic improvement [7]. Photosynthesis is of vital interest to the survival of life on our planet. The relationship between photosynthesis and mineral nutrient supply is complex. Although mineral deficiency may impact growth rapidly, certain leaves on the plant may be able to continue photosynthesize at high rates.

Materials and Methods

On the basis of phosphorus content (%) in grains, leaves and straw, extracted from phosphorus deficient and phosphorus sufficient soils the varieties UPRI-95-49, Tilakchandan, Babunand and Narendra 359 were considered to be phosphorus tolerant whereas, varieties UPR-2284-9-2, UPR-2253-4-1-1, IR-30 and Saket-4 were considered phosphorus susceptible. These varieties were further used for RuBisco Characterization studies using $^{14}C(NaH^{14}CO_3)$ as a tool.RuBisco activity was estimated essentially as described by Fair et al. [6]. The three replicates of leaf samples were pooled so as to obtain about 500 mg of leaf material. 500 mg of freshly harvested leaves were ground with extraction buffer (50 mMTrisHCl, 1mM EDTA, 1mM PMS and 0.1% BSA) and centrifuged. The enzyme present in the supernatant was activated by incubating the extract at room temperature with activation buffer (5mM Glutathione, 0.1mM EDTA, 50mM Tris-HCl, 10 mM $MgCl_2$ and 10mM $NaHCO_3$). Assay medium (30 M TrisHCl, 3.03 M $MgCl_2$, 0.1 M EDTA, 0.2 MRuBP, $NaH^{14}CO_3$ Specific activity 125.17GBq mol^{-1}) without RuBP served as blank for each assay. The reaction was started by addition of RuBP in vials and terminated after 10 min with the addition of 0.2 mL of 6N acetic acid. The contents of vials were evaporated to dryness at 65^0C. The acid stable ^{14}C was subsequently counted in a liquid scintillation counter (Packard TRICARB-model 1600TR, Meriden, USA) after adding 10 mL of scintillation fluid (4 g PPO and 100 mg POPOP in 1litre toluene).

Polyacrylamide Gel Electrophoresis (Native PAGE) of RuBisco

Partially purified RuBisco was run along with the crude extract protein in the crude extract was separated on a 6% native PAGE with discontinuous electrophoresis buffer. 4% stacking gel was used. An electrophoretic current of 10 mA was applied initially and then increased to 30 mA. The gel was run under refrigerated conditions. After full run, the gel was removed and stained overnight with 0.1% (w/v) CBB (R-250). The gels were destained in 3% (w/v) NaCl solution.The amount of RuBisco protein was estimated by cutting the stained band of RuBiscoholo-protein from the non-denaturating gels and extracting in 4 cm of 1% (w/v) aqueous SDS solution for 24h at 4^0C in a shaking water bath. The absorbance was measured at 585 nm and the amount of RuBisco was determined. RuBisco subunits, large and small, were separated according to the method of Mummenhoff and Hurka [1] using SDS-PAGE on 12% resolving gel. Rest of the procedure was similar to that used for native-PAGE.

Experimental Results

Native PAGE Analysis of RuBisco

The results showed thatRuBisco bands in phosphorus susceptible cultivars were less intense as compared to the tolerant cultivars. The RuBisco bands were isolated and used for SDS-PAGE analysis for subunit separation in phosphorus tolerant and susceptible varieties. Large sub unit (LSU) and small sub unit (SSU) were separated using SDS-PAGE analysis. Molecular size of LSU and SSU was confirmed comparing with protein marker (PMW-B). LSU of phosphorus susceptible varieties were less intense as compared to tolerant varieties. In case of zinc LSU showed similar intensity in tolerant and susceptible varieties. SSU showed similar intensity in all varieties.

Soluble leaf protein content, RuBisco content and activity in phosphorus tolerant and phosphorus susceptible varieties

The data showed a significant variation among all the varieties in all the traits. Varieties Babunand and Saket-4 showed the maximum and the minimum protein content whereas varieties UPR-95-49 and UPR-2284-9-2 showed the maximum and the minimum RuBisco content. RuBisco activity was found maximum in UPRI-95-49 and the minimum in UPR-2253-4-1-1. Specific activity was found the maximum in UPRI-95-49 and minimum in IR-30. All the values were higher in case of tolerant varieties when compared to susceptible varieties.

Summary

The varieties (UPRI-95-49, Tilakchandan, Babunand and Narendra 359) have shown relatively higher RuBisco content and RuBiscoactivity and shown satisfactory biochemical symptoms, which is a healthy sign for rice plants grown under phosphorus deficient conditions. These varieties, thus can, perform better photosynthesis even in low soil phosphorus conditions. These varieties can,therefore, be recommended for the phosphorus deficient soils conditions to contribute higher production.

References

[1] K. Mummenhoff and H. Hurka, Plant Syst. Evol. (1986) 281.

[2] S. Abel, C. A. Ticconi, C.A. and Delatorre, Physiol.Plant, (2002) 1.

[3] Cakmak, Plant Soil, (2002) 3.

[4] R.C. Chowdhary, Int. Rice Commission Newsletters, (2000) 22.

[5] T. Fairhurst and A. Dobermann, Bettre crops international, (2002) 3-6

[6] P. Fair, J. Tew, and C.F. Creswell, Ann. Bot. (1973) 831.

[7] H.R. Lofffite, Field Crop Res..56 (1998) 223.

[8] N.D. Majumdar, Oryza., (1995) 83.

[9] H. Marschner, Field Crop Res, (1998) 203.

[10] Li YueNa, HouliGang, Qi Chun Yan, Sun Hong Jiao, Liu Liang, Sui Peng Ju, Guo Xi Miang, Zhzo Guo Chen Agricultural Science & Technology - Hunan, (2010) 11.

Investigation of Liquid-Solids Fluidized Bed of Different Particle size through Radioactive Particle Tracking Techniques

Shubham Jain[1], Priyam Saraswat[1], Harish J. Pant[2] and Rajesh K. Upadhyay[1]

1. *Department of Chemical Engineering, Indian Institute of Technology Guwahati, Guwahati 781039, Assam, India*
2. *Isotope Applications and Radiopharmaceuticals Division, Bhabha Atomic Research Centre, Trombay, Mumbai 400085, India; E-mail: rkupadhyay@iitg.ac.in*

Radioactive particle tracking technique (RPT) has proven to be a powerful and versatile technique both in terms of the richness of information it provides as well as the variety of multiphase flow situations it has been successfully employed. This work reports the execution of RPT technique for investigation of liquid-solid fluidized bed of different particle sizes (1.2 mm and 0.6 mm). Experiments are performed in a 10 cm ID cylindrical column for different liquid velocities. Further, radioactive particle tracking (RPT) experiments are performed for both the solids and effect of liquid velocity and particle size on flow behaviour of bed is quantified.

Introduction

Liquid-solids fluidized beds are widely used in chemical, petrochemical, food, biological and many other industries [1]. Despite of wide application and usage in many industries, the design of liquid solids fluidized bed is mainly depends on empirically developed model due to poor understanding of fluid-particle and particle-particle interactions. The effective design and scale-up of liquid-solids reactor mainly depends on accurate measurement and prediction of flow profiles and mixing characteristics of solids as a function of liquid velocity [2]. However, at present these understanding are far from the complete mainly due to the lack of suitable measurement techniques. Large presence of solids (volume fraction of solids >30-40%) in liquid-solid fluidized bed preclude the use of optical based techniques like LDA (Laser Doppler Animonetry) or PIV (Particle Image Velocimetry).

In current work, a non-invasive radiation based measurement technique, Radioactive Particle Tracking (RPT) [3], is implemented on a liquid solids fluidized bed to decipher the complex flow characteristics of these beds. Further, effect of liquid velocity on mixing characteristic of these beds is investigated. Finally effect of particle size on behavior of liquid-solid fluidized bed is quantified by tracking different size of tracer particle used in RPT experiments.

Experimental Setup and Technique

Experiments are performed in 10 cm ID and 1.5 m long perspex column. A perforated plate liquid distributor having holes of 1 mm diameter on a square pitch with 6 mm centre to centre distance is used in all the experiments. The liquid flow rate is regulated with the help of a rotameter. A 600 mesh size filter cloth is used above the distributor to prevent the particles from falling into the calming section. Glass beads of two different sizes, 1.2 mm and 0.6 mm, having density 2500 kg/m^3 is used as a solid and water having density 998 kg/m^3 is used as a liquid phase. Figure 1 shows the photograph of liquid-solid fluidized bed used in current study with RPT test facility.



Fig. 1 Photograph of experimental setup with RPT test facility

In the RPT technique, a single radioactive particle (a gamma ray source) is used as the marker of the phase whose velocity field is to be mapped. In current study, SC-46 embedded in glass beads is used as a tracer particle to track the motion of glass beads present in the bed. The motion of this tracer particle is catechize by an array of scintillation detector (NaI(Tl)) which are strategically placed around the vessel of interest. In current study total 8 number of scintillation detectors are used to record the photon counts emitted by the tracer particle during its path. Subsequently, a suitable reconstruction algorithm is used to decipher the Lagrangian tracer of the tracer particle from the

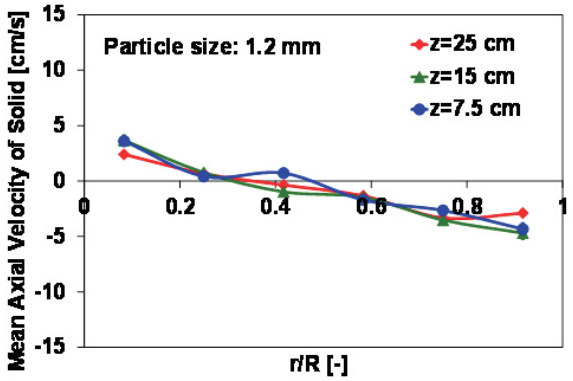


Fig. 2 Variation in mean axial velocity of solids with column diameter at different axial locations (U=0.03 m/s; U/U_{mf} = 3)

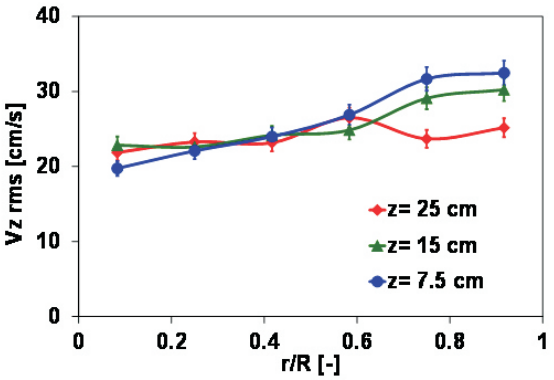


Fig. 3 Variation in axial rms velocity of solids with column diameter at different axial locations (U=0.03 m/s; U/U_{mf} = 3)

recorded information. Further, the instantaneous velocity time series, mean velocity fields, kinetic energies of the turbulence, shear stresses, dispersion coefficients and other parameters that represent the prevailing flow regimes and flow characteristics are evaluated [4].

Results

Experiments are performed in a liquid-solids fluidized bed for different superficial velocities of liquid and different solid sizes to quantify the effect of inlet fluid velocity and particle size on hydrodynamic behavior of fluidized bed. For all the cases RPT experiments are performed by tracking one particle at a time. Figure 2 shows the variation in mean axial velocity of solids (glass particle of size 1.2 mm) with column diameter at three different axial locations for a liquid velocity 0.03 m/s (at $U/U_{mf} = 3$). Results indicate that solid is moving upward near the centre of the column and falling down near the wall. However, variations in solids velocity at different axial locations are minimal which is contradictory to gas-solids fluidized bed. This suggests that liquid-solid fluidized bed is relatively homogeneous and well mixed compared to gas-solids fluidized bed.

Figure 3 shows the variation in axial rms velocity of solids with non-dimensional column radius at different axial location. It is found that unlike mean axial velocity rms velocity of solids is not same at all position. Axial rms velocities are higher near the wall compared to the centre of the column. Further, near the wall axial rms velocity is also a function of axial location in the bed. This suggests that though in time averaged sense bed looks calm and homogeneous, actually it is not and there are significantly higher fluctuations near the wall.

Owing to constraints of space, only some typical results have been reported here. The final submission would contain detailed discussion of the results obtained from the RPT experiments for different fluid velocities and different particle sizes.

Conclusion

In present work, RPT technique is implemented on liquid-solids fluidized bed to understand the complex flow behavior and mixing characteristics of such reactors. Experiments are performed for different fluid velocity to cover the flow regime important for industrial applications. Experiments are performed for different U/U_{mf} ratio varied from 3 to 5. Further effect of particle size on flow behavior is also investigated by using two different sizes of glass beads 0.6 mm and 1.2 mm. Finally, a detailed analysis RPT data is done to quantify the effect of fluid-particle and particle-particle interaction in liquid-solids fluidized bed. Due to limitation of space only few results are presented here. In the full contribution details of all the experimental result will be presented.

References

[1] N. Epstein, International Journal of Chemical Reactor Engineering 1 (2003) R1.

[2] M.P. Dudukovic, Science 325 (2009) 698.

[3] R.K. Upadhyay and S. Roy, Can. J. Chem. Eng. 88 (2010) 601.

[4] R.K. Upadhyay, H.J. Pant and S. Roy, Chem. Eng. Sci. 96 (2013) 152.

Nanocrystalline Zirconia: A Viable Adsorbent for the Column Chromatography Separation of ^{58}Co from Neutron Irradiated Nickel Targets

K.V. Vimalnath, S. Priyalata, Ramu Ram, S. Chakraborty, Rubel Chakravarty, A. Dash

Isotope Application and Radiopharmaceuticals Division, Bhabha Atomic Research Centre, Trombay, Mumbai 400085, India; E-mail:adash@barc.gov.in

We describe a method for the production of no carrier added (NCA) ^{58}Co, which consists of neutron irradiation of natural Ni target followed by column chromatographic separation of ^{58}Co using tetragonal nano zirconia (t-ZrO_2)as the adsorbent. A careful scrutiny of the adsorption parameters of t-ZrO_2 was carried out and implemented to arrive at a conditions resulting optimum retention of ^{58}Co on a tiny column containing t-ZrO_2 followed by elution of ^{58}Co in 0.01 M HCl. The developed procedure was validated using real samples. The overall recovery of ^{58}Co was >90% with appropriate radiochemical and radionuclide purity.

Introduction

There is a great deal of interest in the use of ^{58}Co ($T_{½}$ = 71.3 d) for the preparation of positron sources [1] and diagnosis of pernicious anemia by administration of ^{58}Co labeled vitamin B12 [2,3] owing to its favorable nuclear decay characteristics. ^{58}Co decays to an excited state of ^{58}Fe by positron emission [E^{+}_{max} = 0.474 MeV (99.92 %)] and by the electron capture process. In order to meet the local demand, development of an indigenous technology for the production of ^{58}Co was felt necessary and pursued. No carrier added (NCA) ^{58}Co is produced in a research reactor by ^{58}Ni(n,p)^{58}Co reaction. ^{58}Ni has a natural abundance 68.077% isotopic composition and the fast neutron cross section of 0.297 b for (n,p) reaction at 3.7 MeV neutron energy. In the light of perceived need to perform the radiochemical separation of ^{58}Co from irradiated Ni in a remotely operated shielded enclosure, the scope of using column chromatography separation technique is not only an interesting proposition but also viewed as a necessity. In the quest for an effective adsorbent to perform the aforementioned separation, our interest was focused towards nano-zirconia (t-ZrO_2) whose pH dependent surface properties features can provide an opportunity to suit our requirement. This concept was simplified in our work directed towards the development of a viable chromatographic technique for the separation of ^{58}Co from irradiated Ni. In this communication, we describe an overview of reactor production of ^{58}Co, the overall separation procedure and assessment of the quality of the ^{58}Co.

Experimental

Materials

All reagents used were of analytical grade and were procured from reputed manufacturers. For radiotracer experiments and determination of distribution ratio (K_d) NCA ^{57}Co and ^{63}Ni were used. NaI (Tl) scintillation counter, HPGe-MCA detector coupled with a multichannel analyser (MCA) was used for radioactivity determination in various experiments.

Nano-zirconia (t-ZrO_2) was synthesized by controlled hydrolysis of zirconium oxy chloride solution in alkaline medium as per the reported procedure [4]. Distribution ratios (K_d) of Co and Ni at different pH were determined using ^{57}Co and ^{63}Ni radiotracers following the reported procedure [5].

Neutron Irradiation of Ni Target

1 g of metallic powder nickel target of natural isotopic composition was weighed, packed in an aluminum container, sealed by cold press welding and irradiated in Dhruva research reactor at a fast neutron flux of 1.13×10^{12} n.cm^{-2}.s^{-1} for 90 days.

Radiochemical Processing and Separation of ^{58}Co

In view of radioactive nature of neutron irradiated Ni target, radiochemical processing was carried out in a 100 mm thick lead shielded isotope processing facility to evade radiation exposure. Al can containing irradiated nickel target was cut open and retrieved into a dissolution flask. The target was dissolved in 30 mL conc. HCl by refluxing for two hours to enable complete dissolution of the powder. The dissolved solution was evaporated to dryness, reconstituted with 20 mL of 10 M HCl and passed through a borosilicate glass column [15 cm (l) × 0.8 cm ( )] containing 3 g of the t-ZrO_2 preconditioned with 10 M HCl. The column containing ^{58}Co was washed with 20 mL of 10 M HCl solution to remove loosely held Ni. The effluent containing radioactive nickel was collected and preserved for recovery of ^{63}Ni. Subsequently, ^{58}Co retained on the column was eluted with 10 mL of 0.01 M HCl, concentrated to ~5 mL and its radioactivity content and radionuclide purity ascertained by gamma ray spectrometric measurement of suitably diluted aliquots for appropriate time at a suitable geometry in a HPGe detector coupled to MCA system.

Results and Discussion

Typically, in one batch about 130 MBq (3.5-3.8 mCi) ^{58}Co could be produced by irradiating 1 g nickel target. In order to dissolve the irradiated metallic nickel target, conc. HCl was preferred to HNO_3 as $NiCl_2$ is not volatile compared to $Ni(NO_3)_2.6H_2O$. Dissolution of Ni in HCl took place according to the following reaction

$$Ni_{(s)} + 2HCl_{(aq)} \quad NiCl_{2(aq)} + H_{2(g)} \qquad (1)$$

Neutron irradiated nickel target dissolves slowly in hydrochloric acid and therefore it was necessary to reflux the solution for two hours to obtain a clear green solution of nickel chloride.

Results of the structural characterization studies revealed that t-ZrO_2 consisting of primary particles of size about 6-10 nm [5]. In light of the explicit need to realize the scope of using t-ZrO_2 as the adsorbent for the column chromatography separation of ^{58}Co from irradiated Ni, their distribution ratio (K_d) at different acidity were determined and results obtained are summarized in Table 1. The K_d value which account for a myriad of chemical and physical adsorption process is important to arrive at the optimum conditions not only for the selective retention of ^{57}Co ion on t-ZrO_2 but also for their subsequent elution.

Table-1: Distribution ratio (K_d) of ^{57}Co and ^{63}Ni in hydrochloric acid solution

HCl concentration (M)	K_d	
	^{57}Co	^{63}Ni
0.01	No uptake	0.2± 0.1
0.1	No uptake	0.1± 0.1
0.5	0.2± 0.1	0.1± 0.1
1	0.2±0.1	0.2± 0.1
2	0.1± 0.1	0.1± 0.1
3	0.4±0.2	0.1 ± 0.05
4	1.9± 0.4	No uptake
5	2.5 ± 0.5	No uptake
6	2.9 ± 0.6	No uptake
7	5.17 ± 0.8	No uptake
8	16.62 ± 1.8	No uptake
9	26.87 ± 2.3	No uptake
10	38.4 ± 3.1	No uptake

From the above results, it is inferred that uptake of the Co and Ni ions on t-ZrO_2 is strongly influenced by the acidity of the adsorbing solution. A careful scrutiny of the Table 1 indicated that at 10 M HCl, the K_d values of Co are maximum and Ni has no uptake indicating the scope for separating microscopic amount of no-carrier added' (NCA) ^{58}Co from macroscopic amount of Ni at this acid concentration. However, equally important is the negligible K_d value of ^{58}Co in 0.1M HCl that offers the possibility for elution using this reagent.

This concept was simplified in our work and process demonstration run was performed using neutron irradiated Ni to evaluate the behavior of the adsorbent in the presence of intense radiation environment with the radiolytic products generated. It was seen that quantitative retention of ^{58}Co was possible under the described experimental condition. Washing of the column with 10 M HCl was essential to remove loosely held Ni. ^{58}Co retained on the column was successfully eluted using 0.1 M HCl. A reproducible elution efficiency of 85-95% has been achieved.

t-ZrO_2 can be considered to consist of discrete metal oxide clusters covered by surface hydroxyl groups. At low pH, these hydroxide groups become protonated and the material surface develops a positive charge. At acidic pH, there is a strong attractive interaction between the positively charged t-ZrO_2 surface and the negatively charged chloro complex [$(CoCl_6)^{3-}$] species of cobalt from the liquid solution and thus gets retained by the sorbent. At 0.1 M HCl, Co mostly exist as Co^{3+}, not retained by the positively charged surface of t-ZrO_2 and gets eluted.

About 130 MBq (3.5 mCi) ^{58}Co per batch could be successfully recovered. Owing to the low reaction cross-section (= 0.297 barn), only low yields of cobalt-58 could be produced by this route. A notable advantage of this procedure is that it provides NCA ^{58}Co and the procedure is amenable for operation in a remotely operated shielded cell. Since natural Ni contains 26% ^{60}Ni, (n,p) reaction on ^{60}Ni would produce ^{60}Co. Owing to the long half life (5.27 year) and low reaction cross section, its contribution in the final product is marginal.

Conclusion

The utility of nano crystalline zirconia as an effective sorbent in the column chromatography separation of ^{58}Co from neutron irradiated nickel metal targets has been successfully exploited and demonstrated. Given the simplicity of using column chromatographic technique and the ability to achieve necessary recovery yield, the reported technique would serve in good stead for realizing regular production ^{58}Co adaptable to the existing and foreseeable demands.

Acknowledgements

The authors sincerely thank Shri J. Udhayakumar, IA&RPhD, BARC for providing NCA ^{57}Co radiochemical for studies pertinent to determination of K_d values. The authors acknowledge the help extended by Dr. S. V. Thakare and Shri K. C. Jagadeesan towards irradiating nickel targets in Dhruva research reactor.

References

[1] R. S. Vallery, et al., Nucl. Instr. Meth. Phy. Res A 353 (1994) 16.

[2] M. S. Pathy, S. Kirkman, M. J. Molloy, J. Clinic. Path., 32 (1979) 244.

[3] K. Hjelt, P.A. Rasmussen, O. Munck, Acta. Medi. Scand. 201(1977)167.

[4] S. F. Yin, B. Q. Xu, Chemphyschem. 3 (2003) 277.

[5] R. Chakravarty, R. Shukla, A.K. Tyagi, A.Dash, Chromatographia. 72(2010) 875

Investigation on the Influence of Metal Ion Impurities on the Complexation behavior of Generator Produced ^{90}Y with bifunctional Chelators

Usha Pandey, Naresh Gamre, Ashutosh Dash*

Isotope Applications & Radiopharmaceuticals Division, Bhabha Atomic Research Centre, Trombay, Mumbai 400085, India; E-mail: adash@barc.gov.in

The ^{90}Sr/^{90}Y generator is the exclusive source of 'no carrier added' ^{90}Y for targeted therapy. However, the concomitant presence of trace metals diminishes the complexation of ^{90}Y with bifunctional chelators (BFCs). A systematic investigation was performed to evaluate the influence of trace metals on the complexation of ^{90}Y (from an electrochemical generator) with BFCs such as p-SCN-Bn-PCTA, p-SCN-Bn-DTPA and p-SCN-Bn-DOTA. Our study indicates that while p-SCN-Bn-DTPA was least affected by most of the trace metals studied, p-SCN-Bn-PCTA was most sensitive to their presence and hence could be the ligand of choice for assessing the chemical purity of generator derived ^{90}Y.

Introduction

Yttrium-90 is an important radionuclide used for targeted therapy due to its attractive nuclear properties. ^{90}Sr/^{90}Y generator is the only source of 'no carrier added' ^{90}Y for receptor-targeted therapy as radiolabeled biomolecules are required at high specific activities. The chemical purity of ^{90}Y is very critical for receptor targeted agents as there are only 1.8 ng of yttrium ions in 37 MBq (1 mCi) of ^{90}Y in solution [1] due to which competing metal ions even at ppb levels reduce the ^{90}Y complexation yields with the ligands. A systematic investigation was carried out on the influence of trace metal ions on the complexation yields of ^{90}Y with the BFCs para isothiocyanato benzyl 3,6,9,15-tetraazabicyclo [9.3.1]pentadeca-1(15),11, 13-triene-3,6,9-triacetic acid (p-SCN-Bn-PCTA), para isothiocyanato benzyl diethylene triamine pentaacetic acid (p-SCN-Bn-DTPA) and para isothiocyanato benzyl 1,4,7,10-tetraaza cyclododecanetetraacetic acid (p-SCN-Bn-DOTA).

Experimental

Complexation of ^{90}Y with the ligands p-SCN-Bn-DTPA, p-SCN-Bn-DOTA and p-SCN-Bn-PCTA

Yttrium-90 for the work was obtained from the in-house ^{90}Sr/^{90}Y electrochemical generator [2]. Complexation of ^{90}Y with the BFCs p-SCN-Bn-PCTA, p-SCN-Bn-DTPA and p-SCN-Bn-DOTA was carried out in acetate buffer at pH ~4.0 using carrier $^{89}YCl_3$ equivalent to 3.7 GBq (100 mCi) of $^{90}YCl_3$ and 37 MBq of $^{90}YCl_3$ using 20 L of the respective ligand solution (1 mg/mL, corresponding to a yttrium to ligand molar ratio of about 15). All the reactions were carried out for 30 min. at 80ºC. These reactions were taken as reference reactions to study the influence of trace metal impurities on the complexation yields.

To determine the influence of trace metallic impurities (Al(III), Co(II), Cu(II), Fe(III), Zn(II) and Zr(IV) on the radiolabeling yields of ^{90}Y complexes with the ligands, each trace metal was added separately in concentrations ranging from 1 to 100 ppm to the buffered solution of [$^{89+90}$Y]yttrium chloride and the ligand. All other reaction parameters were maintained as in the control reaction (absence of trace metals). Characterization of ^{90}Y complexes as well as determination of percentage radiolabeling yields was carried out by HPLC and paper chromatography techniques. HPLC was carried out on a C18 RP column using water and acetonitrile with 0.1% trifluoroacetic acid in a gradient mode of elution. All the radiolabeling reactions were also followed using paper chromatography with 50% aqueous acetonitrile as the mobile phase.

Results and Discussion

Yttrium-90 used in the work was obtained from an electrochemical ^{90}Sr/^{90}Y generator which provided ~3.7 GBq of NCA grade ^{90}Y per batch. Greater than 95% radiolabeling yield could be obtained under the standardized conditions for all the BFCs studied (in absence of trace metals). In the standardized HPLC system for characterization of the complexes, $^{90}YCl_3$ (R_t =3.0 min) could be well differentiated from ^{90}Y-DTPA, ^{90}Y-DOTA and ^{90}Y-PCTA complexes which had retention times at 3.9, 16.5 and 18.2 minutes, respectively. Figure 1 shows the HPLC radiochromatogram of ^{90}Y-PCTA complex. In paper chromatography with 50% aqueous acetonitrile as mobile phase, ^{90}Y complexes migrated towards the solvent front (R_f=0.8-1.0), while free $^{90}Y^{3+}$ remained at the point of application (R_f = 0).

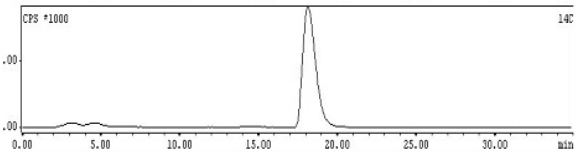


Fig. 1 HPLC radiochromatogram of ^{90}Y-PCTA complex

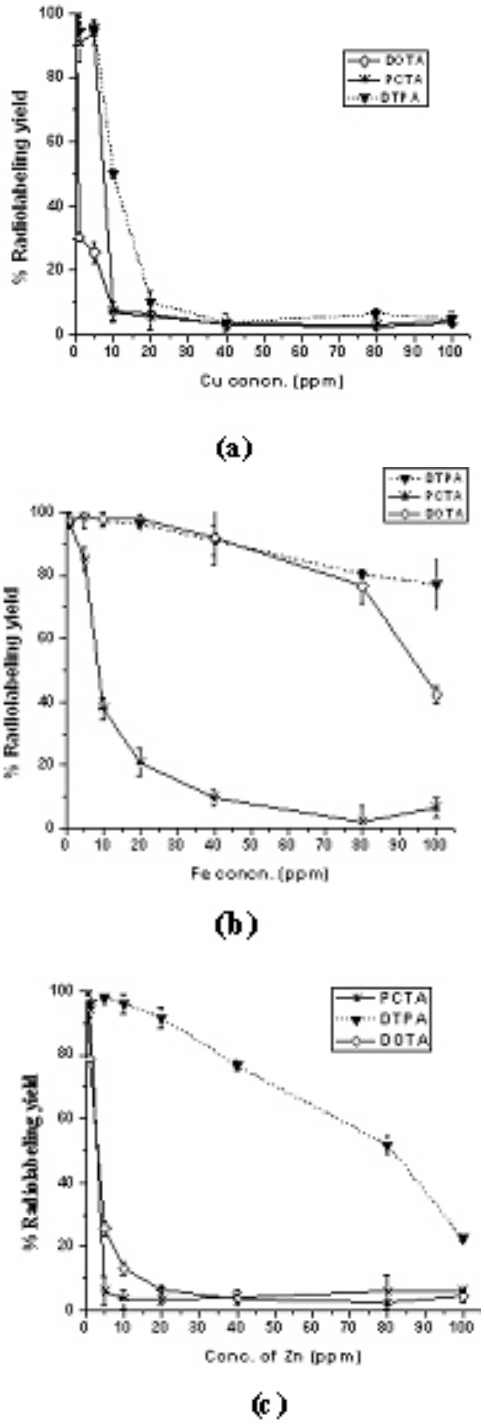


Fig. 2 Influence of (a) Cu(II) (b) Fe(III) and (c) Zn(II) on ^{90}Y complexation with bifunctional chelators

Experiments carried out to study the influence of trace metals on the complexation of ^{90}Y with the ligands showed that in case of p-SCN-Bn-DTPA, except for Cu(II) ion, ^{90}Y complexation yield was unaffected in the presence of each of the other metal ions up to 10 ppm. Most of the metal ions studied were found to interfere significantly with the yields of the ^{90}Y-DOTA complex. p-SCN-Bn-PCTA was found to be most sensitive to the presence of all the trace metal impurities studied except Al(III), most importantly Fe(III), the common metallic impurity found in solutions. Figure 2 (a-c) shows the influence of Cu (II), Fe (III) and Zn (II) ions on the complexation of ^{90}Y with the ligands. A significant point emerging from these findings is that DTPA which is presently being used to ascertain the chemical purity of ^{90}Y solutions from generators may not be the ideal ligand for such purpose. The superior behavior of p-SCN-Bn-DTPA may be due to its acyclic nature leading to facile complexation kinetics with ^{90}Y. However, it would be preferable to use PCTA for quality control owing to its extra sensitivity to the presence of trace metals in ^{90}Y solutions.

Conclusions

While studying the influence of trace metal ions on ^{90}Y radiolabeling with bifunctional ligands, it was observed that p-SCN-Bn-DTPA is least affected by the presence of trace metallic impurities while p-SCN-Bn-PCTA is the most affected and could be used for assessing the chemical purity of ^{90}Y before use for preparation of radiopharmaceuticals.

Acknowledgements

The authors are thankful to Dr. Gursharan Singh, Associate Director(I) and Head, IA&RPhD, RC&I group BARC for his encouragement and support.

References

[1] W. Lynch, R. Clement, J. Deberadinis, J. Forsyth, P. Mayer, L. Murray, L. Vekens, http://www.perkinlmer.com/CMSResources/Images/44-73824PST_Yttrium-99QualityControl.pdf

[2] R. Chakravarty, U. Pandey, R.B. Manolkar, A. Dash, M. Venkatesh, M.R.A. Pillai, Nucl. Med. Biol. 5 (2008) 245.

Sorption of Uranium (VI) by 2-Aminothiazole Functionalized Hydrogels from Aqueous Environment

N. Sivagangi Reddy[1], K.S.V. Krishna Rao[1], T.J. Sudha Vani[1], A.V.R. Reddy[2], Jayshree Ramkumar[2], P.V. Nagendra Kumar[3]

1. *Department of Chemistry, Yogi Vemana University, Kadapa 516 003, India; E-mail: drksvkrishna@yahoo.com*
2. *Analytical Chemistry Division, Bhabha Atomic Research Centre, Trombay, Mumbai, India*
3. *Department of Chemistry, GITAM University, Hyderabad, India*

Hydrogels were synthesized form N-(2-aminothiazolyl)maleamic acid (NATMA) and its copolymers for separation of Uranium (VI) in aqueous environment. Hydrogels are synthesized by free radical polymerisation by azobisisobutyronitrile (AIBN), as initiator and N,N-methylenebisacrylamide MBA, as crosslinker at 55°C. Both Uranyl ion doped and pristine hydrogels were characterized by FTIR for structural confirmation. Studied swelling properties Uranyl ion uptake, pH effect, concentration effect, kinetic studies, isotherm model fittings were studied.

Introduction

Aminothiazole functionalized matrices have found extensive applications especially in the field of separation science, analytical chemistry and biomedical applications [1-5]. Separation science involves the use of the chelating properties of the functional groups for the removal of heavy metal ions. The chelating property is taken advantage of in the sensor and electroanalytical applications which are based on the selective recognition of the target analyte by these reagents. The functional groups also impart the pH dependance nature of these matrices and this in turn has an effect on the removal of metal ions by tuning the pH of the solution.

Uranium is an important element used in the nuclear industry. There are large numbers of important issues like storage of long-term nuclear fuels in deep geological sites, which need to be understood. Separation process plays a major role in treating the radioactive effluents and also for pa concentration from low-level concentration sources. Sorption with different sorbents with enhanced uptake efficiency and selectivity is an attractive procedure adopted for treatment or preconcentration because of the advantages of high efficiency, low cost and the ability to improve selectivity by tuning the structure or functionalization of the matrices. There is always an on-going research in the development of sorbets which have high uptake capacity and selectivity. This can be achieved by increasing the number of chelating sites on the matrix as well as their accessibility. The former can be obtained by selecting ligands of small molecular size and later by altering the cross-linking of polymeric support. Numerous chelating matrices have been reported for their use in the separation of toxic heavy metal ions. Chelating resin with S and N as donor atoms usually has excellent adsorption properties for Uranyl ions [6,7].

In this paper, a comprehensive method developed for the removal of uranium from contaminated soils and wastes has been discussed.

Experimental

Synthesis of the Hydrogels

Reagents used for the synthesis of the hydrogels namely acrylamide (Am), hydroxyl ethylacrylate (HEA), and N-(2-aminothiozolyl) maleamic acid (NATMA) were obtained from EMerck and used as such. The synthesis was carried out by free radical polymerisation at 55°C using Azobisisobutyronitrile (AIBN) as initiator and N-N' methylenebisacrylamide (MBA) as crosslinker. The formed hydrogels were kept in double distilled water in order to remove the unreacted monomers for about a week by changing the water. Then the hydrogels were dried in vacuum oven at 45°C.

Swelling Studies

The swelling characteristics of the hydrogels were studied as follows. The hydrogel samples were dried to obtain xerogels. Known weighed amounts of the xerogels were immersed in 500 mL of double distilled water at 25°C. At specific intervals of time, the swollen hydrogels were weighed after the surface of the gels was air dried. This was repeated until no significant change of weights was observed. Swelling ratio (Q_s) was calculated by following equation, wherein W_s is the weight of the swollen hydrogel and W_d is the weight of the dried hydrogel.

$$Q_s \quad \frac{W_s \quad W_d}{W_d} \qquad (1)$$

Effect of pH on swelling was studied by adjusting the pH of the double distilled water using HCl, NaOH.

Uranyl Ion Uptake Studies

The sorption studies of the Uranyl ion on the NATMA hydrogels were carried out by batch mode equilibrating 30 mL of 300 ppm Uranyl ion solution maintained at pH 6 with 0.05 g of NATMA hydrogels. Various factors like pH, equilibration time and initial metal ion concentration were varied and the results

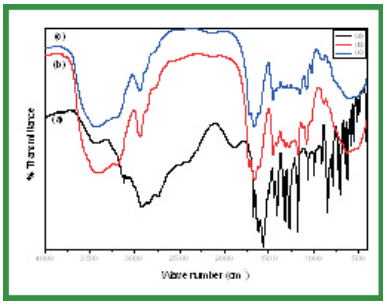
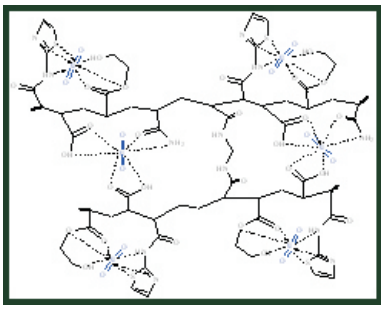


Fig. 1 FTIR spectrum (a) NATMA monomer, (b) NATMA hydrogel and (c) Uranium (VI) adsorbed NATMA hydrogel



Scheme I Schematic representation of possible complexation of NATMA hydrogel with

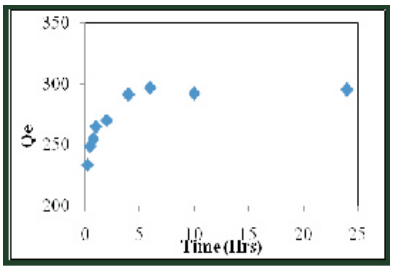


Fig. 2 Effect of contact time on Uranium (VI) sorption

were analyzed. The effect of pH on the uptake was studied in the pH range of 3-9, keeping the equilibration time of 24 h. The amount of uranyl ion left behind in solution was determined spectrophotometrically. The results are based on the average of three replicate measurements. The effect of time of equilibration was studied by equilibrating the uranyl ion solution for different time intervals and the resuidual uranyl ion concentration in solution was determined.

Results and Discussion

The synthesized hydrogels were characterized by IR and degree of swelling. The maximum % of equilibrium swelling was found to be 1112. The IR spectra of the hydrogels, monomers, and Uranium (VI) adsorbed hydrogels are given in Fig. 1. FTIR of NATMA showed characteristic absorption bands at 3450, 2616 cm^{-1}, 1720 cm^{-1}, 1665 cm^{-1} which are assigned to hydroxyl stretching vibrations, carbonyl stretching vibrations, carboxylic acid groups and amide, respectively. Additional characteristic absorption bands of monomer appear at 1449 cm^{-1} and 1301 cm^{-1} due to C-C multiple bond stretching and C-H bending vibrations, respectively. From the spectrum of hydrogel we observed the peak at 1665 cm^{-1} corresponds to -NH- and the peak at 2955 cm^{-1} corresponds to aliphatic -CH stretching vibration. The strong peak at 3450 cm^{-1} is due to the stretching vibrations of the -OH group. The peak at 1733 cm^{-1} is characteristic for the -C=O group of -COOH and ester groups. In the case of uranyl ion adsorbed hydrogel the -C-O bending is shifted to 1150 cm^{-1}. The strong band at 920-930 cm^{-1} confirms the stretching of uranyl ions.

The most probable complexation modes of uranyl ions with hydrogel are presented in Scheme I.

The pH variation studies showed that the optimum pH of uptake was 6. The effect of time of equilibration on uptake (Fig 2) showed that the adsorption is rapid initially and became slower with lapse of time. At the initial stage the process of sorption was fast due to the availability of abundant free sites near the surface where there is less hindrance for the approaching metal ions. Evidently hydrogels have higher sorption ability for the uptake of uranyl ions with respect to contact time all the materials reached saturation after 6 hours.

The effect of initial metal ion concentration variation on the uptake showed that with increasing concentration, the amount taken up increased and then reached saturation. The data of this result fitted well with Langmuir model and the maximum uptake capacity was calculated to be 15 mg/g which matched well with experimentally obtained value.

Conclusions

N-(2-aminothiozolyl)maleamic acid based hydrogels were synthesized and the characterization was carried out using FTIR. Hydrogels were used for removal of Uranyl ions from the aqueous solutions. Various factors like pH, initial concentration and contact time were varied to get maximum uptake. The maximum uptake capacity for uranium was 15 mg/g.

Acknowledgements

Authors gratefully thank to the Board of Research in Nuclear Sciences (BRNS) for financial support for this work (Grant No.: 2010/37C/53BRNS/2538, Dated 23-02-2011).

References

[1] Q.F. Yin, B.Z. Ju, S.F. Zhang, X.B. Wang, J.Z. Yang, Carbohyd. Polym., 72 (2008) 326.

[2] S. Dutta, A. K. Das, J. Sci. Ind. Res., 66(2007)1025.

[3] H. Berbera, G. Alpdogana, B. Asç1a, H. Yildirima, S. Sungura, Analyt. Let., 43 (2010) 2331.

[4] Z. Zhou, Y. Zheng, Q. Wang, Inorg. Chim. Acta, 394 (2013) 127.

[5] E.Sar, H. Berber, B. Asç1, H. Cankurtaran, Electroanalysis, 20 (2008) 1533.

[6] A. Raghavan, M. Santhapa J. Inrg. Nucl. Chem. 35 (1973) 3363.

[7] Y. Kobuke, I. Tabushi, T. Aoki, T. Kamaishi, I. Hagiwara, Ind. Eng. Chem. Res. 27 (1988) 1461.

On the Speciation and Site Symmetry of Uranium in $Sr_2P_2O_7$: A TRFS and Sr K-edge EXAFS Investigation

M. Mohapatra[1], A.K. Yadav[2], S.N. Jha[2], M.J. Kulkarni[1], D. Bhattacharyya[2], V. Natarajan[1] and S.V. Godbole[1]

1. *Radiochemistry Division, Bhabha Atomic Research Centre, Trombay, Mumbai 400 085, India; E-mail: manojm@barc.gov.in*
2. *Atomic and Molecular Physics Division, Bhabha Atomic Research Centre, Trombay, Mumbai 400 085, India*

Uranium speciation was carried in $Sr_2P_2O_7$ matrix by time resolved fluorescence and EXAFS technique. From the fluorescence data it was confirmed that the actinide ion gets stabilized as uranyl in the matrix at two different sites. By correlating with the EXAFS data, it was concluded that the U(VI) ions are replacing the divalent Sr ions at regular sites in SrO_9 polyhedra in the matrix.

Introduction

Time resolved fluorescence (TRF) and Extended X-ray absorption fine structure (EXAFS) spectroscopic techniques are non-invasive methods for speciation studies of metal ions. By virtue of the triple resolution of TRF technique (excitation, emission and life time), it is possible to identify multiple species present simultaneously in a system. Further, through EXAFS, not only the oxidation states, but the coordination geometry of the first and second neighboring atoms along with their numbers can be obtained.

Pyrophosphates of alkaline earth metals (especially Sr) doped with various activator ions have been in limelight recently. The interest in this matrix comes from its applications as ceramics, catalysts, ion exchange and optical materials [1-2]. Among the various actinide ions, U, Am and Cm are known to give efficient fluorescence. Uranium has many oxidation states that show fluorescence including the well known (VI) state. Further, different forms of the U(VI) state, namely uranyl ion (UO_2^{2+}), the octahedral and tetrahedral uranium groups (UO_6^{6-} ,UO_4^{2-} and U^{6+}) are also reported to have intense fluorescence emission. In view of this, speciation studies of U incorporated in $Sr_2P_2O_7$ matrix were carried out using TRF and EXAFS techniques.

Experimental

Undoped and uranium doped $Sr_2P_2O_7$ were prepared via co-precipitation route. The concentration of U in the matrix was adjusted so as to get maximum fluorescence yield and a good edge jump in EXAFS. X-ray diffraction (XRD) studies were done on the samples to check for the phase purity. TRF investigations were done on an Edinburgh FLS-900 unit. The EXAFS measurements were carried out at the dispersive EXAFS beamline (BL-8) in transmission mode at the INDUS-2 Synchrotron Source (2.5 GeV, 100 mA) at Raja Ramanna Centre for Advanced Technology (RRCAT), Indore, India [3]. For the present measurement at Sr K-edge, the Si (111) crystal polychromator has been set at a proper Bragg angle to obtain a band of energy around Sr K edge of 16105 eV.

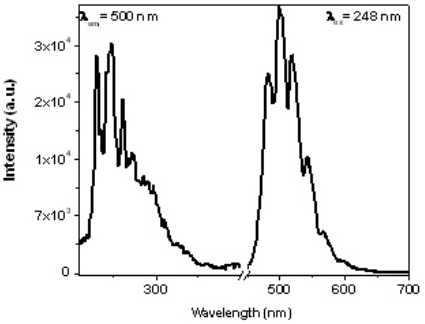


Fig. 1 Excitation and emission spectra

Results and Discussion

XRD patterns for the undoped and uranium doped samples (not showed here) matched with the standard ICDD file no-12-0362 corresponding to $Sr_2P_2O_7$ stabilized in an orthorhombic geometry.

TRF Investigations

Figure 1 shows the excitation and emission spectra of the 1 mol% U doped $Sr_2P_2O_7$ sample giving maximum fluorescence yield. The spectrum is characterized by the presence of peaks at 480, 500, 520, 540 and 565 nm. The peak at 480 nm is attributed to the zero phonon (zp) line of U(VI) and the peaks at higher wavelengths correspond to the vibrational fine structures. The observation of zp line at 480 nm and the occurrence of vibrational fine structures ($_1 \sim 830$ cm^{-1}) at room temperature indicated that U(VI) is getting stabilized as uranyl (UO_2^{2+}) in the matrix.

The luminescence decay profile of the sample (not shown here) could be fitted into bi-exponential decay of 40(fast) and 95(slow) s with 1:1 ratio suggesting the possible stabilization of the uranium at two different sites having different environments. To probe further, a TRES (time resolved emission study) study was carried out with suitable delay times and gate widths. Through this the spectral characteristics of individual species responsible for the 40 and 95 micro second life times was obtained. It can be seen from the spectra that the emission peaks corresponding to the slow decaying species are red shifted by 2-4 nm (Table 1).

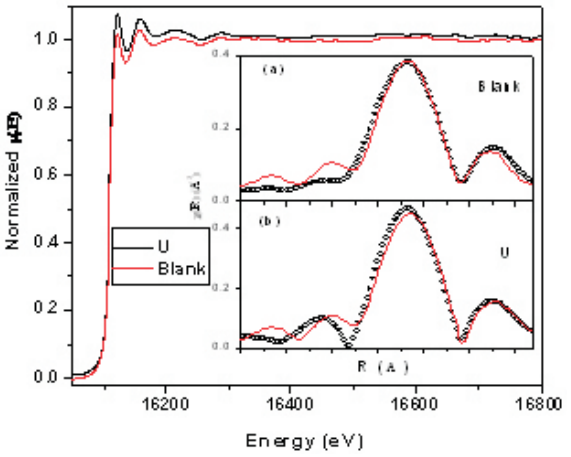


Fig. 2 Normalized EXAFS spectra of undoped and doped $Sr_2P_2O_7$; the inset figure shows the Fourier transformed EXAFS spectra at Sr K-edge (Scatter points) and theoretical fit (Solid line)

Table-1: Peak positions of the fast and slow decaying species from TRES

40 (s) Fast (nm)	482	499	519	542	568
95 (s) Slow (nm)	484	502	523	546	571

The observation of two different emission spectra confirmed the presence of the uranyl ion at two different sites.

EXAFS Investigations

Figure 2 shows the normalized EXAFS spectra ((E) versus E) for blank and U doped $Sr_2P_2O_7$. The data was analyzed using IFEFFIT software package. The inset in Fig. 2 shows (R) versus R spectra of the undoped and doped samples. The structural parameters (atomic coordination and lattice parameters) of $Sr_2P_2O_7$ used for simulation of theoretical EXAFS spectra of the samples have been obtained from reported values in the literature. The bond distances, co-ordination numbers (including scattering amplitudes) and disorder (Debye-Waller) factors (^{2}), which gives the mean square fluctuations in the distances, have been used as fitting parameters. The best fit results are summarized in Table 2.

In the pyrophosphate system, there are two types of PO_4 tetrahedrons, which are linked to each other by a corner and the P_2O_7 groups are isolated by the Sr^{2+} ions. Further, there are two types of Sr^{2+} sites in the host lattice, which are coordinated by nine 'O' atoms.

The first peak in Fourier transform spectra is due to contributions of first and second Sr-O paths at 2.47 Å and 2.60 Å respectively and the second peak is due to the contributions from Sr-O and Sr-P shells. The Debye –Waller factor in case of doped samples are less than the undoped $Sr_2P_2O_7$. It can be seen from the table that there is no change in the first peak bond lengths after U doping; however in case of second Fourier transform peak the average Sr-O and average Sr-P bond lengths are increased for U doped $Sr_2P_2O_7$. The change in the bond lengths in case of Uranium doped samples is possibly due to the smaller ionic radii (0.73 A) of U(VI) ion than Sr^{2+} (1.36 A).

Table-2: structural parameters from EXAFS

	Parameter	SPO	SPO:U
Sr-O	R (Å)	2.47	2.47
	N	1	1
	^{2}	0.012	0.0083
Sr-O	R (Å)	2.60	2.59
	N	4	4
	^{2}	0.007	0.0055
Sr-O	R (Å)	2.97	2.99
	N	2	2
	^{2}	0.0084	0.0061
Sr-O	R (Å)	3.03	3.12
	N	2	2
	^{2}	0.008	0.008
Sr-P	R (Å)	3.10	3.18
	N	2	2
	^{2}	0.012	0.01
Sr-P	R (Å)	3.19	3.18
	N	2	2
	^{2}	0.012	0.0088

Considering the ionic radii, Uranium ions are most likely to replace at regular Sr sites. As mentioned above there are two different types of SrO_9 polyhedra in the matrix and both are nine coordinated with oxygen atoms, since EXAFS will give only average behavior of both sites, based on the bond length changes it is believed that the two uranyl species are replacing two regular sites of Sr^{2+}.

Conclusion

TRFS and EXAFS techniques were used for speciation study of uranium in $Sr_2P_2O_7$. From the fluorescence excitation, emission, decay time and TRES investigations, it was confirmed that the actinide ion gets stabilized as uranyl in the matrix at two different sites. From the EXAFS data, atomic bond distances, radii and Debye-Waller factors were evaluated. From the TRF and EXAFS data, it was concluded that the U(VI) ions are replacing the divalent Sr ions at regular sites in SrO_9 polyhedra.

References

[1] S. Seyyidoglu, M. Ozenbas¸ N. Yazici, A. Yilmaz, J Mater Sci 42 (2007)6453

[2] A.N. Yazici, S. Seyyidoglu, H.Toktamis, A. Yilmaz, J. Lumin. 130 (2010) 1744

[3] S. Basu, S. Varma, A. N. Shirsat, B.N. Wani, S. R. Bharadwaj, A. Chakrabarti, S.N. Jha, D. Bhattacharrya, J. Appl. Phys 113 (2013) 043508

Studies on Evaluation of Modified TRUEX Solvent for the Partitioning of Minor Actinides

Arijit Sengupta, M.S. Murali, P.K. Mohapatra

Radiochemistry Division, Bhabha Atomic Research Centre, Trombay, Mumbai 400085, India;
E-mail: msmurali@barc.gov.in

Preliminary experiments on utilizing isodecanol as a phase modifier in place of TBP, present in the well known TRUEX solvent based on n-octyl(phenyl), N, N-diisobutyl carbamoylmethylphosphine oxide (CMPO) were conducted. It is evaluated for the extraction of trivalent Am and other actinides and a few fission products from nitric acid media. 10% (v/v) isodecanol was chosen as the phase modifier. The Acid uptake constant was determined to be 1.96 which agreed with the literature value. Isodecanol as modifier seems to play an active role in its interaction with the extractant component CMPO.

Introduction

Partitioning of minor actinides (MA= Np, Pu, Am, and Cm) is a part of an envisaged strategy of Partitioning and Transmutation for safe and long-term management of high-level wastes (HLW) originating from nuclear fuel reprocessing [1]. R&D efforts are being directed extensively in India and elsewhere for this purpose. CMPO based TRUEX solvent (0.2M CMPO + 1.2M TBP in dodecane) has been one of the best known organophosphorus reagents based on solvent extraction for the extraction of MA from HLW. Recently, other reagents commonly referred to as diglycolamides (DGAs) are also being developed [1-3]. CMPO has the advantages that there is no need of feed adjustment with respect to acidity and little or no extraction of fission products such as ^{90}Sr. However, the presence of high concentration of TBP (1.2M) in the above TRUEX solvent may be responsible (due to its uptake of acidity) for not-so- easy stripping of trivalent actinides. Long chain alcohols (e.g. Isodecanol) are attractive alternatives for TBP and are part of phase modifiers in DGA systems. The present work deals with a few initial lab-scale experiments with isodecanol as the phase modifier for CMPO for the extraction of Am(III) along with other actinides and a few fission products.

Experimental

CMPO has been synthesized in house and characterized to solvent extraction grade. Isodecanol (>98%) was procured from SISCO labs, India. The tracers ^{233}U, Pu (239 mainly), ^{241}Am, ^{99}Tc, ^{152,154}Eu etc. were used from in-house stock or BRIT (India). They were tested for their radiochemical purity and assayed (alpha or beta) by liquid scintillation counting using toluene scintillator or by NaI(Tl) detector (gamma). The aqueous phase contains appropriate concentrations of nitric acid solutions, prepared by dilution (0.01 to 6.0M) and required radioactive tracers. The oxidation state of Pu was adjusted to IV by the addition of a trace of $NaNO_2$. The equilibration of equal volumes of aqueous and organic phase solutions was carried out in a thermostated water bath. After 30minutes of mixing, phases were centrifuged and aliquots were drawn for radioassay. Distribution ratios (D) were computed as the ratio of activities present in the organic to that in the aqueous phase. The acidities of the aqueous phases were determined by standard acid-base titrations and derived those present in the organic phase by the differences from the original acidity. The error limits generally were within 5%.

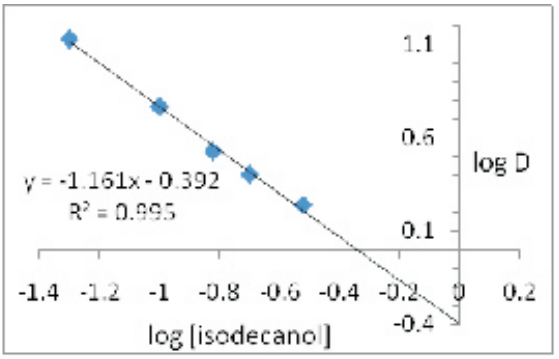


Fig. 1 Variation of logD vs. log [isodecanol], CMPO=0.2M, HNO_3= 3.4M

Results and Discussion

Fig.1 gives the D values of Am(III) at an acidity of ~3.4 M nitric acid with 0.2M CMPO containing various percent values of isodecanol in dodecane. It was seen that no third phase was observed at any combination of the phase modifier with CMPO and the lowest content (5%) gives the maximum D value decreasing with the higher content. This also underlines the fact that isodecanol is not one of the moieties in the extracted complex, but the interaction between CMPO and the phase modifier may result in less D values at higher concentrations of it. For subsequent work, 10% isodecanol was fixed. Fig.2 gives D values for Am(III) as a function of nitric acid concentration. It can be seen that with increase in the acid concentration, the D values increased monotonously up to 6.0M, however, the slope diminished and ultimately the D may reach saturation. However, almost constant D values in the whole acidity range observed with TRUEX solvent attributable to the known intramolecular buffering

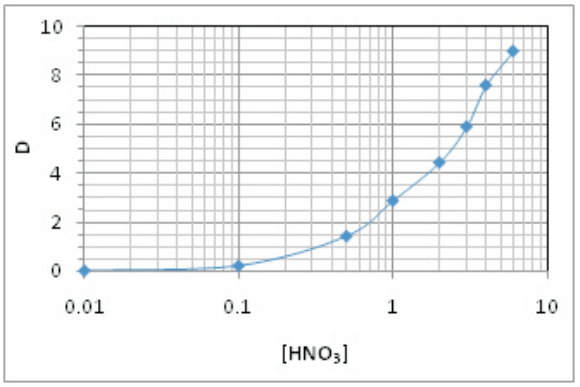


Fig. 2 D values of Am(III) as a function of $[HNO_3]$ with 0.2M CMPO + 10% isodecanol in dodecane

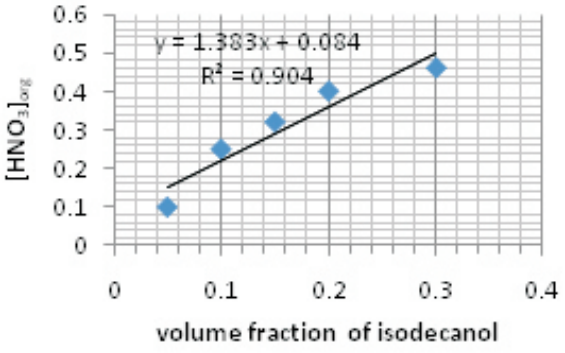


Fig. 3 Variation of uptake of HNO_3 with isodecanol in organic phase

effect of CMPO [4]. The D values between 3 and 4.0M of acid concentration vary from ~ 6.0 to 7.6. This value is for tracer and normally decreases when typical HLW solution with acidity at ~ 3.0M is used for extraction of trivalent actinides. Fig. 3 gives the measure of uptake of acid concentration by the organic phase. It is seen that with increase in the isodecanol fraction, the uptake of the acid varied linearly inferring that isodecanol may be playing a role in the acidity of the organic phase. The intercept would give the acid uptake by bare CMPO in the absence of isodecanol. This value is 0.084M. The acid uptake constant K_H of CMPO was estimated using the equation below.

$$K_H = [CMPO.HNO_3]/([CMPO]_{free}.[HNO_3]_{free})$$

where the numerator is 0.084. If it is assumed that CMPO makes only 1:1 complexes with HNO_3, then $[CMPO]_{free}$ = 0.2-0.084. Applying dissociation constant of 23.5 for HNO_3, free $[HNO_3]$ was found to be 0.37 for 3.4M initial acidity. With these data, K_H was found to be 1.96 which is close to the reported K_H value for CMPO as ~2 [4].

Since the reagent may extract other actinides and to achieve desirable decontamination from the unwanted fission products, the D values are tabulated for the important actinides and two fission products at 3M HNO_3 in Table 1. It can be seen that the D values of fission products such as Tc(VII) and Eu(III) is not insignificant and so adequate scrubbing measures or appropriate complexing agents are needed for a better decontamination.

Conclusions

Isodecanol, in place of TBP as a modifier for 0.2M CMPO in dodecane is used and fixed at 10%(v/v). The distribution ratio, D values of actinides and a few fission products have been determined at ~3.0M nitric acid. The lanthanide fission products represented by Eu may always accompany trivalent Am. Acid uptake by the extraction solvent was also evaluated and was found to agree with that reported in the literature.

Table-1: D values of actinides, lanthanide and fission products with 0.2M CMPO + 10% isodecanol in dodecane at 3.0M HNO_3

Sl. No.	Metal ion	D
1	U(VI)	20.1
2	Pu(IV)	76.0
3	Eu(III)	3.50
4	$^{99}TCO_4^-$	0.23

References

[1] J. N. Mathur, M. S. Murali and K. L. Nash, Solvent Extr. Ion Exch., 2001, 19, 357

[2] Y. Sasaki, Y. Sugo, S. Suzuki, S. Tachimori, Solv. Extr. Ion Exch. 2001, 19, 91

[3] S. A. Ansari, P. N. Pathak, P. K. Mohapatra, V. K. Manchanda, Chem. Rev. 2012, 112, 1751 ; (b) R. B. Gujar, S. A. Ansari, M. S. Murali, P. K. Mohapatra, V. K. Manchanda, J. Radioanal. Nucl.Chem. 2011, 114, 377;(c) S. Manohar, J.N. Sharma, B.V. Shah, P.K. Wattal, Nucl Sci.&Engg., 2007, 156, 96

[4] K.A. Martin, E.P. Horwitz, J.R. Ferraro, Solv Extr and Ion Exch. 1986, 4, 1149

Application of a Simple and Rapid Spectrophotometric method for Uranium analysis in Uranium based waste sample

Bholanath Mahanty, C. D. Karekar, D. K. Das, P.G.Behere, Mohd.Afzal

Advanced Fuel Fabrication Facility, Bhabha Atomic Research Centre, Tarapur 401502, India;
E-mail: bmahanty@barctara.gov.in

A simple and rapid spectrophotometric method is used for the analysis of uranium in uranium based complex waste generated during the analysis of uranium by Davis & Gray method. The method is based on the selective complex formation between U (VI) and Arsenazo (III) at pH 2.0 0.1 which showed maximum absorbance at 651 nm. Interfernce caused by various metal ions, such as V, Mo, Fe, Mn, Cr, K were effectively masked using ethylenediaminetetra acetic acid (EDTA) and tartaric acid. Molar extinction coefficient of 5.68 X 10^4 $moles^{-1}$ lit cm^{-1} is found at 651nm for U(VI)-Arsenazo (III) complex. Mean recovery around 91% is obtained for uranium analysis.

Introduction

Advanced Fuel Fabrication Facility (AFFF), Bhabha Atomic Research Centre is associated with the fabrication of mixed oxide (MOX) fuel for various types of reactors. Chemical quality control (CQC) is an important aspect for checking the quality of the pellet at various stages of fuel fabrication. Uranium is determined in the powder and in the sintered uranium oxide pellet by Davis & Gray method, which involves reduction of U(VI) to U(IV) by Fe(II) in >10 M phosphoric acid medium. Excess Fe (II) is selectively oxidized and U (IV) is titrated with standard potassium dichromate in presence of vanadyl sulphate. Potentiometric method is employed for detecting the end-point of the titration. In this process, a large quantity of uranium waste containing a significant amount of o-phosphate and other various metal ions is generated. Analysis of uranium in this complex mixture is a challenging task for analytical chemist. A very simple and fast spectrophotometric method [1] is employed for the determination of uranium in this matrix. Spectrophotometric method posses many advantages such as simplicity, low cost, sample flexibility, high sensitivity and precision.

The present study is based on the selective complex formation between U(VI) and Arsenazo (III) at pH 2.0 0.1 in presence of ethylenediaminetetraacetic acid and tartaric acid. The absorbance of the pink violet complex of Arsenazo (III) and U(VI) was measured using an optical fiber based UV-Visible spectrophotometer at 651 nm. The accuracy of the current method was checked by recovery study of uranium in the waste sample by analyzing a waste containing known amount of uranium.

Experimental

All the chemicals in this experiment were of analytically pure grade and double distilled water was used to prepare the solution. Uranyl nitrate solution (10 mg ml^{-1} of U) was prepared by dissolving required quantity of U_3O_8 powder in 100 ml of 0.5 M HNO_3 and subsequently it was standardized by potentiometric titration. Arsenazo-III (0.25 %), EDTA solution (2.5%) and tartaric acid (10%) were prepared by dissolving required quantity of the respective reagent in double distilled water.

A waste sample was prepared by analyzing standard uranium solution by Davis & Gray method. Subsequently the waste sample was diluted to 50 mL volumetric flask with double-distilled water to prepare a concentration of 200 ug $mL^{-1}$of uranium. 1 ml of the waste solution was taken in a beaker and dried under infra red lamp. Subsequently it was dissolved in 10 mL of 5 x 10^{-3} M H_2SO_4. An aliquot (2 mL) was transferred into a 10 mL volumetric flask, 240 L arsenazo (III) reagent (0.25%), 200 L tartaric acid (10%) and 400 L EDTA solution (2.5%) were added. The solution was taken up to the mark with dilute H_2SO_4 (pH 2.0). After 5 min., the absorbance of the pink-violet complex was measured at 651 nm in a 1-cm quartz cell with an optical fiber based uv-visible spectrophotometer against a reagent blank as the reference.

Results and Discussion

Working standard of 0.1 to 10 ppm of U was used for the calibration. The correlation coefficient was found to be 0.992. The corresponding linear regression equation was found to be $y = 0.222x + 0.026$. The molar extinction coefficient ( ) of U(VI)-arsenazo (III) complex was calculated from the standard curve and was established to be 5.68 x 10^4 $moles^{-1}$ L cm^{-1}. The effect of variation of concentration of arsenazo(III) on the formation of U(VI)-arsenazo(III) complex was investigated for the range of 1to10 g mL^{-1} of uranium and the results are shown in Fig. 1. It can be seen from the figure that 240 L of arsenazo (III) solution is adequate to complete the formation of colour complex for the range of 1to10 ug ml^{-1} of uranium. The effect of complexing agents (EDTA and Tartaric acid) on the formation of U(VI)-arsenazo (III) complex were also studied by variation of the volume of EDTA and tartaric acid solution for a given concentration of uranium (5 g mL^{-1}) and arsenazo (III) in 10 mL of volumetric flask and are shown in Fig. 2 and Fig. 3 respectively. The results indicated that the variation of concentration of

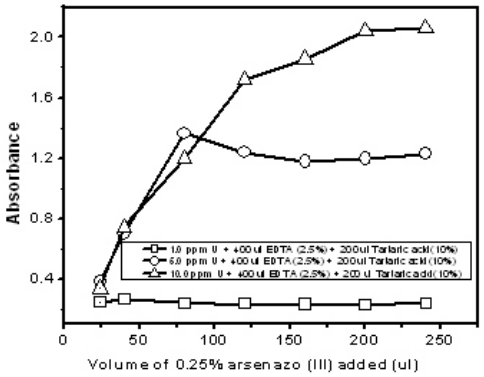


Fig. 1 Effect of variation of volume of arsenazo (III) in the formation U(VI)-arsenazo (III) complex

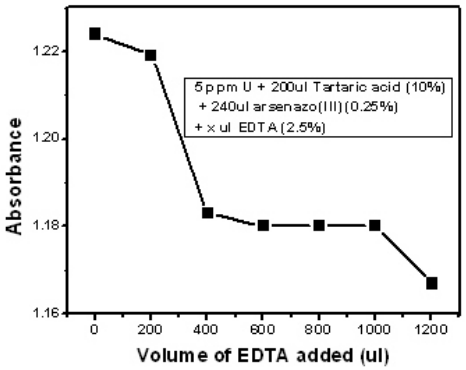


Fig. 2 Effect of variation of volume of EDTA on the formation of U(VI)-Arsenazo(III) complex

complexing agents did not influence considerably the absorbance value. The minimum volume of EDTA (2.5%) and tartaric acid (10%) required for the development of uranium (VI)-arsenazo (III) coloured complex is 400 L and 200 L respectively at 5ppm uranium. The effect of VO^{+2}, Mo (VI), Fe (III) and PO_4^{3-} ions on the determination of uranium with arsenazo (III) were studied and the data are included in Table 1. The results indicated that there is not considerable interference of the metal ions and phosphate on uranium analysis if it is present up to 600 ug and 5 mg respectively. Table 2 revealed the absorbance data and percentage recovery of uranium in the analysis of actual waste containing known amount of uranium. The mean percentage recovery of uranium in the waste sample was found to be 90.7 for 4.0 ppm of uranium with precision expressed in terms standard deviation ( ) as 1.0 (n=5).

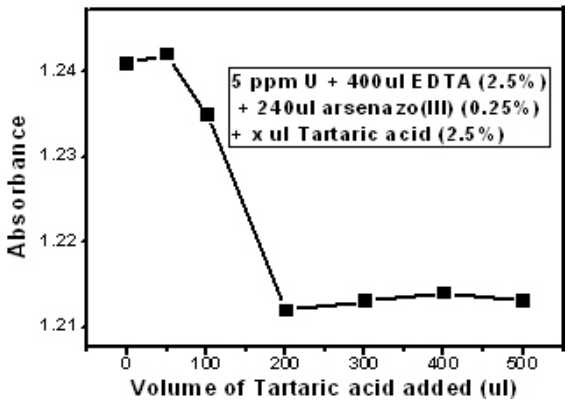


Fig. 3 Effect of variation of volume of Tartaric acid on the formation of U(VI)-Arsenazo(III) complex

Table-1: Interference study of ions in the determination of uranium by arsenazo (III)*

Ions	Amount of Ions added (ug)	Absorbance
VO^{+2}	600	0.981
Mo(VI)	600	1.007
Fe(III)	600	1.008
PO_4^{3-}	5000	0.998

*U= 4 ppm; tartaric acid =200ul; EDTA= 400ul Arsenazo = 240 uL

Table-2: Determination of U in the actual waste sample containing known amount of U (U= 4ppm)

Sl. No.	Absorbance	% Recovery
1	0.820	89.7
2	0.825	90.3
3	0.835	91.4
4	0.821	89.8
5	0.842	92.1

Conclusion

Thus this method can be applied for the uranium determination in uranium based complex waste generated during analysis of uranium by Davis & Gray method.

References

[1] H. Golmohammadi, A. Rashidi, S.J. Sadari, chemistry & chemical technology, 6(3) (2012) 245.

Extraction studies on U(VI) using Tri-n-Octyl Phosphine Oxide Dissolved in Room Temperature Ionic Liquids

D.R. Raut, P.K. Mohapatra

Radiochemistry Division, Bhabha Atomic Research Centre, Trombay, Mumbai 400085, India;
E-mail: mpatra@barc.gov.in

Room temperature ionic liquids (RTILs) are evaluated as diluents for the extraction of U(VI) from nitric acid medium using tri-n-octyl phosphine oxide (TOPO) as the extractant. The solvent consists of 0.05 M TOPO dissolved in C_8mimPF_6 and C_8mimNTf_2. Various parameters like kinetics of U(VI) extraction, effect of feed acidity and TOPO concentration have been studied. Comparatively higher distribution ratio values were obtained for C_8mimPF_6 while no extraction of U(VI) was seen with pure RTILs. Absorption and fluorescence spectroscopic studies were also carried out.

Introduction

Uranium is used world wide as the fuel in nuclear reactors. Due to its strategic nature, recovery of U for various streams emanating from nuclear fuel cycle activities is mandatory. Several solvent extraction methods have been adopted for the recovery of uranium employing various ligands like tri-n-octyl amine, Aliquot-336, tri-n-butyl phosphate, tri-n-octyl phosphine oxide (TOPO) in solvents like n-dodecane or kerosene. There is a growing need to develop 'green' separation processes with low inventory of inflammable and toxic volatile organic compounds (VOCs).

Of late, room temperature ionic liquids (RTILs) have been found to be used extensively in actinide separations including that of uranium. The room temperature ionic liquids appear attractive alternatives due to the fact that their chemical properties can be easily tuned by the judicious choice of cation and anion, having low flammability, and stability towards radiation and heat [1-3]. Therefore, it was of interest to investigate the extraction of U(VI) with RTILs as the diluents and TOPO as the extractant, which is reported for the first time.

Experimental

All ionic liquids, used in present work, were procured from Ioli Tec, Germany while TOPO was procured from E. Merck, Germany. ^{233}U (lab stock) was used as the tracer while natural uranium was used for studies involving macro concentrations of the metal ion. Solvent extraction studies were carried out in airtight polypropylene tubes with 2.5 mL capacity. The solvent extraction studies were carried out by equilibrating equal volumes of the organic and aqueous phase (usually 0.5 mL) which contained the extractant and the radiotracer, respectively. Subsequently, the tubes were centrifuged and assaying of the samples was done by liquid scintillation counting. The distribution ratio for U(VI) was calculated as the ratio of the concentration of uranium (expressed in terms of counts per unit time per unit volume) in the organic phase to that in the aqueous phase. All extraction studies were carried out in duplicate and are found to be reproducible with an error limit of ± 5 %.

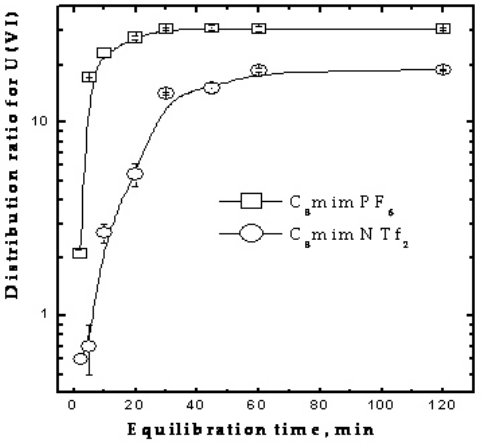


Fig. 1 Kinetics of extraction of U(VI) with 0.05 M TOPO dissolved in RTILs, feed: 3 M HNO_3

Results and Discussion

Figure 1 gives the extraction profiles of the U(VI) by 0.05 M TOPO dissolved in C_8mimPF_6 and C_8mimNTf_2 as a function of the equilibration time.

Kinetics of extraction was slow as compared to molecular diluents like n-dodecane. It took about 30 minutes to reach the equilibrium for C_8mimPF_6 and 60 min for C_8mimNTf_2. Figure 2 shows the extraction profiles of U(VI) at various feed acidities for 0.05 M TOPO dissolved in the two RTILs and n-dodecane. The extraction of U(VI) from aqueous phase to ionic liquid phase can proceed through the cationic exchange mechanism, anionic exchange mechanism or neutral partitioning depending upon nitric acid concentration. In the present case, rise in distribution ratio for U(VI) was noted up to 2 M HNO_3 followed by decrease thereafter which indicated extraction mechanism including solvated species. Similar observations were noted by Yang et al for extraction of rare earth elements by TOPO [4].

The extraction of U(VI) was negligible with pure RTIL in all acidities though a marginal increase in

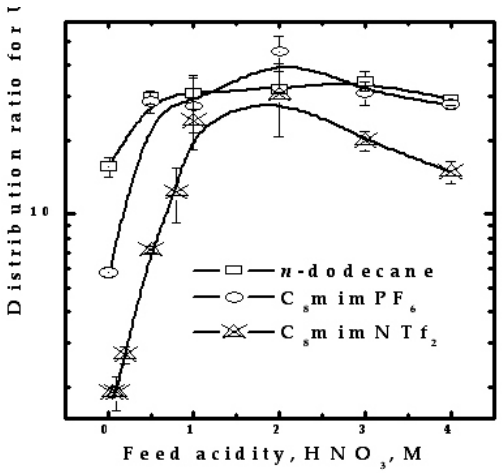


Fig. 2 Effect of feed acidity on distribution ratio for U(VI) with 0.05 M TOPO as extractant, diluents: RTILs

extraction was seen with increasing acidity. As shown in Fig. 2, the extraction of U increased with increasing nitric acid concentration in the feed which is in line with solvation mechanism as follows:

$$UO_2^{2+}{}_{(aq.)} + 2NO_3^-{}_{(aq.)} + nTOPO_{(IL.)} \quad (UO_2(NO_3)_2 .nTOPO)_{(IL)}$$

where (aq.) denotes species in aqueous phase and (IL.) denotes species in ionic liquid phase.

Table-1: Determination of ligand-metal stoichiometry at various acidities for TOPO-RTIL system

RTIL	Feed acidity, HNO_3, M	Slope of log-log fit	R^2
C_8mimPF_6	0.01	1.66	0.95
	3	1.83	0.97
$C_8mimNTf_2^-$	0.01	0.94	0.98
	2	2.09	0.99
	3	2.22	0.99

To understand the metal ligand stoichiometry in the extracted species, distribution coefficient values were determined at varying concentration of TOPO in ionic liquid phase and the slopes of the log D_U vs log [TOPO] plots are presented in Table 1. In case of $C_8mim\ PF_6$, about two TOPO molecules were found to be associated in the extracted species, while for $C_8mimNTf_2$, one molecule of TOPO was found to participate in the extraction process at 0.01 M HNO_3 which increased to two at 3 M HNO_3.

To understand the nature of species and the complexation of uranyl ion with TOPO in RTIL and n-dodecane, absorption and fluorescence spectroscopic studies were also carried out (Fig. 3). Significant difference in the pattern of the spectra was observed for uranyl ion in HNO_3 medium, UO_2^{2+}-TOPO complex in

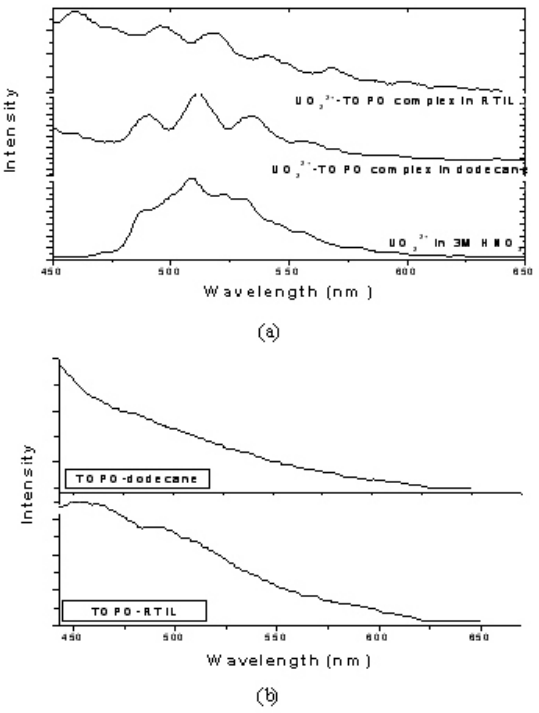


Fig. 3 Fluorescence measurement studies (a) Emission profile of uranium (b) Emission profile of organic phase without metal ion

n-dodecane and UO_2^{2+}-TOPO complex in $C_8mimNTf_2$. On complexation with TOPO, the stretching frequency of O=U=O bond decreases to 392.99 cm^{-1} which further decreases for ionic liquid media 382.13 cm^{-1}. The decay profiles revealed the presence of single species for all the systems.

Conclusions

Extraction of U(VI) with TOPO in ionic liquids was studied for the first time and found to follow solvation mechanism. Metal ligand stoichiometry was found to be dependent on the feed acidity. Fluorescence studies suggested significant difference in the TOPO complexation with ionic liquid and n-dodecane.

Acknowledgement

Authors are thankful to Mr. Arijit Sengupata, RCD, BARC for carrying out florescence studies and valuable discussion. They also thank Head, Radiochemistry Division for his keen interest.

References

[1] P.K. Mohapatra, D.S. Lakshmi, D. Mohan, V.K. Manchanda, Sep. Purif. Technol., 51 (2006) 24.

[2] J.N. Mathur, G.R. Choppin, Solv. Extr. Ion Exch. 16 (1998) 739.

[3] T.J. Bell, Y. Ikeda, Dalton Trans., 40 (2011) 10125.

[4] F. Yang, F. Kubota, N. Kamiya, M. Goto, Sol. Extr. Res. Dev., Japan 20 (2013) 225.

Assay of Actinide Mixtures by Hybrid K-edge Densitometer

M. Bootharajan, K. Swaminathan and C.R. Venkata Subramani

Fuel Chemistry Division, Chemistry Group, Indira Gandhi Centre for Atomic Research, Kalpakkam 603 102, India; E-mail: venkat@igcar.gov.in

This paper describes the Hybrid K-edge densitometer system set up at RCL, IGCAR and results of experiments obtained to assay the concentrations of uranium and plutonium in mixtures. It discusses the procedures used to obtain the concentration of actinides present in higher amounts by K-edge and in lower amounts by K-XRF.

Introduction

A nondestructive and noninvasive technique that can be used for characterization of the spent fuel solutions in the reprocessing plants is K absorption edge densitometry cum K-XRF. This method can be used for spent fuel solutions having high dose levels. A system has been recently commissioned at the Radiochemistry Laboratory, IGCAR for this purpose. This paper describes the system and the results obtained using mixtures of uranium and plutonium solutions using both absorption edge densitometry and XRF.

Theory

In K-edge absorption densitometry, a continuous-energy beam of photons from a tungsten-anode X-ray tube is transmitted through a liquid solution kept in a vial or cuvette Photon transmission through the sample is measured at two photon energies that closely bracket the K-absorption edge of the element of interest. The concentration of the measured element is a simple function of the photon transmission below and above the absorption edge and the path length of X-rays through the sample. This is given by the following expression

$$_s \quad \frac{1}{x} \text{Ln} \frac{T_L}{T_U} \qquad _m \quad \frac{\quad}{m} \qquad (1)$$

Where $_s$ and $_m$ are the concentration of the element and matrix respectively and and $_m$ are the mass absorption coefficient of the element of interest and matrix respectively. T_L and T_u are the transmission at lower and upper side of the edge respectively. As there is no discontinuity in the plot of energy dependence of the photon mass attenuation coefficient for the matrix at the absorption edge of the actinides, the second term in the above equation vanishes since $_m$ is equal to zero.

In the case of actinides, the uranium K-edge appears at 115.6kev and the plutonium K-edge appears at 121.8kev. The K-edge and the L_{III} absorption edges have been used in the assay of special nuclear material. In a hybrid K-edge/K-XRF densitometer system, KED is augmented by a simultaneous X-ray fluorescent measurement of the sample. The concentration of the most abundant actinide is determined by KED and the XRF detector measures the fluoresced X-rays from the sample. Concentration of the other actinide is derived from the ratio of the XRF peak areas. A typical schematic of the K-edge/K-XRF hybrid system is shown in Fig. 1.

Experimental

For both K-edge and K-XRF measurements a 220 kV, 10 mA X-ray generator (YXLON MG226 / 2.25kW) was used to generate the continuum required for this work. The X-ray continuum was suitably tailored by means of beam filters (0.5 mm Cd + 1 mm Ta + 1 mm SS planchette) and the collimated X-rays were allowed to be incident on the sample solution contained in a sample container with a path length of 30.6mm. The X-rays after traversing through the solution were allowed to impinge on a well shielded low energy photon spectrometer (Baltic Scientific, 500 mm^2, 520 eV at 122 keV) through a tungsten collimator of 2mm diameter to ensure that only radiation that had passed through the sample was seen and all scattered radiations were cut off. The spectra were collected using an ITECH quad ADC which is an embedded Linux based high performance ADC with a MCA card. Measurements using various concentrations of mixtures of uranium and thorium solutions by K-edge absorption densitometry have been reported earlier [1].

Mixtures of plutonium and uranium solutions were used for these experiments. These mixtures were obtained by mixing appropriate volumes of standard uranium (195 mg mL^{-1}) and plutonium (81 mg mL^{-1}) solutions. The measurements were carried out with the operating voltage of the X-ray tube maintained at 180 kV and at a current of 1mA and the counting time was fixed as 3000 s. The blank was obtained using 4 M nitric acid only. In each case, the transmission was obtained in the energy ranges of interest. The extrapolation procedure described elsewhere [2] was used to determine the jump ratio of each element of interest. The jump ratio for uranium and plutonium are calculated and the concentrations obtained using equation (1).

The energy dispersive analysis of tube excited K X-rays from the actinide mixtures is carried out with the same X-ray generator. The low energy photon detector was positioned at the largest possible backward angle relative to the primary X-ray beam, as shown in the Fig. 1, in order to remove the inelastically scattered radiation in the energy region (90-120keV) of interest.

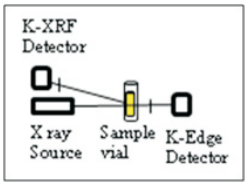


Fig. 1 A typical schematic block diagram of Hybrid system

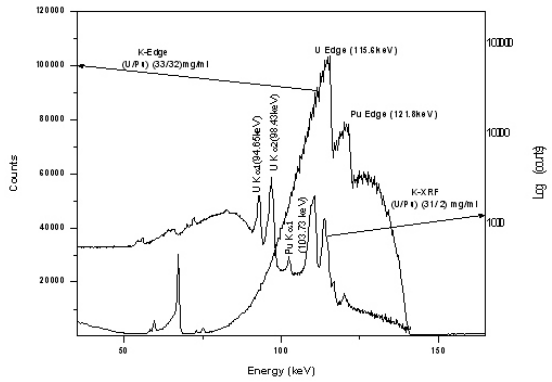


Fig. 2 A typical K-edge/K-XRF spectrum of Uranium & Plutonium mixture

To determine the concentration of plutonium present in lower amounts, XRF spectroscopy was used. The ratio of the peak areas of the 103.7 keV of plutonium and 98.4 keV of uranium was first obtained using higher concentrations of the actinides. From the ratio of these two peaks obtained with higher concentrations of actinides the calibration factor was arrived at. Using the calibration factor, the concentration of plutonium present in the mixtures was determined from the ratio of the peak areas of plutonium and uranium present in the mixtures and the concentration of uranium that was assayed simultaneously by K-edge densitometry.

A typical K-edge/K-XRF spectrum is shown in Fig. 2.

Results and Discussions

This combined technique (Hybrid) allows the measurement of dissolver solutions in plants reprocessing PHWR and LWR fuels having higher concentration of uranium and lower concentration of plutonium. However this method can also be used for dissolver solutions in which one actinide is present in higher concentrations while the others are present in lower concentrations.

Table 1 shows the results of the assay of mixtures of uranium and plutonium by K-edge densitometry. As can be seen from this table that the error in the assay of concentration of uranium and plutonium present in the mixtures is within acceptable limits. It was observed that the error obtained in the estimation is higher when the actinide concentration is less than 10 mg.mL^{-1}. Hence for such mixtures the K-XRF estimation was resorted to.

Table 2 presents the results of the assay of the concentration of plutonium in the mixtures present in less than 10 mg mL$^{-1.}$ It is seen from this table that the error in the measurement by K-XRF is within 6%. However if the of concentration of plutonium present in the mixture is less than 1 mg mL^{-1}, the error in this estimation goes up, since the background in the energy region of K of plutonium is higher compared to signal and can not be distinguished from noise. One way of circumventing this problem is the improvement of the geometry by placing the detector closer to the sample and use of other suitable filters of appropriate thickness.

Table-1: The results of the assay of Uranium in the mixture by K-edge densitometry.

Concentration (mg/mL)				/	
Actual		Experimental			
U	Pu	U	Pu	U	Pu
79.22	27.16	79.84	27.94	0.01	0.03
74.27	20.37	75.07	20.65	0.01	0.01
66.02	16.30	66.88	15.80	0.01	-0.03
66.02	13.58	66.84	13.54	0.01	-0.003
56.59	11.64	57.46	11.80	0.02	0.01
30.30	9.02	30.91	8.56	0.02	-0.05
32.0	4.35	31.84	3.66	-0.005	-0.16
31.07	2.16	30.84	1.54	-0.007	-0.29

Table-2: The results of the assay of Plutonium in the mixture by K-XRF.

Concentration (mg/mL)			/
Actual		Experimental	
U	Pu	Pu	Pu
30.30	9.02	9.47	0.05
32.00	4.35	4.56	0.05
37.11	3.47	3.66	0.05
31.07	2.16	2.26	0.05
31.98	1.09	1.11	0.02
32.96	0.45	0.11	-0.77

References

[1] M.Bootharajan, et.al., Nucl. Radiochem. Symp. (NUCAR-2013) Jabalpur, p147 (2013)

[2] S.T. Hsue and M. Collins, LA-12874-MS.

Studies on Actinide Ion Uptake and Transport using Polymer Inclusion Membranes Containing TODGA as the Extractant

B.N. Mahanty[1], D.R. Raut[2], D.K. Das[1], P.G. Behere[1], Md. Afzal[1] and P.K. Mohapatra[2]

1. *Advanced Fuel Fabrication Facility, Bhabha Atomic Research Centre, Tarapur, Maharastra 401502, India*
2. *Radiochemistry Division, Bhabha Atomic Research Centre, Trombay, Mumbai 400 085, India; E-mail: mpatra@barc.gov.in*

Separation of several actinide ions such as Am^{3+}, Pu^{4+}, UO_2^{2+} and Th^{4+} was studied from dilute nitric feed solutions using CTA based polymer inclusion membranes (PIM). The solid phase extraction studies using PIM pieces indicated the following trend: Am(III) > Pu(IV) > Th(IV) >> U(VI). The metal ion uptake showed an increasing trend at lower acidities up to 2 M HNO_3 followed by a decrease at higher acidities. Membrane transport studies were also carried out using two compartment cells and the results were positive for actinide separation from acidic radioactive wastes.

Introduction

Radioactive waste processing has been one of the most challenging processes involved in the back end of the nuclear fuel cycle. There have been several separation processes such as precipitation, solvent extraction, ion-exchange, etc. which have been used routinely for such applications. However, there is a growing interest in other upcoming techniques which may act viable alternatives. Membrane separation studies for radioactive waste remediation are being carried out in many laboratories for possible applications [1].

We have carried out extensive studies in this direction as well and found TODGA (N,N,N',N'-tetraoctyl diglycolamide) as one of the most promising extractants for actinides in supported liquid membrane based separation methods [2]. Due to the concerns about the stability of liquid membranes, there have been attempts to use plasticized membranes containing the carrier extractant, also known as polymer inclusion membrane (PIM). In this paper, we report the uptake behaviour of TODGA based PIMs for actinide ions such as Am^{3+}, Pu^{4+}, UO_2^{2+} and Th^{4+} from dilute nitric acid feed solutions.

Experimental

TODGA was procured from Thermax Ltd, Pune while CTA was obtained from Alpha Biochem. >97% NPOE (2-nitrophenyloctyl ether) was obtained from Fluka and was used as such while the other reagents were of AR grade. The PIMs were prepared using a previously reported method using cellulose triacetate (CTA) as the base polymer and NPOE by Sugiura [3]. The PIMs were transparent and were found to have uniform thickness (45 to 50 microns). The solid phase extraction studies were carried out using 1 cm^2 PIMs which were contacted with the dilute acid solutions containing the respective radiotracer. Transport studies were carried out using two-compartment cells as reported previously [4].

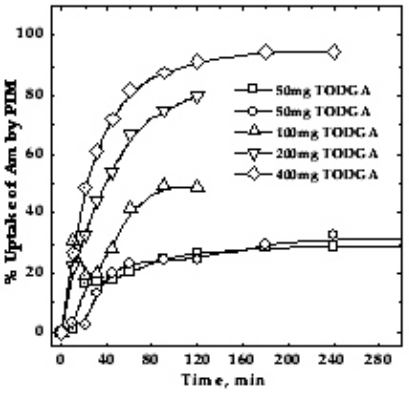


Fig. 1 Optimisation of parameters for PIMs containing TODGA. Feed: ^{241}Am tracer in 1 M HNO_3

Results and Discussion

In order to study the effect of plasticizer concentration, the PIMs were prepared using 80 mg CTA and 200 L NPOE and varying amounts of NPOE. The results are shown in Fig. 1 which indicated that increasing the amount of NPOE, usually showed an increase in Am(III) uptake by the membranes. The optimizing membrane contained 12% CTA, 59% TODGA and 29% NPOE. The metal ion uptake efficiency followed the trend at 1 M HNO_3: Am(III) > Pu(IV) > Th(IV) >> U(VI). The metal ion uptake tendency increased with increasing acidity from 0.5 M to 2.0 M HNO_3 while a decrease was seen at higher acidities. However, with further increase in the HNO_3 concentration resulted in degradation of the PIMs. Fig. 2 shows the effect of nitric acid concentration on Am(III) transport while using a mixture of $NaNO_3$ and HNO_3. It was observed previously by us [5] that Am(III) extraction increased with a mixture of HNO_3 and $NaNO_3$ while pure HNO_3 and pure $NaNO_3$ yielded lower extraction. Similar trends were also observed in the present study while using the TODGA containing PIMs (Fig. 2).

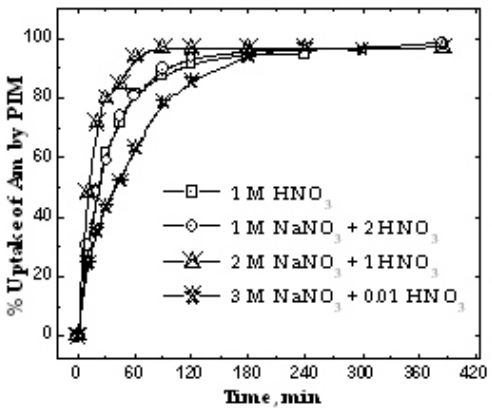


Fig. 2 Effect of feed composition on Am(III) uptake. PIM composition: 80 mg CTA + 40 mg of TODGA + 200 uL of NPOE

The loaded radioactivity could be efficiently stripped from the PIM films by using 1.0×10^{-2} M EDTA at pH 3.0. The stripped membranes could be reused for further metal ion uptake studies. The surface morphology of the membranes were compared from their AFM profiles of the pristine PIMs and those after several usages (Fig. 3). As shown by the AFM pictures, there is hardly any difference in the profiles suggesting that the PIMs can be reused for a long time for this application.

The PIMs were also used for the transport of the actinide ions using two-compartment transport cells and the transport rates followed the same order as that of the uptake as mentioned above. The diffusion coefficients were calculated for the Ann+ - TODGA complexes across the PIMs using a time-lag method [4]. Results on the PIMs will be compared with those reported previously using supported liquid membranes containing TODGA as the carrier extractants.

Conclusions

From this study it can be concluded that TODGA containing PIMs can be effectively used for actinide ion uptake from acidic feed solutions. This holds promise for application of the PIMs for removal of radioactivity from lean radioactive waste solutions.

References

[1] J.F. Dozol, J. Casa, A.M. Sastre; Sep. Sci. Tech., 28, (1993) 2007.

[2] P.K. Mohapatra and V.K. Manchanda; Ind. J. Chem., 42A (2003) 2925.

[3] M. Sugiura and M. Kikawaqa, J. Membrane Sci. 42 (1989) 47.

[4] S. Sriram, P.K. Mohapatra, A.K. Pandey, V.K. Manchanda, L.P. Badheka, J. Membrane Sci. 177 (2001) 163.

[5] S.A. Ansari, P.K. Mohapatra, D.R. Prabhu and V.K. Manchanda, J. Membrane Sci. 282 (2006) 133.

[6] J. Crank, The Mathematics of Diffusion, 2nd ed., Oxford University Press Inc, New York, (1975), p. 414.

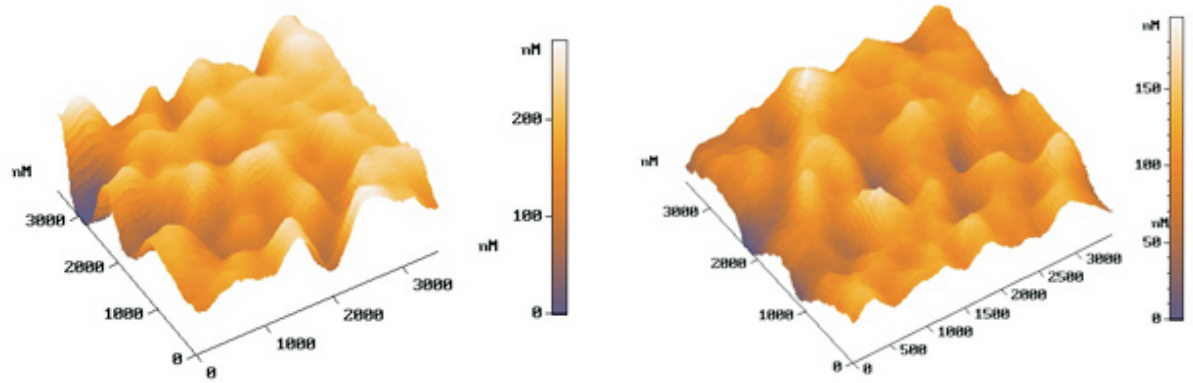


Fig. 3 AFM profiles of (left) pristine PIMs and (right) those used several times for Am recovery from dilute HNO_3 feeds

N,N,N',N'-Tetraoctyl Diglycolamide Coated Fe_3O_4 Nanoparticles for Americium Preconcentration and Determination with -Spectrometry

V. Chavan[1], T. Vasudevan[2], A. Pandey[1*], A. Goswami[1]

1. *Radiochemistry Division, Bhabha Atomic Research Centre, Trombay, Mumbai 400085, India; E-mail: ashokk@barc.gov.in*
2. *Research Reactor Services Division, Bhabha Atomic Research Centre, Trombay, Mumbai 400085, India*

N,N,N',N'-tetraoctyl diglycolamide (TODGA) was coated on Fe_3O_4 nanoparticles under different chemical conditions. TODGA coated on magnetic nanoparticles Fe_3O_4 captured representative actinide ^{241}Am at 3-4 M HNO_3 with a very high efficiency. However, it has been observed that HNO_3 induced preorganization plays an important role in sorption of Am(III) ions even in its self-assembled monolayer on magnetic nanoparticles. As Am(III) sorption in TODGA coated Fe_3O_4 found to be quantitative (90%), this material was used for preconcentration of ^{241}Am from aqueous sample and subjecting it for direct quantification with -spectrometry. A linear variation of -activity of ^{241}Am sorbed in TODGA coated Fe_3O_4 with amount of ^{241}Am spiked in equilibrating solution indicated potential application of this method for monitoring ultra-trace concentration of ^{241}Am in large volume of aqueous samples using magnetically assisted separation.

Introduction

Nuclear waste treatment is at present one of the most important ecological problems faced by nuclear energy industries. The effective solution to this problem not only involves development of efficient method for high level waste partitioning and disposal but also isolation and determination of radionuclides from a variety of complex aqueous matrices. Recently, interest has been focused on magnetic fluidized bed separation technology and the development of magnetically assisted chemical separation (MACS) systems for nuclear waste remediation [1]. They combine the selectivity of a ligand developed for liquid-liquid extraction and improved separation due to the magnetic field, resulting in an effective system suitable for use at low concentrations. The magnetic-sorbent have larger surface area, can be quickly recovered from the medium using external magnetic field, and secondary waste is not generated.

The ether linkage makes a diglycolamide (DGA), a tridentate ligand, having a high extractability for trivalent actinides. Since nitric acid promotes the complexation of diglycolamides with f-element ions, this class of extractants, and especially N,N,N',N'-tetraoctyl diglycolamide (TODGA), has been explored extensively for the partitioning of minor actinides from radioactive high-level liquid wastes at high nitric acid concentrations [2,3]. Therefore, it would be very interesting to study how TODGA molecules behave in self-assembled monolayer on superparamagnetic Fe_3O_4 nanoparticles. TODGA-functionalized nanoparticles are not only of interest for designing new strategies for actinide partitioning [4,5], but also for developing chemical sensors [6] and preorganized multidentate sequestering agents for actinides in biological systems [7].

In present work, a method has been developed for quantification of ^{241}Am at ultratrace concentration in highly acidic waste normally encountered in nuclear reprocessing plants by preconcentration in TODGA coated Fe_3O_4 followed by direct quantification with -spectrometry.

Experimental

In the present work, coating of TODGA on Fe_3O_4 nanoparticles (20-30 nm) was carried out with 0.1M TODGA in n-dodecane and mixture of n-dodecane and 1-decanol with and without subjected to acid treatment. For acid treatment, 0.1M TODGA in dodecane was equilibrated with equal volume of 3M HNO_3 for 30 min under shaking conditions at room temperature. After centrifugation, aqueous layer was discarded. 0.1 g of Fe_3O_4 nanoparticles (20-30 nm) were dispersed in pre-equilibrated 10 mL 0.1M TODGA in dodecane. It was equilibrated at room temperature under shaking condition for 24 hr. Another set of TODGA coating was carried out with 0.1M TODGA in dodecane without acid treated. Organic layer is then removed and the particles were washed 3 times with 1 mL methanol. It was then dried in air at room temperature overnight. Weighed amount of TODGA coated Fe_3O_4 nanoparticles were equilibrated with ^{241}Am activity spiked in feed having acid concentration varying from 3.0 M HNO_3. The radioactivity of the aqueous phase before and after equilibration was used to determine the D value with knowledge of weight of TODGA coated Fe_3O_4 nanoparticles and volume of equilibrating solution as reported in literature for solid sorbent. Linearity was studied by equilibrating Fe_3O_4@TODGA with varying amount of Am activity. The radioactivity of ^{241}Am was counted by -spectrometry using a NaI(Tl) detector coupled to a multichannel analyzer.

Results and Discussion

The Fe_3O_4 nanoparticles were coated with TODGA dissolved in solvent, as such and after equilibration with 3 mol L^{-1} HNO_3 (see Table 1). With uncoated Fe_3O_4 nanoparticles Am(III) uptake could not be detected. The extraction with the TODGA-coated Fe_3O_4 nanoparticles was quite reproducible, since the spread in the D_{Am} values was only 10% using TODGA-coated Fe_3O_4 nanoparticles from different batches. Also, there was no significant (1%) loss of iron content from DGA-coated Fe_3O_4 during equilibration with 3 mol L^{-1} HNO_3. It is interesting to see from Table 1 that D_{Am} is highly dependent upon coating conditions i.e. pre-treatment with HNO_3, temperature, and solvent.

Table-1: Sorption of ^{241}Am in "TODGA-coated Fe_3O_4" prepared using different conditions.

Procedure used for coating TODGA on Fe_3O_4	DAm (mL g^{-1})		% Efficiency
	(without treated)	(HNO_3 treated)	
0.1 mol L^{-1} TODGA in n-dodecane at 25°C	8	684	88.07
0.1 mol L^{-1} TODGA in n-dodecane at 40°C	9	672	87.89
0.1 TODGA mol L^{-1} in 10:1 n-dodecane and 1-decanol at 25°C	8	506	83.64
0.1 mol L^{-1} TODGA in 10:1 n-dodecane and 1-decanol at 40°C	3	1148 50	92.52

The fixed amounts of TODGA-coated Fe_3O_4 were equilibrated with solutions having 3 M HNO_3 and varying concentrations of ^{241}Am. The -activities of ^{241}Am preconcentrated in TODGA-coated Fe_3O_4 were obtained by direct counting of particles collected by applying magnetic field using using a NaI(Tl) detector coupled to a multichannel analyzer. As can be seen from Fig. 1, the -activity of ^{241}Am sorbed in TODGA coated Fe_3O_4 vary linearly with amount of ^{241}Am spiked in equilibrating solution. This seems to suggest that extraction efficiency of TODGA-coated Fe_3O_4 remains fairly constant and method is highly reproducible.

Conclusions

TODGA was successfully coated on Fe_3O_4 nanoparticles using optimized chemical conditions. TODGA coated Fe_3O_4 nanoparticles show quantitative

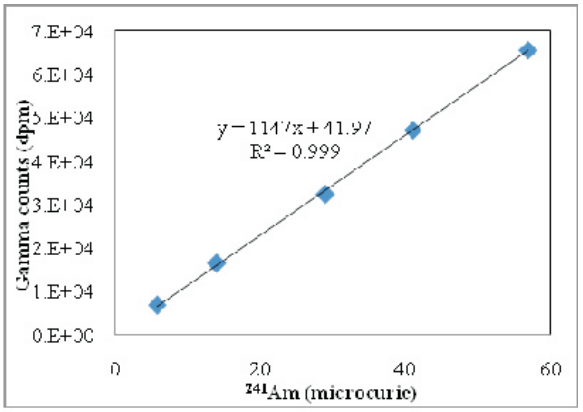


Fig. 1 Variation of -activity (dpm) of 241Am preconcentrated in TODGA coated Fe3O4 as a function of amount of ^{241}Am in equilibrating solution

uptake of Am from solution having 3 M HNO_3 that is normally encountered in nuclear reprocessing plants. The -activity of ^{241}Am sorbed in TODGA coated Fe_3O_4 varied linearly with amount of ^{241}Am spiked in equilibrating solution. This indicates potential application of this method for monitoring ultra-trace concentration of ^{241}Am in large volume of aqueous samples using magnetically assisted separation.

References

[1] L. NuZez, M. D. Kaminski, CHEMTECH, (1998) 41.

[2] Y. Sasaki, Y. Sugo, S. Suzuki, S. Tachimori, Solvent Extr. Ion Exch. 19 (2001) 91.

[3] S. A. Ansari, P. Pathak, P. K. Mohapatra, V. K. Manchanda, Chem. Rev. 112 (2012) 1751.

[4] A. K. Johnson, J. Kaczor , H. Han, M. Kaur, G. Tian, L. Rao, Y. Qiang, A. J. Paszczynski, J. Nanopart. Res., 13 (2011) 4881.

[5] C. Grüttner, V. Böhmer, A. Casnati, J.-F. Dozol, D. N. Reinhoudt, M. M. Reinoso-Garcia, S. Rudershausen, J. Teller, R. Ungaro, W. Verboom, P. Wang, J. Magn. Magn. Mater. 293 (2005) 559.

[6] R. Banerjee, Y. Katsenovich, L. Lagos, M. Senn, M. Naja, V. Balsamo, K. H. Pannell, C.-Z. Li, Electrochim. Acta 55 (2010) 7897.

[7] A. E. V. Gorden, J. Xu, K. N. Raymond, Chem. Rev. 103 (2003) 4207.

Separation of Lanthanides and actinides from Simulated High Level Waste using diglycolamide-functionalized calix[4]arene

Arijit Sengupta[1], P.K.Mohapatra[1], Mudassir Iqbal [2], Jurrian Huskens [2], Willem Verboom[2]

1. *Radiochemistry Division, Bhabha Atomic Research Centre, Trombay, Mumbai 400085, India; E-mail: mpatra@barc.gov.in*
2. *Laboratory of Molecular Nanofabrication, MESA+ Institute for Nanotechnology, University of Twente, P.O. Box 217, 7500 AE Enschede, The Netherlands*

Solutions of several diglycolamide(DGA)-functionalized calix[4]arenes (Calix-DGA) in room temperature ionic liquid were evaluated for actinide separation from Simulated High Level Waste (SHLW) solutions. Studies on Am^{3+} extraction indicated a cation exchange mechanism for all the ligands while an acid independent extraction was observed with the both side DGA-functionalized ligand. The time to attain equilibrium was found to be dependent on the equilibration temperature. Overall, the solvent systems were found to be quite promising for the recovery of actinide ions from HLW.

Introduction

With rapidly growing energy demands, nuclear energy is emerging as one of the most viable and sustainable alternatives to the fossil fuel. The major concern involving nuclear energy is the safa management of the large volumes of the resulting radioactive wastes. The currently accepted strategy of actinide partitioning involves the separation of actinides and long-lived fission product nuclides followed by their transmutation in high flux reactors. Out of the extractants being tested for actinide partitioning, diglycolamides (DGA) such as TODGA (N,N,N',N',-tetraoctyldiglycolamide) appears to be the most promising. The unusually high extraction coefficients for the trivalent actinide ions compared to the tetra- and hexavalent actinide ions with TODGA is due to reverse micelle formation with four TODGA molecules. In DGA-functionalized calix [4]arenes (termed as Calix-DGA hereafter) four diglycolamide pendent arms are anchored on a calyx [4]arene scaffold.

Due to favourable properties like low vapour pressure, high boiling point, wide liquid range, wide range of solubility for organic and inorganic materials, large potential window, room temperature ionic liquids have already gained world-wide acceptance as alternative to conventional diluents and explored even for nuclear fuel cycle [1-3]. The present paper deals with the evaluation of five different structurally modified Calix-DGA ligands (Fig. 1) in room temperature ionic liquid for actinide partitioning from Simulated high level waste. Attempts were made to understand extraction mechanism, extraction kinetics of Am^{3+} and inter comparison of the performances of those ligands in ionic liquid was studied.

Experimental

Radiotracers from laboratory stcks were used after ascertaining their radiochemical purity. The Clix-DGA ligands were synthesized as reported previously {ref]. Ionic liquids were procured from Iolitec, Germany and were used as such. $5X10^{-4}M$ concentration of ligands in $[C_8mim][NTf_2]$ was taken as organic phase for extraction purpose. Spectro Arcos ICP-AES was used for SHLW analyses.

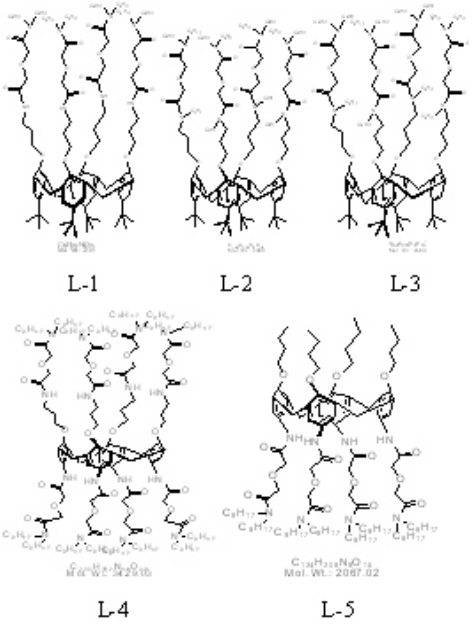


Fig. 1 Structure of the calix-DGA ligands used in the present work

Results and discussion

Separation from SHLW

All the Calix-DGA ligands were found to extract the rare earth ions e.g. Y^{3+}, Pr^{3+}, La^{3+}, Sm^{3+}nd Nd^{3+} along with the tri and teravalent actinide ions from the SHLW into the ionic liquid phase. Ce, Pd, Ru, Sr, Na, K were not at all extracted into the organic phase while Mn, Mo, Cr, Fe and Ba were partially extracted by some of the ligands into aqueous phase. Table-1 represents the analytical data showing extraction behavior of different metal ion from SHLW into ionic liquid phase with RSD < 5%.

Table 1: Analytical results of extraction of metal ion form SHLW

Metal	SHLW	L-I	L-2	L – 3	L-4	L-5
Na	5.9	5.4	5.8	5.6	5.9	5.5
K	0.20	0.073	0.17	0.12	0.11	0.120
Cr	0.13	0.075	0.09	0.035	0.036	0.081
Mn	0.50	0.5	0.45	0.168	0.171	0.047
Fe	0.86	0.19	0.64	0.258	0.26	0.067
Sr	0.034	0.029	0.021	0.022	0.029	0.030
Ru	0.026	0.022	0.026	0.025	0.026	0.007
Pd	0.011	0.011	0.01	0.01	0.01	0.020
Mo	0.16	0.008	0.007	0.009	0.009	0.005
Ba	0.06	0.01	0.024	0.027	0.028	0.06
Y	0.06	0.004	0.001	0.016	0.008	0.002
La	0.08	0.016	0.02	0.028	0.019	0.019
Zr	0.073	0.070	0.032	0.021	0.011	0.052
Nd	0.11	0.039	0.03	0.031	0.035	0.023
Sm	0.077	0.048	0.041	0.042	0.044	0.034
Ce	0.055	0.053	0.051	0.052	0.052	0.044
Pr	0.087	0.027	0.039	0.042	0.028	0.035

Concentrations are in g/L

Extraction Mechanism

Unlike conventional diluents like n-dodecane, the distribution ratio values of Am^{3+} obtained with L-1, L-2, L-3 and L-5 were found to decrease with increase in feed acidity of the aqueous feed solution. This fact suggests that the well known caion- exchange mechanism is operating in case of ionic liquid based solvent systems. At higher feed acidities, H^+ competes strongly with the metal ion which reduces the concentration of free ligand molecules in organic phase, consequently D values decrease. Fig. 2 represents the extraction profiles of Am^{3+} in different Calix-DGA molecules in ionic liquid. A remarkably high acid independent extraction efficiency of Am^{3+} was observed in case of L-4 in ionic liquid.

Extraction Kinetics

Comparatively slower kinetics of extraction was observed in the case of ionic liquid based solvent systems (vis-B-vis conventional solvent like n-dodecane). This can be attributed to the high viscosity coefficient of the ionic liquids compared to the molecular diluents. On increasing temperature, the kinetics were found to be faster. Fig. 3 presents the

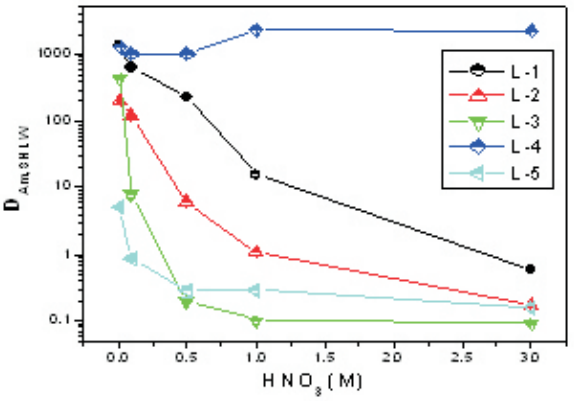


Fig. 2 Extraction profiles Am^{3+} using Calix-DGA ligands in ionic liquid

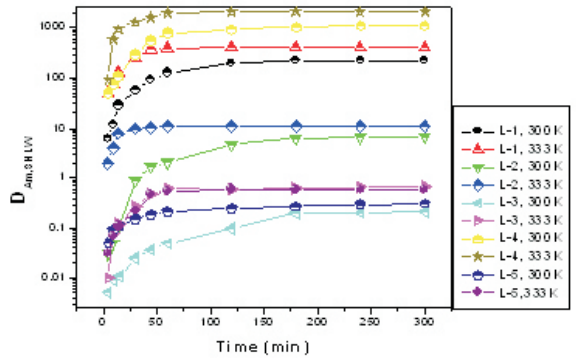


Fig. 3 Extraction kinetics of Am3+ with CDGAs in ionic liquid

extraction kinetics of Am^{3+} with the Calix-DGA ligands in ionic liquid.

Conclusions

L-1 and L-2 in ionic liquid are found to be suitable for actinide partitioning from SHLW. The extraction behavior found to follow ion exchange mechanism with slower kinetics

References

[1] K. Binneman, Chem Rev, 2007, 107, 2592-2614,

[2] A.V. Mudring, S.Tang, Eur. J. Inorg. Chem, 2010, 2569-2581,

[3] M.L. Dietz, Separation Science and Technology, 2007, 2047-2063,

[4] A.E. Visser, R.P. Swatloski, W.M. Reichert, R. Mayton, S. Sheff, A. Wierzbicki, J.H. Davis, R.D. Rogers, Chem. Commun. (2001) 135–136.

Bioaccumulation of Natural Radionuclides and Dose Transfer to Human Population in the Parangipettai Coastal Ecosystem, Tamil Nadu, India

P. Raja[1] and P. Shahul Hameed[2]

1. *Department of Zoology, H.H.Rajah's College, Pudukkottai 001, Tamil Nadu, India; E-mail: rajazoo75@ yahoo.co.in*
2. *Envir. Research Centre, J.J. College of Eng. & Technology, Ammapettai, Trichy 620 009.TN. India.*

This paper presents the Committed Effective Dose (CED) from Po-210 and Pb-210 to the coastal human population of Parangipettai coastal area due to the consumption of sea foods such as prawns, lobster, crabs, gastropods, bivalves, cephalopods and fishes. The Po-210 and Pb-210 were non uniformly distributed with specific bioaccumulation capability. The Po-210 concentration was decisively higher in the muscles of the food organism while Pb-210 maintained a low level. The total radioactivity intake depended both on the concentration and the amount of food consumed. Shell fishes (prawns, crabs and molluscs) contributed a substantial level of alpha radiation to the public (range: 3.37 – 54.99 Sv/y) as compared to that by fishes (range:3.71 – 94.51 Sv/y). The internal dosage received by the public of Parangipettai coastal area was 753.8 Sv/y from Po-210 and 148.8 Sv/y from Pb-210.

Keywords: Radionuclide, Parangipettai coastal ecosystem, ^{210}Po and ^{210}Pb, Dose, CEDE

Introduction

Parangipettai coast where River Vellar is confluencing north Bay of Bengal is located 233 km south of Chennai city of Tamil Nadu (Lat. 110 29' N; Long 790 46' E) Fig.1. The Parangipettai coast near vellar estuary is a true estuary subjected to long term fluctuations in physical and chemical features depending upon the seasonal tidal amplitude and freshwater influx and all resulting in a continuous exchange of organic, inorganic, plant and animal matters. The Parangipettai coast is a resourceful place for phyto and zooplankton and also has rich potential for fin and shellfish production1 [1-3].

Materials and Methods

Po-210 determinations were made by the standard technique of acid digestion, spontaneous deposition of Po-210 from an acid solution on to both sides of a polished silver disc and counting of the Po-210 alpha activity on the disc [4,5]. Pb-210 was estimated by allowing equilibrium growth of Bi-210 (T1/2=5d) separation of $BiPO_4$ and counting in a low beta counter [6]. The counting instruments used were an alpha counter with ZnS (Ag) detector with a background of 0.1 – 0.2 cpm and a counting efficiency of 25% and a low beta counter with a background of 1.5 to 2.0 cpm and efficiency of 40 %. Knowledge of the local dietary habits and per capita intake of diet components is required for assessing radioactivity intake through the seafood. A survey was carried out at the Parangipettai coast region, which has a coastal population covering in coastal villages. Detailed information about the diet was known from the population consisting mainly of fishermen. The activity levels of Po-210 and Pb-210 were analysed in all sea food organism consumed by local population. The radioactivity data of the seafoods

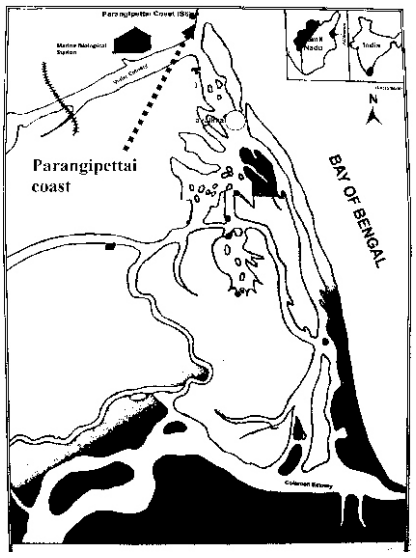


Fig. 1 Study area showing the sampling station

and the data from the diet information survey, the intake of Po-210 and Pb-210 were arrived at. The dose factors (ICRP, 1997) for the natural radionuclides are given below. Po-210: 1.2 x 10-6 Sv/Bq ; Pb-210: 6.9 x 10-7 Sv/Bq . Using the activity intake data and ICRP dose factors, the dose to the individual members of the population was calculated [7].

Conclusions

The present study has generated a database on the bioaccumulation of natural radionuclide and dose transfer to human population in parangipettai coastal ecosystem in the marine province for the first time. Water, sediment and biota (plankton, seaweeds, prawn,

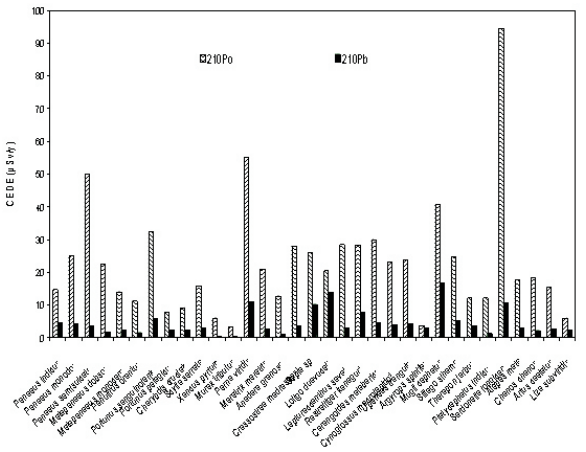


Fig. 2 Committed Effective Dose Equivalent (CEDE) to human population due to seafood intake in the Parangipettai coastal environment

crabs, gastropods, bivalves and fish) samples were subjected to analyses of Po-210 and Pb-210. The results showed a non-uniform distribution of these radionuclides in the biota, in a descending order: molluscs > crustaceans> fishes. The concentration of Po-210 and Pb-210 were 1.65 mBq/L and 3.38 mBq/L in water samples and 4.38 Bq/kg and 2.31 Bq/kg in sediment samples, respectively. The soft tissues and muscle of animals accumulated higher level of Po-210, while shells and bones contained more Pb-210. The bivalve mollusc Perna viridis accumulated higher concentrations of both Po-210 and Pb-210 thus suggesting that this species can probably serve as a bioindicator of radioactive pollution in marine environment. The concentration factor of Po-210 for the biotic components ranged from ~ 10^3 to ~10^4 while for Pb-210, it ranged from ~ 10^2 to ~ 10^3. The total dose transferred by Po-210 and Pb-210 amounted to 902.61 Sv/y and Po-210 contributed 83.5% and Pb-210 contributed 16.5% Sv/y. Po-210, the internal dose due to intake of seafood organisms ranged from 3.37 to 94.51 Sv/y whereas for Pb-210 it varied between 0.43 and 16.66 Sv/y. The committed effective dose to public due to sea food intake of Po-210 was estimated to be 753.82 Sv/y and of Pb-210 to be 148.8 Sv/y. Among the invertebrate seafood organisms consumed by the coastal population, a higher CED was recorded for Po-210 by bivalve Perna viridis (54.99 Sv/y) even though average consumption was found to be minimum of 3.8 kg/cap/y. Generally the average consumption of fish is found to be higher than that of other seafood animals. Among the 15 species of fish analysed, the fish Sardinella longiceps recorded a maximum CED (94.51 Sv/y) and Argyrops spinifer recorded a minimum (3.71 Sv/y). Despite the higher consumption of fish is found compared to other seafood organisms, it result in lesser CED to the public. The results of this study suggest that Po-210 contributes greater dose of 9.02 mSv/y to the coastal population through the consumption of sea foods. The generated data would be a valuable input for the assessment of changes in levels of radioactivity in the Parangipettai coastal ecosystem due to the operation of nuclear power plants in east coast of India.

Acknowledgement

Our sincere thanks are due to Department of Zoology, Jamal Mohamed College for institutional support, Dr. V. Meenakshisundaram, Section Head, Indira Gandhi Centre for Atomic Research, Kalpakkam for technical support and Dr. T. Manoharan, Principal, H.H. The Rajah's College, Pudukkottai for the constant encouragement in acadamic works.

References

[4] Flynn W.W., Anal. Chim. Acta., 43 (1968) 221.

[7] ICRP. Age-dependent Doses to Members of the Public from Intake of Radionuclides: Part 5 Compiation of Ingestion and Inhalation Dose Coefficients. Publication-72, Pergamon press, Oxford.(1997).

[5] Iyengar M.A. R., Ph.D. Thesis, University of Bombay, Bombay, (1983).

[6] Kamath P.R., Bhat I. S., Kamala Rudran, Iyengar M.A. R., Koshy E., Waingankar U.S. and Khanolkar V.S., Proc. of Symposium on Assessment of Radioactivity in man, Heidelberg, IAEA, Vienna, (1964).

[1] Krishnamurthy K. and Prince Jeyaseelan M.J., Int. J. Ecol. Envir. Sci. 9 (1983) 79.

[6] Raja P., Sadiq Bukhari A., Krishnamoorthy R., Shahul Hameed P. and Shahul Hameed M.M., National Symposium on Environment, (2004).

[7] Shahul Hameed P. and Raja P., J. Environmental Geochemistry, 8(1&2) (2005) 330.

Pb Isotopes Induced Bremsstrahlung in Bone Muscle and Teeth

H.C. Manjunatha

Department of Physics, Government College for Women, Kolar-563101, Karnataka, India; E-mail: manjunathhc@rediffmail.com

Introduction

The few isotopes of lead such as ^{210}Pb, ^{211}Pb, ^{212}Pb, ^{213}Pb, ^{214}Pb and ^{215}Pb are good beta emitters. These beta emitting Pb isotopes induce bremsstrahlung radiation and could have different energies and intensities. The Bremsstrahlung yield is a function of two components namely internal Bremsstrahlung and external Bremsstrahlung. The intensity of external Bremsstrahlung (EB) largely depends on the energy of the emitted beta particles and atomic number of the surrounding matrix material. On the other hand, internal Bremsstrahlung component inherently depends on the interaction of the emitted beta particle with the nucleus of the source radionuclide itself. The shapes of bremsstrahlung spectra are a basic ingredient in the understanding and quantification of beta-ray dosimetry. It is useful to have a convenient reference on the shapes of bremsstrahlung spectra from various nuclides. It is important to study the radiation hazards of lead isotopes. Hence in the present work we have formulated the method to study the bremsstrahlung dose induced by the lead isotopes in human bone, muscle and teeth.

Present Work

Estimation of EB cross section

Markowicz et al. [1] proposed an expression for modified atomic number (Z_{mod}) of compound target defined for bremsstrahlung process to take into account the self absorption of Bremsstrahlung and electron back scattering

$$\text{Here, } Z_{mod} = \frac{\sum_i^l \frac{W_i Z_i^2}{A_i}}{\sum_i^l \frac{W_i Z_i}{A_i}} \qquad (1)$$

Here, W_i, A_i and Z_i are atomic weight, weight fraction and atomic number of ith element respectively. The EB cross section is evaluated using Lagrange's interpolation technique, Seltzer-Berger [3] theoretical EB cross section data given for elements using the following expression

$$_{Z_{mod}} \quad \frac{Z_{mod} \quad Z}{Z' \quad Z} \quad _z \qquad (2)$$
$$z \quad Z$$

Where lower case z is the atomic number of the element of known EB cross section $_z$ adjacent to the modified atomic number (Z_{mod}) of the compound whose EB cross section $_{Z_{mod}}$ is desired and upper case Z are atomic numbers of other elements of known EB cross section adjacent to Z_{mod}. The estimated $_{Z_{mod}}$ (milli barn/MeV) is used for evaluation of spectrum.

Evaluation of Bremsstrahlung Spectrum

The number n(T,k) of EB photons of energy k when all of the incident electrons of energy T are completely absorbed in thick target is given by

$$n(T,k) = N \int_k^T \frac{E,k}{dE/dx} dE \qquad (3)$$

where (E, k) is EB cross section at photon energy k and electron energy E, N is the number of atoms per unit volume of target and E is the energy of an electron available for an interaction with nucleus of the thick target after it undergoes a loss of energy per unit length (-dE/dx). For a beta emitter with end point energy T_{max}, spectral distribution of EB photons [S (k)] is given by

$$S(k) = \frac{\int_T^{T_{max}} n\ T,k\ P\ T\ dT}{\int_T^{T_{max}} P\ T\ dT} \qquad (4)$$

where P(T) is the beta spectrum. Evaluated results of (E, k) of eq. (2) and tabulated values of (-dE/dx) of Seltzer-Berger[3] data are used to get S(k) for the target compounds.

Evaluation of Bremsstrahlung Dose

We used the following expression [3] for the calculation of specific absorbed fraction of energy at distance x from the point source monoenergetic photon emitter

$$x \quad \frac{_{en} \exp \quad x\ B_{en}}{4\ x^2} \qquad (5)$$

Here $_{en}$ is linear absorption coefficient of photons of given energy, is linear attenuation coefficient of photons of given energy, B_{en} is energy absorption build up factor; is density of the medium. The energy absorption build up factors have been computed using Geometric progression (GP) fitting method. The specific absorbed fraction for a given beta source was estimated by integrating over the entire bremsstrahlung spectrum.

$$x \quad \int_0^{T_{max}} _T\ x\ dT \qquad (6)$$

where T_{max} is the maximum energy of beta. Estimation of the value of allows calculation of the absorbed

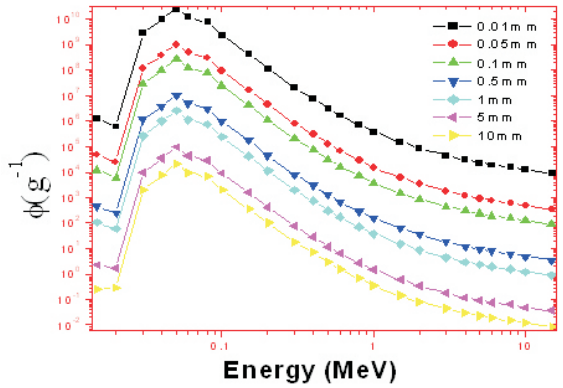


Fig. 1 The variation of specific fraction of absorbed energy ( ) with incident photon energy in bone at penetration depth = 40 mfp

dose at fixed distances from the point source in the infinite, homogeneous medium

$$D(x) = \sum_i \quad _i(x) \qquad (7)$$

where D(x) is the absorbed dose at distance x per unit initial activity (Gy/MBq); is the residence time of activity; and is the mean energy emitted per unit cumulated activity and it is numerically equal to (2.13 n_iE_i), where n_i is the frequency of occurrence of emissions with energy E_i; the quantities n and E are provided by the calculated bremsstrahlung spectrum using equation (4). It has been estimated D(x) between x = 0.01mm and x = 10mm, through complete decay of a given beta isotopes.

Results and Discussion

The specific absorbed fraction of energy (g^{-1}) is computed and it is shown in shown in Fig.1. It is observed that also increases up to the E_{pe} and then decreases. Here E_{pe} is the energy value at which the photo electric interaction coefficients match with Compton interaction coefficients for a given material. For muscle E_{pe} is almost equal to 0.1MeV. The variation of with energy is due to dominance of photoelectric absorption in the lower end and dominance of pair production in the higher photon energy region. In the lower energy end photoelectric absorption is dominant photon interaction process; hence values minimum. As the energy of incident photon increases, Compton scattering overtakes the photoelectric absorption. It results multiple Compton scattering events which increases the value of up to the E_{pe} and becomes maximum at E_{pe}.Thereafter (above E_{pe}), pair production starts dominating (absorption process) which reduces the value of to minimum.

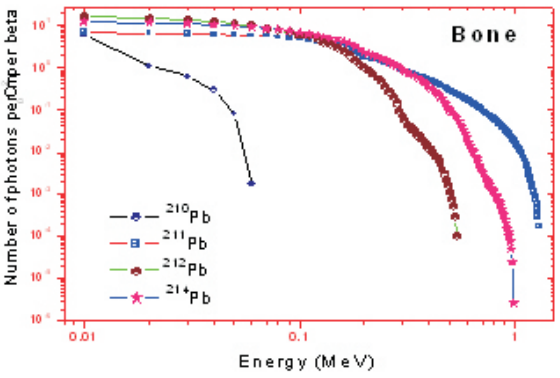


Fig. 2 Bremsstrahlung spectrum of beta emitting lead isotopes in bone

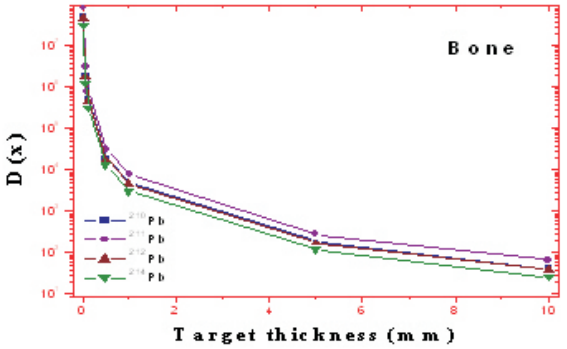


Fig. 3 Absorbed dose (in Gy/MBq) of Bremsstrahlung radiation in bone by beta emitting lead isotopes

During the calculation of values thickness of penetration depth is considered up to 40 mean free paths.

The computed bremsstrahlung spectrum and specific absorbed fractions of energy are used in the evaluation of bremsstrahlung dose. The evaluated Beta bremsstrahlung dose as a function distance for the studied nuclides is also presented. The beta bremsstrahlung dose decreases with the increase of distance. The presesnt work is useful to analyse the radiation hazards of lead isotopes.

References

[1] A.A.Markowicz, R.E.VanGriken.Anal. Chem. 56 (1984) 2049.

[2] ICRU Report No. 44, (1989)

[3] H.C.Manjunatha, B.Rudraswamy. NIM A 621 (2010) 581

Dose Assesment of Bremsstrahlung Induced by Beta-Emitter Radioisotopes of Uranium-238 Series in Human Tissues

H.C. Manjunatha

Department of Physics, Government College for Women, Kolar 563101, Karnataka, India;
E-mail: manjunathhc@rediffmail.com

In the natural Uranium-238 decay series, pure beta isotopes such as ^{234}Th, ^{234}Pa, ^{214}Pb, ^{214}Bi, ^{210}Pb and ^{210}Bi are released. These beta isotopes having maximum beta energies and it induces the bremsstrahlung radiation. The bremsstrahlung component of these beta isotopes has been traditionally ignored in dosimetry calculations. This may be due to a lack of available methods for including this component in the calculations or to the belief that the contribution of this component is negligible compared to that of other emissions. The resulting hazard of bremsstrahlung radiation may therefore be some of concern, at least theoretically, and should be systematically evaluated.

In the present investigation, it has been estimated that the bremsstrahlung dose of beta isotopes of Uranium-238 series such as ^{234}Th, ^{234}Pa, ^{214}Pb, ^{214}Bi, ^{210}Pb and ^{210}Bi in various body organs (incomplete sentence) (Adrenals, Brain, Breasts, Gallbladder Wall, LLI Wall, Small Intestine, Stomach, ULI Wall, Heart Wall, Kidneys, Liver, Lungs, Muscle, Ovaries, Pancreas, Red Marrow, Bone Surfaces, Skin, Spleen, Testes, Thymus, Thyroid, Urin Bladder Wall, Uterus, Fetus, Placenta and Total Body).

Present Work

Computations of the bremsstrahlung dose rate have been divided into three parts, which are as follows; computation of bremsstrahlung efficiency, computation of bremsstrahlung intensity and computation of bremsstrahlung dose rate.

Computation of Bremsstrahlung Efficiency

Markowicz et al. (1984) proposed an expression for modified atomic number (Z_{mod}) of compound target defined for bremsstrahlung process to take into account the self absorption of bremsstrahlung and electron back scattering

$$Z_{mod} = \frac{\sum_i \frac{W_i Z_i^2}{A_i}}{\sum_i \frac{W_i Z_i}{A_i}} \qquad (1)$$

Here, W_i, A_i and Z_i are atomic weight, weight fraction (whether atomic weight and weight fraction are reversed?) and atomic number of ith element respectively. Z_{mod} is evaluated using equation (1) and their composition (ICRU-44). The bremsstrahlung efficiency gives the total fraction of a beta/electron energy that will appear as bremsstrahlung radiation (it is also called as yield) and it can be expresses as

$$\frac{3 \quad 10^{-4} Z_{mod} E_{max}}{1 \quad 3 \quad 10^{-4} Z_{mod} E_{max}} \qquad (2)$$

The above equation is used to estimate the bremsstrahlung efficiency/yield and it is useful to estimate the bressstrahlung hazard. The fraction appearing as bremsstrahlung radiation is linearly (the equation 2 does not predict a linear dependence on Zmod) related to the modified atomic number of the medium.

Computation of Bremsstrahlung Intensity

The rate of energy emission by the source of beta particles with maximum energy of beta (E_{max}) in MeV is (this should be for a given amount of radioactivity, it should be made clear)

$$E \quad 3.7 \quad 10^{11} \quad E_{max} \ \text{MeVs}^{-1} \qquad (3)$$

The rate of energy emission in the form of bremsstrahlung photons is therefore

$$E \quad 3.7 \quad 10^{11} \quad E_{max} \ \text{MeVs}^{-1} \qquad (4)$$

We next compute the exposure rate from bremsstrahlung, treated as coming from a source at a distance r in cm. The intensity at a distance r is given by

$$I \quad \frac{E}{4 \quad r^2} \ \text{MeVcm}^{-2}\text{s}^{-1} \qquad (5)$$

Above equation is used to evaluate the bremsstrahlung intensity.

Computation of Bremsstrahlung Dose Rate

The dose rate in air is

$$D \quad \frac{en}{} I \quad \frac{en}{} \quad \frac{E}{4 \quad r^2} \ \text{MeVg}^{-1}\text{s}^{-1} \qquad (6)$$

Converting units and remembering that 1R=0.0088Gy in air

$$X \quad \frac{en}{} \quad \frac{E}{4 \quad r^2} \quad 6.546 \quad 10^{-5} \text{Rh}^{-1} \qquad (7)$$

Above equation is used to evaluate the bremsstrahlung dose rate by various pure beta nuclides in human tissues.

Results and Discussion

The modified atomic number (Z_{mod}) of compound target defined for bremsstrahlung process is considerd

for the computation of bremsstrahlung efficiency. Bremsstrahlung intensity and bremsstrahlung dose rate also increase with E_{max} of beta nuclide and modified atomic number of target tissue.While estimating the Bremsstrahlung radiation hazard, Bremsstrahlung yield is also important and with out this it is difficult to come for conclusion. The efficiency (yield), intensity and dose rate of bremsstrahlung in Cortical bone is higher than that of all other studied tissues. The efficiency (yield), intensity and dose rate of Bremsstrahlung in yellow marrow is lower than that of all other studied tissues.We have considerd bone and muscle is target organs. These estimated values shows that the bremsstrahlung radiation absorbed dose contribution from an organ to itself is very small compared to that from the beta source, but contribution to other organs is not always negligible. Hence the compnent of bremsstrahlung dose to total dose should be considered in the envirnmental radiactvity dose calculations.

The penetration depth (distance moved by the beta in target tissue) of the beta can be calculated from the estimated Bremsstrahlung dose rate. The thickness x needed to reduce the exposure rate to 1 mR h^{-1} is given by

$$1 = X \quad e \quad ^{x} \qquad (7)$$

and ì are bremsstrahlung dose rate in mR/h and linear attenuation in per cm respectively.

$$x \quad \frac{1}{-} \ln \; X \; cm \qquad (8)$$

Penetration depth of bremsstrahlung (x) is calculated from the above equation (8). Bremsstrahlung efficiency, intensity and penetration depth, determine the quality and quantity of the radiation (known as the source term). Precise estimation of this source term is very important in planning for radiotherapy and diogonisis. The given data may be useful in the field of radiation dosimetry and radiotherapy. The calculations employed the accurate energy absorption buildup factors and the Bremsstrahlung photon spectrum.

Tissue	Zmod	Tissue	Zmod
Adipose tissue	5.505	Spongiosa	7.498
Blood	6.548	Yellowmarrow	5.41
Brain	6.43	Skin	6.369
Breast	6.054	Spleen	6.515
Cell nucleus	6.459	Testis	6.278
Eye lens	6.397	Thyroid	6.512
GI track	6.466	Skeleton-cortical bone	10.991
Heart	6.517	Skeleton-cranium	10.012
Kidney	6.496	Skeleton-femur	8.618
Liver	6.491	Skeleton-humerus	9.214
Lung	6.540	Skeleton-mandible	10.194
Lymph	6.598	Skeleton-ribs(2nd,6 th)	8.929
Muscle	6.481	Skeleton-ribs(10th)	9.487
Ovary	6.307	Skeleton-sacrum	8.196
Pancreas	6.376	Skeleton-spongiosa	7.494
Cartilage	6.648	Skeleton-vertibral column(c4)	8.545
Redmarrow	5.952	Skeleton-vertibral column(D6,L3)	8.503

References

[1] Matthew Hough, Perry Johnson, Didier Rajon, Derek Jokisch, Choonsik Lee, Wesley Bolch, Phys. Med. Biol. 56 (2011) 2309–2346

[2] C. Lee, A.P. Shah, W.E. Bolch, Phys. med. biol., 51(21)(2006) 5391-407

[3] Amish P. S, Wesley E.B, Didier A. R, Phillip W.P, Derek W. J., J. Nucl. Med. 45 (2005) 344-353

[4] M. G. Stabin, K. F. Eckerman, J.C. Ryman, L.E.Williams, J NucI.Med. 35 (1994) 1377-1380

[5] L.Williams, J.Wong, D.Findley, B.Ford. J.Nucl. Med. 30(1989)1373-1377.

[6] Turner. J, Atoms, radiation, and radiation protection. New York: Pergamon Press; (1986)90

[7] A.A.Markowicz, R.E.VanGriken, Anal. Chem. 56(1984) 2049

[8] ICRU Report No. 44, (1989)

[9] M.G. Stabin, Radiation Protection and Dosimetry; an Introduction to Health Physics, Springer publication, 55

Treatment of Radioactive Liquid Waste Containing Mn^{2+} by Synthetic Hydroxyapatite

Diganta Gogoi[1], A.G. Shanmugamani[2], S.V.S. Rao[2], T. Kumar[1], B. Sreekumar[1], P.K. Sinha[3]

1. *Kalpakkam Reprocessing Plant, Nuclear Recycle Board, Bhabha Atomic Research Centre, Kalpakkam 603102*
2. *Centralized Waste Management Facility, Nuclear Recycle Board, Bhabha Atomic Research Centre, Kalpakkam 603102*
3. *Waste Management Division, Bhabha Atomic Research Centre, Mumbai 400085, E-mail: digantogogoi1@gmail.com*

The removal of manganese from a simulated radioactive liquid waste was evaluated using a radiotracer, ^{54}Mn in a batch method by synthetic Hydroxyapatite (HAP). The influences of different parameters such as solution pH, and sodium concentration, on manganese removal were studied. In the presence of sodium ions, the sorption of manganese on HAP was not affected. The sorption of manganese on HAP was pH independent in the range from 4 to 6, because of its buffering properties.

Introduction

Radioactive manganese (^{54}Mn) is produced in the structural and clad materials of fast nuclear reactors due to the high neutron flux encountered in the core. Both radioactive as well as the inactive manganese have significant influences on our environments. ^{54}Mn is having a half-life of 312.5 days and gamma energy of 835keV. Manganese in aqueous solutions can affect both human beings and the aquatic life. High concentration of manganese in human beings can cause brain damage and neural problems. In case of sodium cooled fast breeder reactors, during cleaning of reactor components, ^{54}Mn is removed from the components which results in liquid alkaline waste in the form of aqueous solution of sodium carbonate and sodium bicarbonate where sodium concentration is around 2.1g/L [1].

There are some inorganic sorbents which are used for the removal of manganese such as Kaolinite [2], fly ash [3], Carbon nanotube [4] etc.

Hydroxyapatite (HAP), $Ca_{10}(PO_4)_6(OH)_2$ has been used for the removal of cobalt, copper and other ions. Here, a series of experiments were done to find out the feasibility of synthetic hydroxyapatite for Mn removal from a simulated radioactive waste solution.

Experimental

The HAP was synthesized by a precipitation technique described elsewhere [5]. The precipitate formed was washed with distilled water and it was dried at room temperature for around one week. The material was characterized by XRD, using a Siemens D-500 diffractometer (Germany), FT-IR using an IR Spectrometer Bomem MB 100, with the KBr disc method, thermogravimetric analysis using a TG/DT STA 1500 (Rheometric Scientific Ltd., UK).The simulated sodium carbonate solutions containing 0.001M of Mn (II) were prepared from $MnSO_4.H_2O$ salt where concentration of Na was 2.1g/L.

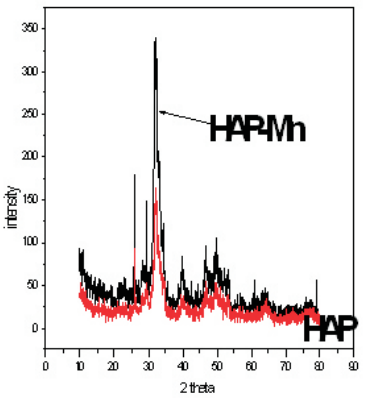


Fig. 1 The XRD spectrum of HAP and HAP-Mn

The experiments were carried out in the batch mode by mixing in beakers containing 1 g of HAP and 100 mL of the above ^{54}Mn spiked solution with continuous stirring. In order to get information on the sorption of manganese ions, small aliquots of the supernatants were taken from the extraction beaker after each 10 minutes of stirring. These samples were analyzed for their gamma activities using a Single Channel Analyzer of Electronic Corporation of India (ECIL), INDIA make. The pH of the final solutions was adjusted by addition of aqueous solutions of NaOH or HNO_3. The initial gamma activities were found to be around 30 -35Bq/mL.

Results and Discussion

HAP Characterization

The XRD spectrum indicates that the HAP synthesized has low crystallineity as shown in Fig.1. The thermo gravimetric analysis (Fig.2) indicates that below 200°C, there is a sharp weight loss which is due to the loss of surface water while below 500^0C the weight loss is due to the loss of interstitial water molecules.

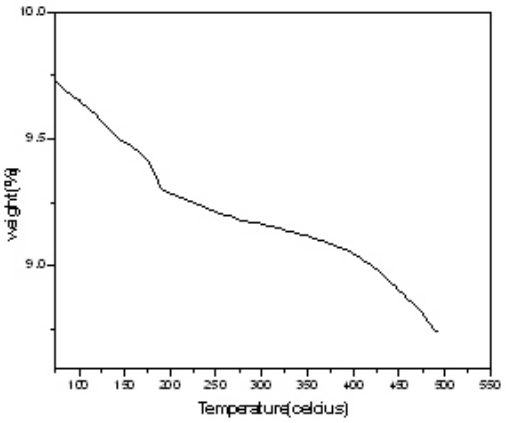


Fig. 2 The TG spectrum of HAP

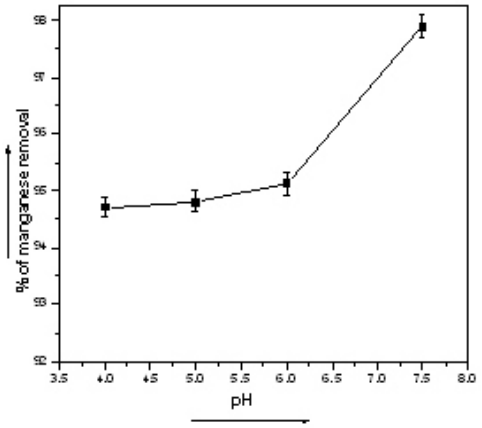


Fig. 3 Effect of solution [pH]

Effect of Solution pH on Metal Sorption

As shown in Fig.3, it was observed that between pH 4 and 6, there was almost no change in manganese ions extraction by HAP. This was due to the buffering properties of synthetic HAP. Beyond pH 6, the removal of manganese suddenly increases which is attributed to the precipitation of manganese as its hydroxides [6]. The buffering capacity of HAP is the results of acid–base reactions of accessible chemical groups on its surface. The chemical composition of the surface phase of HAP is constant in solution of pH within the range 4–10[7]. The mechanisms of the metal cations retention by HAP are different and include ion exchange processes, adsorption, dissolution, precipitation and substitution of Ca^{2+} ions in HAP by other metals during co-precipitation [5].

Effect of sodium ion concentration: It is found (Fig.4) that sodium ions are not having any influence towards removal of manganese by HAP in the sodium concentration range of 0-100g/L.

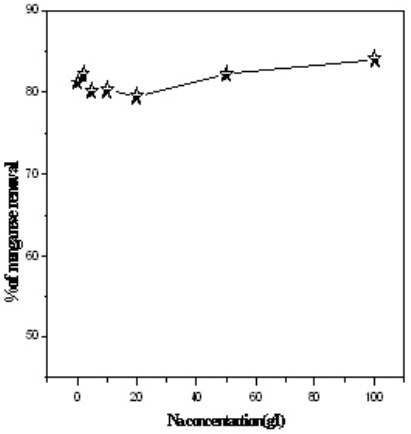


Fig. 4 Effect of sodium ions

Conclusion

The study shows that synthetic HAP can be used for the effective removal of manganese (II) ions in presence of sodium ions which is favored by pH in between 4 and 6.

Acknowledgement

The authors express sincere thanks to S. Chitra, Laboratory Superintendent, CWMF, and Biplob Paul, Plant Superintendent, CWMF, Kalpakkam, for their continuous encouragement.

References

[1] Muralidharan,P.et.al., CG/MCD/2001/12/R-O (2001)

[2] O. Yuvuz, et al., Water Res., 37 (2003) 948.

[3] Y.C. Sharma, Uma, S.N. Singh, Paras, F. Gode, Chem. Eng. J., 132 (2007) 319.

[4] Stafiej, et al., Sep. Purif. Technol. (2007) 5849.

[5] Diganta Gogoi, A. G. Shanmugamani, S. V. S. Rao, T. Kumar, P. K. Sinha, J Radioanal Nucl Chem, DOI 10.1007/s10967-012-2378-6.

[6] N.N. Greenwood, A. Earnshow, Pergamon Press, Oxford, (1984) 1211.

[7] O. Rosskopfova´, M. Galambos¡, J. Ometa´kova´, M. C ¡ aplovic¡ova´ , P. Rajec, 2012. 293:641–647, DOI 10.1007/s10967-012-1711-44.

Isolation, screening and characterization of Uranium microremediable actinomycetes from fallen leaves of Azadirachta indica in Western Ghats.

Mrinalini.J.Singh[1], Dr.S.Padmavathy[2]

1. *Research Scholar, Department of Botany, Nirmala College for Women, Coimbatore 641 018, Tamil Nadu, India; Email: mrinalini.singh50@gmail.com*
2. *Associate Professor of Botany, Nirmala College for Women, Coimbatore 641 018, India.*

Objective

The aim of this study was to isolate and screen the actinomycetes from fallen leaves of Azadirachta indica (Neem) in Western Ghats, India that has the capacity to microremediate radioactive waste Uranium. The influence of different temperature and pH on Uranium removal was also studied.

Methodology

Isolation

Actinomycetes was isolated from the surface sterilized fallen leaves of Azadirachta indica (Neem) plated on Humic acid Vitamin agar supplemented with nystatin and nalidixic acid to inhibit the growth of fungi and bacteria respectively.

Uranium Bioremediation Study

Uranium bioremediation study was carried out to screen the isolated actinomycetes that showed the capacity to microremediate radioactive waste Uranium. Culture media containing uranium which was added as uranyl nitrate was inoculated with 1% (v/v) freshly prepared inoculum of isolated strain. Estimation of residual uranium contents in the filtrate were measured spectrophotometrically at different time intervals. The screened isolate was then characterized by using morphological and biochemical methods. The influence of temperature and pH on uranium removal by the screened actinomycetes isolate was also studied.

Result

A total of six actinomycetes isolates were isolated from surface sterilized fallen leaves of Azadirachta indica. One strain, A5, was selectively screened due to its remarkable microremediation of radioactive waste uranium since the microbe could remove 70% uranium in 12 hours of growth. Uranium removal was better at 30°C and at pH 9. Colony characteristics on Yeast extract

Malt extract agar (ISP2) and biochemical characteristics showed that A5 belonged to the Streptomyces sp.

Significance and Impact

There was no scientific report before on actinomycetes from plant leaves that can microremediate uranium. Hence, isolation and screening of actiomycetes from plants in optimum condition could be the promising resource of potential eco-friendly radionuclide microremediating agent. Further characterization, purification and structural elucidation are recommended to know the novelty of the microbe and quality of the product. Even, its

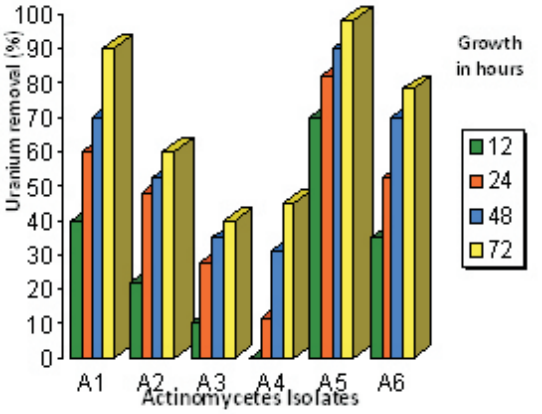


Fig. 1 Uranium Bioremediation study

Table 1: Effect of temperature in Uranium removal

Temp.	A5 Uranium removal (%)			
	12 hrs	24 hrs	48 hrs	72 hrs
10	0	0	0	0
25	60	71	82	90
30	70	82	90	98
45	40	48	56	62
60	0	0	0	0

Table 2: Effect of pH in Uranium removal

pH	A5 Uranium removal (%)			
	12 hrs	24 hrs	48 hrs	72 hrs
3	0	4	7	10
5	10	24	53	70
7	65	78	89	98
9	70	82	90	98

microremediation capacity with other radionuclides and heavy metals may also be investigated.

Acknowledgment

We are thankful to authorities of Nirmala College for Women, Coimbatore, Tamil Nadu and Yaazh Xenomics, Chennai for providing necessary facilities. The first author is sincerely grateful to University Grants Commission, Government of India, for providing the award of Junior Research Fellowship in Science to pursue the research work.

References

[1] Takehiko Tsuruta, American Journal of Environmental Sciences 3 (2) (2007) 60.

[2] Takehiko Tsuruta, J. Nucl. Radiochem.l Sci., 6(1) (2005) 81.

[3] Takehiko Tsuruta, J. Nucl. Radiochem.l Sci., 7(1) (2006) 1.

[4] Takehiko Tsuruta, Journal of bioscience and bioengineering , 97(4) (2004) 275.

[5] Sarkar & Ghosh J. BioSci. Biotech., 1(2) (2012) 141.

[6] M. A. Abu-Eid, et al, An-Najah J. Res., II(13) (1994).

[7] Pranvera Lazo et al., Asian Journal of Chemistry 12(3) (2000) 732.

Annual effective dose due to Natural radioactivity in drinking water

P Padma Savithri[1], S K Srivastava[1], A Y Balbudhe[1], K Vishwa Prasad[1], P M Ravi[2] and R M Tripathi[2]

1. *Health Physics Unit, NFC, Health Physics Division, Bhabha Atomic Research Centre, PO: ECIL, Hyderabad 500062, India; E-mail: pps@nfc.gov.in*
2. *Health Physics Division, Bhabha Atomic Research Centre, Trombay, Mumbai 400085, India*

Natural radioactivity concentration in drinking water supply in and round Hyderabad, Secunderabad was determined. The observed gross alpha activity found in water samples vary from 0.027±0.014 Bq/L to 0.042±0.015 Bq/L with average 0.035 Bq/L while beta activity in all the samples are less than 0.076 Bq/l. Contributions of the drinking water samples to total annual effective dose equivalent from ^{238}U, ^{234}U, ^{230}Th, ^{226}Ra, ^{210}Po, ^{232}Th, ^{228}Th ^{210}Pb and ^{228}Ra are 1.14, 1.24, 5.30, 7.07, 30.3, 5.81, 1.82, 38.3 and 38.3 Svy^{-1} for adults. The results indicate that the annual effective doses are below the WHO recommended reference level for and in food and drinking samples .

Introduction

Natural radioactivity such as U, Th, and their daughter products and ^{40}K exists in the various environmental matrices, though the concentration may vary from place to place. Compared to the natural sources, addition of radionuclide into drinking water stream due to man made activities including operation of nuclear facilities is insignificant. WHO has recommended a screening levels of 0.5 Bq/litre for gross alpha activity and 1 Bq/litre for gross beta activity for drinking water below which no further action is required [1].

Source of drinking water in twin cities of Hyderabad and Secunderabad is mainly dam water built on river or collected rainwater. Hyderabad Metro Water Supply and Sewerage Board reveals around 1 crore population residing in and around twin cities use tap water as the principal source of water supply. Water samples from dam built on river or rain water has been collected and analyzed for gross alpha and beta radioactivity. The main aim of this study is to determine the natural radioactivity levels in drinking water supplied to the twin cities and estimate annual effective dose equivalent due to different source of drinking water.

Material and Method

Water samples were collected in pre cleaned polythene bottle and filtered through 0.45 micron Millipore filter paper followed by gross alpha and gross beta estimation.

Gross Alpha

2 ltr. of filtered water sample is acidified with 5 ml of conc. HCl. 3mg of Fe carrier and 2 mg of Ba carrier is added to it. While heating 5 mL of 50% of ammonium sulphate is added followed by addition of 1:1 NH_3 solution till pH –7 to get precipitate. The distilled water washed precipitate is transferred to previously weighed SS planchet and count for alpha activity on ZnS(Ag) scintillation based alpha counter manufactured by ECIL make No. RCS-4037. Self attenuation correction factor has been assessed by standard addition method (natural uranium) and applied in activity estimation.

Gross Beta

2 litre of filtered sample is acidified with 5 mL of conc. HCl. 100 mg of Ca carrier is added to it to adjust the pH of water sample to 4 -5. 25 mL of Sulkowich reagent (25 g oxalic acid + 25 gm ammonium oxalate + 50ml acetic acid, dissolved in 600 ml distilled water and heated at 40-50°C. Cooled and made up to 750 mL) is added till to get precipitate. The distilled water washed precipitate is transferred to previously weighed SS planchet and counted for beta activity using G M based beta counter manufactured by ECIL make No. RCS-4037.

Result and Discussion

The measured activity concentrations of gross alpha in water samples of different locations in twin cities of Hyderabad are presented in Table 1. The observed gross alpha activity found in water samples vary from 0.027±0.014 Bq/L to 0.042±0.015 Bq/L with average 0.035 ±0.007 Bq/L. The highest gross alpha activity in the water was found in Himayath Sagar and the lowest gross alpha activity in water samples was found in Manjra. The gross alpha activity in water sample is primarily comprised uranium and thorium decay products such as ^{238}U, ^{234}U, ^{230}Th, ^{226}Ra, ^{210}Po, ^{232}Th, and ^{228}Th.

WHO recommends the parameter of gross alpha activity concentration to be 0.5 Bq/L [1]. Bureau of Indian Standards recommends to be 0.1Bq/L [2]. The results obtained show that the measured activity concentrations of gross alpha in all tap water samples is meeting both standards.

The measured activity concentrations of gross beta in tap water samples of different locations in twin cities tap water supply source are shown in Table 1. The observed gross beta activity found in tap water samples less than 0.076 Bq/L. The gross beta activity in water sample is primarily comprised uranium and thorium decay products such as ^{210}Pb and ^{228}Ra. WHO recommends the levels of gross beta activity

Table 1: Gross alpha, Gross beta and annual effective dose for alpha and beta emitters

Sample	Gross Alpha (Bq/L)	Alpha Emitters (Sv/y)							Gross Beta (Bq/L)	Beta Emitters (Sv/y)	
		^{238}U	^{234}U	^{230}Th	^{226}Ra	^{210}Po	^{232}Th	^{228}Th		^{210}Pb	^{228}Ra
Osman Sagar	0.029 ±0.015	0.95	1.04	4.45	5.93	25.4	4.87	1.52	<0.076	<38.3	<38.3
Himayath Sagar	0.042 ± 0.016	1.38	1.50	6.44	8.58	36.8	7.05	2.21	<0.076	<38.3	<38.3
Singur	0.033 ± 0.014	1.08	1.18	5.06	6.75	28.9	5.54	1.73	<0.076	<38.3	<38.3
Manjira	0.027 ± 0.014	0.89	0.97	4.14	5.52	23.7	4.53	1.42	<0.076	<38.3	<38.3
Nagarjuna Sagar	0.042 ± 0.015	1.38	1.50	6.44	8.58	36.8	7.05	2.21	<0.076	<38.3	<38.3
Mean	0.035 ± 0.007	1.14	1.24	5.30	7.07	30.3	5.81	1.82	<0.076	<38.3	<38.3

concentration to be 1.0 Bq/L [1]. The results obtained show that the measured activity concentrations of gross beta in all tap water samples are less than 1.0 Bq/L which is the limit recommended by WHO and BIS.

The total indicative dose was calculated for and emitters as following [3,4].

$$DRw = Aw \times IRw \times DC$$

Where DRw annual effective dose equivalent (Sv year^{-1}), Aw gross and gross activities (Bq L^{-1}), IRw intake of 730 litre of water for adult person in 1 year, DC dose coefficient (SvBq^{-1})

Assuming gross activity to be from any one of ^{238}U, ^{234}U, ^{230}Th, ^{226}Ra, ^{210}Po, ^{232}Th, ^{228}Th respectively and gross activity to be from any of ^{210}Pb and ^{228}Ra respectively Annual effective dose equivalent was calculated. [5].

Contributions of the drinking water samples to total annual effective dose equivalent from ^{238}U, ^{234}U, ^{230}Th, ^{226}Ra, ^{210}Po, ^{232}Th, ^{228}Th, ^{210}Pb and ^{228}Ra are 1.14, 1.24, 5.30, 7.07, 30.3, 5.81, 1.82, 38.3 and 38.3 Svy^{-1} for adults. The results from this study indicate that the annual effective doses are below the WHO recommended reference level of 300 Svy^{-1} due to food and drinking water [1].

Conclusion

Drinking water supply to twin cities of Hyderabad and Secunderabad is mainly dam water built on river or collected rainwater. The observed gross alpha and gross beta activity in drinking water samples is within WHO recommended limit of 0.5 Bq/L for alpha and 1.0 Bq/L for beta activity. The data obtained in this study is baseline which can be used to evaluate possible future changes. This study is useful to know the radiological impact on the public from naturally occurring radio nuclides in drinking water and can also serves to assess hydro geochemical changes to the environment.

Reference

[1] WHO, Guidelines for Drinking-water Quality, third ed. In: Radiological Quality of Drinking Water. World Health Organization, Geneva (2004), Switzerland.

[2] IS 10500; Indian Standard Drinking Water-Specification (2004)

[3] ICRP 119 Compendium of dose coefficient based on ICRP publication 60 (2012)

[4] Sajo-Bohus L, Gomez J, Capote T, Greaves ED, Herrera O, Salazar V, Smith A, J Environ Radioactivity 35 (1997) 305.

[5] F Korkmaz Gorur, R Keser, S Dizman, N T Okumusoglu, Desalination 279 (2011) 135.

Natural Radioactivity in Soil and Dose Rate around Hyderabad, India

A.Y. Balbudhe[1], K. Vishwa Prasad[1], S.K. Srivastava[1], P Padma Savitri[1], P.M. Ravi[2] and R.M. Tripathi[2]

1. *Health Physics Unit (NFC), Health Physics Division, Bhabha Atomic Research Division, Hyderabad-62; E-mail: ayb@nfc.gov.in*
2. *Health Physics Division, Bhabha Atomic Research Division, Mumbai*

Natural radioactivity in soil is significant component of the natural radiation exposure to the population inhabiting that area. Activity of ^{226}Ra, varies from 10.1±2.8 to 80.4±3.5 Bq/kg with mean of 40.2Bq/kg, activity of ^{232}Th varies between 73.5±2.3 and 192.3±2.2 Bq/kg with mean value of 144.7Bq/kg and that of ^{40}K varies between 200.2±10.7 and 1297.8±9.9 Bq/kg with mean value 921.9 Bq/kg. Ratio of ^{226}Ra to ^{232}Th activity varies from 0.06 to 0.47. Computed gamma dose rate varies from 83.27 to 195.60 nGy/h. This is higher than world average and may be due to higher levels of ^{232}Th and ^{40}K in soil.

Introduction

Natural radionuclides in soil generate a significant component of the natural radiation exposure to the population inhabiting that area. The earth's crust is the principle source of natural radionuclides in soils and rocks [1,2]. Igneous rocks of granitic composition are strongly enriched in uranium and thorium, compared to rocks of basaltic or ultramafic composition [3,4].

Since natural background radiation is the main source of human exposure, studies on the levels of natural radioactivity in the environmental matrices and the dose from this source will be useful to compare the radiation exposure from manmade exposures. Hence a study was carried out to determine prevalent natural radioactivity in surface soil around twin cities.

Study Area

Twin cities of Hyderabad and Secunderabad are located on Deccan plateau region of India and lies between N17^0 30' to E78^0 35'. Geologically it is situated on granite gneisses formation of archaean and proterozoic rocks covering a vast time span from 3800 to 570 million years [5]

Materials and Methods

Standard procedures were followed for collection and preparation of samples [6]. Filled containers were weighed and sealed hermitically. The sealed containers were stored for 4-5 weeks before counting to attain secular equilibrium between ^{226}Ra and ^{222}Rn and its decay products.

The samples were analysed using high resolution gamma spectrometery system based on high purity germanium (HPGe) detector. The spectra were analysed for photopeaks due to ^{226}Ra, ^{232}Th daughter products and ^{40}K. Activity of radionuclides was calculated from the prominent gamma energies.

Apart from measurement of radionuclide concentration, radium equivalent activity (Ra_{eq}) [1], radioactivity level index ($I_{\gamma r}$) [4,7,8], external hazard index (H_{ex}) [4,6,7], internal hazard index (H_{in}) [4,7,8], annual gonadal dose equivalent (AGDE) [2,4,7,8,9] and the total gamma absorbed dose rate (D) due to the activity concentration of ^{226}Ra, ^{232}Th and ^{40}K at 1m height were also determined using standard methods [2].

Results and Discussion

The results of analysis of activity concentration of ^{226}Ra, ^{232}Th and ^{40}K in surface soil samples around the twin cities of Hyderabad and Secunderabad are presented in Table 1. Activity of ^{226}Ra, varies from 10.1±2.8 to 80.4±3.5 Bq/kg with mean of 40.2 Bq/kg, activity of ^{232}Th varies between 73.5±2.3 to 192.3±2.2 Bq/kg with mean value of 144.7 Bq/kg and that of ^{40}K varied between 200.2±10.7 to1297.8±9.9 Bq/kg with mean value 921.9 Bq/kg. Ratio of ^{226}Ra to ^{232}Th activity varies from 0.06 to 0.47. The average values for concentration of ^{226}Ra, ^{232}Th and ^{40}K in Indian soil reported earlier by Mishra and Sadasivan were 15.2, 18.4 and 435.3 Bq/kg respectively [10] and the world average values are 30, 45 and 420 Bq/kg respectively [2].

As observed in Table 1, higher radioactivity levels reflects the influence of weathered material from rocks that contain elevated levels of natural radioactivity. In comparison to world average, mean values of ^{226}Ra, ^{232}Th and ^{40}K are higher by a factor 1.3, 3.2 and 2.2 respectively[2]. Concentration of ^{226}Ra and ^{232}Th depends to a large extent on the mineral composition of host rocks. The rocks in this region are granite which has more of ^{226}Ra than most of the other rock types.

The plot of natural thorium to uranium concentration in surface soil samples at different sampling points is shown in Fig. 1. R^2 found to be 0.147 which indicates poor correlation between thorium and uranium in the surface soil samples. Mean of Th/U ratio observed to be 11.03 which is in good agreement with earlier values reported for Hyderabad [10].

It is seen from the Fig. 2 that ^{238}Uand ^{40}K follow some what definite pattern but ^{232}Th do not show any definite pattern with ^{40}K. Similar observations were reported earlier in countrywide survey of Indian soil [10].

Table 1: Results of analysis of soil samples for natural radioactivity

Location	^{226}Ra (Bq/kg)	^{232}Th (Bq/kg)	^{40}K(Bq/kg)
APOU(1)	41.5±3.3	105.2±2.4	1089.2±11.9
Bongulur(2)	28.4±3.1	73.5±2.3	617.7±10.3
Gandipet(3)	39.6±2.0	85.3±1.5	939.0±7.1
Golkonda(4)	49.0±3.7	175.9±3.0	876.4±12.3
Ibrahimpatnam(5)	45.7±2.6	192.3±2.2	1297.8±9.9
Shameerpet(6)	61.1±3.1	147.7±2.4	882.3±10.1
Yapral(7)	10.1±2.8	176.9±3.6	994.6±11.1
Shameerpet Lake(8)	80.4±3.5	172.8±2.6	1296.6±12.2
Bolaram(9)	17.9±3.6	180.4±3.2	200.2±10.7
M Bolaram(10)	28.2±3.2	136.9±2.6	1025.2±11.8

Table 2: Computed radiation hazard indices.

Location	Ra_{eq} (Bq/kg)	^{226}Ra /^{232}Th	I_{mr}	H_{ex}	H_{in}	AGDE (Sv/y)	Dose rate (nGy/h)
1	275.80	0.39	2.05	0.74	0.86	909.98	128.13
2	181.07	0.39	1.34	0.49	0.57	588.94	83.27
3	233.84	0.46	1.74	0.63	0.74	773.63	108.95
4	368.07	0.28	2.67	0.99	1.13	1162.01	165.45
5	420.60	0.24	3.09	1.14	1.26	1352.48	191.37
6	340.25	0.41	2.47	0.92	1.08	1083.23	154.23
7	339.70	0.06	2.50	0.92	0.94	1083.11	153.01
8	427.38	0.47	3.13	1.15	1.37	1377.98	195.60
9	291.22	0.10	2.06	0.79	0.83	872.03	125.55
10	302.91	0.21	2.24	0.82	0.89	981.29	138.47

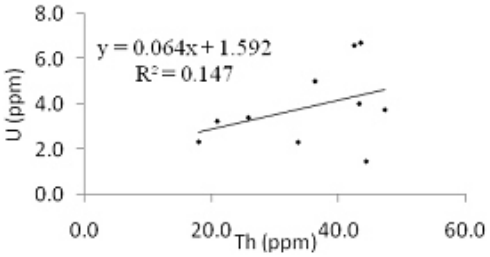


Fig. 1 Natural Th vs U in different samples

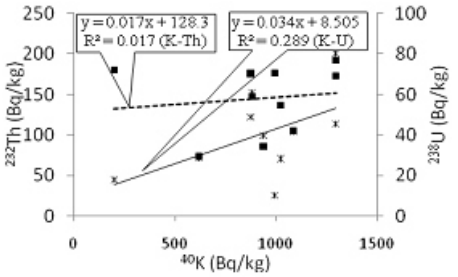


Fig. 2 ^{232}Th and ^{238}U vs ^{40}K in different samples

The computed hazard indices are given in Table 2 along with measured gamma radiation dose levels. The distribution of natural radionuclides is not always uniform. The Ra_{eq} activity is an index that was introduced to represent the specific activities of ^{226}Ra, ^{232}Th and ^{40}K by a single quantity. Mean value of Ra_{eq} is 318.08 Bq/kg. Ra_{eq} is less than the 370Bq/kg for safe use of the material. I_{mr} can be used to estimate the gamma radiation hazard levels. The mean value of I_{mr} is 2.32. I_{mr} is found on higher side due to higher activity of ^{232}Th and ^{40}K in soil of the area. H_{ex} radiation hazard index is used to evaluate the radiation dose rate due to external exposure to gamma radiation from natural radionuclides in construction materials of dwellings. Mean value of H_{ex} is 0.86 which is less than 1. H_{in} quantifies the internal exposure hazard from ^{226}Ra and ^{232}Th viz. radon and thoron and their short lived daughter products. Mean value of H_{in} was observed to be 0.97 in the present study is also less than 1. The gonadal, active bone marrow and bone surface are considered to be organs of interest by UNSCEAR [2]. Mean value of AGDE in the study area observed to 1018.47 Sv/y. Absorbed dose rate in air at 1m height from ground due to the presence of ^{226}Ra, ^{232}Th and ^{40}K in the soil samples in their natural form was computed and found to vary from 83.27 to 195.60 nGy/h with a mean value of 144.40 nGy/h.

Conclusion

In the present study soil samples were analysed using HPGe based gamma spectrometry system. The range of activity of ^{226}Ra, ^{232}Th and ^{40}K in soil found to be 10.1±2.8 to 80.4±3.5 Bq/kg, 73.5±2.3 to 192.3±2.2 Bq/kg and 200.2±10.7 to1297.8±9.9 Bq/kg. Mean of activity concentration of ^{226}Ra, ^{232}Th and ^{40}K in soil found to be 40.2, 144.7 and 921.9 Bq/kg respectively. Mean values of natural radionuclides are higher than the average values for normal background areas of India and the world average values possibly due to the host rock of granite gneisses formation. Mean values of computed radiation hazard indices except I_{mr} are within the respective acceptability criteria.

References

[1] Tahir S. N, Jamil K, Zaidi J. H, Arif M, Nasir Ahmad Sayed Arif Ahmad. Radit Prot Dosimetry 113 (2005) 421.

[2] UNSCEAR, Exposure from natural radiation sources, Annex-B. New York (2000).

[3] Faure G. Principles of isotope geology, 2nd ed. Hoboken, New Jersey: John Wiley & Sons; (1986).

[4] Beretka J, Mathew P.J. Health Phys 48(1985) 87.

[5] Sankaran A V, Jaiswal b, Nambi K S V, Sunta C N, BARC technical report (1986).

[6] IAEA/RCA.BARC Kalpakkam, India (1989) 85.

[7] Mamont-Ciesla K, Gwiazdowski B, biernacka M, Zak A. In: Vohra G, PillaiK C, Sadasivan S,editors. Natural radiation Environment. (1988) New York.

[8] NEO-OECD. Nuclear energy agency,OECD(1979) Paris.

[9] Arafa W. J. Environ Radioact 75 (2004) 315.

[10] Mishra, U.C., Sadasivan, S.,1971.Journal of Scientific and Industrial Research 30(2) (1979) 59.

Utilization of Arsenazo-III for Spectrophotometric Determination of Thorium in Soil Samples

S.K. Srivastava[1], N. Sreenivasa Rao[1], A.Y. Balbudhe[1], K.Vishwa Prasad[1], P. Padma Savithri[1], P.M. Ravi[2] and R.M. Tripathi[2]

1. *Health Physics Unit, NFC, Health Physics Division, Bhabha Atomic Research Centre, PO: ECIL, Hyderabad 500062, India; E-mail: sks@nfc.gov.in*
2. *Health Physics Division, Bhabha Atomic Research Centre, Trombay, Mumbai 400085, India*

The paper discusses the application of arsenazo-III for thorium estimation in soil samples. The basic parameter as stability of complex, linear working range, method detection limit and conditioning for complex formation are discussed. Quality assurance parameter for thorium estimation in soil samples using this reagent is also discussed. The result demonstrates the utilization of arsenazo-III for the accurate and reliable estimation of thorium in soil samples.

Introduction

Thorium is a naturally occurring radioactive element of very long lifetime ($T_{1/2}$=1.4 x 10^{10}y). The average elemental concentration in earth crust is reported to be approx. 6 ppm. The thorium can be determined by many instrumental techniques based on different principles including mass spectrometry with inductively coupled plasma [1], electrochemical methods [2], atomic emission spectrometry with inductively coupled plasma [3], atomic absorption spectrometry [4], chromatography [5] and others. A necessary part of most analytical determinations of elements in real matrices is separation and preconcentration. With reference to spectrophotometric determination of Th the most promising ones belong the disodium Arsenazo III method [6] which has been successfully applied for determination of thorium at ppm in ore samples.

In this paper some basic parameters as optimal concentration of HCl, stoichiometry of relevant complex, method detection limit, detection range, time stability of formed complex and quality assurance parameter for application of reagent for thorium determination in soil samples have been discussed.

Material and Method

All the measurements were performed using the Schimadzu double beam spectrophotometer. Thorium(IV) stock solution (AR grade) containing 10 ppm was used. The concentration of solution of the Arsenazo III (AR grade) was 0.02% (w./v.).

Soil samples were acid digested in a hot 1:1 HF: HNO_3 mixture for 6 hours evaporated to near dryness and treated with $HClO_4$ to remove any remaining organics. Residues were re-dissolved in 8 M HNO_3. The U/Th present in the sample solutions were subjected to passed through columns containing chloride form anion exchange resin (Dowex, 1x8, 100-200 mesh, pre-conditioned with ~50 mL 8 M HNO_3) for U/Th separation. After rinsing with 5x 10 mL 8M HNO_3 to ensure all U and Fe had been flushed, Th adsorbed by the resin was eluted with 100 mL 8 M HCl. The eluted samples were then evaporated to near dryness and the residue is dissolved in 5M 10 mL HCl. The samples were prepared in flasks of 10 mL by adding specific sample volume and 1.0 mL of 0.02% solution of Arsenazo III while maintaining the acidity of 5M HCL of measuring solution.

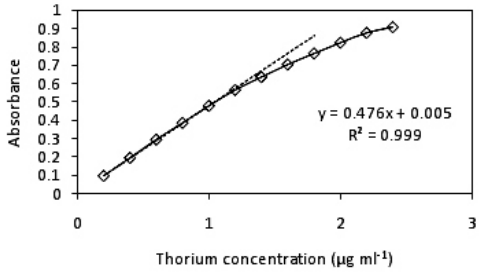


Fig. 1 Absorbance of thorium-arsenazo complex at 660 nm

Result and Discussion

The absorption maximum of the thorium-arsenazo-III complex in diluted hydrochloric acid showed two peaks, namely at 611 nm and 660 nm. The latter one was used for the determination. The molar extinction coefficient for complex at 660 nm is equal to 1.1 x 10^5 L mol^{-1} cm^{-1}.

The validity of Beer's law was checked for 0.2-2.4 gmL^{-1} thorium concentrations (Fig. 1). As the figure indicates, the linear range for accurate determination of thorium extends up to 1 gmL^{-1}.

Method detection Limit (MDL) has been calculated by Hubaux and Vos method at a 95% confidence level and observed to be 0.026 gmL^{-1}.

The thorium - Arsenazo III complex stoichiometry has been established by the mole ratio method (Fig.2). Results indicates formation of a 1:2 complex.

The optical density was found constant for 25 minutes under normal laboratory conditions (Fig.3)

Thorium-arsenazo complex at 660 nm shows maximum absorbance in the 3-7 M HCl condition (Fig. 4).

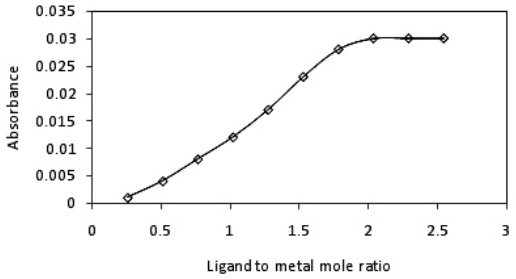


Fig 2 Mole ratio method

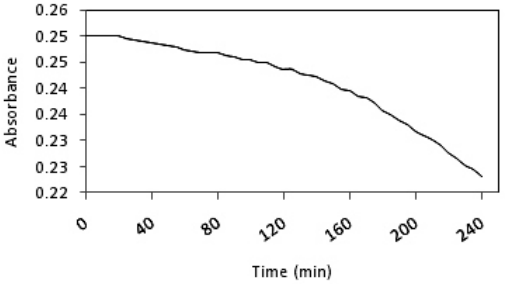


Fig. 3 Time dependence of thorium complex

The accuracy and reliability of the spectrophotometric estimation of thorium in soil is verified by cross method analysis and spike recovery study. Soil sample were analysed by both ICPAES (Inductively Coupled Plasma Atomic Emission Spectroscopy) and UV/VIS Spectrophotometry for thorium estimation.

Table 1: Analysis of thorium in soil samples by UV-VIS spectrophotometry and ICPAES

Sample	UV-VIS(gmL^{-1})	ICPAES (gmL^{-1})
S-1	56	44
S-2	132	122
S-3	54	64
S-4	69	61
S-5	23	20
S-6	15	20
S-7	112	108
S-8	123	120

For validating the result, paired t-test has been applied. Since the calculated t value (1.19) is less than the tabulated value of t (1.89 at 10% probability) there is no significance difference between the two methods.

Spike recovery study for thorium estimation by spectrophotometry has been carried out (Fig.5). The recovery of spiked thorium was found to be in the range of 90% to 97% with an average recovery of 94±2%. This value is in the acceptable range as the samples undergo multiple steps in the preparation and purification of thorium.

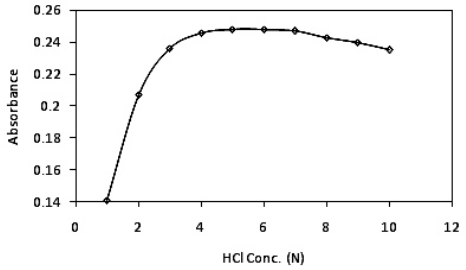


Fig. 4 variation of absorbance of complex with HCl concentration

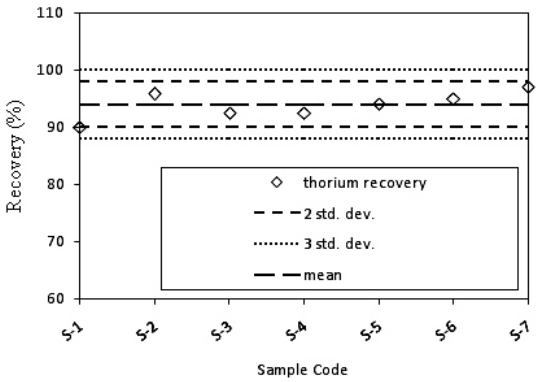


Fig. 5 Thorium spike recovery form the soil samples

Conclusion

Thorium determination in soil samples using Arsenazo III enable the quantification of the analyte. The most suitable working range is observed to be in the range of 3-7 M HCl concentration. The study reaffirmed the formation of ML_2 type of complex between thorium metal and arsenazo ligand at 5M HCl condition. Application of arsenazo for thorium estimation in soil samples shows a better agreement with that of ICPAES technique. Also the recovery of spiked thorium in the present method shows very satisfactory results. Thus arsenazo-III can be satisfactorily utilized for thorium estimation in soil samples.

Reference

[1] Zheng Y, Weinman B; Croninc T; Fleisher M Q; Anderson R F; Appl. Geochem., 18 (2003) 539

[2] Liu, S., Li, J., Xun, M., Gao, P.:Anal. Lett. 36 (2003) 1381

[3] Fujino O., Umetani S.: Anal. Chim. Acta, 420 (2000) 65

[4] Castro M. A., Aller J. A., McCabe, A., Smith W. E., Littlejohn D.: J. Anal. At. Spectrom; 22 (2007) 310

[5] Al-Swathi W. A., Dahl R.: J. Chromatogr. A, 706 (1995) 175

[6] Khan M., Ali A., Khan, N. N.;J. Radioanal. Nucl. Chem., 50 (2001) 353

Results of Measurement of the Tritium in the Western Caucasus

T. Tsvetkova, I. Nevinsky, V. Nevinsky, B. Suyatin

Private Establishment Research Centre of Natural Radioactivity, set. Kholmsky, Abinsk Distr., Krasnodar region, 353309, RUSSIA; E-mail: nevinsky@list.ru

Measurement of the tritium for tasks of hydrogeology, engineering geology, ecology and seismology in water of springs, wells, mud volcanoes and in the rivers and lakes of the Western Caucasus (South Russia) was carried out since 1997. For tritium concentration measurements the electrolytic cell of a new design with electrodes as a spiral and the big proportional chamber were used. The enrichment factor of 64.0 1.5% was received. Correlation of the tritium concentration with regional seismicity was observed. The long-term tritium data in natural waters in South Russia are shown.

Introduction

Measurement of the tritium for tasks of hydrogeology, engineering geology of ecology and seismology in water of springs, wells, mud volcanoes and in the rivers and lakes of the Western Caucasus (South Russia) was carried out since 1997 [1]. The electrolytic cell of a new design and the big proportional chamber were used for tritium concentration measurements.

Instrumentations

For enrichment of tritium samples electrodes as a spiral are made in the electrolytic cell. At electrolytic process with initial volume 500 mL of the sample, the final volume may vary from 7 up to 18 mL in dependence of the quantity of replaceable tephlon plates at the bottom of the cell. In this case the enrichment factor of (64.0 1.5)% was received. The enrichment factor of 220.0 with 2% mistake is received at electrolytic process at 2000 ml to 7 mL. In the device SL-4000 with liquid scintillator beta activity of samples was measured. For fast measurement of tritium in the rivers and lakes during the expeditions the proportional chamber with full volume of 26.6 l (21 cm in diameter x 77 cm lengths) and with working volume 21 l was used. All working volume of the chamber was divided [2] on 37 cells. For reduction of a background from cosmic rays the chamber was placed in the pipe with scintillation plastic in thickness of 5 cm with photomultipliers. The chamber is filled by hydrogen received from the water samples, without a preliminary enrichment. The background of the chamber is 0.5 cpm. The minimal determined activity of tritium was 6 TU with error of 20 %. Concentration 3 1 TU (0.42 Bq/L) of tritium may be determined during 3 hours of measurement.

Results

The increased concentrations of tritium in natural sources in the faults at the big depth were found out.

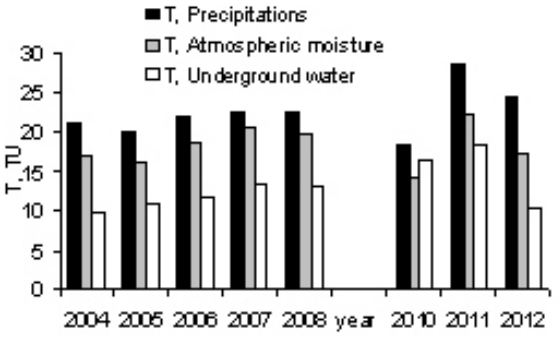


Fig. 1 Average annual concentration of tritium in atmospheric precipitations (snow, rains), moisture and underground water (well of the depth in 30 m) in distance of 30 km in the North from the Black Sea coast

Correlation of the tritium concentration with regional seismicity was observed. The long-term tritium data in natural waters in South Russia are shown (Fig.1). The increase of the tritium concentration in rains in March 2011 may be connected with Fukushima Daiichi NPP effect.

Conclusions

The opportunity of measurement of tritium in natural waters with high accuracy may be used for engineering – geological, seismological and ecological application.

References

[1] I. Nevinsky, V. Nevinsky, V. Ferronsky, T. Tsvetkova. Rad. Meas. 34 (2001) 349.

[2] V. Barnov et al.. Nuclear-chemical phenomena in firm bodies. Academy of Sciences of Georgia, «Mecniereba», Tbilisi (1980) 91.

Successful Application of the Nuclear Analytical Chemistry (NAC) Methods in Seismological Researches of Mud Volcanoes and Springs in the Black Sea Zone.

T. Tsvetkova1, I. Nevinsky1, B. Suyatin1, I. Akkurt[2], F. Kulali[2]

1. *Private Establishment Research Centre of Natural Radioactivity, set. Kholmsky, Abinsk Distr., Krasnodar region, 353309, RUSSIA; E-mail: nevinsky@list.ru*
2. *Suleyman Demirel University, Isparta-Turkey*

For research of an opportunity of earthquakes and eruptions of mud volcanoes forecasting, monitoring of a ^{222}Rn, ^{226}Ra in the springs and gryphones of the mud volcanoes and ^{222}Rn, ^{220}Rn in the soil in the Taman Peninsula were carried out since 1995. Simultaneous measurements in two springs of the Western Caucasus and in two thermal sources of Southwest Turkey ^{222}Rn are also begun. Simultaneous changes of ^{222}Rn concentration in water in Southwest Turkey and South Russia before regional earthquakes are obtained. Reduction of soil ^{222}Rn concentration at mapping of mud volcanoes before occurrence of new gryphones is revealed.

Introduction

For research of an opportunity of earthquakes and eruptions of mud volcanoes forecasting, monitoring of a ^{222}Rn, ^{226}Ra in the springs and gryphones of the mud volcanoes and ^{222}Rn, ^{220}Rn in the soil in the Taman Peninsula (the Western Caucasus) were carried out since 1995 [1]. Simultaneous (at 9:00 GMT daily) measurements in two springs of the Western Caucasus and in two thermal sources of Southwest Turkey [2] ^{222}Rn are also begun.

Instrumentations and Methods

For ^{222}Rn measurement degassing of water samples in volume of 0.5 L and the further alpha – counting are used. The background of the scintillation chambers is 1.7 0.5 cpm. Minimal determination of the ^{222}Rn concentration in water is 0.05 Bq/L. For measurement of low concentration of ^{222}Rn and ^{226}Ra in water a method of degassing, sedimentation of the ^{222}Rn in a cold coal trap and measurement of alpha - activity of ^{222}Rn in the quartz proportional counter (Fig. 1a) is used. The background of the counter is 2 0.5 cph. For measurement of small concentration of ^{226}Ra in water (n x 10^{-2} Bq/L) 1 L of sample in a vessel of degassing 3 for removal of ^{222}Rn was blown by air in volume 25 L with speed of 1 L/min. The vessel of degassing 3 together with a sample was preserved in 1 month and than was connected to the device (Fig. 1a). Saved up in water sample ^{222}Rn from ^{226}Ra was picking out by gas (Ar) from a bottle 1 in a cooling (-30^{0}C) coal trap 6. For clearing of gas from steams of water and of acids and alkalis, traps 4,5 were used. 25 L of Ar during 25 minutes were passed through the sample for allocation of ^{222}Rn. Ar after the trap 6 go out in an atmosphere. Further the trap 6 was heated up to 100^{0}C. During 30 minutes ^{222}Rn from a trap 6 was moved in the cooling (-30^{0}C) quartz proportional counter 8 through a hot trap with magnesium 7. Further for measurement of alpha - activity of allocated ^{222}Rn the quartz counter was filled by gas of 90% Ar + 10%CH_4 up to pressure 1 atmosphere (the circuit of filling in Fig.1a is not shown).

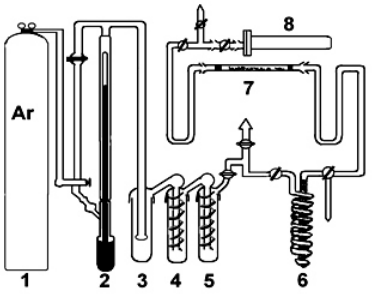


Fig. 1a The device for extraction and measurements of Rn in water: 1 - bottle with Ar; 2 - reometer; 3 – the degassing vessel; 4 - the trap for clearing of gas from steams of water; 5 - the trap for clearing of gas from steams of acids and alkalis; 6 - the coal (3 g) trap; 7 - the trap with magnesium; 8 - the cooled quartz counter;

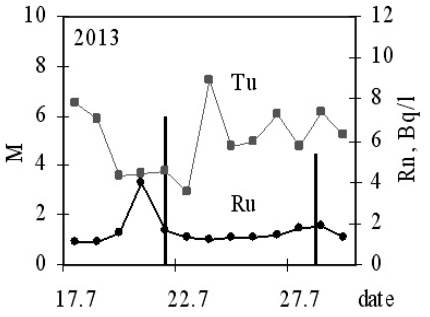


Fig. 1b Changes of Rn concentration in water of springs in South Russia (Ru) and Southwest Turkey (Tu) during the regional earthquakes

Measurement of an alpha activity of ^{222}Rn usually 2 hours in the low background metal screen with a scintillation device of anticoincidence was carried out.

For ^{222}Rn - ^{220}Rn – mapping of the territories of mud volcanoes SSNTDs are applied. Continuous monitoring of soil ^{222}Rn with application semi-conductor as detector (CLIPPERTON II) and scintillation Rn-probe [3] in mud volcanoes was carried out.

Results

In the springs in the territory of mud volcanoes different methods of measurements of Rn concentration for comparison were used simultaneously. Some methodological questions were considered. Sampling and gamma rays measurement of spring water and degassing and measurement of alpha activity of gryphone water were carrying out simultaneously. Sampling or measurement of water alpha activity directly in a spring is the most successful for monitoring. Simultaneous changes of ^{222}Rn concentration in water in Southwest Turkey and South Russia before regional earthquakes are obtained (Fig. 1b). Vertical lines in Fig. 1b show earthquakes of July 21, 2013 (Italy, M5.5, 43.63N13.82E) and July 28, 2013 (Turkey, M4.5, 40/99N34.29E). Concentration of ^{222}Rn in water of a hot (50^0C) spring in Turkey (37.96N29.10E) has increased on July 17 and July 23 before these earthquakes accordingly. Concentration of ^{222}Rn in water of a cold ($13\ ^0C$) spring in South Russia (44.50N38.25E) has increased before earthquake of July 21. But only small (it is no more 5 %-mistakes) increase of the Rn data from this spring during the earthquake of July 28 was observed. As an example, Fig. 1b shows, that water Rn concentration in a hot source and in a cold source change variously before earthquakes of a different magnitude and a different distance from sources. Before earthquakes in a distance up to 1500 km concentration of soil ^{222}Rn in the territory of mud volcanoes 2-3 days before earthquakes increases and then decreases. Reduction of soil ^{222}Rn concentration at mapping of mud volcanoes before occurrence of new gryphones is revealed.

Conclusions

So, NAC methods allow finding out changes of concentration of natural isotopes in springs and mudding volcanoes and may be successfully used for seismological application.

References

[1] I. Nevinsky, V. Nevinsky, V. Ferronsky, T. Tsvetkova. Rad. Meas. 34 (2001) 349.

[2] H. A. Yalim, İ. Akkurt, F.B. Özdemir, R. Unal, A. Sandýkcýoglu, A. Akkurt. Ind. Build. Env. 16 (2007) 77.

[3] V. Nevinsky, I. Nevinsky, T. Tsvetkova. Rad. Meas. 47 (2012) 281.

Study of Radon, Thoron and their Progeny levels in Indoor Environment of Firozabad city in U.P., India

Mukesh Kumar[1], Anshu Agrawal[2] and Rajesh Kumar[3]

1. *Department of Physics, S.V. (P.G.) College, Aligarh 202001, India; E-mail: mksvc@rediffmail.com*
2. *Department of Chemistry, N.R.E.C. College, Khurja 203131, India*
3. *University School of Basic & Applied Sciences, Guru Gobind Singh Indraprastha University, New Delhi 110078, India*

Radon measurements in homes gain importance because of its lethal effects on human health. In the present work, Solid State Nuclear Track Detector's (SSNTD's) based twin cup dosimeters were used to measure concentration levels of radon and thoron in the dwellings of Firozabad city of Uttar Pradesh State in India. From measured values of radon and thoron concentration levels, progeny concentration levels in terms of Potential Alpha Energy Concentrations (PAECs) and annual dose received by the inhabitants were calculated. The measured average values of radon and thoron concentration were found to be 37.4 Bqm^{-3} and 13.7 Bqm^{-3} respectively. The average value of radon and thoron progeny PAECs were found to be 4.0 mWL and 1.5mWL respectively. The average value of annual dose due to inhalation of radon, thoron and their progeny was found to be 1.1 mSv.

Keywords: SSNTD; Radon; Thoron; Twin Cup Dosimeter, Annual dose

Introduction

The most significant terrestrial source of human exposure to ionizing radiations is radon, a noble radioactive gas that arises from the decay of radium, a radioactive element in the decay series of uranium or thorium occurring naturally in varying amounts in all rocks and soil, all over the planet.

Radon has three naturally-occurring radioactive isotopes namely ^{219}Rn (Actinon) with half-life of 3.96 sec, ^{220}Rn (Thoron) with half-life of 55.6 sec and ^{222}Rn (Radon) with half-life of 3.82 days, belonging to the decay chain of ^{235}U, ^{232}Th and ^{238}U respectively. Because of low activity concentration of ^{235}U and the short half-life, ^{219}Rn is not significant for human exposure and only two isotopes ^{222}Rn and ^{220}Rn are of our interest because of their presence indoors. It was estimated that inhalation of radon and its short lived decay products accounts for on an average about one half of the effective dose from all natural sources of radiation [1]. The dominant component of the dose comes from the decay products of radon and the contribution of thoron decay products is of the order of 10 to 20% compared with those of radon [2]. Ramachandran and Sathish (2011) reported nationwide indoor radon and thoron map for India. According to their results 20% of the total indoor inhalation dose rates are due to thoron and its progeny [3].

The health hazard from radon does not come primarily from radon itself, but rather from its short lived radioactive progeny. The health problems arise when radon progeny are inhaled, deposited in the airways, and bombard nearby cells with alpha particles as the atoms transform through the decay chain. These alpha particles can deliver a large localized radiation dose and may lead to malignant transformation and the formation of lung cancer. As radon and its daughter products are identified as a cause of lung cancer among the miners, there exists concern about lung cancer risks among people exposed to lower levels of radon in homes. Residential radon and lung cancer studies have confirmed a smaller but detectable increase in lung cancer risk at residential exposure levels [4,5].

The primary goal of this study was to measure the long term average concentration of radon and thoron gas in the dwellings of Firozabad city to know the radiological risks for local population. Firozabad city is located in north central India, in western Uttar Pradesh, at 27^{0}09 N78^{0}24 E. It is a major hub of manufacturing different glass based items and about four hundred glass industries are registered in this city. The fuel used in industries is either natural gas or coal. For measurements forty different houses in Firozabad city were carefully chosen, so that their construction and operation do not vary significantly.

Experimental Details

Solid State Nuclear Track Detectors (SSNTD's) based twin-cup dosimeters were used to estimate the radon and thoron concentration in the dwellings. Cellulose nitrate films (LR-115, Type-II) were used as detectors. The dosimeters were suspended in the selected houses at a height of about 1.5 m from the floor and at least 10 cm away from any surface for a period of 95 days. Bedrooms were preferred because of maximum occupancy. After proper exposure the detectors were retrieved and etched chemically in a 2.5 N sodium hydroxide (NaOH) solution at 60 ± 1^{0}C for 80 min. in a specially designed constant temperature bath having temperature stability within 1^{0}C. Alpha tracks developed on LR -115 cellulose nitrate films were then counted by using a Polltech make spark counter. For fully developing the partially etched track holes, the pre- sparking voltage of the counter was 900 volts and

Table-1: Radon, Thoron and their Progeny concentration levels and Annual dose in the dwellings of Firozabad city, U.P., India.

	Radon Concentration (Bqm^{-3})	Thoron Concentration (Bqm^{-3})	Radon Progeny concentration (mWL)	Thron Progeny concentration (mWL)	Annual dose (mSv)
MIN.	16.9	3.3	1.8	0.4	0.6
MAX.	58.6	27.6	6.3	3.0	1.7
Average (S.D.)	37.4 (12.6)	13.7 (5.5)	4.0 (1.4)	1.5 (0.6)	1.1 (0.4)

track counting voltage was 450 volts, which corresponds to the plateau region of the counter. The measured track densities were corrected for background and converted in to actual radon and thoron gas concentrations using appropriate calibration factors for pin hole and filter compartments [6]. From measured values of radon and thoron gas concentrations, radon and thoron progeny concentrations in terms of Potential Alpha Energy Concentration (PAECs) and annual dose received by the inhabitants were calculated by using appropriate relations [1,7,8].

Results and Discussion

The results of observed radon, thoron and their progeny concentration along with estimated annual dose received by the inhabitants in the dwellings of Firozabad city, U.P., India are given in the Table-1. It was found that radon and thoron concentration varied from 16.9 Bqm^{-3} to 58.6 Bqm^{-3} with an average value of 37.4 Bqm^{-3} (SD = 12.6) and 3.3 $Bqm^{-3}$to 27.6 Bqm^{-3} with an average value of 13.7 Bqm^{-3}(SD =5.5) respectively. The progeny concentration of radon and thoron in terms of PAECs ranged from 1.8 mWL to 6.3 mWL with an average value of 4.0 mWL (SD = 1.4) and from 0.4 mWL to 3.0 mWL with an averagre value of 1.5 mWL (SD = 0.6) respectively. The annual dose received by inhabitants due to inhalation of radon, thoron and their progeny in indoor air varied from 0.6 mSv to 1.7 mSv with an average value of 1.1 mSv (SD = 0.4). It was found that thoron and its progeny contribute 3.7% to 20% to the total dose due to inhalation of radon, thoron and their decay products.

Conclusions

On the basis of radon surveys conducted in many countries, the International Commission on Radiation Protection (ICRP) has set guidelines for indoor radon concentrations. For dwellings this range is between 200 - 600 Bqm^{-3} [9]. From the present study, it was observed that in studied dwellings, maximum concentration of radon was below the lower reference concentration prescribed by ICRP. Further the average value of annual dose for inhabitants due to inhalation of radon, thoron and their progeny was below the global average value of 1.2 mSv for indoor air as given by UNSCEAR (2000) [1] and below the range of action level (3-10 mSv) recommended by ICRP [9]. Apparently in the opinion as generated through this study, there is presently no significant radiological risk for the inhabitants of studied regions, as of now.

Acknowledgements

The authors would like to thank University Grants Commission, Govt. of India., New Delhi, India for providing financial support under a Minor Research Project [F. NO. 8-2 (179) / 2011 (MRP/NRCB)] for this work. We are also thankful to the residents of Firozabad city for deployment of detectors in their houses.

References

[1] UNSCEAR, United Nations Scientific Committee on the Effects of Atomic Radiation, Annex E: Exposures from natural radiation sources, New York (2000).

[2] T. Martinez, G. Martinez, F. Juarez et al., J. Radioanal. Nucl. Chem. 264(2) (2005) 511.

[3] T. V. Ramachandran, L. A. Sathish , J. Environ. Radioact. 102(11) (2011) 975.

[4] UNSCEAR, United Nations Scientific Committee on the Effects of Atomic Radiation, Annex E: sources-to-effects assessment for radon in homes and workplaces, New York (2006).

[5] L. T. Bliss, K. Daniel, C. Jing et al., Journal of Toxicology and Environmental Health, Part A, 69 (2006) 735.

[6] P. C. Rohmingliana, V. Lalmuanpuia, R. K. Thapal et al., Sci. Vis. 10(4) (2010) 148.

[7] L. A. Sathish, K. Nagaraja, T. V. Ramachandran, International J. Phys.Sci. 6(18) (2011) 4348.

[8] L. A. Sathish, S. Sundareshan, T. V. Ramachandran, Physical Review & Research International 2(2) (2012) 36.

[9] ICRP, International Commission for Radiological Protection, Publication No. 65, (Oxford Pergamon Press), (1993).

Effect of Tsunami on the Natural Radioactivity content in the Beach Sands along the entire East Coast of Tamilnadu State, India

K.S. Lakshmi[1], V. Meenakshisundaram[1], J. Punniyakotti[2,3]

1. *Meenakshi Sundararajan Research Centre, Meenakshi College for Women, Chennai 600 024, India*
2. *Department of Physics, Anna University (M.I.T. Campus), Chennai 600 025, India*
3. *Department of Physics, Meenakshi Sundararajan Engineering College, Chennai 600 024, India; E-mail: kotti_jpk@yahoo.co.in*

As a consequence of devastating tsunami, studies were undertaken on the environmental radioactivity profile along the entire east coast region of Tamilnadu State covering both beach sands and the adjoining inland regions and compared with previously established pre-tsunami distribution profile. Though many parameters were studied in depth, the change in the natural radioactivity content in the beach sands alone is presented in this paper. The results of the present study indicate that the radioactivity content of Th and U in beach sands registered a lower value (85% and 70% respectively) whereas the ^{40}K activity has increased by 25%. This is attributed to the hydrodynamics of tsunami waves which removed huge quantities of beach minerals that have been built up over a few decades. The individual activity concentration of the three primordial radionuclides, total activity content, comparison between pre and post tsunami data for all the 33 sites and their statistical analyses would be covered in the full paper.

Introduction

It is well known that the coastal areas of southern part of India are interspersed with surface deposits of monazite, a thorium bearing mineral. An extensive environmental radioactivity monitoring of entire east coast region of Tamilnadu State, India covering around 1000 km was done earlier in 2002 prior to Tsunami [1]. However, the catastrophic tsunami waves that swept the Tamilnadu coast could have completely or atleast partially altered the natural radioactivity profile picture. Hence, the same study area was chosen and investigated whether the profile has changed as a consequence of devastating Tsunami. The study area covers from Kanyakumari to Pulicat (situated 30 km north of Chennai). The east coast region of Tamilnadu State lies between 8°11' N and 13°04' latitude and 77°29' E and 80°17'' longitude as shown in Fig.1. Thirty three sites were selected and the distance between each site is about 30 km. It may be noted that all the 33 sampling sites selected for both the studies i.e., before and after the tsunami, are exactly the same. Though many investigations have been done as part of this post-tsunami study, the natural radioactivity profile in the beach sands alone is covered in this paper.

Experimental

A 3"x3" NaI(Tl) detector based gamma-ray spectrometer is used for spectral measurements. IAEA reference Standards were used for efficiency determination. Also, 20% of sand samples were analyzed at RSD, IGCAR, an AERB accredited lab, and the activity values compared, thus ensuring the accuracy of the results, which was within ± 3%. The estimated MDA values are 2.22 Bq.kg^{-1} for ^{238}U, 2.15 Bq.kg^{-1} for ^{232}Th and 8.83 Bq.kg^{-1} for ^{40}K.



Fig. 1 Fig.1. The map of study area (S1 to S33)

Results and Discussion

The statistical data corresponding to the activities measured for ^{238}U, ^{232}Th and ^{40}K in beach sand samples collected at all the 33 sites are presented in Table 1. The highest activities (extreme values) of ^{238}U, ^{232}Th, and ^{40}K detected in beach sand samples collected at three sites viz., Kanyakumari, Mamallapuram and Overi have been excluded for the evaluation of statistical parameters. Frequency distribution of activity concentrations for ^{238}U, ^{232}Th, and ^{40}K was plotted. In Table 1, the statistical data pertaining to both pre and post tsunami studies are presented for comparison.

It may be seen from Table 1 that in the present study (post-tsunami), the mean activity content of ^{40}K is the highest followed by ^{232}Th and ^{238}U. Also, the values of skewness for ^{238}U & ^{232}Th are not closer to the null value, indicating the non-existence of normal

Table-1: Comparison on statistical data for activity concentrations of primordial radionuclides (in Bq.kg^{-1}) Pre and Post Tsuanmi (Seashore sand samples)

Stati-stics	Present Study (Post-Tsunami)			Previous study (Pre-Tsunami)		
	^{238}U	^{232}Th	^{40}K	^{238}U	^{232}Th	^{40}K
Mean	11	57	288	40	386	216
Min	BDL	BDL	BDL	BDL	13	15
Max	815	9587	946	254	3576	524
SD	15	86	126	13	100	136
Skew.	2.16	2.31	0.13	1.2	1.4	0.08
Kurt.	4.13	5.53	0.72	0.54	0.99	-0.82
Freq.	L-N	L-N	N	L-N	L-N	N

Note: L-N: Log-Normal; N- Normal

distribution; since the values of kurtosis coefficient are >3, it represents leptokurtic distribution, i.e., sharper than normal distribution.

If one compares the data given in Table 1, the activity content of both ^{238}U and ^{232}Th found to decrease during post-tsunami by around 85% and 70% respectively as compared to Pre-Tsunami; however, the activity concentration of ^{40}K is found to increase (25%) as compared to Pre-Tsunami as shown in Fig.2

The reduction in thorium/uranium activity content and the variation in the activities of ^{40}K must be due to the washing of top layer sand (upto 30 cm) and other particulates containing heavy minerals by tsunami waves and replacing with the bottom layer of sand. Several investigators have reported the depth distribution of radionuclides in soil and sand. Iyer et al [2] have studied the variation of monazite content in beach sand of Kalpakkam in the depth intervals of 0 to 20 cm and 20 to 40 cm and observed a decrease in monazite content over 30% from the first interval to the second interval. Lakshmi et al [1] reported that ^{40}K concentration increases with depth in sand though marginally. ^{40}K is generally associated with ordered crystalline oxide material, resistant organic matter and clay lattices [3]. The lower concentration of ^{40}K in the upper layer sand might be due to physical removal of the above fractions and the mineral muscovite, which is enriched in potassium, due to wind and wave action. Ramasamy et al [4] also reported a marginal increase of potassium content with depth in river sediments. In the present study also, as may be seen in Table 1, that the activity content of Th and U in beach sand registered a lower value whereas ^{40}K activity has increased. Post-tsunami studies on the distribution and bio-accumulation of natural radionuclides in south east

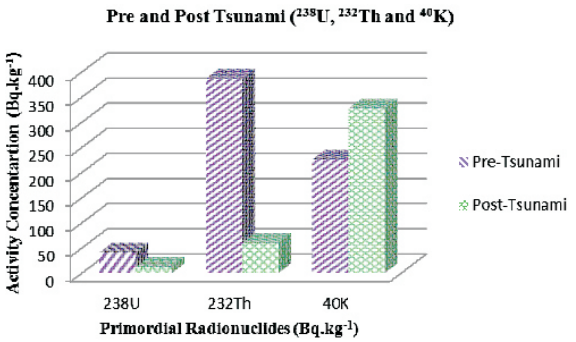


Fig. 2 Mean activity values of ^{232}Th, ^{238}U and ^{40}K

coast of Tamilnadu, India by Satheeshkumar et al [5], reported that one of the major reasons that can be attributed for the reduced level of radioactivity in the beach sands of east coast of Tamilnadu is the hydrodynamics of the Tsunami waves which removed huge quantities of beach materials that have been built up over a few decades; they also reported that there was no enrichment of monazite in the tsunamigenic sediment and hence the reduction in the background radiation of the ecosystem. Hence, the radiological profile becomes modified reducing background radiation levels of the environment. In our earlier study (pre-tsunami), the ^{232}Th concentration is always higher than ^{238}U. The ratio of ^{232}Th/^{238}U was recorded to be 8.9. But Post-Tsunami study recorded the ratio as 4.7.

Conclusions

The tsunami had reduced the mean activity level of thorium and uranium content to a large extent (85% and 70% respectively) in the beach sands.

Acknowledgement

The authors are thankful to Director, IGCAR and Head, RSD, IGCAR, Kalpakkam, for their guidance and constant encouragement.

References

[1] Lakshmi, K.S., Selvasekarapandian, S., Khanna, D, Meenakshisundaram, V, Int. Congr. Ser. 1276 (2005) 323.

[2] Iyer, M.R., Iyengar, M.A.R., Ganapathy, S, (BARC/I-138) (1974).

[3] Cook G.T., Baxter, M.S., Duncan, H.J., Malcolmson, R, J. Environ. Radioact. 1(2) (1984) 119.

[4] Ramasamy, V., Suresh, G, Meenakshisundaram, V, Ponnusamy, V., Appl. Radiat. Isot. 69 (2011) 184.

[5] Satheeshkumar, G., Shahul Hameed, P., maidenideen, M., Kannan, V, Radiation Protection and Environment. 34(2) (2011) 96.

Study on the Spatial Distribution of ^{137}Cs Content in Bottom Sediment and Benthic Species of Mumbai off Coast

S. Sugandhi, V.M. Joshi, S.K. Jha and R.M. Tripathi

Environmental Radioactivity Measurement Section, Health Physics Division, Bhabha Atomic Research Centre, Trombay,Mumbai 400 085, India; E-mail: sugandhi@barc.gov.in

The sediment compartment in marine system is receptor of radionuclides, is considered as indicator matrice. ^{137}Cs is globally distributed in the environment as a fallout of atmospheric nuclear explosions carried out in 60_s by USA,USSR and in 70_s by China. Bottom sediment and benthic species from various locations of Mumbai off coast were collected between 2007 to 2012 and the observed ^{137}Cs content in them varied between 2 to 370.3 Bq/kg$_{(dry)}$,<0.08 to 0.9 Bq/kg$_{(wet)}$ respectively. The average estimated ingestion dose to 'general public' due to the consumption of benthic species is 0.02-0.03 Sv/y, is infinitesimally smaller in comparison to the internationally accepted public dose limit of 1000 Sv/y.

Introduction

Naturally occurring and anthropogenic radionuclides exists both in the terrestrial and marine environment. Ionizing radiation from radionuclides can be harmful to humans as well as to environment. Hence, it is important to understand the long-time behavior of radionuclides in nature to protect both people and surrounding environment. Anthropogenic sources include those from fall out due to the atmospheric nuclear explosion experiments conducted during 1960s by USA,USSR, in 1970s by China and that from operating nuclear installations. Bottom sediment in a marine system is formed from organic and inorganic particles which settle from water of aquatic media. The uptake of radionuclide by marine sediment depends on their physical and chemical properties. The radionuclides introduced into the aquatic system are subjected to dilution, dispersion, removal through sorption by bottom sediment and biota [1]. Most radionuclides are sorbed directly on to sediment within 1 to 2 years [2]. Sediment compartment in marine system acts as a sink for accumulation of radionuclides and it indicates the impact of pollution [3]. Measurement of anthropogenic radionuclides in marine sediment can provide good estimates of past and present radioactive contamination. ^{137}Cs has often been chosen as the most significant representative of anthropogenic radionuclide found in the marine environment which is considered to be the largest contributor to dose among the anthropogenic radionuclides.Benthic species due to their pedantry habits, they are exposed to the radioactive pollutants. Thus, the study of benthic species contributes to an understanding of redistribution of the radionuclides between seawater, sediment and benthic species. The primary objective of this study was to investigate the spatial distribution of ^{137}Cs content in bottom sediment and benthic species from Mumbai off coast and to estimate the ingestion dose to 'general public' due to consumption of it.

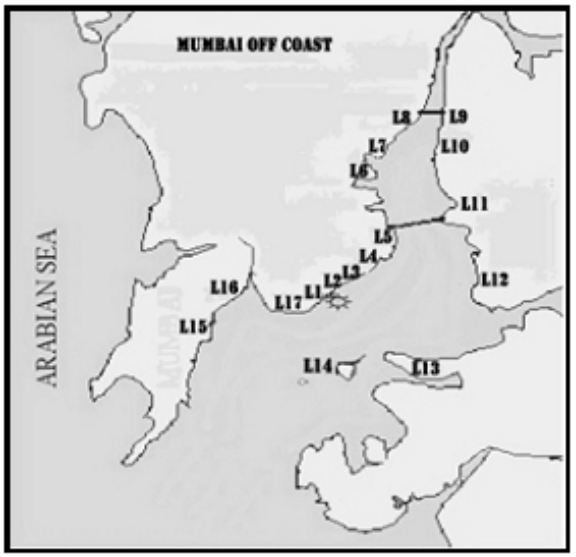


Fig. 1 Mumbai off coast

Description of Sampling Location

The study area (Fig.1), Mumbai off coast (Lat. 18 53' to 19 04'N, Long. 72 48' to 73 00'E) which belongs to the category of land locked mass of water concentrated at the broad southern end with the Arabian Sea is located in the west coast of India, is a recipient of low level treated effluents from BARC,Trombay and also a recipient of domestic and industrial wastes from the city of Mumbai and adjoining areas.

Sampling and Sample Preparation

Approximately 50-100 m away from the Mumbai off coast, bottom sediment (0-20cm depth level, total of 204 nos.) were collected from seventeen different location and benthic species (total of 18nos.- arca, crab, mudskipper) were collected from location 4 and 5 as shown in Fig. 1 between 2007 to 2012 (total 12 surveys).

From each location, three subsamples of sediment were collected, combined, dried, pulverized and homogenized. These samples after drying in an oven at

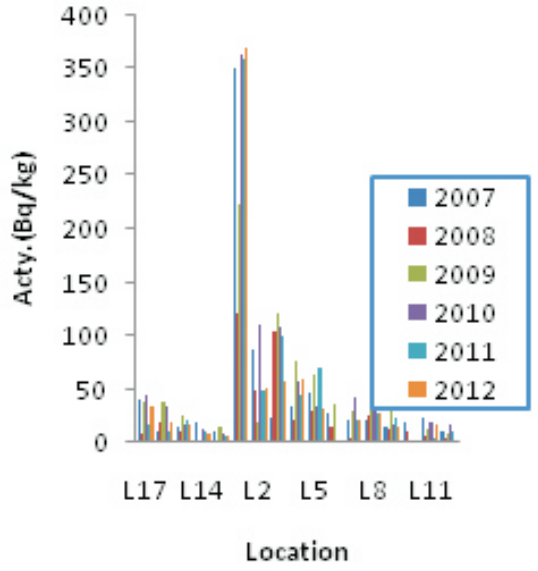


Fig. 2 Spatial distribution of ^{137}Cs content in bottom sediment from Mumbai off coast

110 C for 48h to ensure that moisture is completely removed. A known aliquot (~250g) was taken in a predefined geometry and counted for ^{137}Cs content by gamma spectrometry.

The various varieties of benthic species collected were separated into edible and non-edible parts. The edible part was weighed, dried and powdered. A known aliquot was taken in a predefined geometry and counted for ^{137}Cs content by gamma spectrometry.

Gamma-ray Spectrometry

^{137}Cs content in bottom sediment and benthic species was measured using High Purity Germanium detector (p-type HPGe, Relative Efficiency 50% and resolution 1.8 keV for 1332.0 keV of ^{60}Co). The gamma ray transition of energy at 661.6 keV was used to determine ^{137}Cs concentration.

Result and Discussion

Figure 2, represents spatial distribution of ^{137}Cs content in bottom sediment collected from Mumbai off coast. The ^{137}Cs content in it has varied between 2 to 370.3 Bq/kg$_{(dry)}$ which is almost similar to earlier study done (8 to 480 Bq/kg) at Mumbai Harbour Bay[4]. Table 1 gives the observed ^{137}Cs content in different benthic species which has ranged between < 0.08-0.9 Bqkg^{-1} and is similar to that observed along the coast of Brazil (0.1-0.3 Bqkg^{-1}) [5], Spain (0.08-0.2 Bq kg^{-1}) [6], Greece (0.1–0.2 Bqkg^{-1}) [6]. The average estimated ingestion dose to 'general public' due to the consumption of benthic species is 0.02-0.03 Sv/y.

Table-1: ^{137}Cs content in benthic species and ingestion dose to 'General Public'

Location	^{137}Cs (Bq/kg$_{(wet)}$)	Ingestion Dose to 'General Public' (Sv/y)
4	<0.08-0.9 (15)*	0.03
5	<0.08-0.1 (3)*	0.02

( )* indicate the number of samples analyzed

Conclusions

The spatial distribution of ^{137}Cs content in bottom sediment fom Mumbai off coast, clearly indicates that the concentration level decreases on either side of the maximum observed ^{137}Cs content (L1). This indicates that as soon as the sediment is exposed to low level treated wastes with cesium activity, immediate exchange/uptake of it takes place with/on the sediment, thus immobilizing the activity by acting as a sink for ^{137}Cs.

The estimated internal dose due to consumption of marine benthic species received by the 'general public' is a small fraction (0.001%) of the average annual effective dose due to exposure to natural radiation sources (2.4 mSv) [7] but also a very small fraction (0.003%) of the public dose limit (1000 Sv/y) set by agencies like ICRP and AERB (National Regulatory agency).Thus, the consumption of benthic sea food is safe from the radiological point of view.

References

[1] P.Hemalatha and M.V.M.Desai BARC/2000/I/012.

[2] AjayKumar,Rupali Karpe,Sabyasachi Rout,Vikram Joshi,. R.K Singhal and P.M Ravi J.Radioanal. Nucl. Chem,295(2)(2013) 835.

[3] S.Sugandhi,Sonal Wankhede and P.M.Ravi, Proceedings of Indian Asso. For Radi. Prot.(2012).

[4] R.K.Singhal,A.Kumar,N.Usha,A.V.R.Reddy,Radn.Prot.Dosi.133(4) (2009) 214.

[5] I.L.Cunha,C.S.Minita,R.P.Paiva,A.Teixeria,Sci Tot Env140(1993) 431.

[6] Herve Thebault, M.R.Alessia,Y.,Baena et al Mar Poll Bull 57(6-12)(2008) 801.

[7] UNSCEAR(2000),Sources,Effects and Risks of Ionization radiation, United Nations Scientific Committee on the Effects of Atomic Radiation,New York

Natural Radioactivity Measurement in Soil Samples of Gogi Region, Shahapur, Karnataka

S. Rajesh[1], P. Avinash[1], B. R. Kerur[1,*] and S. Anilkumar[2]

1. *Department of Physics, Gulbarga University, Gulbarga, Karnataka 585 106, India; E-mail: kerurbrk@yahoo.com*
2. *Radiation Safety Systems Division, Bhabha Atomic Research Centre, Mumbai 400 085.India*

The natural radioactivity levels in the environmental samples around the Gogi area have been assessed. The radioactivity in the soil samples was measured using 4"X 4" NaI(Tl) detector based gamma spectrometry system and the radiation levels using RadEye PRD survey meter. The activity of ^{238}U, ^{232}Th and ^{40}K in the soil samples collected from study area were comparable with world average values. The annual effective doses for the sampling locations were estimated from the activity of the soil samples. The average radium equivalent activity and dose measurements were found to be within the permissible limits. The in-situ measured values showed a good agreement (0.9627) with the estimated values obtained in laboratory measurements.

Introduction

Gamma radiations from ^{238}U, ^{232}Th and ^{40}K represent the main external source of the irradiation to the human beings. It is important to study the concentration of natural radionuclides in the environment and its distribution, pathways, mobility, transfers, etc. in various components. The inhalation and ingestion of these radionuclides and their daughter products through air and food is also of concern. Therefore, monitoring and assessment of these radio nuclides in the environment is very important at all level. In the present work activity of ^{238}U, ^{232}Th and ^{40}K was determined in soil samples collected from different locations of Gogi region using NaI(Tl) scintillation detector based gamma spectroscopy. The Gogi area of Karnataka, India has been identified as potential location of uranium deposits. Geologically, this region falls on Bhima river basin. Samples were collected from about twelve villages covering area of radius ranges up to 12 km. The radiation level or the absorbed dose rate also have been measured and compared with that evaluated using the natural activity at the study area.

Materials and Methods

Sample Preparation

Standard procedures were adopted for the collection and preparation of samples from the study area. At each sampling location the geographic coordinates and elevation was recorded using a Garmin portable hand held GPS. The samples were air dried and pulverized to fine powder. The powdered soil samples was transferred to a 250 mL plastic container, sealed using adhesive and were stored for a period of about four to five weeks for radium and their progenies to attain secular equilibrium. After the completion of dormancy period the samples were subjected for gamma spectrometric analysis.

Gamma Spectrometry

Activity measurements were performed using a 4"x4" NaI(Tl) scintillation detector based gamma spectrometric system (manufactured by thermo fishers) for all the samples. The detector was shielded with 3" thick lead bricks to reduce the spectral background due to surrounding building materials and cosmic rays [1]. The gamma ray spectrum was recorded using PC based 1 k multichannel pulse height analyzer. The system was calibrated for the gamma energy range from 661.62 keV – 2.614 MeV using standard gamma sources (^{60}Co, ^{137}Cs and Thorium ore). Activity of radionuclides in each sample was measured using the net photopeak area counts in the peak and efficiency data. The gamma ray absorbed dose rate in air 1 m above the ground level for all the sampling locations were estimated using the equation

$$D = (0.604C_{Th} + 0.462C_U + 0.0417C_K)\ nGy\ h^{-1}$$

Where C_{Th}, C_U and C_K are the activity concentrations ($Bqkg^{-1}$) of Thorium, Radium and Potassium in the samples. The annual effective dose equivalent was also estimated using the conversion of 0.7 $SvGy^{-1}$ to absorbed dose rate as provided by [2].

In-situ Measurements

In-situ dose measurements were also performed using radiation survey meter (RadEye PRD-ER Type, Thermo fisher). The survey meter is held at 1 m above the ground level and the dose rate is measured. The measurement is repeated and the mean value of the dose rate is recorded along with GPS data. This procedure was repeated at all the sampling locations where the soil samples were collected. This instrument is calibrated to give the dose rate due to gamma photons of wide energy range.

Results and Discussion

Data on activity measurement of natural radionuclides such as ^{238}U, ^{232}Th (assuming secular equilibrium with their daughter products) and ^{40}K in the

Table-1: Activity of ^{238}U, ^{232}Th and ^{40}K, Comparison between the Estimated and Measured AED (mSv y^{-1})

Sample No	Sample Location	Activity concentration (Bq kg^{-1})			Raeq (Bq kg^{-1})	AED (mSv y^{-1})	
		^{238}U	^{232}Th	^{40}K		Estimated	Measured
SL01	Karakalli	65.0 ± 1.9	118.9 ± 1.3	917.11 ± 22.7	305.7	0.859	0.919
SL02	Rabanalli	66.9 ± 1.3	52.2 ± 0.8	436.81 ± 12.9	174.3	0.495	0.613
SL03	Karakalli Tanda	61.9 ± 2.0	125.7 ± 1.4	1243.6 ± 19.5	335.3	0.950	0.858
SL04	Gogi	53.2 ± 1.7	102.2 ± 1.1	1015.7 ± 16.8	277.6	0.789	0.797
SL05	Gogi Plant	58.3 ± 1.9	111.3 ± 1.3	805.90 ± 17.7	279.5	0.783	0.858
SL06	Gogi Tanda	40.0 ± 1.9	128.9 ± 1.6	706.90 ± 12.4	278.8	0.771	0.797
SL07	Singnalli	39.8 ± 0.9	20.50 ± 0.6	463.20 ± 9.70	104.8	0.307	0.551
SL08	Kanchinakai	55.1 ± 1.1	48.60 ± 0.7	393.30 ± 10.3	154.9	0.437	0.490
SL09	Maddaraki	23.0 ± 0.8	64.65 ± 1.0	336.39 ± 9.57	141.4	0.391	0.350
SL10	Darshanapur	46.3 ± 1.5	282.5 ± 1.5	873.15 ± 18.5	517.5	1.400	1.314
SL11	Gogi Cross	70.0 ± 0.8	62.42 ± 0.6	487.26 ± 9.61	196.8	0.554	0.526
SL12	B Gudi	23.1 ± 0.9	42.85 ± 0.4	238.03 ± 6.06	102.8	0.288	0.350

samples collected from different locations around the study area are presented in Table 1. The ^{238}U activity ranged from 23.0 to 70.0 Bq kg^{-1}, ^{232}Th activity ranged from 20.5 to 282.5 Bq kg^{-1} and ^{40}K activity ranged from 238.03 to 1243.6 Bq kg^{-1}. The world average activity and range of ^{238}U, ^{232}Th and ^{40}K in soils are 25 (10–50), 25 (7–50) and 370 (100–700) Bq kg^{-1} [2] respectively. Though the activity of radio nuclides from our study was slightly high but the average radium equivalent activity (239.12 Bq kg^{-1}) was found to be within the permissible limits of activity 370 Bq kg^{-1} [3]. The annual effective dose (AED) calculated for the sampling locations in the present work are much less than the limit of 1 mSv y^{-1} for the general public. A Correlation between measured AED (in-situ) and estimated (laboratory) from sample activity are in good correlation as shown in Fig 1.

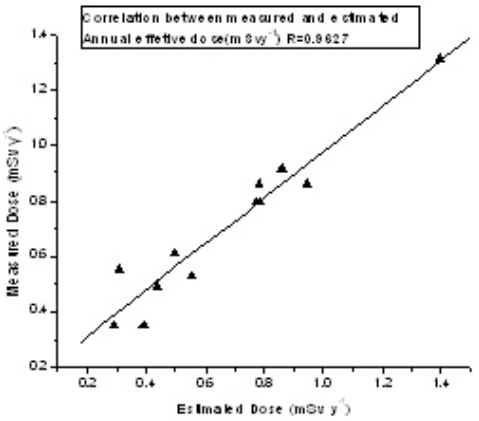


Fig. 1 Correlation between Measured and Estimated Annual effective dose (mSv y^{-1}).

Conclusion

The natural radioactivity levels in the soil samples collected from different locations around Gogi region were estimated using the NaI(Tl) detector based gamma ray spectrometric system. The absorbed dose rate estimated from the activity of the soil samples and directly measured dose rate using RadEye PRD survey meter (excluding cosmic ray) are in good agreement. The results obtained from the present study contribute to the baseline radiological data of the region for future environmental assessment.

Acknowledgement

The authors express their thanks to Board of Research in Nuclear Science (BRNS) for providing the financial support to carry out this work.

References

[1] Anilkumar, S, Narayani Krishnan, S, Sharma, D N, and Abani, M C, Radiation Protection and Environment, 24 (1&2) (2001) 195.

[2] UNSCEAR Sources and effects of ionizing radiation, United Nations Scientific Committee on the effects of atomic radiation, New York, UN. (2000)

[3] OECD, Report by a group of experts of the OECD, Nuclear Energy Agency, Paris, France (1979).

Distribution of Natural Radioactivity in Soil Samples around Tarapur, India

C. B. Dusane, S. Mishra, S. K. Sahu and G. G. Pandit

Environmental Monitoring & Assessment Section, Health Safety & Environment Group, Bhabha Atomic Research Centre, Trombay, Mumbai 400085, India; E-mail: ggp@barc.gov.in

Natural radioactivity around Tarapur, India has been studied. Natural radioactivity was determined in 17 soil samples collected from different locations around Tarapur, India using 50% high purity germanium (HPGe) detector. The radioactivity concentration of ^{238}U, ^{226}Ra, ^{232}Th and ^{40}K varies from 11.5 2.6 - 50.3 6.6 Bq/kg, 14.9 0.6 - 40.5 1.2 Bq/kg , 18.1 0.4 - 75.0 1.5 Bq/kg and 130.1 1.6 - 295.1 2.6 Bq/kg respectively.

Introduction

Natural radioactivity is wide spread in the earth's environment and it exists in various geological formations in soil, rocks, water and air. Natural environmental radioactivity and the associated external exposure due to gamma radiation depends primarily on the geological and geographical conditions, and appear at different levels in the soils of each region in the world [1]. The exposure of human beings to ionizing radiation from natural sources is a continuing and inescapable feature of life on the earth. For most individuals, this exposure exceeds that from all man-made sources combined. There are two main contributors to natural radiation exposures: high-energy cosmic ray particles incident on the earth's atmosphere and radioactive nuclides that originated in the earth's crust and are present everywhere in the environment, including the human body itself. The world population is also exposed to radiation resulting from releases to the environment of radioactive material from man-made sources, and from the use of fuels or inatenals containing naturally occurring radionuclides [2].

In the present study distribution of natural radioactivity were determined in soil samples collected from 17 different locations around Tarapur, India using 50% HPGe detector.

Experimental

Sampling Location

Soil samples were collected from 17 different locations around Tarapur, India. Tarapur is a census town Thane district in the Indian state of Maharashtra. It is an industrial town located some 45 km north of Virar, on the Western Railway line of Mumbai suburban division. Tarapur is located at 17°42'N, 75°28'E to 17.7°N, 75.47°E. It has an average elevation of 456 meters (1496 feet).

Sample Processing

Collected soil samples were dried at 100°C in electric oven and sieved below 2 mm using electromagnetic sieve shaker (EMS 8). Around 250 gram of dried below 2 mm soil samples were packed in plastic container. The containers were made air tight using insulation tape and kept for one month.

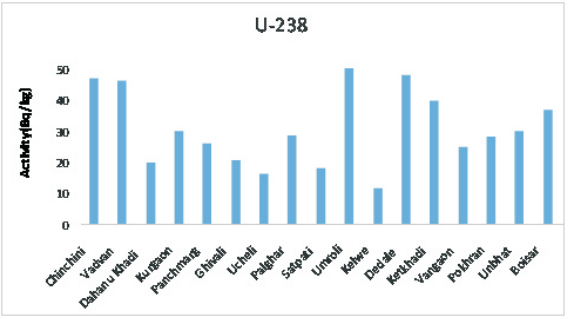


Fig. 1 Distribution of U-238 in soil samples

Sample Analysis

Samples were analyzed using high resolution gamma spectrometry system having 50% relative efficiency with respect to 7.62 cm x7.62 cm NaI (Tl) detector. The certified reference material IAEA RGU-I and RGTh-I have been used for the energy and efficiency calibration of the system in the energy range of 46.5-2614.5 keV. The spectra were acquired for 100000s and the photo peaks were evaluated using the MCAS emulation software.

Results and Discussion

The activity concentration of natural radio nuclides ^{238}U, ^{226}Ra, ^{232}Th and ^{40}K in soil samples of different locations around Tarapur, India are shown in Figs. 1, 2, 3 and 4 respectively. The activity concentration of ^{238}U and ^{226}Ra in six locations was higher compare to world average (33 Bq/kg for ^{238}U and 32 Bq/kg for ^{226}Ra). The activity concentration of ^{238}U and ^{226}Ra was found lower in the remaining eleven sites than the world average value. The activity concentration of ^{232}Th in nine locations of Tarapur found higher compare to the world average values (45 Bq/kg).

In all the sites activity concentration of ^{40}K was found lower than world average value (420 Bq/Kg). However, in India the ^{40}K in soil varies from 38-760 Bq/kg [1].

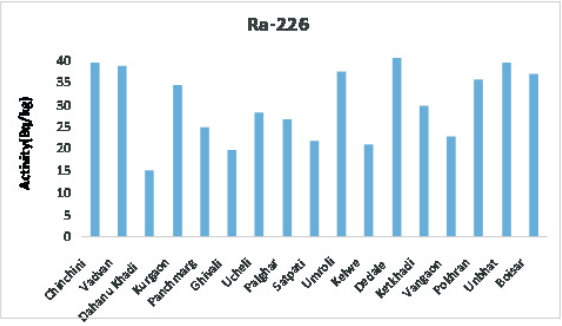


Fig. 2 Distribution of Ra-226 in soil samples

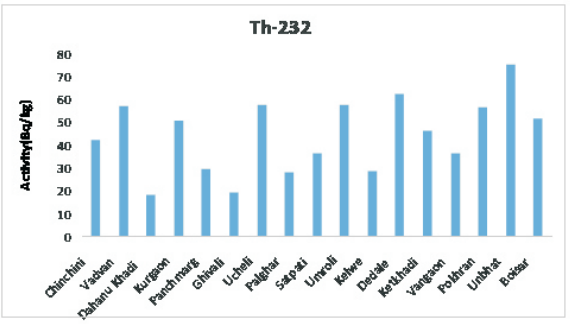


Fig. 3 Distribution of Th-232 in soil samples

The detected activity concentration of ^{238}U, ^{232}Th and ^{40}K in our study is well matched with the Indian average values (29 Bq/kg, 64 Bq/kg and 400 Bq/kg respectively) [3].

References

[1] UNCSEAR United Nations Scientific Committee on the Effects of Atomic Radiation 2000, Sources, Effects and Risks of Ionizing radiation, United Nations, NewYork.

[2] UNSCEAR 2008 Report Vol. I. Sources of Ionizing Radiation, United Nations Scientific Committee on the Effects of Atomic Radiation UNSCEAR 2008 Report to the General Assembly, with scientific annexes.

[3] R. Ravishankar, A. Chandrasekaran, P. Vijaygopalan, B. Venkatraman, G. Senthilkumar, P. Eswaran, A. Rajalakshmi, Radiation Physics and Chemistry. (2012).

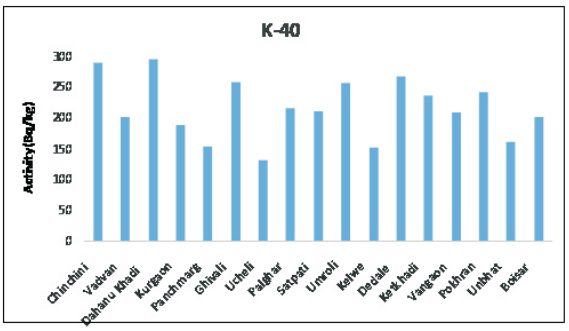


Fig. 4 Distribution of K-40 in soil samples

Environmental Gamma Radiation Monitoring at Visakhapatnam using Thermoluminescence Dosimeters

M. Swarnkar, S.K. Sahu, P.G. Shetty, R.A. Takale, G.G. Pandit

Environmental Monitoring & Assessment Section, Health Safety & Environment Group, Bhabha Atomic Research Centre, Trombay, Mumbai 400085, India; E-mail: sksahu@barc.gov.in

The external background radiation levels at Visakhapatnam have been measured. The measurements were performed using $CaSO_4$: Dy thermoluminiscence dosimeters at 15 locations in and around Visakhapatnam at one meter above the ground. The range of annual average dose rate measured was 0.79-1.86 mGy/year in air based on the analysis of thermoluminiscence dosimeters. Spot readings of the background radiation levels were taken using hand held radiation survey meter.

Introduction

The dose in environment mainly depends upon two factors, natural radiation and manmade or artificially produced radiation. Naturally occurring radionuclides are the major contributors to the total effective dose of ionizing radiation received by the population[1].The natural radiation dose mainly arises from the cosmic radiation (galactic and solar) and from Earth (terrestrial) surface. The two major components contributing about 85% of the total dose are external gamma radiation arising from cosmic rays and primordial radionuclide and inhalation dose due to radon, thoron and their progenies [2]. The gamma rays are the most significant part of environmental dose, due to its large range and deep penetrating power.

The variation in the daily dose rate is primarily influenced by environmental and atmospheric conditions, but it can also be affected by anthropogenic activities. Other influences on the daily dose rate are cosmic-ray ionization and fallout from nuclear weapons testing.

In the last few decades there is a growing concern all over the world about radiation and their exposure to population. Thus it is necessary to conduct radiological environmental surveillance around the proposed nuclear facility. The pre-operational monitoring helps in assessing the impact of operations of facility during its operational phase and also serves as the basis for estimation of radiation doses to public due to releases from plant. The radiation survey data are useful to establish the ambient gamma radiation levels in environment of nuclear site.

Extensive gamma radiation survey was carried out in and around villages located in the surroundings of new BARC complex, Vishakhapatnam site up to a distance of 30 km. The survey was carried out by using a calibrated radiation survey meter. Thermo luminescence Dosimeters (TLDs) were deployed on quarterly basis for a year to obtain the cumulative gamma background radiation levels in the study area.

Study Area

The current study area situated around N17 31.401 and E83 02.161 at Visakhapatnam in the state of Andhra Pradesh, India. The campus is located at Atchuthapuram mandal adjacent to seashore about 35 km from Visakhapatnam City. A survey has been done to find out the existing background gamma radiation levels in and around the campus covering a radial distance of 30 km from the centre (Fig.1) using survey meter and TLDs. The granitic rocks that are predominant in the southern region of India are the kind of rocks that serve as good geochemical hosts for U, Th and high K. A major portion of this region is occupied by proterozoic rocks covering a vast time span from 3800 to 570 million years. The crust in this region shows an enrichment of rare earths with which U and Th are invariably associated in the form of minerals like monazite, samarskite, fergusonite and allanite. Sandstones, limestones, quartzites, slates with poor amounts of U, Th and K will also contribute to the low radiation dose [3].



Fig. 1 Sampling area

Materials and Methods

Thermoluminescence dosimeters were used for measurement of cumulative environmental gamma radiation dose rate. The advantages of passive TL dosimeters for environmental monitoring are that they are small, cheap and do not require power supply during application [4]. The $CaSO_4$:(0.2 mole %) Dy Teflon TLD discs, specifically designed for environmental thermoluminescent dosimetric purpose were used. This disc containing 70 mg of $CaSO_4$: Dy and 210 mg of Teflon powder. Two such discs are mechanically clipped over two symmetrical circular holes on nickel

plated aluminum card. These TLD badge are having very high TL sensitivity, a negligible fading rate and a stable TL response. The TLD badge was covered with and sealed in a polythene pouch to protect the card from rough environment. This system has been thoroughly characterized and the results of this badge have been proved to be highly satisfactory for environmental gamma radiation monitoring. These annealed TLDs, bearing an identification number were deployed at a pre-designated sampling location for a period of three months and was replaced by new TLDs of the next batch. The TLDs after exposure for about three months were evaluated using standard protocol.

The radioactivity content in the soil samples collected from site locations were analyzed by gamma spectrometry technique using High purity germanium detector. The instantaneous environmental gamma radiation levels were also measured in and around the study area using radiation survey meter (target fieldspec) at 1 meter height above the ground. The survey meter has NaI (Tl) Scintillation detector. The detector has an internal Cs-137 source for calibration. Dose-rate ranges that can be measured are 10 $nGyh^{-1}$ - 1 Gyh^{-1}.

Result and Discussion

The gamma radiation levels are furnished in Table 1. It gives annual gamma dose rate in mGy/yr with standard deviation for all the locations currently being monitored. The annual dose rates were computed from quarterly values actually found and normalised to 365 days. It is clearly seen from the results that location to location there is a large variation in external gamma radiation levels. Maximum and minimum dose were found 1.86 mGy/yr at nagulpalli and 0.79 mGy/yr at koppka village. At proposed site for new BARC dose rate is found 1.5 mGy/yr. Table 2 shows natural radioactivity contents in soil samples. From the table: 2 it may be obeserved that vizag soil samples contain higher levels of ^{232}Th and ^{40}K activity it may contributing to the high background gamma radiation levels as measured by TLDs. During the cycle of the TLD survey programe, spot readings of the background radiation levels were taken, both while placing the TLDs and while removing them. The instantaneous dose rates measured using survey meter, are also following the large variation as found in TLDs. It vary 110 nGy/hr to 210 nGy/hr. The large variation in the dose rates may be due to change in cosmic radiation intensities with time and altitude or latitude, non-uniformity in fallout deposite, uneven distribution of natural radionuclides in soil at different locations. The results of this survey will provide baseline data for the assessment of exposure to the population.

Table 1: External gamma radiation dose rates in and around Vishakhapatnam

Sl. No.	Location	Annual dose rate(mGy/yr)
1	Parvada	1.06±0.12
2	Avasomavaram	0.85±0.10
3	Achutapuram	1.12±0.18
4	Yalaminchalli	1.70±0.23
5	Rambilli	1.44±0.14
6	Gobburu	1.26±0.26
7	Nutulaguntlapalem	1.29±0.04
8	Tallapallem	1.66±0.12
9	Bayyavaram	1.60±0.06
10	Nagulapalli	1.86±0.10
11	Munakabaka	1.84±0.09
12	Tummapalla	1.00±0.13
13	Koppaka	0.79±0.03
14	Jogannapalem	1.53±0.26

Table 2: Natural radioactivity contents in soil samples in Bq/kg.

Location	U-238	Ra-226	Th-232	K-40
Parvada	30±2	28±2	241±37	500±184
Achutapuram	29±5	23±4	194±24	486±13
Avasomavaram	39±9	35±11	257±79	511±65
Joganpalem	52±7	41±4	276±28	466±167
Gandivanipalem	39±11	32±8	236±70	328±19
Rambilli	34±2	31±2	219±51	581±146
Yelamanchilli	28±4	24±2	141±24	759±15
Nutuguntelapalem	49±12	48±12	335±87	808±180
Gobburu	36±2	33±2	238±23	775±71
Bayyavarm	33±1	30±3	218±22	733±36
Nagulpalli	34±7	29±7	279±50	794±163
Talaplem	33±1	29±1	226±48	736±144

References

[1] UNSCER: Sources, Effects and Risks of Ionizing Radiation, Report to General Assembly, United Nations, New York, (1993)

[2] UNSCER: Report to the General Assembly, with scientific annexes, I (2000).

[3] A.V. Sankaran, B. Jayaswal, K.S.V. Nambi, and C.M. Sunta, BARC report, (1986).

[4] Ranogajec-Komor, M., Radiat. Safety Manage., 2(1) (2003) 2.

Indoor and Outdoor Gamma Radiation Monitoring at High Background Area of Kerala Using TLDs

P.G. Shetty, S.K. Sahu, R.A. Takale, M. Swarnkar, G.G. Pandit

Environmental Monitoring & Assessment Section, Health Safety & Environment Group, Bhabha Atomic Research Centre, Trombay, Mumbai 400085, India; E-mail: sksahu@barc.gov.in

Indoor and outdoor gamma radiation monitoring was carried out on the population residing in Elevated naturally Radioactive Areas (ENRA).This area is in the Sothern coastal belt of peninsular India in the state of Kerela. For this study hundred houses of different construction types were selected. Indoor and Outdoor measurements were carried out using Thermoluminescence dosimeters (TLDs). This paper presents the results of the dosimetric analysis and effect of different construction types on indoor gamma radiation levels.

Introduction

The natural radiation environment is the major source of radiation exposure to man and consists of both internal and external sources. The main contributors to external exposure from gamma radiation are the members of Uranium (radium) and Thorium series together with potassium. These nuclides are present in all soils and rocks with strong variation from one place to another. Traditional construction materials are derived from these soils and rocks.

There exist some areas in the world where the natural radiation levels are found to be higher than the general background levels found elsewhere. Epidemiolodists and radiobiologist world over have been working over the past few decades to study health effects of chronic radiation exposure in population living in ENRAs. Radiation dosimetry in the ENRAs has therefore become an important tool for the radiobiologists in the epidemiological analyses. These studies include large scale surveys of population exposed to elevated natural background radiations. In India, the monazite bearing regions of Kerala, having significant resident populations living for generations at comparatively higher background levels is suitable for such studies. In this paper indoor and outdoor gamma radiation monitoring was carried in Neendkara village in Kollam district, Kerala. For this study hundred houses of different construction types were selected. Indoor and Outdoor measurements were carried out using Thermoluminescence dosimeters (TLDs). This paper presents the results of the dosimetric analysis and effect of different construction types on indoor gamma radiation levels.

Materials and Methods

Hundred dwellings of different construction types at Needkara Village, Kerela were selected for the survey. The dose levels at a height of 1m above the ground as well as at ground level were recorded both during the deployment as well as retrieval of the TLDs using survey meter. The exposed TLDs were analyzed and evaluated for doses using standard procedure [1]. The gamma-spectrometry system having an n-type coaxial HPGe detector (DSG, Germany) shielded with 7.5 cm thick lead having 50% relative efficiency and a resolution of 2.1 keV at 1.33 MeV gamma energy of ^{60}Co was used to measure soil radioactivity.

Table-1: Soil radioactivity

	Activity (Bq/kg)
^{238}U	41 to 1453
^{234}Th	112 to 9070
^{40}K	70 to 140

Results and Discussion

Soil activity in Neendkara is given in table 1.The values obtained from TLD analysis a was first normalized in terms of absorded dose (mGy/a) and is given in column a and b of Table 1. Using an indoor occupancy factor of 0.8 and outdoor occupancy factor of 0.2 these values were converted in to dose (column c). Using the UNSCEAR [2] conversion coefficient of 0.7Sv/Gy, the doses were then converted to effective dose for the respective house (column d). The effective dose rate was calculated using the formula,

Indoor effective dose rate (mSv y) = D(nGy h–1) x 8760 (h y–1) x 0.8 x 0.7 (Sv Gy–1) x 10–6 (1)

Outdoor effective dose rate (mSv y–1) = D(nGy h–1) x 8760 (h y–1) x 0.2 x 0.7 (Sv Gy–1) x 10–6 (2)

The indoor effective dose was found to vary from 2.14 mSv/a to 9.73 mSv/a. As seen in the table, the gamma radiation levels outside the houses in 42 % cases were less than 10 mGy/a and 37 % cases the gamma radiation were found to exceed 20 mGy/a. The gamma radiation levels inside the house in 84 % cases were less than 10 mGy/a. In 2% cases the gamma radiation were found to exceed 20 mGy/a. However with the occupancy factor of 0.2 and 0.8 for outdoor and indoor dose respectively, the effect of these levels is reduced to a considerable extent.

Majority of the houses under survey (69%) were constructed with brick walls, the remaining houses had either wooden (15%) or thatched walls (16%) with or

Table-2: Environmental gamma radiation levels in Neendkara village

Absorded Dose (mGy/a)		
	Indoor (%) (a)	Outdoor (%) (b)
< 10	84	42
10 to 20	14	21
> 20	2	37

	Absorded Dose (c)		Effective Dose (d)	
	Indoor (%)	Outdoor (%)	Indoor (%)	Outdoor (%)
	mGy/a (a)*0.8	mGy/a (b)*0.2	mSv/a (a)*0.8*0.7	mSv/a (b)*0.2*0.7
< 5	71	75	84	90
5 to 10	20	20	13	10
> 10	9	5	3	

without being plastered and painted. As for the roof, 37% of the houses were made of concrete roof, 20 % were thatched, 30% were tiled and the remaining 13% were made of either asbestos cement or galvanized iron (GI) sheets. About 86% of the houses had cement flooring made directly on the soil, 8% had tiles and 6% were of bare flooring. Indoor gamma radiation level depends mainly upon the type of material used for the construction. This construction material acts both as shielding factor and as source for indoor gamma radiation level. For majority of the houses under survey the construction materials were brought from outside region having less radioactivity content than the surrounding soil. Table 2 gives the radiation dose rate at outdoor and indoor areas for different type building material. It is seen that wooden houses with tiled and Gi sheet provide little shielding from the radiation, due to natural radioactivity outside the house. The shielding factor for houses using concrete roof and brick wall was found to be highest, by factor of 4.

Table-3 : Effect of different construction materials on the indoor gamma radiation level.

Type of House	Indoor (Gy/h)	Outdoor (Gy/h)	Avg.Outdoor to Indoor factor
Brick-concrete	2.9	7.3	
	0.6	2.5	
	0.5	2.2	4
	0.8	4.0	
	0.9	2.5	
	0.4	2.5	
Wooden-tiled	0.22	0.40	
	0.40	0.78	2
	2.16	4.20	
Wooden- Gi sheet	0.24	0.38	
	1.37	2.09	2

Conclusions

The results of the external gamma radiation survey using TLDs and survey meter in the village of Kerala indicate that

1. More than Eighty percent of external indoor gamma radiation dose was within 10 mGy/a and only Two percent was above 20 mGy/a
2. From Our preliminary work on the effect of different types of construction material on the indoor gamma radiation level shows that the shielding factor for houses using concrete roof and brick wall is highest by factor of 4. Whereas make shift houses and provide minimum shielding against external radiation.

References

[1] Nambi, K.S.V., Bapat, V.N., David, M., Sundaram, V.K., Sunta, C.M., and Soman, S.D., Natural background radiation and population dose distribution in India., BARC report (1986).

[2] UNSCEAR United Nations Scientific Committee on the Effect of Atomic Radiation., Annex A; Exposure from Natural Sources., New York (2000)

Optimizations of Teflon Embedded $CaSO_4$: Dy based TLD for Environmental Monitoring Applications

R.A. Takale, S.K. Sahu, M. Swarnkar, P.G. Shetty, G.G. Pandit

Environmental Monitoring & Assessment Section, Health Safety & Environment Group, Bhabha Atomic Research Centre, Trombay, Mumbai 400085, India; E-mail: sksahu@barc.gov.in

In India environmental gamma radiation monitoring, using TLDs is being carried out since last four decades on regular basis. This study discusses the optimization of $CaSO_4$: Dy phosphor for its use in large scale environmental monitoring programe. Investigations are (have been carried out) made to determine optimum thickness of Teflon disc and doping concentration. Teflon disc with 0.8mm thick was found to be the optimum thickness for highest sensitivity with linear dose response. Some of the applications in selected area of normal background in the country are presented in this paper.

Introduction

The thermo luminescent dosimeters (TLDs) are most suitable for environmental monitoring because of its advantages over other systems. Environmental gamma radiation monitoring, using TLDs around all the nuclear installations in India is being carried out using powder based CaF_2 dosimeters. In order to cater to large scale requirement, this system was labor intensive. Phosphor embedded Teflon discs provides one of the key as it offers many advantages over loose powder handling. $CaSO_4$: Dy Teflon TLD discs, has been found to be 35 times more sensitive than TLD 100 [1]. Due to very high TL sensitivity, a negligible fading rate and a stable TL response of $CaSO_4$: Dy Teflon TLD discs, they are routinely used in personal monitoring. The performance criteria for TLDs in environmental monitoring are different from those required in personnel monitoring, as exposure levels are low, long exposure times are required along with extreme sensitivity. Permanent efforts were made in order to increase the sensitivity of $CaSO_4$: Dy phosphor for its use in environmental monitoring. This paper discusses the various characterization studies of $CaSO_4$: Dy TLD system.

Materials and Methods

$CaSO_4$: Dy phosphor embedded Teflon discs of 0.1 mm, 0.2 mm, 0.5 mm, 0.8 mm , 1.2 mm, 1.8 mm and 2.3 mm thickness of 13.3 mm dia were made using respective Teflon tape. These discs were fixed in machine identifiable aluminum card. The set of twenty cards of each thickness were annealed at 250°C for three hours and irradiated to various exposures by Cs-137 gamma radiation source. They were read off using automated TLD badge reader after 2 days, by integrating the output of the photo multiplier for 30seconds, which covered the dosimetric peak at 210°C only. The details of reader and its performance were discussed in detail elsewhere [2].

$CaSO_4$ phosphors doped with 0.05, 0.1, 0.2, 0.3, 0.5, 1 mol percent Dy concentrations were prepared following the re-crystallization technique [3]. For irradiation, Co-60 gamma source with a dose rate 4 Gy/min was used. TL measurements were made with 4 mg of powder, with a linear heating.

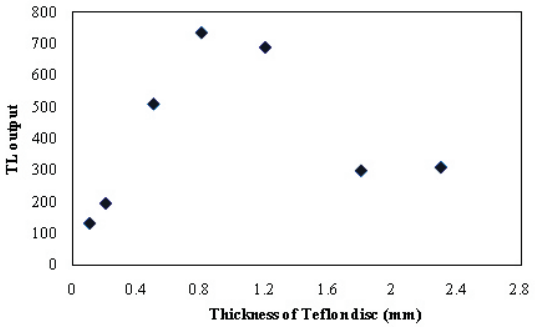


Fig. 1 Variation of TL response with respect to thickness of Teflon discs

The energy dependence was assessed by exposing TLDs to X-ray/gamma radiation of various energies. Three sets of readings were taken, (i) only bare cards, (ii) cards only with plastic cassettes and (iii) cards with 1mm copper filters in the plastic cassettes.

Result and Discussion

To study the effect of Teflon thickness on the performance of the TLD, discs of different thickness were exposed to 100, 200, 400 Gy of Cs-137 gamma rays were read and average TL counts with spread ±5% was considered. The variation of TL response with respect to thickness of Teflon discs for 400 Gy gamma exposure is shown in Fig. 1. It is seen that response to gamma ray increases as thickness increases and after reaching a peak at 0.8mm the increase in thickness results in response declined. The dose response curve drawn using the TLD output against the exposure imparted is as shown in Fig. 2. It is observed from the figure that 0.8mm disc shows the linear dose response in the range up to 400 Gy, the range useful for routine environmental gamma radiation monitoring. It is clear from the Fig. 1 and Fig. 2 that Teflon disc with 0.8 mm thick is the optimum thickness for highest sensitivity with linear dose response.

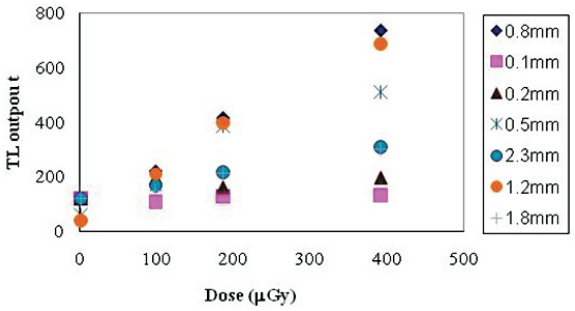


Fig. 2 Dose response curve for various thicknesses

The effect of doping concentration on the sensitivity of $CaSO_4$ has been investigated. Fig.3 denotes the normalized TL output of $CaSO_4$: Dy with different doping concentration. It is clear from these figures that 0.2 mole percent of Dy is the optimum concentration that characterized by the maximum TL-intensity and after which a concentration quenching occurs.

Hence $CaSO_4$: Dy with 0.2 mole % dopant concentration was found to be most suitable for environmental gamma radiation monitoring.

Annealing of the dosimeters becomes necessary because a significant thermo luminescence is left out after the readout which causes interference in their subsequent reuse. Different annealing temperatures have been tried for higher exposures and the optimum was 250^0C for three hour. Reusability of TLD cards which are used for ten cycles were checked with fresh TLD cards. It was found that there is no loss in the TL sensitivity even after ten cycles of reuse. From the typical batch of 100 freshly annealed TLDs the minimum measurable exposure was found be 5 Gy.

Fig. 4 shows the normalized response of three sets of TLDst against the various X-ray/gamma radiation energies. It is seen from the graph that the copper filter of 1 mm thickness was quite suitable. The TL response of these TLDs for exposures at various angles of incidence is within 30% of the true values, which is acceptable as per ANSI criteria.

Applications

Presently $CaSO_4$ based TLDs are being used for continuous environmental gamma radiation monitoring

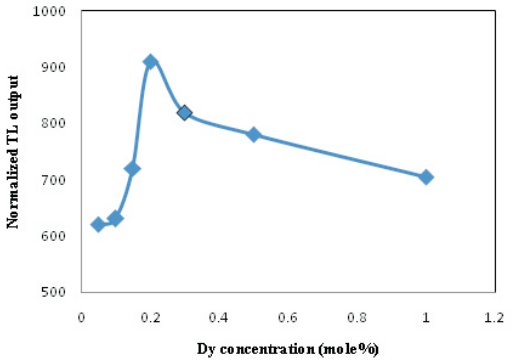


Fig. 3 Normalized TL output of $CaSO_4$: Dy with different doping concentration

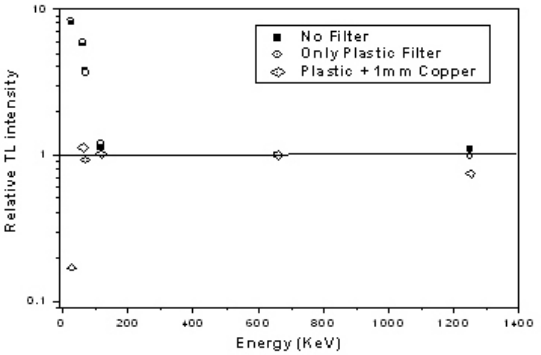


Fig. 4 Normalized response of three sets of TLDs against the various X-ray/gamma radiation energies

across the country. The results obtained by the Teflon embedded $CaSO_4$ based TLD discs were comparable with the earlier used CaF_2 powdered TLDs.

References

[1] K.S.V Nambi, V. N. Bapat, M. David, V. K. Sundaram, C. M. Sunta and S. D. Soman, Radiat.Prot.Dosim. 28(1) (1987) 31.

[2] S. Kannan, P. Ratna and M. S. Kulkarni in Rad. Prot and Env. 26 (2003) 251.

[3] T. Yamashita, N. Nada, H Onishi and S. Kitamura in Proc. 2nd Int. Conf. Lum. Dod. Gatlinburg, T.N. 4-7.

Distribution of Uranium & Thorium in Fractionated Sediment Samples Obtained from Different Locations across Thane Creek Area, Mumbai, India

Sukanta Maity, S.K. Sahu and G.G. Pandit

Environmental Monitoring and Assessment Section, Bhabha Atomic Research Centre, Mumbai 400085, India; E-mail: ggp@barc.gov.in

Distribution of uranium and thorium in different size fractionated sediment samples were carried out using differential pulse adsorptive stripping voltammetry (DPASV) and inductively coupled plasma atomic emission spectrometry (ICP-AES) respectively. Concentration of uranium varies from 5.92 to 16.12 g/g in the coarse sand fraction, 3.80 to 14.03 g/g in the fine sand fraction and 4.33 to 12.96 g/g in the silt and clay fraction respectively. Concentration of thorium varies from 15.17 to 35.95 g/g in the coarse sand fraction, 13.44 to 30.44 g/g in the fine sand fraction and 9.27 to 33.10 g/g in the silt and clay fraction respectively.

Introduction

Metals occur naturally in the environment and are widely distributed, as free ions or forming part of complexes or compounds (U. Fiirstner, 1981). The shore and bottom sediments accumulate radionuclides by sorption from seawater or by sedimentation of suspended radioactive solids. The radionuclides that remain associated with sediments are influenced greatly by the chemical, biochemical and microbiological changes that take place in the environment. In the dynamic process of exchange of these nuclides with other matrices of the aquatic environment, it is the labile components that are involved. In sediments, such labile constituents can be composed of the exchangeable or removable ions on the surface, or the hydrous precipitates that undergo dissolution by the complexing action of the chemicals in the environment (K. C. Pillai, 1975). Uranium is stably dissolved in oxic seawater as the U(VI) uranyl carbonate species, $UO_2(CO_3)_3^{4-}$, and has a 400,000 year residence time in the oceans. Under reducing conditions U may be reduced to the more reactive U(IV). Uranium is a naturally occurring element with an average abundance in the earth crust of about 2 mg per kg (range 0.1 to 20 mg/kg). It is more abundant than silver or gold. It has adverse effects on the human health. The major health effect of uranium is its chemical toxicity, rather than its radiological hazard (D. M. Taylor, 1997).Thorium occurs only in the +4 oxidation state in nature. In aqueous solutions, especially in natural waters, the concentrations of dissolved thorium are very low. Dissolved thorium forms a variety of hydroxyl species, and undergoes extensive chemical interaction with water and most anions. Thorium can form various aqueous complexes with inorganic anions such as dissolved carbonate, fluoride, phosphate, chloride, and nitrate. Thorium (Th^{4+}) is rapidly removed from solution onto particles with a mean residence time of <100 years.

In the present study uranium and thorium were analyzed using DPASV and ICP-AES respectively in different size fractionated sediment samples collected from different locations across Thane Creek area, Mumbai, India.

Experimental

Sampling Location and Physical Characterization

Fourteen sediment samples were collected from different locations across Thane Creek area, Mumbai, India. After collection of the sediment samples were fridge dried. The dried samples were used for physical characterization. At first the dried sediment samples were sieved below 2 mm using electromagnetic sieve shaker (EMS 8). The dried sediment samples (below 2 mm) were size segregated using electromagnetic sieve shaker into different size fractions like coarse sand (between 2.0 mm and 250 m), fine sand (between 250 ìm and 53 m), silt and clay (below 53 m).

Sample Processing

For the estimation of distribution of uranium and thorium in marine sediment, the different size fractions of the sediment samples (between 2.0 mm and 250 m, between 250 m and 53 m, below 53 m) were acid digested in microwave digestion system (Ethos 1). One certified reference material (IAEA-405) sediment sample was also digested through microwave digestion system for the analysis of uranium and thorium to know the percentage recovery of the digestion procedure. After microwave digestion the sample is diluted into 25 ml volumetric flask using 0.25% electronic grade nitric acid. In prepared sample solution (0.25% electronic grade nitric acid solution) uranium and thorium were analyzed.

Sample Analysis

Uranium was analyzed using DPASV (Metrohm multifunction instrument model 693 VA Processor equipped with a 663 VA stand). Measurements were carried out with a hanging mercury drop electrode

(HMDE) in a three-electrode arrangement. The auxiliary electrode was a wire of platinum. Ag/AgCl (KCl 3M) was used as reference electrode. Thorium was analyzed using ICP-AES (Horiba Jobin Yvon model). The reliability of the procedure was further assessed by analyzing standard reference materials IAEA-405 (sediment). The results agreed very well with the certified values.

Results and Discussion

In all the grab sediment samples, it was observed that the predominating portion is the fine sand although from sample to sample its percentage varied. Exception observed in case of sample collected from locations 8, 10 and 14, here predominating portion is coarse sand. The particle size distribution was found to be 15.21-54.76% coarse sand, 39.72 - 66.99% fine sand and 3.36-17.8% silt and clay content respectively shown in figure 1.

Analyzing the uranium and thorium concentration in different size fractionated sediment samples it can be predicted the distribution of uranium and thorium in different particle size of sediment. For quality assurance of the analytical data along with sediment samples certified reference material (IAEA-405) was also analysed. The analysed uranium and thorium concentration were matched very well (94% and 92% respectively) with the certified values. Variation of concentration of uranium and thorium are shown in Figs. 2 and 3 respectively. From Fig. 2, it is clearly observed that uranium concentration is higher in coarse sand fraction in the locations 1, 2, 3, 4, 5, 8, 10, and 13. Whereas in the fine sand fraction uranium concentration is higher in the locations 6, 9 and 14. In the sediment samples collected from locations 7, 11 and 12 uranium concentration is higher in the silt and clay fraction. From Fig. 3, it is clearly observed that thorium concentration is higher in coarse sand fraction in the locations 4, 5, 8, 9, 10, 13 and 14. Whereas in the fine sand fraction thorium concentration is higher in the locations 1, 3 and 6. In the sediment samples collected from locations 2, 7, 11 and 12 thorium concentration is higher in the silt and clay fraction.

Conclusions

It is clearly observed that uranium and thorium concentration vary randomly in different size fractionated sediment samples collected from different locations across Thane Creek area, Mumbai, India. These results will help to know the distribution of uranium and thorium in different size fractionated sediment samples

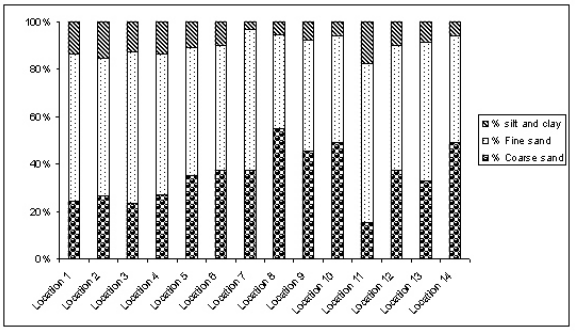


Fig. 1 Percentage distribution of different size fractions of sediment samples

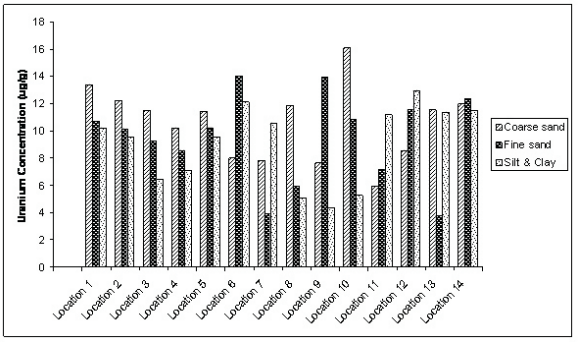


Fig. 2 Concentration distribution of U in different size fractionated sediment samples

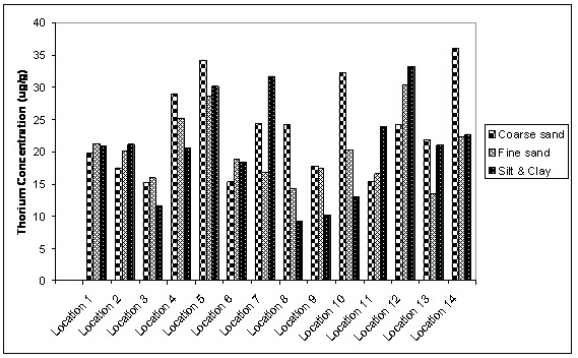


Fig. 3 Concentration distribution of Th in different size fractionated sediment samples

References

[1] Fiirstner U. and Wittman G.T., Metal Pollution in the Aquatic Environment. Springer-Verlag, London, (1981) 486.

[2] Pillai K.C., Dey N.N., Mathew E., Kothari B.U., Behaviour of discharged radionuclides from fuel reprocessing operations in the aquatic environment by Bombay Harbour Bay, in: Impacts of Nuclear Releases into the Aquatic Environment: Proceedings, IAEA, 30 June- 4 July, (1975).

[3] Taylor D.M. and Taylor S.K., Environmental uranium and human health. Rev Environ Health, (1997) 147157.

Estimation of Sensitivity Factor for Direct Thoron Progeny Sensors in Occupational Environments of a Reprocessing Facility

R. Prajith[1], S. Jalaluddin[1], R.P. Rout[1], R. Mishra[1], K. Kannan[2], M.R. Shankaran[2] and B.K. Sapra[1]

1. *Radiological Physics and Advisory Division, Bhabha Atomic Research Centre, Trombay, Mumbai 400085, India; E-mail: rama_barc@yahoo.co.in*
2. *Kalpakkam Reprocessing Plant, Kalpakkam, Tamilnadu 603102, India*

Direct Thoron progeny sensors are deposition based absorber mounted track detector, which can be used for measuring the long time-averaged progeny concentrations. Extensive measurements had been carried out in the indoor environments using these detector systems. In the present work, the field studies of these dosimeter systems carried out in the ADU Processing areas of Kalpakkam Reprocessing Plant has been reported. Since the sensitivity factor of these dosimeters is dependent on the deposition of progeny particulates on the detector surface, hence the various environmental processes governing the deposition, affect the sensitivity factor, especially the air exchange rates. Since higher air exchange rates are generally maintained in the Thorium processing plants, these dosimeters were first calibrated for the plant environment, and the calibration factor was obtained as 2.5 Tr $cm^{-2}d^{-1}$ / EETC (Bq m^{-3}).

Introduction

It is known that in the Indian Nuclear Power Programme, the processing of the spent PHWR fuel is carried out at the reprocessing Plants. It has been observed that in some areas of the plant, especially at the ADU facilities, activity concentrations due to thoron and its progeny was very high [1]. Earlier approach has been either to measure the thoron progeny concentration by grab filter-paper sampling followed by alpha counting, or by estimating the progeny concentration from the measured thoron gas using an assumed equilibrium factor. But, in the case of thoron, it is extremely important to measure both gas as well as progeny, since equilibrium does not exist between the parent and the daughter owing to the shorter half-life of the thoron gas. Secondly, active measurements are not the representative values for calculating the inhalation doses. Hence in the present work, recently developed Direct progeny sensors have been used, which are passive and can give time averaged progeny concentrations.

As discussed in [2], the sensitivity factor (k_T) of this system is dependent on the environmental parameters, especially on the air exchange rates. A scenario of the dependency of sensitivity factor on particle concentration at different air exchange rates in indoor environment is shown in Fig. 1. It shows that, k_T becomes increasingly dependent on air exchange rates at low particle concentrations.

Mathematically, (k_T) of DTPS is defined as [2],

$$k_T \quad \frac{V_d}{0.95 \quad _2} \qquad (1)$$

Where, is the track registration efficiency of the DTPS system,is the decay constant of ^{212}Pb and V_d is the effective deposition velocity of the thoron progeny defined as follows [2].

$$V_d \quad \frac{J}{C} \qquad (2)$$

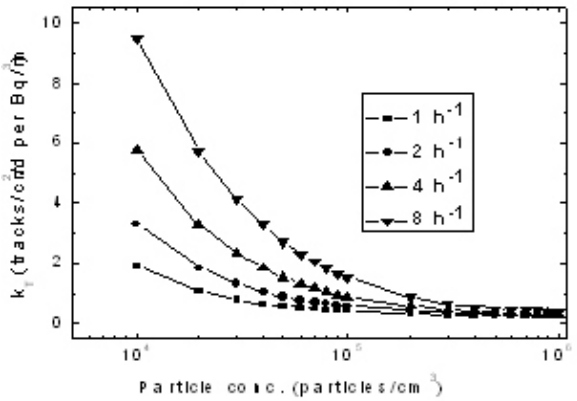


Fig. 1 Sensitivity factor k_T versus Particle concentration Z at different air exchange rates

where, J is the deposited atom flux (atoms/cm^2/s) on the surfaces and C is the atom concentration (atoms/cm^3) in atmosphere.

k_T depends on V_d which being a field parameter varies with the aerosol concentration (Z) and ventilation rate/ air exchange rate (Fig. 1).

In this paper, experiments were carried out to measure V_d and thereby estimate k_T of DTPS system in different locations of the ADU facility, essentially to typify these systems for efficient deployment and the right estimation of inhalation dose in these facilities.

Materials and Methods

For estimation of V_d at a particular location of the ADU Plant, the total progeny atom concentration was measured at that location using a flow mode DTPS loaded integrated sampler [3] and the total progeny atom deposition flux was obtained from the passive DTPS System deployed in the same locations.

The integrated sampler consists of a DTPS placed before the filter paper in an array. In each of the

locations, sampling was carried out at a flow rate of 2 lpm. The sensors are then subjected to etching and counting following the standard protocol to convert the latent tracks created on the sensor to the deposited progeny atom concentration as shown in the table1.

Table1: Deposition atom flux measured at different locations of ADU facility.

Location	Tr/cm^2/d	J (At/cm^2/s)
Loc1	224	0.032
Loc2	87	0.012
Loc3	188	0.027
Loc4	76	0.011
Loc5	90	0.013

Similarly, the passive DTPS system deployed at the same locations were retrieved and subjected to standard etching and counting procedures to convert the track density produced to total atom deposition flux. Measured deposition atom flux at different locations of ADU plant is shown in table 2. V_d was then estimated from the graph between J versus C which yield a straight line (Fig. 2) and the slope of this gives the value of V_d. From Fig. 2, V_d was found to be (0.0061±0.001) cm/s or (0.220±0.036) m/h. This value is found to be about three times higher as compared to that measured in indoor environment 0.075 m/h [2]. Using this value of V_d in Eq. 2, k_T was calculated to be 2.53 tr/cm^2/d per Bq/m^3 which is very close to 2.5 as reported earlier for occupational environments of IRE, Alwaye [2].

Table 2: Deposited progeny atom concentration (atoms cm^{-3}) obtained from integrated sampler.

Location	Tr/cm^2/h	EETC (Bq/m^3)	C (At/cm^3)
Loc1	1950	88.66	4.87
Loc2	754	34.28	1.88
Loc3	1495	67.98	3.73
Loc4	847	38.50	2.11
Loc5	1039	47.25	2.59

By considering ventilation rate of 4-6 h^{-1} and Z around 10^4 p/cc (which is the normal condition in ADU facility), the theoretical model also predict k_T around 2.5 (Fig. 1). Hence value of k_T as 2.5 may be used for this DTPS system in-order to measure thoron progeny concentrations and thus inhalation dose due to thoron progeny in these environments.

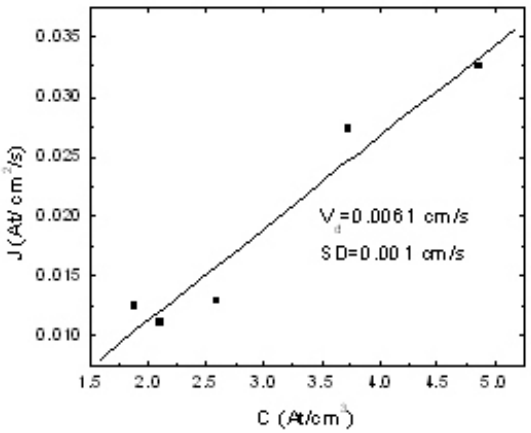


Fig. 2 Graph between J (At/cm^2/s) and C (At/cm^3)

Conclusion

Deposition velocity measured in KARP, ADU facility found to be about 3 times higher the indoor environment. The sensitivity factor of the DTPS system which is used for inhalation dose estimation due to thoron progeny was found to be 2.53 tr/cm^2/d per Bq/m^3.

References

[1] M. D. Deshpande, S. Krisnamony and K. Pendarkar, Bulletin of Rad. Prot. 17 (1994) 23.

[2] R. Mishra and Y. S. Mayya, Rad. Measurements 43 (2008) 1408.

[3] R. Mishra, R. Prajith, B. K. Sapra and Y. S. Mayya, NIM B 268 (2010) 671.

Environmental Radiation Levels at NARL, Gadanki

Charan Kumar K.[1], Manikiam B.[2], Rajendra Prasad T.[3] and Kamsali Nagaraja[1*]

1. *Atmospheric & Space Science Research Laboratory, Department of Physics, Bangalore University, Bangalore 560 056, India; E-mail: kamsalinagaraj@bub.ernet.in*
2. *Sir MV- ISRO Chair, Department of Physics, Bangalore University, Bangalore 560056, India*
3. *National Atmospheric Research Laboratory, Gadanki 517 112, India*

Radioactivity in the atmosphere is a considerable parameter now-a-days due to the health risks and atmospheric research with radon as tracer. The measurements were made using AlphaGUARD and AlphaPM in open space at NARL, Gadanki, India during February to December, 2012. The Average radon concentration observed in Bq/m^3 is 12.86 and ranges between 1 and 195, while radon progeny in mWL shows a mean of 5.19 with variability of 0.13 and 24.32. Both concentrations show a similar trend with peaks during early morning and minima in the afternoon with positive correlation for relative humidity and anti-correlation for ambient temperature due to temperature inversions. The average dose rate observed is 178.1 nSv/hour.

Introduction

Radon is an inert and radioactive gas with half-life of 3.82 days descending from ^{238}U decay series and is ubiquitous in the Earth's crust. ^{222}Rn further decays to its progenies such as ^{218}Po, ^{214}Pb, ^{214}Bi and ^{214}Po. Radon exhaled from soil gets mixes with air and is transported by diffusion or convection [1] and natural radioactivity acts as a significant tracer in the atmospheric boundary layer. There are many evidences that the inhalation of air associated with progenies in the form of radioactive aerosols leads to health problems. Progenies being materials particles, during the respiratory tract deposits energy on to the cells of bronchial epithelium [2] and continuous deposition may leads to the damage of cells. Decay products can also cause direct effect on the DNA structure and indirect effect due to the production of active chemical radicals in the vicinity of DNA [3].

Radon being a Nobel gas does not chemically react with other elements and its origin is restricted almost to land surface [4]. It is also used as a tracer for investigating atmospheric circulation. Studies on the stability and on thermal and mechanical motions of air masses in the low troposphere are of great interest, both to improve understanding of these processes and also for modeling the distribution of pollutants over a territory and evaluating regional and global chemical transport models.

In the present study, the concentrations of radon-222 and progeny were measured at a height of 1m from the surface of earth during February to December 2012. An effort is made to present the preliminary results of measurements of radon and its progeny and their dependence on meteorological parameters. This study shows the variation of radioactivity and becomes a data set for the climate and pollution modeling studies.

Experimental Methodology

Several techniques have been established for the measurement of concentrations of radon. Precision, accuracy and efficiency of different techniques make important issues since the environmental radon and its progenies exhibit usually, low concentration. The AlphaGUARD is a compact portable measuring system for the continuous determination of the radon and selected meteorological parameters including gamma dose rate. The AlphaGUARD uses the proven principle of the pulse ionization chamber of alpha – spectroscopy.

However, the concentrations of progenies were made using AlphaPM in association with AlphaGUARD. The air is sucked and radon progenies are adhered onto the filter paper. The alpha-emissions from the filter are counted by a detector. Based on the flow rate, volume and number of pulses registered during the cycle, the radon progeny concentration is calculated [5]. The sampling was done for every 10 min at a fixed location and height that were not investigated before. Isotopes of radon furnish a unique set of tracers for the study of transport and mixing processes in a wide variety of atmospheric phenomena, particularly in understanding the chemistry of the atmosphere.

Study Area

The measurements were made at National Atmospheric Research Laboratory (NARL), Gadanki, a rural place about 120 km northwest of Chennai on the east coast of the southern peninsula India. The station is surrounded by hills with a maximum height of 400 m and the station is at a height of 375 m above mean sea level. The local topography is complex with a number of small hillocks and an irregular mix of agriculture and small population centers. However, there also exists a high hill of ~1 km about 30 km from the site in the northeast direction. The influence of the sea on the east may not be present at the Gadanki location as it is located far inland.

Results and Discussions

The Fig. 1 shows the variation of radon concentration for a typical day of 28 November 2012.

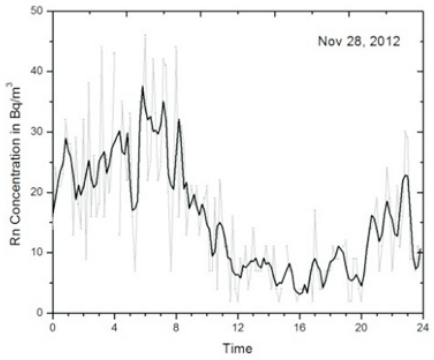


Fig. 1 Diurnal variation of Radon

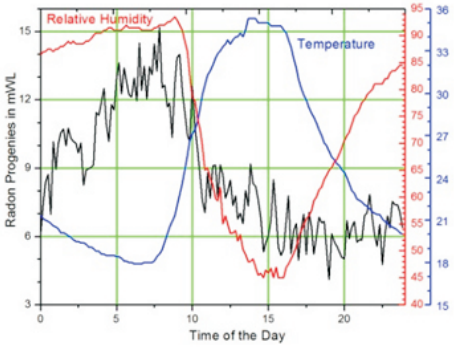


Fig. 2 Diurnal variation of progeny and meteorological parameters

The dark black line represents the mean concentration of radon for every 1-hour and the background line shows the fine mode variation for every 10-minutes. It is clearly seen that radon is high during early morning hours around 05 to 07 hours of IST where as minimum during 14 to 17 hours. The peak in concentration in the early morning hours is due to the temperature inversion.

As a consequence, the gas particles and the aerosols to which its progeny are attached will be present at higher concentrations at ground level. After sunrise the solar radiation warms the lower atmosphere and results in the breakup of inversion that leads to a substantial decline in concentration. Concentrations remain low until late afternoon and the trend agrees well with the elsewhere observations [5,6]. The radon concentration (Bq/m^3) in air varies from 2 to 46 with a mean value of 15.8 showing significant diurnal variation almost by a factor of 23. However, the fluctuations observed may be due to the frequency of observations and the effect of wind.

The diurnal variations of radon progeny with temperature and relative humidity for 28 November 2012 are shown in Fig. 2.

The progeny concentration follows the trend of radon and shows positive correlation with relative humdity and anti-correlation with ambient temperature and is due to the fact explained for radon behaviour. Progeny concentration in air varies from 0.26 to 18.50 mWL with a mean value of 8.72 mWL. On the same day the dose rate is also monitored and shows a mean of 179.69 nSv/hour.

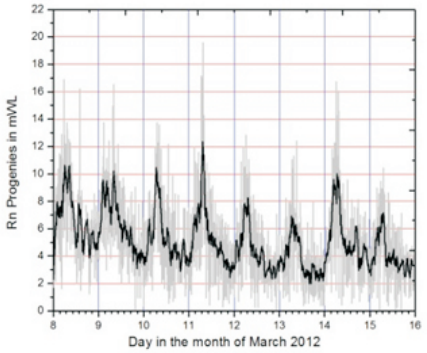


Fig. 3 Continuous variation of progeny for the duration 9-16, March 2012

For consistency, the radon progenies for the duration 9-16, March 2012 is shwon in Fig 3.

The diurnal variation for all the days can be observed clearly with relatively high concentrations during night and early morning hours compared to the day-time. The startistical variations of radon, progenies and meteorological parameters are mentioned in Table 1.

Table-1: Statistiscal variation of radon and its prameters

Statis-tics	Radon (Bq/m^3)	Progeny (mWL)	Temp (^{o}C)	RH (%)	Pres-sure (m bar)	Dose Rate (nSv /hr)
Mean	12.8	5.19	28.8	64.7	968	178
Min	1.0	0.13	12.2	13	800	106
Max	195	24.32	46.8	99	979	386
Std Dev	9.33	4.08	6.23	21.8	14.3	18.3
Median	11.0	4.22	28.1	66	970	177

Skewness is the degree of asymmetry of a distribution around its mean and radon and its progeny shows skewness more than one and indicates that higher values were observed more from its mean values.

Acknowledgment

Authors are thankful to the ISRO for funding and to the Director, NARL for constant encouragement and permitting to carry out experiments at NARL, Gadanki.

References

[1] Yasutaka Omori, Izumi Tohbo , Hiroyuki Nagahama Yoichi Ishikawa, Masato Takahashi, Hiroaki Sato, Tsutomu Sekine., Rad. Meas. 44 (2009) 1045.

[2] H. Tempfer, W.Hofmann, A.Schoher, H.Lettner, A.L. Dinu, Radiat. Environ. Biophys. 49 (2010) 249.

[3] UNSCEAR (1993) Report to the General Assembly.

[4] M.H. Wilkening and W.E.Clements., J.Geophys. Res., 80 (1975) 3828.

[5] K. Nagaraja, L.A. Sathish in SSNTD and their Applications, Ed. N.L. Singh, Narosa Publishing House, New Delhi (2013) 71.

[6] K. Nagaraja, B.S.N. Prasad, M.S. Chandrashekara, L. Paramesh, M.S. Madhava, Ind. J. Pure Appl. Phys. 44 (2006) 353.

Analysis of Cow Dung Samples for Natural Radioactivity

E. Mahiban Ross[1,2] and S. Godwin Wesley[1]

1. *Department of Zoology, Scott Christian College (Autonomous), Nagercoil, 629201, India; E-mail:mahibanross@gmail.com;*
2. *Present Address: Sam Higginbottom Institute of Agriculture Technology and Sciences, Allahabad, 211007, India*

Introduction

Cow dung is the undigested residue of plant matter which has passed through the animal's gut, which is rich in minerals. Along with the minerals, heavy metals are added to soil through animal manure, may directly or indirectly affect the chemical composition of crops grown, by affecting soil and water supplies [1]. The inventory of heavy metal inputs to agricultural land has shown that agricultural soils are at risk from heavy metal accumulation through the application of organic manures [2]. In consideration of the ever increasing pressure being placed on land by more intensive land management practices and the increasing use of agricultural land for waste management, it is important to study the heavy metal content in animal manure [3]. Much focus is on the heavy metal content of cow dung and the radionuclides content are often ignored as if they are not present. Natural radionuclides are present in plant material on varying activity concentrations and can be expected in the cow dung in a similar proportion. Analysis of cow dung samples for natural radioactivity has not been carried out around Kudankulam and no relevant literature is available in the Indian subcontinent on cow dung. So an attempt has been made to study the natural radionuclides in the cow dung, which is widely used as manure for sustainable agriculture. The present study was aimed to analyse the natural radioactivity levels of ^{40}K, ^{228}Ra and ^{226}Ra in cow dung samples.

Experimental

About 1.5 kg of cow dung sample was collected in a polythene bag and taken to the laboratory for radionuclide analysis. The cow dung samples, after drying, were charred and finally made to ash in a muffle furnace at 425ºC. The ash samples were ground to a fine powder and transferred to separate cylindrical vials (dia.19mm_ ht.100 mm); Soil samples were packed in 250 mL containers. The activity concentration of the radionuclide was measured one month later to ensure a secular equilibrium between the ^{238}U and ^{232}Th series and most of their daughter products. A well-type HPGe coaxial detector (EGPC-390-P21-Canberra make, active volume 390 cc, well dimension of 65 mm depth by 21 mm diameter) was used for counting. The radioactivity in the ash soil samples was counted for 50,000 s. Radioactivity was measured by a 16 K EAGLE standalone multichannel analyser with a digital spectrum stabilizer (Model EC-5015). The determination of the peak area and the background subtraction was carried out using APTEC NRC software. The count per second of each radionuclide of interest was obtained based on the resemblance of a Gaussian distribution. The individual peaks were located using Genic software along with CANBERRA which resolves the overlapping of peaks into individual components. All the values are reported at 95% confidence levels. ^{228}Ra and ^{226}Ra activity concentration were determined from ^{228}Ac (911 keV) and ^{214}Bi (609.3 keV), respectively. The activity concentration of ^{40}Kwas determined from 1460.8 keV [4,5]. The software ProUCL4.0 was used for identifying outliers and further analyses were done with the outlier-censored data. The activity concentration for the radionuclides was reported in Bq kg^{-1} fresh weight.

Results and Discussion

Pottasium-40

^{40}K activities in the cow dung samples ranged from 131 ± 43.3 to 271 ± 125 Bq kg^{-1}, with a mean value of 176.4 ± 47.5 Bq kg^{-1}. The activity in the cow dung samples was the lowest in Alagappapuram and the highest in Perumanal which is a coastal village. The samples followed a lognormal distribution, with a 95% UCL of 203.9 Bq kg^{-1}. One-way ANOVA indicated the lack of variation in the ^{40}K activities between the sampling locations ($F = 0.85$; $df = 9, 24$, $P > 0.05$; Table 4.27). ^{40}K in the cow dung samples had showed a significant positive correlation with ^{228}Ra and ^{226}Ra ($r = 0.44$; $P < 0.05$ and $r = 0.57$; $P > 0.05$ respectively). ^{40}K in the cow dung samples could not be compared with globally reported values because of lack of data. The activity of ^{40}K content in cow dung was compared with its activity of grass samples. The ^{40}K content was about three times higher in grass than in cow dung, indicating its absorption by the cow and excretion through urine and also through milk. One-way ANOVA indicates that there is no variation in ^{40}K activity in the cow dung samples between the sampling stations. This is indicative of a similar pattern of excretion of ^{40}K through cow dung in the study area.

Radium-228

^{228}Ra activities in the cow dung samples ranged from 2.23 ± 1.18 to 43.17 ± 32.38 Bq kg^{-1}, with a mean value of 20.4 ± 12.5 Bq kg^{-1}. The lowest ^{228}Ra activity was observed in Alagappapuram and the highest in Aralvoimozhi. The samples followed a normal distribution, with a 95% UCL of 27.55 Bq kg^{-1}. One way ANOVA indicated that there is no significant variation between the sampling locations ($F = 0.41$; $df = 9, 24$, $P > 0.05$). The ^{228}Ra and ^{226}Ra content of cow

dung also had significant positive correlations between them ($r = 0.84$; $P < 0.05$). ^{228}Ra activity in the cow dung samples could not be compared with globally reported values because of lack of data. The activities of the ^{228}Ra in cow dung were compared with that of grass samples. ^{228}Ra in the cow dung samples was higher than grass ^{228}Ra content of this region. This indicates the other possible sources for the intake of ^{228}Ra and the excretion through cow dung. Another reason for the higher ^{228}Ra content in cow dung could be due to the removal of this nuclide by the pectin and fibre content of the diet [6]. Significant positive correlations between cow dung ^{228}Ra and ^{40}K content in milk indicate that the excretion of ^{40}K is high through milk, and that of ^{228}Ra through cow dung which could be studied in detail in future One-way ANOVA indicates that there is no variation in the ^{228}Ra content in the cow dung samples between the sampling stations. This is indicative of a similar pattern of excretion of ^{228}Ra through cow dung in the study area.

Radium-226

^{226}Ra activities in the cow dung samples ranged from 0.25 ± 0.32 to 2.89 ± 1.72 Bq kg^{-1}, with a mean value of 1.57 ± 0.77 Bq kg^{-1}. The lowest ^{226}Ra activity was observed in Alagappapuram and the highest in Aralvoimozhi, like the radionuclide ^{228}Ra. The samples followed a normal distribution, with a 95% UCL of 2.02 Bq kg^{-1}. One-way ANOVA indicated that there is no variation between the sampling locations ($F = 0.57$; $df = 9, 24$, $P > 0.05$). ^{226}Ra in the cow dung samples has not been compared with globally reported values because of little studies on this nuclide. The activity of ^{226}Ra content in cow dung was correlated with its activity in grass samples. In the cow dung ^{226}Ra content was lower and the grass ^{226}Ra content was higher. This indicates that the ^{226}Ra taken by cow may be deposited in bone or excreted. The difference of ^{228}Ra and ^{226}Ra in cow dung could be due to chemical form of the radium nuclides, which behave differently in the intestine of the cow.

Conclusions

This study records the activity concentrations of ^{40}K, ^{228}Ra and ^{226}Ra and to the scientific literature of the present levels in Kudankulam region. This matrice has agricultural importance as it is used as manure. Further, the study of cowdung matrice reveals the pattern of animal nutrition and the cycling of essential and non-essential nuclides. The activity concentration of ^{228}Ra over ^{226}Ra indicates the higher availability of this nuclide in this region. Future studies can focus on the chemical form of the above mentioned radionuclides and to find the exact source of these radionuclides.

References

[1] Singh, B. R. and Steinnes, E., Soil and water contamination by heavy metals. In: Soil processes and water quality. Eds. Lal, R. and Stewart, B. A. CRC Press, Florida (1994) 233.

[2] Nicholson, F. A. and Chambers, B. J. DIAS report Plant production no. 123 (2006) 41,.

[3] Wijewardena, J. D. H. and Gunaratne, S. P. Ann. Sri Lanka Dept. Agric., 6 (2004) 245,.

[4] DueZas, C., Fernández, M. C., CaZete, S., Carretero, J. and Liger, E. Atmos. Environ., 33 (1999) 501,.

[5] Silva, P. S. C., Mazzilli, B. P. and Fávaro, D. I. T. Radioanal. Nuc. Chem., 269 (2006) 739,.

[6] Johnson, J. E., Tyler, T. R. and Ward, G. M. J. Anim. Sci., 29 (1969) 695,.

Estimation of Air to Grass - Dry and Wet Deposition Rates, Velocities, and Mass Interception Factors For Iodine for a Postulated Accidental Scenario

Karunakara N.[1], Ujwal P.[1], Yashodhara I.[1], Sudeep Kumara K.[1], Geetha P.V.[2], Dileep B.N.[3], Joshi P. James[3] and Ravi P.M.[4]

1. *University Science Instrumentation Centre, Mangalore University, Mangalore, India; E-mail: drkarunakara@gmail.com*
2. *Nuclear Power Corporation of India Limited, Anushaktinagar, Mumbai 400 094*
3. *Environmental Survey Laboratory, Kaiga Generating Station, Kaiga 581 400*
4. *Health Physics Division, Bhabha Atomic Research Centre, Trombay, Mumbai 400 085*

Introduction

Measurements of air to grass - dry and wet deposition rates, velocities, and mass interception factors for iodine are sparse in India. Data on these parameters are the basic input for the estimation of radiation dose to the public around a nuclear power plant. We have carried out systematic studies on air to grass - dry and wet deposition rates, velocities, and mass interception factors for iodine for a postulated emergency situation. The main objective of this study was to generate air to grass transfer factors for iodine for the environmental conditions prevailing in Kaiga.

Materials and Method

A walk-in type environmental chamber was designed and fabricated for the studies with facilities for exposing the plants grown in pots to controlled levels of radionuclides/stable elements (Fig. 1). The temperature, humidity, and airflow inside the environmental chamber can be controlled to required values. The chamber has the facility for generating artificial rainfall. It is also provided with ports for air sampling, and the entire system is fabricated from food grade stainless steel.

Grass grown in pots was kept inside the environmental chamber. Stable iodine (elemental form) was sublimed and injected into the environmental chamber suddenly to generate known concentration of iodine in the air inside the chamber. This simulated an accidental release of iodine to the environment. The environmental parameters such as humidity, temperature, and air circulation were controlled to required values. The concentration of iodine in the air inside the chamber was monitored continuously by drawing air from the environmental chamber through a bubbling setup (bubbling air through 1% sodium carbonate solution). The iodine from the bubbled solution was chemically separated (through toluene layer separation) and the concentration was measured by UV-VIS spectrometry [1]. The concentration of iodine inside the chamber was monitored for every 30 min and the mean value of concentration was considered. The grass was exposed to iodine inside the chamber for 3 h after which the leaves were sampled and analysed for iodine concentration. From the concentration values of iodine in the air and grass - the dry deposition rate, deposition velocity, and mass interception rates were estimated.

The fallout through rain is also an important route of entry for iodine into the grass from air. Hence, wet deposition rate of iodine was measured using the environmental chamber. Grass grown in pots was kept inside the chamber and iodine was injected into it as outlined above, and after obtaining a uniform concentration inside the chamber, rainfall was generated for a known time. The leaf samples were then collected and analysed for stable iodine concentration [1].

Calculation

The deposition velocity (m s^{-1}) is the coefficient of dry/wet deposition rate and elemental concentration in air (mg.m^{-3}) and it is calculated as under [1]:

$$V_d = d_i / C_a \quad (1)$$

Where V_d - is the dry/wet deposition velocity, d_i – dry/wet deposition rate (mg.m^{-2}.s^{-1}), C_a - Iodine concentration in air (mg m^{-3}).

The mass interception factor ( ) (m^2. kg^{-1}) is the fraction of total concentration of radionuclide deposited the on ground by the dry/wet deposition process, intercepted by the unit mass of vegetation/grass/pasture and it is an important factor in the estimation of air to grass transfer of radionuclides. It was calculated by using the following equation [1]:

$$= C_g / C_d \quad (2)$$

Where C_g – concentration in grass leaves (mg.kg^{-1}), C_d – total iodine concentration deposited per unit area of ground/tray (mg m^{-2}).

Results

The dry deposition velocity on the grass leaves varied in the range of $0.5x10^{-5}$–$3.3x10^{-5}$ m s^{-1} with a mean value of $1.7x10^{-5}$ m s^{-1}. Not many literature values are available on dry deposition velocity of iodine and the available values vary in the range of 10^{-7}-10^{-2} m s^{-1} [2, 3, and 4]. The dry deposition velocity reported from studies conducted in India [5] for bean leaves was 5.4 10^{-7} m s^{-1}. Experiments conducted under the present study yielded consistent results for different trails. The mass interception factor varied in the range



Fig. 1 A view of the environmental chamber (a) under normal conditions, and (b) after injecting stable iodine

of 0.25-13 $m^2 kg^{-1}$ with a mean value of 4.2 $m^2 kg^{-1}$ with respect to fresh weight. In all these experiments, the temperature of the air inside the environmental chamber was maintained at 20, 25 or 30 C.

The wet deposition velocity of iodine varied in the range of 0.6 10^{-4} -6.7 10^{-4} m s^{-1} with a mean value of 2.2 10^{-4} m s^{-1}. The wet deposition velocity of iodine was higher by an order of magnitude when compared to the dry deposition velocity. The mass interception factor for wet deposition varied in the range of 0.6-10.3 m^2 kg^{-1} with a mean value of 2.6 m^2 kg^{-1}. The experiments conducted using the environmental chamber provided valuable data on the air to grass transfer of iodine, which will be very important for the estimation of concentration of iodine in the grass in case of any emergency. Finally, it may be noted that this is perhaps the first systematic study conducted in India on dry and wet deposition rates, deposition velocities, and mass interception factors using a large scale environmental chamber.

Acknowledgement

Thanks are due to the NPCIL, BRNS, officials and scientific staff of the Kaiga Generating Station, Sri S. G. Ghadge, Director, Safety, NPCIL; Sri Malhotra, Associate Director, Safety, NPCIL and Sri M. Kansal, Chief Engineer, Safety NPCIL.

References

[1] Karunakara, N., Ujwal, U. P., Yashodhara, I., Somashekarappa, H. M., Balakrishna K. M., Geetha, P. V., Dileep, B. N., and Ravi, P. M, Final Report, NPCIL sponsored research project, Mangalore University, (2012).

[2] Chamberlain, A.C. and Chadwick, R.C., Tellus (Online library), 18(2-3) (1966) 226.

[3] Wershofen, H., Aumann, D.C, J. Radioanal. Nucl. Chem., Letters 137(5) (1989) 373.

[4] Handge, P., Hoffmann, F. O., IAEA-SM-180/29 (1974).

[5] Singhal., R. K., Narayanan, Water, air and soil pollution, 158 (1-4) (2004) 181.

Determination of level of radioactivity and Evaluation of Radiation Hazardous in Coastal Sediments of East Coast of Tamilnadu, India

S. Sivakumar[1], R. Ravisankar[2], B. Govardhanan[3] and Prince Prakash Jebakumar[4]

1. *Department of Physics, Mailam Engineering College, Mailam, Tamilnadu - 604304, India*
2. *Post Graduate and Research Department of Physics, Government Arts College, Tiruvannamalai,Tamilnadu 606603, India; E-mail: ravisankarphysics@gmail.com*
3. *Department of Physics, Arunai Engineering College, Tiruvannamalai-606603, Tamilnadu*
4. *National Institute of Ocean Technology, Chennai-601302, Tamilnadu, India*

The natural radioactivity concentrations of ^{238}U, ^{232}Th and ^{40}K were measured by gamma spectrometry in sediment samples collected from Thazhankuda (Cuddalore) to Kodiyakkarai of East Coast of Tamilnadu. The radiation hazard due to the total natural radioactivity in the study area was estimated by different approaches. From the analysis, it is found that the activity concentration of ^{232} Th is slightly greater where as the ^{238}U and ^{40}K were less than the recommended safe and criterion limits by UNSCEAR.

Introduction

Radionuclides have been constituents of the earth since its creation. The earth is still being heated through the decay of long lived natural radionuclides e.g. uranium, thorium and potassium which occur in nature as complexes of oxides, carbonates, phosphates, vanadates and silicates. Using natural and artificial radionuclides require an understanding of their environmental behavior. Such knowledge is needed for their effective applications as in situ tracers and for estimation of human health risks. Gamma radiation emitted from naturally occurring radioisotopes, terrestrial back ground radiation represents the main external source o irradiation of human body. Gamma ray spectrometry has been used in various studies such as soil and sediment radioactivity and environmental impact evaluation. The aim of this work is to measure the natural radionuclide activity in sediment samples at various locations in East coast of Tamilnadu.

Materials and Methods

Sample Collection

The Sediment samples were collected at a depth of about 10 cm by Grab sampler. The sediment samples were collected from 20 locations as given in Fig. 1. The samples were conned, quartered, sieved and dried in oven. The homogenized sample was packed in a standard 250 mL airtight PVC plastic container. The samples were kept aside for about four weeks to ensure equilibrium between ^{226}Ra and its daughters and ^{228}Ra and its daughters before being taken for gamma spectrometric analysis.

Gamma ray Spectrometric Analysis

All samples were subjected to gamma spectral analysis with a counting time of 10,000 secs. A 3" x 3" NaI (Tl) detector was employed with adequate lead shielding which reduced the background by a factor of about 95%. The concentrations of various

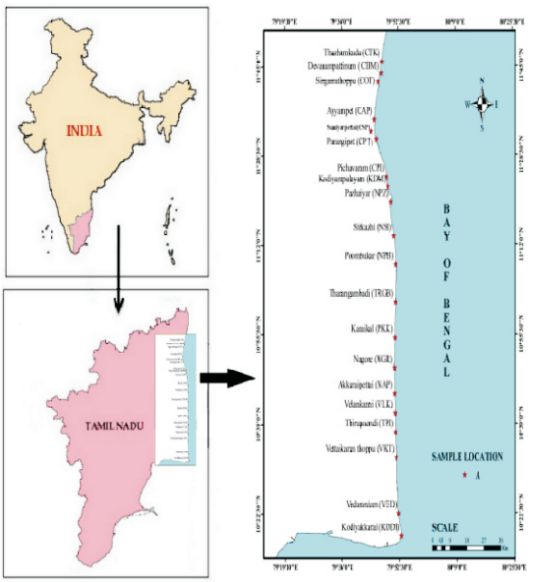


Fig. 1 Samples collected at Different Locations of East coast of Tamilnadu, India

radionuclides of interest were determined in Bq kg^{-1} using the count spectra.

The gamma-ray photo peaks corresponding to 1.46 MeV (^{40}K), 1.76 MeV (^{214}Bi) and 2.614 MeV (^{208}Tl) were considered in arriving at the activity of ^{40}K, ^{238}U and ^{232}Th in the samples. The detection limit of NaI(Tl) detector system for ^{40}K, ^{238}U and ^{232}Th are 8.5, 2.21 and 2.11 Bq kg^{-1}, respectively for a counting time of 10, 000 secs.

Results and Discussions

Activity Concentrations

The results for the activity concentrations of natural radionuclides ^{238}U, ^{232}Th and ^{40}K in coastal sediment samples of different locations of East coast Region is reported in Table 1. The activity concentrations of ^{238}U, ^{232}Th and ^{40}K ranges from 2.21

Table-1: Activity Concentration (Bq kg^{-1}), Absorbed Dose rate (D_R), Annual Effective Dose Rate (H_R)

S. No.	Location	Activity concentration (Bq/Kg)			Absorbed Dose Rate (DR) (nGy/h)	Annual Effective Dose Rate(HR) (mSv/y)
		^{238}U	^{232}Th	^{40}K		
1.	Thazhankuda	BDL	49.24	387.24	49.06	0.060
2.	Devanampattinum	BDL	16.22	374.89	26.55	0.033
3.	Singarrathoppu	BDL	24.48	366.79	31.71	0.039
4.	Ayyampet	BDL	8.24	327.38	19.24	0.024
5.	Samiyarpet	BDL	8.56	358.15	20.74	0.026
6.	Parangipet	BDL	9.92	339.4	20.86	0.026
7.	Pichavaram	BDL	88.78	313.29	72.29	0.089
8.	Kodiyampalayam	BDL	10.03	396.89	23.35	0.029
9.	Pazhiyar	BDL	BDL	372.06	15.63	0.019
10.	Thirumullaivasal	BDL	16.08	439.51	29.17	0.036
11.	Poombukar	BDL	11.55	399.77	24.48	0.030
12.	Tharangambadi	BDL	106.84	355.67	86.09	0.106
13.	Karaikal	20.95	233.94	383.91	180.94	0.223
14.	Nagore	BDL	18.57	413.98	29.75	0.037
15.	Nagapatiinum	12.44	34.83	401.43	45.41	0.056
16.	Velankanni	BDL	13.9	351.31	24.01	0.030
17.	Thirupoondi	BDL	47.22	353.61	46.30	0.057
18.	Vettaikaranthoppu	BDL	10.33	459.26	26.17	0.032
19.	Vedaranium	BDL	18.61	466.47	31.99	0.039
20.	Kodiyakkarai	BDL	15.09	482.45	30.31	0.037
Average					41.70	0.051

to 20.95 Bq kg^{-1}, 2.11 to 233.94 Bq kg^{-1} and 313.29 to 482.95 Bq kg^{-1}, respectively. The mean Activity of ^{232}Th is slightly higher compared to ^{238}U and ^{40}K series of world average values [1]. Figure 1 shows the variation of activity concentration.

Absorbed Gamma Dose Rate (D_R)

The absorbed gamma dose rates (D_R) were calculated in air from the activity concentrations of ^{238}U, ^{232}Th and ^{40}K in the samples. The conversion factors of gamma-dose rate at 1 m above the surface for ^{238}U, ^{232}Th and ^{40}K are 0.462, 0.604 and 0.042 nGy h^{-1}/Bg kg^{-1}, respectively. Therefore, the absorbed dose rate (in nGy h^{-1}) in air can be estimated using the following equation,

$$D_R\,(nGyh^{-1}) = 0.462A_U + 0.604\,A_{Th} + 0.042A_K \quad (1)$$

where A_U, A_{Th} and A_K are the activity concentrations of ^{238}U, ^{232}Th and ^{40}K in Bq kg^{-1}, respectively. The absorbed dose rate values ranged between 15.63 and 180.94, with a mean value of 41.70 nGy h^{-1} were given in Table 1 which was lower than the world average value 84 nGy h^{-1} [2]. Figure 2 shows the variation of absorbed gamma dose rate at different locations of the sampling site.

Annual Effective Dose Rate (H_R)

The annual effective dose rate resulting from the absorbed dose values (D_R) was calculated in mSv/y using the following formula [3]

$$H_R = D_R\,(nGyh^{-1}) \times 8760\ h \times 0.2 \times 0.7SvGy^{-1} \times 10^{-6} \quad (2)$$

It ranged between 0.019 and 0.223 with an average value of 0.051 mSv y^{-1} is lower than the world average value 0.46 mSv y^{-1}. Figure 3 shows the variation of indoor effective dose.

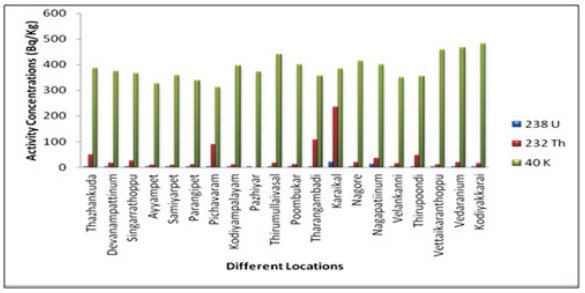


Fig. 1 Shows the variation of activity concentration.



Fig. 2 Variation of Absorbed Gamma Dose Rate



Fig. 3 Variation of Annual Effective Dose Rate

Conclusion

The Activity concentration of natural terrestrial radionuclides of ^{238}U, ^{232}Th, and ^{40}K were measured by gamma-ray spectrometry system for sediment samples collected from the East Coast of Tamilnadu. Gamma spectrometric analysis of sediment samples indicates that the activities due to radionuclides in the thorium are slightly higher when compared to potassium and uranium series. The Absorbed Dose rate and Annual Effective Dose rate values are less compared to the recommended values.

References

[1] UNSCEAR,United Nations Scientific Committee on the effects of Atomic Radiation, United Nations, New York (2000).

[2] R.Ravisankar, K.Vanasudari, A.Chandrasekaran, A.Rajalakshmi, M.Suganya, App.Radi.Iso.70 (2012) 699.

[3] R.Ravisankar, A.chandrasekaran, P.vijayagopal, B.venkatraman, G.Senthilkumar, P.Eswaran, A.Rajalakshmi, Rad. Physics and Chemistry. 81 (2012) 1789.

Spatial Distribution of Gamma Radiation Levels in Yelagiri Hills, Tamilnadu, India by Gamma Ray Spectrometry

A. Chandrasekaran[1*], R. Ravisankar[2], B. Govardhanan[3], P. Vijayagopal[4], S.N. Bramha[4] and B. Venkatraman[4]

1. *Global Institute of Engineering &Technology, Vellore 632509, Tamilnadu, India.*
2. *Post Graduate and Research Department of Physics, Government Arts College, Thiruvanamalai-606603, Tamilnadu, India; E-mail: ravisankarphysics@gmail.com*
3. *Department of Physics, Arunai Engineering College, Tiruvannamalai 606603, Tamilnadu*
4. *Radiation Safety Section, Radiological Safety Division. Indira Gandhi Centre for Atomic Research, Kalpakkam 603102, Tamilnadu, India.*

The Concentration of natural radionuclides in surface soil samples around Yelagiri Hills were determined by gamma ray spectrometry using NaI(Tl) detector. The spatial distribution of uranium and thorium was investigated in soils from the cultivated and undisturbed areas in Yelagiri Hills, Tamil nadu, India. The average absorbed dose rate in the study area was estimated to be 88.62 nGyh^{-1}. To establish the level of radioactivity at different areas isodose map is drawn between the different sampling locations of Yelagiri hills and the absorbed gamma dose rate.

Introduction

Radioactivity of soil environment is one of the main sources of exposure to humans. Hence it is important to know its distribution; gamma radiation comes mainly from radionuclides viz. ^{40}K, ^{232}Th and ^{238}U series. Therefore it is important to measure the concentration of these radionuclides in soil. The level of the natural radioactivity in the soil and in the surrounding environment a well as the associated external exposure due to gamma radiation depends primarily on the geological and geographical conditions of the region [1]. The prime objective of this work is to establish the radioactivity isodose map which is drawn between the different locations of Yelagiri hills and the absorbed gamma dose rate.

Materials and Methods

Sample Collection

The soil profiles were sampled using an automatic core driller. Cores extruded and sectioned at 0.1m diameter and 0.25 m depth were used to take soil samples [2]. The soil sampling locations illustrated in Fig. 1. The soil samples were collected from 25 different sites. The conned, quartered and sieved soil samples were dried in oven. The homogenized samples were then packed in a standard 0.25 L airtight PVC plastic container. Each sample weight about 0.4 kg. The samples were kept aside for about a month to ensure equilibrium between ^{226}Ra and its daughters and ^{228}Ra and its daughters before being taken for gamma spectrometric analysis

Gamma ray Spectrometric Analysis

A 3" x 3" NaI (Tl) detector was employed with adequate lead shielding which reduced the background by a factor of about 95%. Standard sources obtained from IAEA in the same geometry and having the same density, as that of the prepared soil samples, were used to determine the efficiency of the detector for various

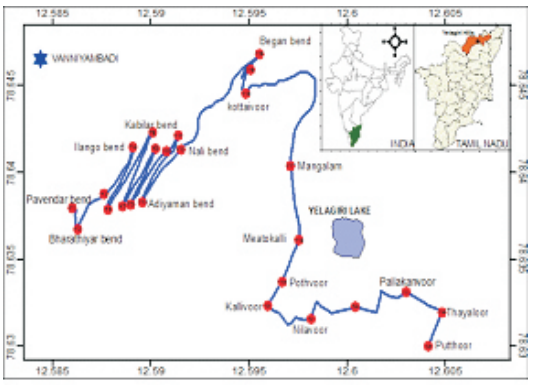


Fig. 1 Samples collected at different sampling points of Yelagiri Hills,Tamilnadu

energies. The activity contents of the standards are known within ±3% accuracy The concentrations of various radionuclides of interest were determined in Bq kg^{-1} using the count spectra.

The gamma-ray photo peaks corresponding to 1.46 MeV (^{40}K), 1.76 MeV (^{214}Bi) and 2.614 MeV (^{208}Tl) were considered in arriving at the activity of ^{40}K, ^{238}U and ^{232}Th in the samples. The detection limit of NaI(Tl) detector system for ^{40}K, ^{238}U and ^{232}Th are 8.5, 2.21 and 2.11 Bq kg^{-1} respectively for a counting time of 20, 000 s.

Results and Discussions

The results for the activity concentrations of natural radionuclides viz. ^{238}U, ^{232}Th and ^{40}K in the soil samples of different locations of Yelagri Hills, Tamilnadu are reported in Table 1. The activity concentrations of ^{238}U, ^{232}Th and ^{40}K ranges from 2.17 to 53.23 Bq kg^{-1}, 13.54 to 114.75 Bq kg^{-1} and 261.11 to 2207.3 Bq kg^{-1}, respectively. The activity concentrations of the natural radionuclides do not provide an exact indication of radiation hazard associated with the materials. So there is a need to

assess the radiological hazards by calculating the radiological parameters such as absorbed gamma dose rate (D_R) and to establish the gamma radiation istodose map.

Table-1:Activity Concentration (Bq kg^{-1}) and Absorbed gamma dose rate (D_R) at various locations of Yelagiri Hills

Sample Id	Locations	Activity Concentration (Bq kg^{-1})			D_R (nGyh^{-1})
		^{238}U	^{232}Th	^{40}K	
YS1	Pavendar bend	BDL	24.47	2207.3	109
YS2	Bharathiyar bend	BDL	21.1	656.51	41.63
YS3	Thiruvalluvar bend	BDL	13.54	851.13	44.77
YS4	Ilango bend	18.93	83.77	1137	111.68
YS5	Kambar bend	25.55	36.24	913.95	73.51
YS6	Kabilar bend	6.24	28.45	1391.6	80.08
YS7	Oviyar bend	23.35	38.95	872.86	72.64
YS8	Paari bend	18.45	89.48	1025.2	110.59
YS9	Kaari bend	33.39	114.75	936.11	130.1
YS10	Oori bend	BDL	22.81	1143.8	63.23
YS11	Aayai bend	21.2	100.42	1128.8	123.41
YS12	Adiyaman bend	15.76	71.31	1250.2	106.78
YS13	Nali bend	BDL	28.05	1455.5	79.81
YS14	Began bend	BDL	26.06	2165.5	108.31
YS15	Arthanavoor	BDL	41.45	1137.8	75.39
YS16	kottaivoor	10.1	43.34	2105.4	121.63
YS17	Mangalam	13.13	29.52	1219.1	76.51
YS18	Meatokalli	23.76	13.78	1263	72.44
YS19	pothvoor	23.79	61.69	700.93	80.75
YS20	Kallivoor	34.93	46.79	2052.8	132.4
YS21	Nilavoor	39.89	57.6	630.41	81.99
YS22	Meatokanivoor	39.55	50.24	625.09	76.72
YS23	Pallakanvoor	49.72	35.95	261.11	56.29
YS24	Thayaloor	20.45	44.47	983.08	79.7
YS25	Putthoor	53.23	89.89	557.88	106.19
Average		19.16	48.56	1146.8	88.62

BDL=2.21Bq/kg

Absorbed Dose Rate (D_R)

To provide a characteristic of the external terrestrial gamma radiation, we have calculated the absorbed dose rates in air at 1m above the ground using the formula [3]

$$D_R(nGyh^{-1}) = 0.43A_U + 0.666A_{Th} + 0.042A_K$$

where A_U, A_{Th} and A_K are the activity concentrations of ^{238}U, ^{232}Th and ^{40}K in Bq/kg, respectively The absorbed gamma dose rate estimate of soil for Indian sub-continent is about 69 nGy h^{-1} and the world average value is 84 nGy h^{-1}. In the present study, the outdoor gamma dose rate for soil ranged from 41.63 to 132.40 nGy h^{-1} with an average of 88.62 nGy h^{-1} which agrees well with global value.

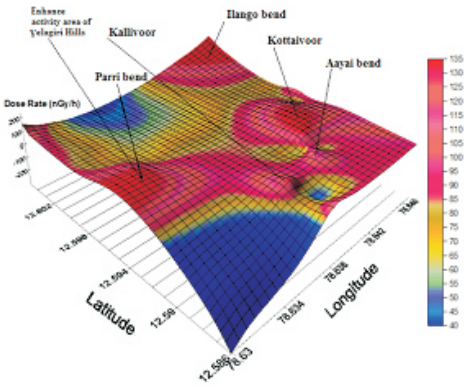


Fig. 2 The 3D plots of Isodose map Yelagiri Hills showing the sampling locations

Gamma Isodose Rate Map

The terrestrial gamma dose rates at each sampling locations are plotted using SURFER (software version 8). Fig. 2 shows the 3D plot of the gamma dose map of different locations of study area with absorbed dose rate. The Enhanced activity areas are indicated with higher peaks with red color regions in the plotted map.

Conclusion

The spatial distribution of natural terrestrial radionuclides of ^{238}U, ^{232}Th, and ^{40}K were measured by gamma-ray spectrometry system for surface soil samples collected from Yelagiri hills of Tamilnadu. The results of the present study were subsequently compared with global average value. The future work plans are to calculate more radiological parameters with statistical approach.

References

[1] UNSCEAR,United Nations Scientific Committee on the effects of Atomic Radiation, United Nations, New York (2000).

[2] R. Ravisankar, A. Rajalakshmi, P. Eswaran, V. Gajendrian, V. Meenakshisundram, Nucl. Sci. Tech. 18 (2007) 372.

[3] R.Ravisankar, A.Chandrasekaran, Vijayagopal, B.Venkatraman, G.Senthilkumar, P.Eswaran and A.Rajalakshmi. Rad.Phy and Chem.81 (2012) 1789.

Determination of Uranium in Groundwater using Liquid Scintillation and Cerenkov Counting Techniques

Sonali P.D.Bhade[1], Ajaykumar[2], P.J. Reddy[1], Rupali Karpe-Kamat[2], R.V. Kolekar[1], Rajvirsingh[1], K.S. Pradeepkumar[1]

1. *Radiation Safety Systems Division, Bhabha Atomic Research Centre, Trombay, Mumbai 400085, India; E-mail: sonali@barc.gov.in*
2. *Health Physics Division, Bhabha Atomic Research Centre, Trombay, Mumbai 400085, India*

Liquid scintillation Extraction and Cerenkov counting techniques were used for determination of Natural Uranium in ground water samples. Various parameters such as effect of sample pH, quench, recovery and sensitivity were studied. These techniques were tested for tracer solutions as well as real samples and the results were compared. Ultra low level liquid scintillation counting coupled with extractive scintillator and Cerenkov counting techniques were proved to be simple, fast yet reliable techniques for the determination of natural U content in ground water samples.

Introduction

Determination of uranium is important in environmental safety monitoring and geochemical studies. Several methods like photometry, laser fluorimetry, gamma and alpha spectrometry for the determination of uranium have been used [1]. Alpha spectroscopy is considered to be a very precise, versatile and sensitive method for -emitters such as uranium, but preparation of the counting samples is laborious, time consuming, and correction factors are needed for self-absorption and geometry [2]. Liquid scintillation methods have been widely used for -emitters and uranium has been determined in several types of samples, e.g. geological samples, water sample and environmental samples associated with uranium mining and milling [3,4]. In most of these methods, uranium is introduced into the counting vial by extracting it with solvents such as TBP (tributyl phosphate), TOPO (trioctylphosphine oxide) and HDEHP (diethylhexyl phosphoric acid], which are miscible with scintillation solution [5]. The advantages of liquid scintillation methods [especially with pulse-shape analysis (PSA)] are low background (and, therefore, a lower limit of detection) and nearly 100% efficiency. In the present study, Liquid Scintillation Counting (LSC) and Cerenkov techniques were employed for the determination of natural uranium in ground water samples and the results obtained were compared.

Experimental

Measurements were carried out in Ultra Low Quantulus 1220 LSC (Wallac, Finland) which has two programmable Multi Channel Analyzers (MCAs). It has built in Pulse Shape Analysis (PSA) circuitry which enables discrimination of and events. Pulse shape discrimination is accomplished by optimizing PSA parameter that can be varied from 1 to 256. In the present study, Optiphase Hisafe-3, a Di-isopropyl Naphthalene (DIN) based commercial cocktail was used. To this scintillation cocktail, 60 g/L of bis (2-ethylhexyl) Phosphoric acid (HDEHP) was added, to prepare an extractive cocktail. Counting was done with Low-diffusion High Density Polyethylene (HDPE) vials (Packard Bioscience). Acidity measurements (pH) were done with Eutech PC 2700 pH meter. Acid blanks were prepared to provide meaningful background subtraction.

Quenching in LSC is a process that interferes with the production or transmission of light photons [6]. Quenching was quantified using Spectral Quench Parameter of External standard (SQP(E)). Counting efficiencies were later determined from these SQP(E) values by constructing calibration curves. A plot of optimized PSA settings against SQP(E) was plotted using various quenched natural Uranium standard sources as shown in Fig. 1. For each quench level, corresponding alpha and beta counting efficiencies were derived. In order to minimize the effect of

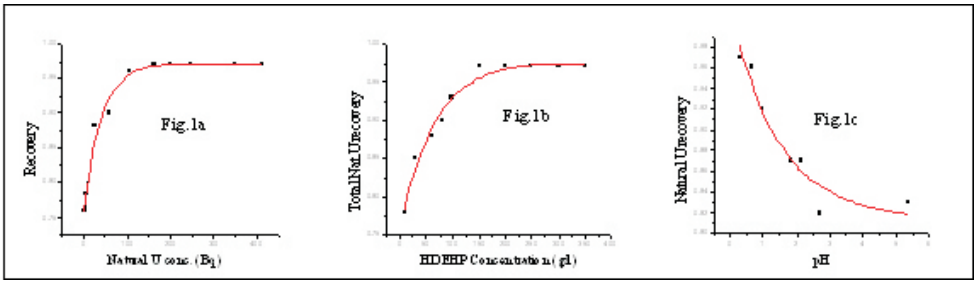


Fig. 1 Effect of activity concentration (Fig.1a), amount of HDEHP (Fig.1b) and pH (Fig.1c) on natural uranium recovery in LSC-solvent extraction technique

background, we define a narrow counting window for as 460-590 channels in alpha MCA which is region of Interest (ROI) with less background and interference. The -window was set from 250-1024 channels in beta MCA. Cerenkov radiations were observed in 0-300channels.

Water samples were acidified with nitric acid to a pH 1-2. These acidified samples were purged with pure argon gas to remove ^{222}Rn. Liquid-liquid solvent extraction procedure with extractive scintillation cocktail was carried out for each sample. 5 mL of Organic phase was gravimetrically decanted into scintillation vial and counted for 500 minutes on the optimized PSA setting.

Extraction recovery for each sample was evaluated by counting acidified water samples after spiking them with natural uranium standard source. For Cerenkov measurements, the groundwater samples (10 mL) were directly measured in low diffusion HDPE vials for a counting time of 500minutes. Recovery of Natural Uranium in organic fraction is a function of various parameters such as sample pH, uranium activity concentration and amount of HDEHP (g/L) in extractive scintillation cocktail. These parameters were studied in detail to check their significance in determination of U recovery. For Cerenkov measurements, ground water samples (10 mL) were directly measured in low diffusion HDPE vials for a counting time of 500minutes.

Result and Discussion

In the present work, Natural U activity was determined by measuring the Cerenkov radiation emitted by ^{234m}Pa (energy-2.23MeV) activity which is in secular equilibrium with its parent radionuclides (^{238}U and ^{234}Th). The directional emission of Cerenkov photons limits the counting efficiencies to ~15% for natural uranium.

Recovery of Natural Uranium in the organic extract was determined for different activity concentrations of uranium standard sources (2Bq to 400 Bq). Rise in Natural Uranium recovery was observed from 70%-96% with increase in activity concentration from 2-100 Bq, above which recovery was found to be independent of the U activities and was found to be >95% as illustrated in Fig. 1a. Exponential rise in recovery was observed for HDEHP concentrations up to 100 g/L after which recovery was found to be independent of the amount of HDEHP in extractive cocktail as shown in Fig. 2b. Effect of amount of HDEHP added to scintillation cocktail, on the recovery of uranium was checked by preparing different extractive scintillation cocktails containing varying amount of HDEHP (10-400 g/L). Exponential rise in recovery was observed for HDEHP concentrations up to 100 g/L after which recovery was found to be independent of the amount of HDEHP in extractive cocktail. Dependence of recovery on pH of the water sample is shown in figure 1c. On the pH scale (pH1-2), more than 85% of U recovery was observed while fall in recovery was observed for pH range 2-5. MDA values obtained for extraction technique and Cerenkov counting were 19 ppb and 40 ppb respectively.

Table 1: Natural uranium content in ground water samples determined Cerenkov and extractive scintillation counting techniques.

Sample Id	Nat.U content(ppb) ± Cerenkov	Nat.U content(ppb) ± LSC
GW1	112.3 ± 4.2	96.0 ± 9.7
GW2	114.0 ± 4.3	111.0 ± 10.7
GW4	131.0 ± 4.9	123.0 ± 10.0
GW5	153.2 ± 4.5	116.4 ± 10.2
GW6	103.4 ± 5.0	85.8 ± 10.5
GW8	87.3 ± 4.2	138.1 ± 10.2
GW9	137.4 ± 3.4	187.8 ± 9.5
GW10	124.0 ± 5.9	109.1 ± 11.0
GW11	65.5 ± 3.4	60.0 ± 8.2
GW12	70.8 ± 3.4	65.0 ± 9.1
GW13	94.8 ± 5.2	190.7 ±16.0
GW14	113.3 ± 6.2	98.2 ± 14.4
GW15	189.6 ± 6.6	168.3 ± 12.5
GW16	91.3 ± 4.0	106.7 ± 9.7
GW18	147.7± 6.0	142 ± 11.3
GW19	79.4 ± 3.3	80.0 ± 9.8
GW21	106.5 ± 5.2	83.0 ± 10.2

Conclusion

Ultra low level LSC coupled with extractive scintillator and PSA was proved to be suitable technique for the determination of natural uranium content in ground water samples. Low background (0.04 cpm) in alpha window, ~100% counting efficiency, lack of self absorption characterizes the extraction procedure. Cerenkov counting has proved to be simple but precise technique that characterized with, easy sample preparation and least generation of organic liquid waste as counting was done without adding scintillation cocktail. The results obtained by both of these techniques were found to be comparable.

References

[1] Z. Tosheva, K. Stoyanova, L. Nikolchev, J. Environ.Radioact., 72 (2004) 47.

[2] M Galán-López, A Martín-Sánchez, Z Tosheva, A Kies, Advances in Liquid Scintillation Spectrometry LSC, Edited by Staniaw Chaupnik, Franz Schönhofer, John Noakes, (2005) 165.

[3] K.Bower, A. Angel, R.Gibson, T.Robinson, D.Knobeloch, B.Smith, J. of Radioanal. and Nucl.Chem. 181 (1) (1994) 97-107

[4] Laina Salonen, The Science of Total Environment 130/131 (1993) 23.

[5] V.Gomez Escobar, F. Vera Tome, J.C.Lozano and A.Martin Sanchez; Applied radiation and isotope 49 (7) (1998) 875.

[6] Pujol L, Snchez-cabeza JA; Analyst 122(1997) 383.

Simultaneous determination of gross alpha and gross activities in water samples using Ultra Low Level Liquid Scintillation Spectrometer

P.J. Reddy, Vandana Pulhani[1], S.P.D. Bhade, R.V. Kolekar , Rajvir Singh, S.K. Jha[1] and K.S. Pradeepkumar

Radiation Safety Systems Division, [1]Health Physics Division, Bhabha Atomic Research Centre, Trombay, Mumbai 400 085; E-mail: pjreddy@barc.gov.in.

Gross alpha and beta activities were determined in water samples using Ultra Low Level LKB Wallac Quantulus 1200 Liquid Scintillation Spectrometer. The instrument was calibrated using ^{241}Am as alpha standard and $^{90}Sr/^{90}Y$ as beta standard. The method was validated using IAEA reference standards. The gross alpha and beta activities determined in water samples lies in the range of 0.2± 0.18 to 0.53± 0.068 Bq L^{-1} with average 0.481± 0.17 Bq L^{-1} and 1± 0.18 to 6.3± 0.75 Bq L^{-1} with average 2.9 ± 0.43 Bq L^{-1} respectively. The results obtained using LSS were compared with the radiochemical separation technique. Minimum Detectable Activity as obtained using LSS were calculated considering efficiencies, counting time and the amount of sample were 0.022 Bq L^{-1} for gross alpha and 0.076 Bq L^{-1} for gross beta.

Introduction

Measurement of gross alpha and beta activity in the environment is an important factor in understanding the natural radiation exposure in humans [1]. Gross activity measurements are carried out in pre-operational survey of proposed nuclear sites and also around plant sites during normal operations. Environmental matrices like soil and water are monitored for gross activity and they help to estimate the radiological impact in the area of interest. Most alpha and beta measurements are performed by direct transferring an aliquot of sample and counted using gas flow proportional counter or by radiochemical procedure followed by detection with ZnS(Ag) and Low background Gas flow or GM counter. This method has its own drawbacks such as self absorption as the water sample is reduced to solid material through evaporation [2] or pre-concentration. The radiochemical procedures lead to losses in recovery of the activity or even self absorption at times which have to be accounted for. The low background liquid scintillation equipped with / discriminator provides an alternative for gross alpha and gross beta activity determination and offers several advantages over the conventional procedure. The counting geometry is essentially 4 , providing high counting efficiencies nearly 100% and eliminating matrix effects [3,4]. This study is aimed at applying the gross alpha and gross beta measurement to water samples using Liquid Scintillation Spectrometer (LSS).

Experimental

Measurements were carried out using Ultra Low Level LKB Wallac Quantulus 1220 LSS which has built-in Pulse Shape Discriminator and external standard ^{152}Eu which allows the measurement of External Quench Parameter (SQP(E)). 25 mL high density polyethylene vials and Optiphase Hi-Safe III scintillation cocktail were used. The radioactive

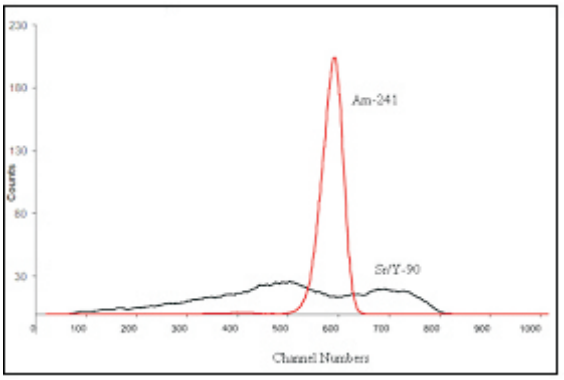


Fig. 1 Alpha and Beta spectra of the standards from LSS

solutions were prepared by weight from ^{241}Am standard solution 542 ± 3 Bqg^{-1} and $^{90}Sr/^{90}Y$ standard solution 270.95 ± 2.1 Bqg^{-1}. Water and effluents samples were collected from different locations in Trombay. They were acidified with HNO_3 (1.25 mL L^{-1}) for preservation. 100 mL of the acidified samples were concentrated by evaporation to 10 mL in order to remove radon and its short lived daughters. Measurements were done by mixing 8 mL of the treated sample and 12 mL scintillation cocktail. Blank was prepared by applying the same procedure as for the samples to 100 mL double deionized water. Counting was done for 500 min. LSS was calibrated to set the Pulse Shape Analysis (PSA) using ^{241}Am and $^{90}Sr/^{90}Y$ reference standards prepared in (8 mL standard + 12 scintillation cocktail) composition as real samples (Fig. 1). The optimum PSA was found as the value in which total misclassification + is lower (Fig. 2). The method was validated using International Atomic Energy (IAEA) water samples distributed for an inter comparison study in 2008 and 2010 by IAEA. Table 1 shows the comparison of results by performing the analysis on IAEA inter-comparison samples and the

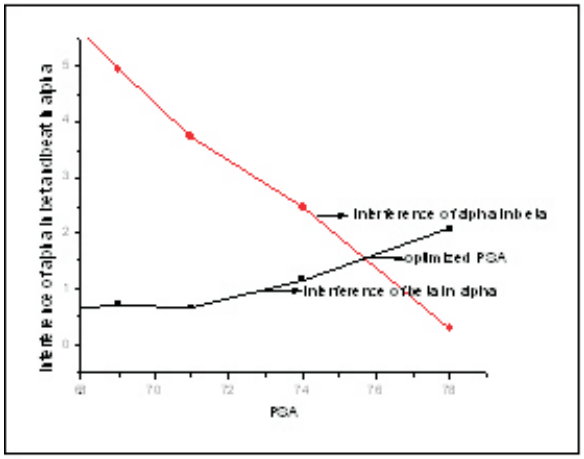


Fig. 2 Alpha and Beta misclassification versus PSA value.

reference values reported by IAEA. Samples were also estimated by conventional method as per EPA protocol [5]. The results of the two methods were compared.

Results and Discussion

The measured activity concentrations of gross alpha and beta samples are shown in Table 2. The observed gross alpha activity found in the water samples varies from 0.464 ± 0.266 $Bq.L^{-1}$ to 0.726 ± 0.074 $Bq.L^{-1}$. The observed gross beta activities found in the water samples vary from 0.966 ± 0.176 $Bq.L^{-1}$ to 6.31 ± 0.745 $Bq.L^{-1}$. The gross beta activity primarily comprises Uranium decay products and $^{90}Sr/^{90}Y$, ^{40}K. The Minimum Detectable Activity (MDA) was calculated considering efficiencies, counting time and the amount of sample. MDA values were 0.022 $Bq.L^{-1}$ for gross alpha and 0.076 Bq L^{-1} for gross beta. The RCA method using the same volume of sample as LSC can achieve an MDA of 0.3 $Bq.L^{-1}$ for gross alpha and <0.87 $Bq.L^{-1}$ for gross beta. The RCA detection limit can be lowered by taking larger amount of sample and longer counting time.

Table 1: Comparison of the results for gross alpha and gross beta activities in IAEA inter-comparison samples.

Sample ID	A	B	C	D
Sample No.4, IAEA-CU-2010 -03	4.8±0.1	5.19± 0.28	9.1±0.22	10.4±0.15
Sample No.4, IAEA-2008-03	3.9±0.08	3.02±0.15	15.7±0.3	18.35±0.34
Sample No.5, IAEA-CU-2010 -03	8.5±0.2	10.33±0.21	11.1±0.3	13.23±0.3

A= Reference value for gross alpha ± (Bq L^{-1}), B = Gross alpha ± (Bq L^{-1}) by LSS, C=Reference value for gross beta ± (Bq L^{-1}), D= Gross beta ± (Bq L^{-1}) by LSS

Table 2: Comparison of Gross alpha and gross beta activities in water samples using LSS and RCA technique.

Sl. No.	Gross ± activity (Bq/L)		Gross ± activity (Bq/L)	
	LSS	RCA	LSS	RCA
1	0.528±0.068	<0.3	1.318±0.181	1.25±0.5
2	0.726±0.074	<0.3	0.966±0.176	<0.87
3	0.197±0.181	<0.3	2.011±0.591	2.23±0.8
4	0.506±0.216	<0.3	6.311±0.745	5.9±0.4
5	0.466±0.211	<0.3	5.437±0.714	5.1±0.4
6	0.464±0.266	<0.3	1.3501±0.180	1.02±0.3

The RCA method gave comparable results with the liquid scintillation method. The majority of the gross alpha results by conventional EPA method were below the detection limit. Reliable beta estimation with good certainty was obtained with gas flow low background detector. Direct evaporation of 10 ml sample on planchet was also done but the activity obtained was below detection limit. Since, in this method for gross alpha and gross beta measurement, the radioactivity of the sample is not separated from the solids of the sample, the solids concentration is very much a limiting factor in the sensitivity of the method. A solid density thickness of 5 mg/cm^2 in the counting planchet is allowed for alpha and (20 mg/ cm^2) for beta for a 2-inch diameter counting planchet. Liquid Scintillation method provides a fast and accurate alternative for determination of gross activity.

References

[1] Alberto Malanca et al. J. Appl. Rad. Isot. 49(7) (1998) 893.

[2] A. Martin Sanchez et al. Applied Radiation and Isotpes, 67 (2009) 817.

[3] Sanchez-Cabeza J.A et al. Radiocarbon, (1993) 43.

[4] Sanchez-Cabeza J.A et al. Health Phys., 68 (1995) 674.

[5] USEPA. Multi-Agency Radiological Laboratory Analytical Protocols Manual, Volume II: Chapters 10-17 and Appendix F, EPA/402/B-04/001B (NUREG-1576).

Estimation of Committed Effective Dose due to Tritium in Ground Water in some places of Maharashtra

P.J. Reddy, S.P.D. Bhade, R.V.Kolekar, Rajvir Singh and K.S.Pradeepkumar

Radiation Safety Systems Division, Bhabha Atomic Research Centre, Trombay, Mumbai 400 085, India; E-mail: pjreddy@barc.gov.in

In the present study Tritium concentration in well and bore well water samples were analyzed for the samples collected from the villages of Pune, Kolhapur and Ratnagiri. The activity concentration ranged from 0.55 - 3.66 Bq L^{-1}. The associated age-dependant dose from water ingestion in the study area was estimated. The effective committed dose recorded for different age classes is negligible compared to World Health Organization and U.S. Environmental Protection Agency dose guidelines. The Minimum Detectable Activity achieved was 1.5 Bq L^{-1} for a total counting time of 500minutes.

Introduction

Tritium is the only radioisotope of hydrogen (atomic no.:1; atomic weight: 3). The natural production of tritium mainly arises from reactions induced by cosmic rays in the upper atmosphere. The radiological impact of tritium results from radiological and biological behavior of the radionuclide. Some parameters enhance the radio toxicity of tritium: for example, it's radioactive half-life (12.33 y), the fact that it's uptake by humans is easy and as an isotope of hydrogen it has a high biological importance [1]. The maximum energy of electrons emitted from tritium decay is 18.6 keV [2], which gives a maximum track length of 6 m in water or tissue. This prevents it from being an external exposure hazard. As a result, it is associated to radiological risk only if absorbed by the human body. Elemental tritium becomes oxidized to water (HTO) and then exist mainly in this form. In the present study, committed effective dose was estimated taking into consideration the obtained tritium concentration and annual water consumption. The present paper also summarizes the criteria for selecting a blank, optimizing the liquid scintillation counting window to reach better sensitivity of recently installed liquid scintillation counter at BARC.

Experimental

A calibrated source of ^{3}H provided by Packard with activity concentration 3331.7 (1.6%) Bq (reference date June 1st, 2008) was diluted to obtain a daughter water of ^{3}H activity 26.9 Bq g^{-1} to serve for preparation of series of quench standards. Optiphase HiSafe-III scintillation cocktail and 20 mL high density polyethylene vials were used for the study. An Ultra Low Level Liquid Scintillation Counter Quantulus 1220 (Wallac, Finland) was used for the measurement. Quenching was observed with the standard quench indicating parameter, the Spectral Index Of External Standard (SQP(E)). The sample to scintillation cocktail volume ratio used was 8 to12[3]. Well and bore water samples in different villages of Pune, Kolhapur and Ratnagiri were collected for the analysis of ^{3}H. The packaged drinking waters selected were some of the most commonly produced and consumed water.

Dose Estimation

The Committed Effective Dose (CED) value for general public was evaluated by considering the radioactivity material that would be ingested by drinking the water from the said well/bore well water as given below:

$$CED\ (Sv\ y^{-1}) = A.B.C$$

where A is the radionuclide concentration (Bq L^{-1}), B is the rate of annual drinking water consumption (L y^{-1}) and C is Dose Conversion Factor (DCF) for the radionuclide ingested (Sv Bq^{-1}).

Blank Samples

The very important step to study is the selection of the best sample that could be used as a blank to define the detector background. Commercially available packaged drinking waters (Aquafina, Baielly, Aqplus, Vedica, Kinley and Bislery packaged drinking waters) samples were considered for the analysis and the one that had the lowest ^{3}H content was selected as a blank. The distillation process reported by Paloma et al.,[4] was followed.

Results and Discussion

Counting Window Optimization and Calibration

The usual criteria used to select the optimum counting conditions in liquid scintillation counting is the signal-to-background ratio expressed as the square of the detection efficiency divided by the background (E^2/B) and is termed as the Figure Of Merit (FOM). Counting region optimization is used to maximize the E^2/B and thereby improve the detection limit. An unquenched ^{3}H standard of 26.9 Bq g^{-1} along with the blank samples was counted for 50 min and 10cycles (total counting time 500 min). Detector background, counting efficiency and FOM was calculated for different combinations of lower level and upper level window. The best FOM (883.8) in our apparatus was obtained for optimal channels 20-162 counting window, with counting efficiency 21.05% and background count rate of 0.501 0.036 cpm using

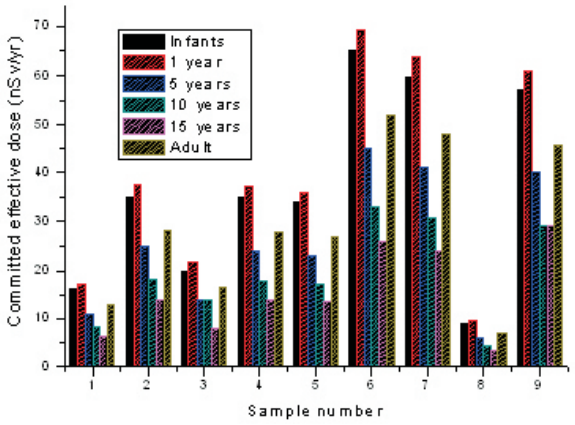


Fig. 1 Variation in the CED dose for ^3H for various age groups in the study area

Aqplus packaged drinking water for ^3H measurement. The count rate for all water samples are in the range of 0.501 0.036 to 0.624 0.04 cpm. We finally chose Aqplus packaged drinking water since it was easily obtainable. The Minimum Detectable Activity achieved using Aqplus packaged drinking water was 1.5Bq L^{-1} for total counting time of 500 minutes. For calibrating the LSC, series of quenched ^3H standards were counted in the optimized channel. A relation between SQP(E) and counting efficiency was used to obtain the percent counting efficiency corresponding to the quench associated with the different water samples analyzed. The yield of distillation was found be 95% as calculated by directly measuring the ^3H activity without distillation stage and measuring the same ^3H activity with distillation by LSC.

Application to Real Samples

An attempt has been made to estimate the ^3H concentration in waters from different environment origins (well and bore well) intended for human consumption.

Well and bore wells

Atmospheric precipitations can deposit ^3H in superficial waters. The tritiated water deposited on the ground can filter through internal layers. The extent of this filtration depends on such factors as the type and permeability of the ground and water content etc. Therefore various tritium levels are found in different waters. To study the tritium content of this kind of sample, waters from different wells and bore wells were analyzed in different villages of Pune, Kolhapur and Ratnagiri. The ^3H content of the Bota, Ahemdnagar samples is found to be 3.656 0.534 Bq L^{-1}. The ^3H content in different villages of Pune varies from 1.239 0.414 Bq/L to 3.948 0.534 Bq L^{-1} with an average of 2.253 0.46 Bq L^{-1}. The ^3H content estimated in New Dhanvad village of Kolhapur is 0.605 0.38 Bq L^{-1} whereas Malvan, Ratnagiri exhibits an average value of 3.496 0.529 Bq L^{-1}. The ^3H concentration in the open well of Jejuri and Malvan indicate somewhat higher values compared to the concentration obtained in the other places of study area. The ^3H concentration recorded in the study area indicated in Table 1 are negligible compared to the WHO [6] and EPA [5] recommended guideline levels for ^3H in portable/drinking water of 10,000 Bq L^{-1} and 740 Bq L^{-1} respectively. These guideline levels referred are based on recommended reference level of WHO and EPA's effective committed dose of 0.1 and 0.04 mSv per year respectively from one year consumption of drinking water. The CED estimates for reference individuals derived from the average activity concentrations of ^3H annually ingested in the study area are presented in Fig. 1. In the present study the committed effective dose calculated is in the range of 3.6 to 65 nSv y^{-1}, which are extremely low and of no radiological significance compared to EPA [5], WHO [6] and ICRP standards with guideline dose limits of 0.04, 0.1 and 1 mSv y^{-1}, respectively, recommended for public consumption due to natural sources of radiation.

Table-1: Sampling sites along with specific ^3H activities (in Bq L^{-1}).

Village name	Source	Specific tritium activity ± 1 (Bq l^{-1})
Vodgaon (Pune)	OW1	0.994 ± 0.498
	BW2	2.15 ± 0.444
Bori (Pune)	BW3	1.24 ± 0.414
Kandli (Pune)	OW4	2.12 ± 0.442
Pimpalvandi(Pune)	OW5	2.057 ± 0.443
Jeijuri(Pune)	OW6	3.948 ± 0.554
Bota(Ahmednagar)	OW7	3.66 ± 0.534
New Dhanvad (Kolhapur)	OW8	0.551 ± 0.366
Malvan (Ratnagiri)	OW9	3.496 ± 0.529

OW= Open well; BW = Bore well

Conclusion

Health hazard and dose assessment due to ingestion of ^3H in bore well and open well sample is not a concern. The annual effective doses to humans from the ingestion of ^3H in these water samples are very low and of no radiological significance. The data depicted in the present study is preliminary and more detailed monitoring program should be initiated in the study area in order to deepen the understanding about drinking waters radioactive content to increase awareness and mitigate possible hazards.

References

[1] Rohwer P.S, Wilcox W.H. Nuclear Safety, 17 (2) (1976) 216.

[2] National Council on Radiation protection and Measurements. A handbook of radiation measurements procedure. 2nd ed. Bethesda, MD: NCRP; Report No. 58 (1985) 368.

[3] Schonofer F. WorldScientific, Singapore, 155 (1994).

[4] Paloma M, et., al.Applied Radiation and Isotopes, 65 (2007) 1048.

[5] US Environmental protection Agency(USEPA), In: Macro Antonio PV MORAES, Marcelo Sartatto, Barbara EL (1975).

[6] World Health Organization (WHO).Guidelines for drinking water quality, Chap 9, 3rd edn, Geneva (2004).

Studies on Sorption of Uranium on Chitin- A Solid State Microextractant-Application to Preparation of Uranium Free Ground Water

Beena Sunilkumar and G. Chakrapani

Chemistry Laboratory, Atomic minerals Directorate for Exploration and Research, Department of atomic Energy, Hyderabad 500 016; E-mail: beenasunilkumar@gmail.com

Studies were carried out to remove uranium based on the solid phase extraction of uranium by chitin from aqueous systems. Investigations were carried out to optimise the parameters like pH, contact time, and amount of chitin. The studies with synthetic samples and real water samples showed that U was easily sorbed on chitin at pH 5. The effects of other cations and anions, which are present in the water samples, were also studied. The method is simple, fast and environmental friendly and it is unaffected by the other ions present in the natural waters. The accuracy of the method was evaluated by applying the present method on ground water samples containing uranium in the range of 100-2200 ppb. The uranium remained in water samples is <20 ppb after treatment with chitin, which is below the WHO and AERB limits given for uranium in drinking water.

Introduction

Chitin is becoming increasingly important natural polymer because of their unique combination of properties like biodegradability, biocompatibility and bioactivity, in addition to attractive physical and mechanical properties. Chitin and its derivative chitosan have a variety of applications in biomedical products, cosmetics, food processing. These products have found good application for removal of metal impurities in waste waters. Many other materials like activated carbon, fly ash, silica gel, zeolites, lignin, seawood, clay materials, agricultural wastes,powdered activated carbon etc. have also been extensively studied for the removal of pollutants from aqueous streams, especially for heavy metals like Cd, Cr, Hg, Pb [1-5]. Adsorption of high field strength elements like Zr, Hf, Mo, W, Nb, Ta in geological samples were studied by chitin [6,7]. Literature survey shows that much of earlier work on adsorption of U has been carried out using derivatives of chitin like chitosan and chitin phosphate [8,9]. The authors tried to optimise the parameters to remove uranium from water systems by using the bio- sorbent chitin.

Experimental

Instrumentation

The instrument used for the uranium analysis is the LED based Uranium Analyser UA-2 by Quantalase Enterprises Pvt. Ltd.

Reagents

Chitin obtained as flakes (from Loba Chemie ltd., Mumbai, india) was powdered in a shatter box. All other reagents used were of analytical grade. The uranium standard solution was prepared from uranyl nitrate of analytical grade.

Solid Phase Extraction Experiments

10 00 mL of tap water was taken in a beaker, 1 mL of 1 mg/mL U_3O_8 was added to the water and the sorption experiments were carried out at different conditions, like varying the pH, contact time and amount of chitin to establish the optimum conditions for sorption of uranium. All of these experiments were conducted at normal atmospheric temperature and pressure.

Resuts and Discussion

Studies of Optimal Conditions

The effects of several experimental parameters on the sorption of uranium were studied using spiking 1000ml tap water with 1000ng uranium. The parameters like pH, weight of chitin, contact time were studied and the optimal parameters are given in Table 1.

Table-1: Optimal conditions

Sample volume	1000 mL
Optimum pH	5
Quantity of Chitin	2g
Contact time	2 hours

Volume of solution -1000mL, pH 5, Time-2 hr

Effect of pH

The effect of pH on the sorption of uranium onto chitin was studied in the pH range of 1-10 maintaining the other parameters as given in the Table 1. The sorption is above 95% at pH range of 3-6 and is shown in Fig. 1.

Effect of Contact Time on the Sorption of Uranium on Chitin

The contact time of chitin with water was varied from 10 minutes to 24 hours by maintaining the other parameters as in the Table 1. The quantitative sorption

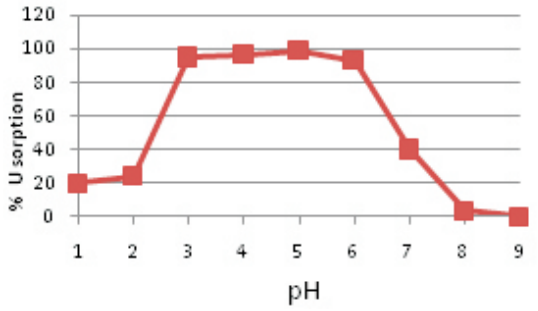


Fig. 1 Effect of pH on sorption of U on Chitin

was evident from 1 hour onwards and 2 hours contact time was chosen as optimum in order to allow sufficient time for sorption of uranium on chitin, considering higher concentration of total dissolved solids.

Effect of Chitin

The quantity of powdered chitin was varied from 500 mg to 10g by maintaining the other parameters in Table 1. 1g of chitin was quite sufficient to remove the U from water at pH 5; keeping in view of the enrichment factor, 2g chitin was used for 1000 mL of water. The experiments conducted on real water samples (1000 mL) effectively removed 2000 ng/mL U by 2g chitin.

Optimum Conditions for Removal of U in Water

From the above results, an optimum amount of 2g of powdered chitin with 2 hr contact time was selected for further studies using 1000 mL water sample.

Desorption Studies

The uranium was sorbed onto chitin by maintaining the experimental conditions in the Table 1. Uranium from chitin can be quantitatively recovered by ashing the sorbed chitin after filtering and the dissolution with nitric acid.

Accuracy of the Method

The accuracy of the present method was evaluated by applying the present method on ground water samples containing uranium in the range of 100-2200 ng/ml. After sorption the uranium remained in water samples is <20 ng/mL, which is below the WHO and AERB limits given for uranium in drinking water. The sorption of U was found to be above 95% in the samples and the values are given in Table 2. The values are an average of five replicate measurements, with an RSD of + 10 ng/mL at 100 ng/mL U.

Application of Sorption Studies to Hydrogeochemical Samples

Environmental samples containing U ranging from 100 ppb to 2200 ppb were selected for the removal of U. and the results are given in the Table 2. The data shows that 98% of U was removed by chitin. It was found that the higher concentration of major cations and anions does affect the quantitative sorption of uranium on chitin.

Conclusion

Chitin effectively removes uranium from water samples in the pH range of 3-6. 2 g chitin can remove 4600 ng/mL uranium from 1000 mL water at pH 5. As chitin is a natural bio-sorbent, this method is environmental friendly, no hazardous chemicals are involved. The time consuming method preparing derivatives of chitin like chitosan and chitin phosphate is avoided. This can also be used as a preconcentration method for uranium determination in water samples. The blank levels were found to be <10 ng/mL ou U in 2g chitin which is negligible.

References

[1] S.E.Bailey, T.J.Olin, R.M. Bricka, , D.D. Adrian Water Research 33(11) (1999) 2469.

[2] A. J. varma, S. V. Deshpande and J. F. Kennedy, Carbohydrate Polymers, 55 (2004) 77.

[3] D.S.R. Murty, G. Chakrapani, J.Anal.At.Spectrometry, 11(1996) 815.

[4] G.Chakrapani, Unpubl.PhD thesis, Bangalore University, India.

[5] G. Chakrapani, D.S.R.Murty, P.L.Mahanta and R.Rangaswamy, Journal of geochemical exploration, 63(1998) 145.

[6] V. Padmasubashini and D S R Murty, Atomic spectroscopy, 30(1) (2009) 32.

[7] V. Padmasubashini and D S R Murty, Atomic spectroscopy, 32(1) (2011) 17.

[8] Valerie Camel, Spectrochimica acta, Part B, 58 (2003), 1177.

[9] Takashi Sakaguchi, Takao Horikoshi and Akira Nakajima, Agricultural Biological Chemistry, 45(10) (1981) 2191.

Table-2: Application to ground water samples for the removal of uranium

Sample No	U in ppb in ground water (by LED Fluorimeter)	U in ppb in ground water (by pellet Fluorimeter	U in ppb left behind after sorption on chitin
1	120	-	2
2	1370	1360	14
3	1800	1795	14
4	2211	2215	18

Estimation of Heavy Metal Pollution in Coringa Mangrove Sediments using PIXE

M. Mahaboob Pacha[1], P. Anil Kumar[2]

1. *Department of Chemistry, Petrochemicals & P.G. Courses, P. R. Government College (Autonomous), Kakinada 533001, India; E-mail: mahaboobpacha@gmail.com*
2. *Department of Zoology, P. R. Government College (Autonomous), Kakinada 533001, India*

Introduction

Coringa Mangrove is on the deltaic branches of Gautami and Godavari Rivers at Kakinada bay, situated in Andhra Pradesh of India. It swamps along the coastal tracts and acts as buffer zone between land and sea and provides habitats and sustenance to many fauna and flora. During the last thirty years or so, sediments and nutrients through runoff have increased by various land disturbances particularly the urban development. Kakinada canal, through which the town's sewage enters the Bay, is the major source of organic pollution. A consequence of all the above has been greater public concern for protection of Coringa mangrove forest. Industrial prominence coupled with agriculture practices, oil and natural gas drilling, port expansion episodes, mechanized fishing and organized tree felling to build shrimp farms proved deterrent to the ecosystem.

The geochemical characteristics of the sediments can be used to infer the weathering trends and the sources of pollution. Sediments are important carriers of trace metals in the hydrological cycle and because metals are partitioned with the surrounding waters, they reflect the quality of an aquatic system. Coastal estuarine regions are the important sinks for persistent pollutants and they accumulate in organisms and bottom sediments

Experimental

Four sediment cores were collected from Coringa mangroves (S1, S2, S3) and Godavari estuary (G1) (Fig. 1) in June 2012 during low tide, in order to determine the variation of mass accumulation of sediments and vertical profile distribution of trace metals. Elemental composition of the sediment cores were estimated using AAS of Perkin Elmer AA800 instrument and the results will be compared with the analytical technique particle-induced X-ray emission (PIXE). The PIXE technique allows the identification of the elements present in the sample and to determine their mass concentrations. Organic Carbon was estimated by titrimetric method using Hydrogen Peroxide as an oxidising agent.

Results and Discussion

The concentrations of heavy metals (Cd, Co, Pb, Cr, Zn, Ni, Mn, Cu & Fe) were measured in different samples of different Mangroves sediments along the coastal area and was found that the concentration of heavy metals in the Mangrove sediments is very high.

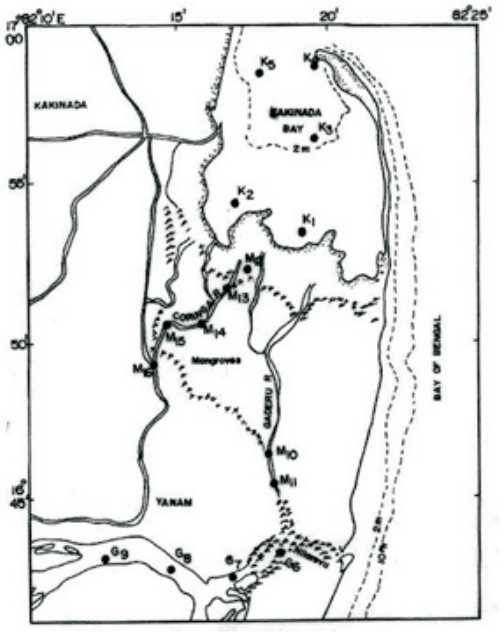


Fig. 1 Location of map showing the study area

The geochemical data of sediment samples from these mangrove swamps revealed that the swamps act as repositories of organic carbon and associated heavy metals through adsorption and complexation processes. Values of organic carbon showed very strong positive correlations with most of the elements as revealed by correlation matrix (r) values. The inter-elemental relationship revealed the identical behaviour of element during its transport in the estuarine environment. The overall variation in concentration can be attributed to discharge of untreated effluents originating from industrial, agricultural, and aqua cultural sources as well as from domestic sewage along with the fishing and boating activities. The resulting compositional dataset was analyzed by multivariate statistical methods, including Pearson correlation matrix. Statistical analysis was performed using statistical software SPSS version 16.0 for Windows shown in Table 1. Component 1 describes the general loading of the bottom sediment with heavy metals. It accounts for 22.6% of the variance and is characterized by high levels of Cd, Ni, Pb and Zn i.e. metals of chalcophylic nature. The combustion of fossil fuels, notably coal are main sources of lead, cadmium, nickel and zinc in water reservoirs. Substantial amounts of those elements enter reservoirs together with municipal wastewater [1].

Component 2 accounted for 20.1% of the total variance and is characterized by high copper concentration. Component 3 accounted for 15.0% of the total variance and are characterized by high manganese and copper concentrations are resulted from their presence in atmospheric precipitation. A correlation of all the trace metals with organic carbon is due to the distribution of trace elements and its association within the sediments.

Conclusions

The investigations carried out revealed a considerable loading of the bottom sediment with cadmium, lead, zinc and copper. The use of PCA enabled us to find that the elevated cadmium, lead, nickel and zinc concentrations may result from the inflow of the contaminated water from the river Godavari and long-range transport. Cd, Pb, Co, and Cu were enriched in the sediments of both estuarine and mangrove ecosystems, which have harmful or dangerous effects on these sensitive ecosystems. These metals also pose eco-toxicological risk through bio-magnification ultimately causing severe health risk to humans. The spatial distributions of trace elements in sediments in the estuarine environment are influenced by so many factors including geochemical and biogeochemical processes like sedimentation, precipitation. The results of our study suggest that an effective environmental management is required to safeguard the health of the ecosystems.

Table-1: VARIMAX rotated factor matrix for trace elemental composition of mangrove and estuarine cores

Trace	Component		
Metal	1	2	3
Zn	0.751	0.288	
Cu		0.846	0.81
Cr		0.447	
Ni	0.516		
Co			
Mn			0.966
Pb	0.723		
Cd	0.827		
Fe		0.896	
OC	0.761	0.478	0.413

Reference

[1] Nriagu, J.O. and J.M. Pacyna, Nature, 333(6169), (1988)134.

Study of Naturally Occurring Radioactive Material (NORM) in Soil using Low Background Gamma ray Spectrometry

A. Srivastava[1], F. Knolle[2], F. Hoyler[3], U.W. Scherer[3] and E.W. Schnug[4]

1. *Chemistry Department, Panjab University, Chandigarh 160014, India; E-mail: alok@pu.ac.in*
2. *GeoPark Harz . Braunschweiger Land . Ostfalen Network, Grummetwiese 16, D-38640 Goslar, Germany*
3. *Aachen University of Applied Sciences, Heinrich Mussmann-Strasse 1, D-52428 J ich, Germany,*
4. *Department of Life Sciences, Technical University, Pockelsstra 14, D-38106 Braunschweig,Germany*

There has been an increasing concern in the state of Punjab arising due to naturally occurring radioactive material (NORM) after high concentration levels of uranium was observed in ground water besides nails and hair of children. The concentration levels of ^{238}U, ^{232} Th and ^{40}K in top soil were measured using low background gamma ray spectrometric setup The concentration of NORM was found to be similar to what is expected as a result of their normal abundance but was found to be lower than what has been observed in the state of Jharkhand. In addition to NORM the fall out radionuclide ^{137}Cs was also observed in soil samples.

Introduction

There has been an increasing concern about toxicity arising due to naturally occurring radioactive material (NORM) in some districts of Punjab State located in the North Western part of India after the publication of a report by Blaurock-Busch et al. [1] which showed that the concentration of uranium in hair and urine of children suffering from physical deformities, neurological and mental disorder from Malwa region was manifold higher than the reference ranges. A detailed study of ground water samples in Malwa by Kumar et al. [2] using fluorescence spectrometry showed that concentration of uranium in subsurface water samples from Malwa region ranged from 2 to 644 ppb with a mean of 73.1 ppb: more than five times higher than the permissible limit of 15 ppb prescribed by the World Health Organization [3]. The uranium concentration in water from Nawanshahr region of Punjab too has been reported around threshold level by Bajaj et al. [4]. In the present work concentration of NORM top soil from affected as well as unaffected region is reported using low background gamma ray spectrometry.

Experimental

Nine samples of top soil from different locations in Punjab State lying between 29.5°N and 32.5°N latitude and between 73.8°E. and 76.9° longitude representing region mostly having increased level of uranium in ground water were collected. The samples were dried for a day in an oven at 60°C until moisture was driven out and then further pulverized and homogenized. 50 gm of the dried, pulverized and homogenized soil samples were then packed in leak proof PET containers. The sealed containers were kept aside for four weeks for attainment of secular equilibrium between radium, thorium and their daughter products before carrying out measurements using direct gamma spectrometry. The background counting was carried out for 625000 s whereas the sample counting was varied between 80,000 s and 170,000 s. Table 1 gives the details of gamma lines used in the present work. The samples were measured using a 40% high purity germanium detector shielded by 10 cm of lead and coupled to a 16 K multi channel analyzer. The resolution of the detector was found to be 1.7 keV at 1332 keV gamma peak of ^{60}Co. The spectral analysis was carried out using the GENIE 2000 software program (Canberra Co., USA).

Results and Discussion

Table 2 shows the activity of the naturally occurring radioactive materials from top soil from different locations in Punjab State. The activity of the radionuclide of interest is expressed in terms of disintegration per kilogram (Bq/kg) of soil. The uncertainty on the reported value based on counting statistics is in the range of three to five percent. The activity for ^{238}U ranges from 16.2 Bq/kg to 33.9 Bq/kg with a mean of 24.8 Bq/kg whereas the activity of ^{232}Th ranges from 31.2 Bq/kg to 61.4 Bq/kg with a mean of 40.2 Bq/kg. The activity of ^{40}K is observed to vary from 313 Bq/kg to 1050 Bq/kg with a mean of 500.7 Bq/kg. If one removes the exceptionally single high value of 1050 Bq/kg obtained in the present work the mean value reduces to 432 Bq/kg . In addition to detecting the activity of naturally occuring radionuclides it is interesting to note that the activity of ^{137}Cs which has its origin in fall out was also detected by the low background gamma ray spectrometric setup used in the present work. The activity of ^{137}Cs ranged from 0.5 Bq/kg to 2.9 Bq/kg with a mean value of 1.1 Bq/kg which is significantly lower than the activity of naturally occuring radionuclides. A comparison of the data obtained in the present work namely 24.8 Bq/kg, 41.0 Bq/kg and 432 Bq/kg respectively for ^{238}U, ^{232}Th and ^{40}K with that of generally considered global average i.e 35 Bq/kg, 45 Bq/kg and 420 Bq/kg respectively shows that the data is comparable to the global average. However if the data is compared with that obtained by Maharana et al [5] namely 53.8 Bq/kg, 44.2 Bq/kg and 464.2 Bq/kg from Jharkhand State for

^{238}U, ^{232}Th and ^{40}K respectively it is observed that the value for ^{238}U obtained in the present work is significantly lower which is not surprising as the region of Jharkhand State studied by the aforementioned researchers is known to have moderate grade uranium deposits. In conclusion it can be stated that the uranium concentration observed in Panjab soil seems to be normally distributed. Therefore the NORM present in soil might not be the factor responsible for the observation of high level of uranium in ground water, hair and nails. It would be interesting to carry out further work in this region as the body of data obtained in the present work is still small to make a definite conclusion.

Table-1: Gamma Lines of Radionuclides of Interest

Radionuclide	Gamma Line (keV)
^{40}K	1460.8
^{226}Ra	186.1
^{214}Pb	295.2, 351.9
^{214}Bi	609.3, 1120.3, 1764.5
^{228}Ac	338.3,463.0, 911.2, 968.9
^{212}Bi	727.3
^{212}Pb	238.6
^{137}Cs	661.7

Table-2: Activity of different naturally occurring radionuclides (Bq/kg) in top soil samples from different locations

Sample	^{238}U	^{232}Th	^{40}K	^{137}Cs
1	26.8	38.9	425	1.7
2	21.8	42.0	461	1.4
3	28.3	31.2	313	3.0
4	22.1	38.0	400	0.4
5	16.2	32.0	432	0.4
6	26.0	34.0	427	0.4
7	22.0	34.7	426	0.4
8	25.9	61.4	1050	1.1
9	33.9	49.7	522	0.5

Acknowledgement

One of the authors (A.S.) would like to place in record his special thanks to Alexander von Humboldt Foundation, Bonn, Germany for providing him financial support to carry out the experimental part of the reported research work in Germany.

References

[1] E. Blaurock-Busch, A. Friedle, M.Godfrey, C.E. Schulte-Uebbing and C. Smit, Clinical Therapeutics 2 (2010) 655

[2] Kumar, A., Usha, N., Sawant, P. D., Tripathi, R. M., Raj, S. S., Mishra, M., Rout, S., Supreeta, P., Singh, J., Kumar, S. and Kushwaha, H. S., Human and Ecological Risk Assessment 17(2011) 381.

[3] WHO, Guidelines for Drinking-water Quality, 4th Ed., Geneva, Switzerland (2011).

[4] M. Bajaj, E.Eiche, T. Neumann, J. Winter and C. Gallert, J Hazardous Materials, 189 (2011) 640.

[5] M.Maharana, N.Krishnan and D.Sengupta, Journal of Medical Physics 35 (2010) 235.

Source Depletion Model for Deposition from a Gaussian Plume

Arun Aravind, H. Seshadri, V. Balasubramaniyan

Environmental and Nuclear Fuel Chemistry Section, Safety Research Institute, Kalpakkam 603102, India;: E-mail: aravind@igcar.gov.in

In atmospheric dispersion modeling, it is important to account for the dry deposition of radionuclides onto the ground surface, for more realistic estimation of radionuclide concentration. Under precipitation or snow fall, wet deposition of radionuclides also contributes towards the source depletion. In this study, radionuclide depositions from a Gaussian plume were determined using a model developed in FORTRAN language and source depletion fraction, (Q'_x / Q) were estimated as a function of distance from the source, for different atmospheric stability classes and release heights. For all the cases studied, it has been found that, for a given stability class, wind velocity and deposition velocity, plume depletion is more predominant for lower release heights.

Introduction

Dry and wet depositions are important processes which depletes the contaminant plume. The dry deposition is caused by a combination of mechanical processes such as gravitational setting, turbulent and molecular diffusion, and inertial impaction, while the mechanism of wet deposition is such that, the plume is "washed out" by rain or snow. Under precipitation or snow fall, source depletion is considered as a function of both dry and wet depositions.

Source Depletion Model

Dry deposition flux can be assumed to be directly proportional to the pollutant concentration at the immediate ground level. And the source depletion due to dry deposition at a distance, x downwind can be formulated as shown in Eq. (1) [1],

$$Q'_{x,DRY} \quad Q\exp \quad \frac{2}{} \quad ^{1/2} \frac{v_d}{\overline{U}_p} \int_0^x \frac{dx}{{}_x \exp\ H_p^2 / 2\ {}_z^2} \quad (1)$$

Where, $Q'_{x,DRY}$ is the depleted source term at a distance x, due to dry deposition (Bq/s). Q is the initial source term (Bq/s). $\overline{U}_p$ is the mean wind speed at the effective release height (m/s). $_z$ is the vertical dispersion coefficient (m) and H_p is the effective release height (m).

Under rainfall or snow, source depletion at a distance, x downwind can be obtained as in eqn. (2) [2],

$$Q'_{x,} \quad Q\exp \quad \frac{x}{U_p} \quad \frac{2}{} \quad ^{1/2} \frac{v_d}{\overline{U}_p} \int_0^x \frac{dx}{{}_x \exp\ H_p^2 / 2\ {}_z^2} \quad (2)$$

First term in the square bracket in eqn. (3), corresponds to the wet deposition. is the washout coefficient as defined in Eq. (3),

$$= \quad R \quad (3)$$

is a constant and R is the rainfall rate (mm/hr).

Eqns. (2) and (3) are used to evaluate the depleted source term for dry deposition and under wet conditions respectively. The integral expression in eqns. (2) and (3) were evaluated numerically by using the Briggs formula for dispersion coefficient [3]. Numerical method employed for evaluating the integral expressions in eqns. (2) and (3) was Simpson's 1/3 rule and the model developed has been encoded in FORTRAN language.

Results and Discussion

Source depletion fraction, (Q'_x / Q) for dry deposition and under wet condition were determined as a function of distance from the source for stability classes A (Extremely unstable), D (Neutral) and F (Very stable). The mean wind speed was assumed to be 1.0 m/s and deposition velocity 10^{-2} m/s for all the cases studied. For the determination of source depletion fraction under wet condition, rainfall rate was assumed to be 1 mm/hr.

Estimated (Q'_x / Q) for dry deposition, for different release heights were compared against the corresponding literature values and are shown in Figs. 1-3, which shows that they are in good agreement [4]. Q'_x / Q estimated as a function of distance from the source under wet condition for stability class F, for different source release heights are shown in Fig. 4. The comparison of Q'_x / Q estimated as a function of distance from the source, for source release height 10 m for stability classes D and A are shown in Fig. 5. In all

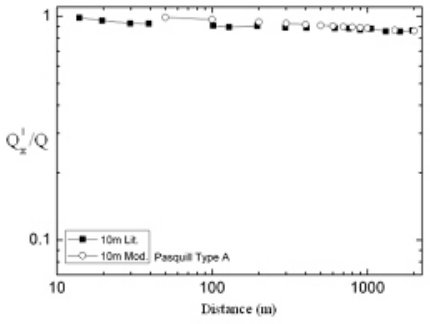


Fig. 1 Source depletion fraction, as a function of distance from the source for Pasquill type A

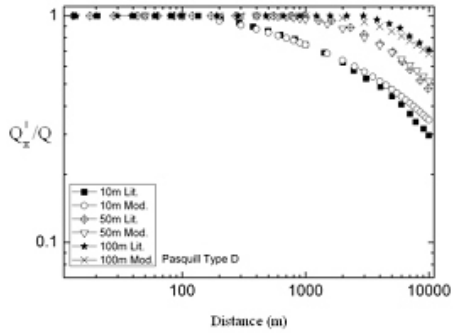


Fig. 2 Source depletion fraction, as a function of distance from the source for Pasquill type D

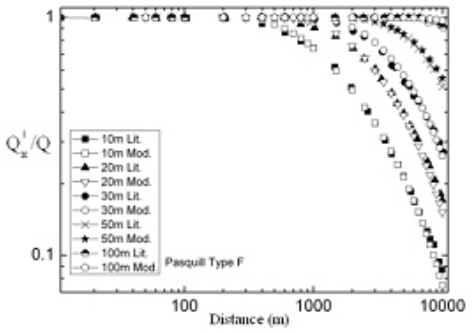


Fig. 3 Source depletion fraction, as a function of distance from the source for Pasquill type

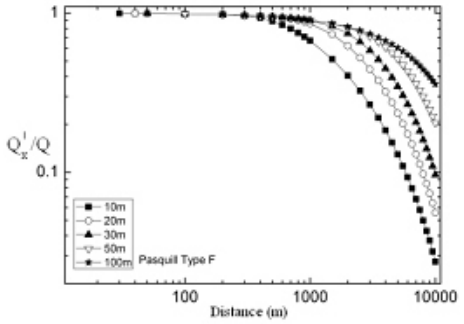


Fig. 4 Source depletion fraction as a function of distance from the source for Pasquill type F

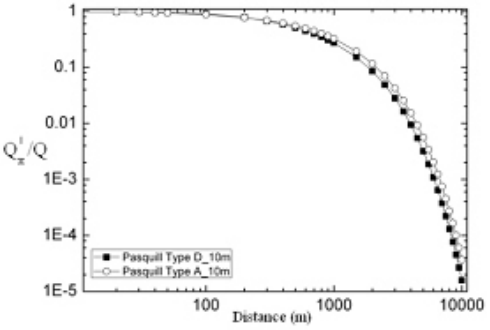


Fig. 5 Comparison of variation of $(Q_x^{'}/Q)$ as a function of distance from the source for stability classes D and A

the cases studied, for a given stability class, plume depletion were found to be more predominant for source release height closer to the ground. This is because, ground level pollutant concentration will be more for lower release heights. Since dry deposition is proportional to the ground level pollutant concentration, plume depletion will more for lower release heights.

Conclusions

Radionuclide depositions from a Gaussian plume were studied using a model developed in FORTRAN language and source depletion fractions, $(Q_x^{'}/Q)$ were estimated as a function of distance from the source, for different cases. It has been found that, for a given stability class, plume depletion is more predominant for lower release heights.

References

[1] David H. Slade, Meteorology and Atomic Energy, U. S. Atomic Energy Commission, Report TID-24190, National Technical Information Service (1968) p.204.

[2] C. Yu, et al., User's Manual for RESRAD-OFFSITE, Version 2 (2007) 4.

[3] Arun Aravind, P. T. Rakesh, H. Seshadri, Source Depletion Model for Dry Deposition from a Gaussian Plume, SRI Internal Report, AERB-SRI/2013/4004(Rev-0) (2013).

[4] I. Van der Hoven, Deposition of Particles and Gases, in Meteorology and Atomic Energy, D. H. Slade, Ed., U. S. Atomic Energy Commission, Report TID-24190, National Technical Information Service (1968) 202.

Occurrenceof the Radionuclides in Groundwater of Crystalline Hard Rocks Regions of Central Part Tamil Nadu, India

C. Thivya[1], S. Chidambaram[1], K. Tirumalesh[2], M. V. Prasanna[3], R. Thilagavathi[1] andM. Nepolian[1]

1. *Department of Earth Sciences, Annamalai University, Annamalai Nagar 608 002, India; E-mail: thivyac1988@gmail.com*
2. *Isotope Applications and Radiopharmaceuticals Division, Bhabha Atomic Research Centre, Mumbai 400 085, India*
3. *Department of Applied Geology, School of Engineering and Science, Curtin University, Sarawak Malaysia*

Samples were collected in hard rock region central parts of Tamilnadu, South India to assess the U and ^{222}Rn levels in groundwater belonging to various lithologies and evaluate their correlations with other water quality parameters. The order of dominance of U in groundwater is; Granite> Charnockite> Fissile Hornblende biotite gneiss> Flood Plain Alluvium> Quartzite, while that of ^{222}Rn is: Granite> Quartzite> Charnockite > Fissile Hornblende biotite gneiss> Flood Plain Alluvium.Both U and ^{222}Rn concentrations were compared with drinking water standards and a few samples show levels above the permissible limits. High degree of weathering of granitic rocks and long contact time of groundwater with the aquifer matrix could be the reason for enhanced U and ^{222}Rn levels in groundwater.

Introduction

U is the primordial radionuclide with longhalf-life of $4.5X10^9$ years and present in all types of rocks whereas ^{222}Rn is a daughter product of U series with a half-life of 3.8 days. Both these elements are present in groundwater in variable concentrations, which is dependent on the fractures, degree and the angle of inclination to the bedrock [1]. The exposure of U and ^{222}Rnto humankind causes kidney problems and lung cancer respectively, therefore groundwater needs to be analysed for these elements before being used for drinking purposes. The study area falls in Madurai district of Tamil Nadu and mainly covers crystalline hard rocks. In this regiongroundwater is the main source of drinking and domestic purposesinspite of its limited availability.Studies have reported higher amount of U in granitic rocks of this district [2] but there was no report available for U levels in groundwaters of this region. In this study,an attempt has been madeto assess the occurrence of U along with ^{222}Rn in groundwaterfrom various lithologies and postulate release mechanism.

Methodology

A total of 33 groundwater samples were collected from different lithological units, 15 from gneissic rock, 12 from Charnockite, 3 from Quartzite, 2 from Granite and one from Flood plain alluvium. The pH, electrical conductivity (EC), Temperature were analyzed in situ using hand held instruments (Eutech instruments).Umeasurements were made using a ICP-MS spectrometer (Perkin- Elmer Sciex® ELANTM 5000).100 mg $L^{-1}$of Uranium Stock solution was prepared from $UO_2(NO_3)_2 \cdot 6(H_2O)$ 99.999%. 10 $mgL^{-1}$of Rh solution was used as an internal standard and it was prepared for $RhCl_3 \cdot 3H_2O$ 38%. A few samples were cross checked by laser fluorimeter.Smart Radon Meter(SRM) has been used for monitoring Radon concentration in water, which employs a closed loop aeration scheme [3].The statistical summary of U, ^{222}Rn, pH, EC and Temperature is given in Table.1

Table-1: Maximum, minimum and average values

Parameter	Maximum	Minimum	Average
Uranium (g L^{-1})	46.7	1.7	6.8
Radon (Bq L^{-1})	211.6	0.1	14.3
pH	8.5	6.6	7.2
EC (s cm^{-1})	4011.0	132.4	1499.3
Temperature (^oC)	32.7	27.7	31.0

Results and discussion

In the study area 2 samples from Charnockite and 1 sample from Granite are above the WHO permissible limit of 15 ppb [4] and rest of the samples are within the limits.In the case of ^{222}Rn, 3 samples from Gneissic rock, 1 sample from Charnockite, Quartzite and granite are above the USEPA permissible limit of 11.1 Bq/l [5] while rest of the samples are within the permissible limit.It is found that ^{222}Rnand Ulevels are positively correlated in groundwater. The higher concentration is observed in the Granitic terrains while the minimum values are noticed in Charnockite lithounits.Granitic rocks often have higher average concentration of U in the order of 5 ppm [6]. The major primary ores of U are UO_2 and U_2O_5. Pitchblende an ore of uranium is generally formed as a result of alteration and redistribution of U oxides by groundwater. In an oxidizing environment the groundwater in fracture contains an appreciable amount of dissolved oxygen, this oxidizes U to hexavalent U, which is mobile and easily leaches intowater and transported.Groundwater

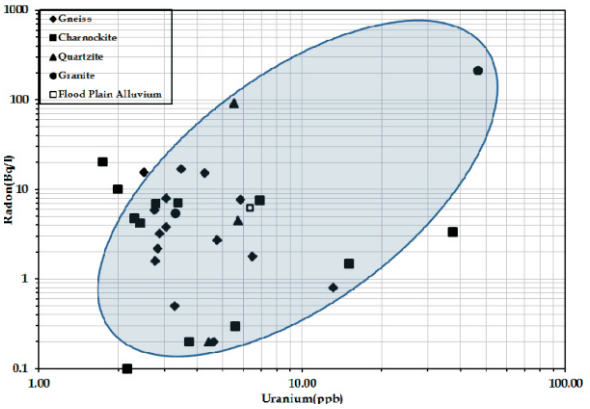


Fig. 1 U Vs ^{222}Rn for groundwater samples

in contact with U rich crystalline rocks show elevated ^{222}Rn levels, which depends on factors like emanation, diffusion and permeability.

The spatial distribution of the higher concentration of U and ^{222}Rn is observed in the northern part of the study area, where the granites are predominant rocks (Figs. 2 & 3). It is observed that U and ^{222}Rnlevels decrease with the increase of pH in groundwater. The higher concentration of U and ^{222}Rn is observed in the near neutral pH of groundwater. On the contrary, U and ^{222}Rn concentration increases with the increase EC values. Inter elemental correlations indicate that U has good correlation with^{222}Rn, EC, Na and SO_4, which indicates that the weathering process and residence time of groundwater enhances the U and ^{222}Rn levels in groundwater.

Conclusion

This study reports of U and ^{222}Rnlevels in groundwater from different rock types of Madurai district and evaluate their correlation with other water quality parameters. A positive correlation were observed between U and ^{222}Rn. Among various rock types high U and ^{222}Rn levels were found in Granitite followed by Gneiss and Charnockite. From inter-elemental correlations it can be found that leaching of weathered products, redox conditions and fracture systems are governing mechanisms for the presence of U and ^{222}Rn in groundwater.Since there are some locations where high U and ^{222}Rn are noticed, it can be suggested that groundwater should be testedfor these radionuclideprior to consumption. There is also a need for further research on prediction models in this

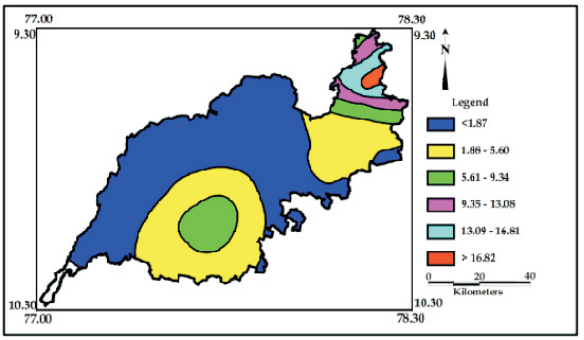


Fig. 2 Spatial distribution of U in groundwater samples

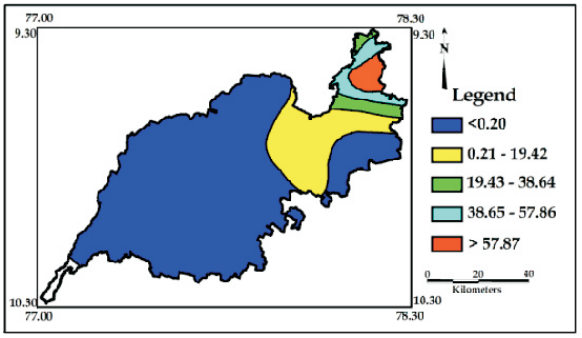


Fig. 3 Spatial distribution of ^{222}Rn in groundwater samples

areaespecially from rock types where the higher U and ^{222}Rn levels are observed.

References

[1] K. Skeppstrom,B. Olofsson. European water 17/18 (2007) 51.

[2] U.K. Pandey, P.Krishnamurthy, Current science, 68(8) (1995).

[3] JJ. Gaware, BK. Sahoo, BK.Sapra, YS. Mayya, Radiat.Prot.Environ, 34 (2011) 37.

[4] WHO (World Health Organization) Guidelines for drinking-water quality. Third edition.Vol 1, Recommendations. Geneva,(2006) ISBN 92 4 154696.

[5] USEPA, National primary drinking water regulations: radionuclides; proposed, EPA. Federal Reg. 56 (1991) 33050.

[6] G. Akerblom and J. Lindgren. European Geologist 5 (1997) 13.

Assessment of Environmental Radioactive Elements (U, ^{222}Rn, ^{3}H) in Groundwater in parts of Nalgonda district, Andhra Pradesh

K.Tirumalesh[1], H.V. Mohokar[1], B.K. Sahoo[2], G. Mallesh[3]

1. *Isotope applications & Radiopharmaceuticals Division, Bhabha Atomic Research Centre, Trombay, Mumbai, India; E-mail: tirumal@barc.gov.in*
2. *Radiological Physics & Advisory Division, Bhabha Atomic Research Centre, Trombay, Mumbai, India*
3. *DHAN Foundation, Hyderabad, Andhra Pradesh, India*

The objective of this work was to assess the concentration of radioactive elements in groundwater of hard rock regions of Nalgonda district, Andhra Pradesh. Radon activity was measured in water samples using smart radon monitor, uranium was measured using ICP-MS and tritium was measured using liquid scintillation counting after electrolytic enrichment. Results indicate that tank water has the minimum in ^{222}Rn activity and groundwater from shallow and deep zones shows significant ^{222}Rn activity. An increasing ^{222}Rn activity trend is noticed along the well depth while EC showed inverse trend. U and HCO_3^- concentrations also decrease along the well depth and show positive correlation. Environmental tritium data indicates modern recharge to groundwater.

Introduction

Nalgonda district falls under semi-arid region (~900 mm total rainfall) and most of the water supply to irrigation is met by groundwater and natural tanks. Since the rainfall is mostly confined to a few intense rain events lasting only for a short duration in a year, storage and proper utilization of this vital source is very important. Tanks play a major useful role in confining the surface run-off and enhancing the groundwater recharge especially in shallow zones. This study presents the data on uranium, ^{222}Rn and ^{3}H along with EC and bicarbonate and their interrelations. This data can be useful as baseline data for the study site and also in understanding the Tank water contribution to groundwater.

Study Site Description

Tanks belonging to Chityal taluka of Nalgonda district were chosen for the study with an area of ~ 50 sq. km. Top zone is mostly weathered ranging from 5-10 m thick while the deeper zones are dominated by fractured granitic rocks. There are 15 natural tanks in these villages which are connected in a cascade fashion and benefit about 250 acres of land for irrigation and domestic purposes. About 100 bore/dug-cum-bore wells exist in and around these villages for extracting groundwater for irrigation purposes. Wells (Hand pumps & dug wells) tapping shallow weathered zone range from 10 to 100 ft bgl (below ground level) while deeper wells (bore wells) tap up to 60 to 350 ft bgl. About 29 samples were collected from hand pumps, bore wells, dug wells and tanks during November 2011.

Methodology

Radon ($t_{½}$, 3.8 d) is an important tracer that has increased in usage over the past two decades, produced from Ra as part of the U decay series. Rn activities are commonly two or three orders of magnitude higher than those of surface water, hence it can act as a potential geochemical tracer for evaluating the groundwater surface water interactions [1]. On the other hand environmental tritium is commonly used as qualitative tracer for assessing the recent recharge to groundwater. Uranium is naturally found in the environment as a mixture of radioisotopes and its presence in groundwater has raising public health as well as environmental concerns.

Measurements

Radon in groundwater is measured using an indigenously developed Smart Radon Monitor (SRM). Water samples were collected from different water sources in a leak tight glass bottle (100 ml). While sampling water into the bottle from water sources, caution was taken to avoid formation of bubble/agitation in the water. Subsequent to sampling, measurements were carried out using the SRM by following the bubbling technique [2]. The radon concentration in water (C_w) from the measured concentration (C_{air}) with SRM was estimated using the following equation,

$$C_w = C_{air}\ \ k + \frac{V_{air}}{V_w} \qquad (1)$$

where, V_{air} and V_w denote air and water volume of the set up respectively, K is the distribution factor of radon concentration between water and air. Typical value of K is 0.2 which can be neglected as comparison to V_{air}/V_w ratio (2.0 in this case).

For tritium measurement, 500 mL water samples were collected in airtight polyethylene bottle. 250 mL of distilled sample was electrolytically enriched at a low temperature of about 1 to 4°C and sample - scintillator mixture (8:12 mL) taken in a 20 mL polythene vial was counted in an ultra low background (0.5 cpm) liquid scintillation counter (Quantulus model 1220). The ^{3}H values are expressed in tritium unit (TU). One TU of sample has $^{3}H/^{1}H$ ratio equals to $1/10^{18}$, which corresponds to 0.12 Bq/kg of water. The minimum

detection limit for this method is 0.5 TU (3) for 500 minutes counting. The counting efficiency and the calibration factor of the counter were about 25% and 70 TU/cpm respectively. Uranium was measured by ICP-MS the detection limit was 0.5 gl^{-1}.

Results and Discussion

Summary of U, Rn, ^{3}H and EC data along with other physical parameters is given in table 1. The radon activities found to vary significantly depending on source of water. It is observed that bore well samples contain higher Rn activity compared to other sources like Hand Pumps, Dug Wells and Tank water. A few samples also show ^{222}Rn activities above permissible limits for drinking [5]. Majority of the samples show significant U concentrations in groundwater which could be attributed to the presence of granitic rocks that are rich in U minerals. It is commonly noticed that groundwater from granitic terrains consists of elevated levels of U and high values are reported earlier in this state [3].

Radon levels increase with depth of the well (Fig. 1a). Very low values are recorded in the tank and dug wells and radon levels seem to increase in groundwaters with increasing well depth. This variation can be attributed to diffusion in tanks and dug wells, whereas in the case of groundwater contribution from surface sources in shallow zones may result in decreased Rn levels. These trends signify that radon can be used as a promising tool to understand the surface water and groundwater interactions. In contrast, an inverse trend is noticed in the EC variation with depth (Fig. 1b) except a few samples from tanks and dug wells (shown in box). Higher EC in the shallow zones could be due to pronounced soil-water interaction while in the case of deep zones water-rock interactions are slow and less pronounced leading to lower mineralization of groundwater in deep zones.

In the case of U, majority of groundwater samples show decreasing trend. A few samples from surface sources show low U concentration, which are shown in box (Fig. 1c). Bicarbonate concentration in groundwater shows decreasing trend with depth similar to U variation (Fig. 1d). A few samples belonging to surface sources show low bicarbonate concentration (shown in box in Fig. 1d). It is observed that groundwater with high bicarbonate values also show higher U concentrations, but there is no systematic

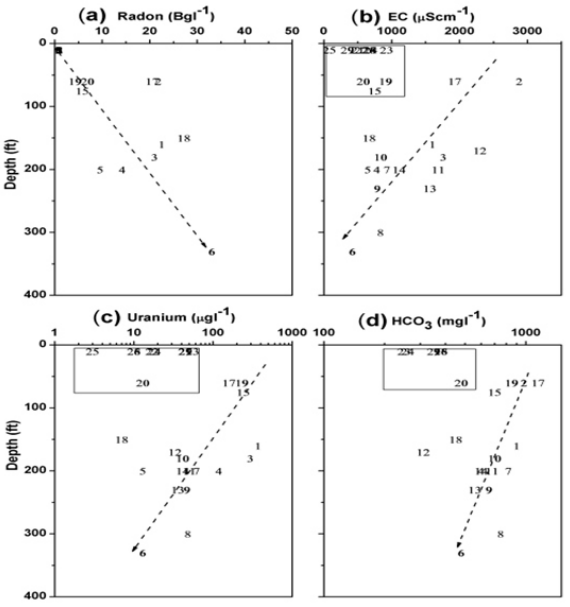


Fig. 1 Vertical distribution of a) Rn, b) EC, c) U and d) HCO_3 in water samples, no. 1-14 (BW), 15-20 (HP &DW) 21-29 (Tank)

trend between U and Rn levels. Presence of high bicarbonate concentration enhances leaching of U from geologic matrix while the probability of diffusion of Rn produced from U decay is high in soil zone. This leads to lower activities of Rn in shallow groundwater compared to deeper parts. Environmental tritium data suggest majority of groundwaters have 4-6 T.U. which indicates modern recharge to these groundwaters. Only one sample showed 0.5 T.U. value, which indicates old water.

Acknowledgements

Authors thank Dr. U. Saravana Kumar, Head, Isotope Hydrology Section, IA & RPhD and Dr. Gursharan Singh, Associate Director, RC&IG, BARC for their constant support during this study.

References

[1] Natasha T. Dimova et al., Jour. Hydrol. 486 (2013) 112.

[2] Jong-Mi Lee, Guebuem Kim, J. Env. Radio., 89 (2006) 219.

[3] Singh et al. J. Geochem. Explor. 76 (2002) 71.

Table 1: Summary of U, Rn, ^{3}H, EC and HCO_3 data of water samples collected from different sources

Source	BW (14)			HP and DW (6)			Tank (9)		
	Min	Max	Mean	Min	Max	Mean	Min	Max	Mean
Depth	60	330	202	60	150	81		15	
Uranium	13	370	89	7	296	157	3	55	27
Radon	9.6	33.1	20	4.3	27.2	12	0.04	0.3	0.15
Tritium	0.5	4.2		4.5	6		4	4.5	
EC	423	2879	1250	582	2982	1320	83	925	530
HCO_3	310	980	670	450	1150	765	250	380	330

Units: Depth (ft), U ($g L^{-1}$), Radon ($Bq L^{-1}$), ^{3}H (T.U.), EC ($S cm^{-1}$), HCO_3^- ($mg L^{-1}$)

Radon and Thoron exhalation measurements in flyash samples collected from dumping area of Panipat Thermal Power Station, India using Smart Radon and Thoron monitor

Lalit Mohan Singh[1], B.K.Sahoo[2], B.K. Sapra[2], Mukesh kumar[3], Rajendra Prasad[4], Rajesh Kumar[1]

1. *University School of Basic & Applied Sciences, Guru Gobind Singh Indraprastha University, New Delhi-110078, India; E-mail: rajeshkumaripu@gmail.com*
2. *Radiological Physics and Advisory Division, Bhabha Atomic Research Centre, Mumbai-400085, India*
3. *Department of Physics, S.V. (P.G.) College, Aligarh 202001, India*
4. *Vivekanand College of Technology and Management, Aligarh 202002, India.*

Subsequent to finding of radiological hazards due to inhalation of environmental radon and thoron, attempts have been made to identify various source matrices of radon and thoron and quantify their emission into environment from those sources. One of such sources is fly ash, which is being widely used for manufacturing of bricks, sheets, land filling etc. In the present work, radon and thoron exhalation measurements have been carried out for Fly ash samples collected from nearby area of Panipat Thermal Power Station, Haryana using BARC developed radon and thoron monitor. It has been found that radon mass exhalation rate varies from 37.5 mBq/kg/h to 212.5 mBq/kg/h with an average value of 112.3 mBq/kg/h .Thoron surface exhalation rate varies from 427.0 Bq/m^2/h to 1418.6 Bq/m^2/h with an average value of 930.8 Bq/m^2/h.

Keywords: Radon, Thoron, Exhalation rate, Flyash

Introduction

Flyash, a coal combustion product contains radionuclide's which arises from uranium and thorium series. Pesky carbon and other impurities and their subsequent emission to the atmosphere are one of the technologically exposure to human being from these radionuclide's. In India approximately 90 million tons (mt) flyash is generated per annum at present. Flyash is largely responsible for environmental pollution and use of flyash as distemper, fertilizer, road construction and ceramics etc. has created various adverse effects on the environment. Concentration of radionuclide's in flyash grows 3-4 times as compared with the original matter. When flyash is used in building construction material (bricks, cement etc.), it becomes potentially hazardous [1-6]. Due to small size and hence large surface area flyash has a tendency to absorb trace elements that are transferred from coal to waste product during combustion. Radon exhalation is an important parameter for estimating radiation hazards from Fly ash samples.

In present study, radon and thoron exhalation rate have been measured using BARC developed Smart Radon and Thoron monitor [7]. A total of 10 Fly ash samples collected from different location of dumping areas of Panipat Thermal Power Station (PTPS), Haryana have been subjected to analysis, aiming to quantify the radon and thoron exhalation source term.

Experimental Method

The accumulation based technique [8] was used to measure the radon mass exhalation while thoron surface exhalation is measured using a scintillation based Smart Thoron Monitor (STM). About 500 g of sample was taken in the accumulation chamber for carrying out measurements. For Radon mass exhalation rate measurement, radon in accumulation chamber is sampled into the scintillation cell (150cc) of the Smart Radon Monitor through a "progeny filter" and "thoron discriminator" eliminating radon progenies and thoron. The thoron discriminator based on "diffusion time delay" does not allow the short lived thoron ^{220}Rn (half life 55.6 sec) to pass through. The alpha scintillations from radon and its decay products form inside the cell are continuously counted for a user –programmable counting period by the PMT and the associated counting electronics. The alpha counts obtained are processed by a microprocessor unit as per the developed algorithm to display the concentration of radon. The build up radon concentration was measured at a time intervals of 1 hour till to attain saturation of radon concentration. On the other hand, thoron concentration was measured at a regular time interval of 15 minutes till equilibrium is reach for thoron concentration.

Calculation Methodology

The radon concentration C (t) in a closed chamber builds up with time according to the equation 1 [8].

$$C(t) \quad \frac{J_m M}{V_e}\left(1 - e^{-\lambda_e t}\right) \quad C_0 e^{-\lambda_e t} \qquad (1)$$

where, C_0 is the ^{222}Rn concentration (Bq/m^3) in the chamber volume at t=0, M is the total mass of the sample, V_e is the effective volume (volume of chamber +internal volume ^{222}Rn monitor – volume of sample) (m^3), λ_e is the effective decay constant for ^{222}Rn, which is the sum of the leak rate (if existing) and the

radioactive decay constant of ^{222}Rn (h^{-1}), t is the measurement time (h).The mass exhalation rate of ^{222}Rn (J_m) of the sample can be determined by fitting the observed build up data of ^{222}Rn concentration inside the chamber to the exponential growth curve given in Eq. (1)

The thoron concentration in the chamber will reach equilibrium in a short time period and the equilibrium thoron concentration (C) is given by the equation 2 [9].

$$C \quad \frac{J_s A}{V} \qquad (2)$$

Where J_s is the thoron surface exhalation rate, V is the effective volume (volume of chamber + internal volume of ^{220}Rn monitor – volume of sample) (m^3), is the radioactive decay constant for ^{220}Rn, A is the surface area of sample is the measurement time (h). Hence by knowing the value of equilibrium thoron concentration, the thoron surface exhalation rate can be estimated.

Results and Conclusion

Table 1 shows the variation in exhalation rate of different flyash samples. Radon mass exhalation rate varies from 37.5mBq/kg/h to 212.5 mBq/kg/h with an average value of 112.3 mBq/kg/h. Thoron surface exhalation rate varies from 427.0 $Bq/m^2/h$ to 1418.6 $Bq/m^2/h$ with an average value of 930.8 $Bq/m^2/h$. The radon exhalation rate of the flyash samples from Panipat Thermal Power Station (PTPS) are within the limit prescribed by Radiation Protection Agencies. Thus flyash appears to be safe and can be used in building materials without posing significant radiological threat to population.

Acknowledgements

Author's are thankful to Panipat Thermal Power Station (PTPS), Haryana for granting the permission for collecting flyash samples. This work is carried out at University School of Basic and Applied Science, Guru Gobind Singh Indraprastha University, New Delhi. Financial assistance provided by Board of Research in Nuclear Science (BRNS) Project Sanction No.2011/36/09-BRNS/197 is gratefully acknowledged.

Table-1: Radon mass exhalation rate and Thoron surface exhalation rate of flyash samples

Sample Code	Sample Weight (gm)	Radon Mass Exhalation Rate (mBq/kg/h)	Thoron Surface Exhalation Rate (Bq/m2/h)
PTPSFA1	500	55.4	900.5
PTPSFA2	500	212.5	1418.6
PTPSFA3	500	165.6	1384.2
PTPSFA4	500	77.1	566.6
PTPSFA5	500	98.9	465.4
PTPSFA6	500	59.5	427.0
PTPSFA7	500	139.9	1341.7
PTPSFA8	500	129.3	1123.1
PTPSFA9	500	147.3	1191.9
PTPSFA10	500	37.5	489.7
Average		112.3	930.8

Reference

[1] Manas Ranjan Senapati Current Science, 100 (2011) 12.

[2] Blaton-Albicka K & Pensko J, Health Physics, 41(1981) 548.

[3] Somali J, Horvath M, Kanyar B, Lendvai Z & Nemeth Cs, Health Physics, 75 (1998) 648.

[4] Kant K, Upadhyay S B, Sharma G S & Chakarva -rti S K. Indoor and Built bEnviron, 15 (2006) 177.

[5] Kumar A. Narayani K S, Sharma D N &Abani M C, Radiat Prot. Environ., 24 (2001) 195.

[6] Gulec N, Gunal (Calci) B & Erler A. Environ Geology, 40 (2001) 331.

[7] Gaware JJ, Sahoo BK, Sapra BK, Mayya YS., BARC News Letter, 318 (2011) 51.

[8] Sahoo B.K., Nathwani D., Eappen K.P., Ramachandran T.V., Gaware J.J. & Mayya Y.S. Radiation Measurements. 42 (2007) 1422.

[9] Sahoo B.K., Mayya Y.S., Agric. and Forest Meteorol, 150 (2010) 1211.

Uranium Leaching from Mining Wastes: Effects of Contact Time, pH and Particle Size

A.C. Patra, P.M. Ravi and R.M. Tripathi

Health Physics Division, Bhabha Atomic Research Centre, Trombay, Mumbai 400 085, India;
E-mail: aditichem@gmail.com

Dynamic short term leaching tests were carried out for mining wastes generated from the uranium mining industry over a period of 0-80 hrs under different leaching conditions. Leaching was fast in the initial stage being followed by a slow stage before attaining a near equilibrium condition. Leaching intensity was observed to be high in acidic pH and for lower particle sizes. The leaching intensity in all the cases was in general weak, indicating slow uranium leaching in the simulated environmental conditions.

Introduction

Uranium is a radiologically and chemically toxic element present in ppm levels in soils to a few percentages in minerals/ rocks used in the mining industry. It becomes mobile in the environment due to geological processes, like leaching and erosion. The fraction of leached uranium apart from the total uranium content, is essential to assess the impact of any soil, sediment etc. Many leaching procedures have hence been developed [1] with the aim of assessing the risk associated with such matrices.

The main wastes generated in large quantities due to the mining and milling of metals, which are to be dealt with in the long term, are the tailings. The ore body configuration and mining methods have an influence on the quantity of tailings [2]. Leaching, due to ingress of water into the tailings piles, acts as the main process of transfer of uranium from the tailings [2].

Hence it is extremely important to understand the leaching of uranium from metallurgical wastes. The effect of different physico-chemical factors on uranium leaching from the wastes also needs to be studied.

Sample Collection

Uranium bearing tailings were collected from the uranium mines in the Singhbhum thrust belt. This area hosts vein or disseminated uranium deposits [3]. Multiple samples were collected from a location and homogenized to make one representative sample. Samples were sieved through an electronic sieve shaker in five particle size classes and stored in polythene containers.

Experimental

The bulk density, pH, moisture content, organic matter content of uranium tailings were 1.43 ± 0.12 g/cm^3, 6.2 ± 1.9, 2.65 ± 0.82% and 1.37 ± 1.13% LOI. The sand, silt and clay content of the tailings were 32.6%, 66.9% and 0.5%, respectively. The total uranium content of the tailings, determined by INAA, was 96.10 ± 3.52 ppm.

The physical variables included in the short term dynamic leaching test were contact time, pH of the leachant solution and particle size of the material. Samples were shaken with water (solid: liquid-1:20) at intervals of 2-80 h on a horizontal shaker at 80-100rpm. Water was used as the leachant to simulate ambient environmental conditions [4]. Samples were subjected to leaching at different pH (pH 3, pH 7 and pH 10) and different particle sizes (<36 m, 36-63 m, 63-125 m, 125-212 m and 212-500 m). Leachant was sampled out at regular time intervals after filtration (0.22 m membrane filter) and replaced with fresh solvent. Laser fluorimetry was used to determine the total uranium content in the leachates. Details of the technique are given elsewhere [5].

Results and Discussion

The variation in pH from neutral-acidic-basic showed pronounced effects on the leached uranium concentrations. Uranium concentrations in the leachant ranged from 0.42-6.58 ppb, 15.80-195.04 ppb and 0.22-2.44 ppb under neutral, acidic and basic pH conditions, respectively. Highest uranium concentrations were leached under acidic conditions due to pyritic nature of the waste.

Uranium concentrations in leachate varied from 0.88-3.42 ppb, 0.38-6.74 ppb, 0.76-2.87 ppb, 0.53-6.47 ppb, and 0.40-4.72 ppb for <36 m, 36-63 m, 63-125 m, 125-212 m and 212-500 m particle sizes (Fig. 1).

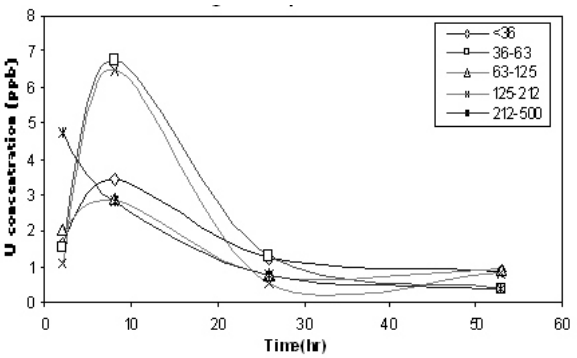


Fig. 1 Time evolution of U with particle size

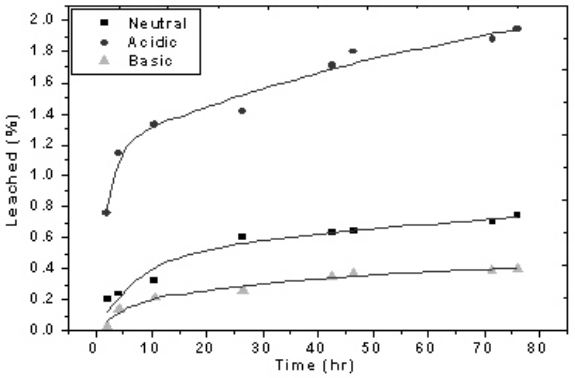


Fig. 2 Cumulative U% leached at different pH

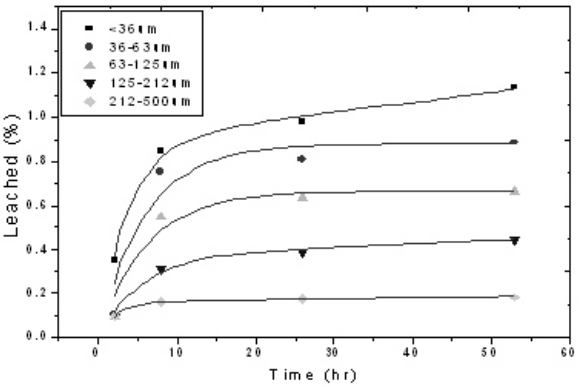


Fig. 3 Cumulative U% leached for different particle sizes

The cumulative fraction of U leached was 0.75, 1.94 and 0.40% under neutral, acidic and basic pH, respectively as observed in Fig. 2.

The maximum cumulative fraction of U leached out from different particle sizes of tailings followed the order <36 m > 36-63 m > 63-125 m > 125-212 m > 212-500 m (Fig. 3).

It can be noted from Figs. 2 and 3 that the leaching of uranium from the tailings followed a similar pattern, an initial fast stage followed by a slower stage. Any leaching process comprises of three main stages. The first stage is approach of the leachant to the solid surface through either molecular diffusion or convection. In the second stage, chemical reactions take place at the solid-liquid interface, followed by the third stage, the ions or molecules of the sample being dissolved are withdrawn to the solution bulk [6]. If the whole process rate is limited by the rate of the first or third stage, diffusion kinetics governs the course of the process. If the second stage is rate- limiting, the process follows the laws of chemical kinetics [6]. Many environmental processes obey mixed order kinetics.

The leaching intensity was calculated as [7]:

$$I\ (h^{-1}) = \frac{[U]_{leachate}\ \ g/mL\ \ \text{leachate volume mL}}{[U]_{sample}\ \ g/g\ \ \text{sample weight g}\ \ \text{time h}} \quad (1)$$

The values of I were 0.16±0.34, 6.34±3.18 and 0.07±0.1 h^{-1} for neutral, acidic and basic pH, respectively. Hence the leaching intensity is strong for acidic and very weak for other pH conditions [7].

The values of I were 1.09±0.65, 0.61±0.4, 0.49±0.25, 0.38±0.13 and 0.35±0.12 h^{-1} for, 63-125 m, 125-212 m and 212-500 m, respectively. Hence leaching intensity is medium for <36 m, 36-63 m and very weak for the other particle sizes [7].

It was observed that the leaching intensities were high in the initial stages and reduced with time, similar to the trend in Fig. 1. This may be due to the initial rapid process of leaching being taken over by the later slower processes.

Conclusion

The leaching intensities obtained from dynamic leaching experiments were mostly medium to very weak, indicating that the mobility of uranium from the waste matrices is low. Hence there is a low chance of groundwater transport of uranium.

The uranium bearing tailings showed increased leaching in acidic pH due to pyritic nature of the wastes. Increased surface area in smaller particle sizes caused enhanced leaching in these particle size fractions.

The leaching intensities showed a decreasing trend in general, due to an initial faster process of leaching being followed by a slower process. The leaching process can thus be considered to obey mixed order kinetics.

References

[1] V. H. Kennedy, A. L. Sánchez, D. H. Oughton, A. P. Rowland, Analyst. 122 (1997) 89.

[2] IAEA-TECDOC-370, (1986) 7.

[3] G. R. Dikshitulu, R. Dhana Raju, R. Gajapathi Rao; Journal of Atomic mineral science, 5 (1997) 81.

[4] Townsend, Timothy, Jang, Yong-Chul, Tolaymat, Thabet. Report #03-01(A), Gainesville, Florida (2003).

[5] A. Chakrabarty, S. Mohapatra, R.M. Tripathi, V.D. Puranik, H. S. Kushwaha, Accred Qual Assur, 15(2) (2010) 119.

[6] P. S. Fedotov, B. Y. Spivakov. Russ Chem Rev, 77 (2008) 649.

[7] Y. Wang, International Journal of Coal Geology, 40 (1999) 103.

Determination of ^{210}Po in Leafy Vegetables and Annual Effective Dose Assessment to the Inhabitants of Mumbai city, India

J.S. Dubey[1], S. K. Sahoo[1], A. Nair[2], S. Mohapatra[1], A.C. Patra[1], P. Lenka[1], P.M. Ravi[1] and R.M. Tripathi[1]

1. *Health Physics Division, Bhabha Atomic Research Centre, Trombay, Mumbai 400085, India; E-mail: jay14982@gmail.com*
2. *SIES College of Arts, Science and Commerce, Nerul, Navi Mumbai*

Present study deals with the measurement of activity concentration of ^{210}Po in leafy vegetable of Mumbai city and corresponding ingestion dose assessment to the population. ^{210}Po activity levels ranged from 44.5-183.3 with an average value of 81.8 mBq/kg. Minimum activity of ^{210}Po was found in shepu and maximum in methi. The concentration reported here is slightly more than the UNSCEAR value. The estimated total effective dose was found to vary from 0.3 – 1.4 with an average value of 0.6 Sv/y, which is about 1% of global average total ingestion dose due to ^{210}Po.

Introduction

Natural radioactivity is ubiquitous and a fact of life which mainly arises from the disintegration of uranium (^{238}U and ^{235}U), thorium (^{232}Th) and their radioactive decay products and potassium (^{40}K) present in the earth's crust. Globally the annual average radiation dose received by members of the public is 2.4 mSv and it varies in the range of 1 – 13 mSv [1]. Out of the ingestion dose due to ^{238}U, ^{235}U and ^{232}Th series radionuclides, about 80% of the dose is due to ^{210}Po and ^{210}Pb. The half-life of ^{210}Po is 138.38 days and has a specific activity of 4.6 Ci/g for ^{210}Po. The toxicity of ^{210}Po is comparable to ^{239}Pu and about 5 times greater than that of ^{226}Ra [2]. ^{210}Po is a well known human carcinogen. Many studies are available on the effect of ^{210}Po on kidney and liver [3]. The main source of ^{210}Po in the environment is ^{222}Rn gas which diffuses into the atmosphere from rocks and soil where it ultimately decays to ^{210}Pb, ^{210}Bi and then to ^{210}Po in the atmosphere. ^{210}Po attaches itself further electrostatically to aerosol particles and are transported back to earth's surface to soil, aquatic environments and subsequently to plants by dry deposition and wash out [4-6]. ^{210}Po is directly taken up by plants either from the soil through the root system or by foliar absorption from the air. [5]. Main exposure routes of the radionuclides are inhalation and ingestion of foods and drinking water. The intake of radionuclides through ingestion of leafy vegetables depends on the elemental concentrations in the leafy vegetables and the dietary habits of the population. The present work deals with the ^{210}Po activity concentration estimation in leafy vegetables of Mumbai city and estimation of the radiation dose to members of the public.

Experimental

Considering the dietary preferences of the local population of Mumbai six varieties of green leafy vegetables in triplicate, 1 kg each were collected from three wholesale markets (Byculla, APMC and Navi Mumbai) in the city of Mumbai. These are the largest wholesale markets for vegetables and fruits and the local suppliers for the city of Mumbai and Navi Mumbai. Hence collection of samples from these markets ensured that the vegetable consumption by the entire city of Mumbai and Navi Mumbai was considered for the present study. Samples were processed as per IAEA recommendations [7]. Spontaneous chemical deposition technique among all other techniques produces a thin uniform layer for ^{210}Po determination by high resolution alpha spectroscopy. In the present work determination of ^{210}Po was optimized for a thin source preparation using the autodeposition on silver disk technique. Six grams dry weight of each dried sample was spiked with ^{209}Po as a yield tracer. Each sample was digested using concentrated nitric acid and per-chloric acid. When the sample was cleared, it was evaporated to dryness. The ^{210}Po was autodeposited onto a silver disk under conditioning of 250 mL of 0.5 M hydrochloric acid with constant temperature of 80°C with a two and half hour deposition time after reduction of iron with ascorbic acid (200 mg). The silver disc was counted with the alpha spectrometer (Passivated ion-implanted silicon detector, active area of 450 mm^2). Details of the instrumentation are given elsewhere [8]. The ^{210}Po activity concentration was calculated with tracer yield varied typically between 70 - 80%.

Result and Discussion

The specific activity of ^{210}Po in leafy vegetables consumed by residents of Mumbai City, India was varied from 44.5 - 183.3 of fresh weight with mean value of 81.4 mBq/kg. The maximum and minimum ^{210}Po concentrations were observed in Methi and shepu, respectively. A graph of mean ^{210}Po concentration in leafy vegetable of different locations is given in Fig. 1. Statistical parameters of the data showing a large variation of the observed ^{210}Po concentration in leafy vegetables may be attributed to local geology and uptake characteristic of different plant species (Table 1). The concentrations reported in the present study are lower than the reported value of Kalpakkam [9], but slightly higher than the UNCEAR value [1]. The annual effective ingestion radiation dose to members of the Public (adult, age > 17 y) was calculated using IAEA

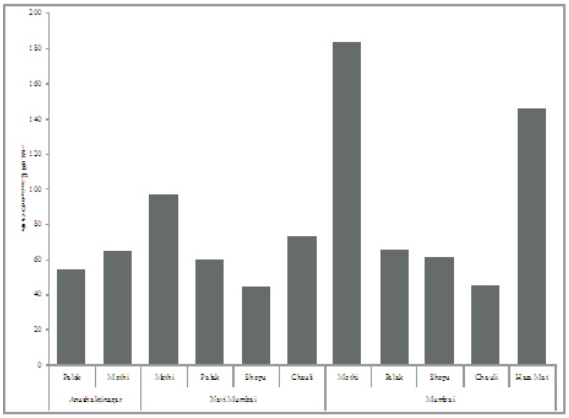


Fig. 1 Mean activity concentration of ^{210}Po in leafy vegetables of different locations

dose conversion factor for ^{210}Po [10] and national intake rates of vegetables (17 gm/d) [11]. The estimated total effective dose due to ^{210}Po through leafy vegetable consumption was found to vary from 0.3 – 1.4 with an average value of 0.6 Sv/y which is about 1% of global average total ingestion dose due to ^{210}Po.The individual contribution of different leafy vegetables to the total dose is shown in Fig. 2. The lower value of dose may be attributed to low activity concentration observed as compared to other reported values and less intake rate of leafy vegetables. ^{210}Po being a naturally occurring radioisotope, there is no national and international prescribed limits on annual effective dose.

Table 1: Summary statistics of the observed data

Statistical parameters	^{210}Po (mBq/kg)
Mean	81.4
Median	64.7
Standard error	13.3
Standard Deviation	44.3
Sample variation	1960.2
Kurtosis	2.0
Skewness	1.7

Conclusion

The activity concentration of ^{210}Po in leafy vegetables consumed by residents of Mumbai City, India was varied from 44.5 - 183.3 of fresh weight with mean value of 81.4 mBq/kg. The estimated total

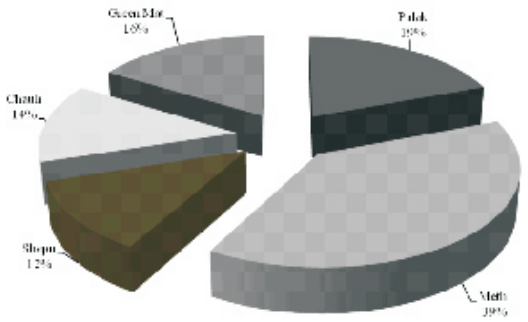


Fig. 2 Individual contribution of different leafy vegetables to the total dose

effective dose due to ^{210}Po through leafy vegetable consumption was found to vary from 0.3 – 1.4 with an average value of 0.6 Sv/y which is about 1% of global average total ingestion dose due to ^{210}Po. The lower value of dose may be attributed to low activity concentration observed as compared to other reported values and less intake rate of leafy vegetables.

References

[1] UNSCEAR, Sources and Effects of Ionising Radiation, United Nations, New York, (2008).

[2] NRC. BEIR IV. Washington, D.C.: National Academy of Sciences, National Research Council, Academy Press; (1988).

[3] International committee for research on cancer, IARC, (1988) 43.

[4] PL Santos, RC Gouvea, IR Dutra, VA Gouvea. J Environ Radioact (1990) 141.

[5] T. Karali, S. Olmez G. Yener. Appl Radiat Isot., 47 (1996) 409.

[6] Pietrzak-Flis Z, Skowronska-Smolak M. Sci Total Environ., 162 (1995) 139.

[7] International Atomic Energy Agency. Technical Report Series(Vienna: IAEA) (1989) 295.

[8] S. Mohapatra, S.K. Sahoo, J.S. Dubey, P. Lenka, R.M. Tripathi and V.D. Puranik. IARP-(2012) 54.

[9] Kannan, M.A.R. Iyengar, R. Ramesh, Applied Radiat Isot., 54 (2001) 663.

[10] IAEA, BSS, Safety Series no. 115 (1996).

[11] R. M. Tripathi, A. Vinod Kumar, S. T. Manikandan, S. Bhalke, T. N. Mahadevan, V. D. Puranik, Atmospheric Environ, 38 (2004) 135.

^{226}Ra Estimation Using A Continuous Radon Monitor of Semi Conductor Detector Type

C.G. Sumesh[1], S.K. Sahoo, A. Vinod Kumar[2], P. M. Ravi, and R.M. Tripathi

1. *Health Physics Division,Bhabha Atomic Research Centre, Trombay, Mumbai 400 085, India; E-mail: sumeshcg@barc.gov.in*
2. *Radiation Safety Systems Division, Bhabha Atomic Research Centre, Trombay, Mumbai 400 085, India*

The estimation of radium using emanometry technique is an established procedure for low level of radium measurement. The utility of a continuous radon in air monitor works on the principle of alpha spectrometry of deposited radon progenies on the detector surface has been studied in detail for radium estimation. The radium concentration measurement using this monitor is found to be convenient, simple as compared to the emanometry technique. The volume of the sample for analysis can be increased thereby minimum detection limit of the measurement can be brought down. The interference of other radium isotopes can also be avoided.

Introduction

Radium is one of the significant naturally occurring radionuclide having four isotopes. These are -emitting ^{226}Ra ($T_{1/2}$ = 1,600 years) in the uranium series, -emitting ^{223}Ra ($T_{1/2}$ = 11.43 days) in the actinium series and -emitting ^{228}Ra ($T_{1/2}$ = 5.75 years) and -emitting ^{224}Ra ($T_{1/2}$ = 3.66 days) in the thorium series. Radium isotopes are radiologically significant, because of the following reasons (i) their decay a number of other alpha producing short lived daughter nuclides are produced and (ii) radium is easily incorporated in the bones of mammals due to their chemical and biological behavior, similar to that of other alkaline earth metals (Ca, Sr, Ba) and can cause enhanced radiation dose to man. Studies on natural background radiation show that the major contribution of radiation dose received by population is through inhalation pathway contribution from radon (^{222}Rn) gas. Since radium (^{226}Ra) is the parent of radon, it is imperative to measure radium content in various matrices that are present in the environment. Among the various methods available for the measurement of radium, gamma spectrometry and radiochemical method are the two extensively used measurement methods. In comparison with these two methods, the radon emanometry technique is a simple and convenient method for low levels of ^{226}Ra estimation.

The presence of thorium isotopes in environmental samples cannot be neglected. Measuring radium from radon emanation using scintillation cells will over estimate the radium content of sample. Therefore an instrument measuring both radon and thoron discriminatively will be useful in determination of accurate amount of radium (^{226}Ra) present in the sample.

Materials and Methods

The radium (^{226}Ra) concentration of any sample can be estimated by measuring the buildup activity of its progeny radon (^{222}Rn) in the sample (Raghavayya, 1977). Samples are loaded in a bubbler in liquid form. The sample will leave for buildup of radon gas in the sample. After attaining equilibrium with radium, radon gas is collected in a scintillation cell. Photomultiplier tube assembly counts the photon events from the scintillation cell and the events are converted into respective concentrations. However, in scintillation cell radon concentration is measured without energy discrimination of alpha particles may have some interference due to the presence of thoron. This leads to the over estimation of the radon concentration. A silicon-based semi-conductor detector (RAD7, Durridge Company Inc) works on the principle of alpha spectrometry technique has been utilized to measure radium in liquid samples. The detail of the instrument is given else were (Sumesh et al., 2012). The concentration of the gases can be calculated using the counts due to ^{218}Po (sniffer mode: 0.324 CPH/Bq m^{-3}) or from the sum of the counts in both windows due to ^{218}Po and ^{214}Po (normal mode: 0.649 CPH/Bq m^{-3}).

Results and Discussion

Standard radium solution diluted with double distilled water in different concentration used to calibrate the method. RAD7 was operated in sniff mode. The result of the study is shown in Fig. 1. A good correlation has been obtained. The comparison of the methods is shown in Table 1. In the table the minimum detection limit (MDL) is calculated using a radon build up period of 7 half life, counting period of 10 minutes, delay period of 200 minutes in scintillation cell. In RAD7, volume of the sample is 250 mL, background concentration 10 Bq m^{-3}, volume of the system 1000 mL, partition coefficient 0.26 and concentration of the measured sample is 10 Bq m^{-3}. The MDL is nearly equal in both the measurement set up however; a more accurate radium concentration can be achieved by RAD7 measurement.

Conclusion

Commercial radon thoron discriminating monitor has been utilized for radium estimation of liquid samples utilizing the radon emanation property. One to

one correlation has been observed between the methods. In RAD7 monitor, large volume of the sample can be used for radon estimation thereby decreasing the minimum detection limit of the method. In addition to this large size of the volume decreases the effective time required for sample preparation. Instrument can be continuously used for measurement of radon since the background build up of ^{214}Po will not affect the concentration measurement.

References

[1] Raghavayya M (1977). A study on the distribution of radon in uranium mines. Report No. BARC I/452, Bhabha Atomic Research Centre, Bombay.

[2] Sumesh, C. G., Vinod Kumar, A., Tripathi, R.M., and Puranik, V.D., Radiation Protection Dosimetry, pp. 1-7 doi:10.1093/rpd/ncs118.

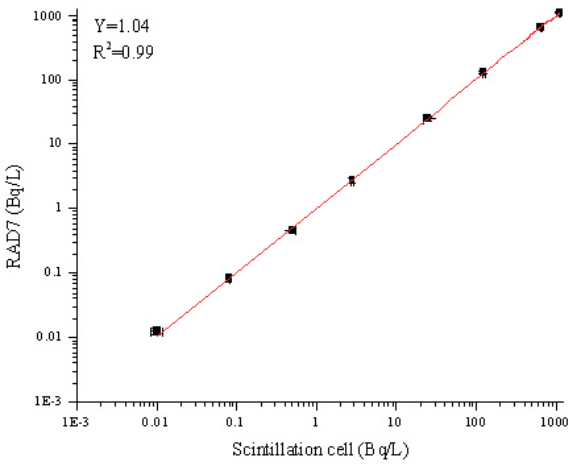


Fig. 1 Linear fit of radium concentration measured using scintillation cell and RAD7

Table-1: Comparison of Emanometry methods using Scintillation cell and Continuous radon monitor

Emanometry method		
	Scintillation cell	RAD7
1	Gross counting of alpha emitting radon and progeny	Counting of Po-218 and Po-214 alphas
2	Vacuum collection of sample is required	Vacuum collection is not required
3	Waiting period of 200 minutes after collection of the sample is required for good no of counts	Sample can be counted immediately
4	Volume of sample is limited 50 ml	Any volume can be used
5	Partition coefficient need not be applied for radon concentration in water medium	Partition coefficient need to be applied for radon concentration in water medium
6	MDL 1 mBq/L	1 mBq/L
7	Thoron interference	Thoron interference is nil since spectrometry is done.

Estimation of Age Dependent Effective Dose due to intake of ^{226}Ra from Drinking Water in Vizag, India

V.K. Thakur, S.K. Sahoo, S. Mohapatra, N.S. Krishna, P. Lenka, A.V. Kumar, P.M. Ravi and R.M. Tripathi

Health Physics Division, Bhabha Atomic Research Centre, Trombay, Mumbai 400 085, India;
E-mail: virendert@rediffmail.com

As a part of the ongoing baseline survey, present work deals with the measurement of ^{226}Ra concentration in ground water samples collected around Bhabha Atomic Research Center (BARC) site Vizag by emanometry technique and subsequent estimation of age dependent effective dose to the people inhabited in that area. The mean activity concentration of ^{226}Ra was 15.8 mBq/L which is much lower than the WHO guideline value of 1 Bq/L. The highest dose was observed for the age group of 14-18 yr (male). The dose for all age group are ranged between 2.2-56 which is well below the WHO recommended dose level of 100 Sv/y.

Introduction

Radium is widely distributed in small amount in the earth's crust and present in all uranium and thorium mineralization. Radium transfers from solid to aqueous phase through alpha recoil process and its concentration in aqueous bodies is controlled by sorbtion–desorbtion with the aquifer surfaces [1]. ^{226}Ra is an alpha emitter and a daughter product of ^{238}U series and the most abundantly found radium isotope due to its long half life (1600 yrs) [2]. ^{226}Ra is the most important radionuclide of concern in uranium series. Exposure due to this natural alpha emitter is of a matter of concern as radium is a bone seeker and a calcium homologue. Radium in water may leads to two main radiological concerns viz. intake of ^{226}Ra through drinking water and high level of ^{226}Ra in water may indicates the soil contamination or elevated radium concentration in deep geological formation. Thus accurate estimation of ^{226}Ra in various environmental matrices is essential in order to assess the dose to the inhabited population. Water intake is an essential part of human diet may contribute to chronic radiation exposure [3]. The contribution of drinking water radioactivity to the total exposure may be small but important as it directly enters human digestive system. Intake of water may vary due to age, sex, metabolic activities of humans. The establishment of baseline radiation level before commencement of any nuclear facility in any region is a prerequisite. The objective of the present study is to generate a baseline database and estimate the age dependent effective dose to the general population due to ^{226}Ra from intake of water around the BARC site at Vizag.

Experimental

Drinking water samples were collected upto 30 radius surrounding the BARC campus following the standard protocol [4]. The period of sampling was between 2009-2013 and it's an ongoing part of the baseline survey. Samples were all from ground water sources as ground water is the major drinking water source in the study area. Details of the study area are given elsewhere [5]. Twenty liter of water samples was collected at different depths in pre-acid cleaned polyethylene containers to avoid wall absorption. The water samples were preserved after filtration and acidification. Determination of ^{226}Ra was done by emanometry technique using scintillation cell and radon bubbler [6]. Pre concentrated water samples were allowed in a bubbler for the growth of ^{222}Rn (7 half lives of ^{222}Rn) gas and then subsequently build up radon gas collected in a scintillation cell for alpha counting, after attaining equilibrium with daughters. The ^{226}Ra content of the sample can be derived by using the appropriate build up and decay factors for ^{222}Rn, which are a function of the buildup period and decay constant of ^{222}Rn [6]. The efficiency of the radon stripping from the solution depends on factors such as bubble size and the total volume of flushed gas. Stirring the solution enhances the radon removal [7]. Details of the instrument and experimental procedure are given elsewhere [8].

Results and Discussion

The activity concentration of ^{226}Ra was varied between 8.0-31.4 with an average value of 15.8 mBq/L which is well below the guideline value of water quality parameter of 1000 mBq/L provided by WHO [9]. According to WHO drinking water containing ^{226}Ra below 1 Bq/L is acceptable for lifetime consumption. The repeatability of the measurement varied between 2-5%.

Effective dose due to ingestion of ^{226}Ra through drinking water pathway for population of all age groups can be computed by using the activity concentration, IAEA dose conversion factors [10] and water intake rates [2, 11]. The water intake rates taken for the infants (0-6 months old), children (7-12 months old), 1-3 and 4-8 are 0.7, 0.8, 1.3 and 1.7 L day^{-1}, respectively. While the water intake rate considered for the age groups of males, 9-13, 14-18 and > 18 year old were 2.4, 3.3 and 3.7 L day^{-1} respectively. The water intake rate considered for the age group of females, 9-13, 14-18 and > 18 year old were 2.1, 2.3 and 2.7 L day^{-1}. For pregnancy and lactation duration the water intake rates considered were 3.0 and 3.8 L day^{-1}. The effective dose estimated for all age groups are ranged between

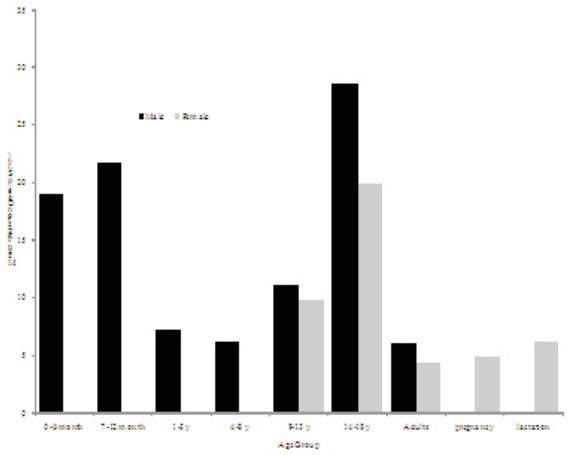


Fig. 1 Mean value of effective dose due to ^{226}Ra intake through drinking water with age group

2.2-56.7 Sv/y. The highest ^{226}Ra effective dose from drinking water intake per year (56.7 Sv/y) received by the population of age group 14-18 yr (male) which is well below than the WHO dose limit of 100 Sv/y. According to Fig. 1 the effective dose for infants is about 4 times that of adult population. This may be attributed to higher dose coefficient for infants (less than 12 months) than the adult group that means infants more radiosensitive. The dose in case of male is higher as compared to female which is due to higher water intake rates. The higher dose during lactation period may be attributed to the need of more water over the period. There is a decreasing trend with age upto 8 years and then it increases. The observed higher average ingestion dose for 14-18 year age group than infant is mainly due to higher intake rate because of higher metabolic rate, though the dose coefficient is lower than infants. The present value of ^{226}Ra concentration in drinking water and the effective age dependent dose is compared with the reported values of Brazil, Croatia and Florida [6, 12 and 13]. The value of ^{226}Ra concentration in present study is much lower than the reported value of ^{226}Ra concentration in ground water of Jaduguda uranium mining region, India [14].

Conclusion

Constant and periodic monitoring of natural radioactivity concentration in drinking water is important since chronic exposure may fatal to population health risk point of view. The result of the present study depicts that, the ^{226}Ra concentration in drinking water samples is well below the WHO limit of lifetime acceptable consumption. The effective dose estimated for all age groups are ranged between 2.2-56.7 Sv/y. The highest ^{226}Ra effective dose from drinking water intake per year (56.7 Sv/y) received by the population of age group 14-18 yr (male) which is well below than the WHO dose limit of 100 ìSv/y. Thus the ^{226}Ra concentration in the present study, as a part of baseline survey is acceptable for all age groups and there is no radiological protection problem associated with the consumption of radium in drinking water.

References

[1] Aleksandra Onishchenko, Michael Zhukovsky, Nenad Veselinovic, ZoraS.Zunic. Applied Radiation Isot. 68 (2010) 825.

[2] Boonsom Porntepkasemsan ,Kanitha Srisuksawad. Applied Radiat and Isot. 66 (2008) 1654.

[3] International Commission on Radiological Protection. Annals of the ICRP, 29, Nos. 1-2, Pergamon Press, Oxford 82 (1999) .

[4] IAEA. Technical Report Series 295. Vienna, Austria (1989).

[5] S. Mohapatra, S. K. Sahoo, A. V. Kumar, A. C. Patra, P. Lenka, J. S. Dubey, V. K. Thakur, R. M. Tripathi and V. D. Puranik. Radiat Protect Dosim, doi:10.1093/rpd/nct108, (2013) 1.

[6] Fa´ bio de Oliveira Lucas, Fernando Brenha Ribeiro. Applied Radiation Isot. 64 (2006) 735.

[7] H. Lucas, F. Markun, R. Boulenger,. The Environmental Behavior of Radium. 1, International Atomic Energy Agency Technical Reports series no 310, Vienna, 149–172 (Chapter 3-2) (1990).

[8] S.K. Sahoo, B.K. Rana, S.Mohapatra, J.S. Dubey, V.K. Thakur, P. Lenka, V.N, Jha, R.M. Tripathi and V.D. Puranik, Proc. of National Symposium on Environment 18 (2013) 57.

[9] World Health Organization, 3rd ed. (2003).

[10] IAEA, BSS. Safety Series no. 115 (1996).

[11] Dietary reference intakes for water, Washington, D.C. USA, (www.npa.edu).

[12] M. Bronzovic, G. Marovic. Health Phys. 88 (2005), 480.

[13] Joseph M. Smoak, James M. Krest. J. Environ Radioact. 89 (2006) 102.

[14] R. M. Tripathi, V. N. Jha, S. K. Sahoo, N. K. Sethy, A. K. Shukla, V. D. Puranik and H. S. Kushwaha. Radiat Protect Dosim. 148(2) (2012) 211.

Measurement of Environmental Radon at Mangalore Karnataka, India

T.K. Agarwal, B.K. Sahoo, B.K. Sapra

Radiological Physics and Advisory Division, Bhabha Atomic Research Centre, Mumbai 400085, India;
E-mail: tarun@barc.gov.in

Soil is the major contributing source for Radon. A comprehensive study has been carried out at Mangalore, Karnataka, under which radon soil gas concentration, radon surface and mass exhalation rate from the soil has been measured. Data generated in this study would be useful to obtain the multi parameter such as source term, radon diffusion length, soil properties etc. as well as to validate the diffusion-time model.

Introduction

It is well known that inhalation of radon (^{222}Rn), thoron (^{220}Rn) and their decay products contributes the largest fraction (52%) of radiation dose to humans, received from natural background radiation [UNSCEAR 2000]. That is why, it is important to study the environmental radon, thoron and their decay products. This paper presents the radon-thoron studies conducted at Mangalore region. In this study, experiments were carried out for measuring radon concentration in soil gas, in situ radon flux at different locations in the Mangalore city.

Materials and Method

In situ measurement of radon flux from the soil was carried out with accumulator technique and indigenously developed portable radon monitor (SRM) monitor. Also, Radon mass exhalation rate was measured from the soil samples, collected from the different location at Mangalore. Besides, Radon concentration in soil gas was measured using soil probe and SRM.

In situ Radon Flux Measurement from Soil Surface

Experimental set up for the in situ measurement of radon flux is shown in the Fig. 1. At the end of the measurement, data for transient variation of radon concentration was retrieved. Figure 2 shows the build-up of radon concentration in the accumulator with time.

Least square fitting has been carried out using the appropriate models to yield the value of radon flux.

The following equation was used for this purpose:

$$C(t) = C_0 + C_m (1 - e^{t/\tau_e}) \quad (1)$$

where, C_m $kf\frac{A}{V}$ τ_e, C_0 is the initial radon concentration inside the accumulator (at t = 0) which is assumed to be the same as the steady atmospheric radon concentration and τ_e is the time constant of radon build-up. τ_e has a complicated dependence upon the dimensions of the chamber and the radon diffusion coefficient D in the matrix. It can vary from a few minutes for small chambers to several hours for large chambers. The value of k is typically about 0.88.



Fig. 1 Experimental set up for the In situ measurement of radon flux

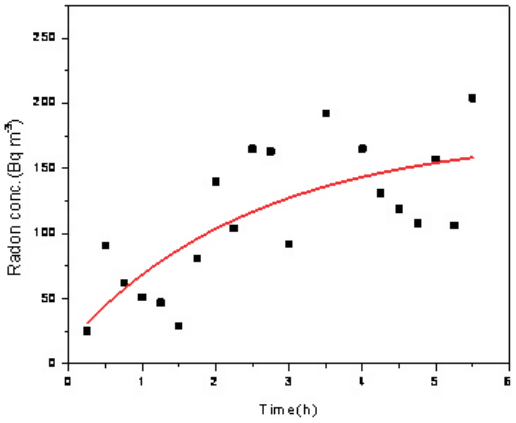


Fig. 2 Transient variation of radon concentration in the accumulator

Upon fitting the radon concentration data measured at regular intervals to Eq.1, flux f was calculated by estimating the parameters C_0, C_m and τ_e.

Radon Mass Exhalation Rate from Soil Sample

Experimental set up for measuring the radon mass exhalation rate from the soil is given in the Fig. 3.



Fig. 3 Experimental set up for measuring the mass exhalation rate from the soil sample

Buildup of radon concentration with respect to time is shown in the Fig. 4.

The radon concentration C (t) at time t since closing the chamber builds up according to the formula

$$C(t) \quad \frac{J_m M}{V_e} 1 \quad e \quad {}_e t \qquad C_0 e \quad {}_e t \qquad (2)$$

where, C_0 is the ^{222}Rn concentration (Bq m^{-3}) present in the chamber volume at t = 0, M is the total mass of the dry sample (kg). V is the effective volume (volume of chamber+ internal volume of ^{222}Rn monitor – volume of sample) (m^3). $_e$ is the effective removal rate for ^{222}Rn, which is sum of the leak rate (if existing) and the radioactive decay constant ( ) of ^{222}Rn (h^{-1}) and t is the measurement time (h). Here, leakage rate is negligible so effective removal rate ($_e$) equals to decay constant of radon ( ). For the shorter duration of measurements, Eq.2. can be approximated as:

$$C(t) \quad \frac{J_m M}{V} t \quad C_0 \qquad (3)$$

This represents a straight line having slope $\frac{J_m M}{V}$.

The mass exhalation rate was estimated using the slope obtained by the linear fitting of the concentration data with respect to time.

Measurement of Radon Concentration in Soil Gas

Concentration of radon in soil gas was measured at different location in Mangalore. For this purpose, soil gas was sampled by inserting the soil probe at varying depths. Radon concentration was then measured using SRM.

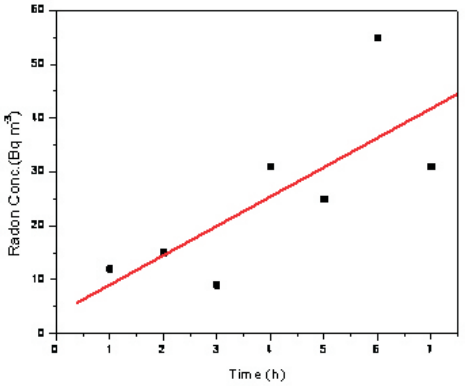


Fig. 4 Linear fitting of radon concentration data with time

Results and Discussion

In situ Radon flux varied from 6.34 1.95 to 49.17 7.73 Bq m^{-2} h^{-1}. Radon mass exhalation rate from the collected soil samples ranged from 9.61 2.5 to 18.5 3.2 Bq kg^{-1}h^{-1}. The values of radon concentration in soil gas were found to be varying from 2.35 0.45 to 76.45 3.15 k Bq m^{-3} at the depth of 20 cm to 70 cm respectively.

Acknowledgements

Authors would like to thank Shri DAR Babu, Head, RP&AD BARC for his encouragement and support.

Reference

[1] UNSCEAR, United Nations scientific committee on the effects of atomic radiation. Sources and effects of ionizing radiation. Report to the General Assembly of the United Nations with Scientific Annexes, United Nations, New York (2000).

[2] Sahoo B.K., Mayya Y.S., Agricul. and fores. metro. 150 (2010) 1211.

Spatial Distribution of Tritium in Surface Water and Assessment of Ingestion Dose

C.K. Rupali[1], B. Sonali[2], Priyanka Reddy[2], S.K. Jha[1] and R.M. Tripathi[1]

1. *Health Physics Division, Bhabha Atomic Research Centre, Trombay, Mumbai 400085, India; E-mail: chakor@barc.gov.in*
2. *Radiation Safety Systems Division, Bhabha Atomic Research Centre, Trombay, Mumbai 400085, India*

The present study focuses on the distribution of tritium in drinking water samples from Mumbai and other suburban areas. Measurement of tritium in the drinking water was carried out using an ultra-low background LKB Quantulus Spectrometer, model 1220.The concentration of tritium in the drinking water ranged between 12.3-19.8TU with a geometric mean of 13.3TU.The observed values doesn't indicate any fresh input of tritium and are well within prescribed limit of 740 Bq/L (approx. 6,271.2 TU) given by USEPA for tritium ingestion through drinking water. The estimated dose due to tritium ingestion through drinking was 0.02 Sv/y which is negligible when compared to the limit of 1000 Sv/y assigned to general public.

Introduction

Tritium (^{3}H) is a radioactive isotope of hydrogen with a half life of 12.3 years and emits beta particles with a maximum energy of 18.6 keV (average 5.7 keV) and it decays to ^{3}He. Hydrogen is the most abundant element in the universe, comprising approximately 90% of the luminous universe by weight. Ordinary hydrogen (^{1}H) accounts for greater than 99.985% of all naturally-occurring hydrogen, whereas deuterium (^{2}H) comprises approximately 0.015%. By comparison, tritium (^{3}H) represents only approximately 10^{-16} % of naturally occurring hydrogen. Chemical properties of tritium are identical to those of hydrogen. It is produced both naturally and artificially [1].Tritium is naturally produced primarily through the interaction of cosmic ray protons and neutrons with gases (including nitrogen, oxygen and argon) in the upper atmosphere. Around 99% of the tritium produced in the upper atmosphere is oxidised to tritiated water (HTO) and dispersed into surface water. Tritiated vapour mixes with water vapour and enters the hydrosphere, and thereafter circulates as an integral part of water cycle. Tritium production through natural processes has resulted in a global steady-state inventory of approximately 2.65 kg, corresponding to about 9.6 x 10^5 TBq during pre nuclear era [1]. The quantity of tritium present in the biosphere considerably increased due to number of anthropogenic sources which account for the dominant portion of the global tritium inventory. Anthropogenic tritium sources include thermonuclear detonations during nuclear weapons testing, special fusion bombs and commercial production for medical diagnostics, radiopharmaceuticals etc. [1]. Global inventory of tritium due to these weapon testing was estimated to be about 640 kg and one sixteenth of this quantity i.e. 40 kgs remains on the earth surface even today [2]. Most of the bomb produced tritium has been deposited to World Ocean either by precipitation, surface run off or by molecular exchange. Of the total natural tritium inventory, almost 99% has been estimated to occur in the oceans, with less than 1% occurring in the atmosphere and in the groundwater [1]. According to UNSCEAR 2000 report, drinking water is considered to be an important factor in increasing the natural radiation exposure in humans. The determination of natural radionuclides in drinking water is crucial, when these radionuclides are taken in to the body by ingestion. Tap water is used for domestic work as well as for consuming. Therefore it is important to access the radioactivity content in the water frequently to check the compliance with regulatory guidelines [3].

This paper describes the spatial distribution of specific activity of tritium in drinking water samples collected from Mumbai and other suburban areas and assessment of ingestion dose.

Materials and Methods

Study Area, Sample Collection and Preparation

Tap water samples were collected from different locations in Navi Mumbai and Mumbai. Approx.100 mL of samples were collected in clean and dry plastic bottles. All the water samples were filtered through Whatman filter paper No.42 and distilled to remove the nutrients and dissolved salts. This step is essential prior to counting, as the direct counting of the samples can lead to quenching and chemiluminiscence owing to the presence of more salt. The contribution from ^{40}K, associated with potassium content of water, is also eliminated through this method. The distillate thus obtained was used for estimation of tritium contents. The tritium content of all these samples was determined by liquid scintillation counting, using an ultra-low background LKB Quantulus Spectrometer, model 1220. A known aliquot (8 mL) of the sample was mixed with 12 mL of commercially available scintillator (Quick Safe 400) in a 22 ml High Density Polyethylene (HDPE) counting vial, thoroughly mixed and analysed for tritium response. Each sample was counted for 50 min. and was repeatedly counted 10 times to get better statistics. The background of the detector system was

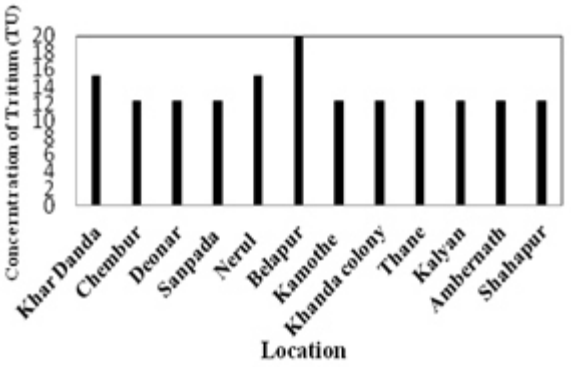


Fig. 1 Plot of Activity of tritium in drinking water samples from different locations in Mumbai & suburban areas

determined using tritium free water (Mili-Q water). Counting efficiency for each analysis was determined using a tritium standard source [4]. The activity of tritium was calculated using the formula as given below

$$\text{Tritium Activity } \frac{\text{Bq}}{\text{L}} = \text{Netcps} \quad \text{SD} \quad \frac{100}{\text{E}} \quad \frac{1}{\text{V}} \quad (1)$$

Result and Discussion

The Ultra-low Background LKB Quantulus Spectrometer, Model 1220 (Wallac, Finland) has an advantage over the other liquid scintillation counter as it is having an ability to detect the lower level upto12.3TU (BDL) in drinking water. In this system, background is minimized by an optimized combination of active and passive shields. Fig.1, gives the concentration of tritium in drinking water collected from Mumbai and other suburban areas. In the present study, the concentration of tritium in water samples collected from Mumbai and other suburban areas ranged between 12.3-19.8TU with a geometric mean of 13.8TU. These results are comparable with the previous survey which was ranging from 8.8-61TU with a geometric mean of 25.3TU [5]. This value for drinking water is lower than ^{3}H the limit of 740 Bq L^{-1} established by EPS (USA) [6].

The estimated values were much lower than that observed in water samples of Centro Nuclear ARAMAR, Brazil [7] and in the Yenisei river water, Russia [8] where the background ^{3}H concentration is 219.5TU and 33.1TU respectively.

Methodology for Ingestion Dose Assessment

The ingestion dose due to tritium in drinking water is estimated by

$$\text{Ingestion dose} = C \ \frac{\text{Bq}}{\text{L}} \quad \text{C.R.} \ \frac{\text{L}}{\text{Y}} \quad \frac{\text{Sv}}{\text{Bq}} \qquad (2)$$

Where, C is concentration of tritium in drinking water, C.R is consumption rate, and DCF is Dose Coefficient for tritium (1.8×10^{-11} Sv/Bq).The water consumption rate is considered as 2 L/day for an Indian reference man.

Fig.2, gives the dose due to tritium in drinking water to the public staying at different locations of

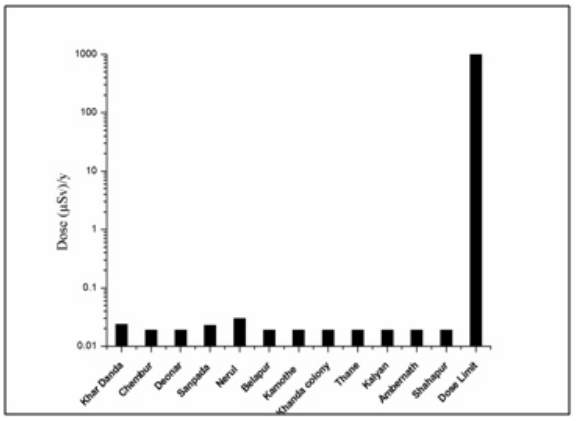


Fig. 2 Plot of Dose due to tritium in drinking water to the public staying at different locations in Mumbai & suburban areas

Mumbai and other suburban areas. In view of the new limits (0.3 Sv/y) for the tritium in drinking water proposed by the Ontario Drinking Water Advisory Council (ODWAC) is based on the three times the dose from naturally occurring tritium. In the present study, the obtained dose of 0.05 Sv/y can be assigned to the dose from the naturally occurring tritium.

Conclusion

It is concluded from the present study that the activity concentration in all the water samples was within acceptable levels. A large variation in the concentration of tritium in the water samples may be due to non-uniform distribution of tritium in continental water masses compared to oceanic masses. The estimated ingestion dose due to tritium in drinking water received by the public is negligible and can be assigned due to naturally occurring tritium.

References

[1] The Tritium Studies Project INFO-0792, Canada's Nuclear Regulator, Report prepared for the CNSC by EcoMetrix Incorporated in association with RWDI Air Inc.(2009).

[2] Robert L. Michel, Nature 263 (1976) 103.

[3] Sources and Effects of Ionizing Radiation, United Nations Scientific Committee on the Effects of Atomic Radiation, New York NY USA (2000).

[4] A.G.Hegde,L.N.Sharma,S.Chandramouli, D.D.Rao, V.M.Matkar, P.C.Verma and M.P.Rajan, ESL Procedure Manual (1998).

[5] S.S.Gogate, S.H.Sadarangani, T.M.Krishnamoorty and S.D.Soman India Journal of Pure and Applied Physics, 22 (1984) 729.

[6] ASTM, Standard Methods for the Examination of Water and Wastewater, 19th ed., (1995) 739.

[7] Moraes, M.A.P.V. Sartoratto, M., Sartoratto, B.E.L., Oliveira, C.B., Mendes, V.A., Radiat. Meas. 35 (2002) 333.

[8] M Bolsunvsky, A.Y., Bondarev, L.G., J. Environ. Radioactivity 66 (2003) 285.

Role of Lead (Pb^{2+}ion) as modifier as well as former on the properties of Lead-Iron Phosphate and Borosilicate Simulated nuclear waste glasses

G. Hazra[1], P. Mitra[2], T. Das[3], P. P. Malik[4]

1. *Department of Chemistry, Kalna College, Burdwan 713409, W. B., India; E-mail: hazragoutam1980@rediffmail.com*
2. *Department of Physics, The University of Burdwan, Burdwan 713 104, W.B., India*
3. *Department of Chemistry, The University of Burdwan, Burdwan 713 104, W.B.,India*
4. *Department of Chemistry, B. B. College, Asansol, Burdwan 713303, W.B., India*

Lead-iron phosphate glasses (LIP) are a promising new waste form for the safe immobilization of radioactive waste for long term disposal due to lower aqueous corrosion rate (10^2 to 10^3 times lower), lower processing temperature etc. LIP glass can be prepared at temperatures as low as 750°C. The leaching study of such glasses under Soxhlet condition shows lead (Pb^{2+}) to be a superior candidate as modifier towards leach resistance, $Fe^{3+/2+}$ and Pb^{2+} have the dual role as glass formers/ modifier which ultimately has an effect on the chemical durability of these glasses.

Introduction

The future development of nuclear energy depends largely on the success programmes and management of radioactive wastes generated at various stages of the nuclear fuel cycle. Nuclear waste glasses are to be stored for several thousand years under such conditions before the radioactivity die down, corrosion study of such glasses under varying environmental conditions will be helpful in understanding the durability and fission product release from such glasses[1]. In the present works simulated glass both phosphate and borosilicate composition as that of the waste are selected and melted from batch oxides. Finally these glasses after setting proper melting conditions are subjected to leaching studies under Soxhlet condition. Based on the findings of such studies recommendation will be forwarded in terms feasible glass composition which will be selected as nuclear waste glass. In this study composition of the glasses melted with PbO as modifier are given as a special emphasis.

Experimental

Preparation of Glass Batches and Melting Operation

The glass batches were prepared from the AR graded ingredients, were dried and taken in high alumina crucibles and fired in a muffle furnace fitted with programmer in the range 750-1000°C for soaking periods of 30 min-60 min under ambient condition. In melting operation, the temperature and time of meting are the principal factors and are to be monitored (Table 1).

pH Study

For the pH determination of the leachate solution, the bulk glass was powdered to 0.3-0.425 mm size. 1 g of the glass powder was taken in a beaker with a fixed volume of 40 mL of distilled water. It was stirred with a magnetic stirrer for a definite period of time of 2 mins. The pH of the liquid was determined by a pH meter (Systronics digital pH meter 335) [ASTM: E70]. Such measurements of pH were done at regular intervals of 1 h, 2 h, 3 h, 4 h and 5 h respectively, the mixture being stirred after each 15 min. Results of such pH study are shown in Table 2.

Table-1:Compositions of different glasse (Wt.%)

Glass	SiO_2	$Na_2B_4O_7$	PbO	BaO	Fe_2O_3	CeO_2	SrO	P_2O_5	M.P. (±20C)
BS4	39.6	20	33.4	7	-	-	-	-	800
BS6	29.6	20	38.4	-	-	7	5	-	800
BS7	40	24	-	-	13	-	20	-	
LIP1	5	-	16.7	25	12.5	-	-	40.8	1000
LIP2	17.6	-	16.7	25	12.5	-	-	28.2 (H_3PO_4)	Not glass formed
LIP3	-	-	49 (Pb_3O_4)	-	8	10	-	33	950
LIP4	-	-	52.4	-	7.9	6.5	-	33.2	750
LIP5	-	-	49 (Pb_3O_4)	-	8	-	10	33	900
LIP6	-	-	49 (Pb_3O_4)	-	8	5	5	33	900
LIP7	-	-	49 (Pb_3O_4)	10	8	-	-	33	950

Leaching Study

For leaching study about 0.5 gm of each sample glass accurately weighed which was earlier crushed to 300-425 mesh was taken in a nylon net, the dimension of which was such that the glass powder did not pass out through it. Next it was vapour distilled in Soxhlet apparatus with a r.b. flask (500 mL capacity) fitted with condenser for varying period of time maximum upto 24 h, the heating being done by a heating mantle. [ASTM: C1285-02(2008)]

Table-2: pH of different glasses at different time intervals

Glass	1 hr.	2 hr.	3 hr.	4 hr.	5 hr.
LIP1	6.85	6.89	7.03	6.95	6.43
LIP3	7.05	7.25	7.35	7.25	7.07
LIP4	7.36	7.25	7.26	7.24	7.24
LIP5	7.02	7.06	7.09	7.13	7.12
LIP6	6.15	6.39	6.54	6.64	6.76
LIP7	5.78	5.84	5.76	5.80	5.63
BS4	7.18	7.33	7.53	7.06	6.96
BS6	7.95	7.48	7.44	7.27	7.28
BS7	7.79	7.44	7.51	7.37	7.39

Percent Weight Loss

The weight loss after each run of leaching was measured by a four-decimal electronic balance (Satorius) and was converted into % wt. loss and are as shown in Table 3.

Table-3: % weight loss of glasses at different time intervals

Glass	4 hr.	8 hr.	12 hr.	16 hr.	20 hr.	24 hr.
LIP1	1.3	0.84	0.33	0.07	0.20	0.49
LIP3	.139	0.0569	0.1194	0.0796	0.0	0.0
LIP4	0.08	0.3596	0.6817	0.1200	.1212	.1214
LIP5	0.65	0.14	0.0	0.0	0.0	0.0
LIP6	0.20	0.40	0.48	0.36	0.44	0.20
LIP7	0.00	0.0295	0.00	0.0886	0.0985	0.00
BS6	0.20	0.18	0.04	0.22	0.30	——-
BS7	0.23	0.89	1.2	1.4	0.57	——-

Results and Discussion

As a source of lead two ingredients were tried, viz., PbO and Pb_3O_4 with mixed results. For the formation of phosphate glasses two materials were tried e.g., P_2O_5 and H_3PO_4. As the earlier is a sticky material it was difficult to handle. The pH increase can be distinguished and correlated to the schematic phosphate network. At the beginning the P–O–M (M= Pb, Sr, Ce, Ba) bonds could be preferentially corroded with a release of phosphate groups in the leaching solution contributing to make up a drop in pH. Later on, the acidic medium could involve a corrosion enhancement with partial hydrolysis of P–O–P band P–O–Pb bonds. It is seen from leaching study(Table 3) that there is a decreasing trend in percent weight loss for the glasses BS6 and LIP1 both having PbO in their compositions whereas for the glass BS7 without PbO there is an increasing trend with time. Thus the role of Pb^{2+} as modifier in both borosilicate and phosphate systems is very distinct in enhancing its leach resistance. It was reported [2] that for lead iron phosphate (LIP) glasses a decrease in leach rate is observed, a finding being in good agreement with our finding. From Tables 3 it is evident that those glasses melted with Pb_3O_4 as source of Pb are found to be more leach resistant in comparison to other glasses melted with PbO as the source of Pb. The advantage of using Pb_3O_4 as batch material is that above 550°C it dissociates into PbO and O_2

$$\text{as, } 2Pb_3O_4 \quad 6\,PbO + O_2 \qquad (1)$$

which generates O_2 and ultimately take part into network O- sites additionally liberating PbO [3].

Conclusions

Lead was found to act as a good modifier and former as leach resistant [4]. The findings on pH of leachate solution have been explained in terms of ionic size, ionic radii and ionic potential of the modifier ions incorporated into the glass network. The dissolution of these glasses tends to decrease slightly with increasing O/P ratio and increasing (Fe+Pb)/P ratios.[5] A lead ion can react with an NBO and inhibit the reaction that destroys the structural component in the glass. Lead-iron phosphate glasses (LIP) are a potential candidate for immobilization of high level commercial and defence radioactive waste with leach rate $10^2 – 10^3$ times lower than the leach rate of a comparable borosilicate waste glass.

References

[1] J. Mukerji and A. S. Sanyal, Glass Technol. 45 (2004) 117.

[2] Kamizono I., Hayakawa S. and Muraoka S., J. Materials Science Letters. 10 (1993) 423.

[3] S. Jana, B. Karmakar and P.Kundu., Matt.Sc. of Poland, 25 (2007) 1127.

[4] Sales B.C., Boatner L.A., Science 226 (1984) 4670

[5] S.T. Reis, M. Karabulut b, D.E. Day, J. Nu. Materials 304 (2002) 87.

Active Measurement of Radon and Thoron Exhalation from Soil and Building Materials Samples and Effect of Grain Size

Neetika Chauhan[1], R.P. Chauhan[1], B.K. Sahoo[2], M. Joshi[2], B.K. Sapra[2]

1. *Department of physics, National Institute of Technology, Kurukshetra 136119, India; E-mail: neetika.nit@gmail.com*
2. *Radiological Physics & Advisory Division, Bhabha Atomic Research Centre, Mumbai 400 094*

Radon (^{222}Rn) and Thoron (^{220}Rn) emission from soil and building materials is considered as primary sources for inhalation dose to a person in indoor environment In view of this, experiments have been carried out to determine radon and thoron emission from samples of soil and building materials using BARC developed smart radon and thoron monitor. Samples that were subjected to analysis included soil, sand, cement, flyash, POP, snewcem, lime powder, chalk putty and wallputty Each sample was kept in a leak tight metal chamber, connected to a radon/thoron monitor to measure radon and thoron concentration at different time interval. Thoron being short-lived (half life of 55.6 s), a minimum thickness of building material was maintained such that the thoron surface exhalation rate will be independent of sample size. In case of radon, the air volume of the set up was kept sufficient enough to neglect the possible back diffusion effect. The influence of grain size on radon and thoron exhalation rates in soil and fly ash samples has been investigated by measuring the packing density and % porosity of samples

Introduction

Among many aspects for assuring healthy living zone like temperature, Humidity, tobacco smoke, vapor intrusion, ventilation, volatile organic compounds (VOCs): indoor radioactivity is one of the major issues. In the international radiation safety regime, ICRP, UNSCEAR, WHO, IAEA performed important role in estimating levels, effects and risks of ionizing radiation along with providing helpful safety standards, protection philosophy and recommendations for society. Ionizing radiation received by the living organism because of the presence of significant amount of indoor and outdoor environmental radioactivity have many health's implications [1-2]. In the present busy scenario, people use to spend a large fraction of their life time in the dwellings of house, school, offices and industry etc and the risk of health degradation increases because of the high probability to radiation exposure (internal or external) from the radioactive elements such as ^{222}Rn , ^{220}Rn and theirs decay products. The presence of radon and thoron in indoor environment gives rise to significant contribution to radiation dose to a person which is more than 50% of the total background dose. The main source of indoor thoron is the exhalation from the commonly used building construction materials and soils [3]. In the present study, experiments were carried out to estimate the radon and thoron exhalation source term due to various soil and building materials available in Kurukshetra, Haryana, India.

Materials and Method

Radon mass exhalation from building materials samples was measured by accumulation techniques (Fig. 1) using a large volume cylindrical chamber (about 10 times larger than the sample volume) to ignore the back diffusion effect. Radon mass exhalation rate was estimated by least square fitting of Eq. (1) to the buildup data of radon in the chamber. BARC developed Smart Radon Monitor [4] was used for the radon concentration measurement with the measurement cycle of 1 hour.

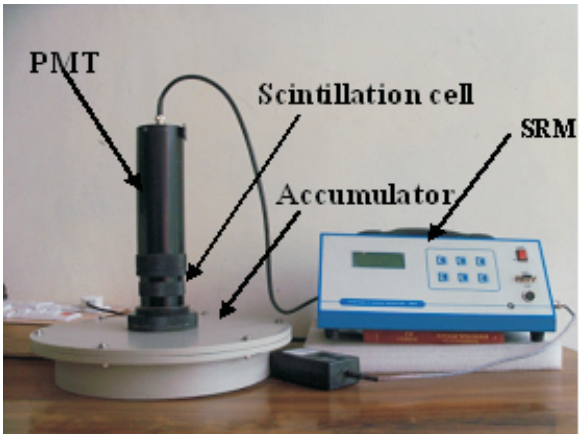


Fig. 1 Experimental Arrangement of Radon exhalation rate measurement

Equation for growth of radon concentration inside sealed chamber is given as [5]:

$$C(t) = \frac{J_M M}{V_e}\left(1 - e^{-\lambda_e t}\right) + C_0 e^{-\lambda_e t} \qquad (1)$$

Where, C(t), radon concentration inside the chamber measured at time t (Bq/m^3). J_M, radon mass exhalation rate from the sample (Bq/kg/h). M, mass of the sample (kg). V, air volume in the measurement system (m^3). $_e$, effective decay constant (h^{-1}). C_0, concentration in the air space of measurement system before starting the experiment (Bq/m^3). t, measurement time (h).

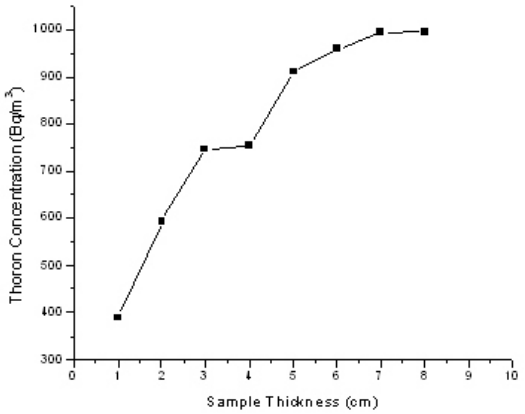


Fig. 2 Variation of thoron concentration with thickness of sand sample

The diffusion length of the thoron is very less, so it was assumed that thoron gas will exhale from the upper surface of small thickness of the examined building material. The exhalated thoron gas decay fast due to the short half life 55.6 seconds before the steady state is reached. The thoron gas concentration (Bq/m^3) measured by the Smart Thoron Monitor was used to calculate exhalation rate from equation (2) [6].

$$JS = (C.V.)/A \quad (2)$$

C, thoron concentration inside the chamber measured by thoron monitor, V is the total empty volume inside the close loop path of experimental arrangement, is thoron decay constant ($0.0126\ s^{-1}$), A is the surface area. To optimize the sample thickness to measure the thoron concentration effectively the measurement was done for 1 cm, 2 cm, 3 cm up to 9 cm thickness for the sand sample. It was observed experimentally that the thoron concentration become independent of sample thickness at the height above 6 cm. The results are shown in Fig. 2.

Results

Table 1 and Table 2 present the results of grain size, packing density, porosity, radon mass exhalation and thoron surface exhalation rate measured for soil samples and Fly ash samples. As may be seen from Table 1, exhalation rate of radon and thoron decreases with increasing in soil grain size and from Table 2, there is random pattern observed with the increasing in fly ash grain size. This needs to be investigated through proper mathematical modeling.

Table-1: Grain size effect on ^{222}Rn and ^{220}Rn exhalation rates in soil sample

Grain Size (m)	Packing density $10^3 kgm^{-3}$	Porosity (%)	^{222}Rn Mass Exhalation mBq/kg/h	^{220}Rn Surface Exhalation $Bq/m^2/h$
<50	1.61	40.97	84±13	3812±437
50-100	1.98	44.45	66±06	3091±291
100-200	2.05	46.56	31±09	2576±146

Table 3 present results of packing density, porosity, radon mass exhalation and thoron surface exhalation from various building materials samples. The radon exhalation was found to be varying from 4 mBq/kg/h to 61 mBq/kg/h while thoron surface exhalation rate was found to be varying from 76 $Bq/m^{2/}h$ to 5151 $Bq/m^2/h$. The maximum value of radon and thoron exhalation rate was observed for the soil samples.

Table-2: Grain size effect on ^{222}Rn and ^{220}Rn exhalation rates in fly ash sample

Grain Size (m)	Packing density $10^3 kgm^{-3}$	Porosity (%)	^{222}Rn Mass Exhalation mBq/kg/h	^{220}Rn Surface Exhalation $Bq/m^2/h$
<20	1.45	41.46	09±0.9	480±102
20-50	1.50	40.22	11±1.1	468±86
50-100	1.36	45.31	04±1.5	179±46
100-200	1.61	36.16	25±0.4	742±367

Table-3: ^{222}Rn and ^{220}Rn exhalation rates of building materials

Building material	Packing density, $10^3 kgm^{-3}$	Porosity (%)	^{222}Rn Mass Exhalation mBq/kg/h	^{220}Rn Surface Exhalation $Bq/m^2/h$
Soil	1.52	46.15	61±6	5151±1030
Sand	2.39	36.74	37±4	2034±54
Cement	1.93	47.94	17±1	565±43
Fly ash	1.44	45.31	10±1	711±118
POP	1.27	46.35	25± 1	806±241
Snewcem	1.66	ND	04±3	120±41
Lime	1.12	47.15	09±3	76±23
Chalk	1.37	44.89	41±14	1603±317
Wall putty	2.03	43.79	39±10	464±43

ND- not detected

Acknowledgement

The authors are thankful to Board of Research in Nuclear Science (BRNS), Department of Atomic Energy, Mumbai, India for providing the funds in form of major research projects

References

[1] UNSCEAR (United Nations Scientific Committee on the Effects of Atomic Radiation), (2006)

[2] WHO (World Health Organization), (2009).

[3] Tuccimei, P., Moroni, M., Norcia, D., 2006. Appl. Radiat. Isot. 64, (2006) 254.

[4] Gaware JJ, Sahoo BK, Sapra BK, Mayya YS. Radiat. Prot. Environ, 34(2011) 37.

[5] Sahoo, B.K., Nathwani, D., Eappen, K.P., Ramachandran, T.V., Gaware, J.J., Mayya, Y.S. Radiation Measurements 42 (2007) 1422.

[6] Sahoo B.K., Mayya Y.S. Agricul. and fores. metro.150 (2010) 1211.

A Correlation Study between Indoor Radon-Thoron Concentration and Soil Exhalation Rates from Indian Dwellings

Amit Kumar[1], R. P. Chauhan[1], Manish Joshi[2]

1. *Department of Physics, National Institute of Technology, Kurukshetra-136119, Haryana, India; E-mail: amit.vera@gmail.com*
2. *Radiological Protection and Advisory Division, Bhabha Atomic Research Centre, Mumbai, India*

The measurements of indoor radon and thoron concentration in some north Indian dwellings were carried out using pin hole based radon thoron dosimeters. The inhalation doses were calculated by ICRP recommendations. The radon and thoron exhalation rates from the soil collected from the same dwellings area were also carried out with closed chamber technique using active measurement by scintillation radon monitor and scintillation thoron monitor. The indoor radon and thoron concentration varied from 12 to 90 Bq/m^3 and 20 to 140 Bq/m^3 respectively. A good positive correlation was found between indoor radon thoron concentration and their exhalation rates.

Introduction

Indoor radon and thoron present in the environment is a major contributor to inhalation dose which are produced in the decay series of uranium, thorium present in the soil and rocks. The radon and thoron levels in dwelling depend upon the soil, radioactivity content in building materials and house ventilation. The inhalation of these gases may cause lung cancer due to their alpha emitting nature. However, the half life of thoron is very small but it cannot be neglected in the environment because the thoron progeny which exist in solid particulate are more dangerous as compare to thoron itself. The indoor radon and thoron concentration strongly depends upon the radium content and hence radon and thoron exhalation rates of soil. Thus it is necessary to monitor these gases in the dwellings and exhalation rates from soil.

Materials and Methods

The indoor radon and thoron concentration in some north Indian dwelling were carried out using pin hole based radon thoron dosimeters (Fig. 1) and radon mass exhalation rates from the soil samples were found by active technique using scintillation radon monitor and thoron surface exhalation rates by scintillation thoron monitor (Fig. 2). A typical radon growth in closed chamber is shown in Fig.3.

Calibration and Equlibrium Factors

The indoor radon and thoron concentration were calculated according to following relations.

$$C_T \quad \frac{T_2 \quad d \quad C_R \quad K'_R}{d \quad K_T} \qquad (1)$$

$$C_R \quad \frac{T_1}{d \quad K_R} \qquad (2)$$

Where C_R and C_T are radon and thoron concentration, T_1 (Tr.cm^{-2}) is the track density observed in 'radon' compartment. K_R is the calibration factor of radon in 'radon' compartment for radon (0.017 ± 0.002 Tr. cm^2

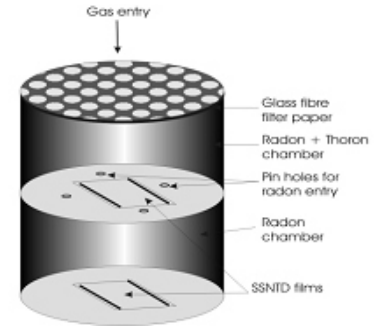


Fig. 1 Pin hole radon thoron dosimeter

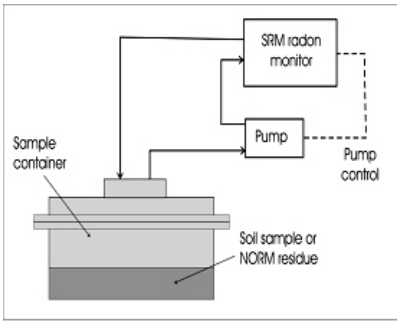


Fig. 2 Experiment set for exhalation rates

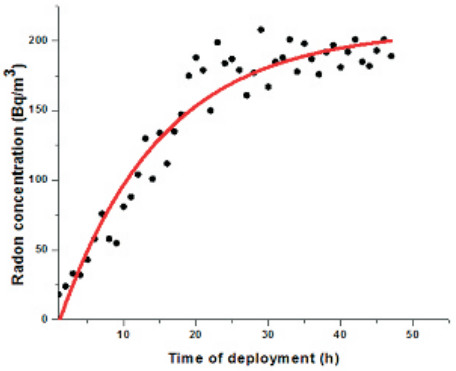


Fig. 3 Growth of radon in closed chamber for soil samples

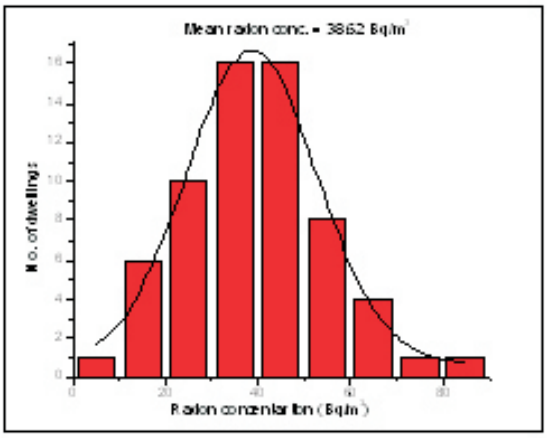


Fig. 4 Frequency distribution curve for radon concentration

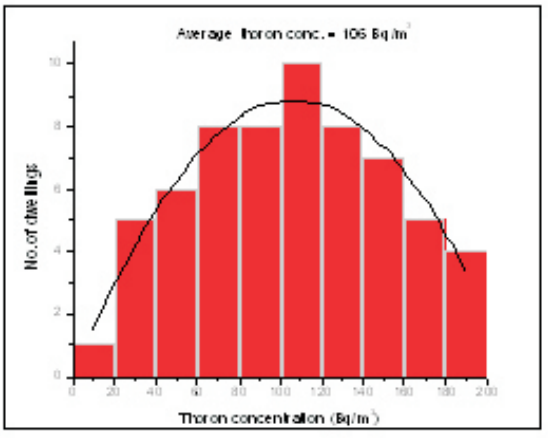


Fig. 5 Frequency distribution curve for thoron concentration

per Bq.d.m ^{3}) d is the number of days of exposure. T_2 (Tr.cm^{-2}) is the track density observed in the 'radon + thoron' compartment K_R (0.0172 ± 0.002 Tr. cm ^{2} per Bq.d.m ^{3}) and K_T (0.010 ± 0.001 Tr. cm ^{2} per Bq.d.m ^{3}) are the calibration factors of radon and thoron in 'radon + thoron' compartment [1]. The inhalation dose due to radon and thoron, was calculated by using conversion coefficient 9 and 40 nSv with equilibrium factor F_R = 0.4 and F_T = 0.1 for radon and thoron, respectively. The dose coefficient for radon and thoron are calculated using conversion coefficient 0.17 nSv for radon and 0.11 nSv for thoron. Finally an estimation of the inhalation dose in mSv yr^{-1} may be calculated using the formula [2-6]

$$D\ (mSv) = \{(0.17+9F_R)\ C_R + (0.11+40F_T)\ C_T\} \times 7000 \times 10^{-6} \quad (3)$$

Results and Discussion

The results of indoor radon and thoron from some dwellings from north India and radon and thoron exhalation rates from soil samples were calculated. The indoor radon and thoron concentration varied from 12 to 90 Bq/m^3 and 20 to 190 Bq/m^3 respectively as shown in frequency distribution curve (Fig. 4 and 5).

The radon and thoron frequency distribution curve showed that the most of dwellings have radon concentration 30-40 Bq/m^3 which is worldwide average, while 90% dwellings have thoron concentration lower than the limit recommended by ICRP, 1993. The radon mass exhalation rates are well below the worldwide average. A good positive correlation was found between indoor radon thoron concentration and their exhalation rates.

Conclusion

1. The indoor radon concentration varied from 12 to 90 Bq/m^3 with an average of 38 Bq/m^3.
2. The indoor radon concentration varied from 20 to 190 Bq/m^3 with an average of 106 Bq/m^3.
3. The indoor radon and thoron concentration are below the recommended value.
4. A good positive correlation was found between indoor radon thoron concentration and their exhalation rates.

References

[1] B.K. Sahoo, B.K. Sapra, S.D. Kanse, J.J. Gaware, Y.S. Mayya, Radiation Measurements (2013), doi: 10.1016/j.radmeas.2013.08.003.

[2] UNSCEAR, (1993) p. 73

[3] UNSCAER (2000)

[4] UNSCAER (2006)

[5] Y.S. Mayya, K.P. Eappen, K.S.V. Nambi, Radiation Protection Dosimetry. (1998) 77 (3)

[6] J. Sannappa, M.S. Chandra Shekara, L.A. Sathish, L. Paramesh, P. Venkataramaiah Radiation Measurement 37(2003) 55.

[7] ICRP, (1993).

Particle size distribution and Natural Radionuclide's Association in the Mumbai Harbour Bay Bottom Sediment

Hemalatha.P, Madhuparna D, Sanu.S.Raj, S. K Jha and R.M.Tripathi

Environmental Radiation Monitoring Section, Health Physics Division, Bhabha Atomic Research Centre, Mumbai 400 085, India; E-mail: hemlathap@gmail.com

Natural radioactivity level in the Mumbai Harbour bay sediment was estimated and their association with particle size was investigated. Seven different particle size fractions from <63 m to >300 m were separated by wet sewing using electromagnetic sieve shaker and particle size distribution was studied in the marine sediment. The particle size fractions were analysed for Ra-226, Ra-228 and K-40 content using 50% relative efficiency p-type Co-axial HPGe detector. It was observed that, 71.8 % of the total sediment contained <63 m size particles. Higher percentage of K-40 was observed to be associated in the size fraction of <60 to 90 m size particles.

Introduction

Natural radioactivity in the environment occurs mainly due to the presence of primordial parent nuclides ^{238}U, ^{232}Th and ^{235}U, which give rise to chain of decay products and also from natural K-40. The behaviour of radium in seawater is based on longest-lived isotopes ^{226}Ra and ^{228}Ra. Natural radioactivity is highly variable throughout the world depending upon the geological history of the region. Estimation of radioactivity in the environment provides information on their mobility and mechanism of physico, bio-geo chemical processes through diffusion, adsorption, accumulation, and assimilation [1]. Studying the distribution of radionuclides in marine environment assumes importance due to the fact that; gamma radiation from the sediment represents the main external source of irradiation to the human body. Mumbai Harbour bay is dominated by clay mineral particle[2]. Sorption of radionuclide in the sediment depends on various factors [3] such as particle size, mineral composition of the sediment, sedimentation rate, organic matter content, pH etc [4]. Particle size plays an important role as a potential carrier with the tidal actions in transporting radionuclide to surrounding coastal areas. This paper presents the particle size distribution of the marine sediment and the association of natural radioactivity with different particle sizes of bottom sediment of Mumbai Harbour bay.

Material and Method

Bottom sediment was collected from Trombay Naval Jetty, a location representative for the study in Mumbai Harbour Bay. A grab sampler was used to collect bulk sediment from the shore. A homogenous sediment slurry was prepared with a known amount of sediment. The slurry was passed through a set of seven sieves of different Particle size fractions from >300 m to <63 by wet sieving method using electromagnetic sieve shaker. By this way eight different size fractions such as >300 m, 250-300 m, 180-250 m, 150-180 m, 125-150 m, 125-90 m, 90-63 m and <63 m were obtained. Each particle size fraction was separately collected, dried at 105°C, and each fraction was quantitatively filled in counting boxes and sealed well. The gamma radioactivity content of the sample was measured by using a high resolution, 50% relative efficiency p-type Co-axial HPGe detector, (Eurisys Measures) coupled to a 8 K multichannel analyser. All the samples were counted for a period of 80,000 seconds. The detector was calibrated using standard samples supplied by International Atomic Energy Agency (IAEA) Vienna. The concentrations of natural radioactivity of the sediment particle were measured through the decay chain isotopes of ^{232}Th and ^{238}U. The activity of Ra-226 was measured from the gamma energy of 186 keV, and Ra-228 content was estimated through Ac-228 from the gamma energies of 911 and 969 keV. A direct measurement at 1,462 keV was achieved to get the concentration of ^{40}K.

Results and Discussion

The particle size analysis of the sediment revealed that the sediment was dominated by fine particles. It was observed that about 71.8% of the total sediment contained <63 m size particles and other particle size fractions were observed to be in the range of 2 to 6%. Ra-226 concentration was observed to be distributed in the seven particle size fractions in the range of 10 to 21%. While Ra-228, the daughter product of ^{232}Th was observed to be higher in the size fraction of 90 and 180 m. It was observed to be 30%, and in the other size fractions it was in the range of about 5%. Similarly K-40 was observed to be differentially distributed in the different size fractions of the sediment in the range of Higher percentage of K-40 was observed to be associated in the size fraction of <60 to 90 m size particles. Radioactive isotopes behave chemically similar to their stable counter elements or their analogous elements. Similarly radioactive materials find a different route to reach humans and it is usually dictated by the chemistry of the elements in the environment. The paper gives the details of particle size distribution of the bottom sediment and discusses the quantity of natural radionuclides Ra-228, Ra-226, and

K-40 association with different particle size of the sediment with respect to physico chemical parameters of the environment.

Table-1: Particle size distribution of Mumbai Harbour Bay sediment

Particle Size fraction of Sediment (m)	% Weight of the fraction
<63	71.83
63-90	2.11
90-125	5.85
125-150	3.87
150-180	2.80
180-250	2.07
250-300	5.99
>300	5.48

References

[1] Baskaran, M. and Santschi, P.H., The role of particles and colloids in the transport of Radionuclides in coastal environments of Texas, Marine Chemistry, 43 (1993) 95.

[2] P.Hemalatha & M.V.M.Desai, Ecological & Physico chemical studies of Mumbai Harbour Bay' -2000 BARC/2000/I/012 (2000).

[3] Ligero, R.A., Ramos-Lerate, I., Barrera, M., Casas-Ruiz, M., J. Environ. Radioact. 57 (2001) 7.

[4] R.A.Horne, Marine Chemistry, Woodshole Oceanographic Instititution.Wiley- Interscience. N.Y. (1969).

Studies on Concentration of Radionuclides in Medicinal Plants

Chandra Shekara K.[1],Yashodhara I.[2], Karunakara N.[2] ,Radhakrisna A.P.[1],·Somashekarappa H.M.[2]

1. *Department of Physics, St.Philomena College, Puttur 574202, Karnataka, India; E-mail:carrtmu@gmail.com*
2. *University Science and Instrumentation Centre (USIC), Mangalore University, Mngalagangotri 574199*

The concentration of radionuclides in medicinal plants exhibiting important medicinal properties collected from coastal Karnataka region were analysed and estimated. It is found that these plants have significant activity concentration of radionuclides. Measurement of concentration of radionuclides has been carried out using HPGe gamma spectrometer. The study has revealed that the activity of ^{40}K is maximum as compared to ^{226}Ra, ^{210}Pb, ^{232}Th, and ^{137}Cs concentrations present in the medicinal plants.

Introduction

The Earth on which we live is the beautiful collection of variety of plants. Among these many are medicinal plants. Ayurvedic medicine proved its efficacy for the treatment of various diseases and these medicines are from plant origin and they are found to have minimum side effects. Therapeutic use of medicinal plants in human health is in regular practice even from Vedic period. There are many references [1] to the curative properties of medicinal plants in the ancient literature. 'CharakaSamhitha' and 'SushruthaSamhitha' are two major literatures of Ayurveda system dealing with the medicine and treatment. Many investigations [2, 3] have been made to know the basic contents of the plants in different region.

The medicinal plants are abundantly available in coastal and malnad region of Karnataka. Most of this region is a part of Western Ghats which is very rich in its biodiversity. Interior regions such as Puttur,Bantwal,Sullia and Belthangady of west coast of Karnataka are known for using traditional and folklore medicine in which medicinal plants are used as main ingredients. The detailed studies of uses of these plants are yet to be performed in this geographical area. This study aims at the analysis of medicinal plants available in this region with different curative properties. The medicinal plants—Curcumalonga(L.),Eupatorium odoratum (L.), Ficus racemosa(L.) and Alstonia scholaris (L.) which are commonly known as Turmeric, Devil weed, Atti and Haale respectively are selected in present study. These plants have got very high medicinal value and they are being used extensively by ayurvedic practitioners of this region. The following Table gives the medicinal properties of the above mentioned plants [4]

Medicinal Plant	Medicinal Property
Curcuma longa(L.)	Antiseptic
Eupatorium odoratum(L.)	Cures skin diseases and wounds
Ficus racemosa(L.)	Astringent, Tonic
Alstonia scholaris(L.)	Anti periodic, Astringent

Materials and Methods

The plants are collected from the selected area, processed using the standard methods given in EML procedure manual [5] and analysed for ^{226}Ra, ^{210}Pb, ^{232}Th, ^{40}K and ^{137}Cs concentrations following the standard methods and procedures. All the above listed radionuclides have been estimated using gamma spectrometric method [6]. The spectrometer was calibrated using standards obtained from IAEA.

Results and Discussions

The activity concentrations of ^{226}Ra, ^{210}Pb, ^{232}Th, ^{40}K and ^{137}Cs have been measured in the above listed medicinal plants and also from soil samples collected from the corresponding sampling locations. In plants the activity concentration of ^{226}Ra is found to vary from 0.998±0.14 Bq kg^{-1} to 40.45 ± 8.755 Bq kg^{-1}, ^{210}Pb activity is found to vary from BDL to 51.80s±1.35 Bq kg^{-1}, ^{232}Th activity varies between BDL and 43.08±6.35 Bq kg^{-1}, ^{40}K activity varies between 557±5.94 Bq $kg^{-1}$and 1910.76 ± 14.87 Bq kg^{-1} and ^{137}Cs is found to BDL level except in Turmeric (0.2498±0.0001 Bq kg^{-1}). However, the concentration of ^{40}K in all the plants is found to be orders of magnitude higher than the activities of ^{226}Ra, ^{210}Pb, ^{232}Th, and ^{137}Cs.The higher concentration of ^{40}K in both medicinal and non medicinal plants is evident and similar results have been reported by other investigators [7,8]. Potassium is one of the important nutrients of the plants and ^{40}K being its isotope it is expected to be higher in its concentration. In the soil samples collected from same area the activity concentration of ^{226}Ra varies from 10.92±0.86Bqkg^{-1} to 41.72±4.15 Bq kg^{-1}. ^{210}Pb from 33.78±5.76 to122.84±7.30 Bq kg^{-1}, ^{232}Th from 40.72±1.86 to 90.55± 2.79 Bq kg^{-1}.^{40}K from 162.36 ±8.83 to 355.2±11.83 Bq kg^{-1} and ^{137}Cs varies from BDL to 14.36±0.76 Bq kg^{-1}.

Conclusion

The study shows that the medicinal plants have certain significant activity concentrations of radionuclides. There is a possibility of ingestion of these radionuclides along with medicines prepared using these plants. If these radionuclides are not going to play any role in curing the diseases, they may contribute an additional radiation dose to human.

References

[1] Parchure S. N. Charaka Samhita. Sagar Publications. PuneIn dia. (1983).

[2] Karunakara N., Somashekarappa H.M., Narayana Y., Avadhani D.N., Mahesh H.M., Siddappa K., J. Environ. Radioactivity, 65 (2003) 255.

[3] Somashekarappa H.M., NarayanaY, Radhakrishna A.P., Karunakara N., Balakrishna K.M.& Siddappa K J.Environ. Radioactivity, 31(2) (1996) 189.

[4] Shetty B.V., Kaveriappa K.M. and Gopalakrishna Bhat K., Pilikula Nisarga Dhama Society .Mangalore (2002).

[5] Herbert L.Volchok and Gail De PlanqueEML Procedure Manual, 26th Edn. Environmental Measurement Laboratory (EML). (1983).

[6] Ramachandran, T.V. & Mishra U.C., Bull. Radiat. Prot., 12 (1989) 51.

[7] Karunakara,N., Studies on radionuclide distribution and uptake in the environment of Kaiga PhD Thesis, Mangalore University.(1997)

[8] Donatella Desideri, Maria Assunta Meli, Caria Roselli, J. Environ. Radioactivity, 101 (2010) 751.

Seasonal Variation of Radioactivity in Ground Water at Trombay

Vandana Pulhani, Joyeeta Mukherjee, S K Jha and R M Tripathi

Health Physics Division, Bhabha Atomic Research Centre, Trombay, Mumbai 400 085, India;
E-mail: vanpulh@barc.gov.in

Surveillance of bore well water for radioactivity is a regular process to assess the migration of radioactivity into groundwater. Numerous bore wells are dug inside Trombay area and concentration of the radionuclides like ^{137}Cs and ^{90}Sr in ground water is recorded every quarter. The observations for the last five years were compiled and trend in the activity levels in the different quarters was studied.

Introduction

The safe and normal operation of numerous units in a nuclear plant is ensured by regular environmental surveillance around these plants. The different matrices like air, water, vegetation, soil are regularly assessed for radioactivity content. A number of bore wells are dug at numerous locations and bore well water assayed for radionuclides like ^{137}Cs and ^{90}Sr, to study and assess the migration of radionuclides in the ground water. The regular surveillance data at Trombay has been compiled to understand the trend of variation in the activity levels obtained in the bore wells in a year. The seasonal dependence of the radioactivity concentration was investigated.

Material and Methods

The analytical techniques and instrumentation used for the radiochemical assay was based on standard procedures as described below [1]. For the qualitative and quantitative measurement of gamma emitting radionuclide, samples were concentrated from 500 ml to 250 ml by evaporation and taken in a plastic container (250ml) of standard geometry for gamma spectrometry using HPGe Detector. The detector is a co-axial 50cc p-type high purity Germanium crystal with a resolution of 2 KeV and a relative efficiency of 15% for 1.332 MeV gamma energy of Co-60. Strontium was separated from the sample as strontium carbonate and estimated by beta counting of ^{90}Y obtained in secular equilibrium after radiochemical separation.

The activity measured in the four quarters for 5 years was compiled and the ratio of levels in second, third and fourth each was calculated with respect to that in the first quarter for each year. The comparison of ratios gave the seasonal variation of the radioactivity in the bore well water.

Results and Discussion

Figs. 1 and 2 give the average activity concentration ratios for ^{137}Cs and ^{90}Sr from the years 2008 to 2012. It was observed that ^{137}Cs activity concentration ratio in the months of April-June i.e. the second quarter with respect to that of the first quarter i.e. January-March was more among the three ratios between second, third and fourth. In majority of the bore wells during the summer months there is lowering of the water table due to negligible recharge and increased discharge towards sea, hence the activity in ground water gets concentrated and increases. In the next quarters i.e. third (July-Sept) and fourth (Oct-Dec), the activity ratio decreased with respect to that obtained in the first quarter, due to higher recharge during monsoon. Among the activity ratios of the fourth and third, the ratio of fourth was more than that in the third because the water table goes down due to reduced recharge. But this ratio is still lower than that in the second quarter. The majority of the bore wells in the fourth quarter show an activity ratio of around or less than 1 with respect to first. This indicates that there is no fresh input of ^{137}Cs activity in the bore well. ^{137}Cs has the tendency to get incorporated in the soil crystal lattice, fixed by clay minerals in the mineral soil layers almost irreversibly and become less labile for migration in to groundwater [2,3]. Hence there was no major change in the concentration of ^{137}Cs in the groundwater. Any individual bore well showing higher ratio can be

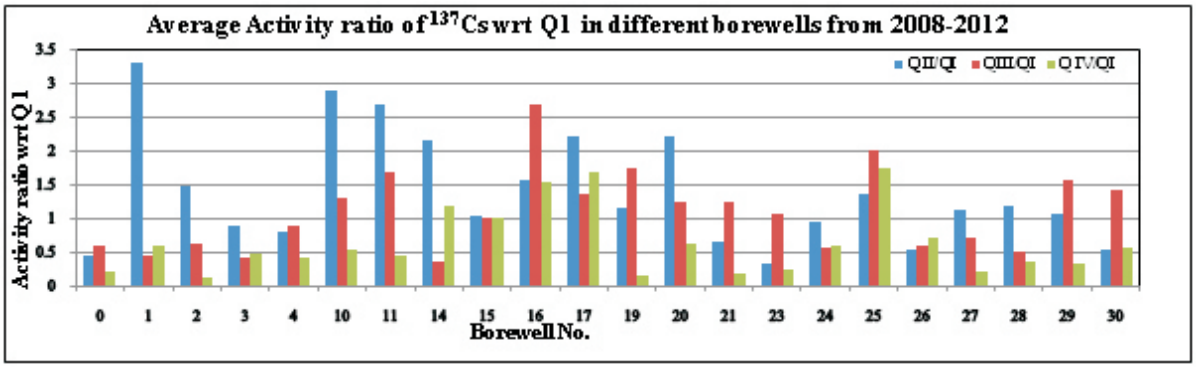


Fig. 1 Seasonal Variation of Cs-137 in Ground water

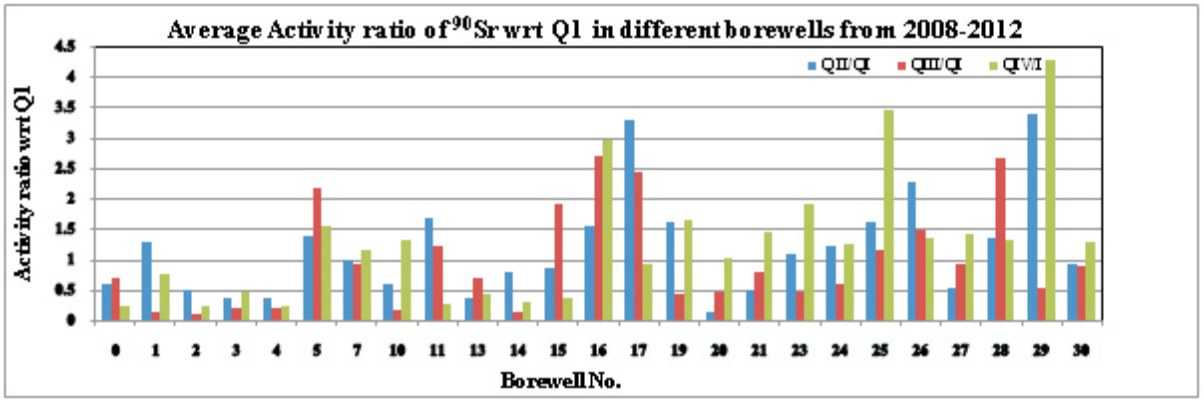


Fig. 2 Seasonal Variation of ^{90}Sr in Ground water

assumed to have fresh leaching of the radionuclide from the surroundings. The changes in groundwater physicochemical characteristics may also favor release of cesium held in the soil to the water. As some evidence suggests that a considerable percentage of ^{137}Cs remains in mineral soil layers as an easily exchangeable form over a prolonged period of time [4,5].

^{90}Sr is more mobile and does not follow the same trends as cesium, as seen from Fi.g 2. ^{90}Sr activity ratio in most of the bore wells was more than 1 in second and fourth quarter and comparable. In some bore wells the ratio was observed to be higher in the III quarter than the other two, indicating migration from surroundings. Sr which is labile may be getting dissolved due to ingress of rain and seawater and migrating in to the groundwater. The effect of seawater ingress on the migration of Sr and its seasonal variations can be co-related to the water quality parameters of the bore well water. A complete study of the physicochemical parameters of the groundwater is being carried out to completely explain the seasonal variations.

Conclusions

The specific chemical properties of the radionuclides are seen to have an effect on their migration in the ground water. Cesium is retained in soil matrix and hence its concentration does not change much even after rainwater ingress whereas strontium is mobile and can be clearly seen from its variation in bore well water over the year. Strontium activity is not showing a common or similar trend in all the bore wells and is probably affected by other factors.

References

[1] USEPA. Multi-Agency Radiological Laboratory Analytical Protocols Manual, Volume II: Chapters 10-17 and Appendix F, EPA/402/B-04/001B (NUREG-1576) Washington,DC (2004).

[2] Cremers A., Elsen A., De Preter P. & Maes A. Quantitative analysis of radiocaesium retention in soils. Nature, 335 (1988) 247.

[3] Valcke E. & Cremers A. Sorption-desorption dynamics of radiocaesium in organic matter soils. Sci. Total Environ.157 (1994) 275.

[4] Andersson K. G. & Roed J, J. Environ. Radioact. 22 (1994) 183.

[5] Bunzl K., Kracke W., Schimmack W. & Zelles L, J. Environ. Radioact.39 (1998) 55.

Radiological Measurement of Phosphate Rock, and Phosphogypsum from Fertilizer Industries in India

S. J. Sartandel, S. V. Bara, S. Chinnaesakki, S. K. Jha and R. M. Tripathi

Health Physics Division, Bhabha Atomic Research Centre, Trombay, Mumbai 400085, India; E-mail: sangjs@barc.gov.in

Natural radionuclides from the uranium and thorium series were measured, using high-resolution gamma-spectrometry in phosphate rock and phosphogypsum samples from the phosphate fertilizer industry in India. Equilibrium was found to be disrupted during the chemical processing of phosphate rock with 83 % of the ^{226}Ra and only 5 % of ^{238}U fractionating to phosphogypsum. Activity concentrations of ^{238}U and ^{226}Ra in phosphogypsum produced from various fertilizer industries of India showed levels <1000 Bq kg^{-1} and pose no restriction for use in building / construction material or agricultural use.

Introduction

Phosphate deposits are generally characterized by high levels of natural radionuclide concentrations. Processing of this phosphate ore redistribute radionuclides and introduce them into phosphoric acid starting material for phosphate fertilizers and by-product phosphogypsum. The radium that is found naturally associated with phosphate rock (PR) becomes associated with the phosphogypsum (PG) after the rock is reacted with sulphuric acid. Depending on radioactivity levels in PG it may be used as a raw material in building products. It has only been in recent years that the question of radioactivity has been raised and this question now influences every decision relative to potential use in building materials.

Radiological assessment of PG would be important if it is used as either land-filling or building material. The knowledge will also help in predicting the occupational exposures that may occur during processing of PR and its corresponding by-products [1]. The Atomic Energy Regulatory Board (AERB), India has been examining the radiological safety implications of adding PG in building and construction materials and use in agriculture. In compliance with these draft regulations, representative samples of PR ore drawn from the consignment used for processing in fertilizer plants and its corresponding by-product PG were assessed for concentration of natural radionuclides. The present study was carried to find range of natural radioactivity concentrations in PR and PG samples of various fertilizer industries in India using imported and Indian PR.

Method

125 samples of PR and PG received from fertilizer industries using indigenous (Indian) PR and ore imported from different countries were considered. The samples were processed and sealed in gas tight, radon impermeable, cylindrical polyethylene plastic containers (6.5 cm diameter and 7 cm height) to achieve radioactivity equilibrium of short-lived progeny of ^{226}Ra and ^{224}Ra.

Gamma Spectrometry Measurement

Activity concentrations of ^{238}U, ^{226}Ra, ^{210}Pb, ^{228}Ra, ^{232}Th, and ^{40}K were measured in samples of PR and PG by gamma-ray spectrometry. Gamma-ray measurements were carried out using HPGe detector with a relative efficiency of 50% coupled to a PC-based spectrum stabilized 8K channel analyzer (PHAST, Electronics Division, BARC). ^{238}U activity was estimated from 1001 keV of ^{234m}Pa and 63 keV (^{234}Th) peak. ^{226}Ra was estimated through its daughter products ^{214}Pb (352 keV) and ^{214}Bi (609 keV and 1764 keV), ^{210}Pb was estimated using gamma energy 46.5 keV. Assuming secular equilibrium between ^{232}Th and ^{228}Th for PR samples, thorium activity concentration was estimated by using the gamma-ray line 2614 keV of ^{208}Tl which is a daughter of ^{228}Th. ^{228}Ra activity concentration in the PR and PG samples were determined by measuring the intensity of the 911 keV gamma-ray peak from ^{228}Ac. ^{40}K activity was estimated using 1460 keV gamma peak. The samples were acquired for 100,000 s and the photo peaks were evaluated by using the PHAST MCA emulation software and activity of the sample was calculated.

Results and Discussion

Activity concentrations of ^{238}U, ^{226}Ra, ^{210}Pb, ^{232}Th, and ^{40}K in phosphate rock were found to range from 53-1490 Bq kg^{-1}, 51-1449 Bq kg^{-1}, 52-1306 Bq kg^{-1}, 7-85 Bq kg^{-1} and 18-392 Bq kg^{-1}, respectively, while the concentration of ^{238}U, ^{226}Ra, ^{210}Pb, ^{228}Ra, and ^{40}K in phosphogypsum samples ranged from 10-76 Bq kg^{-1}, 35-695 Bq kg^{-1}, 37-681 Bq kg^{-1}, 5-24 Bq kg^{-1} and 12-205 Bq kg^{-1}, respectively. Imported PR used in industries A, B, C and D showed higher Uranium series radionuclide concentrations than PR of Indian origin used in industries E and F. The radioactivity concentration observed in PR for ^{228}Ra, ^{232}Th, and ^{40}K are quite similar except that of industry F showing comparatively higher radioactivity concentration of ^{40}K which can be attributed to geological origin of PR.

A good correlation is observed in activity concentration of ^{238}U with ^{226}Ra and ^{210}Pb (Fig. 1), thus confirming the radioactive equilibrium of radionuclides ^{238}U - ^{226}Ra - ^{210}Pb of the ^{238}U decay series in the PR

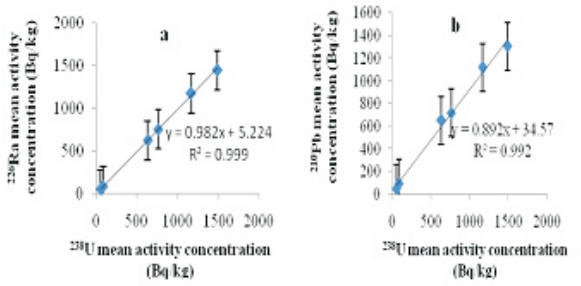


Fig. 1 Relation between the mean activity concentration of (a) ^{238}U and ^{226}Ra (b) ^{238}U and ^{210}Pb in phosphate rock samples

samples. Equilibrium is significantly disrupted during the chemical processing of PR. This disruption is clearly seen through plots of mean activity concentration of ^{226}Ra, ^{228}Ra, ^{210}Pb, ^{40}K, and ^{238}U in PG samples versus activity concentration in the corresponding PR. Good correlation is observed between PG and PR for activities of ^{226}Ra, ^{210}Pb, and ^{40}K while, ^{238}U content of PG shows no correlation with the ^{238}U content of the PR. Hull and Burnett (1996) [2] also have reported no correlation between the concentrations of Uranium in the PG and the PR. The extent of incorporation of these radionuclides into PG is primarily controlled by the concentration supplied by the ore rock as well as by the acidification process efficiency. Based on the principles followed internationally and AERB Directive No. 01/09, 2009 [3] industries can sell PG for use in building and construction materials, if the activity concentration of ^{226}Ra in it is less than or equal to 1000 Bq kg^{-1}. If ^{226}Ra concentration in PG is more than 1000 Bq kg^{-1}, the seller must mix it with other ingredients such that the ^{226}Ra activity concentration in bulk material is less than or equal to 1000 Bq kg^{-1}. Mean activity concentration of ^{226}Ra in the PG samples of different fertilizer industries were observed to less than guidance level of 1000 Bq kg^{-1} prescribed by AERB Directive No. 01/09, 2009 and pose no restriction in use as building/construction material.

Radium Equivalent Activity (Ra_{eq})

The radium equivalent, $Ra_{(eq)}$ is a common index used to compare the specific activities of samples containing ^{226}Ra, ^{232}Th, and ^{40}K, that takes into account the radiation hazards associated with them. Comparatively high $Ra_{(eq)}$ activity was observed in PR and PG samples of industries using imported phosphate than the industries using PR ore of Indian origin.

Gamma Index (I)

The activity concentration index (I) also called as gamma index, has been defined by the European Commission [4] to help control external radiation exposure due to natural radionuclides in building materials.

$$I = A_{Ra}/300 + A_{Th}/200 + A_K/3000$$

where A_{Ra}, A_{Th}, and A_K are the specific activities of ^{226}Ra, ^{232}Th, and ^{40}K.

Gamma Index (I) has been calculated for PG samples analysed in this work and range between 0.1-2.4 (Table 1). The screening criteria for this index, which are based on dose rates of 0.3 or 1.0 mSv y^{-1}, [4] were used. PG samples produced from ore of Indian origin show the level well within the recommended upper limit I 0.5 for the excessive gamma dose of 0.3 mSv y^{-1} and material can be used in bulk quantities [4]. PG originating from industries using imported ore showed gamma index ranging from 1.3 - 2.4 and can have superficial or restricted use of material [4].

Conclusion

Equilibrium in PG samples was found to be disrupted due to the chemical processing of PR, with 83% of ^{226}Ra and only 5% of ^{238}U fractionating to PG. Radioactivity concentration and radium equivalent activity were found to be higher in PR and PG samples processed from imported ores as compared to those processed from Indian ore. This study suggests no restriction for use of this materials as building/ construction material.

Acknowledgments

The authors would like to thank Dr. D. N. Sharma, Director, HS & EG, BARC, for his constant encouragement and support towards this work.

Table 1: Activity Index (I) in phosphogypsum from Indian fertilizer plants

Industry (no. of samples)	Origin of PR samples	Activity index (I) (Bq kg^{-1})
A (30)	imported ore	2.4
B (35)	imported ore	2.2
C (20)	imported ore	1.3
D (15)	imported ore	1.3
E (15)	Indian ore	0.1
F (10)	Indian ore	0.3

References

[1] UNSCEAR Ionizing radiation: Sources and biological effects (1988).

[2] Hull C.D., Burnett W.C., J. Env. Rad. 32(3) (1996) 213

[3] AERB Directive No. 01/09, Use of Phosphogypsum in Building and Construction Materials and in Agriculture. Atomic Energy (Radiation Protection) Rules (2009).

[4] Radiation Protection No. 112, . European Commission, Radiological protection principles concerning the natural radioactivity of building materials. Directorate-General Environment, Nuclear Safety and Civil Protection (1999).

A Simple spectrophotometric method for the determination of Uranium in industrial and environmental samples using 1-(benzo[d]thiazol-2-yl)thiourea

Y. Harinath[1], K. Seshaiah[1], A.V.R. Reddy[2]

1. *Inorganic and Analytical Chemistry Division, Department of Chemistry, Sri Venkateswara University, Tirupati - 517 502, India.Email:seshaiahsvu@gmail.com*
2. *Analytical Chemistry Division, Bhabha Atomic Research Centre, Trombay, Mumbai 400 085, India.*

Uranium is an important element in the actinides series due to its wide applications in nuclear industry as a nuclear fuel. The primary source of uranium is naturally occurring uranium ore present in the earth crust. The recovery of uranium from ore is carried out via two step process viz. (a) acid, alkali or bio leaching, and (b) separation from the ore leach solution [1-6]. Monitoring of uranium concentration in ore leach solution is an important aspect for its effective and efficient recovery.

A large number of analytical techniques have been used for the determination of uranium in a wide variety of samples such as environmental, seawater, process streams, effluent/waste streams, ores and ore leach solutions. The availability of power full instrumentals techniques such as neutron activation analysis (NAA), energy dispersive X-ray fluorescence (EDXRF), inductively coupled plasma emission spectrometry (ICPAES), inductively coupled plasma mass spectrometry (ICP-MS) has enabled the analysis of complex mixtures with high accuracy and precision [7–11]. However, these advanced techniques require sophisticated, high value instruments.

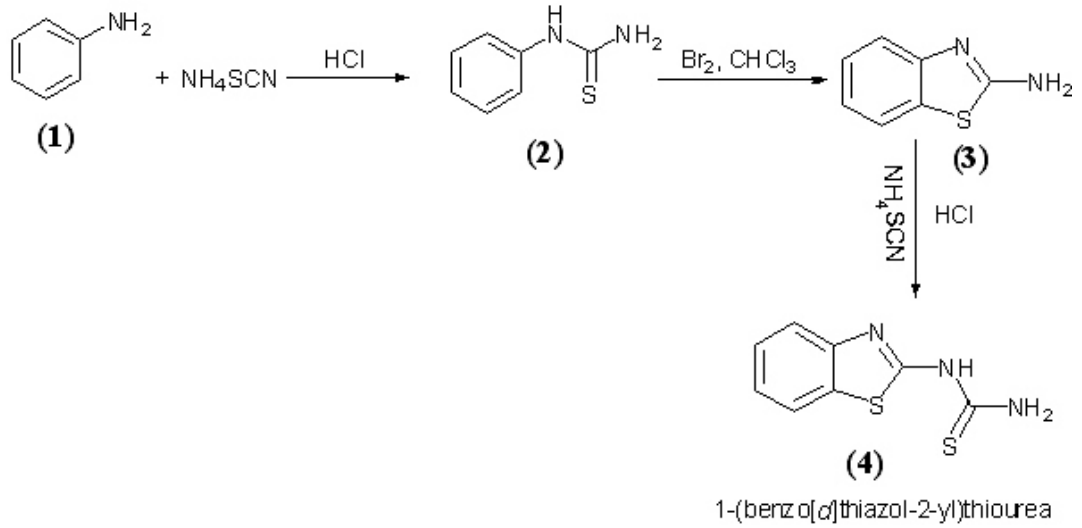
The association of spectrophotometric techniques employing chelating agents and chemometric methods offers outstanding advantages for the analysis of uranium in complex matrices [12, 13]. In this context we have developed a simple and sensitive spectrophotometric method for the determination of uranium in environmental samples using a new ligand, 1-(benzo[d]thiazol-2-yl)thiourea (btt). 1-(benzo[d]thiazol-2-yl)thiourea was prepared by the addition reaction of 2-amino benzthiazole with ammonium isothiocynate shown in scheme 1. The colorimetric method is based on the reaction of uranium with 1-(benzo[d]thiazol-2-yl)thiourea in acidic medium. The reagent reacts with uranium to form pale green colored 1:2 (M:L) complex. The color reaction is instaneous and color is stable for more than 24 hours with constant absorbance. Beer's law was obeyed in the uranium concentration range of 15 ìg L^{-1} to 100 ìg L^{-1}, with a molar absorptivity, 5.35×10^4 mol^{-1} cm^{-1} and Sandell's sensitivity 0.0016 Fg cm^{-2} at 24 ± 2 EC. The accuracy was checked by determining uranium from standard solutions in the range 20–70 ìg L^{-1}. Since the proposed method is sensitive it was applied for determination of Uranium in industrial and environmental samples.

References

[1] Uranium and uranium compounds, Encyclopedia of Chemical Technology, 3rd ed., 23 (1983) 514.

[2] J.A. Brierley, C.L. Brierley, Hydrometallurgy 59 (2001) 233.

[3] R.G. McCready, W.D. Gould, Bioleaching of uranium, in: H.L. Ehrlich, C.L. Brierley (Eds.), Microbial



Scheme 1 Synthetic route for the ligand

Mineral Recovery, McGraw-Hill, New York, (1990) 107.

[4] H.M. Lizama, M.J. Fairweather, Z. Dai, T.D. Allegretto, Hydrometallurgy, 69 (2003) 109.

[5] K.L. Narayana, K.M. Swamy, K.S. Rao, J.S. Murty, Miner. Process. Extr. Metall. Rev., 16 (1997) 239.

[6] K.M. Swamy, L.B. Sukla, K.L. Narayana, R.N. Kar, V.V. Panchanadikar, Ultrason. Sonochem. 2 (1995) S5.

[8] A. El-Taher, Appl. Radiat. Isot. 68 (2010) 1189.

[9] A. El-Taher, A. Nossair, A.H. Azzam, K-L. Kratz, A.S. Abdel-Halim, J. Environ. Prot. Eng. 29 (2004) 19.

[10] M. Afzal, J. Hanif, M. Saleem, I. Hanif, R. Ahmed, J. Radioanal. Nucl. Chem. 152 (1991) 251.

[11] P. Shrivastav, S.K. Menon, Y.K. Agrawal, J. Radioanal. Nucl. Chem. 250 (2001) 459.

[12] S. Ku, N. Obarski, Z. Marczenko, Anal. Sci. 8 (1992) 213.

[13] Ali Niazi, J. Braz. Chem. Soc. 17 (2006) 1020.

Determination of Effective Vertical Migration Velocity and Residence Times of ^{137}Cs in Sediments of Mumbai Harbor Bay using Compartment Models

Ajay Kumar, Sabyasachi Rout P.M. Ravi and R.M.Tripathi

Health Physics Division, Bhabha Atomic Research Centre, Mumbai 400 085, India; E-mail: ajaykls@barc.gov.in

The vertical concentration profile of ^{137}Cs in core sediment of Mumbai Harbour Bay has been studied by the compartment models. Based on the measured concentrations of ^{137}Cs in the sediment layers, the transport parameters as residence half life and effective migration velocity were determined. The residence half lives were observed to be 5 years and 13.6 years in cores L-3 and L-5 respectively. The corresponding effective migration velocity was obtained to be 7.2 cm/y and 3.23 cm/y over the core length of 36 cm and 44 cm respectively. The migration velocities obtained were well within reported values in literatures.

Introduction

The compartment model is a model that has been widely used to study radionuclide migration and behavior in the soil or sediment [1,2]. The model justifies the use of migration rates which are different for each soil/sediment layer because it is assumed that soil/sediment properties are uniform for each horizon. A single migration rate is therefore associated with each soil/sediment horizon. The model can be applied with ease because it does not require detailed information on the actual transport processes of the radionuclide in the soil/sediment such as the sorption properties, water infiltration etc. It has the disadvantage that only the residence times and migration velocity of the radionuclide with the soil/sediment layers can be obtained.

^{137}Cs is known to be the most abundant fallout radionuclide present in the marine environment, the concentration varying from region to region, according to the specific sources of contamination and the geographical location. In most sedimentary environments, ^{137}Cs is deposited as fallout which is rapidly and strongly fixed by sediment particles [3].

Materials and Methods

In the present study, two core sediment samples were collected from locations namely L-3 and L-5 within 1 nautical mile area from the discharge location of CIRUS using a sediment corer. The depth of the core was upto 40 cm with a diameter of 45 mm. The core was cut into ten fractions of 4cm each and brought to the laboratory. Each fraction was washed with deionised water, dried at 110ºC for 24 h, ground with a mortar and pestle, homogenized and sieved through a 2 mm mesh sieve. About 100-250 g of meshed samples were transferred to a pre-weighed cylindrical acrylic container with dimension of 75 mm diameter x 75 mm height (331cm^3), sealed. Finally, the activity of ^{137}Cs was determined using photopeak at 662 keV using gamma spectrometry system based on a co-axial high purity germanium detector (HPGe, 50% relative efficiency). The residence half life of ^{137}Cs in the various sediment layers were evaluated with compartmental models [1].

The multi compartment model [2] assumes that the sediment depth is split into a series of N horizontal layers which are connected by a downward transport rate of the particular radionuclide being investigated. In this case, the transfer of activity A_i of a particular radionuclide in the compartment i in a small time interval dt can be mathematically expressed as:

$$\frac{dA_i}{dt} = K_{i-1} A_{i-1} - K_i A_i - \quad A_i \qquad (1)$$

Where K_i is the fractional rate of transfer from one compartment i and is the disintegration constant of the radionuclide.

For the first compartment eq. (1) becomes

$$\frac{dA_i}{dt} = (\quad + K_i)A_i \qquad (2)$$

The solution of above equation is given by

$$A_i = A_0 \quad e^{\quad K_i \ t} \qquad (3)$$

The above equation can be rewritten in terms of the depth x (cm) and sedimentation rate, below the sediment-water interface,

$$A_i = A_0 \quad e^{\quad K_i \ \frac{x}{S}} \qquad (4)$$

Where, A_i = activity of radionuclides in the sediment at any depth (x), A_0 = activity of radionuclides in the freshly deposited sediment at depth x = 0 (the sediment-water interface), S = sedimentation rate in cm/year.

Results and Discussions

A plot of log activity of ^{137}Cs verses arithmetic sediment depth yielded a straight line (Fig. 1 and Fig. 3) and the sedimentation rate was determined to be 1.61cm/y and 1.03 cm/y by the slope of lines obtained in cores L-3 and L-5 respectively. The value of K_i was calculated to be 0.137 y^{-1} and 0.051 y^{-1} for core L-3 and L-5 respectively using the obtained values of

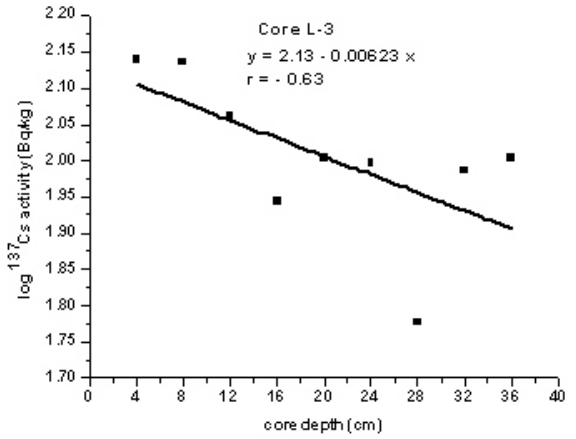


Fig. 1 Logarithmic plot of ^{137}Cs content against depth in core L-3

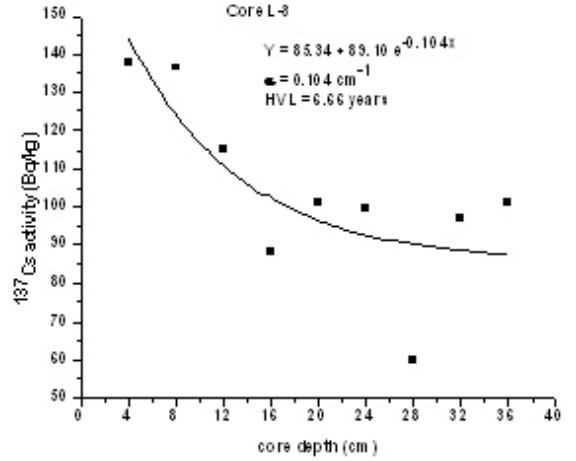


Fig. 2 Depth profile distribution of ^{137}Cs in core L-3

coefficient of x by fitting the exponential curve of activity of ^{137}Cs with depth by least square methods (Fig. 2 and Fig. 4).

The residence half life of the radionuclide in layer i was calculated using the equation $_i \frac{0.693}{K_i}$ [4] and found to be 5 years and 13.6 years in cores L-3 and L-5 respectively. With the help of the equation: $v_i \frac{L_i}{i}$, the corresponding effective migration velocity ($_i$) was obtained to be 7.2 cm/y and 3.23 cm/y over the core lengths (L_i) of 36 cm and 44 cm respectively.

Conclusions

In the core L-5, the residence time of ^{137}Cs was observed to be about 60% higher than in core L-3.

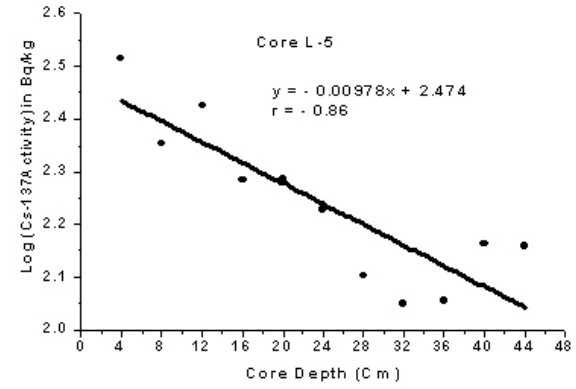


Fig. 3 Logarithmic plot of ^{137}Cs content against depth in core L-5

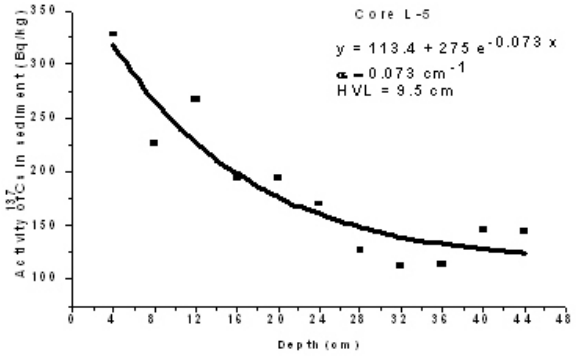


Fig. 4 Depth profile distribution of ^{137}Cs in core L-5

Since, the residence half life of radionuclide is reciprocal to effective migration velocity, therefore it is concluded that larger the residence time, lower the scavenging / removal rate of radionuclides in the sediment layers.

References

[1] Bunzl K., Forster H., Kracke W. and Schimmack W., J. Environ. Radioactivity 22 (1994) 11.

[2] Kirchner, G., J. Environ. Radioact. 38 (3) (1998) 339.

[3] Kristic D., Nikezic D., Stevanovic N., Jelic M.,Appl. Radiat. Isotopes 61 (2004) 1487.

[4] Boone F.W., Kantello V. Martti, Mayer G. Paul and Palms M. John., Health Phys 48(4) (1985) 401.

Distribution and Retention of Cs Radioisotopes in Soil Affected by Fukushima Nuclear Plant Accident

S. Mishra[1,2], H. Arae[1], A. Sorimachi[3], M. Hosoda[4], S. Tokonami[3], T. Ishikawa[1], and S.K.Sahoo[1]

1. *Project for Environmental Dynamics and Radiation Effects, National Institute of Radiological Sciences, 4-9-1 Anagawa, Inage-ku, Chiba 263-8555, Japan; E-mail: sahoo@nirs.go.jp*
2. *Environmental Monitoring and Assessment Section, Bhabha Atomic Research Centre, Trombay, Mumbai, 400085, India*
3. *Institute of Radiation Emergency Medicine, Hirosaki University, Aomori 036-8564, Japan*
4. *Graduate School of Health Sciences, Hirosaki University, Aomori 036-8564, Japan*

There was a large release of radio cesium (Cs-134 and Cs-137) to the atmosphere during Fukushima Daiichi Nuclear Power Plant (FDNPP) accident and contaminated soil over a vast area, due to fallout activity. Therefore, studies on the behavior of radio cesium especially migration in soil and its retention on soil particles is very important for external dose assessment and root uptake. We have determined the sorption coefficient (K_d) for Cs using laboratory batch method in soil samples collected from a contaminated area affected by FDNPP accident and the effect of various soil parameters on the K_d value has been studied. We have noticed that Cs sorption is mostly influenced by cation exchange process and sorbed on the surface of clay particles. From vertical depth profile of Cs in soil shows most of it is retained on the top layer within 5cm thickness. Sequential extraction of soil using various reagents may be helpful to understand better on the mechanism of Cs retention.

Introduction

A catastrophic earthquake followed by Tsunami on 11 March 2011 resulted a serious nuclear accident at Fukushima Daiichi Nuclear Power Plant (FDNPP) about 250 km north to Tokyo, Japan. As a consequence, huge amount of radioactive Cs (Cs-134 and Cs-137) released into the atmosphere and caused radioactive contamination of soils over a wide area [1,2]. From the viewpoint of radiation protection and dose assessment, it important to know the fate and geochemical behavior of Cs in soil. Radiological half life of Cs-137 is about 30 years. The retention of cesium on soil occurs through many different mechanisms, e.g. sorption, ion exchange, bonding to iron oxides and organic matter [3]. The migration rate of Cs in soils is very low since it could retain on clay minerals efficiently [4]. Factors, those affect the migration and retention of cesium in soil, are soil texture, pH, mineralogy, organic matter content and exchangeable ions [5]. Therefore, we have carried out a systematic study in a contaminated area within 20 km zone of FDNPP accident site to understand the fate of Cs and important factors affecting the migration and retention behavior in soil. Chemical characterization of soil and its effect on sorption of Cs has been studied in details. Depth profile distribution of Cs has been carried out in some selected sites in order to find out the migration rate. To understand the mechanism of Cs retention, leaching studies using sequential extraction technique have been applied.

Experimental

Surface soil and core soil samples have been collected within 20 km evacuated zone of FDNPP accident site during July and November, 2012. Ground water samples were also collected from the corresponding sites to measure the distribution coefficient (K_d) of Cs. Cs radioisotopes were analysed in soil (oven dried and <2mm size) and water (filtered through 0.45 μ membrane filter) using gamma spectrometry. Laboratory batch method was used for K_d estimation and used stable Cs as a tracer. Soil parameters affecting the retention of Cs mainly pH, organic content (OC), cation exchange capacity (CEC), $CaCO_3$ and particle size have been measured using standard analytical procedure. Soil characterization with respect to elemental and oxide composition has been carried out using inductively coupled plasma mass spectrometry (ICPMS) and X-ray fluorescence technique (XRF) respectively. Modified Tessier method has been applied for sequential extraction of radio Cs to find out the distribution of Cs in different soil components.

Results and Discussion

Activity concentrations of Cs-134 and Cs-137 in soil samples varied from 0.63-841 kBq/kg and 0.62-819 kBq/kg, respectively. The wide variation in activity concentration of Cs is mainly attributed to the radioactivity plume movement and high activity was observed in North West direction. The isotopic ratio ($^{137}Cs/^{134}Cs$) was found to vary from 0.93-1.16 indicating the activity of Cs in soil is mainly from FDNPP accident. Major elements of soil samples are given in Table 1. Distribution coefficient (K_d) values for Cs in soil varies from 55-646 L/kg. K_d values shows significant correlation with CEC and fine particles where as a reverse correlation with K_2O and positive correlation with P_2O_5. These observations suggest, sorption may be mainly controlled by ion exchange process on the clay surfaces. However, further studies

are necessary to establish the mechanism. The results of sequential extraction may support on this studies. A weak correlation observed for Cs-K_d with organic content.

Table-1: Major oxide composition of soil (mass%) analyzed by XRF

	Mean	SD	Min	Max
SiO_2	59.8	9.23	42.1	82.9
TiO_2	0.55	0.11	0.35	0.77
Al_2O_3	15.8	2.39	12.1	21.4
Fe_2O_3	4.84	1.24	3.02	8.11
MgO	1.14	0.26	0.71	1.48
CaO	1.60	0.79	0.47	3.28
Na_2O	1.72	0.58	0.82	2.70
K_2O	1.85	0.54	0.83	2.49
P_2O_5	0.13	0.09	0.01	0.42
MnO	0.09	0.03	0.04	0.15

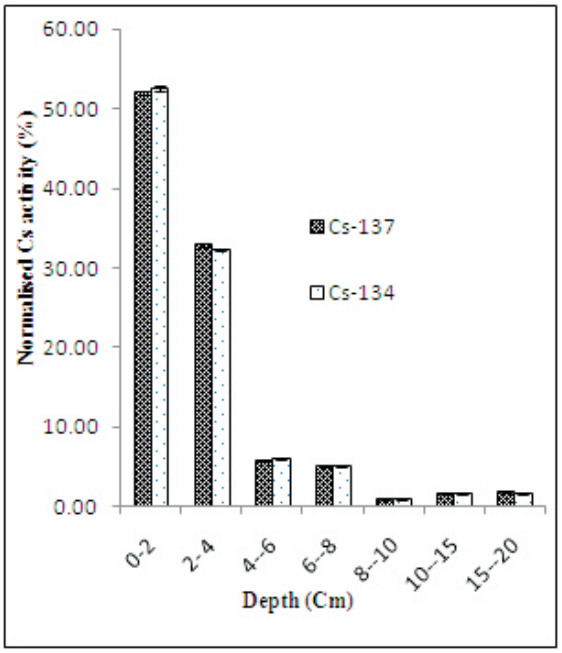


Fig. 1 Soil depth profile distribution of Cs-134 andCs-137 in a typical grassland soil affected by FDNPP accident

We have observed from depth profile studies that most of the Cs activity is retained on the top 5 cm of soil layer as shown in Fig.1. Migration rate was found more in forest soil in comparison with grassland soil. However, presence of litter in forest soil (mostly rich in organics) strongly influences the retention of Cs thereby restricting its migration into deeper soil layer.

Conclusion

Distribution coefficients of Cs found to be significantly correlated with CEC. The present field area covers mainly near terrains. We have noticed a large variation can be attributed to different soil environments. The study shows Cs isotopes are strongly retained on the surface soil mostly within 5cm thickness. However, presence of thick litter in forest favors the accumulation of Cs restricting migration into deeper soil layer. It is therefore necessary to carry out more studies to understand the mechanism of Cs retention which is in progress.

Acknowledgement

This research was supported by a Grant-in-Aid for Scientific Research from the Japan Society for the Promotion of Science. SM is thankful to the Japan Society for the Promotion of Science for the award of post-doctoral fellowship.

References

[1] T. Watanabe, N. Tsuchiya, Y. Oura, M. Ebihara, C. Inoue, N. Hirano, R. Yamada, S. Yamasaki, A. Okamoto, F. Watanabe Nara and K. Nunohara. Geochemical Journal, 46 (2012) 279.

[2] N. Yoshida and Y. Takahashi,Elements, 8(3) (2012) 201.

[3] N. H. M. Kamel and J. D. Navratil, Journal of Radioanal. Nucl. Chem. 254 (2002) 421.

[4] J. K ya, N. M. Nagy and Z. Nemes, Journal of Colloid and Interface Science 290(2005) 350.

[5] H. J. Cha, M. J. Kang, G. H. Chung, G. S. Choi and C. W. Lee, Journal of Radioanal. Nucl. Chem. 267 (2006) 349.

Tracking of Activity of Major Daughter Products (^{212}Bi , ^{212}Pb & ^{228}Ac) in Thorium Ore with time in a Hermetically Sealed Container

H. Basu, R.K.Singhal, M.V.Pimple, P.K. Sharma and A.V.R.Reddy

Analytical Chemistry Division, Bhabha Atomic Research Centre, Trombay, Mumbai 400085, India;
E-mail: hirak@barc.gov.in

During this work activities of ^{212}Bi, ^{212}Pb and ^{228}Ac were tracked at different time intervals for 30 days in hermetically sealed closed container. IAEA-RGTh-1 reference materials having 2.89% Th with floated silica powder of similar grain size distribution (< 100 m) was used for this work. Concentration of ^{232}Th in the composite sample (ore) is 3250 ± 270 Bq kg^{-1}. Gamma measurement was carried on a high-purity p-type germanium (HPGe) detector having a relative efficiency of 50%. Data obtained during this work clearly shows that there is only minor variation in the concentration of ^{212}Bi, ^{212}Pb and ^{228}Ac from the time of sealing to 30th day. Mean concentration of ^{232}Th evaluated using gamma energy line of ^{228}Ac (912 keV) and ^{212}Bi (728 keV) shows a deviation of only 0.05%, and 5.66% respectively from the certified mean value of ^{232}Th, whereas a large negative deviation of 29.9% was observed in the case of ^{212}Pb (239 keV).

Introduction

Thorium is a naturally occurring radioactive element which undergoes alpha decay with a half-life of about 14.05 billion years. In nature, virtually all thorium is found as ^{232}Th. Other isotopes of thorium are short-lived intermediates in the decay chains of higher elements, and only found in trace amounts. Radon-220 (^{220}Rn) is one of its decay products and it is in gaseous form while radium and actinium are its secondary decay products. Quantification of Thorium (^{232}Th) in the environmental samples by gamma ray spectrometry is generally carried out in closed container which are hermetically sealed and kept to equilibrium for 30 days. Content of thorium in the sample was determined by taking the average from all three gamma lines.

Thorium is estimated to be about three to four times more abundant than uranium in the Earth's crust. Thorium is found in small amounts in most of the rocks and soils whereas as granite rocks contain up to 80 g g^{-1} of thorium [1]. Because thorium oxide is highly insoluble, very little of this element is mobile in the aquatic environment. Exposure to thorium internally leads to an increased risk of liver diseases. Thorium contribution is approximately 40% in the total external gamma exposure from the Earth crust. This is mainly due to Thallium 208 (^{208}Tl) and Actinium-228 (^{228}Ac) daughters from Thorium which are very hard gamma ray emitters. In view of the above, it is very much important to quantify the content of thorium in various environmental samples by using rapid & non destructive assay techniques [1,2].

Experimental

Dried ore samples were weighed accurately and transferred to a cylindrical transparent polypropylene container (75 mm dia. and 75 mm H). Sample containers were placed on the active volume of a shielded high-purity p-type germanium (HPGe) detector with an efficiency of 50% and activity was measured for a counting time of 2,000 s. The energy calibration of the instrument was done with a mixture of ^{133}Ba, ^{137}Cs and ^{60}Co source, while the efficiency calibration was done with reference standard uranium ore IAEA-RGU-1. (7.09% U).

The energy resolution (FWHM) achieved in the calibration measurements was 1.8 keV at the 1.33 MeV reference transition of ^{60}Co. Depending on the background of the measured spectra, the Minimum Detectable Activity (MDA) was calculated to be 1.0×10^{-2} Bq kg^{-1} for ^{232}Th. From these values, a detection limit of 2.5×10^{-3} g g^{-1} was derived, for thorium.

Results & Discussion

Direct determination of ^{232}Th in solid sample without any chemical treatment using semiconductor gamma ray spectrometer is very difficult because ^{232}Th does not have intense gamma rays (lines) of it own. But there are several daughter products which have more intense lines and activities equal to those of their parents in the state of secular equilibrium. In the case of the thorium series, the existence of the equilibrium can be assumed throughout the series for any soil and rock if the emanation of thoron (^{220}Rn) is prevented. As a general belief, this can be achieved if the sample is hermetically sealed.

While quantifying a radionuclide by using gamma spectrometry, the preference will be given to only those lines which were free from interferences. In general thorium in powdered soil and rock samples was quantified using ^{212}Pb (239 keV and a gamma yield of 43.1%), ^{212}Bi (728 keV and gamma yield of 6.64%) and ^{228}Ac (912 keV and gamma yield of 29%). While doing so, it was assumed that secular equilibrium was reached between ^{232}Th and their decay products. The concentration of ^{232}Th was determined from the average concentrations of ^{212}Pb, ^{212}Bi and ^{228}Ac in the samples. Two of the radionucides ^{212}Bi and ^{212}Pb are the progeny

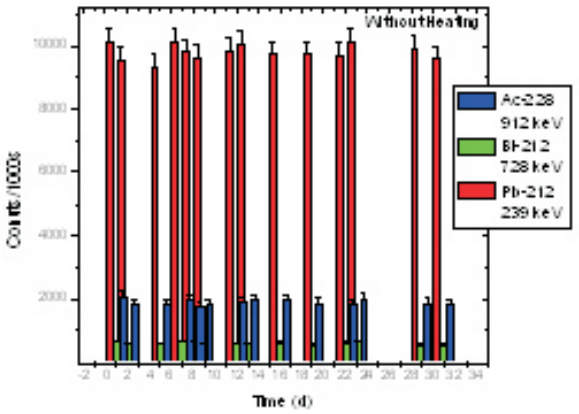


Fig. 1 Variation in counts observed in 2000 seconds for gamma line of ^{212}Bi (728keV), ^{212}Pb (239kev) and ^{228}Ac (912 keV) with time in hermetically sealed container having uranium ore

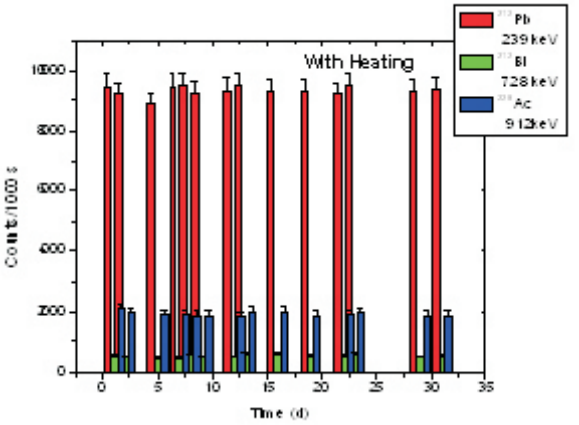


Fig. 2 Variation in counts observed in 2000 second for gamma line of ^{212}Bi (728keV), ^{212}Pb (239 keV) and ^{228}Ac (912 keV) with time in hermetically sealed container having uranium ore

of ^{220}Rn which is a gas while ^{228}Ac is directly in the secular equilibrium with ^{232}Th. Fig.1 gives the variation in counts for all three radionuclides observed at different time intervals after the hermetically sealing the container. From this Fig. 1 it is clear that there is no variation in counts with time in all the radionuclides (^{212}Bi ^{214}Pb and ^{228}Ac). The observed minor variation of 1-3% is statistical in nature. From the observation, it can be concluded that there is no substantial build up of ^{212}Bi and ^{212}Pb with time in the container.

In order to remove earlier remains of radon if any in ore grains, ore sample was heated in an oven at 90°C for eight hours and after cooling at room temperature the sample was transferred to the same cylindrical containers as used in the previous study. The similar patterns of counts were observed and thus there was no build of these radionuclides (Fig. 2). But it was interesting to note that there was 5% less counts in the case of ^{212}Pb and ^{212}Bi as compared to counts obtained without heating which may be within experimental limits.

Table 1 gives average activities of thorium (Bq kg^{-1}) evaluated from all three gamma lines at different time intervals. It is clear that mean concentration of ^{232}Th evaluated using gamma energy lines ^{228}Ac (912 keV) and ^{212}Bi (728 keV) shows only 0.05% and 5.66% respectively from the certified mean value of ^{232}Th whereas a large negative deviation of 29.9% was observed in the case of ^{212}Pb (239 keV).

Table-1: Evaluated concentration of ^{232}Th based on counts obtained for gamma energy lines ^{228}Ac (912 keV) and ^{212}Bi (728 keV) and ^{212}Pb (239 keV) at different time intervals

Time (days) elapsed after hermetically sealing of the container	^{212}Pb	^{212}Bi	^{228}Ac
0	2370	3478	3267
5	2205	3442	3124
9	2270	3236	3236
16	2280	3489	3459
22	2284	3588	3207
31	2255	3376	3217
Mean value	2277.33 ±53.71	3434.81 ±119.42	3251.67 ± 112.21
Percentage deviation from the mean value	-29.9%	5.66%	0.05%

Conclusion

Work carried out under this programme clearly indicates that quantification of thorium in mineral/solid powder samples can be carried out by using gamma line of ^{212} Bi (728 keV) and ^{228}Ac (912 keV) without any time delay whereas it is advisable to avoid ^{212}Pb (239 keV) gamma line.

References

[1] Kumar, Ajay Singhal R.K., Preetha J., Rupali K, Narayanan U Suresh Sughandhi, Manish K. Mishra, A.K. Ranade. (2008) Water Air Soil Pollut. 192 293.

[2] Z. Papp. Z. Dezso, Daroczy (1997) Journal of Radioanalytical and Nuclear Chemistry, 222(1-2) 171-176.

Determination of $^{134}Cs/^{137}Cs$ activity in the shore sand and soil samples collected around Fukushima

H. Basu[1], R.K.Singhal[1], M.V.Pimple[1], D.V. Borole[2], Nobuyoshi Yamashita[3], A.V.R. Reddy[1]

1. *Analytical Chemistry Division, Bhabha Atomic Research Centre, Trombay, Mumbai 400085*
2. *National Institute of Oceanography, Dona Paul, Goa (Ex)*
3. *National Institute of Advanced Industrial Science and Technology (AIST) Research Institute for Environmental Management Technology, Onogawa 16-1, Tsukuba, Ibaraki 305-8569, JAPAN, E-mail: hirak@barc.gov.in*

Fresh inventories of ^{137}Cs in the ambient environment are of great interest due to its importance in dating the age of the sediment. During Fukushima Dai-ichi Nuclear Power Plant (FDNPP) nuclear accident there was a large amount of input of ^{137}Cs in Pacific Ocean along the coast of Fukushima, Japan. During this work ratios of ^{134}Cs and ^{137}Cs were determined in shore sand samples along the coast of Fukushima. Determination of ^{134}Cs and ^{137}Cs was carried out using n-type detector having a relative efficiency of 50%. Activity ratios of ^{134}Cs and ^{137}Cs observed at various locations were in the range of 0.79 -0.84 with an average value of 0.81which was seen to be almost constant.

Introduction

An important environmental application of radioisotopes is to date sediments and the contaminants associated with sediments. The technique called "geochronology" is based on the radioisotope ^{210}Pb, part of the uranium decay series. Second isotopic method, often used in conjunction with ^{210}Pb geochronology to verify the age-dating of the sediments, relies on ^{137}Cs, which is a fission product mainly from atmospheric nuclear testing. The use of ^{137}Cs as an indicator of sedimentation processes is consistent, with the fact that it binds almost irreversibly to clay and silt particles and has a long half-life (30.2 years). The ^{137}Cs record begins in about 1953, and the amount in the sediment core peaks at a level corresponding to 1963, the year of the Limited Test Ban Treaty for atmospheric testing. In Europe region a second peak in 1986 is observed because of the Chernobyl event. ^{137}Cs is often used as a second independent method to age-date contaminants in sediments. An input of 1.5 x 10^{16} Bq of ^{137}Cs is estimated as entered in the ambient environment during nuclear accident at the Fukushima Dai-ichi Nuclear Power Plant (FDNPP) of Japan on 11 March 2011[1]. Therefore in the near future, there would probably be good signature of ^{137}Cs in environment, released from Fukushima, Japan.

Experimental

Samples were collected in April 2012 from nineteen different locations as shown in the Fig. 1. Samples were dried in an oven at 60°C for 48 hrs. Dried samples were passed through a sieve of having 2000 m pore size. Sieved samples were weighed accurately and transferred to cylindrical transparent polypropylene containers (75 mm D and 75 mm H). Sample containers were placed on the active volume of a shielded high-purity n-type germanium (HPGe) detector with an efficiency of 50 % and activity measured for a counting time of 80,000 s. The energy calibration of the

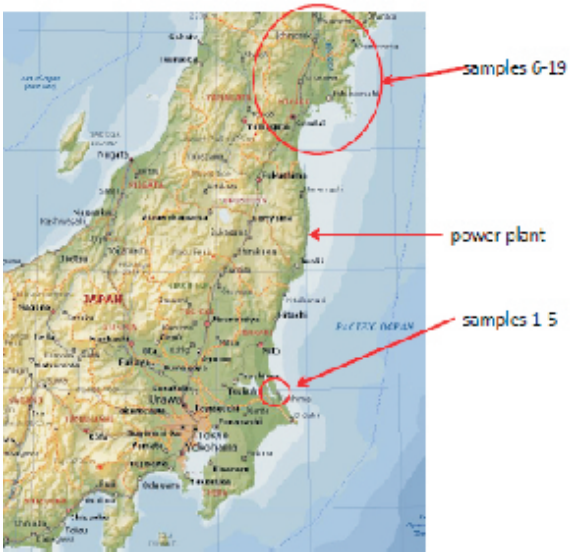


Fig. 1 Sampling locations

instrument was carried out with a mixture of ^{133}Ba, ^{137}Cs and ^{60}Co sources, while the efficiency calibration was done with reference standard uranium ore (IAEA-RGU-1).

Results and Discussion

The chemistry of ^{137}Cs in soil & shore sand is well understood. In general, deposition of ^{137}Cs in these matrices occurs primarily in association with precipitation and its initial depth distribution in the soil/sand layer is affected by infiltration of precipitation into soil/sand and adsorption of radionuclides by the soil/sand particles of the surface horizon. Knowledge of the initial distribution of fallout radionuclides in surface sample as well as the post-depositional redistribution in soil/sand sample is essential to understand their fate in the terrestrial environment. Total released amount of ^{137}Cs in Fukushima Prefecture due to the Fukushima

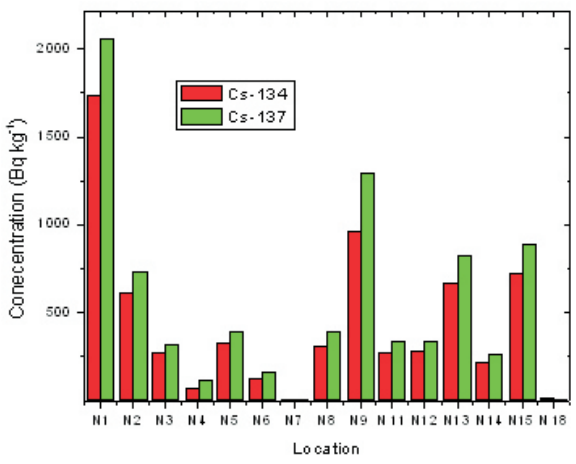


Fig. 2 Concentration of ^{137}Cs and ^{134}Cs at different locations as on March 2011

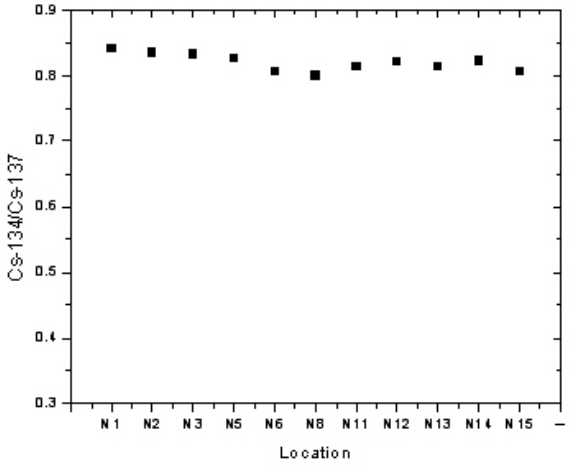


Fig. 3 Activity ratios of $^{134}Cs/^{137}Cs$

Dai-ichi Nuclear Power Plant (FDNPP) accident is estimated to be approximately $1.5X10^{17}$ Bq [2]. This radioactivity is about 7% of the 5.2×10^{18} Bq released from the Chernobyl NPP accident in April 1986. Soil, vegetation and other ecological compartments are, as expected, highly contaminated by the deposited radionuclides which were released from the FDNPP accident. Fig.2 shows the concentration of ^{137}Cs and ^{134}Cs recorded at different locations around the FDNPP.

From this Figure its clear that air driven activity settled widespreadly in a 50-100 km radial zone of Fukushima, Japan. Most of the Fukushima-derived radionuclides, which were transported from the Fukushima Dai-ichi NPP by northeast wind, were deposited on land surface by rainfall during March 21-23, 2011. Fig. 3 shows the observed activity ratios of ^{134}Cs and ^{137}Cs on March, 2011 at different locations ranged 0.79-0.84 with an average of 0.81.The ratios are seen to be almost constant throughout, independent of the locations.

However as per the work carried out by Katsumi Hirose, $^{134}Cs/^{137}Cs$ activity ratios in samples collected in different regions around Fukushima ranged from 0.99 to 1.09 with an average of 1.03[2]. The result suggests that there were no spatial and temporal variations of the $^{134}Cs/^{137}Cs$ activity from March 2011 to April 2012. It must be noted that ^{137}Cs and ^{134}Cs deposited at almost same ratio in various locations in Japan because the $^{134}Cs/^{137}Cs$ activity in the Fukushima derived radionuclides was nearly 1.0, which values are higher than that in the Chernobyl fallout ($^{134}Cs/^{137}Cs$ ratio: 0.5) [3,4].

Conclusion

Radioactivity originating from the Fukushima Dai-ichi NPP accident dominantly spread in & around Fukishima Plain by southwest and northeast wind. As the samples were collected almost a year after the incident and similar pattern of $^{134}Cs/^{137}Cs$ ratios were observed in all the nineteen locations clearly indicates no spatial and temporal variations due to local geochemical variations.

Reference

[1] Chino, M., Nakayama, H., Nagai, H., Terada, H., Katata, G., Yamazawa, H., Journal of Nuclear Science and Technology 48 (7) (2011) 1129.

[2] Katsumi Hirose. 2011 Journal of Environmental Radioactivity 111 (2012) 13.

[3] UNSCEAR, Sources and Effects of Ionizing Radiation, vol. 1:Sources, United Nations, New York, (2000) 654.

[4] IAEA. 1986. Summary report on the post-accident review meeting on the Chernobyl accident, Safety Series No. 75-INSAG-1, (1986).

Mobile Radiation Mapping of Indian West Coast by Railway Route

Laxmidhar Sahoo, Anil Otari, Shashank S.Saindane, Suri M.M.K, Rajvir Singh, Pradeepkumar K.S

Radiation Safety Systems Division, Bhabha Atomic Research Centre, Trombay, Mumbai 400085, India;
E-mail: laxmisd@barc.gov.in

Environmental radiation mapping of the Indian west coast was carried out by installing various state of the art radiation monitoring instruments and systems in a coach of the train. The objective of this monitoring was to generate the base line dose rate data of the coastal region of the four states and also to demonstrate the methodology of environmental monitoring for locating the presence of orphan sources, if any. This paper discusses the environmental radiation background mapping being carried out on Indian west coast from Thiruvanthapuram, Kerala to Kurla Terminus, Mumbai using rail route. An average dose rate recorded during this route was 104 07 nGy h^{-1} with a maximum of 184 11 nGy h^{-1}. This mobile monitoring methodology adopted and base line dose rate data generated will be useful during the radiological impact assessment, if required during any suspected radiological emergency in the region.

Keywords: Environmental Mobile Radiation Mapping, Radiation Survey, GPS

Introduction

The environmental radiation background varies from place to place due to the change in content of naturally occuring radio isotopes and concentration of radio-nuclides like K-40, decay products of naturally occuring radioactive series of U-238 and Th-232 in the earth's crust and high energy cosmic radiation. The objective of radiation monitoring during emergencies is to obtain timely and comprehensive information on the environmental radiation levels for assessment of radiological status for implementing countermeasures. Environmental mobile radiation monitoring is also an important tool to locate the presence of hot spot or any orphan radiation source or radioactive contamination. This paper describes the mobile radiation monitoring of Indian West Coast by installing radiation monitors inside a train compartment. Variation in radiation levels at different railway stations are shown in Figure1 and average radiation levels with respect to different state's coastal region, measured by different instruments are shown in Table 1.

Methodology

Radiological mapping (Saindane et al) was carried out for West Coast Thiruvanthapuram, Kerala to Kurla Terminus, Mumbai by rail route by installing state of the art radiation monitoring instruments in the train.

(a) CARMS (Compact Aerial Radiation Monitoring System) a Geiger Muller (GM) tube based real time (online) Dose Logging System with Global Positioning System (GPS), developed by RSSD, BARC (Raman et al). Energy compensated multiple GM detectors are used to enhance the sensitivity. The system was connected to an external battery which can continuously work up to 36 hours for monitoring and storing of data. The calibration factor for the system is 0.32cps per 10 nGy/h. The GPS was positioned inside the Coach near the glass window to get a uniform coverage

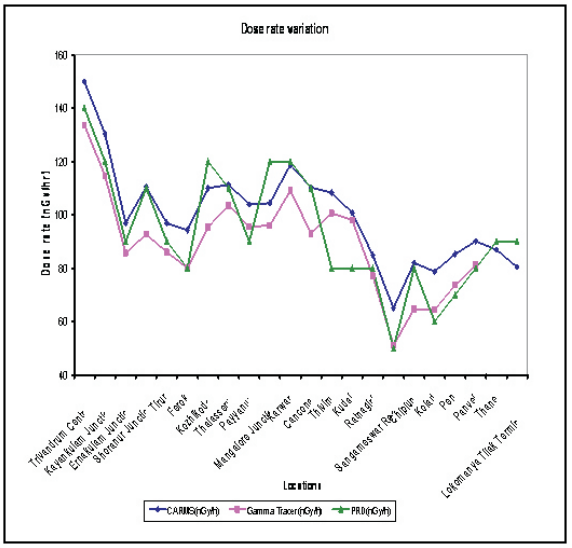


Fig. 1 Dose rate variation at different Railway stations during the radiation mapping program

of satellites. Data acquisition interval for CARMS was optimized as 10 seconds, and each dose rate data is tagged with positional co-ordinates

(b) Gamma Tracer (GT) is an offline battery operated GM based portable dose logging system. It has dose rate range of 20nGy/h - 10mGy/h.

(c) Personal Radiation Detector (PRD) is a NaI(Tl) scintillation detector based monitor with miniature photomultiplier for detection of very low radiation levels.

Maximum dose rate 184.8 nGy/h was observed at Thiruvanthapuram, Kerala.

Results and Discussion

The data acquired during this survey, the radiation background level varied from 83.28 to 114.76nGy/h in

western coastal region of the country due to terrestrial radiation. Radiation level observed was high in Kerala region and lower while coming in Maharashtra region during the monitoring period.

Table-1: State wise Radiation Levels

Coastal region	Distance (km)	Range of dose rate level CARMS(nGy/h) GT(nGy/h)	
Kerala	574	56.6 - 184.8	42 - 172
Karnataka	399	59.8 - 175.4	44 - 164
Goa	147	62.5 - 156.6	51 - 154
Maharashtra	684	53.1 - 166.0	42 - 142

Conclusions

The environmental dose rate data can be used as a base line environmental radiation level data for the region. In addition to Gamma Tracer & Personal Radiation Detector, CARMS were used for the mobile monitoring. This information can be used for assessing the impact of any radiological consequences due to any abnormal event occurrence, presence of any orphan sources or transboundary radiation emergencies.

References

[1] Saindane et al, Bulletin of Radiation Protection, 28(1-4) (2005) 266.

[2] Raman et al, Proceedings of symposium CNIRD-2005.

Uranium in Fossils and Palaeosols from Siwaliks

A. Srivastava[1], R. Patnaik[2] , P.K. Sharma[3], D.K. Avhad[3], M.K.T. Bassan[3], M.V.Pimple[3] and A.V.R.Reddy[3]

1. *Department of Chemistry, Panjab University, Chandigarh 160014; E-mail: alok@pu.ac.in*
2. *Department of Geology, Punjab, University, Chandigarh 160014*
3. *Analytical Chemistry Division, Bhabha Atomic Research Centre, Trombay, Mumbai 400085*

Paleosol and Fossil Samples from well dated Shivalik sections have been measured for their uranium content with a view to understand the role of geogenic factors in enhancing the levels of uranium in ground water bodies of Malwa region in Punjab State in North Western India. The concentration of uranium has been found to vary between 2.98 ppm to 106.86 ppm. The data so far obtained show that there may be a possibility that there could be a geogenic contribution in the enhancement of uranium concentration in ground water.

Introduction

The concern about toxicity related to uranium in Malwa region of Punjab State located in North Western part of India is increasing day by day. Kumar et al. (1) have shown that the mean concentration of uranium in groundwater is 73.1 ppb: more than five times higher than the permissible limit of 15 ppb prescribed by the World Health Organization (2). Rohit Kumar (3) has also reported that the concentration of uranium in ground water samples collected from Bathinda District in Malwa region varied between 139 and 295 ppb. Alrakabi et al. (4) too found elevated level of uranium in ground water samples obtained from this region. Several hypotheses have been postulated to explain the higher level of uranium concentration in ground water which range from fly ash to fertilizers to geogenic. In the present work an attempt has been made to look into the geogenic aspect of the problem by determining the concentration of uranium in fossils and palaeosols obtained from Siwalik palaeo-channel and floodplain deposits suspected to have been feeding the ground water of the Malwa region.

Material and Methods

Samples of fossils and paleosol were collected from the geologically well dated palaeomagnetically and biostratigraphically besides tephrachronologically sections of the Siwaliks exposed between Nahan (H.P) and Jammu (J&K). Table 1 gives the name of locations along with concentration of uranium in g/kg (ppm).These sample sites have been marked using a Global Positioning system (GPS) and are situated well above the present-day water table of the areas. The samples were dried for a day in an oven at 60 °C until moisture was driven out and then further pulverized and homogenized. 50 g of the dried, pulverized and homogenized soil samples were then put in a platinum crucible and digested using concentrated nitric acid till a clear solution was obtained. The digested sample was used directly as well as after the separation of uranium using n-tributyl phosphate (TBP) for measuring the concentration of uranium using Inductively coupled plasma optical emission spectrometry ICP (OES) and UV – Visible Absorption Spectrophotometry Jasco(V-530). The standardization of the technique was carried out by using Standard Reference Material.

Result and Discussion

Our results show that fossils and palaeosols presently situated at higher elevations, far above the present day water table, acquired anomalous quantity of uranium millions of years ago while they were buried deep inside the earth and ground water containing uranium flowing through them under anaerobic conditions. Taking cue from the above mentioned postulate it is proposed that the kind of high concentration of uranium the ground water in the Malwa region of Punjab has acquired, could only be perhaps due to uranium bearing water percolating through the recharge region (Himalayan foothills) and feeding the ground water of Punjab for millions of years. The other the possibility could be existence of uranium rich palaeo-channels of ancient river, that subsequently got dried up buried below the water table of this region which on and off kept feeding the

ground water of this region. It is worth noting that the Malwa region being waterlogged and semiarid, experiences high surface evaporation, low mobility of the ground water, high soil salinity and high concentration of Total Dissolved Salts (TDS) in the ground water, creating some sort of anaerobic conditions, which in turn may facilitate uranium enrichment.

It would be interesting to carry out further work in this direction to arrive at definitive conclusion about the source of the present uranium toxicity problem in the Malwa region of Punjab State.

Acknowledgments

The authors thank the Chairman of the Geology Department, Punjab University, Chandigarh for the help rendered by way of supporting the field trip during which the samples used in the present work were collected. The scientific discussion with Prof. R. Ramesh from Geophysics Division of Physical Research Laboratory, Ahmedabad is also duly acknowledged.

Table-1: Concentration of U in fossil and palaeosol.

Sr. No.	Name and Sample ID	Location	Siwalik Formation and Age	U by Spectrophoto metry (ppm)	U by ICP – OES with separation (ppm)	U by ICP - OES without separation (ppm)
1	Fossil DKB - 2	Devni Khadri (H.P.) 30° 31' 08.23" 77° 15' 39.54"	Tatrot 2.5 Ma	10.00 ± 1.00	9.02± 0.91	9.83 ± 0.97
2	Palaeosol KHPS	Khetpurali 30° 40' 41.50" 76° 59' 43.75"	Tatrot 2.5 Ma	ND	ND	ND
3	Fossil MEJ	Masol 30° 49' 41.78" 76° 50' 51.79"	Tatrot 2.5 Ma	106.86 ± 5.39	104.86± 5.28	105.3 ± 5.30
4	Palaeosol HPS - D	Haritalyangar, H.P. 31° 31' 27.91" 76° 38' 10.89"	Dhok Pathan 8.85 Ma	13.08 ± 1.78	12.73 ± 1.27	12.91 ± 1.29
5	Fossil DKB - 1	Devni Khadri (H.P.) 30° 31' 08.23" 77° 15' 39.54"	Tatrot 2.5 Ma	11.58 ± 1.16	9.86 ± 0.96	9.93 ± 0.97
6	Fossil MT	Masol 30° 49' 41.78" 76° 50' 51.79"	Tatrot 2.5 Ma	62.11 ± 2.21	59.34 ± 1.36	59.60 ± 1.40
7	Palaesol MPS-N	Moginand (H.P.) 30° 31' 01.5" 77° 13' 14.4"	Tatrot 2.5 Ma	2.99 ± 0.18	2.88 ± 0.11	2.98 ± 0.12
8	Sandstone (between palaeosols) HSST	Haripur Khol (H.P.) 30° 28'02.52" 77° 23' 31.25"	Tatrot 2.5 Ma	24.89 ±2.49	21.66 ± 1.04	21.85 ± 1.05
9	Palaesol MPS	Moginand (H.P.) 30° 31' 01.5" 77° 13' 14.4"	Tatrot 2.5 Ma	ND	ND	ND
10	Soil - 5	SRM - 1	SRM - 1	3.52 ± 0.32	3.22 ± 0.25	3.52 ± 0.32

References

[1] A. Kumar, N. Usha, P.D. Sawant, R.M. Tripathi, S.S. Raj, M. Mishra, S. Rout, P. Supreeta, J. Singh, S. Kumar and H.S. Kushwaha, H. S., Human and Ecological Risk Assessment, 17(2011) 381 .

[2] WHO Guidelines for Drinkingwater Quality, 4th Ed., Geneva, Switzerland, (2011).

[3] Rohit Kumar M.Sc Thesis, Chemistry Department, Panjab University, Chandigarh (2012).

[4] M. Alrakabi, G. Singh, A. Bhalla, S. Kumar, A. Srivastava, B. Rai, N. Singh, J. S. Shahi, and D. Mehta, J Radioanal Nucl Chem 294 (2012) 221.

Radiation Levels and Radionuclide Distributions In Terrestrial, Atmospheric and Aquatic Environs of Gogi Uranium Mining Region of North Karnataka

Yashodhara I.[1], Sudeep Kumara K.[1], Karunakara N.[1] and Tripathi R.M.[2]

1. *University Science Instrumentation Centre, Mangalore University, Karnataka, India; E-mail: drkarunakara@gmail.com*
2. *Environmental Assessment Division, Bhabha Atomic Research Centre, Mumbai 400 085*

A comprehensive study to generate a database on baseline radiation levels and radioncuclides distribution was carried out around the proposed Gogi uranium mining region of Shahpur taluk of Yadgiri district in North Karnataka. The Baseline database on radioactivity and trace elements concentrations in different environmental matrices around the proposed uranium mining region is essential because such a study would help to assess radiological impact of long term mining operations on the environment. The gamma absorbed dose rate, activity concentrations of primordial radionuclides in terrestrial, atmospheric and aquatic environmental samples were measured by employing standard methods. The results observed for the Gogi region are compared with the literature values reported for other parts of India and worldwide average values.

Keywords: Gogi, Uranium, soil, water, air.

Introduction

The two prominent sources of external radiation are cosmic rays and terrestrial gamma rays. Terrestrial gamma rays derived essentially from ^{40}K and the radionuclides belonging to ^{238}U and ^{232}Th series that are present in earth's crust. Uranium is the heaviest naturally occurring element present in the crust of the earth. It leaches out from rocks and minerals, mixes with water and gets transported along with ground water. Consequently, uranium is found in small quantities in dissolved and suspended particulate forms in surface and underground water. Radium-226 is a long-lived ($T_{1/2}$=1600 y) and ^{222}Rn is a short lived ($T_{1/2}$=3.8 d) daughters of the ^{238}U decay series and these radionuclides also found in the water in trace quantities.

Gogi (16 44' 00" N, 76 45' 00" E), a village in Shahapur taluk in Yadgiri district of Karnataka, India has been identified as a prospective uranium mining area. Studies aimed at establishing the baseline data on radiation levels and radionuclides distribution in various environmental matrices around proposed mining region is important because such a study would help to assess the impact of our scientific and technological activities on the environment. This paper presents the results of the comprehensive study undertaken to generate database on baseline radiation levels and radioncuclides distribution around the proposed Gogi region.

Materials and Methods

The study covered entire area in the 0-5 km Core Zone, 5-15 km Buffer Zone I and 15-30 km Buffer Zone II with Gogi village as the common centre of all the 3 zones (Fig. 1). The gamma absorbed dose rates were measured by (i) using a portable RDS-31 (Mirion, France) gamma survey meter (for short term measurements), and (ii) TLD's for long term measurements. The activity concentrations of ^{40}K, ^{232}Th and ^{226}Ra in soil samples, were measured using a 42% relative efficiency n-type or a 38% relative efficiency p-type HPGe gamma spectrometers. Concentration of uranium in the water samples was measured using LED based laser fluorimeter. The activity concentration of ^{226}Ra in water samples was measured by pre-concentration using MnO_2 powder and subsequent gamma spectrometry. The ^{222}Rn concentration in the water was measured by emanometry method. High volume air sampler (APM 460 BL, Envirotech) was employed for air sampling and the activity concentrations of different long lived radionuclides in the air samples were measured by HPGe gamma spectrometry. The indoor and outdoor radon concentration in air was measured using AlphaGuard and Scintillation based radon monitors (SRM). Long term measurements of ^{222}Rn



Fig. 1 Map of Gogi uranium mining region and sampling locations

concentration in air were performed using pin-hole cup dosimeters.

Results and Discussion

The gamma absorbed dose rates were found to vary in the range of 59 – 274 nSv h^{-1} with a median value of 115 nSv h^{-1}. The median value of gamma absorbed dose rate was higher in core zone because of natural mineralization of heavy elements in this zone. The median value of gamma absorbed dose rates observed for Gogi region was higher when compared to the mean values of 56.5 nSv h^{-1} [1] and 62.1 nSv h^{-1} [2] reported for different regions of India and the world average value of 39.2 nSv h^{-1} [3]. The activity concentrations of ^{40}K, ^{232}Th and ^{226}Ra in the soil samples varied in the ranges of 56.2–1371.1 Bq kg^{-1}, 10.2–576.9 Bq kg^{-1} and 5.8– 154.8 Bq kg^{-1} with corresponding median values of 778.9±18.1 Bq kg^{-1}, 84.4±2.2 Bq kg^{-1} and 33.3±1.0 Bq kg^{-1} respectively. The mean values of activity concentrations of primordial radionuclides were higher for core zone when compared to other zones. The study showed highly non uniform distribution of primordial radionucildes in the region with activity concentrations varying significantly within a small area, which is due to highly localized mineralization in this area. The concentration of ^{40}K and ^{232}Th observed in the present study was higher when compared to the all-India average value and the worldwide average value [3]. The activity concentrations of ^{238}U, ^{226}Ra and ^{222}Rn in the water samples varied in the range of 11.1 – 33198.8 mBq L^{-1}, 19.5–10506 mBq L^{-1} and 0.4 – 2115.3 Bq L^{-1} with the median values of 106.3±10.0 mBq L^{-1}, 52.6±4.5 mBq L^{-1} and 17.4±0.6 Bq L^{-1}, respectively and these values are higher when compared to the values reported for other regions of India and the world [3-6]. The median value of ^{222}Rn concentration in the water samples of Tube-wells of Gogi region were higher when compared to those reported for other regions of India [7]. The activity concentrations of ^{7}Be and ^{210}Pb in air samples varied in the ranges of 1.1–6.5 mBq m^{-3} and <0.1 – 4.0 mBq m^{-3} with the corresponding mean values of 3.7±0.3 mBq m^{-3} and 1.2±0.2 mBq m^{-3}. The indoor and outdoor radon concentration in air varied in the ranges of <5.0 – 24.0 Bq m^{-3} and 5.5–12.7 Bq m^{-3} with the mean values of 11.9±5.0 Bq m^{-3} and 8.3±4.5 Bq m^{-3} respectively. The indoor radon concentration observed in the present study was comparable with the All-India and worldwide average values [8 and 9].

Aknowledgements

The authors are thankful to the Board of Research in Nuclear Sciences (BRNS), Mumbai for sponsoring the research project which has helped in undertaking this study.

References

[1] U.C. Mishra and S. Sadasivan, J. Sci. Ind Res., 30 (1971) p. 59.

[2] K.S Nambi, V.N Bapat, M. David, V.K. Sundaram, C.M. Santa and S.D. Soman, Radiation Protection Desimetry, (1987).

[3] United Nations Scientific Committee on the Effects of Atomic Radiation (UNSCEAR-2008). Report to the General Assembly, Vol. 1. (2008), Annex. B.

[4] N.Nagaiah, S. Malini, L. Paramesh, P. Venkataramaiah and M. Raghavayya, Engineering Geology and the Environment, Balkema, Rotterdam, (1996) 2033.

[5] M. J. Frissel, R. O. Blaauboer, H. W. Koster, H. Pleenhouts, J. F. Stoutjesdu and L. H. Vaas, Radiation Physics Chemistry, 34 (1989) 327.

[6] Z. Vukovic, M. Mandic and D. Vokovic, J. Radioact., 33(1) (1996) 41.

[7] K. Siddappa, H. M. Somashekarapaa, Y. Narayana, N. Karunakara, D. N. Avadhani and H. M. Mahesh. Final Report, BRNS-DAE Research Project. (2000).

[8] T. V. Ramachandran and L. A. Sathish, J. Environ. Radioact., 102 (2011) 975.

[9] United Nations Scientific Committee on the Effects of Atomic Radiation (UNSCEAR). Sources and effects of ionizing radiation. Report to the General Assembly, (2000), Annexe B.

Radiological Characterization of Drinking Water in Jaduguda Uranium Mining Area and Assessment of Effective Dose to Member of Public

S.K. Sahoo, S.Mohapatra, J.S. Dubey, V.K. Thakur, P. Lenka, A.C. Patra, V.N. Jha, P.M. Ravi and R.M. Tripathi

Health Physics Division, Bhabha Atomic Research Centre, Trombay, Mumbai-400 085, India; E-mail: sksbarc@gmail.com

Present work deals with measurement of the radionuclide concentrations like total uranium, ^{226}Ra, ^{210}Po and ^{210}Pb in drinking water of Jaduguda uranium mining area and assessment of the corresponding ingestion dose to member of public. Total uranium concentration varied between 0.2-11.6 with an average value of 4.2 g/L. The concentration of ^{226}Ra, ^{210}Po and ^{210}Pb ranged between 3.5-79.0, 1.5-18.8 and 20.1-50.7 with average values of 15.3, 9.8 and 26.7 mBq/L respectively. The mean value of total effective dose to member of public due to these radionuclides via drinking water ingestion was found to 57.2 with a range of 25.8-102.7 Sv/y.

Introduction

Natural radionuclides present in every compartment of environment with wide variation in concentration depending on regional geological formation, prevailing environmental conditions etc. Natural radioactivity arises mainly due to ^{238}U and ^{232}Th series isotopes and ^{40}K in the environment. Natural radiation is the largest contributor to the total radiation dose to population. About 20% of the natural radiation dose is due to external radiation from terrestrial radioactivity [1]. The radionuclides that are present in soils and host rocks can be leached to the corresponding aquifers depending upon their solubility and concentration and hence prevails in surface and ground water bodies. Estimation of concentration of these radioactive elements in various environmental matrices is pivotal and of major concern. The natural radioactivity scenario may modify drastically due to uncontrolled anthropogenic activities. Mineral mining is one of the anthropogenic practices which has the potential to redistribute the minerals in the adjoining area and may enhance natural radioactivity if adequate safety measures are not implemented [2]. The levels of terrestrial environmental radiations are related to the type of rocks from which the soil originates [1]. Extraction of ores and subsequent processing technology may lead to enhanced levels of NORM in the sourrounding areas and hence mining activities in that particular area may redefine the radiological scenario and modify the environment. Water intake is an essential part of human diet, may contribute to chronic natural radioactivity exposure. Drinking water consumption may be crucial in the areas prone to exposure of natural alpha emitters [1]. Measurements of natural radioactivity in drinking water are essential for assessment of the ingestion dose to members of the public. The exposure due to ingestion of naturally occurring radioactive materials, especially the alpha emitters of ^{238}U and ^{232}Th series is the area where relatively less studies carried out due to its tedious radio-chemical processing and occurrence of low levels in water. Present study deals with measurement of the radionuclide concentrations like total uranium, ^{226}Ra, ^{210}Po and ^{210}Pb in drinking water of Jaduguda uranium mining area and assessment of the comprehensive ingestion dose to members of the public. These are the most significant radionuclides typically found in drinking water with respect to radiation dose evaluation.

Experimental

Drinking water samples were collected from the local drinking water sources (mostly tube well) in Jaduguda uranium mining area as per the IAEA standard protocol [3]. Details of the study area are given elsewhere [4]. Samples were analysed by laser fluorimeter for total uranium concentration. Detail methods of sample processing, instrumnet calibration and analysis are given elsewhere [5]. ^{226}Ra concentration was estimated by emanometry technique. Details of the instrumentation are given elsewhere [6]. ^{210}Po isotopic concentration was estimated by autodeposition on silver planchet followed by counting in alpha spectrometry. As the alpha energy is used for detection and measurement, the ^{210}Po requires separation from the bulk matrix and preparation of a thin, uniform monomolecular source for accurate measurement [7]. The sample source preparation for the alpha spectrometric determination of ^{210}Po is optimized, in order to achieve highly reproducible alpha sources with high resolution. The concentration of ^{210}Pb was measured by gross alpha counting system after radiochemical separation [8].

Results and Discussion

The measured activity concentration of total uranium in drinking water samples varied between 0.2-11.6 with an average value of 4.2 g/L. The activity concentration of ^{226}Ra, ^{210}Po and ^{210}Pb ranged between 3.5-79.0, 1.5-18.8 and 20.1-50.7 with average values of

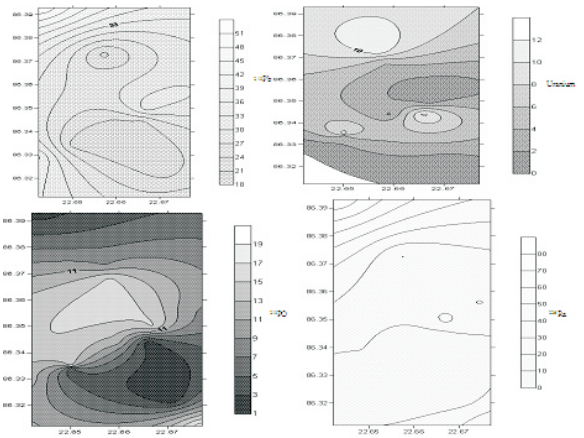


Fig. 1 Contour map of radionuclide concentration distribution

15.3, 9.8 and 26.7 mBq/L, respectively. The contour map of radionuclide concentration distribution is shown in Fig. 1. The uranium and ^{226}Ra level in drinking water samples was found to be well within the national (AERB) and international (WHO, US EPA) guideline values. The reason for wide variation of activity concentration may be due to heterogeneous distribution of uranium deposits in the region. The concentration of uranium and ^{226}Ra obtained in the present study is comparable with the other reported studies of the same region [4,6]. The concentration of ^{226}Ra, ^{210}Po obtained is comparable with the reported values of Syria [9].

Effective dose due to drinking water ingestion for adult population (> 17 yrs) can be computed [5] by using the yearly intake of drinking water (4.05 l/d) and IAEA, BSS dose conversion factors for the concerned radionuclides [10]. Mass concentration of natural uranium observed in groundwater can be expressed in activity concentration using a conversion factor of 25 Bq/mg assuming natural uranium composition. The ingestion dose due to U, ^{226}Ra, ^{210}Po and ^{210}Pb to adult population residing around Jaduguda mining complex from drinking water sources works out to be 0.3-19, 1.4-32.7, 2.7-33.3 and 20.5-51.7 Sv/y, respectively. The mean value of total effective dose to member of public due to these radionuclides via drinking water ingestion was found to 57.2 with a range of 25.8-102.7 Sv/y. The average effective dose is well below the WHO reference level of 100 Sv/y. The individual contribution of radionuclides to the total dose is shown in pie chart (Fig. 2). ^{210}Pb and ^{210}Po are the main contributors towards the total dose received by the population.

Conclusion

The reason for wide variation of activity concentration may be due to heterogeneous distribution of uranium deposits in the study area. The mean value of total effective dose to member of public due to these

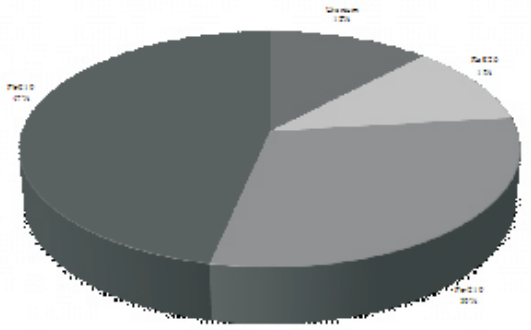


Fig. 2 Contribution of radionuclides to total ingestion dose from drinking water

alpha emitting radionuclides via drinking water ingestion was found to 57.2 with a range of 25.8-102.7 Sv/y. The average effective dose is well below the WHO reference level of 100 Sv/y. The drinking water which is mostly the ground water (tube well) is not affected by the mining industry and the activity concentration is due to natural distribution of radioanuclides.

Acknowledgement

Authors are thankful to the authorities of Uranium Corporation of India Limited for providing necessary facilities and support. The help and support provided during sampling, by the colleagues of Health Physics Unit, Jaduguda is also acknowledged.

References

[1] UNSCEAR, Sources and Effects of Ionising Radiation, United Nations, New York, (2008).

[2] M. Gavrilescu, L. V. Pavel, I. Cretescu. J. Hazard. Mater., 163 (2009) 475.

[3] IAEA. Technical Report Series 295, Vienna, Austria, (1989).

[4] N. K. Sethy, R. M. Tripathi, V. N. Jha, S. K. Sahoo, A. K. Shukla, V. D. Puranik. J of Environ Protect, 2 (2011) 1002.

[5] S.K.Sahoo, S. Mohapatra, A.Chakrabarty, Sumesh C.G., V.N. Jha, R.M. Tripathi and V.D. Puranik. Radiat Protect and Dosim, 136(2) (2009) 108.

[6] S.K. Sahoo, B.K. Rana, S.Mohapatra, J.S. Dubey, V.K. Thakur, P. Lenka, V.N, Jha, R.M. Tripathi and V.D. Puranik, Proc. of National Symposium on Environment-18 (2013) 57.

[7] IAEA. Analytical Quality in Nuclear Applications Series, (2009), No. 12.

[8] J. S. Dubey, S. K. Sahoo, P. Lenka, S. Mohapatra, V.N. Jha, B.K. Rana, R. M. Tripathi, and V. D. Puranik. Proc. of National Symposium on Environment-18, (2013), 53.

[9] I. Othman and T. Yassine. Environment International, (1996), 22, suppl. 1, S355.

[10] BSS. International Atomic Energy Agency, (1996), Safety series no. 115.

Comparative Evaluation of Different Extractants towards Cloud Point Extraction of Metal Ions

Neelam Kumari, P.N. Pathak, P.K. Mohapatra

Radiochemistry Division, Bhabha Atomic Research Centre, Trombay, Mumbai 400 085, INDIA; E-mail: ppathak@barc.gov.in)

The cloud formation behavior of nonionic surfactant Triton X-114 (1,1,3,3-Tetramethylbutyl) phenyl-polyethylene glycol; t-Oct-C_6H_4-$(OCH_2CH_2)_xOH$, x = 7-8) was investigated in Na-acetate medium. The effects of organic dopents (often added for metal extractions) such as dibenzoylmethane (DBM), and thenoyltrifluoroacetone (HTTA) on metal ions (viz. U(VI), Am(III), Sr(II), and Cs(I)) extraction were investigated. Extraction (%) of metal ions followed the order: U(VI) > Am(III) > Sr(II) > Cs(I).

Introduction

There is a growing interest in the development of environmentally benign techniques for the determination of low concentrations of toxic / radioactive elements in environmental samples. This is particularly relevant for the routine control measurements of the total radioactivity in aqueous solutions and in the assessment of radiological impact of various anthropogenic activities. These measurements have to be performed on very dilute solutions and therefore often require pre-concentration of the radionuclides / toxic metal ions from relatively large volumes of the sample solutions [1]. In this context, cloud point extraction (CPE) appears attractive as an environmentally benign liquid–liquid extraction method due to inherent features like low cost, safety and a high preconcentration factor. This extraction technique is based on the clouding phenomenon of nonionic surfactants in aqueous solutions after an increase in temperature or the addition of a salting-out agents. This method has shown promise for the separation / pre-concentration of trace metals in various samples with complicated matrices [2]. The temperature at which the separation of an aqueous micellar solution of a surfactant into a concentrated phase (coacervate) containing most of the surfactant, and a dilute aqueous phase is referred to as the cloud point (CP). The metal (solute) extraction is dependent on its micellar solubilization and often requires large amounts of the surfactant compared to the solute. CPE is generally performed in the presence of an additional chelating agent, capable of forming a lipophilic metal complex and favors its partitioning in the micellar phase.

This paper presents the cloud formation and extraction of different metal ions such as U(VI), Am(III), Sr(II), and Cs(I) employing a nonionic surfactant Triton X-114 (1,1,3,3-tetramethylbutyl) 1phenyl-polyethylene glycol; t-Oct-C_6H_4-$(OCH_2CH_2)_x$ OH, x = 7-8) in Na-acetate medium. The relative performance of different extractants such as dibenzoylmethane (DBM), and thenoyltrifluoro-acetone (HTTA) on cloud formation and on metal ions (viz. U(VI), Am(III), Sr(II), and Cs(I)) extraction have been evaluated.

Experimental

All the extraction studies were performed in duplicate in polypropylene (PP) tubes of 15 mL capacity. The desired radionuclides were spiked in 0.1 M Na-acetate (generally 5 mL) containing 0.12 % (w/v) of Triton X 114 surfactant, which was optimized on the basis of cloud formation behavior, without/with extractants molecules. Solutions of DBM or HTTA in methanol were used (on v/v basis) for studies. The loss of radioactivity for ^{233}U and ^{241}Am (due to their hydrolysis) on the walls was within (±10-20%) under different experimental conditions of the present study. This loss was confirmed by washing the tubes with dilute HNO_3 solutions and counting the activity in the washings. The radioactivity loss was corrected by blank experiments under identical experimental conditions without the surfactant. The metal ion concentration (expressed in terms of counts, A_i) in the sample solutions before CP were taken as initial concentration, and those present in the supernatant (after CPE experiments, A_f) were treated as concentration after extraction. After CPE, the sample tubes were centrifuged for about 20 minutes for phase separation and cooled to allow the settlement of the heavy surfactant phase in the bottom. The extent of the extraction of the metal ions was determined by counting their radioactivity by LSC (sample size: 0.1 mL for ^{233}U) or by gamma spectrometry (sample size: 1.0 mL for ^{241}Am, ^{137}Cs, and $^{85,89}Sr$) in the samples collected from the respective stock solutions and the supernatants. The percentage extraction (% E) was defined as:

$$\%E = \frac{A_i \quad A_f}{A_i} \quad 100 \qquad (1)$$

Material balance and the reproducibility of the metal ion extraction data were within the error limits of ±10%.

Results and Discussion

The clouding behavior of Triton X 114 in presence of DBM and HTTA (up to $1x10^{-3}$ M in

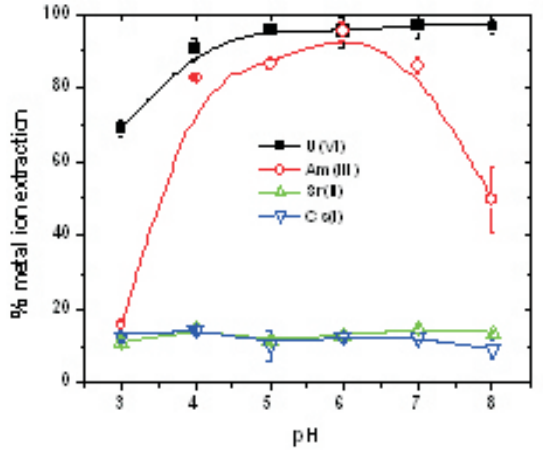


Fig. 1 CPE of metal ions as a function of aqueous phase pH; Aqueous phase: 0.1 M Na-acetate; [DBM]: 5 x 10^{-3} M in methanol; Triton X-114: 0.12% (w/v); T:50°C

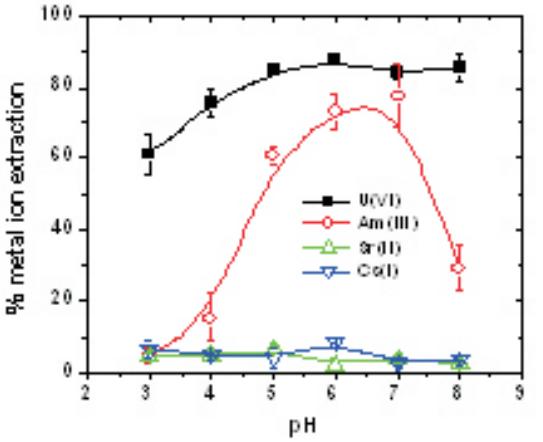


Fig. 2 CPE of metal ions as a function of aqueous phase pH; Aqueous phase: 0.1 M Na-acetate; [HTTA]: 1 x 10^{-3} M in methanol; Triton X-114: 0.12% (w/v); T:50°C

methanol) in 0.1 M Na-acetate solution at pH 8 was investigated. The presence of DBM molecules along with methanol in the sample solutions suppressed the CP of Triton X 114 from 25°C to 4±1°C. This behavior can be attributed to the dehydration of the ether groups of the surfactant molecules. The extractant and methanol molecules may react with water molecules through H-bonding. There may be a mutual competition for hydration by water molecules between the ethylene oxide group of nonionic micelles and the additives resulting in the less hydrated micelles. These micelles approach each other and coalesce at the CP. However, similar experiments using HTTA (in methanol) showed only marginal influence on the clouding behavior (CP: 21±2°C) of the surfactant micelles in the aqueous medium. It appears that HTTA (being more acidic in nature) induces repulsion between the charged micelles and its deprotonated form leading to minor change in the cloud point.

The recovery of ^{233}U, ^{241}Am, ^{85,89}Sr, ^{137}Cs radionuclides from aqueous samples (0.1 M Na-acetate) was studied employing DBM and HTTA as the extractants and Triton X 114 as the nonionic surfactant. The choice of these extractants was based on the fact that both are acidic extractants and can perform well in low acidic solutions. In addition, these two extractants displayed clear cloud formation behavior which could be easily separated for the analysis of the radionuclides. Extraction studies of metal ions (viz. ^{233}U(VI), ^{241}Am(III), ^{85,89}Sr(II) and ^{137}Cs(I)) at tracer concentrations, were carried out from 0.1 M Na-acetate solutions containing Triton X 114 (0.12 %, w/v) + 5x10^{-3} M DBM (methanol) in pH range of 3 to 8 at T = 50 °C (Fig.1). The extraction of U(VI) increased gradually from 69 % (at pH 3) to 98 % (at pH 8). Similarly, Am(III) extraction increased from 16.1 % (at pH 3) to 95.2 (at pH 6) beyond which a decrease was observed. This decrease was attributed probably to the hydrolysis of Am(III) and HTTA at higher pH. It appears that even though U(VI) may be hydrolyzed at higher pH, the formation of cationic species like $UO_2(OH)^+$ may still be extracted. However, there was negligible extraction (~10(±2)%) of Sr(II) and Cs(I) ions under identical experimental conditions. Similar observations were made using HTTA as the extractant (Fig.2). The extraction profile is consistent with the fact that metal ions with higher charge display better extraction.

Conclusions

The cloud formation behavior of Triton X-114 was investigated in 0.1 M Na-acetate in the presence of DBM, and HTTA (dissolved in methanol). There was a sharp decrease in CP of Triton X-114 (25°C) for DBM (4±1°C) in comparison to HTTA (21±2°C) system. CPE experiments showed that DBM and HTTA can be used for the recovery of ^{233}U and ^{241}Am from aqueous solutions. It will be of interest to compare a series of beta diketones for their cloud formation behavior and evaluate their potential for metal ion uptake studies from environmental samples.

References

[1] Larpent, C., Prévost, S., Berthon, L., Zemb, T., Testard, F. New J. Chem., 31 (2007) 1424.

[2] Wen, X., Zhao, Y., Deng, Q., Ji, S., Zhao, X., Guo, J. Spectrochim. Acta Part A, 89 (2012) 1.

Applicability of Analytical Instrument in Trace Evidence Analysis

Mukesh Sharma[1] and Shailendra Jha[2]

1. *Physics Division, State Forensic Science Laboratory, Jaipur 302 016, Rajasthan, India; E-mail: mksphy@gmail.com*
2. *State Forensic Science Laboratory, Jaipur 302 016, Rajasthan, India*

In the present paper, we explain the importance of the analytical instrument used in the field of forensic science for the analysis of the trace evidences collected from the scene of occurrence. The forensic scientist has to rely upon these instrumental analyses of trace amounts of materials like drugs, toxicological specimens, GSR, fibres, glass, paints, soil etc. Through this paper, reviews on these techniques which are extensively used in forensic sciences are reported. Our report summaries on the basis of analytical problem facing for a forensic expert and techniques employed to tackle them like XRD/XRF, inductively coupled plasma (ICP) techniques, Raman spectroscopy and microscopy (optical, GRIM, electron microscopy, TEM).

Introduction

The analysis of a crime scene involves the participation of experts in both the physical and biological sciences as well as in many areas of technology and law enforcement. Forensic chemists study fingerprint patterns and fiber, glass, gunshot, and other types of residues; analyze drugs and poisons; examine possible forgeries; analyze residues for possible arson and explosive crimes; and carry out DNA analyses to identify possible criminal suspects.

In this paper, we have tried to explain the analytical instruments available for analysis of trace evidence analysis.

Elemental Chemical Analysis using XRD /XRF

The X-ray fluorescence (XRF)/ X-rays Diffarction techniques have been used in forensic science for several decades [1-3]. Unlike many other analytical techniques, XRF does not affect samples as it is a non-destructive method.

Forensic science involves the application of science to law. The physical traces can commonly include paint flakes, glass fragments, fibers, slivers of metal, soils, building materials, stains of any description, corrosion products, loose powdered materials, gun shot residue (GSR), etc. [4]. Possible applications of the XRF/XRD technique on different kind of forensic samples are summarized in the Fig. 1.

Inductively Coupled Plasma (ICP) Mass Spectrometry Technique

The discrimination of sheet glass exposed to high temperature by the determination of trace impurities using ICPMS was reported. The determination of iron in glass by laser ablation and solution sampling comparing dynamic reaction cell-ICPMS and high resolution (sector field) ICPMS was also reported [5]. Several reports on the analysis of glass by LIBS, including a comparison of the results from LA-ICPMS, ìXRF, and LIBS for the analysis of the same set of samples [6], the comparison of different irradiation wavelengths for the analysis of glass [7], and two other research studies on the application of LIBS to glass analysis [8] were published.

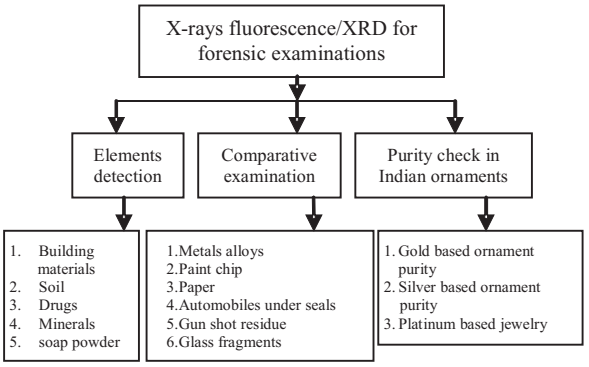


Fig. 1 Summary of use of X-ray techniques in forensic sciences [4]

Raman Spectroscopy Techniques

There has been resurgence in Raman spectroscopy for its application in forensic science. This method allows for the measurement of the inelastic scattering of light due to the vibrational modes of a molecule when irradiated by an intense monochromatic source such as a laser. The Raman technique presents advantages such as its non-destructive nature, its fast analysis time, and the possibility of performing microscopic in situ analyses. In its forensic application, it is a versatile technique that covers a wide spectrum of samples such as drugs of abuse, trace evidence, fibers and inks [9-10].

Instruments characterized by a high sensitivity and coupled to light microscopes supply a high potential for the micrometric and in situ analysis of many types of materials of forensic interest. The analysis of textile fibers constitutes a clear example. The usefulness of this technique for the forensic analysis of fibers mainly focuses on the detection of dyes.

Microscopy and Electron Microscopy

Microanalysis is the application of a microscope and micro scopiea / techniques to the observation, collection, and analysis of micro evidence that cannot be clearly observed or analyzed without such devices. Microanalysis today generally deals with samples in the milligram or microgram size ranges. Microscopes and the techniques to be discussed will be limited to those that employ light in the visible, ultraviolet (UV), and infrared (IR) frequency ranges or use electrons for illumination. Analysis with a microscope may be limited to observations of morphology or involve the collection of more sophisticated analytical data, such as optical properties, molecular spectra, or elemental analysis [11,12]. A wide verity of microscopes is available for use in a forensic laboratory and they can examine a wide variety of materials.

Traces such as fragments of glass, paints or gunshot residues most often occur in very small quantities. Thus, sensitive analytical methods are required in order to obtain satisfactory results from small amounts of sample. For the selection of proper analytical methods one should take into account the fact that the method is not allowed to destroy the samples because the material might be re-used. One of these non-destructive methods is scanning electron microscopy with an energy dispersive X-ray spectrometry (SEM DX) [9]. It is a powerful tool for forensic purposes because one can examine objects considering their morphology and the elemental composition. Moreover, the obtained results can be evaluated by using suitable methods of chemometric analysis [13]. The paint coat of a car body consists of a number of successively overlaid paint layers. These layers differ from each other in terms of their ingredients, i.e., resin, pigments and fillers. The number of layers making up a car covering depends on its type. In brand new cars and in those that have not been repainted there are only three to four layers.

Discussions

The analytic techniques initiated by forensic experts have continued to expand in complexity and improve in reliability. Many new analytic tools have been applied to analytical problems in almost all areas of the field, and the technology continues to open new areas of research. Over the last two decades, a new analytical tool has been developed. Forensic examiners continue to be concerned about conducting unequivocal identification of toxic substances in such a manner that the results can withstand a legal challenge. The problems of substance abuse, designer drugs, increased potency of therapeutic agents, and widespread concern about pollution and the safety and health of workers present challenges to the analyst skills. Today investigators have a wide range of analytical tests and sophisticated equipment with which to study microscopic pieces of evidence collected at such crime scenes. As disgruntled individuals and terrorists continue to use fire and explosives to disrupt society, forensic chemists will go on developing methods for identifying the persons responsible for such events.

Reference

[1] R.E. Van Griken and A.A. Markowicz, Handbook of X-Ray Spectrometry, Marcel Dekker, New York (1992); Also R. Jenkins, An Introduction to X-Ray Spectrometry, Heyden, London (1970).

[2] J. M. Jaklevic, J. R. French, T. W. Clarkson and M. R. Greenwood, Adv. X-Ray Anal. 21 (1978) 1971.

[3] R. Jenkins, An Introduction to X-Ray Spectrometry, Heyden, London (1970);R. Jenkins, Comparison of Wavelength and Energy Dispersive Spectrometers. in: X-Ray Fluorescence Spectrometry, 2nd ed., Wiley-Interscience, New York pp. 111–121 (1999).

[4] Shailendra Jha, M. Sharma, R K Kothari and B K Sharma Role of importance of X-ray fluorescence analysis of forensic Samples, Proceedings of ICNX (2009) Malasiya.

[5] Castro, W.; Trejos, T.; Naes, B.; Almirall, J. R. Anal. Bioanal. Chem., 392(4) (2008) 663.

[6] Naes, B. E.; Umpierrez, S.; Ryland, S.; Barnett, C. Almirall, J. R.Spectrochim. Acta, Part B, 63B (10) (2008) 1145.

[7] Barnett, C.; Cahoon, E.; Almirall J. R. Spectrochim. Acta, Part B, 63B (10) (2008) 1016.

[8] Bouffard SP, Sommer AJ, Katon JE, Godber S. Use of Molecular Microspectroscopy to Characterize Pigment-loaded Polypropylene Single Fibers. Applied Spectroscopy, 48(11) (1994) 1387.

[9] Keen IP, White GW, Fredericks PM. Characterization of Fibers by Raman Microprobe Spectroscopy. Journal of Forensic Sciences, 43(1) (1998) 82.

[10] Miller J, Bartick E G. Forensic Analysis of Single Fibers by Raman Spectroscopy. Applied Spectroscopy, 55(12) (2001) 1729; Also Jochem G, Lehnert RJ. On the Potential of Raman Microscopy for the Forensic Analysis of Coloured Textile Fibres. Science & Justice, 42(4) (2002) 215.

[11] G. Zador, Z. Brozek-Mucha, EM DX-a useful tool for forensic examinations Materials Chemistry and Physics, 81 (2003) 345.

[12] G. Zadora, Z. Bro zek-Mucha, A. Parczewski, Prob. Forensic Sci. XLVII (2001) 137.

[13] Role of Electron microscope in Forensic Science Mukesh Sharma and Shailendra Jha, IEMSI–2010, BARC during 8th-10th Mar. (2010).

Combating Nuclear Terrorism in India: Preventive Nuclear Forensic Perspectives

N.K. Raghav[1], J.S. Lad[2] A.V. Deshmukh[2] and S.S.Jagtap[3]

1. *Department of Forensic Medicine & Toxicology, S.N. Medical College Agra*
2. *Assistant Professor, Govt. Institute of Forensic Science, Aurangabad, E-mail: avdeshmukhgifsa@gmail.com*
3. *Assistant Professor, Institute of Forensic Science, Mumbai*

Nuclear Terrorism is constant threat to India by many terrorist organization and neighboring country. These organizations are directly or indirectly aided with nuclear material by terrorism supporting country. Such organization has a significant potential source for acquiring nuclear and other radioactive Material. Possibility of leakage is widely feared because of the deterioriorating law and order condition, great spur of nuclear proliferation after the cold war and disintegration of USSR. Terrorist could gain access to Nuclear and radioactive material and smuggle to India through porous borders. Preventive Forensic approach in screening and searching Nuclear and Radioactive material will play cardinal role to prevent nuclear disaster happening in India. Future plans could be extracted from terrorists through their narco-tests, brain Fingerprinting and a data base on this could be prepared, which could later be used to help prevent any attacks. In present paper authors strongly recommend setting up Preventive Forensic Units in India so that any Internal or external nuclear attack could be aborted.

Keywords: Nuclear Terrorism, Preventive Forensic, Nuclear Attack

Introduction

The threat of nuclear attack by terrorist has high probability in India. Nuclear attack is capable to inflict mass casualty, long term radiation sickness, cancer, radioactive contamination in the environment. India is facing multifacet militancy in Jammu and Kashmir, Assam, Andhra Pradesh, Chhattishgarh, Jharkhand, and West Bengal. These terrorist groups are guided by religious, quasi religious, regional sentiments rather than country well being [1]. To launch a nuclear attack terrorist group can steal, buy or build nuclear bomb. Pakistan's Inter Services Intelligence Agency sympathize with Taliban, Al Qaida. Pakistan's ISI has access to Pakistan's nuclear arsenal. Dr. Abdul Qadir Khan, father of Pakistan's nuclear program ran a nuclear distribution network in Iran, Libya and North Korea [2]. Under such potential threatening situation India should display extensive preventive machinery across borders, airports, nuclear installations and places of National Importance.

Nuclear Forensic in Prevention of Nuclear Attack

Preventive Nuclear Forensic can play important role before dealing with real time nuclear attack or simulating situation in several ways. The first scenario involves detection of nuclear and radioactive material or an intact device. Secondly, The radiological dispersal device in which high explosive is mixed with radioactive substance. It can lead to casualty along with radioactive contamination in the surrounding. The third scenario involves fissile material or primitive device in which nuclear explosion takes but distribution is limited to few blocks.

Nuclear Forensic is a comprehensive set of measures for detection, interception, categorization, characterization and attribution of Nuclear and radioactive material collected from nuclear scene [3]. The primary concern of Nuclear Forensic is to determine the motivations of terrorists, specialists whose assistance they got in nuclear operation, supplier state role in whole or in part, intermediaries to provide support, funding, shelter, cover activities etc. Nuclear Forensic contributes. Nuclear Forensic contributes prevention of terrorist attack by increasing chances of failure of terrorist mission. If Nuclear or radioactive material or weapon is intercepted before terrorist act, it should be traced to its original state and possibility of group or person designed the weapon should be determined with accuracy. Once design and origin is determined intelligence and Law enforcement agencies can focus on people associated with that kind of source. If Nuclear Forensic Expert along with intelligence information are able to identify where device was made, the experts that helped with mechanizing assembly may be more easily identified [4].

Control and continious search of nuclear and radioactive material at border reuire lot of attention. Borders in india are safeguarded by border security force(BSF), Indotibetan Border Police(ITBP). In insurgent areas Indian Military take hold of border secrurity. For further protection from any nuclear or radiological attack it is need of hour to that Government of India establish Nuclear search squad to deployed at border check points, airports, bus stands and places of national importance. they should be adequately trained in nuclear searching, detection, and radiohazards protection. Radioactive material could be detected and their movement could be monitored. The instument used for this purpose are-

(a) Fixed Radiation Portal monitors: RPMs are sinle or dual piller or slab containing gamma radiation and neutron detectors. These are semipermanent pass through monitors installed at checkpoints. RPMs are supported by CCTV cameras. These are very effective device for pedestrian, vehicle, cargo traffic. RPMs have aglorythms, when skillfully operated data could be stored and transmitted to Nuclear forensic Laboratory for correct interpretation to identify and charecterize nuclear and radioactive material.

(b) Personal Radiation Detectors: PRD are lightwaight compact hand held device to be essentailly keep by Nuclear Search Squad. PRD are simple display and alarm device fit for petrolling purpose.

(c) Hand held gamma and neutron search detector: gamma and neutron search detectors are compact detector which provide greater flexibility and discrimination even in low concentration . This is primary detection instrument and require periodic calibration.

In event of seizure of nuclear and radioactive material or nuclear device intact, the role of Nuclear Forensic scientist is to-

1. Identify nature of nuclear and radioactive material
2. to access immediate danger and advise Intelligence and law enforcement agencies
3. Locate the original source of material
4. Give opinion on intended use of nuclear and radioactive material or device.

Nuclear and radioactive material seized is screened by nuclear fingerprint. Characterization involves

A. Macroscopic Parameters
B. Isotopic composition
C. Elemental Composition
D. Microscopic parameters

When sample consist of mixtures of component to deceive intelligence or law enforcement agencies each component shall separated out analyzed individually to determine relevant information.

For execution of nuclear attack involved terrorist group must have cooperation with number of intermediaries who can provide money, material , safe place to work for at least weeks and most likely months, instrumentation, transport, transport across guarded borders, people who can evade law enforcement agencies in target country and who speak target country language, local regional language. Some such intermediaries belong to terrorist organization some will not. All involved must be recognized and interrogated scientifically to know their respective role in planning execution of nuclear attack. Intelligence and law enforcement agencies should seek cooperation from INTERPOL, EUROPOL, WCO, FBI, Wide international collaboration to implement and improve Nuclear Forensic effort both in pre event and post event can enhance incentives for government to be more vigil about nuclear security and against infiltrations by or influence from terrorist elements [5]. Promoting and sharing of international database will also boost nuclear material source determination.

Conclusion

In order to effectively combat nuclear terrorism effort is needed to enhance security and surveillance system. Detection capability can be boosted up by installation of affordable sensitive detectors in large number in border crossing points, air ports, major railway stations, Bus Stands and places of National importance. Interface with Forensic Science characterization techniques need to be optimized. Development of Database on Nuclear and Radioactive substances used in Nuclear weapons, power reactors, and research is also need of time for enhanced prevention of nuclear attack.

References

[1] Trager RF, Zagorcheva D P, International Security, 30(3) (2007) 87.

[2] Basrur R M, Steinhausler, Risk potential and counter measures, (2010) 1.

[3] Mayer K, Wallenious M, Ray I., The Analyst, 130 (2005) 433.

[4] Blackdar J.M., Garner S.E., Bounds J.A., Casson W.H., Mercer D.J., Evaluation of commercial detectors. INMM 44th annual meeting, Phoenix, (2003) 13.

[5] Fergusion C.D., Preventing Catastrophic Nuclear Terrorism, CSR11, Couyncil on Foreign relation, New York, (2006) 1.

A Review on Nuclear Forensic Methodology for Analysis of Nuclear Material of Unknown Origin

A.V. Deshmukh[1], N.K Raghav[1] N.M Fatangare[1] and S.S. Jagtap[2]

1. *Dept of & Forensic Science, Institute of Forensic Science, Aurangabad, E-mail: avdeshmukhgifsa@gmail.com*
2. *Institute of Forensic Science, Mumbai*

With the growing use of nuclear power and threat from illegal nuclear smuggling nuclear forensic provides an aid to the law enforcement to trace back modus operandi of such threats. Extensive nuclear proliferation, race among countries to acquire nuclear capability and global terrorism scenario has mandated Nuclear Forensic Science technology to tackle nuclear threats. Gamma spectrometry, alpha spectrometry, thermal ionization mass spectrometry, inductively coupled plasma mass spectrometry are employed for charecterization and relative isotopic composition determinant of Nuclear material and techniques like SEM transmission electron TEM, FT-IR, GC-MS, Electrophoretic technique are used to characterize the contaminated materials in order to deceive investigative agencies. The present paper provide systematic Forensic methodology for Nuclear and radioactive materials encountered at any crime scene due to any accidental discharges or military activities.

Keywords: Nuclear Forensic, Nuclear Proliferation, Nuclear and Radioactive mater.

Introduction

The development in the field of science and technology resulted in remarkable change in our society. Nuclear and radioactive material has extensive application in every sector such as power generation, medicine, agriculture, space exploration and warheads. On the other hand, nuclear material is smuggled for terrorism which has got active after the cold war. Cold war was a race between United State of America and Soviet Union (USSR) that dominated both super powers until early 1990s. Both the country focused on Research and development for the design of more advance, efficient and powerful nuclear weapons followed by Britain, France and china. Recently India and Pakistan has also joined the nuclear power race. During the 1945 to 1998 world was showered by more than 2000 nuclear test on land and 500 detonations in the atmosphere. It resulted into large deposition of fission products and actinides throughout the biosphere. In 1991 the end of the Cold War and crumbling of Soviet Union form 12 new independent states along with these nuclear sources got distributed most of them became orphan. States like Russia, Belarus, Ukraine, and Kazakhstan form Former Soviet Union (FSU) struggling economic and disgraceful social conditions in FSU stimulated illegal smuggling and black marketing of nuclear material. The nuclear smuggling is the biggest threat and challenge for every country.

Nuclear Forensic-Nuclear Forensic Deals with determination of attributes of suspected radioactive exhibits by both nuclear and conventional methods. The object of analysis is to provide fingerprint information regarding source, path of synthesis and procedure. Attribution includes the identity, quality and origin of the material along with the related information as involvement of black market network, frequency of shipments and trafficking route. India is a leading nuclear country which uses nuclear material in many agricultural applications, nuclear weapons. As far as Nuclear Forensic is concerned, there is no existence of Nuclear Forensic Laboratory throughout the country. The nuclear forensic analysis starts from the full pelage radiochemical forensic laboratories which consist of every facility such as analytical instruments, radiation counters, systems free from contamination and cosmic-rays as well as counter shielding, powerful system for the removal of cryogenic and counting gas effluents during analysis. High level security is maintened in Nuclear Forensic Laboratory in order to avoid any type of accident or injury.

Nuclear Forensic Analysis for determination of nuclear signature and attribution of any suspected, illegally smuggled or orphan nuclear or radiological material is performed through radiochemical examination. The examination results in spectral data list modes involves recoding individuals, time-tagged energy events. Particle detection-Beta-particle counters used for most of the short life â and ã emitting samples to characterize decaying nuclides. A single gas-filled â counter along with eight-position turret is useful. Alpha counting is implemented in case of heavy elements such as uranium, polonium etc. Gamma-Counting for the forensic sample is achieved using two types of gamma counter detector – Al-windowed coaxial detector and LEPS Planar detector. Neutron counting can be used in case of any unknown sample suspected for emission of neutron i.e. polonium. Microscopy, spectroscopy, chromatography, mass spectrometric, x-ray and electrophoretic techniques are equally valuable in radio forensic analysis. Microscopy is used to exaggerate the image of sample or to magnify trace nuclear samples. Optical microscopy provides primary details of color, shape, size, texture, surface morphology and

mineralogy. Scanning electron microscopy proved grater resolution, more depth of focus and can combined with x-rays. The result of SEM is depending on sample preparation and coating usually done with carbon. SEM can be used to study other traditional forensic evidence such as tool marks, striation mark. Transmission electron microscopy is bit tedious to use and required long and expensive sample preparation. TEM is still important for nuclear forensic investigations and provide great magnification in comparision to optical and SEM. TEM provides very fine details which can provide source information and use for impurity profiling. X-Ray Microanalysis works on the interaction between the energetic (KeV) electrons and the sample in SEM and TEM. This technique provides valuable information on chemical composition and elemental concentration at lower limits. The role of X-ray microanalysis in nuclear forensic investigations is valuable due to accuracy in quantifying the yield of elemental concentration in the suspected nuclear materials. Fourier-transform infrared spectroscopy is known for structural determination and identification of organic and inorganic compounds by molecular bonds vibrations at fingerprint frequency. From the infrared spectrum the bonds and functional groups are identified. A wide-range library of nuclear forensic samples and other related compounds is very essential which for accurate identification of unknown samples. Recent development in analytical instrumentaction leads to hyphenated techniques for better detection at lower level. Isotope mass spectrometry is one of new tool to nuclear forensic investigation for determinaction of isotopic, elemental, molecular abundance and split ratio with a high precision with more accuracy. Isotope –Ratio MS commonly used to determine the isotopic abundance of specific element in the suspected nuclear sample. Previously thermal-isolation mass spectrometry was used to detect trace sample. Now a days it is replaced by multicollector-inductive coupled plasma-mass spectrometer in which the suspected sample is dissolved in acid and fine spray with the nebulizer and plasma of high temperature is created for the break down its atomic constituent for the detection by MS. Similarly elemental composition mass spectrometry is used for determination and abundance of ultra traces of nuclear material in the seized samples. Gas Chromatography coupled with mass spectrometry is widely used in routine forensic analysis for the detection of organic compounds such as narcotic and psychotropic substance, drugs, high explosives. GC-MS is more sensitive and detects at the level of PPB which can provide unique signature of compound. Such fingerprint information can be used to trace source to nab nuclear criminals. All the information generated after the interpretation of the analytical results of sized or suspected nuclear material yields valuable information that directly or indirectly useful in nuclear investigation.

Conclusion

Nuclear Forensic Science in India is fascinating discipline which requires a lot of support from government due to the vulnerability of nuclear proliferation and nuclear smuggling. New methodologies are needed to be developed and implemented in order to determine nuclear and radioactive material with high accuracy and precision. Author strongly recommends that further research is needed in this field to identify new characteristics in order to prove beyond reasonable doubt before court of law.

References

[1] P. Williams and P.N. Woessner, The real threat of nuclear smuggling, Sci. Am 272,40.1996

[2] P.M. Grant, K.J. Moody,I.D. Hutcheon, Forensic analysis of suspected illicit nuclear material, Journal of Forensic Science, 43(3),680,1998

[3] T.R. England, B.F. Rider, Evaluation and complication of fission product yields,1993.

[4] L. Reimer, Scanning Electron microscope, Springer, 1985.

[5] K.J. Moody, I.D. Hutcheon and P.M. Grant, Nuclear Forensic Analysis, Taylor and Francis, 2005.

Thoron Mitigation Using Charcoal Based System

Sudeep Kumara K.[1], Karunakara N.[1], Yashodhara I.[1], Sapra B. K.[2], Sahoo B. K.[2], Gaware J. J.[2], Kanse S. D.[2], and Mayya Y. S.[3]

1. *University Science Instrumentation Centre, Mangalore University, India; E-mail: drkarunakara@gmail.com*
2. *Radiological Physics & Advisory Division, BARC, Mumbai 400 081*
3. *Department of Chemical Engineering, IIT, Mumbai-400 076*

Introduction

Thorium rich sand (monazite) need to be mined and processed for the nuclear power generation programme. In thorium processing plants, the ^{220}Rn generated during the processing of monazite sand is a source of concern to the workers. The dose delivered by ^{220}Rn and its progeny is orders of magnitude higher than that of ^{222}Rn because of its very short half-life (55.6 seconds) and high specific activity. The removal of ^{220}Rn gas from workplaces has received increased attention and efforts are on to develop mitigation/removal systems for this radioactive gas.

We have developed a ^{220}Rn removal/mitigation system for use in workplaces. The system uses activated charcoal as an adsorbing medium. It is well known that activated charcoal is a good adsorber of ^{222}Rn and ^{220}Rn gases. Experiments on removal of ^{220}Rn using coconut shell-based granular activated charcoal were conducted for various flow rates and adsorber beds of varying height and diameter. Breakthrough curves were generated and performance parameters such as, breakthrough time and adsorption coefficient 'K_a' were evaluated. Theoretical calculations were performed and based on these an optimised prototype charcoal based mitigation system is being designed and developed. The prototype system which can be scaled up for actual use in workplaces, offer numerous advantages for the removal of ^{220}Rn for site remediation activities. The details of these studies are presented and discussed in this paper.

Materials and Methods

Experimental Arrangements

The main aim is to study the characteristics of a charcoal adsorber bed. Since ^{220}Rn is a short lived radioisotope it cannot be used for studying adsorption characteristics of a charcoal bed. Therefore, for studying the adsorption bed characteristics and to generate the breakthrough curve ^{222}Rn should be used. The experimental arrangement for studying the ^{222}Rn and ^{220}Rn adsorption characteristic of activated charcoal bed is shown in Fig. 1. Coconut shell-based granular activated charcoal was filled in cylinders and used as adsorber beds. The cylinders were filled with charcoal ensuring that no void space was left inside, and this was accomplished through packing density measurements as well as holding the cylinder vertically during the experiment. The ^{222}Rn and ^{220}Rn gases were drawn from soil gas and injected in to the adsorber bed using a dry air pump. The pumping of ^{222}Rn and ^{220}Rn was continued till the ^{222}Rn concentration breakthrough occurred from the charcoal bed. The techniques for obtaining ^{222}Rn and ^{220}Rn from soil gas are available in our earlier publication and it has been seen that soil gas is an excellent source capable of providing steady high concentrations of these gases [1,2]. The concentration of these gases in the inlet and outlet of the adsorber bed was measured simultaneously using an AlphaGuard (Genitron, Germany) and a Smart Radon Monitor (SRM developed by RP&AD, BARC). The performance and accuracy of the measuring systems were checked frequently through inter-comparison measurements between AlphaGuard, SRM and RAD 7.

Mathematical Formulation

The basic model for ^{222}Rn and ^{220}Rn adsorption mechanism on charcoal consists of solving convective transport equations in packed bed media taking into account the various system and flow parameters. The model formulated by Madey et al. [3] considering the net flow of gaseous atoms into the volume element, diffusion of gaseous atoms, adsorption and desorption of gaseous atoms by the adsorber, and the radioactive decay of ^{222}Rn and ^{220}Rn was adopted in the present study for generating theoretical breakthrough curves. The breakthrough curve for radon adsorption in charcoal was generated theoretically for different charcoal adsorber beds and the adsorption coefficients were evaluated by the best fit method.

Results and Discussion

Results of ^{222}Rn and ^{220}Rn Mitigation using Charcoal Columns

The experimentally obtained ^{222}Rn breakthrough curves for different adsorber beds are presented in Fig. 2. For comparison the ^{222}Rn and ^{220}Rn concentrations in the inlet air (which remains the same for all the adsorber beds) are also presented in the figure. These results are for a flow rate of 10 L min^{-1}, temperature of 32 C, and relative humidity of 85% (constant for all the adsorber beds).

The profile of ^{222}Rn concentration in the outlet air of the charcoal bed is shown in Fig. 2. Initially there is complete adsorption of all ^{222}Rn and ^{220}Rn by the charcoal and after some time sudden concentration breakthrough occurs for ^{222}Rn. The time at which ^{222}Rn breakthrough occurs depends on the dimension of the adsorber bed and in turn the volume of charcoal in the column. From the saturation region of the breakthrough curves for different columns, it is clear that the

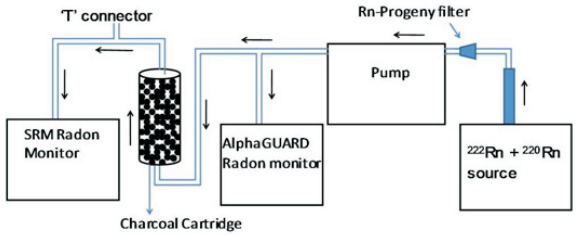


Fig. 1 Experimental arrangements for the ^{222}Rn and ^{220}Rn mitigation studies using charcoal beds

concentration breakthrough occurs only for ^{222}Rn, and the results clearly indicate complete mitigation of ^{220}Rn from the inlet air. The details of these studies are presented elsewhere [4]. Studies were also carried out for different flow rates and it was found that the breakthrough time decreased with the increase of the flow rate.

From the experimentally generated breakthrough curves the ^{222}Rn adsorption capacity (K_a) for charcoal was estimated [4] and this varied in the range of 2.2-3.4 m^3 kg^{-1}. Cosma et al. [5] have reported ^{222}Rn adsorption studies on a carbon molecular sieve and the K_a value reported by them varied in the range of 1.1-7.1 m^3 kg^{-1} for different types of charcoal. It should be noted that the value of adsorption coefficient depends largely on the humidity, temperature, and carrier gas conditions [6]. The degassing properties and temperature dependence of the adsorption were also studied in detail.

Design of a Prototype ^{220}Rn Mitigation System

Based on the parameters derived from the experiments and from the theoritical calculations, a prototype ^{220}Rn mitigation system was designed and fabricated. The prototype system which can be scaled up for use in workplaces, offer numerous advantages for the removal of ^{222}Rn and ^{220}Rn for site remediation activities in uranium and thorium processing industries. Extensive studies are now under progress to characterise the mitigation system. The details are discussed in the full length paper.

Acknowledgements

The investigators would like to thank BARC, Mumbai and Mangalore University for the MoU programme to undertake this study. The investigators are thankful to Dr. D. N. Sharma, Director, HS&E, BARC, Dr. A.K. Ghosh and Shri H. S. Kushwaha, former Directors, HS&E, BARC for their encouragement.

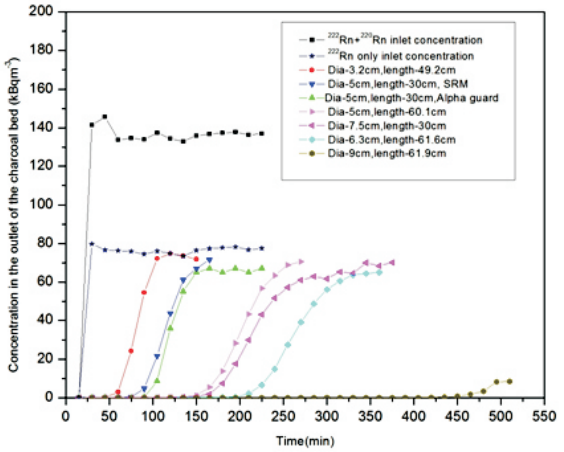


Fig. 2 ^{222}Rn breakthrough curves for charcoal beds of different dimensions

References

[1] Al-Azmi D and Karunakara N.,. J. Radiation Meas. 42 (2007) 486.

[2] Karunakara N. and Darwish Al-Azmi, Health Physics, 98(4) (2010) 621.

[3] Madey Richard, Jan-Chan Huang, Eugene Pflumm, Nuclear Science and Engineering. 78 (1981) 205.

[4] Sudeep Kumara, Yashodhara I, Karunakara N, Mayya Y S, Sapra B K, Sahoo B K, Gaware J, Kanse S D, 19th National Symposium on Radiation Physics (NSRP-19), Chennai, December 12-14, (2012).

[5] Cosma C., Van Deynse A., Poffijn A., Radiation Measurements 31 (1999) 351.

[6] Coleman R. D., Holday D. A., Kuznetz H. L., Woolrich P. F. Radon and radon daughter hazards in mine atmosphere. Am Ind. Hyg. Assn. Q 17:405-410 (1956).

Establishing the Lung Counting Facility - An Experience

S. Rajaram[1], J. Thulasi Brindha[1], K.R.Sreedevi[1], P.M. Ravi[2] and R.M. Tripathi[3]

1. *Environmental Survey Laboratory, Health Physics Division, Bhabha Atomic Research Centre, Kalpakkam 603 102; E-mail: srajaram@igcar.gov.in*
2. *Environmental Studies Section, Bhabha Atomic Research Centre, Mumbai 400 085*
3. *Health Physics Division, Bhabha Atomic Research Centre, Mumbai 400 085*

The lung counting facility at Kalpakkam, used for the estimation of transuranics, consists of an array of three large area Germanium detectors fixed in a single assembly. The new door less steel room is designed to reduce the background in the low energy region. The efficiency calibration was carried out using ^{241}Am and ^{232}Th lung sets LLNL phantom. Efficiency as a function of MEQ-CWT was calculated for array of detectors. The 4.65 MDA of the high resolution HpGe detectors with low background due to steel room is 14 Bq for ^{241}Am. The successful setting up of the lung facility enabled the in-vivo measurement of around 200 personnel annually.

Introduction

Kalpakkam site (12° 33' N and 80° 11' E) situated on the east coast is growing into a major nuclear complex comprising of Madras Atomic Power Station (MAPS) , Fast Breeder Test Reactor (FBTR), Centralised Waste Management Facility (CWMF), Reprocessing and Development Laboratory (RDL), Kalpakkam Reprocessing Plant (KARP) and a host of allied facilities. In the vicinity of the nuclear installations environmental monitoring is carried out by Environmental Survey Laboratory (ESL) to monitor the radioactivity concentration in both biotic and abiotic media. In addition to this, in-vivo monitoring of personnel working in the nuclear installations is also being carried out at ESL. Towards this, a lung counting facility to measure the lung burden due to transuranics has been established by Environmental Survey Laboratory, Kalpakkam1with the guidance of IDD, BARC Mumbai. The successful setting up of the lung facility enabled the in-vivo measurement of around 200 personnel annually

Materials and Methods

Measurement of internal contamination of transuranics through in vivo monitoring is a challenge in radiation protection. Detection of ^{239}Pu through ^{241}Am measurement is a widely used technique world over. This involves measurement of 60 keV gamma photon in the presence of low-energy X-rays and high background in low energy regions of interest, which is very difficult. While setting up the lung counting facility many factors were taken into account viz. reduction of background radiation, improving the sensitivity.

The dimension of the building housing the lung counting facility including the steel room is 20m x 8m. The natural radiation level at this location is 20 R/h due to monazite deposits. To reduce this natural background radiation the upper layer of soil upto 1m was removed and replaced with monazite free river sand of 5 R/h radiation level. The steel room (2.5 m x 2 m x 2 m) was constructed with optimized shield

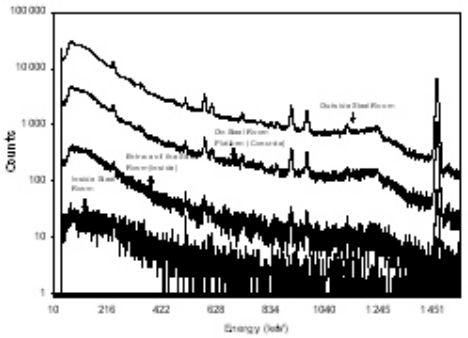


Fig. 1 Background Reduction due to Steel Room

thickness of 20 cm. This was fabricated from Mild Steel grade No. 2062 from Steel Authority of India (SAIL) weighing around 100 tonnes. Mild steel is generally free from any radioactive contamination (particularly Co-60) which was cross cheeked using gamma spectrometry. The inside of the steel room was lined with graded shielding material viz. 3mm Pb + 2mm Cd + 0.5 mm Cu to cut off low energy X-rays emitted by the shielding materials.

Generally the steel rooms are made with doors which may lead to claustrophobia of the subjects due to confinement for long time in a closed room. This was resolved by designing a steel room without door.

To find the background reduction due to steel room, 33% Co-axial HpGe Detector was used. The background spectrum was taken at four different locations inside the lung counting room which is shown in Fig.1. From the figure it can be seen that the background reduction for the energy range of 10 to 1500 keV was about 99.5%. The background counts in 59.5 keV ROI of Am-241 using the array of HPGe planar detectors is 0.02 counts per second.

An array of three HpGe detectors is used in the lung counting facility at Kalpakkam. Although the detection area of HPGe array is much lower as compared to Phoswich scintillation detector, the inherently superior energy resolution compensate for

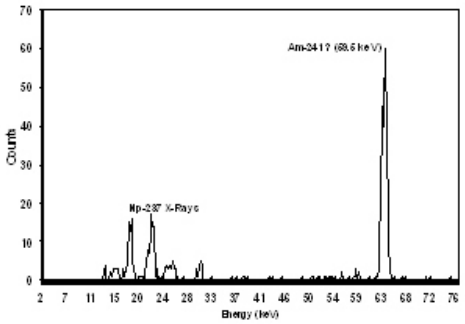


Fig. 2 Am-241 Source Spectrum

the smaller area, as the identification of the radionuclides is possible at much lower level. The individual detector outputs are connected to individual Multi Channel Anlayser (Target Make, Model No. dMCA pro-GN) for analysis. The Array of detectors attached to 30 litre Dewar flask which is mounted on a SS platform fixed on the steel room wall. This assembly as such, is movable in the vertical direction using synchronous motor coupled with gear system. In addition, the subject bed is also movable in horizontal and vertical direction.

Energy calibration of the system was done using the energies 17.8 keV and 59.5 keV of ^{241}Am Source. Calibration factor of the system is around 0.2 keV/channel. A typical energy calibration spectrum of one of the detectors is shown in Fig.2 in which the 59.5 keV gamma along with low energy X-rays are clearly visible.

The phantom used for efficiency calibration is the third generation Lawrence Livermore National Laboratory (LLNL) [1] phantom. ^{241}Am and ^{232}Th lung sets supplied along with LLNL phantom, were used to calibrate the detectors.

The efficiency is a function of Muscle equivalent chest wall thickness (MEQ-CWT) [2].

$$\text{MEQ-CWT} = \text{CWT}\left[\frac{\mu_{adp}}{\mu_{msc}}\frac{\text{AMF}}{100} + \frac{\mu_{msc}}{\mu_{msc}}\frac{(1-\text{AMF})}{100}\right]$$

Where MEQ-CWT is the muscle equivalent chest wall thickness (mm), CWT is the physical chest wall thickness (mm), AMF is the adipose mass fraction (%), $_{adp}$ is the linear attenuation coefficient at a given energy for adipose tissue (cm^{-1}) and $_{msc}$ is the linear attenuation coefficient at a given energy for muscle tissue (cm^{-1}) [3].

Minimum Detectable Activity (MDA)

The MDA for the actual subject was calculated using subject background and efficiency of B series overlay plate of the LLNL phantom. MDA (4.65) for ^{241}Am was calculated to be 14 Bq for a period of 3600 sec.

JAERI Phantom

The Japanese Atomic Energy Research Institute (JAERI) Phantom was received at Radiation Safety Division, IGCAR, Kalpakkam as part of IAEA intercomparison exercise. For comparison between the lung counting facility at RSD,IGCAR, and ESL, Kalpakkam this phantom was used . The ^{241}Am activity was calculated to be 597 Bq which is in good agreement with 546 Bq estimated by RSD, IGCAR, Kalpakkam [4].

Table-1: Counting Efficiency of Am-241 (59.5 keV) for the large area germanium detector array as a unction of MEQ-CWT using LLNL Phantom

MEQ-CWT (mm)	Efficiency (cps/Bq)
16.2	1.1 X 10^{-3}
22.63	9.0 X 10^{-4}
26.42	7.9 X 10^{-4}
32.99	6.4 X 10^{-4}
40.81	5.0 X 10^{-4}

Conclusion

Measurement of internal contamination of transuranics through in vivo monitoring using an array of HpGe detectors was successfully established at ESL, Kalpakkam. The new door less designed steel room was implemented at Kalpkkam. The array of HpGe detectors was used to improve the sensitivity of in vivo monitoring and resolution for well defined peak. The detector was calibrated using the LLNL phantom for various chest wall thickness. In the intercomparison exercise of JAERI phantom the Am-241 activity agreed with that obtained by RSD, IGCAR. Around 200 personnel were lung monitored annually. The MDA for the lung counting facility was found to be 14 Bq for one hour counting period.

Acknowledgements

The authors would like to thank Dr. D.N. Sharma, Director, HS&E Group, BARC for the keen interest and constant encouragement.. Authors gratefully acknowledge the contribution by Dr. V. Kannan, ex-OIC, ESL, Kalpakkam and Dr. S.P. Garg, IDS, BARC. Authors would like to express their gratitude to Dr.B.Venkatraman, Associate Director, Radiological Safety and Environmental Group, IGCAR, Shri. R.Mathiyarasu and Smt. M. Manohari, RSD, IGCAR, Kalpakkam. The authors would also like to thank the staff members of the laboratory for their support.

References

[1] Griffith, R.V., Dean, P.N., Anderson, A.L., Fischer, J.C., Proc. IAEA Conf. Vienna : IAEA; IAEA-SM-229/56, 4493-504; 1978; 1-16. (1978).

[2] Kramer, G.H.,Health Physics, 77(2) (1999) 207.

[3] Rajaram S., Thulasi Brindha J., Sreedevi K.R. and Hegde A.G., Radiation Protection Dosimetry, 148(I) (2012) 121.

[4] Manohari, M, Mathiyarasu, R, Rajagopal, V, Meenkshisundaram, V and Indira, R., Radiation Protection Dosimetry, 144(1-4) (2011) 427.

Performance Evaluation of HPGe detector for Environmental Sample analysis at different Shielding Conditions.

T.J. Jaison[1], A.K. Patra[1], P.M. Ravi[2] and R.M. Tripathi[2]

1. *ESL (ESS, Health Physics Division, BARC), Kakrapar Atomic Power Station, Gujarat 394651; E-mail: jaisontjohn@npcil.co.in*
2. *Health Physics Division, Bhabha Atomic Research Centre, Mumbai 400 085.*

This work describes the influence of different shielding conditions during -ray spectrometric measurements at Environmental Survey Laboratory, Kakrapar site. The HPGe system (100% RE) was used for obtaining background spectra in three different conditions. Spectral analysis shows that a significant reduction in overall background and background peak count rates with fabricated shield against no shielding condition and also against standard Pb bricks shielding. The estimated Minimum Detectable Activity for ^{137}Cs was lowered seven times with fabricated Cu-Cd lining shield from no shield conditions and lowered three times from standard Pb brick shielding. Significantly lowered MDA for ^{40}K was also achieved.

Introduction

In this work, we describe influence of different shielding conditions during low-background -ray spectrometric studies conducted at the Environmental Survey Laboratory of Health Physics Division at Kakrapar, with the goal of providing surveillance of natural and anthropogenic radioactivity.

The primary task of an environmental analyst is to lower the detection limit for a given system. To improve the detection limit for a specific system, the background has to be reduced as much as possible. The background in spectra is caused by cosmic rays and associated processes, radioactive impurities in the detector assembly, rays from external natural radioactivity, radon etc [1]. In this work we have evaluated the HPGe system, at three different counting conditions; no shielding condition, shielding with locally obtained standard Pb bricks (4cm x 7cm x 15cm) and fabricated Pb shielding with Cu and Cd lining.

Material and Methods

The coaxial HPGe system used in this experiment is of 100% RE (BSI, Riga) with 417cc active volume. The system resolution measured as FWHM at 1332 keV is 2.1 keV and peak to Compton ratio is 83:1. The Al end cap is of thickness 2.0 mm. The system is of J configuration, facilitating preamplifier away from the detector and shielding. Background spectra for 1,50,000 sec in three conditions were obtained. First without employing any kind of shielding to the detector, then by employing a two layered standard Pb brick shielding (140mm thickness) around the detector with a cover of 1cm thick MS plate. Then a fabricated (Technocare, Mumbai) shield of 150 mm Pb thicknes with 2.0 mm Cu and 1.5 mm Cd lining enclosed in 15 mm MS vessel was installed and a background spectrum was obtained. The system was calibrated using mixed liquid source traceable to NIST international standard for energy, FWHM and efficiency. All the experiments were conducted within a week so that variations in spectra due to radon or cosmic origin are minimized.

Results and Discussion

The spectra obtained at different conditions were analysed manually in channel by channel basis as well as using the analytical software, according to the merit. The integral count rate over the entire (50-3450 keV) region for no shield condition was 230.31 cps, 8 times higher than the standard Pb bricks shielding (28.36 cps), which in turn is 8 times higher than the same for fabricated Pb shield with Cu-Cd lining (3.49 cps). The 242.00 keV ^{210}Pb peak and 300.09 keV ^{212}Pb peaks could be observed only when no shielding was provided. The 338.32 keV ^{228}Ac peak and 860.56 ^{208}Tl peak were not detected with the fabricated shield. The background counts for ^{137}Cs were 0.048 cps (no shielding), 0.007 cps (standard Pb brick shield) and 0.001 cps (fabricated shield) where as same for ^{40}K were 3.276 cps, 0.349 cps & 0.012 cps at respective conditions. This indicates a significant reduction in overall background and background peak count rates due to the fabricated shield against other conditions. The % area error was subsequently increased from no shield to standard brick condition and then to fabricated shield for all detected background peaks. Conventional -spectrometry at ground level, consisting of a Ge detector and passive shielding, can provide an integrated background of 0.4 cps/ 100 cm^3 of Ge volume [2]. We could achieve only 0.84 cps per 100 cm^3 for fabricated Pb shielding with Cu-Cd lining. This could be due to higher ^{210}Pb content in the lead obtained from Indian market used in the fabricated shielding.

It is then important to check the detection levels for the tested conditions. The minimum detectable activity (MDA[1]) of the measurements was calculated according to the Currie [3] formula, where - 1.645 (confidence level 95%). MDA[3] also was calculated by using = 3 (99.87% confidence level). According to the equations given by Gilmore [4], if gross counts in

Table-1: Parameters of detection limit

	Description	L_C	L_U	L_D	A_U (Bq/kg)	MDA^1 (Bq/kg)	MDA^2 (Bq/kg)	MDA^3 (Bq/kg)
^{137}Cs (661.7 keV)	no shielding	819	11943	1641	29.3	1.25	4.03	2.28
	Pb shielding	319	1575	641	3.9	0.48	1.57	0.88
	Cu-Cd liner	113	238	228	0.6	0.17	0.56	0.31
^{40}K (1460.8 keV)	no shielding	416	491383	835	13409.8	32.05	22.78	58.46
	Pb shielding	171	53179	344	1451.3	10.63	9.40	19.39
	Cu-Cd liner	69	1817	140	49.6	2.13	3.81	3.89

the peak region (n channels) is G, Compton counts on both sides of n from 2x m channels is S, the background counts B is n*S/2m and net peak area counts A is G-B; then for = 0.05, Critical Limit L_C, Upper Limit L_U, Detection Limit L_D, MDA^2 and Activity Limit A_U can be estimated. The obtained spectra for 1,50,000 sec in all three conditions were used to calculate above mentioned terms for ^{137}Cs and ^{40}K and tabulated in Table 1, assuming a sample weight of 0.3 kg in 250 ml bottle geometry, as they are among the most important radionuclides mentioned in the environmental surveillance of natural and anthropogenic radioactivity. The results show that MDA for ^{137}Cs was lowered by seven times with fabricated Cu-Cd lining shield from no shield conditions and lowered by three times from standard Pb brick shielding. And for ^{40}K was lowered by fifteen times with fabricated Cu-Cd lining shield from no shield conditions and lowered by five times from standard Pb brick shielding. Figure 1 shows the comparison of background gamma spectra using HPGe detector in three different conditions (without shielding, with Pb bricks shielding and with fabricated shielding).

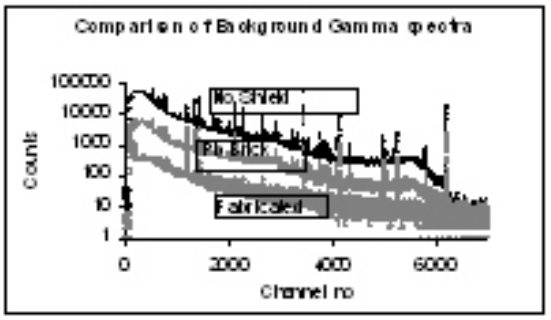


Fig. 1 Comparison of background gamma spectra using HPGe detector

Conclusion

Background spectra obtained using 417 cc standard coaxial HPGe of 100% relative efficiency based -spectrometry system for 1,50,000 sec at three different conditions were used for performance evaluation of the system in the context of environmental monitoring. Spectra analysis shows that a significant reduction in overall background and background peak count rates due to the shielding with standard Pb bricks around the detector, where as the fabricated shield could reduce both drastically further. The results also shows that MDA for ^{137}Cs was lowered by seven times with fabricated Cu-Cd lining shield from no shield conditions and lowered by three times from standard Pb brick shielding. And for ^{40}K was lowered by fifteen with fabricated Cu-Cd lining shield from no shield conditions and lowered by five times from standard Pb brick shielding.

Acknowledgment

The authors would like to thank Dr. D. N. Sharma Director Health, Safety and Environment Group, BARC for keen interest and encouragement. Authors are grateful to Shri. L. K. Jain, Site Director, KAPS for his continuous support. Thanks are also due to other colleagues in Environmental Survey Laboratory, KAPS for their help and co-operation.

References

[1] T.M. Semkow, P.P. Parekh, C.D. Schwenker, A.J. Khan, A. Bari, J.F. Colaresi, O.K. Tench, G. David, W. Guryn., App. Radiat. Isot. 57 (2002) 213.

[2] F. Cannizzaro, G. Greco, M. Raneli, M.C. Spitale, E. Tomarchio, Nucl. Instrum. Methods A 390 (1997) 167.

[3] L.A. Currie, Anal. Chem. 40 (1968) 586.

[4] G. Gilmore, Practical Gamma Ray Spectrometry. John Wiley & Sons, New York. (2008). ISBN: 978-0-470-86196-7.

Quantification of Measurement Uncertainty in Determination of Uranium in Magnesium Diuranate by Titrimetry

B. Narasimha Murty, G. Brahmananda Reddy and H.R. Ravindra

Control lab, Nuclear Fuel Complex, Hyderabad 500 062, India; E-mail: ravindra@nfc.gov.in

Various sources of uncertainty involved in the determination of uranium content in magnesium diuranate by titrimetry were identified and the measurement uncertainty was quantified in terms of the expanded combined uncertainty at 95% confidence level as 0.25%, thus, uranium content in magnesium diuranate sample in terms of % U_3O_8 = 74.30 ± 0.25%.

Introduction

For any industrial laboratory the main objective is to extend uninterrupted and reliable analytical support on a routine basis. For accomplishing this unique task, it becomes essential to look for simple, rapid, rugged and reliable analytical methods to determine various analytical parameters. Thus, quantification of measurement uncertainty in determination of analytical parameter employing a particular method obviously would provide reasonable confidence on the reported analytical result. In this paper, the measurement uncertainty involved in the determination of content of uranium in magnesium diuranate by a titrimetric method is quantified. For the purpose, the methodology given in EURACHEM/CITAC Guide CG-4 is followed. According to this, it is required (i) to formulate the measurand (ii) identification of all the independent variables that can influence the value of the measurand (iii) calculation of the standard uncertainty in the measurement of each variable (iv) calculation of the combined standard uncertainty (v) calculation of expanded uncertainty.

Experimental

Determination of content of uranium in magnesium diuranate by titrimetry involves (i) Accurate weighing of sample (about 15 g) (ii) Dissolution in nitric acid and making up to accurate volume (iii) Drawing of sample aliquot using a bulb pipette (iv) Addition of various reagents in order as per the procedure (v) Titration against standard potassium dichromate solution (vi) Detection of end point visually. For determining Type A uncertainty, repeated measurements were made on various portions drawn from the same magnesium diuranate sample and standard deviation was calculated to be ± 0.22187%.

Quantification of Measurement Uncertainty

The measurand in this present case is content of uranium in terms of $\%U_3O_8$ present in magnesium diuranate sample, which is determined by the titrimetric method using the following expression.

$\%U_3O_8 = 100 \times V_T \times K \times L$ where

$$K \quad \frac{V_i}{V_a} \quad \frac{W_{KD}}{W_{MDU}}$$

$$L \quad \frac{M_{U_3O_8}}{M_{KD}} \quad \frac{P_{KD}}{V_{KD}}$$

V_T = volume of standard potassium dichromate consumed in the titration of sample (mL); W_{KD}= weight of potassium dichromate taken for preparing the standard solution (g); $M_{U_3O_8}$ = molar mass of triuranium octaoxide(g mol^{-1}); W_{MDU} = weight of the sample taken for analysis(mg); P_{KD} = purity as a mass fraction of potassium dichromate primary standard used; M_{KD}= molar mass of potassium dichromate primary standard used (g mol^{-1}); V_{KD} = total volume of the standard potassium dichromate solution (mL); V_i = total volume of the completely dissolved solution to which the completely dissolved MDU is made; V_a = aliquot of the MDU solution sample taken (mL)

To calculate "Type B uncertainty", the identified sources of uncertainty are in the measurement of P_{KD}, W_{KD}, W_{MDU}, V_T, M_{KD}, , V_{KD}, V_i and V_a.The standard uncertainty(SU) in each of the identified sources are calculated as below.

1. SU in P_{KD} is given by

$$u(P_{KD}) = \frac{0.001}{\sqrt{3}} = 0.000577350269$$

2. SU in W_{KD} is given by

$$u(W_{KD}) = \sqrt{2\ 0.0577350269^{\ 2}}$$
$$= 0.081649658 \text{ mg}$$

3. SU in W is given by

$$u(W_{MDU}) = \sqrt{2\ 0.057735^{\ 2}} = 0.081649658 \text{ mg}$$

4. SU in V_T is given by

$$u(V_T) = \sqrt{a^2 \quad b^2} = 0.02220070819 \text{ mL}$$
where a = 0.00879536; b = 0.020412414 mL

5. SU in M_{KD} is given by

$$u(M_{KD}) = \sqrt{c^2 \quad d^2 \quad e^2} = 0.08732000806 \text{ g mol}^{-1}$$
where c = 0.0069220323; d = 0.000519615; e = 0.00011547 g mol^{-1}

6. SU in $M_{U_3O_8}$ is given by

Table-1: Values of variables and uncertainties in them

Variable	Value	Standard Uncertainty	Relative Std uncertainty
Rep	1.0	9.4954×10^{-4}	0.0949
W(KD)	2.4516 g	8.165×10^{-5} g	0.0033
P(KD)	1.0	5.774×10^{-4}	0.0577
$M(U_3O_8)$	842.082 g mol^{-1}	0.0351 g mol^{-1}	0.0042
M(KD)	294.185 g mol^{-1}	0.0873 g mol^{-1}	0.0297
V_{KD}	1000 mL	0.2451 mL	0.0245
W(MDU)	8.5000 g	0.0000817 g	0.001
V_i	250 mL	0.04082 mL	0.0163
V_a	5 mL	0.00475 mL	0.095
V(T)	18 mL	0.022 mL	0.1233

$$u\ M_{U_3O_8} \quad \sqrt{(0.00034641)^2 \quad (0.0000577)^2}$$
$$= 0.03511882991 \text{ g mol}^{-1}$$

7. SU in V_{KD} is given by

   $u(V_{KD}) = 0.245104473$ mL

8. SU in V_i is given by

   $u(V_i) = 0.0408248290464$ mL

9. SU in V_a is given by

   $u(V_a) = \sqrt{(0.00242487)^2 \quad (0.004082483)^2}$
   $= 0.004748333041$ mL

From the spreadsheet calculation, the standard combined uncertainty in $\%U_3O_8$ is 0.1235% From the data furnished in the Table, it is easy to know that the contribution of various factors quantitatively towards the overall uncertainty in measurement of content of uranium by titrimetric method. They can be placed in decreasing order of magnitude as (i) volume of the potassium dichromate solution consumed (ii) volume of aliquot of sample taken (iii) repeatability (iv) purity as a mass fraction of potassium dichromate primary standard used (v) molar mass of potassium dichromate (vi) volume of potassium dichromate standard solution prepared (vii) volume of MDU sample stock solution made (viii) molar mass of triuranium octaoxide (ix) weight of potassium dichromate primary standard taken for preparing standard solution (x) weight of MDU sample taken for analysis

Conclusion

The measurement uncertainty involved in the determination of uranium content in magnesium diuranate by titrimetry thus can be quantified in terms of the expanded combined uncertainty at 95% confidence level as 0.25%, thus, uranium content in MDU sample in terms of $\%U_3O_8 = 74.30 \pm 0.25\%$.

Acknowledgements

The authors express their deep sense of gratitude to Sri N. Saibaba, Chief Executive, NFC and to Sri B. Prahlad, DCE(QA, TS, HRD & Lib) for their encouragement and support in the present investigation.

Quantification of Measurement Uncertainty in the Determination of O/U ratio of UO_{2+x} Powders by Titrimetry

B. Narasimha Murty, G. Brahmananda Reddy and H.R. Ravindra

Control lab, Nuclear Fuel Complex, Hyderabad 500062, India; E-mail: ravindra@nfc.gov.in

Various sources contributing to measurement uncertainty involved in the determination of O/U ratio of hyperstoichiometric uranium dioxide powder were identified, the relative contribution of each was quantified and the measurement uncertainty quantified in terms of the expanded combined uncertainty at 95% confidence level as 0.0036, thus O/U of the sample = 2.043 ± 0.004.

Introduction

For any industrial laboratory the main objective is to extend uninterrupted and reliable analytical support on a routine basis. For accomplishing this unique task, it becomes essential to look for simple, rapid, rugged and reliable analytical methods to determine various analytical parameters. Thus, quantification of measurement uncertainty in determination of analytical parameter employing a particular method obviously would provide reasonable confidence on the reported analytical result. In this paper, the measurement uncertainty involved in the determination of O/U ratio of hyperstoichiometric uranium dioxide powders employing a titrimetric method is quantified. For the purpose, the methodology given in EURACHEM/CITAC Guide CG-4 is followed. According to this, it is required (i) to formulate the measurand (ii) identification of all the independent variables that can influence the value of the measurand (iii) calculation of the standard uncertainty in the measurement of each variable (iv) calculation of the combined standard uncertainty (v) calculation of expanded uncertainty

Experimental

For determining O/U ratio of hyperstoichiometric uranium dioxide by titrimetry, accurately weighed sample (of about 100 mg) is dissoled in a non-oxidizing medium such as 4.5 M sulphuric acid containing few drops of hydro fluoric acid on hot plate followed by addition of ferric ions and titrate against standard potassium dichromate using barium diphenyl amine as a visual indicator. From the sample weight and titre value O/U ratio is calculated. For determining Type A uncertainty, repeated measurements were made on the same hyperstoichiometric uranium dioxide sample and standard deviation was calculated to be ± 0.00377.

Quantification of Measurement Uncertainty

The measurand in this present case is O/U ratio of a hypostoichiometric uranium dioxide, which can be determined by the titrimetric method using the following expression.

$$\frac{O}{U} \quad 3 \quad \frac{A}{B \quad C} \text{ where}$$

$$A = 3 \quad V_T \quad W_{KD} \quad P_{KD}$$

$$B = 3 \quad V_T \quad W_{KD} \quad P_{KD} \quad 1 \quad \frac{M_{UO_2}}{M_{UO_3}}$$

$$C = \frac{W \quad M_{KD}}{M_{UO_3}}$$

V_T= volume of standard potassium dichromate consumed in the titration of sample (mL); W_{KD} = weight of potassium dichromate taken for preparing the standard solution (g); M_{UO_3} = molar mass of uranium trioxide (g mol^{-1}); M_{UO_2} = molar mass of uranium dioxide (g mol^{-1}); W= weight of the sample taken for analysis (mg); P_{KD} = purity as a mass fraction of potassium dichromate primary standard used.

To calculate "Type B uncertainty", the identified sources of uncertainty are P_{KD}, W_{KD}, V_T, M_{KD}, M_{UO_2} M_{UO_3} and W the quantification of the uncertainty in the variables are as follows.

1. The standard uncertainty in P_{KD} is given by

$$u(P_{KD}) = \frac{0.001}{\sqrt{3}} = 0.000577350269$$

2. The standard uncertainty in W_{KD} is given by

$$u(W_{KD}) = \sqrt{2 \quad 0.0577350269^{\ 2}} = 0.081649658 \text{ mg}$$

3. The standard uncertainty in W is given by

$$u(W) = \sqrt{2 \quad 0.0577350269^{\ 2}} = 0.081649658 \text{ mg}$$

4. The standard uncertainty in V_T is given by

$$u(VT) = \sqrt{(0.01164)^2 \quad (0.01225)^2}$$
$$= 0.01689601142 \text{ mL}$$

5. The standard uncertainty in M_{KD} is given by

$u(M_{KD}) = \sqrt{a^2 \quad b^2 + c^2} = 0.08732000806$ g mol^{-1}
where a = 0.0069220323; b = 0.000519615;
c = 0.00011547 g mol^{-1}

6. The standard uncertainty in M_{UO_2} is given by

$$u \ M_{UO_2} \quad \sqrt{(0.00035)^2 \quad (0.000058)^2}$$
$$= 0.03511882991 \text{ g mol}^{-1}$$

7. The standard uncertainty in M_{UO_3} is given by

Table-1: Values of variables and uncertainties in them

Variable	Value	Standard Uncertainty	Relative Std uncertainty
Rep	1.0	0.000584	0.05844
W(KD)	1.226 g	0.0000817 g	0.00661
P(KD)	1.0	5.7735×10^{-4}	0.00577
$M(UO_3)$	286.0271 g mol^{-1}	5.228×10^{-2} g mol^{-1}	0.01828
$M(UO_2)$	270.0 g mol^{-1}	3.5118×10^{-2} g mol^{-1}	0.01301
M(KD)	294.2 g mol^{-1}	8.732×10^{-2} g mol^{-1}	0.02968
V_T	24.0 mL	0.0169 mL	0.07040
W	84.9 mg	0.0000817 g	0.09617

$$u\ M_{UO_3} \quad \sqrt{(0.00052)^2 \quad (0.000058)^2}$$
$$= 0.05228126639 \text{g mol}^{-1}$$

Conclusion

The measurement uncertainty involved in the determination of O/U ratio of hyperstoichiometric uranium dioxide powder thus can be quantified in terms of the expanded combined uncertainty at 95% confidence level as 0.0036, thus O/U of the sample = 2.043 ± 0.004.

Acknowledgements

The authors express their deep sense of gratitude to Sri N. Saibaba, Chief Executive, NFC and to Sri B. Prahlad, DCE(QA, TS, HRD & Lib) for their encouragement and support in the present investigation.

Certification of Biological Reference Materials by Instrumental Neutron Activation Analysis

Mamata R. Lanjewar[1] and R.B. Lanjewar[2]

1. *Department of Chemistry, R.T.M. Nagpur University, Nagpur, (M.S.), India; E-mail: rb_lajewar@rediffmail.com*
2. *Department of Chemistry, Dharampeth M.P.Deo Memorial Science College, Nagpur, (M.S.) India*

A multielemental instrumental neutron activation analysis (INAA) method by short and long irradiation has been employed for the determination of 21 minor and trace elements in two standard Reference Materials P-RBF and P-WBF from Institute of Radioecology and Applied Nuclear Techniques, Czekoslavakia. Also some biological standards such as Bowen's kale, cabbage leaves (Poland) including wheat and rice flour samples of local origin were analysed. It is suggested that INAA is an ideal method for the certification of Reference Materials of Biological Matrices.

Introduction

The deficiency of essential micronutrients and excess of toxic metals in cereals, an important food items for human nutrition, can cause public health risk. Therefore, before their consumption and adoption of soil supplementation, concentrations of essential micronutrients and metals in cereals should be monitored.

Well characterized reference materials have to be extremely useful in verifying the accuracy of analytical procedures and quality of data. A number of SRMs/ CRMs have been developed by NIST(USA), IAEA(Vienna), NIES(Japan) and other agencies. Nowadays trace element analysis of foods and related materials has gained importance from both toxicological and nutritional point of view [1]. Accurate measurement of trace elements in foodstuffs is of crucial importance to estimate dietary intake of essential elements required for normal human growth. NAA has been widely used for the certification of SRMs due to its multielemental capability and high sensitivity for most elements [2]. We have employed INAA for the determination of 18 elements in two proposed SRMs, P-RBF and P-WBF from Czechoslavakia. Also wheat and rice flour samples of local origin were analysed for comparison.

In recent years, a variety of biological materials including lichens have been suggested for use as biomonitors of environmental pollution [3]. However, the control of analytical quality in this field is hampered by non existence of suitable SRMs. In this regard, we have analyzed two intercomparison run samples of Lichen (IAEA-336) and control material of cabbage leaves (IAEA-359) for trace elements. Several biological standards were also analysed for quality assurance of our data.

Experimental

Institute of Radioecology and Applied Nuclear Techniques Czechoslovakia had distributed two samples of Rye bread flour (P-RBF) and Wheat bread flour (P-WBF). Its moisture content was determined by drying at 60°C in an electric oven for 6 h. IAEA (Vienna) and Portugese National Laboratory of Energy and Indutrial Technology (LNETI) had distributed lichen reference material (IAEA-336) and a control material of cabbage leaves (IAEA-359). 15-25 mg each of P-RBF, P-WBF, Lichen, a synthetic standard[4] and biological standards (Bowen Kale and NIST SRM wheat flour) were packed in high purity Al foil, irradiated for 15 min and 1 hrs at thermal neutron flux of 10^{12} n $cm^{-2}s^{-1}$ followed by high resolution gamma spectroscopy using 80 cm^3 HPGe detector. For long irradiation of 1 week, 35-50 mg each of sample and the standards were encapsulated in High purity quartz ampoules and irradiated for one week in CIRUS reactor at BARC, Mumbai. After about 1 week delay, samples were counted on 113 cm^3 HPGe (PGT) detector.

Result and Discussion

National Institute of Standards and Technology (NIST), USA and International Atomic Energy Agency (IAEA), Vienna are the two prime organizations actively involved in the development of Reference Materials (SRM or CRM) of biological, geological, environmental and other matrices. Whereas at NIST these SRMs are characterized within their own laboratories at Gaithersburg employing various analytical techniques at IAEA CRMs are also distributed to various laboratories around the world through Analytical Quality Control Services (AQCS). For the certification of concentration of an element in an SRM, it is essential that atleast two independent analytical techniques should be adopted. A critical literature survey has shown that NAA has been extensively use for the certification. It is essential due to its ability to assess homogeneity efficiently and essentially blank free nature which make it extremely valuable tool for use in SRM certification [5-7].

Our INAA data for two proposed standards (P-RBF and P-WBF), wheat and rice flour of local origin, Lichen (IAEA-336), cabbage leaves (IAEA-359) and the two standards Bowen's Kale and NIST SRM wheat flour listed in Table.1. It is observed that our concentration in two standards are in good agreement with the certified values. Elemental

Table-1: Concentration of elements in Biological Standards and Samples

Element	Bown Kale	Wheat flour (SRM-1567)	P-RBF	P-WBF	Wheat Flour	Rice Flour	Lichen (IAEA-336)	Cabbage (Control IAEA-359)
Br, g/g	26.05 0.6 (24.9)	7.78 0.06 (9)	0.63 (0.541)	1.45	-	-	-	7.3 0.5
Cl, g/g	3080 (3560)	396 (-)	360 (436)	693 (656)	-	-	1.84 0.15 (1.91)	8.68 0.57
Co, ng/g	73.9 18 (63.2)	71 10 -	180 (76.9)	79 (23.3)	61	42	170 10 (290)	171 10 (120)
Cr, g/g	0.28 0.02 (0.37)	0.21 0.02 (-)	0.59 (0.446)	0.40 (0.11)	0.83	0.19	1.65 0.06 (1.60)	1.12 0.14 (1.30)
Cs (ng/g)	78 (76.3)	0.024	34 (6)	29 (4.75)	36	25	-	-
Cu, g/g	4.92 0.6 4.92	3.14 0.3 (2.0)	3.45 (2.43)	3.35 (2.77)	-	-	5.19 1.1 (3.57)	4.22 0.8 (5.22)
Fe, g/g	109 9 (119)	18.1 4.6 (18.3)	87.3 (20.8)	48.8 (23.8)	61.1	15.0	372 68 (430)	133 23 (155)
Hg, ng/g	106 (171)	6 (9)	3.6 (2.42)	4.0 (2.7)	-	-	372 68 (430)	133 23 (155)
K, mg/g	23.8 2.3 (24.4)	13.7 0.1 (13.6)	3.16 (2.67)	2.85 (2.55)	-	-	2.0 0.1 (1.8)	31.3 2.3 (31.9)
Mg, g/g	2.07 (1.67)	1.73 0.20 (-)	2.0 (0.41)	1.24 (0.556)	-	-	1.0 0.06 (0.58)	1.30 0.08 (2.0)
Mn, g/g	14.2 0.2 (14.8)	9.35 2.7 (8.5)	27.8 (18)	18.9 (22.6)	-	-	11.8 0.8 (62.3)	12.3 0.8 (31.3)
Na, mg/g	2.29 0.14 (2.36)	7.73 0.5 (8.0)	3.0 (1.3)	9.0 (2.1)	-	-	0.83 0.19 (0.32)	0.99 0.12 (0.57)
P, mg/g	4.90 0.37 (4.48)	1.88 0.35 (-)	2.47 (1.71)	2.72 (2.28)	3.89 (-)	1.98	0.75 0.06 (0.61)	2.71 0.09 (5.26)
Rb, g/g	57.2 3.7 (53.4)	1.15 0.08 (1.0)	1.66 (1.25)	1.69 (1.53)	4.03	3.49	1.5 0.2 (1.8)	6.0 0.7 (6.0)
Sb, ng/g	-	-	4.6 (5.29)	20 (21.4)	21	9	-	-
Sc, ng/g	13.1 (9.48)	7 (-)	8.6	4.4	106	4.8	-	-
Se, ng/g	119 2.0 (134)	- (1.11)	26.0 (29.2)	30.5 (38.4)	192	61	240 10 (220)	220 9 (110)
Zn, g/g	31.6 1.4 (32.29)	15.1 1.0 (10.6)	18.5 (16)	21.3 (17.9)	41.1	5.8	39.9 1.5 (30.2)	36.5 2.9 (37.9)

Note: Values in parenthesis are the certified or literature values

concentration in various standards were calculated using synthetic standards provided by Prof. Suzuki[4] and Bowen's kale. Later other standards were also used as comparator and finally mean values were calculated. Standard deviations in most of the cases are <10% suggesting high precision except in few cases like Fe due to interferences. Therefore, a radiochemical procedure need to be adopted.

Our elemental concentration in four flour samples are likely to be accurate within +10%. A comparison of elemental contents in two proposed standards with their accepted mean values show fairly good agreement. In some cases, however, large deviations have been observed. Element content in two bread flour (P-RBF and P-WBF) shows that these differs widely in Na, P, Br, Cr, Sb and Co whereas other elements such as K, Mn, Zn and Hg are similar. Also wheat and rice flour show striking differences in Cr, Sb, Fe, Zn and Se which are quite obvious.

A close look at the data in Table 1 show that in case of Lichen (IAEA-336) and cabbage (IAEA-359) our elemental contents for most elements are in good agreement with their accepted mean values. However, concentration of K, Mg and Mn differ from accepted mean values. In case of Lichen, it is observed our values for Br, Cl, Cr and Rb are in excellent agreement with that of accepted mean values. Our values for Cu, Fe, Hg and Zn differ by ~20% from the accepted values. Also the standard deviation for most elements are <10% thus suggesting precision of our data.

In view of our data presented here, it can be concluded that INNA is suitable method for the certification of elemental contents in samples of biological origin.

Reference

[1] K. Okamoto, Sci. Total Environ., 107 (1991) 29.

[2] C. Vandeecasteele, Microchim Acta, 2 (1991) 379.

[3] P.Ila, J. Radioanal. Nucl. Chem., 120 (1988) 247.

[4] N. Suzukim, Y. Iwata and H Imura, Anal.Sci., 2 (1986) 335.

[5] R.R. Greenberg, Anal. Chem., 58 (1986) 2511.

[6] C. Galinha, H.M. Anawar, M.C. Freitas, A.M. Pacheco, M. Almeida-Silva, J. Coutinho, B. Macns, A.S. Almeida, 69(11) 2011, 1596.

[7] Saad A. AL-Kahtani and Omar A. F. Ald-dayel, Int. J. Chem. Sci, 6(3), (2008) 1653.

Recent Advances in Microwave Heating Assisted Sample Preparation Methodologies in Chemical Quality Control of ThO_2 based MOX Fuels

G. Singh, R.K. Malav, R.B. Bhong, A.B. Name, A. Pandey, D.K. Das, P.G. Behere and Mohd. Afzal

Advanced Fuel Fabrication Facility, Nuclear Fuels Group, Bhabha Atomic Research Centre, Tarapur, 401502, India; E-mail: gitendars@barctara.gov.in

An insight into recent developments in microwave heating assisted sample preparation for representative, accurate and precise analytical measurements in radio-analytical and quality control laboratories for ThO_2 based MOX fuels at AFFF has been illustrated. The pressure vessel dissolution parameters were optimized for liquid sample preparation whereas a co-denitration technique was developed for solid sample preparation for metallic impurity determination by DC-arc-AES. It was demonstrated that the microwave heating assisted sample preparation (liquid and solid) is a novel technique for representative sample preparation. The pros and cones of the conventional methods vis-à-vis microwave heating assisted sample preparation have also been discussed.

Introduction

Among the actinide oxides of interest in the nuclear industry, dielectric properties of ThO_2 make it microwave transparent whereas UO_2 and PuO_2 as microwave absorbers [1-2]. ThO_2 and ThO_2 based mixed oxide (MOX) fuels are relatively stable, inert and less susceptible to dissolve [3]; the methodologies for their quantitative and rapid dissolution is the research matter for which an actinide chemist is looking for.

In this paper, the scope of the application is discussed in liquid and solid sample preparation for ThO_2 based MOX fuels in wider context. The pressure vessel dissolution parameters were optimized for liquid sample preparation whereas a co-denitration technique was developed for solid sample for metallic impurity determination by DC-arc-AES. The pros and cones of the conventional methods of sample preparation vis-à-vis microwave heating assisted sample preparation have been discussed.

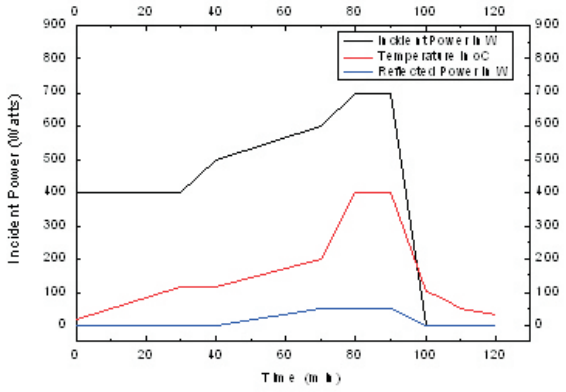


Fig. 1 A typical power and temperature profile during microwave co-denitration of ThO_2 based MOX sample

Experimental

Materials and Instruments

Non-sintered ThO_2, PuO_2 and UO_2/U_3O_8 and sintered ThO_2, (Th, Pu)O_2 and (Th,U)O_2 pellets. Two indigenously designed and developed microwave heating systems (MHS-I: 0.8KW and MHS-II: 3KW) and a commercial (MHS-III: 1.6KW dual magnetron) @ 2450 MHz were used in the present study.

Moisture Removal from Fuel Samples

Samples were heated in microwave cavity for 5-10 minutes to remove moisture and other volatiles at specified incident power.

Sample and Standard Preparation

Working standards of Th, U and Pu were prepared by dissolving respective nuclear grade oxides in A. R. grade 16M HNO_3. Dissolution of standards and samples was performed in PTFE safety pressure vessels operated upto 40 bars for quality control analysis requiring sample in solution form. The co-denitrated solid samples of ThO_2, (Th,U)O_2 and (Th,Pu)O_2 were prepared in quartz vessels using a specific microwave power program for analyzing metallic impurities by DC-arc-AES (Fig. 1).

Analyses requiring Sample in Solution Form

Actinide Determination: In the microwave digested samples thorium in the presence of plutonium was determined by Ethylenediamminetetraacetic acid (EDTA) complexometric titration using Xylenol Orange as visual indicator of titration end point [4] after oxidizing Pu to Pu(VI) by AgO [5]. The dissolved uranium was quantified by modified Davies and Gray redox titrimetric method [6] followed by potentiometric end point determination and Ti^{3+} reduction of U in H_2SO_4 medium [7] and Bi-amperometric end point detection. The plutonium was determined by Drummond and Grant redox titrimetric method [8]

Table-1: Various quality control analyses and microwave versus conventional sample preparation w.r.t. analytical outcomes.

Sample type	Analysis required	Conventional method of sample preparation	Microwave heating assisted sample preparation	Results
ThO_2, (Th, Pu)O_2, (Th,U)O_2	Heavy metal content	In Pt. dishes under IR lamp	In PTFE pressure vessels	Comparable
ThO_2, (Th, Pu)O_2, (Th,U)O_2	MI by ICP-OES, IC	In Pt. dishes under IR lamp	In PTFE pressure vessels	Comparable
UO_2/ PuO_2	Iso Comp TIMS	In Pt. dishes under IR lamp	In PTFE pressure vessels	Comparable
Liquid waste	Activity (gross alpha)	As such	In PTFE pressure vessels	Conventional showed negative bias
ThO_2, (Th, Pu)O_2, (Th,U)O_2	MI by DC-Arc-AES	Grinding/ milling	Dissolution and co-denitration to oxide powder	Conventional showed negative bias

MI- metallic impurity, IC- Ion chromatography, IR- Infra red

where titration end point was detected potentiometrically.

Metallic Impurity: The metallic impurities were determined by ICP-OES [9] and ion chromatography (IC) after solvent extraction of major matrix.

Isotopic composition: The isotopic composition of Pu was determined by TIMS after dissolution of samples in HNO_3 by microwave in pressure vessels.

Activity assay: The activity (gross alpha) was measured in aqueous waste samples after microwave heating assisted dissolution [10]. Small samples (0.25ml) were fixed on SS disks by hot plancheting technique and activity was measured by ZnS (Ag) scintillation counter.

Analyses requiring Sample in Solid / Powder Form

The metallic impurities were determined by DC-Arc-AES in microwave co-denitrated mixed oxide powder samples of ThO_2, (Th,1%Pu)O_2, and (Th,8%Pu)O_2.

Results and Discussion

As microwaves can penetrate deep into core of the materials and heats uniformly, moisture/ volatiles were removed rapidly and quantitatively from the samples.A comparison of microwave and conventional sample preparation for chemical quality control of ThO_2 based MOX fuel is presented in Table 1. The results were compared using appropriate statistical tools.

The liquid waste generated in various MOX fuel fabrication stages, contains agglomerates/ chips of MOX and a small fraction in dissolved form. The activity measurement after microwave dissolution of samples could help in accurate categorization and hence treatment of various liquid wastes.

The DC-Arc-AES requires homogeneous sample in powder form. UO_2 and UO_2 based MOX samples (low PuO_2%) are easily pulverized by oxidation whereas in ThO_2 based MOX, the oxidative pulverization is not feasible. The crushing and milling of samples will not yield sufficiently homogeneous samples usually. The microwave dissolution in HNO_3 and co-deniration of nitrate solutions to get homogeneous oxide powder was developed. It was observed that the metallic impurity content in the samples prepared by grinding/ milling method shows lower values and there was no loss of metallic impurities by microwave co-denitration.

Conclusions

It has been demonstrated that microwave heating assisted sample preparation (liquid and solid) is a novel technique for representative sample preparation and hence precise/ accurate analytical measurements in the chemical quality control of ThO_2 based MOX fuel. The microwave co-denitrated MOX powder can be used for determination of metallic impurities by DC-arc-AES technique.

Acknowledgement

Authors express their sincere thanks to all colleagues of chemical quality control section of AFFF for extending their help during the experimental work and preparing the manuscript. We are extremely grateful to sh. Arun Kumar, Director, Nuclear Fuels Group, for his keen interest and constant encouragement during the course of this work.

References

[1] Holocombe C. E., American Ceramic Society Bulletin, 62 (1983) 1388.

[2] Hass P. A., American Ceramic Society Bulletin, 58 (1979) 873.

[3] Bond W. D., ORNL-2519, Oak Ridge National Laboratory, (1958).

[4] Vogel A. I., Text book of Quantitative Inorganic Analysis, 3rd edition, Logmans, Green and Co.Ltd, London 442.

[5] S. P. Hasilkar, N.Gopinath et. al., J. of Radioanalytical and Nuclear Chemistry, 122 (1988) 69.

[6] Davies W. and Gray W., Talanta 11 (1964) 1203.

[7] N. Gopianth et. al., J. of Radioanalytical and Nuclear Chemistry, 96(3) (1985) 273.

[8] Drummond J. L. and Grant R. A., Talanta, 13 (1966) 477.

[9] N. D Save, S Ghosh, Rohit Malav, G. Singh, R. K Jaiswal, Neeraj Kumar, A. Prakash, Md. Afzal and J. P. Panakka, Proceedings of ICAS Kochi, (2010).

[10] R. K. Malav, G. Singh, D.K. Das, Amrit Prakash, P.G. Behere and Mohd. Afzal: pp-363, NUCAR, (2013).

Analysis of Titanium in D9 alloy- An Inter Comparison Study and Application to Radioactive Sample

S. Sriram, S. Annapoorani, V. Hemalatha and K. Sankaran

Analytical Chemistry & Spectroscopy Section, Materials Chemistry Division, Chemistry Group, Indira Gandhi Centre for Atomic Research, Kalpakkam 603 102; E-mail: ksran@igcar.gov.in

Titanium modified Austenitic Stainless steel alloy (D9) is well known for its swelling resistance under demanding reactor ambience. Chemical characterization of such important alloy carries much larger role in the quality control aspects. This work compares various analytical procedures and techniques envisaged to determine titanium concentration in D9 samples and further extending the analysis to radioactive D9 wrapper and clad of MOX test fuel sub assembly.

Introduction

The material under present study, namely a Titanium modified, controlled carbon content austenitic stainless steel is currently a candidate material for the fuel clad and wrapper tubes of 500 MWe PFBR. This steel is designated as D9 alloy. The nominal composition of this alloy is designed to be around that of AISI 316, but with the important exception of having high nickel, correspondingly low chromium, besides controlled titanium additions. It is believed that the matrix/TiC interface would be playing a significant role in accommodating the radiation damage. Hence a precise chemical quantification of titanium is necessary.

Analytical Techniques and Experimental Procedure

The following analytical techniques were used for analysis viz. RFGDOES, Spark OES, ICPOES, EDXRF, CNAA and LIBS. The material for this study was obtained from RML, IGCAR in the form of flattened specimens of wrapper and clad. Apart from solid specimens, respective metal chips were also readied for dissolution purposes. A known weight of these chips was dissolved using aqua regia/HF and made upto 100mL. This solution was analysed using ICPOES and concentration of titanium was obtained. Solid specimens were analysed using RFGDOES, Spark OES,LIBS and ED-XRF and the results are tabulated. Based on the procedures followed for the inactive samples, a radioactive wrapper and clad specimens from MOX test fuel sub-assembly were analysed for its titanium content using ICPOES.

Calibration

Certified Reference Materials of Stainless Steel (NIST and BAS) are used as standards for Calibration curves for the direct solid analysis. The standards are surface finished and then sparked with the conditions selected and the intensities of the light radiation emitted by the individual elements are acquired by the photomultiplier tubes. This is linearly related to the concentration of the elements. In order to offset probable fluctuation in the operating parameters, the intensities of the individual elements obtained by sparking are then ratioed with the intensity of the matrix iron line and calibration curves are plotted between intensity ratio (I_e/I_{Fe}) versus concentration by fitting the values to the suitable equation. The polynomial for which the standard deviation is minimum and which will accommodate maximum number of the data points in the curve is used to plot the calibration curves. Similarly, methods were standardized using solution standards (SRM) for ICPOES technique.

Precision and Accuracy

The precision of the result expressed in percentage RSD (relative standard deviation in %) is given by the equation RSD = (sd/mean) x 100, where 'sd' is the standard deviation. Each specimen was sampled on different places and the mean of a minimum of three best replicate analyses is used for each sample to calculate the precision. Typical values of 1-2% RSD is routinely obtained for major elements like Cr, Ni, Mn, Mo and Si while 2-5% is obtained for other minor and trace elements like Ti, C, S, P, V, Nb, Al etc., by RFGDOES and Spark OES techniques. Since Certified Reference Materials are used for drawing calibration curves, the results obtained are very accurate.

Application to Radioactive Samples of Wrapper and Clad

A cut section from fuel pin "00P0" of MOX test fuel sub assembly was characterized for its titanium concentration after dissolution and analysed using ICPOES.

Dissolution Procedure

About 400 mg of sample was taken in a Teflon beaker and 5 mL of aqua regia was added to it. The sample was heated using hot plate for about 20 min and at the end of the dissolution, 2 drops of HF was added. After cooling, the sample was made upto 50 mL in a PP standard flask. The dose rate was measured in this standard flask at a distance of about 5 cm, and found to be 200 mR/h. The final solution was analysed using ICPOES inside a glovebox.

Table-1:

D9 Wrapper Analysis		D9 Clad Analysis	
Technique	Conc. of Ti (%)	Technique	Conc. of Ti (%)
RFGDOES (CG)	0.19 ± 0.01	RFGDOES[CG]	0.2 7± 0.01
SPARK OES (CG)	0.18 ± 0.01	SPARKOES [CG]	0.28 ± 0.01
ICPOES (CG)	0.17 ± 0.01	ICPOES [CG]	0.28 ± 0.01
EDXRF (RSD)	0.18 ± 0.01	LIBS [CG]	0.29 ± 0.01
ICPOES (NFC)	0.17 ± 0.02	ICPOES[NFC]	0.28 ± 0.02
ICPOES(BARCF)	0.17 ± 0.01	CNAA(CG)	0.25 ± 0.02

Table-2: Radioactive samples from MOX test fuel sub assembly using ICPOES:

D9 Wrapper_T Analysis		D9 Clad_T Analysis	
Titanium	0.18 ± 0.01 %	Titanium	0.31 ± 0.02 %

Results and Discussion

Table 1 compares the concentration of titanium in D9 alloy obtained from various analytical techniques. It is found that the values of Titanium agreed well for both solution based and direct solid analytical techniques within the acceptable limits.

Acknowledgement

The authors are greatful to Mr. Ran vijay kumar and Mr. Karthik for providing us the D9 alloy specimens used in this study.

Uncertainty Budget in Internal Monostandard NAA for Small and Large Size Samples Analysis

K.B. Dasari, R. Acharya

Radiochemistry Division, Bhabha Atomic Research Centre, Trombay, Mumbai 400 085, India; E-mail: racharya@barc.gov.in

Total uncertainty budget evalution on determined concentration value is important under quality assurance programme. Concentration calculation in NAA or carried out by relative NAA and k0 based internal monostandard NAA (IM-NAA) method. IM-NAA method has been used for small and large sample analysis of clay potteries. An attempt was made to identify the uncertainty components in IM-NAA and uncertainty budget for La in both small and large size samples has been evaluated and compared.

Introduction

Instrumental Neutron Activation Analysis (INAA) is a nuclear analytical technique for quantitative determination of elements in different matrices and offers simultaneous multi-elemental capabilities. Every quantitative result should be reported with corresponding uncertainty, which reflects the quality of results. Inherently NAA method has few sources of errors compared to many instrumental and wet chemical methods. In relative INAA method most of the parameters are not affected to combined uncertainty due sample and standard are irradiated together and counted at identical geometry. Unlike relative method, the k_0 methodology, several uncertainty parameters should be considered into combined uncertainty like mass of the samples and standards, counting statistics, peak fitting error, detector efficiency ( ) and geometry, coincidence, flux parameters, nuclear constants, etc.

In 2003, k_0-based internal monostandard NAA (IM-NAA) method was developed at RCD, BARC. The advantage of method is that it doesn't require any external standard for getting elemental concentration ratios in order to calculate total uncertainty using following equation for small size sample

$$\frac{m_x}{m_y} \quad \frac{(S.D.C.)\ (f \quad Q_0(\ ))_y}{(S.D.C.)\ (f \quad Q_0(\ ))_x} \frac{P_{Ax}}{P_{Ay}} \quad \frac{\ \ _y}{\ \ _x} \frac{k_{0,Au}(y)}{k_{0,Au}(x)} \quad (1)$$

where P_A is the net peak area under the gamma line of interest, S is the saturation factor, D is the decay factor, C is the counting factor for correcting the decay during counting period, f is the thermal to epithermal neutron flux ratio, is the epithermal shape parameter, $Q_0(\ )$ is the resonance intergral to 2200 m/s cross section ratio, $k_{0,Au}$ is the literature $k_{0,Au}$-factor and is the in-situ relative detection efficiency.

In the IM-NAA using highly thermalized neutrons, the ratio of the mass (m) of an element x to the element y present in the sample is given by the following expression for large size non-geometry samples analysis,

$$\frac{m_x}{m_y} \quad \frac{S.D.C._y}{S.D.C._x} \frac{P_{Ax}}{P_{Ay}} \quad \frac{\ \ _y}{\ \ _x} \frac{k_{0,Au}(y)}{k_{0,Au}(x)} \quad (2)$$

Among the above discussed INAA methods relative NAA and IM-NAA methods are best than the single comparator k_0-based NAA method. The error contribution in relative NAA and IM-NAA methods comparison are given in Table 1.

Table-1: Uncertainty components in small and large samples, and its typical values using INAA methods

Parameters	Small samples		Large sample IM-NAA
	Relative NAA	IM-NAA	
Sample mass	✓	✓	X
Std. mass	✓	✓	X
Conc. Std	✓	✓	X
P_A analyte	✓	✓	✓
P_A standard	✓	✓	✓
(element efficiency)	X	✓	✓
(Internal std. efficiency)	X	✓	✓
$k_{0,\ Au}$ factor (element)	X	✓	✓
$k_{0,\ Au}$ factor (IS: Na, Sc)	X	✓	✓
f	X	✓	X
, Q_0	X	✓	X

In the present work, we have calculated combined uncertainty in IM-NAA for small and large size pottery samples. In IM-NAA, elemental concentrations / ratios such as Cr, Fe, Co, Cs, La, Ce, Zn, Eu, Lu, Hf and Th with respect to Sc were calculated. As a case study, uncertainty budget for a La has been calculated.

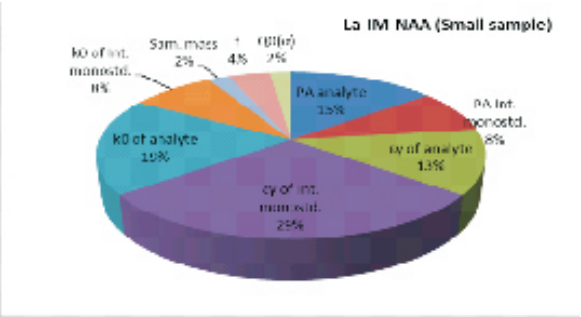


Fig. 1 Pie chart of relative combined uncertainty contribution parameters in IM-NAA method applied to small samples for La analysis

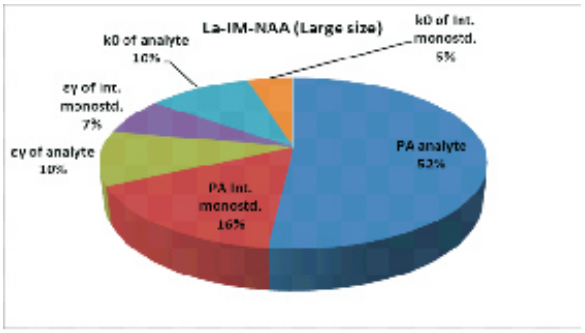


Fig. 2 Pie chart of relative uncertainty contribution parameters in IM-NAA method applied to large size samples

Results and Discussion

The combined uncertainties for elements were calculated applying error propagation rules as per concentration determination equations of NAA methods (Eq.1 and 2).

k_0-based IM-NAA Applied to Small Size Samples

IM-NAA method doesn't require any external standard thus standard concentration parameter will be negligible which major uncertainty contributor is in relative method. A pie chart of relative uncertainty contribution of different parameters for La concentration ratio determination using IM-NAA method is shown in Fig. 1. The combined uncertainty is 3.0 %.

k_0-based IM-NAA Applied to Large Size Samples

IM-NAA application to large size sample is advantage than application to small samples. Most of the parameters are negligible such as mass of the sample due large sample (100g), f + Q_0( ) factor due to samples irradiated in highly thermalized neutrons. A pie chart of relative uncertainty contribution of different parameters for La concentration ratio determination using IM-NAA method applied to large size samples is shown in Fig. 2. The combined uncertainty for La elements is 4.9 %.

Scandium concentration was determined using relative NAA. Elemental concentration of La/Sc was converted into absolute concentration. La concentration in small samples is 44.9 (2.1) ppm and in large size sample is 48.8 (4.8) ppm. Total uncertainty percentages quoted in brackets are in within 5%. Uncertainty in large samples is higher due to higher counting statistics error.

The following precautions should be considered to reduce the uncertainty budget.

1. All significant -ray lines should be identified qualitatively with proper energy calibration.
2. Identification of radionuclides should be confirmed by re-determining their half-lives.
3. Correction for dead time should be as small as possible < 5 %.
4. The counting efficiency of the detector for the sample and standard should be as close as possible.
5. Reproducible counting geometry in terms of distance and sample size.
6. Self shielding effects due to sample size and its composition.
7. Instability in the instrument with regard to resolution and energy calibration should be minimum.

Conclusion

Compared to relative method, total uncertainty of IM-NAA is comparatively higher. LSNAA is advantages than small samples by IM-NAA as f, , Q_0 are not considered as input parameters.

Acknowledgements

Authors thanks to Dr. A. Goswami, Head, Dr. P.K. Pujari, Head, NCS, Radiochemistry Division, BARC for his support and encouragement.

References

[1] AGC Nair et.al, Anal. Chem., 75 (2003) 4868.

[2] K.B. Dasari, et al., J. Radioanal. Nucl. Chem. 286 (2010) 525.

[3] B. Smodiš and T. Bucar J. Radioanal. Nucl. Chem. 269 (2006) 311.

Quantification of Measurement Uncertainty in the Determination of O/U Ratio of Sintered Uranium Dioxide Fuel Pellets by Spectrophotometry

B. Narasimha Murty, U.B. Misra, M. Dutta and H.R. Ravindra

Control lab, Nuclear Fuel Complex, Hyderabad 500 062, India; E-mail: ravindra@nfc.gov.in

Various sources of contributing to the measurement uncertainty involved in the determination of O/U ratio of hyperstoichiometric uranium dioxide powder were identified, their relative contribution to the total measurement uncertainty was quantified and the total measurement uncertainty was quantified in terms of the expanded combined uncertainty at 95% confidence level as 0.0036, thus O/U of the sample = 2.043 ± 0.004.

Introduction

For any industrial laboratory the main objective is to extend uninterrupted and reliable analytical support on a routine basis. For accomplishing this unique task, it becomes essential to look for simple, rapid, rugged and reliable analytical methods to determine various analytical parameters. Thus, quantification of measurement uncertainty in determination of analytical parameter employing a particular method obviously would provide reasonable confidence on the reported analytical result. In this paper, the measurement uncertainty involved in the determination of O/U ratio of hyperstoichiometric uranium dioxide sintered pellets employing a spectrophotometric method is quantified. For the purpose, the methodology given in EURACHEM/CITAC Guide CG-4 is followed. According to this, it is required (i) to formulate the measurand (ii) identification of all the independent variables that can influence the value of the measurand (iii) calculation of the standard uncertainty in the measurement of each variable (iv) calculation of the combined standard uncertainty (v) calculation of expanded uncertainty

Experimental

For determining O/U ratio of hyperstoichiometric uranium dioxide sintered fuel pellets by spectrophotometry, the sintered fuel pellet was powdered manually in a mortar and pestle under the flow of argon gas. Portion of powdered sample was transferred into a dissolver flask provided with a vent for purging of inert gas. To this about 40 mL of 2M sulphuric acid containing few drops of hydrofluoric acid (from which the dissolved oxygen was expelled previously by purging argon gas) and contents were allowed to heat on a water bath while continuing the purging of inert gas continuously for about forty minutes. Then the dissolver flask was removed from water bath and the contents were allowed to cool to room temperature under argon gas purging only. The absorbance of the solution so obtained was measured at 535 nm and also at 285 nm in a matched 1 cm quartz cells. For determining Type A uncertainty, repeated measurements were made on the same hyperstoichiometric uranium dioxide fuel pellet sample and standard deviation for the excess oxygen content was calculated to be ± 0.0013

Quantification of Measurement Uncertainty

The measurand in this present case is excess oxygen content in a hypostoichiometric uranium dioxide fuel pellet, which can be determined by spectrophotometric method using the following expression.

$$x \quad \frac{A_6 \quad {}_4}{A_6 \quad {}_4 \quad A_4 \quad {}_6} \qquad (1)$$

Where A_6, A_4 are the absorbance values recorded for the sample solution at 285 and 535 nm, ${}_6$, ${}_4$ are molar absorptivity values for U(VI) and U(IV) at 285 and 535 nm respectively. To calculate "Type B uncertainty", the identified sources of uncertainty are A_6, A_4, ${}_6$, ${}_4$. For determining the molar absorptivity of U(IV), uranium(IV) stock solution in 2M sulphuric acid medium was made using the degreased nuclear grade uranium metal turnings. Similarly, stock solution of U(VI) was also prepared in 2M sulphuric acid devoid of nitrate. The calibration curve obtained for various concentrations of U(IV) is Y = 6.8067 (X)+ 0.0008; R^2=0.9999 where Y is absorbance of the solution at 535 nm and X is the concentration of U(IV) in mole L^{-1}. Similarly, the calibration curve obtained for various concentrations of U(VI) is A = 584.9563 (B) – 0.0029; R^2 = 0.9998 where A is the absorbance value for the solution at 285 nm and B is the concentration of U(VI) in mole L^{-1}.

For a given calibration curve Y = mX + c, we can calculate the standard deviation in the slope,

$$S_m \quad \sqrt{\frac{S_r^2}{S_{xx}}} \quad \text{where } S_r \quad \sqrt{\frac{S_{yy} \quad m^2 S_{xx}}{N \quad 2}}$$

$$S_{xx} \quad x_i^2 \quad \frac{x_i \quad {}^2}{N}$$

$$S_{yy} \quad y_i^2 \quad \frac{y_i \quad {}^2}{N}$$

The standard deviations in determining the molar absorptivities $_6$, $_4$ for U(VI) and U(IV) at 285 and 535 nm calculated to be 0.038911376 and 6.442849848 L mole^{-1} cm^{-1} respectively. The general relationship between the combined standard uncertainty $u_C(y)$ of a value y and the uncertainty of the independent parameters x_1, x_2, x_3,……., x_n on which it depends is given by

$$u_c (y (x_1, x_2, x_3,……., x_n) = \sqrt{\sum_{i\ 1,n} c_i^2\ u(x_i)^2}$$

$$= \sqrt{\sum_{i\ 1,n} u(y, x_i)^2}$$

where y (x_1, x_2, x_3,……., x_n) is a function of several parameters x_1, x_2, x_3,……., x_n and c_i is a sensitivity coefficient evaluated as $c_i = \frac{y}{x_i}$, the partial differential of y with respect to x_i and u(y,x_i) denotes the uncertainty in y arising from the uncertainty in x_i mm

From the spreadsheet calculation, the standard combined uncertainty in O/U ratio is 0.0018 From the data furnished in the Table, it is easy to know that the contribution of various factors quantitatively towards the overall uncertainty in measurement of hypostoichiometric uranium dioxide powder by titrimetric method. They can be placed in decreasing order of magnitude as (i) Weight of the sample (ii) volume of standard potassium dichromate solution consumed in the titration of sample (iii) repeatability (iv) purity as a mass fraction of potassium dichromate primary standard used (v) molar mass of potassium dichromate (vi) molar mass of uranium trioxide (vii) molar mass of uranium dioxide and (viii) weight of potassium dichromate primary standard taken for preparing standard solution

Conclusion

The measurement uncertainty involved in the determination of O/U ratio of hyperstoichiometric uranium dioxide powder thus can be quantified in terms of the expanded combined uncertainty at 95% confidence level as 0.0036, thus O/U of the sample = 2.043 ± 0.004.

Acknowledgements

The authors express their deep sense of gratitude to Sri N. Saibaba, Chief Executive, NFC and to Sri B. Prahlad, DCE(QA, TS, HRD & Lib) for their encouragement and support in the present investigation.

Author index

Abdul Sattar S. 194
Abhijit Saha 284, 286
Abirami N. 226
Acharya R. 5, 65, 75, 98, 102, 104, 106, 108, 110, 112, 114, 116, 118, 124, 126, 208, 210, 212, 214, 224, 298, 557
Adur B. 114
Adya V.C. 290, 300
Afzal Mohd. 408, 414, 553
Agarwal A.. . . . . 206, 212
Agarwal Chhavi 280, 314
Agarwal Ram K. 228
Agarwal T.K. 328, 497
Aggarwal S.K. 42, 102, 180, 182, 304
Agrawal Anshu 439
Ahuja B.L. 12, 146, 192
Ahuja Sumedha 364
Ajay Kumar 469, 517,
Ajmal P.Y. 140, 142
Akkarakaran J J. 118
Akkurt I. 437
Akshatha 342, 344
Alam Md. Nayer 356
Alamelu D. 102
Alpa Dashora 192
Amit Kumar 505
Anand Vivek J. 350
Anil Kumar P. 477
Anil kumar S. 154, 156, 162, 445
Annapoorani S. 555
Ansari S.A.. 110
Arae H. 519
Archana Mukherjee 278
Arjune Rajkanya. M.. . . . 348
Arun Aravind 481
Arun Kumar 294
Asai M 20
Ashok Kumar G.V.S. . . . 298
Avhad D.K. 527
Avinash P. R. 322
Avinash P. 445
Ayushi Dudwadkar 288
Babu K S. 246
Badigera N. M.. 324
Baghyalakshmi C.M. . . . 226
Bagla Hemlata 62, 388
Balaji Rao Y.. . . . . 152, 254, 256, 258, 260
Balasubramaniyan V. . . . 481
Balbudhe A.Y. 430, 432, 434
Bamankar Y.R. 352
Bandyopadhyay T.. . . . . 318, 334
Banerjee M. 390
Banerjee Sharmila 282, 292
Bara S.V.. 513
Barot Nisha 388
Basavaiah N.. 176
Bassan M.K.T.. 527
Basu H. 521, 523
Basu S.. 390
Basu Sandip 28
Behera A. 208
Behere P.G. 408, 414, 553
Belegya T. 114
Bentoumi G. 3
Bhade S.P.D.. . . . . 471, 473
Bhade Sonali P.D. 154
Bhadwal Mohini 292
Bhamra N.S. 112
Bhangare R.C. 140, 142
Bhanumurthy K. 382
Bhar T.. 390
Bhardwaj S. 98
Bhatta B.C. 240
Bhattacharya D. 216, 404
Bhong R.B. 553
Bhuloka Reddy S. 198, 218
Biswal Jayashree. 369
Biswal R.R. 108
Biswas D.C. 280
Biswas H.S. 220
Bohra Archna 386
Bootharajan M. 412
Borole D.V. 523
Brahmaji Rao J.S. 94, 296
Brahmananda Reddy G. . . 252, 547, 549
Bramha S.N. 567
Buddhadev Kanrar 182
Cantle John 44
Chajduk E 53
Chakrabarty K.. 112
Chakraborty Sudipta, . . . 380, 398
Chakrapani G. 475
Chakravarty R.. 377

Chakravarty Rubel 398
Chandra Shekara K 509
Chandrasekaran A. 150, 188, 467
Chandrasekhar D. 104
Chandrashekar K.R. 342, 344
Charan Kumar K. 459
Chatt A. 26, 88, 90, 120
Chattopadhyay Sankha . . 356
Chaturvedi T. P. 104
Chauhan Neetika 503
Chauhan R. P. 503, 505
Chavan T. 98, 172, 178
Chavan V. 416
Chhillar Sumit 210, 212, 214, 224
Chidambaram S. 483
Chinnaesakki S. 513
Chinnusamy A. 226
Chirag K. Vyas 320, 338
Chopra S. 386
Chowdhury D.P. 220
Daisy Joseph 216
Dalvi Aditi.A. 100, 178
Danko B 53
Danu Laxman S. 280
Dararutana P. 77, 144
Das D. K. 408, 414, 553
Das M.K. 302
Das Malay Kanti 356
Das Sujata Saha 356
Das T. 501
Das Tapas 70, 292
Dasari K. B. 102, 104, 116, 208, 557
Dash Ashutosh 377, 380, 398, 400, 31, 278, 350, 352
Dash S C 55
Datta J. 220
De S K.. 116
Deb S.B. 284, 286, 302
Deolekar S S. 246
Deshmukh A.V. 537, 539
Devarajan M.C. 226
Dey G.K.. 196
Dey M K 308
Dhal Soumya Praksh. . . . 386
Dhami P.S.. 300
Dhanik Jyotsna. 392
Dhawale B.A. 272
Dileep B. N. 463
Dimayuga F. 3
Drishty Satpati 282
Dubey J.S. 330, 491, 531
Durgaprasad Rao A.. . . . 148
Dusane C. B.. . . . . 190, 447
Dutta D. 184
Dutta M. 559
Dutta R K 75, 186
Dybczyñski R S 53
Eappen K. P.. 338
Fatangare N.M 539
Fukushima M. 72, 90
Ganesh S. 242, 264, 316
Gangopadhyay Kaushik . . 17
Gaur Diwakar 122
Gautam Sanghdeep 358
Gaware J. J. 541
Gayatri 358
Geetha P. V. 463
Gey Y. 132
Ghaleb A.M. 146
Ghare P T. 246
Godbole S. V. 270, 290, 330, 404
Godwin Wesley S. 461
Gogoi Diganta 426
Gopalakrishnan R K.. . . . 246, 248
Goswami A. 132, 248, 280, 314, 414
Goswami Sunil. 367, 369, 371, 373
Gothankar S. S. 136, 174
Govardhanan B. 465, 467
Granthali S. 310
Greenberg Robert R.. . . . 49
Guha Sameer Kumar. . . . 363
Gupta S. K. 206, 212
Haba H 22
Halder R.. 196
Hani Baek 68
Hareendran K. N. 172
Harinatha Y. 515
Hazra G. 501
Hemalatha V. 555
Hemalatha.P 164, 507
Hemamalini R.. 176
Hosoda M. 519
Hoyler F.. 479
Hubli R. C. 182
Humera Shaikh 134, 375
Huskens Jurrian 418
Iqbal Mudassir. 418
Ishikawa T. 519

Jae Won Shin 320, 338
Jagadeesan K. C.. 352
Jagasia Poonam 300
Jagrati Sahariya 146, 192
Jagtap S.S. 537, 539
Jain Shubham 396
Jaison T. J. 346, 545
Jalaluddin S. 336, 457
Jat J.R. 254
Jayachandran. 354
Jena S. 204
Jeyakumar S.. 302
Jha S K. 136, 164, 174, 443, 471, 499, 507, 511, 513
Jha S.N. 14, 216, 404
Jha Shailendra 535
Jha V. N.. 531
John R. 132
Jose M.T. 150
Joshi Akhilesh C. 128
Joshi C.P. 348
Joshi D.S. 318, 334
Joshi M 503
Joshi Manish 505
Joshi P. James 463
Joshi V.M. 443
Junghans A. 132
Jyeshtharaj B. Joshi 171
Kademani B. S. 382
Kadwad V.B. 312
Kalaga Dinesh V. 371
Kalyane G. N. 160
Kamachi Mudali U. 226, 238, 240, 264, 316
Kamsali Nagaraja 459
Kanagasabapathy K.V. . . 188
Kanan K. 457
Kanekar A.S.. 92
Kanse S. D. 541
Karekar C. D. 408
Karhadkar C.G. 112
Karpe-Kamat Rupali 469
Karunakara N 463, 509, 429, 541
Kaur N. 214
Kaushik Sanyal 180
Kaustab Ghosh 266
Keila Isaac-Olive 120
Kerur B. R.. . . . . 162, 322, 445
Khan K B 294
Khilnani Roshan 388
Kim G S 68
Kim G. N. 132
Kim K. 132
Knolle F. 479
Kolekar R.V.. . . . . 154, 469, 471, 473
Korde Aruna 282
Kore Prashant S. 134, 138
Koteswara Rao K 402
Koteswara Rao V 86
Kothai P. 168, 190
Krishna N. S.. 495
Krishna Reddy L. 126
Kulali F. 437
Kulkarni M.J. 404
Kumar A. V. 495
Kumar N. 180
Kumar R. 298
Kumar S. 220
Kumar Sangita D. 288, 306, 310
Kumar T.. 426
Lad J.S. 536
Lad Shila N. 244
Ladhaf Bibifatima M. . . . 134, 138, 162, 375
Lagad Rupali A. 102
Lahiri Susanta 17, 266
Lakshmana Das N.. 208
Lakshmia K.S. 441
Lakshminarayana P.V.. . . 148
Lanjewar Mamata R. . . . 360, 551
Lanjewar Ratnakar B. . . . 360, 551
Laoharojanaphand S. . . . 82
Lee E J 68
Lee M. W. 132
Lee Y W 68
Lenka P. 491, 495, 531
Li G. 3
Li L. 3
Lindstrom Richard M. . . . 49
Lokhande Rajkumar M. . . 138
Lokpati Mishra. 160
Luna Barua, ... 356
Madhavi Adiga 344
Madhuparna D. 164, 507
Madhuri Adiga. 344
Madhusmita, ... 356
Madhusudhana Rao P. V. . 94, 194
Mahaboob Pacha M. . . . 477
Mahanty B.N. 414
Mahanty Bholanath 408

Maharia R.S. 75
Maheswari P. 184
Mahiban Ross E. 46
Mahur A. K. 326
Maiti Moumita 17, 266
Maity Sukanta 455
Maji S. 234, 236
Malav R.K.. 553
Mali H B. 114
Malik P. P. 501
Mallesh G. 485
Manchanda V. K. 320, 338
Manikiam B. 459
Manish Chand 296
Manisha V. 310
Manjunatha H.C.. . . . . 422, 424
Massavczyh R. 132
Matsue H. 90
Matsutani T. 72
Maurice Navodita 365, 394
Mayya Y. S. 541
Meenakshisundarama V.. . 441
Mete U. 98
Mhatre Amol 262
Minal Nadar 160
Mishra Shuddhodan P. . . 379
Mishra P.K. 276
Mishra R. 336, 457
Mishra S.. . . . . 447, 519
Mishra Sandeep 358
Mishra Sujata 232, 240
Misra N.L. 180, 182
Misra Pragati. 358, 365, 394
Misra U.B. 559
Mithlesh kumar 270, 272
Mitra P. 501
Mohamad Daud 1
Mohammad F.M. 146
Mohan N.I.G.N. 373
Mohapatra M. 80
Mohapatra P.K. 92, 300, 406, 410, 414, 418, 533
Mohapatra S.. . . . . 330, 491, 495, 531
Mohapatra C. 306
Mohite Baburao S.. 244
Mohokar H.V. 485
Mondal S. 182
Mukesh Kumar 439, 487
Mukherjee A. 377
Mukherjee Joyeeta 511
Mukherjee S.. 184
Mukherjee S.K. 180, 210
Murali M.S. 248, 406
Murthy P.K. 306
Naga Raju G. J. 198, 218
Nagame Y 20
Nagar B.K. 284, 286
Nagendra Kumar P.V. . . . 126, 402
Naik H.. . . . . 10, 132
Nair A. 491
Name A.B. 553
Nanda B.B. 108
Nandita Panda 232
Narasimha Murty B. 252, 547, 549, 559
Narayana P.V.L. 386
Narayani K. 156
Naresh Gamre 278, 400
Naseerutheen A. 188
Natarajan D. 226
Natarajan R. 242, 264, 316
Natrajan V.. . . . . 80, 216, 270, 272, 404
Nayak A.K. 256, 258
Nayak C. 216
Nayeem M.A. 122
Neelam Kumari 533
Nemoto T. 72
Nepolian M. 483
Nevinsky I.. . . . . 436, 437
Nevinsky V. 436
Nicy Ajith 98
Nidhi Gupta 262
Niharbala Devi 232
Nimai Pathak 270
Nuwad Jitendra 352
Ohtsuki T 30, 74
Otari Anil 525
Padma Savithri P 430, 432, 434
Padmavathy S. 428
Pai Rajesh V. 180
Pandey Usha 278
Pandey A. 416, 553
Pandey A.K. 38, 110, 304
Pandey B.K. 86, 122
Pandey K.L. 268
Pandey N.K. 266, 242, 264, 316
Pandey Renu 364
Pandey U. 377, 400
Pandit G.G. 140, 142, 158, 168, 190

Pankaj Kumar B.. 386
Pant A.D. 154, 246
Pant H. J.. . . . . 34, 367, 369, 371, 373, 384, 396
Pant R.C.. 394
Papu Samanta 284
Patel Renuka 112
Pathak P.N. 92, 533
Patil Rajashekar K 354
Patnaik R. 527
Patra A. C. 489, 531
Patra A. K.. . . . . 436, 348, 545
Patra Sabyasachi 314
Paul S. 334
Paul Sabyasachi 318
Pavelka S. 78, 340
Pawar Pravina P. 130, 134, 138, 166, 375
Pillai S N. 294
Pillay R. H. 136
Pimple M.V. 521, 523, 527
Polkowska-Motrenko H . . 53
Pradeepkumar K.S. 46, 154, 156, 246, 469, 471, 473, 525
Prahlad B. 258
Prajith R.. . . . . 336, 557
Prakash A 294
Pranav M. Joshirao 320, 338
Prasad M. V. R. 188
Prasad R. S. 294
Prasad K.L. 306
Prasanna M. V. 483
Premachand K.. 148
Premadas A. 250
Prince Prakash Jebakumar . 465
Pritty Rao 200
Priya Srinivasan 248
Priyadarshini N. 238
Priyalata S.. 398
Priyanka Reddy 499
Pujari P.K. 104, 108, 112, 114, 116, 184, 210, 212, 214, 224
Pulhani Vandana 246, 471, 511
Punniyakotti J.. 441
Pyszynska M. 53
Radha Rani 226
Radhakrisna A. P. 509
Raghav N.K. 537, 539
Raghavendra Y. 276
Raja Annamalai G.. 188
Raja P. 420
Rajaram S. 443
Rajeeta Joseph 216
Rajendra Prasad 487
Rajendra Prasad T.. 459
Rajesh Kumar 439, 487
Rajesh S. 322, 445
Rajesh Sankhla 170
Rajput P. 216
Raju M.K. 94
Rajurkar Nilima 96, 110
Rajurkar Umesh S. 138
Rajvir Singh 469, 471, 473, 525
Ram S.S. 186
Ramakumar K.L.. 268
Ramamoorthy N.. 382
Ramana B. V. V. 152
Ramana J. V. 222
Ramanjaneyulu P.S. 268
Ramkumar Jayshree 402
Ramnarayan K. 194
Ramteke P.W. 358, 365
Ramu Ram 350, 398
Rana Y.S. 112
Rao A.D.P. 386
Rao A.K.. 306
Rao A.S. 306
Rao D. D. 160, 170
Rao I.N. 386
Rao S.V.S. 426
Rasmi R.R.. 312
Ratna Raju M. 94, 148
Raut D.R. 410, 414
Raut V V. 302
Ravi P M 330, 346, 348, 430, 432, 434, 463, 489, 491, 493, 495, 517, 531, 543, 545
Ravindra H. R.. . . . . 152, 258, 254, 256, 258, 260, 547, 549, 559
Ravisankar R. 150, 188
Ray D. K. 204, 208
Ray N.R. 220
Reddy A. V. R 5, 75, 98, 106, 112, 116, 124, 126, 220, 230, 288, 298, 308, 310, 402, 515, 521, 523, 527
Reddy G. L. N. 222
Reddy N. Sivagangi 402
Reddy P.J. 154, 469, 471, 473

Remya Devi P.S. 100
Revay Z. 114
Rita 122
Rogge R. 3
Rosaline Mishra 322
Rout G.B. 86, 122
Rout P. C. 210
Rout R. P. 336, 457
Rout Sabyasachi 517
Roy Shantanu 371
Rufus A.L. 128
Rupa N. 86
Rupali C.K. 499
Rupvate V. H. 172
Sagar Anil 382
Sagar D.V. 330
Sagar Veena 262
Sahoo B. K. 328, 485, 487, 497, 503, 541
Sahoo G.S. 318, 334
Sahoo Laxmidhar 525
Sahoo S. K. 84, 330, 491, 493, 495, 519, 531
Sahoo S. 308
Sahu S. K. 140, 142, 168, 190, 240, 447, 449, 451, 453, 455
Saibaba N. 258
Samajdar I. 196
Samantaray J.S. 367, 369, 373
Sampath M. 238
Samuel G. 377
Sandeep S. 168
Sangita Dhara 180
Sanjay Kumar S. 180, 182
Sanjiv Kumar 200, 202, 222
Sankaran K. 234, 236, 555
Sanu S. Raj. 164, 507
Sapra BK 328, 336, 457, 487, 497, 503, 541
Saradhi I.V. 158
Sarangi A.K. 122
Saraswat Priyam 396
Sarbjit Singh 262
Sarita 206
Sarita P. 198, 218
Sarkar S. 75, 186
Sarma H.D. 377
Sarma Haladhar Dev . . . 278
Sarnaik Jayula 312
Sartandel S. J. 513
Satendra Kumar 234, 236
Sato T K 20
Satpathy K. K. 188
Satpati A K 308
Satyam P. V. 196
Satyanarayana G. 256
Saurabh Sneha 392
Saxena A. 216
Saxena M.K. 268, 284, 286, 302
Saxena Sanjay Kumar . . . 350, 352
Schädel M 20
Scherer U.W. 479
Schnug E.W. 479
Schwengner R. 132
Seetharamireddy B. 194
Sengupta Arijit 290, 406, 418
Sengupta A. 300
Sengupta D. 326
Sengupta P. 196
Seshadreesan N.P. 94, 296
Seshadri H.. 481
Seshaiaha K. 515
Seung-Woo Hong 320, 338
Shagufta Khan 230
Shah R.V. 304
Shahul Hameed P. 420
Shaikh Humera. B 138
Shailesh Kantak 96
Shakir Khan M. 332
Shankaran M. R. 457
Shanmugamani A.G.. . . . 426
Sharanabasappa 162
Sharma P.K. 521, 527
Sharma Anil 326
Sharma Mukesh 535
Sharma Rajveer 386
Sharma S. K. 184
Sharma V.K. 367, 369, 373, 384
Shashank S. Saindane . . . 525
Shehanaz Bano 260
Shekhar Kumar 238
Shenoy K Bhaskar 354
Shenoy K. B.. 312
Sheshshayee M.S. 365
Shetty P.G.. . . . . 449, 451, 453
Shin S.G. 132
Shinde Amol D. 106, 108, 124, 214
Shinde Rakesh N. 110, 118

Shrivastava H.B. 86
Shukla Narayani 358, 394
Shukla Pradeep K 358, 365, 394
Singh K.P. 112
Singh A. 206
Singh A. K. 182
Singh Bhupinder 362, 363, 364, 394
Singh D. 214
Singh G. 553
Singh Gursharan 373
Singh H.P. 306
Singh I.S. 160
Singh Lalit Mohan 487
Singh Mrinalini J. 428
Singh P. 212
Singh Rajvir 154, 156
Singh Tej 112
Singhal R.K. 362, 364, 521, 523
Singhal Sourabh 369
Sinha Amar 8
Sinha P.K. 426
SitaMahalakshmi N. V. . . 148
Sivakumar S. 465
Sivaprasad N. 312
Smodiš B. 51
Sodaye S. 210, 212, 224
Sola P. 82
Solapurkar M. N. 294
Somashekarappa H M . . . 312, 354, 509
Sonali B. 499
Sonali P.D. Bhade 469
Sonar N.L. 274
Soni P.K. 206
Sonkawade R.G. 326
Sonu Sharma 192
Sorimachi A. 519
Sreedevi K.R. 543
Sreekumar B. 426
Sreenivasa Rao N. 434
Srikantha G. A. 365
Srinivasu N. 379
Srinuttrakul W. 82
Sriram G.. 55
Sriram S. 555
Srivastava A.. . . . . 98, 206, 214, 479, 525
Srivastava S. 118
Srivastava S.K.. . . . . 430, 432, 434
Subbarao R.V. 226
Sudarsan V. 196
Sudarshan K. 210
Sudarshan M. 75, 186
Sudeep Kumara K.. . . . . 463, 529, 541
Sudha Vani T.J. 402
Sugandhi S. 443
Sukumar A.A. 202
Suman V. 334
Sumana Paul 304
Sumedha 362, 363
Sumesh C. G. 330, 493
Sun G M.. 68
Sunil C. 334
Sunil kumar Beena 475
Sunitha Y. 202
Suprasanna P. 118
Sur B. 3
Suresh Gandhi M. 150
Suri M.M.K 525
Surung Bharat S.. 130
Suwankot N. 82
Suyatin B. 436, 437
Swain K.K. 98, 100, 112, 116, 178
Swaminathan K. 412
Swarnkar M. 449, 451, 453
Swaroop K. 354
Takale R.A. 449, 451, 453
Takamiya K. 74
Tamilarasu S. 176
Tancharakorn S. 144
Tanuja Nesari 96
Tapase A. S. 350
Thakur D.A. 274
Thakur V. K.. . . . . 495, 531
Thilagavathi R. 483
Thivya C. 483
Thulasi Brindha J. 543
Thulasidas S.K. 270
Tirumalesh K. 483, 485
Tirupathi Naidu 373
Tiwari M. 140, 142
Tokonami S. 519
Tomar B. S. 60, 268, 302
Tomer R. P. S 55
Toyoshima A. 20
Tripathi R.M. 136, 164, 174,330, 346, 348, 430, 432, 434, 443, 489, 491, 493, 495, 499, 507, 511, 513, 517, 529, 531, 543, 545

Tripathy S. K. 330
Tripathy S.P. 318, 334
Tsukada K 20
Tsvetkova T. 436, 437
Tupe Vandana A. 166
Tyagi S.K. 392
Ujwal P. 463
Upadhyay Rajesh K. 396
Vaishali De 276
Vajpyee L K.. 246
Valsala T.P. 274, 276
Vashisht B.. 98
Vasudevan T. 416
Velavendan P. 242, 264, 316
Velmurugan S. 128
Velraj G. 176
Venkata Subramani C. R. . 24, 94, 296, 298, 412
Venkatakumaran B. 150
Venkatesan V. 294
Venkatesh K.. 310
Venkatraman B. 467
Venki Bejawada 306
Verboom Willem 418
Verma A.K. 156
Verma Deepak 332
Verma G.P. 154
Verma R.. . . . . 100, 112,
Verma S K. 116
Vijayagopal P. 467
Vijayakumar V. 226
Vijayalakshmi D. 94
Vijayalakshmi I. 150
Vikram Kumar S. 200, 202, 222
Vimalnath K. V. 380, 398
Vinod Kumar A. 493
Vishwa Prasad K 430, 432, 434
Vishwanath P. Singh . . . 324
Vishwaraj I. 274, 276
Vithal G.K.. 306,
Vivekanand Kain 230
Wagh D. N. 98, 172, 178
Wagner A. 132
Won-in K. 144
Yadav A.K. 404
Yadav R. K. B.. 246
Yamashita Nobuyoshi . . . 523
Yang J. H. 68
Yashodhara I. 463, 509, 529, 541
Yogendra Kumar. 350, 352
Zaman M. 132
Zhang W. 88